Photoinduced Hydrogen Atom Transfer Strategies for C-H Activation of Organic Molecules

Dissertation

Zur Erlangung des Doktorgrades der Naturwissenschaften
(Dr. rer. nat.)
an der Fakultät für Chemie und Pharmazie
der Universität Regensburg

vorgelegt von

Daniel Franz Kolb

aus Traunstein

2025

The experimental work for this thesis was conducted at the Institute of Organic Chemistry at the University of Regensburg under the supervision of Prof. Dr. Burkhard König from May 2022 to March 2025.

Date of submission:	02.04.2025
Date of colloquium:	26.05.2025

Board of examiners:

PD Dr. Jonathan O. Bauer	chair
Prof. Dr. Burkhard König	1st referee
Prof. Dr. Oliver Reiser	2nd referee
Prof. Dr. Frank-Michael Matysik	examiner

Table of Contents

Part I – Photoreactions in Water

1. Anthraquinone Sulfonates as Water-Soluble Photocatalysts: Synthetic Applications and Perspectives

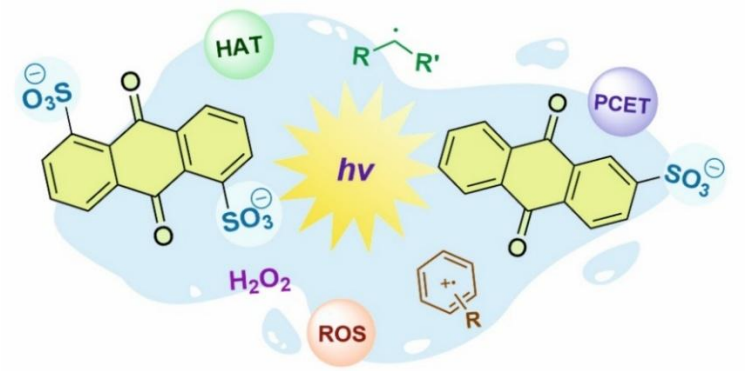

Abstract: Anthraquinone sulfonates (AQS) are water-soluble and cost-effective photocatalysts that have been attracting increasing interest due to their unique features. Their sulfonate groups unlock the application of the photoactive anthraquinone core in aqueous solution. Moreover, these readily available catalysts can engage with substrates through different activation modes, such as hydrogen atom transfer (HAT) and proton-coupled electron transfer (PCET) events. However, to date, their reactivity has not been fully explored, and further applications are expected to emerge. In this perspective, we outline existing synthetic applications and discuss future perspectives.

[i] Reproduced from manuscript submitted to *ChemPhotoChem*, D. Kolb,‡ A. Fedulin,‡ B. König,* with permission from Wiley-VCH GmbH. Schemes, tables, and text may differ from the submitted version.

[ii] Author contributions: D. Kolb and A. Fedulin contributed equally to this work. D. Kolb conceived the concept of this study. D. Kolb and A. Fedulin investigated the scientific background and wrote the manuscript. B. König reviewed the manuscript and is the corresponding author.

1.1 Introduction

Organic photoredox catalysts have become cost-effective alternatives to metal-based catalysts for the C–H activation of organic molecules.[1–3] Herein, even relatively simple quinone derivatives such as naphthoquinones,[4,5] anthraquinones,[6,7] or DDQ[8,9] showcase a rich photochemistry, as these are able to interact as catalysts with substrates through different activation modes, including hydrogen atom transfer (HAT), single electron transfer (SET), and triplet energy transfer (EnT).[4–9]

However, despite the versatility of these quinone-based photocatalysts, due to solubility issues in aqueous media, their use is often restricted to organic solvents. Accordingly, introducing ionizable substituents into these scaffolds can be a fruitful strategy to unlock their application in water, as a sustainable solvent.[10] An example of this approach is anthraquinone sulfonates (AQS), which gather several desirable properties. Their high solubility in aqueous environments, commercial availability, and tunable redox properties make them interesting options for the development of photochemical reactions in water. Herein, the low pKa values of the sulfonate groups of AQS enable the full ionization of these substances in this medium. This simplifies their catalytic systems, as the existence of different species in equilibrium is precluded, as it is the case of other catalysts displaying phosphate or carboxylate groups, whose speciation in water depends on the pH of the solution.[11] Regarding their general structure, AQS display a photoactive anthraquinone core attached to one or multiple sulfonate groups commonly coupled to an ammonium or sodium counteraction (Scheme 1). In organic synthesis, the most commonly used are sodium anthraquinone sulfonates (SAQS) such as sodium anthraquinone-2-sulfonate (**SAQS-1**), sodium anthraquinone-2,6-disulfonate (**SAQS-2**), sodium anthraquinone-2,7-disulfonate (**SAQS-3**)

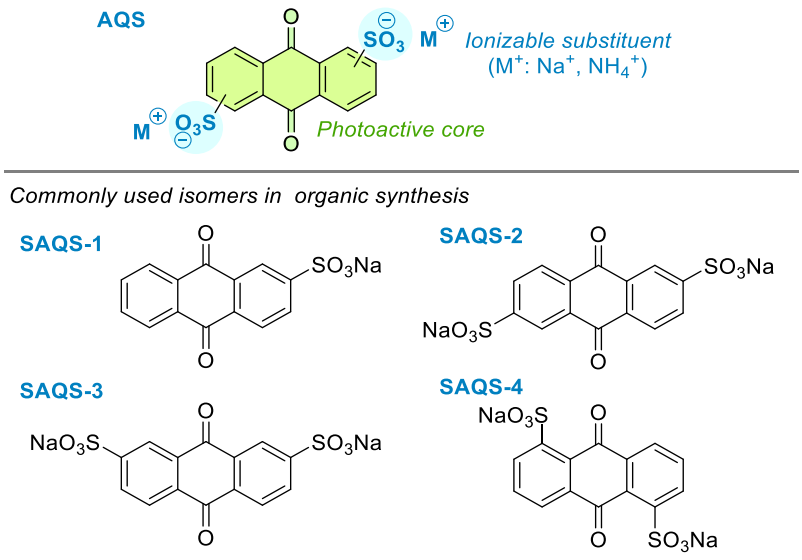

Scheme 1. General structure of AQS and most common isomers used in light-driven synthetic methodologies.

and sodium anthraquinone-1,5-disulfonate (**SAQS-4**). Herein, the number of sulfonate groups, the symmetry, and the substitution pattern have a great impact on the solubility in water of these catalysts, which ranges from 0.0197 M for the monosulfonated derivative **AQS-1** to 0.74 M for the disulfonated derivative **SAQS-3**.[11,12] Moreover, their commercial availability and easy preparation by sulfonating anthraquinone make these catalysts attractive options when developing new reactions in water.

The quinone/semiquinone/hydroquinone redox system is, to date, one of the most studied.[13] Due to their rapid redox kinetics and chemical tunability, AQS have found widespread application as electrolytes in the design of redox flow batteries (RFBs)[13,14–17] or as exogenous redox mediators (RMs) for biological systems.[18–21]

The photophysical properties of AQS were investigated as early as the 1950s.[22] The valuable mechanistic understanding gathered during this stage laid the foundation for the later development of their synthetic photochemical applications. Initially, AQS were almost exclusively employed as catalysts for the photooxidation of alcohols,[22] and as photoinitiators for polymerizations.[23–26] More recently, several catalytic functionalization protocols have been reported, including tandem processes and photoelectrochemistry. Upon irradiation, the photoactive anthraquinone core leads to excited states that can engage with substrates via HAT or proton-coupled electron transfer (PCET) events. For the latter, the excited states of AQS have been found to display oxidation potentials up to +2.3 V in the case of **SAQS-1**.[27] Furthermore, due to their ability to generate reactive oxygen species (ROS),[28,29] AQS can be employed for the oxidation of organic compounds in water.[30,31] Thus, these photocatalysts have promising potential applications in environmental remediation.[7]

To date, these substances have been predominantly employed as photoexcitable HAT agents for the activation of C–H bonds. However, in our opinion, the full potential of these water-soluble catalysts has not been fully explored yet. We expect significant progress in this field, especially as notable efforts are currently underway to further develop photochemical reactions in water.[10,32–38] Accordingly, our intention is to provide the reader with a roadmap of the multiple opportunities offered by AQS.

In this perspective, we outline the general properties of AQS, present existing synthetic applications, showcase recent advances, and discuss future perspectives. For each presented synthetic method, selected substrate scope examples are provided, plausible reaction mechanisms are discussed, and their eventual application in the late-stage functionalization of natural products and pharmaceuticals is showcased.

1.2 Aqueous Photochemistry of Anthraquinone Sulfonates

Despite the many advantages provided by the solubility of AQS in water and their ability to engage with substrates via HAT and ET events, it is of uttermost importance to understand the different ways in which AQS can react with water itself.

Photoinduced reactions between AQS and water have been attracting attention for over 50 years. In the late 1960s it was observed that the irradiation of aqueous solutions of AQSs with near-ultraviolet and visible light yields a mixture of hydroxylated anthraquinone sulfonate derivatives.[39,40] Multiple studies have been conducted to demystify the nature of this aqueous photoreactivity. In early reports,[39–41] the hydroxylating ability of AQS was explained by the generation of free hydroxy-radicals derived from water (Fenton-type chemistry). However more recent studies ruled out the formation of free hydroxy-radicals in aqueous solution of AQS.[42–45] Although until now there is no consensus on the exact mechanism, elaborated spectroscopic studies (including laser flash photolysis) allow us to draw the following photoreaction scheme for sodium anthraquinone-2,6-disulfonate (**SAQS-2**) (Scheme 2a).[43]

First, upon irradiation, **SAQS-2** undergoes photoexcitation to form the triplet species (**SAQS-2***) featuring a lifetime of less than 1 µs. Triplet **SAQS-2*** undergoes a fast reaction

a) Photohydroxylation of **SAQS-2** in in aquesous solution. Mills 1981.[43]

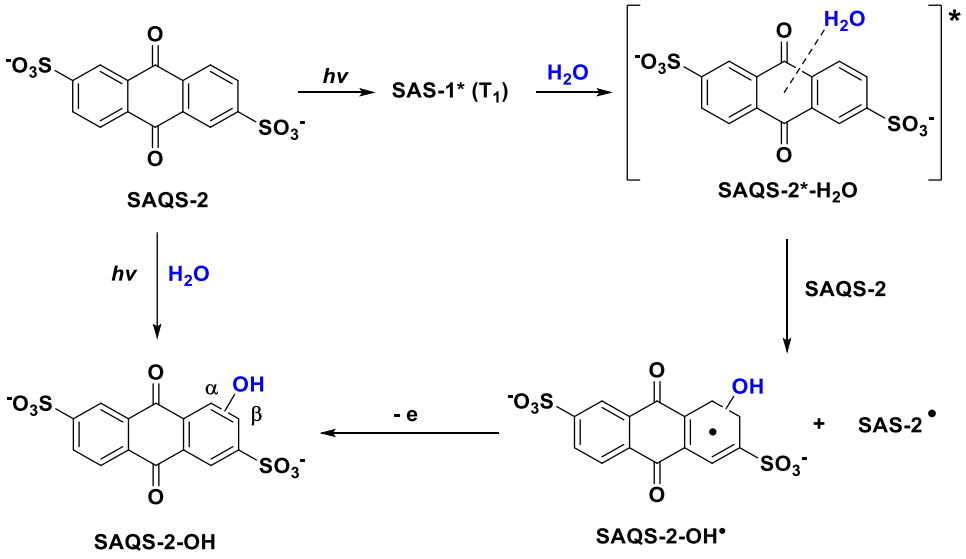

b) Photohydroxylation of arenes with **SAQS-1**. Minero 2008[30] & Sarakha 2010[45]

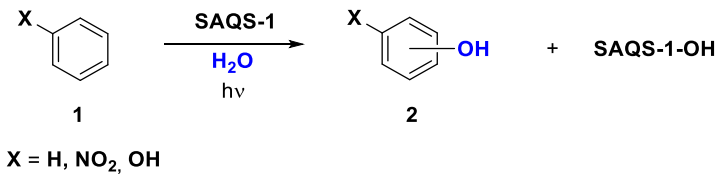

Scheme 2. Aqueous photochemistry of AQS.

with water to form two spectroscopically distinct anthraquinone-water adducts **SAQS-2*-H_2O** (reported as transients B and C).[46] Due to their short lifetimes, exact structures of **SAQS-2*-H_2O** were not clearly determined however, time-resolved resonance Raman spectroscopy provided some hints).[47] Further, **SAQS-2*-H_2O** might undergo oxidation by ground state **SAQS-2** to form an anthraquinone-hydroxy radical adduct **SAQS-2-OH•** and semiquinone radical **SAQS-2•**. The semiquinone species **SAQS-2•** can then be quenched in the presence of molecular oxygen, or, alternatively, under inert conditions, disproportionate to give the parent anthraquinone **SAQS-2** and the corresponding fully reduced hydroquinone (**SAQS-2-H_2**). Oxidation of **SAQS-2-OH•** in aqueous solution by oxygen or another oxidant leads to the formation of stable hydroxylated products **SAQS-2-OH**. The α/β-OH regioisomer distribution depends on the pH of the solution and oxygen concentration.[40] Noteworthy, the photoreactivity and the intermediates observed for monosubstituted **SAQS-1** are almost equivalent to that proposed for disulfonate **SAQS-2**.[45,46,48–53]

Interestingly, light-excited **SAQS-1** species can induce hydroxylation of aromatic compounds (**1**) such as benzene, nitrobenzene, or phenols (Scheme 2b).[30,45] As a result, despite their many advantages, AQS also have an important drawback: they can react with water. Accordingly, these catalysts might not be suitable for reactions requiring prolonged periods of time. Alternatively, an increased catalytic loading can be employed to account for undesired catalyst losses. On the other hand, the photohydroxylating ability of aqueous AQS towards substituted benzenes holds promise for synthetic applications, especially if operated in a catalytic regime.

1.3 Photochemical Applications of Anthraquinone Sulfonates

Photooxidation of Alcohols to Carbonyls

AQS absorb light in the near-UV and visible range to form excited states capable of engaging with substrates in HAT events through homolytic C–H bond cleavage. Some advantages of performing such reactions in water are the inert nature of this solvent towards HAT events (due to the high BDE of its HO-H bond),[54] and the increased lifetimes of the formed open-shell species in this medium, as neutral C-centered radicals do not react with water.[55]

Once these C-centered radicals are formed by AQS, a wide array of transformations can be accessed depending on the presence of radical traps. For instance, molecular oxygen is prone to react with these open-shell species to form peroxyl radicals as reactive intermediates. These, due to their instability, can further collapse to form stable carbonyl derivatives (aldehydes and ketones) or carboxylic acid products upon hydrogen peroxide extrusion.[56,57] Therefore, it is no surprise that the first synthetic applications of AQS were developed under air atmosphere, making use of this ubiquitous external oxidant. Additionally, this aerobic

photooxidative approach has been proven efficient for the design of tandem sequences that make use of the formed carbonyl compounds as electrophilic reactants.

Due to the relatively low bond-dissociation energy (BDE) displayed by α-alkoxy C–H bonds,[54] alcohols are particularly attractive substrates for HAT-based transformations. Moreover, the polarity of these functional groups allows to employ small alcohol molecules in aqueous environments.

Pioneering work by the Cooper group in 1954 provided the first example of the application of AQS for the photooxidation of an alcohol.[22] The authors successfully employed sodium antraquinone-2,6-disulfonate (**SAQS-2**) in aqueous solution under aerobic conditions and 365 nm irradiation. Under these conditions, the photooxidation of ethanol (**2**) yielded a mixture containing acetaldehyde (**3**) as the main product, hydrogen peroxide as by-product, and significant amounts of acetic acid (**4**) (Scheme 3a). The latter formed presumably due to the overoxidation of the formed acetaldehyde product, as the aldehydic C–H bond displays a rather low BDE and is therefore prone to undergo HAT in the presence of **SAQS-2**. Shortly after and building on these results, Wells reported a series of kinetic experiments regarding the photooxidation of several alcohols (**5**) (methanol, ethanol, isopropanol, and *tert*-butanol) with sodium anthraquinone-2-sulfonate (**SAQS-1**) in aqueous solution (Scheme 3b).[58,59] Accordingly, this work expanded the scope of the photooxidation of alcohols to the preparation

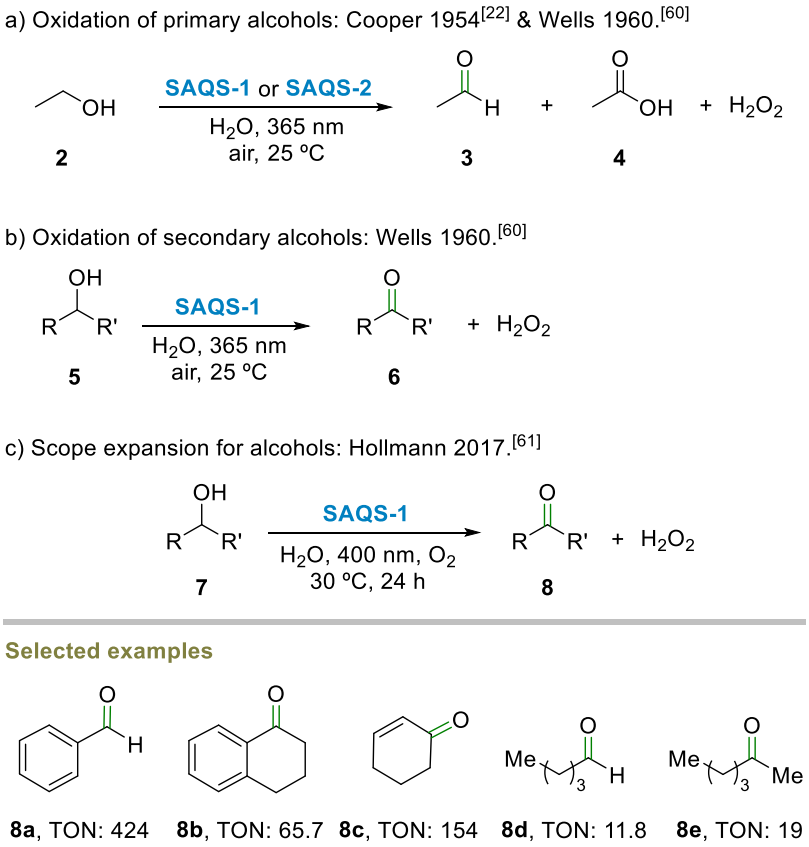

Scheme 3. AQS catalyzed photooxidation of alcohols.

of a ketone (**6**) (in this case, acetone, obtained by oxidizing isopropanol). Altogether, these initial findings were followed by significant mechanistic speculation, wherein Newton concluded that the photooxidation of alcohols proceeded through H-atom abstraction from the alcohol by the electronically excited anthraquinone in its n,π* triplet state.[60]

More recently, inspired by the previously discussed findings, Hollmann and coworkers developed a general method for the photooxidation of alcohols (**7**) using **SAQS-1** as HAT catalyst (Scheme 3c). By activating a wide array of benzylic (**7a** and **7b**), allylic (**7c**), and aliphatic (**7d** and **7e**) α-alkoxy C–H bonds, the corresponding aldehydes, and ketones were successfully prepared (**8a**-**8e**) with reasonable turnover numbers (TON) (Scheme 3c).[61] Herein, the authors proposed a mechanism based on the quenching of C-centered radicals by molecular oxygen and the formation of peroxyl radicals as key intermediates.

Oxygenation of Aliphatic C–H Bonds

Additionally, the Hollman group applied the same approach with **SASQS-1** for the oxygenation of aliphatic C–H bonds (**9**) to give the corresponding carbonyl products (**10a**-**10d**) (Scheme 4).[61] Herein, the experiments performed with alkyl benzenes (**10a**-**10d**) delivered the best turnover numbers (TON) for **SAQS-1**, presumably due to the relatively low BDEs displayed by their benzylic C–H bonds. Less activated C–H bonds displaying notably higher

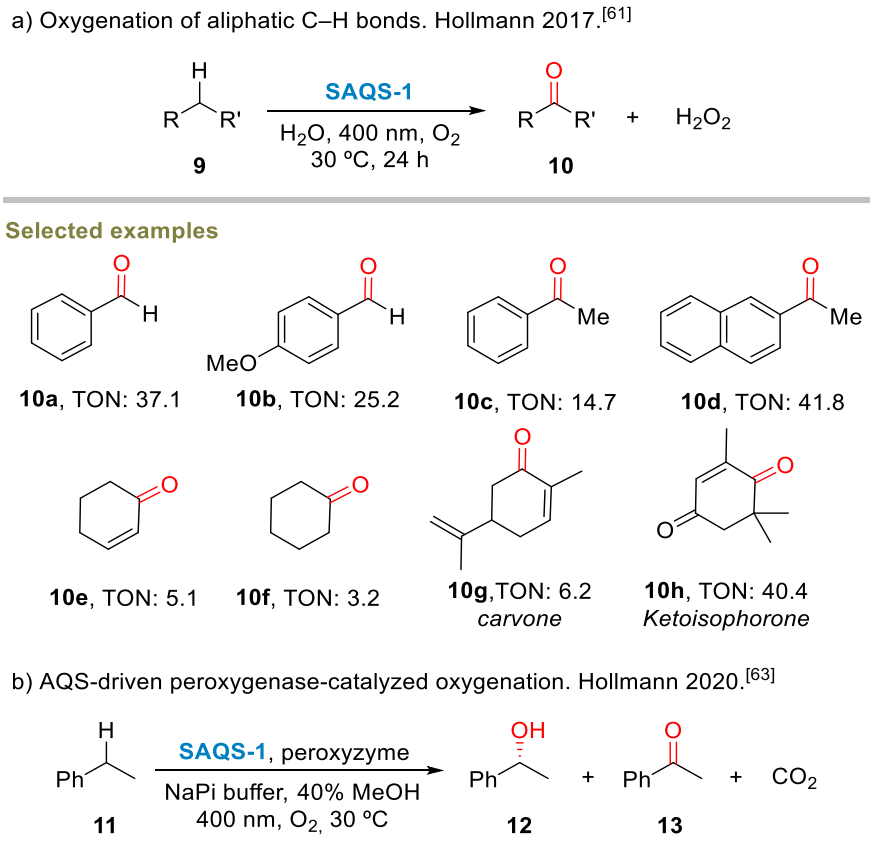

Scheme 4. AQS-driven oxygenation methodologies.

BDEs proved to be suitable as well (**10e**-**10h**), although with notably lower TON, as showcased, for instance, by the oxidation of cyclohexene (**10e**) or cyclohexane (**10f**). Furthermore, the methodology was successfully applied for the selective oxygenation of two natural terpenes: limonene (**9g**) to carvone (**10g**), and isophorone (**9h**) to ketoisophorone (**10h**). Similarly to the photooxidation of alcohols to carbonyl compounds, Hollmann suggested the formation of peroxyl radicals in the presence of oxygen. However, the oxygenation of aliphatics by anthraquinones is still the subject of ongoing investigations and mechanistic speculation.[62]

In a later publication, Hollman and coworkers reported **SAQS-1** as an efficient catalyst for driving the peroxygenase-catalyzed oxygenation of ethylbenzene (**11**) to give 1-phenylethanol (**12**) and acetophenone (**13**) (Scheme 4b), showcasing the combined advantages of water-solubility, excellent reactivity, and compatibility with peroxyzymes as enzymatic systems.[63] Moreover, the initial oxidation of ethylbenzene (**11**) to 1-phenylethanol (**12**) was performed in an asymmetric fashion, although with low enantioselectivity (34% ee). This same approach was applied to the oxidation of cyclohexane to cyclohexanol and cyclohexanone with similar results.

Tandem Photooxidative Processes

Based on the facile photooxidation of alcohols to carbonyls by AQS, such transformations can be coupled to additional steps, thus utilizing the formed aldehydes as reactive electrophilic intermediates. As a result, tandem photooxidative processes (TPP) in alignment with the principles of green chemistry[64,65] can be easily designed, thus circumventing tedious intermediate purification steps.

Such an approach was successfully implemented with **SAQS-1** by the Itoh group in 2015.[66] Herein, the photooxidation of benzyl alcohols (**14**) to benzaldehydes (**Int-1**) under aerobic conditions was coupled with a subsequent aldol condensation with cyclic ketones (**15**). Accordingly, the authors prepared several β-hydroxy ketones from benzyl alcohols displaying various substitution patterns and cyclic ketones of different ring sizes (**16a**-**16e**) (Scheme 5). Furthermore, by employing a derivative of L-proline as a water-soluble asymmetric organocatalyst (**OC***), the corresponding products were obtained with high diastereo- and enantioselectivities. For this tandem process, the authors proposed the *in situ* generation of benzaldehydes (**Int-1**) accompanied by concomitant hydrogen peroxide formation as a key step. Once the aldehyde is formed, it is proposed to undergo a condensation reaction with the enolate of the corresponding cyclic ketone. This final step is catalyzed by **OC***, which transfers its chiral information to the substrate, thereby enabling the nucleophilic attack of the enolate to occur in an asymmetric fashion.

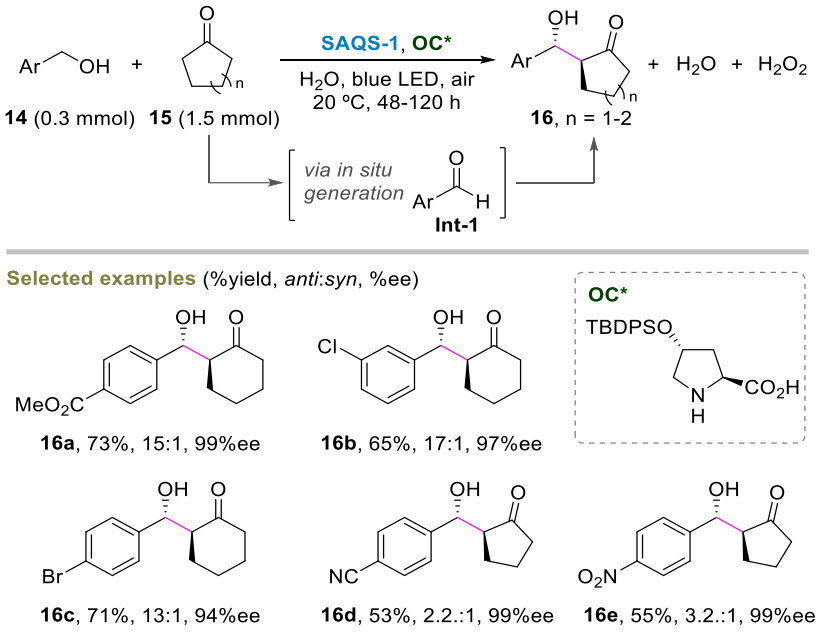

Scheme 5. Asymmetric photooxidative aldol condensation of benzyl alcohols.

More recently, the König group applied a similar strategy for the preparation of benzylidenemalononitrile derivatives (**19**) from benzyl alcohols (**17**) and malononitrile (**18**) (Scheme 6).[67] For this, the photooxidation of the benzyl alcohols to the corresponding

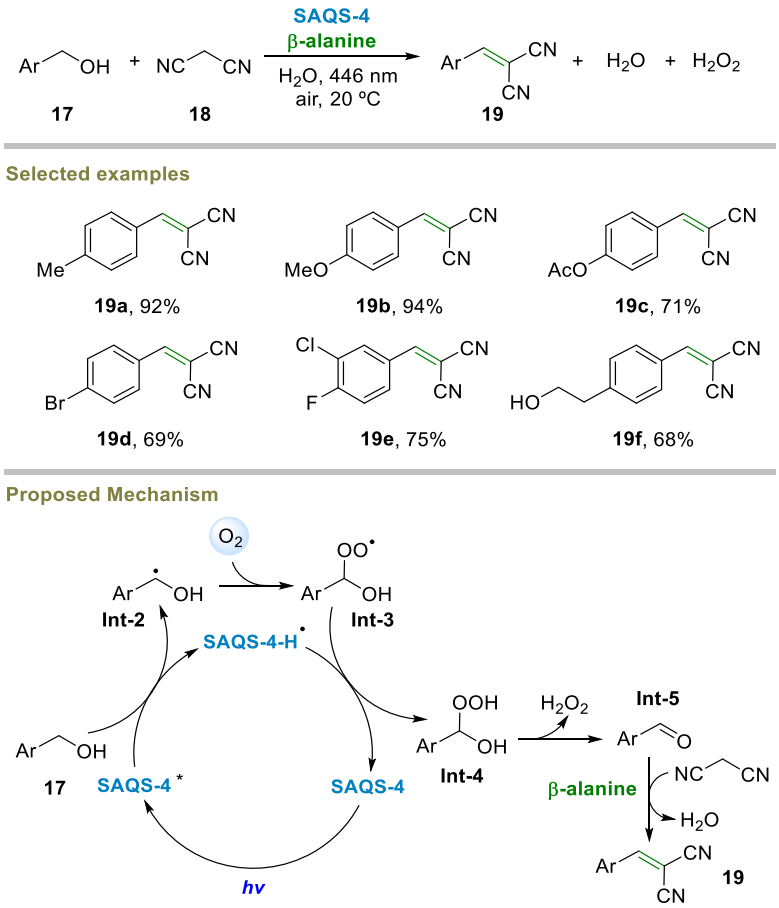

Scheme 6. Tandem synthesis of benzylidenemalononitriles in/on water under visible light.

benzaldehydes intermediates, was coupled with a Knoevenagel condensation reaction. As a result, hydrogen peroxide and water are generated as by-products. This dual catalytic system comprises sodium anthraquinone-1,5-disulfonate (**SAQS-4**) as HAT catalyst and β-alanine as a green and inexpensive organocatalyst. Regarding the substrate scope, benzyl alcohol and its derivatives with electron-donating groups gave particularly good results in terms of yield and short reaction times (**17a** and **17b**). Additionally, the system was found to be compatible with various other substituents (**17c**-**17e**). Moreover, this methodology was demonstrated to be efficient for the selective functionalization of benzylic- over aliphatic alcohols (**17f**). Due to the low solubility of the formed products in an aqueous medium, they can be easily isolated in most cases by filtering the reaction mixture, resulting in an operationally simple protocol. Referring to the results published by Hollmann[61] and Itoh,[66] the König group proposed a plausible reaction mechanism for this transformation.

First, the photoexcited anthraquinone sulfonate (**SAQS-4***) engages with the benzyl alcohol (**17**) via HAT to generate an α-alkoxy benzylic radical (**Int-2**). This species can then be quenched by molecular oxygen to generate a peroxyl radical (**Int-3**). The resulting *O*-centered radical is proposed to reoxidize the reduced **SASQS-4-H**$^{\bullet}$ to its ground state (**SASQS-4**), and the formed peroxide intermediate (**Int-4**) to decompose to the corresponding aldehyde (**Int-5**), releasing hydrogen peroxide. The aldehyde, in the presence of β-alanine as an organocatalyst, undergoes condensation with malononitrile, which results in the formation of the corresponding benzylidenemalononitrile product (**19**).

Bromination of Arenes

As an alternative to HAT activation, the excited triplet state of AQS can engage in sequential proton-coupled electron transfer (PCET) processes. These sequences are initiated by a single electron transfer (SET) event between the excited AQS and an aromatic substrate with an accessible oxidation potential. The generated radical aryl cation intermediate then undergoes subsequent proton transfer (PT). Despite of the great oxidative power of AQS, the synthetic applications of this activation mode are limited to just a few examples.

Due to their carbonyl groups, the electron density of anthraquinones can be easily altered by protonation, leading to modifications in their redox properties. As a result, particularly high redox potentials can be achieved, which would otherwise be almost exclusively attainable by notably more expensive photocatalysts such as iridium complexes or acridinium dyes.

This strategy was successfully implemented by the König group for the bromination of electron-rich arenes (**20**) via aromatic C–H activation through PCET (Scheme 7).[27] By protonating **SAQS-1** with trifluoroacetic acid (TFA), the authors claimed to achieve a redox potential of +2.3 V, able to engage with a variety of arenes via ET. The generated radical cation

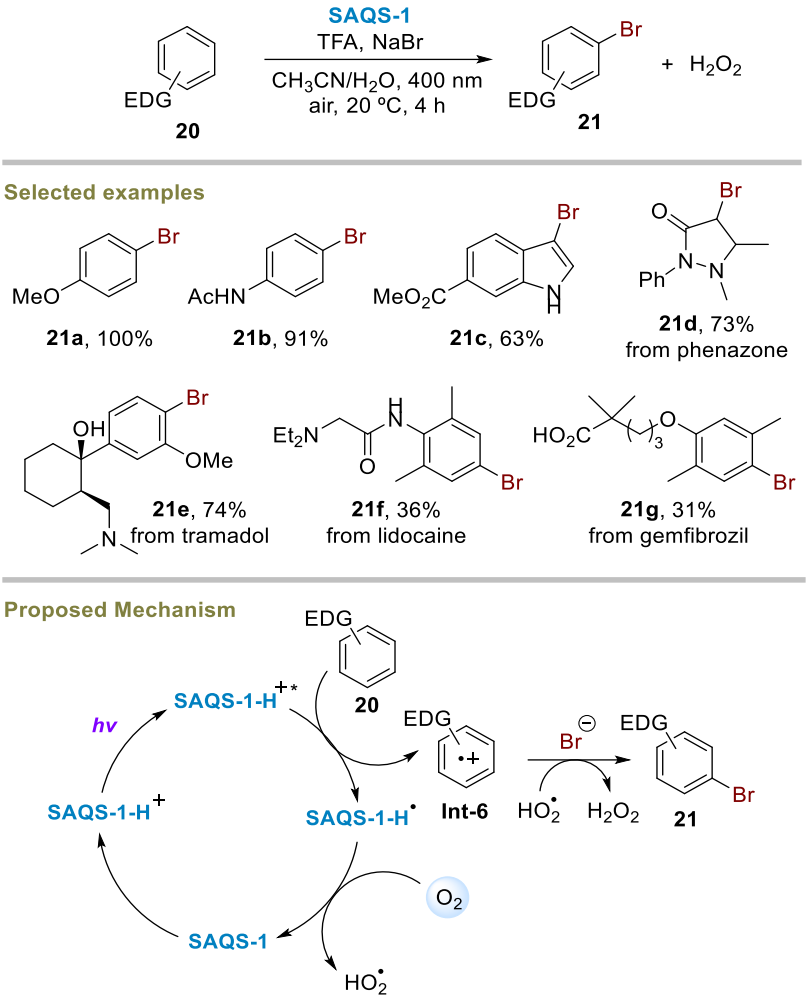

Scheme 7. Photocatalytic bromination of electron-rich arenes.

aryl species (**Int-6**) are postulated to undergo nucleophilic attack in the presence of bromide anions. As a result, the corresponding aryl bromide (**21**) is formed while hydrogen peroxide is formed as a by-product of the process since oxygen is used as an external oxidant for the regeneration of the photocatalyst. This example showcases the versatility of AQS, as their redox properties can be easily tuned in the presence of certain additives such as acids.

However, to date, the modification of the redox properties of these catalysts via protonation of hydrogen-bonding events remains relatively unexplored. Regarding the substrate scope, the methodology was successfully applied for the preparation of a wide array of products (**21a-21g**), including bioactive molecules such as phenazone (**21d**), tramadol (**21e**), lidocaine (**21f**) and gemfibrozil (**21g**). Interestingly, a similar enhancement in reactivity by protonation was reported for AQs in a photooxygenation process of alkanes.[62]

Regarding AQS-driven brominations, the Hollmann group demonstrated more recently the application of **SAQS-1** for the bromination of thymol (**22**) using peroxidase (Scheme 8), which proceeds through the *in situ* generation of hypobromite as the oxidizing agent.[63] Herein, methanol is used as the sacrificial electron donor to drive this bromination process.

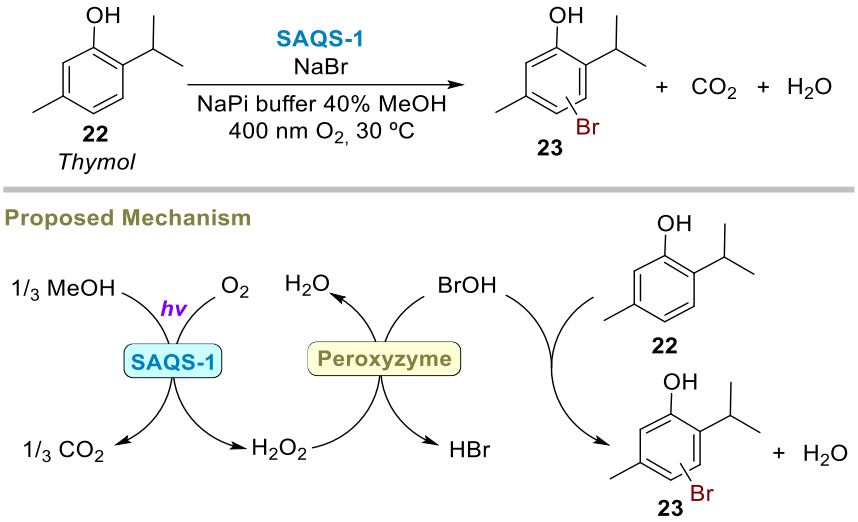

Scheme 8. AQS-driven peroxidase catalyzed bromination of thymol.

Photoelectrochemical Asymmetric Cyanation of Benzylic C–H Bonds

Another interesting application of anthraquinone sulfonates is their combination with photoelectrochemistry. Herein, the Xu group disclosed a versatile cyanation protocol for benzylic C–H bonds (**24**).[68] While trimethylsilyl cyanide (TMSCN) is used as cyanation agent, the dual catalytic system is based on the interplay between sodium anthraquinone-2,7-disulfonate (**SAQS-3**) for benzylic radical generation and a copper complex employed for radical trapping (Scheme 9). As an alternative to other cyanation protocols based on photoinduced HAT,[69–71] Xu and coworkers employed **SAQS-3** for a two-step sequential electron/proton transfer. In this process, the applied current was used for regenerating both catalysts. By employing a chiral ligand (**L1***) in combination with a copper salt, the transformation was carried out in an asymmetric fashion, with high enantioselectivities. In addition, formic acid was employed for enhancing the reactivity of **SAQS-3** by increasing its oxidation potential, a similar strategy that has already been discussed for the bromination of electron-rich arenes by **SAQS-1**.[27]

Due to the mild reaction conditions, the system exhibited broad functional group tolerance (**25a**-**25j**). Its scope included, for instance, a peptide derivative (**25e**) and highly reactive groups such as azides (**25f**) or epoxides (**25g**). Furthermore, the methodology was applied for the late-stage functionalization of bioactive molecules such as ibuprofen- (**25h**) D-glucose- (**25i**) or penicillanic acid (**25j**) derivatives.

Regarding the proposed mechanism, the catalytic cycle is initiated with **SAQS-3** being excited by light to give **SAQS-3*,** which can engage through ET with the alkyl-arene substrate. As a result, an ion-radical pair is formed between the benzylic radical cation and the reduced semiquinone radical. Next, a PT event takes place between both species which results in the

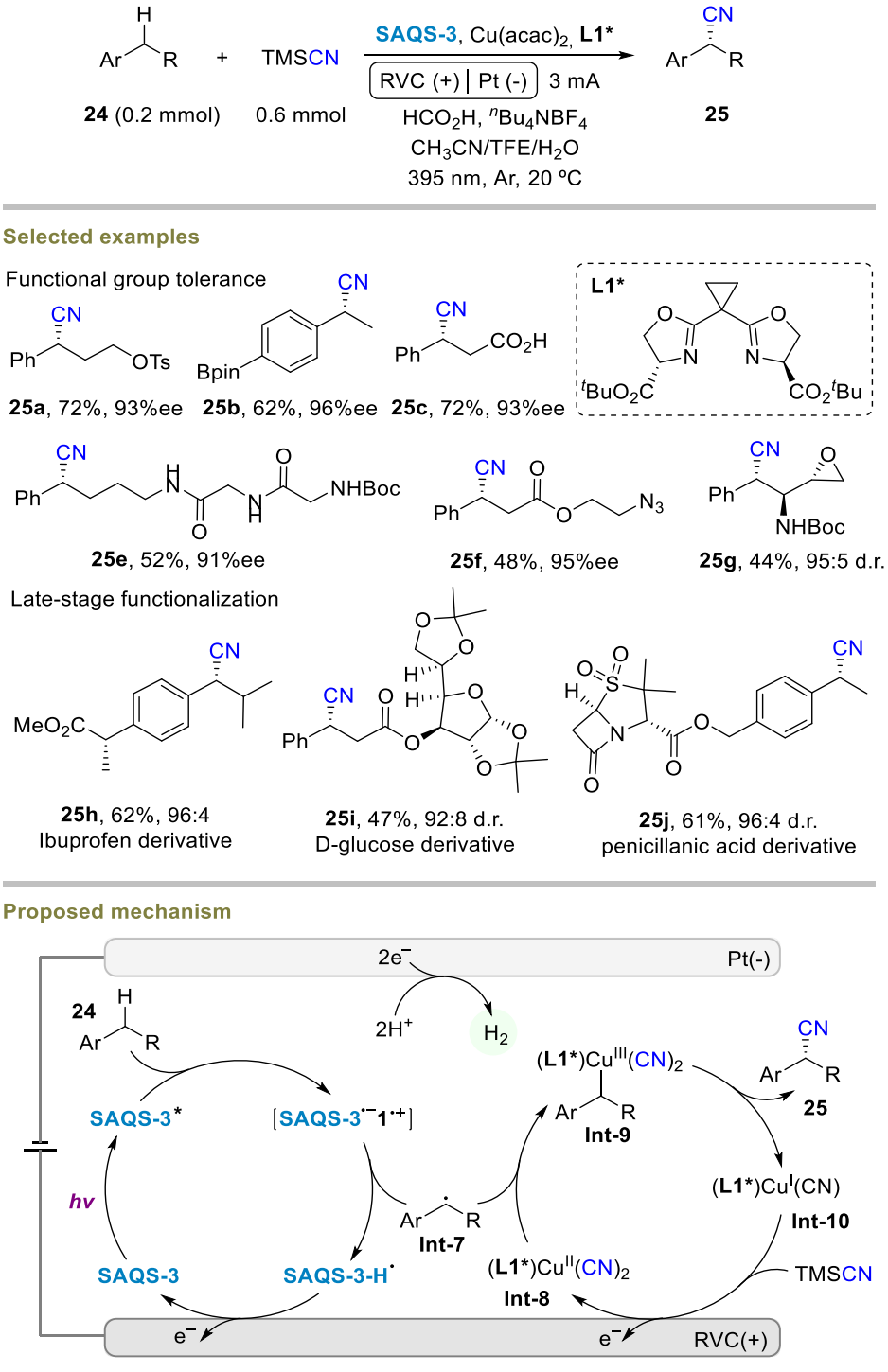

Scheme 9. Photoelectrochemical asymmetric cyanation of benzylic C–H bonds.

formation of a benzylic radical (**Int-7**). Subsequently, this open-shell species can be trapped by the copper (II) complex (**Int-8**) to form a copper (III) intermediate (**Int-9**). This complex then releases the desired cyanated product (**25**), simultaneously getting reduced to a copper (I) intermediate (**Int-10**), which is further oxidized by the cathode and reacts with TMSCN to regenerate the copper (II) complex (**Int-8**). Similarly, the previously formed semiquinone species is also oxidized by the cathode, thus closing the photocatalytic cycle. The electrons gained during both steps are used for proton reduction at the anode.

Although, as mentioned, alternative photochemical cyanation methodologies employing a HAT approach are available,[69–71] Xu's system offers a clear advantage over these by regenerating the photocatalyst electrochemically. Furthermore, similarly to Itoh's work,[66] the combination of AQS photocatalysts with asymmetric catalysts has proven to be an efficient strategy for preparing products with high enantioselectivities.

Environmental Applications

As discussed, upon irradiation, AQS can reach excited states from which they can react as strong oxidants via SET or as excellent HAT agents. Moreover, these catalysts stand out for their ability to generate ROS species,[7,28,29] in aqueous medium.

In addition, **SAQS-1** has been successfully employed for the degradation of organic dyes (immobilized on treated nylon as a heterogeneous catalyst),[31] and its application in wastewater treatment has also been investigated due to its ability to generate ROS under irradiation.[28] Furthermore, **SAQS-1** has also been reported as an efficient microbial photosensitizer for removing inorganic pollutants, such as nitrates, from aqueous solutions. Herein, Zhou and coworkers reported a semi-artificial system involving this catalyst as a photosensitizer for bacterial denitrification reactions.[72]

1.4 Future Perspectives

In The current trends in synthetic organic chemistry point towards the further development of photocatalysis as an indispensable tool for performing organic transformations in a sustainable fashion. Prioritizing the use of green solvents is another of the key pillar of this strategy. However, in the case of water, the options regarding available photocatalysts are limited. Consequently, the demand for water-soluble catalysts is on the rise. In this context, AQS are emerging as promising candidates that contribute to this shift in organic synthesis, unlocking the application of the photoactive anthraquinone core in aqueous media. Accordingly, these catalysts enable adapting quinone photochemistry to water such as benzylic or aromatic functionalizations.

Although this feature is relatively underexplored for AQS, when we direct our attention toward other sulfonated photocatalysts, it becomes apparent that their water solubility can be a significant advantage when aiming to transform highly polar biologically derived molecules. An excellent example of this application is provided by the structurally resembling photocatalysts to AQS, benzophenone-3,3'-bis(sodium sulfonate) (BPSS). Herein, this catalyst has been successfully employed as a HAT agent for the alkylation of α,β-unsaturated compounds,[73,74] and the isomerization of aldoses.[75] Hereof, an example that might support

a potentially similar application of AQS in the future is the recent report by the Murai group on the oxidation of ascorbic acid by anthraquinone-2,6-disulfonate.[76]

Another feature of AQS that might be further exploited is their excellent compatibility with other catalysts. To date, AQS have been successfully employed in combination with a wide array of other catalysts, ranging from simple organocatalysts such as β-alanine,[67] to more complex catalysts such as the proline derivative employed by the Itoh group,[66] or the chiral copper complex reported by Xu and coworkers.[68] This compatibility is also extended to biological systems, in which due to the low pKa values of the sulfonate groups, speciation issues are precluded. Herein, apart from their application as electron shuttles in biological systems,[19] AQS have also been employed for synthetic purposes in the presence of enzymes,[63] or as bacterial photosensitizers for denitrification processes.[72]

Furthermore, as showcased by Xu's cyanation protocol,[68] the application of current can be a fruitful strategy for the regeneration of AQS and the design of transformations with high atom economies. Although this approach remains relatively underexplored to date, it also holds great potential, as photoelectrochemistry is rising as a powerful tool for synthetic purposes.[77,78] Herein, the pioneering work by the Xu group might serve as inspiration for the development of more sustainable methodologies, precluding the need for sacrificial oxidants.

The ability of AQS, to generate a wide array of ROS species and their compatibility with biological systems such as bacteria has enabled the application of these photosensitizers for the degradation of a wide array of pollutants ranging from organic molecules such as organic dyes.[31] to inorganic pollutants such as nitrates.[72] Herein, AQS might be a metal-free and more cost-effective alternative to other photocatalysts that have been investigated for similar purposes, such as the decatungstate anion, previously reported for the photodegradation of pesticides in water.[79]

In contrast, a particularly interesting but underexplored feature of AQS is the modification of their reactivity by protonation. This strategy was showcased by the bromination and cyanation protocols of the König[27] and Xu[68] groups respectively, and it can render excellent results in the enhancement of the oxidative power of these catalysts by the addition of acids. AQS can easily replace certain oxidative catalysts as an inexpensive and water-compatible option. Moreover, the protonation of AQS significantly enables these photocatalysts to target a much broader range of substrates, thus expanding the synthetic chemist's toolbox.

Lastly, in our opinion, the photophysical properties of AQS should be further investigated to provide valuable insights and guidance in selecting different AQS isomers based on their synthetic applications. Accordingly, the combination of experimental results, spectroscopic studies and computational investigations might be a good strategy for drawing relationships between structure and reactivity of these promising photocatalysts.

1.5 Conclusions

AQS entail a class of photoorganocatalysts with outstanding properties and great potential applications in organic synthesis. To date, their application in oxygenation reactions has been particularly prominent, being tandem photooxidative processes of great interest, as they allow to build molecular complexity from relatively simple molecules. Moreover, AQS have been successfully combined with chiral catalysts, enabling the development of asymmetric transformations in aqueous media. Furthermore, the electrochemical regeneration of these photocatalysts appears to point to the future development of more sustainable photoelectrochemical reactions. Additionally, due to the ability of AQS to generate ROS, their application for degrading of organic compounds holds great potential. Altogether, we expect that further investigations and a better understanding of the reactivity of these catalysts might bolster the development of their synthetic applications in water in the upcoming years.

1.6 References

[1] A. Romero, D. A. Nicewicz, *Chem. Rev*. **2016**, *116*, 10075–10166.

[2] I. K. Sideri, E. Voutyritsa, C. G. Kokotos, *Org. Biomol. Chem*. **2018**, *16*, 4596–4614.

[3] T. Bortolato, S. Cuadros, G. Simionato, L. Dell'Amico, *Chem. Commun*. **2022**, *58*, 1263–1283.

[4] A. E. Alegría, A. Ferrer, G. Santiago, E. Sepúlveda, W. Flores, *J. Photochem. Photobiol. A* **1999**, 127, 57–65.

[5] R. I. Teixeira, J. S. Goulart, R. J. Corrêa, S. J. Garden, S. B. Ferreira, J. C. Netto-Ferreira, V. F. Ferreira, P. Miro, M. L. Marin, M. A. Miranda, N. C. de Lucas, *RSC Adv.* **2019**, *9*, 13386–13397.

[6] J. Cervantes-González, D. A. Vosburg, S. E. Mora-Rodriguez, M. A. Vázquez, L. G. Zepeda, C. Villegas Gómez, S. Lagunas-Rivera, *ChemCatChem* **2020**, *12*, 3811–3827.

[7] C.-X. Chen, S.-S. Yang, J.-W. Pang, L. He, Y.-N. Zang, L. Ding, N.-Q. Ren, J. Ding, *Environ. Sci. and Ecotechnol*. **2024**, *22*, 100449.

[8] S. Das, P. Natarajan, B. König, *Chem. Eur. J*. **2017**, *23*, 18161–18165.

[9] P. Natarajan, B. König, *Eur. J. Org. Chem*. **2021**, *2021*, 2145–2161.

[10] M. Cortes-Clerget, J. Yu, J. R. A. Kincaid, P. Walde, F. Gallou, B. H. Lipshutz, *Chem. Sci*. **2021**, *12*, 4237–4266.

[11] J. Mao, W. Ruan, Q. Chen, *J. Electrochem. Soc*. **2020**, *167*, 70522–70525.

[12] S. N. Garcia, X. Yang, L. Bereczki, D. Kónya, *Molecules* **2021**, *26*, 1203–1213.

[13] F. Hasan, V. Mahanta, A. A. A. Abdelazeez, *Adv. Mater. Interfaces* **2023**, *10*, 2300268.

[14] B. Huskinson, M. P. Marshak, C. Suh, S. Er, M. R. Gerhardt, C. J. Galvin, X. Chen, A. Aspuru-Guzik, R. G. Gordon, M. J. Aziz, *Nature*, **2014**, *505*, 195.

[15] M. R. Gerhardt, L. Tong, R. Gómez-Bombarelli, Q. Chen, M. P. Marshak, C. J. Galvin, A. Aspuru-Guzik, R. G. Gordon, M. J. Aziz, *Adv. Energy Mater.* **2017**, *7*, 1601488.

[16] W. Ruan, J. Mao and Q. Chen, *Curr. Opin. Electrochem*. **2021**, *29*, 100748.

[17] J.-M. Fontmorin, S. Guiheneuf, T. Godet-Bar, D. Floner, F. Geneste, *Curr. Opin. Colloid Interface Sci.* **2022**, *61*, 101624.

[18] W. Liu, Y. Wu, T. Liu, F. Li, H. Dong and M. Jing, *Front. Microbiol.*, **2019**, *10*, 464.

[19] Y. Bai, A. Mellage, O. A. Cirpka, T. Sun, L. T. Angenent, S. B. Haderlein, A. Kappler, *Environ. Sci. Technol*. **2020**, *54*, 4131–4139.

[20] Z. Ren, P. Ma, L. Lv, G. Zhang, W. Li, P. Wang, X. Liu and W. Gao, *J. Clean. Prod.*, **2022**, *372*, 133527.

[21] L. Yu, C. Ju, K. Jing, Z. Wang, S. Niyazi and Q. Wang, *J. Environ. Manage.* **2023**, *333*, 117455.

[22] J. L. Bolland, H. R. Cooper, *Proc. R. Soc. Lond*. A **1954**, *225*, 405–426.

[23] N. Geacintov, V. Stannett, E. W. Abrahamson, J. J. Hermans, *J. Appl. Polym. Sci*., **1960**, *3*, 54–60.

[24] Q. Anwaruddin, M. Santappa, *J. Polym. Sci. B Polym. Lett*. **1967**, *5*, 361–365.

[25] G. Geuskens, A. Etoc, P. Di Michele, *Eur. Polym. J*. **2000**, *36*, 265–271.

[26] N. Liu, G. Sun, S. Gaan, P. Rupper, *J. Appl. Polym. Sci*. **2010**, *116*, 3629–3637.

[27] D. Petzold, B. König, *Adv. Synth. Catal*. **2017**, *360*, 626–630.

[28] N. Liu, G. Sun, *Ind. Eng. Chem. Res*. **2011**, *50*, 5326–5333.

[29] M. Le Bechec, T. Pigot, S. Lacombe, *ChemPhotoChem* **2018**, *2*, 622–631.

[30] V. Maurino, D. Borghesi, D. Vione and C. Minero, *Photochem. Photobiol. Sci*. **2008**, *7*, 321–327.

[31] N. Liu and G. Sun, *ACS Appl. Mater. Interfaces* **2011**, *3*, 1221–1227.

[32] K. Sun, Q.-Y. Lv, X.-L. Chen, L.-B. Qu, B. Yu, *Green Chem*. **2021**, *23*, 232–248.

[33] S. Barata-Vallejo, D. E.Yerien, A. Postigo, *ACS Sustain. Chem. Eng*. **2021**, *9*, 10016–10047.

[34] Y.-M. Tian, E. Hofmann, W. Silva, X. Pu, D. Touraud, R. M. Gschwind, W. Kunz, B. König, *Angew. Chem. Int. Ed*. **2023**, *62*, e202218775.

[35] Q. Dou, H. Zeng, Curr. Opin. Green Sustain. Chem. **2023**, *40*, 100766.

[36] A. M. Ghouse, S. M. Akondi, *Org. Biomol. Chem*. **2023**, *21*, 5351–5355.

[37] C. Chatgilialoglu, S. Barata-Vallejo, T. Gimisis, *Molecules* **2024**, *29*, 569.

[38] Y.-M. Tian, W. Silva, R. M. Gschwind, B. König, *Science* **2024**, *383*, 750–756.

[39] A. D. Broadbent, *Chem. Commun*. **1967**, 382–383.

[40] A. D. Broadbent, R. P. Newton, *Can. J. Chem*. **1972**, *50*, 381–387.

[41] A. D. Broadbent, H. Matheson, R. P. Newton, *Can. J. Chem*. **1975**, *53*, 826–830.

[42] J. L. Charlton, R. G. Smerchanski, C. E. Burchill, *Can. J. Chem*. **1976**, *54*, 512–515.

[43] A. H. and A. Mills, Photochem. Photobiol. **1981**, *33*, 619–626.

[44] I. Loeff, A. Trelnln, *J. Phys. Chem*. **1983**, *1569*, 2536–2544.

[45] P.R. Maddigapu, A. Bedini, C. Minero, V. Maurino, D. Vione, M. Brigante, G. Mailhot, M. Sarakha, *Photochem. Photobiol. Sci*. **2010**, *9*, 323–330.

[46] K. P. Clark, H. I. Stonehill, J. Chem. Soc., *Faraday Trans*. **1972**, *68*, 577–590.

[47] D. Phillips, J. N. Moore, R. E. Hester, *J. Chem. Soc. Faraday Trans. 2 Mol. Chem. Phys*. **1986**, *82*, 2093–2104.

[48] K. P. Clark, I. Stonehill, H, *J. Chem. Soc., Faraday Trans. 1* **1972**, *68*, 1676–1686.

[49] S. A. Ansuman Roy, *J. Indian Chem. Soc*. **1982**, *59*, 585–590.

[50] A. Wakisaka, T. W. Ebbesen, H. Sakuragi, K. Tokumaru, *J. Phys. Chem.* **1987**, *91*, 6547–6551.

[51] A. Bedini, E. De Laurentiis, B. Sur, V. Maurino, C. Minero, M. Brigante, G. Mailhot, D. Vione, *Photochem. Photobiol. Sci*. **2012**, *11*, 1445–1453.

[52] G. L. Zhu, L. W. Zhang, Y. C. Liu, Z. F. Cui, X. S. Xu, G. Z. Wu, *Chinese J. Chem. Phys*. **2016**, *29*, 140–146.

[53] S. Goia, M. A. P. Turner, J. M. Woolley, M. D. Horbury, A. J. Borrill, J. J. Tully, S. J. Cobb, M. Staniforth, N. D. M. Hine, A. Burriss, J. V. Macpherson, B. R. Robinson, V. G. Stavros, *Chem. Sci*. **2022**, *13*, 486–496.

[54] Y. -R. Luo, *Comprehensive Handbook of Chemical Bond Energies*, CRC Press, Boca Raton **2007**.

[55] C. Chatgilialoglu, S. Barata-Vallejo, T. Gimisis, *Molecules* **2024**, *29*, 569.

[56] N. F. Nikitas, D. I. Tzaras, I. Triandafillidi, C. G. Kokotos, *Green Chem.* **2020**, *22*, 471–477.

[57] C. S. Batsika, C. Koutsilieris, G. S. Koutoulogenis, M. G. Kokotou, C. G. Kokotos, G. Kokotos, *Green Chem*. **2022**, *24*, 6224–6231.

[58] C. F. Wells, *Trans. Faraday Soc*. **1961**, *57*, 1703–1718.

[59] C. F. Wells, *Trans. Faraday Soc.* **1961**, *57*, 1719–1731.

[60] A. Broadbent, R. Newton, *Can. J. Chem*. **1971**, *50*, 381–387.

[61] W. Zhang, J. Gacs, I. W. C. E. Arends, F. Hollmann, *ChemCatChem* **2017**, *9*, 3821–3826.

[62] H. Yin, Y. Yuan, Y. Li, J. Tang, W. Zhong, L. Mao, *Green Chem*. **2023**, *25*, 2757–2770.

[63] B. Yuan, D. Mahor, Q. Fei, R. Wever, M. Alcalde, W. Zhang, F. Hollmann, *ACS Catal*. **2020**, *10*, 8277–8284.

[64] T. J. Collins, Green Chemistry, *Macmillan Encyclopedia of Chemistry*, Macmillan, New York **1997**.

[65] P. Anastas, N. Eghbali, *Chem. Soc. Rev*. **2010**, *39*, 301–312.

[66] A. Fujiya, T. Nobuta, E. Yamaguchi, N. Tada, T. Miura, A. Itoh, *RSC Adv*. **2015**, *5*, 39539–39543.

[67] D. Kolb, K. Friedmann, B. König, *ChemCatChem* **2024**, e202400936.

[68] C.-Y. Cai, X.-L. Lai, Y. Wang, H.-H. Hu, J. Song, Y. Yang, C. Wang, H.-C. Xu, *Nature Catal* **2022**, *5*, 943–951.

[69] S. Kamijo, T. Hoshikawa, M. Inoue, *Org. Lett*. **2011**, *13*, 5928–5931.

[70] T. Hoshikawa, S. Yoshioka, S. Kamijo, M. Inoue, *Synthesis* **2013**, *45*, 874–887.

[71] X.-Z. Fan, J.-W. Rong, H.-L. Wu, Q. Zhou, H.-P. Deng, J. Da Tan, C.-W. Xue, L.-Z. Wu, H.-R. Tao, J. Wu, *Angew. Chem. Int. Ed.* **2018**, *57*, 8514–8518.

[72] M. Chen, Q. Cai, X. Chen, S. Huang, Q. Feng, T. Majima, R. J. Zeng, S. Zhou, *Environ. Sci. Technol.* **2022**, *56*, 5161–5169.

[73] D. Dondi, I. Caprioli, M. Fagnoni, M. Mella, A. Albini, *Tetrahedron* **2003**, *59*, 947–957.

[74] D. Dondi, S. Protti, A. Albini, S. M. Carpio, M. Fagnoni, *Green Chem*. **2009**, *11*, 1653–1659.

[75] Y. Masuda, H. Tsuda, M. Murakami, *Angew. Chem. Int. Ed*. **2020**, *59*, 2755–2759.

[76] F. Ema, Z. Fu, H. Murai, *ACS Omega* **2019**, *4*, 5601–5608.

[77] S. Wu, J. Kaur, T. A. Karl, X. Tian, J. P. Barham, *Angew. Chem. Int. Ed*. **2022**, *61*, e202107811.

[78] L. Qian, M. Shi, *Chem. Commun*. **2023**, *59*, 3487–3506.

[79] I. Texier, C. Giannotti, S. Malato, C. Richter, J. Delaire, *Catalysis Today*, **1999**, *54*, 297–307.

2. Tandem Synthesis of Benzylidenemalononitrile Derivatives in/on Water under Visible Light

Abstract: Tandem processes are valuable tools that allow to build molecular complexity while reducing waste production and the number of steps of synthetic routes. In this work, the in situ photooxidation of benzyl alcohols to the corresponding benzaldehydes is coupled with a Knoevenagel condensation for the preparation of benzylidenemalononitrile derivatives. In this rapid one-pot tandem process, sodium anthraquinone-1,5- disulfonate (SAQS) and β-alanine are employed as safe and inexpensive catalysts, while air is used as a terminal oxidant. Moreover, using water as reaction medium results in most cases in the precipitation of the target products, thus facilitating their isolation.

[i] Reproduced from D. Kolb, K. Friedmann, B. König,* *ChemCatChem* **2024**, *16*, e202400936. with permission from Wiley-VCH GmbH. Schemes, tables, and text may differ from the published version.

[ii] Author contributions: D. Kolb conceived the concept of this study and investigated the scientific background. D. Kolb and K. Friedmann optimized the reaction conditions, synthesized the starting materials, and conducted the mechanistic investigations. D. Kolb performed the photoreactions with the assistance of K. Friedmann. D. Kolb wrote the manuscript and supporting information. B. König supervised the project, reviewed the manuscript, and is the corresponding author.

2.1 Introduction

Currently, the chemical and pharmaceutical industries are experiencing a notorious shift in terms of sustainability, wherein reducing the energy input of reactions, and restricting the use of hazardous chemicals have become first-order priorities.[1] In addition, shortening the length of synthetic routes by performing multiple steps in a single vessel can improve the overall efficiency of the process while circumventing intermediary purification steps and reducing waste production.[1c,2]

Due to their low cost, bench stability, and natural prevalence, alcohols are particularly attractive synthetic building blocks. In addition, their facile oxidation to the corresponding aldehydes enables the design of tandem oxidative processes (TOP), wherein their initial oxidation is coupled with an additional step.[3] While most of these processes rely on thermal conditions, the relatively low C–H bond-dissociation energy (BDE) displayed by α-alkoxy positions can be easily exploited via photoinduced H-atom transfer (HAT).[4] Herein, equivalent aldehyde intermediates can be accessed under notably milder reaction conditions in the presence of a photoexcitable HAT agent and oxygen.[5] Accordingly, tandem photooxidative processes (TPP) constitute a more sustainable alternative to conventional TOP, allowing to build molecular complexity by using light. However, despite their potential applications, to date, these remain unexplored to a large extent. In addition to the design of tandem reactions, the replacement of hazardous organic solvents remains a major challenge. As a result, efforts are being made to prioritize the use of green solvents such as water.[1a,1c,6] Unfortunately, this medium is often associated with solubility issues or revealed as incompatible with photocatalytic systems. To overcome these limitations, water-soluble photoexcitable HAT agents can be employed.[5a,7] For instance, sulfonated anthraquinones have been successfully implemented in TPP, as showcased by the Itoh group in their work on the photooxidative tandem condensation between benzyl alcohols and ketones in aqueous medium.[5a]

Benzylidenemalononitrile derivatives, also known as tyrphostins, display a broad range of biological properties.[8] In addition, these electron-poor olefins are regarded as versatile radical traps for the elucidation of reaction mechanisms and valuable substrates for Giese-type reactions.[9] Although a plethora of different reaction conditions have been reported so far,[10] their synthesis mainly relies on the classic Knoevenagel condensation, wherein an aldehyde and an active C–H methylene compound undergo a condensation reaction in the presence of an organocatalyst (Scheme 1a).[11] More recently, several tandem methodologies have been developed to access equivalent products from benzyl alcohols.[12] Inspired by these previous works,[5a,12] and the concept of TPP, we envisioned an alternative method to the classical reaction in alignment with the principles of green chemistry.[13] Herein, we hypothesized that benzyl alcohols could be employed as benzaldehyde precursors in designing a Knoevenagel

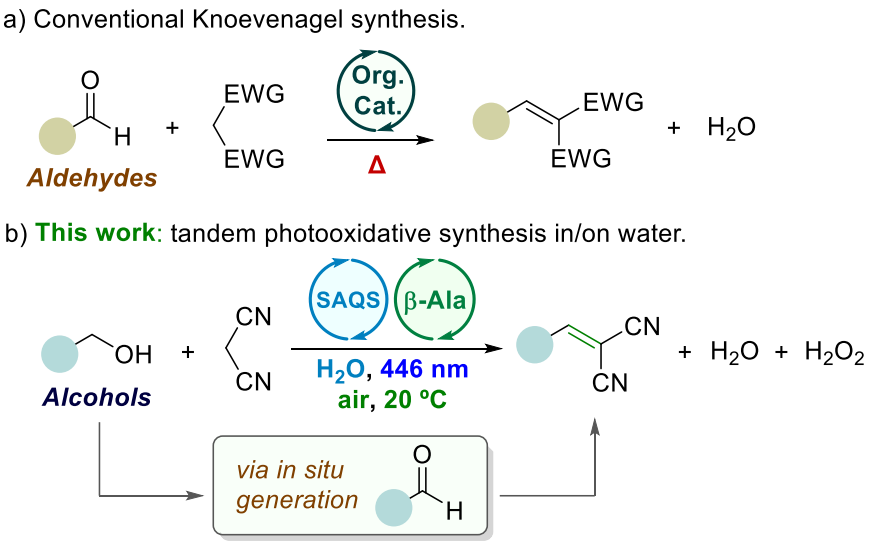

Scheme 2. Synthesis of benzylidenemalononitrile derivatives. SAQS: sodium anthraquinone-1,5-disulfonate. β-Ala: beta-alanine.

cascade reaction in water, thus precluding organic solvents and replacing heat with light (Scheme 1b).

2.2 Results and Discussion

Taking the lead from Itoh's work,[5a] we set out to test the envisioned transformation with a dual catalytic system involving sodium anthraquinone-2-sulfonate (**SAQS1**), L-proline, and water as solvent. Accordingly, due to their solubility in this medium, benzyl alcohol (**1a**) and malononitrile (**2**) were chosen as model substrates for the preparation of benzylidenemalononitrile (**3a**). At first, the reaction mixture was subjected to 405 nm (0.7 W) irradiation, under air (Table 1; entry 1). To our delight, after 2 h, the formation of a white precipitate was observed (Figure S4). Extraction of the reaction mixture with EtOAc and subsequent analysis via GC-FID revealed the formation of 3a in low yield (39%) (Figure S6). In addition, the presence of unreacted starting materials (1a and 2) and the formation of the postulated benzaldehyde intermediate were corroborated.

Motivated by these promising results, we proceeded to optimize the system by surveying different water-soluble photocatalysts (Table 1; entries 2-4). While riboflavin (**RF**) proved compatible under blue light irradiation (entry 4), sulfonated anthraquinones delivered notably better results. In particular, sodium anthraquinone-1,5-disulfonate (**SAQS3**) was revealed as the best choice, providing **3a** in 63% yield (entry 3). Next, the replacement of L-proline by piperidine, a base commonly used for Knoevenagel condensations,[10b] led to a significant drop in yield (entry 5). This might be attributed to the oxidation of the non-protonated amine by the excited state of the photocatalyst. In contrast, other amino acids such as glycine, β-alanine, γ-aminobutyric acid (**GABA**) gave better results (entries 6-8). Accordingly, β-alanine was

Table 1. Optimization of reaction conditions.[a]

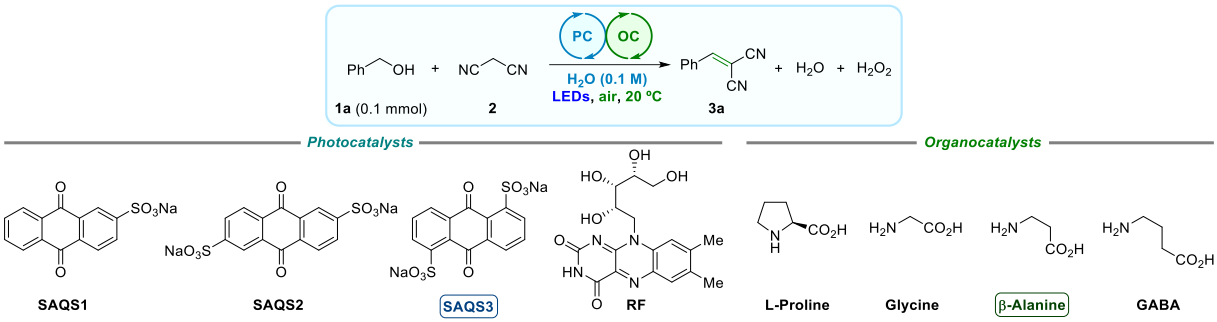

Entry	equiv. **2**	PC (mol%)	OC (mol%)	t (h)	LEDs	Yield of **3a** (%)[b]
1	1	SAQS1 (10)	L-Proline (10)	2	405 nm (0.7 W)	39
2	1	SAQS2 (10)	L-Proline (10)	2	405 nm (0.7 W)	58
3	1	SAQS3 (10)	L-Proline (10)	2	405 nm (0.7 W)	63
4	1	RF (1)	L-Proline (10)	3	446 nm (0.7 W)	22
5	1	SAQS3 (10)	Piperidine (10)	2	405 nm (0.7 W)	9
6	1	SAQS3 (10)	Glycine (10)	2	405 nm (0.7 W)	50
7	1	SAQS3 (10)	β-Alanine (10)	2	405 nm (0.7 W)	65
8	1	SAQS3 (10)	GABA (10)	2	405 nm (0.7 W)	43
9	1.2	SAQS3 (10)	β-Alanine (10)	2	405 nm (0.7 W)	71
10	1.5	SAQS3 (10)	β-Alanine (10)	2	405 nm (0.7 W)	77
11	1.5	SAQS3 (10)	β-Alanine (10)	2	446 nm (0.7 W)	81
12	1.5	SAQS3 (10)	β-Alanine (10)	2	528 nm (0.2 W)	n.d.
13	1.5	SAQS3 (10)	β-Alanine (5)	2	446 nm (0.7 W)	86
14	1.5	SAQS3 (10)	β-Alanine (1)	2	446 nm (0.7 W)	68
15	1.5	SAQS3 (5)	β-Alanine (5)	2	446 nm (0.7 W)	66
16	**1.5**	**SAQS3 (10)**	**β-Alanine (5)**	**3**	**446 nm (0.7 W)**	**91**

[a]Reaction conditions: **1a** (0.1 mmol), **2**, photocatalyst, organocatalyst, H_2O (1 mL), LEDs (radiant power), air, 20 ºC. [b]GC-FID yields determined using α,α,α-trifluorotoluene as internal standard upon extraction of the reaction mixture with EtOAc (1 mL).

identified as the best option (**3a**, 65% yield) (entry 7). This safe and inexpensive naturally occurring amino acid has been previously reported for catalyzing condensation reactions even at mild temperatures.[14]

The reaction yield was further improved up to 77% by increasing the number of equivalents of **2** from 1 to 1.5 (entry 10). In addition, alternative irradiation sources were examined, wherein 446 nm (0.7 W) LEDs delivered the best performance (81%) (entry 11). In contrast, when irradiating with 523 nm (0.2 W) LEDs, **1a** remained unreacted (entry 12), as **SAQS3** does not absorb in this region of the visible light spectrum (Figure S7). Afterward, the catalyst loadings

were optimized (entries 13-15), being the loading of β-alanine reduced to 5 mol% (entry 13). Regarding the photocatalyst, reducing its loading to 5 mol% led to a drop in yield (66%) (entry 15). As a result, a loading of 10 mol% of **SAQS3** was maintained. Conducting the reaction for an additional hour led to excellent results (91%) (entry 16). Analysis of the reaction mixture via GC-FID (Figure S8) revealed complete consumption of **1a**, while only traces of benzaldehyde intermediate were detected. Lastly, the product was isolated via filtration of the reaction mixture, obtaining **3a** as a white solid in very good yield (87%). Lastly, the methodology was successfully scaled up using 8 mmol of **1a**, which resulted in the isolation of **3a** in acceptable yield (59%).

With the optimized conditions in hand, we explored the substrate scope of the transformation (Scheme 2). First, alkyl-substituted benzyl alcohols (**3b**-**3e**) were tested, wherein very good to excellent yields were achieved (82-95%). Interestingly, neither the relatively low BDE of the C–H bonds of the methyl group substituents nor their disposition had a significant impact on the reaction yield (**3b**-**3d**). However, in the case of *ortho*-methyl benzyl alcohol (**1b**) additional reaction time was required to achieve a similar yield to the *meta*- and *para*-substituted homologues (**1c** and **1d**), presumably due to increased steric hindrance. 4-Ethylbenzyl alcohol (**1e**) required longer reaction times, presumably due to its lower solubility in water. To our delight, product **3f**, also known the drug tyrphostin A1,[8b] was prepared in

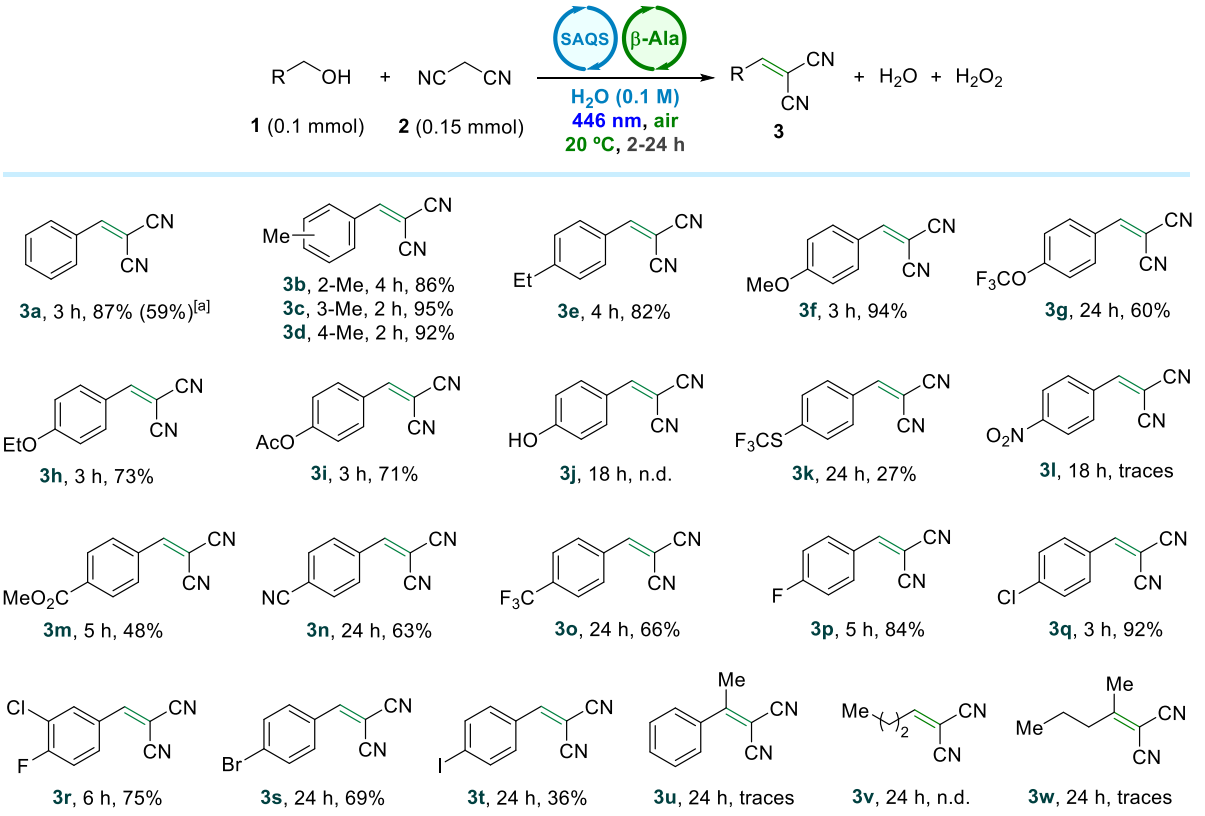

Scheme 2. Substrate scope. Reaction conditions: **1** (0.1 mmol), **2** (0.15 mmol) **SAQS3** (10 mol%), β-alanine (5 mol%), H_2O (1 mL), 446 nm (0.7 W), air, 20 ºC. [a]Isolated yield of 8 mmol scale reaction after 7 h of irradiation at 24 ºC.

excellent yield (94%)from anisyl alcohol (**1f**). Similarly, 4-trifluoromethoxy- (**1g**), 4-ethoxy- (**1h**), and 4-acetoxy benzyl alcohol delivered satisfactory results (**3f-3h**). In contrast, the presence of an unprotected hydroxy group (**1j**) impeded reaction progress, as the starting material remained unreacted. According to a previous study, anthraquinone sulfonates can undergo rapid degradation under similar reaction conditions, in the presence of phenol derivatives.[15]

Next, the compatibility of different heteroatoms and functional groups was further explored. Herein, 4-(trifluoromethylthio)benzyl alcohol (**1k**) gave the corresponding product (**3k**) in poor yield. In addition, strong electron-withdrawing groups such as nitro (**1l**), ester (**1m**), cyano (**1n**), or trifluoromethyl (**1o**) were evaluated. However, only limited success was achieved, as these groups seemed to hinder the initial oxidation event of the alcohol. For instance, the nitro derivative (**3l**) could only be detected in traces amounts (Figure S9).

Other halogenated starting materials (**1p**-**1t**) generally performed well in the tandem process, delivering the target products in moderate to excellent yields (36-92%). While fluoro- and chlorinated substrates (**1p**-**1r**) reacted in short reaction times, bromo- (**1s**) and iodo- (**1t**) substituents led to a significant reaction time increase accompanied by yield decrease. In the case of 4-iodobenzyl alcohol (**1t**), for instance, the formation of degradation products such as the corresponding benzoic acid was confirmed. Here, no correlation could be drawn between the electron-donating/withdrawing ability of the halogen atoms and the obtained yields.

Subsequently, the methodology was tested on a secondary benzyl alcohol (**1u**) to give the corresponding ketone as a reactive intermediate. Although the formation of acetophenone was confirmed by GC-MS analysis, the aimed condensation product (**3u**) was only observed in trace amounts (Figure S10). This might be attributed to the lower electrophilicity, and higher steric hindrance displayed by acetophenone compared to benzaldehyde as a reactive intermediate.

Lastly, two aliphatic alcohols were surveyed. While 1-pentanol (**1v**) remained unreacted, 2-pentanol (**1w**) delivered the aimed product (**3w**) in trace amounts (Figure S11). The scope was further explored with **1a** and different active C–H methylene compounds as nucleophiles (Scheme S6). Unfortunately, all alternatives to malononitrile failed.

Afterward, the selectivity of the methodology was investigated. Accordingly, an intramolecular competition experiment between an aliphatic and a benzylic alcohol was carried out (Scheme 3a). As a result, only the monofunctionalized product **3x** could be isolated in good yield (68%). The alternative monofunctionalized product **3y** (derived from the oxidation of the aliphatic alcohol) or the bifunctionalized product **3z** were not observed by GC-MS analysis (Figure S12). Additionally, an intermolecular competition experiment between benzyl alcohol and 1-pentanol was set (Scheme 3b), wherein **1a** delivered **3a** in very good yield (79%), while 1-pentanol remained unreacted (Figure S13).

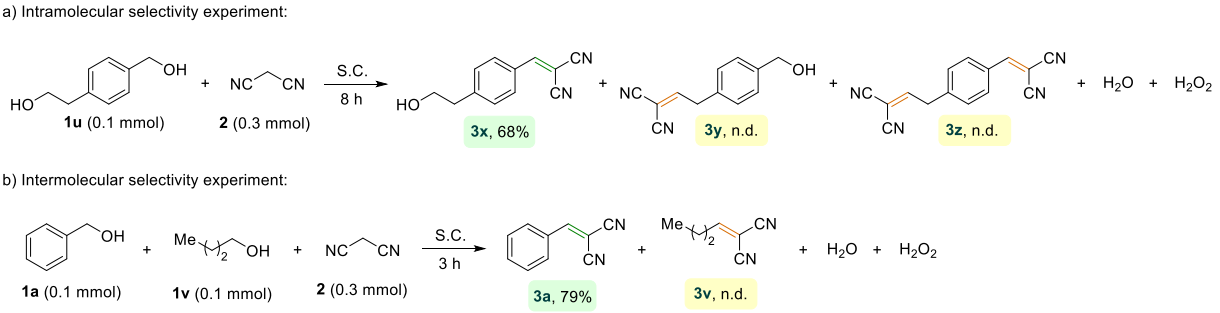

Scheme 3. Selective functionalization of benzyl alcohols over aliphatic alcohols. Standard conditions (S.C.): **SAQS3** (10 mol%), β-alanine (5 mol%), H_2O (1 mL), 446 nm (0.7 W), air, 20 ºC.

Next, we set out to unveil the reaction mechanism of the transformation by analyzing the reaction mixture of **3a** (Scheme 4). Herein, GC-MS analysis (Figure S14) revealed the presence of traces of benzaldehyde, thus supporting the postulated tandem process, wherein this species is generated in situ as a key intermediate. Furthermore, TLC analysis indicated the presence of benzoic acid as the sole side product, presumably derived from the overoxidation of the observed benzaldehyde intermediate. According to literature, aldehydes can readily oxidize to the corresponding acids upon exposure to air and light,[16] a process that might be accelerated in the presence of radical initiators such as HAT catalysts.[17] In addition, the presence of hydrogen peroxide as by-product was confirmed. Its concentration in the reaction mixture could be determined in the range of 2-5 mg/mL (0.06-0.15 M) employing semiquantitative peroxide test stripes (Figure S15).

A series of control experiments were carried out to get additional insight into the reaction mechanism (Table 2). When conducting the reaction in the absence of light (entries 2 and 3) or photocatalyst (entry 4), no product was observed. In contrast, the preclusion of β-alanine (entry 5) led to significant product formation (33%), however, in lower yield compared to the standard reaction conditions (91%). Herein, the reaction between benzaldehydes and malononitrile has been previously reported to proceed even without catalysts.[18] Furthermore, benzyl alcohol (**1a**) was subjected to the optimized conditions in the absence of **2** (entry 6) (Figure S16), which resulted in the oxidation of **1a** to benzoic acid, as the aldehyde intermediate can undergo an additional oxidation step.[16,17]

Conducting the reaction under nitrogen atmosphere led to product formation in almost stoichiometric amounts, referred to the photocatalyst loadings (entries 7 and 8). Under these

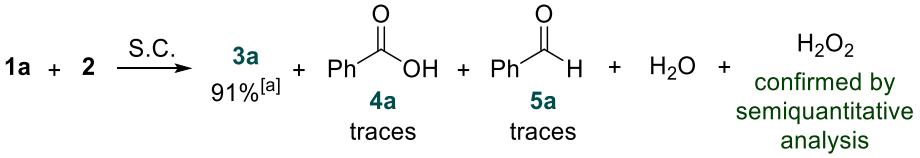

Scheme 4. Analysis of the reaction mixture of **3a**. S.C.: standard conditions. [a]GC-FID yield determined using α,α,α-trifluorotoluene as internal standard.

Table 2. Control experiments.

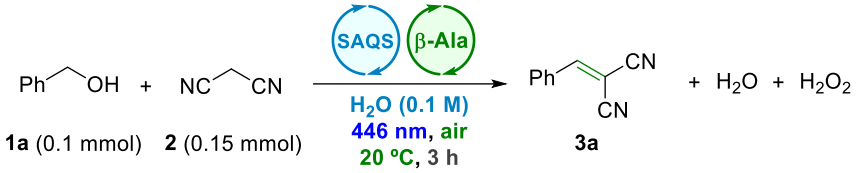

Entry	Deviation from conditions	Yield of **3a** (%)[a]
1	-	91
2	No light	n.d.
3	No light; 60 ºC	n.d.
4	No **SAQS3**	n.d.
5	No β-alanine	33
6	No **2**	n.d.
7	Under N_2	9
8	Under N_2; 15 mol% **SAQS3**	12
9	Under O_2 (1 atm.)	63
10	TEMPO (1 equiv.)	Traces

[a]GC-FID yields determined using α,α,α-trifluorotoluene as internal standard.

conditions, no H_2O_2 generation was detected (Figure S17). This suggests that in the absence of oxygen, the reduced form of the photocatalyst cannot be regenerated due to the lack of a terminal oxidant. Instead, **SAQS3** might be reduced to the corresponding hydroquinone (Scheme S7). Using an oxygen balloon instead of ambient air atmosphere (entry 9) led to a satisfactory yield of **3a** (63%), however inferior to the optimized conditions (91%). This might be attributed to the quenching of the photocatalyst in the presence of a significant excess of oxygen, as well as the undesired oxidation of the benzaldehyde to benzoic acid (as revealed by TLC-analysis). Lastly, the reaction was conducted in the presence of TEMPO as a radical scavenger (entry 10), which hampered reaction progress. Unfortunately, no radical trapping adduct could be isolated or detected.

In accordance with the performed mechanistic studies and previous reports,[5,7c,19] a plausible reaction mechanism was proposed for the tandem photooxidative process (Scheme 5). At first, the alcohol starting material (**I**) engages with the photoexcited anthraquinone (**SAQS***) via HAT to deliver a benzylic radical (**II**), which is postulated to further react with molecular oxygen to give a peroxyl radical (**III**). This intermediate then reacts with the reduced form of the photocatalyst (**SAQSH**$^{\bullet}$) via HAT, regenerating its ground state (**SAQS**) while giving the corresponding peroxide (**IV**), which, upon H_2O_2 release, forms benzaldehyde (**V**). This electrophilic intermediate then undergoes a condensation reaction with

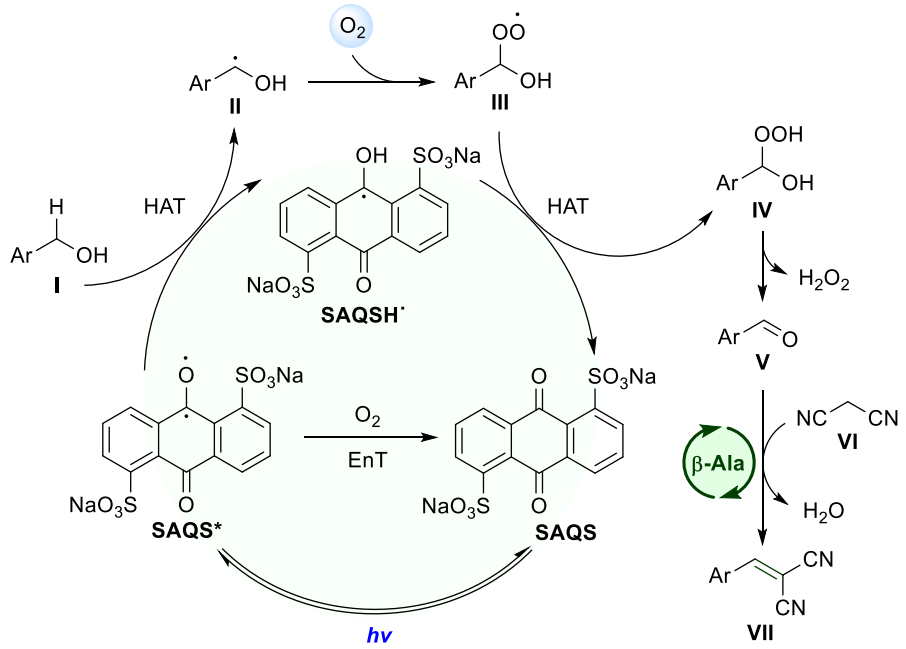

Scheme 5. Proposed reaction mechanism.

malononitrile (**VI**), catalyzed by β-alanine to give the corresponding benzylidenemalononitrile derivative (**VII**) and water as by-product.

2.3 Conclusions

To summarize, we have developed a light-driven cascade reaction for the preparation of benzylidenemalononitrile derivatives using water as reaction medium. Herein, benzyl alcohols are employed as bench-stable starting materials and oxidized by air to benzaldehydes in a photooxidative process catalyzed by sodium anthraquinone-1,5-disulfonate. The in situ generated electrophilic intermediates are then reacted with malononitrile in the presence of β-alanine as a green and inexpensive organocatalyst. Due to the solubility of both catalysts in water, the reaction is carried out in this medium, which results in several cases in the direct precipitation of the final condensation products. Overall, the methodology is operationally simple, prioritizes the use of non-hazardous chemicals, and proceeds in short reaction times at room temperature.

2.4 Experimental Section

2.4.1 General Information

Chemicals and solvents: All commercially available chemicals were purchased in high quality and used without further purification. Solvents for column chromatography were distilled before use. Petrol ether is abbreviated as PE, while ethyl acetate is abbreviated as EtOAc. Moisture-sensitive reactions were carried out using dry solvents in oven-dried glassware. Solvents were removed in a rotary evaporator at temperatures below 40 ºC under reduced pressure.

Manual Column Chromatography (CC): flash silica gel 60 M (particle size 40–63 µm, 230–440 mesh, Merck) was used as the stationary phase. Binary eluent mixtures are reported as v/v solutions normalized to 100 volume units.

Flash Column Chromatography (FCC): flash silica gel (Merck, 40-63 µm) was used as the stationary phase. Binary eluent mixtures are reported as v/v solutions normalized to 100 volume units. Purification by automated flash column chromatography was performed on a Biotage® IsoleraTM Spektra One device using either pre-packed Biotage® columns or silica gel 60 M (particle size 40–63 µm, 230–440 mesh, Merck) self-packed columns.

Analytical TLC: performed on silica gel pre-coated aluminium sheets (Macherey-Nagel©, silica gel 60 G/UV254, 0.2 mm). Visualization was accomplished by exposure to UV light (254 nm) or dipping the plate in $KMnO_4$ stain. Eluent mixtures for TLC are reported as v/v solutions normalized to 100 volume units.

Nuclear magnetic resonance (NMR): spectra were recorded at room temperature (20 ºC) using a Bruker Avance 400 (400 MHz for ^{1}H, 101 MHz for ^{13}C, 376 MHz for ^{19}F) NMR spectrometer. Chemical shifts are reported in δ-scale as parts per million [ppm] relative to the solvent residual peaks as internal standard. Coupling constants *J* are given in Hertz [Hz], and the multiplicity of the signals is abbreviated as singlet (s), broad singlet (bs), doublet (d), doublet of doublets (dd), triplet (t), doublet of triplets (dt), triplet of doublets (td), quadruplet (q), or multiplet (m). Signals are reported as follows: (multiplicity, coupling constant *J*, number of protons). Spectra were analyzed using MestReNova 6.0.2.

High Resolution Mass Spectrometry (HRMS): spectra were obtained from the central analytical mass spectrometry facilities of the Faculty of Chemistry and Pharmacy, University of Regensburg. All mass spectra were recorded on a Finnigan MAT 95, Thermo Quest Finnigan TSQ 7000, Finnigan MATSSQ 710 A, or an Agilent Q-TOF 6540 UHD instrument.

GC-FID and GC-MS**:** GC measurements were performed on a GC 7890 from Agilent Technologies. Data acquisition and evaluation were done with Agilent Chem Station Rev.C.01.04. GC–MS measurements were performed on a 7890A GC system from Agilent Technologies with an Agilent 5975 MSD Detector. Data acquisition and evaluation were done

with MSD Chem Station E.02.02.1431. A capillary column HP-5MS/30 m x 0.25 mm/0.25 µM film and helium as carrier gas (flow rate of 1 mL/min) were used. The injector temperature (split injection: 40:1 split) was 280 ºC, and the detection temperature was 300 ºC (FID). GC measurements were made and investigated via the integration of the signal obtained. The GC oven temperature program was adjusted as follows: initial temperature of 40 ºC was kept for 3 min, the temperature was increased at a rate of 15 ºC/min over 16 minutes until 280 ºC was reached and maintained for 5 min, the temperature was again increased at a rate of 25 ºC/min throughout 48 s until a final temperature of 300 ºC was reached and maintained for 5 min.

Semiquantitative H_2O_2 determination: the H_2O_2 concentration of the reaction mixture was determined semiquantitatively using Quantofix© peroxide test sticks. Upon reaction completion, an aliquot of 100 µL of reaction mixture was diluted with distilled water (dilution factor = 100), and the peroxide test strip was immersed in the resulting solution for 1 s. After 15 s, a picture was taken from the test stick.

Photoreactor setup in batch: photoreactions were irradiated with LEDs (EAGLERISE© ELP8X3LS, λ = 446 nm (± 45), average radiant flux 690 ± 10 mW, 36 V, 700 mA). Reaction mixtures were exposed to light under stirring (250 rpm, magnetic stirrer) from the bottom side of the vial. The system's temperature was controlled by a cooling circuit consisting of an aluminium cooling block connected to a cryostat (Figure S1).

The optical power of the LEDs was determined using a FieldMaxII-TOTM laser power meter equipped with a PM3 sensor. The emission spectrum of the LEDs (Figure S2) was recorded using an Ocean Optics HR4000CG-UV-NIR Glass fiber and diffusor.

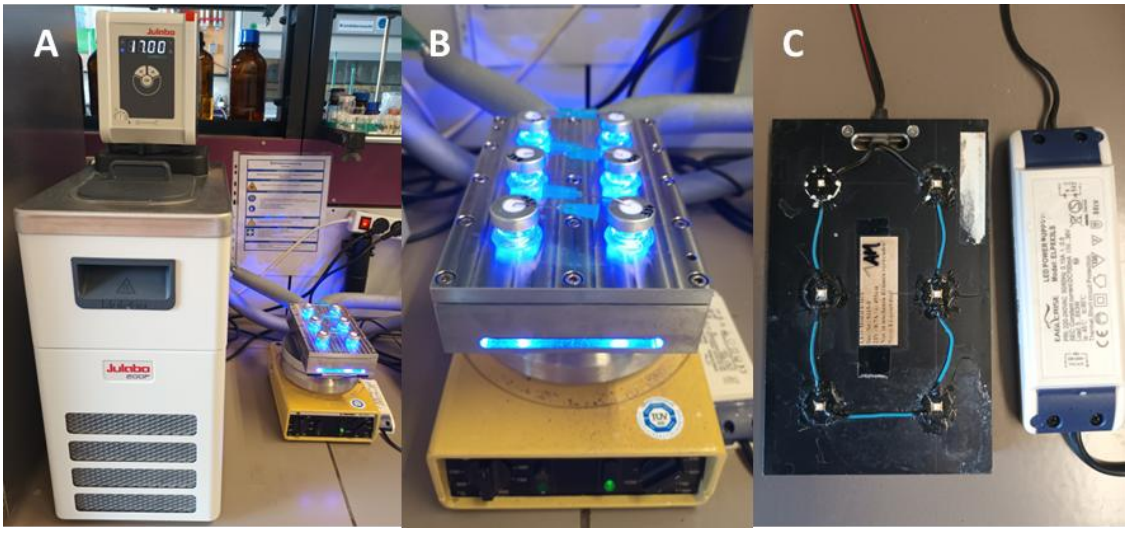

Figure S1. Photoreactor setup. **A**: cryostat connected to the aluminium cooling block. **B**: cooling block and LED on top of the stirrer. **C**: LED module.

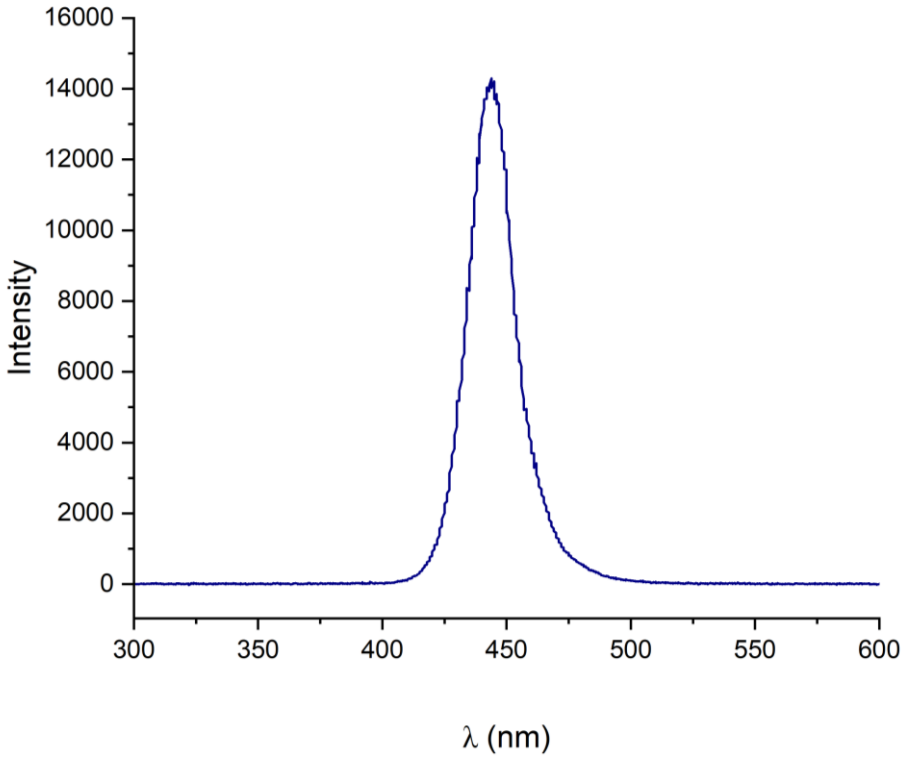

Figure S2. Led emission spectrum of the LED used for the photoreactions.

Glassware absorption: photoreactions were carried out in WICOM 20 mm crimp-cap vials (5 mL, 38.5 x 22.0 mm) made of borosilicate glass. The vials transmit 100% of incident light above 350 nm (Figure S3).

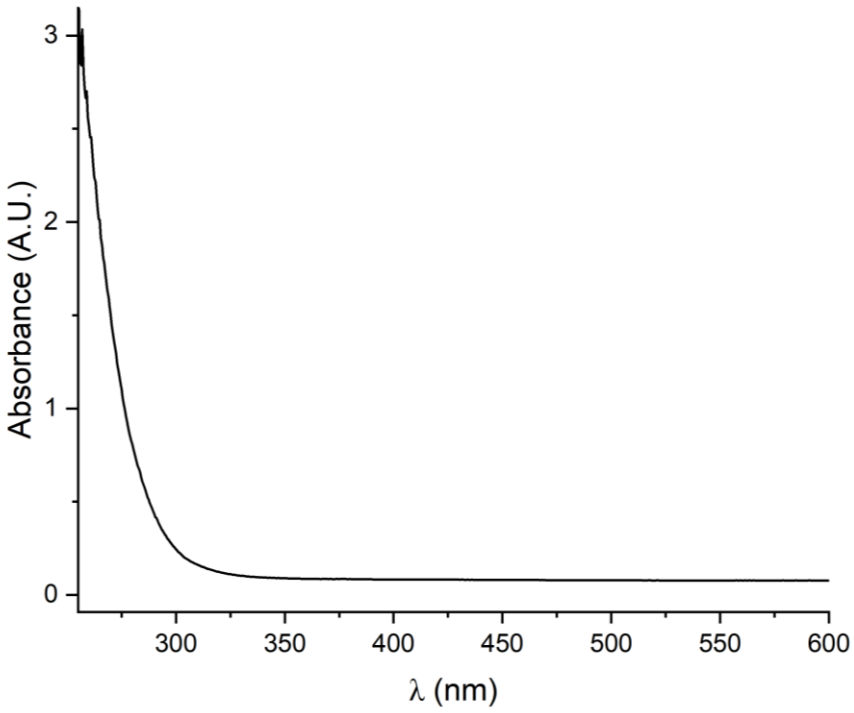

Figure S3. Absorption spectrum of vials used for photoreactions.

2.4.2 General Synthetic Procedures

General Procedure for Photoreactions (GP1)

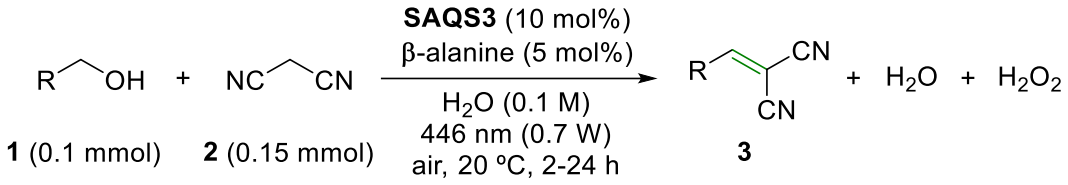

Scheme S1. General procedure for photocatalytic reactions in batch. SAQS3: sodium anthraquinone-1,5-disulfonate.

A 5 mL crimp-cap vial equipped with a PTFE-coated stirring bar was loaded with the corresponding alcohol (0.1 mmol, 1.0 equiv.), malononitrile (10.1 mg, 0.15 mmol, 1.5 equiv.), β-alanine (0.5 mg, 5 µmol, 5 mol%), sodium anthraquinone-1,5-disulfonate (3.7 mg, 10 µmol, 10 mol%) and distilled water (1 mL). The vial was sealed with a PTFE septum, sonicated for 10 s, and the reaction was kept open to air via a needle. Lastly, the reaction mixture was stirred (250 rpm) under irradiation using a blue LED set-up (λ = 446 nm (± 45), optical power = 0.7 W) at 20 ºC (temperature controlled by an aluminium cooling block connected to a cryostat). Reaction progress was monitored by TLC or GC analysis. Depending on the product, different work-up procedures were followed:

GP1a (compounds **3a**-**3f**, **3h, 3l, 3m, 3n, 3p**-**3s**): after 2-24 h, the mixture was filtered under reduced pressure using a Büchner funnel and the resulting solid washed with distilled water (1 mL). The obtained solid was dissolved in $CHCl_3$ (5 mL), and the solvent was removed under reduced pressure to give the corresponding product as a solid. For product **3s**, further purification via CC (PE/EtOAc = 96/4) was required.

GP1b (compounds **3g**, **3k**, **3o**, **3t**, **3x**): after 8-24 h, 100 mg of NaCl were added to the reaction mixture, and the product was extracted with EtOAc (3 x 1 mL). The combined organic layers were dried over Na_2SO_4, and the solvent was removed under reduced pressure. The crude product was purified via CC.

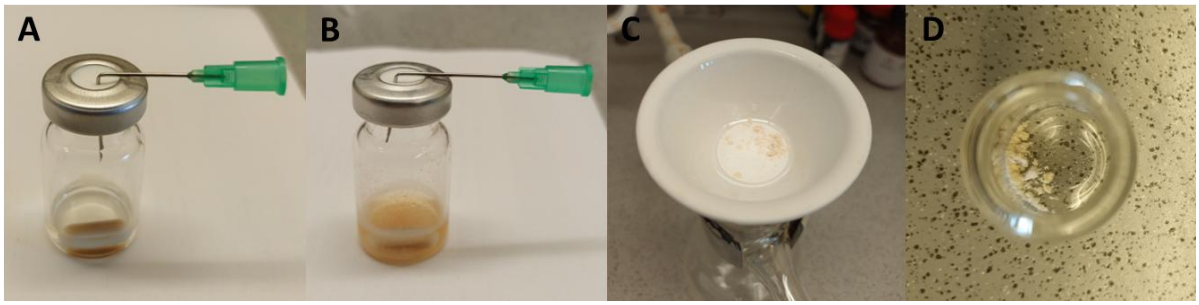

Figure S4. Reaction of **1a**. **A**: reaction mixture before irradiation. **B**: reaction mixture after 3 h irradiation. **C**: Filtered product. **D**: Isolated product.

Scale-up Procedure for Photoreactions

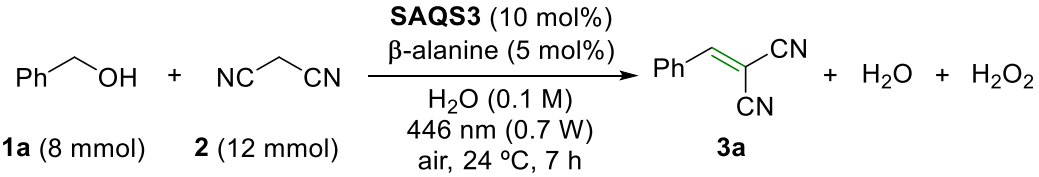

Scheme S2. Scale up for the photocatalytic synthesis of **3a**.

A 900 mL crystallizer (height 75 mm, Ø 140 mm) equipped with a PTFE-coated stirring bar was loaded with benzyl alcohol (680 µL, 8 mmol, 1.0 equiv.), malononitrile (792 mg, 12 mmol, 1.5 equiv.), β-alanine (40 mg, 0.4 mmol, 5 mol%), sodium anthraquinone-1,5-disulfonate (296 mg, 0.8 mmol, 10 mol%) and distilled water (80 mL). The resulting reaction mixture was stirred (400 rpm) under irradiation using a plate equipped with six blue LEDs (each one: λ = 446 nm (± 45), optical power = 0.7 W) placed on top of the crystallizer at 24 ºC. After 7 h, the mixture was filtered under reduced pressure using a Büchner funnel, and the resulting solid was washed with distilled water (20 mL). The obtained solid was dissolved in $CHCl_3$ (50 mL) and dried over Na_2SO_4. Lastly, the solvent was removed under reduced pressure to give **3a** as a pale brown solid (726 mg, 59%).

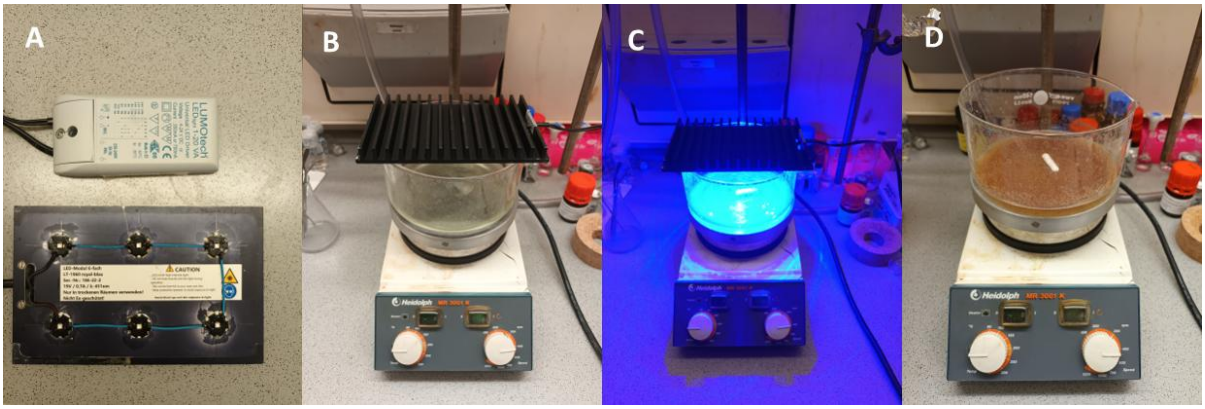

Figure S5. Photoreactor scale-up setup. **A**: LED module. **B**: reaction mixture before irradiation. **C**: reaction mixture during irradiation. **D**: reaction mixture after 7 h irradiation.

General Procedure for the Synthesis of Starting Materials (GP2)

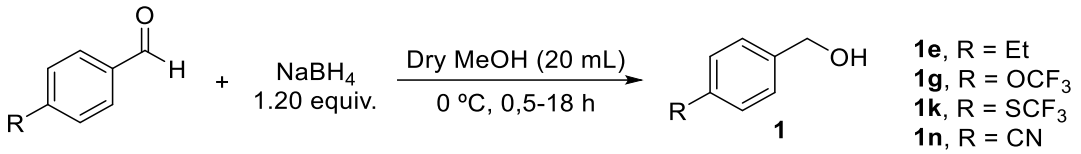

Scheme S3 General procedure for the synthesis of benzyl alcohols as starting materials.

Based on a procedure previously reported in our laboratories.[20] In an oven-dried round bottom flask, the corresponding benzaldehyde (2.50 mmol, 1.00 equiv.) was dissolved in dry MeOH (10 mL). The mixture was cooled to 0 °C and a solution of $NaBH_4$ (114 mg, 3.00 mmol, 1.20 equiv.) in dry MeOH (10 mL) was added dropwise. The resulting mixture was stirred at 0 °C for 0,5-18 h. After confirming reaction completion by TLC analysis, the reaction was quenched with water (10 mL), and the product was extracted with EtOAc (5 x 10 mL). The combined organic layers were dried over Na_2SO_4, and the solvent was removed under reduced pressure. For **1e**, **1g**, and **1k,** the crude product was purified via CC or FCC (PE/EtOAc).

2.4.3 Synthesis and Analytical Data of Starting Materials

Synthesis of 4-ethylbenzyl alcohol (**1e**)

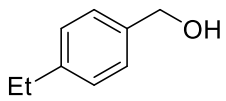

Prepared according to **GP2**. Reaction time: 30 min. Purification via FCC (PE/EtOAc = 80/20).

Isolated yield: 60% (204 mg, clear oil).

^{1}H-NMR (400 MHz, $CDCl_3$): δ (ppm) = 7.29 (d, *J* = 8.0 Hz, 2H), 7.20 (d, *J* = 8.0 Hz, 2H), 4.65 (s, 2H), 2.66 (q, *J* = 7.6 Hz, 2H), 1.80 (bs, 1H), 1.24 (t, *J* = 7.6 Hz, 3H). **^{13}C-NMR** (101 MHz, $CDCl_3$): δ (ppm) = 143.8, 138.1, 128.1, 127.2, 65.3, 28.6, 15.6. **R_f** = 0.30 (PE/EtOAc = 80/20) [$KMnO_4$]. **HRMS** (EI-MS): $[C_9H_{12}O]^{\cdot+}$ $[M]^{\cdot+}$ calcd: 136.08827; found: 136.08820.

Synthesis of 4-(trifluoromethoxy)benzyl alcohol (**1g**)

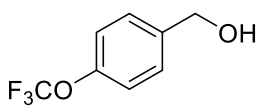

Prepared according to **GP2**. Reaction time: 18 h. Purification via CC (PE/EtOAc = 80/20).

Isolated yield: 82% (394 mg, clear oil).

^{1}H-NMR (400 MHz, $CDCl_3$): δ (ppm) = 7.31 (d, *J* = 8.7 Hz, 2H), 7.13 (d, *J* = 8.0 Hz, 2H), 4.61 (s, 2H), 1.86 (s, 1H). **^{13}C-NMR** (101 MHz, $CDCl_3$): δ (ppm) = 148.6 (q, *J* = 1.7 Hz), 139.5, 128.3, 124.3, 121.7, 120.5 (q, *J* = 257.0 Hz), 64.4. **^{19}F-NMR** (376 MHz, $CDCl_3$): δ (ppm)= -58.5. **R_f** = 0.34 (PE/EtOAc = 80/20) [$KMnO_4$]. **HRMS** (EI-MS): $[C_8H_7O_2F_3]^{\cdot+}$ $[M]^{\cdot+}$ calcd: 192.03927; found: 192.03978.

Synthesis of 4-acetoxybenzyl alcohol (**1i**)

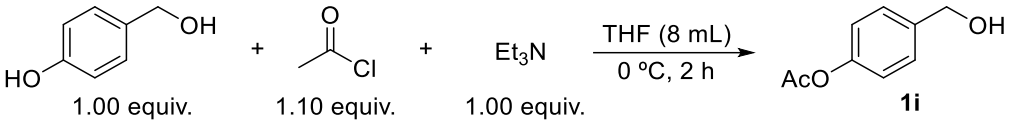

Scheme S4 Procedure for the synthesis of 4-acetoxybenzyl alcohol (**1i**).

Prepared according to a procedure from Nie et al.[21] In an oven-dried Schlenk flask, 4-hydroxybenzyl alcohol (253 mg, 2.00 mmol, 1.00 equiv.) was dissolved in dry THF (4 mL), and Et_3N (280 µl, 2.00 mmol, 1.00 equiv.) was added under inert atmosphere. The mixture was cooled to 0 °C and a solution of acetyl chloride (160 µl, 2.20 mmol, 1.10 equiv.) in THF (4 mL) was slowly added. The resulting mixture was stirred at 0 °C for 2 h. Afterward, the reaction mixture was filtered, and the solid was washed with THF (5 mL). The solvent was evaporated, the crude redissolved in CH_2Cl_2 (10 mL) and washed with water (10 mL). The organic layer was dried over Na_2SO_4, and the solvent was removed in vacuo. The crude product was purified via FCC (PE/EtOAc = 75/25) to obtain **1i**. **Isolated yield:** 38% (126 mg, clear oil).

^{1}H-NMR (400 MHz, $CDCl_3$): δ (ppm) = 7.36 (d, *J* = 8.5 Hz, 2H), 7.10 – 7.03 (m, 2H), 4.66 (s, 2H), 2.29 (s, 3H), 1.92 (s, 1H). **^{13}C-NMR** (101 MHz, $CDCl_3$): δ (ppm) = 169.6, 150.0, 138.5, 128.0, 121.6, 64.7, 21.1. **R_f** = 0.26 (PE/EtOAc = 75/25). **HRMS** (EI-MS): $[C_9H_{10}O_3]^{\cdot+}$ $[M]^{\cdot+}$ calcd: 166.06245; found: 166.06221.

Synthesis of 4-((trifluoromethyl)thio)benzenemethanol (**1k**)

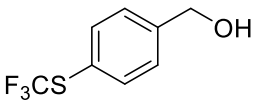

Prepared according to **GP2**. Reaction time: 18 h. Purification via CC (PE/EtOAc = 80/20).
Isolated yield: 88% (460 mg, white solid).

^{1}H-NMR (400 MHz, $CDCl_3$): δ (ppm) = 7.64 (d, *J* = 8.1 Hz, 2H), 7.41 (d, *J* = 8.5 Hz, 2H), 4.73 (s, 2H), 2.00 (s, 1H). **^{13}C-NMR** (101 MHz, $CDCl_3$): δ (ppm) = 143.9, 136.5, 129.6 (q, *J* = 308.1 Hz), 127.6, 123.3 (q, *J* = 2.1 Hz), 64.4. **^{19}F-NMR** (376 MHz, $CDCl_3$): δ (ppm)= -43.4. **R_f** = 0.28 (PE/EtOAc = 80/20) [$KMnO_4$]. **HRMS** (EI-MS): $[C_8H_7OF_3S]^{\cdot+}$ $[M]^{\cdot+}$ calcd: 208.01642; found: 208.01628.

Synthesis of 4-cyanobenzyl alcohol (**1n**)

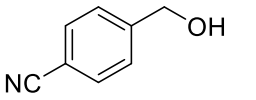

Prepared according to **GP2**. Reaction time: 2 h.
Isolated yield: 56% (186 mg, clear oil).

^{1}H-NMR (400 MHz, $CDCl_3$): δ (ppm) = 7.61 (d, *J* = 8.3 Hz, 2H), 7.46 (d, *J* = 8.3 Hz, 2H), 4.75 (s, 2H), 2.32 (s, 1H). **^{13}C-NMR** (101 MHz, $CDCl_3$): δ (ppm) = 146.3, 132.2, 127.0, 118.8, 110.9, 64.1. **HRMS** (EI-MS): $[C_8H_7NO]^{\cdot+}$ $[M]^{\cdot+}$ calcd: 133.05222; found: 133.05199.

Two-step synthesis of 2-(4-(hydroxymethyl)phenyl)ethan-1-ol (**1x**)

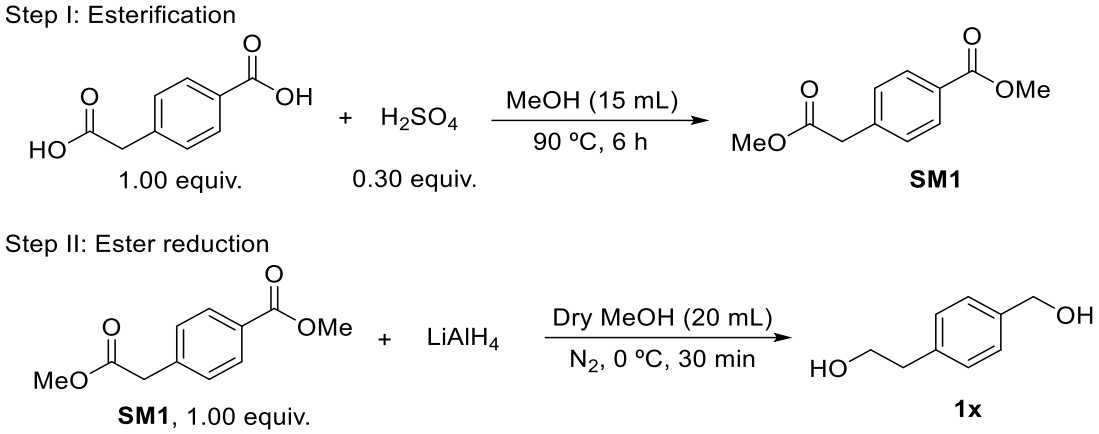

Scheme S5. Synthesis of 2-(4-(hydroxymethyl)phenyl)ethan-1-ol (**1x**).

Step I: synthesis of methyl 4-(2-methoxy-2-oxoethyl)benzoate (**SM1**)

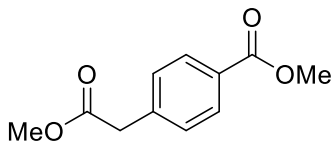

In a 50 mL crimp-cap vial equipped with a Teflon-coated stirring bar, 4-(carboxymethyl)benzoic acid (676 mg, 3.75 mmol, 1.00 equiv.) and concentrated H_2SO_4 (60 µL, 1.12 mmol, 0.30 equiv.) were dissolved in MeOH (15 mL) and stirred at 90 °C for 6 h. Upon reaction completion, MeOH was removed under reduced pressure, and the crude product was redissolved in EtOAc (50 mL) and washed with saturated aq. Na_2CO_3 (2 x 50 mL), water (50 mL) and brine (50 mL). The organic phase was dried over Na_2SO_4, and the solvent was removed under reduced pressure. Lastly, the crude product was purified via CC (PE/EtOAc = 80/20) to obtain **SM1**. **Isolated yield:** 97% (755 mg, clear oil).

^{1}H-NMR (400 MHz, $CDCl_3$): δ (ppm) = 8.02 – 7.95 (m, 2H), 7.35 (d, *J* = 8.4 Hz, 2H), 3.90 (s, 3H), 3.69 (s, 3H), 3.68 (s, 2H). **^{13}C-NMR** (101 MHz, $CDCl_3$): δ (ppm) = 171.2, 166.8, 139.0, 129.8, 129.3, 129.0, 52.1, 52.0, 41.1. **R_f** = 0.28 (PE/EtOAc = 90/10). **HRMS** (EI-MS): $[C_{11}H_{12}O_4]^{\cdot+}$ $[M]^{\cdot+}$ calcd: 208.07301; found: 208.07285.

Step II: synthesis of 2-(4-(hydroxymethyl)phenyl)ethan-1-ol (**1x**)

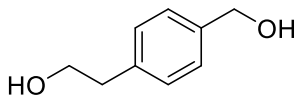

Based on a procedure from Ernst et al.[22] In a pressure tube equipped with a Teflon-coated stirring bar, substrate **SM1** (312 mg, 1.50 mmol, 1.00 equiv.) was dissolved in dry Et_2O (5 mL) and added dropwise to a suspension of $LiAlH_4$ (91 mg, 2.40 mmol) in dry Et_2O (15 mL) under N_2 atmosphere. After refluxing the resulting mixture at 35 °C for 2 h, the mixture was quenched with water (0.1 mL), aq. 0.3 M NaOH (0.1 mL) and water again (0.2 mL). After 10 min, Na_2SO_4 was added, and the resulting suspension was stirred for additional 10 min. Afterward, the mixture was filtered through a celite plug and rinsed with Et_2O (5 mL). The filtrate was washed

with brine (20 mL), the organic phase dried over Na_2SO_4, and the solvent was removed under reduced pressure. The crude product was purified via CC (PE/EtOAc = 50/50) to obtain **1x**. **Isolated yield:** 92% (210 mg, clear oil).

^{1}H-NMR (400 MHz, $CDCl_3$): δ (ppm) = 7.34 (d, *J* = 8.1 Hz, 2H), 7.25 (d, *J* = 8.1 Hz, 2H), 4.68 (s, 2H), 3.87 (t, *J* = 6.5 Hz, 2H), 2.89 (t, *J* = 6.6 Hz, 2H), 1.93 (s, 1H), 1.64 (s, 1H). **^{13}C-NMR** (101 MHz, $CDCl_3$): δ (ppm) = 139.1, 138.0, 129.2, 127.3, 65.1, 63.6, 38.8. **R_f** = 0.30 (PE/EtOAc = 50/50) [$KMnO_4$]. **HRMS** (EI-MS): $[C_9H_{12}O_2]^{\cdot+}$ $[M]^{\cdot+}$ calcd: 152.08318; found: 152.08298.

2.4.4 Optimization Studies

Work-up Protocol and Analysis of Reaction Mixtures by GC-FID

The system was optimized via GC-FID analysis, using α,α,α-trifluorotoluene as internal standard. For this, a four-point calibration curve was made using commercial benzylidenemalononitrile (**3a**).

After 2-3 h of reaction, the vial was opened, and a 0.1 M solution of α,α,α-trifluorotoluene in EtOAc (1 mL) was added. The vial was sealed with parafilm foil and shaken vigorously for 10 s. Then, the seal was removed, and 100 mg NaCl were added. The vial was sealed again with parafilm foil and shaken vigorously for 20 s. After removing the seal, the phases were allowed to separate for 1 min. Then, an aliquot of 200 µL of the organic phase was taken with a syringe and microfiltered. Lastly, the aliquot was analyzed via GC-FID analysis and its content in product **3a** was determined using the before-mentioned calibration curve.

GC-FID Analysis of the Initial Experiment with 3a

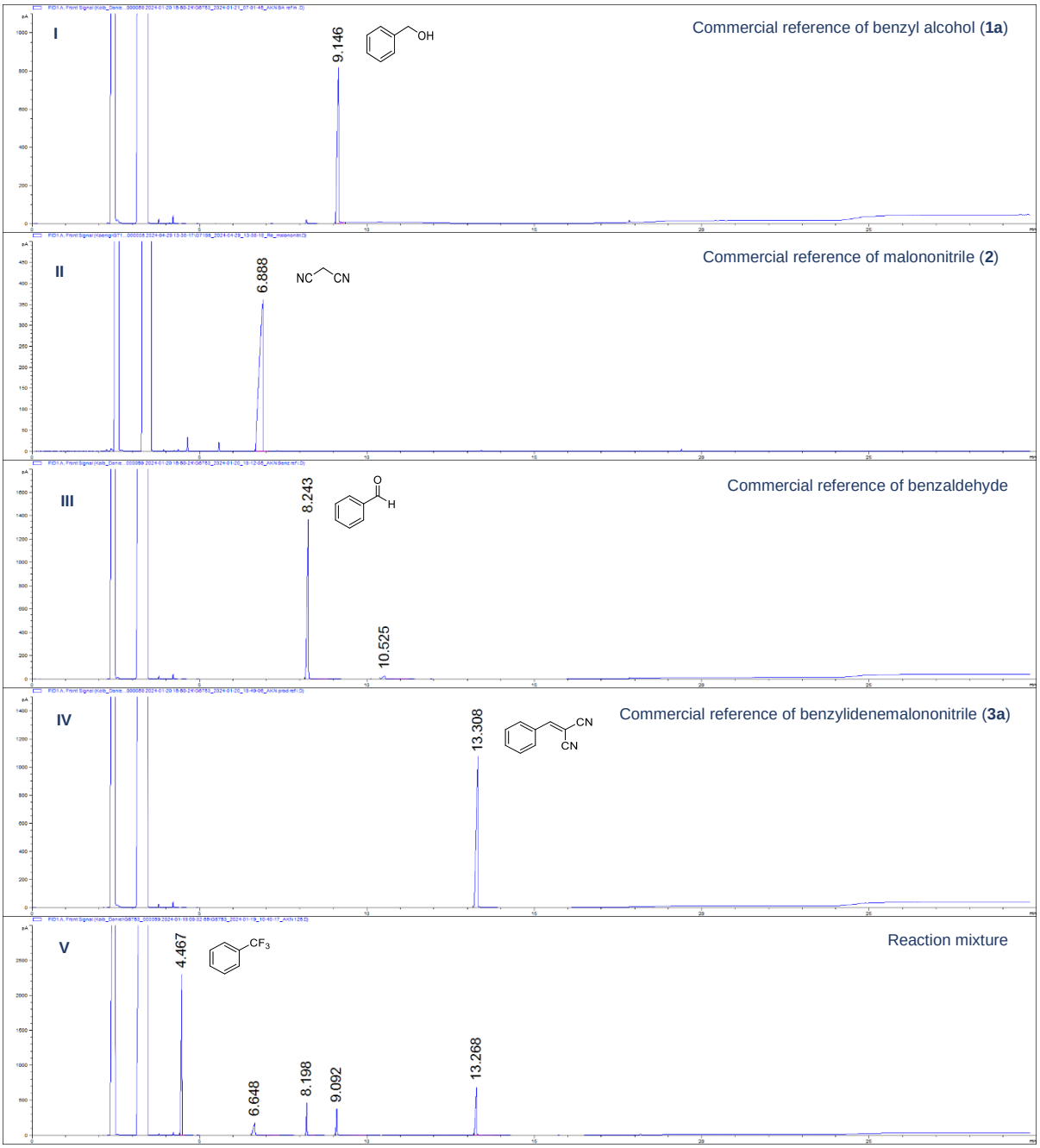

Figure S6. GC-FID chromatograms for the initial experiment with **3a**. **I**: commercial reference of **1a** (9.1 min). **II**: commercial reference of **2** (6.9 min). **III**: commercial reference of benzaldehyde (8.2 min). **IV**: commercial reference of **3a** (13.3 min). **V**: reaction mixture of **3a** (13.3 min) containing α,α,α-trifluorotoluene as internal standard (1 equiv.; 4.5 min).

2.4.5 UV-Vis Spectrum of Sodium Anthraquinone-1,5-disulfonate

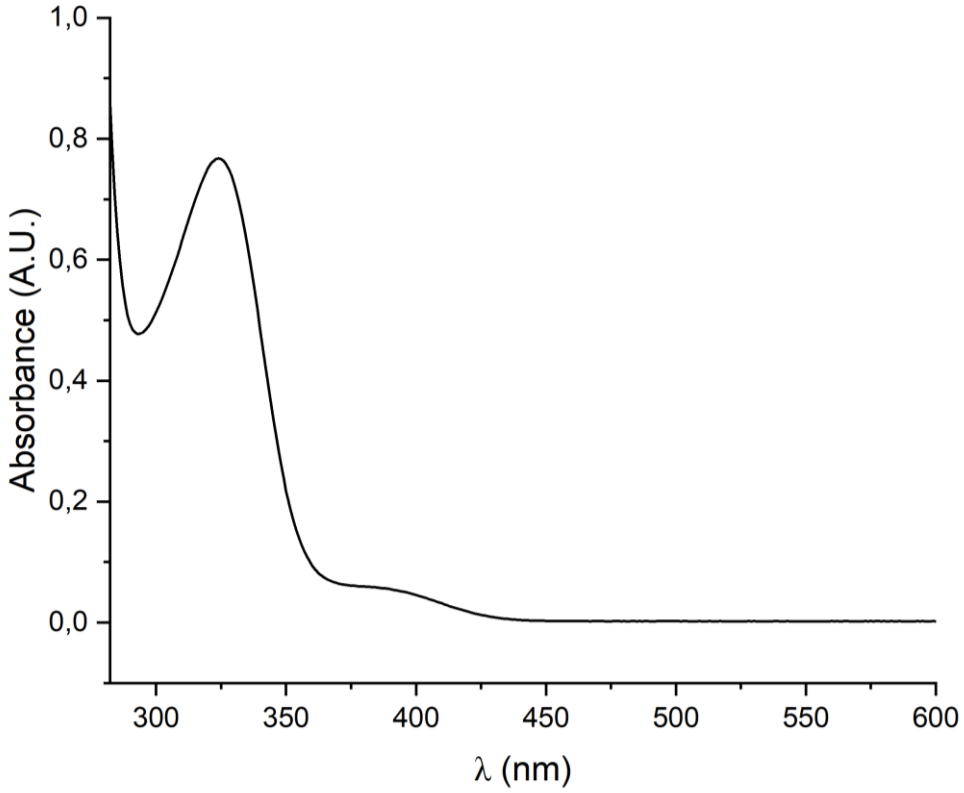

Figure S7. UV-Vis absorption spectrum of sodium anthraquinone-1,5-disulfonate (1 mM) in H_2O.

2.4.6 GC-FID Analysis of Experiment with Optimized Conditions with 3a

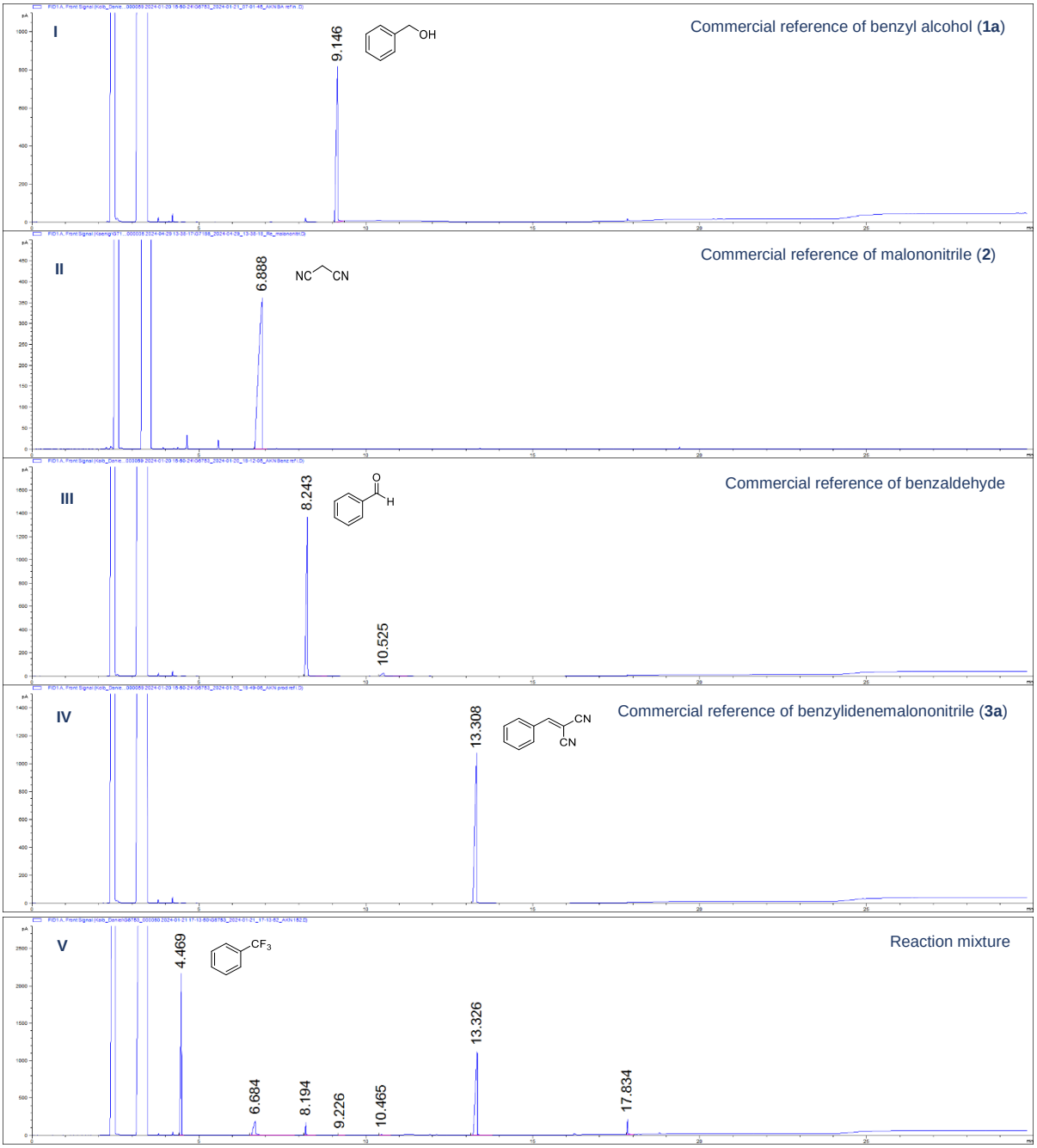

Figure S8. GC-FID chromatograms for experiment with optimized conditions with **3a**. **I**: commercial reference of **1a** (9.1 min). **II**: commercial reference of **2** (6.9 min). **III**: commercial reference of benzaldehyde (8.2 min). **IV**: commercial reference of **3a** (13.3 min). **V**: reaction mixture of **3a** (13.3 min) containing α,α,α-trifluorotoluene as internal standard (1 equiv.; 4.5 min).

2.4.7 GC-MS Analysis of Reaction Mixtures of non-isolated Products

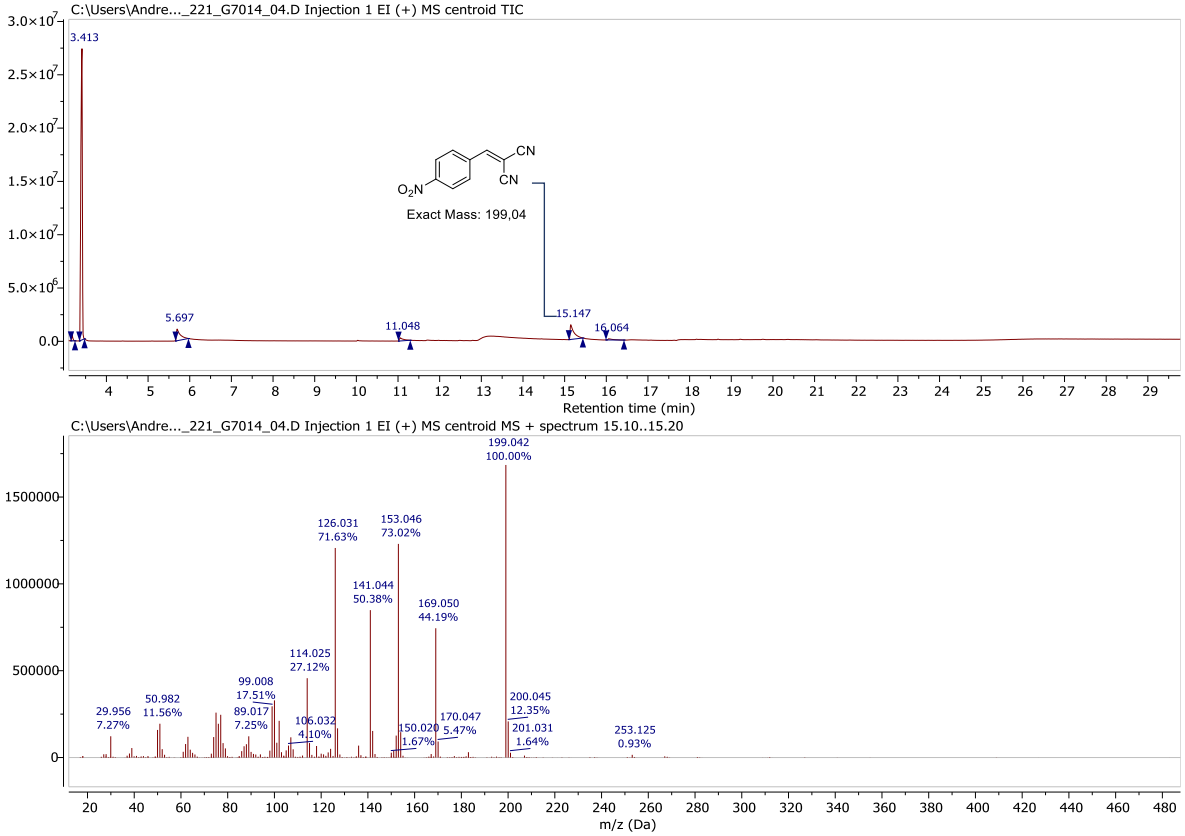

Figure S9. GC-MS chromatogram for **3l**. Fragmentations for the interval 15.1-15.2 min.

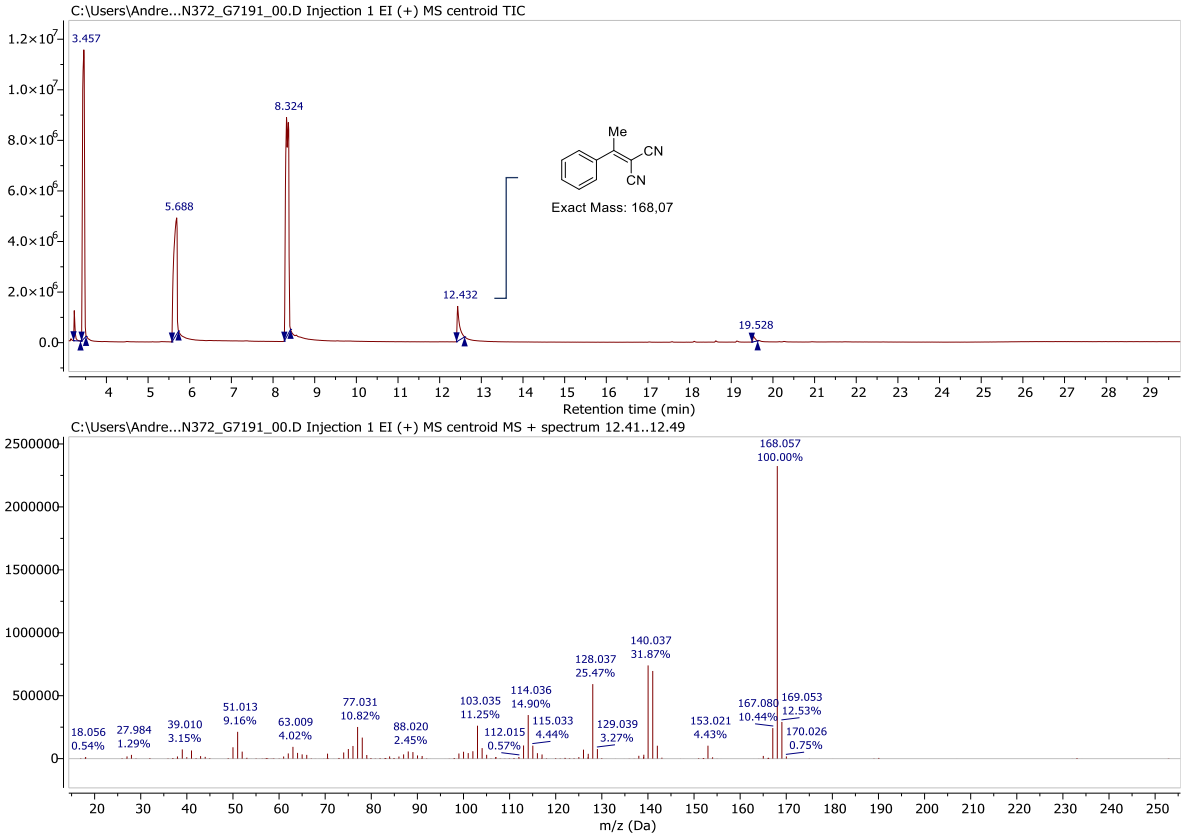

Figure S10. GC-MS chromatogram for **3u**. Fragmentations for the interval 12.4-12.5 min.

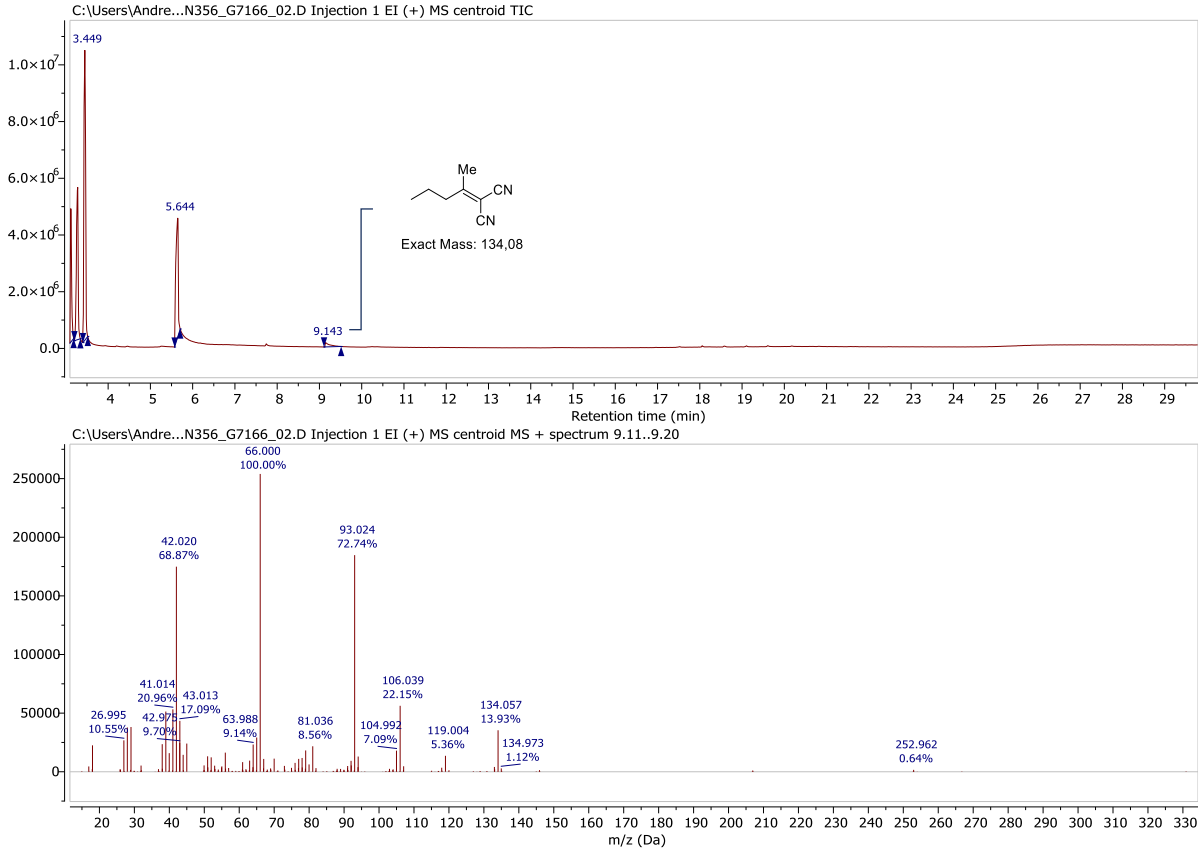

Figure S11. GC-MS chromatogram for **3w**. Fragmentations for the interval 9.1-9.2 min.

2.4.8 Substrate Scope of Failed Active C–H Methylene Compounds

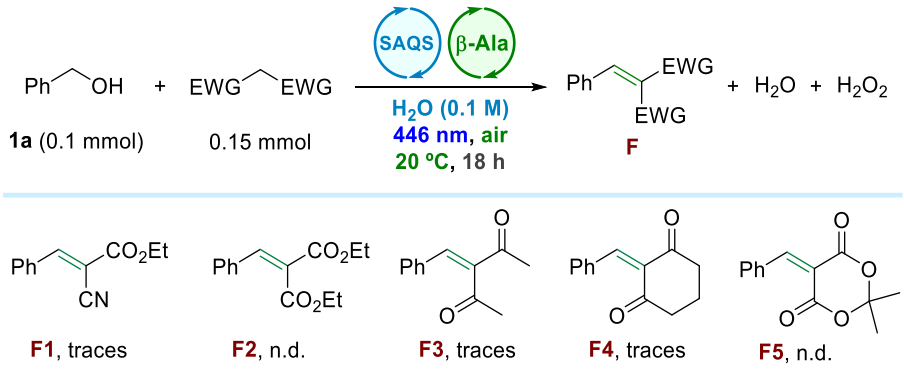

Scheme S6. Failed substrate scope. Reaction conditions: **1a** (0.1 mmol), **2** (0.15 mmol) **SAQS3** (10 mol%), β-alanine (5 mol%), H_2O (1 mL), 446 nm (0.7 W), air, 20 ºC, 18 h.

2.4.9 Mechanistic Studies

GC-MS Analysis of Intramolecular Competition Experiment

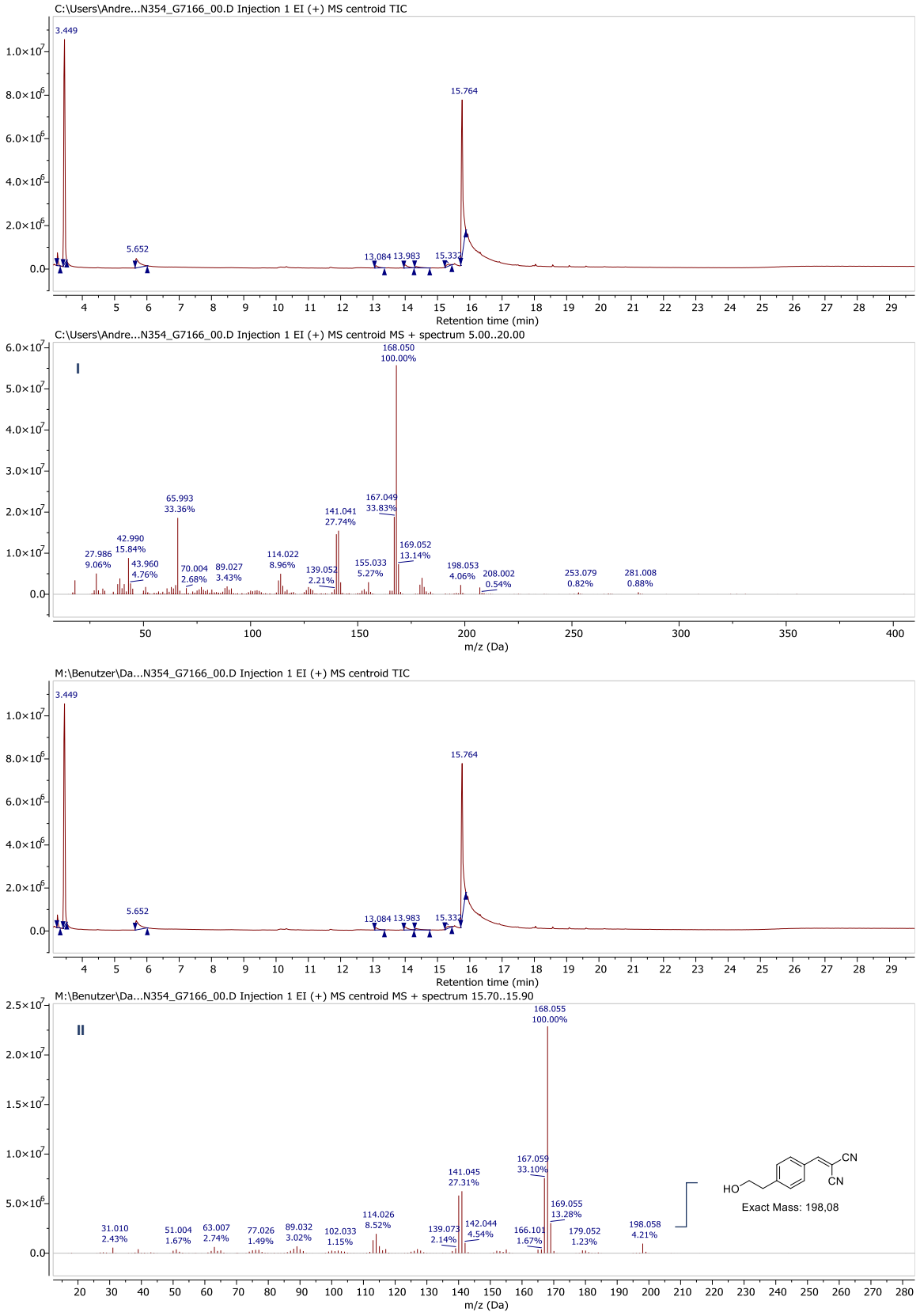

Figure S12. GC-MS chromatograms for **3x**. **I**: Fragmentations for the interval 5.0-20.0 min. **II**: Fragmentations for the interval 15.7-15.9 min.

GC-MS Analysis of Intermolecular Competition Experiment

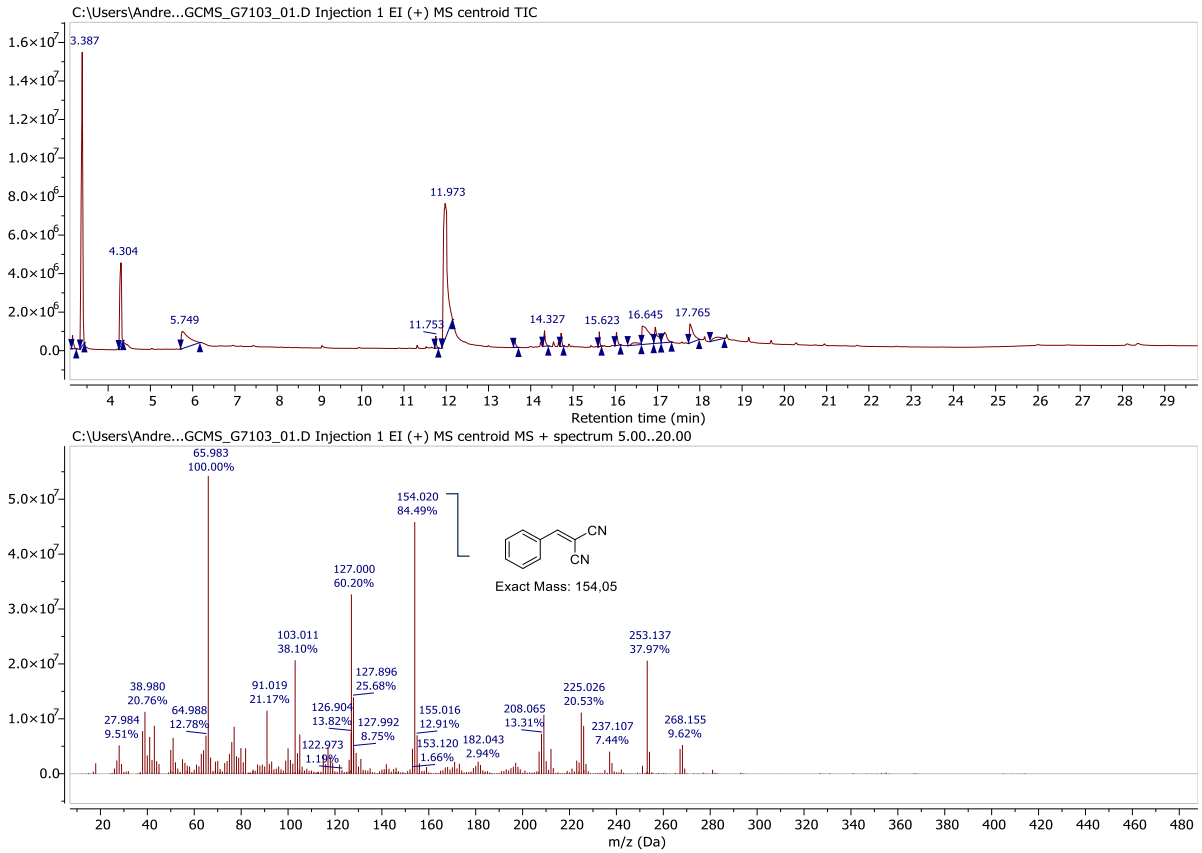

Figure S13. GC-MS chromatogram for intermolecular competition experiment. Fragmentations for the interval 5.0-20.0 min.

GC-MS Analysis of Reaction Mixture of 3a

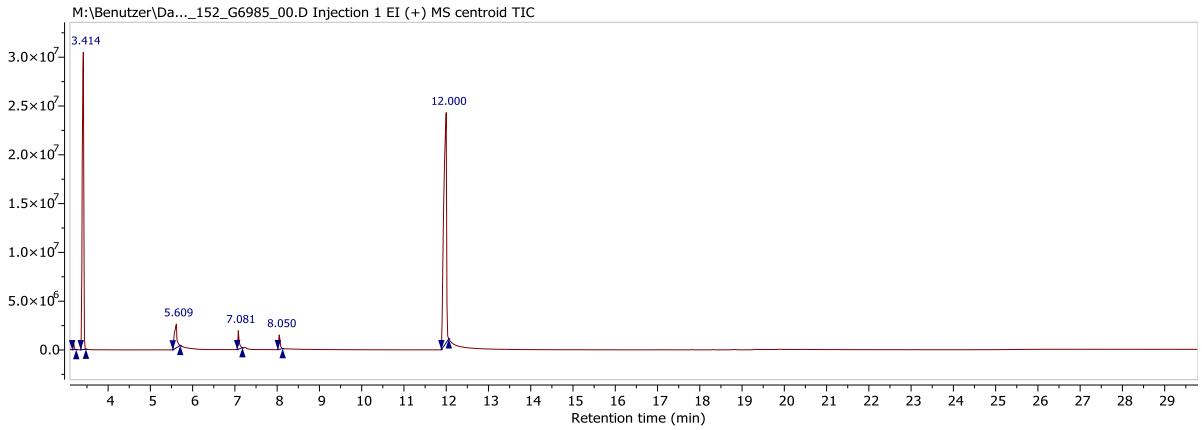

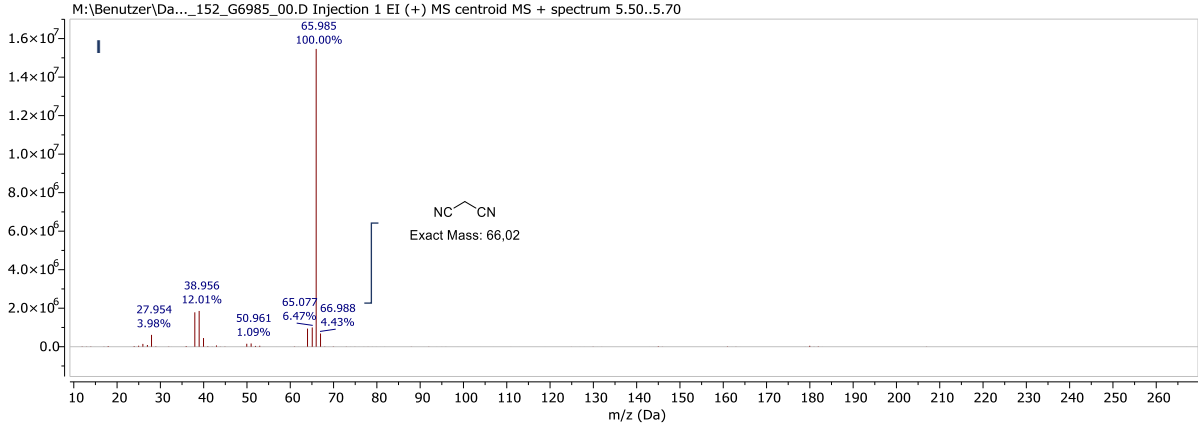

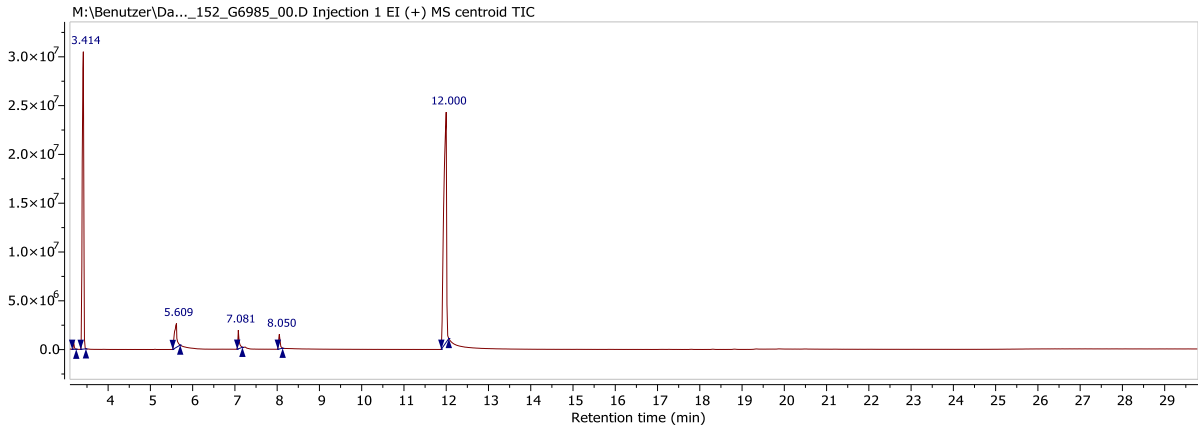

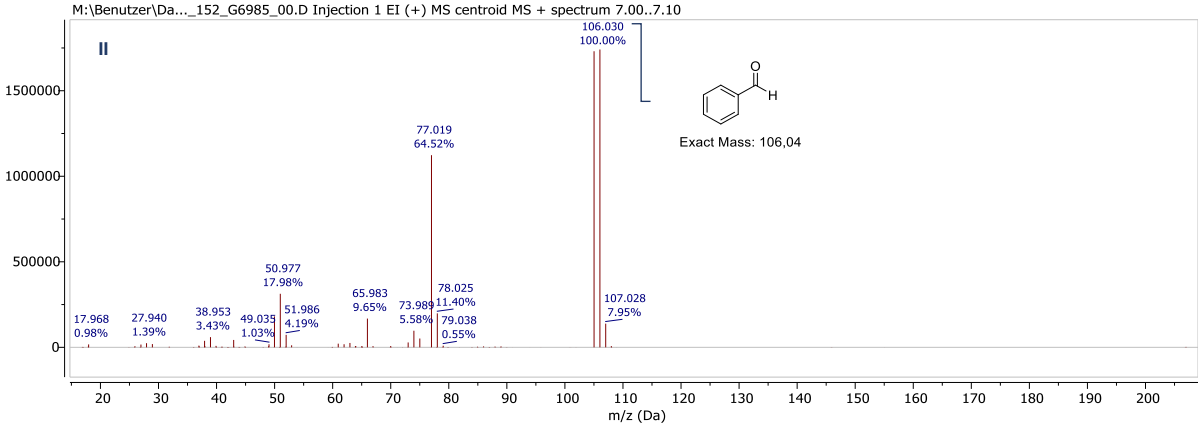

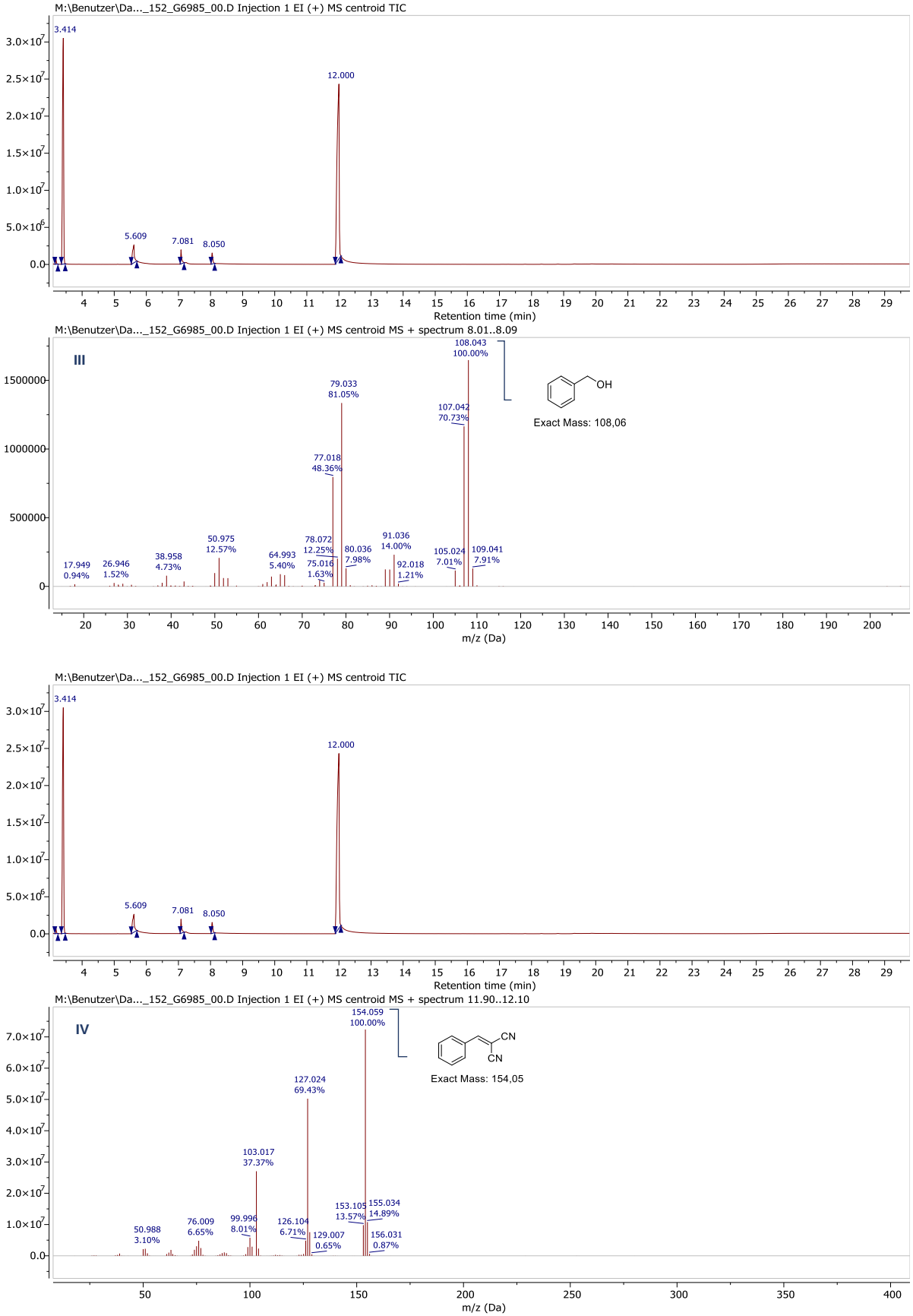

Figure S14. GC-MS chromatogram for the reaction mixture of **3a**. **I**: Fragmentations for the interval 5.5-5.7 min. **II**: Fragmentations for the interval 7.0-7.1 min. **III**: Fragmentations for the interval 8.0-8.1 min. **IV**: Fragmentations for the interval 11.9-12.1 min.

Semiquantitative Hydrogen Peroxide Determination

The hydrogen peroxide concentration of the reaction mixture of **3a** was determined semiquantitatively using Quantofix© peroxide test sticks (Figure S15). Upon reaction completion, an aliquot of 100 µL of reaction mixture was diluted with distilled water (dilution factor = 100) and the peroxide test strip was immersed in the solution for 1 s. After 15 s a picture was taken from the test stick. Upon visual evaluation, the concentration of H_2O_2 in the reaction mixture of **3a** can be established in the range of 2-5 mg/mL (0.06-0.15 M).

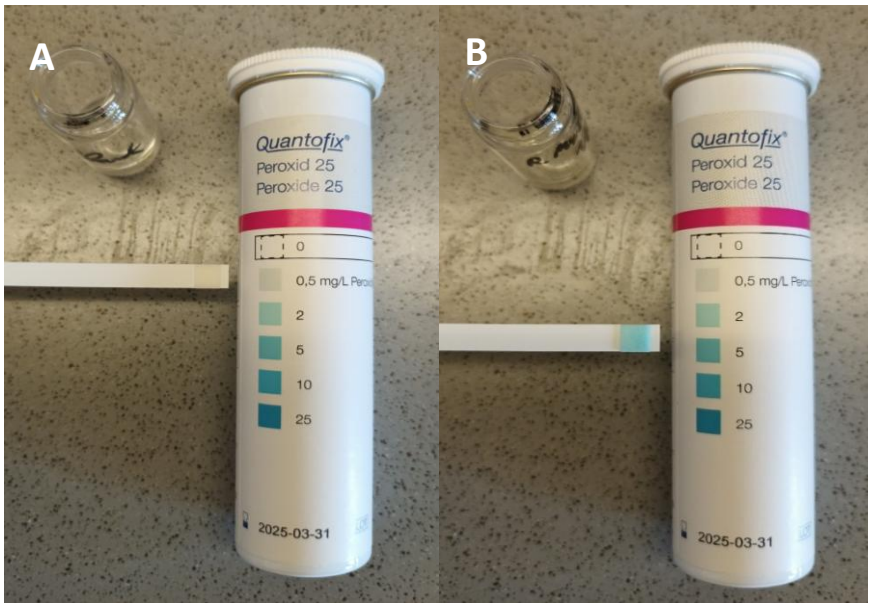

Figure S15. Hydrogen peroxide test. **A**: test result for distilled water (blank). **B**: test result for a reaction mixture of **3a** after 3 h of irradiation.

GC-MS Analysis of Reaction in the Absence of 2

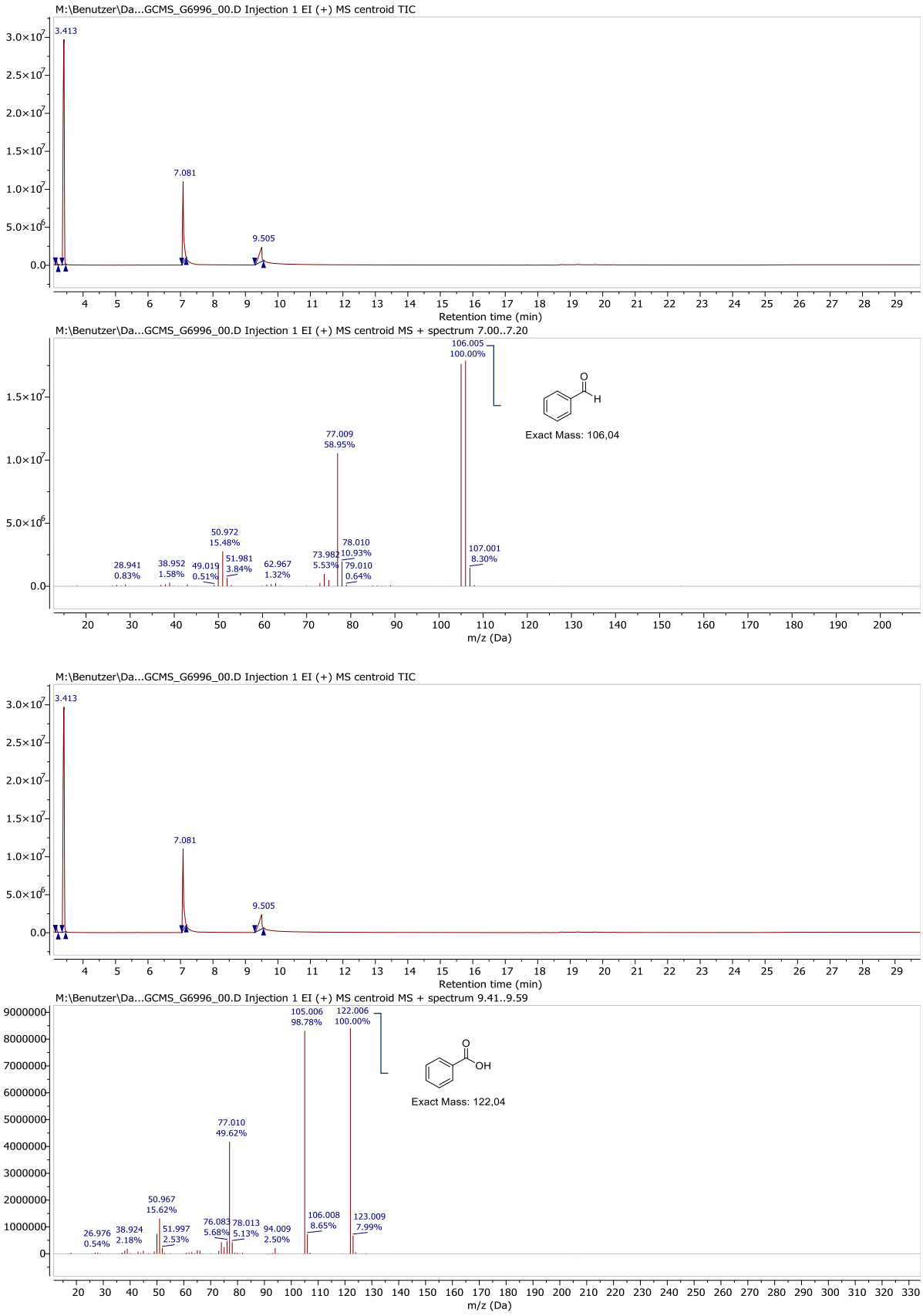

Figure S16. GC-MS chromatogram of control experiment in the absence of **2**. **I**: Fragmentations for the interval 7.0-7.2 min. **II**: Fragmentations for the interval 9.4-9.6 min.

Semiquantitative Hydrogen Peroxide Determination of Reactions Carried out under N_2 Atmosphere

The hydrogen peroxide concentration of the reaction mixtures of **3a** conducted under N_2 atmosphere was determined semiquantitatively using Quantofix© peroxide test sticks (Figure S17). Upon reaction completion, an aliquot of 100 µL of the reaction mixture was diluted with distilled water (dilution factor = 100), and the peroxide test strip was immersed in the solution for 1 s. After 15 s, a picture was taken from the test stick. Upon visual evaluation, the reactions conducted under inert atmosphere gave a negative result.

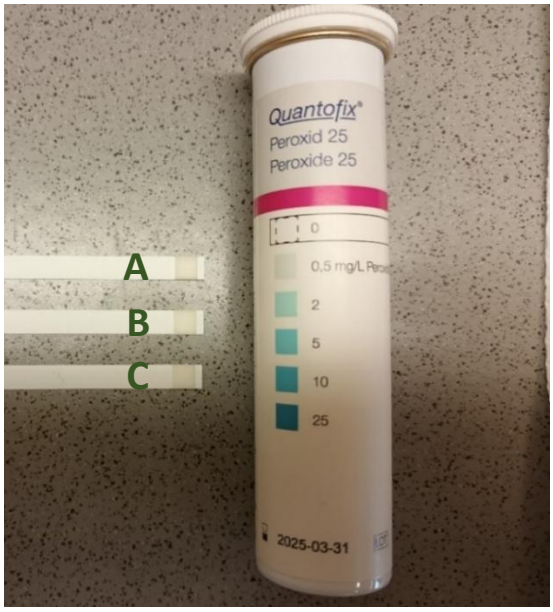

Figure S17. Hydrogen peroxide test. **A**: test result for distilled water (blank). **B**: test result for a reaction mixture of **3a** after 3 h of irradiation under N_2. **C**: test result for a reaction mixture of **3a** containing 15 mol% **SAQS3** after 3 h of irradiation under N_2.

Mechanistic Proposal in the Absence of Oxygen for the Tandem Photooxidative Transformation

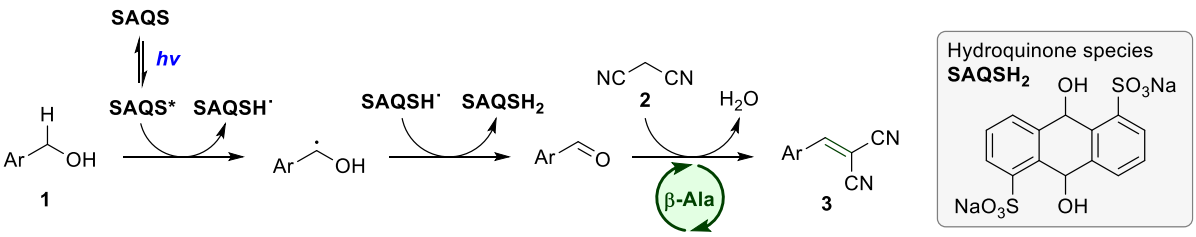

Scheme S7. Mechanistic proposal for the reaction in the absence of oxygen.

2.4.10 Synthesis and Analytical Data of Products

Benzylidenemalononitrile (**3a**)

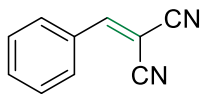

Prepared according to **GP1a**.
Reaction time: 3 h.
Isolated yield: 87% (13.4 mg, white solid).

^{1}H-NMR (400 MHz, $CDCl_3$): δ (ppm) = 7.91 (dd, *J* = 8.2, 0.8 Hz, 2H), 7.78 (s, 1H), 7.67 – 7.60 (m, 1H), 7.54 (dd, *J* = 10.6, 4.7 Hz, 2H). **^{13}C-NMR** (101 MHz, $CDCl_3$): δ (ppm) = 159.9, 134.6, 130.9, 130.7, 129.6, 113.7, 112.5, 82.9. **HRMS** (EI-MS): *m/z* for $[C_{10}H_6N_2]^{\cdot+}$ $[M]^{\cdot+}$ calcd: 154.05255, found: 154.05225.

2-Methylbenzylidenemalononitrile (**3b**)

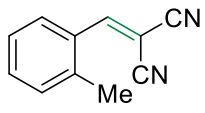

Prepared according to **GP1a**.
Reaction time: 4 h.
Isolated yield: 86% (14.4 mg, white solid).

^{1}H-NMR (400 MHz, $CDCl_3$): δ (ppm) = 8.16 – 8.01 (m, 2H), 7.54 – 7.44 (m, 1H), 7.35 (dd, *J* = 15.7, 7.8 Hz, 2H), 2.45 (s, 3H). **^{13}C-NMR** (101 MHz, $CDCl_3$): δ (ppm) = 158.2, 139.8, 134.2, 131.4, 129.9, 128.3, 127.1, 113.8, 112.5, 84.0, 19.8. **HRMS** (EI-MS): *m/z* for $[C_{11}H_8N_2]^{\cdot+}$ $[M]^{\cdot+}$ calcd: 168.06820, found: 168.06851.

3-Methylbenzylidenemalononitrile (**3c**)

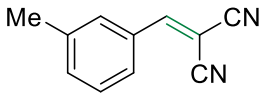

Prepared according to **GP1a**.
Reaction time: 2 h.
Isolated yield: 95% (16.0 mg, brownish solid).

^{1}H-NMR (400 MHz, $CDCl_3$): δ (ppm) = 7.76 – 7.71 (m, 2H), 7.69 (s, 1H), 7.47 – 7.40 (m, 2H), 2.43 (s, 3H). **^{13}C-NMR** (101 MHz, $CDCl_3$): δ (ppm) = 160.1, 139.6, 135.5, 131.2, 130.9, 129.5, 127.9, 113.8, 112.6, 82.4, 21.2. **HRMS** (EI-MS): *m/z* for $[C_{11}H_8N_2]^{\cdot+}$ $[M]^{\cdot+}$ calcd: 168.06820, found: 168.06831.

4-Methylbenzylidenemalononitrile (**3d**)

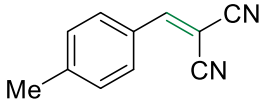

Prepared according to **GP1a**.
Reaction time: 2 h.
Isolated yield: 92% (15.5 mg, brownish solid).

^{1}H-NMR (400 MHz, $CDCl_3$): δ (ppm) = 7.81 (d, *J* = 8.1 Hz, 2H), 7.72 (s, 1H), 7.34 (d, *J* = 8.0 Hz, 2H), 2.46 (s, 3H). **^{13}C-NMR** (101 MHz, $CDCl_3$): δ (ppm) = 159.8, 146.4, 130.9, 130.3, 128.4, 114.0, 112.8, 81.2, 22.0. **HRMS** (EI-MS): *m/z* for $[C_{11}H_8N_2]^{\cdot+}$ $[M]^{\cdot+}$ calcd: 168.06820, found: 168.06842.

4-Ethylbenzylidenemalononitrile (**3e**)

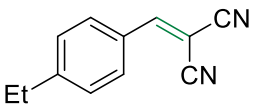

Prepared according to **GP1a**.
Reaction time: 4 h.
Isolated yield: 82% (14.9 mg, pale yellow solid).

^{1}H-NMR (400 MHz, $CDCl_3$): δ (ppm) = 7.84 (d, *J* = 8.3 Hz, 2H), 7.73 (s, 1H), 7.36 (d, *J* = 8.2 Hz, 2H), 2.75 (q, *J* = 7.6 Hz, 2H), 1.27 (t, *J* = 7.6 Hz, 3H). **^{13}C-NMR** (101 MHz, $CDCl_3$): δ (ppm) = 159.8, 152.4, 131.0, 129.2, 128.6, 114.0, 112.8, 81.2, 29.2, 14.9. **HRMS** (EI-MS): *m/z* for $[C_{12}H_{10}N_2]^{\cdot+}$ $[M]^{\cdot+}$ calcd: 182.08385, found: 182.08338.

4-Methoxybenzylidenemalononitrile (**3f**)

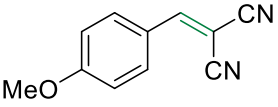

Prepared according to **GP1a**.
Reaction time: 3 h.
Isolated yield: 94% (17.3 mg, pale yellow solid).

^{1}H-NMR (400 MHz, $CDCl_3$): δ (ppm) = 7.91 (d, *J* = 8.9 Hz, 2H), 7.65 (s, 1H), 7.01 (d, *J* = 8.9 Hz, 2H), 3.91 (s, 3H). **^{13}C-NMR** (101 MHz, $CDCl_3$): δ (ppm) = 164.8, 158.8, 133.4, 124.0, 115.1, 114.4, 113.3, 78.5, 55.8. **HRMS** (EI-MS): *m/z* for $[C_{11}H_8N_2O]^{\cdot+}$ $[M]^{\cdot+}$ calcd: 184.06311, found: 184.06265.

4-(trifluoromethoxy)benzylidenemalononitrile (**3g**)

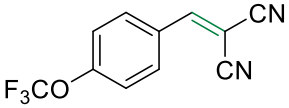

Prepared according to **GP1b**.
Reaction time: 24 h.
Isolated yield: 60% (14.2 mg, white solid).

^{1}H-NMR (400 MHz, CD_2Cl_2): δ (ppm) = 8.01 – 7.96 (m, 2H), 7.82 (s, 1H), 7.42 – 7.35 (m, 2H). **^{13}C-NMR** (101 MHz, CD_2Cl_2): δ (ppm) = 158.2, 153.0, 132.7, 129.3, 121.1, 120.2 (q, *J* = 259.5 Hz), 113.5, 112.4, 83.7. **^{19}F-NMR** (376 MHz, CD_2Cl_2): δ (ppm)= -57.9. **R_f** = 0.24 (PE/EtOAc = 96/4). **HRMS** (EI-MS): *m/z* for $[C_{11}H_5N_2OF_3]^{\cdot+}$ $[M]^{\cdot+}$ calcd: 238.03485, found: 238.03419.

4-Ethoxybenzylidenemalononitrile (**3h**)

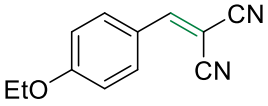

Prepared according to **GP1a**.
Reaction time: 3 h.
Isolated yield: 73% (14.5 mg, white solid).

^{1}H-NMR (400 MHz, $CDCl_3$): δ (ppm) = 7.89 (d, *J* = 8.9 Hz, 2H), 7.64 (s, 1H), 6.99 (d, *J* = 8.9 Hz, 2H), 4.14 (q, *J* = 7.0 Hz, 2H), 1.46 (t, *J* = 7.0 Hz, 3H). **^{13}C-NMR** (101 MHz, $CDCl_3$): δ (ppm) = 164.3, 158.9, 133.5, 123.8, 115.5, 114.5, 113.4, 78.2, 64.3, 14.5. **HRMS** (EI-MS): *m/z* for $[C_{12}H_{10}N_2O]^{\cdot+}$ $[M]^{\cdot+}$ calcd: 198.07876, found: 198.07927.

4-Acetoxybenzylidenemalononitrile (**3i**)

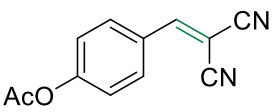

Prepared according to **GP1a**.
Reaction time: 3 h.
Isolated yield: 71% (15.1 mg, white solid).

^{1}H-NMR (400 MHz, $CDCl_3$): δ (ppm) = 7.95 (d, *J* = 8.7 Hz, 2H), 7.74 (s, 1H), 7.30 (d, *J* = 8.8 Hz, 2H), 2.34 (s, 3H). **^{13}C-NMR** (101 MHz, $CDCl_3$): δ (ppm) = 168.4, 158.5, 155.2, 132.3, 128.4, 123.0, 113.6, 112.5, 82.6, 21.1. **HRMS** (EI-MS): *m/z* for $[C_{12}H_8N_2O_2]^{\cdot+}$ $[M]^{\cdot+}$ calcd: 212.05803, found: 212.05760.

4-(trifluoromethyl)thio)benzylidenemalononitrile (**3k**)

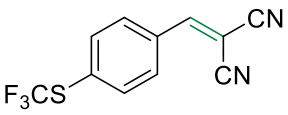

Prepared according to **GP1b**.
Reaction time: 24 h.
Isolated yield: 27% (6.9 mg, white solid).

^{1}H-NMR (400 MHz, CD_2Cl_2): δ (ppm) = 7.96 – 7.92 (m, 2H), 7.85 (s, 1H), 7.81 (d, *J* = 8.5 Hz, 2H). **^{13}C-NMR** (101 MHz, CD_2Cl_2): δ (ppm) = 158.3, 136.0, 132.6, 131.4 (q, *J* = 4.2, 1.9 Hz), 131.1, 129.2 (q, *J* = 308.6 Hz), 113.3, 112.2, 85.3. **^{19}F-NMR** (376 MHz, CD_2Cl_2): δ (ppm) = - 41.7. **R_f** = 0.28 (PE/EtOAc = 95/5). **HRMS** (EI-MS): *m/z* for $[C_{11}H_5N_2F_3S]^{\cdot+}$ $[M]^{\cdot+}$ calcd: 254.01200, found: 254.01243.

Methyl 4-(2,2-dicyanovinyl)benzoate (**3m**)

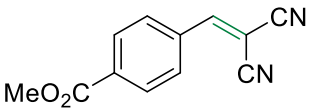

Prepared according to **GP1a**.
Reaction time: 5 h.
Isolated yield: 48% (10.1 mg, pale yellow solid).

^{1}H-NMR (400 MHz, $CDCl_3$): δ (ppm) = 8.18 (d, *J* = 8.1 Hz, 2H), 7.96 (d, *J* = 8.1 Hz, 2H), 7.83 (s, 1H), 3.96 (s, 3H). **^{13}C-NMR** (101 MHz, $CDCl_3$): δ (ppm) = 165.4, 158.5, 134.9, 134.3, 130.5, 130.4, 113.2, 112.0, 85.3, 52.7. **HRMS** (EI-MS): *m/z* for $[C_{12}H_8N_2O_2]^{\cdot+}$ $[M]^{\cdot+}$ calcd: 212.05803, found: 212.05753.

4-Cyanobenzylidenemalononitrile (**3n**)

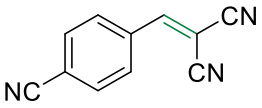

Prepared according to **GP1a**.
Reaction time: 24 h.
Isolated yield: 63% (11.3 mg, white solid).

^{1}H-NMR (400 MHz, $CDCl_3$): δ (ppm) = 8.00 (d, *J* = 8.3 Hz, 2H), 7.87 – 7.80 (m, 3H). **^{13}C-NMR** (101 MHz, $CDCl_3$): δ (ppm) = 157.3, 134.2, 133.1, 130.7, 117.3, 117.2, 112.7, 111.7, 86.9. **HRMS** (EI-MS): *m/z* for $[C_{11}H_5N_3]^{\cdot+}$ $[M]^{\cdot+}$ calcd: 179.04780, found: 179.04802.

4-trifluoromethylbenzylidenemalononitrile (**3o**)

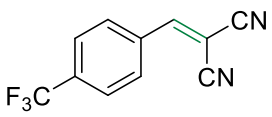

Prepared according to **GP1b**. Reaction time: 24 h. The crude product was purified via CC (PE/Acetone = 92/8).
Isolated yield: 66% (14.7 mg, white solid).

^{1}H-NMR (400 MHz, $CDCl_3$): δ (ppm) = 8.02 (d, *J* = 8.4 Hz, 2H), 7.85 (s, 1H), 7.81 (d, *J* = 8.4 Hz, 2H). **^{13}C-NMR** (101 MHz, $CDCl_3$): δ (ppm) = 158.0, 135.3 (q, *J* = 33.3 Hz), 133.7, 130.7, 127.1, 126.55 (q, *J* = 3.7 Hz), 124.4, 121.7, 119.0, 112.9, 111.9, 86.0. **^{19}F-NMR** (376 MHz, $CDCl_3$): δ (ppm)= -64.0. **R_f** = 0.25 (PE/Acetone = 92/8). **HRMS** (EI-MS): *m/z* for $[C_{11}H_5N_2F_3]^{\cdot+}$ $[M]^{\cdot+}$ calcd: 222.03993, found: 222.04039.

4-Fluorobenzylidenemalononitrile (**3p**)

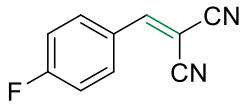

Prepared according to **GP1a**.
Reaction time: 5 h.
Isolated yield: 84% (14.4 mg, white solid).

^{1}H-NMR (400 MHz, $CDCl_3$): δ (ppm) = 8.05 – 7.91 (m, 2H), 7.77 (s, 1H), 7.32 – 7.20 (m, 2H). **^{13}C-NMR** (101 MHz, $CDCl_3$): δ (ppm) = 167.4, 164.8, 158.3, 133.4 (d, *J* = 9.5 Hz), 127.33 (d, *J* = 3.3 Hz), 117.5 (d, *J* = 22.3 Hz), 113.0 (d, *J* = 7.6 Hz), 82.41 (d, *J* = 2.7 Hz). **^{19}F-NMR** (376 MHz, $CDCl_3$): δ (ppm)= -100.5. **HRMS** (EI-MS): *m/z* for $[C_{10}H_5N_2F]^{\cdot+}$ $[M]^{\cdot+}$ calcd: 172.04313, found: 172.04347.

4-Chlorobenzylidenemalononitrile (**3q**)

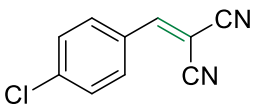

Prepared according to **GP1a**.
Reaction time: 3 h.
Isolated yield: 92% (17.3 mg, white solid).

^{1}H-NMR (400 MHz, $CDCl_3$): δ (ppm) = 7.86 (d, *J* = 8.6 Hz, 2H), 7.73 (s, 1H), 7.52 (d, *J* = 8.6 Hz, 2H). **^{13}C-NMR** (101 MHz, $CDCl_3$): δ (ppm) = 158.3, 141.2, 131.9, 130.1, 129.3, 113.5, 112.4, 83.4. **HRMS** (EI-MS): *m/z* for $[C_{10}H_5N_2Cl]^{\cdot+}$ $[M]^{\cdot+}$ calcd: 188.01358, found: 188.01386.

3-Chloro-4-fluorobenzylidenemalononitrile (**3r**)

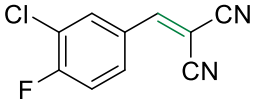

Prepared according to **GP1a**.
Reaction time: 6 h.
Isolated yield: 75% (15.4 mg, pale-brown solid).

^{1}H-NMR (400 MHz, $CDCl_3$): δ (ppm) = 7.96 (dd, *J* = 6.8, 2.3 Hz, 1H), 7.88 (ddd, *J* = 8.6, 4.4, 2.3 Hz, 1H), 7.69 (s, 1H), 7.33 (t, *J* = 8.5 Hz, 1H). **^{13}C-NMR** (101 MHz, $CDCl_3$): δ (ppm) = 162.7, 160.1, 156.9, 133.3, 130.8 (d, *J* = 8.6 Hz), 128.1 (d, *J* = 4.1 Hz), 123.2 (d, *J* = 18.5 Hz), 118.1

(d, *J* = 22.1 Hz), 112.5 (d, *J* = 110.3 Hz), 84.1. **^{19}F-NMR** (376 MHz, $CDCl_3$): δ (ppm) = - 103.3. **HRMS** (EI-MS): *m/z* for $[C_{10}H_4N_2FCl]^{\cdot+}$ $[M]^{\cdot+}$ calcd: 206.00416, found: 206.00367.

4-Bromobenzylidenemalononitrile (**3s**)

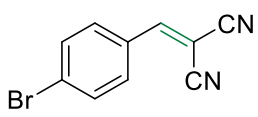

Prepared according to **GP1a**. Reaction time: 24 h. The filtered solid was purified via CC (PE/EtOAc = 96/4).
Isolated yield: 69% (16.1 mg, white solid).

^{1}H-NMR (400 MHz, $CDCl_3$): δ (ppm) = 7.80 – 7.75 (m, 2H), 7.73 – 7.67 (m, 3H). **^{13}C-NMR** (101 MHz, $CDCl_3$): δ (ppm) = 158.4, 133.1, 131.8, 130.0, 129.7, 113.5, 112.3, 83.5. **R_f** = 0.28 (PE/EtOAc = 96/4) [$KMnO_4$]. **HRMS** (EI-MS): *m/z* for $[C_{10}H_5N_2Br]^{\cdot+}$ $[M]^{\cdot+}$ calcd: 231.96306, found: 231.96278.

4-Iodobenzylidenemalononitrile (**3t**)

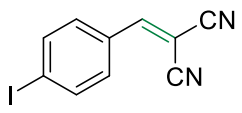

Prepared according to **GP1b**. Reaction time: 24 h. The crude product was purified via CC (PE/Acetone = 92/8).
Isolated yield: 36% (10.1 mg, white solid).

^{1}H-NMR (400 MHz, $CDCl_3$): δ (ppm) = 7.96 – 7.85 (m, 2H), 7.69 (s, 1H), 7.60 (d, *J* = 8.4 Hz, 2H). **^{13}C-NMR** (101 MHz, $CDCl_3$): δ (ppm) = 158.7, 139.1, 131.5, 130.2, 113.5, 112.4, 102.9, 83.6. **R_f** = 0.23 (PE/Acetone = 92/8). **HRMS** (EI-MS): *m/z* for $[C_{10}H_5N_2I]^{\cdot+}$ $[M]^{\cdot+}$ calcd: 279.94919, found: 279.9898.

2-(4-(2-hydroxyethyl)benzylidene)malononitrile (**3x**)

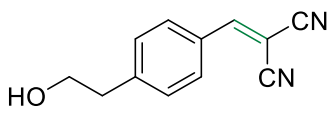

Prepared according to **GP1b**. Reaction time: 8 h. The crude product was purified via CC (PE/Acetone = 75/25).
Isolated yield: 68% (14.8 mg, pale-yellow oil).

^{1}H-NMR (400 MHz, $CDCl_3$): δ (ppm) = 7.88 – 7.82 (m, 2H), 7.74 (s, 1H), 7.41 (d, *J* = 8.1 Hz, 2H), 3.91 (t, *J* = 4.7 Hz, 2H), 2.96 (t, *J* = 6.1 Hz, 2H), 1.63 (bs, 1H). **^{13}C-NMR** (101 MHz, $CDCl_3$): δ (ppm) = 159.7, 147.1, 131.0, 130.4, 129.3, 127.4, 127.0, 113.9, 112.8, 81.9, 62.9, 39.3. **R_f** = 0.31 (PE/Acetone = 75/25). **HRMS** (EI-MS): *m/z* for $[C_{12}H_{10}N_2O]^{\cdot+}$ $[M]^{\cdot+}$ calcd: 198.07876, found: 198.07879.

2.5 References

[1] a) C. J. Clarke, W.-C. Tu, O. Levers, A. Bröhl, J. P. Hallett, *Chem. Rev*. **2018**, *118*, 747–800; b) K. N. Ganesh, D. Zhang, S. J. Miller, K. Rossen, P. J. Chirik, M. C. Kozlowski, J. B. Zimmerman, B. W. Brooks, P. E. Savage, D. T. Allen, A. M. Voutchkova-Kostal, *Org. Process Res. Dev*. **2021**, *25*, 1455–1459; c) S. Kar, H. Sanderson, K. Roy, E. Benfenati, J. Leszczynski, *Chem. Rev*. **2022**, *122*, 3637–3710; d) J. Colberg, K. Kuok Hii, S. G. Koenig, *ACS Sustainable Chem. Eng*. **2022**, *10*, 8239–8241.

[2] a) J.-C. Wasilke, S. J. Obrey, R. T. Baker, G. C. Bazan, *Chem. Rev.* **2005**, *105*, 1001–1020; b) Y. Hayashi, *Chem. Sci.* **2016**, *7*, 866–880; c) H. Ren, K. M. Maloney, K. Basu, M. J. Di Maso, G. R. Humphrey, F. Peng, R. Desmond, D. A. L. Otte, E. Alwedi, W. Liu, S.-W. Zhang, S. Song, R. A. Arvary, M. A. Zompa, D. Lehnherr, G. E. Martin, H. Y. D. Chang, A. E. Mohan, F. J. Guzman, L. Jellett, A. Y. Lee, G. Spencer, E. S. Fisher, J. R. Naber, H. Gao, S. Lohani, R. T. Ruck, L.-C. Campeau, *Org. Process Res. Dev*. **2020**, *24*, 2445–2452; d) J. C. Caravez, K. S. Iyer, R. D. Kavthe, J. R. A. Kincaid, B. H. Lipshutz, *Org. Lett*. **2022**, *24*, 9049–9053.

[3] a) V. Jeena, R. S. Robinson, *RSC Adv*. **2014**, *4*, 40720–40739; b) O. O. Kovalenko, H. Lundberg, D. Hübner, H. Adolfsson, *Eur. J. Org. Chem*. **2014**, *30*, 6639–6642; c) B. Paul, M. Maji, K. Chakrabarti, S. Kundu, *Org. Biomol. Chem*. **2020**, *18*, 2193–2214.

[4] Y. -R. Luo, *Comprehensive Handbook of Chemical Bond Energies*; CRC Press: Boca Raton, 2007.

[5] a) A. Fujiya, T. Nobuta, E. Yamaguchi, N. Tada, T. Miura, A. Itoh, *RSC Adv.* **2015**, *5*, 39539–39543; b) M. Du, G. Zeng, J. Huang, D. Sun, Q. Li, G. Wang, X. Li, *ACS Sustainable Chem. Eng*. **2019**, *7*, 9717–9726; c) N. F. Nikitas, D. I. Tzaras, I. Triandafillidi, C. G. Kokotos, *Green Chem*. **2020**, *22*, 471–477; d) I. Krivtsov, A. Vazirani, D. Mitoraj, R. Beranek, *ChemCatChem* **2023**, *15*, e202201215.

[6] a) K. Sun, Q.-Y. Lv, X.-L. Chen, L.-B. Qu, B. Yu, *Green Chem*. **2021**, *23*, 232–248; b) M. Cortes-Clerget, J. Yu, J. R. A. Kincaid, P. Walde, F. Gallou, B. H. Lipshutz, *Chem. Sci*. **2021**, *12*, 4237–4266; c) S. Barata-Vallejo, D. E. Yerien, A. Postigo, *ACS Sustainable Chem. Eng*. **2021**, *9*, 10016–10047.

[7] a) I. Texier, C. Giannotti, S. Malato, C. Richter, J. Delaire, *Catal. Today* **1999**, *54*, 297–307; b) M. D. Tzirakis, I. N. Lykakis, M. Orfanopoulos, *Chem. Soc. Rev*. **2009**, *38*, 2609–2621; c) W. Zhang, J. Gacs, I. W. C. E. Arends, F. Hollmann, *ChemCatChem* **2017**, *9*, 3821–3826; d) Y. Masuda, H. Tsuda, M. Murakami, *Angew. Chem. Int. Ed*.

2020, *59*, 2755–2759; e) B. Yuan, D. Mahor, Q. Fei, R. Wever, M. Alcalde, W. Zhang, F. Hollmann, *ACS Catal.* **2020**, *10*, 8277–8284.

[8] a) F. Michel, L. Mercklein, A. Crastes de Paulet, J. C. Doré, J. Gilbert, J. F. Miquel, *Prostaglandins* **1984**, *27*, 69–84; b) A. Gazit, P. Yaish, C. Gilon, A. Levitzki, *J. Med. Chem.* **1989**, *32*, 2344–2352; c) A. grodsky, A. Vanichkin, M. Patya, A. Gazit, N. Osherov, A. Levitzki, *Science* **1994**, *264*, 1319–1322; d) Y. Zlotnik, M. Patya, A. Vanichkin, *Br J Cancer* **2005**, *92*, 294–297; e) A. Levitzki, E. Mishani, *Annu. Rev. Biochem*. **2006**, *75*, 93–109; f) A. Novogrodsky, M. Weisspapir, M. Patya, A. Meshorer, A. Vanichkin, *Cancer Res*. **1998**, *58*, 2397–2403; g) A. Sidhu, J. R. Sharma, M. Rai, *Indian J. Chem. Sect. B Org. Med. Chem*. **2010**, *49*, 247–250; h) K. Turpaev, M. Ermolenko, T. Cresteil, J. C. Drapier, *Biochem. Pharmacol*. **2011**, *82*, 535–547.

[9] A. L. Gant Kanegusuku, J. L. Roizen, *Angew. Chem. Int. Ed*. **2021**, *60*, 21116–21149.

[10] a) R. Trotzki, M. M. Hoffmann, B. Ondruschka, *Green Chem*., **2008**, *10*, 873–878; b) K. van Beurden, S. de Koning, D. Molendijk, J. van Schijndel, *Green Chem. Lett. Rev*. **2020**, *13*, 349–364; c) C. Salvitti, M. Bortolami, I. Chiarotto, A. Troiani, G. de Petris, *New J. Chem*. **2021**, *45*, 17787–17795; d) R. Tokala, D. Bora, N. Shankaraiah, *ChemMedChem* **2022**, *17*, e202100736; e) A. Das, K. R. Justin Thomas, *Green Chem*. **2022**, *24*, 4952–4957; f) K. M. Uddin, M. Sakib, S. Siraji, R. Uddin, S. Rahman, A. Alodhayb, K. A. Alibrahim, A. Kumer, M. M. Matin, M. M. H. Bhuiyan, *ACS Omega* **2023**, *8*, 25817–25831; g) H. Zhao, C. D. Campbell, *J. Chem. Technol. Biotechnol*. **2024**, *99*, 780–787.

[11] E. Knoevenagel, *Dtsch. Chem. Ges*. **1894**, *27*, 2345–2346.

[12] a) T. Toyao, M. Saito, Y. Horiuchi, M. Matsuoka, *Catal. Sci. Tech*. **2014**, *4*, 625–628; b) Chen Chen, H. Yang, J. Chen, R. Zhang, L. Guo, H. Gan, B. Song, W. Zhu, L. Hua, Z. Hou, *Catal. Commun*. **2014**, *47*, 49–53; c) Y. Horiuchi, D. Do Van, Y. Yonezawa, M. Saito, S. Dohshi, T.-H. Kim, M. Matsuoka, *RSC Adv.* **2015**, *5*, 72653–72658; d) W. J. Ang, Y. S. Chng, Y. Lam, *RSC Adv*. **2015**, *5*, 81415–81428; e) Y.-A. Li, S. Yang, Q.-K. Liu, G.-J. Chen, J.-P. Ma, Y.-B. Dong, *Chem. Commun*. **2016**, *52*, 6517–6520; f) J.-S. Wang, F.-Z. Jin, H.-C. Ma, X.-B. Li, M.-Y. Liu, J.-L. Kan, G.-J. Chen, Y.-B. Dong, *Inorg. Chem*. **2016**, *55*, 6685–6691; g) C.-C. Cao, C.-X. Chen, Z.-W. Wei, Q.-F. Qiu, N.-X. Zhu, Y.-Y. Xiong, J.-J. Jiang, D. Wang, C.-Y. Su, *J. Am. Chem. Soc*. **2019**, *141*, 2589–2593; h) F.-F. Zhu, L.-J. Chen, S. Chen, G.-Y. Wu, W.-L. Jiang, J.-C. Shen, Y. Qin, L. Xu, H.-B. Yang, *Chem*. **2020**, *6*, 2395–2406.

[13] a) T. J. Collins, *Green Chemistry*, Macmillan Encyclopedia of Chemistry, Macmillan: New York, **1997**; b) P. Anastas, N. Eghbali, *Chem. Soc. Rev*. **2010**, *39*, 301–312.

[14] a) F. S. Prout, *J. Org. Chem.* **1953**, *18*, 928–933; b) L. Zhu, N. Lei, Z. Miao, C. Sheng, C. Zhuang, J. Yao, W. Zhang, *Chin. J. Chem*. **2012**, *30*, 139–143; c) D. W. Domaille, G. R. Hafenstine, M. A. Greer, A. P. Goodwin, J. N. Cha, *ACS Sustainable Chem*. *Eng*. **2016**, *4*, 671–675; d) G. R. Hafenstine, K. Ma, A. W. Harris, O. Yehezkeli, E. Park, D. W. Domaille, J. N. Cha, A. P. Goodwin, *ACS Catal*. **2017**, *7*, 568–572.

[15] V. Maurino, D. Borghesi, D. Vione, C. Minero, *Photochem. Photobiol. Sci*., **2008**, *7*, 321–327.

[16] a) R. A. Sheldon, J. K. Kochi, *Metal-Catalysed Oxidations of Organic Compounds*, Academic Press, New York **1981**; b) M. Sankar, E. Nowicka, E. Carter, D. M. Murphy, D. W. Knight, D. Bethell, G. J. Hutchings, *Nat. Commun*. **2014**, *5*, 3332; c) H. Shi, J. Li, T. Wang, M. Rudolph, A. S. K. Hashmi, *Green Chem*. **2022**, *24*, 5835–5841; d) C. S. Batsika, C. Koutsilieris, G. S. Koutoulogenis, M. G. Kokotou, C. G. Kokotos, G. Kokotos, *Green Chem.* **2022**, *24*, 6224–6231.

[17] N. Tada, K. Hattori, T. Nobuta, T. Miura, A. Itoh, *Green Chem*. **2011**, *13*, 1669–1671.

[18] V. Campisciano, F. Giacalone, M. Gruttadauria, *ChemCatChem* **2022**, *14*, e202200696.

[19] a) C. F. Wells, *Trans. Faraday Soc.* **1961**, *57*, 1703–1718; b) K. P. Clark, H. I. Stonehill, *J. Chem. Soc., Faraday Trans*. 1 **1972**, *68*, 577–590; c) Z. Yu, J. Zhao, Y. Wu, L. Guo, C. Ma, H. Zhu, J. Li, L. Duan, Z. Liu, H. Sun, G. Zhao, Q. Meng, *ACS Sustainable Chem. Eng*. **2023**, *11*, 13320–13332.

[20] D. Kolb, A. A. Almasalma, M. Morgenstern, L. Ganser, I. Weidacher, B. König, *ChemPhotoChem* **2023**, *7*, e202300167.

[21] X. Nie, L. Xia, H. L. Wang, G. Chen, B. Wu, T. Y. Zeng, C. Y. Hong, L. H. Wang, Y. Z. You, *ACS Appl. Mater. Interfaces* **2019**, *11*, 31735–31742.

[22] Z. Pechlivanidis, H. Hopf, L. Ernst, *Eur. J. Org. Chem*. **2009**, *2*, 223–237.

Part II – Dual HAT-Cobalt Photocatalysis

3. Synthesis of Linear Enamides and Enecarbamates via Photoredox Acceptorless Dehydrogenation

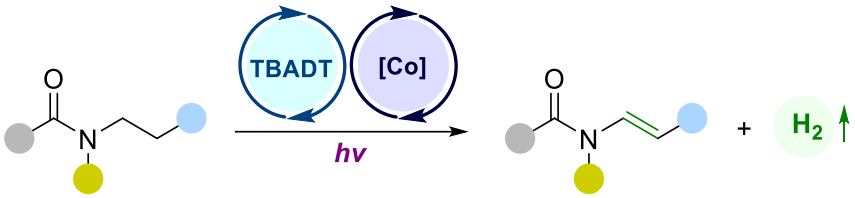

Abstract: In recent years, several methods for the direct desaturation of aliphatic compounds have been developed, facilitated by the unique combination of photoredox and transition-metal catalysis. Hereby, alkenes with high functionalization potential can be prepared in a straightforward fashion. We adapted a previously reported system involving tetrabutylammonium decatungstate (TBADT) as hydrogen atom transfer (HAT) agent and a cobaloxime co-catalyst for dihydrogen evolution for the dehydrogenative preparation of linear enamides and enecarbamates from saturated precursors. The substrate scope includes several natural products and drug derivatives. The reaction does not require noble metal catalysts, exhibits short reaction times compared to previous methods and is suitable for the late-stage functionalization of drug derivatives.

[i] Reproduced from Ritu,‡ D. Kolb,‡ N. Jain,* B. König,* *Adv. Synth. Catal*. **2023**, *365*, 605–611. with permission from Wiley-VCH GmbH. Schemes, tables, and text may differ from the published version.

[ii] Author contributions: Ritu and D. Kolb contributed equally to this work. Ritu conceived the concept of this study, carried out the photoreactions, optimized the reaction conditions, performed the mechanistic studies, and wrote the mechanistic discussion of the manuscript. D. Kolb synthesized the starting materials, wrote the introduction and substrate scope discussion of the manuscript, and added the characterization data to the supporting information. X-ray crystallographic analysis was performed by the X-Ray structure analysis department of the University of Regensburg. N. Jain and B. König supervised the project, reviewed the manuscript and are the corresponding authors.

3.1 Introduction

The direct dehydrogenation of aliphatic compounds to olefins carried out by enzymes is an essential transformation in living systems, and is involved in several biosynthetic pathways such as the desaturation of fatty acids or carotenoids.[1] The emulation of these reactions by chemists has remained unmet, since the activation of two relatively inert C(sp^3)–H bonds in a single process is kinetically and thermodynamically disfavoured.[2] As a result, direct desaturations often require harsh reaction conditions involving the combination of transition metal catalysts with external oxidants/H-acceptors,[3] or in situ generation of intramolecular radicals as H-acceptors, often at high temperatures.[4]

In view of this, the development of alternatives with better atom- and energy efficiency for a conversion of alkanes to alkenes is highly desirable.[5] Over the last decade, photochemistry has emerged as a technique by which transformations under milder reaction conditions can be achieved. Heat is replaced by light for generating radicals,[4a,4c,4d,4e,6] and the use of oxidizing agents/H-acceptors can be precluded by the design of acceptorless catalytic systems which release dihydrogen instead.[7-9] Preoxidized or prefunctionalized starting materials[10] can be avoided. Acceptorless cooperative HAT-based protocols for instance, have been applied for the desaturation of aliphatic substrates including even unactivated cycloalkanes[7a] to alkenes[7] and aromatics.[7c,8,9] Even though some of these methodologies involve organocatalysts as HAT-mediators,[9] most systems rely on a dual catalytic approach by combining a photoexcitable HAT-catalyst, which upon irradiation is capable of generating a C-centered radical, and a transition-metal complex required for dihydrogen evolution.[7,8]

In the context of alkene synthesis, cobaloxime complexes have proven their efficiency as co-catalysts in combination with photoexcitable hydrogen atom abstractors, such as 2-chloroanthraquinone,[7c] or tetra-*n*-butylammonium decatungstate (TBADT).[7a]

Enamide and enamine scaffolds are valuable synthetic building blocks, which are ubiquitous among agrochemicals, natural products, pharmaceuticals, and as monomers for the preparation of polymeric materials.[11] The synthetic strategies for their access commonly employ heating, activated substrates or expensive catalysts and ligands.[3d,12] This has partly been circumvented with the development of novel photochemical methodologies relying on dehydrogenation processes. In this regard, the Tunge group published a protocol for the elimination of *N*-acyl amino acids via a dual catalytic approach involving an acridinium-based photocatalyst and a cobalt complex.[7b] In the same year, the Gevorgyan group reported a site-selective protocol for the desaturation of amines, wherein the position of the double bond is controlled by the effect of a directing group attached to the substrate. The photoexcitation of a palladium catalyst leads to an intramolecular 1,n-HAT process and a subsequent desaturation (Scheme 1a).[4e] More recently, the El-Sepelgy group reported

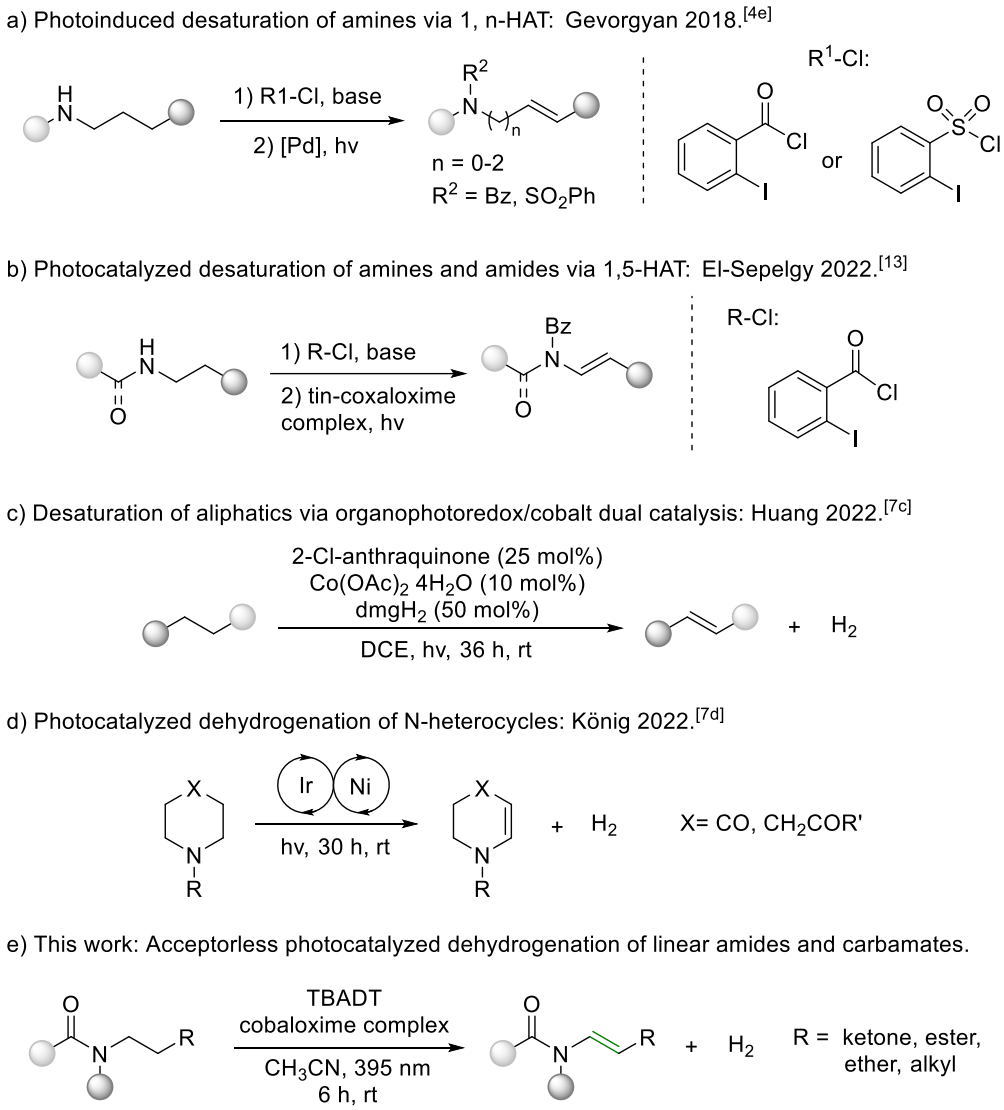

Scheme 3. Photochemical preparation of enamides and enecarbamates via HAT-mediated desaturations.

an alternative methodology based on the same principle for the desaturation of a variety of amines and amides, using a tin-cobaloxime complex instead (Scheme 1b).[13] Although both protocols give access to a wide array of synthons in good yields, the incorporation of the directing group requires an additional step which limits their application in late-stage functionalization or even for the desaturation of biologically relevant molecules. As an alternative to these approaches, the Huang group reported a versatile protocol for the desaturation of a wide array of aliphatics. However, the system requires a particularly high-catalyst loading, long reaction times and is limited in terms of enamide and enecarbamate scope (Scheme 1c).[7c]

In this context, our group recently reported the dehydrogenation of aliphatic *N*-heterocycles such as cyclic enamides and enecarbamates via a novel cooperative catalytic approach between an iridium photocatalyst and a nickel complex (Scheme 1d).[7d] This reaction proceeds regioselectively under mild conditions, and with perfect atom economy.

Building on the above-mentioned methodologies developed by the Huang and the König group,[7c,7d] we decided to further expand the scope of these protocols. For this purpose, we adapted the synergistic system reported by Sorensen,[7a] for the preparation of challenging linear enamides and enecarbamates (Scheme 1e).

3.2 Results and Discussion

We began our study with *N*-methyl-*N*-(3-oxobutyl) benzamide (**1a**) as the model substrate by subjecting it to the dehydrogenation reaction conditions recently published by our group.[7d] Unfortunately, only trace amounts of the desired product **1b** were observed. Inspired by a recent report from the Sorensen group,[7a] we hypothesized that photoexcitable TBADT could act as a HAT agent to form radical intermediate **I**. The resulting reduced form of TBADT is oxidized by a Co(II) complex, thus closing the catalytic cycle. We found that with 2 mol% of TBADT as the photocatalyst, and 5 mol% of $Co(dmgH)_2(pyr)Cl$ (COPC) as the co-catalyst in acetonitrile (50 mM) under 395 nm blue LED, the desired dehydrogenated product **1b** was formed in 9% yield after 24 h at 25 ℃. Encouraged by this result, we decided to further optimize the reaction conditions.

Different photocatalysts were screened and only decatungstate based photocatalysts were active (Table S1, supporting information). The reaction time was optimized, and 6 h was found to be ideal since extending the reaction time did not increase the product yield (Table S2).

Table 1. Screening of reaction conditions.

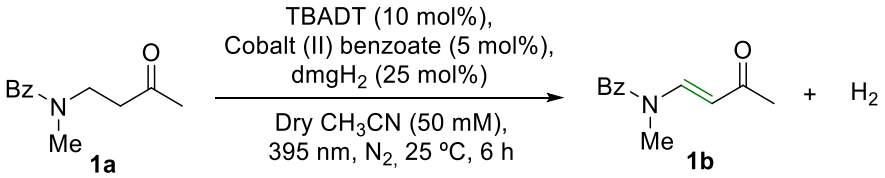

Entry	Deviation from conditions	Yield of **1b** (%) [b]
1	-	71
2	No light	n.d.
3	50 ℃ instead of irradiation	n.d.
4	No photocatalyst	n.d.
5	No cobalt catalyst	n.d.
6	No $dmgH_2$	n.d.
7	15 mol% TBADT	65

[a]Reaction conditions: **1a** (0.1 mmol), TBADT (10 mol%), cobalt benzoate (5 mol%), $dmgH_2$ (25 mol%), CH_3CN (2 mL), 395 nm LED (2.1 W), 25 ºC, N_2. [b]Yields determined via GC-FID analysis using benzonitrile as I.S.

Next, the light source, solvent, co-catalyst, and catalyst loadings were tested (Table S3-S7, supporting information). Gratifyingly, after these optimizations, the yield of the desired dehydrogenated product **1b** increased to 71% yield in presence of 10 mol% TBADT, 5 mol% cobalt benzoate and 25 mol% of dimethylglyoxime ($dmgH_2$) in acetonitrile (50 mM) under 395 nm blue LED for 6 h at 25 ℃ (Table 1, entry 1). No reaction occurred in the dark either at room temperature or at 50 ℃ (Table 1, entries 2-3) confirming a visible light mediated transformation. Similarly, no product was observed in the absence of the photo- or cobalt-catalyst (Table 1, entries 4-5). Only trace amounts of the product were obtained when the reaction was carried out without adding $dmgH_2$ (Table 1, entry 6), suggesting the critical role of the $dmgH_2$ ligand framework in the hydrogen evolution process.[14] Furthermore, a higher catalyst loading of 15 mol% of TBADT (Table 1, entry 7) did slightly decrease the product yield.

Inspired by our recently published desaturation protocol for *N*-heterocycles,[7d] several linear structural analogues were prepared for attaining equivalent transformations (Scheme 2). Accordingly, the optimized catalytic system was initially tested with tertiary *N*-substituted scaffolds featuring an electron-withdrawing carbonyl group at the desaturation site.

Hereby, the presented methodology delivered enamide **1b** and *N*-protected enamines (**2b**-**8b**) as the corresponding desaturation products in moderate to good yields (30-71%). In addition, the structure of **7b** in the crystal was determined by X-ray analysis.[15] Notably, enamide **1b** afforded the best result (71% yield), presumably due to the high electron-withdrawing ability of its aromatic moiety which can stabilize the C-centered radical formed at α-position to the nitrogen atom.[16] Although the aromatic carbamate moiety in **8b** seemed to have a similar effect on the reaction yield (64%), no clear correlation between reactivity and structural or electronic properties could be identified.

With these preliminary results in hand, the methodology was applied to secondary amides, furnishing several to date unreported enamides (**9b**-**17b**) in satisfactory yields (49-77%). A possible electronic effect on the aromatic amide moiety was investigated. For this, various *para*-substituted aromatic amides were prepared displaying different EDGs (**9a**-**12a**). However, no clear trend was observed, as the reaction yield did not show a direct correlation with the variation in the electronic properties of the tested substituents (**9b**-**12b**). The ether group in compound **16b,** and the β-alanine ester substructure featured by **17b** were well tolerated. Interestingly, while for the previously discussed tertiary *N*-substituted derivatives the *E*-isomer was exclusively obtained, secondary moieties besides **16b** and **17b**[17] afforded solely the corresponding *Z* isomer. Even though the *E*-configuration of these olefinic products is thermodynamically favoured,[18] the predominance of the *Z*-configuration among secondary enamides suggests that *Z*-isomer formation might be favoured due to intramolecular hydrogen bonding between the nitrogen and the carbonyl group. The same argument might be valid for

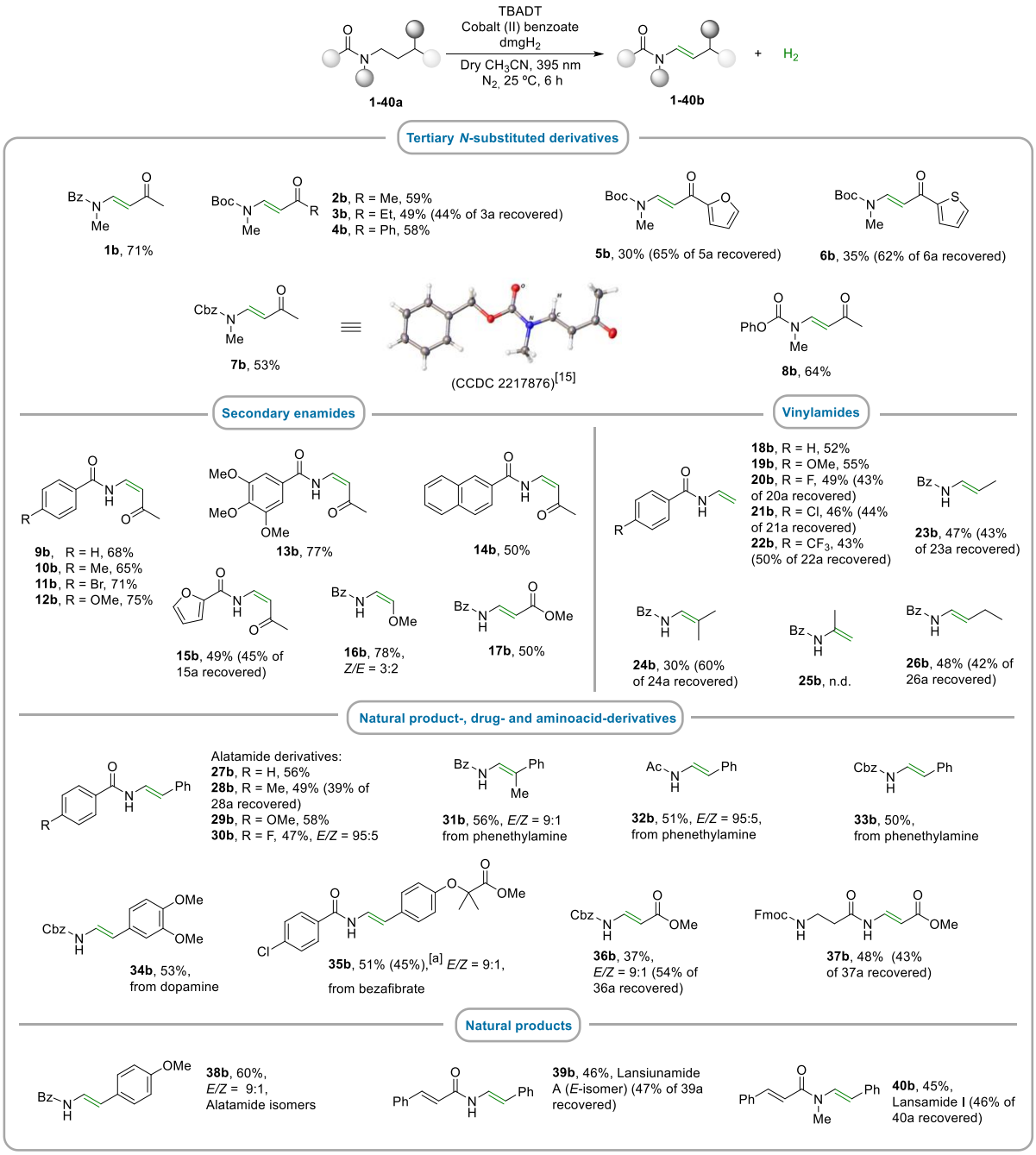

Scheme 2. Substrate scope. Reaction conditions: **1a** (0.1 mmol), TBADT (0.01 mmol), cobalt benzoate (0.005 mmol), $dmgH_2$ (0.025 mmol), CH_3CN (2 ml), 395 nm LED, 6 h, 25 ℃, N_2. Given yields are Isolated. [a]Reaction at 500 mg scale.

explaining the predominant formation of the *Z*-isomer of **16b**, as it features a methoxy group which can act as a hydrogen bond acceptor.

Aromatic alkylamides proved suitable too, giving the corresponding vinylamides (**18b**-**25b**) in moderate yields (30-55%). Herein unreported desaturations of relatively simple molecules could be carried out in a mild and straightforward fashion. These results suggest that apart from nitrogen, an additional EWG attached to the aliphatic desaturation site is not essential for promoting the dehydrogenation process. No electronic effect of the aromatic amide moiety was observed (**18b**-**22b**). However, a certain steric effect was identified, as the reaction yield

dropped notably with increasing substitution on the aliphatic C-end of the substrate (**23b** and **24b**). In addition, further investigations revealed that α-substituted amides such as **25a** did not render the expected products (**25b** in this case). This is presumably due to the increased steric hindrance, as cobaloxime complexes involving tertiary carbon centers are not common. Contrary to the substitution degree of the carbon atoms attached to the desaturation site, the chain length, as observed for products **18b**, **23b** and **26b** has no relevant impact on the reaction yield. Also, for **26a** only the mono-desaturation product **26b** was observed.

The reaction scope for the synthesis of biologically relevant scaffolds was also examined. Alatamide, phenethylamine, and dopamine derivatives (**27a**-**34a**) seemed particularly attractive targets as they have many synthetic and pharmacological applications.[19] The desaturation of several substrates bearing these motifs were carried out, giving access to products with potential biological activity (**27b**-**34b**) in moderate yields (47-58%) and exclusively (**27b**-**29b**, **32b**, **33b**) or predominantly (**30b**, **31b**, **34b**) in *E*-configuration.

Likewise, the desaturation of the methyl ester of the commercial drug bezafibrate, a potent hypolipidemic agent,[20] gave a novel derivative of this drug (**35b**), predominantly in its *E*-configuration. Furthermore, the scalability of our methodology was demonstrated by carrying out the desaturation of **35a** on a 0.5-gram scale, giving the product **35b** (45%), in slightly lower yield than the small-scale reaction (51%). Based on the successful desaturation of **17a** to **17b**, two β-alanine derivatives were prepared. Herein, the dehydrogenation of an aminoacid ester (**36a**) and a dipeptide (**37a**) was accomplished. Regarding the dipeptide, the desaturation proceeded chemoselectively as a single desaturation product was isolated (**37b**) while the corresponding two-fold desaturation product was only observed in trace amount by GC-MS.

Lastly, three natural products were successfully prepared by the dehydrogenation of their saturated precursors. Alatamide (**38b**) for instance, an amide derived from β-phenylethylamine[18a,20] could be prepared through a facile two-step approach in moderate yield as a diastereoisomeric mixture (*E*/*Z* = 9:1). Similarly, Lansiunamide A (**39b**) and Lansamide I (**40b**), two naturally occurring cinnamamides,[21b,22] were prepared following a two-step synthetic scheme, hereby circumventing tedious total synthesis protocols.[21b,23]

Although our method is highly efficient for the desaturation of secondary aliphatic carbon centers, tertiary C-centers at α- or β-position to the nitrogen (except for **24b** and **31b**) react less efficient, as sterics seem to prohibit the reaction (Scheme S7). In addition, as observed for failed substrates **SM-A** and **SM-C** that did not deliver the corresponding desaturated products, the protocol is only suitable for substrates displaying electron-withdrawing *N*-protecting groups such as amides and carbamates with generally high oxidation potentials. Free amines do not yield the desired products as the excited decatungstate anion with an oxidation potential of around +2.44 V vs SCE acts as an oxidant via SET. As a result, if a free

amine was subjected to the given system, most likely, a *N*-centered radical cation is generated instead of a HAT event taking place.[24c]

To demonstrate the synthetic utility of the products, a postfunctionalization reaction was carried out. Herein, the *E*-isomer of natural product **38b** was used for the preparation of oxazole **41** (70%) via an hypervalent-iodine mediated oxidative cyclization (Scheme 3).

Spectroscopic studies, control experiments, and kinetic isotope effect (KIE) studies were performed to investigate the reaction mechanism. An UV-Vis kinetic study was chosen to gain insight into the combined catalyst system. A solution of substrate **1a** and TBADT in acetonitrile was irradiated (Figure S3). After 2 minutes of irradiation, an immediate growth of a broad band (absorbance maximum at 450 nm, 630 nm, and 780 nm), characteristic for the reduced form of TBADT was observed. Further, no significant change was observed when a solution of **1a** and cobalt complex in acetonitrile, and a solution of cobalt complex and TBADT in acetonitrile was irradiated (Figure S4-S5). Additionally, when we irradiated **1a**, TBADT, and the cobalt complex (Figure S6), the peak at 430 nm was observed which indicated the reduction of Co (III) to Co (II). The results suggested that the oxidation of the reduced photocatalyst took place by single electron transfer to Co (III). The peak at 780 nm indicated the presence of reduced TBADT in the reaction solution. The hydrogen evolved quantitatively as determined by GC analysis of the crude product mixture (Fig. S7-S8). Light "on−off" experiments suggested that continuous light irradiation is required for the reaction to proceed (Fig. S11). Kinetic isotope effects (KIE) were calculated by estimating the parallel rates of the reaction for substrates **1a** and **1a-D$_5$** (Scheme 4a), as well as from competition experiments between **1a**

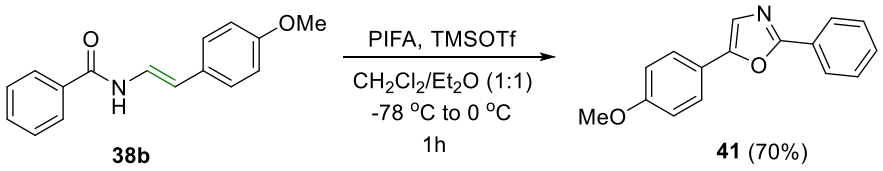

Scheme 3. Synthetic application of Alatamide (*E*-isomer) for the preparation of an oxazole.

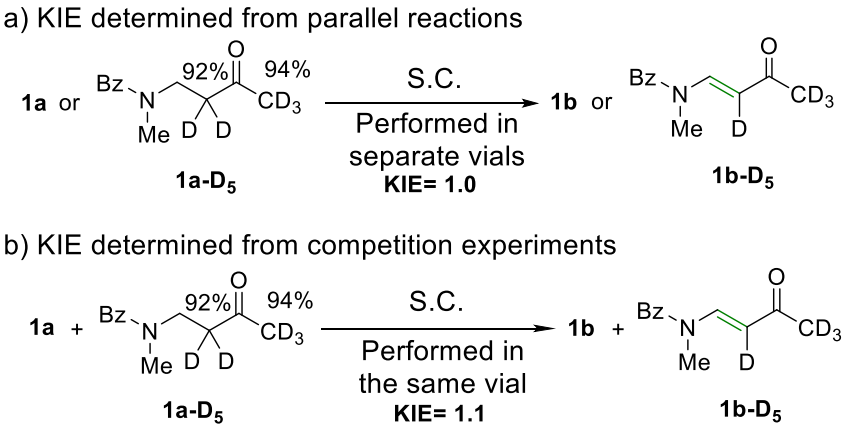

Scheme 4. Kinetic Isotope Effect **(**KIE) measurements.

and **1a-D$_5$** (Scheme 4b). Small KIE values of the order 1-1.1 units were observed in both cases. These results exclude the hydrogen evolution step as the rate determining step of the reaction.

Based on the mechanistic routes reported in the literature,[7c,14,24-27] we proposed a plausible mechanism for the photocatalytic dehydrogenation of aliphatic *N*-hetero acyclic systems as shown in Scheme 5. Photoexcitation of decatungstate anion $[W_{10}O_{32}]^{4-}$ produces a triplet excited state $*[W_{10}O_{32}]^{4-}$, which abstracts a hydrogen atom from substrate **I**, producing alkyl radical **II** and the protonated reduced decatungstate $[W_{10}O_{32}]^{5-}H^+$.[24] Alkyl radical **II** is subsequently trapped by the Co(II) complex, yielding an alkyl Co(III) intermediate **III**.[24] Irradiation of **III** delivers the alkene product **IV** along with a Co (III)-H intermediate.[7c,25a,25c,26] The intermediate **V** then engages with another proton to evolve hydrogen gas and releases a Co(III) complex.[14,27]

Lastly, the oxidation of the protonated reduced photocatalyst $[W_{10}O_{32}]^{5-}H^+$ takes place by single electron transfer (SET) from the Co(III) intermediate ($E_{1/2}$ Co^{III}/Co^{II} = −0.68 V vs Ag/Ag^+ in MeCN, $E_{1/2}$ $[W_{10}O_{32}]^{4-}$/ $[W_{10}O_{32}]^{5-}$= -0.96 V vs Ag/Ag^+ in MeCN), regenerating both catalysts in their ground states.[28]

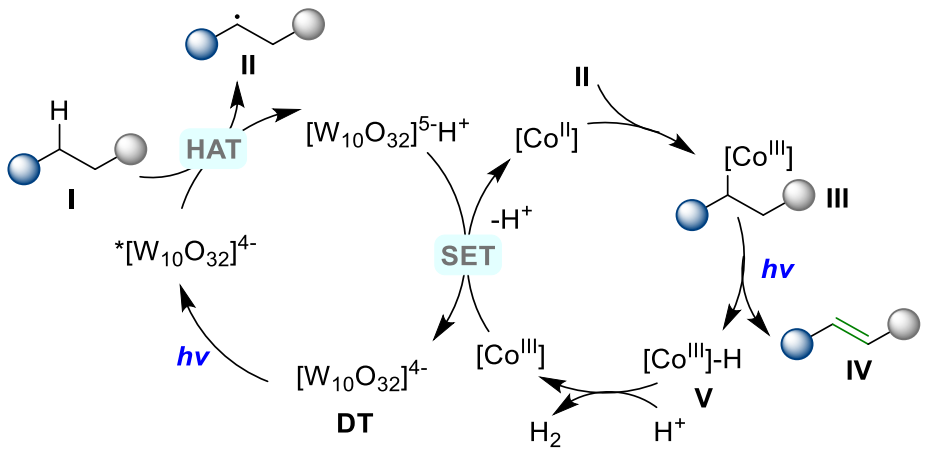

Scheme 5. Proposed plausible reaction mechanism.

3.3 Conclusions

In conclusion, we report a light-driven acceptorless cooperative HAT method for the dehydrogenation of aliphatic carbamates and amides to the corresponding enecarbamates and enamides. TBADT and a cobaloxime complex have been used as H-abstractor and β-hydride elimination agent respectively. The method features short reaction times and exhibits broad functional group tolerance, making it suitable for late-stage functionalization of drug derivatives.

3.4 Experimental Section

3.4.1 General Information

Chemicals and solvents: all commercially available chemicals were purchased in high quality and used without further purification. Solvents for column chromatography were distilled prior to use. Moisture and oxygen-sensitive reactions were carried out using dry solvents in oven-dried glassware under inert atmosphere of pre-dried nitrogen. The evaporation of solvents was carried out in a rotary evaporator at temperatures below 40 ºC, under reduced pressure.

Flash Column Chromatography (FCC): flash silica gel (Merck, 40-63 µm) was used as the stationary phase. Eluent mixtures are reported as v/v solutions normalized to 100 volume units. Purification by automated flash column chromatography was performed on a Biotage® IsoleraTM Spektra One device using either pre-packed Biotage® columns or silica gel 60 M (particle size 40‑63 μm, 230‑440 mesh, Merck) self-packed columns.

Analytical TLC: performed on silica gel pre-coated aluminium sheets (Machery-Nagel, silica gel 60 G/UV254, 0.2 mm). Visualization was accomplished by exposure to UV-light (254 nm or 365 nm), or by dipping the plates in a staining solution (potassium permanganate stain, 2,4-dinitrophenylhydrazine (2,4-DNPH) stain or ninhydrin stain) eventually accompanied by heating. Eluent mixtures for TLC are reported as v/v solutions normalized to 100 volume units.

Nuclear magnetic resonance (NMR): spectra were recorded at room temperature using a Bruker Avance 400 (400 MHz for ^{1}H, 101 MHz for ^{13}C, 376 MHz for ^{19}F) NMR spectrometer. Chemical shifts are reported in δ-scale as parts per million [ppm] relative to the solvent residual peaks as internal standard. Coupling constants *J* are given in Hertz [Hz] and the multiplicity of the signals is abbreviated as: singlet (s), broad singlet (bs), doublet (d), doublet of doublets (dd), triplet (t), doublet of triplets (dt), triplet of doublets (td), quadruplet (q), septet (sept) or multiplet (m). Signals are reported as follows: (multiplicity, coupling constant *J*, number of protons). Spectra were analyzed using MestReNova 6.0.2.

High Resolution Mass Spectrometry (HRMS): spectra were obtained from the central analytic mass spectrometry facilities of the Faculty of Chemistry and Pharmacy, University of Regensburg. All mass spectra were recorded on a Finnigan MAT 95, Thermo Quest Finnigan TSQ 7000, Finnigan MATSSQ 710 A or an Agilent Q-TOF 6540 UHD instrument.

GC-FID and GC-MS: GC measurements were performed on a GC 7890 from Agilent Technologies. Data acquisition and evaluation was done with Agilent Chem Station Rev.C.01.04. GC‑MS measurements were performed on a 7890A GC system from Agilent Technologies with an Agilent 5975 MSD Detector. Data acquisition and evaluation was done with MSD Chem Station E.02.02.1431. A capillary column HP-5MS/30 m x 0.25 mm/0.25 µM film and helium as carrier gas (flow rate of 1 mL/min) were used. The injector temperature (split

injection: 40:1 split) was 280 °C, detection temperature 300 °C (FID). GC measurements were investigated via integration of the signal obtained. The GC oven temperature program was adjusted as follows: initial temperature 40 ^{0}C was kept for 3 minutes, the temperature was increased at a rate of 15 °C/min over a period of 16 minutes until 280 °C was reached and kept for 5 minutes, the temperature was again increased at a rate of 25 °C/min over a period of 48 seconds until the final temperature (300 °C) was reached and kept for 5 minutes.

Cyclic Voltammetry: CV measurements were carried out with a three-electrode potentiostat galvanostat PGSTAT302N from Metrohm Autolab. Glassy carbon was used as the working electrode, a platinum wire counter electrode, and a silver wire as the pseudo reference electrode. Also, tetrabutylammonium tetrafluoroborate Fluka 0.1 M was used as the supporting electrolyte. Prior to the measurement, the solvent (CH_3CN) was degassed with argon. All experiments were performed under argon atmosphere with a scan rate of 50 mV s^{-1} using ferrocene as the internal reference.

Crystallographic Description: Full structural information has been deposited with the Cambridge Crystallographic Data Centre as CCDC-2217876.

UV-Vis Spectroscopy: In situ UV-Vis Kinetic measurements were recorded with an-Agilent 8453 spectrophotometer in acetonitrile as solvent.

Photoreactor setup: photoreactions were irradiated with LEDs (Engine LZ4-40UB00-00U5, λ = 395 nm (± 15), average radiant flux 2168 ± 30 mW, 89 V, 700 mA). Reaction mixtures were exposed to light under stirring (400 rpm, magnetic stirrer) from the bottom side of the vial. The temperature of the system was controlled by a water-cooling circuit consisting of an aluminium cooling block connected to a thermostat (Figure S1).

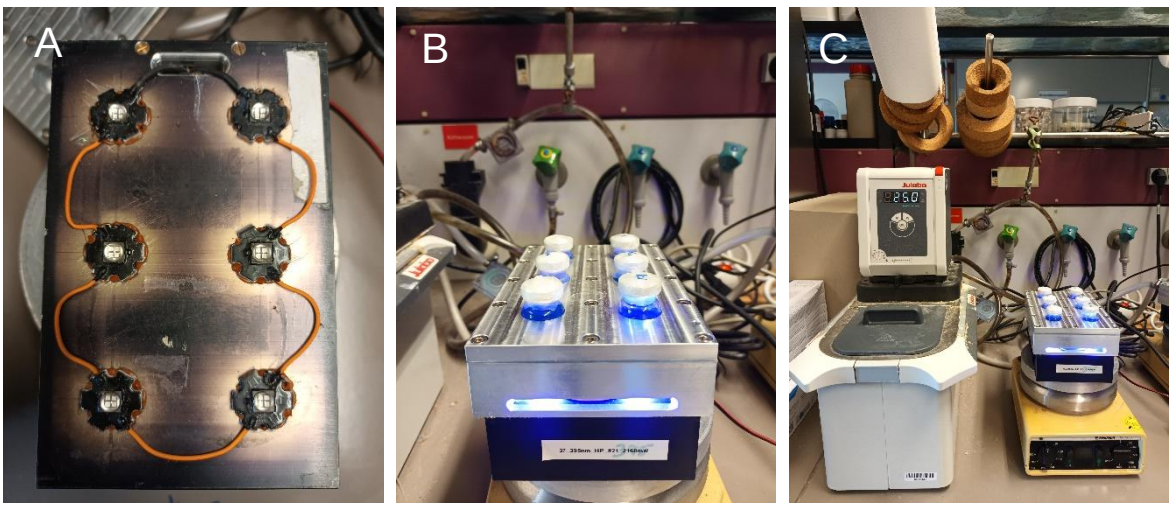

Figure S1. Photoreactor setup. A: LED module. B: Cooling block on top of stirrer. C: Thermostat connected to the aluminium cooling block.

The optical power of the LEDs was determined using a FieldMaxII-TOTM laser power meter equipped with PM3 sensor. The emission spectrum of the LEDs (Figure S2) was recorded using an Ocean Optics HR4000CG-UV-NIR Glass fibre and diffusor.

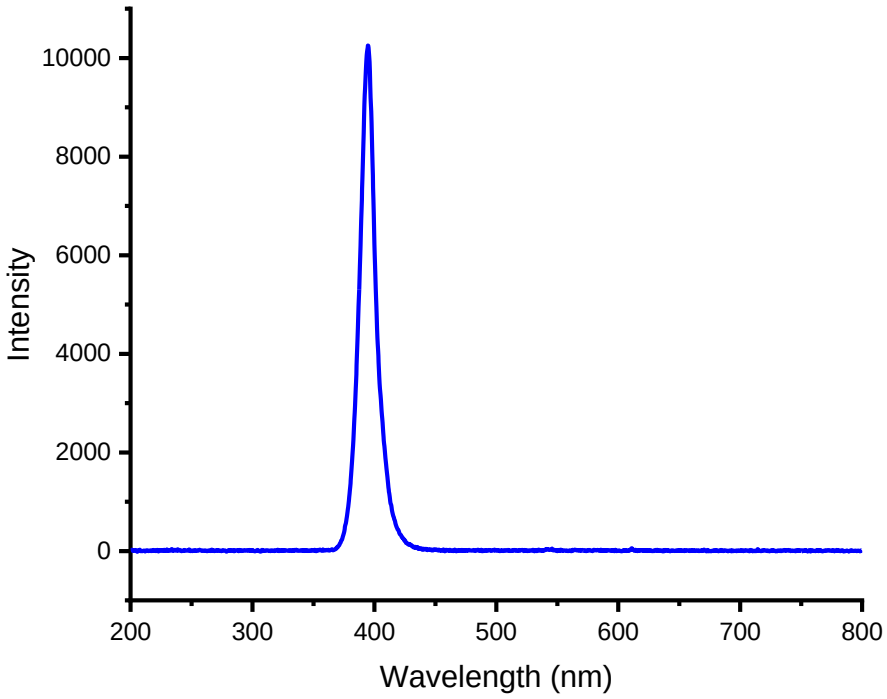

Figure S2. Led emission spectrum of employed LEDs.

3.4.2 General Synthetic Procedures

General Procedure 1 (GP1) for the Synthesis of Boc-Protected Amines as Starting Materials (2a, 3a)

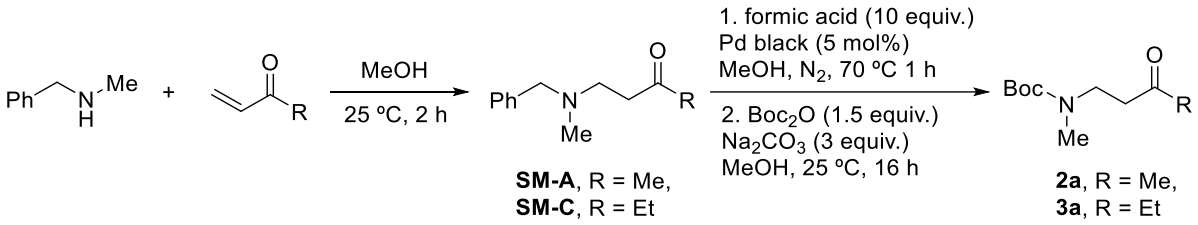

Scheme S1. General procedure 1 for the synthesis of Boc-protected amines.

The two-step synthesis was carried out based on a procedure published by Zhan et al.[29]

Step 1. Synthesis of benzylamines (**SM-A** and **SM-C**): To a solution of vinyl ketone (1.05 equiv.) in MeOH, *N*-methyl-1-phenylmethanamine (1.00 equiv.) was added dropwise at 0 ºC and the resulting mixture was stirred at 25 ºC for 2 h. Afterwards, the solvent was evaporated, and the crude product was purified via flash column chromatography (FCC) to obtain the corresponding benzylamine.

Step 2. Synthesis of Boc-protected amines (**2a** and **3a**): To a solution of benzylamine (1.00 equiv.) in dry MeOH, formic acid (1.00 equiv.) and palladium black (0.05 equiv.) were added at 0 ºC under N_2 atmosphere. After heating the suspension to reflux for 30 min, the reaction crude was filtered through celite and rinsed with MeOH. To the filtrate, Na_2CO_3 (3.00 equiv.) and Boc_2O (1.50 equiv.) were added successively, and the resulting mixture was stirred at 25 ºC for 16 h. Afterwards, the solvent was evaporated, the residue redissolved in EtOAc and washed with water. The product was extracted with EtOAc (3 x), and the combined organic layers were successively washed with brine, dried over $MgSO_4$, and filtered through a silica plug. After evaporating the solvent, the crude product was purified via flash FCC to obtain the corresponding Boc-protected amine.

General Procedure 2 (GP2) for the Synthesis of Amides as Starting Materials (1a, 7a, 8a, 9a, 10a, 11a, 12a, 13a, 14a, 15a, 17a, 18a, 19a, 20a, 21a, 22a, 26a, 39a)

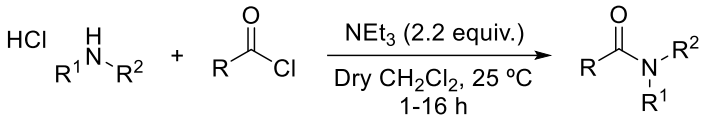

Scheme S2. General procedure 2 for the synthesis of amides.

In an oven dried Schlenk flask, the corresponding amine hydrochloride (1.00 equiv.) was suspended in dry CH_2Cl_2 and NEt_3 (2.20 equiv.) was added under N_2 atmosphere. Next, the reaction mixture was cooled to 0 °C and the corresponding acyl chloride (1.10 equiv.) was added. After stirring the suspension at 25 °C for a given time, the mixture was diluted with CH_2Cl_2 and washed with water. The aqueous phase was extracted with CH_2Cl_2 (3 x), and the combined organic layers were washed with brine and dried over Na_2SO_4. Lastly, the solvent was evaporated under reduced pressure, and the crude product was purified via FCC.

General Procedure 3 (GP3) for the Synthesis of Boc-Protected Amines as Starting Materials (4a, 5a, 6a)

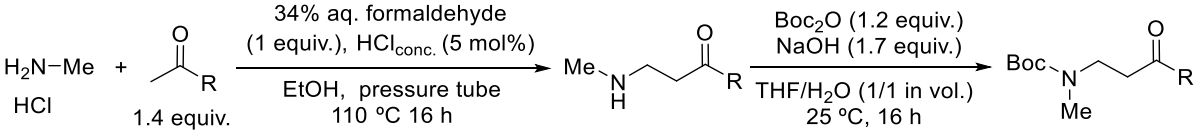

Scheme S3. General procedure 3 for the synthesis of Boc-protected amines.

Substrates **4a**-**6a** were prepared based on a two-step synthesis reported by Buitrago *et al*.[30]

Step 1: In a crimp-cap vial, to a solution of ketone (1.40 equiv.) in EtOH, ethylamine hydrochloride (1.00 equiv.), 34% aqueous formaldehyde solution (1.00 equiv.) and concentrated hydrochloric acid (0.05 equiv.) were added. The vial was sealed, and the mixture refluxed at 110 ºC for 16 h. Afterwards, the mixture was cooled to room temperature and the solvent was removed under reduced pressure. Next, EtOAc was added, and the resulting suspension was stirred for 3 h. Lastly, the precipitate was filtered and dried over high vacuum to obtain the corresponding free amine which was used without further purification.

Step 2: In a round-bottom flask, to a solution of amine (1.00 equiv.) in THF/H_2O (1/1 in Vol.), NaOH (1.70 equiv.), and Boc_2O (1.20 equiv.) were added. After stirring the mixture at 25 ºC for 16 h, THF was removed under reduced pressure and the product was extracted with CH_2Cl_2 (3 x). The combined organic layers were washed with brine and dried over Na_2SO_4. Lastly, the solvent was evaporated, and the crude product purified via FCC to obtain the corresponding Boc-protected amine.

General Procedure 4 (GP4) for the Synthesis of Amides as Starting Materials (16a, 23a, 24a, 25a, 27a, 28a, 29a, 30a, 31a, 32a, 33a, 34a, 36a, 38a)

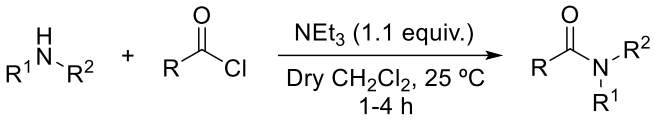

Scheme S4. General procedure 4 for the synthesis of amides.

In an oven-dried Schlenk flask, the corresponding amine (1.00 equiv.) was dissolved in dry CH_2Cl_2, and NEt_3 (1.10 equiv.) was added under N_2 atmosphere. Next, the reaction mixture was cooled to 0 °C and the corresponding acyl chloride (1.10 equiv.) was added dropwise. After stirring the suspension at 25 °C for a given time, the mixture was diluted with CH_2Cl_2 and washed with water/brine (1/1 in Vol.). The organic layer was dried over Na_2SO_4, and the solvent evaporated. The obtained crude product was then purified via FCC.

General Synthetic Procedure 5 (GP5) for Photoreactions

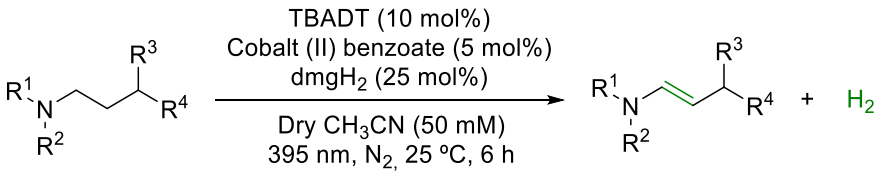

Scheme S5. General procedure for the photocatalyzed dehydrogenation of aliphatics.

A 5 mL crimp-cap vial equipped with a stirring bar, was loaded with the corresponding aliphatic substrate (100 µmol, 1.00 equiv.), TBADT (33.3 mg, 10 µmol, 10 mol%), cobalt (II) benzoate (1.5 mg, 5 µmol, 5 mol%) and $dmgH_2$ (3.0 mg, 25 µmol, 25 mol%). The vial was sealed, evacuated, and backfilled with N_2 (3x) before adding dry CH_3CN (2 mL). The reaction mixture was subsequently purged with N_2 for 15 min and stirred under irradiation using a 2.2 W 395 nm (± 15 nm) LED set-up for 6 h at 25 °C (temperature controlled by a thermostat). Reaction progress was monitored by TLC or GC analysis. Afterwards, the solvent was evaporated under reduced pressure and the crude product was purified via FCC.

General Procedure 6 (GP6) for 0.5-gram Scale Photoreaction

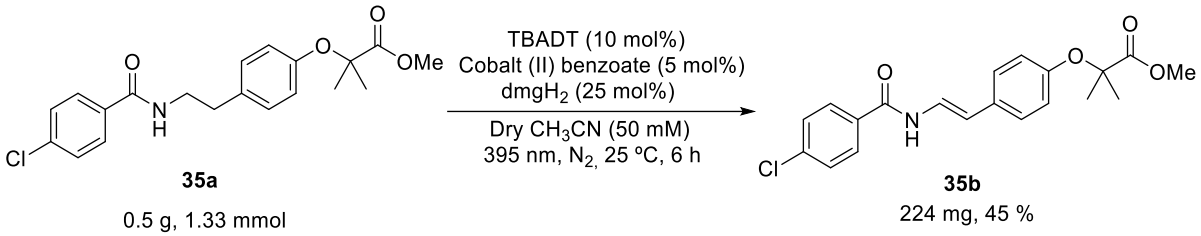

Scheme S6. General procedure for the photocatalyzed dehydrogenation of **35a** on 0.5-gram scale.

A photoreactor equipped with a stirring bar, was loaded with the corresponding aliphatic substrate (1.33 mmol, 1.00 equiv.), TBADT (0.133 mmol, 10 mol%), cobalt (II) benzoate (0.066 mmol, 5 mol%) and $dmgH_2$ (0.332 mmol, 25 mol%). The vial was sealed, evacuated, and back filled with N_2 (3x) before adding dry CH_3CN (50 mM). The reaction mixture was subsequently purged with N_2 for 15 min and stirred under irradiation using a 2.2 W 395 nm (± 15 nm) LED set-up for 6 h at 25 ºC (temperature controlled by a thermostat). Reaction progress was monitored by TLC or GC analysis. Afterwards, the solvent was evaporated under reduced pressure and the crude product was purified via FCC.

Preparation of Tetra-*N*-Butylammonium Decatungstate (TBADT)

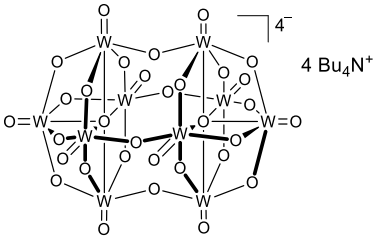

The synthesis was carried out using modified known procedures from the literature.[31] Tetrabutylammonium bromide (2.4 g, 7.40 mmol, 1.0 equiv.) (dried overnight under high vacuum) and sodium tungstate dihydrate $Na_2WO_4 \cdot 2H_2O$ (5.0 g, 15.2 mmol, 2.0 equiv.) were added in separate Erlenmeyer flasks. Then, deionized water (150 mL) was added to each flask. Both solutions were rapidly stirred and heated to 90 °C using a heating oil bath. When both solutions reached 90 °C (checked by thermometers), concentrated HCl was added to each solution until their pH was stabilized at 2. The solutions were then combined and stirred at 90 °C for 30 min. A white suspension of TBADT is formed. The reaction mixture was cooled to room temperature and the white solid was filtered off on a Buchner funnel. After washing with water, the wet solid was lyophilized overnight. The solid was then suspended in dichloromethane (90 mL) and stirred at room temperature for 4 h. After filtration through a Buchner funnel, TBADT was obtained as a white solid (4.3 g, 1.29 mmol, 86%). Electroanalytical data is matched with literature data.[31]

3.4.3 Reaction Conditions Optimization

Table S1. Screening of photocatalyst.

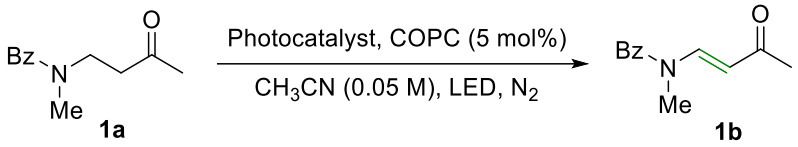

Entry	Photocatalyst (mol%)	LED	COPC	Yield of **1b** (%)[a]
1[b]	[Ir{dF(CF$_3$)ppy}$_2$(dtbpy)]PF$_6$ (2)	450 nm	NiBr$_2$.dtbbpy instead of COPC	Traces
2	[Ir{dF(CF$_3$)ppy}$_2$(dtbpy)]PF$_6$ (2)	450 nm	Yes	N.d.
3	Ru(bpy)$_3$Cl$_2$ 6H$_2$O (2)	450 nm	Yes	Traces
4	2-chloroanthraquinone (5)	400 nm	Yes	Traces
5	Eosin Y (5)	450 nm	Yes	Traces
6	Benzophenone (5)	365 nm	Yes	Traces
7	4CZIPN (5)	450 nm	NiBr$_2$.dtbbpy instead of COPC	N.d.
8	NaDT (2)	395 nm	Yes	8
9	TBADT (2)	395 nm	Yes	9
10	TBADT (2)	395 nm	NiBr$_2$.dtbbpy instead of COPC	N.d.

1a (0.1 mmol), TBADT (0.002 mmol), COPC (5 mol%), CH$_3$CN (2 mL), 395 nm LED, 25 ºC, 6 h, N$_2$. [a]Yields determined via GC-FID analysis using benzonitrile as I.S.[b]Using EtOAc as solvent.

Table S2. Screening of reaction time**.**

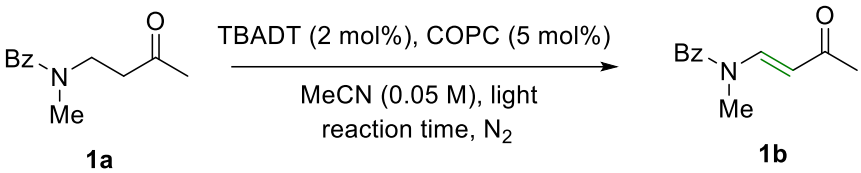

Time (min)	30	120	240	360	480	1440
Yield of **1b** (%)[a]	7	14	16	18	17	9

1a (0.1 mmol), TBADT (0.002 mmol), COPC (0.005 mmol), CH$_3$CN (2 mL), 395 nm LED, 25 ºC, N$_2$. [a]Yields determined via GC-FID analysis using benzonitrile as I.S.

Table S3. Screening of light source.

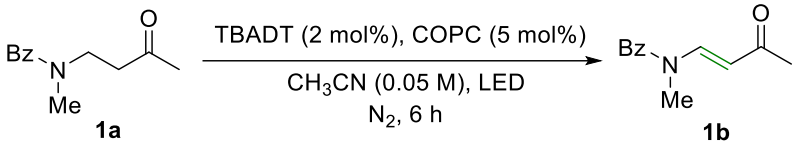

Entry	LED	Yield of **1b** (%)[a]
1	395 nm	18
2	365 nm (low power)	Traces
3	365 nm (high power)	Traces
4	385 nm (low power)	11

1a (0.1 mmol), TBADT (0.002 mmol), COPC (0.005 mmol), CH_3CN (2 mL), 395 nm LED, 25 ºC, 6 h, N_2. [a]Yields determined via GC-FID analysis using benzonitrile as I.S.

Table S4. Control experiments.

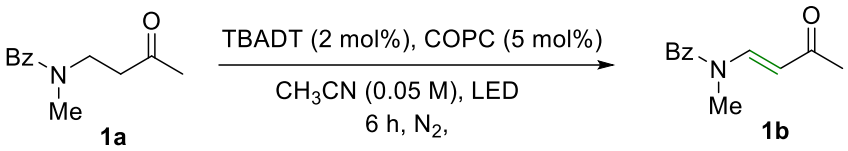

Entry	TBADT	COPC	LED (395 nm)	Yield of **1b** (%)[a]
1	yes	yes	no	N.d.
2	no	yes	yes	N.d.
3	yes	no	yes	Traces
4	no	no	yes	N.d.
5	yes	yes	No light, 50 ℃	N.d.
6	yes	yes	Yes at 40 ^{0}C	12

1a (0.1 mmol), TBADT (0.002 mmol), COPC (0.005 mmol), CH_3CN (2 mL), 395 nm LED, 25 ºC, 6 h, N_2. [a]Yields determined via GC-FID analysis using benzonitrile as I.S.

Table S5. Screening of Solvents**.**

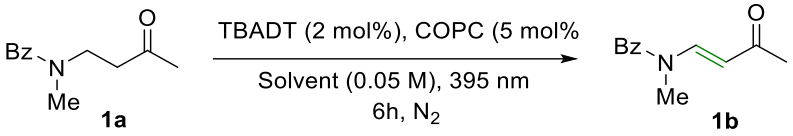

Entry	Solvent	Yield of **1b** (%)[a]
1	CH_3CN	18
2	CD_3CN	19
3	DCE	Traces
4	Acetone	10
5	DMSO	Traces
6	CH_3CN/H_2O (9:1)	16
7	DMF	N.d.

1a (0.1 mmol), TBADT (0.002 mmol), COPC (0.005 mmol), Solvent (0.05 M), 395 nm LED, 25 ºC, 6 h, N_2. [a]Yields determined via GC-FID analysis using benzonitrile as I.S.

Table S6. Screening of co-catalysts.

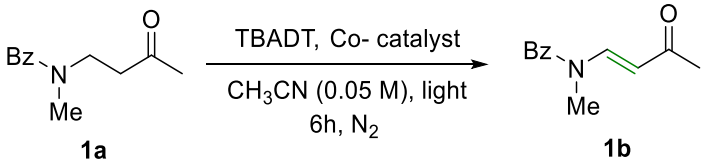

Entry	Co-catalyst (5 mol%)	Additive (50mol%)	Yield of **1b** (%)[a]
1	COPC	-	18
2	CO (dmgH)Cl_2	-	16
3	Co $(OAc)_2$.4 H_2O	$dmgH_2$	18
4	$Co(dmgH)_2Py_2PF_6$	-	6
5	Co (Sep)CF_3SO_3	-	Traces
6	Co $(acac)_2$. xH_2O	$dmgH_2$	13
7	$NiBr_2$.dtbbpy	-	N.d.
8[b]	Vitamin B_{12}	-	9
9[c]	Co $(OAc)_2$	$dmgH_2$	17
10[d]	Cobalt (II) Benzoate	$dmgH_2$	19
11[e]	$Co(dmgBF_2)$ $MeCN_2$	-	18
12[f]	Co (III) 2,4- pentanedionate	$dmgH_2$	13
13	$CoCl_2$	$dmgH_2$	9
14	$CuCl_2$	$dmgH_2$	6

1a (0.1 mmol), TBADT (0.002 mmol), Co-catalyst (0.005 mmol), additive (0.05 mmol), CH_3CN (2 mL), 395 nm LED, 25 ℃, 6 h, N_2. [a]Yields determined via GC-FID using benzonitrile as I.S.

Table S7. Screening of catalysts loading.

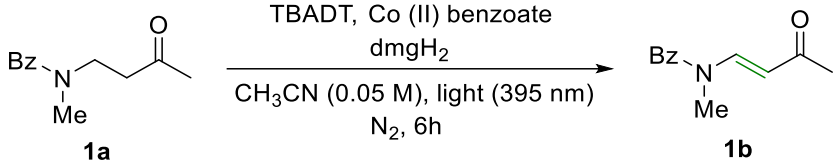

1a **1b**

Entry	mol% TBADT	mol% Co^{II} benzoate	mol% $dmgH_2$	Yield of **1b** (%)[a]
1	2.0	5.0	50	19
2	2.0	5.0	25	23
3	5.0	5.0	50	45
4	5.0	5.0	25	57
5	5.0	10	50	46
6	5.0	25	25	34
7	10.0	5.0	25	71 (78)
8[b]	10.0	5.0	25	N.d.
9[c]	10.0	5.0	25	N.d.
10[d]	-	5.0	25	N.d.
11[e]	10.0	-	25	N.d.
12[f]	10.0	5.0	-	5
13	10.0	2.5	12.5	59
14	10.0	10	50	60
15[g]	10.0	5	25	65
16[h]	10.0	5	25	68
17	15.0	5.0	25	68 (85)

1a (0.1 mmol), TBADT, Co (II) benzoate, $dmgH_2$, CH_3CN (2 mL), 395 nm LED, 25 ºC, 6 h, N_2. [a]Yields were determined by GC-FID analysis using benzonitrile as internal I.S. [b]In the dark. [c]50 ºC instead of light. [d]Without TBADT. [e]Without cobalt benzoate. [f]Without $dmgH_2$ ligand. [g]CH_3CN (0.1 M), [h]CH_3CN (0.025 M).

3.4.4 Mechanistic Studies

Online UV-Vis Kinetics Spectra

UV-Vis kinetic studies were performed chosen to gain insight into the dual catalytic system (results were consistent with the observations of reported methods).[32] Firstly, a solution of substrate **1a** (0.1 mmol) and TBADT (0.01 mmol) in 2 mL acetonitrile was irradiated (Figure S3). After 2 min of irradiation, an immediate growth of a broad characteristic of reduced TBADT (absorbance maximum at 450 nm, 630 nm, and 780 nm) is observed. The growth of this feature increases over 1 hour course of the photolysis. After 1 h, it remained same over the time. This observation suggests that TBADT is consumed significantly during this reaction.

A solution of substrate **1a** (0.1 mmol), cobalt benzoate (0.005 mmol), and $dmgH_2$ (0.025 mmol) in 2 mL acetonitrile was irradiated (Figure S4). As can be seen in the absorbance spectrum, there is essentially no change observed following 180 minutes of reaction mixture irradiation. This result is consistent with the finding in table S7, entry 10.

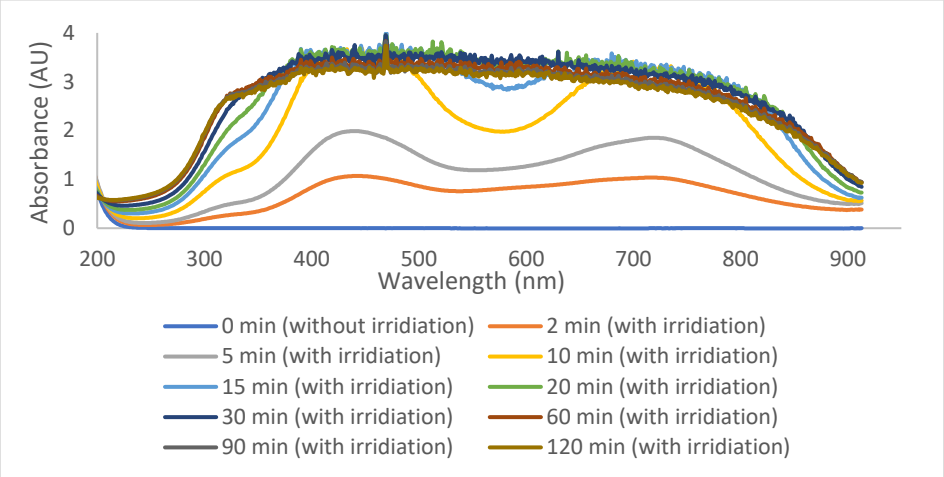

Figure S3. Absorbance spectrum from the continuous photolysis of a solution of **1a**, and TBADT.

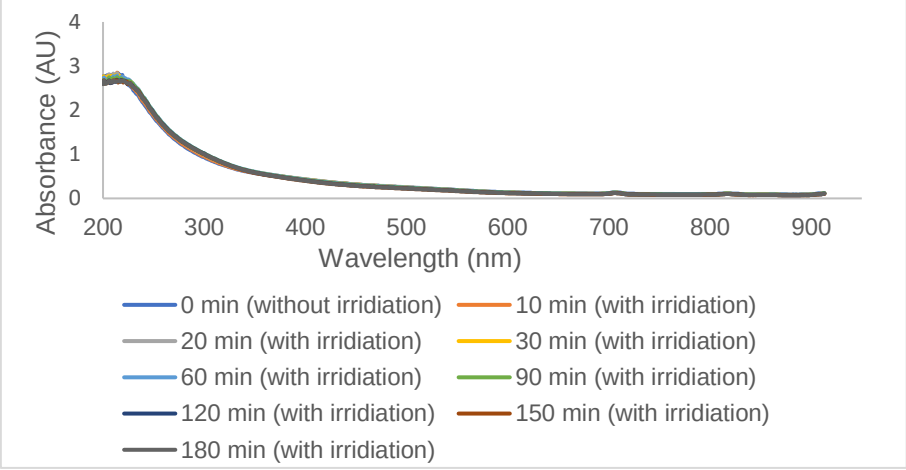

Figure S4. Absorbance spectrum from the continuous photolysis of a solution of **1a**, and Cobalt benzoate and $dmgH_2$.

A solution of TBADT (0.01 mmol), cobalt benzoate (0.005 mmol) and $dmgH_2$ (0.025 mmol) in 2 ml acetonitrile was irradiated (Figure S5). Further, there is essential no change observed following 300 min of irradiation. Which suggested that no electron transfer takes place between the photocatalyst and cobaloxime complex in absence of **1a** under light.

A solution of substrate **1a** (0.1 mmol), TBADT (0.01 mmol), cobalt benzoate (0.005 mmol) and $dmgH_2$ (0.025 mmol) in 2 ml acetonitrile was irradiated (Figure S6). Interestingly, the appearance of absorbances relating to reduced TBADT is delayed approximately 60 min of irradiation, with earlier unobserved peaks at 430 nm, 590 nm, and 780 nm growing in during the preceding time. The peak at 430 nm is consistent with the reduction of the Co (III) to Co (II). Which suggested that oxidation of reduced photocatalyst would take place by single electron transfer from Co (III) form.

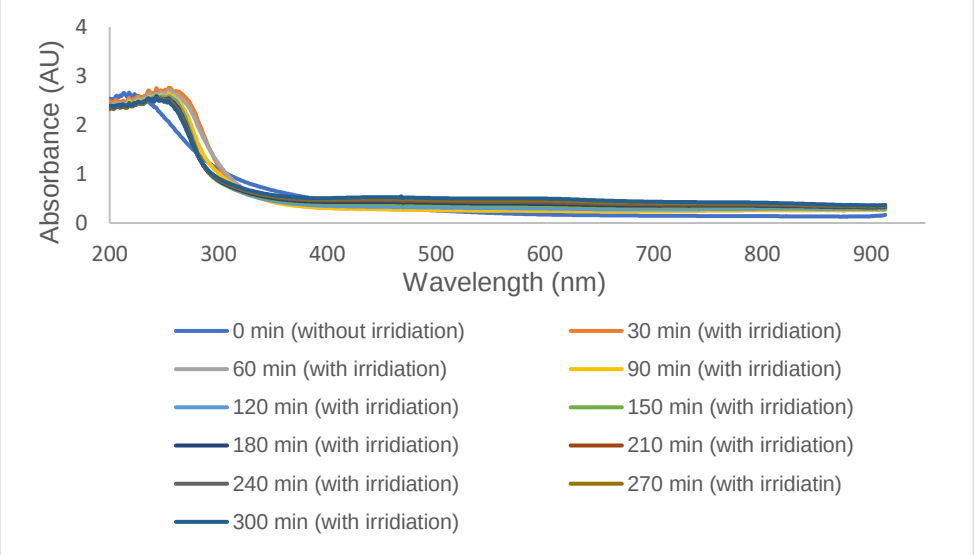

Figure S5. Absorbance spectrum from the continuous photolysis of a solution of TBADT, Cobalt benzoate, and $dmgH_2$.

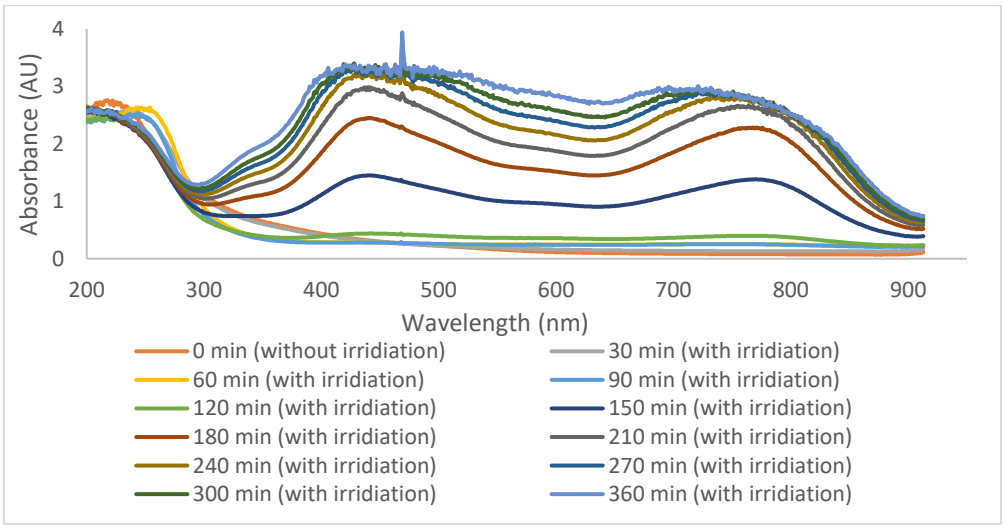

Figure S6. Absorbance spectrum from the continuous photolysis of a solution of **1a**, TBADT, Cobalt benzoate and $dmgH_2$.

Quantitative Analysis of Evolved Hydrogen Gas

Example 1:

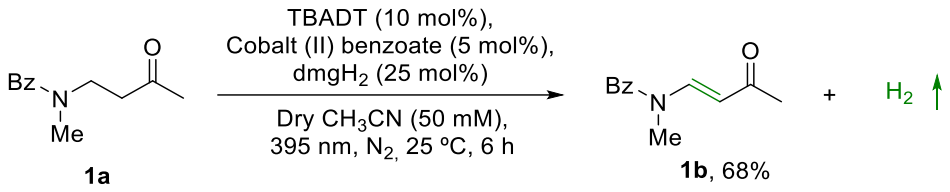

A 5 mL crimp-cap vial equipped with a stirring bar, was loaded with **1a** (50 µmol, 1.00 equiv.), TBADT (16.7 mg, 5 µmol, 10 mol%), cobalt (II) benzoate (0.75 mg, 2.5 µmol, 5 mol%) and $dmgH_2$ (1.5 mg, 12.5 µmol, 25 mol%). The vial was sealed, evacuated, and back filled with N_2 (3x) before adding dry CH_3CN (1 mL). The reaction mixture was subsequently purged with N_2 for 15 min and stirred under irradiation using a 2.1W 395 nm LED set-up at 25 ° C (temperature controlled by a thermostat). The upper atmosphere was analyzed by headspace GC after 6 h of irradiation. In addition, the sample was subjected to GC-FID analysis and the yield of **1b** was determined.

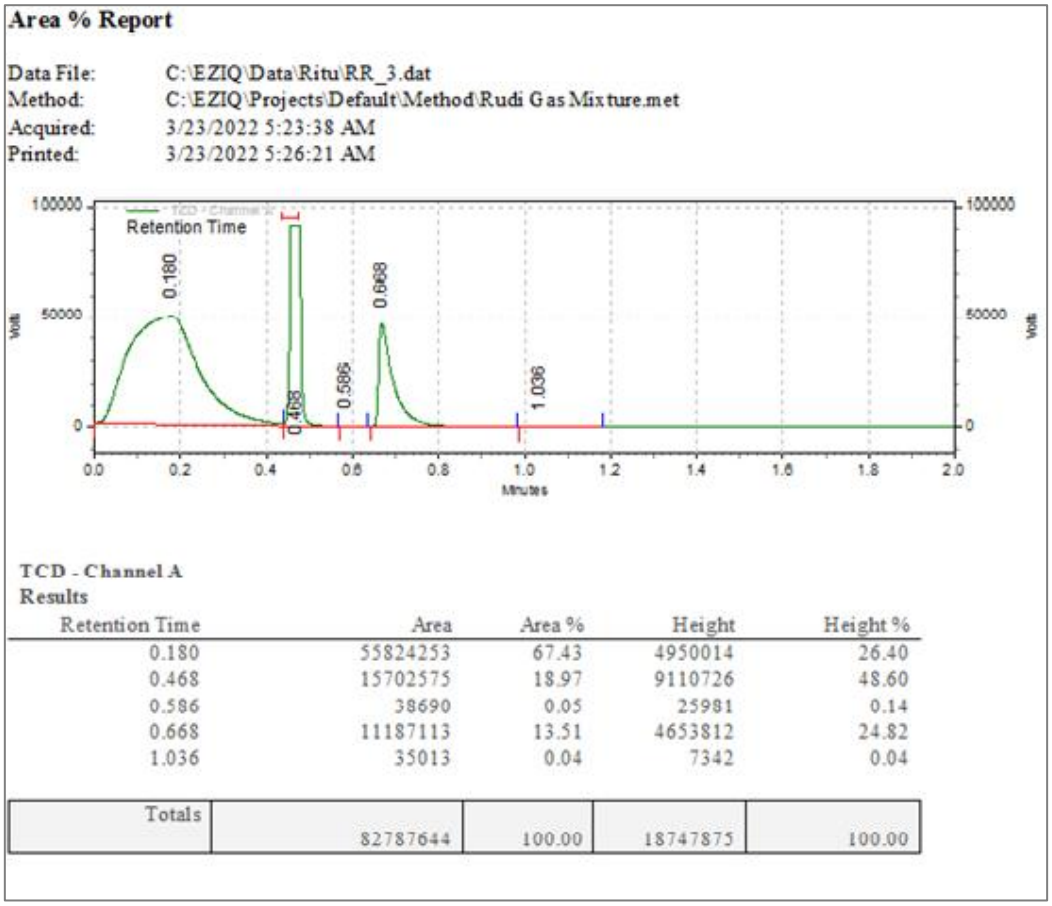

Figure S7. Detection of hydrogen gas by INFICON 3000 Micro GC Gas Analyzer.

Example 2:

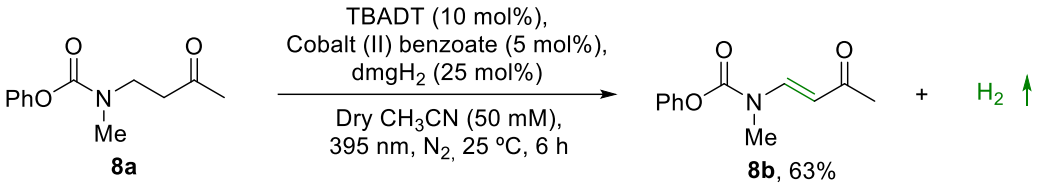

A 5 mL crimp-cap vial equipped with a stirring bar, was loaded with **8a** (50 µmol, 1.00 equiv.), TBADT (16.7 mg, 5 µmol, 10 mol%), cobalt (II) benzoate (0.75 mg, 2.5 µmol, 5 mol%) and $dmgH_2$ (1.5 mg, 12.5 µmol, 25 mol%). The vial was sealed, evacuated, and back filled with N_2 (3x) before adding dry CH_3CN (1 mL). The reaction mixture was subsequently purged with N_2 for 15 min and stirred under irradiation using a 2.1W 395 nm LED set-up at 25 ºC (temperature controlled by a thermostat). The upper atmosphere was analyzed by headspace GC after 6 h of irradiation. In addition, the sample was subjected to GC-FID analysis, and the yield of **8b** was determined.

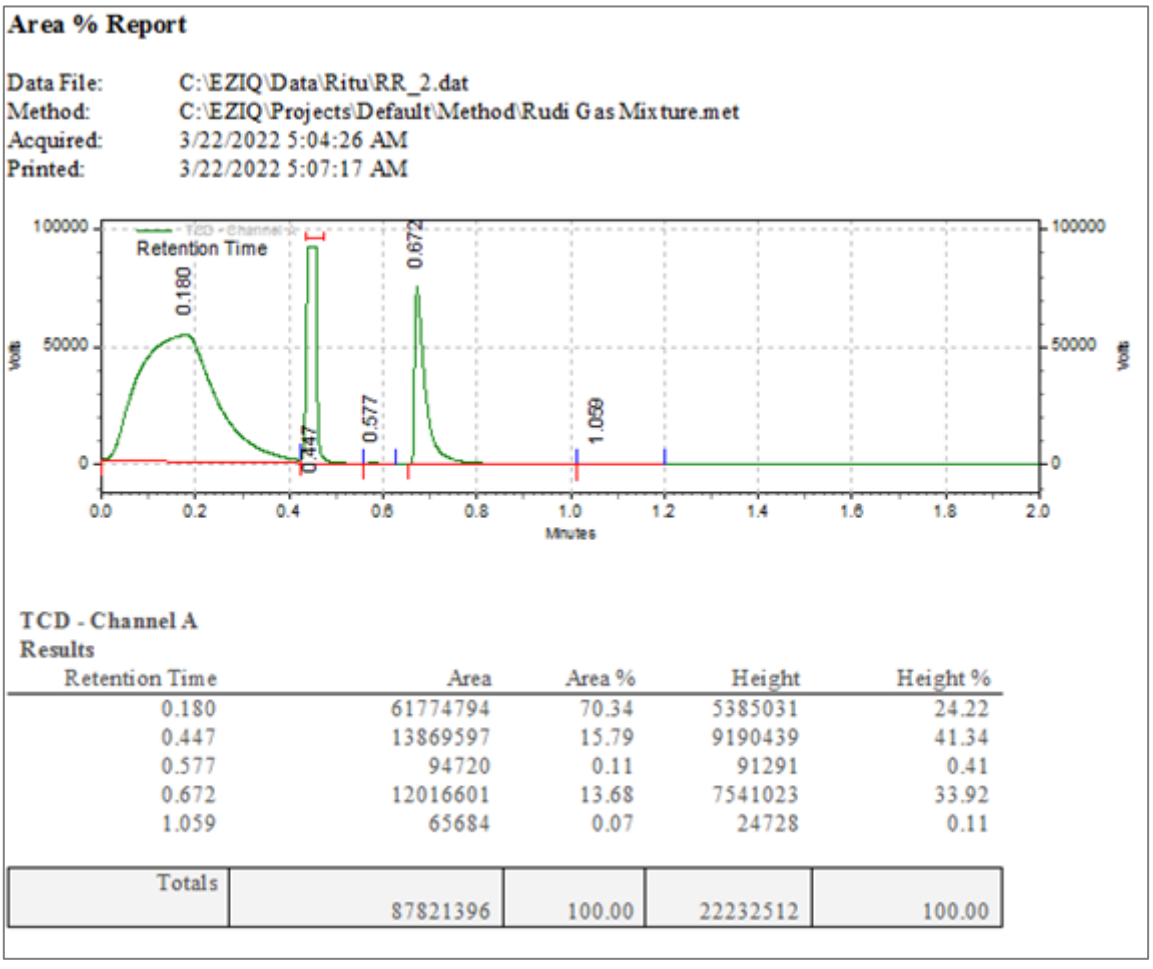

Retention Time	Area	Area %	Height	Height %
0.180	61774794	70.34	5385031	24.22
0.447	13869597	15.79	9190439	41.34
0.577	94720	0.11	91291	0.41
0.672	12016601	13.68	7541023	33.92
1.059	65684	0.07	24728	0.11
Totals	87821396	100.00	22232512	100.00

Figure S8. Detection of hydrogen gas by INFICON 3000 Micro GC Gas Analyzer.

Independent-Rate KIE Experiments of 1a and 1a-D_5

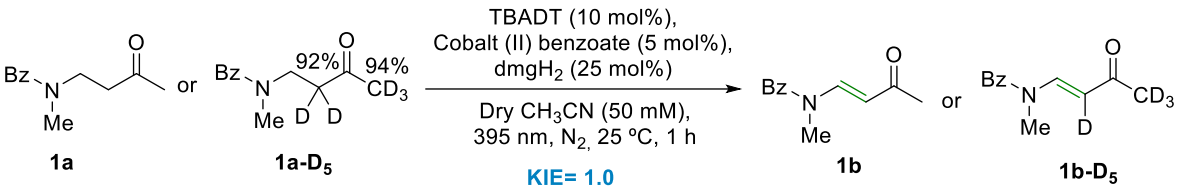

A 5 mL crimp-cap vial equipped with a stirring bar, was loaded with 4-(methyl(phenyl)amino) butan-2-one **1a** (100 µmol, 1.00 equiv.) or 4-(methyl(phenyl)amino)butan-2-one-1,1,1,3,3-d_5 **1a-D_5** (100 µmol, 1.00 equiv.), TBADT (33.3 mg, 10 µmol, 10 mol%), cobalt (II) benzoate (1.5 mg, 5 µmol, 5 mol%) and $dmgH_2$ (3.0 mg, 25 µmol, 25 mol%). The vial was sealed, evacuated, and back filled with N_2 (3x) before adding dry CH_3CN (2 mL). The reaction mixture was subsequently purged with N_2 for 15 min and stirred under irradiation using a 395 nm (2.1 W) LED set-up for 6 h at 25 º C (temperature controlled by a thermostat). Samples were taken with syringe and filtered through a disposable syringe filter. All samples were analyzed via GC-FID to determine the yield.

Table S8. Independent KIE experiments.

Entry	Time (min)	Yield **1b** (%)[a]	Yield **1b-D_5** (%)[a]
1	0	0	0
2	15	12	12
3	30	17	17
4	46	22	20
5	60	24	24

[a]GC-FID yields determined using benzonitrile as internal standard.

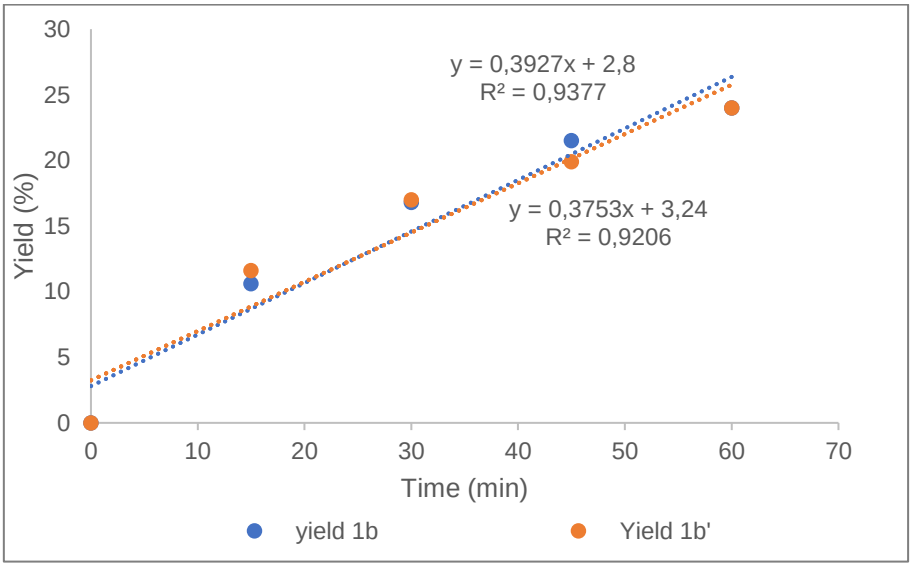

Figure S9. Reaction time-course data for independent rate KIE of **1b** and **1b-D_5**.

Intermolecular Competition KIE Experiment of 1a and 1a-D_5

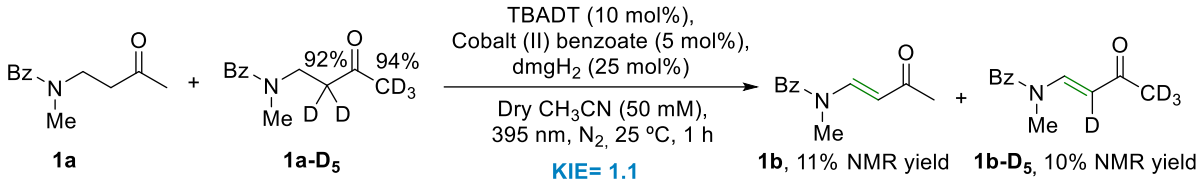

A 5 mL crimp-cap vial equipped with a stirring bar, was loaded with 4-(methyl(phenyl)amino) butan-2-one **1a** (100 µmol, 1.00 equiv.), 4-(methyl(phenyl)amino)butan-2-one-1,1,1,3,3-d_5 **1a-D_5** (100 µmol, 1.00 equiv.), TBADT (33.3 mg, 10 µmol, 10 mol%), cobalt (II) benzoate (1.5 mg, 5 µmol, 5 mol%) and $dmgH_2$ (3.0 mg, 25 µmol, 25 mol%). The vial was sealed, evacuated, and backfilled with N_2 (3x) before adding dry CH_3CN (2 mL). The reaction mixture was subsequently purged with N_2 for 15 min and stirred under irradiation using a 395 nm (2.1 w) LED set-up for 6 h at 25º C (temperature controlled by a thermostat). After 1h, the reaction mixture was filtered through a thin silica gel pad using PE/EtOAc (70/30) as eluent. The solvent was evaporated at a reduced pressure to give mixture of products and starting materials. The yield and the deuterium distribution of the products were calculated by ^{1}H NMR of [**1a** + **1b** + **1a-D_5** +**1b-D_5**].

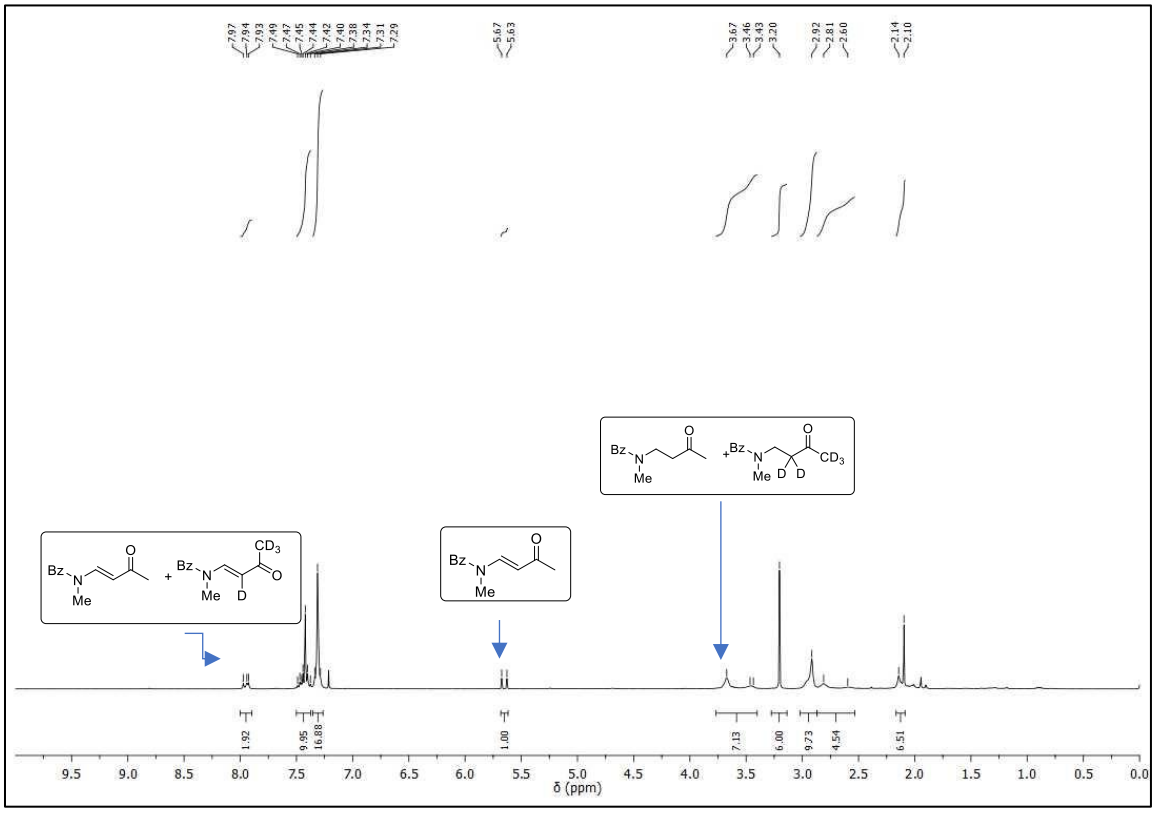

Figure S10. ^{1}H NMR spectrum of [**1a** + **1b** + **1a-D_5** + **1b-D_5**].

Light On-Off Experiment

A 5 mL crimp-cap vial equipped with a stirring bar, was loaded with **1a** (100 µmol, 1.00 equiv.), TBADT (33.3 mg, 10 µmol, 10 mol%), cobalt (II) benzoate (1.5 mg, 5 µmol, 5 mol%) and $dmgH_2$ (3.0 mg, 25 µmol, 25 mol%). The vial was sealed, evacuated, and back filled with N_2 (3x) before adding dry CH_3CN (2 mL). The reaction mixture was subsequently purged with N_2 for 15 min and stirred under irradiation using a 2.1W 395 nm LED set-up for 6 h at 25 º C (temperature controlled by a thermostat). Reaction progress was monitored by TLC or GC analysis. Parallel reactions were carried out for various reaction times. The yield of product **1b** was determined by GC analysis.

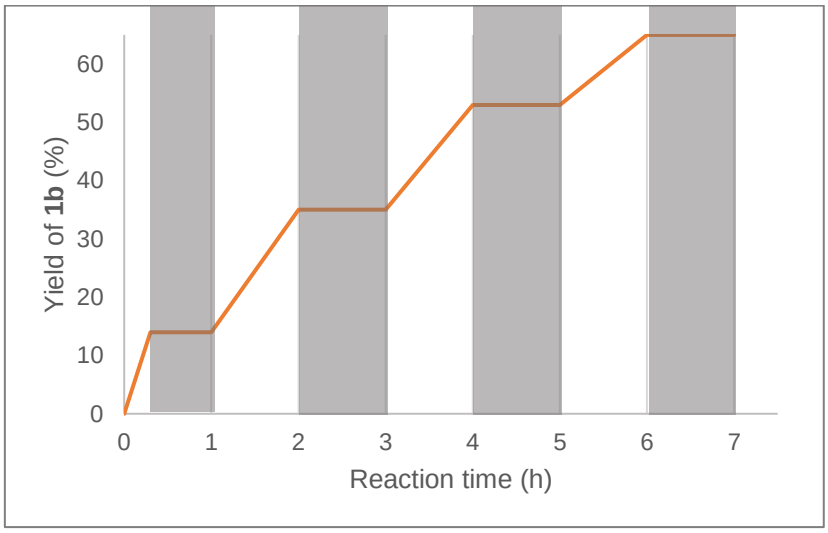

Figure S11. Conversion of **1b** at different times with 395 nm light irradiation (white region) and without light irradiation (grey region).

3.4.5 Failed Substrates for Photoreactions

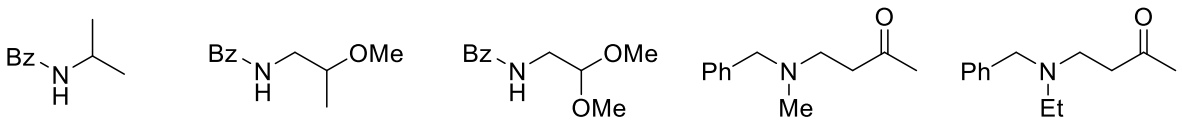

25a **F2** **F3** **SM-A** **SM-C**

Scheme S7. Unsuccessful substrates. Reactions performed according to **GP 5**.

3.4.6 Synthesis and Analytical data of Starting Materials

tert-butyl methyl(3-oxobutyl)carbamate (**2a**)

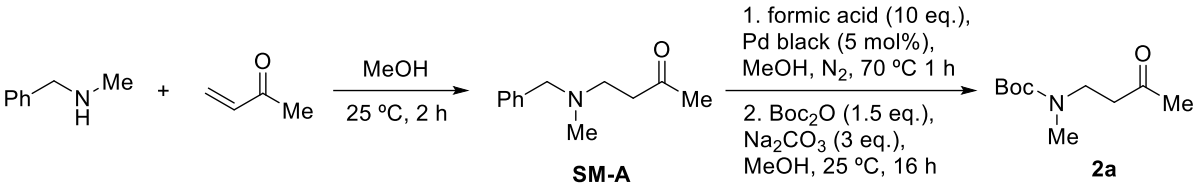

SM-A and **2a** were prepared according to general procedure **GP1** via a two-step procedure.

Step 1. Synthesis of 4-(benzyl(methyl)amino) butan-2-one (**SM-A**): Prepared from methyl vinyl ketone (3.5 mL, 41.6 mmol) and *N*-methyl-1-phenylmethanamine (5.1 mL, 39.1 mmol) in MeOH (30 mL). The crude product was purified via FCC (PE/EOtAc = 70/30), to obtain compound **SM-A** as a pale brown liquid (5.85 g, 78% yield).

^{1}H-NMR (400 MHz, CD_2Cl_2): δ (ppm) = 7.38 – 7.20 (m, 5H), 3.49 (s, 2H), 2.68 (t, *J* = 6.7 Hz, 2H), 2.60 (t, *J* = 6.7 Hz, 2H), 2.17 (s, 3H), 2.11 (s, 3H). **^{13}C-NMR** (101 MHz, CD_2Cl_2): δ (ppm) = 207.7, 139.3, 128.9, 128.1, 126.9, 62.2, 52.1, 41.9, 41.7, 29.7. **R_f** = 0.22 (PE/EtOAc = 70/30) [2,4-DNPH]. **HRMS** (EI-MS): $[C_{12}H_{17}NO]^{\cdot+}$ $[M]^{\cdot+}$ calcd: 191.1310; found: 191.1307.

Step 2. Synthesis of *tert*-butyl methyl(3-oxobutyl)carbamate (**2a**): Prepared from **SM-A** (5.83 g, 30.5 mmol, 1.00 eq.), formic acid (11.7 mL, 304.8 mmol) and palladium black (160 mg, 1.5 mmol) in dry MeOH (200 mL). To the filtrate, Na_2CO_3 (9.68 g, 91.4 mmol) and Boc_2O (9.97 g, 45.7 mmol) were added. The crude product was purified via FCC (PE/EtOAc = 80/20) to obtain **2a** as a pale brown oil (5.03 g, 82% yield for the two steps).

^{1}H-NMR (400 MHz, $CDCl_3$): δ (ppm) = 3.20 (s, 2H), 2.69 – 2.51 (m, 3H), 2.43 (s, 2H), 1.91 (d, *J* = 18.6 Hz, 3H), 1.35 – 1.02 (m, 9H). **^{13}C-NMR** (101 MHz, $CDCl_3$): δ (ppm) = 206.6, 154.9, 78.8, 43.5, 41.6, 41.4, 34.3, 33.9, 29.6, 27.8. **R_f** = 0.30 (PE/EtOAc = 80/20) [2,4-DNPH]. **HRMS** (APCI-MS): $[C_{10}H_{20}NO_3]^+$ $[M + H]^+$ calcd: 202.1438; found: 202.1437.

Synthesis of 4-(methylamino)butan-2-one hydrochloride (**SM-B**)

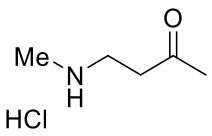

In a schlenk flask, compound **2a** (5.02 g, 25.0 mmol) was dissolved in a 1 M solution of HCl in EtOAc (60 mL) under N_2 atmosphere and the reaction mixture was stirred at 25 ºC for 16 h. Afterwards, the solvent was evaporated, and the remaining solid was triturated and washed with cold Et_2O (3 x 5 mL), obtaining **SM-B** as a white solid (3.11 g, 90% yield).

^{1}H-NMR (400 MHz, $CDCl_3$): δ (ppm) = 9.36 (s, 2H), 3.20 (bs, 2H), 3.11 (t, *J* = 6.0 Hz, 2H), 2.70 (s, 3H), 2.21 (s, 3H). **^{13}C-NMR** (101 MHz, $CDCl_3$): δ (ppm) = 205.2, 44.0, 39.3, 33.6, 30.1. **Mp** = 87–90 °C. **HRMS** (ESI-MS): for free amine $[C_5H_{12}NO]^+$ $[M + H]^+$ calcd: 102.0919; found: 102.0913.

Synthesis of *N*-methyl-*N*-(3-oxobutyl)benzamide (**1a**)

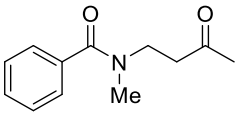

Prepared according to general procedure **GP2** from **SM-B** (1.15 g, 8.40 mmol), benzoyl chloride (1.08 mL, 9.20 mmol) and NEt_3 (2.6 mL, 18.70 mmol) dissolved in CH_2Cl_2 (40 mL) in 1 h. The crude product was purified via FCC (PE/EtOAc = 40/60), to obtain **1a** as a pale brown oil (1.33 g, 78% yield).

^{1}H-NMR (400 MHz, $CDCl_3$): δ (ppm) = 7.36 (d, *J* = 7.4 Hz, 5H), 3.63 (m, 2H), 2.97 (s, 3H), 2.75 (m, 2H), 2.14 (m, 3H). **^{13}C-NMR** (101 MHz, $CDCl_3$): δ (ppm) = 207.3, 171.4, 136.2, 129.4, 128.2, 126.8, 126.4, 43.1, 41.1, 38.3, 30.0. **R_f** = 0.29 (PE/EtOAc = 40/60) [2,4-DNPH]. **HRMS** (EI-MS): $[C_{12}H_{15}NO_2]^{\cdot+}$ $[M]^{\cdot+}$ calcd: 205.1103; found: 205.1097.

Synthesis of *tert*-butyl methyl(3-oxopentyl)carbamate (**3a**)

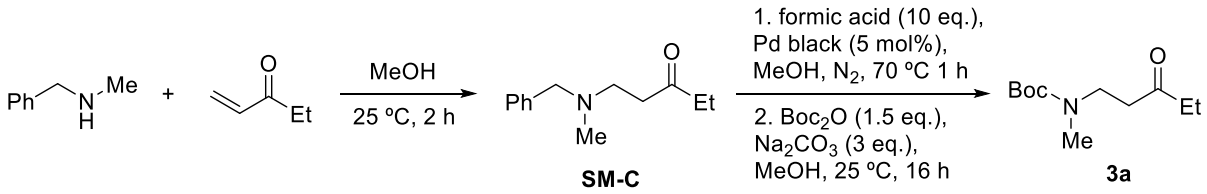

SM-C and **3a** were prepared according to general procedure **GP1**.

Step 1. Synthesis of 1-(benzyl(methyl)amino)pentan-3-one **SM-C**: Prepared from ethyl vinyl ketone (320 µL, 3.10 mmol) and *N*-methyl-1-phenylmethanamine (390 µL, 3.00 mmol) in MeOH (3 mL). The crude product was purified via FCC (PE/EOtAc = 75/25), to obtain compound **SM-C** as a pale brown liquid (518 mg, 84% yield).

^{1}H-NMR (400 MHz, $CDCl_3$): δ (ppm) = 7.32 – 7.15 (m, 5H), 3.46 (s, 2H), 2.69 (t, J = 7.1 Hz, 2H), 2.57 (t, J = 7.0 Hz, 2H), 2.39 (q, J = 7.1 Hz, 2H), 2.16 (s, 3H), 1.02 (td, J = 7.3, 0.5 Hz, 3H). **^{13}C-NMR** (101 MHz, $CDCl_3$): δ (ppm) = 210.2, 138.5, 128.7, 127.9, 126.7, 62.0, 51.9, 41.7, 40.3, 35.6, 7.4. **R_f** = 0.23 (PE/EtOAc = 75/25) [2,4-DNPH].

Step 2. Synthesis of *tert*-butyl methyl(3-oxopentyl)carbamate (**3a**): Prepared from **SM-C** (494 mg, 2.40 mmol), formic acid (930 µL, 24.10 mmol) and palladium black (12.6 mg, 118 µmol) in dry MeOH (15 mL). To the filtrate, Na_2CO_3 (762 mg, 7.20 mmol) and Boc_2O (785 mg, 3.60 mmol) were added. The crude product was purified via FCC (PE/EtOAc = 80/20) to obtain **3a** as a colourless oil (466 mg, 90%).

^{1}H-NMR (400 MHz, $CDCl_3$): δ (ppm) = 3.35 (d, *J* = 6.8 Hz, 2H), 2.73 (t, *J* = 7.6 Hz, 3H), 2.55 (d, *J* = 6.7 Hz, 2H), 2.39 – 2.26 (m, 2H), 1.33 (t, *J* = 7.8 Hz, 9H), 0.93 (dd, *J* = 8.0, 6.5 Hz, 3H). **^{13}C-NMR** (101 MHz, $CDCl_3$): δ (ppm) = 209.8, 155.3, 79.2, 44.1, 40.5, 36.0, 34.6, 28.1, 7.4. **R_f** = 0.27 (PE/EtOAc = 85/15) [2,4-DNPH]. **HRMS** (APCI-MS): $[C_{11}H_{22}NO_3]^+$ $[M + H]^+$ calcd: 216.1560; found: 216.1597.

Synthesis of *tert*-butyl methyl(3-oxo-3-phenylpropyl)carbamate (**4a**)

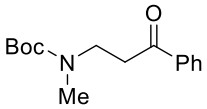

Prepared according to general procedure **GP3**.

Step 1: carried out using acetophenone (450 µL, 3.80 mmol), ethylamine hydrochloride (182 mg, 2.70 mmol), 34% aqueous formaldehyde solution (240 µL, 2.70 mmol), concentrated hydrochloric acid (10 µL, 125 µmol) and EtOH (1.5 mL).

Step 2: carried out using NaOH (184 mg, 4.6 mmol), Boc_2O (700 mg, 3.2 mmol) and THF/H_2O (8 mL; 1/1 in vol.). The crude product was purified via FCC (PE/EtOAc = 80/20) to obtain **4a** as a colourless oil (605 mg, 85% for two steps).

^{1}H-NMR (400 MHz, $CDCl_3$): δ (ppm) = 7.89 (dd, *J* = 5.2, 3.3 Hz, 2H), 7.49 (t, *J* = 7.2 Hz, 1H), 7.39 (t, *J* = 7.6 Hz, 2H), 3.57 (t, *J* = 7.0 Hz, 2H), 3.15 (s, 2H), 2.83 (s, 3H), 1.37 (s, 9H). **^{13}C-NMR** (101 MHz, $CDCl_3$): δ (ppm) = 198.9, 198.5, 155.4, 136.6, 133.0, 128.4, 127.9, 79.3, 44.8, 37.0, 28.2. **R_f** = 0.24 (PE/EtOAc = 80/20) [2,4-DNPH]. **HRMS** (ESI-MS): $[C_{15}H_{21}NO_3Na]^+$ $[M + Na]^+$ calcd: 286.1414; found: 286.1415.

Synthesis of tert-butyl (3-(furan-2-yl)-3-oxopropyl)(methyl)carbamate (**5a**)

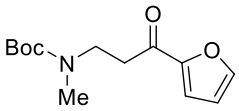

Prepared according to general procedure **GP3**.

Step 1: carried out using 2-furyl methylketone (385 mg, 3.50 mmol), ethylamine hydrochloride (169 mg, 2.50 mmol), 34% aqueous formaldehyde solution (220 µL, 2.50 mmol), concentrated hydrochloric acid (10 µL, 125 µmol) and EtOH (1 mL).

Step 2: carried out using NaOH (170 mg, 4.3 mmol), Boc_2O (648 mg, 3.0 mmol) and THF/H_2O (7 mL; 1/1 in vol.). The crude product was purified via FCC (PE/EtOAc = 90/10) to obtain **5a** as a white solid (126 mg, 20% for two steps).

^{1}H-NMR (400 MHz, $CDCl_3$): δ (ppm) = 7.59 (d, *J* = 0.9 Hz, 1H), 7.20 (s, 1H), 6.54 (s, 1H), 3.60 (t, *J* = 6.9 Hz, 2H), 3.05 (s, 2H), 2.88 (s, 3H), 1.43 (s, 9H). **^{13}C-NMR** (101 MHz, $CDCl_3$): δ (ppm) = 187.9, 155.5, 152.7, 146.6, 117.7, 117.3, 112.3, 79.6, 44.9, 37.4, 34.6, 28.4. **R_f** = 0.22 (PE/EtOAc = 90/10) [2,4-DNPH]. **HRMS** (ESI-MS): $[C_{13}H_{19}NO_4Na]^+$ [M + Na]$^+$ calcd: 276.1206; found: 276.1204.

Synthesis of tert-butyl methyl(3-oxo-3-(thiophen-2-yl)propyl)carbamate (**6a**)

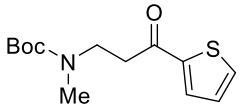

Prepared according to general procedure **GP3**.

Step 1: carried out using 2-acetyl tiophene (390 µL, 3.50 mmol), ethylamine hydrochloride (169 mg, 2.50 mmol), 34% aqueous formaldehyde solution (220 µL, 2.5 mmol), concentrated hydrochloric acid (10 µL, 125 µmol) and EtOH (1 mL).
Step 2: carried out using NaOH (170 mg, 4.30 mmol), Boc_2O (648 mg, 3.00 mmol) and THF/H_2O (7 mL; 1/1 in vol.). The crude product was purified via FCC (PE/EtOAc = 90/10) to obtain **6a** as a white solid (274 mg, 41% for two steps).

^{1}H-NMR (400 MHz, $CDCl_3$): δ (ppm) = 7.73 (d, *J* = 12.8 Hz, 1H), 7.64 (d, *J* = 4.7 Hz, 1H), 7.13 (t, *J* = 4.3 Hz, 1H), 3.61 (t, *J* = 6.9 Hz, 2H), 3.13 (d, *J* = 10.8 Hz, 2H), 2.88 (s, 3H), 1.43 (s, 9H). **^{13}C-NMR** (101 MHz, $CDCl_3$): δ (ppm) = 191.5, 155.5, 144.2, 133.9, 132.4, 132.1, 128.2, 79.7, 45.3, 38.0, 28.4, 23.8. **R_f** = 0.29 (PE/EtOAc = 90/10) [2,4-DNPH]. **HRMS** (ESI-MS): $[C_{13}H_{19}NO_3SNa]^+$ [M + Na]$^+$ calcd: 292.0978; found: 292.0980.

Synthesis of benzyl methyl(3-oxobutyl)carbamate (**7a**)

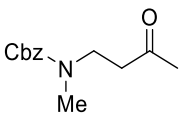

Prepared according to general procedure **GP2** from **SM-B** (240 mg, 1.70 mmol), benzyl chloroformate (280 µL, 1.90 mmol) and NEt_3 (540 µL, 3.90 mmol) dissolved in CH_2Cl_2 (10 mL) in 16 h. The crude product was purified via FCC (PE/EtOAc = 70/30), to obtain **7a** as a colourless oil (339 mg, 83% yield).

^{1}H-NMR (400 MHz, $CDCl_3$): δ (ppm) = 7.41 – 7.27 (m, 5H), 5.11 (s, 2H), 3.52 (t, *J* = 6.9 Hz, 2H), 2.93 (s, 3H), 2.70 (m, 2H), 2.14 (m, 3H). **^{13}C-NMR** (101 MHz, $CDCl_3$): δ (ppm) = 207.3, 206.9, 156.2, 136.8, 128.5, 128.0, 127.8, 67.0, 44.6, 43.8, 42.2, 41.8, 35.2, 35.0, 30.2. **R_f** = 0.28 (PE/EtOAc = 70/30) [2,4-DNPH]. **HRMS** (EI-MS) m/z: $[M]^{\cdot+}$ $[C_{13}H_{17}NO_3]^{\cdot+}$, calcd: 235.1203; found, 235.1205.

Synthesis of phenyl methyl(3-oxobutyl)carbamate (**8a**)

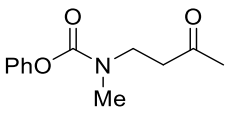

Prepared according to general procedure **GP2** from **SM-B** (250 mg, 1.80 mmol), phenyl chloroformate (260 µL, 2.00 mmol) and NEt_3 (560 µL, 4.00 mmol) dissolved in CH_2Cl_2 (10 mL) in 4 h. The crude product was purified via FCC (PE/EtOAc = 60/40), to obtain **8a** as a colourless oil (320 mg, 80% yield).

^{1}H-NMR (400 MHz, $CDCl_3$): δ (ppm) = 7.35 (t, *J* = 7.8 Hz, 2H), 7.19 (t, *J* = 7.3 Hz, 1H), 7.10 (d, *J* = 7.7 Hz, 2H), 3.64 (dt, *J* = 41.2, 6.8 Hz, 2H), 3.06 (m, 3H), 2.81 (q, *J* = 6.6 Hz, 2H), 2.19 (d, *J* = 5.8 Hz, 3H). **^{13}C-NMR** (101 MHz, $CDCl_3$): δ (ppm) = 207.3, 206.7, 154.7, 151.3, 129.3, 125.4, 125.3, 121.7, 44.9, 44.3, 42.3, 41.7, 35.6, 35.4, 30.3, 30.2. **R_f** = 0.28 (PE/EtOAc = 60/40) [2,4-DNPH]. **HRMS** (ESI-MS): $[C_{12}H_{16}NO_3]^+$ $[M + H]^+$ calcd: 222.1130; found: 222.1126.

Synthesis of 2-(3-oxobutyl)isoindoline-1,3-dioneone (**SM-D**)

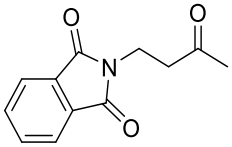

Compound **SM-D** was prepared based on a procedure described by Dailler et al.[33] A crimp-cap vial was charged with phthalimide (4.46 g, 30.0 mmol, 1.00 eq.), and under nitrogen atmosphere, EtOAc (20 mL) and methyl vinyl ketone (2.01 mL, 31.5 mmol, 1.05 eq.) were added. After stirring the resulting suspension at 65 ºC for 10 min, triton B (40% benzyltrimethylammonium hydroxide in MeOH; 680 µL, 1.50 mmol, 0.05 eq.) and the mixture was stirred at 65 ºC for additional 30 min. The resulting precipitate was then filtered, triturated, and washed with Et_2O (3 x 6 mL), to obtain **SM-D** as a white solid (5.39 g, 83% yield).

^{1}H-NMR (400 MHz, $CDCl_3$): δ (ppm) = 7.83 (dd, *J* = 5.4, 3.1 Hz, 2H), 7.71 (dd, *J* = 5.5, 3.0 Hz, 2H), 4.01 – 3.89 (m, 2H), 2.87 (t, *J* = 7.4 Hz, 2H), 2.18 (s, 3H). **^{13}C-NMR** (101 MHz, $CDCl_3$): δ (ppm) = 205.8, 168.1, 134.0, 123.3, 41.6, 33.0, 29.9. **R_f** = 0.28 (Toluene/EtOAc = 90/10) [2,4-DNPH]. **HRMS** (EI-MS): $[C_{12}H_{11}NO_3]^{\cdot+}$ $[M]^{\cdot+}$ calcd: 217.0733; found: 217.0732.

Synthesis of 4-aminobutan-2-one hydrochloride (**SM-E**)

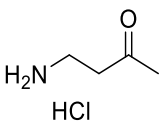

Compound **SM-E** was prepared based on a procedure described by Li et al.[34] A crimp-cap vial was charged with **SM-D** (5.39 g, 24.8 mmol, 1.00 eq.) and a mixture of $HCl_{conc.}$/formic acid/water (100 mL; 3/1/1 in vol.). The vial was sealed, and the mixture refluxed at 100 ºC for 16 h. Afterwards, the vial was cooled to 0 ºC and the mixture was filtered. Next, the filtrate was concentrated under reduced pressure, the resulting residue was dissolved in 1N HCl (3 mL), and the remaining suspended solid was filtered again. Lastly, the filtrate was concentrated to obtain compound **SM-E** as a hygroscopic pale brown slurry (2.39 g, 78% yield).

^{1}H-NMR (400 MHz, D_2O): δ (ppm) = 3.08 (t, *J* = 6.2 Hz, 2H), 2.87 (t, *J* = 6.2 Hz, 2H), 2.11 (s, 3H). **^{13}C-NMR** (101 MHz, D_2O): δ (ppm) = 211.4, 39.5, 34.3, 29.3. **HRMS** (ESI-MS): for free amine $[C_4H_{10}NO]^+$ $[M + H]^+$ calcd: 88.08; found: 88.0757.

Synthesis of *N*-(3-oxobutyl)benzamide (**9a**)

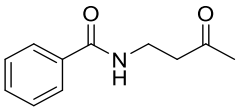

Prepared according to general procedure **GP2** from **SM-E** (124 mg, 1.00 mmol), benzoyl chloride (120 µL, 1.12 mmol) and NEt_3 (310 µL, 2.20 mmol) dissolved in CH_2Cl_2 (7 mL) in 1 h. The crude product was purified via FCC (PE/EtOAc = 50/50), to obtain **9a** as a colourless oil (134 mg, 70% yield).

^{1}H-NMR (400 MHz, $CDCl_3$): δ (ppm) = 7.73 (dd, *J* = 5.2, 3.3 Hz, 2H), 7.50 – 7.44 (m, 1H), 7.44 – 7.36 (m, 2H), 6.85 (s, 1H), 3.67 (dd, *J* = 11.5, 6.0 Hz, 2H), 2.79 (t, *J* = 5.6 Hz, 2H), 2.16 (s, 3H). **^{13}C-NMR** (101 MHz, $CDCl_3$): δ (ppm) = 208.7, 167.3, 134.3, 131.4, 128.5, 126.9, 42.9, 34.5, 30.1. **R_f** = 0.21 (PE/EtOAc = 50/50) [2,4-DNPH].

Synthesis of 4-methyl-*N*-(3-oxobutyl)benzamide (**10a**)

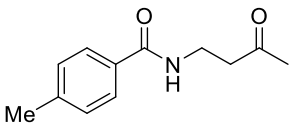

Prepared according to general procedure **GP2** from **SM-E** (124 mg, 1.00 mmol), 4-methylbenzoyl chloride (150 µL, 1.10 mmol) and NEt_3 (310 µL, 2.20 mmol) in CH_2Cl_2 (7 mL) in 2 h. The crude product was purified via FCC (PE/EtOAc = 50/50), to obtain **10a** as a white solid (151 mg, 74% yield).

^{1}H-NMR (400 MHz, $CDCl_3$): δ (ppm) = 7.63 (d, *J* = 8.2 Hz, 2H), 7.19 (d, *J* = 7.9 Hz, 2H), 6.82 (s, 1H), 3.65 (dd, *J* = 11.5, 6.0 Hz, 2H), 2.79 (t, *J* = 5.6 Hz, 2H), 2.37 (s, 3H), 2.16 (s, 3H). **^{13}C-NMR** (101 MHz, $CDCl_3$): δ (ppm) = 208.8, 167.3, 141.8, 131.4, 129.1, 127.4, 126.9, 42.9, 34.4, 30.1, 21.4. **R_f** = 0.23 (PE/EtOAc = 50/50) [2,4-DNPH]. **HRMS** (EI-MS): $[C_{12}H_{15}NO_2]^{\cdot+}$ $[M]^{\cdot+}$ calcd: 205.1097; found: 205.1096.

Synthesis of 4-bromo-*N*-(3-oxobutyl)benzamide (**11a**)

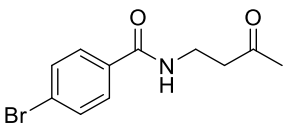

Prepared according to general procedure **GP2** from **SM-E** (124 mg, 1.00 mmol), 4-bromobenzoyl chloride (246 mg, 1.10 mmol) and NEt_3 (310 µL, 2.20 mmol) in CH_2Cl_2 (7 mL) in 1.5 h. The crude product was purified via FCC (PE/EtOAc = 50/50), to obtain **11a** as a white solid (82 mg, 30% yield).

^{1}H-NMR (400 MHz, $CDCl_3$): δ (ppm) = 7.62 – 7.59 (m, 2H), 7.56 – 7.52 (m, 2H), 6.83 (s, 1H), 3.66 (dd, *J* = 11.4, 6.0 Hz, 2H), 2.80 (t, *J* = 5.6 Hz, 2H), 2.18 (s, 3H). **^{13}C-NMR** (101 MHz, $CDCl_3$): δ (ppm) = 208.8, 166.3, 133.1, 131.7, 128.5, 126.2, 42.8, 34.6, 30.2. **R_f** = 0.27 (PE/EtOAc = 50/50) [2,4-DNPH]. **HRMS** (APCI-MS): $[C_{11}H_{13}NO_2Br]^+$ $[M + H]^+$ calcd: 270.0124; found: 270.0125.

Synthesis of 4-methoxy-*N*-(3-oxobutyl)benzamide (**12a**)

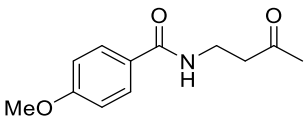

Prepared according to general procedure **GP2** from **SM-E** (124 mg, 1.00 mmol), 4-methoxybenzoyl chloride (160 µL, 1.10 mmol) and NEt_3 (310 µL, 2.20 mmol) in CH_2Cl_2 (7 mL) in 2 h. The crude product was purified via FCC (PE/EtOAc = 40/60), to obtain **12a** as a white solid (140 mg, 63% yield).

^{1}H-NMR (400 MHz, $CDCl_3$): δ (ppm) = 7.74 – 7.67 (m, 2H), 6.92 – 6.86 (m, 2H), 6.72 (s, 1H), 3.83 (s, 3H), 3.66 (dd, *J* = 11.4, 6.0 Hz, 2H), 2.79 (t, *J* = 5.6 Hz, 2H), 2.17 (s, 3H). **^{13}C-NMR** (101 MHz, $CDCl_3$): δ (ppm) = 208.8, 162.2, 129.3, 128.7, 126.6, 113.7 (d, J = 8.5 Hz), 55.4, 43.0, 34.4, 30.2. **R_f** = 0.25 (PE/EtOAc = 40/60) [2,4-DNPH]. **HRMS** (EI-MS): $[C_{12}H_{15}NO_3]^{\cdot+}$ $[M]^{\cdot+}$ calcd: 221.1046; found: 221.1047.

Synthesis of 3,4,5-trimethoxy-*N*-(3-oxobutyl)benzamide (**13a**)

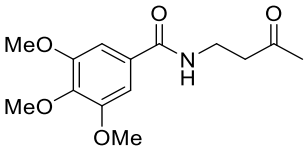

Prepared according to general procedure **GP2** from **SM-E** (124 mg, 1.00 mmol), 3,4,5-trimethoxybenzoyl chloride (257 mg, 1.10 mmol) and NEt_3 (310 µL, 2.20 mmol) in CH_2Cl_2 (7 mL) in 6 h. The product was purified via FCC (PE/EtOAc = 30/70), to obtain **13a** as a white solid (125 mg, 44% yield).

^{1}H-NMR (400 MHz, $CDCl_3$): δ (ppm) = 6.96 (s, 2H), 6.76 (bs, 1H), 3.89 (s, 6H), 3.86 (s, 3H), 3.66 (dd, *J* = 11.4, 5.8 Hz, 2H), 2.80 (t, *J* = 5.6 Hz, 2H), 2.17 (s, 3H). **^{13}C-NMR** (101 MHz, $CDCl_3$): δ (ppm) = 208.9, 167.0, 153.2, 140.9, 129.8, 104.3, 60.9, 56.3, 42.9, 34.7, 30.2. **R_f** = 0.30 (PE/EtOAc = 30/70) [2,4-DNPH]. **HRMS** (ESI-MS): $[C_{14}H_{20}NO_5]^+$ $[M + H]^+$ calcd: 282.1336; found: 282.1338.

Synthesis of *N*-(3-oxobutyl)-2-naphthamide (**14a**)

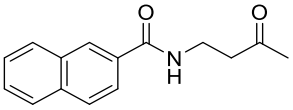

Prepared according to general procedure **GP2** from **SM-E** (124 mg, 1.00 mmol), 2-naphthoyl chloride (246 mg, 1.10 mmol) and NEt_3 (310 µL, 2.20 mmol) in CH_2Cl_2 (7 mL) in 1.5 h. The crude product was purified via FCC (PE/EtOAc = 50/50), to obtain **14a** as a pale-yellow oil (97 mg, 40% yield).

^{1}H-NMR (400 MHz, $CDCl_3$): δ (ppm) = 8.26 (s, 1H), 7.89 (ddd, *J* = 20.9, 11.1, 5.6 Hz, 5H), 7.60 – 7.51 (m, 3H), 6.99 (s, 1H), 3.74 (dd, *J* = 11.5, 5.9 Hz, 2H), 2.85 (t, *J* = 5.6 Hz, 2H), 2.19 (s, 3H). **^{13}C-NMR** (101 MHz, $CDCl_3$): δ (ppm) = 208.8, 167.3, 132.6, 128.9, 128.4, 127.7, 127.6, 127.4, 126.7, 123.5, 43.0, 34.6, 30.2. **R_f** = 0.24 (PE/EtOAc = 50/50) [2,4-DNPH]. **HRMS** (APCI-MS): $[C_{15}H_{16}NO_2]^+$ $[M + H]^+$ calcd: 242.1176; found: 242.1176.

Synthesis of *N*-(3-oxobutyl)furan-2-carboxamide (**15a**)

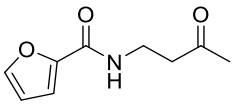

Prepared according to general procedure **GP2** from **SM-E** (124 mg, 1.00 mmol), 2-furoyl chloride (120 µL, 1.10 mmol) and NEt_3 (310 µL, 2.20 mmol) dissolved in CH_2Cl_2 (7 mL) in 1.5 h. The crude product was purified via FCC (PE/EtOAc = 50/50), to obtain **15a** as a pale-yellow oil (99 mg, 55% yield).

^{1}H-NMR (400 MHz, $CDCl_3$): δ (ppm) = 7.41 (dd, *J* = 1.7, 0.7 Hz, 1H), 7.07 (dd, *J* = 3.5, 0.6 Hz, 1H), 6.90 (s, 1H), 6.46 (dd, *J* = 3.5, 1.8 Hz, 1H), 3.64 (dd, *J* = 11.7, 6.1 Hz, 2H), 2.77 (t, *J* = 5.7 Hz, 2H), 2.17 (s, 3H). **^{13}C-NMR** (101 MHz, $CDCl_3$): δ (ppm) = 208.3, 158.4, 147.9, 144.0, 114.1, 112.0, 43.0, 33.6, 30.1. $\mathbf{R_f}$ = 0.22 (PE/EtOAc = 50/50) [2,4-DNPH]. **HRMS** (APCI-MS): $[C_9H_{12}NO_3]^+$ $[M + H]^+$ calcd: 182.0812; found: 182.0813.

Synthesis of *N*-(2-methoxyethyl)benzamide (**16a**)

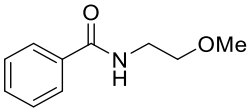

Prepared according to general procedure **GP4** from 2-methoxyethan-1-amine (180 µL, 2.00 mmol), benzoyl chloride (260 µL, 2.20 mmol) and NEt_3 (310 µL, 2.20 mmol) in CH_2Cl_2 (10 mL) in 2 h. The product was purified via FCC (PE/EtOAc = 60/40), to obtain **16a** as a colourless oil (347 mg, 97% yield).

^{1}H-NMR (400 MHz, $CDCl_3$): δ (ppm) = 7.82 – 7.74 (m, 2H), 7.54 – 7.47 (m, 1H), 7.47 – 7.39 (m, 2H), 6.53 (s, 1H), 3.66 (dd, *J* = 10.3, 5.1 Hz, 2H), 3.60 – 3.54 (m, 2H), 3.39 (s, 3H). **^{13}C-NMR** (101 MHz, $CDCl_3$): δ (ppm) = 167.5, 134.5, 131.4, 128.5, 126.9, 71.2, 58.8, 39.7. $\mathbf{R_f}$ = 0.23 (PE/EtOAc = 60/40) [2,4-DNPH]. **HRMS** (APCI-MS): $[C_{10}H_{14}NO_2]^+$ $[M + H]^+$ calcd: 180.1019; found: 180.1015.

Synthesis of methyl 3-benzamidopropanoate (**17a**)

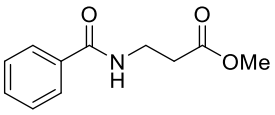

Prepared according to general procedure **GP2** from methyl 3-aminopropanoate hydrochloride (285 mg, 2.00 mmol), benzoyl chloride (260 µL, 2.20 mmol) and NEt_3 (620 µL, 4.40 mmol) dissolved in CH_2Cl_2 (15 mL) in 2 h. The crude product was purified via FCC (PE/EtOAc = 70/30), to obtain **17a** as a white solid (331 mg, 80% yield).

^{1}H-NMR (400 MHz, $CDCl_3$): δ (ppm) = 7.75 (dd, *J* = 5.3, 3.3 Hz, 2H), 7.51 – 7.45 (m, 1H), 7.45 – 7.37 (m, 2H), 6.91 (s, 1H), 3.75 – 3.66 (m, 5H), 2.65 (t, *J* = 6.0 Hz, 2H). **^{13}C-NMR** (101 MHz, $CDCl_3$): δ (ppm) = 173.3, 167.3, 134.3, 131.5, 128.5, 126.9, 51.8, 35.3, 33.7. $\mathbf{R_f}$ = 0.30 (PE/EtOAc = 70/30) [2,4-DNPH]. **HRMS** (APCI-MS): $[C_{11}H_{14}NO_3]^+$ $[M + H]^+$ calcd: 208.0968; found: 208.0971.

Synthesis of *N*-ethylbenzamide (**18a**)

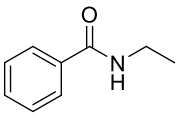

Prepared according to general procedure **GP2** from ethylamine hydrochloride (150 mg, 1.80 mmol), benzoyl chloride (232 µL, 1.98 mmol) and NEt_3 (555 µL, 3.96 mmol) in 1 h. The crude product was purified via FCC (PE/EtOAc = 70/30), to obtain **18a** as a white solid (151 mg, 56% yield).

^{1}H-NMR (400 MHz, $CDCl_3$): δ (ppm) = 7.75 (dd, *J* = 5.2, 3.3 Hz, 2H), 7.47 (ddd, *J* = 6.4, 3.7, 1.3 Hz, 1H), 7.44 – 7.37 (m, 2H), 6.28 (bs, 1H), 3.48 (qd, *J* = 7.3, 5.8 Hz, 2H), 1.24 (t, *J* = 7.3 Hz, 3H). **^{13}C-NMR** (101 MHz, $CDCl_3$): δ (ppm) = 167.5, 134.8, 131.3, 128.5, 126.9, 34.9, 14.9. **R_f** = 0.24 (PE/EtOAc = 70/30). **HRMS** (APCI-MS): $[C_9H_{12}NO]^+$ $[M + H]^+$ calcd: 150.0913; found: 150.0913.

Synthesis of *N*-ethyl-4-methoxybenzamide (**19a**)

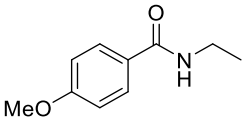

Prepared according to general procedure **GP2** from ethylamine hydrochloride (150 mg, 1.80 mmol), 4-methoxybenzoyl chloride (271 µL, 1.98 mmol) and NEt_3 (555 µL, 3.96 mmol) in 3 h. The crude product was purified via FCC (PE/EtOAc = 70/30), to obtain **19a** as a white solid (315 mg, 98% yield).

^{1}H-NMR (400 MHz, $CDCl_3$): δ (ppm) = 7.77 – 7.68 (m, 2H), 6.92 – 6.85 (m, 2H), 6.26 (bs, 1H), 3.82 (s, 3H), 3.52 – 3.40 (m, 2H), 1.21 (t, *J* = 7.3 Hz, 3H). **^{13}C-NMR** (101 MHz, $CDCl_3$): δ (ppm) = 167.0, 162.0, 128.6, 127.0, 113.6, 55.3, 34.8, 14.9. **R_f** = 0.20 (PE/EtOAc = 70/30). **HRMS** (APCI-MS): $[C_{10}H_{14}NO_2]^+$ $[M + H]^+$ calcd: 180.1019; found: 180.1019.

Synthesis of *N*-ethyl-4-fluorobenzamide (**20a**)

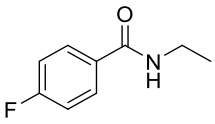

Prepared according to general procedure **GP2** from ethylamine hydrochloride (150 mg, 1.80 mmol), 4-fluorobenzoyl chloride (239 µL, 1.98 mmol) and NEt_3 (555 µL, 3.96 mmol) in 1 h. The crude product was purified via FCC (PE/EtOAc = 70/30), to obtain **20a** as a white solid (294 mg, 98% yield).

^{1}H-NMR (400 MHz, $CDCl_3$): δ (ppm) = 7.84 – 7.70 (m, 2H), 7.13 – 7.01 (m, 2H), 6.26 (bs, 1H), 3.47 (qd, *J* = 7.3, 5.7 Hz, 2H), 1.23 (t, *J* = 7.3 Hz, 3H). **^{13}C-NMR** (101 MHz, $CDCl_3$): δ (ppm) = 166.5, 165.9, 163.4, 131.0 (d, *J* = 3.1 Hz), 129.2 (d, *J* = 8.9 Hz), 115.6, 115.4, 35.0, 14.9. **^{19}F-NMR** (377 MHz, $CDCl_3$): δ (ppm)= -109.1. **R_f** = 0.29 (PE/EtOAc = 70/30). **HRMS** (APCI-MS): $[C_9H_{11}NOF]^+$ $[M + H]^+$ calcd: 168.0819; found: 168.0821.

Synthesis of *N*-ethyl-4-chlorobenzamide (**21a**)

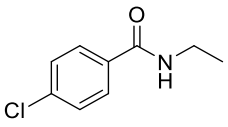

Prepared according to general procedure **GP2** from ethylamine hydrochloride (150 mg, 1.80 mmol), 4-chlorobenzoyl chloride (255 µL, 1.98 mmol) and NEt_3 (555 µL, 3.96 mmol) in 1.5 h. The crude product was purified via FCC (PE/EtOAc = 80/20), to obtain **21a** as a white solid (275 mg, 83% yield).

^{1}H-NMR (400 MHz, $CDCl_3$): δ (ppm) = 7.74 – 7.64 (m, 2H), 7.39 – 7.31 (m, 2H), 6.45 (bs, 1H), 3.45 (qd, *J* = 7.3, 5.7 Hz, 2H), 1.22 (t, *J* = 7.3 Hz, 3H). **^{13}C-NMR** (101 MHz, $CDCl_3$): δ (ppm) = 166.5, 137.4, 133.1, 128.7, 128.3, 35.0, 14.7. **R_f** = 0.22 (PE/EtOAc = 80/20). **HRMS** (APCI-MS): $[C_9H_{11}NOCl]^+$ $[M + H]^+$ calcd: 184.0524; found: 184.0526.

Synthesis of *N*-ethyl-4-(trifluoromethyl)benzamide (**22a**)

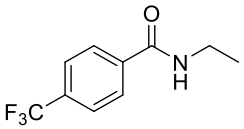

Prepared according to general procedure **GP2** from ethylamine hydrochloride (150 mg, 1.80 mmol), 4-(trifluoromethyl)benzoyl chloride (304 µL, 1.98 mmol) and NEt_3 (555 µL, 3.96 mmol) in 1 h. The product was purified via FCC (PE/EtOAc = 80/20), to obtain **22a** as a white solid (353 mg, 90% yield).

^{1}H-NMR (400 MHz, $CDCl_3$): δ (ppm) = 7.86 (d, *J* = 8.1 Hz, 2H), 7.66 (d, *J* = 8.2 Hz, 2H), 6.38 (bs, 1H), 3.50 (qd, *J* = 7.3, 5.8 Hz, 2H), 1.25 (t, *J* = 7.3 Hz, 3H). **^{13}C-NMR** (101 MHz, $CDCl_3$): δ (ppm) = 166.2, 138.0, 133.0 (q, *J* = 32.6 Hz), 130.3, 127.7, 127.3, 125.5 (q, *J* = 3.7 Hz), 125.0, 122.3, 119.6, 35.1, 14.7. **^{19}F-NMR** (377 MHz, $CDCl_3$): δ (ppm)= -63.5. **R_f** = 0.24 (PE/EtOAc = 80/20). **HRMS** (APCI-MS): $[C_{10}H_{11}NOF_3]^+$ $[M + H]^+$ calcd: 218.0787; found: 218.0788.

Synthesis of *N*-propylbenzamide (**23a**)

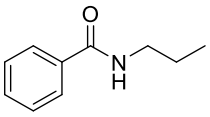

Prepared according to general procedure **GP4** from propan-1-amine (170 µL, 2.03 mmol), benzoyl chloride (260 µL, 2.20 mmol) and NEt_3 (310 µL, 2.20 mmol) dissolved in CH_2Cl_2 (10 mL) in 1 h. The crude product was purified via FCC (PE/EtOAc = 80/20), to obtain **23a** as a white solid (279 mg, 85% yield).

^{1}H-NMR (400 MHz, $CDCl_3$): δ (ppm) = 7.78 – 7.73 (m, 2H), 7.51 – 7.45 (m, 1H), 7.44 – 7.37 (m, 2H), 6.28 (bs, 1H), 3.45 – 3.37 (m, 2H), 1.69 – 1.56 (m, 2H), 0.97 (t, *J* = 7.4 Hz, 3H). **^{13}C-NMR** (101 MHz, $CDCl_3$): δ (ppm) = 167.6, 134.8, 131.2, 128.5, 126.8, 41.7, 22.9, 11.4.167.5, 134.8, 131.3, 128.5, 126.9, 34.9, 14.9. **R_f** = 0.30 (PE/EtOAc = 80/20). **HRMS** (APCI-MS): $[C_{10}H_{14}NO]^+$ $[M + H]^+$ calcd: 164.1070; found: 164.1070.

Synthesis of 2-methylpropan-1-amine (**24a**)

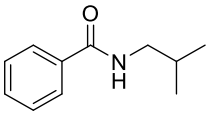

Prepared according to general procedure **GP4** from propan-1-amine (200 µL, 2.00 mmol), benzoyl chloride (260 µL, 2.20 mmol) and NEt_3 (310 µL, 2.20 mmol) in CH_2Cl_2 (10 mL) in 1 h. The crude product was purified via FCC (PE/EtOAc = 90/10), to obtain **24a** as a pale-yellow oil (176 mg, 50% yield).

^{1}H-NMR (400 MHz, $CDCl_3$): δ (ppm) = 7.82 – 7.69 (m, 2H), 7.51 – 7.35 (m, 3H), 6.39 (bs, 1H), 3.26 (t, *J* = 6.5 Hz, 2H), 1.89 (dp, *J* = 13.5, 6.7 Hz, 1H), 0.96 (d, *J* = 6.7 Hz, 6H). **^{13}C-NMR** (101 MHz, $CDCl_3$): δ (ppm) = 167.7, 135.0, 131.3, 128.6, 126.9, 47.4, 28.7, 20.2. **R_f** = 0.32 (PE/EtOAc = 90/10). **HRMS** (ESI-MS): $[C_{11}H_{16}NO]^+$ $[M + H]^+$ calcd: 178.1226; found: 178.1231.

Synthesis of *N*-isopropylbenzamide (**25a**)

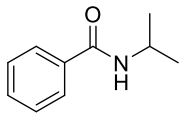

Prepared according to general procedure **GP4** from propan-2-amine (170 µL, 1.98 mmol), benzoyl chloride (260 µL, 2.20 mmol) and NEt_3 (310 µL, 2.20 mmol) dissolved in CH_2Cl_2 (10 mL) in 1.5 h. The crude product was purified via FCC (PE/EtOAc = 90/10), to obtain **25a** as a white solid (290 mg, 89% yield).

^{1}H-NMR (400 MHz, $CDCl_3$): δ (ppm) = 7.74 (dd, *J* = 5.3, 3.3 Hz, 2H), 7.50 – 7.36 (m, 3H), 6.08 (s, 1H), 4.37 – 4.18 (m, 1H), 1.25 (d, *J* = 6.6 Hz, 6H). **^{13}C-NMR** (101 MHz, $CDCl_3$): δ (ppm) = 166.7, 134.9, 131.2, 128.4, 126.8, 41.8, 22.8. **R_f** = 0.30 (PE/EtOAc = 80/20).

Synthesis of *N*-butylbenzamide (**26a**)

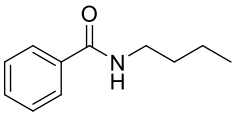

Prepared according to general procedure **GP2** from 1-aminobutane hydrochloride (320 mg, 1.80 mmol), benzoyl chloride (232 µL, 1.98 mmol) and NEt_3 (555 µL, 3.96 mmol) in 2 h. The crude product was purified via FCC (PE/EtOAc = 85/15), to obtain **26a** as a white solid (285 mg, 89% yield).

^{1}H-NMR (400 MHz, $CDCl_3$): δ (ppm) = 7.78 – 7.73 (m, 2H), 7.44 – 7.38 (m, 1H), 7.37 – 7.30 (m, 2H), 6.83 (bs, 1H), 3.44 – 3.33 (m, 2H), 1.60 – 1.49 (m, 2H), 1.39 – 1.27 (m, 2H), 0.88 (t, *J* = 7.3 Hz, 3H). **^{13}C-NMR** (101 MHz, $CDCl_3$): δ (ppm) = 167.5, 134.7, 131.0, 128.2, 126.8 39.7, 31.5, 20.0, 13.6. **R_f** = 0.24 (PE/EtOAc = 85/15).

Synthesis of *N*-phenethylbenzamide (**27a**)

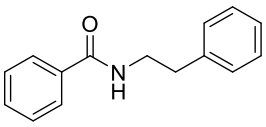

Prepared according to general procedure **GP4** from phenethylamine (260 µL, 1.99 mmol), benzoyl chloride (260 µL, 2.18 mmol) and NEt_3 (310 µL, 2.20 mmol) in CH_2Cl_2 (10 mL) in 2.5 h. The crude product was purified via FCC (PE/Acetone = 90/10), to obtain **27a** as a white solid (308 mg, 68% yield).

^{1}H-NMR (400 MHz, $CDCl_3$): δ (ppm) = 7.69 (dd, *J* = 5.3, 3.3 Hz, 2H), 7.48 (ddd, *J* = 6.5, 3.8, 1.2 Hz, 1H), 7.40 (dd, *J* = 10.2, 4.6 Hz, 2H), 7.33 (dd, *J* = 9.8, 5.1 Hz, 2H), 7.25 (dd, *J* = 8.6, 4.8 Hz, 3H), 6.20 (s, 1H), 3.72 (dd, *J* = 12.9, 6.8 Hz, 2H), 2.94 (t, *J* = 6.9 Hz, 2H). **^{13}C-NMR** (101 MHz, $CDCl_3$): δ (ppm) = 167.5, 138.9, 134.6, 131.4, 128.8, 128.7, 128.5, 126.8, 126.6, 41.1, 35.7. **R_f** = 0.30 (PE/Acetone = 90/10). **HRMS** (APCI-MS): $[C_{15}H_{16}NO]^+$ $[M + H]^+$ calcd: 226.1226; found: 226.1230.

Synthesis of 4-methyl-*N*-phenethylbenzamide (**28a**)

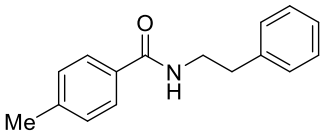

Prepared according to general procedure **GP4** from phenethylamine (260 µL, 1.99 mmol), 4-methyl benzoyl chloride (300 µL, 2.22 mmol) and NEt_3 (310 µL, 2.20 mmol) dissolved in CH_2Cl_2 (10 mL) in 3 h. The crude product was purified via FCC (PE/Acetone = 90/10), to obtain **28a** as a white solid (465 mg, 97% yield).

^{1}H-NMR (400 MHz, CD_2Cl_2): δ (ppm) = 7.60 (d, *J* = 8.1 Hz, 2H), 7.36 – 7.28 (m, 2H), 7.29 – 7.17 (m, 5H), 6.32 (s, 1H), 3.66 (dd, *J* = 13.1, 6.9 Hz, 2H), 2.91 (t, *J* = 7.1 Hz, 2H), 2.38 (s, 3H). **^{13}C-NMR** (101 MHz, CD_2Cl_2): δ (ppm) = 167.1, 141.9, 139.3, 132.1, 129.2, 128.9, 128.6, 126.8, 126.5, 41.2, 35.8, 21.2. **R_f** = 0.28 (PE/Acetone = 90/10). **HRMS** (EI-MS): $[C_{16}H_{17}NO]^{\cdot+}$ $[M]^{\cdot+}$ calcd: 239.1305; found: 239.1300.

Synthesis of 4-methoxy-*N*-phenethylbenzamide (**29a**)

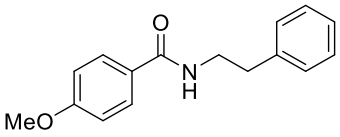

Prepared according to general procedure **GP4** from phenethylamine (260 µL, 1.99 mmol), 4-methoxybenzoyl chloride (300 µL, 2.20 mmol) and NEt_3 (310 µL, 2.20 mmol) dissolved in CH_2Cl_2 (10 mL) in 2 h. The crude product was purified via FCC (PE/Acetone = 85/15), to obtain **29a** as a white solid (369 mg, 72% yield).

^{1}H-NMR (400 MHz, CD_2Cl_2): δ (ppm) = 7.70 – 7.62 (m, 2H), 7.32 (ddd, *J* = 7.1, 4.4, 1.6 Hz, 2H), 7.28 – 7.19 (m, 3H), 6.95 – 6.87 (m, 2H), 6.21 (s, 1H), 3.83 (s, 3H), 3.65 (dd, *J* = 13.0, 7.0 Hz, 2H), 2.90 (t, *J* = 7.1 Hz, 2H). **^{13}C-NMR** (101 MHz, CD_2Cl_2): δ (ppm) = 166.6, 162.1, 139.3, 128.8, 128.5, 128.4, 127.1, 126.4, 113.6, 41.1, 35.8. **R_f** = 0.24 (PE/Acetone = 85/15). **HRMS** (EI-MS): $[C_{16}H_{17}NO_2]^{\cdot+}$ $[M]^{\cdot+}$ calcd: 255.1254; found: 255.1251.

Synthesis of 4-fluor-*N*-phenethylbenzamide (**30a**)

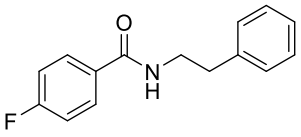

Prepared according to general procedure **GP4** from phenethylamine (260 µL, 1.99 mmol), 4-fluoro benzoyl chloride (260 µL, 2.19 mmol) and NEt_3 (310 µL, 2.20 mmol) in CH_2Cl_2 (10 mL) in 1 h. The product was purified via FCC (PE/Acetone = 85/15), to obtain **30a** as a white solid (467 mg, 96% yield).

^{1}H-NMR (400 MHz, $CDCl_3$): δ (ppm) = 7.96 – 7.83 (m, 2H), 7.52 (t, *J* = 7.3 Hz, 2H), 7.44 (dd, *J* = 13.4, 6.8 Hz, 3H), 7.31 – 7.22 (m, 2H), 6.49 (bs, 1H), 3.89 (dd, *J* = 13.0, 6.8 Hz, 2H), 3.12 (t, *J* = 7.0 Hz, 2H). **^{13}C-NMR** (101 MHz, $CDCl_3$): δ (ppm) = 166.4, 165.8, 163.3, 138.8, 130.8 (d, *J* = 3.1 Hz), 129.1 (d, *J* = 8.9 Hz), 128.7 (d, *J* = 5.9 Hz), 126.6, 115.6, 115.4, 41.2, 35.6. **^{19}F-NMR** (377 MHz, $CDCl_3$): δ (ppm)= -108.9. **R_f** = 0.27 (PE/Acetone = 85/15). **HRMS** (EI-MS): $[C_{15}H_{14}NOF]^{\cdot+}$ $[M]^{\cdot+}$ calcd: 243.1054; found: 243.1056.

Synthesis of *N*-(2-phenylpropyl)benzamide (**31a**)

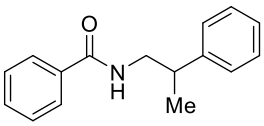

Prepared according to general procedure **GP4** from 2-phenylpropane-1-amine (370 µL, 2.50 mmol), benzoyl chloride (320 µL, 2.74 mmol) and NEt_3 (390 µL, 2.76 mmol) in CH_2Cl_2 (12 mL) in 6 h. The crude product was purified via FCC (PE/Acetone = 90/10), to obtain **31a** as a white solid (550 mg, 92% yield).

^{1}H-NMR (400 MHz, $CDCl_3$): δ (ppm) = 7.56 – 7.48 (m, 2H), 7.35 (dd, *J* = 8.4, 6.3 Hz, 1H), 7.25 (dd, *J* = 15.6, 7.5 Hz, 4H), 7.18 – 7.13 (m, 3H), 6.02 (bs, 1H), 3.72 (dt, *J* = 13.2, 6.5 Hz, 1H), 3.31 (ddd, *J* = 13.5, 8.7, 4.9 Hz, 1H), 3.06 – 2.90 (m, 1H), 1.23 (d, *J* = 7.0 Hz, 3H). **^{13}C-NMR** (101 MHz, $CDCl_3$): δ (ppm) = 167.4, 144.0, 134.6, 131.3, 128.7, 128.4, 127.2, 126.8, 126.7, 46.5, 39.7, 19.2. **R_f** = 0.23 (PE/Acetone = 90/10). **HRMS** (ESI-MS): $[C_{16}H_{18}NO]^+$ $[M + H]^+$ calcd: 240.1383; found: 240.1390.

Synthesis of benzyl phenethylcarbamate (**33a**)

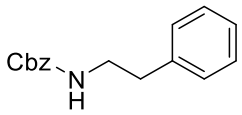

Compound **33a** was prepared based on a procedure published by Yang et al.[35] In an oven dried Schlenk flask, phenethylamine (260 µL, 1.99 mmol, 1.00 equiv.) was dissolved in dry THF (10 mL) and powdered K_2CO_3 (335 mg, 2.40 mmol, 1.20 equiv.) was added under N_2 atmosphere. Next, the reaction mixture was cooled to 0 °C and benzyl chloroformate (320 µL, 2.23 mmol, 1.10 eq.) was added dropwise. After stirring the solution at 25 °C for 2 h, water was added (10 mL), and the product was extracted with CH_2Cl_2 (2 x 10 mL). The combined organic layers were dried over Na_2SO_4, and the solvent evaporated. The crude product was then purified via FCC (PE/EtOAc = 85/15), to obtain **33a** as a white solid (405 mg, 79% yield).

^{1}H-NMR (400 MHz, $CDCl_3$): δ (ppm) = 7.31 – 7.17 (m, 7H), 7.17 – 7.06 (m, 3H), 5.01 (s, 2H), 4.70 (bs, 1H), 3.38 (dd, *J* = 13.1, 6.6 Hz, 2H), 2.73 (t, *J* = 6.9 Hz, 2H).

^{13}C-NMR (101 MHz, $CDCl_3$): δ (ppm) = 156.3, 138.7, 136.5, 128.7, 128.6, 128.5, 128.1, 126.5, 66.6, 42.2, 36.0. **R_f** = 0.22 (PE/EtOAc = 85/15). **HRMS** (EI-MS): $[C_{16}H_{17}NO_2]^{\cdot+}$ $[M]^{\cdot+}$ calcd: 255.1254; found: 255.1248.

Synthesis of benzyl (3,4-dimethoxyphenethyl)carbamate (**34a**)

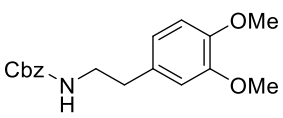

Compound **34a** was prepared based on a procedure reported by Yang et al.[35] In an oven dried Schlenk flask, 2-(3,4-dimethoxyphenyl)ethan-1-amine (340 µL, 2.02 mmol, 1.00 equiv.) was dissolved in dry THF (10 mL) and powdered K_2CO_3 (340 mg, 2.42 mmol, 1.20 equiv.) was added under N_2 atmosphere. Next, the reaction mixture was cooled to 0 °C and benzyl chloroformate (320 µL, 2.23 mmol, 1.10 eq.) was added dropwise. After stirring the solution at 25 °C for 2 h, water was added (10 mL) and the product was extracted with CH_2Cl_2 (2 x 10 mL). The combined organic layers were dried over Na_2SO_4, and the solvent evaporated. The crude product was then purified via FCC (PE/EtOAc = 75/25), to obtain **34a** as a white solid (541 mg, 86% yield).

^{1}H-NMR (400 MHz, $CDCl_3$): δ (ppm) = 7.39 – 7.27 (m, 5H), 6.79 (d, *J* = 8.0 Hz, 1H), 6.71 (d, *J* = 10.0 Hz, 2H), 5.10 (s, 2H), 4.79 (bs, 1H), 3.85 (d, *J* = 5.5 Hz, 6H), 3.44 (dd, *J* = 13.1, 6.6 Hz, 2H), 2.76 (t, *J* = 6.9 Hz, 2H). **^{13}C-NMR** (101 MHz, $CDCl_3$): δ (ppm) = 156.3, 149.0, 147.7, 136.5, 131.1, 128.5, 128.1, 120.6, 111.9, 111.3, 66.6, 55.9, 55.8, 42.3, 35.6. **R_f** = 0.24 (PE/EtOAc = 75/25). **HRMS** (EI-MS): $[C_{18}H_{21}NO_4]^{\cdot+}$ $[M]^{\cdot+}$ calcd: 315.1465; found: 315.1463.

Synthesis of methyl 2-(4-(2-(4-chlorobenzamido)ethyl)phenoxy)-2-methylpropanoate (**35a**)

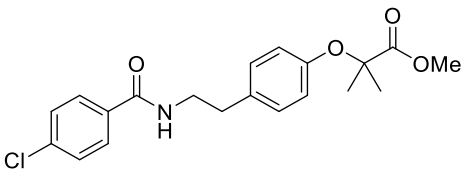

Compound **35a** was prepared based on a procedure published by Zhang *et al*.[36] In a round bottom flask, to a solution of bezafibrate (543 mg, 1.50 mmol, 1.00 equiv.) in MeOH (6 mL) is added concentrated sulfuric acid (30 µL, 535 µmol, 0.35 equiv.). After stirring the solution at 25 °C for 16 h, the solvent was evaporated under reduced pressure and the residue redissolved in EtOAc (50 mL). The organic phase was washed with saturated aqueous Na_2CO_3 solution (2 x 50 mL), water (50 mL), brine (40 mL), and dried over Na_2SO_4. Lastly, the solvent was evaporated to obtain **35a** as a white solid (552 mg, 98% yield).

^{1}H-NMR (400 MHz, $CDCl_3$): δ (ppm) = 7.63 – 7.58 (m, 2H), 7.37 – 7.31 (m, 2H), 7.07 (d, *J* = 8.5 Hz, 2H), 6.77 (d, *J* = 8.6 Hz, 2H), 6.25 (s, 1H), 3.75 (s, 3H), 3.63 (dd, *J* = 12.9, 6.9 Hz, 2H), 2.84 (t, *J* = 6.9 Hz, 2H), 1.57 (s, 6H). **^{13}C-NMR** (101 MHz, $CDCl_3$): δ (ppm) = 174.7, 166.4, 154.0, 137.5, 132.9, 132.5, 129.5, 128.7, 128.2, 119.5, 79.1, 52.4, 41.2, 34.7, 25.3. **R_f** = 0.19 (PE/EtOAc = 80/20). **HRMS** (ESI-MS): $[C_{20}H_{23}ClNO_4]^{+}$ $[M + H]^{+}$ calcd: 376.1310; found: 376.1314.

Synthesis of methyl 3-(((benzyloxy)carbonyl)amino)propanoate (**36a**)

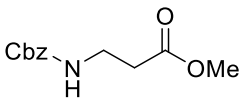

Prepared according to general procedure **GP2** from methyl 3-aminopropanoate hydrochloride (210 mg, 1.50 mmol), benzyl chloroformate (230 µL, 1.64 mmol), NEt_3 (460 µL, 3.30 mmol) and CH_2Cl_2 (8 mL) in 1 h. After washing the residue with water and removing the solvent, compound **36a** was obtained as a colourless oil (323 mg, 91% yield).

^{1}H-NMR (400 MHz, CD_2Cl_2): δ (ppm) = 7.58 (dt, *J* = 6.0, 3.7 Hz, 5H), 5.62 (s, 1H), 5.32 (s, 2H), 3.91 (s, 3H), 3.68 (q, *J* = 6.2 Hz, 2H), 2.78 (t, *J* = 6.2 Hz, 2H). **^{13}C-NMR** (101 MHz, CD_2Cl_2): δ (ppm) = 172.6, 156.2, 137.0, 128.5, 128.0, 128.0, 77.7, 66.5, 51.7, 36.7, 34.3. **R_f** = 0.20 (PE/Acetone = 85/15). **HRMS** (ESI-MS): $[C_{12}H_{16}NO_4]^+$ [M + H]$^+$ calcd: 238.1074; found: 238.1076.

Synthesis of methyl 3-(3-((((9H-fluoren-9-yl)methoxy)carbonyl)amino)propanamido) propanoate (**37a**)

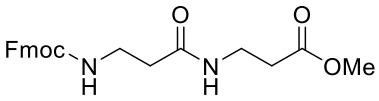

Compound **37a** was prepared based on a procedure published by Boonyarattanakalin *et al*.[37] In a Schlenk flask, to 0 ºC cooled solution of 3-((((9H-fluoren-9-yl)methoxy)carbonyl)amino) propanoic acid (311 mg, 1.50 mmol, 1.00 equiv.) in dry CH_2Cl_2 (30 mL), under N_2 atmosphere was added hydroxybenzotriazole (HOBt) (225 mg, 1.65 mmol, 1.10 equiv.) and 1-Ethyl-3-(3-dimethylaminopropyl)carbodiimide hydrochloride (349 mg, 1.80 mmol, 1.20 equiv.). After stirring the reaction mixture at 0 ºC for 30 min, a solution of methyl 3-aminopropanoate hydrochloride (254 mg, 1.80 mmol, 1.20 equiv.) and DIPEA (280 µL, 1.63 mmol, 1.10 equiv.) in dry CH_2Cl_2 (15 mL) was added. The resulting mixture was stirred at 25 ºC for 16 h. Afterwards, the reaction mixture crude was diluted with CH_2Cl_2 (40 mL) and washed with aqueous 5% HCl solution (50 mL), aqueous 0.1 M NaOH solution (50 mL), water (50 mL) and brine (50 mL). The organic phase was dried over Na_2SO_4, and the solvent removed under reduced pressure, obtaining a white solid which was further washed and triturated with Et_2O (3 x 5 mL), to give **37a** as a white solid (418 mg, 70% yield).

^{1}H-NMR (400 MHz, $CDCl_3$): δ (ppm) = 7.75 (d, *J* = 7.5 Hz, 2H), 7.59 (d, *J* = 7.5 Hz, 2H), 7.39 (t, *J* = 7.4 Hz, 2H), 7.30 (t, *J* = 7.4 Hz, 2H), 6.21 (s, 1H), 5.56 (s, 1H), 4.36 (d, *J* = 7.0 Hz, 2H), 4.19 (t, *J* = 7.0 Hz, 1H), 3.67 (s, 3H), 3.60 – 3.28 (m, 4H), 2.53 (t, *J* = 5.9 Hz, 2H), 2.39 (t, *J* = 5.7 Hz, 2H). **^{13}C-NMR** (101 MHz, $CDCl_3$): δ (ppm) = 172.9, 171.3, 156.5, 143.9, 141.2, 127.6, 127.0, 125.1, 119.9, 66.6, 51.8, 47.2, 37.0, 35.9, 34.8, 33.8. **R_f** = 0.22 (PE/Acetone = 70/30) [ninhydrin]. **HRMS** (ESI-MS): $[C_{15}H_{21}NO_5Na]^+$ [M + Na]$^+$ calcd: 419.1577; found: 419.1581.

Synthesis of *N*-(4-methoxyphenethyl)benzamide (**38a**)

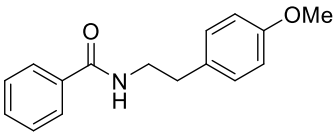

Prepared according to general procedure **GP4** from 2-(4-methoxyphenyl)ethan-1-amine (300 µL, 2.00 mmol), benzoyl chloride (260 µL, 2.18 mmol) and NEt_3 (310 µL, 2.20 mmol) dissolved in CH_2Cl_2 (10 mL) in 4 h. The crude product was purified via FCC (PE/Acetone = 80/20), to obtain **38a** as a white solid (453 mg, 89% yield).

^{1}H-NMR (400 MHz, $CDCl_3$): δ (ppm) = 7.75 – 7.65 (m, 2H), 7.54 – 7.43 (m, 1H), 7.40 (dd, *J* = 10.2, 4.6 Hz, 2H), 7.15 (d, *J* = 8.5 Hz, 2H), 6.91 – 6.80 (m, 2H), 6.20 (s, 1H), 3.80 (s, 3H), 3.68 (dd, *J* = 12.9, 6.8 Hz, 2H), 2.87 (t, *J* = 6.9 Hz, 2H). **^{13}C-NMR** (101 MHz, $CDCl_3$): δ (ppm) = 167.4, 158.3, 134.7, 131.3, 130.8, 129.7, 128.5, 126.8, 114.1, 55.2, 41.3, 34.7. **R_f** = 0.30 (PE/Acetone = 80/20). **HRMS** (EI-MS): $[C_{16}H_{17}NO_2]^{\cdot+}$ $[M]^{\cdot+}$ calcd: 255.1254; found: 255.1247.

Synthesis of *N*-phenethylcinnamamide (lansiunamide C) (**39a**)

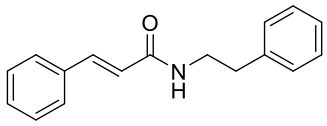

Compound **39a** was prepared following a procedure published by Yao *et al*.[38] In a Schlenk flask, to a solution of *N*-hydroxysuccinimide (173 mg, 1.50 mmol, 1.00 equiv.) in CH_3CN (3 mL) was added *trans*-cinnamaldehyde (190 µL, 1.49 mmol, 1.00 equiv.). Next, iodobenzene diacetate (488 mg, 1.50 mmol, 1.00 equiv.) was added under N_2 atmosphere and after stirring the mixture for 5 min, phenethylamine (190 µL, 1.50 mmol, 1.00 eq.) was introduced. The resulting mixture was stirred at 25 ºC for 7 h. Afterwards, the crude reaction mixture was quenched with water (5 mL) and the aqueous phase was extracted with EtOAc (3 x 5 mL). The combined organic layers were then dried over Na_2SO_4, the solvent removed under reduced pressure and the crude product was purified via FCC (PE/Acetone = 85/15), to obtain **39a** as a pale-yellow solid (180 mg, 48% yield).

^{1}H-NMR (400 MHz, $CDCl_3$): δ (ppm) = 7.54 (d, *J* = 15.6 Hz, 1H), 7.40 (dd, *J* = 6.5, 3.1 Hz, 2H), 7.30 – 7.20 (m, 5H), 7.18 – 7.13 (m, 3H), 6.27 (d, *J* = 15.6 Hz, 1H), 5.73 (bs, 1H), 3.58 (dd, *J* = 13.0, 6.9 Hz, 2H), 2.82 (t, *J* = 6.9 Hz, 2H). **^{13}C-NMR** (101 MHz, $CDCl_3$): δ (ppm) = 165.9, 141.0, 138.8, 134.8, 129.6, 128.8, 128.7, 128.6, 127.7, 126.5, 120.6, 40.8, 35.6. **R_f** = 0.28 (PE/Acetone = 85/15) [$KMnO_4$]. **HRMS** (APCI-MS): $[C_{17}H_{18}NO]^+$ $[M + H]^+$ calcd: 252.1383; found: 252.1386.

Synthesis of *N*-methyl-*N*-phenethylcinnamamide (**40a**)

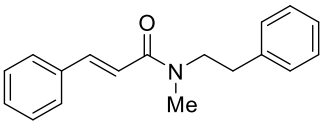

Prepared according to general procedure **GP4** from *N*-methyl-2-phenylethan-1-amine (290 µL, 1.97 mmol), *trans*-3-phenylacryloylchloride (378 mg, 2.20 mmol) and NEt_3 (310 µL, 2.20 mmol) dissolved in CH_2Cl_2 (10 mL) in 3.5 h. The crude product was purified via FCC (PE/Acetone = 85/15), to obtain **40a** as a pale brown oil (285 mg, 58% yield).

^{1}H-NMR (400 MHz, CD_2Cl_2): δ (ppm) = 7.72 – 7.18 (m, 11H), 6.91 (d, *J* = 15.4 Hz, 0.45H), 6.62 (d, *J* = 15.4 Hz, 0.55H), 3.72 – 3.64 (m, 2H), 3.04 (d, *J* = 20.0 Hz, 3H), 2.97 – 2.84 (m, 2H). **^{13}C-NMR** (101 MHz, CD_2Cl_2): δ (ppm) = 166.2, 165.9, 141.8, 141.3, 139.5, 138.6, 135.5, 129.5, 129.4, 128.9, 128.8, 128.7, 128.5, 127.8, 127.7, 126.7, 126.2, 118.1, 117.9, 77.6, 51.8, 50.2, 36.0, 35.4, 34.0, 33.7. **R_f** = 0.23 (PE/Acetone = 85/15) [$KMnO_4$]. **HRMS** (EI-MS): $[C_{18}H_{19}NO]^{\cdot+}$ $[M]^{\cdot+}$ calcd: 265.1467; found: 265.1461.

Synthesis of *N*-methyl-*N*-(3-oxobutyl-2,2,4,4,4-d_5) benzamide (**1a-D$_5$**)

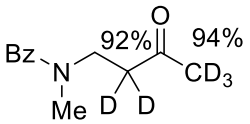

Synthesized according to a reported literature procedure.[39] Product **1a-D$_5$** (85% yield) was isolated with 92%/94% deuterium incorporation.

^{1}H-NMR (400 MHz, $CDCl_3$): δ (ppm) = 7.27 (m, 5H), 3.71-3.42 (m, 2H), 2.90-2.74 (m, 3H). **^{13}C-NMR** (101 MHz, $CDCl_3$): δ (ppm) = 207.4, 171.3, 136.1, 129.3, 128.1, 126.7, 126.2, 45.5, 42.8, 38.1, 32.3. **R_f** = 0.29 (PE/EtOAc = 40/60) [2,4-DNPH]. **HRMS** (ESI-MS): $[C_{12}H_{10}D_5NO_2]^+$ $[M + H]^+$ calcd: 211.1489; found: 211.1491.

3.4.7 Synthesis and Analytical Data of Products

Synthesis of (*E*)-*N*-methyl-*N*-(3-oxobut-1-en-1-yl)benzamide (**1b**)

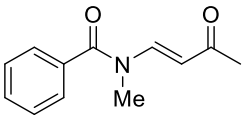

Prepared according to general procedure **GP5** from **1a** (20.6 mg, 100 µmol). The crude product was purified via FCC (PE/EtOAc = 50/50), to obtain **1b** as a viscous colourless oil (14.5 mg, 71% yield).

^{1}H-NMR (400 MHz, $CDCl_3$): δ (ppm) = 8.02 (d, *J* = 14.0 Hz, 1H), 7.57 – 7.44 (m, 5H), 5.72 (d, *J* = 14.0 Hz, 1H), 3.28 (s, 3H), 2.16 (s, 3H). **^{13}C-NMR** (101 MHz, $CDCl_3$): δ (ppm) = 196.8, 171.6, 143.8, 133.4, 131.5, 128.8, 128.3, 109.2, 31.7, 28.0. **R_f** = 0.20 (PE/EtOAc = 50/50) [$KMnO_4$]. **HRMS** (EI-MS): $[C_{12}H_{13}NO_2]^{\cdot+}$ $[M]^{\cdot+}$ calcd: 203.0946; found: 203.0941.

Synthesis of *tert*-butyl (*E*)-methyl(3-oxobut-1-en-1-yl)carbamate (**2b**)

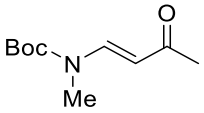

Prepared according to general procedure **GP5** from **2a** (20.1 mg, 100 µmol). The crude product was purified via HPLC, to obtain **2b** as a colourless oil (11.8 mg, 59% yield).

^{1}H-NMR (400 MHz, $CDCl_3$): δ (ppm) = 8.19 (d, *J* = 14.3 Hz, 1H), 5.51 (d, *J* = 14.3 Hz, 1H), 3.07 (s, 3H), 2.24 (s, 3H), 1.53 (s, 9H). **^{13}C-NMR** (101 MHz, $CDCl_3$): δ (ppm) = 197.5, 152.2, 143.5, 130.1, 128.4, 108.2, 83.4, 31.2, 28.0. **R_f** = 0.23 (PE/EtOAc = 85/15) [$KMnO_4$]. **HRMS** (ESI-MS): $[C_{10}H_{18}NO_3]^+$ $[M + H]^+$ calcd: 200.1281; found: 200.1278.

Synthesis of *tert*-butyl (*E*)-methyl(3-oxopent-1-en-1-yl)carbamate (**3b**)

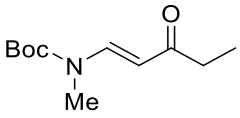

Prepared according to general procedure **GP5** from **3a** (21.5 mg, 99 µmol). The crude product was purified via FCC (PE/EtOAc = 90/10), to obtain **3b** as a colourless oil (10.4 mg, 49% yield).

^{1}H-NMR (400 MHz, $CDCl_3$): δ (ppm) = 8.22 (d, *J* = 14.2 Hz, 1H), 5.50 (d, *J* = 14.2 Hz, 1H), 3.06 (s, 3H), 2.53 (q, *J* = 7.4 Hz, 2H), 1.52 (s, 9H), 1.11 (t, *J* = 7.4 Hz, 3H). **^{13}C-NMR** (101 MHz, $CDCl_3$): δ (ppm) = 200.2, 152.3, 142.3, 106.7, 83.2, 31.1, 28.4, 28.0, 8.6. **R_f** = 0.24 (PE/EtOAc = 90/10) [$KMnO_4$]. **HRMS** (ESI-MS): $[C_{11}H_{20}NO_3]^+$ $[M + H]^+$ calcd: 214.1443; found: 214.1438.

Synthesis of tert-butyl (*E*)-methyl(3-oxo-3-phenylprop-1-en-1-yl)carbamate (**4b**)

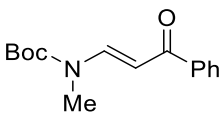

Prepared according to general procedure **GP5** from **4a** (26.3 mg, 100 µmol). The crude product was purified via FCC (PE/EtOAc = 80/20), to obtain **4b** as a white solid (15.2 mg, 58% yield).

^{1}H-NMR (400 MHz, $CDCl_3$): δ (ppm) = 8.45 (d, *J* = 13.6 Hz, 1H), 7.92 (d, *J* = 7.3 Hz, 2H), 7.53 (t, *J* = 7.3 Hz, 1H), 7.46 (t, *J* = 7.4 Hz, 2H), 6.22 (d, *J* = 13.6 Hz, 1H), 3.19 (s, 3H), 1.54 (s, 9H).

^{13}C-NMR (101 MHz, $CDCl_3$): δ (ppm) = 190.2, 163.0, 152.3, 144.8, 139.0, 132.2, 128.7, 128.5, 128.0, 102.6, 83.5, 31.4, 28.1. **R_f** = 0.26 (PE/EtOAc = 80/20) [$KMnO_4$]. **HRMS** (ESI-MS): $[C_{15}H_{20}NO_3]^+$ [M + H]$^+$ calcd: 262.1443; found: 262.1441.

Synthesis of tert-butyl (*E*)-(3-(furan-2-yl)-3-oxoprop-1-en-1-yl)(methyl)carbamate (**5b**)

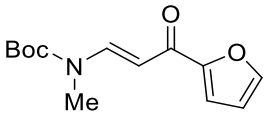

Prepared according to general procedure **GP5** from **5a** (25.1 mg, 100 µmol). The crude product was purified via FCC (PE/EtOAc = 95/5), to obtain **5b** as a colourless oil (7.6 mg, 30% yield).

^{1}H-NMR (400 MHz, $CDCl_3$): δ (ppm) = 8.47 (d, *J* = 13.7 Hz, 1H), 7.56 (s, 1H), 7.19 (d, *J* = 3.4 Hz, 1H), 6.53 (dd, *J* = 3.4, 1.6 Hz, 1H), 6.17 (d, *J* = 13.7 Hz, 1H), 3.18 (s, 3H), 1.54 (s, 9H). **^{13}C-NMR** (101 MHz, $CDCl_3$): δ (ppm) = 178.3, 154.0, 152.3, 145.5, 143.9, 115.8, 112.3, 101.9, 83.5, 31.4, 28.1. **R_f** = 0.24 (PE/EtOAc = 95/5) [$KMnO_4$]. **HRMS** (ESI-MS): $[C_{13}H_{17}NO_4Na]^+$ [M + Na]$^+$ calcd: 274.10; found: 274.1051.

Synthesis of tert-butyl (*E*)-methyl(3-oxo-3-(thiophen-2-yl)prop-1-en-1-yl) carbamate (**6b)**

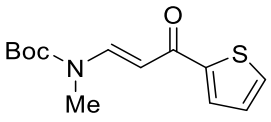

Prepared according to general procedure **GP5** from **6a** (27.0 mg, 100 µmol). The crude product was purified via FCC (PE/EtOAc = 95/5), to obtain **6b** as a white solid (9.5 mg, 35% yield).

^{1}H-NMR (400 MHz, $CDCl_3$): δ (ppm) = 8.45 (d, *J* = 13.5 Hz, 1H), 7.72 (dd, *J* = 3.7, 0.9 Hz, 1H), 7.59 (dd, *J* = 4.9, 0.9 Hz, 1H), 7.12 (dd, *J* = 4.9, 3.9 Hz, 1H), 6.12 (d, *J* = 13.5 Hz, 1H), 3.18 (s, 3H), 1.53 (s, 9H). **^{13}C-NMR** (101 MHz, $CDCl_3$): δ (ppm) = 181.9, 152.2, 145.9, 144.0, 132.6, 130.5, 127.9, 102.0, 83.5, 31.4, 28.0. **R_f** = 0.26 (PE/EtOAc = 95/5) [$KMnO_4$]. **HRMS** (ESI-MS): $[C_{13}H_{18}NO_3S]^+$ [M + Na]$^+$ calcd: 268.1002; found: 268.1002.

Synthesis of benzyl (*E*)-methyl(3-oxobut-1-en-1-yl)carbamate (**7b**)

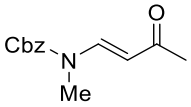

Prepared according to general procedure **GP5** from **7a** (23.5 mg, 100 µmol). The crude product was purified via HPLC, to obtain **7b** as a white solid (12.3 mg, 53% yield).

^{1}H-NMR (400 MHz, $CDCl_3$): δ (ppm) = 8.22 (d, *J* = 14.3 Hz, 1H), 7.45 – 7.33 (m, 5H), 5.56 (d, *J* = 14.3 Hz, 1H), 5.27 (s, 2H), 3.14 (s, 3H), 2.24 (s, 3H). **^{13}C-NMR** (101 MHz, $CDCl_3$): δ (ppm) = 197.1, 153.6, 142.7, 135.1, 128.7, 128.5, 128.4, 128.0, 109.2, 69.0, 31.5, 27.6. **R_f** = 0.21 (PE/EtOAc = 75/25) [$KMnO_4$]. **HRMS** (ESI-MS): $[C_{13}H_{16}NO_3]^+$ [M + H]$^+$ calcd: 234.1130; found: 234.1126.

Synthesis of phenyl (*E*)-methyl(3-oxobut-1-en-1-yl)carbamate (**8b**)

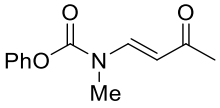

Prepared according to general procedure **GP5** from **8a** (22.1 mg, 100 µmol). The crude product was purified via HPLC, to obtain **8b** as a white solid (14.1 mg, 64% yield).

^{1}H-NMR (400 MHz, $CDCl_3$): δ (ppm) = 8.32 (d, *J* = 13.4 Hz, 1H), 7.41 (dt, *J* = 10.6, 2.2 Hz, 2H), 7.27 (dd, *J* = 10.4, 4.4 Hz, 1H), 7.19 – 7.11 (m, 2H), 5.69 (d, *J* = 14.3 Hz, 1H), 3.27 (s, 3H), 2.29 (s, 3H). **^{13}C-NMR** (101 MHz, $CDCl_3$): δ (ppm) = 197.0, 150.6, 129.6, 126.3, 121.3, 31.9, 28.0. **R_f** = 0.21 (PE/EtOAc = 65/35) [$KMnO_4$]. **HRMS** (ESI-MS): $[C_{12}H_{14}NO_3]^+$ $[M + H]^+$ calcd: 220.0968; found: 220.0971.

Synthesis of (*Z*)-*N*-(3-oxobut-1-en-1-yl)benzamide (**9b**)

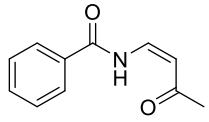

Prepared according to general procedure **GP5** from **9a** (19.1 mg, 100 µmol). The crude product was purified via FCC (PE/EtOAc = 50/50), to obtain **9b** as a pale yellow solid (12.9 mg, 68% yield).

^{1}H-NMR (400 MHz, $CDCl_3$): δ (ppm) = 12.64 – 12.39 (bs, 1H), 7.99 – 7.94 (m, 2H), 7.65 (dd, *J* = 10.8, 8.4 Hz, 1H), 7.61 – 7.56 (m, 1H), 7.49 (tt, *J* = 6.8, 1.4 Hz, 2H), 5.65 (d, *J* = 8.4 Hz, 1H), 2.25 (s, 3H). **^{13}C-NMR** (101 MHz, $CDCl_3$): δ (ppm) = 201.6, 165.2, 138.1, 133.0, 131.9, 128.9, 127.9, 104.7, 30.6. **R_f** = 0.22 (PE/EtOAc = 50/50) [$KMnO_4$]. **HRMS** (APCI-MS): $[C_{11}H_{12}NO_2]^+$ $[M + H]^+$ calcd: 190.0863; found: 190.0862.

Synthesis of (*Z*)-4-methyl-N-(3-oxobut-1-en-1-yl)benzamide (**10b**)

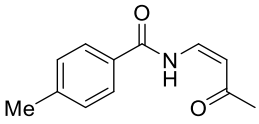

Prepared according to general procedure **GP5** from **10a** (20.5 mg, 100 µmol). The crude product was purified via FCC (PE/EtOAc = 55/45), to obtain **10b** as a pale-yellow solid (13.3 mg, 65% yield).

^{1}H-NMR (400 MHz, $CDCl_3$): δ (ppm) = 12.49 (d, *J* = 8.5 Hz, 1H), 7.87 (d, *J* = 8.2 Hz, 2H), 7.66 (dd, *J* = 10.8, 8.4 Hz, 1H), 7.29 (d, *J* = 8.2 Hz, 2H), 5.64 (d, *J* = 8.4 Hz, 1H), 2.42 (s, 3H), 2.25 (s, 3H). **^{13}C-NMR** (101 MHz, $CDCl_3$): δ (ppm) = 201.6, 165.2, 144.0, 138.3, 130.2, 129.6, 129.1, 128.5, 128.0, 104.5, 30.6, 21.6. **R_f** = 0.19 (PE/EtOAc = 55/45) [$KMnO_4$]. **HRMS** (APCI-MS): $[C_{12}H_{14}NO_2]^+$ $[M + H]^+$ calcd: 204.1019; found: 204.1021.

Synthesis of (*Z*)-4-bromo-N-(3-oxobut-1-en-1-yl)benzamide (**11b**)

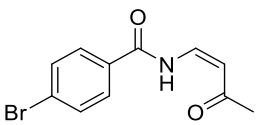

Prepared according to general procedure **GP5** from **11a** (27.0 mg, 100 µmol). The crude product was purified via FCC (PE/EtOAc = 50/50), to obtain **11b** as a white solid (19.0 mg, 71% yield).

^{1}H-NMR (400 MHz, $CDCl_3$): δ (ppm) = 12.53 (d, *J* = 9.2 Hz, 1H), 7.84 (d, *J* = 8.6 Hz, 2H), 7.63 (dd, *J* = 10.7, 8.5 Hz, 3H), 5.68 (d, *J* = 8.4 Hz, 1H), 2.27 (s, 3H). **^{13}C-NMR** (101 MHz, $CDCl_3$):

δ (ppm) = 201.8, 164.4, 138.0, 132.3, 130.8, 129.4, 128.2, 105.1, 30.7. **R_f** = 0.24 (PE/EtOAc = 50/50) [$KMnO_4$]. **HRMS** (APCI-MS): $[C_{11}H_{11}BrNO_2]^+$ $[M + H]^+$ calcd: 267.9968; found: 267.9970.

Synthesis of (*Z*)-4-methoxy-N-(3-oxobut-1-en-1-yl)benzamide (**12b**)

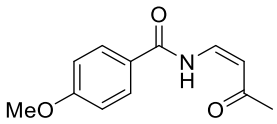

Prepared according to general procedure **GP5** from **12a** (21.9 mg, 100 µmol). The product was purified via FCC (PE/EtOAc = 45/55), to obtain **12b** as a white solid (16.4 mg, 75% yield).

^{1}H-NMR (400 MHz, $CDCl_3$): δ (ppm) = 12.48 (d, *J* = 9.0 Hz, 1H), 8.03 – 7.86 (m, 2H), 7.65 (dd, *J* = 10.8, 8.4 Hz, 1H), 7.04 – 6.88 (m, 2H), 5.63 (d, *J* = 8.4 Hz, 1H), 3.86 (s, 3H), 2.24 (s, 3H). **^{13}C-NMR** (101 MHz, $CDCl_3$): δ (ppm) = 201.6, 164.6, 163.5, 138.5, 130.0, 124.1, 114.1, 104.2, 55.5, 30.6. **R_f** = 0.22 (PE/EtOAc = 45/55) [$KMnO_4$]. **HRMS** (ESI-MS): $[C_{12}H_{14}NO_3]^+$ $[M + H]^+$ calcd: 220.0968; found: 220.0968.

Synthesis of (*Z*)-3,4,5-trimethoxy-N-(3-oxobut-1-en-1-yl)benzamide (**13b**)

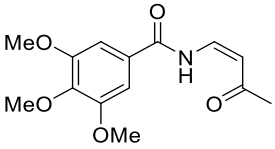

Prepared according to general procedure **GP5** from **13a** (28.1 mg, 100 µmol). The product was purified via FCC (PE/EtOAc = 45/55), to obtain **13b** as a white solid (21.6 mg, 77% yield).

^{1}H-NMR (400 MHz, $CDCl_3$): δ (ppm) = 12.50 (d, *J* = 10.1 Hz, 1H), 7.63 (dd, *J* = 10.7, 8.4 Hz, 1H), 7.20 (s, 2H), 5.65 (d, *J* = 8.4 Hz, 1H), 3.94 (s, 6H), 3.91 (s, 3H), 2.25 (s, 3H). **^{13}C-NMR** (101 MHz, $CDCl_3$): δ (ppm) = 201.7, 164.8, 153.3, 142.3, 138.2, 127.0, 105.1, 104.6, 60.9, 56.3, 30.6. **R_f** = 0.18 (PE/EtOAc = 45/55) [$KMnO_4$]. **HRMS** (APCI-MS): $[C_{14}H_{18}NO_5]^+$ $[M + H]^+$ calcd: 280.1179; found: 280.1180.

Synthesis of (*Z*)-*N*-(3-oxobut-1-en-1-yl)-2-naphthamide (**14b**)

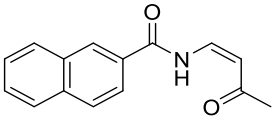

Prepared according to general procedure **GP5** from **14a** (24.1 mg, 100 µmol). The product was purified via FCC (PE/EtOAc = 50/50), to obtain **14b** as a white solid (12.0 mg, 50% yield).

^{1}H-NMR (400 MHz, $CDCl_3$): δ (ppm) = 12.69 (d, *J* = 9.8 Hz, 1H), 8.51 (s, 1H), 8.05 – 7.98 (m, 2H), 7.95 (d, *J* = 8.6 Hz, 1H), 7.90 (d, *J* = 7.9 Hz, 1H), 7.73 (dd, *J* = 10.7, 8.4 Hz, 1H), 7.65 – 7.55 (m, 2H), 5.70 (d, *J* = 8.4 Hz, 1H), 2.29 (s, 3H). **^{13}C-NMR** (101 MHz, $CDCl_3$): δ (ppm) = 201.7, 165.4, 138.3, 135.5, 132.6, 129.5, 129.2, 128.9, 128.6, 127.8, 127.1, 123.7, 104.8, 30.7. **R_f** = 0.23 (PE/EtOAc = 50/50) [$KMnO_4$]. **HRMS** (APCI-MS): $[C_{15}H_{14}NO_2]^+$ $[M + H]^+$ calcd: 240.1019; found: 240.1021.

Synthesis of (*Z*)-N-(3-oxobut-1-en-1-yl)furan-2-carboxamide (**15b**)

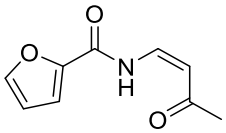

Prepared according to general procedure **GP5** from **15a** (18.1 mg, 100 µmol). The crude product was purified via FCC (PE/EtOAc = 55/45), to obtain **15b** as a white solid (8.8 mg, 49% yield).

^{1}H-NMR (400 MHz, $CDCl_3$): δ (ppm) = 12.30 (s, 1H), 7.60 (dd, *J* = 1.7, 0.8 Hz, 1H), 7.55 (dd, *J* = 11.1, 8.5 Hz, 1H), 7.30 (dd, *J* = 3.5, 0.7 Hz, 1H), 6.57 (dd, *J* = 3.6, 1.7 Hz, 1H), 5.64 (d, *J* = 8.5 Hz, 1H), 2.25 (s, 3H). **^{13}C-NMR** (101 MHz, $CDCl_3$): δ (ppm) = 201.2, 146.5, 145.9, 136.6, 117.3, 112.7, 104.9, 30.7. **R_f** = 0.20 (PE/EtOAc = 55/45) [$KMnO_4$]. **HRMS** (APCI-MS): $[C_9H_{10}NO_3]^+$ $[M + H]^+$ calcd: 180.0655; found: 180.0656.

Synthesis of *N*-(2-methoxyvinyl)benzamide (**16b**)

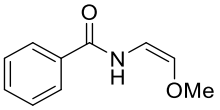

Z

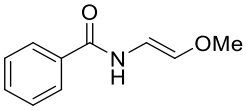

E

Prepared according to general procedure **GP5** from **16a** (17.9 mg, 100 µmol). The crude product was purified via FCC (PE/EtOAc = 60/40), to obtain **16b** (13.8 mg, 78% yield) as a diastereoisomeric mixture (*Z*/*E* = 3:2).

Z isomer: White solid. **^{1}H-NMR** (400 MHz, $CDCl_3$): δ (ppm) = 7.83 (d, *J* = 3.1 Hz, 1H), 7.80 (d, *J* = 1.5 Hz, 1H), 7.53 – 7.40 (m, 3H), 6.38 (dd, *J* = 10.3, 4.7 Hz, 1H), 5.70 (d, *J* = 4.8 Hz, 1H), 3.68 (s, 3H). **^{13}C-NMR** (101 MHz, $CDCl_3$): δ (ppm) = 163.5, 134.0, 133.8, 131.7, 128.6, 127.0, 104.1, 60.1. **R_f** = 0.35 (PE/EtOAc = 60/40) [$KMnO_4$]. **HRMS** (EI-MS): $[C_{10}H_{11}NO_2]^{\cdot+}$ $[M]^{\cdot+}$ calcd: 177.0784; found: 177.0783.

E isomer: White solid. **^{1}H-NMR** (400 MHz, $CDCl_3$): δ (ppm) = 8.07 (d, *J* = 6.7 Hz, 1H), 7.83 – 7.76 (m, 2H), 7.49 – 7.43 (m, 1H), 7.37 (t, *J* = 7.5 Hz, 2H), 6.83 (d, *J* = 12.0 Hz, 1H), 6.56 (dd, *J* = 12.0, 9.1 Hz, 1H), 3.54 (s, 3H). **^{13}C-NMR** (101 MHz, $CDCl_3$): δ (ppm) = 164.9, 140.2, 133.9, 131.5, 128.5, 127.0, 104.9, 56.7. **R_f** = 0.20 (PE/EtOAc = 60/40) [$KMnO_4$]. **HRMS** (EI-MS): $[C_{10}H_{11}NO_2]^{\cdot+}$ $[M]^{\cdot+}$ calcd: 177.0784; found: 177.0783.

Synthesis of methyl (*E*)-3-benzamidoacrylate (**17b**)

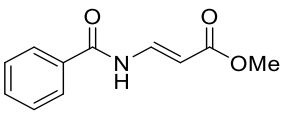

Prepared according to general procedure **GP5** from **17a** (20.7 mg, 100 µmol). The product was purified via FCC (PE/Acetone = 85/15), to obtain **17b** as a white solid (10.3 mg, 50% yield).

^{1}H-NMR (400 MHz, CD_3CN): δ (ppm) = 9.35 (d, *J* = 6.5 Hz, 1H), 8.07 (dd, *J* = 14.3, 11.2 Hz, 1H), 7.89 (dt, *J* = 8.5, 1.7 Hz, 2H), 7.64 – 7.58 (m, 1H), 7.54 – 7.49 (m, 2H), 5.73 (d, *J* = 14.3 Hz, 1H), 3.68 (s, 3H). **^{13}C-NMR** (101 MHz, CD_3CN): δ (ppm) = 168.6, 166.1, 139.3, 133.7, 133.5, 129.7, 128.7, 118.3, 102.1, 51.8. **R_f** = 0.23 (PE/Acetone = 85/15) [$KMnO_4$]. **HRMS** (APCI-MS): $[C_{11}H_{12}NO_3]^+$ $[M + H]^+$ calcd: 206.0812; found: 206.0814.

Synthesis of *N*-vinylbenzamide (**18b**)

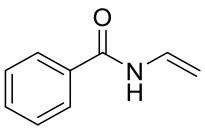

Prepared according to general procedure **GP5** from **18a** (14.9 mg, 100 µmol). The crude product was purified via FCC (PE/EtOAc = 75/25), to obtain **18b** as a white solid (7.7 mg, 52% yield).

^{1}H-NMR (400 MHz, $CDCl_3$): δ (ppm) = 7.95 (s, 1H), 7.81 (d, *J* = 7.3 Hz, 2H), 7.55 – 7.49 (m, 1H), 7.44 (t, *J* = 7.5 Hz, 2H), 7.19 (ddd, *J* = 15.9, 10.6, 8.9 Hz, 1H), 4.78 (d, *J* = 15.8 Hz, 1H), 4.53 (d, *J* = 8.7 Hz, 1H). **^{13}C-NMR** (101 MHz, $CDCl_3$): δ (ppm) = 164.7, 133.5, 132.1, 129.1, 128.7, 127.1, 96.2. **R_f** = 0.21 (PE/EtOAc = 75/25) [$KMnO_4$]. **HRMS** (APCI-MS): $[C_9H_{10}NO]^+$ $[M + H]^+$ calcd: 148.0757; found: 148.0755.

Synthesis of 4-methoxy-*N*-vinylbenzamide (**19b**)

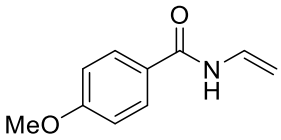

Prepared according to general procedure **GP5** from **19a** (17.9 mg, 100 µmol). The crude product was purified via FCC (PE/EtOAc = 70/30), to obtain **19b** as a white solid (9.8 mg, 55% yield).

^{1}H-NMR (400 MHz, $CDCl_3$): δ (ppm) = 7.80 – 7.76 (m, 2H), 7.72 (d, *J* = 8.5 Hz, 1H), 7.19 (ddd, *J* = 15.8, 10.7, 8.9 Hz, 1H), 6.97 – 6.91 (m, 2H), 4.73 (d, *J* = 15.8 Hz, 1H), 4.50 (d, *J* = 8.7 Hz, 1H), 3.86 (s, 3H). **^{13}C-NMR** (101 MHz, $CDCl_3$): δ (ppm) = 164.0, 162.7, 129.2, 129.0, 125.7, 114.0, 95.4, 55.5. **R_f** = 0.22 (PE/EtOAc = 70/30) [$KMnO_4$]. **HRMS** (APCI-MS): $[C_{10}H_{12}NO_2]^+$ $[M + H]^+$ calcd: 178.0863; found: 178.0862.

Synthesis of 4-fluor-*N*-vinylbenzamide (**20b**)

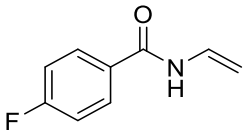

Prepared according to general procedure **GP5** from **20a** (16.7 mg, 100 µmol). The crude product was purified via FCC (PE/EtOAc = 75/25), to obtain **20b** as a white solid (8.1 mg, 49% yield).

^{1}H-NMR (400 MHz, $CDCl_3$): δ (ppm) = 8.10 – 7.67 (m, 3H), 7.22 – 7.03 (m, 3H), 4.78 (d, *J* = 15.8 Hz, 1H), 4.54 (d, *J* = 8.7 Hz, 1H). **^{13}C-NMR** (101 MHz, $CDCl_3$): δ (ppm) = 166.3, 163.8, 163.6, 129.6, 129.5, 129.0, 116.0, 115.7, 96.4. **^{19}F-NMR** (377 MHz, $CDCl_3$): δ (ppm) = -107.5. **R_f** = 0.20 (PE/EtOAc = 75/25) [$KMnO_4$]. **HRMS** (APCI-MS): $[C_9H_9FNO]^+$ $[M + H]^+$ calcd: 166.0668; found: 166.0665.

Synthesis of 4-chloro-*N*-vinylbenzamide (**21b**)

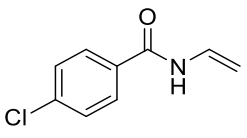

Prepared according to general procedure **GP5** from **21a** (18.4 mg, 101 µmol). The crude product was purified via FCC (PE/EtOAc = 80/20), to obtain **21b** as a pale-yellow solid (8.4 mg, 46% yield).

^{1}H-NMR (400 MHz, $CDCl_3$): δ (ppm) = 7.77 (t, *J* = 15.9 Hz, 3H), 7.43 (dd, *J* = 8.8, 2.0 Hz, 2H), 7.16 (ddd, *J* = 15.8, 10.5, 9.0 Hz, 1H), 4.79 (d, *J* = 15.8 Hz, 1H), 4.56 (d, *J* = 8.7 Hz, 1H).

^{13}C-NMR (101 MHz, $CDCl_3$): δ (ppm) = 163.5, 138.4, 131.8, 129.0, 128.8, 128.5, 96.6. **R_f** = 0.23 (PE/EtOAc = 80/20) [$KMnO_4$]. **HRMS** (APCI-MS): $[C_9H_9ClNO]^+$ [M + H]$^+$ calcd: 182.0373; found: 182.0369.

Synthesis of 4-(trifluoromethyl)-*N*-vinylbenzamide (**22b**)

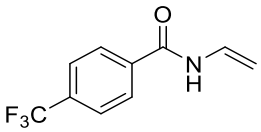

Prepared according to general procedure **GP5** from **22a** (21.7 mg, 100 µmol). The crude product was purified via FCC (PE/EtOAc = 80/20), to obtain **22b** as a white solid (9.2 mg, 43% yield).

^{1}H-NMR (400 MHz, $CDCl_3$): δ (ppm) = 7.92 (d, *J* = 8.1 Hz, 3H), 7.72 (d, *J* = 8.3 Hz, 2H), 7.17 (ddd, *J* = 15.8, 10.6, 8.9 Hz, 1H), 4.83 (d, *J* = 15.8 Hz, 1H), 4.60 (d, *J* = 8.7 Hz, 1H). **^{13}C-NMR** (101 MHz, $CDCl_3$): δ (ppm) = 163.4, 136.8, 133.8 (d, *J* = 32.8 Hz), 128.7, 127.6, 125.8 (q, *J* = 3.7 Hz), 124.9, 97.3. **^{19}F-NMR** (377 MHz, $CDCl_3$): δ (ppm) = -63.6. **R_f** = 0.22 (PE/EtOAc = 80/20) [$KMnO_4$]. **HRMS** (APCI-MS): $[C_{10}H_9F_3NO]^+$ [M + H]$^+$ calcd: 206.0636; found: 206.0633.

Synthesis of (*E*)-N-(prop-1-en-1-yl)benzamide (**23b**)

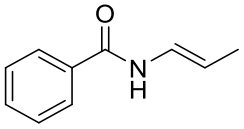

Prepared according to general procedure **GP5** from **23a** (16.3 mg, 100 µmol). The crude product was purified via FCC (PE/EtOAc = 85/15), to obtain **23b** as a white solid (7.6 mg, 47% yield).

^{1}H-NMR (400 MHz, $CDCl_3$): δ (ppm) = 7.90 – 7.68 (m, 3H), 7.56 – 7.46 (m, 1H), 7.46 – 7.37 (m, 2H), 6.95 (ddd, *J* = 14.1, 10.4, 1.7 Hz, 1H), 5.32 (dq, *J* = 13.5, 6.7 Hz, 1H), 1.73 (dd, *J* = 6.7, 1.6 Hz, 3H). **^{13}C-NMR** (101 MHz, $CDCl_3$): δ (ppm) = 164.2, 133.8, 131.7, 128.6, 127.0, 123.6, 108.9, 14.9. **R_f** = 0.24 (PE/EtOAc = 85/15) [$KMnO_4$]. **HRMS** (APCI-MS): $[C_{10}H_{12}NO]^+$ [M + H]$^+$ calcd: 162.0913; found: 162.0915.

Synthesis of *N*-(2-methylprop-1-en-1-yl)benzamide (**24b**)

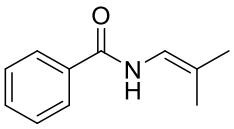

Prepared according to general procedure **GP5** from **24a** (17.7 mg, 100 µmol). The crude product was purified via FCC (PE/EtOAc = 95/5), to obtain **24b** as a white solid (5.3 mg, 30% yield).

^{1}H-NMR (400 MHz, $CDCl_3$): δ (ppm) = 7.79 (dd, *J* = 5.3, 3.3 Hz, 2H), 7.59 – 7.35 (m, 5H), 6.83 – 6.69 (m, 1H), 1.79 – 1.68 (m, 6H). **^{13}C-NMR** (101 MHz, $CDCl_3$): δ (ppm) = 164.1, 134.2, 133.5, 131.7, 130.1, 128.7, 128.4, 126.9, 117.3, 116.4, 22.5, 16.6. **R_f** = 0.19 (PE/EtOAc = 95/5) [$KMnO_4$]. **HRMS** (APCI-MS): $[C_{11}H_{14}NO]^+$ [M + H]$^+$ calcd: 176.1075; found: 176.1074.

Synthesis of (*E*)-*N*-(but-1-en-1-yl)benzamide (**26b**)

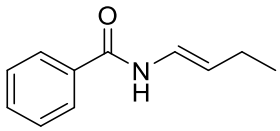

Prepared according to general procedure **GP5** from **26a** (17.7 mg, 100 µmol). The product was purified via FCC (PE/EtOAc = 90/10), to obtain **26b** as a colourless oil (8.4 mg, 48% yield).

^{1}H-NMR (400 MHz, $CDCl_3$): δ (ppm) = 7.90 (d, *J* = 8.1 Hz, 1H), 7.79 (dd, *J* = 5.2, 3.4 Hz, 2H), 7.52 – 7.37 (m, 3H), 7.00 – 6.88 (m, 1H), 5.43 – 5.32 (m, 1H), 2.09 (pd, *J* = 7.4, 1.5 Hz, 2H), 1.02 (t, *J* = 7.4 Hz, 3H). **^{13}C-NMR** (101 MHz, $CDCl_3$): δ (ppm) = 164.4, 133.8, 131.7, 128.6, 128.3, 127.0, 122.2, 116.1, 23.0, 14.2. $\mathbf{R_f}$ = 0.18 (PE/EtOAc = 90/10) [$KMnO_4$].

Synthesis of (*E*)-*N*-styrylbenzamide (**27b**)

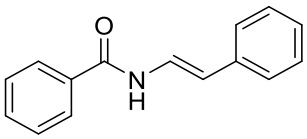

Prepared according to general procedure **GP5** from **27a** (22.5 mg, 100 µmol). The product was purified via FCC (PE/Acetone = 95/5), to obtain **27b** as a pale pink solid (12.6 mg, 56% yield).

^{1}H-NMR (400 MHz, CD_2Cl_2): δ (ppm) = 8.24 (d, *J* = 8.5 Hz, 1H), 8.14 – 8.09 (m, 1H), 7.87 (d, *J* = 7.4 Hz, 1H), 7.73 (dt, *J* = 19.0, 9.5 Hz, 1H), 7.67 – 7.46 (m, 4H), 7.40 – 7.17 (m, 4H), 6.33 (d, *J* = 14.7 Hz, 1H). **^{13}C-NMR** (101 MHz, CD_2Cl_2): δ (ppm) = 164.5, 136.3, 133.7, 133.6, 132.2, 130.1, 128.8, 128.7, 128.6, 127.1, 126.7, 125.6, 123.2, 113.5. $\mathbf{R_f}$ = 0.18 (PE/Acetone = 95/5) [$KMnO_4$]. **HRMS** (APCI-MS): $[C_{15}H_{13}NO]^+$ $[M + H]^+$ calcd: 224.1070; found: 224.1074.

Synthesis of (*E*)-4-methyl-*N*-styrylbenzamide (**28b**)

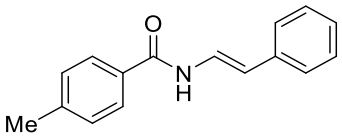

Prepared according to general procedure **GP5** from **28a** (23.9 mg, 100 µmol). The product was purified via FCC (PE/EtOAc = 90/10), to obtain **28b** as a white solid (11.6 mg, 49% yield).

^{1}H-NMR (400 MHz, $CDCl_3$): δ (ppm) = 8.03 (d, *J* = 10.1 Hz, 1H), 7.75 (t, *J* = 6.8 Hz, 3H), 7.36 – 7.26 (m, 6H), 7.19 (t, *J* = 7.2 Hz, 1H), 6.26 (d, *J* = 14.6 Hz, 1H), 2.41 (s, 3H). **^{13}C-NMR** (101 MHz, $CDCl_3$): δ (ppm) = 164.4, 142.8, 136.1, 130.5, 129.5, 128.7, 127.1, 126.7, 125.6, 123.2, 113.3, 21.5. $\mathbf{R_f}$ = 0.24 (PE/EtOAc = 90/10) [$KMnO_4$]. **HRMS** (EI-MS): $[C_{16}H_{15}NO]^{\cdot+}$ $[M]^{\cdot+}$ calcd: 237.1148; found: 237.1145.

Synthesis of (*E*)-4-methoxy-*N*-styrylbenzamide (**29b**)

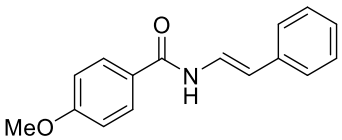

Prepared according to general procedure **GP5** from **29a** (25.5 mg, 100 µmol). The product was purified via FCC (PE/EtOAc = 90/10), to obtain **29b** as a white solid (14.7 mg, 58% yield).

^{1}H-NMR (400 MHz, $CDCl_3$): δ (ppm) = 7.94 – 7.80 (m, 3H), 7.40 – 7.23 (m, 6H), 6.97 (d, *J* = 8.1 Hz, 2H), 6.24 (d, *J* = 14.4 Hz, 1H), 3.87 (s, 3H). **^{13}C-NMR** (101 MHz, $CDCl_3$): δ (ppm) = 163.9, 162.8, 136.2, 130.2, 129.0, 128.7, 128.5, 126.7, 125.6, 123.3, 114.1, 113.0, 55.5. $\mathbf{R_f}$ = 0.20 (PE/EtOAc = 90/10) [$KMnO_4$]. **HRMS** (EI-MS): $[C_{16}H_{15}NO_2]^{\cdot+}$ $[M]^{\cdot+}$ calcd: 253.1097; found: 253.1093.

Synthesis of 4-fluoro-*N*-styrylbenzamide (**30b**)

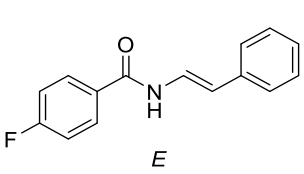

E

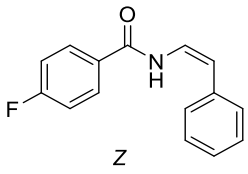

Z

Prepared according to general procedure **GP5** from **30a** (24.3 mg, 100 µmol). The crude product was purified via FCC (PE/EtOAc = 90/10), to obtain **30b** (11.4 mg, 47% yield) as a diastereoisomeric mixture (*E*/*Z* = 95:5).

E isomer: White solid. **^{1}H-NMR** (400 MHz, $CDCl_3$): δ (ppm) = 8.11 (d, *J* = 7.6 Hz, 1H), 7.87 (dd, *J* = 8.6, 5.3 Hz, 3H), 7.72 (dd, *J* = 14.5, 10.8 Hz, 1H), 7.39 – 7.29 (m, 4H), 7.16 (t, *J* = 8.6 Hz, 2H), 6.27 (d, *J* = 14.6 Hz, 1H). **^{13}C-NMR** (101 MHz, $CDCl_3$): δ (ppm) = 166.4, 163.4, 133.7, 130.2, 129.6, 129.5, 128.8, 128.5, 126.9, 125.7, 122.9, 116.1, 115.9, 113.8. **^{19}F-NMR** (377 MHz, $CDCl_3$): δ (ppm) = -107.2. **R_f** = 0.19 (PE/EtOAc = 90/10) [$KMnO_4$]. **HRMS** (ESI-MS): $[C_{15}H_{13}FNO]^+$ $[M + H]^+$ calcd: 242.0981; found: 242.0979.

Z isomer: White solid. **^{1}H-NMR** (400 MHz, $CDCl_3$): δ (ppm) = 8.29 (d, *J* = 8.8 Hz, 1H), 7.77 (dd, *J* = 8.7, 5.3 Hz, 2H), 7.44 (t, *J* = 7.6 Hz, 2H), 7.35 (d, *J* = 7.5 Hz, 2H), 7.29 (t, *J* = 7.4 Hz, 1H), 7.23 – 7.09 (m, 3H), 5.91 (d, *J* = 9.5 Hz, 1H). **^{13}C-NMR** (101 MHz, $CDCl_3$): δ (ppm) = 166.4, 163.3, 135.7, 129.5, 129.4, 129.3, 127.9, 127.2, 122.3, 116.1, 115.9, 111.1. **^{19}F-NMR** (377 MHz, $CDCl_3$): δ (ppm) = -107.2. **R_f** = 0.32 (PE/EtOAc = 90/10) [$KMnO_4$]. **HRMS** (ESI-MS): $[C_{15}H_{13}FNO]^+$ $[M + H]^+$ calcd: 242.0981; found: 242.0981.

Synthesis of *N*-(2-phenylprop-1-en-1-yl)benzamide (**31b**)

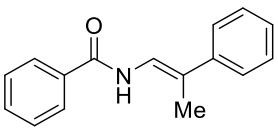

E

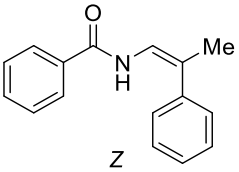

Z

Prepared according to general procedure **GP5** from **31a** (23.9 mg, 100 µmol). The crude product was purified via FCC (PE/EtOAc = 90/10), to obtain **31b** (13.2 mg, 56% yield) as a diastereoisomeric mixture (*E*/*Z* = 9:1).

E isomer: White solid. **^{1}H-NMR** (400 MHz, $CDCl_3$): δ (ppm) = 7.69 (d, *J* = 7.7 Hz, 2H), 7.61 (d, *J* = 10.1 Hz, 1H), 7.38 (t, *J* = 7.3 Hz, 1H), 7.35 – 7.23 (m, 5H), 7.17 (t, *J* = 7.6 Hz, 2H), 7.08 (dd, *J* = 9.4, 4.2 Hz, 1H), 1.96 (s, 3H). **^{13}C-NMR** (101 MHz, $CDCl_3$): δ (ppm) = 164.3, 140.9, 133.9, 132.0, 128.8, 128.4, 127.0, 126.7, 125.4, 119.9, 118.4, 14.5. **R_f** = 0.17 (PE/EtOAc = 90/10) [$KMnO_4$]. **HRMS** (ESI-MS): $[C_{16}H_{16}NO]^+$ $[M + H]^+$ calcd: 238.1232; found: 238.1232.

Z isomer: White solid. **^{1}H-NMR** (400 MHz, $CDCl_3$): δ (ppm) = 7.84 (d, *J* = 9.0 Hz, 1H), 7.66 – 7.62 (m, 2H), 7.50 – 7.31 (m, 8H), 7.10 (dd, *J* = 10.9, 1.4 Hz, 1H), 2.11 (d, *J* = 1.4 Hz, 3H). **^{13}C-NMR** (101 MHz, $CDCl_3$): δ (ppm) = 163.8, 139.5, 133.7, 131.8, 129.3, 128.7, 127.5, 126.9, 119.9, 118.5, 21.9. **R_f** = 0.27 (PE/EtOAc = 90/10) [$KMnO_4$]. **HRMS** (ESI-MS): $[C_{16}H_{16}NO]^+$ $[M + H]^+$ calcd: 238.1232; found: 238.1230.

Synthesis of *N*-styrylacetamide (**32b**)

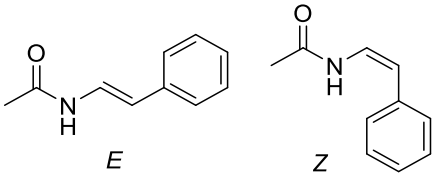

Prepared according to general procedure **GP5** from *N*-acetyl-2-phenylethylamine (16.3 mg, 100 µmol). The crude product was purified via FCC (PE/EtOAc = 75/25), to obtain **32b** (8.2 mg, 51% yield) as a diastereoisomeric mixture (*E*/*Z* = 95:5).

E isomer: White solid. **^{1}H-NMR** (400 MHz, $CDCl_3$): δ (ppm) = 7.64 – 7.43 (m, 2H), 7.24 (dt, *J* = 7.9, 5.7 Hz, 4H), 7.13 (t, *J* = 7.0 Hz, 1H), 6.06 (d, *J* = 14.4 Hz, 1H), 2.08 (s, 3H). **^{13}C-NMR** (101 MHz, $CDCl_3$): δ (ppm) = 167.5, 136.0, 128.6, 126.6, 125.5, 122.6, 112.5, 23.3. **R_f** = 0.22 (PE/EtOAc = 75/25) [$KMnO_4$]. **HRMS** (EI-MS): $[C_{10}H_{11}NO]^{\cdot+}$ $[M]^{\cdot+}$ calcd: 161.0835; found: 161.0840.

Z isomer: White solid. **^{1}H-NMR** (400 MHz, $CDCl_3$): δ (ppm) = 8.11 (d, *J* = 7.2 Hz, 1H), 7.61 (t, *J* = 7.4 Hz, 1H), 7.47 (t, *J* = 7.7 Hz, 1H), 7.40 (t, *J* = 7.7 Hz, 2H), 7.30 – 7.23 (m, 1H), 6.97 (dd, *J* = 11.1, 9.7 Hz, 1H), 5.75 (d, *J* = 9.6 Hz, 1H), 2.07 (s, 3H). **^{13}C-NMR** (101 MHz, $CDCl_3$): δ (ppm) = 167.6, 135.7, 133.6, 130.2, 129.1, 128.5, 127.9, 127.0, 122.1, 109.8, 23.5. **R_f** = 0.31 (PE/EtOAc = 75/25) [$KMnO_4$]. **HRMS** (EI-MS): $[C_{10}H_{11}NO]^{\cdot+}$ $[M]^{\cdot+}$ calcd: 161.0835; found: 161.0834.

Synthesis of benzyl (*E*)-styrylcarbamate (**33b**)

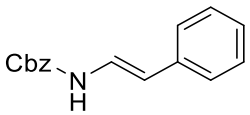

Prepared according to general procedure **GP5** from **33a** (25.5 mg, 100 µmol). The crude product was purified via FCC (PE/EtOAc = 85/15), to obtain **33b** as a white solid (12.7 mg, 50% yield).

^{1}H-NMR (400 MHz, $CDCl_3$): δ (ppm) = 7.44 – 7.33 (m, 5H), 7.27 (dd, *J* = 8.3, 3.5 Hz, 4H), 7.21 – 7.14 (m, 1H), 6.68 (d, *J* = 10.4 Hz, 1H), 5.97 (d, *J* = 14.6 Hz, 1H), 5.20 (s, 2H). **^{13}C-NMR** (101 MHz, $CDCl_3$): δ (ppm) = 153.5, 136.1, 135.8, 128.6, 128.4, 128.3, 126.3, 125.3, 123.9, 110.9, 67.4. **R_f** = 0.23 (PE/EtOAc = 85/15) [$KMnO_4$]. **HRMS** (ESI-MS): $[C_{16}H_{16}NO_2]^+$ $[M + H]^+$ calcd: 254.1181; found: 254.1180.

Synthesis of benzyl (*E*)-(3,4-dimethoxystyryl)carbamate (**34b**)

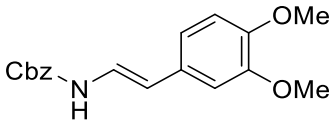

Prepared according to general procedure **GP5** from **34a** (31.5 mg, 101 µmol). The product was purified via FCC (PE/EtOAc = 75/25), to obtain **34b** as a white solid (16.7 mg, 53% yield).

^{1}H-NMR (400 MHz, $CDCl_3$): δ (ppm) = 7.40 – 7.32 (m, 5H), 7.13 (dd, *J* = 14.5, 11.0 Hz, 1H), 6.81 (d, *J* = 15.7 Hz, 3H), 6.69 (d, *J* = 10.8 Hz, 1H), 5.92 (d, *J* = 14.6 Hz, 1H), 5.18 (s, 2H), 3.87 (s, 3H), 3.86 (s, 3H). **^{13}C-NMR** (101 MHz, $CDCl_3$): δ (ppm) = 153.5, 149.1, 147.9, 135.8, 129.1, 128.6, 128.4, 128.3, 122.4, 118.3, 111.3, 110.9, 107.6, 67.4, 55.9, 55.8. **R_f** = 0.21 (PE/EtOAc = 75/25) [$KMnO_4$]. **HRMS** (ESI-MS): $[C_{18}H_{20}NO_4]^+$ $[M + H]^+$ calcd: 314.1392; found: 314.1390.

Synthesis of methyl 2-(4-(2-(4-chlorobenzamido)vinyl)phenoxy)-2-methylpropanoate (**35b**)

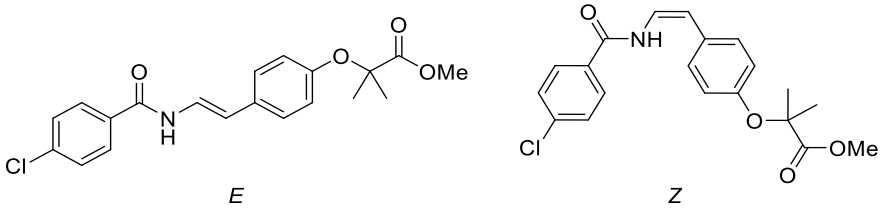

E *Z*

Prepared according to general procedure **GP5** from **35a** (37.6 mg, 100 µmol). The crude product was purified via FCC (PE/EtOAc = 75/25), to obtain **35b** (19.1 mg, 51% yield) as a diastereoisomeric mixture (*E*/*Z* = 9:1).

E isomer: White solid. **^{1}H-NMR** (400 MHz, $CDCl_3$): δ (ppm) = 7.93 (d, *J* = 10.5 Hz, 1H), 7.61 (d, *J* = 8.5 Hz, 2H), 7.39 (dd, *J* = 14.6, 10.6 Hz, 1H), 7.28 – 7.22 (m, 2H), 7.03 (d, *J* = 8.7 Hz, 2H), 6.63 – 6.56 (m, 2H), 6.04 (d, *J* = 14.6 Hz, 1H), 3.60 (s, 3H), 1.42 (s, 6H). **^{13}C-NMR** (101 MHz, $CDCl_3$): δ (ppm) = 174.8, 163.4, 154.4, 138.4, 131.9, 130.0, 129.0, 128.5, 126.5, 121.8, 119.4, 113.6, 79.2, 52.5, 25.3. **R_f** = 0.20 (PE/EtOAc = 75/25) [$KMnO_4$]. **HRMS** (ESI-MS): $[C_{20}H_{21}ClNO_4]^+$ $[M + H]^+$ calcd: 374.1159; found: 374.1158.

Z isomer: Pale-yellow solid. **^{1}H-NMR** (400 MHz, $CDCl_3$): δ (ppm) = 8.22 (d, *J* = 10.7 Hz, 1H), 7.68 (d, *J* = 8.5 Hz, 2H), 7.48 – 7.39 (m, 2H), 7.22 (d, *J* = 8.6 Hz, 2H), 7.15 – 7.05 (m, 1H), 6.92 – 6.83 (m, 2H), 5.84 (d, *J* = 9.4 Hz, 1H), 3.78 (s, 3H), 1.62 (s, 6H). **^{13}C-NMR** (101 MHz, $CDCl_3$): δ (ppm) = 174.6, 163.3, 154.4, 138.5, 131.8, 129.4., 129.1, 128.8, 128.5, 121.5, 119.6, 110.9, 79.2, 52.6, 25.4. **R_f** = 0.29 (PE/EtOAc = 75/25) [$KMnO_4$]. **HRMS** (ESI-MS): $[C_{20}H_{21}ClNO_4]^+$ $[M + H]^+$ calcd: 374.1159; found: 374.1159.

Synthesis of methyl 3-(((benzyloxy)carbonyl)amino)acrylate (**36b**)

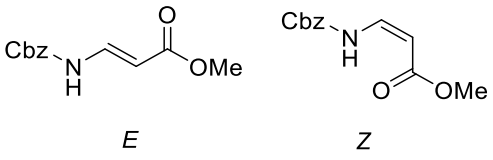

E *Z*

Prepared according to general procedure **GP5** from **36a** (23.7 mg, 100 µmol). The product was purified via FCC (PE/EtOAc = 80/20), to obtain **36b** (8.7 mg, 37% yield) as a diastereoisomeric mixture (*E*/*Z* = 9:1).

E isomer:White solid. **^{1}H-NMR** (400 MHz, $CDCl_3$): δ (ppm) = 7.82 (t, *J* = 13.0 Hz, 1H), 7.42 – 7.31 (m, 5H), 7.01 (d, *J* = 10.7 Hz, 1H), 5.38 (d, *J* = 14.0 Hz, 1H), 5.21 (s, 2H), 3.71 (s, 3H). **^{13}C-NMR** (101 MHz, $CDCl_3$): δ (ppm) = 167.6, 152.7, 139.3, 135.1, 128.7, 128.7, 128.5, 99.8, 68.2, 51.4. **R_f** = 0.19 (PE/EtOAc = 80/20) [$KMnO_4$]. **HRMS** (ESI-MS): $[C_{12}H_{13}NO_4Na]^+$ $[M + Na]^+$ calcd: 258.0742; found: 258.0738.

Z isomer: White solid. **^{1}H-NMR** (400 MHz, $CDCl_3$): δ (ppm) = 9.80 (s, 1H), 7.47 – 7.30 (m, 5H), 7.29 (m, 1H), 5.21 (s, 2H), 5.07 (d, *J* = 8.7 Hz, 1H), 3.71 (s, 3H). **^{13}C-NMR** (101 MHz, $CDCl_3$): δ (ppm) = 169.2, 140.0, 135.3, 128.6, 128.6, 128.3, 67.9, 51.2. **R_f** = 0.30 (PE/EtOAc = 80/20) [$KMnO_4$]. **HRMS** (ESI-MS): $[C_{12}H_{13}NO_4Na]^+$ $[M + Na]^+$ calcd: 258.0742; found: 258.0739.

Synthesis of methyl (*E*)-3-(3-((((9H-fluoren-9-yl)methoxy)carbonyl)amino) propanamido) acrylate (**37b**)

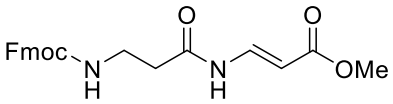

Prepared according to general procedure **GP5** from **37a** (39.6 mg, 100 µmol). Purification via FCC (PE/EtOAc = 60/40) yielded **37b** as a white solid (19.0 mg, 48% yield).

^{1}H-NMR (400 MHz, $CDCl_3$): δ (ppm) = 8.36 (s, 1H), 8.02 (m, 1H), 7.75 (d, *J* = 7.5 Hz, 2H), 7.55 (d, *J* = 7.4 Hz, 2H), 7.39 (t, *J* = 7.4 Hz, 2H), 7.30 (t, *J* = 7.3 Hz, 2H), 5.50 (d, *J* = 14.2 Hz, 1H), 5.40 (s, 1H), 4.38 (d, *J* = 6.4 Hz, 2H), 4.19 (t, *J* = 6.7 Hz, 1H), 3.73 (s, 3H), 3.49 (s, 2H), 2.54 (s, 2H). **^{13}C-NMR** (101 MHz, $CDCl_3$): δ (ppm) = 169.5, 167.7, 156.8, 143.7, 141.3, 137.3, 127.7, 127.1, 125.0, 120.0, 101.6, 66.9, 51.5, 47.1, 36.5. **R_f** = 0.21 (PE/EtOAc = 60/40) [$KMnO_4$]. **HRMS** (ESI-MS): $[C_{22}H_{23}N_2O_5]^+$ $[M + H]^+$ calcd: 395.1607; found: 395.1607.

Synthesis of *N*-(4-methoxystyryl)benzamide (**38b**)

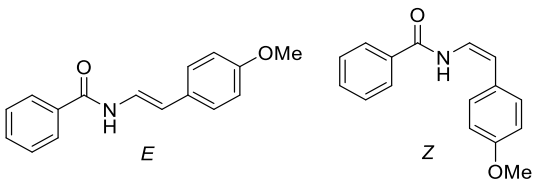

Prepared according to general procedure **GP5** from **38a** (25.5 mg, 100 µmol). Purification via FCC (PE/EtOAc = 75/15) yielded **38b** (15.3 mg, 60% yield) as a diastereoisomeric mixture (*E*/*Z* = 9:1).

E isomer: White solid. **^{1}H-NMR** (400 MHz, $CDCl_3$): δ (ppm) = 7.91 (d, *J* = 10.5 Hz, 1H), 7.86 – 7.83 (m, 1H), 7.67 – 7.44 (m, 5H), 7.30 (d, *J* = 8.7 Hz, 2H), 6.86 (d, *J* = 8.7 Hz, 2H), 6.23 (d, *J* = 14.6 Hz, 1H), 3.81 (s, 3H). **^{13}C-NMR** (101 MHz, $CDCl_3$): δ (ppm) = 164.4, 158.7, 133.6, 133.5, 132.1, 130.2, 128.8, 128.6, 128.5, 127.1, 126.8, 121.4, 114.2, 113.4, 55.3. **R_f** = 0.18 (PE/EtOAc = 75/15) [$KMnO_4$]. **HRMS** (ESI-MS): $[C_{16}H_{16}NO_2]^+$ $[M + H]^+$ calcd: 254.1181; found: 254.1181.

Z isomer: White solid. **^{1}H-NMR** (400 MHz, $CDCl_3$): δ (ppm) = 8.30 (d, *J* = 10.1 Hz, 1H), 7.76 (d, *J* = 7.2 Hz, 2H), 7.54 (dd, *J* = 8.5, 6.2 Hz, 1H), 7.46 (t, *J* = 7.5 Hz, 2H), 7.32 – 7.24 (m, 2H), 7.14 (dd, *J* = 10.8, 9.7 Hz, 1H), 7.01 – 6.92 (m, 2H), 5.85 (d, *J* = 9.4 Hz, 1H), 3.84 (s, 3H). **^{13}C-NMR** (101 MHz, $CDCl_3$): δ (ppm) = 164.3, 158.5, 133.5, 132.1, 129.1, 128.8, 128.1, 127.0, 121.4, 114.7, 110.8, 55.3. **R_f** = 0.23 (PE/EtOAc = 75/25) [$KMnO_4$]. **HRMS** (ESI-MS): $[C_{16}H_{16}NO_2]^+$ $[M + H]^+$ calcd: 254.1181; found: 254.1179.

Synthesis of *N*-((*E*)-styryl)cinnamamide (**39b**)

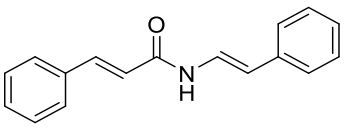

Prepared according to general procedure **GP5** from **39a** (25.1 mg, 100 µmol). The product was purified via FCC (PE/EtOAc = 85/15), to obtain **39b** as a bright yellow solid (11.4 mg, 46% yield).

^{1}H-NMR (400 MHz, $CDCl_3$): δ (ppm) = 7.77 (d, *J* = 15.5 Hz, 1H), 7.69 (dd, *J* = 14.5, 11.0 Hz, 1H), 7.53 (dd, *J* = 6.3, 2.8 Hz, 3H), 7.34 (ddd, *J* = 28.3, 10.8, 5.5 Hz, 7H), 7.19 (t, *J* = 7.2 Hz,

1H), 6.47 (d, *J* = 15.5 Hz, 1H), 6.19 (d, *J* = 14.5 Hz, 1H). **^{13}C-NMR** (101 MHz, $CDCl_3$): δ (ppm) = 162.9, 143.0, 136.0, 134.5, 130.2, 128.9, 128.7, 128.0, 126.8, 125.7, 122.9, 119.4, 113.3. **R_f** = 0.23 (PE/EtOAc = 85/15) [$KMnO_4$]. **HRMS** (APCI-MS): $[C_{17}H_{16}NO]^+$ [M + H]$^+$ calcd: 250.1232; found: 250.1230.

Synthesis of *N*-methyl-*N*-((*E*)-styryl)cinnamamide (**40b**)

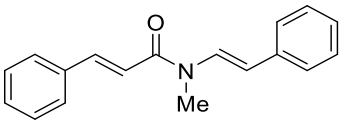

Prepared according to general procedure **GP5** from **40a** (26.5 mg, 100 µmol). The product was purified via FCC (PE/EtOAc = 85/15), to obtain **40b** as a pale green solid (11.9 mg, 45% yield).

^{1}H-NMR (400 MHz, $CDCl_3$): δ (ppm) = 7.77 (s, 1H), 7.58 (dd, *J* = 7.2, 2.1 Hz, 2H), 7.46 – 7.29 (m, 8H), 7.21 (d, *J* = 6.9 Hz, 1H), 7.03 (d, *J* = 15.4 Hz, 1H), 6.08 (d, *J* = 14.4 Hz, 1H), 3.37 (s, 3H). **^{13}C-NMR** (101 MHz, $CDCl_3$): δ (ppm) = 135.0, 130.1, 129.1, 129.0, 128.9, 128.8, 128.6, 128.3, 128.0, 126.6, 125.7, 117.1, 29.7. **R_f** = 0.25 (PE/EtOAc = 85/15) [$KMnO_4$]. **HRMS** (ESI-MS): $[C_{18}H_{18}NO]^+$ [M + H]$^+$ calcd: 264.1388; found: 264.1387.

Synthesis of 5-(4-methoxyphenyl)-2-phenyloxazole (**41**)

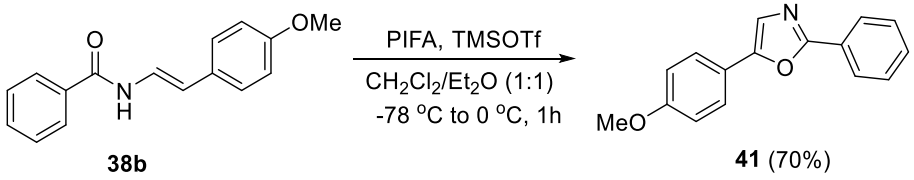

38b **41** (70%)

Compound **41** was synthesized following on a reported literature procedure.[40]

In a two-neck round bottom flask, substrate **38b** (50 mg, 1.00 equiv.) was dissolved in dry CH_2Cl_2/Et_2O (16 mL; 1:1 in Vol.) (8 ml) and the resulting solution was cooled to -78 °C. Next, phenyliodine bis(trifluoroacetate) (PIFA) (0.24 mmol, 1.20 equiv.) and TMSOTf (0.43 mmol, 2.20 equiv.) were added, and the reaction mixture was stirred at 0 °C for 1 h. Afterwards, the reaction mixture was diluted with CH_2Cl_2 (10 mL), washed with saturated aqueous $NaHCO_3$ solution (10 mL) and the product was extracted with CH_2Cl_2 (3 x 10 mL). The combined organic layers were dried over $MgSO_4$, and the solvent removed under reduced pressure. The crude product was purified via FCC (PE/EtOAc), obtaining compound **41** (70%) as a white solid.

^{1}H-NMR (400 MHz, $CDCl_3$): δ (ppm) = 8.10 (dd, *J* = 7.8, 1.5 Hz, 2H), 7.69 – 7.63 (m, 2H), 7.47 (q, *J* = 6.4 Hz, 3H), 7.33 (s, 1H), 6.97 (t, *J* = 5.7 Hz, 2H), 3.86 (s, 3H). **^{13}C-NMR** (101 MHz, $CDCl_3$): δ (ppm) = 160.6, 159.8, 151.3, 130.1, 128.8, 127.6, 126.1, 125.7, 121.9, 120.9, 114.4, 55.4. **HRMS** (APCI-MS): $[C_{16}H_{13}NO_2]^+$ [M + H]$^+$ calcd: 252.1019; found: 252.1019.

3.5 References

[1] a) P. H. Buist, *Nat. Prod. Rep.,* **2004**, *21*, 249–262; b) A. R. Moise, S. Al-Babili, E. T. Wurtzel, *Chem. Rev.* **2014**, *114*, 164–193.

[2] R. Breslow, *Chem. Soc. Rev*. **1972**, *1*, 553.

[3] a) G. E. Dobereiner, R. H. Crabtree, *Chem. Rev.* **2010**, *110*, 681–703; b) A. Kumar, T. M. Bhatti, A. S. Goldman, *Chem. Rev.* **2017**, *117*, *19*, 12357–12384; c) C. B. Bheeter, R. Jin, J. K. Bera, P. H. Dixneuf, H. Doucet, *Adv. Synth. Catal.* **2014**, *356*, 119–124; d) G. Li, P. A. Kates, A. K. Dilger, P. T. Cheng, W. R. Ewing, J. T. Groves, *ACS Catal.* **2019**, *9*, 9513–9517.

[4] a) R. Breslow, S. Baldwin, T. Flechtner, P. Kalicky, S. Liu, W. Washburn, *J. Am. Chem. Soc.* **1973**, *95*, 3251–3262; b) A.-F. Voica, A. Mendoza, W. R. Gutekunst, J. O. Fraga, P. S. Baran, *Nat. chem.* **2012**, *4*, 629–635; c) M. Parasram, P. Chuentragool, D. Sarkar, V. Gevorgyan, *J. Am. Chem. Soc.* **2016**, *138*, 6340–6343; d) M. Parasram, P. Chuentragool, Y. Wang, Y. Shi, V. Gevorgyan, *J. Am. Chem. Soc.* **2017**, *139*, 14857–14860; e) P. Chuentragool, M. Parasram, Y. Shi, V. Gevorgyan, *J. Am. Chem. Soc.* **2018**, *140*, 2465–2468; f) L. Huang, A. Bismuto, S. A. Rath, N. Trapp, B. Morandi, *Angew. Chem. Int. Ed.* **2021**, *60*, 7290–7296.

[5] H. Weissermel, H. J. Arpe in *Industrial Organic Chemistry*, 3rd ed., (Ed.: K. Sora), Wiley-VCH, Weinheim, **1997**, pp. 59.

[6] a) W.-M. Cheng, R. Shang, Y. Fu, *Nature Commun.* **2018**, *9*, 5215; b) S. Yang, H. Fan, L. Xie, G. Dong, M. Chen, *Org. Lett.* **2022**, *24*, 6460–6465.

[7] a) J. G. West, D. Huang, E. J. Sorensen, *Nat. Commun.* **2015**, *6*, 10093; b) K. C. Cartwright, J. A. Tunge, *ACS Catal.* **2018**, *8*, 11801–11806; c) M.-J. Zhou, L. Zhang, G. Liu, C. Xu, Z. Huang, *J. Am. Chem. Soc.* **2021**, *143*, 16470–16485; d) Ritu, S. Das, Y.-M. Tian, T. Karl, N. Jain, B. König, *ACS Catal.* **2022**, *12*, 10326–10332; e) M.-J. Zhou, G. Liu, C. Xu, Z. Huang, *Synthesis* **2022**.

[8] a) K.-H. He, F.-F. Tan, C.-Z. Zhou, G.-J. Zhou, X.-L. Yang, Y. Li, *Angew. Chem. Int. Ed.* **2017**, *56*, 3080–3084; b) Q. Yin, M. Oestreich, *Angew. Chem. Int. Ed.* **2017**, *56*, 7716–7718; c) S. U Dighe, F. Juliá, A. Luridiana, J. J. Douglas, D. Leonori, *Nature* **2020**, *584*, 75–81.

[9] a) S. Kato, Y. Saga, M. Kojima, H. Fuse, S. Matsunaga, A. Fukatsu, M. Kondo, S. Masaoka, M. Kanai, *J. Am. Chem. Soc.* **2017**, *139*, 2204–2207; b) H. Fuse, M. Kojima, H. Mitsunuma, M. Kanai, *Org. Lett.* **2018**, *20*, 2042–2045.

[10] R. C. Larock, *Comprehensive Organic Transformations*, 3rd ed., (Ed.: R.C Larock), Wiley, New York, **2018**.

[11] a) J. E. Moses, J. E. Baldwin, R. Marquez, R. M. Adlington, A. R. Cowley, *Org. Lett.* **2002**, *4*, 3731–3734; b) K. Takasu, N. Nishida, A. Tomimura, M. Ihara, *J. Org. Chem.* **2005**, *70*, 3957–3962; c) L. Dai et al., *Bioorg. Med. Chem. Lett.* **2015**, *25*, 34–37; d) M. J. Caulfield, G. G. Qiao, D. H. Solomon, *Chem. Rev.* **2002**, *102*, 3067–3084; e) Z. Rappopport, in *The Chemistry of Enamines,* Ed.; Wiley: New York, **1994**; f) G. Bernadat, G. Masson, *Synlett* **2014**, *25*, 2842–2867.

[12] a) J. R. Dehli, J. Legros, C. Bolm, *Chem. Commun.,* **2005**, 973–986; b) A. D. Bolig, M. Brookhart, *J. Am. Chem. Soc.,* **2007**, *129*, 14544–14545; c) K. Gopalaiah, H. B. Kagan, *Chem. Rev.,* **2011**, *111*, 4599–4657; d) P. Spieß, M. Berger, D. Kaiser, N. Maulide, *J. Am. Chem. Soc.,* **2021**, *143*, 10524–10529.

[13] C. Wang, L. M. Azofra, P. Dam, M. Sebek, N. Steinfeldt, J. Rabeah, O. El-Sepelgy, *ACS Catal.* **2022**, *12*, 8868–8876.

[14] J. L. Dempsey, B. S. Brunschwig, J. R. Winkler, H. B. Gray, *Acc. Chem. Res.* **2009**, *42*, 1995–2004.

[15] CCDC 2217876 contains the supplementary crystallographic data for this paper. These data can be obtained free of charge from The Cambridge Crystallographic Data Centre via www.ccdc.cam.ac.uk/structures.

[16] J. Hioe and H. Zipse, in *Encyclopedia of Radicals in Chemistry, Biology and Materials*, **2012**.

[17] Isomerization of the olefinic products might take place under the photochemical reaction conditions.

[18] J. R. Hanson, in *Functional Group Chemistry.* UK: The Royal Society of Chemistry, **2001**.

[19] a) M. Sambaiah, P. Thota, S. S. Kottawar, S. Yennam, K. Shiva Kumar and M. Behera, *ChemistrySelect* **2021**, *6*, 5406–5410; b) D. Calina, F. Carvalho, A. Oana Docea, in *Toxicological Risk Assessment and Multi-System Health Impacts from Exposure*, ed. A. M. Tsatsakis, Academic Press **2021**, 545–556; c) R. B. Rothman, J. R. Glowa, *Mol. Neurobiol.* **1995**, *11*, 1–19; d) D. Charvin, R. Medori, R. A. Hauser, O. Rascol, *Nat. Rev. Drug Discov.* **2018**, *17*, 804–822.

[20] a) H. Kusama, M. Nishiyama, S. Ikeda, *Folia Pharmacol. Jpn.* **1988**, *92*, 175–180; b) K. L. Goa, L. B. Barradell, G. L. Plosker, *Drugs* **1996**, *52*, 725–753; c) I. Goldenberg, M. Benderly, U. Goldbourt, *Vasc. Health Risk Manag.* **2008**, *4*, 131–141.

[21] a) A. Chatterjee, M. Chakrabarty, A. B. Kundu, *Aust. J. Chem.* **1975**, *28*, 457–460; b) R. Lin, X. Lin, Q. Su, B. Guo, Y. Huang, M.-A. Ouyang, L. Song, H. Xu, *Molecules* **2019**, *24*, 3764.

[22] J. H. Lin, *Phytochemistry* **1989**, *28*, 621–622.

[23] a) I. Stefanuti, S. A. Smith, R. J. Taylor, *Tetrahedron Lett.* **2000**, *41*, 3735–3738; b) A. E. Pasqua, F. D. Ferrari, J. J. Crawford, R. Marquez, *Tetrahedron Lett.* **2014**, *55*, 6042–6043.

[24] a) V. de Waele, O. Poizat, M. Fagnoni, A. Bagno, D. Ravelli, *ACS Catal.* **2016**, *6*, 7174–7182; b) L. Capaldo, D. Ravelli, *Eur. J. Org. Chem.* **2017**, *2017*, 2056–2071; c) D. Ravelli, M. Fagnoni, T. Fukuyama, T. Nishikawa, I. Ryu, *ACS Catal.* **2018**, *8*, 701–713.

[25] a) B.P. Branchaud, Y. L. Choi, *Tetrahedron Lett.* **1988**, *29*, 6037–6038; b) C. D. Garr, R. G. Finke, *J. Am. Chem. Soc.* **1992**, *114*, 10440–10445; c) H. Cao, Y. Kuang, X. Shi, K. L. Wong, B. B. Tan, J. M. C. Kwan, X. Liu, J. Wu, *Nat. Commun.* **2020**, *11*, 1956.

[26] a) G. N. Schrauzer, J. W. Sibert, R. J. Windgassen, *J. Am. Chem. Soc.* **1968**, *90*, 6681–6688; b) D. N. R. Rao, M. C. R. Symons, *J. Chem. Soc., Faraday Trans. 1* **1984**, *80*, 423–434; c) M. E. Weiss, L. M. Kreis, A. Lauber, E. M. Carreira, *Angew. Chem. Int. Ed.* **2011**, *50*, 11125–11128; d) X. Sun, J. Chen, T. Ritter, *Nat. chem.* **2018**, *10*, 1229–1233; e) H. Cao, H. Jiang, H. Feng, J. M. C. Kwan, X. Liu, J. Wu, *J. Am. Chem. Soc.* **2018**, *140*, 16360–16367; f) K. C. Cartwright, J. A. Tunge, *ACS Catal.* **2018**, *8*, 11801–11806; g) V. T. Nguyen, V. D. Nguyen, G. C. Haug, H. T. Dang, S. Jin, Z. Li, C. Flores-Hansen, B. S. Benavides, H. D. Arman, O. V. Larionov, *ACS Catal.* **2019**, *9*, 9485–9498; h) Q.-Y. Meng, T. E. Schirmer, K. Katou, B. König, *Angew. Chem. Int. Ed.* **2019**, *58*, 5723–5728; i) X. Wang, Y. Li, X. Wu, *ACS Catal.* **2022**, *12*, 3710–3718.

[27] a) P. Du, K. Knowles, R. Eisenberg, *J. Am. Chem. Soc.* **2008**, *130*, 12576–12577; b) T. Lazarides, T. McCormick, P. Du, G. Luo, B. Lindley, R. Eisenberg, *J. Am. Chem. Soc.* **2009**, *131*, 9192–9194.

[28] a) T. Yamase, N. Takabayashi, M. Kaji, *Dalton Trans.* **1984**, 793–799; b) X. Hu, B. S. Brunschwig, J. C. Peters, *J. Am. Chem. Soc.* **2007**, *129*, 8988–8998; c) P. Du, J. Schneider, G. Luo, W. W. Brennessel, R. Eisenberg, *Inorg. Chem.* **2009**, *48*, 4952–4962.

[29] F. Zhan, G. Liang, *Angew. Chem. Int. Ed.* **2013**, *52*, 1266–1269.

[30] E. Buitrago, H. Lundberg, H. Andersson, P. Ryberg, H. Adolfsson, *ChemCatChem* **2012**, *4*, 2082–2089.

[31] a) I. B. Perry, T. F. Brewer, P. J. Sarver, D. M. Schultz, D. A. DiRocco, D. W. C. MacMillan, *Nature* **2018**, *560*, 70; b) F. Babawale, K. Murugesan, R. Narobe, B. König, *Org. Lett*. **2022**, *24*, 4793–4797.

[32] a) C. Tanielian, R. Seghrouchni, C. Schweitzer, *J. Phys. Chem. A*. **2003**, *107*, 1102; b) J. West, D. Huang, E. Sorensen, *Nat Commun.* **2015**, *6*, 10093.

[33] D. Dailler, R. Rocaboy, O. Baudoin, *Angew. Chem. Int. Ed.* **2017**, *56*, 7218–7222.

[34] X. Li, X. Che, G.-H. Chen, J. Zhang, J.-L. Yan, Y.-F. Zhang, L.-S. Zhang, C.-P. Hsu, Y. Q. Gao, Z.-J. Shi, *Org. lett.* **2016**, *18*, 1234–1237.

[35] B. Yang, L. Shi, J. Wu, X. Fang, X. Yang, F. Wu, *Tetrahedron* **2013**, *69*, 3331–3337.

[36] S. Zhang, Y. Li, T. Wang, M. Li, L. Wen, W. Guo, *Org. lett.* **2022**, *24*, 1742–1746.

[37] S. Boonyarattanakalin, S. Athavankar, Q. Sun, B. R. Peterson, *J. Am. Chem. Soc.* **2006**, *128*, 386–387.

[38] H. Yao, Y. Tang, K. Yamamoto, *Tetrahedron Lett.* **2012**, *53*, 5094–5098.

[39] K. I. Galkin, E. G. Gordeev, V. P. Ananikov, *Adv. Synth.Catal.* **2021**, *363*, 1368–1378.

[40] C. Hempel, B. J. Nachtsheim, *Synlett.* **2013**, *24*, 2119– 2123.

4. Decarbonylation of Benzaldehydes by Dual Photoorgano-Cobalt Catalysis

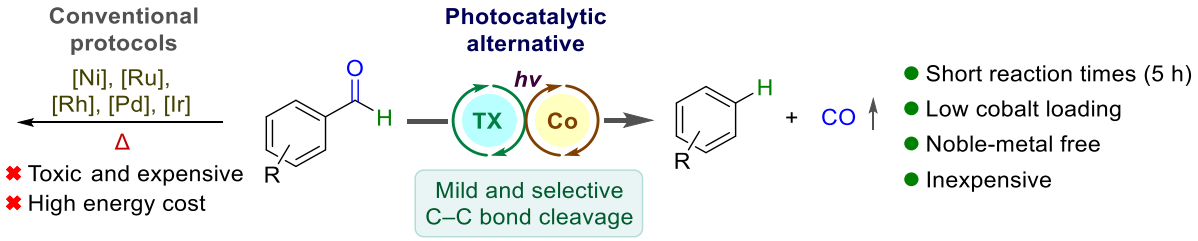

Abstract: We report a mild alternative to thermally driven noble-metal catalyzed decarbonylation protocols for the defunctionalization of benzaldehydes in short reaction times. Our cooperative photocatalytic system involves thioxanthone as an inexpensive HAT-agent and a cobalt complex required for selective C(sp^2)–C(sp^2) bond cleavage. The generated acyl and phenyl intermediates are postulated to be stabilized as cobalt complexes.

[i] Reproduced from D. Kolb, M. Morgenstern, B. König,* *Chem. Commun*. **2023**, *59*, 8592–8595. with permission from RSC. Schemes, tables, and text may differ from the published version.

[ii] Author contributions: D. Kolb and M. Morgenstern conceived the concept of this study and investigated the scientific background. D. Kolb optimized the reaction conditions, performed the photoreactions, and conducted the mechanistic investigations. M. Morgenstern synthesized the starting materials. D. Kolb wrote the manuscript and supporting information with input from M. Morgenstern. B. König supervised the project, reviewed the manuscript, and is the corresponding author.

4.1 Introduction

In nature, the defunctionalization of aldehydes to alkanes is catalyzed by enzymes known as decarbonylases in a mild fashion. Plants for instance apply this transformation for the biosynthesis of long-chain alkane waxes from aldehydes.[1] In the laboratory however, the main strategies in the chemist's repertoire depend on the combination of noble-metal catalysts and high temperatures, wherein C–H insertion of the metal into the aldehyde bond plays a key role (Scheme 1a).[2] In the last years, progress has been made within the field of photochemistry to offer milder and more sustainable alternatives. Simultaneously, there is growing interest for new methodologies designed to defunctionalize and process biologically derived materials, reducing its oxygen content by cleaving syngas (CO + H_2) for instance.[3] While photocatalytic spin center shift-based protocols have been successfully employed for the transformation of natural products such as sugars,[4] there is still a severe lack of photocatalytic procedures.

In this context, pioneering work by the Sorensen group provided a powerful cooperative base metal catalytic system for the sequential dehydroformylation of α-quaternary aldehydes involving a decarbonylation step (Scheme 1b).[5] However, the olefinic products are obtained as regioisomeric mixtures in low yields after long reaction times (48-96 h). This is partly due to the inefficiency of decantungstate as a photocatalyst, as it displays a low absorption coefficient for wavelengths above 365 nm[6] and tends to disproportionate with time.[7] In addition, non-α-

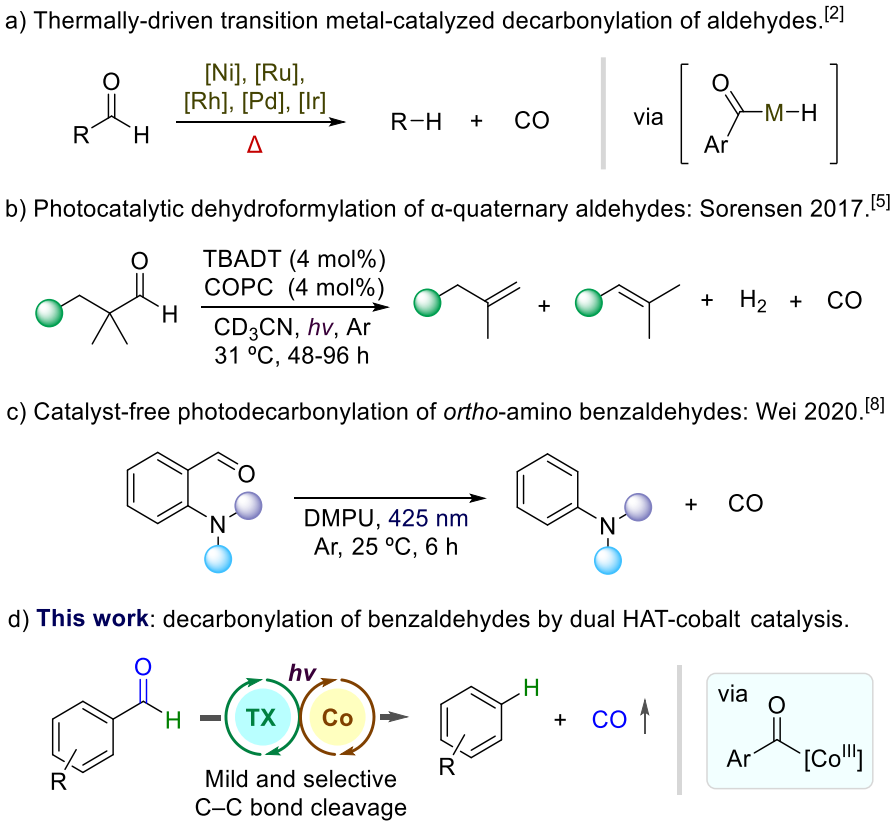

Scheme 4. Conventional and photochemical protocols for the decarbonylation of aldehydes.

quaternary aldehydes only deliver the corresponding alkenes in trace amounts, while benzaldehydes are mentioned as unsuitable substrates as they lead to the formation of "dead-end acyl radicals" which are unlikely to undergo decarbonylation. More recently, the Wei group reported a catalyst-free approach for the facile photodecarbonylation of *ortho*-amino benzaldehydes (Scheme 1c).[8] While several anilines could be prepared in good yields, the reaction is restricted to *ortho*-prefunctionalized substrates. In sight of the limitations of the above-mentioned methodologies, we developed a general method for the defunctionalization of benzaldehydes (Scheme 1d).

In our minds, a decarbonylation protocol compatible with naturally prevalent products would imply an important advance in the field of photocatalysis, as defunctionalization and deoxygenation methodologies have been gaining relevance in the last years. As an alternative to thermally-driven heterolytic metal C–H insertion into the aldehyde bond, we hypothesized that the generation of acyl radicals via hydrogen atom transfer (HAT) might be a milder solution for accessing equivalent acyl complexes. Hereby, the low bond-dissociation energy (BDE) of the aldehyde C–H bond[9] can be easily exploited by homolytic cleavage, simultaneously circumventing expensive noble-metal catalysts and high temperatures. Our system involves thioxanthone (TX) as a photocatalyst and a cobalt complex. TX stands particularly out for its unique properties: it is inexpensive, non-toxic and can mediate a variety of events including HAT.[10] Ultimately, the system allows to selectively cleave stable C(sp^2)–C(sp^2) bonds, operating via photoinduced C–H bond activation.

4.2 Results and Discussion

Inspired by Sorensen's photocatalytic system, we began our search with 4-*tert*-butylbenzaldehyde (**1a**) as model substrate and a synergistic HAT/cobalt system. Herein, TX proved to be the best option as a HAT-agent (Table S1). After optimizing the cobalt

Table 1. Screening of reaction conditions.

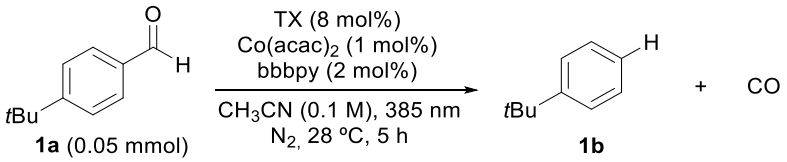

Entry	Deviation of optimized conditions	Yield of **1b** (%)[a]
1	-	94
2	EtOAc instead of CH_3CN	88
3	TBADT instead of TX	27
4	Benzophenone instead of TX	63

[a]GC-FID yields determined using mesitylene as I.S

source (Table S2), ligand (Table S3), solvent (Table S4), catalyst/ligand loadings (Tables S5 and S6), concentration (Table S7), temperature (Table S8), irradiation source (Table S9) and reaction time (Table S10), product **1b** was obtained in excellent yield (94%). Notably, the system worked best when using technical grade acetonitrile (215 ± 6 ppm H_2O) and low loadings of cobalt source (1 mol%) and 4,4′-di-*tert*-butyl-2,2′-dipyridyl (bbbpy) ligand (2 mol%). The reaction rendered excellent results as well when using ethyl acetate as a green solvent[11] (Table 1; entry 2).

With the optimized conditions in hand, we started the substrate scope with benzaldehyde (**2a**) and several naturally occurring alkyl-substituted derivatives (**3a**-**8a**),[12] which delivered the corresponding arenes (**3b**-**8b**) in good to excellent yields (61-95%) (Scheme 2). Interestingly, the benzylic positions of the substituents (**3b**-**8b**) were well tolerated due to the mild nature of TX as a HAT-agent. Even so, a slight decline in the reaction yield was observed when increasing the substitution degree of these positions (**5b**, **7b** and **8b**), presumably due to the weakening of the benzylic C–H bonds displayed by the *para*-substituents.[13] Alkoxy-

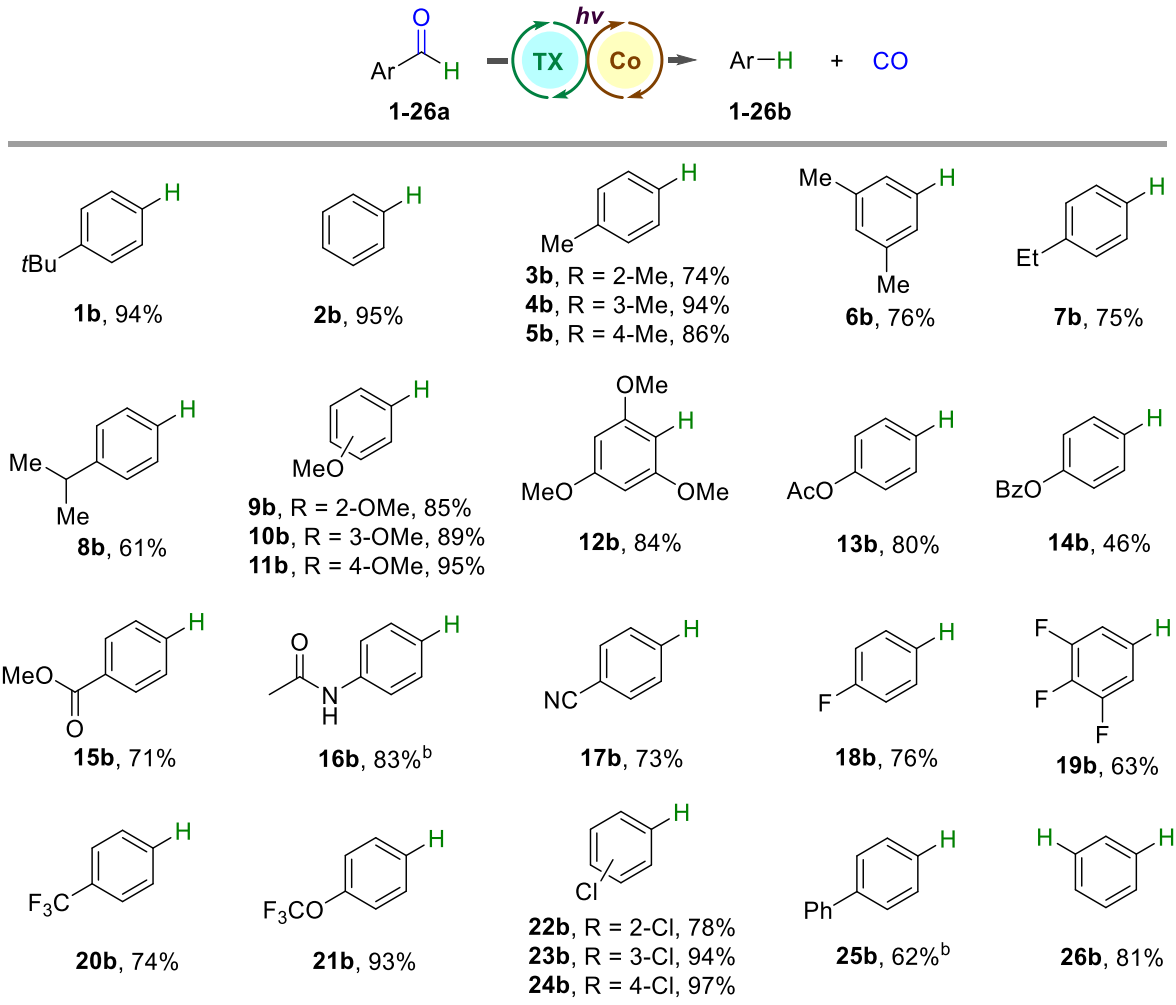

Scheme 2. Substrate scope. [a]Reaction conditions: a (0.05 mmol), TX (8 mol%), $Co(acac)_2$ (1 mol%), bbbpy (2 mol%), CH_3CN (0.5 mL), 385 nm LED (3.6 W), N_2, 28 °C, 5 h. GC-FID yields determined using mesitylene as I.S. [b]Isolated yield.

substituted homologues prevalent in nature (**9a**-**12a**)[14] reacted smoothly as well, giving products **9b** to **12b** with excellent results (84-95%). Remarkably, the sterically more hindered *ortho*-substitution of compounds **9a** and **12a**, had no significant impact on the reaction yield.

The functional group tolerance of the system was further explored with acetoxy- and benzoyloxy- *para*-substituted benzaldehydes, which were successfully decarbonylated to phenyl acetate (**13b**, 80%) and phenyl benzoate (**14b**, 46%) respectively. Substrates bearing ester (**15a**), amide (**16a**), and nitrile groups (**17a**) were tested as well, delivering the corresponding products (**15b**-**17b**) in very good yields (71-83%). Likewise, several halogenated compounds (**18b**-**24b**) were successfully prepared from their aldehyde precursors in high yields (63-97%). Comparably to **9a** and **12a**, the *ortho*-substitution pattern of **22a** had only limited impact on the reaction yield. Lastly, the system was applied for the defunctionalization of biphenyl-4-carboxaldehyde (**25a**) and for the two-fold decarbonylation of **26a**, obtaining biphenyl (**25b**, 62%) and benzene (**26b**, 81%) respectively.

Overall, electron- donating and withdrawing substituents were well tolerated. Regarding the limitations of the methodology, substrates bearing hydroxy- (**f1**), thioether- (**f2**), nitro- (**f3**) and carboxylic acid groups (**f4**) remained unreacted, while amino- (**f5**), and bromo- (**f6**) substituted derivatives degraded (Scheme S1). Moreover, aliphatic aldehydes had only limited success (Scheme S2).

To elucidate the reaction mechanism, a series of control experiments were carried out (Table 2). While the photochemical nature of the transformation could be confirmed (no reaction occurred in absence of light; entry 2), it was found that the use of TX as a light-driven HAT-agent was not essential (entry 3). Hereof, benzaldehydes can act themselves as HAT-agents towards weak C–H bonds under UV irradiation.[15] The overlap of the emission

Table 2. Screening of reaction conditions.

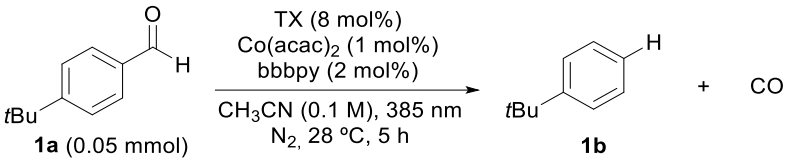

Entry	Deviation from optimized conditions	Yield of **1b** (%)[a]
1	-	94
2	No light	n.d.
3	No TX	46
4	No $Co(acac)_2$	9
5	No bbbpy	7
6	Under air	16

[a]GC-FID yields determined using mesitylene as I.S.

spectrum of the LEDs and the UV-Vis absorption spectrum of 1a (Figure S7) confirmed this self-catalyzed hypothesis as a plausible alternative mechanism to the TX-mediated HAT pathway. In contrast, the absence of our cobalt complex decreased significatively the reaction yield (Table 2, entries 4 and 5), which confirmed its key role in the decarbonylation process. Conducting the reaction under air led to lower yields due to quenching of the photocatalyst by oxygen (entry 6). Furthermore, GC-MS analysis of the reaction mixture revealed the formation of the corresponding benzophenone (**1c**) as by-product in trace amounts (Scheme 3a), suggesting the in situ generation of acyl and phenyl intermediates.[16] Based on this observation, a radical-scavenging experiment with TEMPO was performed (Scheme 3b). Hereby, the formation of the radical trapping products **R1** and **R2** was identified by LC-MS analysis. The corresponding phenyl-radical adduct (**R3**) however was not detected which suggests that the phenyl intermediate is likely to be stabilized as a closed-shell species. While detection of **R1** confirmed the formation of acyl radicals via HAT, **R2** evidenced the generation

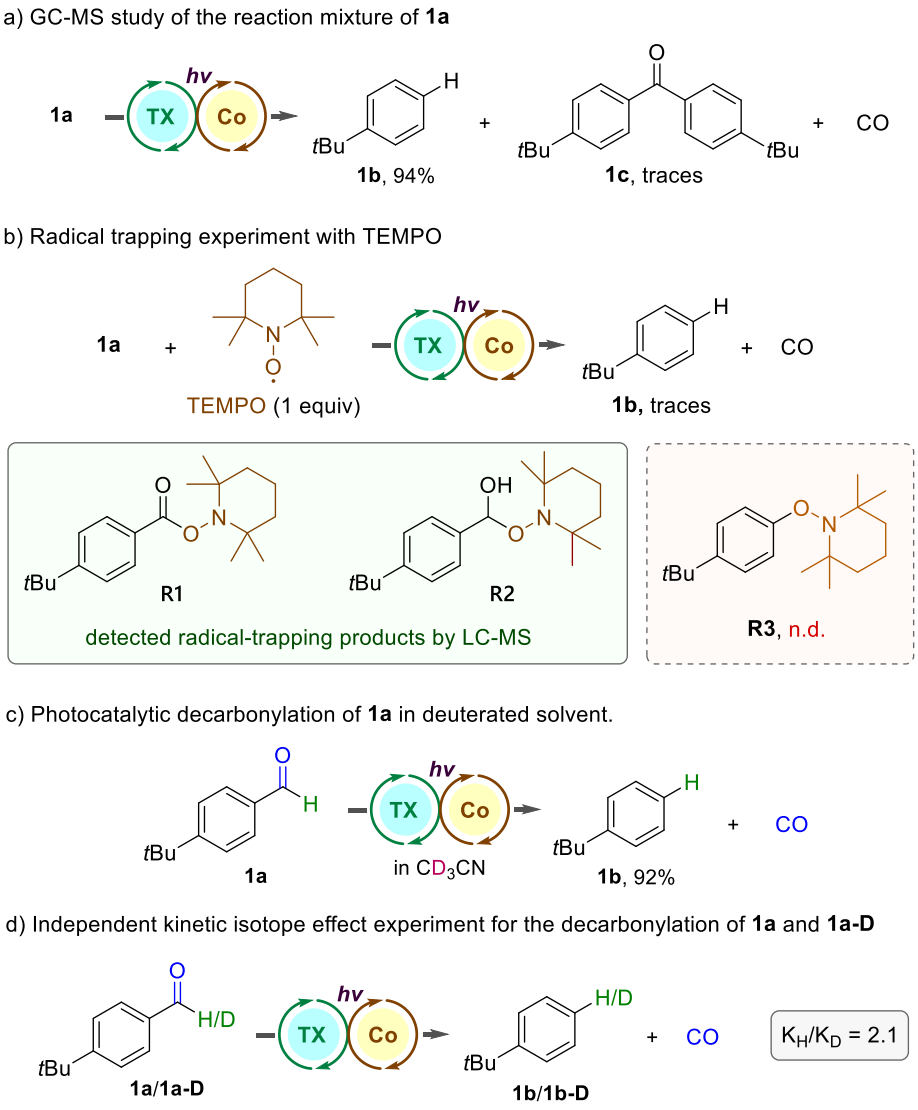

Scheme 3. Mechanistic studies. [a]Conditions: a (0.05 mmol), TX (8 mol%), $Co(acac)_2$ (1 mol%), bbbpy (2 mol%), CH_3CN (0.5 mL), 385 nm (3.6 W), N_2, 28 °C, 5 h. GC-FID yields using mesitylene as I.S.

of benzyl alcohol radicals, consequently supporting the alternative self-catalyzed decarbonylation pathway (Scheme S4). When conducting the decarbonylation of **1a** in deuterated acetonitrile, GC-MS and NMR-analysis revealed the exclusive formation of product **1b** without significant deuterium incorporation (Scheme 3c), ruling out solvent participation in the catalytic cycle. Moreover, an independent kinetic experiment between **1a** and its deuterated homologue **1a-D** was conducted (Scheme 3d). As a result, a significant primary kinetic isotope effect (KIE) was observed (K_H/K_D = 2.1), establishing the HAT event on the aldehydic C–H bond as the rate determining step (RDS) of the overall transformation.

Based on these findings, a general reaction mechanism was proposed (Scheme 4). First, upon excitation of the photocatalyst (PC) to its triplet state (PC*), a HAT-event takes place with benzaldehyde (**I**) leading to the generation of an acyl radical (**II**). This intermediate can then be trapped by the cobalt (II) complex (**III**) to form a cobalt (III) complex (**IV**). According to a previous report,[17] this acyl complex (**IV**) can presumably undergo decarbonylation to give intermediate **V** upon CO extrusion. The formed aryl-cobalt species (**V**) can then engage with the reduced form of the photocatalyst (PC$^{\bullet}$–H) regenerating its ground state (PC) via HAT. This event ultimately leads to the formation of the unfunctionalized arene (**VI**).

Furthermore, carbon monoxide evolution was confirmed by gas chromatography (Figure S17) and by performing an aminocarbonylation as test reaction,[18] wherein the drug moclobemide[19] was obtained in good yield (Scheme 5). Lastly, to demonstrate the potential of the methodology for reducing the oxygen content of natural product mixtures, an equimolar mixture of *ortho*-, *meta*- and *para*-substituted methoxy benzaldehydes was subjected to the optimized conditions. As a result, substrates **9a**, **10a** and **11a** were convergently defunctionalized to anisole in excellent yield (97%) after 16 h of irradiation (Scheme 6).

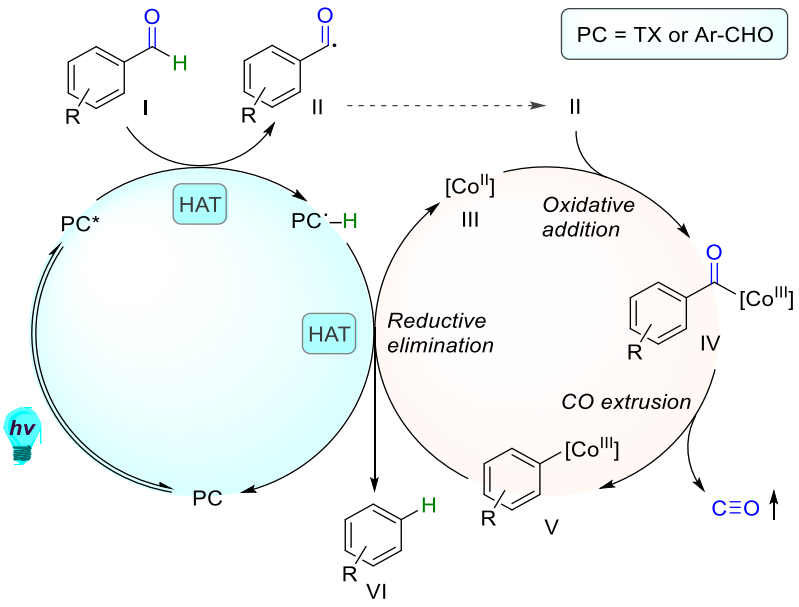

Scheme 4. Proposed general reaction mechanism.

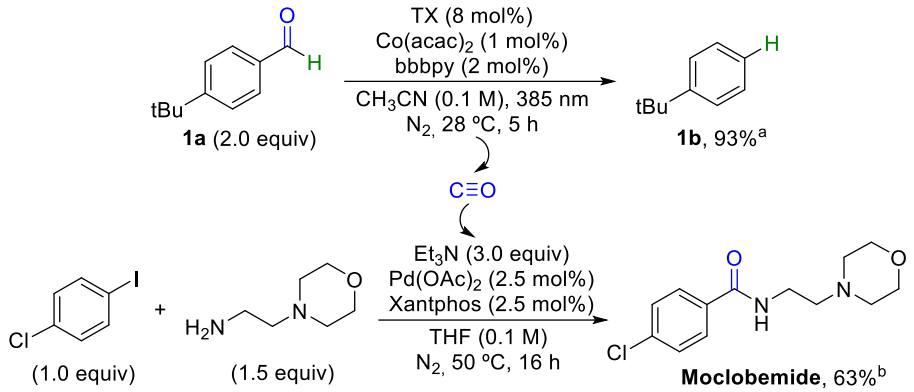

Scheme 5. Test reaction for CO evolution. [a]GC-FID yield using mesitylene as I.S. [b]Isolated yield.

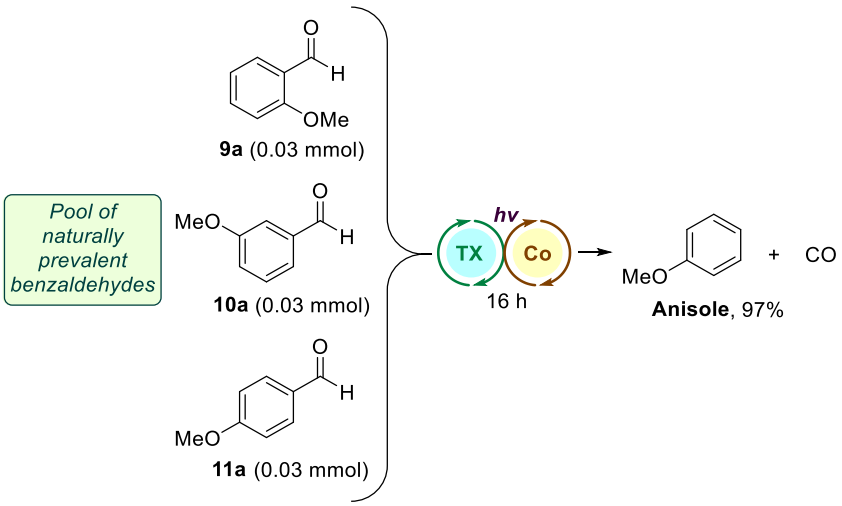

Scheme 6. Convergent defunctionalization of a mixture of methoxy substituted benzaldehydes (**9a**-**11a**). [a]Standard conditions; 16 h.

4.3 Conclusions

To summarize, we have developed a photocatalytic methodology for the decarbonylation of benzaldehydes by mild and selective C(sp^2)–C(sp^2) bond cleavage in short reaction times. The cooperative HAT/cobalt system exhibits broad functional tolerance and circumvents the use of heat and expensive noble-metal catalysts. The conducted mechanistic studies suggest the formation of acyl radicals and a cobalt-aryl complex as key intermediates. Investigations are ongoing for the further functionalization of the generated cobalt-aryl complex and the extension of the substrate scope.

4.4 Experimental Section

4.4.1 General Information

Chemicals and solvents: all commercially available chemicals were purchased in high quality and used without further purification. Solvents for column chromatography were distilled prior to use. Moisture and oxygen-sensitive reactions were carried out using dry solvents in oven-dried glassware under inert atmosphere of pre-dried nitrogen. The evaporation of solvents was carried out in a rotary evaporator at temperatures below 40 ºC, under reduced pressure. The water content of acetonitrile (215 ± 6 ppm water) used for photocatalyzed reactions was determined by Karl Fischer titration.

Flash Column Chromatography (FCC): flash silica gel (Merck, 40-63 µm) was used as the stationary phase. Binary eluent mixtures are reported as v/v solutions normalized to 100 volume units. Purification by automated flash column chromatography was performed on a Biotage® IsoleraTM Spektra One device using either pre-packed Biotage® columns or silica gel 60 M (particle size 40–63 µm, 230–440 mesh, Merck) self-packed columns.

Analytical TLC: performed on silica gel pre-coated aluminium sheets (Machery-Nagel, silica gel 60 G/UV254, 0.2 mm). Visualization was accomplished by exposure to UV-light (254 nm). Eluent mixtures for TLC are reported as v/v solutions normalized to 100 volume units.

Nuclear magnetic resonance (NMR): spectra were recorded at room temperature using a Bruker Avance 400 (400 MHz for ^{1}H, 101 MHz for ^{13}C) NMR spectrometer. Chemical shifts are reported in δ-scale as parts per million [ppm] relative to the solvent residual peaks as internal standard. Coupling constants *J* are given in Hertz [Hz] and the multiplicity of the signals is abbreviated as: singlet (s), broad singlet (bs), doublet (d), doublet of doublets (dd), triplet (t), doublet of triplets (dt), triplet of doublets (td), quadruplet (q), or multiplet (m). Signals are reported as follows: (multiplicity, coupling constant *J*, number of protons). Spectra were analyzed using MestReNova 6.0.2.

High Resolution Mass Spectrometry (HRMS): spectra were obtained from the central analytical mass spectrometry facilities of the Faculty of Chemistry and Pharmacy, University of Regensburg. All mass spectra were recorded on a Finnigan MAT 95, Thermo Quest Finnigan TSQ 7000, Finnigan MATSSQ 710 A or an Agilent Q-TOF 6540 UHD instrument.

GC-FID and GC-MS: GC measurements were performed on a GC 7890 from Agilent Technologies. Data acquisition and evaluation was done with Agilent Chem Station Rev.C.01.04. GC–MS measurements were performed on a 7890A GC system from Agilent Technologies with an Agilent 5975 MSD Detector. Data acquisition and evaluation was done with MSD Chem Station E.02.02.1431. A capillary column HP-5MS/30 mx 0.25 mm/0.25µM film and helium as carrier gas (flow rate of 1 mL/min) were used. The injector temperature (split

injection: 40:1 split) was 280 ºC, detection temperature 300 ºC (FID). GC measurements were made and investigated via integration of the signal obtained. The GC oven temperature program was adjusted as follows: initial temperature 40 ºC was kept for 3 minutes, the temperature was increased at a rate of 15 ºC/min over a period of 16 minutes until 280 ºC was reached and kept for 5 minutes, the temperature was again increased at a rate of 25 ºC/min over a period of 48 seconds until the final temperature (300 ºC) was reached and kept for 5 minutes.

Gas analyzer: evolved carbon monoxide analysis was performed on a micro-GC 3000 series (Inficon) provided with a 5A Molsieve column (10 m x 320 µm x 30 µm) and a TCD detector. Argon was used as carrier gas at 60 ºC for 3 min. Data acquisition and evaluation was done with EZ IQ from Inficon.

UV-Vis Spectroscopy: UV-Vis measurements were recorded with an Agilent 8453 spectrophotometer in acetonitrile as solvent.

Photoreactor setup: photoreactions were irradiated with LEDs (Engine LZ4-40UB00-00U5, λ = 385 nm (± 25), average radiant flux 3610 ± 45 mW, 89 V, 700 mA). Reaction mixtures were exposed to light under stirring (350 rpm, magnetic stirrer) from the bottom side of the vial. The temperature of the system was controlled by a water-cooling circuit consisting of an aluminium cooling block connected to a thermostat (Figure S1).

The optical power of the LEDs was determined using a FieldMaxII-TOTM laser power meter equipped with a PM3 sensor. The emission spectrum of the LEDs (Figure S2) was recorded using an Ocean Optics HR4000CG-UV-NIR Glass fiber and diffusor.

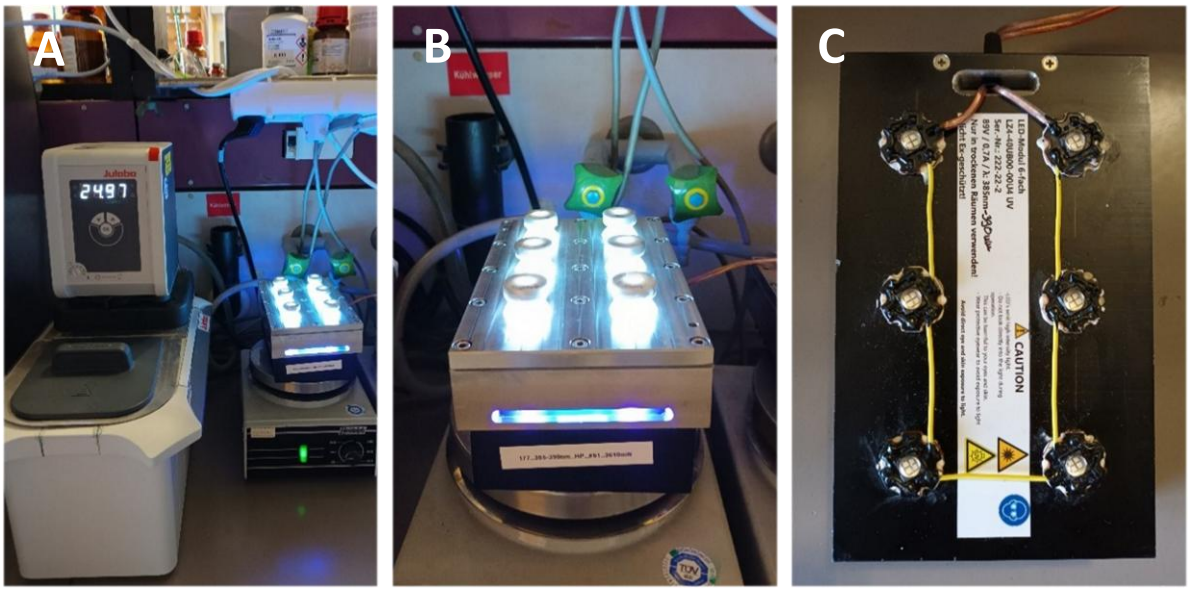

Figure S1. Photoreactor setup. A: Thermostat connected to the aluminium cooling block. B: Cooling block and LED on top of stirrer. C: LED module.

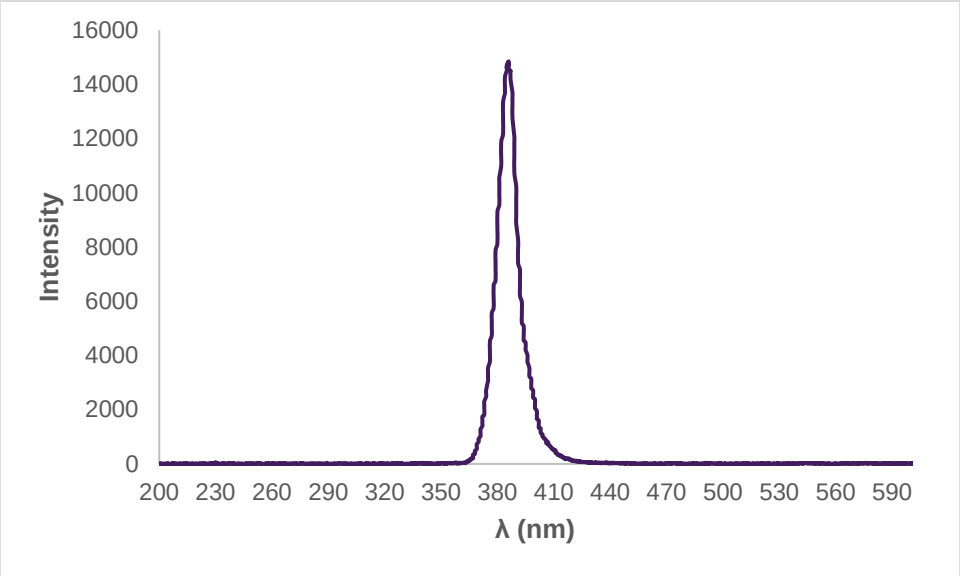

Figure S2. Emission spectrum of the LEDs used for the photoreactions.

Glassware absorption: photoreactions were carried out in WICOM® 20 mm crimp-cap vials (5 mL, 38.5 x 22.0 mm) made of borosilicate glass. The vials transmit 100% of incident light above 350 nm (Figure S3).

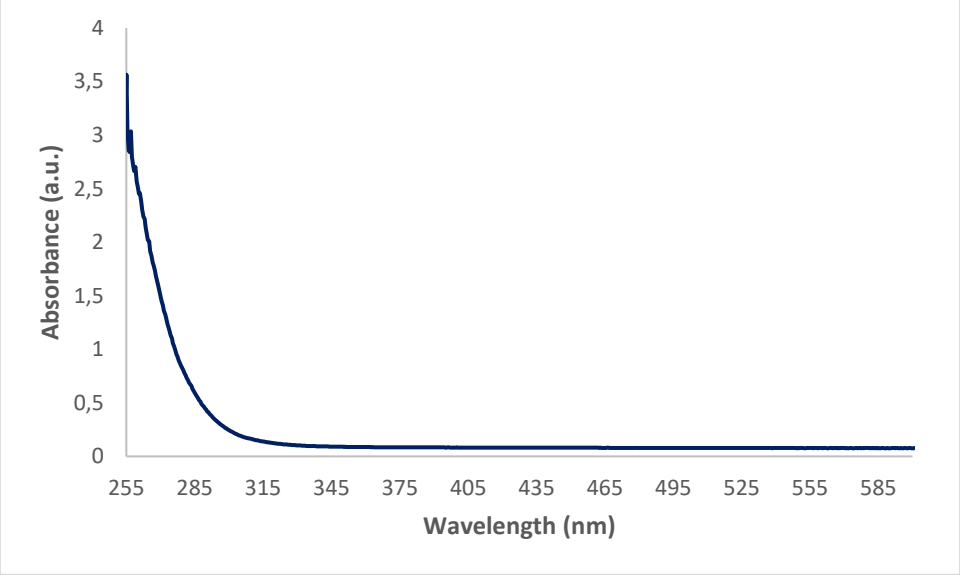

Figure S3. Absorption spectrum of vials used for photoreactions.

4.4.2 General Procedure for Photoreactions (GP1)

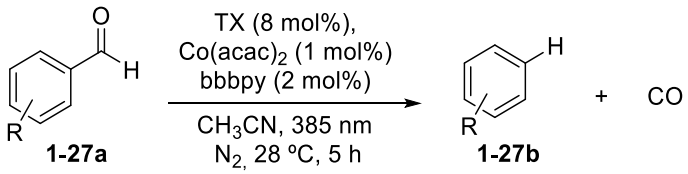

A 5 mL crimp-cap vial equipped with a stirring bar, was loaded with the corresponding benzaldehyde (50 µmol, 1.00 equiv.), thioxanthone (0.9 mg, 4 µmol, 8 mol%), cobalt (II) acetylacetonate (0.13 mg, 0.5 µmol, 1 mol%) and 4,4′-di-*tert*-butyl-2,2′-dipyridyl (0.27 mg, 1 µmol, 2 mol%). The vial was sealed, non-dried CH_3CN (0.5 mL) was added, and the mixture was sonicated for 1 min. After degassing via freeze-pump-thaw cycling (3 x), the reaction mixture was stirred under irradiation using a 3.6 W 385 nm (± 25 nm) LED set-up for 5 h at 28 ºC (temperature controlled by a thermostat). Reaction progress was monitored by TLC or GC-FID analysis. Afterwards, for compounds with relatively high vapor pressure, the reaction yield was determined via GC-FID analysis using mesitylene as internal standard (I.S.). For products **16b** and **25b**, the solvent was evaporated under reduced pressure, and the crude product was purified via FCC.

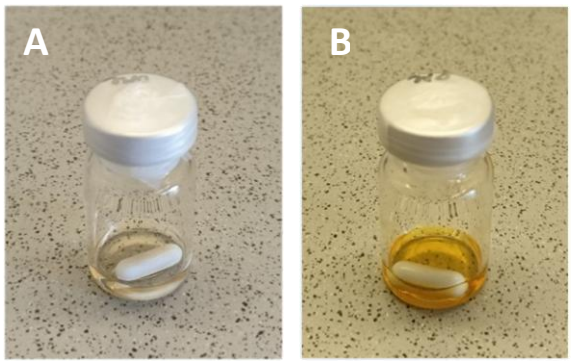

Figure S4. Vial containing reaction mixture of **1a**. A: before irradiation. B: after 5 h irradiation.

4.4.3 Reaction Conditions Optimization

Table S1. Screening of photocatalyst.

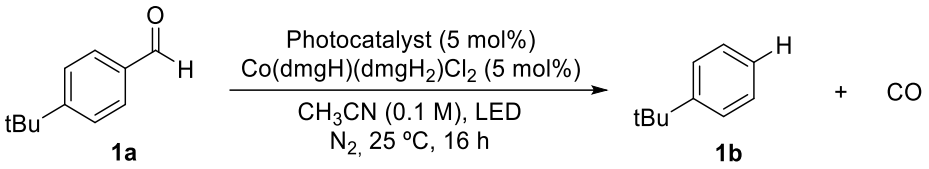

Entry	Photocatalyst	Irradiation	Yield of **1b** (%)[a]
1	Eosin Y	450 nm (1.3 W)	3
2	Rhodamine 6G	450 nm (1.3 W)	7
3	TBADT	395 nm (2.2 W)	52
4	Anthraquinone	395 nm (2.2 W)	11
5	2-Chloroanthraquinone	395 nm (2.2 W)	11
6	Xanthone	395 nm (2.2 W)	19
7	Thioxanthone	395 nm (2.2 W)	62
8	2-chlorothioxanthone	395 nm (2.2 W)	38
9	4-Methoxy-4'-trifluoromethylbenzophenone	365 (3.1 W)	32
10	Anthrone	365 (3.1 W)	19

1a (0.05 mmol), photocatalyst, Co(dmgH)(dmgH$_2$)Cl$_2$ (5 mol%), CH$_3$CN (0.5 mL), LED, 25 °C, 16 h, N$_2$. [a]Yields were determined by GC-FID analysis using mesitylene as I.S.

Table S2. Screening of co-catalyst.

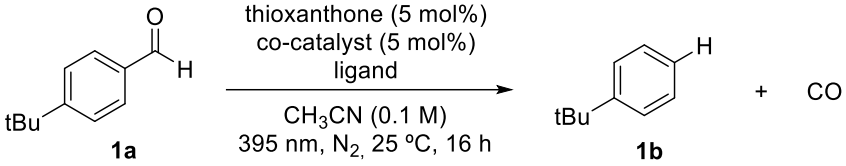

Entry	co-catalyst	Ligand (mol%)	Yield of **1b** (%)[a]
1	$Co(dmgH)(dmgH_2)Cl_2$	-	62
2	COPC	-	58
3	$Co(acac)_2$	-	28
4	$Co(acac)_2$	4,4′-di-*tert*-butyl-2,2′-dipyridyl (bbbpy) (10 mol%)	72
5	$Co(NO_3)_2{\cdot}6H_2O$	bbbpy (10 mol%)	48
6	$Co(OAc)_2$	bbbpy (10 mol%)	67
7	$CoCl_2$	-	37
8	$CoCl_2$	bbbpy (10 mol%)	62
9	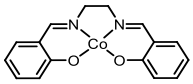	-	54
10	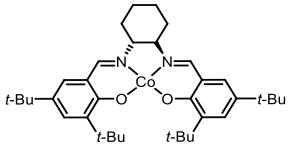	-	20
11	$CuCl_2$	bbbpy (10 mol%)	N.d.
12	$NiCl_2$	bbbpy (10 mol%)	N.d.
13	$FeCl_2$	bbbpy (10 mol%)	N.d.

1a (0.05 mmol), thioxanthone (5 mol%), co-catalyst (5 mol%), CH_3CN (0.5 mL), 395 nm LED (2.2 W), 25 ℃, 16 h, N_2. [a]Yields were determined by GC-FID analysis using mesitylene as I.S.

Table S3. Screening of ligand.

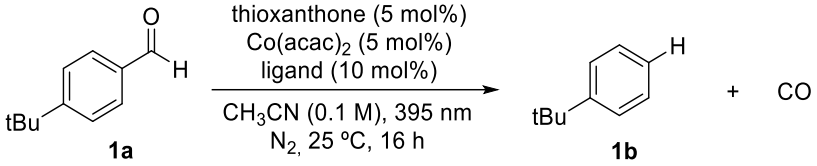

Entry	Ligand	Yield of **1b** (%)[a]
1	bbbpy (10 mol%)	72
2	2,2'-bipyridine	40
3	6,6′-Dimethyl-2,2′-bipyridyl	34
4	Neocuproin	25
5	Pyridine	21

1a (0.05 mmol), thioxanthone (5 mol%), $Co(acac)_2$ (5 mol%), ligand, CH_3CN (0.5 mL), 395 nm LED (2.2 W), 25 ℃, 16 h, N_2. [a]Yields were determined by GC-FID analysis using mesitylene as I.S.

Table S4. Screening of solvent.

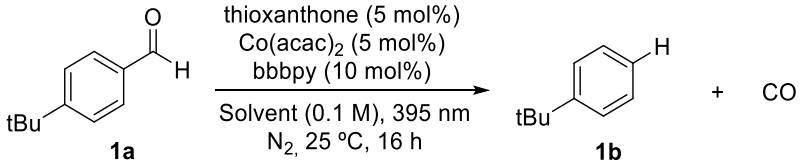

Entry	Solvent	Yield of **1b** (%)[a]
1[b]	Non-dry CH_3CN (215 ± 6 ppm water)	72
2	Dry CH_3CN	66
3	CH_3CN/H_2O (9/1 in vol.)	6
4	EtOAc	70
5	Dry CH_2Cl_2	10
6	Dry acetone	51
7	Dry MeOH	9

1a (0.05 mmol), thioxanthone (5 mol%), $Co(acac)_2$ (5 mol%), bbbpy (10 mol%) solvent (0.5 mL), 395 nm LED (2.2 W), 25 ℃, 16 h, N_2. [a]Yields were determined by GC-FID analysis using mesitylene as I.S. [b]water content determined by Karl-Fischer titration.

.

Table S5. Screening of photocatalyst loading.

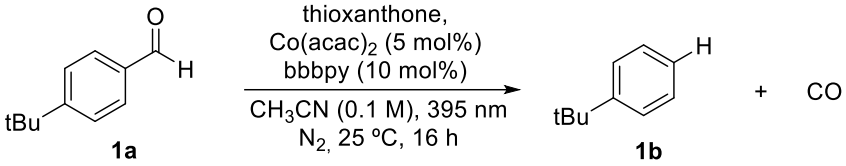

Entry	Photocatalyst (mol%)	Yield of **1b** (%)[a]
1	thioxanthone (2 mol%)	55
2	thioxanthone (5 mol%)	72
3	thioxanthone (8 mol%)	73
4	thioxanthone (11 mol%)	60

1a (0.05 mmol), thioxanthone, $Co(acac)_2$ (5 mol%), bbbpy (10 mol%), CH_3CN (0.5 mL), 395 nm LED (2.2 W), 25 ℃, 16 h, N_2. [a]Yields were determined by GC-FID analysis using mesitylene as I.S.

Table S6. Screening of co-catalyst and ligand loading.

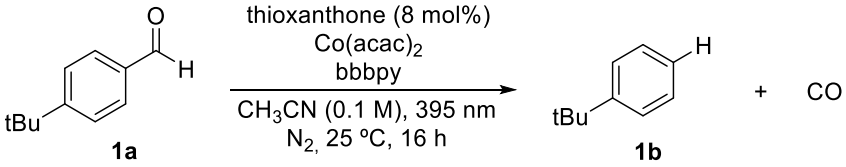

Entry	Co-catalyst (mol%)	Ligand (mol%)	Yield of **1b** (%)[a]
1	$Co(acac)_2$ (1 mol%)	-	17
2	$Co(acac)_2$ (1 mol%)	bbbpy (2 mol%)	77
3	$Co(acac)_2$ (2 mol%)	dtbbpy (4 mol%)	72
4	$Co(acac)_2$ (2 mol%)	dtbbpy (6 mol%)	69
5	$Co(acac)_2$ (5 mol%)	dtbbpy (5 mol%)	70
6	$Co(acac)_2$ (5 mol%)	dtbbpy (10 mol%)	73

1a (0.05 mmol), thioxanthone (8 mol%), $Co(acac)_2$, bbbpy, CH_3CN (0.5 mL), 395 nm LED (2.2 W), 25 ℃, 16 h, N_2. [a]Yields were determined by GC-FID analysis using mesitylene as I.S.

Table S7. Screening of concentration.

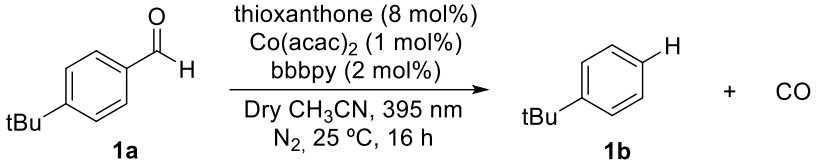

Entry	Concentration (M)	Yield of **1b** (%)[a]
1	0.05	65
2	0.1	77
3	0.15	64

1a, thioxanthone (8 mol%), $Co(acac)_2$ (1 mol%), bbbpy (2 mol%), CH_3CN (0.5 mL), 395 nm LED (2.2 W), 25 ℃, 16 h, N_2. [a]Yields were determined by GC-FID analysis using mesitylene as I.S.

Table S8. Screening of temperature.

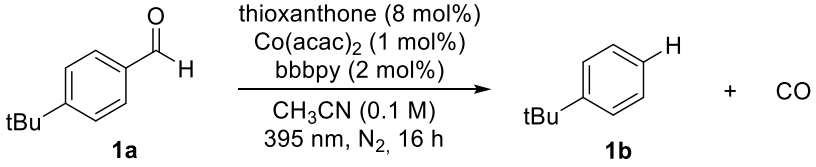

Entry	Temperature (ºC)	Yield of **1b** (%)[a]
1	10	44
2	25	77
3	40	81
4	60	86

1a (0.05 mmol), thioxanthone (8 mol%), $Co(acac)_2$ (1 mol%), bbbpy (2 mol%), CH_3CN (0.5 mL), 395 nm LED (2.2 W), 16 h, N_2. [a]Yields were determined by GC-FID analysis using mesitylene as I.S.

Table S9. Screening of light source.

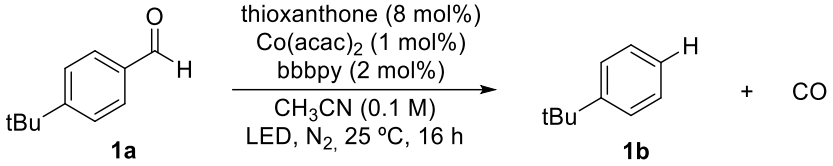

Entry	Light source	Yield of **1b** (%)[a]
1	420 nm (0.5 W)	9
2	395 nm (0.6 W)	22
3	395 nm (2.2 W)	77
4	385 nm (3.6 W)	91
5	365 nm (2.6 W)	69

1a (0.05 mmol), thioxanthone (8 mol%), $Co(acac)_2$ (1 mol%), bbbpy (2 mol%), CH_3CN (0.5 mL), LED, 25 ºC, 16 h, N_2. [a]Yields were determined by GC-FID analysis using mesitylene as I.S.

Table S10. Screening of reaction time.

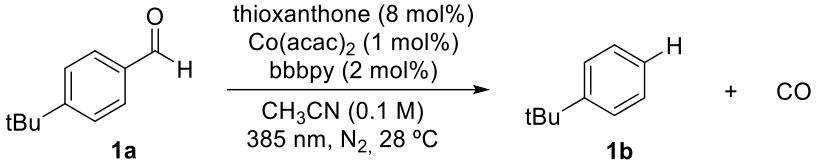

Entry	Reaction time	Yield of **1b** (%)[a]
1	5 min	22
2	15 min	48
3	30 min	59
4	1 h	71
5	2 h	82
6	4 h	88
7	5 h	94
8	6 h	92
9	8 h	92
10	16 h	91

1a (0.05 mmol), thioxanthone (8 mol%), $Co(acac)_2$ (1 mol%), bbbpy (2 mol%), CH_3CN (0.5 mL), 385 nm LED (3.6 W), 28 ºC, N_2. [a]Yields were determined by GC-FID analysis using mesitylene as I.S.

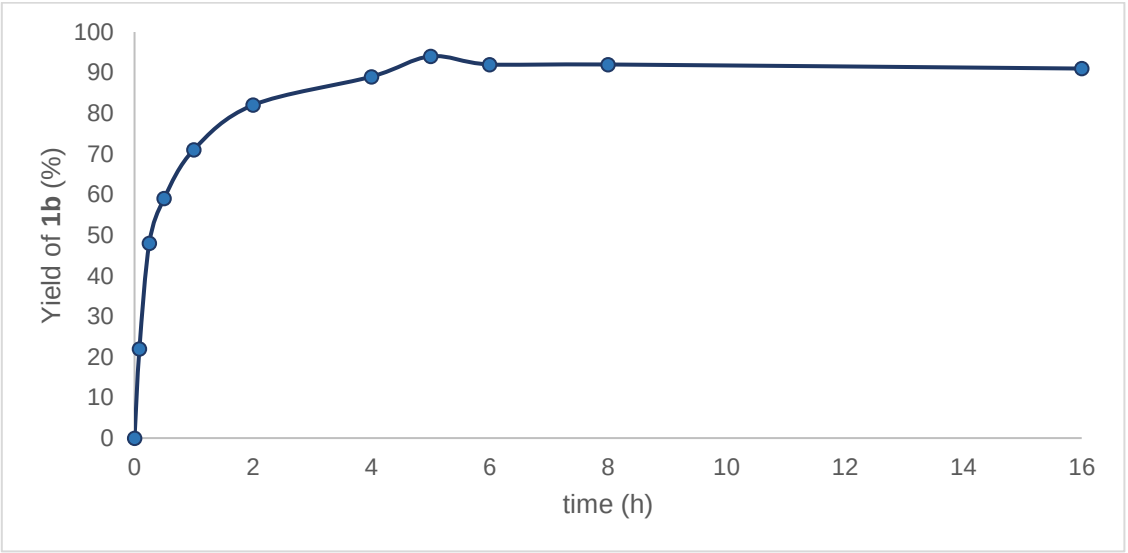

Figure S5. Kinetic profile with optimized reaction conditions for the decarbonylation of **1a**.

4.4.4 Failed Substrates

The presence of certain moieties such as phenol-, amine-, nitro-, bromo-, thioether-, or acid substituents hampered reaction progress. (Scheme S1).

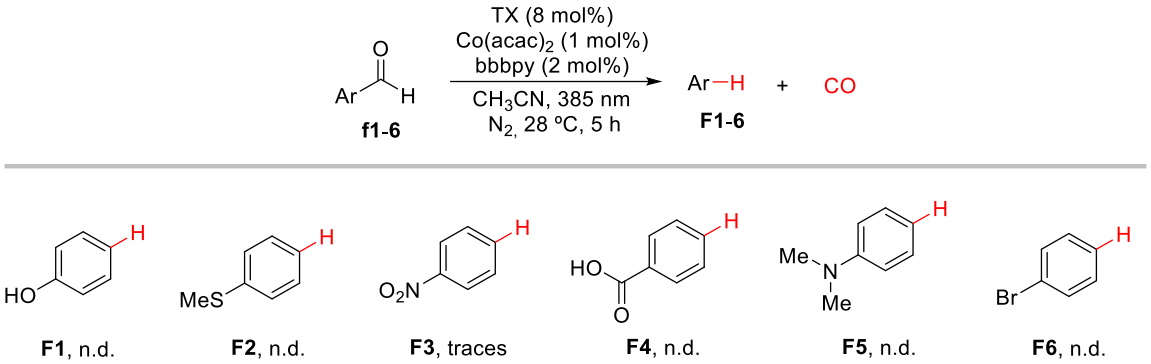

Scheme S1. Failed substrates for the photocatalytic decarbonylation. Reaction conditions: **f** (0.05 mmol), thioxanthone (8 mol%), $Co(acac)_2$ (1 mol%), bbbpy (2 mol%), CH_3CN (0.5 mL), 385 nm LED (3.6 W), 28 ºC, 5 h, N_2. Reaction mixtures analyzed via GC-MS analysis.

4.4.5 Tested Aliphatic Substrates

Similarly to benzaldehydes, the C–H bond of aliphatic aldehydes exhibits relatively low bond dissociation energies. Encouraged by the excellent results achieved with aromatic substrates, a few aliphatic aldehydes were additionally tested. Unfortunately, only acceptable results were obtained with phenylacetaldehyde (**g4**) and 3-phenylpropionaldehyde (**g5**) (Scheme S2). While starting materials **g1** and **g2** remained mostly unreacted, subjecting **g3** to the reaction conditions led to degradation.

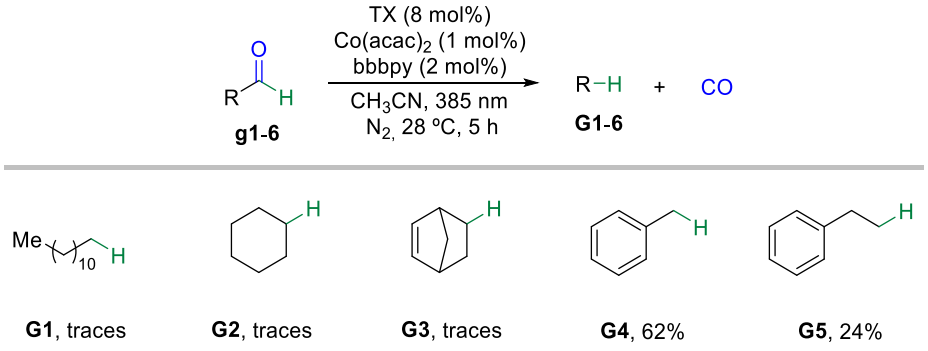

Scheme S2. Tested aliphatic aldehydes. Reaction conditions: **g** (0.05 mmol), thioxanthone (8 mol%), $Co(acac)_2$ (1 mol%), bbbpy (2 mol%), CH_3CN (0.5 mL), 385 nm LED (3.6 W), 28 ºC, 5 h, N_2. Yields determined by GC-FID analysis against mesitylene as internal standard.

4.4.6 Mechanistic Studies

UV-Vis Spectra of Reaction Components

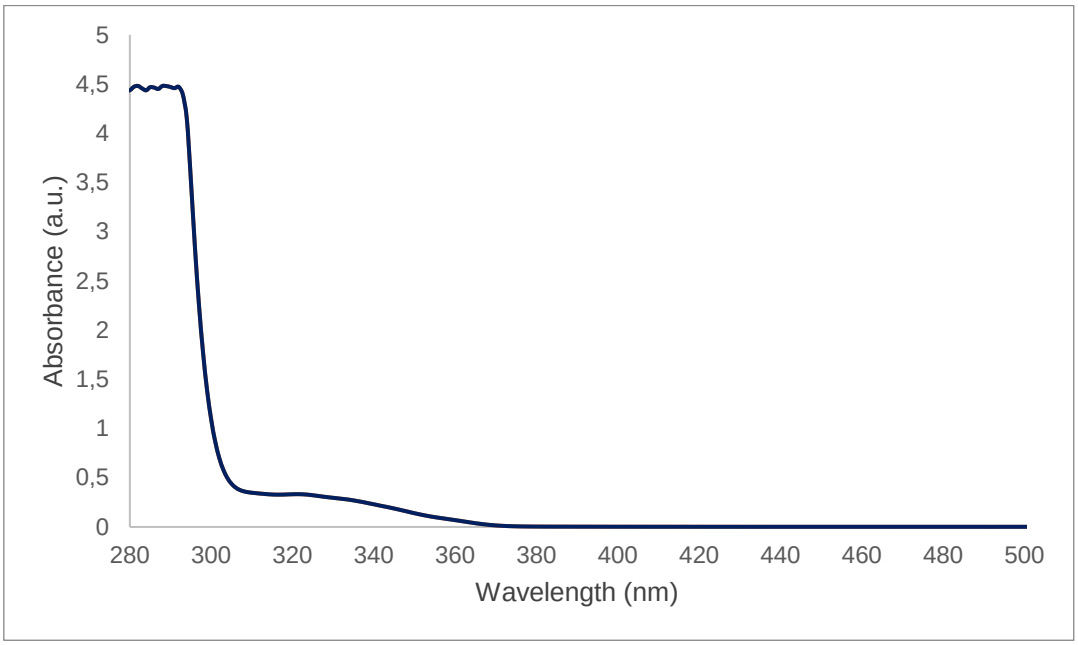

Figure S6. UV-Vis absorption spectrum of **1a** in CH_3CN (1.4 mM).

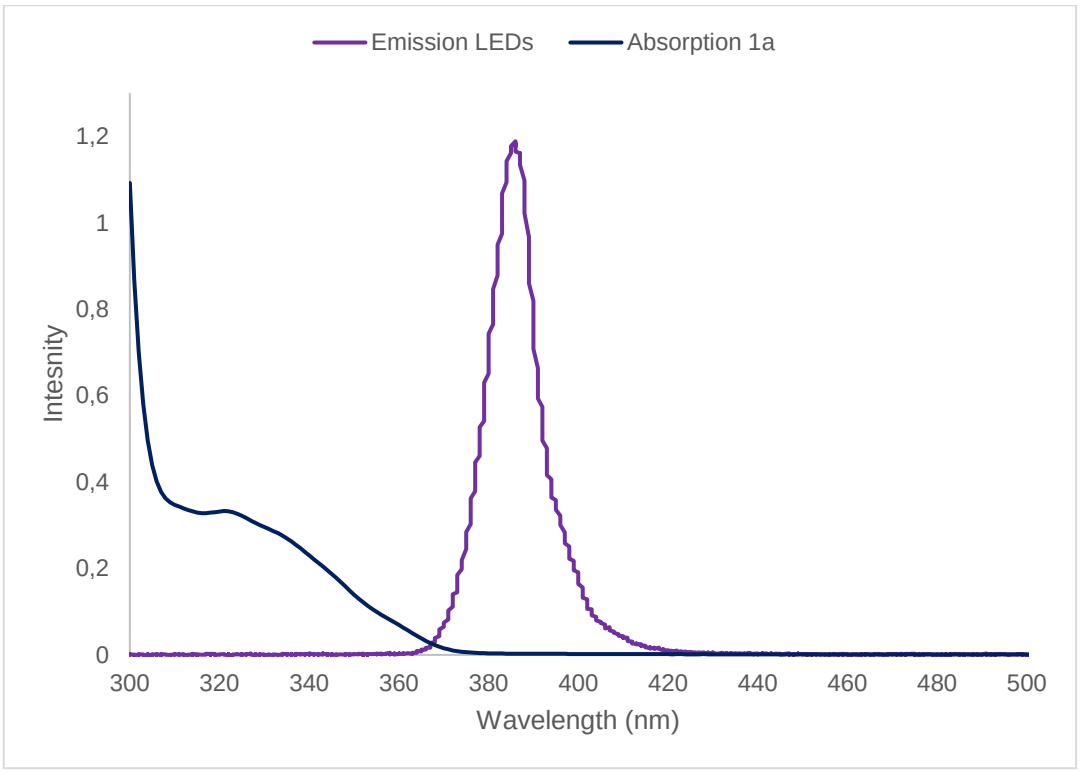

Figure S7. Combined UV-Vis absorption spectrum of **1a** in CH_3CN (1.4 mM) and emission spectrum of the LEDs.

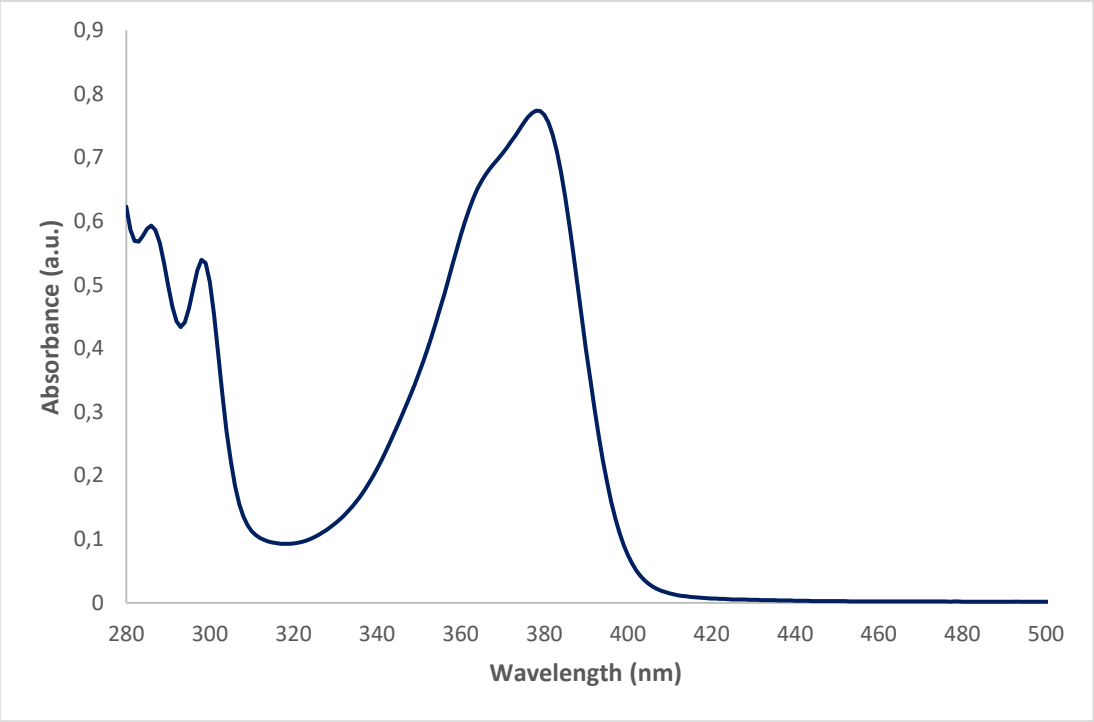

Figure S8. UV-Vis absorption spectrum of TX in CH_3CN (0.5 mM).

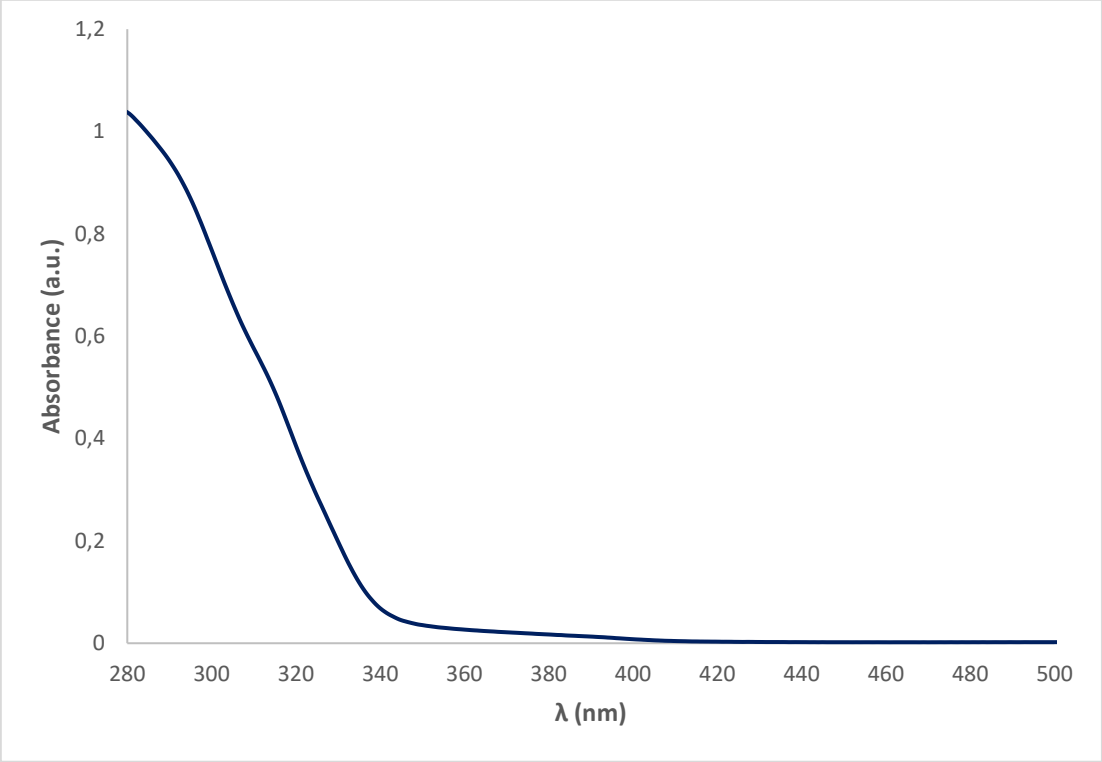

Figure S9. UV-Vis absorption spectrum of $Co(acac)_2$ in CH_3CN (0.1 mM).

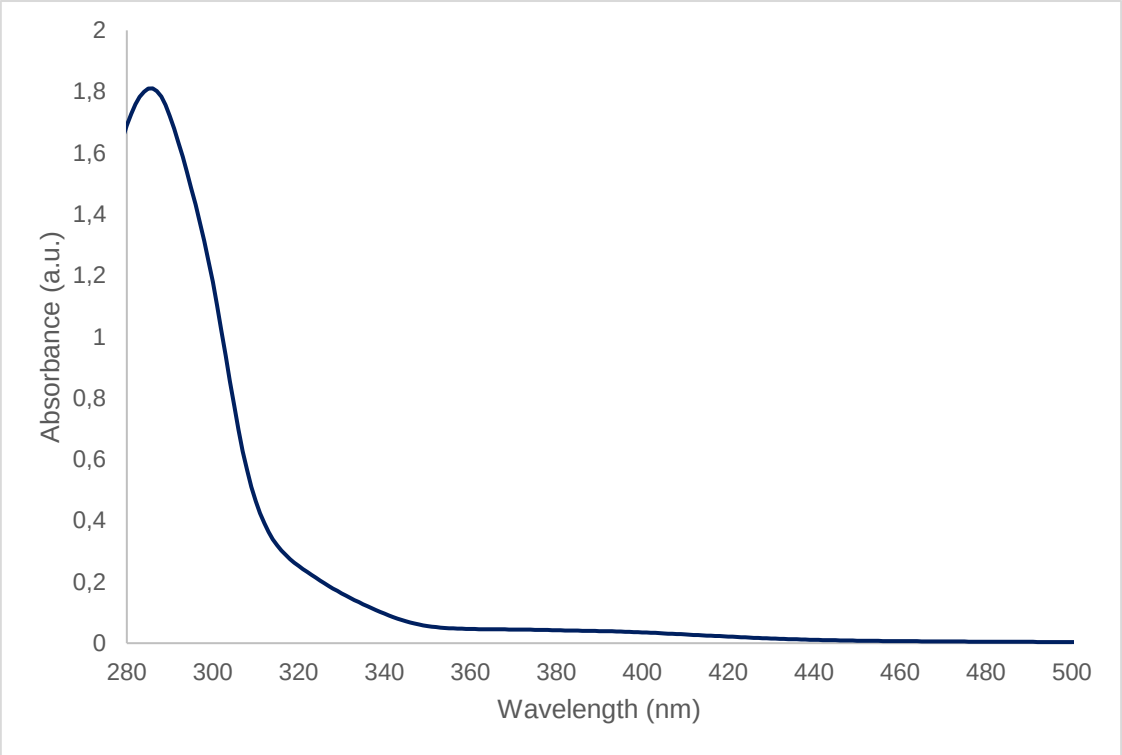

Figure S10. UV-Vis absorption spectrum of $Co(acac)_2$ (0.2 mM) + bbbpy (0.4 mM) in CH_3CN.

GC-MS Study of the Reaction Mixture of 1a

In the case of the reaction mixture of the decarbonylation of **1a**, the mass corresponding to the molecular ion of the benzophenone by-product **1c** can be clearly seen (Figure S11).

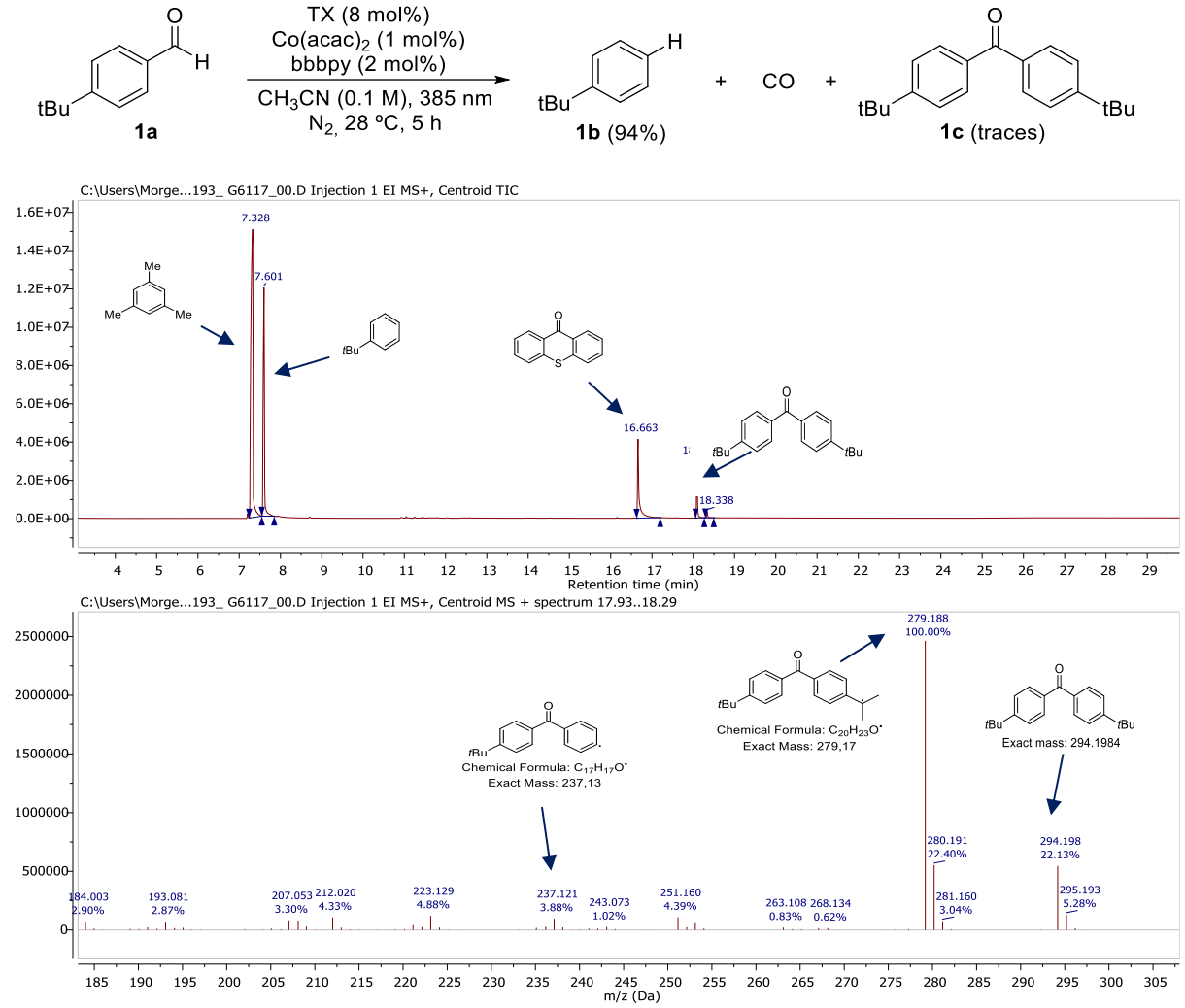

Figure S11. GC-MS chromatogram for the photocatalyzed decarbonylation of **1a** displaying benzophenone **1c** as by-product.

Radical Trapping Experiment with TEMPO

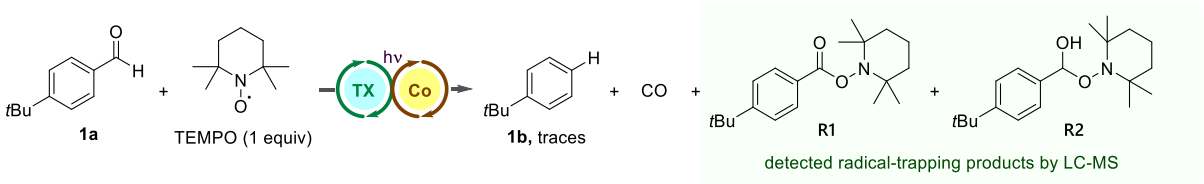

A 5 mL crimp-cap vial equipped with a stirring bar, was loaded with the 4-*tert*butyl benzaldehyde (9 µL, 50 µmol, 1.00 equiv.), thioxanthone (0.9 mg, 4 µmol, 8 mol%), cobalt (II) acetylacetonate (0.13 mg, 0.5 µmol, 1 mol%), 4,4′-di-tert-butyl-2,2′-dipyridyl (0.27 mg, 1 µmol, 2 mol%), and TEMPO (8 mg, 50 µmol, 1.00 equiv.). The vial was sealed, non-dried CH_3CN

(0.5 mL) was added, and the mixture was sonicated for 1 min. After degassing via freeze-pump-thaw cycling (3 x), the reaction mixture was stirred under irradiation using a 3.6 W 385 nm LED set-up for 5 h at 28 º C. The resulting reaction mixture was analyzed via LC-MS and GC-FID. Product **1b** was observed in trace ammounts, thereby indicating a radical pathway. The formation of **R1** and **R2** indicated the in-situ formation of acyl and benzyl radicals.

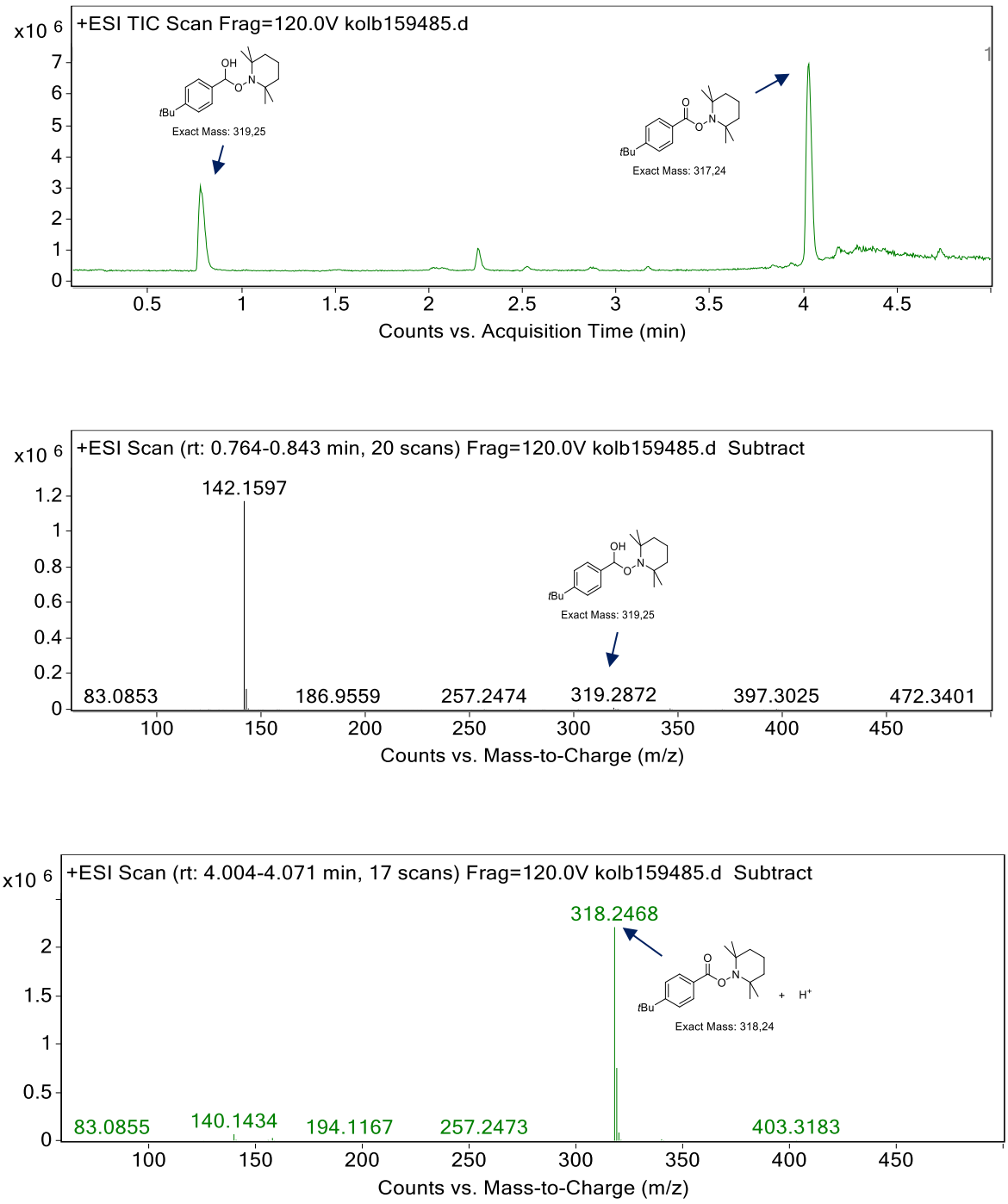

Figure S12. LC-MS chromatogram for the photocatalyzed decarbonylation of **1a** in presence of TEMPO (1 equiv.).

Detailed Mechanistic Pathways

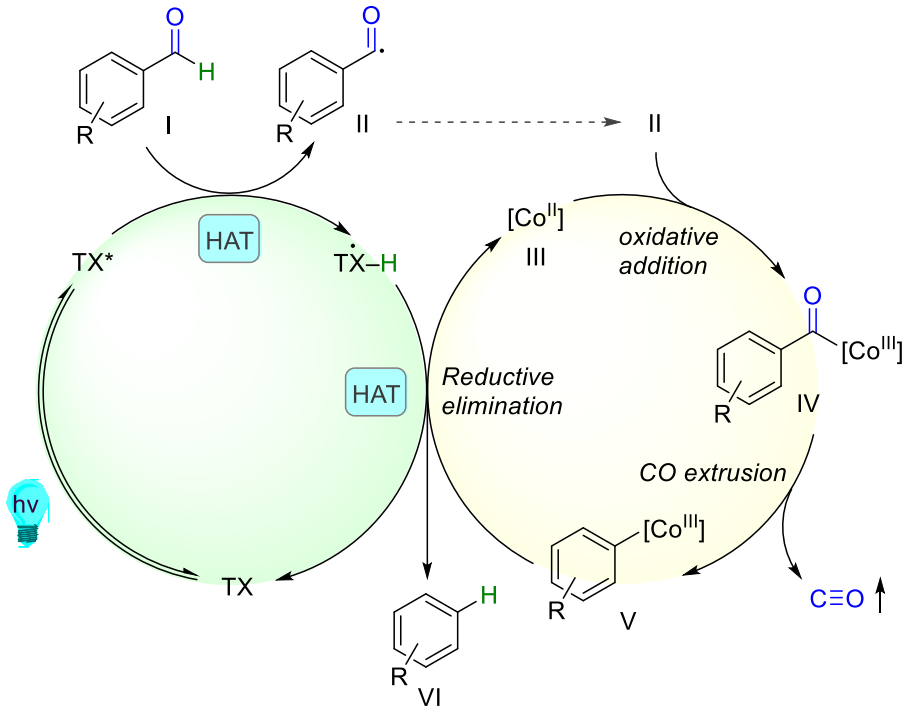

Scheme S3. TX-mediated photocatalyzed decarbonylation pathway.

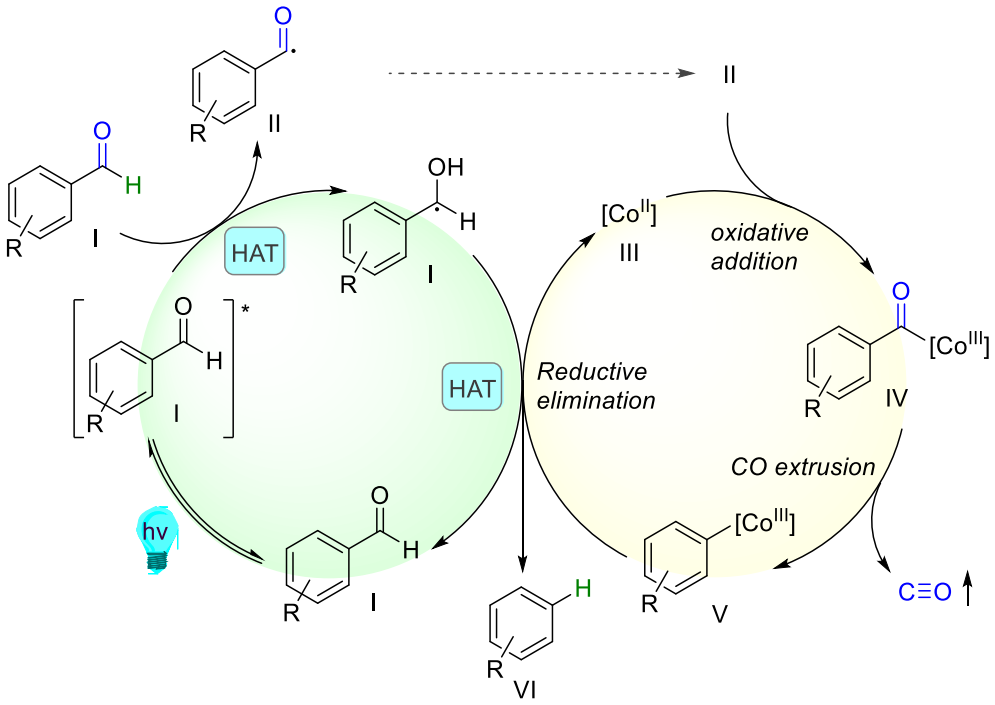

Scheme S4. Self-photocatalyzed decarbonylation pathway.

Photocatalytic Decarbonylation of 1a in CD_3CN

The reaction mixture was prepared according to general procedure **GP1** from 4-*tert*butyl benzaldehyde (9 µL, 50 µmol, 1.00 equiv.), thioxanthone (0.9 mg, 4 µmol, 8 mol%), cobalt (II) acetylacetonate (0.13 mg, 0.5 µmol, 1 mol%) and 4,4′-di-*tert*-butyl-2,2′-dipyridyl (0.27 mg, 1 µmol, 2 mol%), using CD_3CN (0.5 mL) as a solvent.

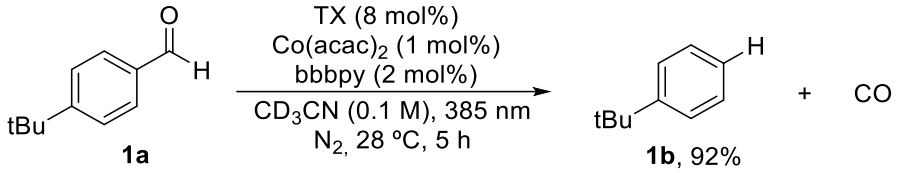

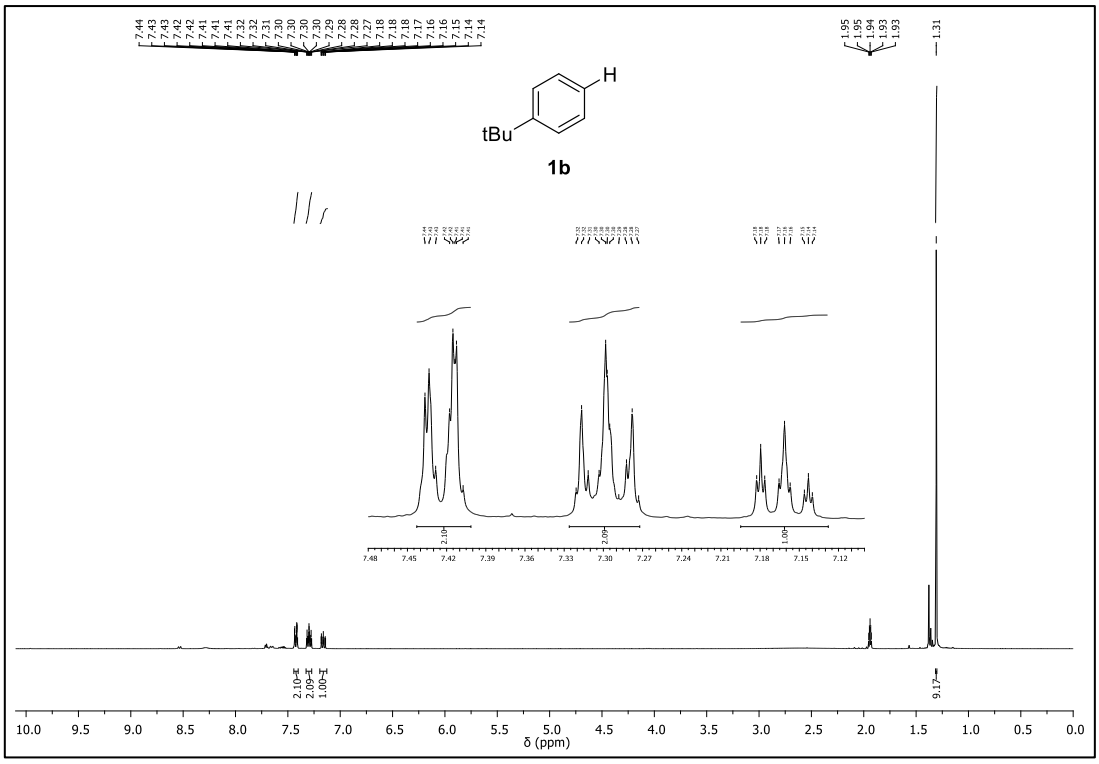

Figure S13. ^{1}H-NMR crude spectrum for the decarbonylation of **1a** in CD_3CN.

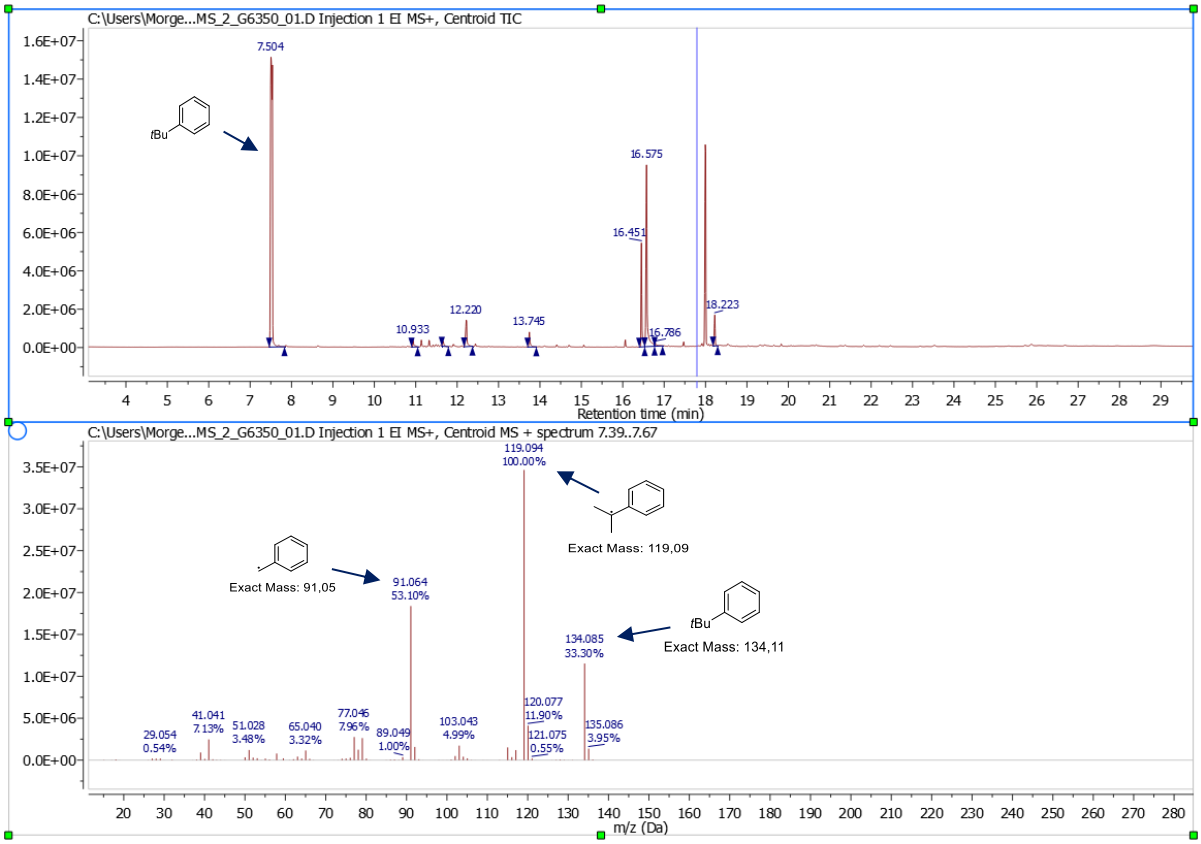

Figure S14. GC-MS chromatogram for the photocatalytic decarbonylation of **1a** in CD_3CN.

Independent KIE Experiments between 1a and 1a-D

For the KIE studies two different sets of reaction mixtures were prepared. The yield of **1b** or **1b-D** was measured at different time intervals via GC-FID.

Decarbonylation of **1a**: according to **GP1**, six vials were set in parallel for the decarbonylation of **1a**. In total, 4-*tert*butylbenzaldehyde (52 µL, 300 µmol, 1.00 equiv.), thioxanthone (5.4 mg, 24 µmol, 8 mol%), cobalt (II) acetylacetonate (0.8 mg, 3 µmol, 1 mol%) and 4,4′-di-*tert*-butyl-2,2′-dipyridyl (1.7 mg, 6 µmol, 2 mol%) in non-dried CH_3CN (3 mL) were used and distributed equally in six different 5 mL crimp-cap vials.

Decarbonylation of **1a-D**: according to **GP1**, six vials were set in parallel for the decarbonylation of **1a-D**. In total, **1a-D** (52 µL, 300 µmol, 1.00 equiv.), thioxanthone (5.4 mg, 24 µmol, 8 mol%), cobalt (II) acetylacetonate (0.8 mg, 3 µmol, 1 mol%) and 4,4′-di-*tert*-butyl-2,2′-dipyridyl (1.7 mg, 6 µmol, 2 mol%) in non-dried CH_3CN (3 mL) were used and distributed equally in six different 5 mL crimp-cap vials.

Table S11. Competition KIE experiments between **1a** and **1a-D**.

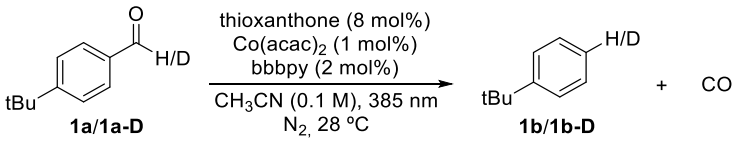

Entry	Time (h)	Yield of **1b** (%)[a]	Yield of **1b-D** (%)[a]
1	0,083	22	5
2	0,5	59	17
3	1	71	24
4	2	82	39
5	4	89	60
6	5,5	94	71

a (0.05 mmol), thioxanthone (8 mol%), $Co(acac)_2$ (1 mol%), bbbpy (2 mol%), CH_3CN (0.5 mL), 385 nm LED (3.6 W), 28 ºC, N_2. [a]Yields were determined by GC-FID analysis using mesitylene as I.S.

Qualitative Analysis of Evolved Carbon Monoxide via Gas Chromatography

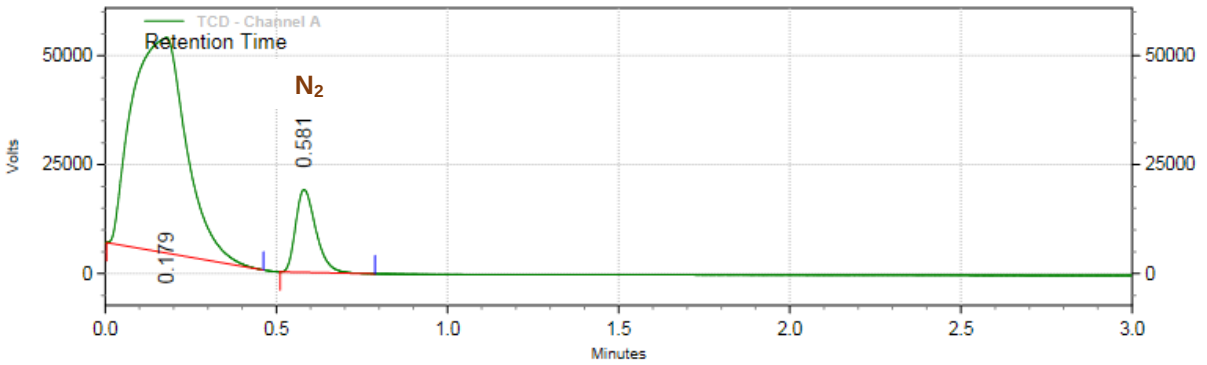

Figure S15. Gas chromatogram of vial filled with pre-dried nitrogen.

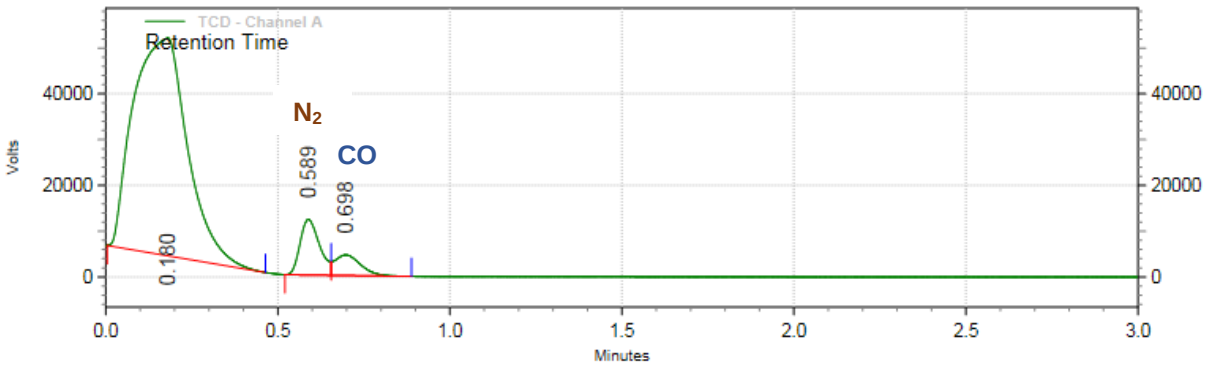

Figure S16. Gas chromatogram of vial filled with a mixture of pre-dried nitrogen and carbon monoxide.

The carbon monoxide used as reference (Figure S16) was generated following a procedure reported by Borggraeve et al.[20]

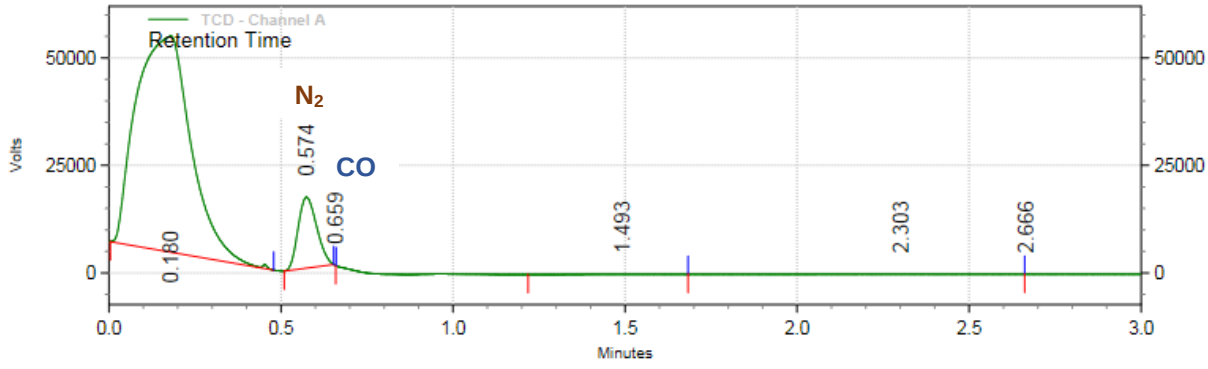

Figure S17. Measurement of evolved carbon monoxide after irradiating 5 h a mixture containing **1a**.

Test Reaction for the Qualitative Determination of Evolved Carbon Monoxide

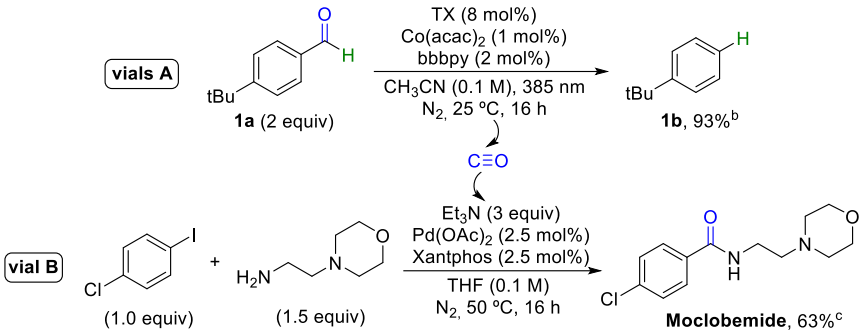

Carbon monoxide generating reaction (**vials A**): According to **GP1**, four vials were set in parallel for the decarbonylation of **1a**. In total, 4-*tert*butylbenzaldehyde (35 µL, 200 µmol, 1.00 equiv.), thioxanthone (3.6 mg, 16 µmol, 8 mol%), cobalt (II) acetylacetonate (0.52 mg, 2 µmol, 1 mol%) and 4,4′-di-*tert*-butyl-2,2′-dipyridyl (1.1 mg, 4 µmol, 2 mol%) in non-dried CH_3CN (2 mL) were used and distributed equally in four different 5 mL crimp-cap vials. Upon reaction completion, the gas phases of the four vials were transferred via syringe to a separate vial containing the test reaction mixture (**vial B**).

Carbon monoxide consuming test reaction (**vial B**): the procedure was inspired by a protocol reported by Uzunlu et al.[21] A 10 mL crimp-cap vial was charged with a cross-shaped stirring bar, $Pd(OAc)_2$ (0.7 mg, 2.5 µmol, 2.5 mol%), xantphos (3.6 mg, 2.5 µmol, 2.5 mol%) and 1-chloro-4-iodobenzene (23.9 mg, 100 µmol, 1.00 equiv.). The vial was sealed, evacuated, and backfilled with N_2. Then, dry THF (1 mL), 4-(2-aminoethyl)morpholine (20 µL, 150 µmol, 1.50 equiv.) and Et_3N (42 µL, 300 µmol, 3.00 equiv.) were added. The resulting mixture was purged with N_2 for 10 min, and the evolved carbon monoxide in **vials A** after 5 h irradiation was transferred via syringe to the sealed **vial B**. The resulting mixture was stirred at 50 °C for 16 h. Afterwards water was added (5 mL) and the product was extracted with EtOAc (3 x 8 mL). The combined organic layers were dried over Na_2SO_4, and the solvent was removed under reduced pressure. The crude product was purified via FCC (PE/EtOAc = 40/60), obtaining **moclobemide** as a white solid (17 mg, 63%).

Analytical data for **moclobemide**:

^{1}H-NMR (400 MHz, $CDCl_3$): δ (ppm) = 7.71 (d, *J* = 8.5 Hz, 2H), 7.42 (d, *J* = 8.5 Hz, 2H), 6.74 (s, 1H), 3.76 – 3.69 (m, 4H), 3.54 (dd, *J* = 11.2, 5.6 Hz, 2H), 2.60 (t, *J* = 6.0 Hz, 2H), 2.55 – 2.46 (m, 4H). **^{13}C-NMR** (101 MHz, $CDCl_3$): δ (ppm) = 166.3, 137.7, 133.0, 128.9, 128.4, 67.0, 56.8, 53.3, 36.1. Spectroscopic data is consistent with literature values.[21] **R_f** = 0.22 (PE/EtOAc = 40/60). **mp** = 135–137 °C. **HRMS** (EI-MS): $[C_{13}H_{17}N_2O_2Cl]^{\cdot+}$ $[M]^{\cdot+}$ calcd: 268.09731; found: 268.09707.

Radical Trapping Experiment with Benzylidenemalononitrile

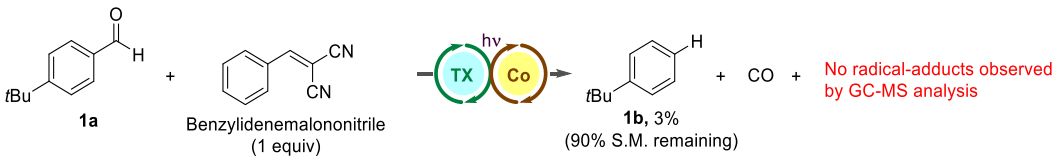

In an attempt to expand the scope of our methodology to the acylation of activated alkenes, the decarbonylation of **1a** was performed in presence of benzylidenemalononitrile.

A 5 mL crimp-cap vial equipped with a stirring bar, was loaded with 4-*tert*butylbenzaldehyde (9 µL, 50 µmol, 1.00 equiv.), thioxanthone (0.9 mg, 4 µmol, 8 mol%), cobalt (II) acetylacetonate (0.13 mg, 0.5 µmol, 1 mol%), 4,4′-di-tert-butyl-2,2′-dipyridyl (0.27 mg, 1 µmol, 2 mol%), and benzylidenemalononitrile (7.9 mg, 50 µmol, 1.00 equiv.). The vial was sealed, non-dried CH_3CN (0.5 mL) was added, and the mixture was sonicated for 1 min. After degassing via freeze-pump-thaw cycling (3 x), the reaction mixture was stirred under irradiation using a 3.6 W 385 nm LED set-up for 5 h at 28 º C. Analysis via GC-MS and GC-FID analysis revealed the presence of unconsumed benzylidenemalononitrile, while the decarbonylation process was significantly inhibited, obtaining 1b in poor yield (..%).

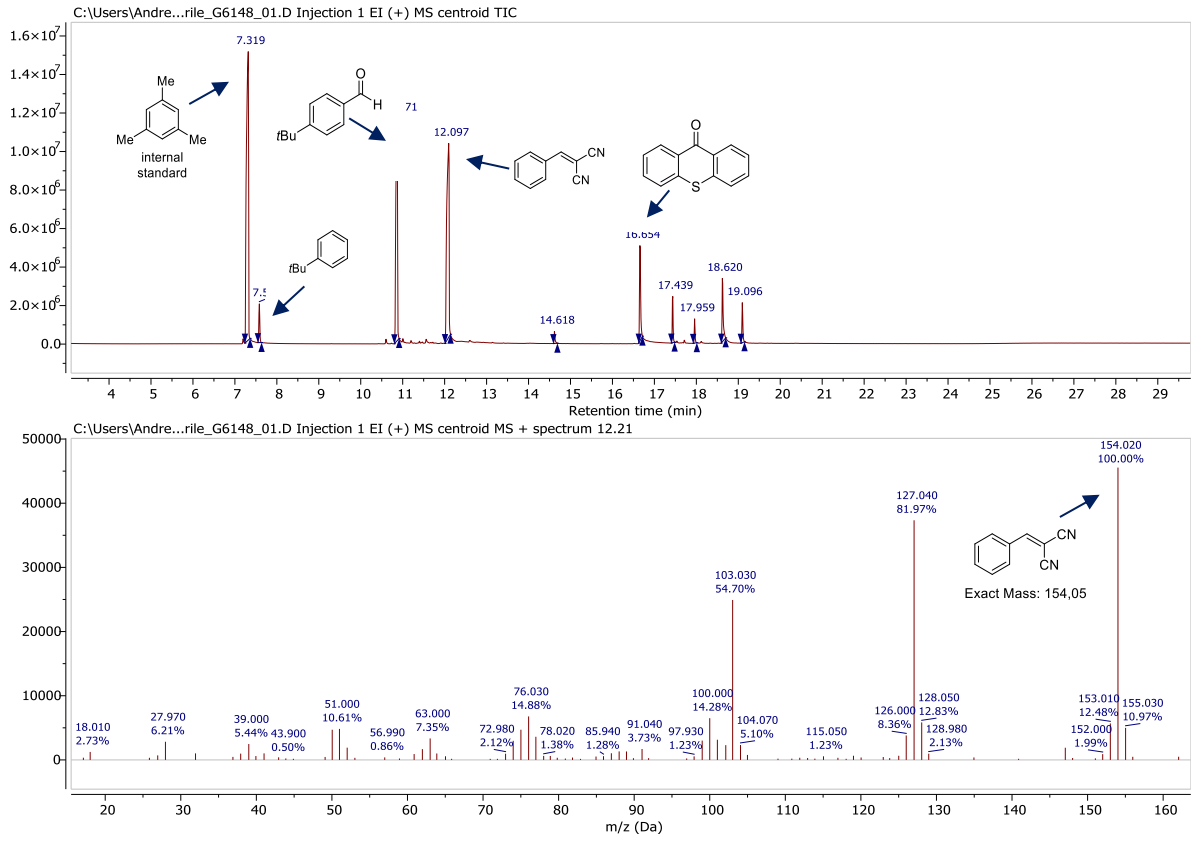

Figure S18. GC-MS chromatogram for the photocatalyzed decarbonylation of **1a** in presence of benzylidenemalononitrile (1 equiv.).

4.4.7 Procedure for the Convergent Decarbonylation of Methoxybenzaldehydes

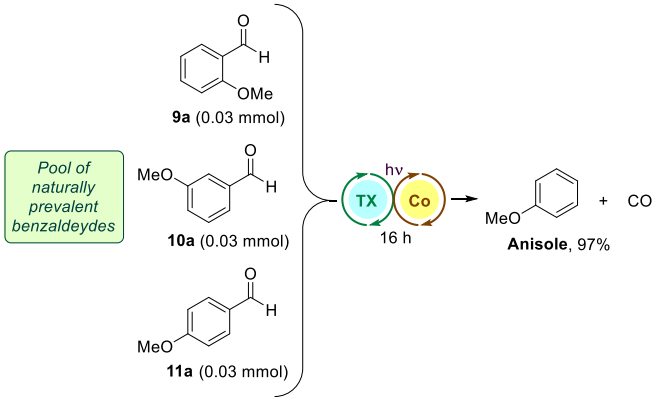

A 5 mL crimp-cap vial equipped with a stirring bar, was loaded with 2-methoxybenzaldehyde (4.2 mg, 30 µmol, 1.00 equiv.), 3-methoxybenzaldehyde (4.2 mg, 30 µmol, 1.00 equiv.), 4-methoxybenzaldehyde (4.2 mg, 30 µmol, 1.00 equiv.), thioxanthone (1.6 mg, 7.2 µmol, 8 mol%), cobalt (II) acetylacetonate (0.23 mg, 0.9 µmol, 1 mol%) and 4,4′-di-*tert*-butyl-2,2′-dipyridyl (0.49 mg, 1.8 µmol, 2 mol%). The vial was sealed, non-dried CH_3CN (0.9 mL) was added, and the mixture was sonicated for 1 min. After degassing via freeze-pump-thaw cycling (3 x), the reaction mixture was stirred under irradiation using a 3.6 W 385 nm LED set-up for 16 h at 28 ° C. Reaction progress was determined via GC-FID analysis against mesitylene as internal standard (97%, GC-FID yield).

4.4.8 Synthesis and Analytical Data of Isolated Compounds

Synthesis of **SM-A**

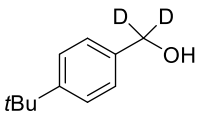

Prepared according to a procedure reported by Nisal et al.[21] In an oven-dried schlenk flask, $LiAlD_4$ (212 mg, 5.05 mmol, 1.50 equiv.) was dissolved in dry THF (30 mL) at 0 ºC under N_2 atmosphere. Next, 4-*tert*butyl benzoic acid (600 mg, 3.37 mmol, 1.00 equiv.) was added and the mixture was stirred at 20 ºC for 18 h. Afterwards, another portion of $LiAlD_4$ (106 mg, 2.52 mmol, 0.75 equiv.) was added and the mixture was stirred for additional 24 h at 20 ºC. Upon reaction completion, the reaction crude was quenched with aqueous 0.05 M NaOH solution (20 mL) and the product was extracted with EtOAc (3 x 10 mL). The combined organic layers were dried over Na_2SO_4 and the solvent was evaporated. The crude product was purified via FCC (PE/EtOAc = 75/25), to obtain **SM-A** as a clear oil (360 mg, 64% yield).

^{1}H-NMR (400 MHz, $CDCl_3$): δ (ppm) = 7.43 – 7.37 (m, 2H), 7.36 – 7.28 (m, 2H), 1.68 (bs, 1H), 1.33 (s, 9H). **^{13}C-NMR** (101 MHz, $CDCl_3$): δ (ppm) = 150.8, 137.9, 127.0, 125.6, 60.5, 34.6, 31.4. Spectroscopic data is consistent with literature values. **R_f** = 0.32 (PE/EtOAc = 75/25). **HRMS** (EI-MS): $[C_{11}H_{14}OD_2]^{\cdot+}$ $[M]^{\cdot+}$ calcd: 166.13212; found: 166.13207.

Synthesis of **1a-D**

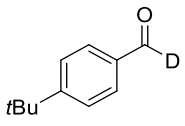

Prepared according to a procedure reported by Luo et al.[22] In an oven-dried schlenk flask, **SM-A** (310 mg, 1.86 mmol, 1.00 equiv.) was dissolved in CH_2Cl_2 (15 mL). Next, $NaHCO_3$ (312 mg, 3.72 mmol, 2.00 equiv.) and Dess-Martin Periodinane (1.10 g, 2.60 mmol, 1.40 equiv.) were subsequently added at 0 ºC under N_2 atmosphere. The resulting mixture was stirred at 20 ºC for 20 h. Afterwards, water (10 mL) and saturated aqueous $NaHCO_3$ solution (10 mL) were added, and the product was extracted with CH_2Cl_2 (4 x 8 mL). The combined organic layers were dried over Na_2SO_4, and the solvent was evaporated under reduced pressure. The crude product was purified via FCC (PE/EtOAc = 95/5), to obtain **1a-D** as a clear oil (252 mg, 83% yield).

^{1}H-NMR (400 MHz, CD_3CN): δ (ppm) = 7.85 – 7.81 (m, 2H), 7.64 – 7.61 (m, 2H), 1.34 (s, 9H). **^{13}C-NMR** (101 MHz, CD_3CN): δ (ppm) = 193.2, 159.3, 135.3, 130.4, 127.1, 36.0, 31.3. Spectroscopic data is consistent with literature values. **R_f** = 0.25 (PE/EtOAc = 95/5). **HRMS** (EI-MS): $[C_{11}H_{13}OD]^{\cdot+}$ $[M]^{\cdot+}$ calcd: 163.11019; found: 163.11038.

Synthesis of 4-acetoxybenzaldehyde (**13a**)

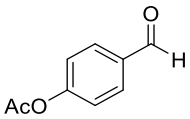

In an oven-dried schlenk flask, to a solution of 4-hydroxybenzaldehyde (1.00 g, 8.19 mmol, 1.00 equiv.) in EtOAc (15 mL) at 0 ºC were added Et_3N (2.85 mL, 20.5 mmol, 2.50 equiv.) and acetylchloride (1.17 mL, 16.4 mmol, 2.00 equiv.). The resulting mixture was stirred at 20 ºC for 2 h. Afterwards, water (10 mL) and saturated aq. $NaHCO_3$ solution (20 mL) were added, and the product was extracted with EtOAc (3 x 10 mL). The combined organic layers were successively washed with saturated aq. $NaHCO_3$ solution (20 mL), saturated aq. NH_4Cl solution (20 mL) and brine (20 mL), dried over Na_2SO_4 and the solvent was evaporated under reduced pressure. The crude product was purified via FCC (PE/EtOAc = 90/10), to obtain **13a** as a clear colourless oil (1.13 g, 84% yield).

^{1}H-NMR (400 MHz, $CDCl_3$): δ (ppm) = 9.96 (s, 1H), 7.91 – 7.86 (m, 2H), 7.28 – 7.21 (m, 2H), 2.31 (s, 3H). **^{13}C-NMR** (101 MHz, $CDCl_3$): δ (ppm) = 190.9, 168.7, 155.4, 134.0, 131.2, 122.4, 21.2. Spectroscopic data is consistent with literature values.[23] **R_f** = 0.29 (PE/EtOAc = 90/10). **HRMS** (EI-MS): $[C_9H_8O_3]^{\cdot+}$ $[M]^{\cdot+}$ calcd: 164.04680; found: 164.04682.

Synthesis of 4-benzoyloxybenzaldehyde (**14a**)

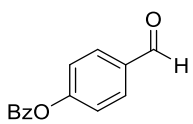

In an oven-dried schlenk flask, to a solution of 4-hydroxybenzaldehyde (1.00 g, 8.19 mmol, 1.00 equiv.) in DCM (15 mL) at 0 ºC were added Et_3N (2.85 mL, 20.5 mmol, 2.50 equiv.) and benzoylchloride (1.90 mL, 16.4 mmol, 2.00 equiv.). The resulting mixture was stirred at 20 ºC for 2 h. Afterwards, water (10 mL) and saturated aq. $NaHCO_3$ solution (20 mL) were added, and the product was extracted with DCM

(3 x 10 mL). The combined organic layers were successively washed with saturated aq. $NaHCO_3$ solution (20 mL), saturated aq. NH_4Cl solution (20 mL) and brine (20 mL), dried over Na_2SO_4 and the solvent was evaporated under reduced pressure. The crude product was purified via FCC (PE/EtOAc = 90/10), to obtain **14a** as a white solid (1.25 g, 67% yield).

^{1}H-NMR (400 MHz, $CDCl_3$): δ (ppm) = 10.03 (s, 1H), 8.24 – 8.19 (m, 2H), 8.02 – 7.95 (m, 2H), 7.71 – 7.64 (m, 1H), 7.57 – 7.51 (m, 2H), 7.45 – 7.39 (m, 2H). **^{13}C-NMR** (101 MHz, $CDCl_3$): δ (ppm) = 191.0, 155.7, 134.0, 131.3, 130.3, 128.9, 128.7, 122.6. Spectroscopic data is consistent with literature values.[24] **R_f** = 0.33 (PE/EtOAc = 90/10). **HRMS** (EI-MS): $[C_{14}H_{10}O_3]^{\cdot+}$ $[M]^{\cdot+}$ calcd: 226.06245; found: 226.06229.

Synthesis of acetanilide (**16b**)

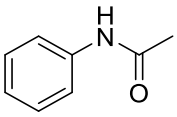

Prepared according to general procedure **GP1** from 4-acetamido benzaldehyde (8.2 mg, 50 µmol). The crude product was purified via FCC (PE/EtOAc = 60/40), to obtain **16b** as a white solid (5.6 mg, 83% yield).

^{1}H-NMR (400 MHz, CD_2Cl_2): δ (ppm) = 7.50 (d, *J* = 7.9 Hz, 3H), 7.31 (t, *J* = 7.9 Hz, 2H), 7.10 (t, *J* = 7.4 Hz, 1H), 2.13 (s, 3H). **^{13}C-NMR** (101 MHz, CD_2Cl_2): δ (ppm) = 168.3, 138.3, 128.9, 124.1, 119.8, 24.4. Spectroscopic data is consistent with literature values.[25] **R_f** = 0.20 (PE/EtOAc = 60/40). **mp** = 114–116 °C. **HRMS** (APCI-MS): $[C_8H_9NO]^+$ $[M + H]^+$ calcd: 136.0757; found: 136.0758.

Synthesis of biphenyl (**25b**)

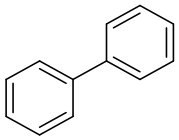

Prepared according to general procedure **GP1** from biphemyl-4-carboxaldehyde (9.4 mg, 50 µmol). The crude product was purified via FCC (*n*-hexane), to obtain **25b** as a white solid (4.8 mg, 62% yield).

^{1}H-NMR (400 MHz, CD_2Cl_2): δ (ppm) = 7.61 (dt, *J* = 8.2, 1.7 Hz, 2H), 7.48 – 7.42 (m, 2H), 7.39 – 7.32 (m, 1H). **^{13}C-NMR** (101 MHz, CD_2Cl_2): δ (ppm) = 141.2, 128.8, 127.4, 127.1. Spectroscopic data is consistent with literature values.[26] **R_f** = 0.53 (*n*-hexane). **mp** = 67–69 °C. **HRMS** (EI-MS): $[C_{12}H_{10}]^{\cdot+}$ $[M]^{\cdot+}$ calcd: 154.0777; found: 154.07733.

4.5 References

[1] a) J. Shanklin, E. Whittle, B. G. Fox, *Biochemistry* **1994**, *33*, 12787–12794; b) E. N. G. Marsh, M. W. Waugh, *ACS Catal.* **2013**, *3*, 2515–2521.

[2] a) H. Lu, T.-Y. Yu, P.-F. Xu, H. Wei, *Chem. Rev.* **2021**, *121*, 365–411; b) Ž. Selaković, A. M. Nikolić, V. Ajdačić, I. M. Opsenica, *Eur. J. Org. Chem.* **2022**, e202101265.

[3] M. Wang, H. Zhou, F. Wang, *Acc. Chem. Res.* **2023**, *56*, 1057–1069.

[4] F.-L. Zhang, B. Li, K. N. Houk, Y.-F. Wang, *JACS Au*, **2022**, *2*, 1032–1042.

[5] D. J. Abrams, J. G. West, E. J. Sorensen, *Chem. Sci.* **2017**, *8*, 1954–1959.

[6] I. Texier, C. Giannotti, S. Malato, C. Richter, J. Delaire, *Catal. Today* **1999**, *54*, 297–307.

[7] a) V. de Waele, O. Poizat, M. Fagnoni, A. Bagno, D. Ravelli, *ACS Catal.* **2016**, *6*, 7174–7182; b) I. B. Perry, T. F. Brewer, P. J. Sarver, D. M. Schultz, D. A. DiRocco, D. W. C. MacMillan, *Nature* **2018**, *560*, 70–75.

[8] J. Zhou, L. Li, S. Wang, M. Yan, W. Wei, *Green Chem.* **2020**, *22*, 3421–3426.

[9] a) J. Simões, D. Griller, *Chem. Phys. Lett.* **1989**, *158*, 175–177; b) A. Banerjee, Z. Lei, M.-Y. Ngai, *Synthesis*, **2019**, *51*, 303–333.

[10] N. F. Nikitas, P. L. Gkizis, C. G. Kokotos, *Org. Biomol. Chem.* **2021**, *19*, 5237–5253.

[11] F. P. Byrne, S. Jin, G. Paggiola, T. H. M. Petchey, J. H. Clark, T. J. Farmer, A. J. Hunt, C. Robert McElroy, J. Sherwood, *Sustain. Chem. Process.* **2016**, *4*, 7.

[12] a) C. E. Turner, M. A. Elsohly, E. G. Boeren, *J. Nat. Prod.* **1980**, *43*, 169–234; b) K. H. Baser, M. Kürkçüoglu, T. Özek, *J. Essent. Oil Res.* **1992**, *4*, 133–138; c) T. Du Loots, F. H. van der Westhuizen, L. Botes, *J. Agric. Food Chem.* **2007**, *55*, 6891–6896; d) Z.-Z. He, J.-F. Yan, Z.-J. Song, F. Ye, X. Liao, S.-L. Peng, L.-S. Ding, *J. Nat. Prod.* **2009**, *72*, 1198–1201; e) X. Zhang, H. Gao, L. Zhang, D. Liu, X. Ye, *Ind Crops Prod.* **2012**, *39*, 162–169.

[13] J. Hioe, H. Zipse, *Org. Biomol. Chem.* **2010**, *8*, 3609–3617.

[14] a) M. Muchalal, J. Crouzet, *Agric. Biol. Chem.* **1985**, *49*, 1583–1589; b) L.-K. Sy, G. D. Brown, *J. Nat. Prod.* **1998**, *61*, 987–992; c) B. D'Abrosca, M. DellaGreca, A. Fiorentino, P. Monaco, A. Zarrelli, *J. Agric. Food Chem.* **2004**, *52*, 4101–4108; d) M. B. C. Gallo, W. C. Rocha, U. S. Da Cunha, F. A. Diogo, F. C. Da Silva, P. C. Vieira, J. D. Vendramim, J. B. Fernandes, M. F. d. G. Da Silva, L. G. Batista-Pereira, *Pest. Manag. Sci.* **2006**, *62*, 1072–1081.

[15] a) X. Si, L. Zhang, A. S. K. Hashmi, *Org. Lett.* **2019**, *21*, 6329–6332; b) L. Zhang, X. Si, Y. Yang, M. Zimmer, S. Witzel, K. Sekine, M. Rudolph, A. S. K. Hashmi, *Angew. Chem. Int. Ed.* **2019**, *58*, 1823–1827; c) M. A. Theodoropoulou, N. F. Nikitas, C. G. Kokotos, *Beilstein J. Org. Chem.* **2020**, *16*, 833–857.

[16] In contrast, the formation of acyl- or aryl-radical homocoupling products such as biphenyls was not observed.

[17] S. Yuan, H. Sun, S. Zhang and X. Li, *Inorganica Chim. Acta* **2016**, *439*, 100–105.

[18] N. Uzunlu, P. Pongrácz, L. Kollár and A. Takács, *Molecules*, **2023**, *28*. DOI: 10.3390/molecules28010442.

[19] A. Fitton, D. Faulds and K. L. Goa, *Drugs*, **1992**, *43*, 561–596.

[20] C. Veryser, S. van Mileghem, B. Egle, P. Gilles, W. M. de Borggraeve, *Reac. Chem. Eng.* **2016**, *1*, 142.

[21] R. Nisal, M. Jayakannan, *Biomacromolecules*, **2022**, *23*, 2667.

[22] S. Luo, C. Weng, Y. Ding, C. Ling, M. Szostak, X. Ma, J. An, *Synlett*, **2020**, *32*, 51.

[23] B. Schmidt, N. Elizarov, R. Berger, F. Hölter, *Org. Biomol. Chem.* **2013**, *11*, 3674–3691.

[24] S. Nasri, I. Zahou, I. Turowska-Tyrk, T. Roisnel, F. Loiseau, E. Saint-Amant, H. Nasri, *Eur. J. Inorg. Chem.* **2016**, *31*, 5004–5019.

[25] B. Karimi, H. Behzadnia, *Synlett* **2010**, *13*, 2019–2023.

[26] J.-H. Li, B.-X. Tang, L.-M. Tao, Y.-X. Xie, Y. Liang, M.-B. Zhang, *J. Org. Chem.* **2006**, *71*, 7488–7490.

.

5. Photocatalytic Dehydroformylation of Benzyl Alcohols to Arenes

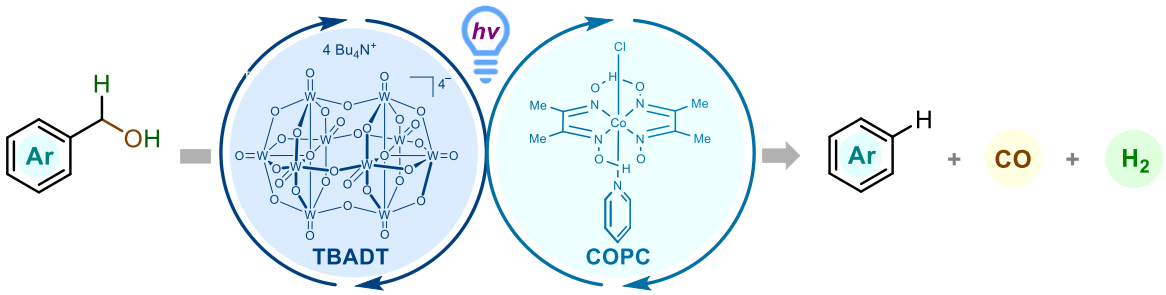

Abstract: The combination of photoinduced hydrogen atom transfer (HAT) and cobalt catalysis gives access to a mild dehydroformylation sequence for the defunctionalization of benzyl alcohols to arenes. The transformation proceeds through a stepwise radical pathway, wherein benzylic and acyl radicals are generated as key intermediates. As a result, stable C−C bonds can be cleaved while generating concomitant syngas ($CO+H_2$).

[i] Reproduced from D. Kolb, A. A. Almasalma, M. Morgenstern, L. Ganser, I. Weidacher, B. König,* *ChemPhotoChem* **2023**, *7*, e202300167. with permission from Wiley-VCH GmbH. Schemes, tables, and text may differ from the published version.

[ii] Author contributions: D. Kolb, A. A. Almasalma, and M. Morgenstern conceived the concept of this study and investigated the scientific background. D. Kolb optimized the reaction conditions, synthesized the starting materials, and conducted the mechanistic investigations. D. Kolb performed the photoreactions with the assistance of L. Ganser and I. Weidacher. D. Kolb wrote the manuscript and supporting information with input from M. Morgenstern. B. König supervised the project, reviewed the manuscript, and is the corresponding author.

5.1 Introduction

Hydroformylation, the functionalization of an alkene with carbon monoxide and hydrogen to generate the corresponding aldehyde, is one of the largest chemical transformations employed in industry, with an overall output of 10.4 megatons of products generated in the year 2008.[1] As a result, this process gives access to a myriad of intermediates with indispensable industrial applications such as methacrolein (acrylic glass manufacture),[2] or 2-methyl butanal (isoprene precursor).[3] Moreover, the rich reactivity profile of the aldehyde functionality gives rise to a plethora of follow-up transformations, such as oxidation to acids, amides, and lactones, or reductions to amines and alcohols.[4] In contrast, the reverse transformation, cleaving off syngas (CO + H_2) to form an alkene, has historically been less relevant, as aldehydes are generally less available substrates.

The fossil fuel-based chemical industry of the last century was focused on building molecular complexity from simple, unfunctionalized aliphatics and olefins. Going forward, future chemical production will employ complex, biologically derived starting materials like sugars or lignin, transforming them into simpler building blocks. As an example, photocatalytic deoxygenations involving gas evolution can be fruitful strategies that allow to modify complex natural products such as sugars,[5] or degrade polymers in a straightforward fashion.[6]

Initially, the dehydroformylation reaction was explored with aldehydes, using stoichiometric or catalytic amounts of metal complexes.[7] More recently, primary alcohols were reported to undergo dehydroformylation and oxidative dehydroxymethylation in the presence of ruthenium and rhodium complexes respectively.[8] In this context, pioneering work by the Sorensen group provided a photocatalytic version of these transformations by employing a dual HAT-cobalt system under mild conditions.[9] Herein, alkenes could be prepared from α-quaternary aldehydes via dehydroformylation, and in a single instance from an alcohol via dehydroxymethylation (Scheme 1a). Alternatively, the Zuo group successfully employed cerium complexes for the photocatalytic transformation of alcohols by formaldehyde extrusion.[10]

Inspired by these methodologies and by our previous work on the photocatalytic decarbonylation of benzaldehydes (Scheme 1b),[11] we hypothesized that a two-step dehydroformylation sequence might unlock benzyl alcohols as substrates for their defunctionalization to arenes (Scheme 1c). For this purpose, an acceptorless light-driven HAT-cobalt system held positive prospects. In our opinion, a photochemical hydrogen atom abstraction at the activated benzylic position should be an efficient way to generate a benzylic radical. This open-shell species could then engage in a dehydrogenation event with a cobalt complex, giving the corresponding benzaldehyde, which upon decarbonylation would yield the unfunctionalized arene.

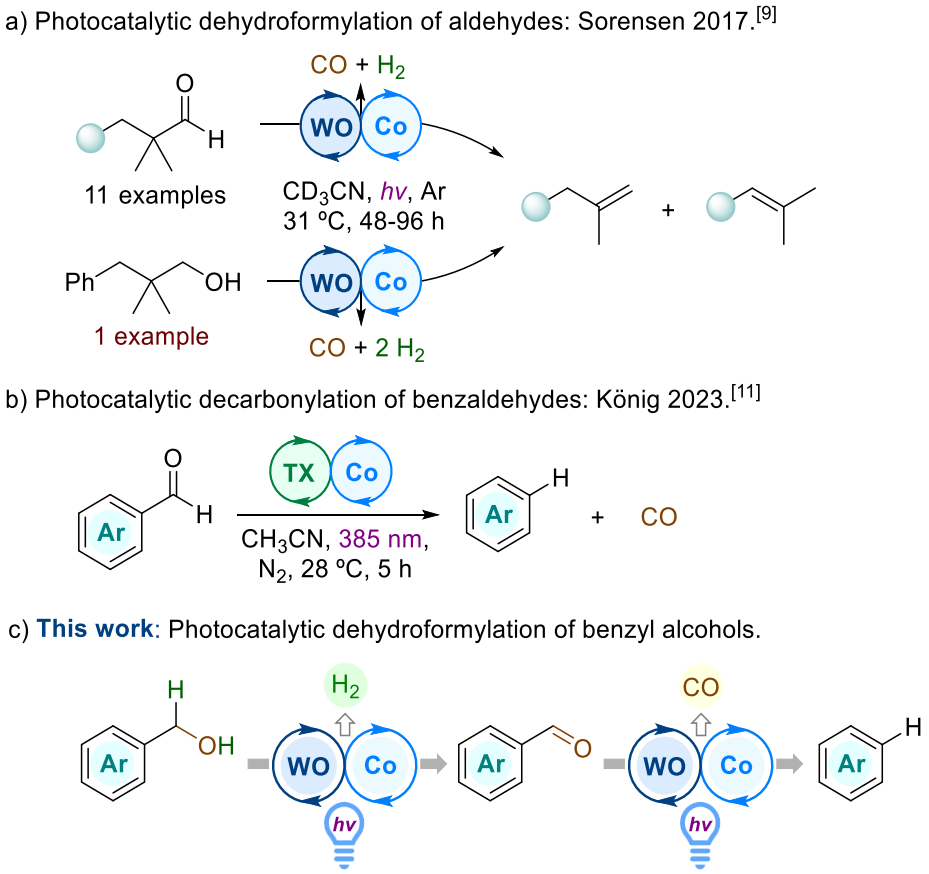

Scheme 5. Photocatalytic dehydroformylation and decarbonylation methodologies. WO = decatungstate. TX = thioxanthone.

5.2 Results and Discussion

4-*tert*-Butylbenzyl alcohol (**1a**) was chosen as model substrate to test the dehydroformylation reaction. At first, a range of photoexcitable HAT-agents and cobalt complexes were screened in different loadings (Tables S1 and S2). Here, the combination of tetra-*n*-butylammonium decatungstate (TBADT) and cobaloxime pyridine chloride (COPC) as hydrogen evolution catalyst proved optimal. When screening different solvents, non-dried acetonitrile was found to be the best option (Table S3), proving the system to be non-moisture sensitive. Additionally, different concentrations (Table S4) and several LEDs were tested (Table S5).

The optimized system was found to involve low loadings of TBADT and COPC, acetonitrile as solvent, and a 385 nm LED (4.7 W) as irradiation source. To our delight, with these conditions, product **1b** was obtained in very good yield after 6 h (85%) (Table 1, entry 1), in a two-step process, corresponding to an average yield of 92% per step. Furthermore, the reaction was successfully conducted on a 0.3 mmol scale, albeit requiring longer reaction times and a higher substrate concentration (entry 2). The replacement of any of the reaction components led in all cases to a significant decrease in yield. Sodium decatungstate (NaDT), despite its similar H-atom abstracting ability to TBADT, led to lower yield presumably due to

Table 1. Screening of reaction conditions.

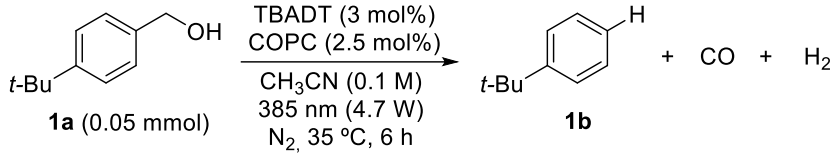

Entry	Deviation of standard conditions	Yield of **1b** (%)[a]
1	None	85
2	0.3 mmol scale, CH_3CN (0.2 M), 48 h	80
3	NaDT instead of TBADT	43
4	Benzophenone instead of TBADT	45
5	Anthraquinone instead of TBADT	17
6	Thioxanthone instead of TBADT	15
7	$Co(dmgH)(dmgH_2)Cl_2$ instead of COPC	47

[a]GC-FID yields determined using mesitylene as internal standard.

its poor solubility in acetonitrile (entry 3). Several cheaper photocatalysts such as benzophenone, anthraquinone, or thioxanthone (entries 4-6) were also found compatible. Similarly, using a different cobalt catalyst (entry 7) rendered acceptable results. With the optimized conditions in hand, we investigated the substrate scope (Scheme 2) with benzyl alcohol (**2a**) and several naturally occurring derivatives.[12]

Both alkyl and alkoxy-substituted substrates (**3a**-**16a**), gave the corresponding arenes in good yields (47-84%). To our delight, the conditions could be easily tuned for sterically hindered *ortho*-substituted derivatives (**3a**, **8a** and **14a**). For these substrates, increasing the reaction time to 16 h led to comparable yields to *para*- and *meta*-substituted homologues. The presence of activated C–H bonds with low bond-dissociation energies (BDEs) such as secondary and tertiary benzylic positions (**6a** and **7a**) was well tolerated. Similarly, the highly activated benzyloxy position displayed by **16a** was found compatible with our system, albeit giving **16b** in low yield after 16 h of irradiation. Herein, the photocatalyst is believed to engage in undesired HAT events with the mentioned position, consequently decelerating the dehydroformylation process. Derivatives with ester groups as substituents (**17a**-**19a**) were successfully converted. Unfortunately, **17a** and **19a** were found to degrade with increasing reaction time. In addition, the methodology was applied for the dehydroformylation of vanillyl alcohol (**20a**). Hereof, guajacol (**20b**) was obtained in low yield, presumably due to the presence of the unprotected phenol moiety. Aryl methanols displaying extended π-systems reacted smoothly, furnishing the corresponding arenes (**21b**-**23b**) in good yields (60-69%). The more sterically hindered 1-naphthalenemethanol (**22a**), required longer reaction times in comparison to 2-naphthalenemethanol (**23a**). The dehydroformylation of substrate **24a** gave

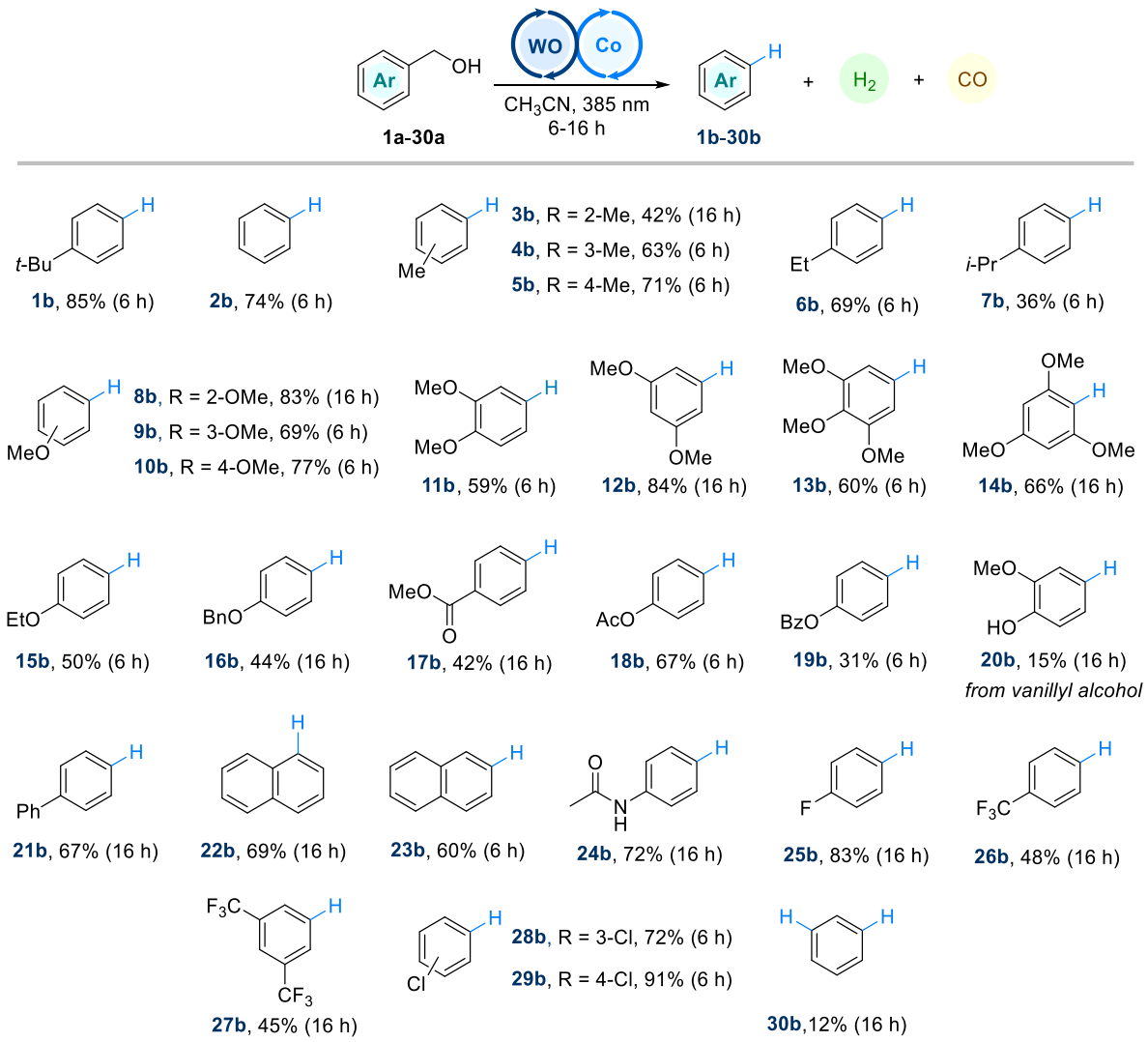

Scheme 2. Substrate scope for benzyl alcohols. [a]Reaction conditions: a (0.05 mmol), TBADT (3 mol%), COPC (2.5 mol%), CH_3CN (0.5 mL), 385 nm LED (4.7 W), N_2, 35 ºC. GC-FID yields determined using mesitylene as I.S.

acetanilide (**24b**) in very good yield (72%). Next, the substrate scope was expanded with several halogenated substrates (**25a**-**29a**), wherein chlorinated derivatives (**28a** and **29a**) gave better results than fluorinated homologues (**25a**-**27a**). According to literature, the electron donating/withdrawing ability of the substituents can have a direct impact on the BDE and overall stability of benzylic radicals.[13] Hereof, radicals with higher lifetimes are more likely to be trapped by cobalt (II), accelerating the first dehydrogenation step of the dehydroformylation sequence. Lastly, the methodology was applied for the two-fold defunctionalization of 1,3-benzenedimethanol (**30a**) to benzene (**30b**), obtaining benzaldehyde as main side product.

Next, a series of control reactions were carried out with model substrate **1a** (Table 4). All reaction components turned out to be essential for the dehydroformylation reaction, confirming its photocatalytic nature. In absence of TBADT, COPC, or light no product was formed (entries 2-4). Instead, in all these cases the starting material remained unreacted. Similarly, the replacement of light by heat prevented the reaction from occurring (entry 5).

Table 2. Control experiments.

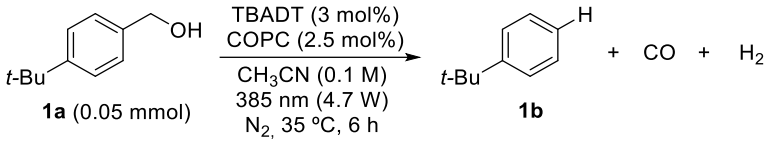

Entry	Deviation of standard conditions	Yield of **1b** (%)[a]
1	None	85
2	No TBADT	N.d.
3	No COPC	N.d.
4	No light	N.d.
5	No light; at 60 ºC	N.d.
6	Under air	18

[a]GC-FID yields determined using mesitylene as I.S.

In addition, conducting the reaction under air led to a notable decrease in the yield presumably due to quenching of the photocatalyst by oxygen (entry 6). Under these conditions, the formation of 4-*tert*-butyl benzoic acid was observed.

To elucidate the reaction mechanism, several additional experiments were performed (Scheme 3). First, gas evolution was confirmed by gas chromatography (Figure S9). While the generation of hydrogen could be observed as a clearly defined peak, the detection of carbon monoxide remained elusive. Further analysis by GC-MS and GC-FID of the reaction mixture of **1a** after 5 h of irradiation revealed the presence of 4-*tert*-butyl benzaldehyde (**1-ald**) (Scheme 3a). In contrast, when concluding the reaction for 6 h, this product was detected only in trace amounts, suggesting its role as an intermediate in the dehydroformylation process. This finding is consistent with the postulated initial oxidation step of the alcohol to the corresponding aldehyde via cooperative HAT-cobalt catalysis (see Scheme 1).

Furthermore, a radical trapping experiment was conducted using TEMPO as a scavenger (Scheme 3b). Consequently, two main radical-derived products were observed (**T-1a** and **T-1-ald**), indicating the in-situ generation of benzylic and acyl radicals via HAT. This finding supported a stepwise radical dehydroformylation sequence, wherein the initial dehydrogenation of the alcohol to give the corresponding aldehyde is essential. To further test this hypothesis, we subjected the proposed aldehyde intermediate (**1-ald**) to our reaction conditions (Scheme 3c), which underwent decarbonylation to give **1b** in excellent yield (93%). According to our previous work on the photocatalytic decarbonylation of benzaldehydes,[11] such a dual HAT-cobalt system performs well in the defunctionalization of aromatic aldehydes. In contrast, subjecting substrate **31a** to our conditions led to no arene formation (Scheme 3d), as the protection of the alcohol group prevents the initial dehydrogenation event.

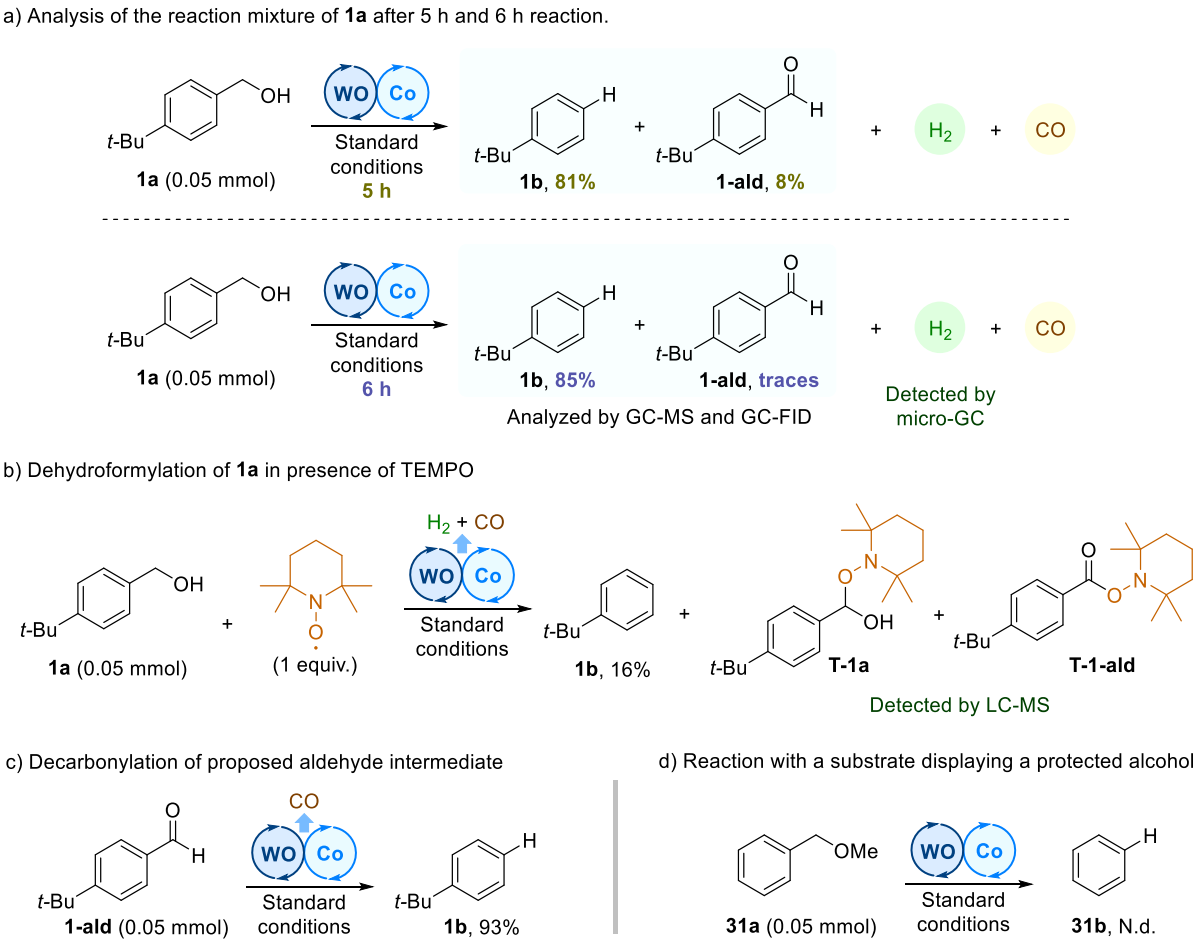

Scheme 3. Mechanistic studies. [a]Standard conditions: substrate (0.05 mmol), TBADT (3 mol%), COPC (2.5 mol%), CH_3CN (0.5 mL), 385 nm LED (4.7 W), N_2, 35 ºC, 6 h. GC-FID yields determined using mesitylene as I.S.

Based on the above observations and according to previous studies,[9],[11],[14] we proposed a plausible mechanism for the dehydroformylation of benzyl alcohols (Scheme 4). In the transformation, a stepwise radical mechanism could be involved, proceeding via photoinduced C–H activation. The overall mechanism can be described as the combination of two pairs of consecutive HAT-cobalt catalytic cycles, which ultimately result in the selective cleavage of the aryl-alkyl C–C bond of the benzyl alcohol (**IV**). Consequently, one equivalent each of hydrogen and carbon monoxide are generated. In the first cycle, the alcohol (**IV**) is initially oxidized to an aldehyde intermediate (**V**) that can further engage in a second cooperative cycle to undergo decarbonylation and give the corresponding arene product (**XIII**).

First, upon irradiation of the photocatalyst (**I**), its excited state (**II**) abstracts a H-atom from the benzyl alcohol (**IV**) via HAT, consequently generating a benzylic radical (**V**). This species can be trapped by cobalt (II) (**VI**) to form a cobalt (III) complex (**VII**). This complex then further reacts, to give a cobalt-hydride complex (**VIII**) and the corresponding benzaldehyde (**IX**). Next, the cobalt hydride complex (**VIII**) reacts with the reduced form of the photocatalyst (**III**) via proton transfer coupled with single electron transfer (SET). Herein, both the cobalt (II) complex

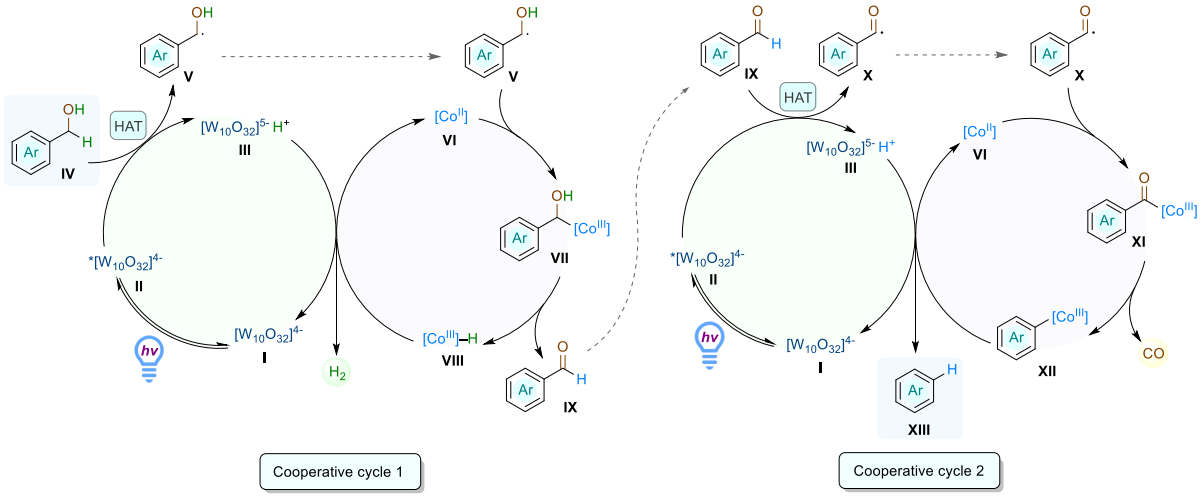

Scheme 4. Proposed mechanism for the sequential dehydroformylation of benzyl alcohols.

(**VI**) and the photocatalyst (**I**) are regenerated. The resulting benzaldehyde (**IX**) can then undergo decarbonylation, as its weak C–H bond is prone to be cleaved by the excited photocatalyst (**II**) to give an acyl radical (**X**). The combination of this species with cobalt (II) (**VI**) leads to the formation of an acyl-cobalt complex (**XI**), which upon extrusion of carbon monoxide yields an aryl-cobalt complex (**XII**). This last species is postulated to engage with the reduced form of the photocatalyst (**III**) via another proton transfer coupled with SET, regenerating it to its ground state (**I**) while giving the aimed unfunctionalized arene product (**XIII**).

5.3 Conclusions

In summary, we have developed a photocatalytic methodology for the sequential dehydroformylation of benzyl alcohols to arenes. The combination of TBADT as photoexcitable HAT-agent and COPC as co-catalyst results in a cooperative photocatalytic system that generates concomitant syngas (CO + H_2). The performed mechanistic studies confirmed the in-situ generation of benzylic and acyl radicals, indicating that the transformation proceeds through a stepwise radical pathway. These open-shell intermediates can then be trapped by a cobalt (II) complex, giving access to further transformations, including dehydrogenation and decarbonylation events. With our proposed reaction mechanism, we postulate that the transformation proceeds via selective C–H bond activation and results in C–C bond cleavage.

5.4 Experimental Section

5.4.1 General Information

Chemicals and solvents: all commercially available chemicals were purchased in high quality and used without further purification. Solvents for column chromatography were distilled prior to use. Petrol ether is abbreviated as PE, while ethyl acetate as EtOAc. Moisture and oxygen-sensitive reactions were carried out using dry solvents in oven-dried glassware under inert atmosphere of pre-dried nitrogen. The evaporation of solvents was carried out in a rotary evaporator at temperatures below 40 ºC, under reduced pressure.

The water content of acetonitrile (245 ± 7 ppm water) used for photocatalyzed reactions was determined by Karl-Fischer titration.

Flash Column Chromatography (FCC): flash silica gel (Merck, 40-63 µm) was used as the stationary phase. Binary eluent mixtures are reported as v/v solutions normalized to 100 volume units. Purification by automated flash column chromatography was performed on a Biotage® IsoleraTM Spektra One device using either pre-packed Biotage® columns or silica gel 60 M (particle size 40–63 µm, 230–440 mesh, Merck) self-packed columns.

Analytical TLC: performed on silica gel pre-coated aluminium sheets (Machery-Nagel, silica gel 60 G/UV254, 0.2 mm). Visualization was accomplished by exposure to UV-light (254 nm). Eluent mixtures for TLC are reported as v/v solutions normalized to 100 volume units.

Nuclear magnetic resonance (NMR): spectra were recorded at room temperature using a Bruker Avance 400 (400 MHz for ^{1}H, 101 MHz for ^{13}C) NMR spectrometer. Chemical shifts are reported in δ-scale as parts per million [ppm] relative to the solvent residual peaks as internal standard. Coupling constants *J* are given in Hertz [Hz] and the multiplicity of the signals is abbreviated as: singlet (s), broad singlet (bs), doublet (d), doublet of doublets (dd), triplet (t), doublet of triplets (dt), triplet of doublets (td), quadruplet (q), or multiplet (m). Signals are reported as follows: (multiplicity, coupling constant *J*, number of protons). Spectra were analyzed using MestReNova 6.0.2.

High-Resolution Mass Spectrometry (HRMS): spectra were obtained from the central analytical mass spectrometry facilities of the Faculty of Chemistry and Pharmacy, University of Regensburg. All mass spectra were recorded on a Finnigan MAT 95, Thermo Quest Finnigan TSQ 7000, Finnigan MATSSQ 710 A or an Agilent Q-TOF 6540 UHD instrument.

GC-FID and GC-MS: GC measurements were performed on a GC 7890 from Agilent Technologies. Data acquisition and evaluation were done with Agilent Chem Station Rev.C.01.04. GC–MS measurements were performed on a 7890A GC system from Agilent Technologies with an Agilent 5975 MSD Detector. Data acquisition and evaluation was done with MSD Chem Station E.02.02.1431. A capillary column HP-5MS/30 m x 0.25 mm/0.25 µM

film and helium as carrier gas (flow rate of 1 mL/min) were used. The injector temperature (split injection: 40:1 split) was 280 ºC, detection temperature 300 ºC (FID). GC measurements were made and investigated via integration of the signal obtained. The GC oven temperature program was adjusted as follows: initial temperature 40 ºC was kept for 3 min, the temperature was increased at a rate of 15 ºC/min over a period of 16 minutes until 280 ºC was reached and kept for 5 min, the temperature was again increased at a rate of 25 ºC/min over a period of 48 s until the final temperature (300 ºC) was reached and kept for 5 min.

Photoreactor setup: photoreactions were irradiated with LEDs (Engine LZ4-40UB00-00U5, λ = 385 nm (± 28), average radiant flux 4702 ± 70 mW, 90 V, 900 mA). Reaction mixtures were exposed to light under stirring (350 rpm, magnetic stirrer) from the bottom side of the vial. The temperature of the system was controlled by a water-cooling circuit consisting of an aluminium cooling block connected to a thermostat (Figure S1).

The optical power of the LEDs was determined using a FieldMaxII-TOTM laser power meter equipped with a PM3 sensor. The emission spectrum of the LEDs (Figure S2) was recorded using an Ocean Optics HR4000CG-UV-NIR Glass fiber and diffusor.

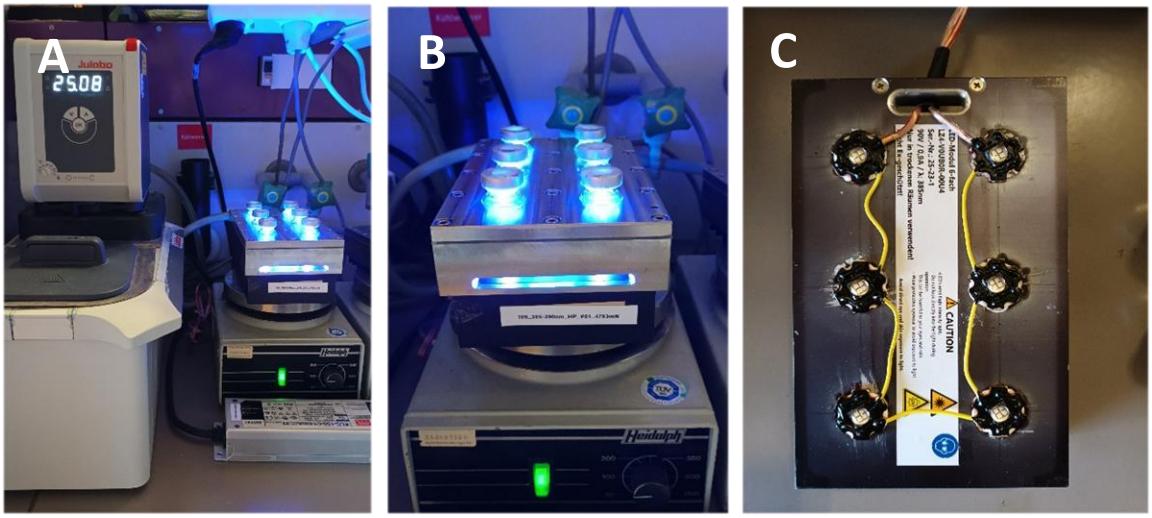

Figure S1. Photoreactor setup. A: Thermostat connected to the aluminium cooling block. B: Cooling block and LED on top of stirrer. C: LED module.

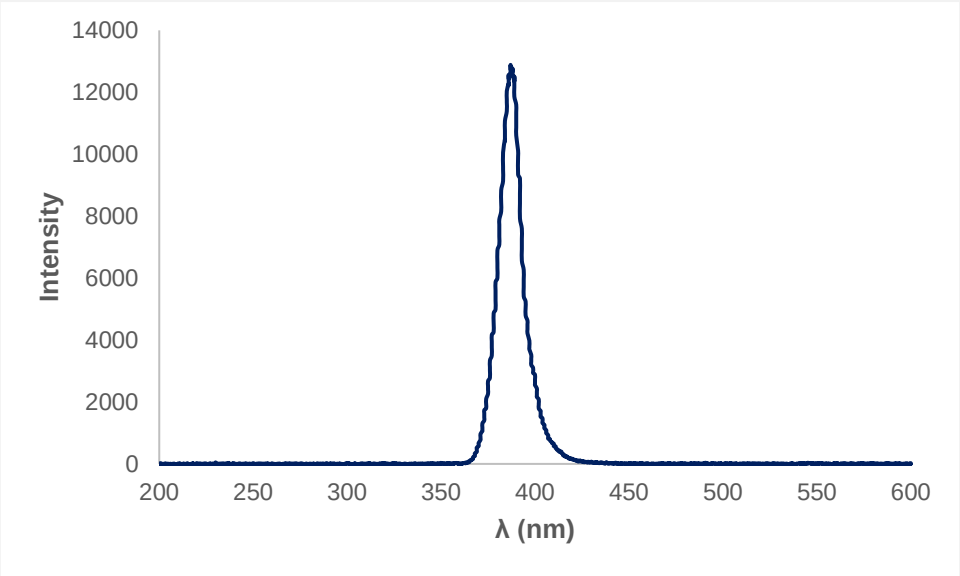

Figure S2. Led emission spectrum of the LED used for the photoreactions.

Glassware absorption: photoreactions were carried out in WICOM 20 mm crimp-cap vials (5 mL, 38.5 x 22 mm) made of borosilicate glass. The vials transmit 100% of incident light above 350 nm (Figure S3).

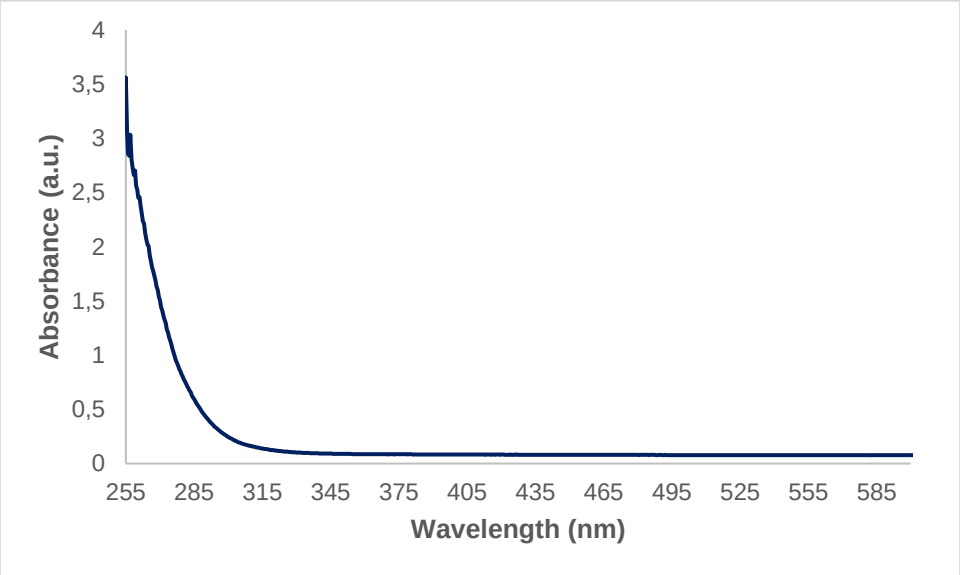

Figure S3 Absorption spectrum of vials used for photoreactions.

5.4.2 General Synthetic Procedures

General Procedure for Photoreactions (GP1)

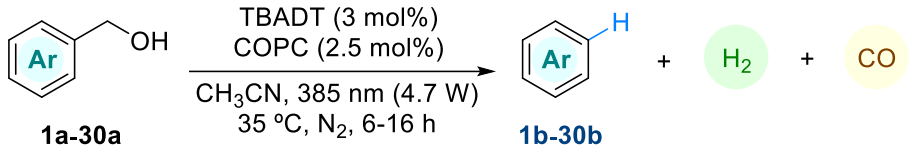

Scheme S1. General procedure for the photocatalytic dehydroformylation of benzyl alcohols.

A 5 mL crimp-cap vial equipped with a PTFE-coated stirring bar, was loaded with the corresponding benzyl alcohol (50 µmol, 1.00 equiv.) (if solid), TBADT (5.1 mg, 1.5 µmol, 3 mol%) and COPC (0.5 mg, 1.25 µmol, 2.5 mol%). The vial was sealed, evacuated, and backfilled with N_2 before adding the corresponding benzyl alcohol (50 µmol, 1.00 equiv.) (if liquid) and non-dried CH_3CN (0.5 mL). The reaction mixture was subsequently purged with N_2 for 10 min and stirred under irradiation using a 4.7 W 385 nm (± 25 nm) LED set-up for 6 h or 16 h at 35 °C (temperature controlled by a thermostat). Reaction progress was monitored by TLC or GC analysis. Afterwards, the reaction yield was determined via GC-FID analysis using mesitylene as internal standard.

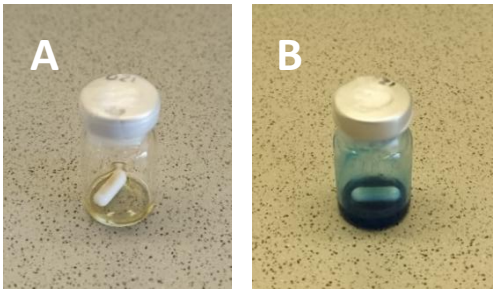

Figure S4. Vial containing reaction mixture of **1a**. A: before irradiation. B: after 6 h irradiation.

General Procedure for the Synthesis of Starting Materials (GP2)

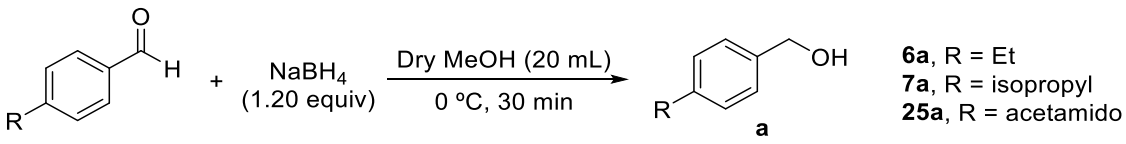

Scheme S2. General procedure for the synthesis of benzyl alcohols as starting materials.

In an oven-dried round bottom flask, the corresponding benzaldehyde (2.50 mmol, 1.00 equiv.) was dissolved in dry MeOH (10 mL). The mixture was cooled to 0 °C and a solution of $NaBH_4$ (114 mg, 3.00 mmol, 1.20 equiv.) in dry MeOH (10 mL) was slowly added. The resulting mixture was stirred at 0 °C for 30 min. After confirming reaction completion by TLC-analysis, the reaction was quenched with water (10 mL) and the product was extracted with EtOAc (5 x 10 mL). The combined organic layers were dried over Na_2SO_4, and the solvent was removed under reduced pressure. The crude product was purified via FCC (PE/EtOAc).

5.4.3 Reaction Conditions Optimization

Table S1. Screening of photocatalyst.

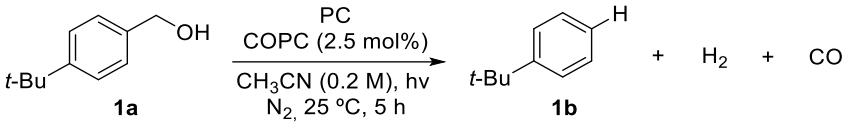

Entry	photocatalyst (mol%)	Irradiation	Yield of **1b** (%)[a]
1	Anthraquinone (5)	395 nm (2.2 W)	Traces
2	Benzophenone (5)	365 (3.1 W)	7
3	Benzophenone (25)	365 (3.1 W)	42
4	4-Methoxy-4'-trifluoromethyl benzophenone (5)	395 nm (2.2 W)	10
5	TBADT (1)	395 nm (2.2 W)	23
6	TBADT (2)	395 nm (2.2 W)	39
7	TBADT (3)	395 nm (2.2 W)	53
8	TBADT (4)	395 nm (2.2 W)	55
9	Thioxanthone (5)	395 nm (2.2 W)	3
10	Xanthone (5)	395 nm (2.2 W)	Traces

1a (0.1 mmol), photocatalyst, COPC (2.5 mol%), CH_3CN (0.5 mL; non-dried), LED, 25 °C, 5 h, N_2. [a]Yields were determined by GC-FID analysis using mesitylene as I.S.

Table S2. Screening of cobalt catalyst.

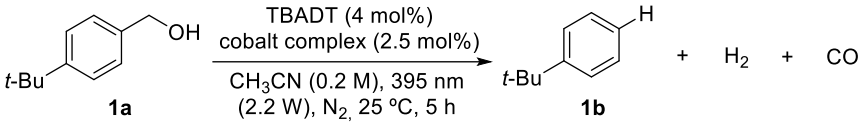

Entry	Cobalt catalyst (mol%)	Yield of **1b** (%)[a]
1	COPC (1.5)	47
2	COPC (2.5)	53
3	COPC (5)	26
4	COPC (10)	9
5	$Co(dmgH)(dmgH_2)Cl_2$ (5)	39

1a (0.1 mmol), TBADT (3 mol%), cobalt complex, CH_3CN (0.5 mL; non-dried), 395 nm (2.2 W), 25 °C, 5 h, N_2. [a]Yields determined via GC-FID analysis using mesitylene as I.S.

Table S3. Screening of solvents.

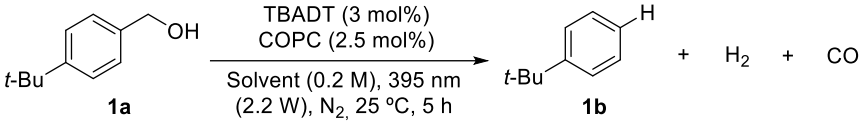

Entry	Solvent	Yield of **1b** (%)[a]
1	DMSO (dry)	2
2	CH_3CN (dry)	51
3[b]	CH_3CN (non-dried)	53
4	EtOAc (dry)	7
5	DMF (dry)	N.d.

1a (0.1 mmol), TBADT (3 mol%), COPC (2.5 mol%), solvent (0.5 mL), 395 nm (2.2 W), 25 ℃, 5 h, N_2. [a]Yields were determined by GC-FID analysis using mesitylene as I.S. [b]Water content (245 ± 7 ppm H_2O) determined by Karl-Fischer titration.

Table S4. Screening of reaction concentration.

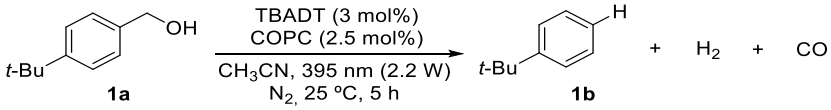

Entry	Concentration	Yield of **1b** (%)[a]
1	0.1 M	58
2	0.2 M	53

1a, TBADT (3 mol%), COPC (2.5 mol%), CH_3CN (0.5 mL; non-dried), 395 nm (2.2 W), 25 ℃, 5 h, N_2. [a]Yields were determined by GC-FID analysis using mesitylene as I.S.

Table S5. Screening of irradiation source.

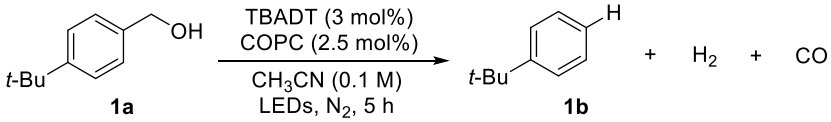

Entry	Irradiation source	Temperature (ºC)[b]	Yield of **1b** (%)[a]
1	395 nm (2.2 W)	25	58
2	385 nm (3.6 W)	29	65
3	385 nm (4.7 W)	35	81
4	365 nm (3.1 W)	30	62

1a, TBADT (3 mol%), COPC (2.5 mol%), CH_3CN (0.5 mL; non-dried), LEDs, 5 h, N_2. [a]Yields were determined by GC-FID analysis using mesitylene as I.S. [b]Temperature of reaction mixture.

Table S6. Reaction time screening.

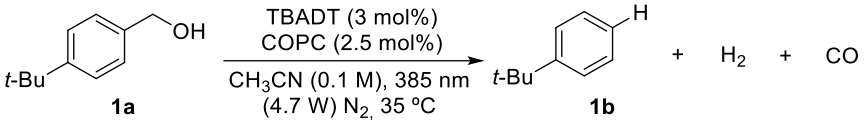

Entry	Time (h)	Yield of **1b** (%)[a]
1	1	48
2	2	62
3	3	75
4	4	78
5	5	81
6	6	85
7	16	82

1a, TBADT (3 mol%), COPC (2.5 mol%), CH_3CN (0.5 mL; non-dried), 385 nm (4.7 W), 35 ℃, N_2. [a]Yields were determined by GC-FID analysis using mesitylene as I.S.

Figure S5. Kinetic profile with optimized reaction conditions for **1a**.

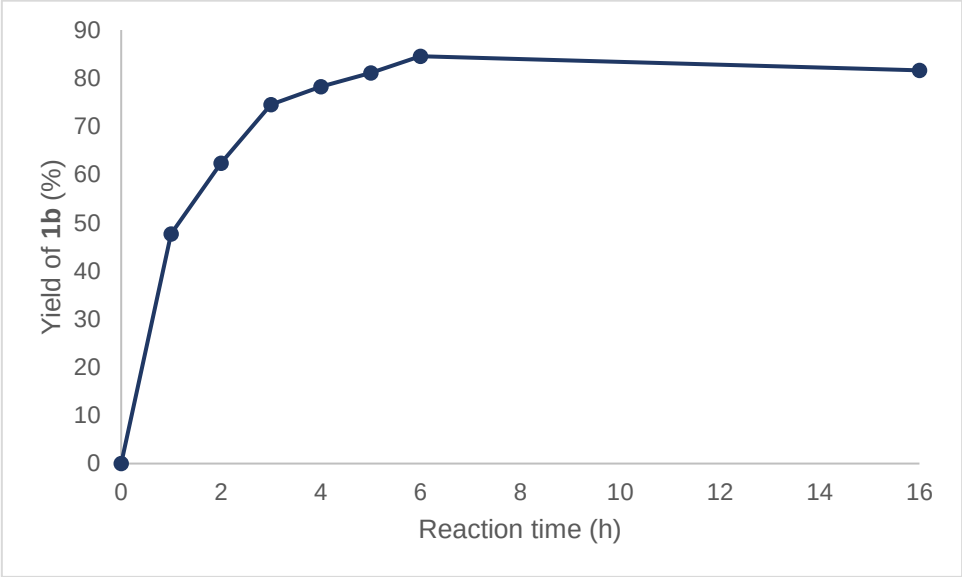

5.4.4 Mechanistic Studies

Control Experiments

The control experiments were set according to general procedure **GP1**.

Table S7. Control experiments.[a]

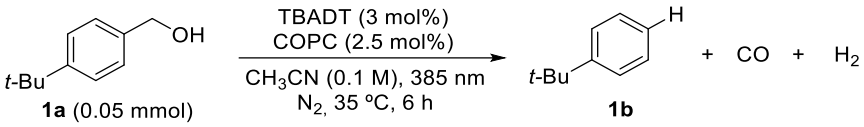

Entry	Deviation from standard conditions	Yield of **1b**[a] (%)
1	None	85
2	No TBADT	N.d.
3	No COPC	N.d.
4	No light	N.d.
5	No light; at 60 ºC	N.d.
6	Under air	18

[a]GC-FID yields determined using mesitylene as I.S.

Qualitative Analysis of Evolved Hydrogen Gas

Photocatalytic reaction set according to **GP1**.

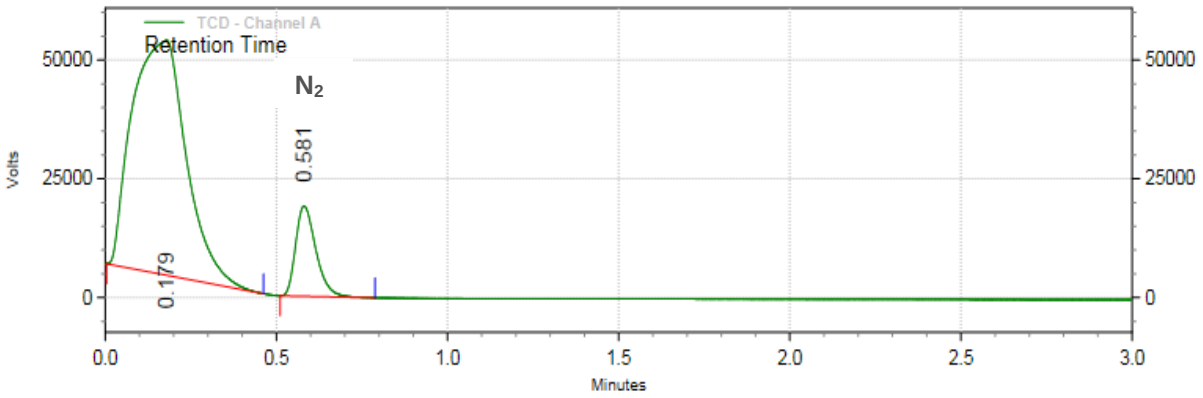

Figure S6. gas chromatogram of vial filled with nitrogen.

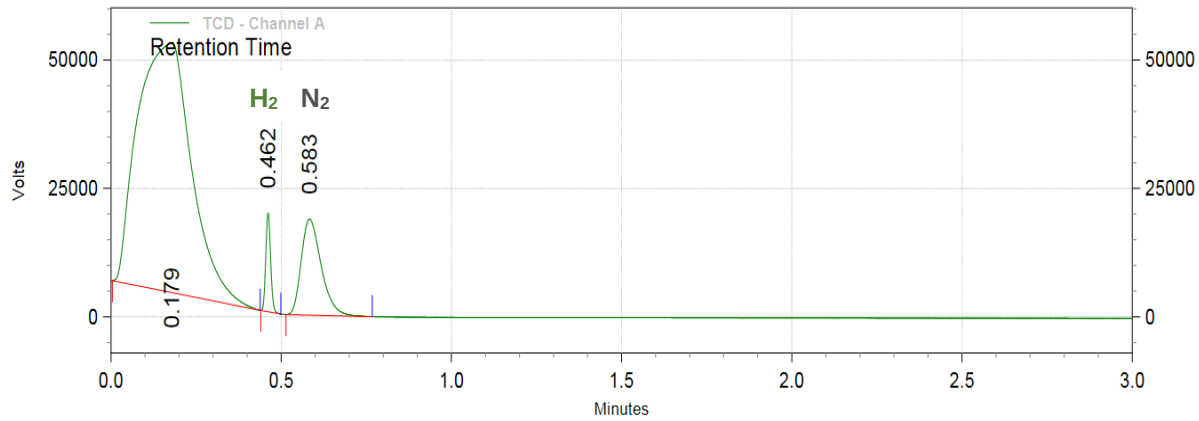

Figure S7 gas chromatogram of vial filled with a mixture of nitrogen and hydrogen.

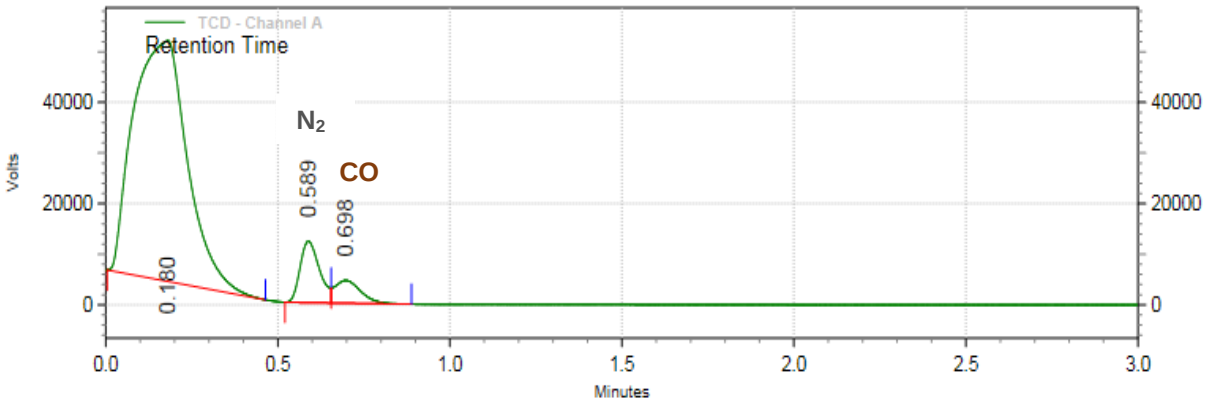

Figure S8. Gas chromatogram of vial filled with a mixture of nitrogen and carbon monoxide.

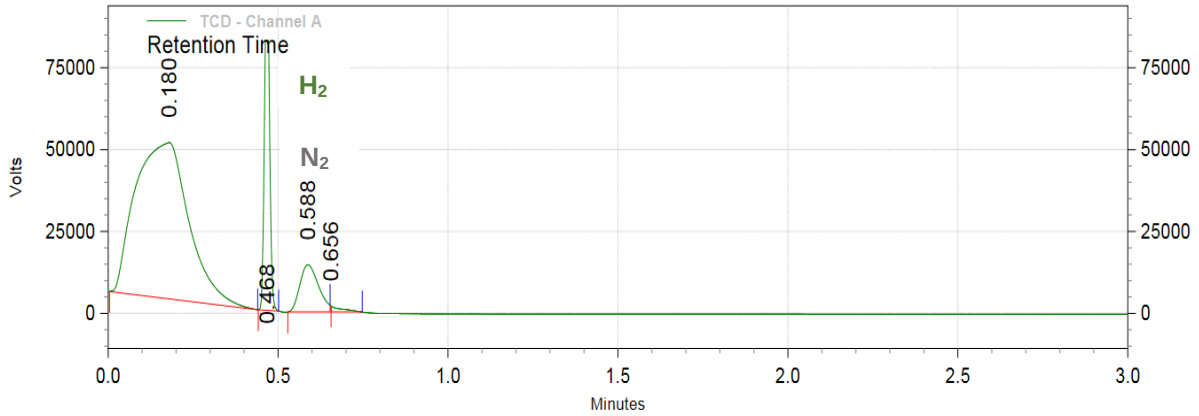

Figure S9. Measurement of gases after irradiating 6 h a reaction mixture containing **1a**.

GC-MS study of the reaction mixture of 1a after 5 h reaction

Photocatalytic reaction set according to **GP1**. In the case of the reaction mixture of the decarbonylation of **1a**, the mass corresponding to the molecular ion of the benzaldehyde intermediate (**1-ald**) could be clearly seen (Figure S10). The yields were determined by GC-FID analysis using mesitylene as internal standard.

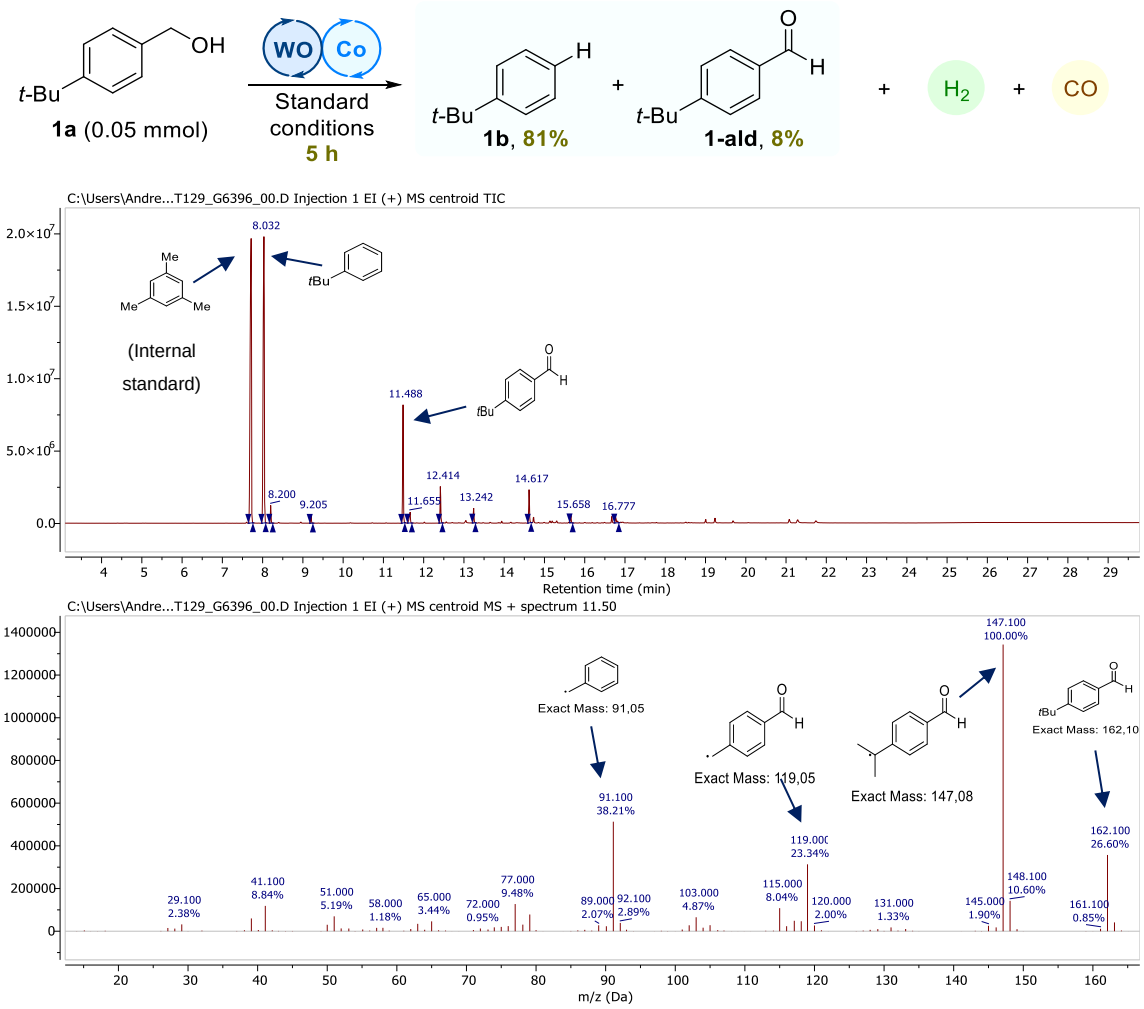

Figure S10. GC-MS chromatogram of the reaction mixture of **1a** after 5 h reaction.

GC-MS study of the reaction mixture of 1a after 6 h reaction

Photocatalytic reaction set according to **GP1**. In the case of the reaction mixture of the decarbonylation of **1a**, after 6 h, the mass corresponding to the molecular ion of the benzaldehyde intermediate (**1-ald**) could be seen (Figure S11), however its proportion was found to be lower in comparison to the reaction mixture of **1a** after 5 h reaction (Figure S10). The yields were determined by GC-FID analysis against mesitylene as internal standard.

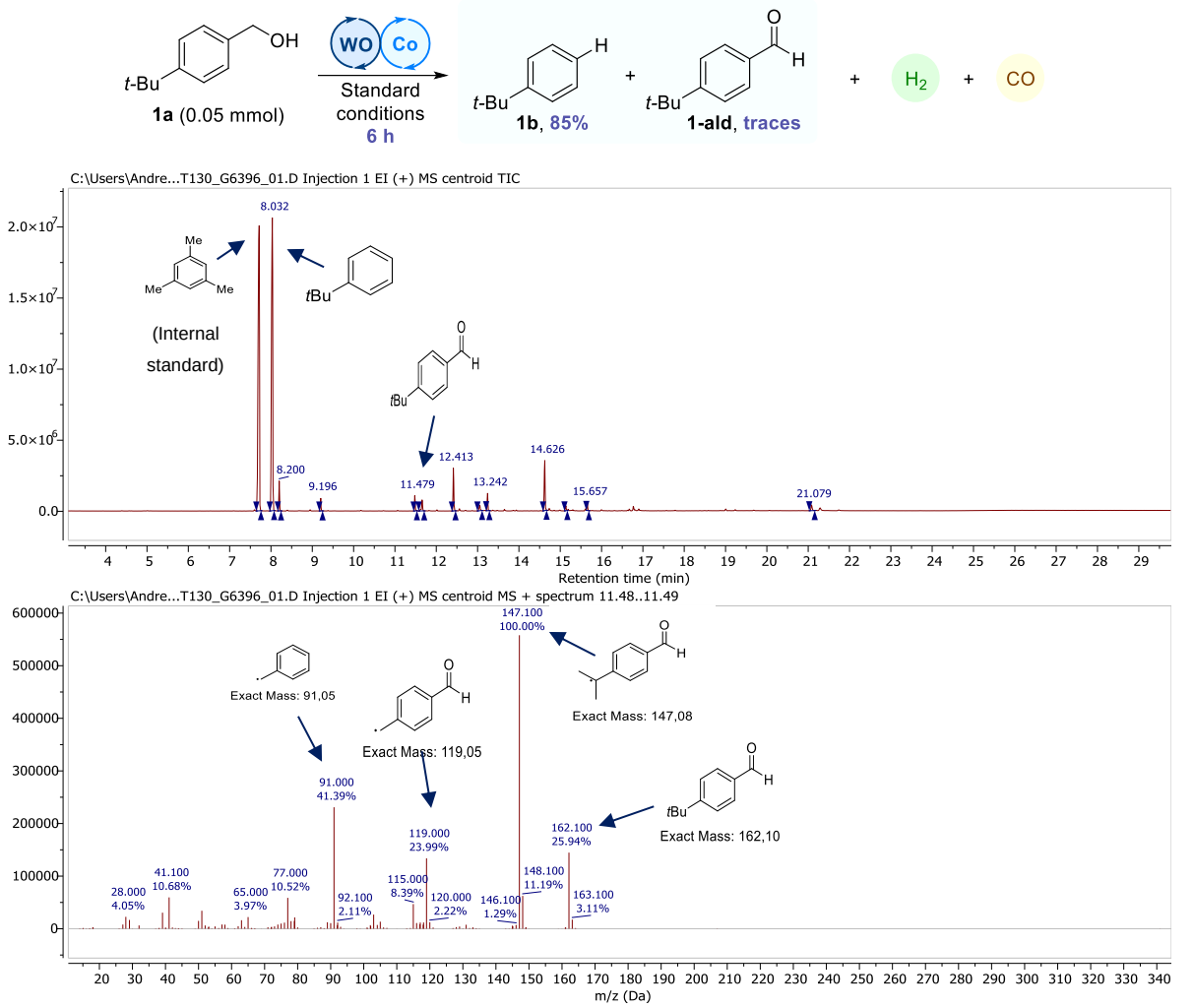

Figure S11. GC-MS chromatogram of the reaction mixture of **1a** after 6 h reaction.

Dehydroformylation of 1a in the presence of TEMPO

A 5 mL crimp-cap vial equipped with a stirring bar, was loaded with TBADT (5.1 mg, 1.5 µmol, 3 mol%), COPC (0.5 mg, 1.25 µmol, 2.5 mol%) and TEMPO (8.0 mg, 50 µmol, 1.00 equiv.). The vial was sealed, evacuated, and back filled with N_2 before adding 4-*tert*butyl benzyl alcohol (9 µL, 50 µmol, 1.00 equiv.), and CH_3CN (0.5 mL). The reaction mixture was subsequently purged with N_2 for 10 min and stirred under irradiation using a 4.7 W 385 nm (± 25 nm) LED set-up for 6 h at 35 ºC. The yield of **1b** was determined by GC-FID analysis and the reaction mixture was analyzed by LC-MS analysis. The addition of TEMPO as a radical scavenger

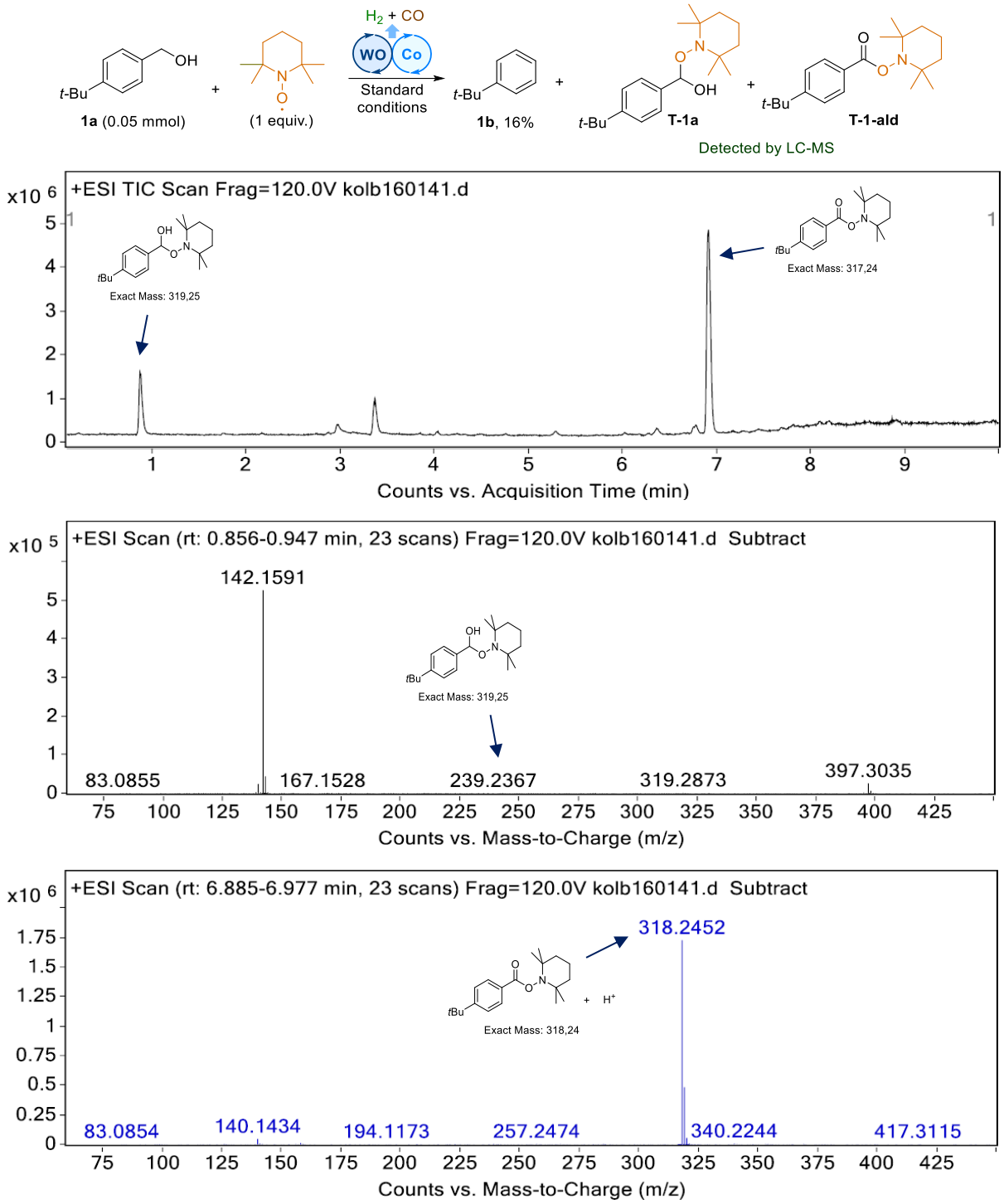

Figure S12. LC-MS chromatogram for the photocatalytic dehydroformylation of **1a** in presence of TEMPO (1 equiv.).

resulted in a significant drop of the reaction yield (16%). Formation of the radical-trapping adducts **T-1a** and **T-1-ald** indicated the in-situ formation of acyl and benzyl radicals.

Decarbonylation of proposed aldehyde intermediate

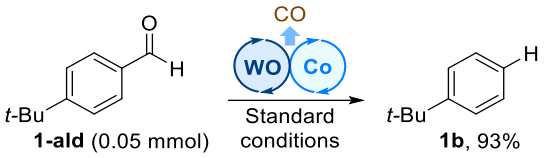

A 5 mL crimp-cap vial equipped with a stirring bar, was loaded with TBADT (5.1 mg, 1.5 µmol, 3 mol%) and COPC (0.5 mg, 1.25 µmol, 2.5 mol%). The vial was sealed, evacuated, and back filled with N_2 before adding 4-*tert*butyl benzaldehyde (9 µL, 50 µmol, 1.00 equiv.), and CH_3CN (0.5 mL). The reaction mixture was subsequently purged with N_2 for 10 min and stirred under irradiation using a 4.7 W 385 nm (± 25 nm) LED set-up for 6 h at 35 ºC (temperature controlled by a thermostat). The yield of **1b** was determined by GC-FID analysis (93%).

Control experiment with 31a

A 5 mL crimp-cap vial equipped with a stirring bar, was loaded with TBADT (5.1 mg, 1.5 µmol, 3 mol%) and COPC (0.5 mg, 1.25 µmol, 2.5 mol%). The vial was sealed, evacuated, and back filled with N_2 before adding benzyl methyl ether (7 µL, 50 µmol, 1.00 equiv.) and CH_3CN (0.5 mL). The reaction mixture was subsequently purged with N_2 for 10 min and stirred under irradiation using a 4.7 W 385 nm (± 25 nm) LED set-up for 6 h at 35 ºC. The reaction mixture was analyzed by GC-MS analysis.

5.4.5 Synthesis and Analytical Data of Isolated Compounds

Synthesis of tetra-*n*-butylammonium decatungstate (TBADT)

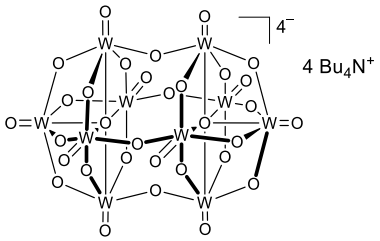

TBADT was synthesized using a modified literature procedure reported in our laboratories before.[15] Tetrabutylammonium bromide (2.40 g, 7.40 mmol, 1.0 equiv.) and $Na_2WO_4 \cdot 2H_2O$ (5.00 g, 15.2 mmol, 2.0 equiv.) were placed into separate 500 ml round bottom flasks. Deionized water (150 ml) was then added to each flask and the resulting solutions were heated to 90 °C. At this temperature, the pH of both solutions was adjusted to a value of 2 by adding conc. HCl. The solutions were combined, and the resulting mixture was stirred at 90 °C for 30 min. The mixture was allowed to cool to 25 ºC and the formed precipitate was filtered off under reduced pressure and washed with water. After removing the remaining water by lyophilization, the solid was suspended in CH_2Cl_2 (100 ml) and stirred at room temperature for 3 h. Lastly, the suspension was filtered under reduced pressure, obtaining TBADT as a white solid (2.40 g, 0.73 mmol, 67 %).

Synthesis of 4-ethylbenzyl alcohol (**6a**)

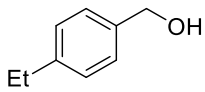

Prepared according to **GP2** from 4-ethylbenzaldehyde (350 µL, 2.50 mmol). The crude product was purified via FCC (PE/EtOAc = 80/20), obtaining **6a** as a clear oil (204 mg, 60%).

^{1}H-NMR (400 MHz, $CDCl_3$): δ (ppm) = 7.29 (d, *J* = 8.0 Hz, 2H), 7.20 (d, *J* = 8.0 Hz, 2H), 4.65 (s, 2H), 2.66 (q, *J* = 7.6 Hz, 2H), 1.80 (bs, 1H), 1.24 (t, *J* = 7.6 Hz, 3H). **^{13}C-NMR** (101 MHz, $CDCl_3$): δ (ppm) = 143.8, 138.1, 128.1, 127.2, 65.3, 28.6, 15.6. **R_f** = 0.30 (PE/EtOAc = 80/20). **HRMS** (EI-MS): $[C_9H_{12}O]^{\cdot+}$ $[M]^{\cdot+}$ calcd: 136.08827; found: 136.08820.

Synthesis of 4-isopropylbenzyl alcohol (**7a**)

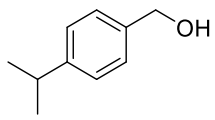

Prepared according to **GP2** from 4-isopropylbenzaldehyde (390 µL, 2.50 mmol). The crude product was purified via FCC (PE/EtOAc = 75/25), obtaining **7a** as a clear oil (194 mg, 52%).

^{1}H-NMR (400 MHz, $CDCl_3$): δ (ppm) = 7.30 (d, *J* = 8.1 Hz, 2H), 7.23 (d, *J* = 8.1 Hz, 2H), 4.66 (s, 2H), 2.92 (dt, *J* = 13.8, 6.9 Hz, 1H), 1.62 (bs, 1H), 1.26 (d, *J* = 6.9 Hz, 6H). **^{13}C-NMR** (101 MHz, $CDCl_3$): δ (ppm) = 148.5, 138.3, 127.2, 126.6, 65.3, 33.9, 24.0. **R_f** = 0.33 (PE/EtOAc = 75/25). **HRMS** (EI-MS): $[C_{10}H_{14}O]^{\cdot+}$ $[M]^{\cdot+}$ calcd: 150.10392; found: 150.10374.

Synthesis of 4-benzyloxybenzyl alcohol (**16a**)

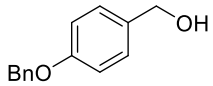

Prepared according to a procedure from Kumar et al. [16] In an oven-dried Schlenck flask, 4-Hydroxybenzyl alcohol (209 mg, 1.65 mmol, 1.00 equiv.) was dissolved in dry acetone (10 mL) under N_2 atmosphere. Next, K_2CO_3 (242 mg, 1.73 mmol, 1.05 equiv.) and benzylbromide (200 µl, 1.65 mmol, 1.00 equiv.) were added and the resulting mixture was stirred at 20 ºC for 24 h. Upon reaction completion, the solvent was removed under reduced pressure and the crude was redissolved in EtOAc (15 ml) and washed with water (15 ml). The aqueous phase was extracted with EtOAc (3 x 15 ml), and the combined organic layers were dried over Na_2SO_4. The solvent was evaporated, and the product was purified via FCC (PE/EtOAc = 75/25), obtaining **16a** as a white solid (152 mg, 43% yield).

1H-NMR (400 MHz, $CDCl_3$): δ (ppm) = 7.47 – 7.36 (m, 4H), 7.36 – 7.26 (m, 3H), 7.00 – 6.94 (m, 2H), 5.08 (s, 2H), 4.62 (s, 2H), 1.58 (s, 1H). **^{13}C-NMR** (101 MHz, $CDCl_3$): δ (ppm) = 158.4, 136.9, 133.4, 128.7, 128.6, 128.0, 127.4, 115.0, 70.0, 65.1. **R_f** = 0.26 (PE/EtOAc = 75/25). **HRMS** (APCI-MS): $[C_{14}H_{18}NO_2]^+$ $[M + NH_4]^+$ calcd: 232.1332; found: 232.1332.

Synthesis of 4-acetoxybenzyl alcohol (**18a**)

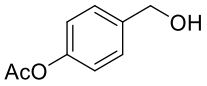

Prepared according to a procedure from Nie et al.[17] In an oven-dried Schlenk flask, 4-hydroxybenzyl alcohol (253 mg, 2.00 mmol, 1 equiv.) was dissolved in dry THF (4 mL) and Et_3N (280 µl, 2.00 mmol, 1 equiv.) was added under inert atmosphere. The mixture was cooled to 0 ºC and a solution of acetylchloride (160 µl, 2.20 mmol, 1.10 equiv.) in THF (4 mL) was slowly added. The resulting mixture was stirred for 2 h at 0 ºC. After confirming reaction completion by TLC analysis, the reaction mixture was filtered, and the solid was washed with THF (5 mL). The solvent was removed under reduced pressure and the crude was redissolved in CH_2Cl_2 (10 mL) and washed with water (10 mL). The organic layer was dried over Na_2SO_4, and the solvent was removed in vacuo. The crude product was purified via FCC (PE/EtOAc = 75/25), obtaining **18a** as a clear oil (126 mg, 38%).

^{1}H-NMR (400 MHz, $CDCl_3$): δ (ppm) = 7.36 (d, *J* = 8.5 Hz, 2H), 7.10 – 7.03 (m, 2H), 4.66 (s, 2H), 2.29 (s, 3H), 1.92 (s, 1H). **^{13}C-NMR** (101 MHz, $CDCl_3$): δ (ppm) = 169.6, 150.0, 138.5, 128.0, 121.6, 64.7, 21.1. **R_f** = 0.26 (PE/EtOAc = 75/25). **HRMS** (APCI-MS): $[C_9H_{14}NO_3]^+$ $[M + NH_4]^+$ calcd: 184.0968; found: 185.1011.

Synthesis of 4-benzoyloxybenzyl alcohol (**19a**)

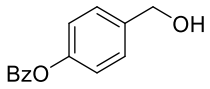

Prepared according to a procedure from Nie et al.[3] In an oven-dried Schlenk flask, 4-hydroxybenzyl alcohol (253 mg, 2.00 mmol, 1 equiv.) was dissolved in dry THF (5 mL) and Et_3N (280 µl, 2.00 mmol, 1 equiv.) was added under inert atmosphere. The mixture was cooled to 0 ºC and a solution of benzoylchloride (233 µl, 2.00 mmol, 1.00 equiv.) in THF (5 mL) was slowly added. The resulting mixture was stirred for 30 min at 0 ºC. After confirming reaction completion by TLC analysis, the solvent was evaporated, and the crude was redissolved in EtOAc (10 mL) and washed with water (10 mL). The aqueous phase was extracted with EtOAc (3 x 10 mL), and the combined organic layers dried over Na_2SO_4. After removing the solvent under reduced pressure, the crude product was purified via FCC (PE/EtOAc = 70/30), obtaining **19a** as a white solid (280 mg, 63%).

^{1}H-NMR (400 MHz, $CDCl_3$): δ (ppm) = 8.28 – 8.14 (m, 2H), 7.64 (ddd, *J* = 7.0, 2.5, 1.3 Hz, 1H), 7.51 (dd, *J* = 10.7, 4.7 Hz, 2H), 7.44 (d, *J* = 8.6 Hz, 2H), 7.25 – 7.18 (m, 2H), 4.72 (s, 2H), 1.80 (s, 1H). **^{13}C-NMR** (101 MHz, $CDCl_3$): δ (ppm) = 165.3, 150.4, 138.6, 133.7, 130.2, 129.5, 128.6, 128.2, 121.9, 64.8. **R_f** = 0.22 (PE/EtOAc = 70/30). **HRMS** (EI-MS): $[C_{14}H_{12}O_3]^{\cdot+}$ $[M]^{\cdot+}$ calcd: 228.07810; found: 228.07852.

Synthesis of 4-acetamidobenzyl alcohol (**24a**)

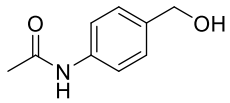

Prepared according to **GP2** from 4-acetamidobenzaldehyde (416 mg, 2.50 mmol). The crude product was purified via FCC (CH_2Cl_2/MeOH = 93/7), obtaining **24a** as a white solid (186 mg, 50%).

^{1}H-NMR (400 MHz, MeOD): δ (ppm) = 7.50 (d, *J* = 8.5 Hz, 2H), 7.28 (d, *J* = 8.6 Hz, 2H), 4.85 (s, 2H), 4.54 (s, 2H), 2.10 (s, 3H). **^{13}C-NMR** (101 MHz, MeOD): δ (ppm) = 171.6, 139.0, 138.5, 128.6, 121.1, 64.8, 23.8. **R_f** = 0.28 (CH_2Cl_2/MeOH = 93/7). **HRMS** (APCI-MS): $[C_9H_{12}NO_2]^+$ $[M + H]^+$ calcd: 166.0863; found: 166.0863.

5.5 References

[1] S. Naqvi, Oxo Alcohols. Process Economics Program Report 21E; SRI Consulting: Menlo Park, CA, **2010**.

[2] F. Merger; H. J. Foerster, (to BASF Aktiengesellschaft) EP Patent 0058927.

[3] H. Fischer, G. Schnuchel, (to Erdölchemie GmbH) German Patent DE 2163396, 1973; *Chem. Abstr*. **1973**, *79*, 106002.

[4] a) R. Franke, D. Selent, A. Börner, *Chem. Rev*., **2012**, *112*, 5675–5732; b) G. M. Torres, R. Frauenlob, R. Franke, A. Börner, *Catal. Sci. Technol.* **2015**, *5*, 34–54.

[5] a) F. L. Zhang, B. Li, K. N. Houk, Y.-F. Wang, *JACS Au* **2022**, *2*, 1032–1042; b) M. Wang, H. Zhou, F. Wang, *Acc. Chem. Res.* **2023**. 56, 1057–1069.

[6] A. B. Korpusik, A. Adili, K. Bhatt, J. E. Anatot, D. Seidel, B. S. Sumerlin, *J. Am. Chem. Soc.* **2023**. *145*, 10480–10485.

[7] a) R. H. Prince, K. A. Raspin, *Chem. Commun*. **1966,** 156–157; b) C. A. McCombs, C. H. Foster, (to Eastman Kodak company) U.S. Patent 4272444A, **1980**; c) D. L. Wertz, M. F. Sisemore, M. Selke, J. Driscoll, J. S. Valentine, *J. Am. Chem. Soc.* **1998**, *120*, 5331–5332; d) Y. Goto, S. Wada, I. Morishima, Y. Watanabe, *J. Inorg. Biochem*. **1998**, *69*, 241–247; e) S. Kusumoto, T. Tatsuki, K. Nozaki, *Angew. Chem. Int. Ed*. **2015**, *54*, 8458–8461.

[8] H.-A. Ho, K. Manna, A. D. Sadow, *Angew. Chem. Int. Ed*. **2012**, *51*, 8607–8610; b) A. Mazziotta, R. Madsen, *Eur. J. Org. Chem.* **2017**, *2017*, 5417–5420; c) X. Wu, F. A. Cruz, A. Lu, V. M. Dong, *J. Am. Chem. Soc.* **2018**, *140*, 10126–10130.

[9] D. J. Abrams, J. G. West, E. J. Sorensen, *Chem. Sci*. **2017**, *8*, 1954–1959.

[10] a) K. Zhang, L. Chang, Q. An, X. Wang, Z. Zuo, *J. Am. Chem. Soc.* **2019**, *141*, 10556–10564; b) Y. Chen, X. Wang, X. He, Q. An, Z. Zuo, *J. Am. Chem. Soc.* **2021**, *143*, 4896–4902.

[11] D. Kolb, M. Morgenstern, B. König, *Chem. Commun.* **2023**, *59*, 8592–8595.

[12] a) J. F. Andersen, *J. Agric. Food Chem*. **1987**, *35*, 60–62; b) N. Dudareva, E. Pichersky, J. Gershenzon, *Plant Physiol*. **2004**, *135*, 1893–1902; c) B. N. Shyamala, M. M. Naidu, G. Sulochanamma, P. Srinivas, *J. Agric. Food Chem*. **2007**, *55*, 7738–7743.

[13] a) Z. Wen, Z. Li, Z. Shang, J. P. Cheng, *J. Org. Chem*. **2001**, *66*, 1466–1472; b) J. Hioe, H. Zipse, *Org. Biomol. Chem.* **2010**, *8*, 3609–3617.

[14] a) J. L. Dempsey, B. S. Brunschwig, J. R. Winkler, H. B. Gray, *Acc. Chem. Res*. **2009**, *42*, 1995–2004; b) J. G. West, D. Huang, E. J. Sorensen, *Nat. Commun*. **2015**, *6*, 10093; c) V. de Waele, O. Poizat, M. Fagnoni, A. Bagno, D. Ravelli, *ACS Catal*. **2016**, *6*, 7174–7182; d) D. Ravelli, M. Fagnoni, T. Fukuyama, T. Nishikawa, I. Ryu, *ACS Catal*. **2018**, *8*, 701–713; e) Ritu, D. Kolb, N. Jain, B. König, *Adv. Synth. Catal*. **2023**, *365*, 605–611; f) Y. Seino, Y. Yamaguchi, A. Suzuki, M. Yamashita, Y. Kamei, F. Kamiyama, T. Yoshino, M. Kojima, S. Matsunaga, *Chem. Eur. J*. **2023**, *29*, e202300804.

[15] a) I. B. Perry, T. F. Brewer, P. J. Sarver, D. M. Schultz, D. A. DiRocco, D. W. C. MacMillan, *Nature* **2018**, *560*, 70–75; b) F. Babawale, K. Murugesan, R. Narobe, B. König, *Org. Lett.* **2022**, *24*, 4793–4797.

[16] P. Kumar, R. A. Fernandes, M. N. Ahmad, S. Chopra, *Tetrahedron* **2021**, *96*, 132375.

[17] X. Nie, L. Xia, H. L. Wang, G. Chen, B. Wu, T. Y. Zeng, C. Y. Hong, L. H. Wang, Y. Z. You, *ACS Appl. Mater. Interfaces* **2019**, *11*, 31735–31742.

Part III – HAT initiated Spin-Center Shift Photocatalysis

6. Photocatalyzed Dehydration of 1-Aryl-1,2-Ethanediols to Methyl Ketones Driven by Eosin Y Fragmentation Products

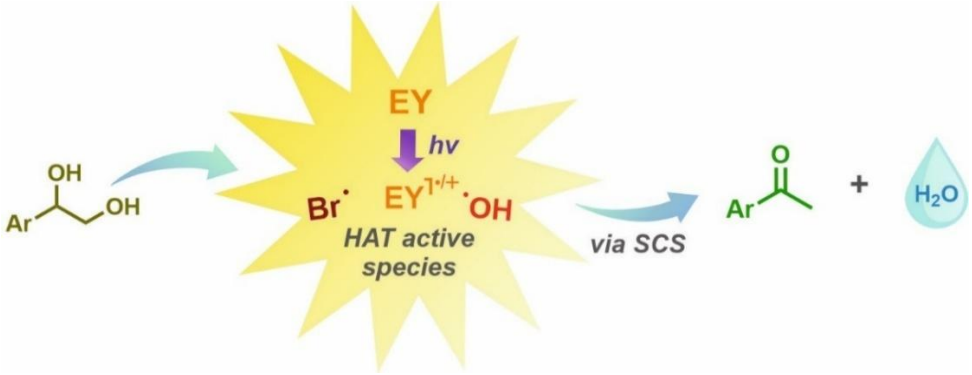

Abstract: Herein, we report a mild photocatalytic redox-neutral dehydration of aryl-1,2-ethanediols forming the respective methyl ketones. In the proposed mechanistic cycle, an initial hydrogen atom transfer (HAT) event is followed by a 1,2-spin center shift (SCS) as key steps. Interestingly, Eosin Y was found to act as a pre-catalyst dissociating into a catalytically active mixture under irradiation. To the best of our knowledge, this exemplifies the first synthetic utilization of Eosin Y degradation products. As a result, our reaction can be realized with a single organic photocatalyst and releases water as a sole by-product.

[i] Reproduced from E. K. Taskinen, D. Kolb, M. Morgenstern, B. König,* *Chem. Eur. J*. **2025**, *31*, e202404200. with permission from Wiley-VCH GmbH. Schemes, tables, and text may differ from the published version.

[ii] Author contributions: E. Taskinen and M. Morgenstern conceived the concept of this study and investigated the scientific background. E. Taskinen and D. Kolb synthesized the starting materials and conducted the mechanistic investigations. D. Kolb optimized the reaction conditions. E. Taskinen performed the photoreactions and isolated the products. E. Taskinen wrote the manuscript and supporting information with input from D. Kolb. B. König supervised the project, reviewed the manuscript, and is the corresponding author.

6.1 Introduction

1,2-Diols and vicinal polyols are widely present in Nature, playing vital roles in the structure and function of life-enabling architectures.[1] For plants and bacteria, carbohydrates represent the main constituent in their cell walls. For mammals, carbohydrates form the backbone for genetic information storage (deoxyribose in DNA) and are a major energy source.[2] Furthermore, glycosylation, the addition of glycans to cell surfaces, has been identified as an efficient means for cell-to-cell signalling and pathogen recognition in the recent years.[3] In society, naturally occurring polyols have found various uses as food additives (Xylitol), dyes (anthocyanins), and cosmetics (glycerine).[4] In chemistry, polyols have served as important building blocks for the chiral pool and provided inspiration for method development for decades.[5] As a result, the reactivity of alcohols has been carefully studied and further utilized in the synthesis of polymers or polyhydroxylated natural products.[6,7]

Recently, the well-established two-electron transformations of alcohols have been enriched further by photochemistry, which provides a mild and easy access to one-electron reaction pathways.[8] The reactivity of oxygen-centered radicals, generated from ligand-to-metal charge transfer (LMCT) or proton-coupled electron transfer (PCET) strategies have unlocked several intriguing transformations ranging from hydrogen atom transfer (HAT) to selective C–C bond cleavage.[8a,8b,8f] For instance, when subjecting diol **I** to cerium LMCT catalysis, the initial formation of an oxygen-centered radical is swiftly followed by a β-scission forming the corresponding aldehyde products **II** and **III** (Scheme 1a).[9] In addition to the alkoxy radical generation, the proximity of a heteroatom also lowers the dissociation energy of the neighbouring C–H bonds[10], thus providing means for highly selective α-O activation strategies (Scheme 1b–1d). Although in many cases the transient carbon-centered radical (such as **VII**) is trapped by radical acceptors, the same intermediate has also been utilized in C–O-epimerizations as elegantly demonstrated by the groups of MacMillan, Phipps and Wendlant (Scheme 1b, compounds **V** and **VI**).[11] Upon further tuning the reaction conditions, the α-oxygen radicals **VII** and **XI** can be directed towards another reaction pathway.

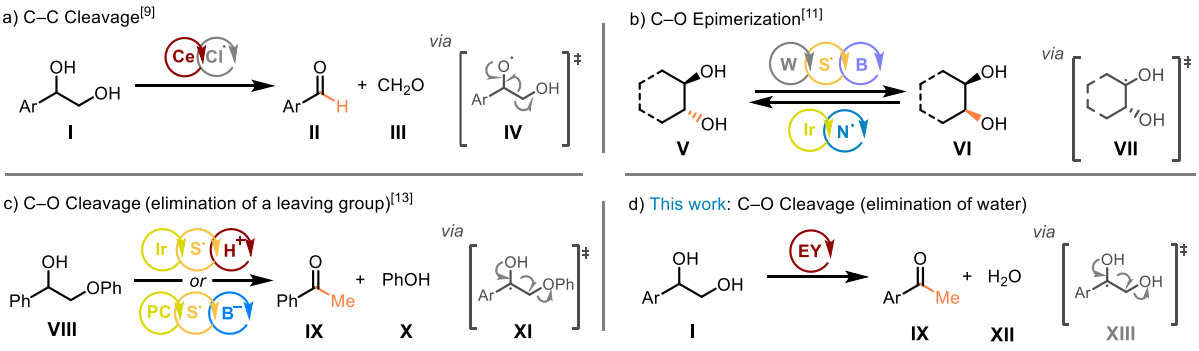

Scheme 1. Previous reported photocatalytic reactions of vicinal diols (a)–c))[9,11,13] and the redox-neutral photocatalytic dehydration (this work, d)).

As first defined by Wessig and Muehlin in their review article, the classical 1,2-spin center shift (SCS) process that can be described as “a 1,2- radical shift accompanied by the elimination of an adjacent leaving group or its corresponding acid”.[12] Inside living cells, the SCS sequence works as a key step in the biosynthesis and repair of DNA, yet due to the effortless engagement of multiple atoms, this process has also found its use in organic chemistry.[12]

For synthetic purposes, the SCS has been used in intermolecular and intramolecular reactions to achieve a wide array of transformations ranging from pyridine alkylations to degradation of lignin model compounds.[13] Towards the latter goal, the groups of König and Nocera have harnessed a dual-catalytic system comprising of a photocatalyst and HAT catalyst for the redox-neutral phenolate elimination (Scheme 1c).[14] Despite the success of this dual catalytic strategy on lignin-like compounds, no reaction could be observed with a free hydroxy group as the leaving group. As summarized by Houk and Wang in their recent review, the general limitation still suppressing the broader applicability of the SCS is its requirement for a good leaving group and/or for additives to assist the elimination.[13a] As converting the β-functionality to a good leaving group adds to the number of synthetic steps and increases the waste generated, the use of strong acids or bases severely limits the functional group tolerance. To address these limitations, we herein report a redox-neutral photocatalytic HAT/SCS sequence for the mild dehydration of aryl-1,2-ethanediols **I** to methyl ketones (Scheme 1d). Our reaction runs with a single organic photocatalyst thus providing a significant simplification to the previously reported catalytic systems. Moreover, substrate pre-activation together with acidic or basic additives can be avoided. As a result, water is released as the sole by-product of our reaction.

6.2 Results and Discussion

We commenced our efforts towards the development of a mild dehydration protocol by choosing the commercially available 1-phenyl-1,2-ethanediol (**1a**) as a starting material (Table 1). Upon screening various HAT catalysts, we were pleased to observe that Eosin Y gave an excellent conversion of the starting material into the product within one hour (Table S1). With further optimization, the loading of Eosin Y could be reduced to 2 mol% while obtaining the product in 91% yield (Entry 1). Intriguingly, the structurally related Fluorescein and product-resembling benzophenone were unable to catalyse the desired transformation (Entries 2 and 3). Bismuth and iron chloride, known to generate chlorine radicals *via* LMCT mechanism,[15] also furnished the product albeit in lowered yields (32% and 11% yield, respectively, Entries 4 and 5). Moving on to solvents, acetonitrile turned out to be the best option, although ethyl acetate also gave good yields despite the reaction was proceedingslightly slower (Entry 6). Unexpectedly, the irradiation with 385 nm LEDs gave the

Table 1. Screening of reaction conditions.

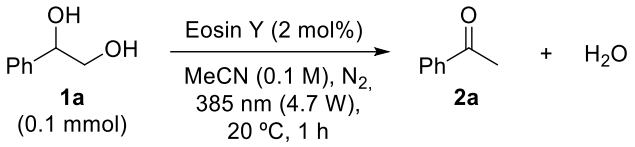

Entry	Deviation from conditions	Yield of **2a** (%)[a]
1	-	91
2	Fluorescein	n.d.
3	Benzophenone	n.d.
4[b]	$BiCl_3$ (20 mol%)	32
5[c]	$FeCl_3$ (20 mol%)	11
6[d]	EtOAc instead of MeCN	73
7	420 nm or 520 nm LEDs	Traces
8	Under air	Traces
9	No light or photocatalyst	n.d.

[a]Calibrated GC-FID yields. [b]$BiCl_3$ (20 mol%) + TBACl (40 mol%). [c]$FeCl_3$ (20 mol%) + TBACl (20 mol%). [d]Reaction time 3 h. TBACl = tetra-*n*-butylammonium chloride.

highest yield, whereas 520 nm or 420 nm irradiation resulted in trace amounts of product (Entry 7). Lastly, the performed control experiments proved the necessity of an inert atmosphere, light, and photocatalyst for the transformation (Entries 8 and 9).

Having established the optimal reaction conditions, we moved on to study the scope of the transformation. Some trends across the reaction scope were identified (Scheme 2). With respect to the steric effects, a methyl substituent on the *para*-and *meta*-positions gave essentially identical yields (71% and 70%), whereas shifting the methyl group to the *ortho*-position decreased the yield to 21% (compound **2b** + **2c** vs. **2d**). These results suggest some degree of sensitivity towards steric hindrance near the reaction center. Further away on the ring, though, a smooth conversion to the product could be achieved even with a *tert*-butyl group in place (compound **2e**).

With respect to the electronic effects, a clear preference was observed for electron-poor groups placed in the *para*-position and electron donating groups located in the *meta*-position (vide infra). For example, the *para*-fluorinated diol furnished the corresponding acetophenone **2f** in a 72% yield whereas the *meta*-fluorinated diol reacted to the product in a mere 32% yield (**2g**). In addition to fluorine, trifluoromethyl and chlorine *para*-substituents were also well tolerated, both giving the desired products with over 70% yields (compounds **2h** and **2i**). In contrast, a methoxy group in a *para*-position led to 15% yield of product **2j** but a methoxy group

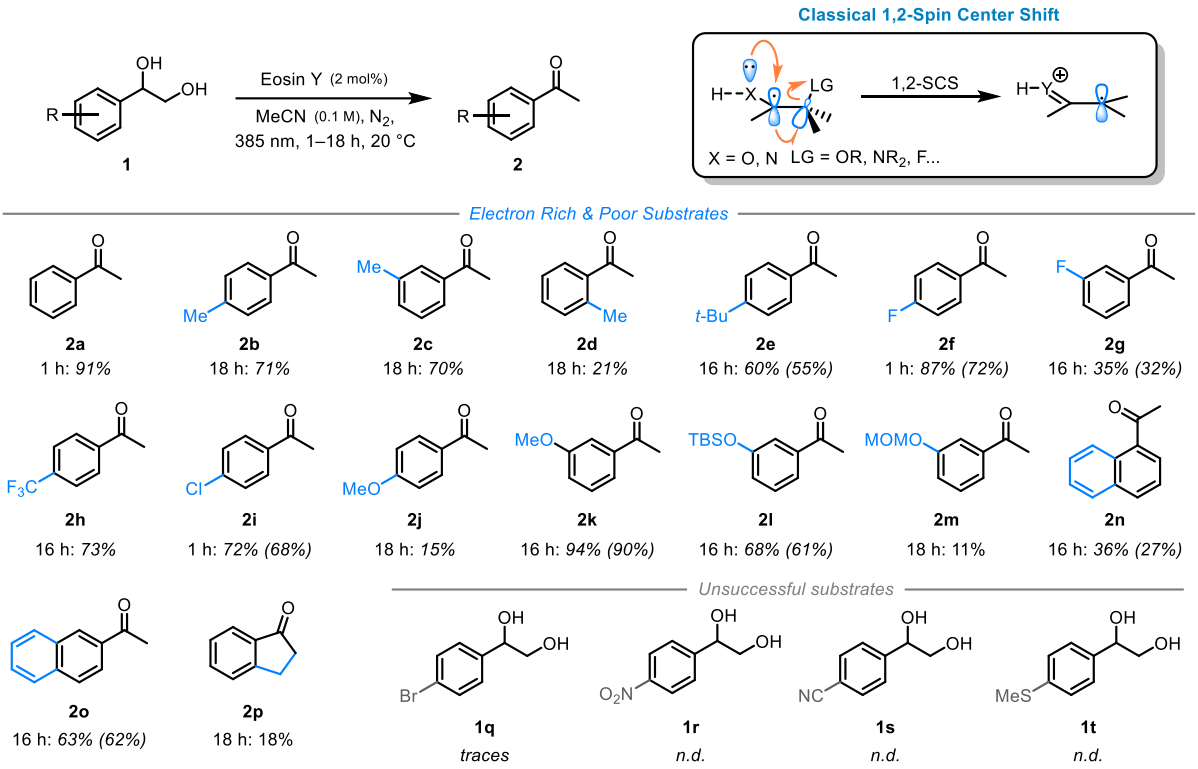

Scheme 2. Scope for the photocatalytic dehydration of diols. Yields reported as calibrated GC-FID yields, isolated yields in parenthesis.

as the *meta*-substituent gave the acetophenone derivative **2k** in excellent yield (91%). Furthermore, a highly electron-rich and acid-labile TBS group could be used to protect the phenolic hydroxy group in the *meta*-position, thus forming the corresponding OH-protected acetophenone **2l** in a 68% yield. A MOM-protected phenol, in turn, gave the product **2m** in 11% yield. Mechanistically speaking, the observed electronic preference seems to support the HAT as a mechanism for the initial radical generation as the alternative aryl oxidation-deprotonation pathway would operate better on electron-rich aromatic systems.[16]

Moving on to the naphthyl system, the sterically hindered 1-napthyl diol reacted to the corresponding acetophenone product **2n** more sluggishly than its 2-napthyl counterpart **2o**. Lastly, the importance of free rotation and antiperiplanar relationship between the leaving group and the benzylic radical were showcased by the thwarting of the reaction with substrate **2p** where the leaving group is located on a secondary carbon (see SI). Regarding limitations, the bromine-containing substrate **1q** decomposed under the reaction conditions, whereas cyano-, nitro- and sulfur-containing groups completely prevented the reaction progress (substrates **1r**–**1t**).

To gain a deeper understanding of our reaction, a set of mechanistic experiments was carried out. Our initial hypothesis was that the neutral Eosin Y, which has been well-established as a HAT catalyst, would be the catalytically active species in our reaction.[17] However, we were puzzled by the identification of 385 nm LEDs as optimal irradiation source and the lack

of reactivity with 420 nm and 520 nm irradiation (Table 1 and Table S4). Therefore, we started out by tracking down the light-absorbing species in our reaction mixture. When dissolved into acetonitrile, the main absorption band of the Eosin Y was found around 540 nm (Figure 1b). As this absorption band has been further assigned to the monoanionic Eosin Y, our observation further demonstrates the dynamic, solvent-dependent acid-base equilibrium of this photocatalyst.[17b,c] Although protonation of Eosin Y with Brønsted acids has been reported to enhance the HAT-activity of the catalyst, in our system, the addition of acetic acid, hydrochloric acid or sulfuric acid did not enable the conversion *trans*-cyclohexane-1,2-diol to cyclohexanone.[17d] This result further implied that our reaction might not proceed *via* excitation of neutral Eosin Y. Upon a careful inspection, an additional absorption feature can be observed around 380 nm.[18] This band was unambiguously identified to stem from Eosin Y (dark orange line), whereas the diol **1a** did not show any absorbance above 300 nm (grey dotted line). However, the addition of **1a** to a solution of Eosin Y resulted in small changes in the absorption spectrum on both sides of the utilized irradiation wavelength, thus indicating a possible hydrogen bonding and/or π-π-stacking interactions between these species.

To better characterize the observed color change of the reaction mixture from bright pink to pale yellow under irradiation (Figure 1a), an *ex-situ* UV-vis monitoring of the reaction was carried out. Irradiation with a 385 nm LED resulted in a smooth decrease in the Eosin Y main absorption band at 520 nm, followed by the rise of a broad absorption band in the blue-light region (Figure 1c). Noteworthily, the diol **1a** had a significant impact on the rate of the spectral changes: a solution containing only Eosin Y retained its green-light absorption band for almost 45 minutes, whereas in the presence of the diol, this band disappeared after 10 minutes of irradiation. Although faster, these spectral changes are in good agreement with those observed

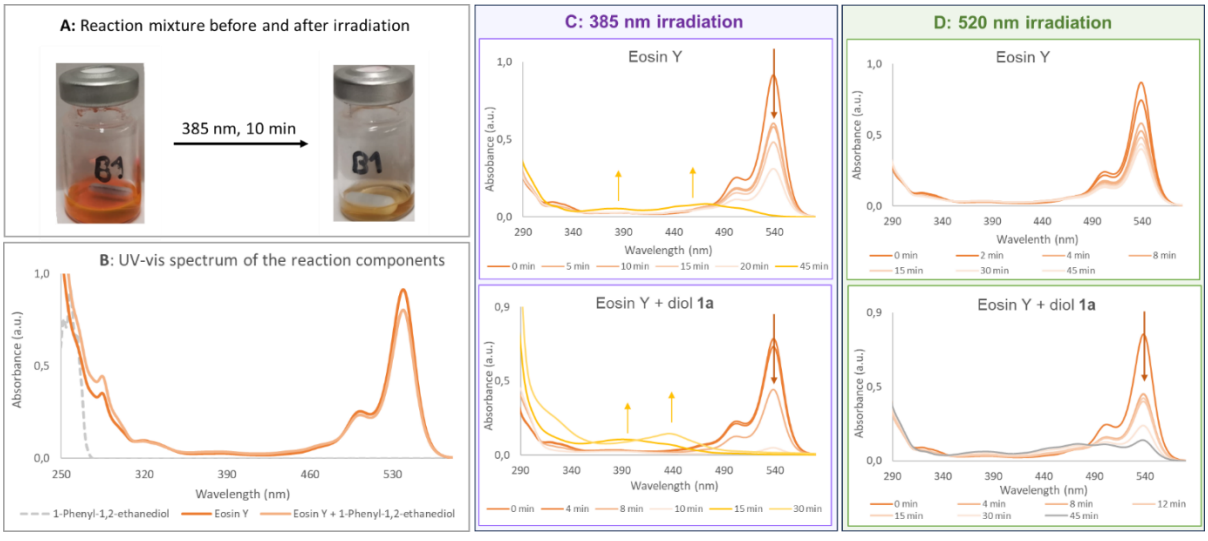

Figure 1. The observed color change of the reaction mixture (a), UV-vis spectrum of the reaction components separately and together in MeCN (b), spectral changes observed in *ex situ* UV-vis measurements upon irradiating with 385 nm LEDs (c) and 520 nm LEDs (d).

by the group of Janssen during their study on the Eosin Y photodegradation under green laser irradiation.[19] Under a green-light LED, however, our spectral changes were significantly slower, and without the diol **1a**, no new absorption features could be observed (Figure 1d). These differences observed with different irradiation sources might stem either from the higher energy and higher light intensity of the 385 nm LEDs and 520 nm laser as compared to 520 nm LEDs or, alternatively, hint towards excitation of an electron to a higher laying orbital when using a lower wavelength irradiation (anti-Kasha behaviour).[20] Further support to the hypothesis of Eosin Y photolysis was obtained from HPLC-MS analysis of the reaction mixture which revealed the emergence of numerous compounds after a 10-minute irradiation period. Based on HRMS, most of these molecules could be categorized into a) debromination, b) dehydration, and c) radical adducts of Eosin Y (Scheme 3a and Figure S10). In this context, it is also worth mentioning that the control experiment of stirring Eosin Y at 60 °C in the dark did not result in any degradation even after prolonged periods of time, thus confirming the photochemical nature of this process.

We then turned our attention to the product-forming events. The kinetic profile of the reaction was measured and was found to display a sigmoidal curve (Scheme 3b). Furthermore, three different stages could be separated from this curve: the reaction starts with an induction period (stage I, 0–10 min), followed by rapid consumption of the substrate (stage II, 10–15 min) and ending with a prolonged period of continuous product formation (stage III, 15–60 min). Strikingly, when comparing the reaction kinetics with the UV-vis studies on Eosin Y degradation discussed above, the time frame for the induction period and photodissociation of the catalyst seem to perfectly align. This synchronism explains the unusual combination of Eosin Y with violet light: the reaction does not proceed *via* the triplet state of Eosin Y, but Eosin Y is rather

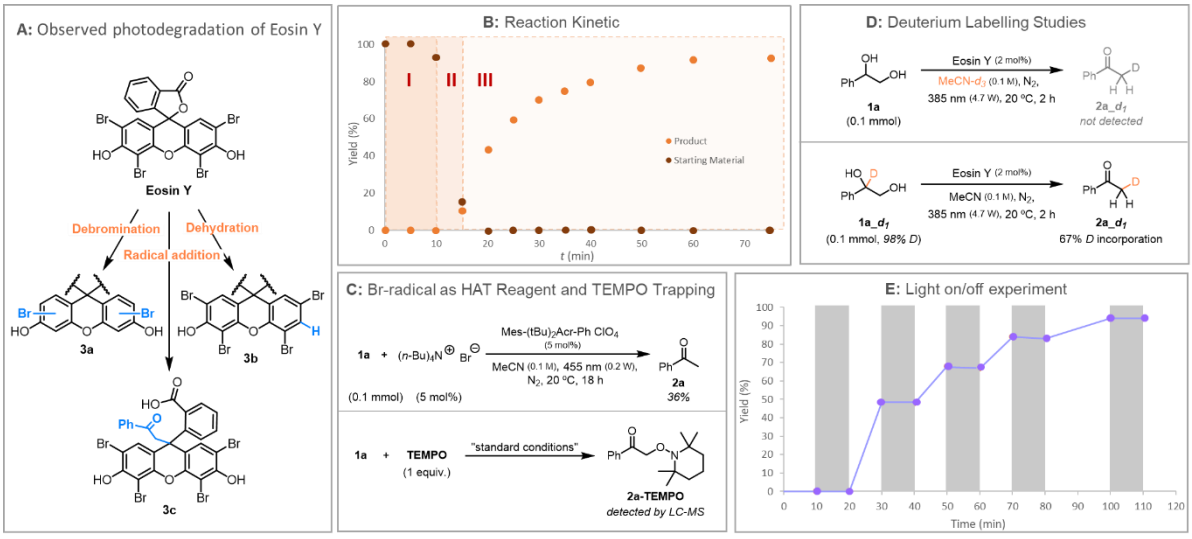

Scheme 3. Observed photodegradation products of Eosin Y in LC-MS analysis (a), kinetic profile of the reaction (b), bromine-radical mediated HAT and TEMPO trapping experiment (c), deuterium labelling experiment (d) and light on/off experiment (e).

a pre-catalyst whose photodissociation forms the actual catalytically active mixture. Interestingly, even though the photolysis of Eosin Y has been previously well characterized together with the establishment of the catalytic activity of the decomposition products of other photocatalysts, to our knowledge, this is the first report detailing the synthetic utilization of Eosin Y degradation products.[19,21] Out of the previously discussed dissociation products, especially the bromine radicals are well known as HAT active species.[21]

To test whether the bromine radicals could indeed catalyse our transformation, we set up control experiments using catalytic amounts of tetra-*n*-butylammonium bromide (TBABr) in combination with a photocatalyst capable of oxidizing the bromide anion into a bromine radical.[22] Indeed, the combination of TBABr with an acridinium-derived photocatalyst gave the desired product **2a** in a 36% yield, whereas the acridinium dye alone was not able to catalyse the reaction (Scheme 3c and Table S8). On one hand, this result confirms the feasibility of the bromine radical as the HAT catalyst, but on the other hand, it leaves room for the coexistence of other catalytically active species to reach the efficiency observed under the optimal reaction conditions. Finally, the autocatalytic mechanism was ruled out as the addition of acetophenone to the reaction mixture before irradiation was found to thwart the reaction (see Table S7).

Next, we investigated the processes taking place during the starting material conversion and the product formation phases (stages II + III of the kinetic curve). Although a clear discrepancy could be observed in the rates of these two events, no intermediates could be detected by GC-FID or ^{1}H-NMR analysis of the reaction progress (see SI). However, a radical trapping experiment with TEMPO was able to identify the adduct stemming from the *alpha*-carbonyl radical (**2a-TEMPO**) supporting the 1,2-spin center shift as a viable reaction pathway (Scheme 3c). Further insights into the behaviour of this radical came from deuterium labelling experiments (Scheme 3d). Running the reaction in deuterated acetonitrile did not result in any deuterium incorporation into the product, which indicates that the solvent does not play any active role in the reaction.[23] Interestingly, a high level of deuterium transfer between the benzylic position and the α-carbonyl position was observed, suggesting that the abstracted hydrogen (or deuterium) atom might end up in the terminal position of the product. This deuteration process could occur either through a back deuterium atom transfer (bDAT) or, through a reductive radical polar crossover, followed by deuteration of the enolate intermediate. Importantly, the former mechanistic pathway, where the *alpha*-carbonyl radical is proposed to abstract a deuterium atom would imminently regenerate the original HAT active species, thus making the process a radical chain reaction. Although the free carbanions have been, in turn, described as superbasic intermediates able to deprotonate acetonitrile, in our reaction, the possibility for enolate formation would significantly reduce the basicity of these reduced species. Moreover, the performed light on/off experiment verified the necessity of

continuous irradiation for the reaction, thus hinting against a radical chain mechanism as the main product-forming pathway (Scheme 3e).

Based on our mechanistic studies and the previous literature on 1,2-spin center shift discussed above, the following reaction mechanism is proposed (Scheme 4). During the induction period of the reaction (stage I), the high energy irradiation forms a highly active catalytic mixture of Eosin Y derivatives **3** and their corresponding elimination products (such as bromine radicals). These HAT active species initiate the product-forming cycle (stages II and III) by abstracting a hydrogen atom from the aryl-1,2-diols **1** forming the benzylic radical **4**. This radical undergoes a rapid 1,2-spin center shift generating an α-carbonyl radical **5** and releasing a molecule of water. The radical intermediate **5** is then reduced to the corresponding enolate **6**, followed by protonation to product **2**, for example, by the initial hydrogen atom abstracting species. Although the final steps of the mechanism could not be fully ascertained, a photocatalytic regeneration step, such as a SET between $\mathbf{3}^{+}$ and Br^{-}, is needed to close the catalytic cycle.

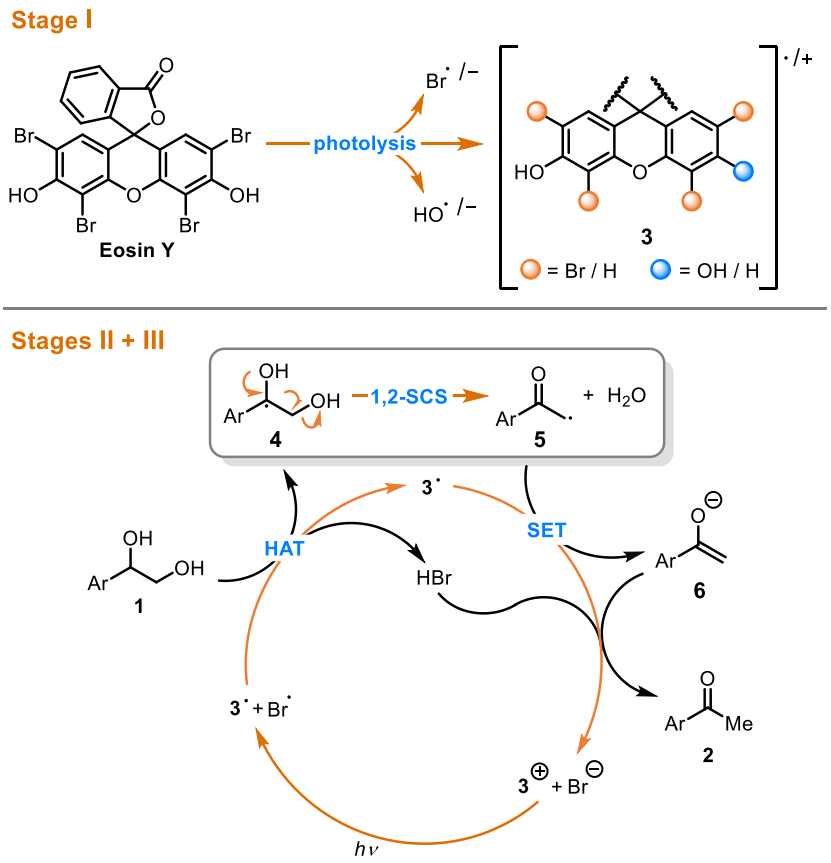

Scheme 4. Proposed reaction mechanism for the photocatalytic redox-neutral dehydration of aryl-1,2-ethanediols.

6.3 Conclusion

In summary, we have developed a protocol for the photocatalytic dehydration of aryl-1,2-diols to the corresponding methyl ketone derivatives. Our system uses Eosin Y as the sole catalyst and achieves cleavage of water under mild reaction conditions, and without activating reagents or pre-functionalization steps. The mechanistic studies revealed that the reaction is driven by a highly active catalytic mixture formed from the photolysis of Eosin Y. The product-forming cycle features a benzylic hydrogen atom abstraction followed by a 1,2-spin center shift, after which the carbonyl radical is reduced to its enolate form and is finally protonated. Considering the sensitivity of complex (bio)molecules and the conditions typically required in dehydration protocols, we hope that our contribution will inspire further development towards improved methods for elimination reactions.

6.4 Experimental Section

6.4.1 General Information

Chemicals and solvents: all commercially available chemicals were purchased in high quality and used without further purification. Solvents for column chromatography were distilled prior to use. Petrol ether is abbreviated as PE, while ethyl acetate as EtOAc. Moisture and oxygen-sensitive reactions were carried out using dry solvents in oven-dried glassware under inert atmosphere of pre-dried nitrogen. The evaporation of solvents was carried out in a rotary evaporator at temperatures below 40 ºC, under reduced pressure.

The water content of acetonitrile (245 ± 7 ppm water) used for photocatalyzed reactions was determined by Karl-Fischer titration.

Flash Column Chromatography (FCC): flash silica gel (Merck, 40-63 µm) was used as the stationary phase. Binary eluent mixtures are reported as v/v solutions normalized to 100 volume units. Purification by automated flash column chromatography was performed on a Biotage® IsoleraTM Spektra One device using either pre-packed Biotage® columns or silica gel 60 M (particle size 40–63 µm, 230–440 mesh, Merck) self-packed columns.

Analytical TLC: performed on silica gel pre-coated aluminium sheets (Machery-Nagel, silica gel 60 G/UV254, 0.2 mm). Visualization was accomplished by exposure to UV-light (254 nm). Eluent mixtures for TLC are reported as v/v solutions normalized to 100 volume units.

Nuclear magnetic resonance (NMR): spectra were recorded at room temperature using a Bruker Avance 400 (400 MHz for ^{1}H, 101 MHz for ^{13}C, 376 MHz for ^{19}F) NMR spectrometer. Chemical shifts are reported in δ-scale as parts per million [ppm] relative to the solvent residual peaks as internal standard. Coupling constants *J* are given in Hertz [Hz] and the multiplicity of the signals is abbreviated as: singlet (s), broad singlet (bs), doublet (d), doublet of doublets (dd), triplet (t), doublet of triplets (dt), triplet of doublets (td), quadruplet (q), or multiplet (m). Signals are reported as follows: (multiplicity, coupling constant *J*, number of protons). Spectra were analyzed using MestReNova 6.0.2.

High Resolution Mass Spectrometry (HRMS): spectra were obtained from the central analytical mass spectrometry facilities of the Faculty of Chemistry and Pharmacy, University of Regensburg. All mass spectra were recorded on a Finnigan MAT 95, Thermo Quest Finnigan TSQ 7000, Finnigan MATSSQ 710 A or an Agilent Q-TOF 6540 UHD instrument.

GC-FID and GC-MS: GC measurements were performed on a GC 7890 from Agilent Technologies. Data acquisition and evaluation was done with Agilent Chem Station Rev.C.01.04. GC–MS measurements were performed on a 7890A GC system from Agilent Technologies with an Agilent 5975 MSD Detector. Data acquisition and evaluation was done with MSD Chem Station E.02.02.1431. A capillary column HP-5MS/30 m x 0.25 mm/0.25 µM

film and helium as carrier gas (flow rate of 1 mL/min) were used. The injector temperature (split injection: 40:1 split) was 280 ºC, detection temperature 300 ºC (FID). Measurements were made via integration of the signal obtained. The GC oven temperature program was adjusted as follows: initial temperature 40 ºC was kept for 3 minutes, the temperature was increased at a rate of 15 ºC/min over a period of 16 minutes until 280 ºC was reached and kept for 5 minutes, the temperature was again increased at a rate of 25 ºC/min over a period of 48 seconds until the final temperature (300 ºC) was reached and kept for 5 minutes.

Photoreactor setup in batch: photoreactions were irradiated with LEDs (Engine LZ4-40UB00-00U5, λ = 385 nm (± 28), average radiant flux 4702 ± 70 mW, 90 V, 900 mA). Reaction mixtures were exposed to light under stirring (400 rpm, magnetic stirrer) from the bottom side of the vial. The temperature of the system was controlled by a water-cooling circuit consisting of an aluminium cooling block connected to a thermostat (Figure S1).

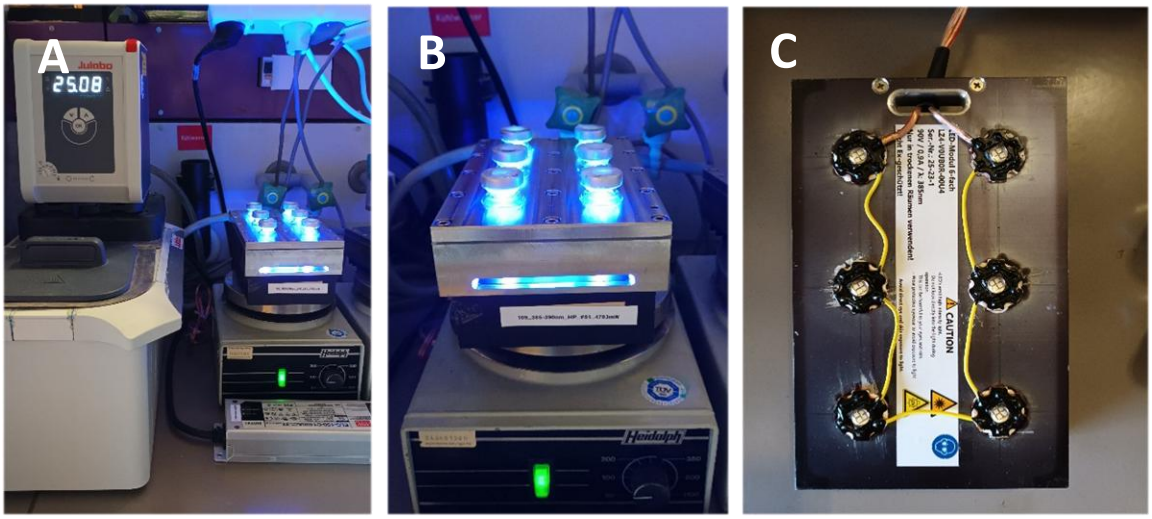

Figure S1. Photoreactor setup. A: Thermostat connected to the aluminium cooling block. B: Cooling block and LED on top of stirrer. C: LED module.

The optical power of the LEDs was determined using a FieldMaxII-TOTM laser power meter equipped with a PM3 sensor. The emission spectrum of the LEDs (Figure S2) was recorded using an Ocean Optics HR4000CG-UV-NIR Glass fibre and diffusor.

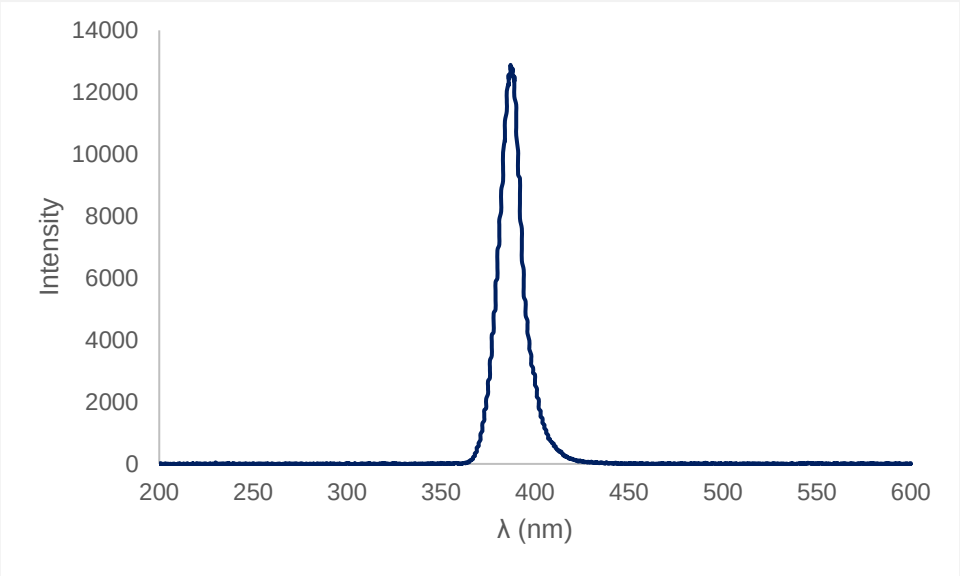

Figure S2. Led emission spectrum of the LED used for the photoreactions.

Glassware absorption: photoreactions were carried out in WICOM 20 mm crimp-cap vials (5 mL, 38.5 x 22.0 mm) made of borosilicate glass. The vials transmit 100% of incident light above 350 nm (Figure S3).

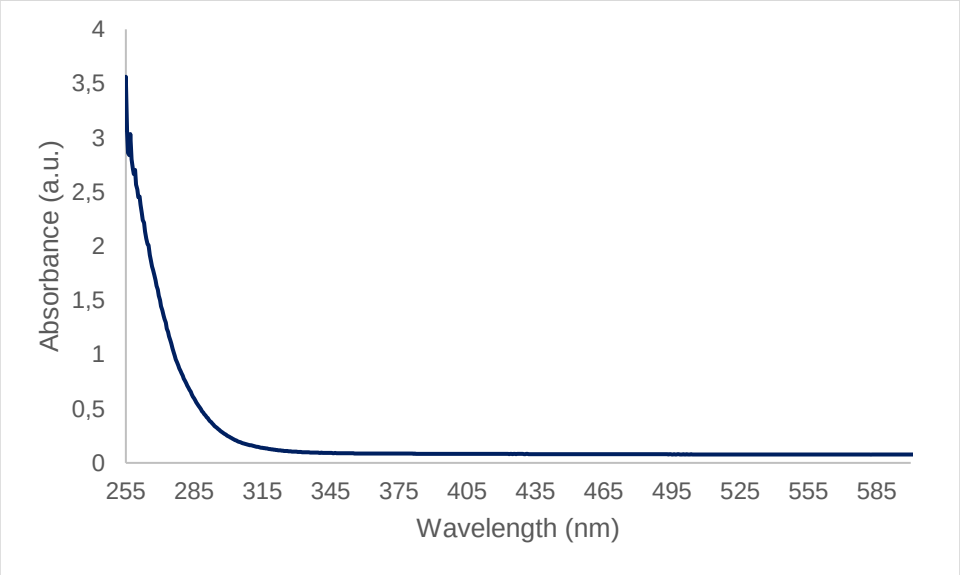

Figure S3. Absorption spectrum of vials used for photoreactions.

6.4.2 General Procedure for Photoreactions (GP1)

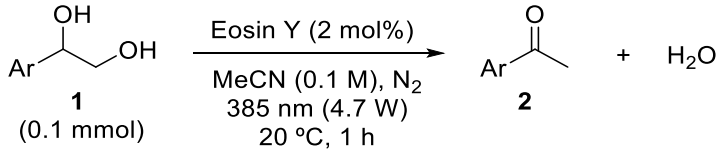

A 5 mL crimp-cap vial equipped with a Teflon-coated stirring bar, was loaded with the corresponding 1,2-ethanediol (0.1 mmol, 1.0 equiv.) and Eosin Y (1.4 mg, 2.0 µmol, 2 mol%). The vial was sealed, evacuated, and back filled with N_2 before adding CH_3CN (1 mL). Then, the resulting mixture was sonicated for 15 s, purged with N_2 for 5 min and subsequently stirred under irradiation using a 4.7 W 385 nm (± 25 nm) LED set-up for 1 to 18 hours at 20 ºC (temperature controlled by a cryostat). Reaction progress was monitored by GC analysis. For the determination of the GC-FID yields, mesitylene (250 µL of 0.4 M stock solution) was added to the crude reaction mixtures, which were then filtered through a syringe filter before subjecting to GC-FID analysis. Final GC-FID yields were calculated with a five-point calibration curve made with each product.

For isolation, two to four identical vials (see exact details from section 2.4) were set parallel according to the **GP1**. After completion, the vials were combined, and major impurities were removed by filtering the mixture through a short silica plug using CH_2Cl_2 as eluent. The volume of the crude was then carefully reduced to around 10 mL, which was then subjected to flash column chromatography using a mixture of Et_2O/PE as eluent. Careful solvent evaporation yielded the desired products.

6.4.3 Reaction Conditions Optimization

All optimization studies were carried out using the conditions described in **GP1** as standard conditions, changes to these conditions are given in each table. The yields reported are calculated from a five-point GC-FID calibration curve of acetophenone using mesitylene (250 µL of 0.4 M stock solution) as internal standard.

Table S1. Screening of photocatalysts.

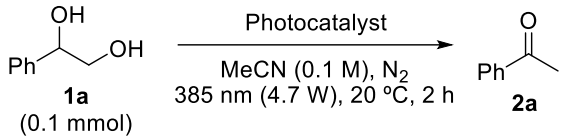

1a (0.1 mmol) **2a**

Entry	Photocatalyst	Yield (%)
1	$FeCl_3$ (20 mol%) + TBACl (20 mol%)	11
2	$BiCl_3$ (20 mol%) + TBACl (40 mol%)	32
3	$BiBr_3$ (20 mol%) + TBABr (40 mol%)	46
4	Eosin Y (2 mol%)	91
5	Eosin Y (1 mol%)	79
6	Eosin Y (5 mol%)	87
7	Eosin Y disodium salt (2 mol%)	N.d.
8	Eosin B (2 mol%)	N.d.
9	Eosin B disodium salt (2 mol%)	N.d.
10	Fluorescein (2 mol%)	N.d.
11	Fluorescein Na-salt (2 mol%)	N.d.
12	Thioxanthone (5 mol%)	Traces
13	Benzophenone (5 mol%)	Traces
14	TBADT (2 mol%)	Traces
15	Xanthone (5 mol%)	N.d.
16	4-Methoxyacetophenone (5 mol%)	N.d.

Yields determined with calibrated GC-FID using mesitylene as I.S.

Table S2. Optimization of Eosin Y loading.

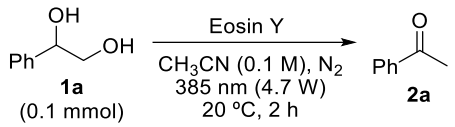

Entry	Eosin Y (mol%)	Yield (%)
1	0.2	N.d.
2	0.5	23
3	1.0	42
4	2.0	89
5	3.0	89
6	4.0	87

Yields determined with calibrated GC-FID using mesitylene as I.S.

Table S3. Screening of solvents.

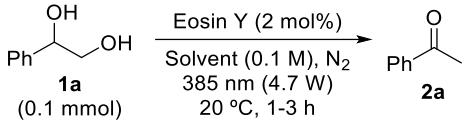

Entry	Solvent (1 mL, 0.1 mM)	Time (h)	Yield (%)
1	CH_3CN	1	89
2	EtOAc	1	22
3	EtOAc	3	73
4	Acetone	1	Traces
5	DMSO	1	N.d.
6	DMF	1	N.d.
7	DMA	1	N.d.
8	CH_2Cl_2	1	46
10	$CHCl_3$	1	12
11	MeOH	1	N.d.

Yields determined with calibrated GC-FID using mesitylene as I.S.

Table S4. Optimization of light source.

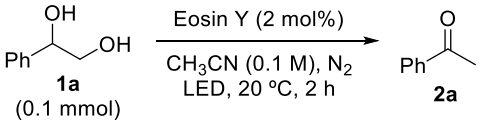

Entry	LED	Yield (%)
1	365 nm	Traces
2	385 nm (4.7 W)	79
3	420 nm (0.6 W)	Traces
4	520 nm	N.d.

Yields determined with calibrated GC-FID using mesitylene as I.S.

Table S5. Optimization of reaction time and reaction mixture concentration.

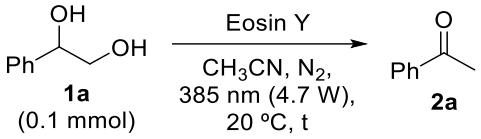

Entry	c (M)	Eosin Y (mol%)	*t* (min)	Yield (%)
1	0.1	1	15	traces
2	0.1	2	60	89
3	0.1	2	70	91
4	0.1	4	90	89
5	0.1	3	120	92
6	0.15	2	120	78
7	0.20	2	120	73

Yields determined with calibrated GC-FID using mesitylene as I.S.

6.4.4 Control Experiments

Table S6. Control experiments.

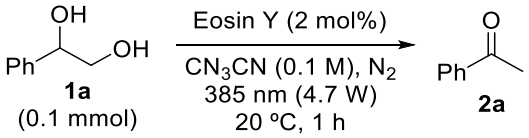

Entry	Deviation from standard	Yield (%)
1	None	89
2	No light	N.d.
3	No Eosin Y	N.d.
4	Under air	traces
5	With TEMPO	traces

Yields determined with calibrated GC using mesitylene as I.S.

6.4.5 Synthesis and Analytical Data of Products

Synthesis of acetophenone (**2a**)

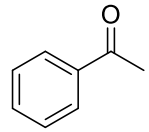

Prepared according to **GP1** from 1-phenylethane-1,2-diol (13.8 mg, 0.10 mmol, 1.00 equiv.), reaction time 1 h. Calibrated GC-FID yield 91%.

Synthesis of 1-(*p*-tolyl)ethan-1-one (**2b**)

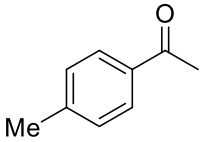

Prepared according to **GP1** from 1-((*p*-tolyl)ethane)-1,2-diol (15.2 mg, 0.10 mmol, 1.00 equiv.), reaction time 18 h. Calibrated GC-FID yield 71%.

Synthesis of 1-(*m*-tolyl)ethan-1-one (**2c**)

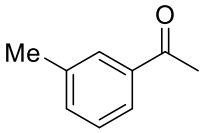

Prepared according to **GP1** from 1-(*m*-tolyl)ethane)-1,2-diol (15.2 mg, 0.10 mmol, 1.00 equiv.), reaction time 18 h. Calibrated GC-FID yield 70%.

Synthesis of 1-(*o*-tolyl)ethan-1-one (**2d**)

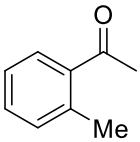

Prepared according to **GP1** from 1-(*o*-tolyl)ethane)-1,2-diol (15.2 mg, 0.10 mmol, 1.00 equiv.), reaction time 18 h. Calibrated GC-FID yield 21%.

Synthesis of 1-(4-(*tert*-butyl)phenyl)ethan-1-one (**2e**)

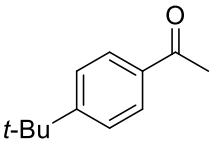

Prepared according to **GP1** from 1-(4-(*tert*-butyl)phenyl)ethane-1,2-diol (58.3 mg, 0.30 mmol, 1.00 equiv.), reaction time 18 h. After the silica plug and evaporation, the crude was purified via FCC (PE/Et_2O = 95/5) giving **2e** as a pale oil. Calibrated GC-FID yield 60%, isolated yield 29 mg, 55%.

^{1}H-NMR (400 MHz, $CDCl_3$): δ (ppm) = 7.84–7.80 (m, 2H), 7.41–7.38 (m, 2H), 2.50 (s, 3H), 1.26 (s, 9H). **^{13}C-NMR** (101 MHz, $CDCl_3$): δ (ppm) = 197.6, 156.8, 134.6, 128.3, 125.5, 35.1, 31.1, 26.6. **R_f** = 0.55 (PE/Et_2O = 90/10), [UV]. **HRMS** (EI-MS): $[M]^{\cdot+}$ $[C_{12}H_{18}O_2]^{\cdot+}$ calcd: 176.11957; found: 176.11966.

Synthesis of 1-(4-fluorophenyl)ethan-1-one (**2f**)

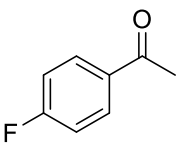

Prepared according to **GP1** from 1-(4-fluorophenyl)ethane)-1,2-diol (62.5 mg, 0.40 mmol, 1.00 equiv.), reaction time 16 h. The crude was purified via FCC (PE/Et_2O = 90/10) giving **2f** as a pale oil. Calibrated GC-FID yield 87%, isolated yield 30 mg, 72%.

^{1}H-NMR (400 MHz, $CDCl_3$): δ (ppm) = 8.01–7.95 (m, 2H), 7.16–7.10 (m, 2H), 2.59 (s, 3H). **^{13}C-NMR** (101 MHz, $CDCl_3$): δ (ppm) = 196.5, 165.7 (d, *J* = 255 Hz), 133.6 (d, *J* = 3.0 Hz), 130.9 (d, *J* = 9.4 Hz), 115.6 (d, *J* = 21.9 Hz), 26.5. **^{19}F-NMR** (376 MHz, $CDCl_3$, $PhCF_3$ as internal standard): δ (ppm) = –106.3 – (–)106.4 (m). **R_f** = 0.59 (PE/Et_2O = 90/10), [UV]. **HRMS** (APCI-MS): $[M]^+$ $[C_8H_7FO+H]^+$ calcd: 139.0559; found: 139.0553.

Synthesis of 1-(3-fluorophenyl)ethan-1-one (**2g**)

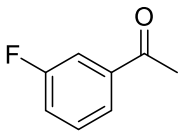

Prepared according to **GP1** from 1-(3-fluorophenyl)ethane)-1,2-diol (62.5 mg, 0.40 mmol, 1.00 equiv.), reaction time 16 h. The crude was purified via FCC (PE/Et_2O = 90/10) giving **2g** as a pale oil. Calibrated GC-FID yield 35%, isolated yield 18 mg, 32%.

^{1}H-NMR (400 MHz, $CDCl_3$): δ (ppm) = 7.72 (ddd, *J* = 7.8, 1.6, 0.9 Hz, 1H), 7.62 (ddd, *J* = 9.5, 2.6, 1.6 Hz, 1H), 7.43 (app. dt, *J* = 8.2, 5.5 Hz, 1H), 7.25 (dtd, *J* = 8.2, 2.6, 0.9 Hz, 1H), 2.58 (s, 3H). **^{13}C-NMR** (101 MHz, $CDCl_3$): δ (ppm) = 196.8 (d, *J* = 2.1 Hz), 162.7 (d, *J* = 248.0 Hz) 139.2 (d, *J* = 6.1 Hz), 130.3 (d, *J* = 7.6 Hz), 124.1 (d, *J* = 3.0 Hz), 120.1 (d, *J* = 21.5 Hz), 114.9 (d, *J* = 22.2 Hz), 26.7. **^{19}F-NMR** (376 MHz, $CDCl_3$, $PhCF_3$ as internal standard): δ (ppm) = –112.93 – (–)113.01 (m). **R_f** = 0.45 (PE/Et_2O = 90/10), [UV]. **HRMS** (EI-MS): $[M]^{\cdot+}$ $[C_8H_7FO]^{\cdot+}$ calcd: 138.04754; found: 138.04756.

Synthesis of 1-(4-(trifluoromethyl)phenyl)ethan-1-one (**2h**)

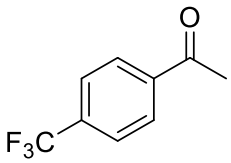

Prepared according to **GP1** from 1-(4-(trifluoromethyl)phenyl)ethane-1,2-diol (20.6 mg, 0.10 mmol, 1.00 equiv.), reaction time 16 h. Calibrated GC-FID yield 73%.

Synthesis of 1-(4-chlorophenyl)ethan-1-one (**2i**)

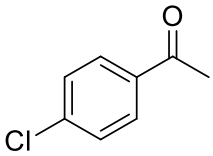

Prepared according to **GP1** from 1-(4-chlorophenyl)ethane-1,2-diol (34.5 mg, 0.20 mmol, 1.00 equiv.), reaction time 1 h. The crude was purified via FCC (PE/Et_2O = 90/10) giving **2i** as a pale yellow oil. Calibrated GC-FID yield 72%, isolated yield 21 mg, 68%.

^{1}H-NMR (400 MHz, $CDCl_3$): δ (ppm) = 7.85–7.81 (m, 2H), 7.39–7.35 (m, 2H), 2.52 (s, 3H). **^{13}C-NMR** (101 MHz, $CDCl_3$): δ (ppm) = 196.8, 139.6, 135.4, 129.7, 128.9, 26.6. **R_f** = 0.41 (PE/Et_2O = 90/10), [UV]. **HRMS** (EI-MS): $[M]^{\cdot+}$ $[C_8H_7OCl]^{\cdot+}$ calcd: 154.01799; found: 154.01789.

Synthesis of 1-(4-methoxyphenyl)ethan-1-one (**2j**)

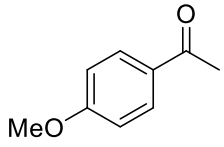

Prepared according to **GP1** from 1-(4-methoxyphenyl)ethane)-1,2-diol (16.8 mg, 0.10 mmol, 1.00 equiv.), reaction time 18 h. Calibrated GC-FID yield 15%.

Synthesis of 1-(3-methoxyphenyl)ethan-1-one (**2k**)

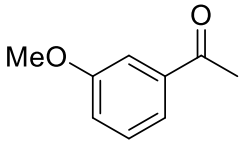

Prepared according to **GP1** from 1-(3-methoxyphenyl)ethane)-1,2-diol (67.3 mg, 0.40 mmol, 1.00 equiv.), reaction time 16 h. The crude was purified via FCC (CH_2Cl_2/Et_2O = 85/15) giving **2k** as a pale yellow oil. Calibrated GC-FID yield 94%, isolated yield 54 mg, 90%.

^{1}H-NMR (400 MHz, $CDCl_3$): δ (ppm) = 7.52 (ddd, *J* = 7.6, 1.7, 1.0 Hz, 1H), 7.47 (dd, *J* = 2.8, 1.7 Hz, 1H), 7.35 (t, *J* = 8.2 Hz, 1H), 7.09 (ddd, *J* = 8.2, 2.8, 1.0 Hz, 1H), 3.84 (s, 3H), 2.58 (s, 3H). **^{13}C-NMR** (101 MHz, $CDCl_3$): δ (ppm) = 196.9, 158.8, 137.5, 128.5, 120.1, 118.6, 111.3, 54.4, 25.7. **R_f** = 0.46 (PE/Et_2O = 90/10), [UV]. **HRMS** (EI-MS): $[M]^{\cdot+}$ $[C_9H_{12}O_2]^{\cdot+}$ calcd: 150.06753; found: 150.06714.

Synthesis of 1-(3-((*tert*-butyldimethylsilyl)oxy)phenyl)ethan-1-one (**2l**)

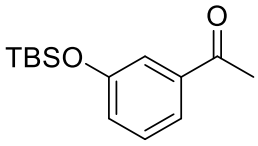

Prepared according to **GP1** from 1-(3-((*tert*-butyldimethylsilyl)oxy)phenyl) ethan-1,2-diol (80.5 mg, 0.30 mmol, 1.00 equiv.), reaction. The crude was purified via FCC (PE/Et_2O = 90/10) giving **2l** as a pale-yellow oil. Calibrated GC-FID yield 68%, isolated yield 46 mg, 61%.

^{1}H-NMR (400 MHz, $CDCl_3$): δ (ppm) = 7.54 (ddd, *J* = 7.7, 1.8, 1.0 Hz, 1H), 7.42 (dd, *J* = 2.6, 1.8 Hz, 1H), 7.31 (t, *J* = 8.0 Hz, 1H), 7.04 (ddd, *J* = 8.0, 2.6, 1.0 Hz, 1H), 2.57 (s, 3H), 0.99 (s, 9H), 0.21 (s, 6H). **^{13}C-NMR** (101 MHz, $CDCl_3$): δ (ppm) = 197.8, 156.0, 138.6, 129.5, 124.9, 121.6, 119.5, 26.7, 25.6, 18.2, – 4.4. **R_f** = 0.40 (PE/Et_2O = 90/10), [UV]. **HRMS** (APCI-MS): $[M+H]^+$ $[C_{14}H_{22}O_2Si+H]^+$ calcd: 251.1467; found: 251.1464.

Synthesis of 1-(3-(methoxymethoxy)phenyl)ethan-1-one (**2m)**

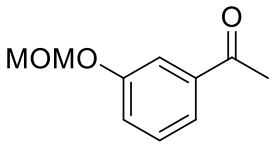

Prepared according to **GP1** from 1-(3-(methoxymethoxy)phenyl) ethane-1,2-diol (18.1 mg, 0.10 mmol, 1.00 equiv.) reaction time 18h. Calibrated GC-FID yield 11%.

Synthesis of 1-(naphthalen-1-yl)ethan-1-one (**2n**)

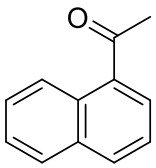

Prepared according to **GP1** from 1-(naphthalen-1-yl)ethane)-1,2-diol (56.5 mg, 0.30 mmol, 1.00 equiv.), reaction time 16 h. After the silica plug and evaporation, the crude was purified via FCC (10% Et_2O/PE) giving **2n** as brownish oil. Calibrated GC-FID yield 36%, isolated yield 14 mg, 27%.

^{1}H-NMR (400 MHz, $CDCl_3$): δ (ppm) = 8.75 (dd, *J* = 8.7, 0.5 Hz, 1H), 8.02–7.87 (m, 4H), 7.63–7.49 (m, 4H), 2.76 (s, 3H). **^{13}C-NMR** (101 MHz, $CDCl_3$): δ (ppm) = 201.9, 135.5, 134.0, 133.0,

130.2, 128.7, 128.4, 128.1, 126.5, 126.0, 124.3, 29.7. **R_f** = 0.44 (PE/Et_2O = 90/10), [UV]. **HRMS** (EI-MS): $[M]^{\cdot+}$ $[C_9H_{12}O_2]^{\cdot+}$ calcd: 170.07262; found: 170.07228.

Synthesis of 1-(naphthalen-2-yl)ethan-1-one (**2o**)

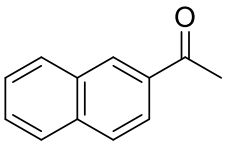

Prepared according to **GP1** from 1-(naphthalen-2-yl)ethane)-1,2-diol (37.6 mg, 0.20 mmol, 1.00 equiv.), reaction time 16 h. The crude was purified via FCC (PE/Et_2O = 90/10) giving **2o** as a pale solid. Calibrated GC-FID yield 63%, isolated yield 21 mg, 62%.

^{1}H-NMR (400 MHz, $CDCl_3$): δ (ppm) = 8.47 (br. s., 1H), 8.04 (dd, *J* = 8.7, 1.8 Hz, 1H), 7.97 (d, *J* = 8.1 Hz, 1H), 7.91–7.87 (m, 2H), 7.63–7.59 (m, 1H), 7.58–7.54 (m, 1H), 2.73 (s, 3H). **^{13}C-NMR** (101 MHz, $CDCl_3$): δ (ppm) = 198.1, 135.6, 134.5, 132.5, 130.2, 129.6, 128.5, 128.4, 127.8, 126.8, 123.9, 26.7. **R_f** = 0.38 (PE/Et_2O = 90/10), [UV]. **HRMS** (EI-MS): $[M]^{\cdot+}$ $[C_{12}H_{10}O]^{\cdot+}$ calcd: 170.07262; found: 170.07221.

Synthesis of 2,3-dihydro-1*H*-inden-1-one (**2p**)

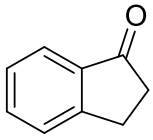

Prepared according to **GP1** from a commercially available 2,3-dihydro-1*H*-inden-1,2-diol (15.0 mg, 0.10 mmol, 1.00 equiv.) reaction time 18 h. Calibrated GC-FID yield 18%.

6.4.6 List of Unsuccessful Substrates

With respect to the limitations of the current method, certain functional groups were found to be incompatible (Figure S4).

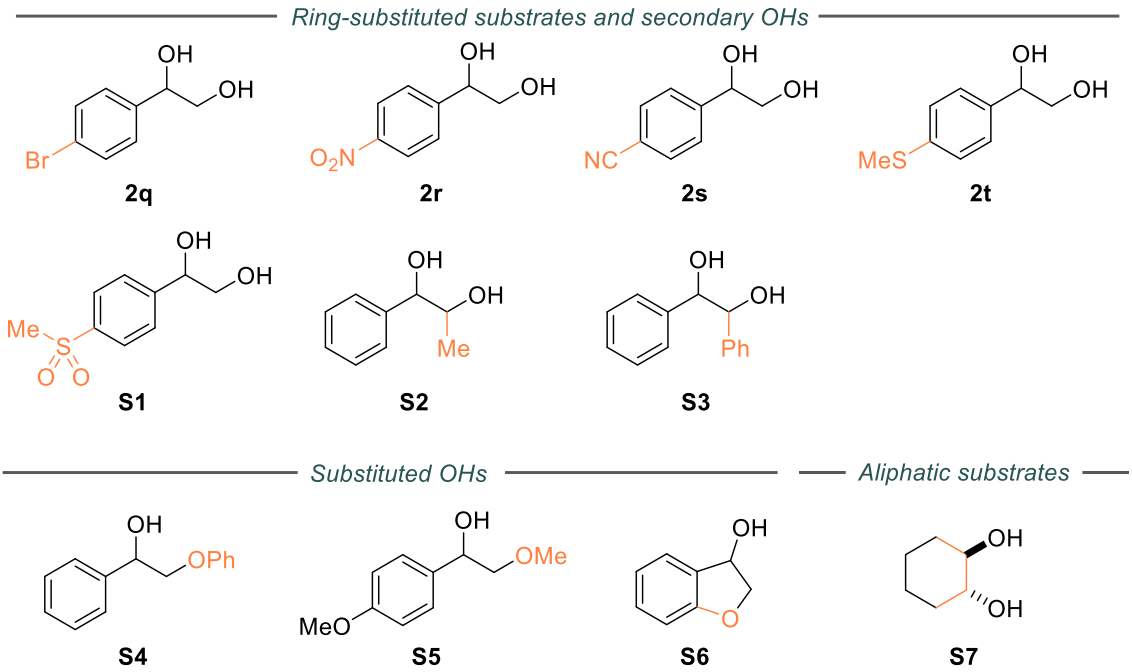

Figure S4. List of noncompatible diols and diol derivatives in the Eosin Y- catalyzed HAT/SCS reaction.

Firstly, brominated starting materials (such as **2q**) underwent debrominative degradation leading to a complex mixture of products. On the other hand, nitro-(**2r**) and cyano-(**2s**) substituents and sulfur-containing functional groups (as in **2t** and **S1**) fully hindered the conversion of starting material. The *ortho*-methoxy substrate **S2** probably suffered from the combined negative electronic (as with *para*-methoxy substrate) and steric (as with *ortho*-methyl substrate) effects thus leading to poor performance of this starting material. Furthermore, steric hindrance around the leaving group, as demonstrated with **S3** and **S4** seemed to thwart the transformation. In stark contrast to many previously reported methods, a hydroxy group was found to be the best-performing leaving group whereas phenoxy (**S5**), methoxy (**S6**) and phenolic (**S7**) containing substrates were mostly unreactive under our reaction conditions. Finally, aliphatic substrates (such as commercially available **S8**) could not be engaged to the transformation most likely due to the stronger aliphatic α-oxygen C–H bond.

6.4.7 Synthesis and Analytical Data of Starting Materials

The model compound **1a** and diol **1p** were commercially purchased and used without further purification. Other diols were synthetized according to the following procedures.

Synthesis of Diols via Alkene Oxidation (GP2)

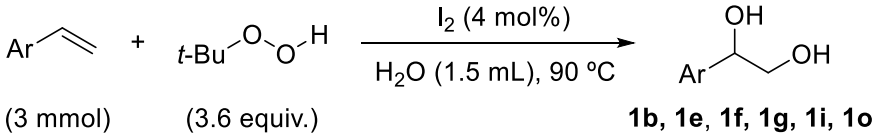

According to a procedure of Liu *et* al.[24] the styrene derivative (3.0 mmol, 1.0 equiv.), I_2 (30 mg, 16 µmol, 4 mol%), distilled water (1.5 mL) and *tert*-butylhydroperoxide (70% solution in H_2O, 1.5 mL, 10.8 mmol, 3.6 equiv.) were added to a 15 ml crimp-cap vial. The vial was sealed, and the reaction mixture was heated at 90 ºC for 24 h. The reaction was quenched with a 2 M $Na_2S_2O_3$ (4 mL) and the product was extracted with EtOAc (5 x 10 mL). The combined organic layers were dried over $MgSO_4$, and the solvent was removed under reduced pressure. The crude product was purified by flash column chromatography using PE/Acetone as eluent.

Synthesis of Diols via Oxidation of Acetophenones (GP3)

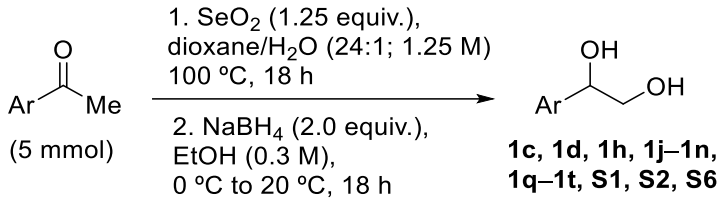

According to a detailed literature procedure by Rygus and Hall.[25] SeO_2 (1.25 equiv.) was suspended into a mixture of 1,4-dioxane and water (24:1, 1.25 M), and warmed to 55 °C until fully soluble. The mixture was then cooled to room temperature, the acetophenone derivative (5 mmol, 1.0 equiv.) was added and the reaction was heated at reflux (100 °C) overnight. Dark (often green) colored reaction mixture with black precipitate at bottom often indicated successful oxidation. After cooling to ambient temperature, the mixture was filtered and concentrated under reduced pressure. The crude was then pressed through a silica plug using EtOAc/PE (1:1) as eluent and evaporated to dryness.

The crude product was then dissolved in EtOH (0.3 M) and cooled to 0 °C. $NaBH_4$ (2.0 equiv.) was added portionwise, and the reaction was stirred overnight while allowing to warm to 20 °C. The reaction was quenched with 2M HCl (or sat. NH_4Cl for acid-sensitive substrates), EtOH was removed under reduced pressure and the remaining aqueous mixture was extracted with EtOAc (3x). After drying with $MgSO_4$, the mixture was filtered, and the solvent evaporated. Purification with flash column chromatography (PE/Acetone) yielded the final products.

Synthesized Successful Diols

Synthesis of 1-(*p*-tolyl)ethane-1,2-diol (**1b**)

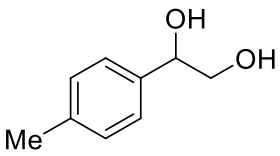

Prepared according to **GP2** from 1-methyl-4-vinylbenzene (350 µL, 2.5 mmol, 1.0 equiv.). The crude product was purified via FCC (PE/Acetone = 70/30), giving **1b** as a white solid (204 mg, 60%).

^{1}H-NMR (400 MHz, $CDCl_3$): δ (ppm) = 7.25 (d, *J* = 7.9 Hz, 2H), 7.17 (d, *J* = 7.9 Hz, 2H), 4.78 (dd, *J* = 8.1, 3.6 Hz, 1H), 3.72 (dd, *J* = 11.5, 3.6 Hz, 1H), 3.64 (dd, *J* = 11.5, 8.1 Hz, 1H), 2.63 (br. s., 2H), 2.34 (s, 3H). **^{13}C-NMR** (101 MHz, $CDCl_3$): δ (ppm) = 137.8, 137.5, 129.3, 126.0, 74.6, 68.1, 21.1. **R_f** = 0.26 (PE/Acetone = 70/30) [PMA stain]. **HRMS** (EI-MS): $[M]^{\cdot+}$ $[C_9H_{12}O_2]^{\cdot+}$ calcd: 152.08318; found: 152.08343.

Synthesis of 1-(*m*-tolyl)ethane-1,2-diol (**1c**)

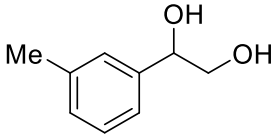

Prepared according to **GP3** from 1-(*m*-tolyl)ethan-1-one (1.3 g, 10 mmol, 1.0 equiv.). The crude product was purified via FCC (PE/Acetone 60/40), giving **1c** as a white solid (668 mg, 44%).

^{1}H-NMR (400 MHz, $CDCl_3$): δ (ppm) = 7.23 (d, *J* = 7.6 Hz, 1H), 7.17–7.09 (m, 3H), 4.77 (dd, *J* = 8.2, 2.5 Hz, 1H), 3.72 (dd, *J* = 11.4, 2.5 Hz, 1H), 3.64 (dd, *J* = 11.4, 8.2 Hz, 1H), 2.97–2.70 (br. s., 2H), 2.35 (s, 3H). **^{13}C-NMR** (101 MHz, $CDCl_3$): δ (ppm) = 140.4, 138.2, 128.7, 128.4, 126.7, 123.1, 74.7, 68.1, 21.4. **R_f** = 0.47 (PE/Acetone = 60/40) [PMA stain]. **HRMS** (EI-MS): $[M]^{\cdot+}$ $[C_9H_{12}O_2]^{\cdot+}$ calcd: 152.08318; found: 152.08282.

Synthesis of 1-(*o*-tolyl)ethane-1,2-diol (**1d**)

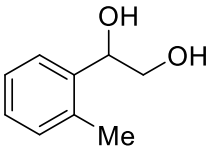

Prepared according to **GP3** from 1-(*o*-tolyl)ethan-1-one (1.3 g, 10 mmol, 1.0 equiv.). The crude product was purified via FCC (PE/Acetone 70/30), giving **1d** as a colorless oil (624 mg, 41%).

^{1}H-NMR (400 MHz, $CDCl_3$): δ (ppm) = 7.49 (dd, *J* = 7.4,1.2 Hz, 1H), 7.25–7.13 (m, 3H), 5.06 (dd, *J* = 8.4, 3.0 Hz, 1H), 3.73 (dd, *J* = 11.4, 3.0 Hz, 1H), 3.62 (dd, *J* = 11.4, 8.4, 1H), 2.35 (s, 3H), 2.29 (br.s., 2H). **^{13}C-NMR** (101 MHz, $CDCl_3$): δ (ppm) = 138.4, 134.7, 130.5, 127.8, 126.3, 125.7, 71.4, 66.9, 19.0. **R_f** = 0.48 (PE/Acetone = 60/40) [PMA stain]. **HRMS** (EI-MS): $[M]^{\cdot+}$ $[C_9H_{12}O_2]^{\cdot+}$ calcd:152.08318; found: 152.08315.

Synthesis of 1-(4-(*tert*-butyl)phenyl)ethane-1,2-diol (**1e**)

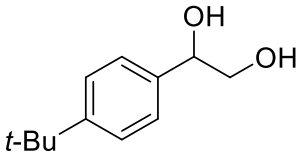

Prepared according to **GP2** from 1-(*tert*-butyl)-4-vinylbenzene (690 µL, 5.0 mmol, 1.0 equiv.). The crude product was purified via FCC (PE/Acetone = 60/40) giving **1e** as a white solid (702 mg, 72%).

^{1}H-NMR (400 MHz, $CDCl_3$): δ (ppm) = 7.41–7.38 (m, 2H), 7.32–7.29 (m, 2H), 4.81 (dd, *J* = 8.0, 3.5 Hz, 1H), 3.77 (dd, *J* = 11.3, 3.5 Hz, 1H), 3.69 (dd, *J* = 11.3, 8.0 Hz, 1H), 2.30 (br. s., 2H), 1.32 (s, 9H). **^{13}C-NMR** (101 MHz, $CDCl_3$): δ (ppm) = 151.1, 137.5, 125.8, 125.5, 74.5, 68.0, 34.6, 31.3. **R_f** = 0.28 (PE/Acetone = 70/30) [PMA stain]. **HRMS** (EI-MS): $[M]^{\cdot+}$ $[C_{12}H_{18}O_2]^{\cdot+}$ calcd: 194.13013; found: 194.13046.

Synthesis of 1-(4-fluorophenyl)ethane-1,2-diol (**1f**)

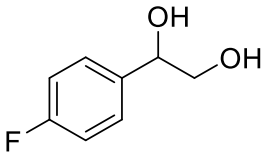

Prepared according to **GP2** from 1-fluoro-4-vinylbenzene (600 µL, 5.0 mmol, 1.0 equiv.). The crude product was purified via FCC (PE/Acetone 70/30), giving **1f** as a white solid (548 mg, 70%).

^{1}H-NMR (400 MHz, $CDCl_3$): δ (ppm) = 7.37–7.31 (m, 2H), 7.08–7.01 (m, 2H), 4.81 (dd, *J* = 8.2, 3.1 Hz, 1H), 3.75 (dd, *J* = 11.3, 3.1 Hz, 1H), 3.63 (dd, *J* = 11.3, 8.2 Hz, 1H), 2.50 (br. s., 2H). **^{13}C-NMR** (101 MHz, $CDCl_3$): δ (ppm) = 162.5 (d, *J* = 247 Hz), 136.1 (d, *J* = 3.1 Hz), 127.7 (d, *J* = 8.1 Hz), 115.4 (d, *J* = 21.5 Hz), 74.0, 68.1. **^{19}F-NMR** (376 MHz, $CDCl_3$, $PhCF_3$ as internal standard): δ (ppm) = –115.25 – (–)115.34 (m) **R_f** = 0.30 (PE/EtOAc = 80/20) [PMA stain]. **HRMS** (APCI-MS): $[M+NH_4]^+$ $[C_8H_9FO_2+NH_4]^+$ calcd: 174.0930; found: 174.0928.

Synthesis of 1-(3-fluorophenyl)ethane-1,2-diol (**1g**)

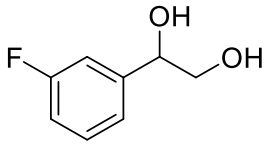

Prepared according to **GP2** from 1-(3-fluorophenyl)ethan-1-one (690 mg, 5.0 mmol, 1.0 equiv.). The crude product was purified via FCC (PE/Acetone 70/30), giving **1g** as a pale yellow solid (286 mg, 37%).

^{1}H-NMR (400 MHz, $CDCl_3$): δ (ppm) = 7.29–7.23 (m, 1H), 7.04–7.00 (m, 2H), 6.98–6.93 (m, 1H), 4.73 (dd, *J* = 8.5, 3.1 Hz, 1H), 4.37 (br. s., 2H), 3.64 (dd, *J* = 11.7, 3.1 Hz, 1H), 3.54 (dd, *J* = 11.7, 8.5 Hz, 1H). **^{13}C-NMR** (101 MHz, $CDCl_3$): δ (ppm) = 162.8 (d, *J* = 246.2 Hz) 143.1 (d, *J* = 6.8 Hz), 130.0 (d, *J*= 8.2 Hz), 121.6 (d, *J* = 2.9 Hz), 114.7 (d, *J* = 21.2 Hz), 113.0 (d, *J* = 21.7 Hz), 74.1 (d, *J* = 1.5 Hz), 67.7. **^{19}F-NMR** (376 MHz, $CDCl_3$, $PhCF_3$ as internal standard): δ (ppm) = –113.59 – (–)113.67 (m). **R_f** = 0.57 (PE/Acetone = 60/40) [PMA stain]. **HRMS** (EI-MS): $[M]^{\cdot+}$ $[C_8H_9FO_2]^{\cdot+}$ calcd: 156.0587; found: 136.0585.

Synthesis of 1-(4-(trifluoromethyl)phenyl)ethane-1,2-diol (**1h**)

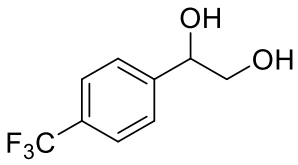

Prepared according to **GP3** from 1-(4-(trifluoromethyl)phenyl)ethan-1-one (1.9 g, 10 mmol, 1.0 equiv.). The product was purified via FCC (PE/Acetone = 60/40), giving **1h** as a white solid (797 mg, 39%).

^{1}H-NMR (400 MHz, DMSO-d_6): δ (ppm) = 7.67 (d, *J* = 8.1 Hz, 2H), 7.57 (d, *J* = 8.1 Hz, 2H), 5.46 (d, *J* = 4.4 Hz, 1H), 4.80 (app. t., *J* = 5.5 Hz, 1H), 4.63 (dd, *J* = 11.9, 5.5 Hz, 1H), 3.52–3.41 (m, 2H). **^{13}C-NMR** (101 MHz, DMSO-d_6): δ (ppm) = 148.8 (app. d, *J* = 1.2 Hz), 127.9 (q, *J* = 31.8 Hz), 127.5, 125.1 (q, *J* = 3.8 Hz), 124.9 (q, *J* = 271 Hz), 73.6, 67.5. **^{19}F-NMR** (376 MHz, DMSO-d_6, $PhCF_3$ as standard): δ (ppm) = –63.32. **R_f** = 0.58 (PE/Acetone = 60/40) [PMA stain]. **HRMS** (EI-MS): $[M+NH_4]^+$ $[C_9H_9F_3O_2+NH_4]^+$ calcd: 224.0898; found: 224.0896.

Synthesis of 1-(4-chlorophenyl)ethane-1,2-diol (**1i**)

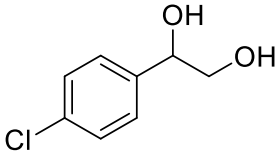

Prepared according to **GP2** from 1-chloro-4-vinylbenzene (600 µL, 5.0 mmol, 1.0 equiv.). The crude product was purified via FCC (PE/Acetone = 70/30), giving **1i** as a pale brown solid (370 mg, 43%).

^{1}H-NMR (400 MHz, $CDCl_3$): δ (ppm) = 7.35 – 7.31 (m, 2H), 7.31 – 7.27 (m, 2H), 4.79 (dd, *J* = 8.2, 3.5 Hz, 1H), 3.73 (dd, *J* = 11.3, 3.5 Hz, 1H), 3.60 (dd, *J* = 11.3, 8.2 Hz, 1H), 2.72 (bs, 2H). **^{13}C-NMR** (101 MHz, $CDCl_3$): δ (ppm) = 138.9, 133.8, 128.7, 127.5, 74.0, 67.9. **R_f** = 0.27 (PE/Acetone = 70/30) [PMA stain]. **HRMS** (EI-MS): $[M]^{\cdot+}$ $[C_8H_9O_2Cl]^{\cdot+}$ calcd: 172.02856; found: 172.02844.

Synthesis of 1-(4-methoxyphenyl)ethane-1,2-diol (**1j**)

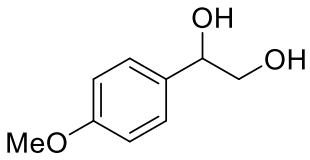

Prepared according to **GP3** from 1-(4-methoxyphenyl)ethan-1-one (1.5 g, 10 mmol, 1.0 equiv.). The 2-oxoacetaldehyde was reduced in wet THF as solvent according to literature,[26] under diluted conditions (M = 0.1 M). NOTE: Typical concentration (M = 0.3 M) on the reduction leads to polymerization indicated by the formation of milky mixture. The crude was purified via FCC (PE/Acetone = 70/30), giving **1j** as a white solid (1.34 g, 53%).

^{1}H-NMR (400 MHz, DMSO-d_6): δ (ppm) = 7.25 (d, *J* = 8.6 Hz, 2H), 6.87 (d, *J* = 8.6 Hz, 2H), 5.11 (d, *J* = 4.1 Hz, 1H), 4.66 (app. t., *J* = 5.7 Hz, 1H), 4.49 (dd, *J* = 12.2, 5.6 Hz, 1H), 3.73 (s, 3H). **^{13}C-NMR** (101 MHz, $CDCl_3$): δ (ppm) = 158.7, 135.9, 127.8, 113.7, 73.8, 68.0, 55.5. **R_f** = 0.37 (PE/Acetone = 60/40) [PMA stain]. **HRMS** (ESI-MS): $[M+Na]^+$ $[C_9H_{12}O_3+Na]^+$ calcd: 191.0684; found: 191.0677.

Synthesis of 1-(3-methoxyphenyl)ethane-1,2-diol (**1k**)

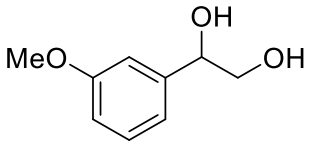

Prepared according to **GP3** from 1-(3-methoxyphenyl)ethan-1-one (1.5 g, 10 mmol, 1.0 equiv.). The crude product was purified via FCC (PE/Acetone = 70/30), giving **1k** as a white solid (1.8 g, 79 %).

^{1}H-NMR (400 MHz, $CDCl_3$): δ (ppm) = 7.29 (app. t., *J* = 8.1 Hz, 1H), 6.96–6.93 (m, 2H), 6.87–6.84 (m, 1H), 4.81 (dd, *J* = 8.2, 2.4 Hz, 1H), 3.83 (s, 3H), 3.77 (dd, *J* = 11.5, 2.4 Hz, 1H), 3.67 (dd, *J* = 11.5, 8.2 Hz, 1H), 2.72 (br. s., 2H). **^{13}C-NMR** (101 MHz, $CDCl_3$): δ (ppm) = 159.8, 142.2, 129.6, 118.3, 113.4, 111.7, 74.6, 68.0, 55.3. **R_f** = 0.36 (PE/Acetone = 60/40) [PMA stain]. **HRMS** (EI-MS): $[M]^{\cdot+}$ $[C_9H_{12}O_2]^{\cdot+}$ calcd: 168.07810; found: 168.07827.

Synthesis of 1-(3-((*tert*-butyldimethylsilyl)oxy)phenyl)ethane-1,2-diol (**1l**)

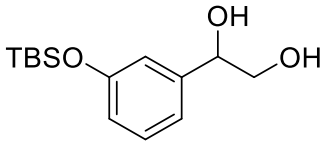

1-(3-((*tert*-butyldimethylsilyl)oxy)phenyl)ethan-1-one was prepared *via* TBS-protection of 3'-hydroxyacetophenone following a literature reported procedure.[27] The title compound was then prepared according to **GP3** from the protected alcohol (1.25 g, 5 mmol, 1.0 equiv.). The crude was purified via FCC (PE/Acetone = 70/30), giving **1l** as a pale solid (677 mg, 50%).

^{1}H-NMR (400 MHz, $CDCl_3$): δ (ppm) = 7.21 (app. t., *J* = 7.8 Hz, 1H), 6.95–9.92 (m, 1H), 6.86–6.84 (m, 1H), 6.77 (dd, *J* = 8.0, 0.8 Hz, 1H), 4.76 (dd, *J* = 8.2, 3.5 Hz, 1H), 3.73 (dd, *J* = 11.4, 3.5 Hz, 1H), 3.63 (dd, *J* = 11.4, 8.2 Hz, 1H), 2.42 (br. s., 2H), 0.98 (s, 9H), 0.19 (s, 6H). **^{13}C-NMR** (101 MHz, $CDCl_3$): δ (ppm) = 155.8, 142.1, 129.5, 119.6, 118.9, 117.8, 74.5, 68.1, 25.7, 18.2, –4.4. **R_f** = 0.66 (PE/Acetone = 60/40) [phosphomolybdic acid]. **HRMS** (APCI-MS): $[M+NH_4]^+$ $[C_{14}H_{24}O_3Si+NH_4]^+$ calcd: 286.1839; found: 286.1838.

Synthesis of 1-(3-(methoxymethoxy)phenyl)ethane-1,2-diol (**1m**)

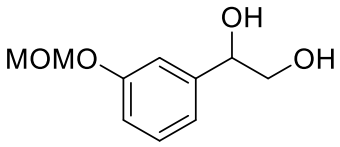

1-(3-methoxymethoxy)phenyl)ethan-1-one was synthetized via MOM-protection of 3'-hydroxyacetophenone following a literature reported procedure.[28] The title compound was then prepared according to **GP3** from the protected alcohol (1.80 g, 10 mmol, 1.0 equiv.). The crude was purified via FCC (PE/Acetone = 70/30), giving **1m** as a viscous yellow oil (785 mg, 40%).

^{1}H-NMR (400 MHz, $CDCl_3$): δ (ppm) = 7.28 (t, *J* = 7.8 Hz, 1H), 7.07–7.05 (m, 1H), 7.02–6.96 (m, 2H), 5.81 (s, 2H), 4.80 (dd, *J* = 8.0, 3.5 Hz, 1H), 3.77 (dd, *J* = 11.2, 3.5 Hz, 1H), 3.66 (dd, *J* = 11.2, 8.0 Hz, 1H), 3.47 (s, 3H), 2.19 (br. s., 2H). **^{13}C-NMR** (101 MHz, $CDCl_3$): δ (ppm) = 157.5, 142.2, 129.7, 119.5, 115.8, 114.0, 94.4, 74.5, 68.0, 56.1. **R_f** = 0.34 (PE/Acetone = 60/40) [PMA stain]. **HRMS** (APCI-MS): $[M+NH_4]^+$ $[C_{10}H_{14}O_4+NH_4]^+$ calcd: 216.1236; found: 216.1235.

Synthesis of 1-(naphthalen-1-yl)ethane-1,2-diol (**1n**)

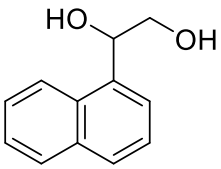

Prepared according to **GP3** from 1-(naphthalen-1-yl)ethan-1-one (1.7 g, 10 mmol, 1.0 equiv.). The crude product was purified via FCC (PE/Acetone = 70/30), giving **1n** as a white solid (1,4 g, 73%).

^{1}H-NMR (400 MHz, DMSO-d_6): δ (ppm) = 8.16 (d, *J* = 8.2 Hz, 1H), 7.93 (dd, *J* = 7.8, 1.6 Hz, 1H), 7.82 (d, *J* = 8.1 Hz, 1H), 7.66 (d, *J* = 7.1 Hz, 1H), 7.57–7.48 (m, 3H), 5.45–5.42 (m, 1H), 5.37–5.32 (m, 1H), 3.67 (ddd, *J* = 11.1, 6.0, 3.8 Hz, 1H), 3.52 (ddd, *J* = 11.2, 6.9, 3.8 Hz, 1H), 3.37 (br.s, 2H). **^{13}C-NMR** (101 MHz, DMSO-d_6): δ (ppm) = 139.4, 133.6, 130.9, 129.0, 127.6, 126.2, 125.8, 125.8, 124.1, 123.9, 71.6, 67.6. **R_f** = 0.74 (PE/Acetone = 60/40) [PMA stain]. **HRMS** (EI-MS): $[M]^{\cdot+}$ $[C_9H_{12}O_2]^{\cdot+}$ calcd: 188.08318; found: 188.08300.

Synthesis of 1-(naphthalen-2-yl)ethane-1,2-diol (**1o**)

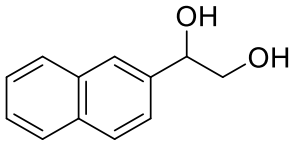

Prepared according to **GP2** from 2-vinylnaphthalene (771 mg, 5.0 mmol, 1.0 equiv.). The crude product was purified via FCC (PE/EtOAc = 60/40), obtaining **1o** as a white solid (586 mg, 62%).

^{1}H-NMR (400 MHz, DMSO-d_6): δ (ppm) = 7.91–7.84 (m, 4H), 7.53–7.46 (m, 3H), 5.37 (d, *J* = 4.2 Hz, 1H), 4.76 (app. t., *J* = 5.8 Hz, 1H), 4.71 (dd, *J* = 11.8, 5.8 Hz, 1H), 3.53 (t, *J* = 5.8 Hz, 2H). **^{13}C-NMR** (101 MHz, DMSO-d_6): δ (ppm) = 141.6, 133.2, 132.8, 128.1, 127.9, 127.7, 126.3, 125.9, 125.5, 125.1, 74.4, 67.8. **R_f** = 0.37 (PE/EtOAc = 60/40) [PMA stain]. **HRMS** (EI-MS): $[M]^{\cdot+}$ $[C_{12}H_{12}O_2]^{\cdot+}$ calcd: 188.08318; found: 188.08317.

Synthesized Unsuccessful Diols

Synthesis of 1-(4-bromophenyl)ethane-1,2-diol (**1q**)

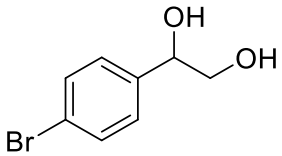

Prepared according to **GP3** from 1-(4-bromophenyl)ethan-1-one (2.0 g, 10 mmol, 1.0 equiv.). The crude product was purified via FCC (PE/Acetone = 70/30), giving **1q** as a white solid (80 mg, 6 %).

^{1}H-NMR (400 MHz, $CDCl_3$): δ (ppm) = 7.49 (d, *J* = 8.4 Hz, 2H), 7.25 (d, *J* = 8.4 Hz, 2H), 4.79 (dd, *J* = 8.0, 3.0 Hz, 1H), 3.75 (dd, *J* = 11.4, 3.0 Hz, 1H), 3.62 (dd, *J* = 11.4, 8.0 Hz, 1H), 2.28 (br.s., 2H). **^{13}C-NMR** (101 MHz, $CDCl_3$): δ (ppm) = 139.4, 131.65, 127.8,121.9, 74.0, 67.9. **R_f** = 0.69 (PE/Acetone = 60/40) [PMA stain]. **HRMS** (APCI-MS): $[M+NH_4]^+$ $[C_8H_9BrO_2 + NH_4]^+$ calcd: 234.0129; found: 234.0121.

Synthesis of 1-(4-nitrophenyl)ethane-1,2-diol (**1r**)

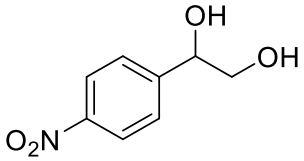

Prepared according to **GP3** from 1-(4-nitrophenyl)ethan-1-one (1.6 g, 10 mmol, 1.0 equiv.). The crude product was first purified via FCC (PE/Acetone = 60/40), and the obtained orange oil was further subjected to reverse-phase column (C18, H_2O+0.5 % TFA / CH_3CN). After evaporation of the solvent and lyophilization product **1r** was obtained as a yellow solid (244 mg, 13%).

^{1}H-NMR (400 MHz, $CDCl_3$): δ (ppm) = 8.20–8.24 (m, 2H), 7.54–7.58 (m, 2H), 4.95 (dd, *J* = 7.9, 3.4 Hz, 1H), 3.84 (dd, *J* = 11.3, 3.4 Hz, 1H), 3.64 (dd, *J* = 11.3, 7.9 Hz, 1H), 2.62 (br. s., 2H). **^{13}C-NMR** (101 MHz, $CDCl_3$): δ (ppm) = 147.7, 147.6, 126.9, 123.7, 73.7, 67.7. **R_f** = 0.42 (PE/Acetone = 60/40) [PMA stain]. **HRMS** (APCI-MS): $[M+NH_4]^+$ $[C_8H_9NO_4+NH_4]^+$ calcd: 201.0875; found: 201.0868.

Synthesis of 4-(1,2-dihydroxyethyl)benzonitrile (**1s**)

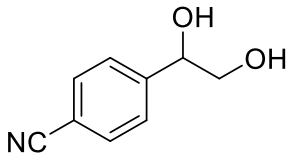

Prepared according to **GP3** from 4-acetylbenzonitrile (1.4 g, 10 mmol, 1.0 equiv.). The crude product was purified via FCC (PE/Acetone = 60/40), giving **1s** as a pale oil (784 mg, 48%).

^{1}H-NMR (400 MHz, $CDCl_3$): δ (ppm) = 7.70–7.67 (m, 2H), 7.55–7.52 (m, 2H), 4.92 (dd, *J* = 7.8, 3.4 Hz, 1H), 3.84 (dd, *J* = 11.2, 3.4 Hz, 1H), 3.65 (dd, *J* = 11.2, 7.8 Hz, 1H), 1.56 (br. s., 2H). **^{13}C-NMR** (101 MHz, $CDCl_3$): δ (ppm) = 146.0, 132.3, 126.8, 118.7, 111.5, 73.9, 67.6. **R_f** = 0.43 (PE/Acetone = 60/40) [PMA stain]. **HRMS** (APCI-MS): $[M+NH_4]^+$ $[C_9H_9NO_2+NH_4]^+$ calcd: 181.0977; found: 181.0973.

Synthesis of 1-(4-(methylthio)phenyl)ethane-1,2-diol (**1t**)

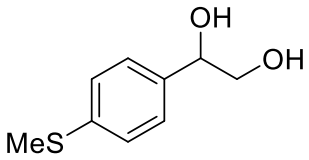

1-(4-methylthio)phenyl)ethan-1-one was synthetized *via* Friedel–Crafts acylation of methylthiophenol ether following a literature reported procedure.[29] Title compound was then prepared according to **GP3** from 4'-(methylthio)-acetophenone (831 mg, 5 mmol, 1.0 equiv.). Purification via FCC (PE/Acetone = 60/40), gave **1t** as a white solid (314 mg, 34%).

^{1}H-NMR (400 MHz, DMSO-d_6): δ (ppm) = 7.31 (d, *J* = 8.3 Hz, 2H), 7.23 (d, *J* = 8.3 Hz, 2H), 4.65 (br. s., 2H), 4.54 (app. t., *J* = 5.9 Hz, 1H), 3.46–3.43 (m, 2H), 2.45 (s, 3H). **^{13}C-NMR** (101 MHz, DMSO-d_6): δ (ppm) = 140.3, 136.2, 127.0, 125.8, 73.5, 67.5, 15.1. **R_f** = 0.26 (PE/Acetone = 60/40) [PMA stain]. **HRMS** (APCI-MS): $[M+NH_4]^+$ $[C_9H_{12}O_2S + NH_4]^+$ calcd: 202.0902: found 202.0894.

Synthesis of 1-(4-(methylsulfonyl)phenyl)ethane-1,2-diol (**S1**)

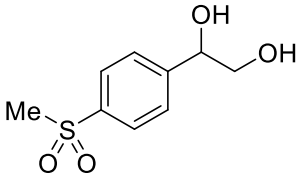

Prepared according to **GP3** from 1-(4-(methylsulfonyl)phenyl)ethan-1-one (1.98 g, 10 mmol, 1.0 equiv.). The crude was purified via FCC (PE/Acetone = 70/30), giving **S1** as a white solid (450 mg, 21%).

^{1}H-NMR (400 MHz, DMSO-d_6): δ (ppm) = 7.88 (d, *J* = 8.0 Hz, 2H), 7.62 (d, *J* = 8.0, 2H), 5.51 (br. s., 1H), 4.83 (br. s., 1H), 4.66 (br. s., 1H), 3.49 (br. s., 2H), 3.19 (s, 3H). **^{13}C-NMR** (101 MHz, DMSO-d_6): δ (ppm) = 149.7, 139.3, 127.3, 126.6, 73.2, 67.1, 43.7. **R_f** = 0.09 (PE/Acetone = 60/40) [PMA stain]. **HRMS** (ESI-MS): $[M+H]^+$ $[C_9H_{13}O_4S]^+$ calcd: 217.0535; found: 217.0530.

Synthesis of 1-phenylpropane-1,2-diol (**S2**)

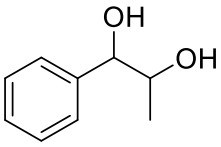

Prepared according to a literature reported procedure.[30] 1-Phenylpropane-1,2-dione (600 mg, 4.0 mmol, 1.0 equiv.) was dissolved in EtOH (10 mL) and cooled to 0 °C. $NaBH_4$ (180 mg, 2.5 mmol, 1.2 equiv.) was added portion-wise over 10 minutes, after which the reaction mixture was stirred for 30 minutes at 0 °C and 1 h at 20 ºC. Reaction was quenched with H_2O, extracted with EtOAc (3x), the combined organic layers dried over $MgSO_4$, followed by filtration and evaporation of solvent. Crude was purified via FCC (PE/Acetone = 75/25) and after solvent evaporation, the product was obtained as pale solid (564 mg, 92%). The ratios of *cis* and *trans* – isomers in the 1H-NMR spectrum were determined using Karplus analysis on the doublets at 4.68 and 4.36 ppm.

^{1}H-NMR (400 MHz, $CDCl_3$): δ (ppm) = 7.38–7.28 (br. m., 8.5H), 4.68 (*cis*, d, *J* = 4.2 Hz, 1H), 4.36 (*trans*, d, *J* = 7.8 Hz, 0.6H), 4.01 (*cis*, dq, *J* = 6.6, 4.2 Hz, 1H), 3.87 (*trans*, dq., *J* = 7.8, 6.4 Hz, 0.6H), 2.82 (br. s., 3H), 1.08 (*cis*, d, *J* = 6.4 Hz, 3H), 1.06 (*trans*, d, *J* = 6.4 Hz, 1.8H). **^{13}C-NMR** (101 MHz, $CDCl_3$): δ (ppm) = 141.0 (*trans*), 140.3 (*cis*), 128.5 (*trans*), 128.3 (*cis*),

128.1 (*trans*), 127.8 (*cis*), 126.9 (*trans*), 126.6 (*cis*), 79.5 (*trans*), 77.4 (*cis*), 72.2 (*trans*), 71.3 (*cis*), 18.7 (*trans*), 17.1 (*cis*). **R_f** = 0.51 (PE/Acetone = 60/40) [PMA stain]. **HRMS** (APCI-MS): $[M+NH_4]^+$ $[C_9H_{12}O_2+NH_4]^+$ calcd: 170.1181; found: 170.1176.

Synthesis of 2-phenoxy-1-phenylethan-1-ol (**S4**)

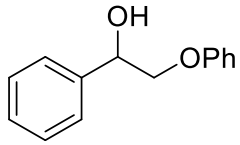

Prepared according to a literature reported procedure.[30] Phenol (1.45 mL, 16.5 mmol, 1.1 equiv.) and K_2CO_3 (3.0 g, 22.5 mmol, 1.5 equiv.) were dissolved in acetone (150 mL) at room temperature. 2-bromo-1-phenyl-ethan-1-one (3.0 g, 15.0 mmol, 1.0 equiv.) was added portionwise to the mixture, and the reaction was refluxed for 4 h. After cooling to room temperature, the suspension was filtered, and the solvent removed under reduced pressure. The obtained crude product was then used in the next step without further purification. For the reduction, crude 2-phenoxy-1-phenylethan-1-one (1.5 g, 15.0 mmol, 1.0 equiv.) was dissolved in the mixture of THF/water (75 mL, 4/1) and cooled to 0 °C. $NaBH_4$ (681 mg, 18.0 mmol, 1.2 equiv.) was added portionwise at 0 °C, after which the reaction was stirred at room temperature for 2 h. The reaction was quenched with sat. NH_4Cl (30 mL) and the aqueous phase was extracted with ethyl acetate (3x). Combined organic phases were dried over $MgSO_4$, filtered, and concentrated. Purification via FCC (PE/EtOAc = 60/40) yielded **S4** as white solid (1.08 g, 72%).

^{1}H-NMR (400 MHz, DMSO-d_6): δ (ppm) = 7.52–7.48 (m, 2H), 7.40–7.35 (m, 2H), 7.32–7.26 (m, 3H), 6.97–6.91 (m, 3H), 5.70 (d, *J* = 4.6 Hz, 1H), 4.07–4.03 (m, 2H), 3.46 (br. s., 1H). **^{13}C-NMR** (101 MHz, DMSO-d_6): δ (ppm) = 159.0, 142.9, 129.9, 128.5, 127.7, 126.9, 121.0, 115.0, 73.5, 71.4. **R_f** = 0.83 (PE/Acetone = 60/40) [PMA stain]. **HRMS** (EI-MS): $[M+H]^{\cdot+}$ $[C_{14}H_{14}O_2]^{\cdot+}$ calcd: 214.0993; found: 214.0990.

Synthesis of 2-methoxy-1-(4-methoxyphenyl)ethan-1-ol (**S5**)

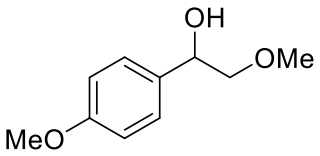

Prepared according to **GP3** from 1-(4-methoxyphenyl)ethan-1-one (1.5 g, 10 mmol, 1.0 equiv.). Reduction of the 2-oxoacetaldehyde intermediate in MeOH led to alkoxylation to the primary alcohol. Purification via FCC (PE/Acetone = 60/40), yielded **S6** as a white solid (480 mg, 26%).

^{1}H-NMR (400 MHz, $CDCl_3$): δ (ppm) = 7.24–7.20 (m, 2H), 6.92–6.88 (m, 2H), 4.25 (dd, *J* = 8.6, 3.8 Hz, 1H), 3.80 (s, 3H), 3.67 (dd, *J* = 11.6, 8.6 Hz, 1H), 3.57 (dd, *J* = 11.6, 3.8 Hz, 1H), 3.27 (s, 3H), 2.34 (br. s., 1H). **^{13}C-NMR** (101 MHz, $CDCl_3$): δ (ppm) = 159.5, 130.2, 128.1, 114.0, 84.1, 67.4, 56.7, 55.3. **R_f** = 0.61 (PE/Acetone = 60/40) [PMA stain]. **HRMS** (EI-MS): $[M]^{\cdot+}$ $[C_{10}H_{14}O_3]^{\cdot+}$ calcd: 182.0943; found: 182.0942.

Synthesis of 1-phenylpropane-1,2-diol (**S6**)

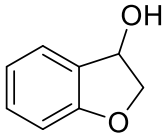

Prepared according to a literature reported procedure.[14a] 3-Coumaranone (0.54 g, 4.0 mmol, 1.0 equiv.) was disolved in MeOH (10 mL) and the mixture was cooled to 0 °C. $NaBH_4$ (1.6 g, 42 mmol, 11.4 equiv.) was added portionwise during 1 h. After the addition, the reaction was stirred for 30 minutes at 0 °C, after which it was allowed to warm to room temperature. The reaction was quenched with aqueous HCl (15 mL, 0.2 M) and the aqueous phase was extracted with chloroform (3×). The combined organic phases were dried over $MgSO_4$, filtered and concentrated. Purification by flash column chromatography (*tert*-butyl methyl ether) gave the title compound as a pale oil (529 mg, 97%).

^{1}H-NMR (400 MHz, $CDCl_3$): δ (ppm) = 7.22 (d, *J* = 7.5 Hz, 1H), 7.12 (app, td, *J* = 7.5, 1.0 Hz, 1H), 6.80 (app. td, *J* = 8.1, 1.0 Hz, 1H), 6.71 (d, *J* = 8.1 Hz, 1H), 5.02 (dd, *J* = 6.6, 2.5 Hz, 1H), 4.26 (dd, *J* = 10.7, 6.6 Hz, 1H), 4.15 (dd, *J* = 10.7, 2.5 Hz, 1H), 3.07 (br. s., 1H). **^{13}C-NMR** (101 MHz, $CDCl_3$): δ (ppm) = 160.1, 130.7, 128.2, 125.6, 121.0, 110.5, 79.0, 71.8. **R_f** = 0.62 (PE/Acetone = 60/40) [PMA stain]. **HRMS** (EI-MS): $[M]^{\cdot+}$ $[C_8H_8O_2]^{\cdot+}$ calcd: 136.0523; found: 136.0517.

Synthesized Diol for Mechanistic Studies

Synthesis of 1-phenylthane-1-*d*-1,2-diol (**1a_*d*$_1$**)

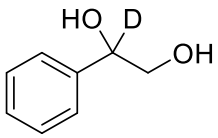

2-Hydroxy-1-phenylethan-1-one (163 mg, 1.20 mmol, 1.00 equiv.) was dissolved in CD_3OD (5 mL) and the resulting mixture was cooled to 0 °C. Then, sodium borodeuteride (98% *D*-atom, 167 mg, 4.00 mmol, 3.33 equiv.) was added portion wise over 10 minutes. The reaction was allowed to slowly warm towards room temperature while stirring for 2h, after which TLC analysis of the reaction showed full consumption of the starting material. The reaction was quenched by adding a few drops of 1M HCl, and methanol was evaporated under reduced pressure. Water (10 mL) was added to the residue and the aqueous phase was extracted with CH_2Cl_2 (5 x 10 mL). The combined organic layers were dried over $MgSO_4$, filtered and the solvents evaporated. The product was dried under high vacuo overnight which afforded the title compound as white solid (29 mg, 17%, 98%-*D*-atom).

^{1}H-NMR (400 MHz, $CDCl_3$): δ (ppm) = 7.37–7.27 (m, 5H), 4.79 (br.s., 0.02H, residual 1H), 3.70 (br. s., 1H), 3.64 (br. s., 1H), 3.16 (br.s., 2H). **^{13}C-NMR** (101 MHz, $CDCl_3$): δ (ppm) = 140.4, 128.5, 128.0, 126.1, 74.3, 67.9.

6.4.8 Mechanistic Studies

UV-Vis Studies

The mechanistic studies were commenced with attempts to identify the light-absorbing species in this photochemical transformation. For this, UV-vis spectra were recorded from the 1-phenylethane-1,2-diol (**1a**, 0.1 mM), Eosin Y (0.25 mM) and a combination of Eosin Y (0.25 mM) and the diol **1a** (0.1 M) and the results are shown in Figure S6. The spectra were recorded using a 10 mm × 1 mm quartz cuvette with 10 mm pathlength from 800 nm to 200 nm at 25 °C. The spectral window was chosen to be 800 nm to 200 nm having data interval of 1 nm and scan rate 600 nm/min. Baseline spectrum of pure non-dried CH_3CN was subtracted from each spectra before measuring.

NOTE**:** Due to the low absorption coefficient of the absorption band around 390 nm, the combination of indicated concentration with 10 mm pathlength were found crucial for separating this small absorbance from the baseline.

As can be seen from Figure S5, Eosin Y appears to be the main light absorbing species in the reaction mixture (bright orange line) whereas the 1-phenylethane-1,2-diol (gray-dottet line) does not have any observable absorption above 300 nm. The comparison between the irradiation wavelengths of 385 nm and 523 nm can be found in the section 4.2, where also the hypothesis for the need of the shorter wavelength are discussed. Addition of a solid diol **1a** to

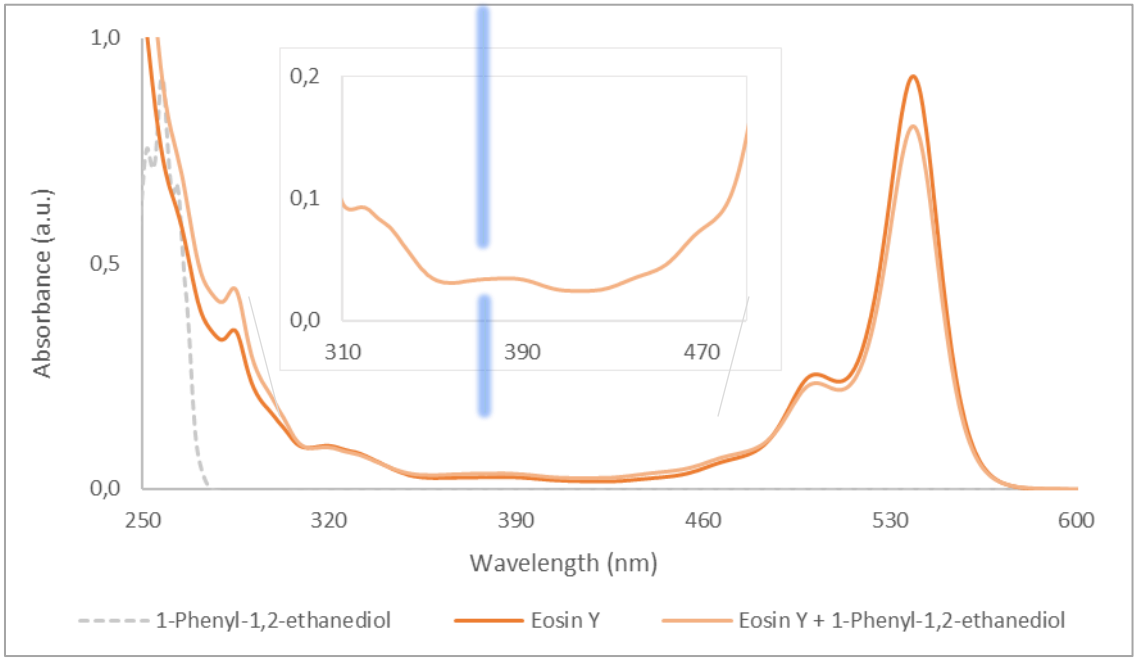

Figure S5. UV-vis spectrum of Eosin Y (0.25 mM), 1-phenylethane-1,2-diol (**1a**, 0.1 M) and a combination of the two (0.25 mM for EY and 0.1 M for diol) in a non-dried CH_3CN (1 mL). UV-vis spectra measured using a 10 mm × 1 mm quartz cuvette, *T* = 25 °C, spectral window 800 nm to 200 nm, data interval 1 nm, scan rate 600 nm/min. Baseline of pure acetonitrile is subtracted from the spectra.

a solution of Eosin Y in CH_3CN appears to slightly reduce the intensity of absorption on the Eosin Y's main absorption band at 520 nm and somewhat intensify the absorption near the UV-region around 300 nm. Although minor, these changes could hint towards a weak interaction between the diol **1a** and Eosin Y.

UV-Vis Monitoring of Eosin Y Photodegradation

Owing to the observed colour change during the first 10 minutes of the reaction, the possibility of (photo)degradation of Eosin Y was studied more closely (Figure S6). For this study, four vials were set up separately according to **GP1** containing either only Eosin Y (1.4 mg, 2.0 µmol) or a combination of Eosin Y (1.4 mg, 2.0 µmol) and 1-phenylethane-1,2-diol (**1a**, 13.8 mg, 0.10 mmol) dissolved in non-dried CH_3CN (1 mL) under N_2 atmosphere. The reaction mixtures were then irradiated with the desired wavelengths (385 nm or 523 nm) at 20 °C (temperature controlled with a cryostate) and a 25 µL probe of the reaction mixture was drawn with a Hamiltonian syringe at noted time points. These probes were diluted with 1 mL CH_3CN before measuring with UV-vis (quartz cuvette 10 mm × 1 mm, pathlength 10 mm, temperature 25 °C).

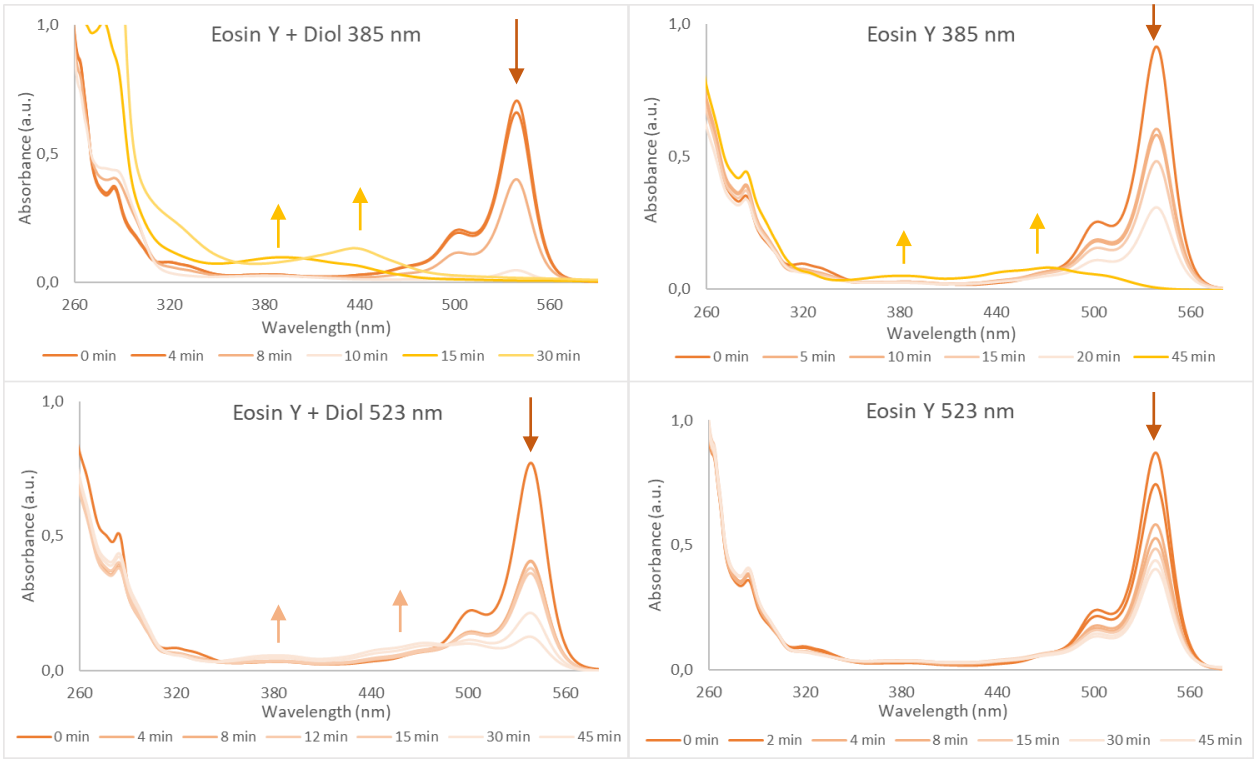

Figure S6. Time-dependent photodegradation of Eosin Y w/o 1-phenylethane-1,2-diol (**1a**) under 385 nm (4.7 W) or 523 nm (0.8 W) irradiation. The reaction mixtures were prepared according to **GP1** and detailed at the beginning of section 4.2. *Ex-situ* measurement of UV-vis spectra from 25 µL reaction mixture diluted to 1 mL of non-dried CH_3CN (concentration 0.25 mM) carried out in a 10 mm × 1 mm quartz cuvette at 25 °C. Spectral window 800 nm to 200 nm, data interval 1 nm, scan rate 600 nm/min. Baseline measured from pure acetonitrile is subtracted from the spectra.

Taken together, the results presented in Figure S6 suggest that a rapid photodegradation of the original catalyst takes place under the high intensity irradiation at 385 nm. The observed changes in the UV-vis spectrum are in good agreement with the literature reported Eosin Y degradation with 520 nm laser irradiation.[19] In the literature, inert atmosphere was found to speed up the photodegradation perhaps by excluding an alternative relaxation pathway *via* singlet oxygen generation, whereas under our conditions the presence of diol **1a** clearly accelerates the degradation perhaps by generating free radicals into the reaction mixture (section 4.4). In contrast, though, the degradation process appears to be significantly slower when irradiating the main absorption band of Eosin Y at 523 nm. This can be either owing to the inherently lowered energy of the irradiation of longer wavelength (Planck–Einstein Relation) or due direct excitation of an electron to a higher unoccupied molecular orbital with higher energy and intensity irradiation (although Kasha's rule would predict a fast relaxation to the lowest LUMO, which would correspond the orbital with excited state energy corresponding 520 nm irradiation). Meanwhile, the thermal control experiment run at 60 °C did not show any significant degradation even at prolonged time periods (1 h), ruling out the possibility of varying degrees of heating with different wavelength LEDs.

Kinetic Profile of the Reaction

The kinetic profile of the reaction was measured from the reaction of 1-phenylethane-1,2-diol (**1a**) under standard reaction conditions (**GP1**). The reaction progress was then monitored by taking 25 µL sample from the reaction mixture at indicated time points, and an internal standard of mesitylene (100 µL of 0.025 M stock solution in CH_3CN) was added. Then, the mixtures were submitted to GC-FID analysis and the final conversion and yields were calculated from five-point calibration curves made for the starting material and product.

Based on the kinetic profile presented in Figure S7, three different stages of the reaction can be separated. The reaction begins with a short induction period (< 10 min) during which neither the starting material gets consumed, nor formation of product is detected. This initiation period for the reaction correlates with the Eosin Y degradation described in the previous chapter. According to the UV-vis degradation studies, the original photocatalyst bleaches within the first ten minutes of the reaction, whereas the starting material consumption starts only shortly before the 10-minute mark. These coincidences could therefore suggest that Eosin Y acts as a precatalytic species in our system and the initial activation leads to the formation of highly efficient catalytic system.

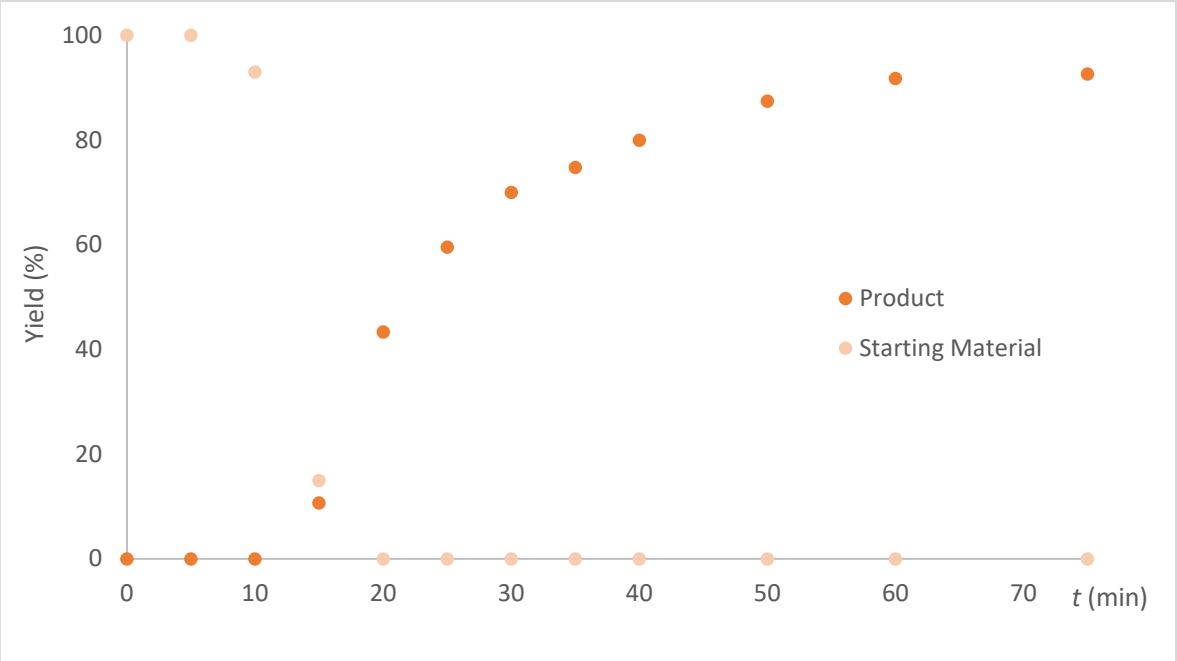

Figure S7. The kinetic profile of the reaction. The conversion and yield in each point was calculated by analyzing a 25 µL sample of the reaction mixture taken at indicated time periods with added stock solution of mesitylene as internal standard (100 µL, 0.025 M) with GC-FID. The reported yields were then calculated against a five-point calibration curve for the starting material and product.

In the second stage of the reactions (t = 10–20 min), the starting material gets rapidly consumed and reaches full conversion at 20 minutes. During this time period, the rate of the product formation displays a logarithmic kinetic, indicative of fast formation of product. However, at the point of 20 minutes where the starting material is fully consumed, the product yield has reached around 40%. In the last stage of the reaction (t = 20–60 min) the product formation is still ongoing, the rate of which starts to slowly plateau and reaching the final yield at 60 minutes.

Reaction Monitoring with *ex situ* ^{1}H-NMR

As the reaction kinetic presented in Figure S7 indicated towards the possibility of a reaction intermediate, an *ex situ* NMR kinetic was measured. For this, one vial was prepared according to **GP1** and the reaction was irradiated with 385 nm (4.7 W) LEDs at 20 °C. At given time points, a 50 µL sample was drawn from the reaction mixture, diluted with CD_3CN and measured via ^{1}H NMR-analysis (300 MHz). The combined spectra are presented in Figure S8.

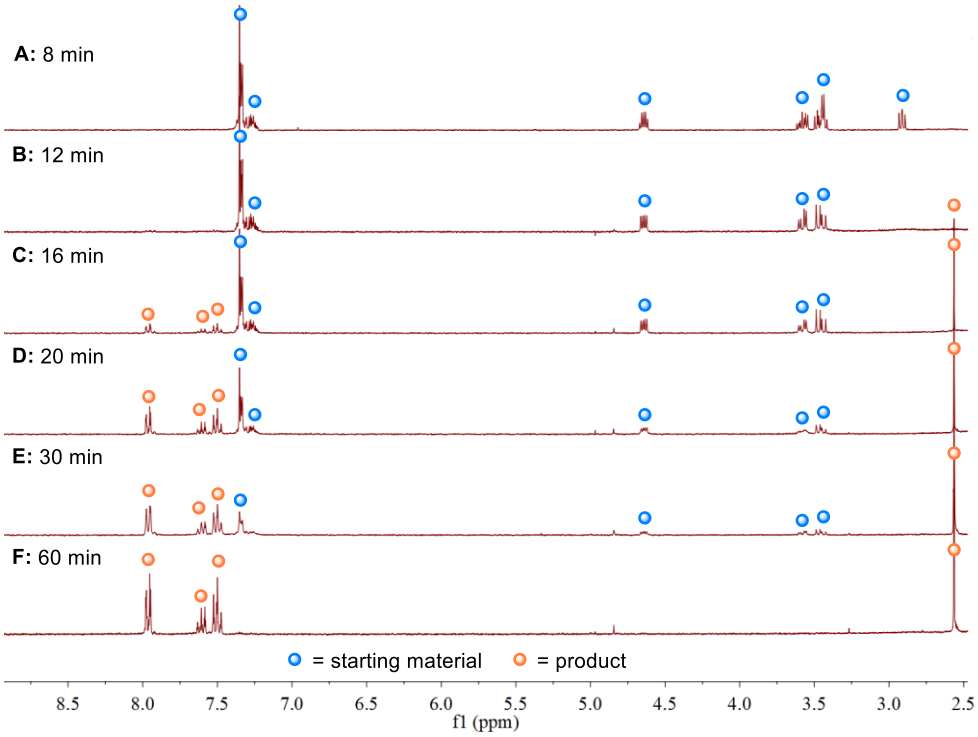

Figure S8. Combined ^{1}H-NMR spectra for the kinetic profile of the reaction. For this study, one vial was set up according to **GP1** and the reaction was irradiated with 385 nm (4.7 W) LEDs at 20 °C. On give time points, a 50 µL sample was drawn from the reaction mixture, diluted with CD_3CN and submitted to ^{1}H NMR-analysis (300 MHz).

Strikingly, before the onset of the reaction the ^{1}H-NMR spectrum might not be on the first glance easily recognizable as 1-phenylethane-1,2-diol (**1a**) due to unexpectedly complex splitting of the proton signals and the occurrence of an additional triplet around 3.0 ppm. Upon deeper analysis of spectra, the additional complexity was attributed to the hydroxy protons of **1a** which under anhydrous conditions appeared to be rather unexchangeable (Figure S8, spectrum A). Furthermore, these OH protons also cause an extra order of splitting in the nearby C–H signals. However, as the reaction commences, the water released as a by-product initiates a fast exchange of the hydroxy protons, illustrated by the simplified ^{1}H-NMR spectrum at 12 minutes (spectrum B). From this point on, the formation of product becomes visible and the growth of the aromatic protons at 8 ppm belonging to **2a** can be observed until 60 minutes (spectra C–F). Unfortunately, though, despite the rapid starting material consumption compared to the product formation, no prominent reaction intermediate could be distinguished.

Reaction Efficiency with Added Acetophenone (Autocatalytic Pathway)

Since the acetophenone formed as the product is also known as a photocatalytic HAT reagent, the possibility of an autocatalyzed reaction was studied.[31] To this end, four reactions were set up according to **GP1** and a varying amount of acetophenone was added to each mixture before irradiating the reactions for 30 minutes with 385 nm LEDs (table S7). Afterwards, mesitylene (250 µL of 0.4 M stock solution) was added as an internal standard and the reaction mixtures were analysed by GC-FID. Yields were calculated using a five-point calibration curve and amounts of originally added acetophenone were subtracted to obtain the final corrected yields.

As can be observed in table S7, the addition of the product to the reaction mixture does not present advantages to the reaction, and indeed the addition of more than 25 mol% begins to show reaction inhibition. Therefore, it seems that the formation of the product does not help to drive the reaction, but on the contrast hinders the productive reaction pathway. One possible explanation could be acetophenone acting as a competing light absorbing species therefore diminishing the excitation efficiency of the reaction catalyzing species.

Table S7. Study of the addition of initial amounts of **2a** to the reaction mixture of **1a**.

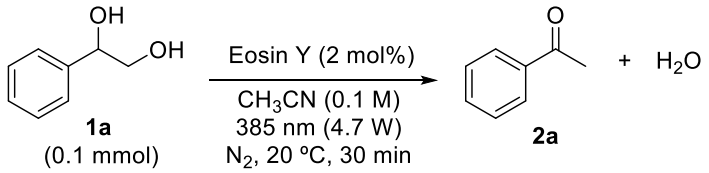

Entry	Initial loading of **2a** (mol%)	Corrected yield of **2a**[a]
1	0	45
2	25	40
3	50	30
4	75	15

[a]The initial loading of acetophenone was subtracted.

Light on/off Experiment

To differentiate between a photoinitiated and photochemical reaction pathways, a light on/off experiment was carried out. Based on the earlier sections, degradation of the original photocatalyst was already proven to be a light-driven process (section 4.2), but the dependency of the later reaction stages (consumption of starting material and especially the conversion of possible intermediate(s) to products) on light irradiation was still unclear. For the light on/off reaction, one vial was set up according to **GP1** and irradiated with 385 nm (4.7 W)

LEDs while cycling between the light and dark periods (ten minutes each) as shown in Figure S9. The progress of the reaction with respect to the product formation was followed by drawing a sample of 25 µL every ten minutes (at the exact points of switching between light and dark phases) to which 250 µL of mesitylene stock solution (0.01 M in acetonitrile) was added. Then, 0.5 mL of CD_3CN was added and the probes were analysed with ^{1}H-NMR (300 MHz). The integrals of the aromatic protons of mesitylene (3H, δ = 6.5 ppm) and the aliphatic methyl group of acetophenone (3H, δ = 2.3 ppm) were used for the calculation of product yield. The results from the light on/off experiment were then combined in Figure S9.

The results shown in Figure S9 clearly show that the reaction proceeds only during the “light” phases, therefore confirming that continuous irradiation is needed for each stage of the process. The ten-minute induction period observed during the measurement of the reaction kinetic (section 4.3.1) also displays in the on/off experiment causing only small amounts of the product being formed during the first irradiation period of 10 minutes. Apart from the light-dependency of the degradation of the photocatalyst, according to the on/off study also the consumption of starting material and the conversion of possible intermediates to the desired product are all light-dependent events.

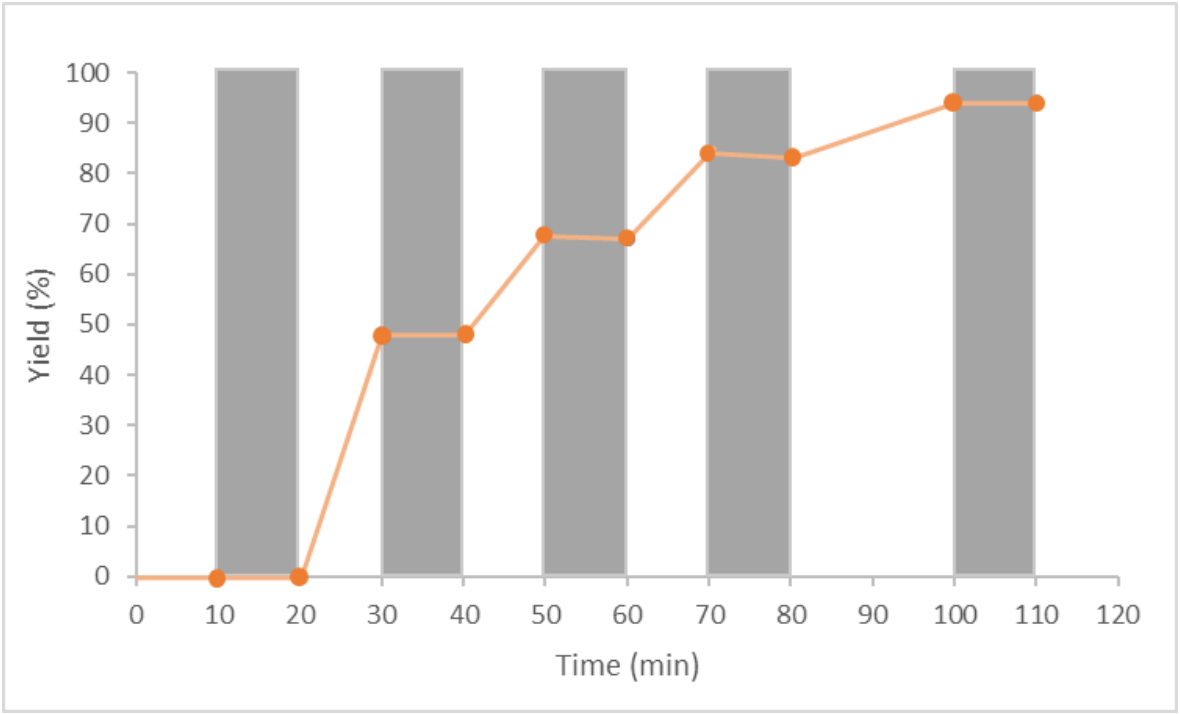

Figure S9. Light on/off experiment of the photocatalytic dehydration reaction of 1-phenylethane-1,2-diol (**1a**). The yield at each point was calculated by taking a 25 µL probe from the reaction mixture, to which 250 µL of mesitylene stock solution (0.01 M) was added. The probes were then filled with 0.5 mL of CD_3CN and analyzed with ^{1}H-NMR (300 MHz) using the aromatic protons of mesitylene (3H, δ = 6.5 ppm) and acetophenone methyl group (3H, δ = 2.3 ppm) for the integration.

HPLC-MS Analysis of Eosin Y Photodegradation

Following up the leads on the possible photodegradation of Eosin Y in the overtime UV-vis measurement as well as the literature precedents, the composition of the reaction mixture was further studied with HPLC-MS. For this, one vial comprising of Eosin Y (69.2 mg, 0.1 mmol, 1.0 equiv.) and diol **1a** (13.8 mg, 0.1 mmol, 1.0 equiv.) in CH_3CN (1 mL) was set up according to **GP1** and was irradiated for 10 minutes with the 390 nm (4.7 W) LEDs at 20 °C (cryostate set at 10 °C). The mixture was then filtered through a syringe filter before submitting for HPLC-Q-TOF-MS analysis. Despite the simplicity of the reaction in terms of the number of reagents, a complex mixture of compounds was obtained (Scheme 3 and Figure S10). Based on the prevailing decomposition/radical addition patterns, some representative examples of the found compounds accompanied by the possible structures are combined in Figure S10.

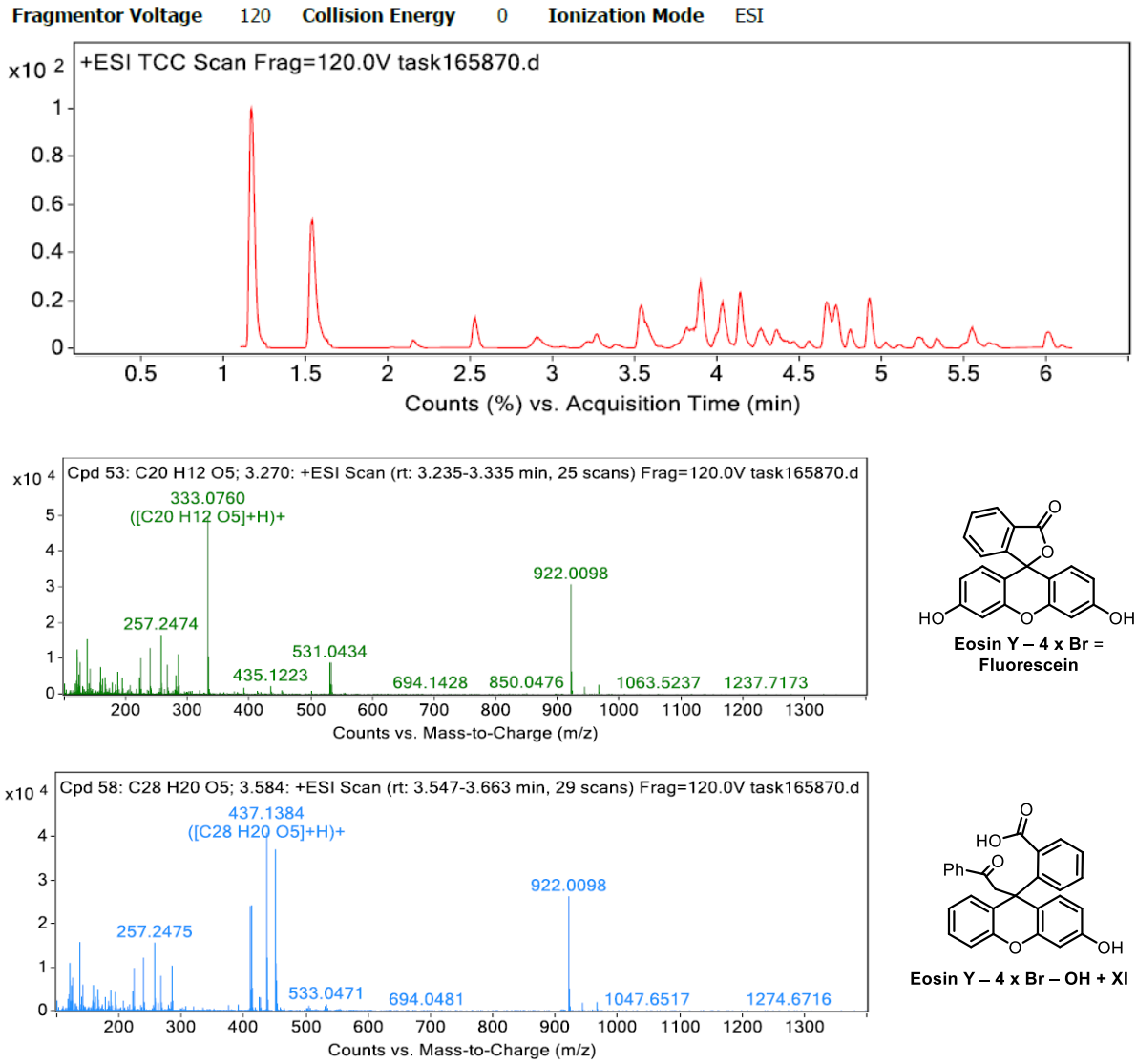

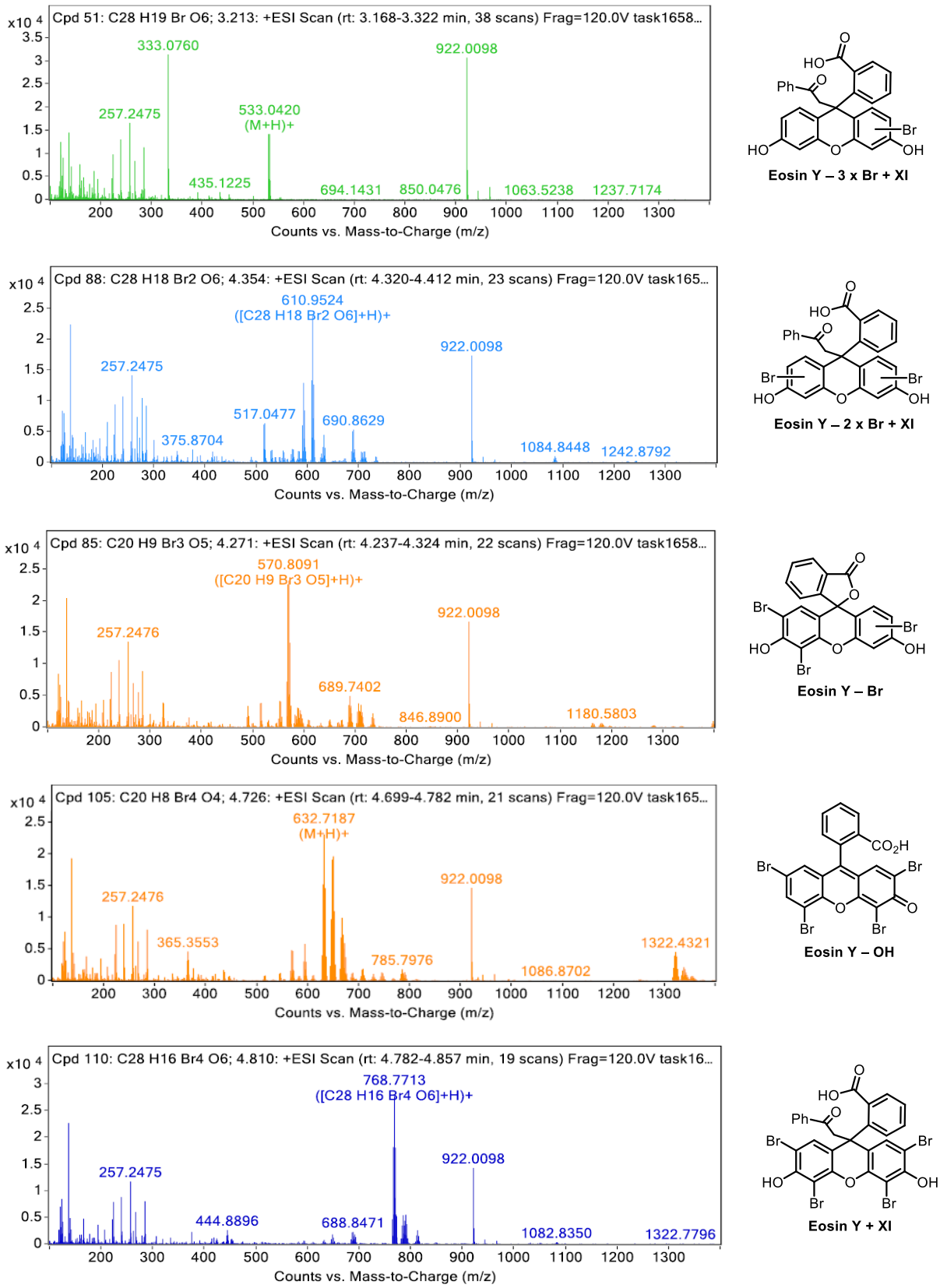

Figure S10. An overview of the HPLC-MS spectrum of Eosin Y and 1-phenylethane-1,2-diol photodegradation (above) combined with selected mass spectra (below). Possible structures of corresponding to each peak are shown on the right.

As can be seen from the Figure S10, most of the degradation products could be classified corresponding to A) different degrees of Eosin Y debromination (1–4 bromines cleaved), B) addition of an α-carbonyl radical to the photocatalyst, and C) further dehydration of the debrominated molecules and radical adducts. Out of these degradation pathways, debromination of Eosin Y has been well established in the literature,[19] whereas significantly less has been discussed about the possible radical addition. However, based on earlier reports disclosing the photosubstitution reactions on 4CzIPN[21a] and photoadditions to Fukuzumi dye,[21c] analogous reactivity with Eosin Y could be imagined. This could also in part explain the increased rate of Eosin Y degradation in the presence of the diol **1a** as observed by UV-vis spectroscopy (previously discussed). The questions regarding the extent and efficiency of this possible process remain outside of the frames of this study.

Studies Towards Br-Radical as a Potential HAT Catalyst

After identifying debromination as one of the main events in the photodegradation of Eosin Y during the initiation period of the reaction, the possibility of the so-generated bromide radical acting as a HAT catalyst was studied. Towards this direction, a bromine radical precursor was added in the reaction as tetrabutylammonium salt, and four photocatalysts were chosen based on literature reports to oxidize the bromide anion to its radical form.[22] Due to the very low catalyst loading of Eosin Y in the standard reaction conditions, the bromide anion loading was kept low to mimic the original reaction conditions. Therefore, we started our studies with the bromide loading of 2.0 mol%. The results of these reactions are summarized in table S8.

Table S8. Screening of bromide anion as HAT precursor in the dehydration reaction of **1a**.

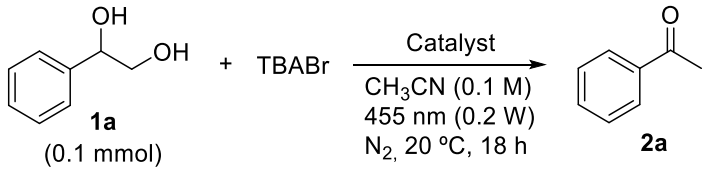

Entry	Catalyst (mol%)	TBABr (mol%)	Yield of **2a** (%)[a]
1	$Ir[dF(CF_3)ppy]_2(dtbbpy)PF_6$ (1)	2.0	n.d.
2	Mes-(^{t}Bu)$_2$Acr-Ph ClO_4 (5)	2.0	28
3	Triphenylpyrylium tetrafluoroborate (5)	2.0	n.d.
4	Mes-(^{t}Bu)$_2$Acr-Ph ClO_4 (5)	5.0	36
5	Mes-(^{t}Bu)$_2$Acr-Ph ClO_4 (5)	–	n.d.
6	$BiBr_3$ (20)	20	46

Reaction conditions: 1-Phenylethane-1,2-diol (13.8 mg, 0.1 mmol), TBABr, catalyst, dry CH_3CN, N_2, 455 nm LED (200 mW) at 25 °C for 18 h. GC-FID yields were calculated using a calibration curve

As can be observed from the table S8, in the presence of 3,6-di-*tert*-butyl-9-mesityl-10-phenylylacridin-10-ium perchlorate the desired acetophenone product was obtained in an unoptimized yield of 28% indicating that the hypothesis of bromide-radical driven HAT is feasible (table S8, entry 2). In contrast, though, $(Ir[dF(CF_3)ppy]_2(dtbbpy)PF_6$ and triphenylpyrylium tetrafluoroborate were not able to catalyze the reaction despite possessing the required redox-potentials to oxidize the bromide anion (entries 1–3). In all the unsuccessful reaction the starting material **1a** remained untouched. Furthermore, increasing the bromide loading to 5.0 mol% led to a positive effect on the reaction and an improved 36% yield was observed (entry 4). As the acridinium dyes are known as strong oxidizing agents (E^*_{red} > 2.0 V) the alternative mechanistic pathway going *via* aryl oxidation followed by benzylic deprotonation was ruled out by the control experiment where no product was detected in the absence of a bromide source (entry 5). Finally, an orthogonal method for the bromide radical generation was studied and a LMCT approach with bismuth bromide was found to give 46% yield of the desired product (entry 6).

Taken together, the productive reactions using orthogonal methods for bromine radical generation would thus hint towards the feasibility of bromine radical to catalyze our HAT/SCS sequence. However, even though the increase in bromide loading does have an advantageous effect on the reaction, the efficiency of this process still clearly falls short of that seen in the optimal reaction conditions with Eosin Y. It is therefore well likely that bromine radical is not the only HAT active species in the reaction, but other fragmentation products of Eosin Y also participate to the product formation.

TEMPO Trapping Experiment

To gather information about the short-lived radical intermediates formed during the reaction, trapping of these possible intermediates were attempted with TEMPO (section 4.5.1) and with different alkenes (section 4.5.2). For the TEMPO trapping studies, one reaction was set up according to **GP1** with the addition of TEMPO (15.6 mg, 0.1 mmol, 1.0 equiv.) as a reagent. After irradiation, the reaction mixture was filtered through a syringe filter and analyzed via LC-MS.

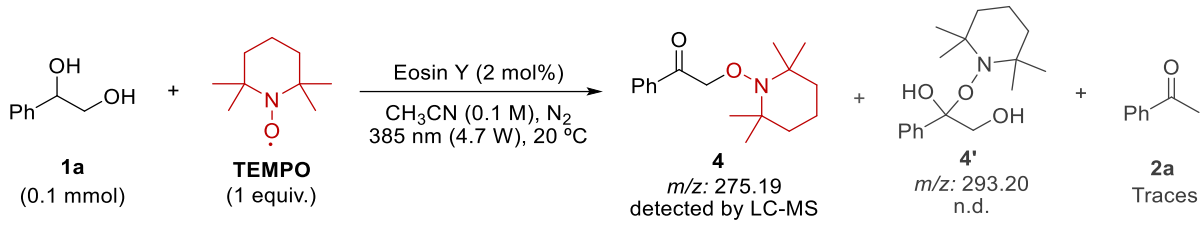

Scheme S1. Schematic representation of the results of TEMPO trapping studies with diol **1a**.

The measured LC-MS from the crude reaction mixture containing TEMPO included several mass peaks (Figure S11). The base peak of the mixture corresponded to the protonated TEMPO adduct **4**, whereas the identity of higher mass peaks were unknown, and the possibility of dimerization during the reaction or measurement was not ruled out. Importantly, any mass peak potentially corresponding to the benzylic radical adduct **4'** was not detected, which might indicate that the radical transfer from the benzylic position to the *alpha*-carbon during the spin center shift could be a very fast process.

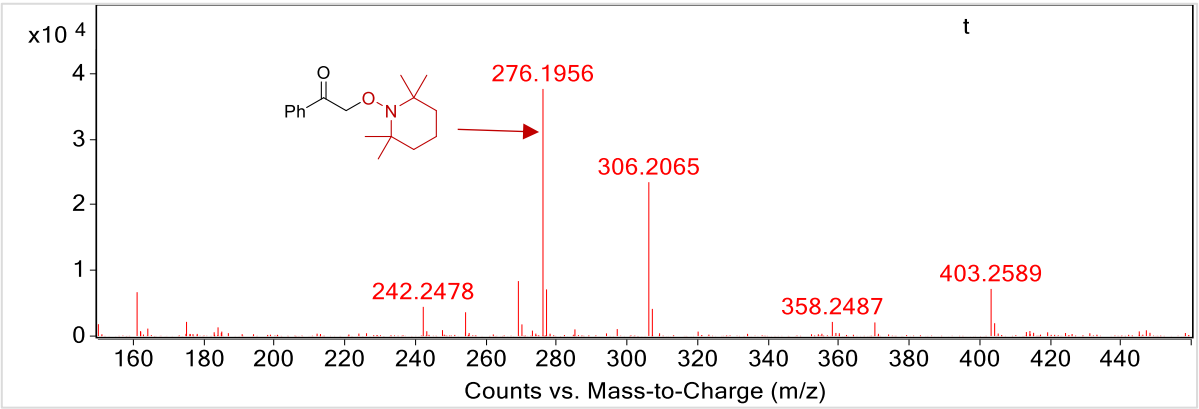

Figure S11. LC-MS chromatogram for the photocatalytic dehydration of **1a** in presence of TEMPO (1 equiv.). Mass spectrum recorded with Q-TOF on positive polarization using electron spray ionization (ESI) as ionization method.

Deuterium Labelling Studies

Finally, the mechanistic studies were concluded with deuterium labelling studies (Scheme S2). The reactions were set according to the **GP1** with modifications highlighted in Scheme below.

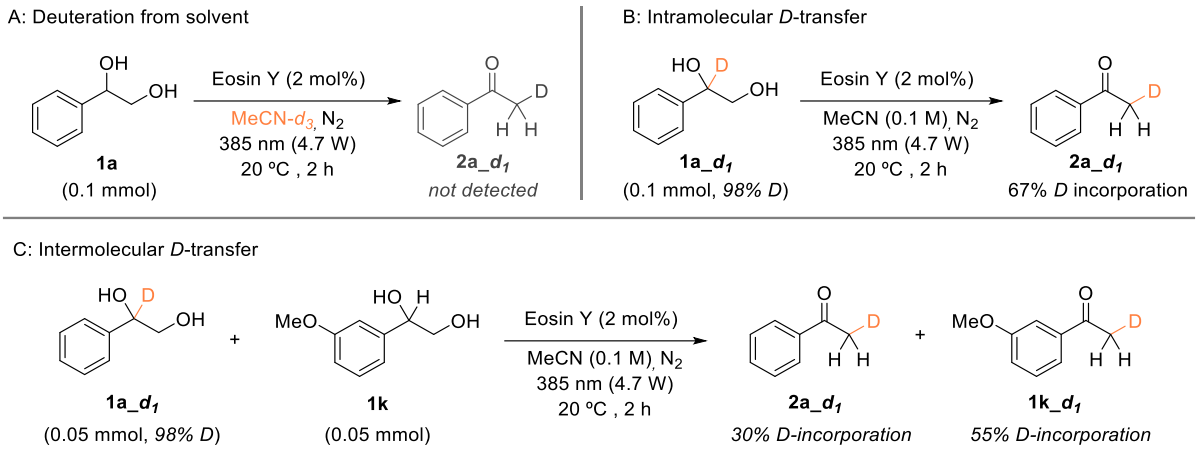

Scheme S2. Summary of deuterium labelling experiments.

Firstly, no deuteration was observed when running the reaction in CD_3CN, suggesting that the solvent does not directly participate the reaction (Scheme S2, A). A recently disclosed publication about the superbasicity of benzylic carbanions demonstrated how in the absence of other reaction partners these intermediates are quenched by deprotonating the solvent.[23] In the context of the afore-mentioned study the intermediacy of carbanions could thus be proven by deuterium transfer from the solvent to the product. Under our reaction conditions, however, similar rationalizations cannot be followed in such a straightforward manner for various reasons; the reduction of *alpha*-carbonyl radical would generate an enolate which is no longer superbasic, and substrates **1**, acetophenone products and Eosin Y are all more acidic than the solvent and would therefore be preferentially deprotonated. On the other hand an intramolecular deuterium transfer from **1a_*d*$_1$** led to a 67% deuterium incorporation to the product demonstrating that the species responsible of the initial HAT can react again with the intermediate and donate back the abstracted atom either in the form of a hydrogen atom or a proton (Scheme S2, B). The intermolecular deuterium transfer furthermore demonstrated that the H/D scrambling takes place when reacting equimolar amounts of deuterated and non-deuterated substrates (Scheme S2, C). This indicates that the HAT catalyst and the reaction intermediate dissociate after the first catalytic event and that other factors such as acidity, precoordination or the rate of BHAT could be more important factors than initial spatial arrangement when determining which species react together in the product forming step.

6.5 References

[1] a) A. C. Weymouth-Wilson, *Nat. Prod. Rep*. **1997**, *14*, 99–110; b) B. La Ferla, C. Airoldi, C. Zona, A. Orsato, C. Cardona, S. Merlo, E. Sironi, G. D'Orazio, F. Nicotra, *Nat. Prod. Rep.* **2011**, *28*, 630–648; c) Y. van Kooyk, G. A. Rabinovich, *Nat. Immunol.* **2008**, *9*, 593–601; d) A. Helenius, M. Aebi, *Science*, **2001**, *291*, 2364–2369.

[2] K. Yamatsugu, M. Kanai, *Chem. Rev*. **2023**, *123*, 6793–6838.

[3] Y. van Kooyk, G. A. Rabinovich, *Nat. Immunol.* **2008**, *9*, 593–601.

[4] a) T. Rice, E. Zannini, E. K. Arendt, A. Coffey, *Crit. Rev. Food Sci. Nurt.* **2019**, *60*, 2034–2051: b) A. R. Pereira, V. C. Fernandez, C. Delerue-Matos, V. de Freitas, N. Mateus, J. Oliveira, *Food Chem.* **2024**, *461*, 140945.

[5] a) Y. Liu, W. Wang and A.-P. Zeng, *Nat. Commun.* **2022**, *13*, 1595; b) H. Tang, Y.-B. Tian, H. Cui, R.-Z. Li, X. Zhang, D. Niu, *Nat. Commun.* **2020**, *11*, 5681; c) C. K. Hill, J. F. Hartwig, *Nat. Chem.* **2017**, *9*, 1213–1221; d) Y. Wang, H. M. Carder, A. E. Wendlant, *Nature*, **2020**, *578*, 403–408.

[6] a) K. R. Kunduru, R. Hogerat, K. Ghosal, M. Shaheen-Mualim, S. Farah, *J. Chem. Eng.* **2023**, *459*, 141211; b) A. Delavarde, G. Savin, P. Derkenne, M. Boursier, R. Morales-Cerrada, B. Nottelet, J. Pinaud, S. Caillol, *Prog. Polym. Sci.* **2024**, *151*, 101805; c) A. C. Weymouth-Wilson, *Nat. Prod. Rep.* **1997**, *14*, 99–110.

[7] B. La Ferla, C. Airoldi, C. Zona, A. Orsato, F. Cardona, S. Merlo, E. Sironi, G. D'Orazio, F. Nicotra, *Nat. Prod. Rep.* **2011**, *28*, 630.

[8] a) A. Hu, J.-J. Guo, H. Pan, H. Tang, Z. Gao, Z. Zuo, *J. Am. Chem. Soc.* **2018**, *140*, 1612–1616; b) A. Hu, Y. Chen, J.-J. Guo, N. Yu, Q. An, Z. Zuo, *J. Am. Chem. Soc.* **2018**, *140*, 13580–13585; c) T. Xue, Z. Zhang; R. Zeng, *Org. Lett.* **2021**, *24*, 977–982; d) W. Liu, Q. Wu, M. Wang, Y. Huang, P. Hu, *Org. Lett.* **2021**, *23*, 8413–8418; e) K. Sumiyama, N. Toriumi, N. Iwasawa, *Eur. J. Org. Chem.* **2021**, *2021*, 2474–2478; f) H. G. Yayla, H. Wang, K. T. Tarantino, H. S. Orbe, R. R. Knowles, *J. Am. Chem. Soc.* **2016**, *138*, 10794–10797; g) E. Tsui, A. J. Metrano, Y. Tsuchiya, R. R. Knowles, *Angew. Chem. Int. Ed.* **2020**, *59*, 11845–11849.

[9] J. Schwarz, B. König, *Chem. Commun.* **2019**, *55*, 486–488.

[10] a) D. F. McMillen, D. M. Golden, *Ann. Rev. Phys. Chem.* **1982**, *33*, 493–532; b) M. M. Suryan, S. A. Kafafi, S. E. Stein, *J. Am. Chem. Soc.* **1989**, *111*, 4594–4600.

[11] a) Y.-A. Zhang, X. Gu, A. E. Wendlandt, *J. Am. Chem. Soc.* **2022**, *144*, 599–605; b) C. J. Ostwood, D. W. C. MacMillan, *J. Am. Chem. Soc.* **2022**, *144*, 93–98;

c) A. S. K. Lahdenperä, J. Dhankhar, D. J. Davies, N. Y. S. Lam, P. D. Bacoş, K. de la Vega-Hernández, R. J. Phipps, *Science* **2024**, *386*, 42–49.

[12] P. Wessig and O. Muehling, *Eur. J. Org. Chem.* **2007**, *2007*, 2219–2232.

[13] a) F.-L. Zhang, B. Lin, K. N. Houk, Y.-F. Wang, *JACS Au* **2022**, *2*, 1032–1042; b) B. Matsuo, A. Granados, J. Majhi, M. Sharique, G. Levitre, G. A. Molander, *ACS Org. Inorg. Au* **2022**, *2*, 435–454.

[14] a) K. Chen, J. Schwarz, T. A. Karl, A. Chatterjee, B. König, *Chem. Commun*. **2019**, *55*, 13144–13147; b) Q. Zhu, D. G. Nocera, *ACS Catal.* **2021**, *11*, 14181–14187; c) Y.-X. Cao, G. Zhu, Y. Li, N. Le Breton, C. Gourlaouen, S. Choua, J. Boixel, H.-P. Jacquot de Rouville, J.-F. Soulé, *J. Am. Chem. Soc.* **2022**, *144*, 5902–5909.

[15] a) Y. Cheng Kang, S. M. Treacy, T. Rovis, *ACS Catal.* **2021**, *11*, 7442–7449; b) D. Birnthaler, R. Narobe, E. Lopéz-Berguno, C. Haag, B. König, *ACS Catal.* **2023**, *13*, 1125–1132.

[16] a) R. Lechner, S. Kümmel, B. König, *Photochem. Photobiol. Sci.* **2010**, *9*, 1367–1377; b) M. A. Ischay, M. S. Ament, T. P. Yoon, *Chem. Sci.* **2012**, *3*, 2807–2811.

[17] a) X.-Z. Fan, J. W. Rong, H.-L. Wu, Q. Zhou, H.-P. Deng, J. Da Tan, C.-W. Xue, L.-Z. Wu, H.-R. Tao, J. Wu, *Angew. Chem. Int. Ed*. **2018**, *57*, 8514–8518; b) D. M. Yan, Q.-Q. Zhao, L. Rao, J.-R. Chen, W.-J. Xiao, *Chem. Eur. J.* **2018**, *24*, 16895–16901; c) M. Majek, F. Filace, A. J. von Wangelin, *Beilstein J. Org. Chem.* **2014**, *10*, 981–989; d) H. Cao, D. Kong, L.-C. Yang, S. Chanmungkalakul, T. Liu, J. L. Piper, Z. Peng, L. Gao, X. Liu, X. Hong, J. Wu, *Nat. Synth.* **2022**, *1*, 794–803.

[18] Due to the low absorption coefficient of the band around 380 nm, concentration and light path length are important parameters to observe this feature. See details in the SI.

[19] A. Alvarez-Martin, S. Trashin, M. Cuykx, A. Covaci, K. De Vael, K. Janssen, *Dyes and Pigments*, **2017**, *145*, 376–384.

[20] P. Kimber, F. Plasser, *J. Chem. Theory Comput.* **2023**, *19*, 2340–2352.

[21] a) S. Grotjahn, B. König, *J. Org. Chem.* **2021**, *23*, 3146–3150; b) Y. Kwon, J. Lee, Y. Noh, D. Kim, Y. Lee, C. Yu, J. C. Roldao, J. Gierschner, R. Wannemacher, M. S. Kwon, *Nat. Commun.* **2023**, *14*, 92; c) Y.-X. Cao, G. Zhu, Y. Li, N. Le Breton, C. Gourlaouen, S. Choua, J. Boixel, H.-P. Jacquout de Rouville, J.-F. Soulé, *J. Am. Chem. Soc.* **2022**, *144*, 5902–5909.

[22] a) Z. Wang, X. Ji, T. Han, G.-J. Deng, H. Huang, *Adv. Synth. Catal.* **2019**, *361*, 5643–5647; b) P. Jia, Q. Li, W. C. Poh, H. Jiang, H. Liu, H. Deng, J. Wu, *Chem*, **2020**, *6*, 1766–1776.

[23] S. Grotjahn, C. Graf, J. Zelenka, A. Pattanaik, L. Müller, R. J. Kutta, J. Rehbein, J. Roithová, R. M. Gscwind, P- Nuernberger, B. König, *Angew. Chem. Int. Ed.* **2024**, *63*, e202400815.

[24] X. Gao, J. Lin, L. Zhang, X. Lou, G. Guo, N. Peng, H. Xu, Y. Liu, *J. Org. Chem.* **2021**, *86*, 15469–15480.

[25] J. P. G. Rygus, D. G. Hall, *Nat. Commun.* **2022**, *14*, 2653.

[26] B. Zeynizadeh, T. Behvar, *Bull. Chem. Soc. Jpn.* **2005**, *78*, 307–315.

[27] B. D. Dond, S. N. Thore, *Tetrahedron Lett.* **2020**, *61*, 151660.

[28] O. Obaro-Best, J. Reed, A. F. B. Norfadilah, R. Monahan, R. Sunasee, *Synth. Commun*, **2016**, *46*, 586–593.

[29] S.-K. Wang, X. You, D.-Y. Zhao, N.-J. Mou, Q.-L. Luo, *Chem. Eur. J.* **2017**, *23*, 11757–11760.

[30] J.-L. Wang, H.-J. Li, H.-S. Wang, Y.-C. Wu *Org. Lett.* **2017**, *14*, 3811–3814.

[31] M. Huix-Rotlant, D. Siri, N. Ferré, *Phys. Chem. Chem. Phys.* **2013**, *15*, 19293–19300.

7. Summary

This thesis presents the application of several photoinduced H-atom transfer strategies for the transformation of organic molecules through C–H Activation. These approaches have been successfully applied for the functionalization and defunctionalization of several substrates, including amides, carbamates, benzyl alcohols, benzaldehydes, and 1-aryl-1,2-ethanediols.

Part I of this thesis focuses on the application of anthraquinone sulfonates as water-soluble photocatalysts in organic synthesis.

In **Chapter 1**, the synthetic applications of anthraquinone sulfonates as photocatalysts are reviewed, and the potential for further applications in organic synthesis is discussed.

In **Chapter 2**, the tandem synthesis of benzylidenemalononitriles from benzyl alcohols and malononitrile is described. In this sequence, the initial photooxidation of a benzyl alcohol, catalyzed by anthraquinone-1,5-disulfonate, yields the corresponding benzaldehyde as a key intermediate. This step is followed by β-alanine-catalyzed condensation between the benzaldehyde and malononitrile. The use of water as the reaction medium and atmospheric oxygen as the terminal oxidant results in an efficient and operationally simple protocol.

Part II of this thesis focuses on the application of light-driven dual HAT-cobalt systems for gas-evolving reactions, including dehydrogenations, decarbonylations, and dehydroformylations.

In **Chapter 3**, the acceptorless dehydrogenation of amides and carbamates to the corresponding enamides and enecarbamates is described. Due to the absence of any sacrificial oxidant, hydrogen gas is generated as the sole by-product. The dual catalytic system comprises TBADT as an H-atom transfer photocatalyst and a cobaloxime complex, which is required for hydrogen evolution. The use of TBADT as a strong HAT agent enables cleaving aliphatic α-amido C–H bonds with relatively high bond dissociation energies.

In **Chapter 4**, the decarbonylation of benzaldehydes to arenes and carbon monoxide is described. This light-driven defunctionalization protocol is based on the interplay of thioxanthone as a H-atom transfer photocatalyst and a cobalt complex.

In **Chapter 5**, the sequential dehydroformylation of benzyl alcohols to arenes is described. This photocatalytic system was conceived as a follow-up of the system described in Chapter 4. However, in this case, TBADT and a cobaloxime complex are used as the essential components of this dual HAT-cobalt system. The transformation proceeds in a stepwise fashion, benzaldehydes being formed as key intermediates and hydrogen and carbon monoxide as byproducts.

Part III of this thesis focuses on the initiation of spin-center shift transformations through photoinduced H-atom transfer.

In **Chapter 6**, after a brief introduction of spin-center shift methodologies, the dehydration of 1-aryl-1,2-ethanediols to the corresponding acetophenones is described. The mechanistic investigations revealed that Eosin Y acts as a pre-catalyst, upon irradiation, yielding a mixture of H-atom transfer active species that can initiate a 1,2-spin-center shift within the substrate.

8. Zusammenfassung

Diese Arbeit stellt die Anwendung mehrerer photoinduzierter H-Atom-Transferstrategien zur Transformation organischer Moleküle durch C–H-Aktivierung vor. Diese Ansätze wurden erfolgreich zur Funktionalisierung und Defunktionalisierung mehrerer Substrate, einschließlich Amide, Carbamate, Benzylalkohole, Benzaldehyde und 1-Aryl-1,2-ethandiole eingesetzt.

Teil I dieser Arbeit befasst sich mit der Anwendung von Anthrachinonsulfonaten als wasserlösliche Photokatalysatoren in der organischen Synthese.

In **Kapitel 1** werden die synthetischen Anwendungen von Anthrachinonsulfonaten als Photokatalysatoren zusammengefasst und die Perspektiven weiterer potenzieller Anwendungen in der organischen Synthese behandelt.

In **Kapitel 2** wird die Tandemsynthese von Benzylidenmalononitrilen aus Benzylalkoholen und Malononitril beschrieben. In dieser Reaktion ergibt die anfängliche Photooxidation des Benzylalkohols, katalysiert durch Anthrachinon-1,5-disulfonat, das entsprechende Benzaldehyd als Zwischenprodukt. Auf diesen Schritt folgt eine β-Alanin-katalysierte Kondensation zwischen Benzaldehyd und Malononitril. Die Verwendung von Wasser als Reaktionsmedium und atmosphärischem Sauerstoff als terminalem Oxidationsmittel führt zu einem effizienten und operativ einfachen Syntheseprotokoll.

Teil II dieser Arbeit befasst sich mit der Anwendung lichtgetriebener dualer HAT-Kobaltsysteme für gasentwickelnde Reaktionen wie Dehydrierungen, Decarbonylierungen und Dehydroformylierungen.

In **Kapitel 3** wird die akzeptorlose Dehydrierung von Amiden und Carbamaten zu den entsprechenden Enamiden und Encarbamaten beschrieben. Aufgrund des Fehlens jeglichen Opferoxidationsmittels entsteht Wasserstoffgas als einziges Nebenprodukt. Das duale katalytische System besteht aus TBADT als H-Atom-Transfer-Photokatalysator und einem Cobaloximkomplex, der für die Wasserstoffentwicklung erforderlich ist. Die Verwendung von TBADT als starkes HAT-Mittel ermöglicht die Spaltung aliphatischer α-Amido-C–H-Bindungen mit relativ hohen Bindungsdissoziationsenergien.

In **Kapitel 4** wird die Decarbonylierung von Benzaldehyden zu Arenen und Kohlenmonoxid beschrieben. Dieses lichtgetriebene Defunktionalisierungsprotokoll basiert auf dem Zusammenspiel von Thioxanthon als H-Atom-Transfer-Photokatalysator und einem Kobaltkomplex.

In **Kapitel 5** wird die sequentielle Dehydroformylierung von Benzylalkoholen zu Arenen beschrieben. Dieses photokatalytische System wurde als Erweiterung des in Kapitel 4 beschriebenen Systems konzipiert. In diesem Fall werden jedoch TBADT und ein

Cobaloximkomplex als wesentliche Komponenten des dualen HAT-Kobaltsystems verwendet. Die Transformation verläuft schrittweise, wobei Benzaldehyde als wichtige Zwischenprodukte und Wasserstoff und Kohlenmonoxid als Nebenprodukte gebildet werden.

Teil III dieser Arbeit befasst sich mit der Initiierung von Spinzentrumsverschiebungstransformationen durch photoinduzierten H-Atomtransfer.

In **Kapitel 6** wird nach einer kurzen Einführung in Spinzentrumsverschiebungsmethoden die Dehydratisierung von 1-Aryl-1,2-ethandiolen zu den entsprechenden Acetophenonen beschrieben. Die mechanistischen Untersuchungen ergaben, dass Eosin Y als Präkatalysator fungiert, der bei Bestrahlung eine Mischung von H-Atomtransfer-aktiven Spezies ergibt, die in der Lage sind, eine 1,2-Spinzentrumsverschiebung innerhalb des Substrats zu initiieren.

9. Appendix

9.1 Abbreviations

A	absorbance
Ac	acetyl
APCI	atmospheric pressure chemical ionization
AQ	anthraquinone
AQS	anthraquinone sulfonate
aq.	aqueous
Ar	aryl
Bbbpy	4,4′-Bis(*tert*-butyl)-2,2′-bipyridin
BDE	bond-dissociation energy
Bn	benzyl
Boc	*tert*-butyloxycarbonyl
bs	broad singlet
Bz	benzoyl
°C	degrees Celsius
calcd.	Calculated
Cbz	Benzyloxycarbonyl
CC	column chromatography
CCDC	Cambridge Crystallographic Data Centre
conc.	concentrated
COPC	cobaloxime pyridine choride
d	doublet
δ	chemical shift
DCE	1,2-dichloroethane
dd	doublet of doublets
DMA	*N*,*N*-dimethylacetamide
DMF	*N*,*N*-dimethylformamide
$dmgH_2$	dimethylglyoxime
DMSO	dimethylsulfoxide
2,4-DNPH	2,4-dinitrophenylhydrazine
dt	doublet of triplets
$E_{1/2}$	reduction potential
EDG	electron-donating group
ee	enantiomeric excess
EI	electron ionization
EnT	triplet energy transfer
equiv.	Equivalent(s)
ESI	electrospray ionization
Et	ethyl
EtOAc	ethyl acetate
EWG	electron-withdrawing group

EY	eosin Y
FCC	flash column chromatography
FID	flame ionization detector
Fmoc	Fluorenylmethoxycarbonyl
GC	gas chromatography
GP	general procedure
h	hour(s)
HAT	hydrogen atom transfer
HPLC	high-performance liquid chromatography
HRMS	high-resolution mass spectrometry
hv	incident photon energy
Hz	Hertz
I.S.	internal standard
i-Pr	isopropyl
J	coupling constant
KIE	kinetic isotope effect
λ	wavelength
LC	liquid chromatography
LED	light-emitting diode
LMCT	ligand-to-metal charge transfer
M	molar
m	multiplet
m	*meta*
Me	methyl
MeCN	acetonitrile
mg	milligram
MHz	megahertz
min	minute(s)
mL	milliliter
µL	microliter
mM	millimolar
mm	millimeter
mmol	millimole
µmol	micromole
MOM	methoxymethylether
mol	mole
mol%	mole percent
Mp	melting point
MS	mass spectrometry
mW	milliwatt
N.d.	not detected
nm	nanometer
*n*Bu	*n*-butyl
NMR	nuclear magnetic resonance
o	*ortho*

OC	organocatalyst
p	*para*
PC	photocatalyst
PCET	proton-coupled electron transfer
PE	petrol ether
Ph	phenyl
PMA	phosphomolybdic acid
ppm	parts per million
q	quadruplet
Q-TOF-MS	quadrupole time-of-flight mass spectrometry
R	substituent
ROS	reactive oxygen species
s	singlet
S.C.	standard conditions
SAQS	sodium anthraquinone sulfonate
SCE	saturated calomel electrode
SCS	spin-center shift
SET	single-electron transfer
t	triplet
TBADT	tetrabutylammonium decatungstate
TBS	*tert*-butyldimethylsilyl
t-Bu	*tert*-butyl
td	triplet of doublets
TEMPO	(2,2,6,6-tetramethylpiperidin-1-yl)oxyl
THF	tetrahydrofurane
TLC	thin-layer chromatography
TMS	trimethylsilyl
Ts	tosyl
TX	thioxanthone
UV	ultraviolet
V	Volt
Vis	visible
Vol.	volume
W	Watt
WO	decatungstate
X	halogen substituent
xantphos	4,5-bis(diphenylphosphino)9,9-dimethylxanthene
XRD	X-ray diffraction
Ø	diameter

9.2 NMR Spectra of Chapter 2

NMR spectra of starting materials

^{1}H-NMR (400 MHz, $CDCl_3$) of **1e**

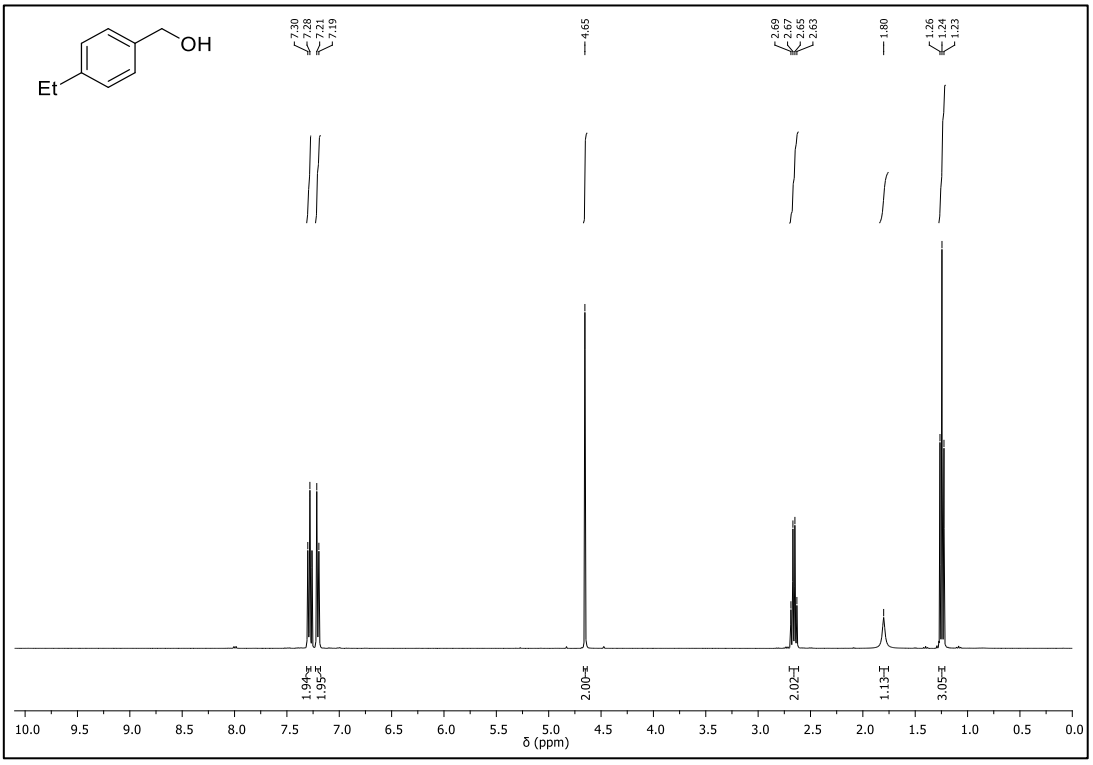

^{13}C-NMR (101 MHz, $CDCl_3$) of **1e**

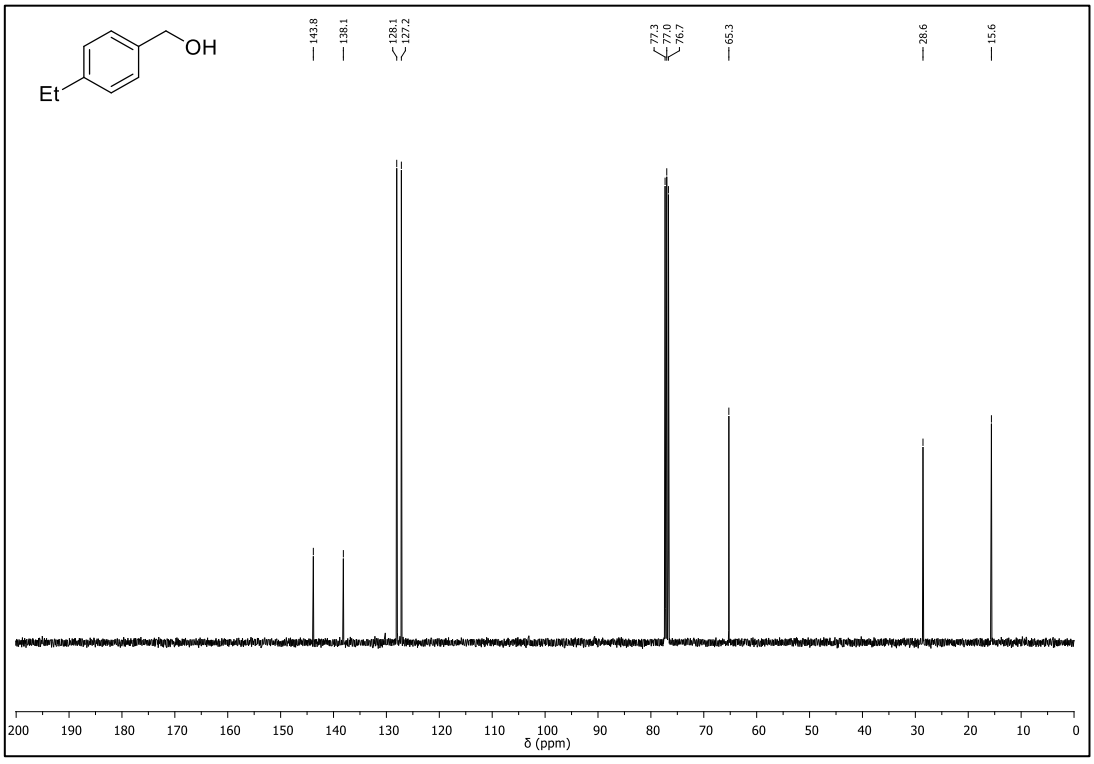

^{1}H-NMR (400 MHz, $CDCl_3$) of **1g**

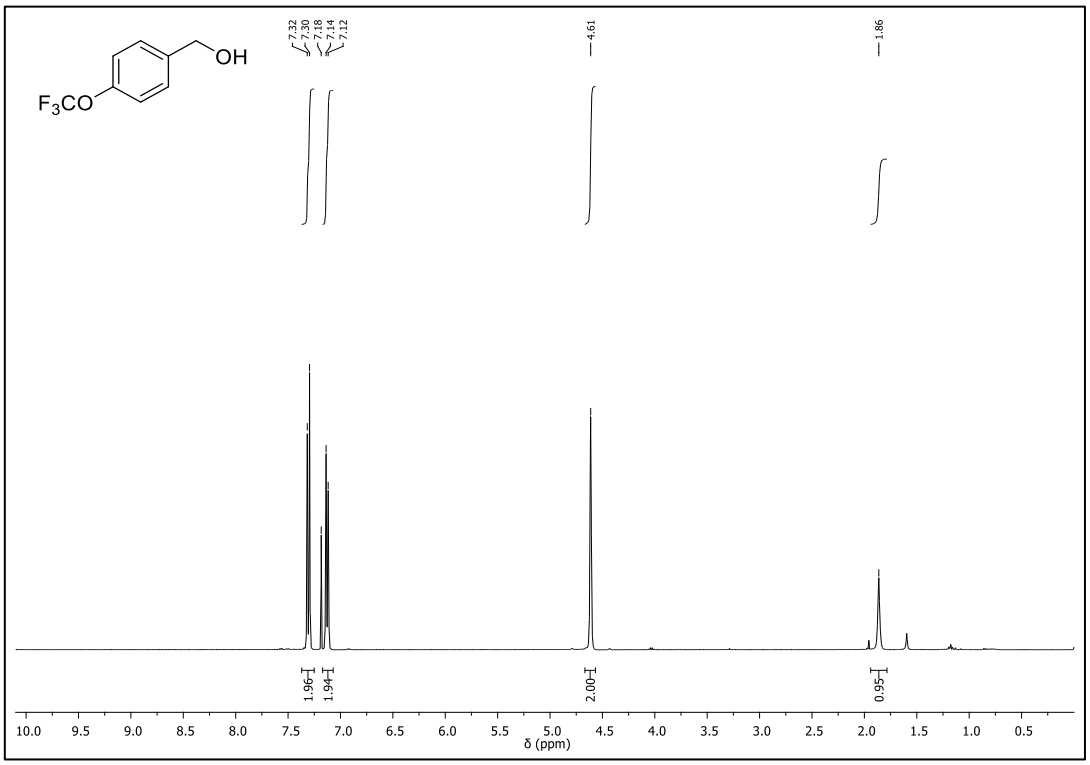

^{13}C-NMR (101 MHz, $CDCl_3$) of **1g**

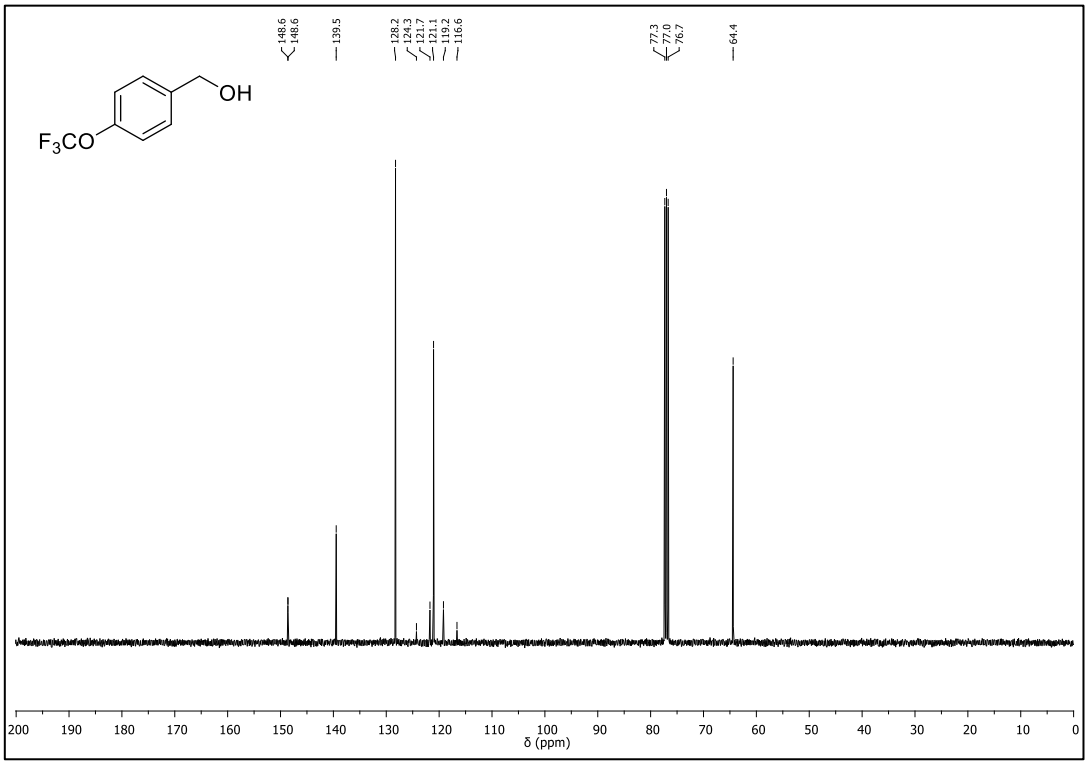

^{19}F-NMR (376 MHz, $CDCl_3$) of **1g**

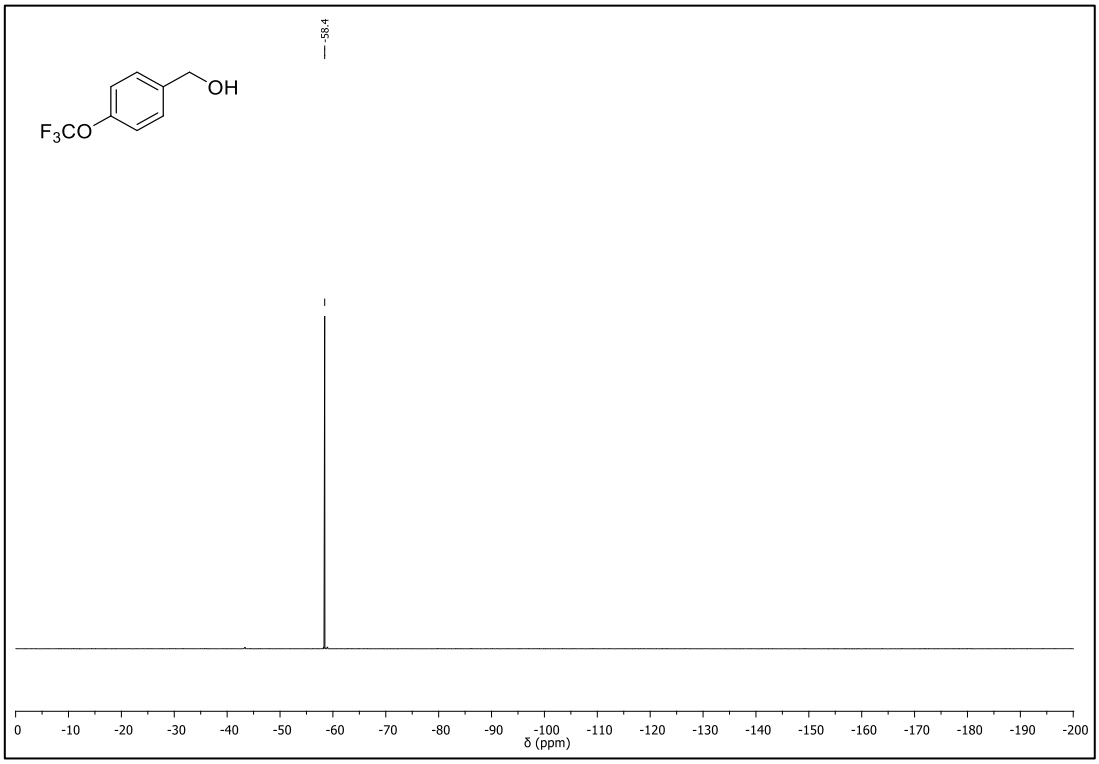

^{1}H-NMR (400 MHz, $CDCl_3$) of **1i**

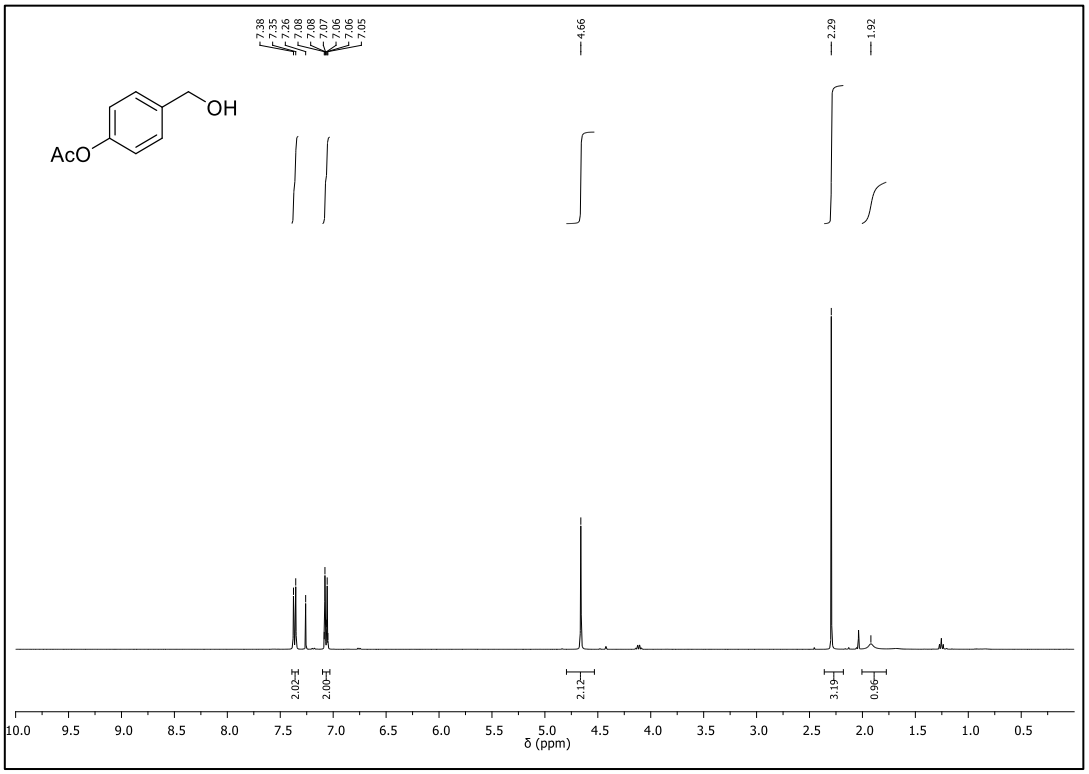

^{13}C-NMR (101 MHz, $CDCl_3$) compound **1i**

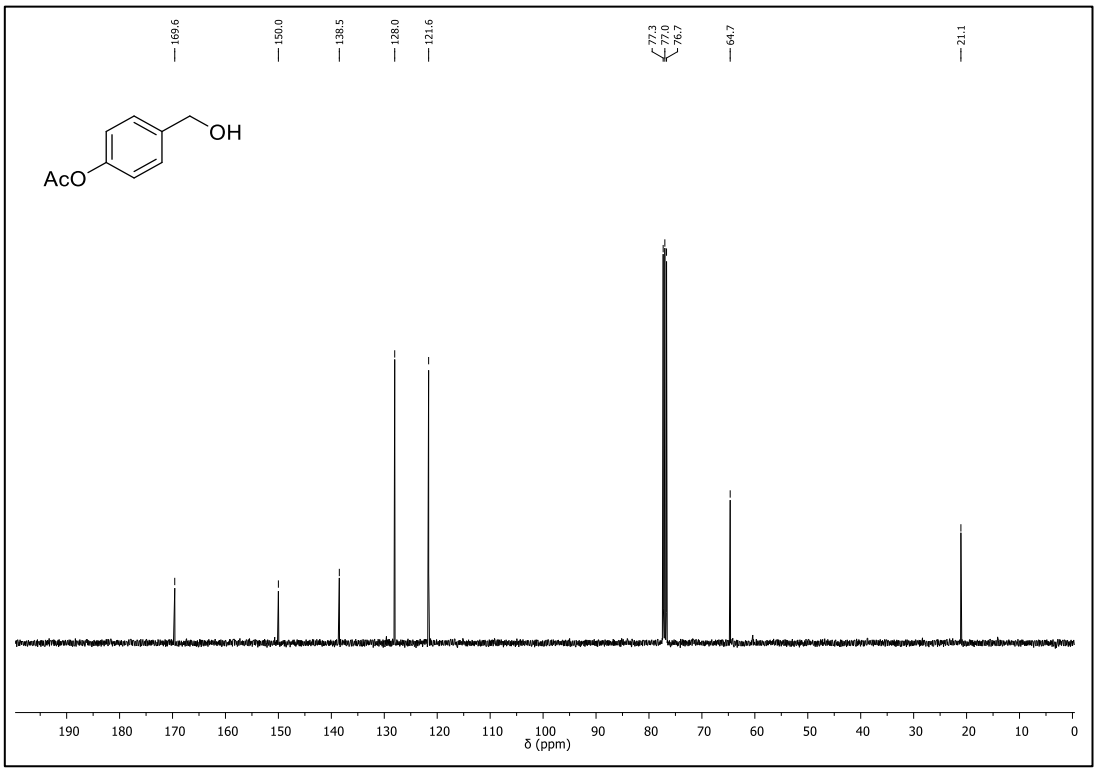

^{1}H-NMR (400 MHz, $CDCl_3$) of **1k**

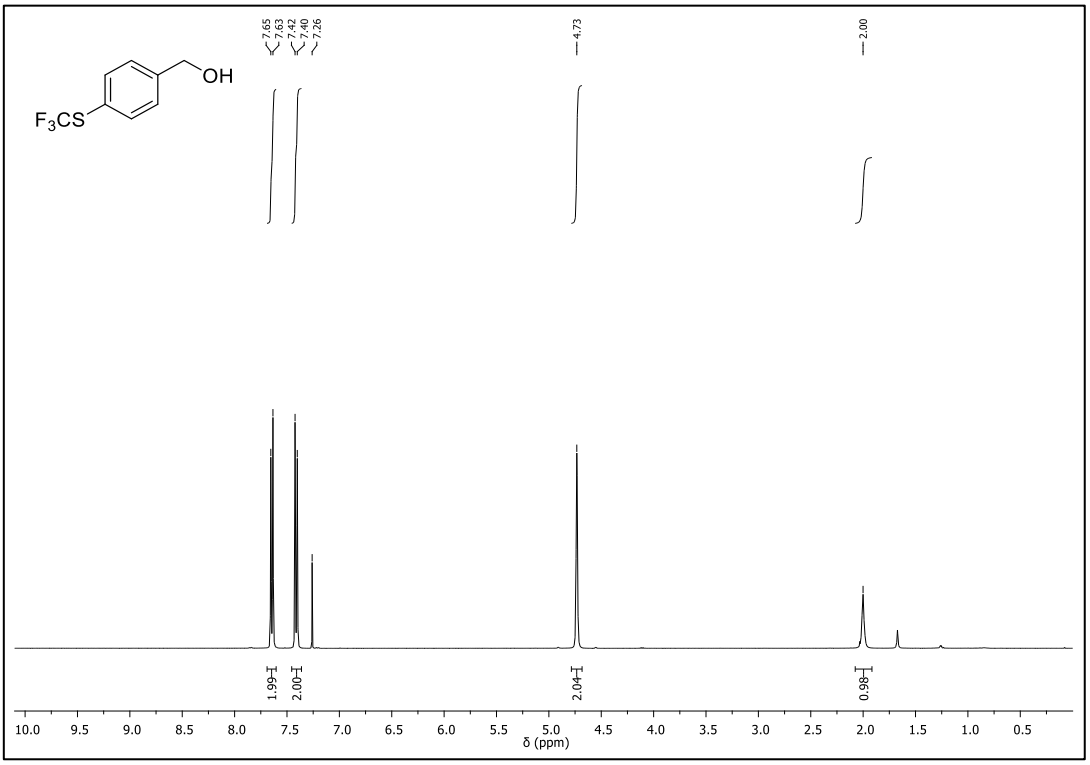

^{13}C-NMR (101 MHz, $CDCl_3$) of **1k**

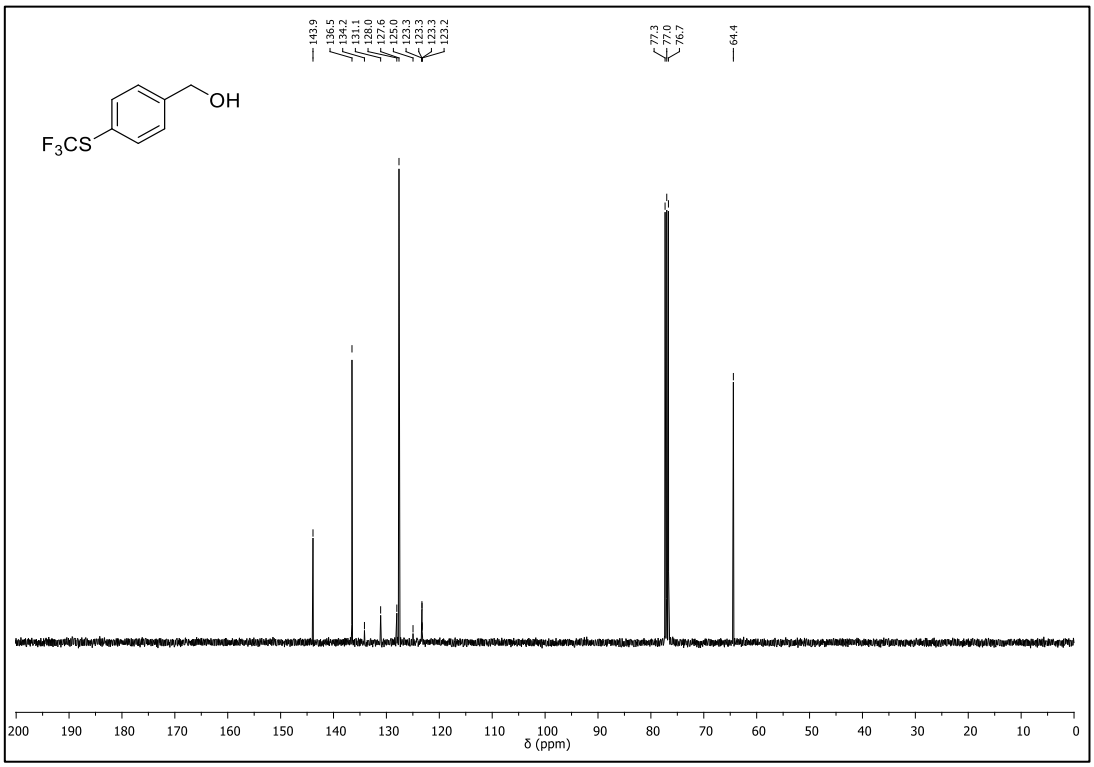

^{19}F-NMR (376 MHz, $CDCl_3$) of **1k**

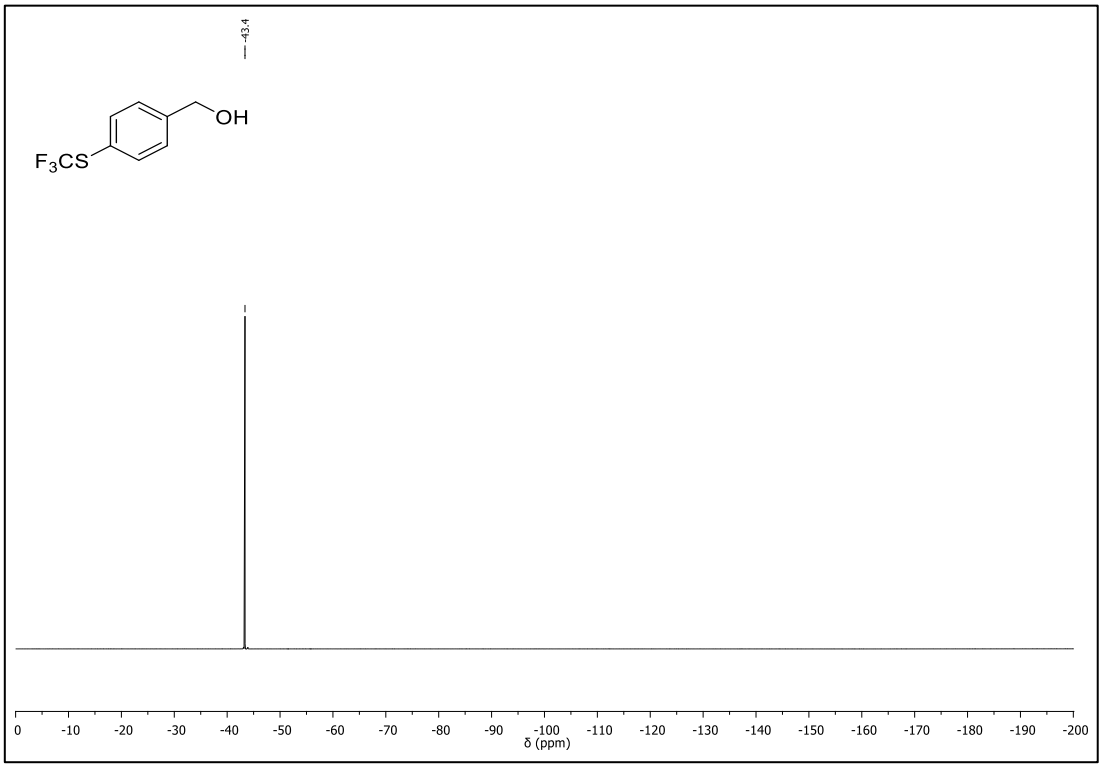

^{1}H-NMR (400 MHz, $CDCl_3$) of **1n**

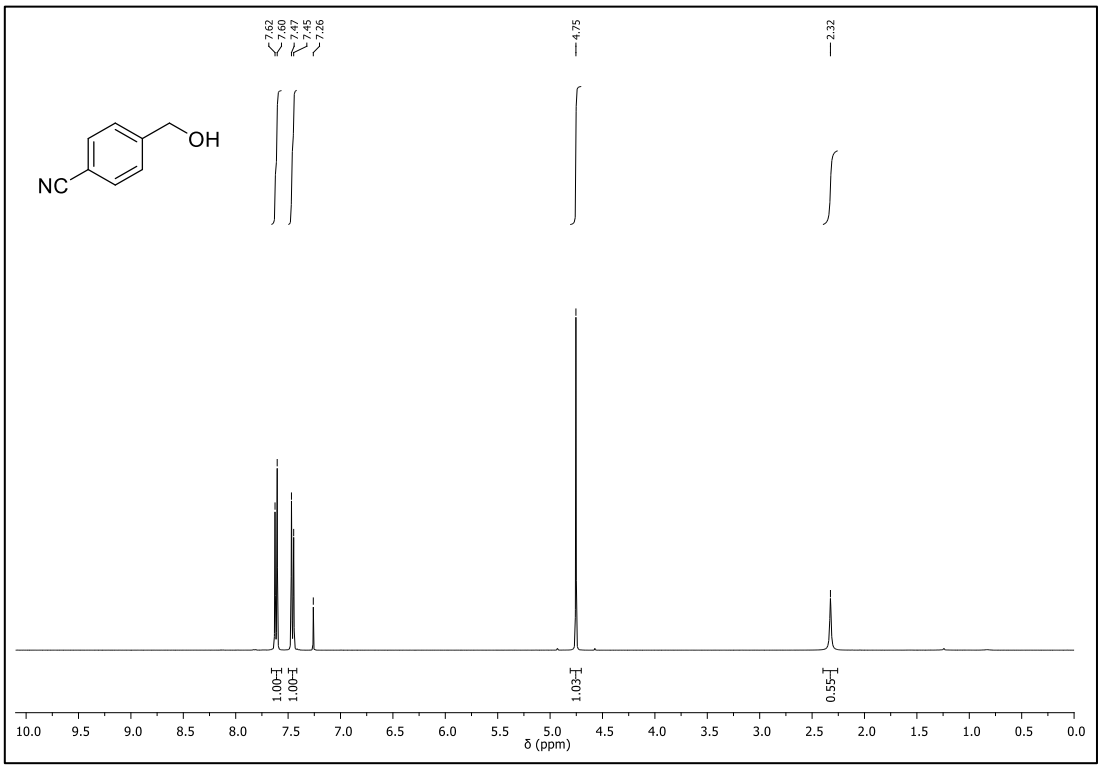

^{13}C-NMR (101 MHz, $CDCl_3$) of **1n**

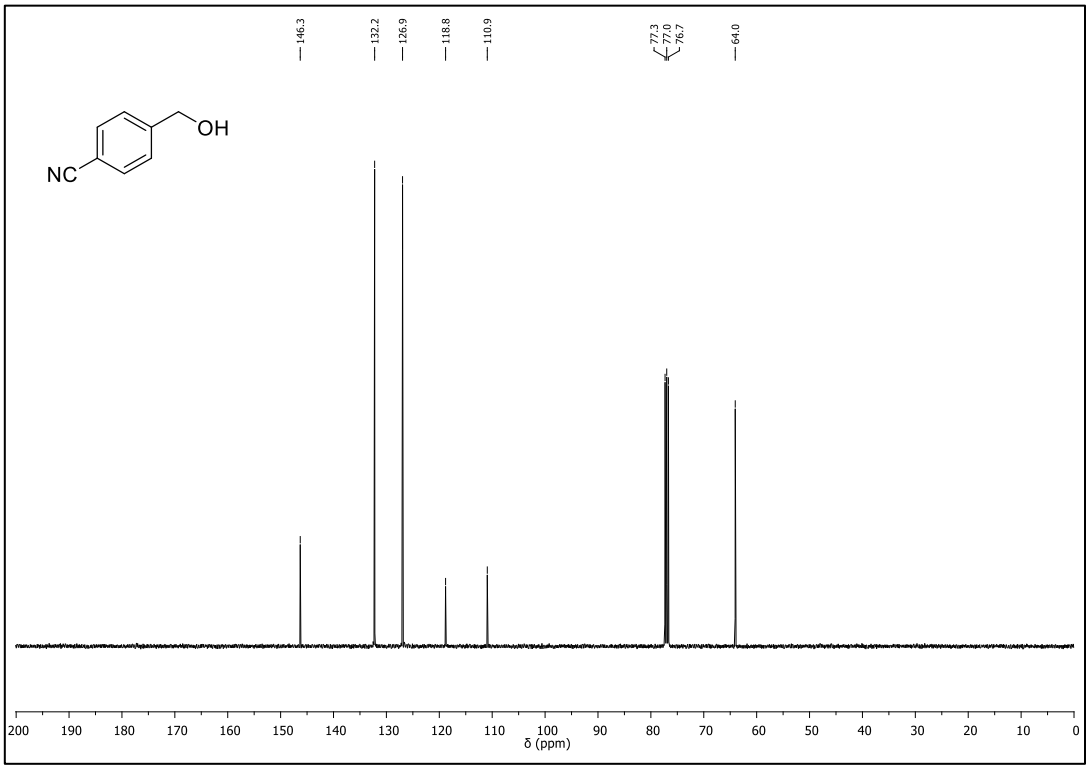

^{1}H-NMR (400 MHz, $CDCl_3$) of **SM1**

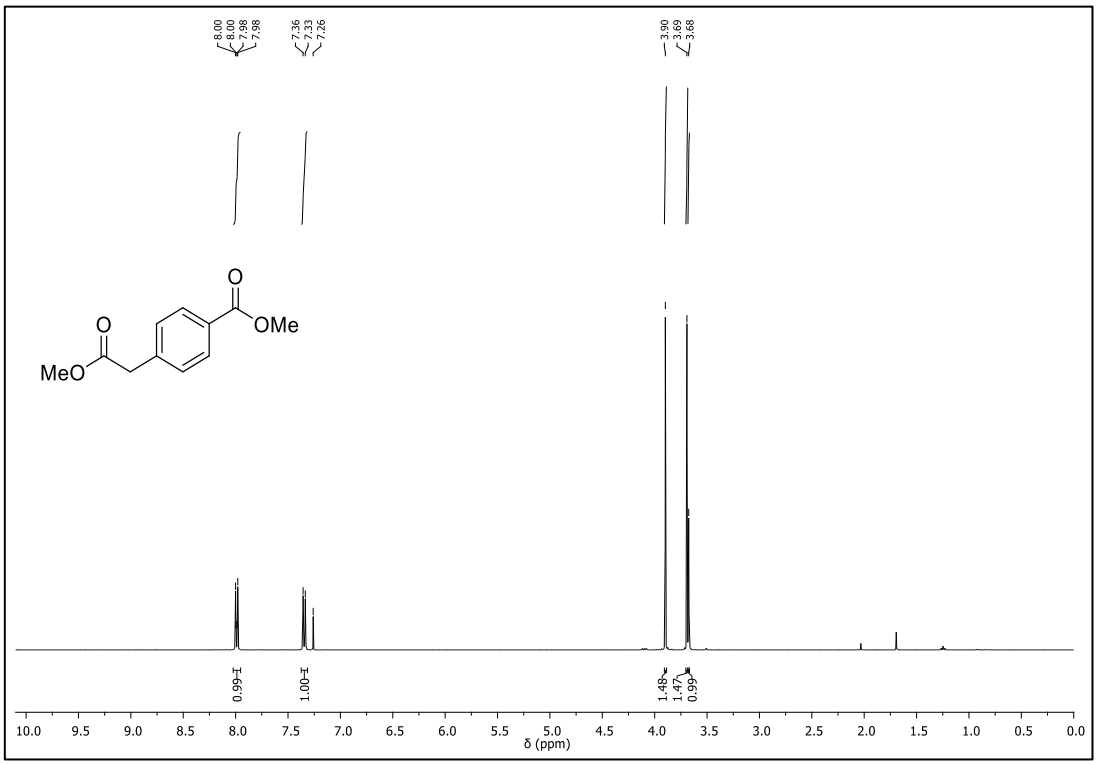

^{13}C-NMR (101 MHz, $CDCl_3$) of **SM1**

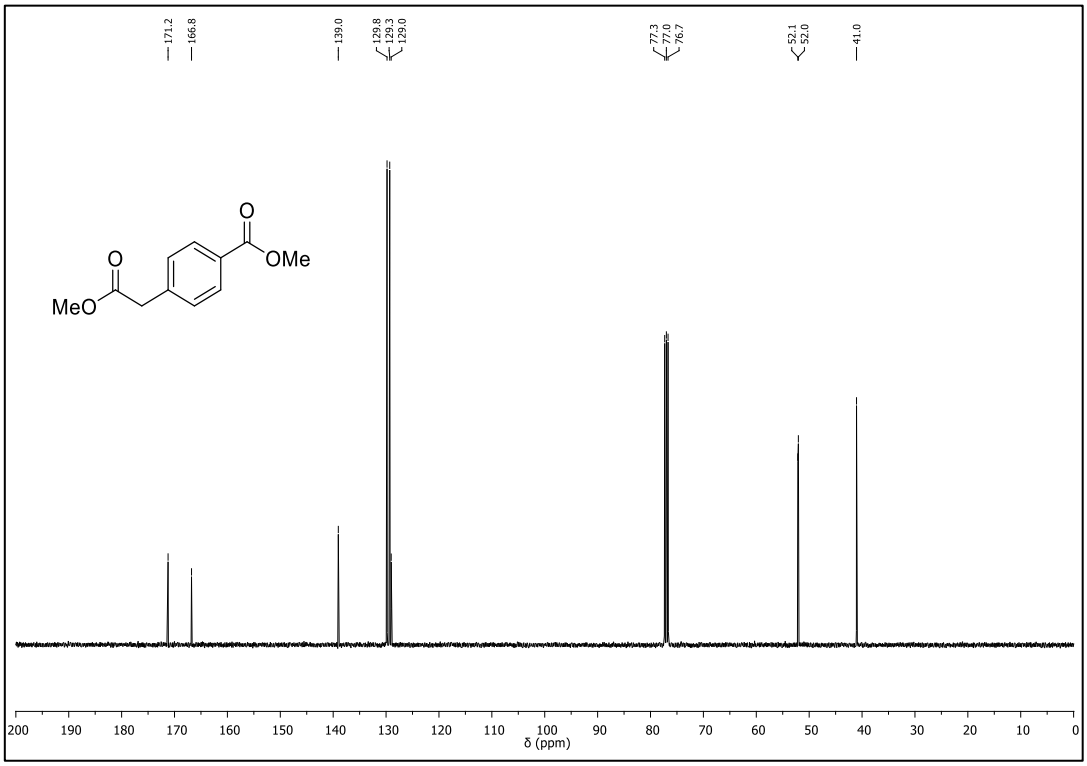

^{1}H-NMR (400 MHz, $CDCl_3$) of **1x**

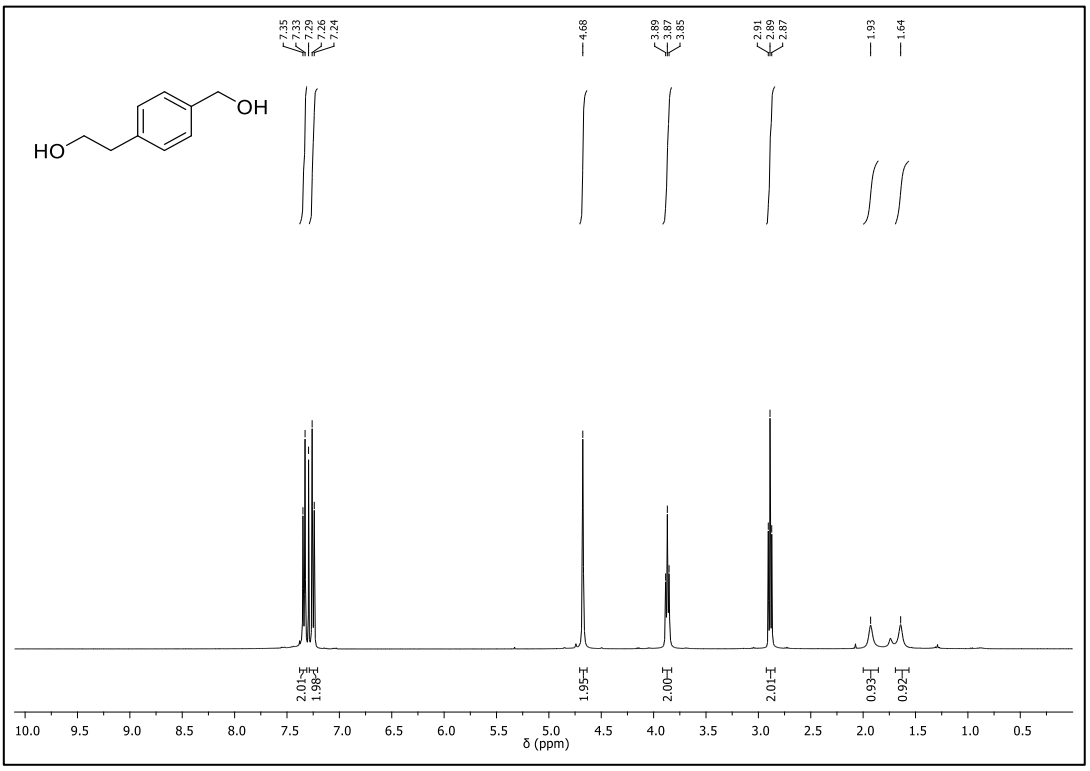

^{13}C-NMR (101 MHz, $CDCl_3$) of **1x**

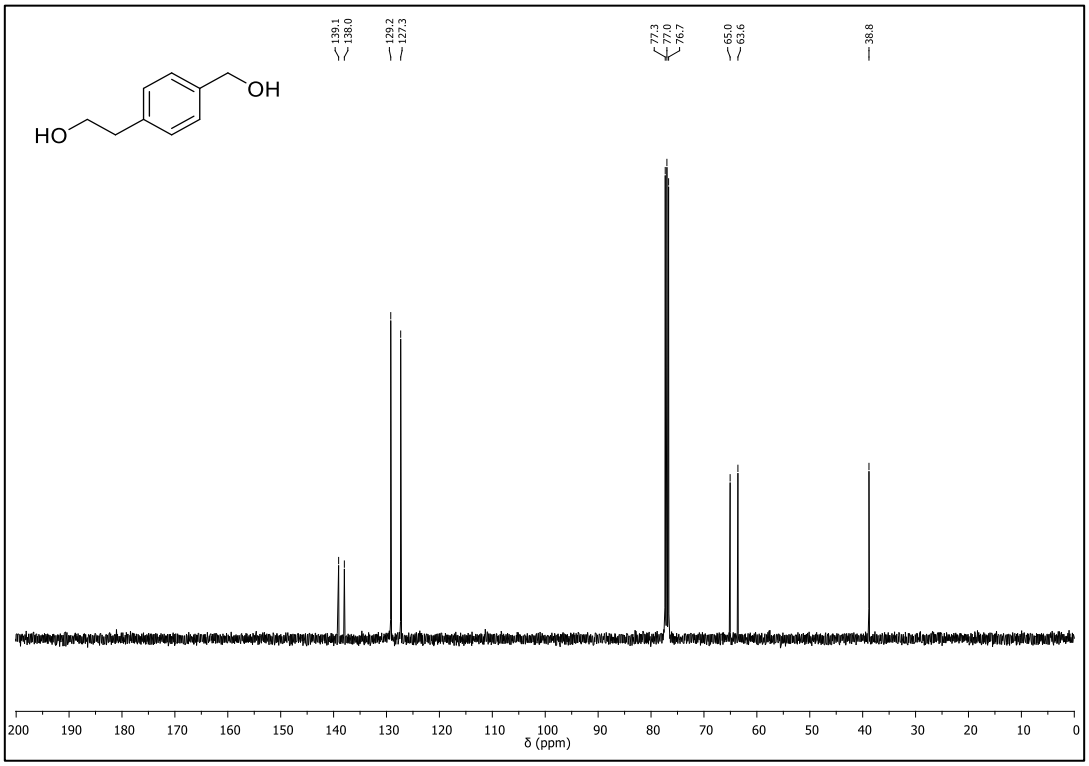

NMR spectra of products

^{1}H-NMR (400 MHz, $CDCl_3$) of **3a**

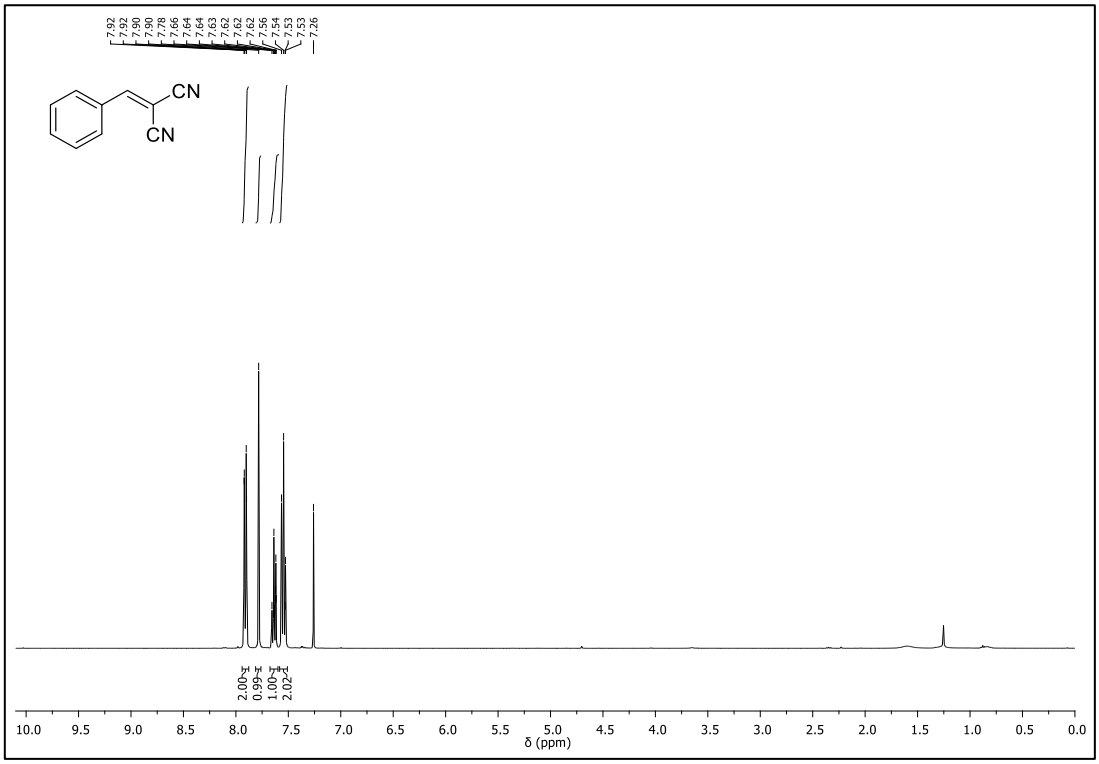

^{13}C-NMR (101 MHz, $CDCl_3$) of **3a**

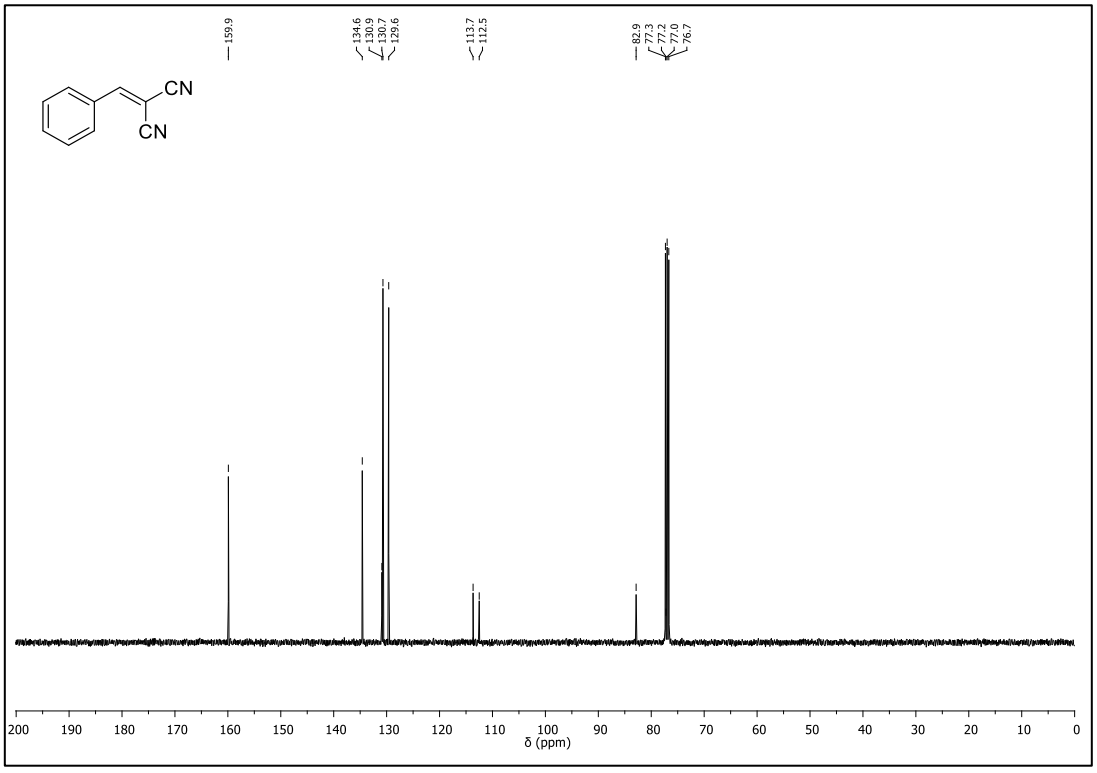

^{1}H-NMR (400 MHz, $CDCl_3$) of **3b**

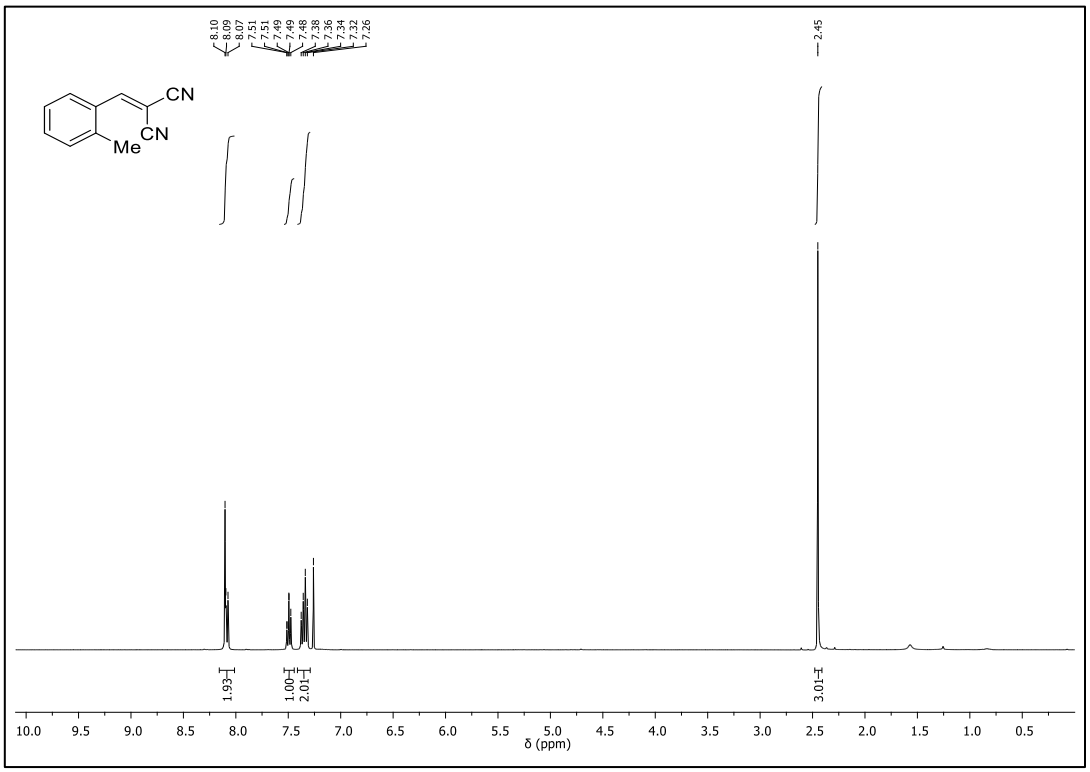

^{13}C-NMR (101 MHz, $CDCl_3$) of **3b**

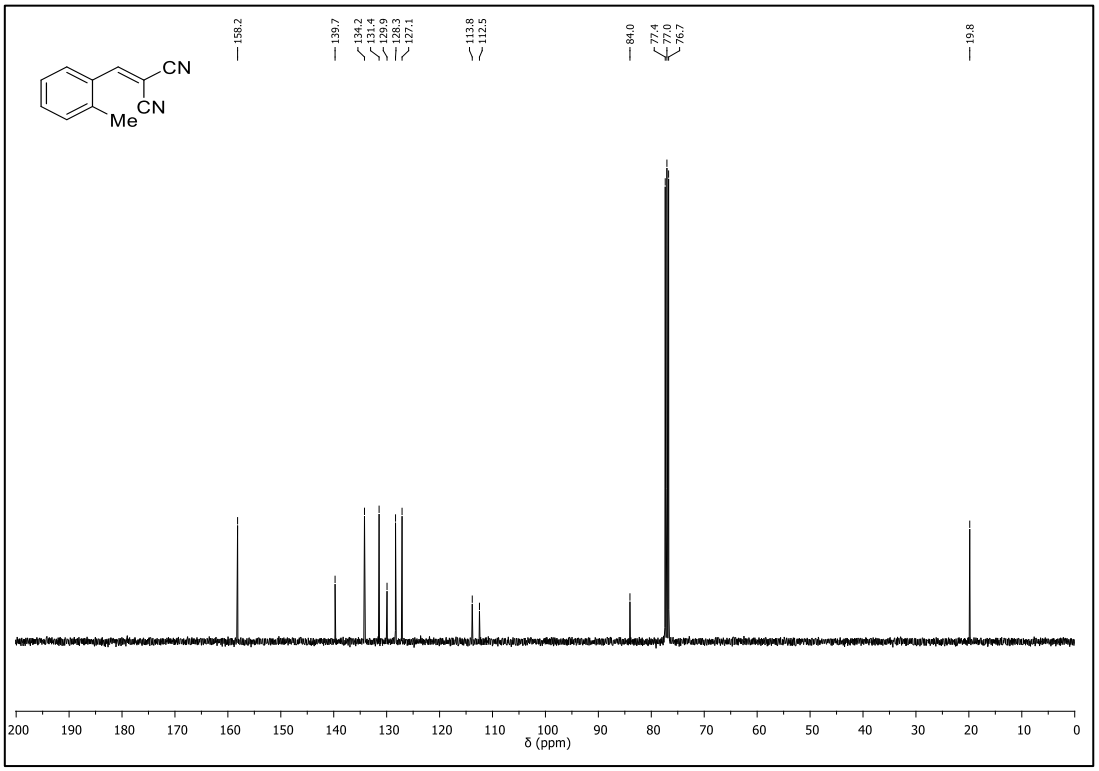

^{1}H-NMR (400 MHz, $CDCl_3$) of **3c**

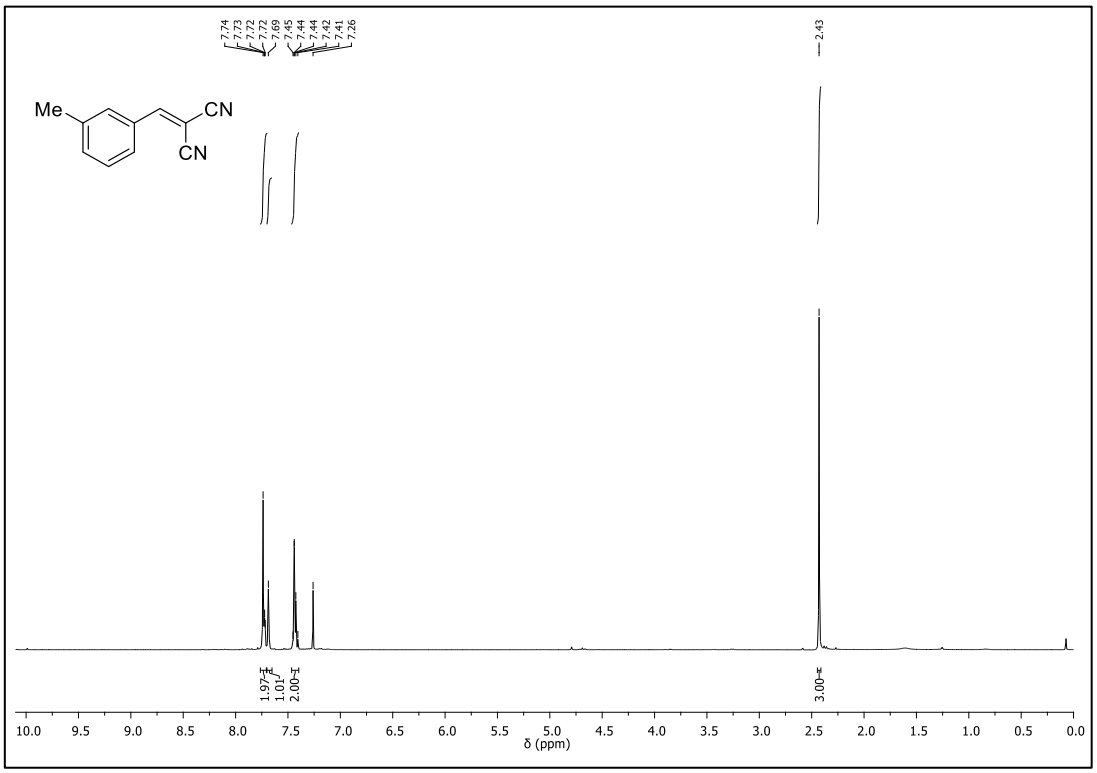

^{13}C-NMR (101 MHz, $CDCl_3$) of **3c**

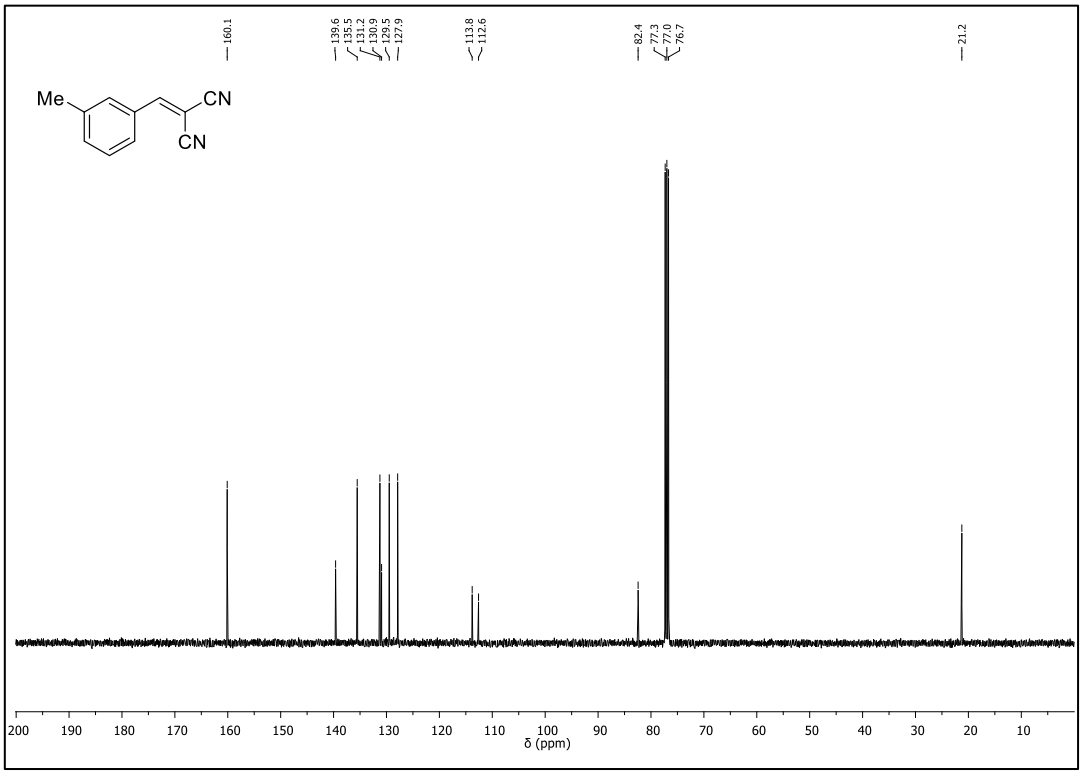

^{1}H-NMR (400 MHz, $CDCl_3$) of **3d**

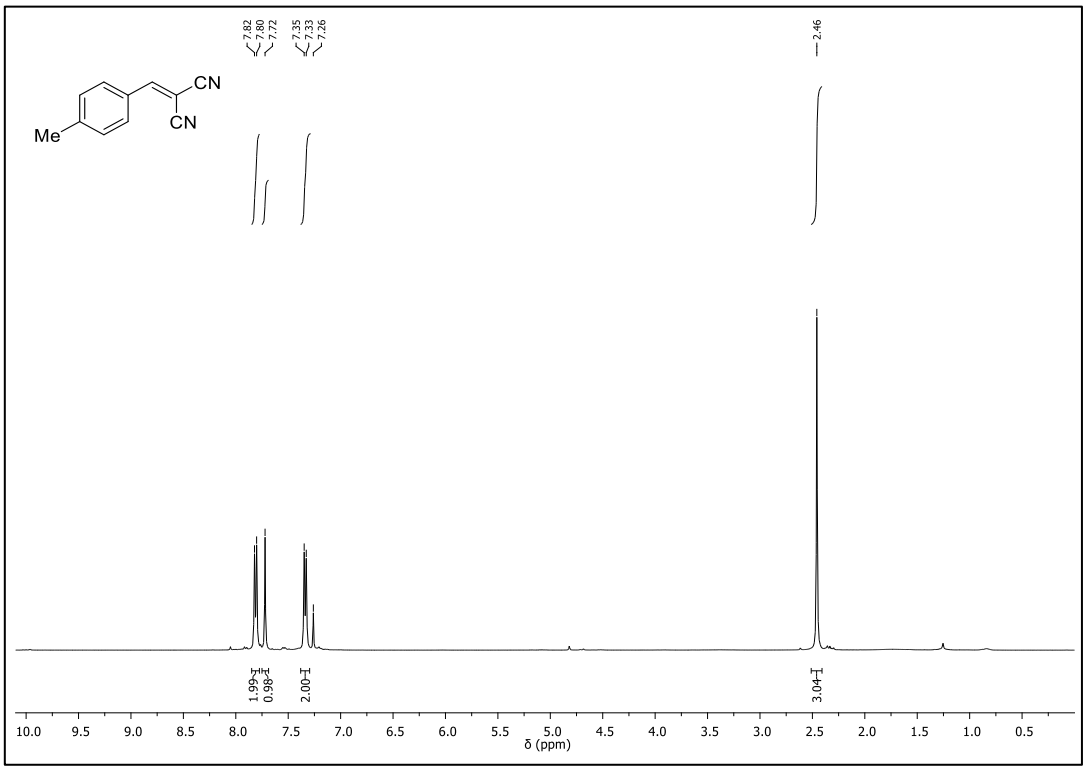

^{13}C-NMR (101 MHz, $CDCl_3$) of **3d**

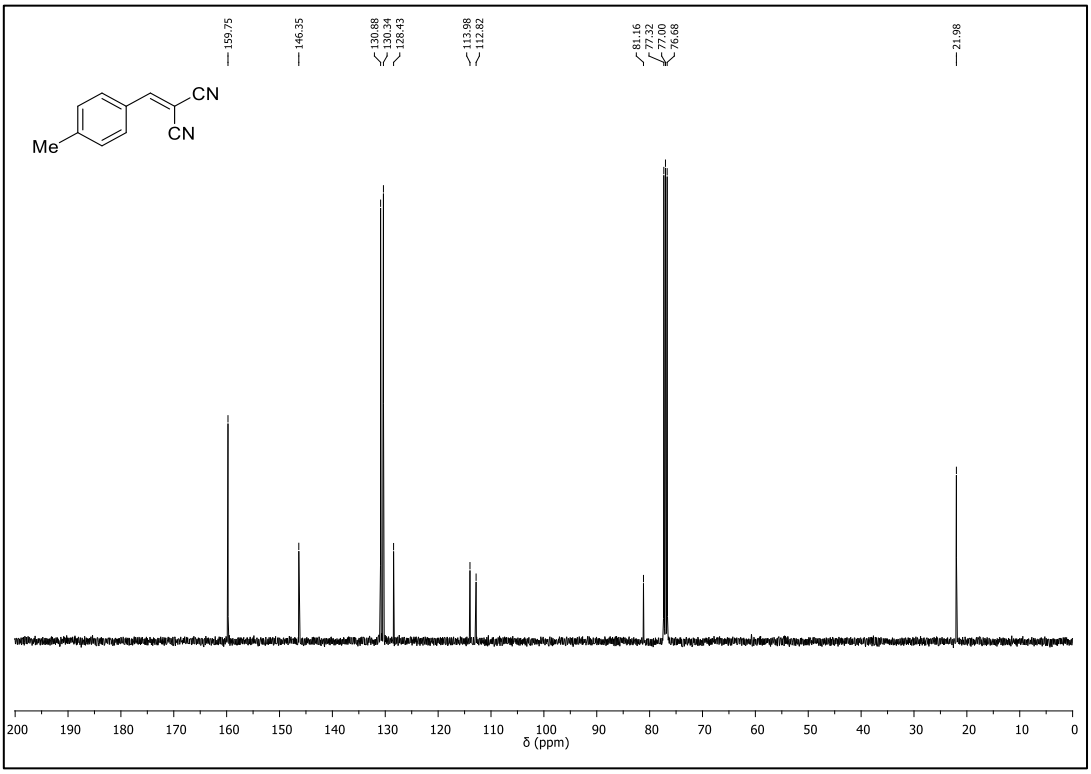

^{1}H-NMR (400 MHz, $CDCl_3$) of **3e**

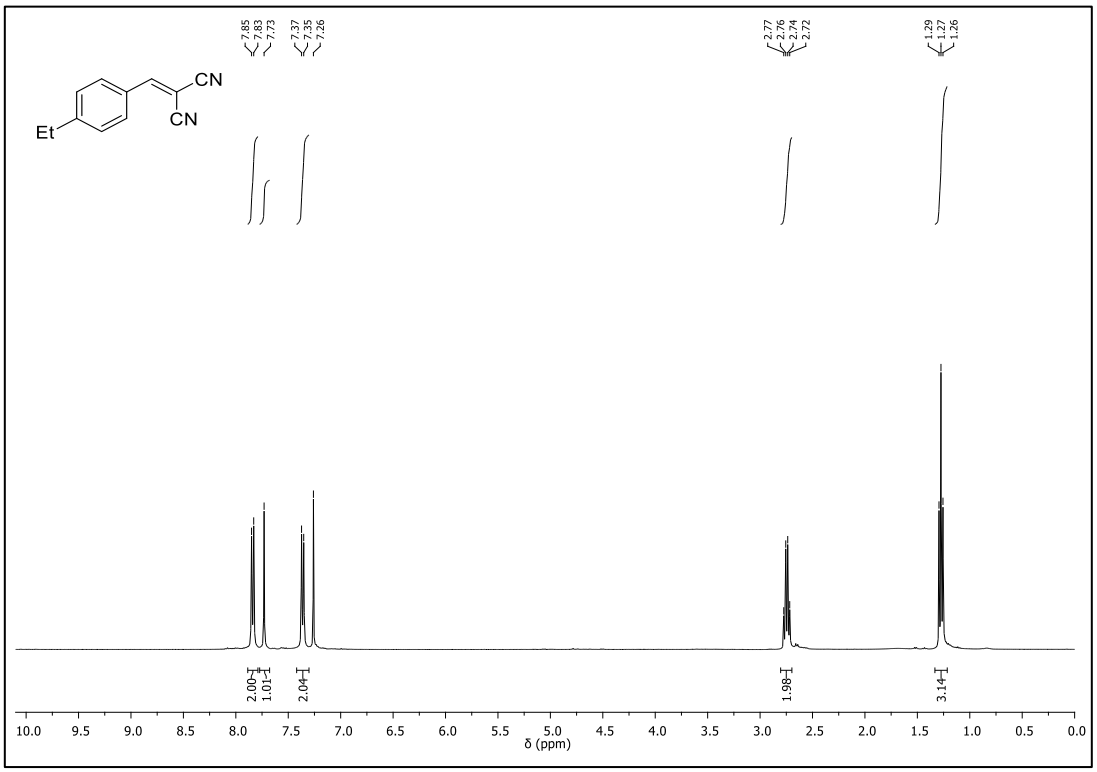

^{13}C-NMR (101 MHz, $CDCl_3$) of **3e**

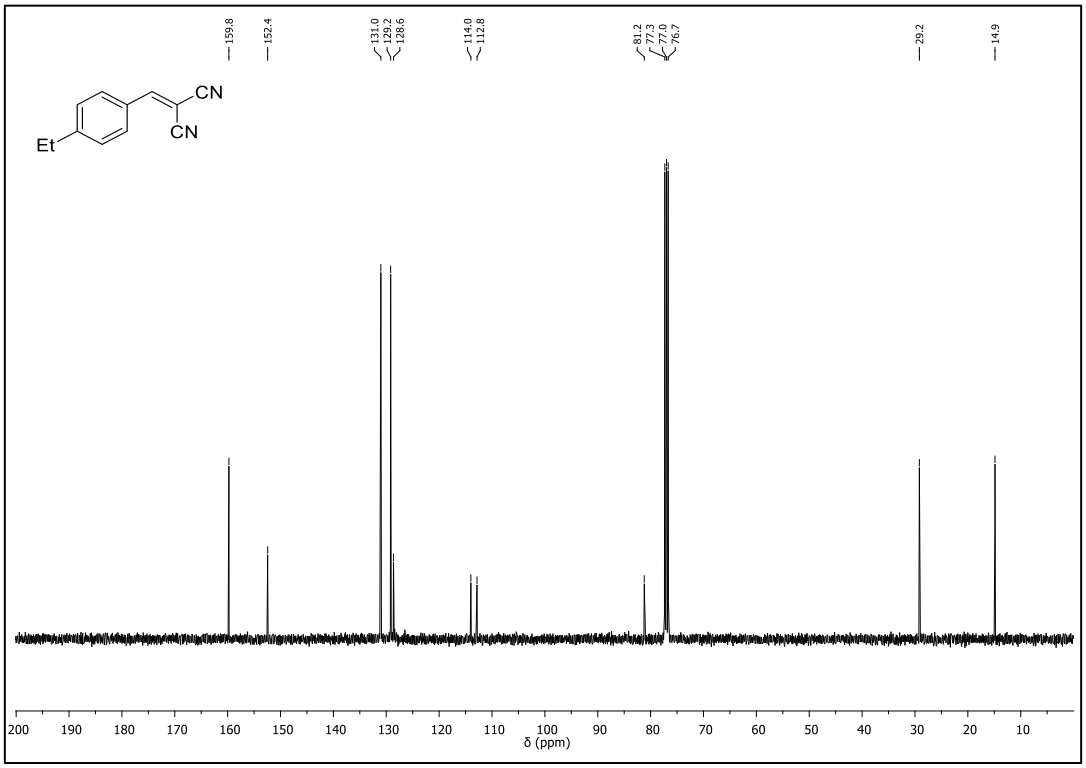

^{1}H-NMR (400 MHz, $CDCl_3$) of **3f**

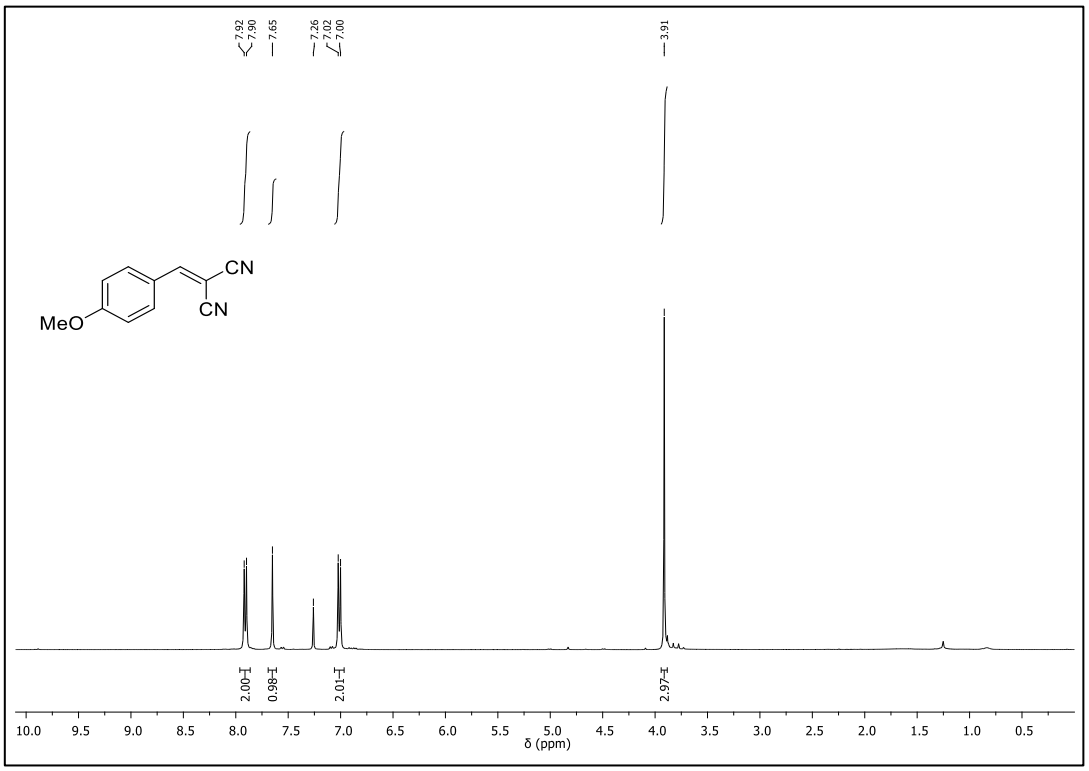

^{13}C-NMR (101 MHz, $CDCl_3$) of **3f**

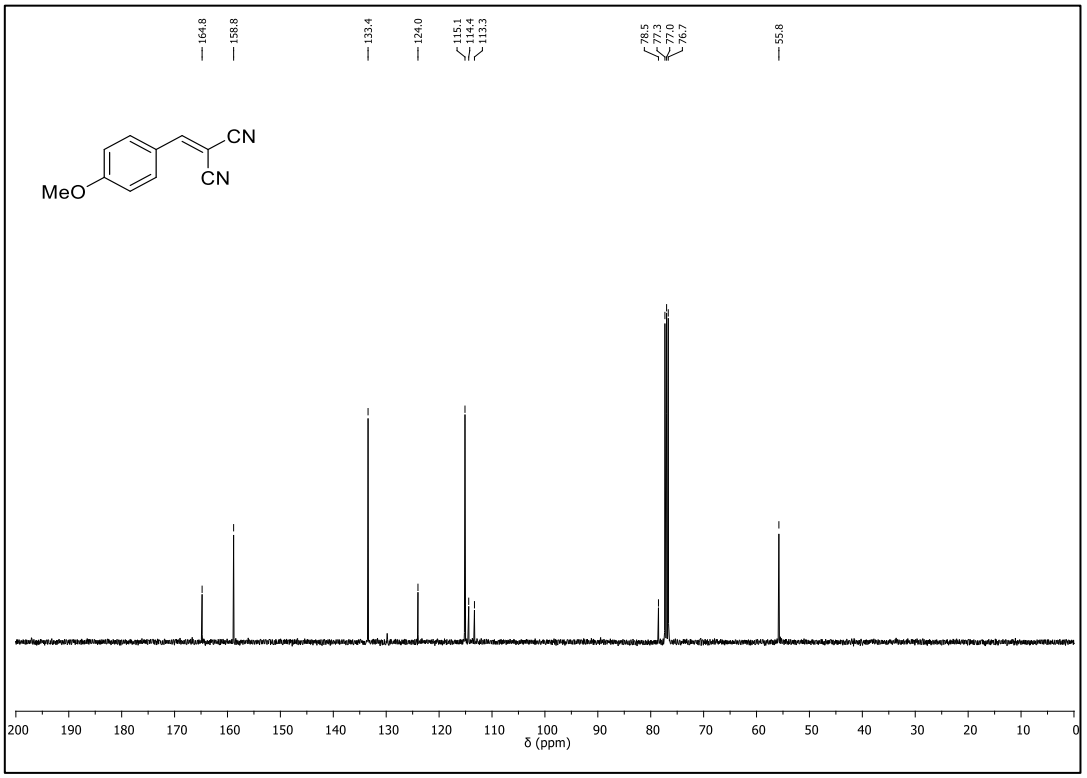

^{1}H-NMR (400 MHz, CD_2Cl_2) of **3g**

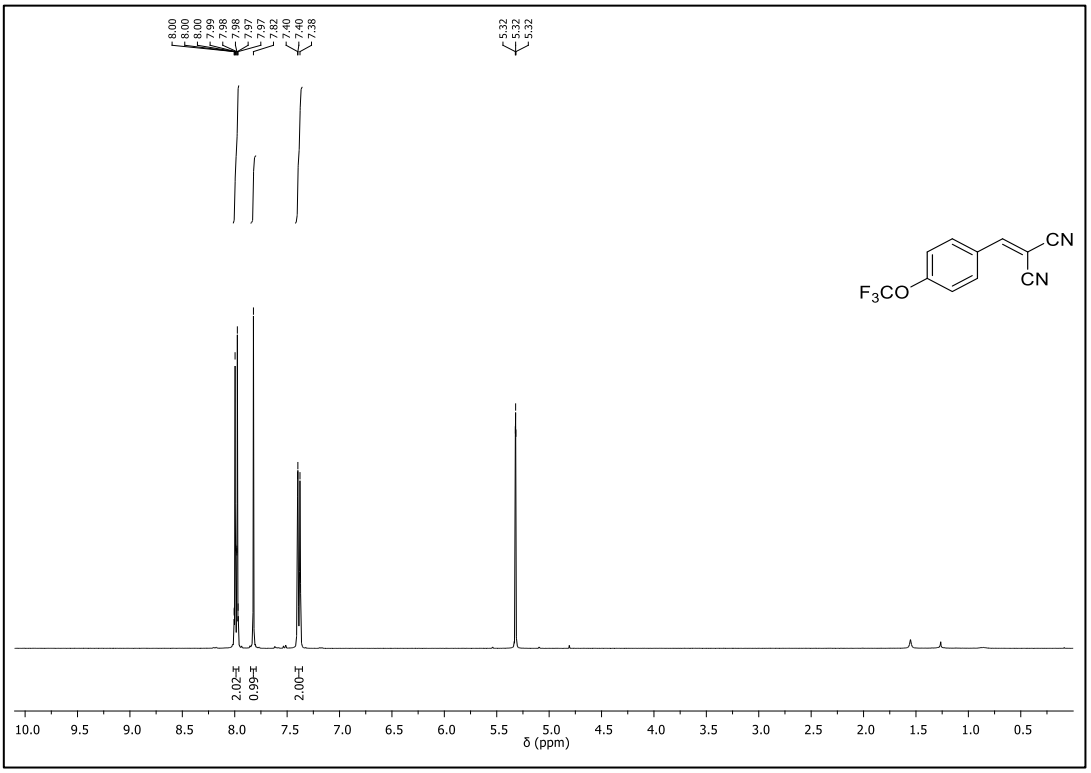

^{13}C-NMR (101 MHz, CD_2Cl_2) of **3g**

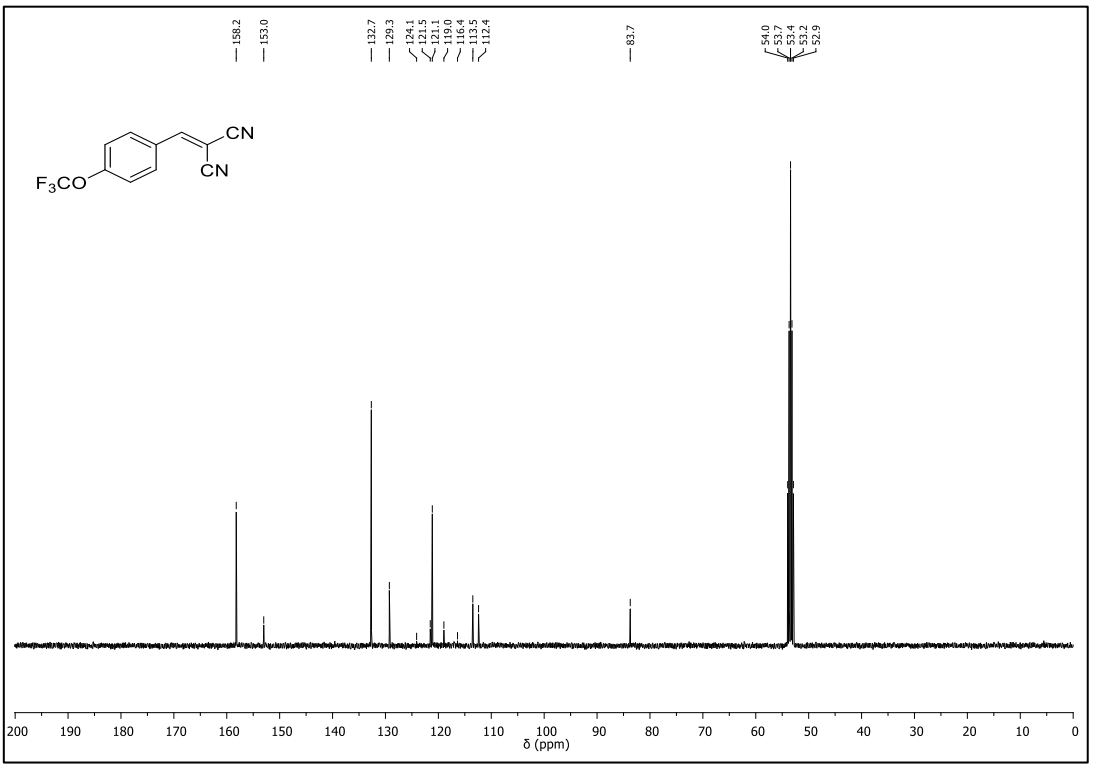

^{19}F-NMR (376 MHz, CD_2Cl_2) of **3g**

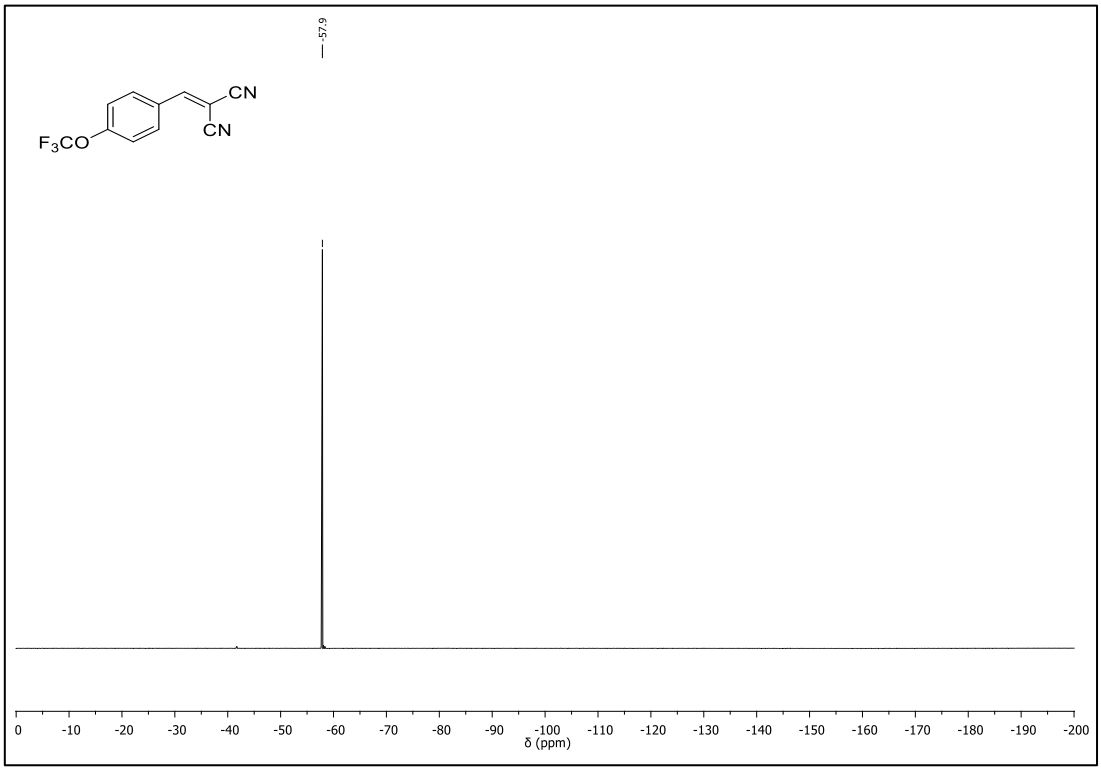

^{1}H-NMR (400 MHz, $CDCl_3$) of **3h**

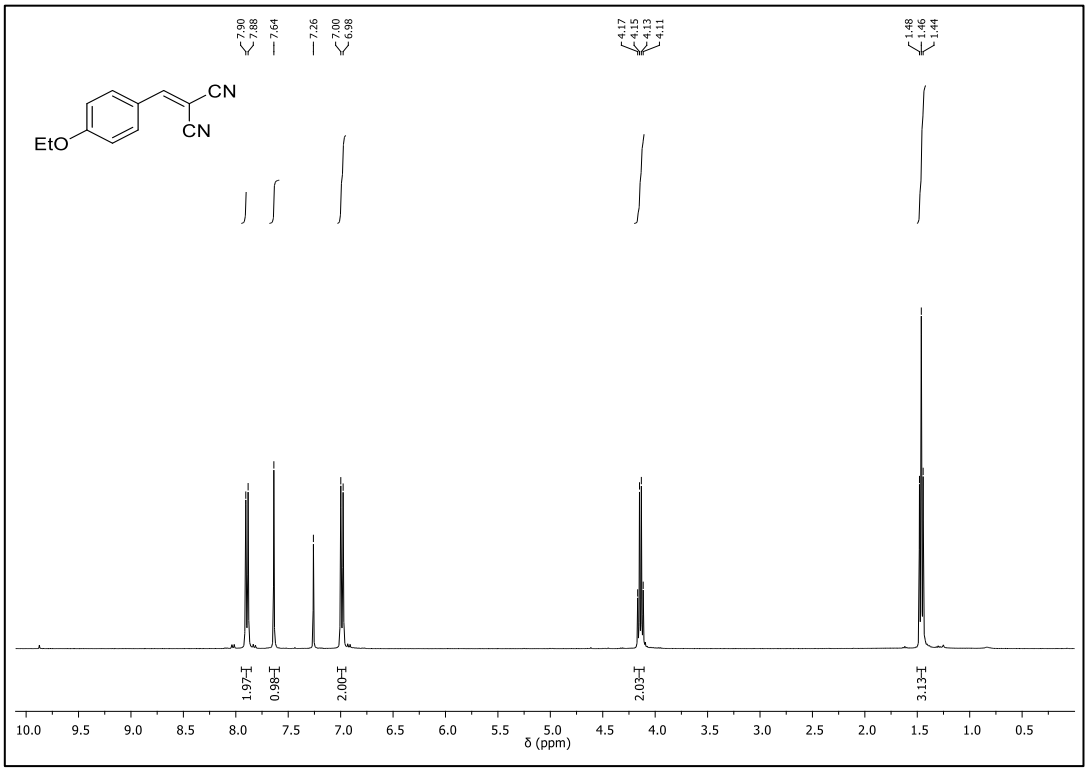

^{13}C-NMR (101 MHz, $CDCl_3$) of **3h**

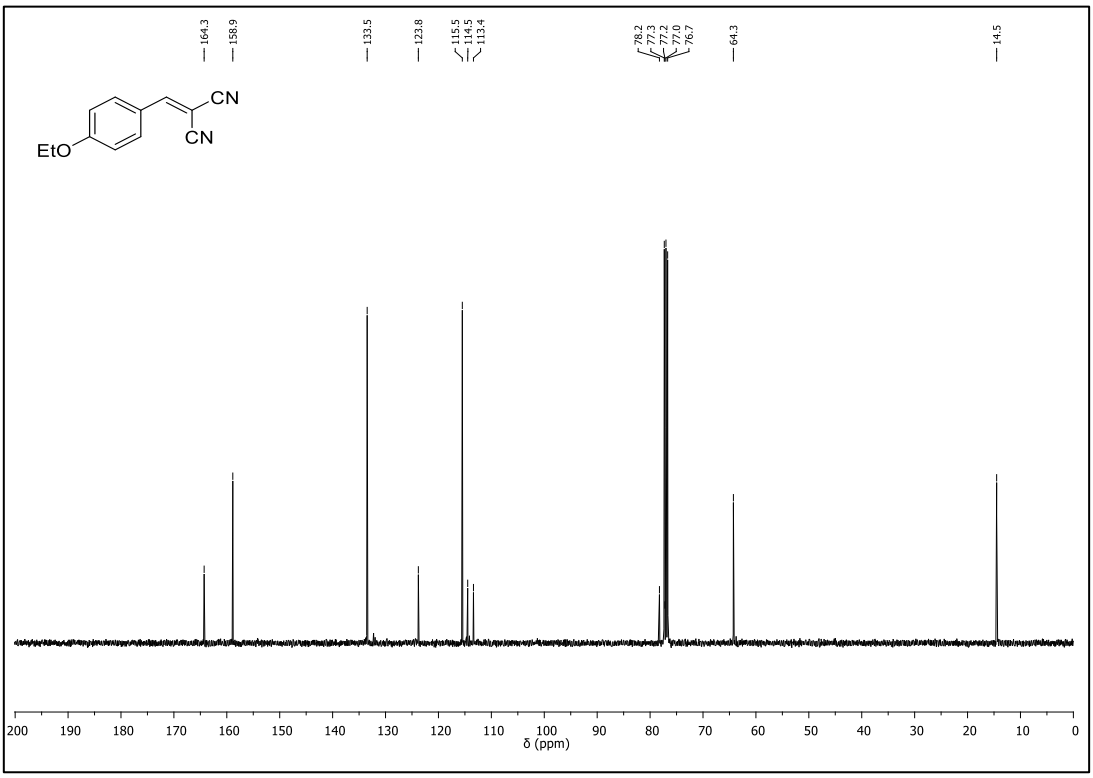

^{1}H-NMR (400 MHz, $CDCl_3$) of **3i**

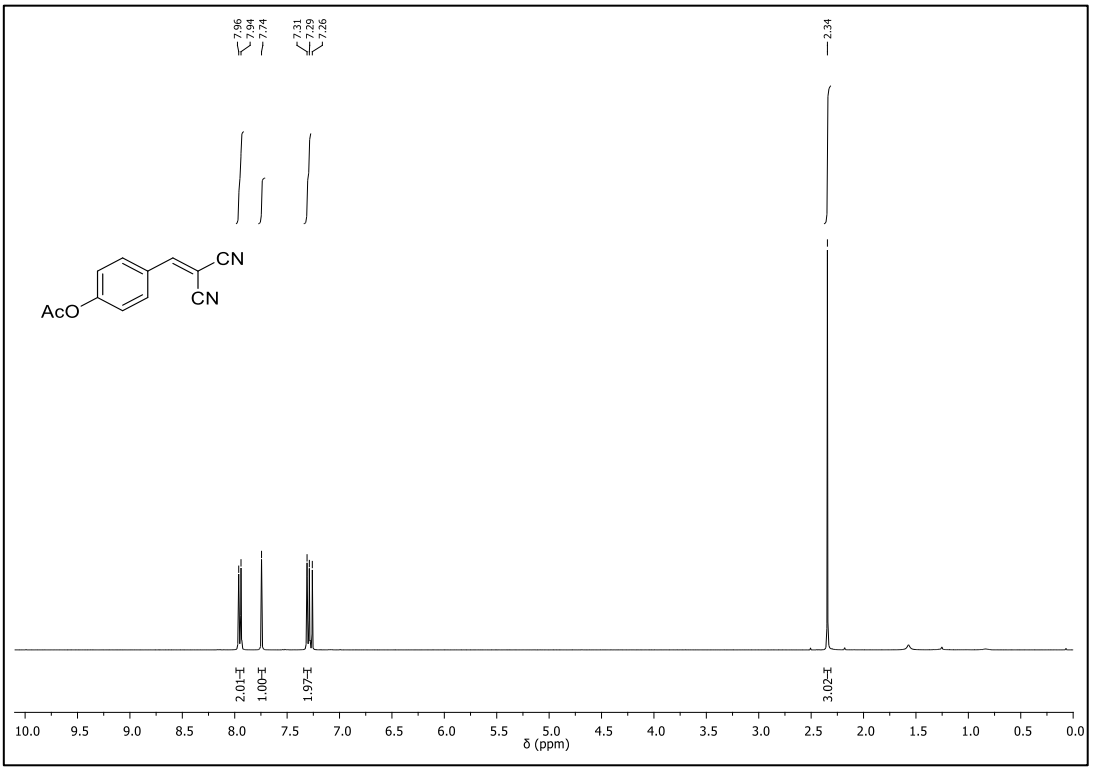

^{13}C-NMR (101 MHz, $CDCl_3$) of **3i**

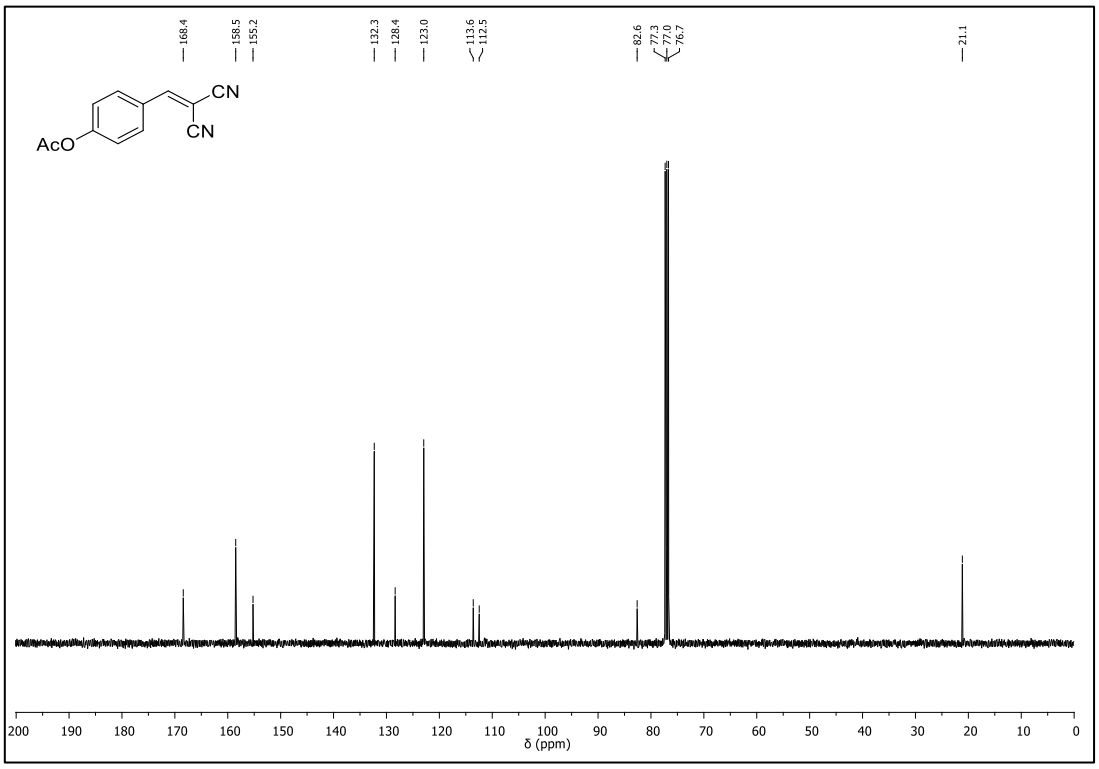

^{1}H-NMR (400 MHz, $CDCl_3$) of **3k**

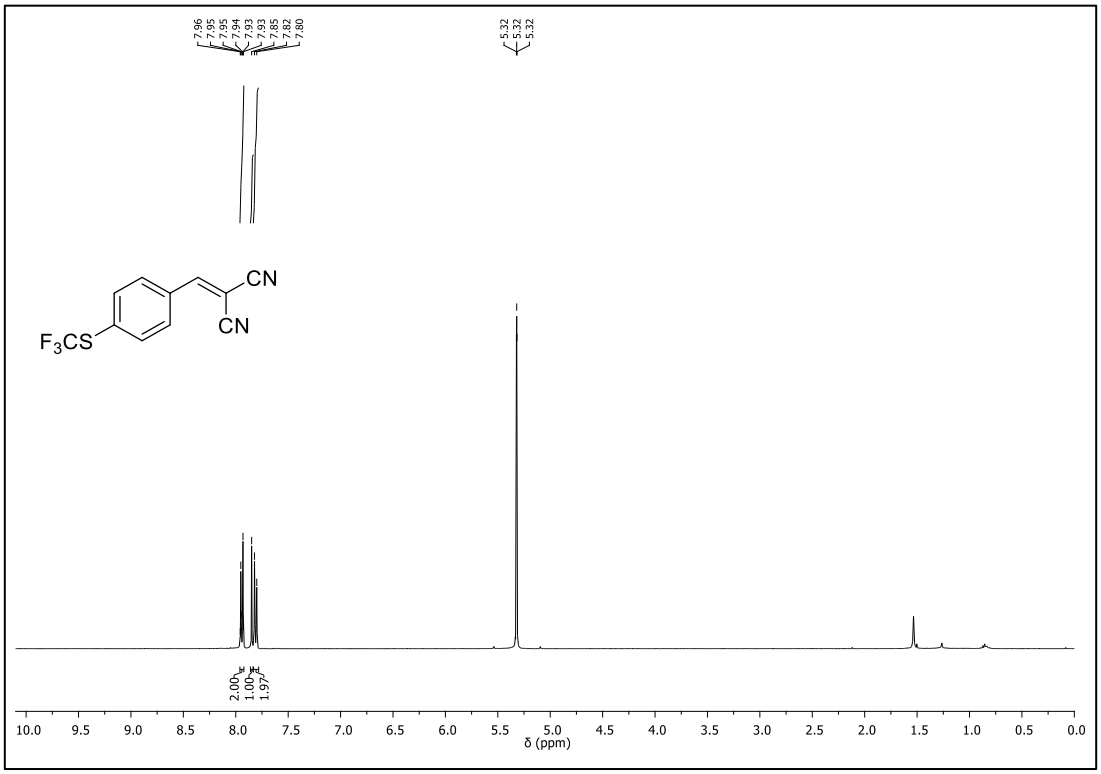

^{13}C-NMR (101 MHz, $CDCl_3$) of **3k**

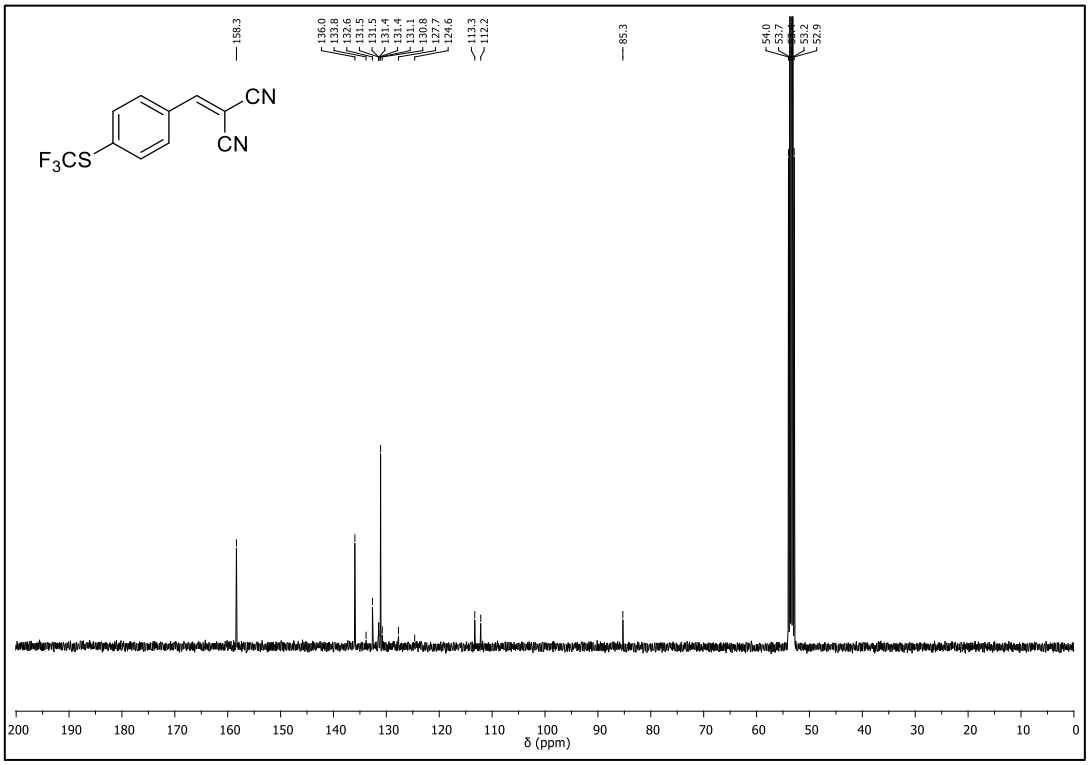

^{19}F-NMR (376 MHz, $CDCl_3$) of **3k**

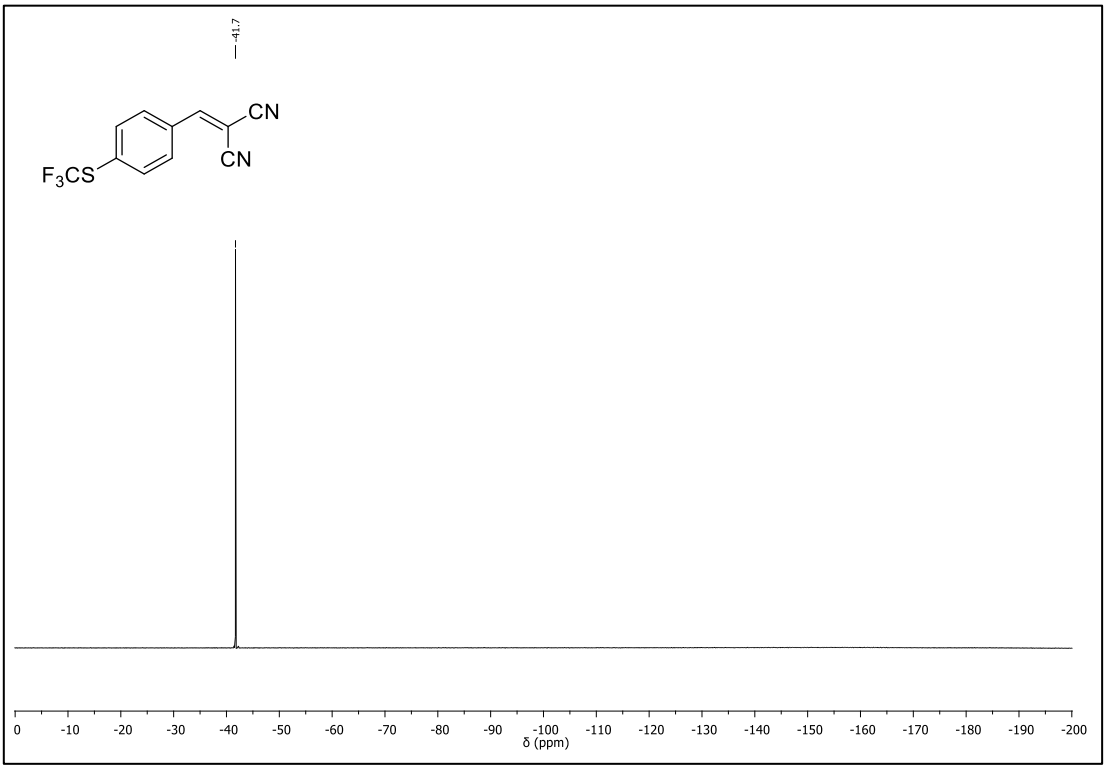

^{1}H-NMR (400 MHz, $CDCl_3$) of **3m**

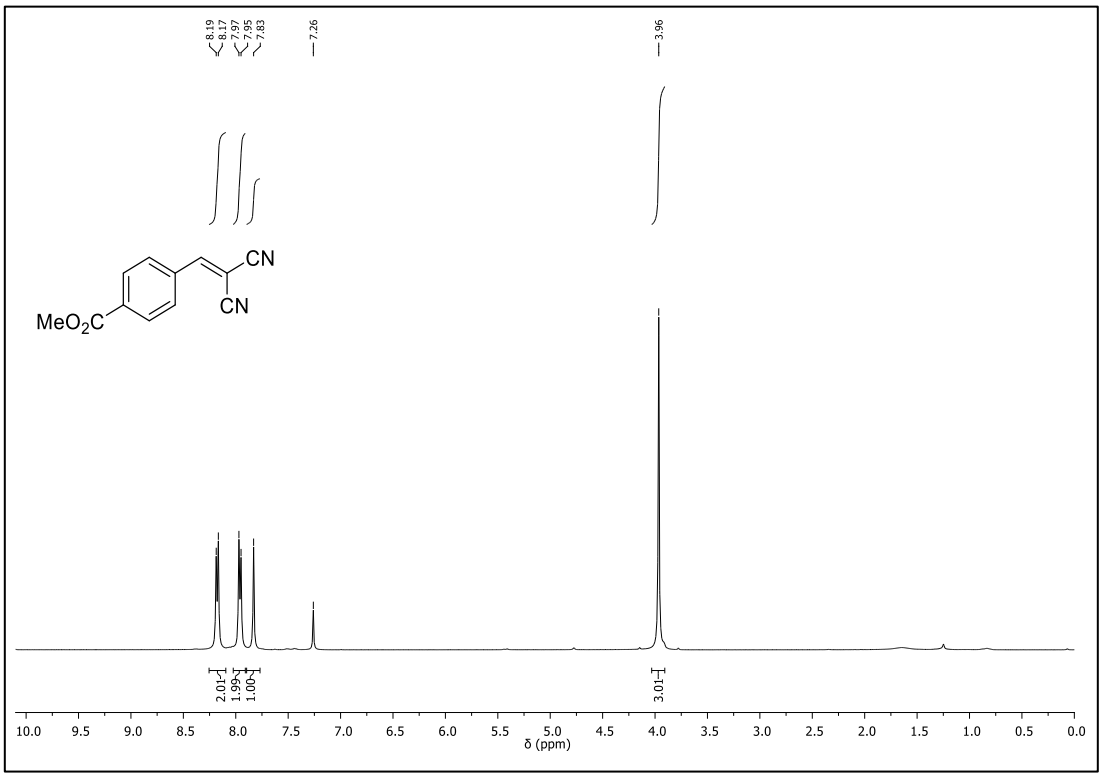

^{13}C-NMR (101 MHz, $CDCl_3$) of **3m**

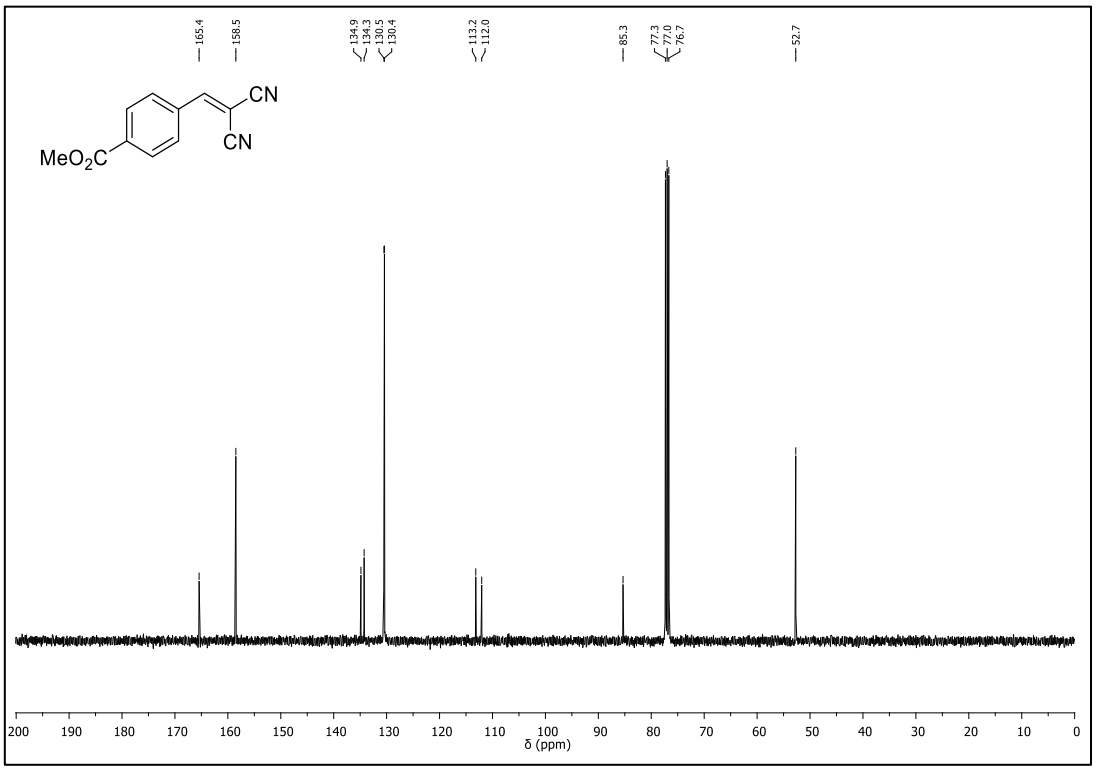

^{1}H-NMR (400 MHz, $CDCl_3$) of **3n**

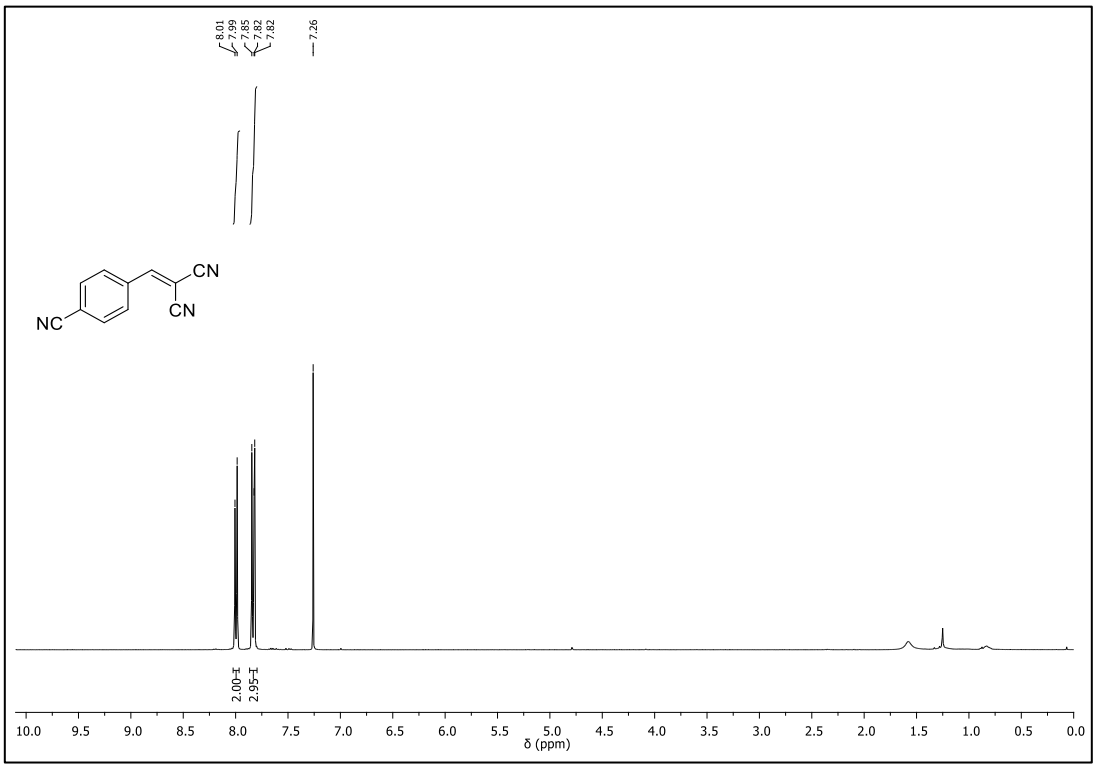

^{13}C-NMR (101 MHz, $CDCl_3$) of **3n**

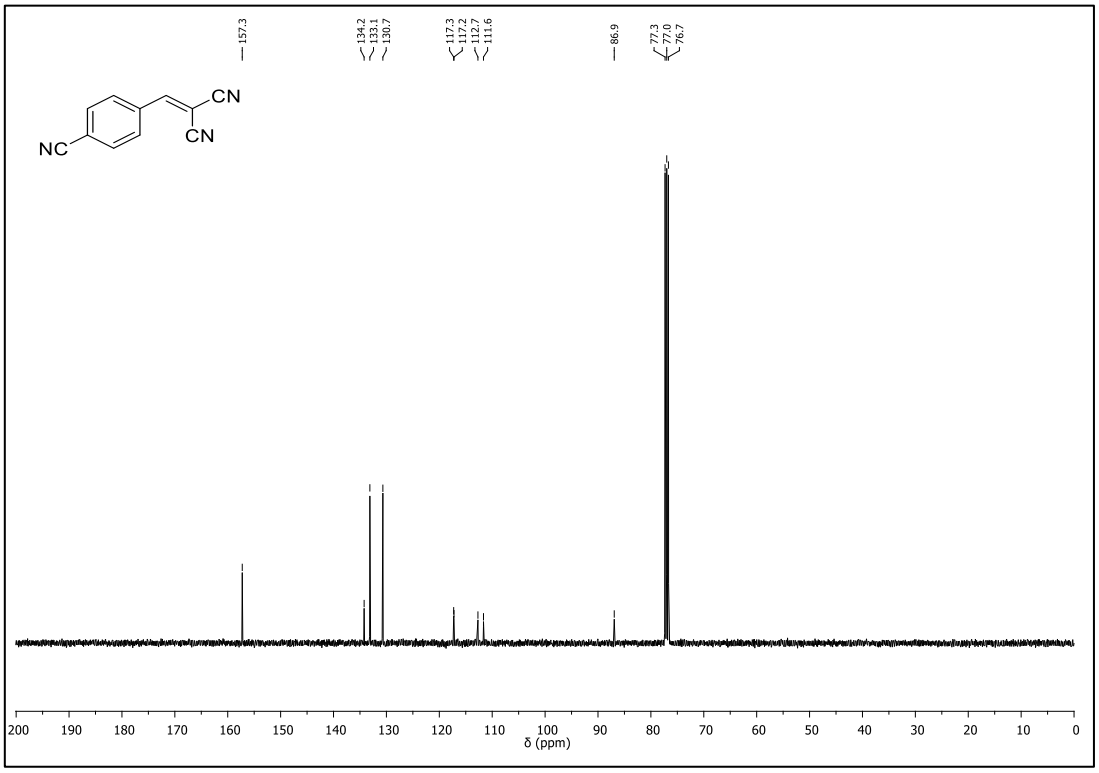

^{1}H-NMR (400 MHz, $CDCl_3$) of **3o**

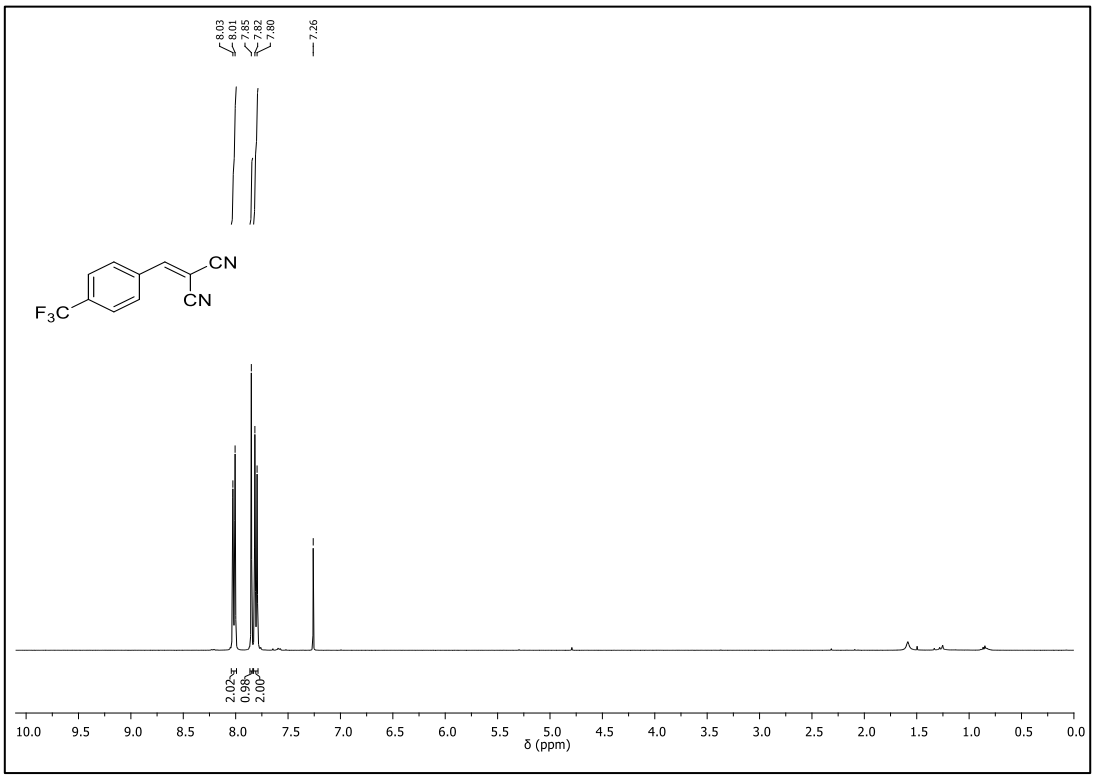

^{13}C-NMR (101 MHz, $CDCl_3$) of **3o**

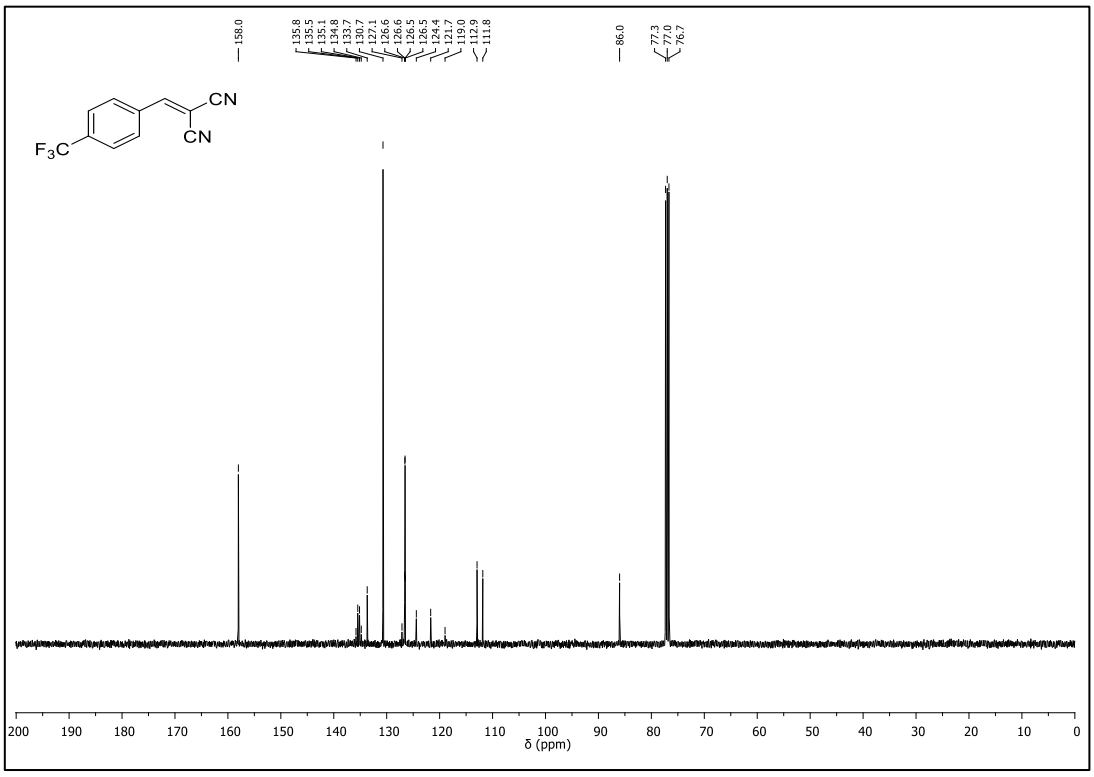

^{19}F-NMR (376 MHz, $CDCl_3$) of **3o**

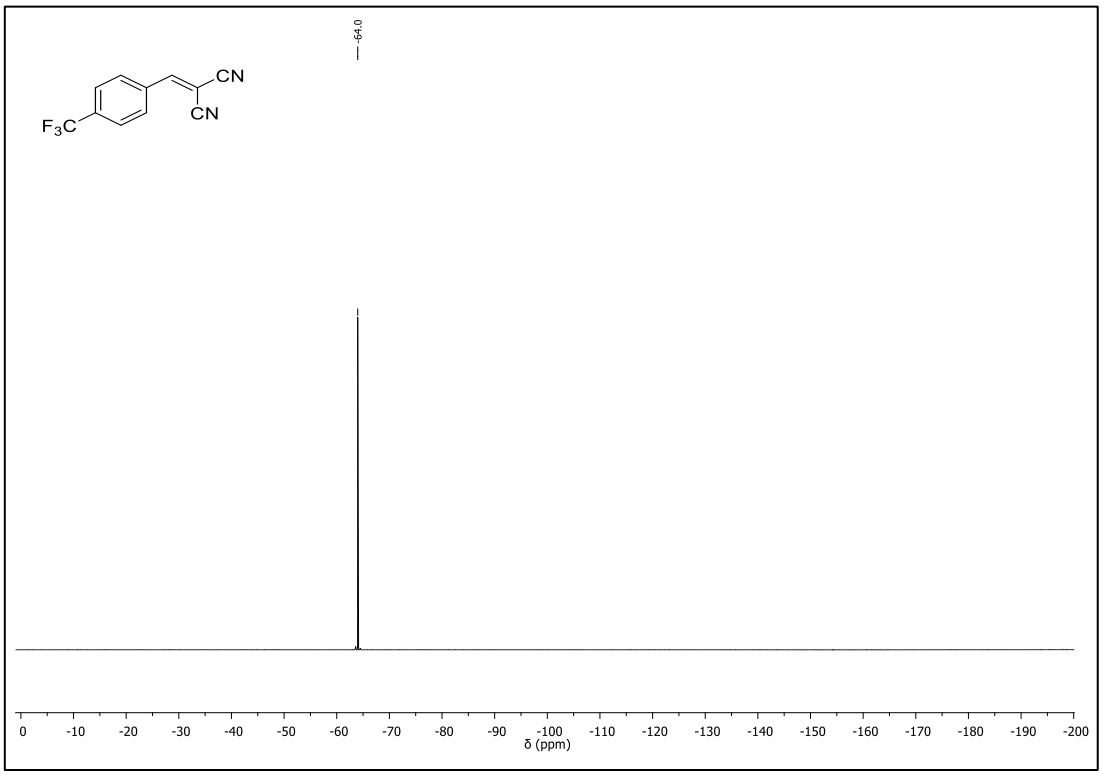

^{1}H-NMR (400 MHz, $CDCl_3$) of **3p**

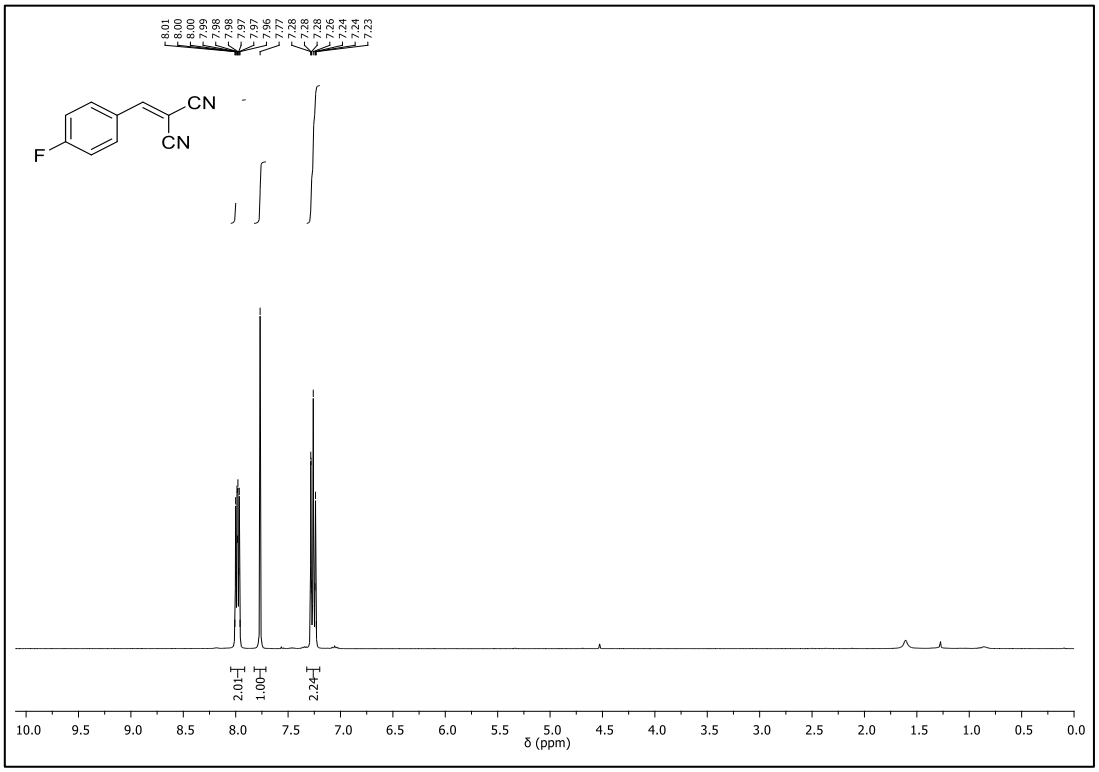

^{13}C-NMR (101 MHz, $CDCl_3$) of **3p**

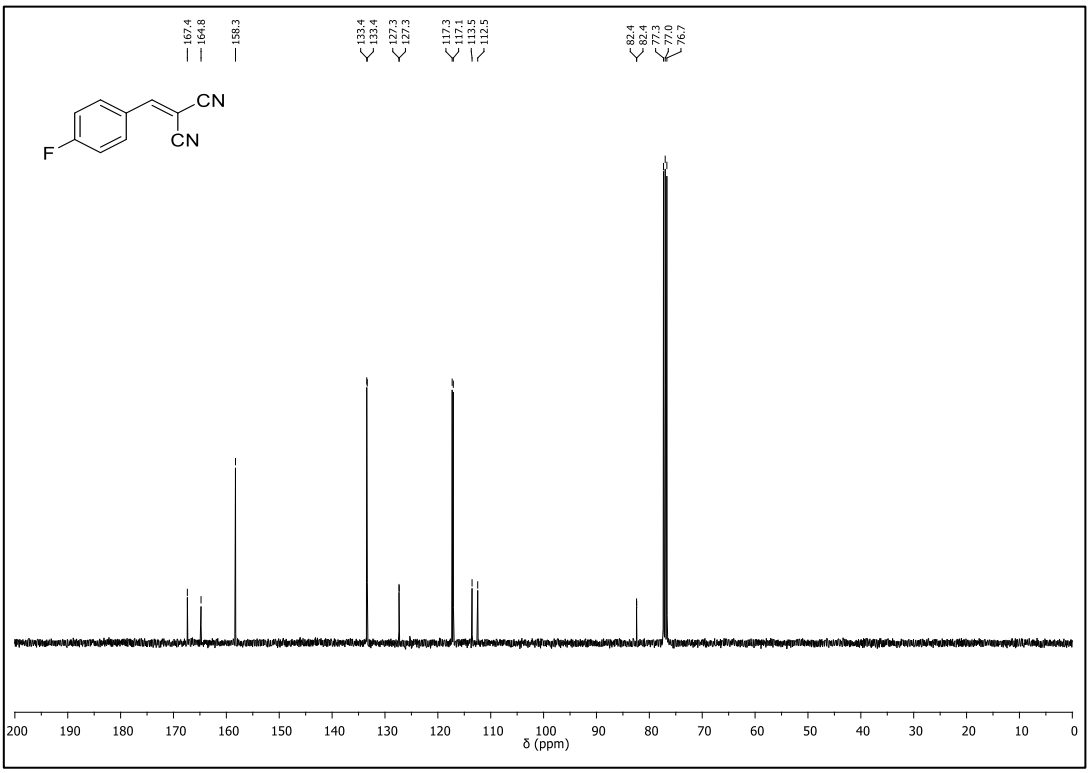

^{19}F-NMR (376 MHz, $CDCl_3$) of **3p**

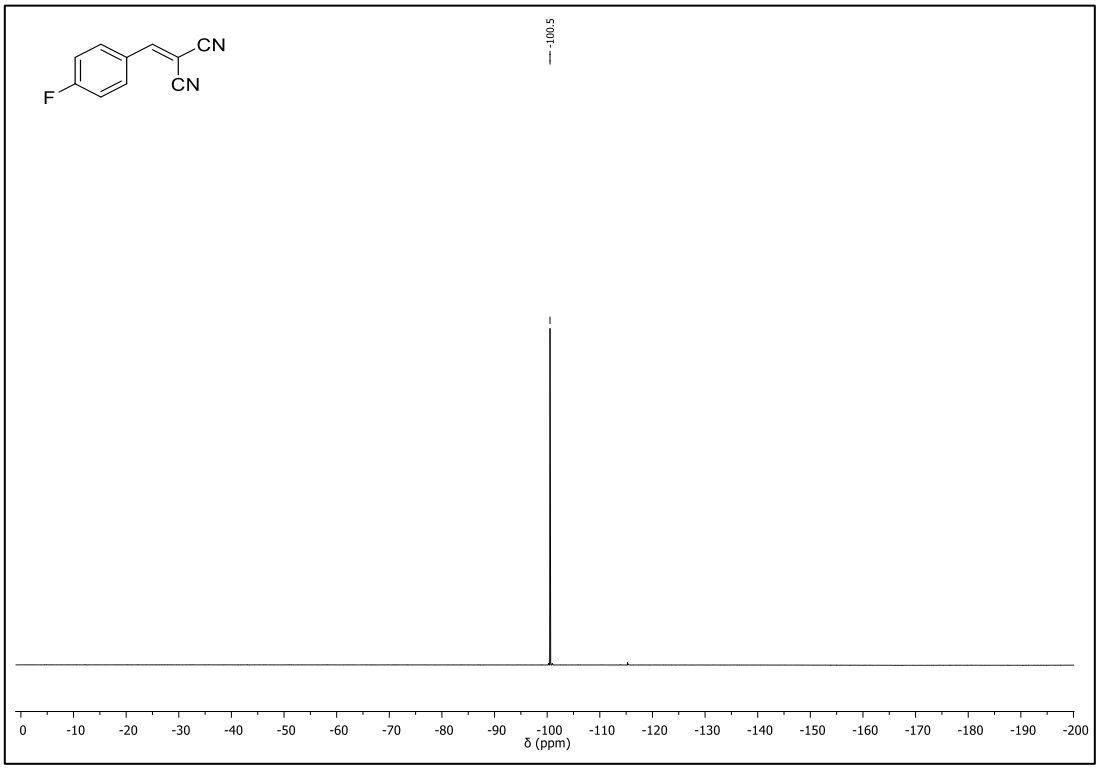

^{1}H-NMR (400 MHz, $CDCl_3$) of **3q**

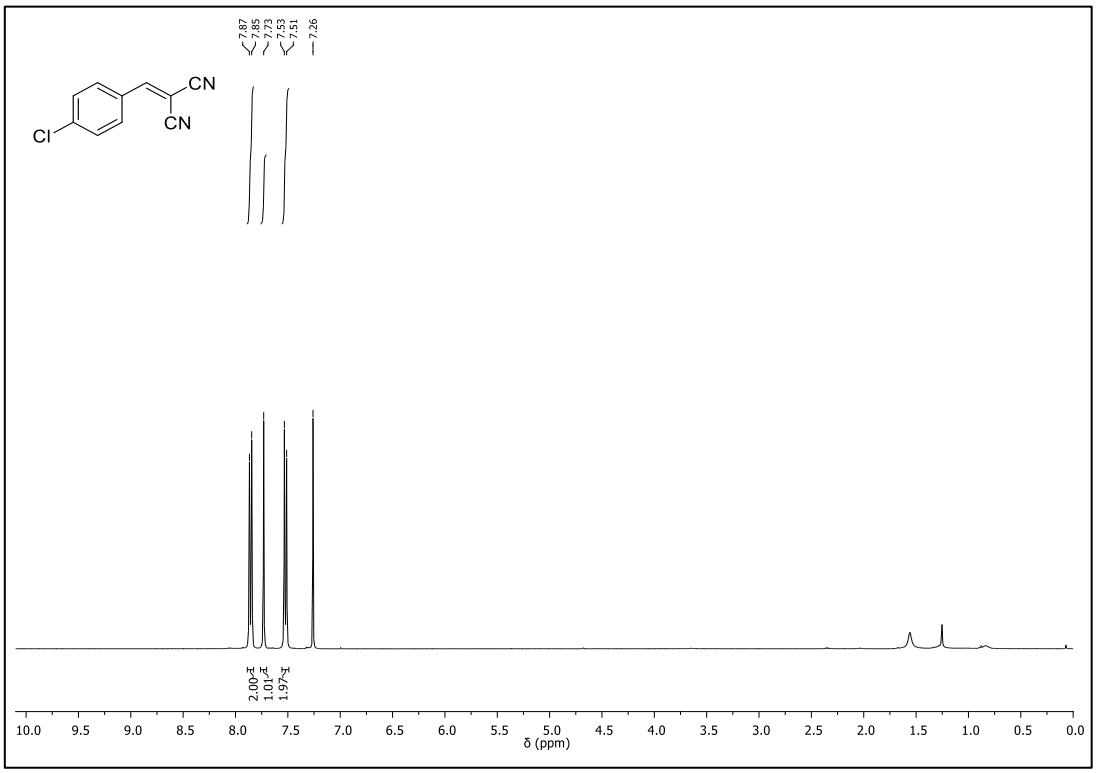

^{13}C-NMR (101 MHz, $CDCl_3$) of **3q**

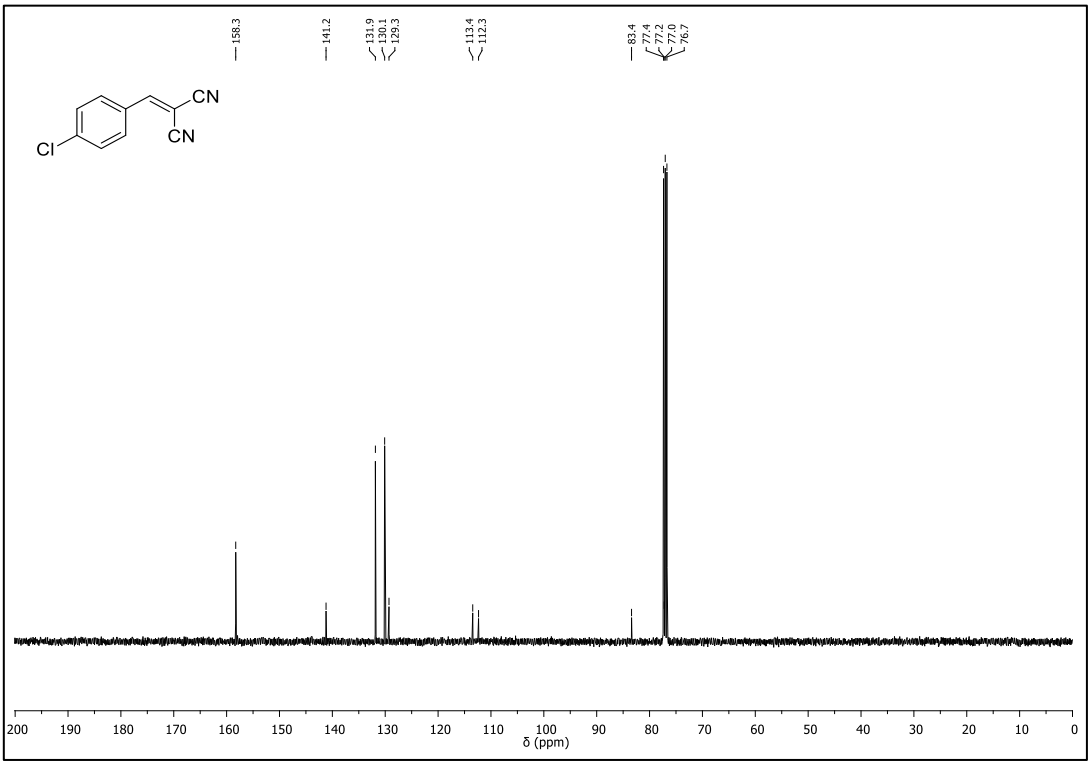

^{1}H-NMR (400 MHz, $CDCl_3$) of **3r**

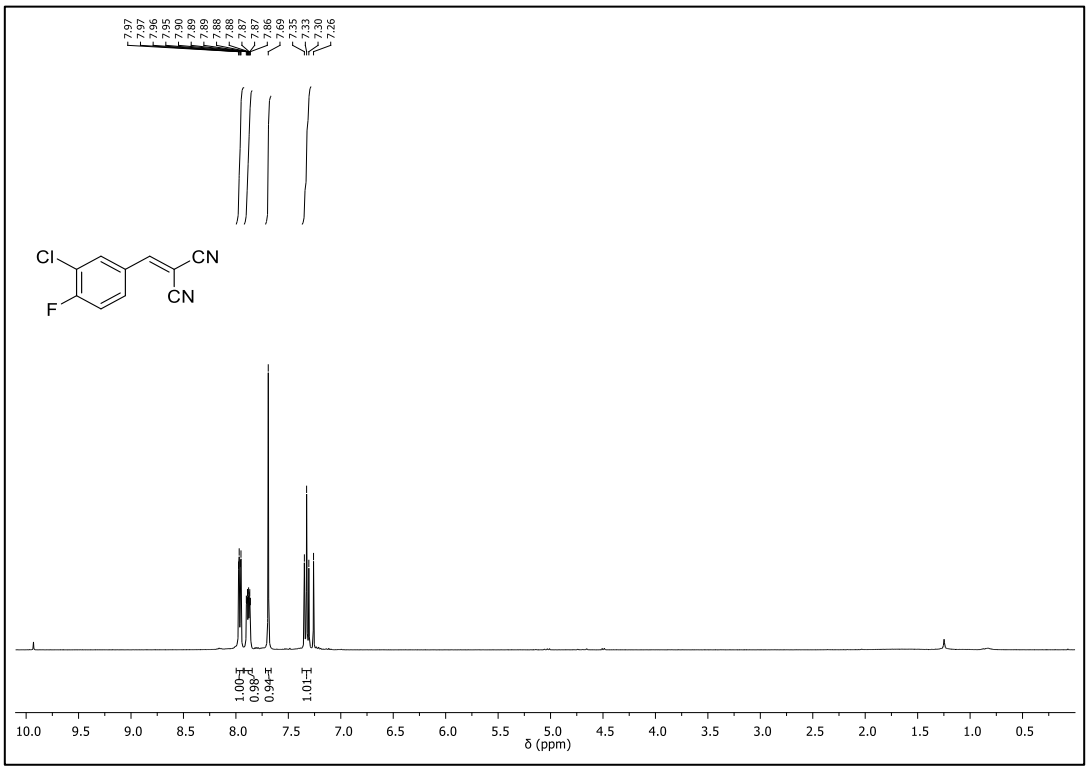

^{13}C-NMR (101 MHz, $CDCl_3$) of **3r**

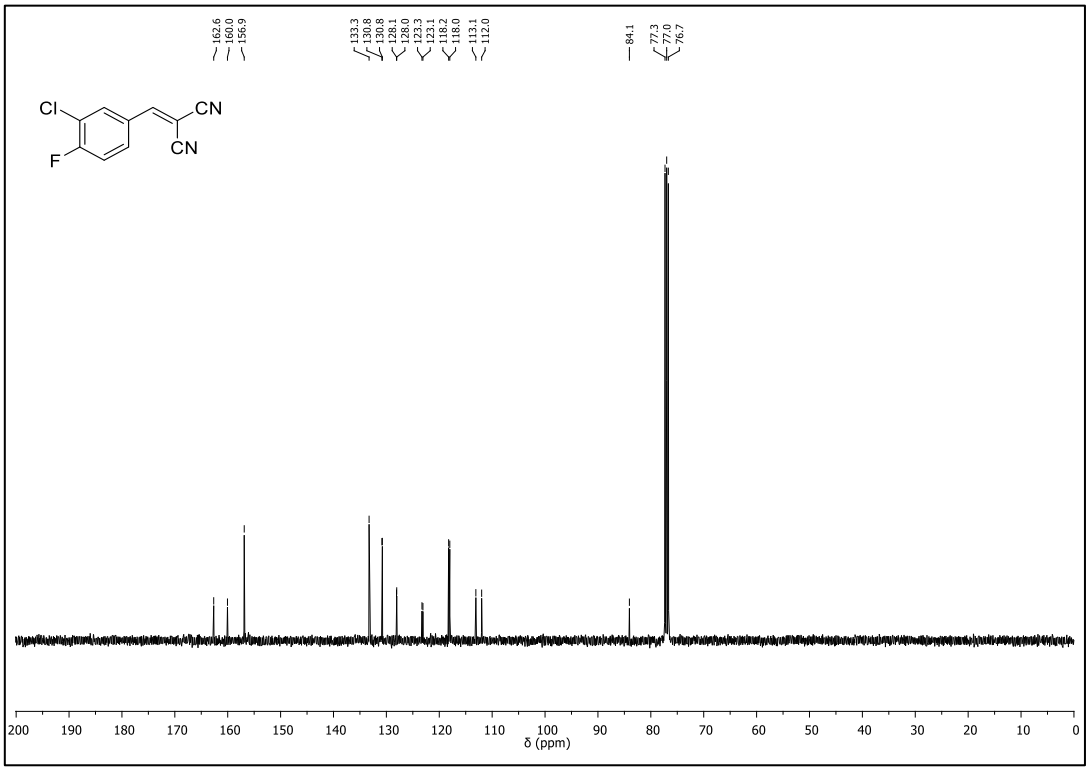

^{19}F-NMR (376 MHz, $CDCl_3$) of **3r**

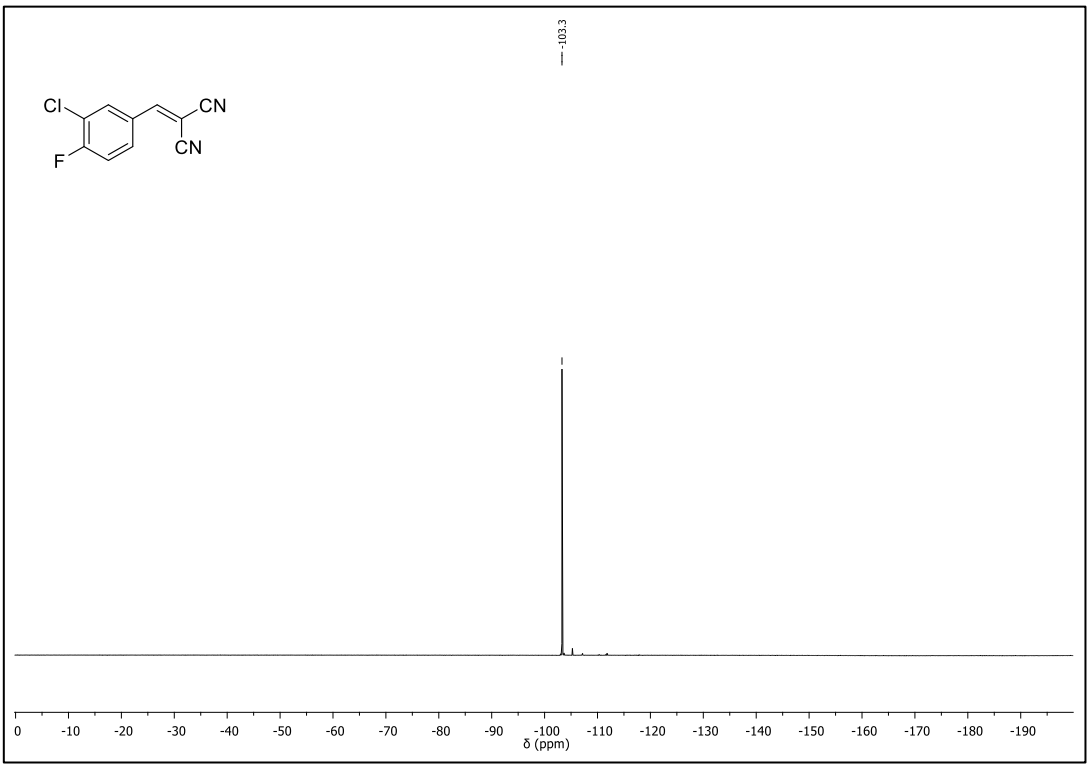

^{1}H-NMR (400 MHz, $CDCl_3$) of **3s**

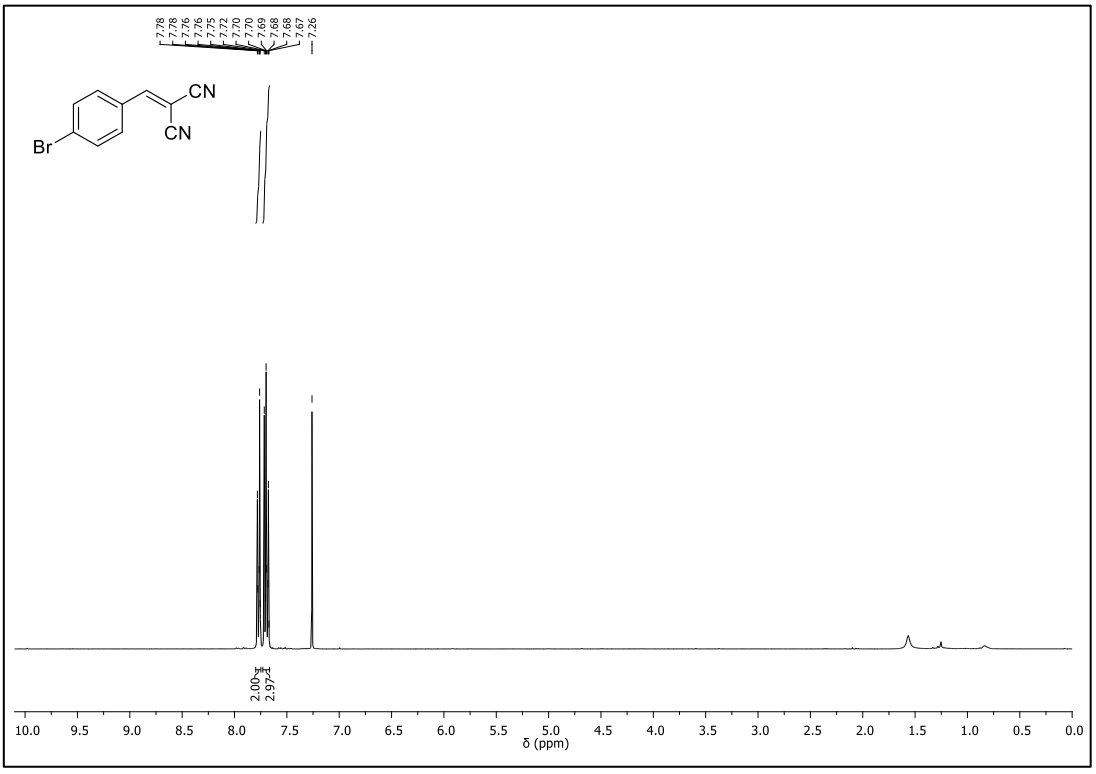

^{13}C-NMR (101 MHz, $CDCl_3$) of **3s**

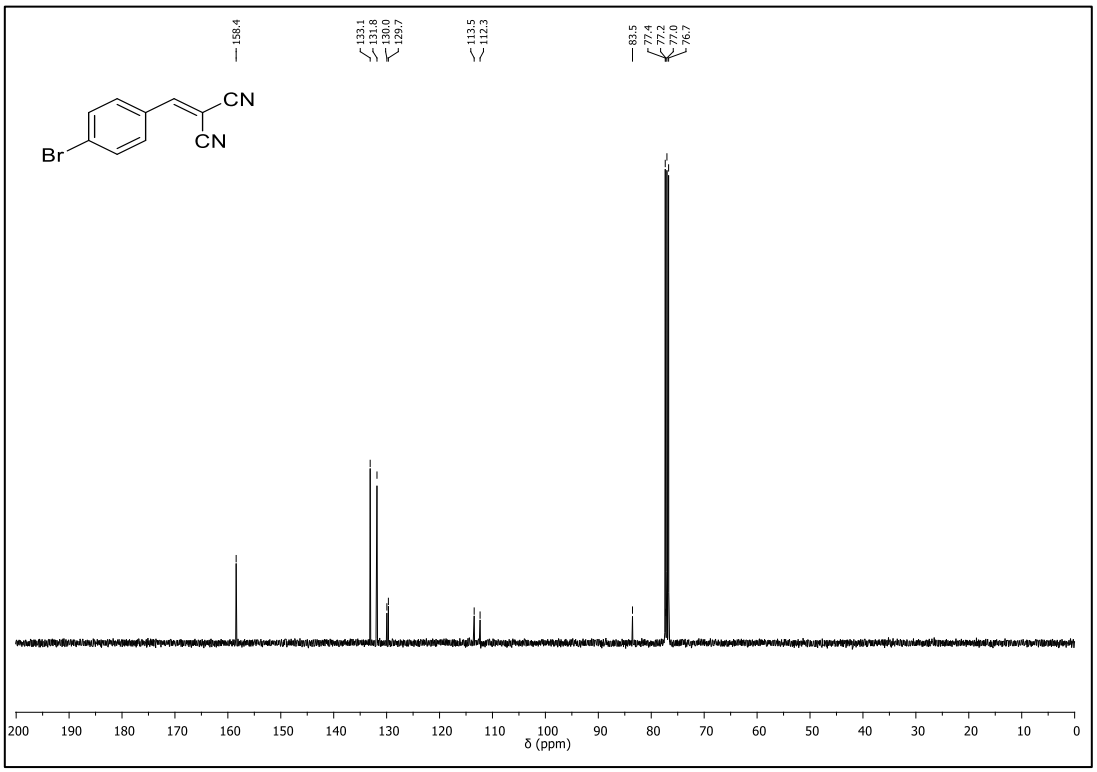

^{1}H-NMR (400 MHz, $CDCl_3$) of **3t**

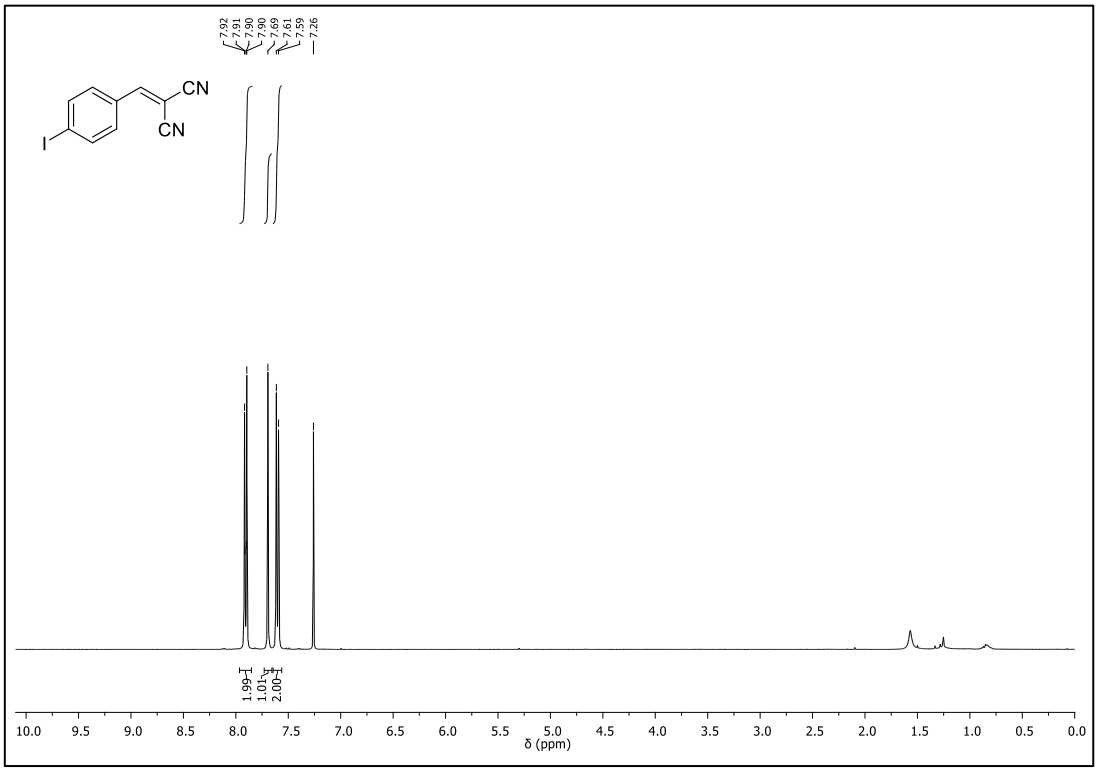

^{13}C-NMR (101 MHz, $CDCl_3$) of **3t**

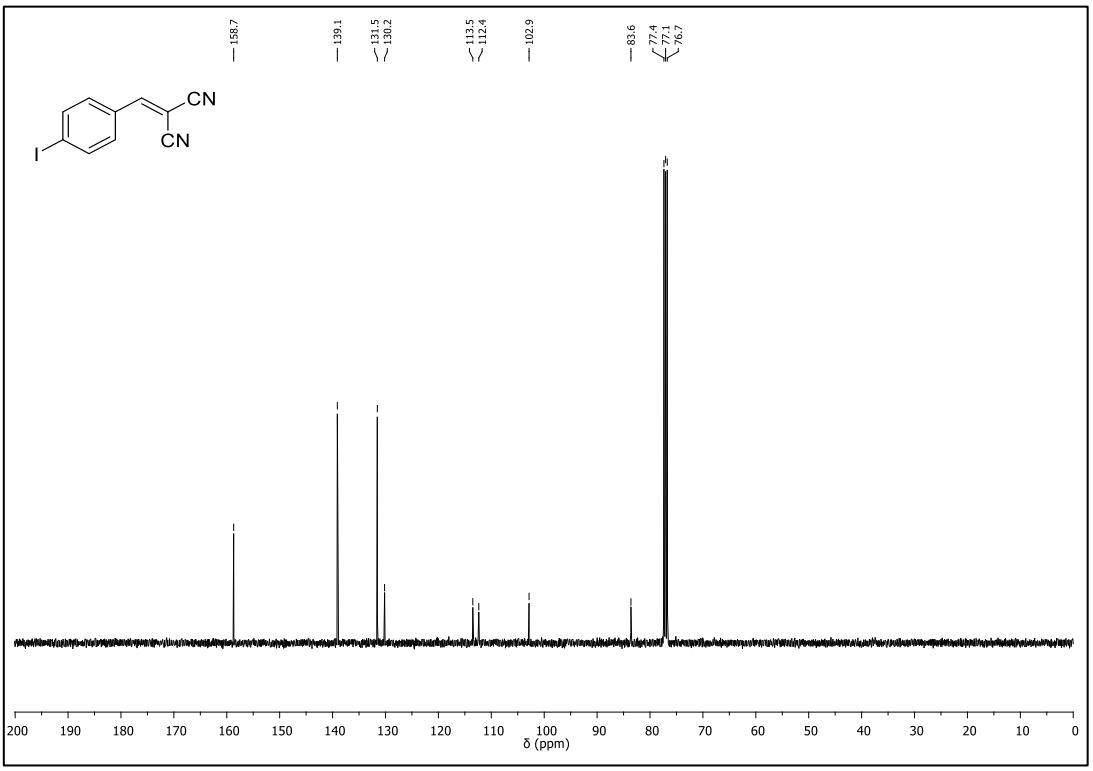

^{1}H-NMR (400 MHz, $CDCl_3$) of **3x**

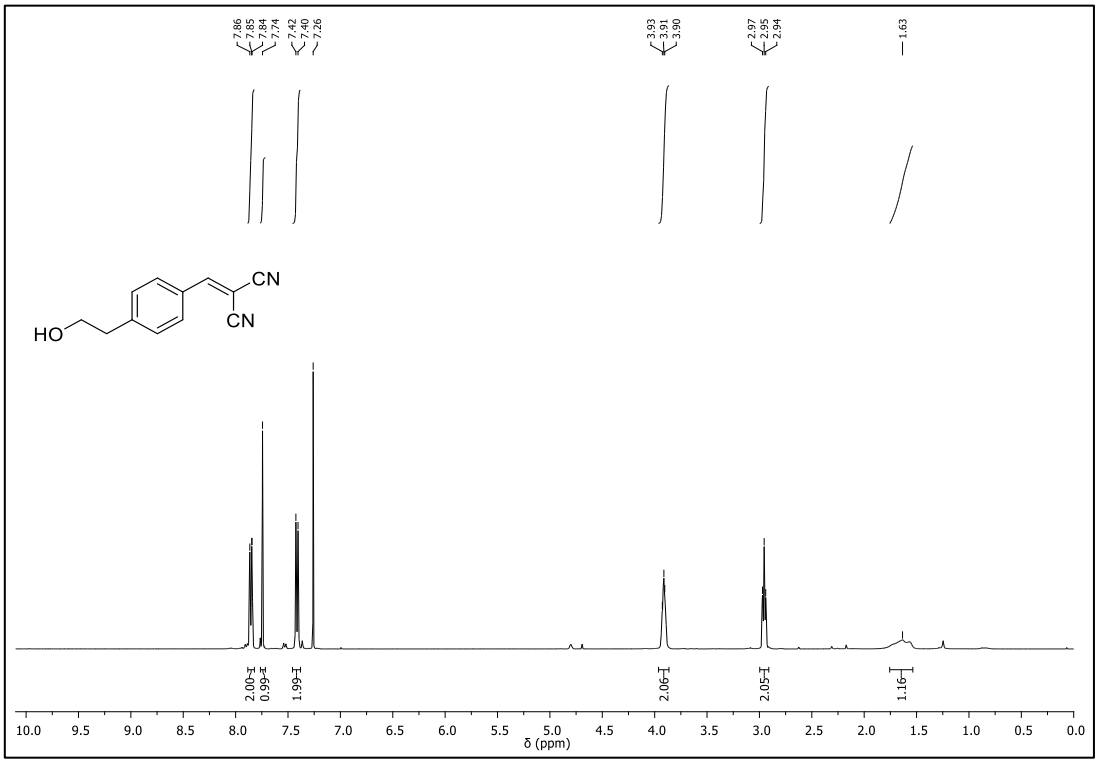

^{13}C-NMR (101 MHz, $CDCl_3$) of **3x**

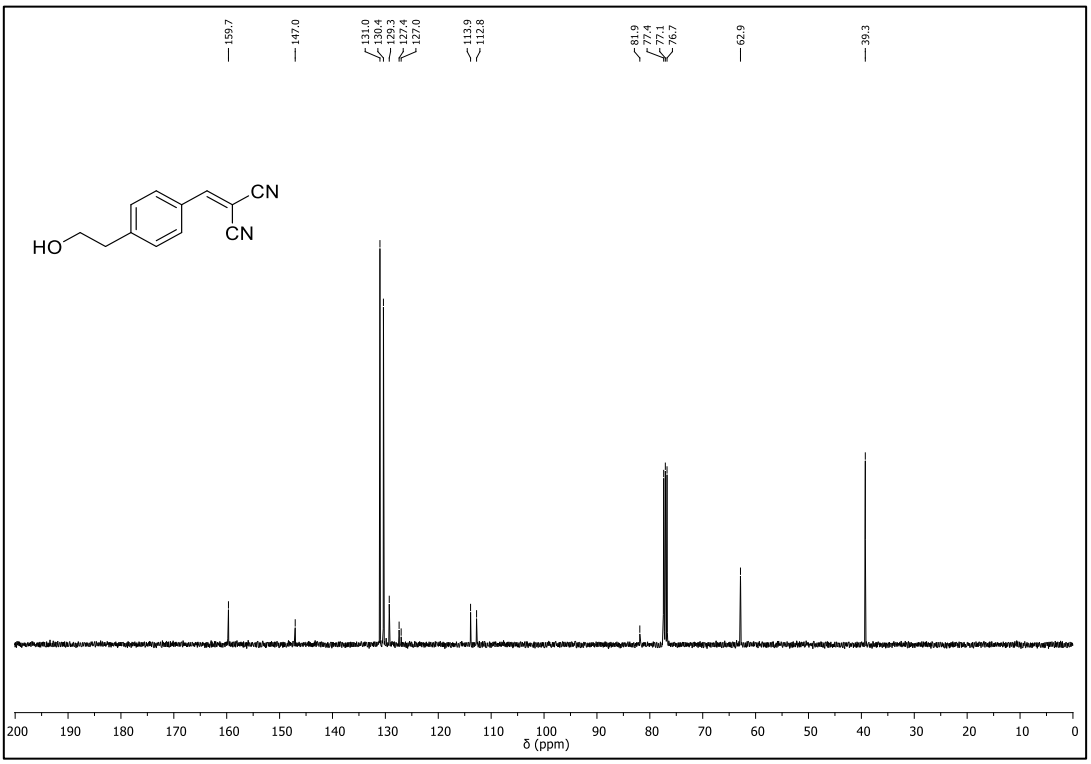

9.3 NMR Spectra of Chapter 3

NMR Spectra of Starting Materials

^{1}H-NMR (400 MHz, CD_2Cl_2) of **SM-A**

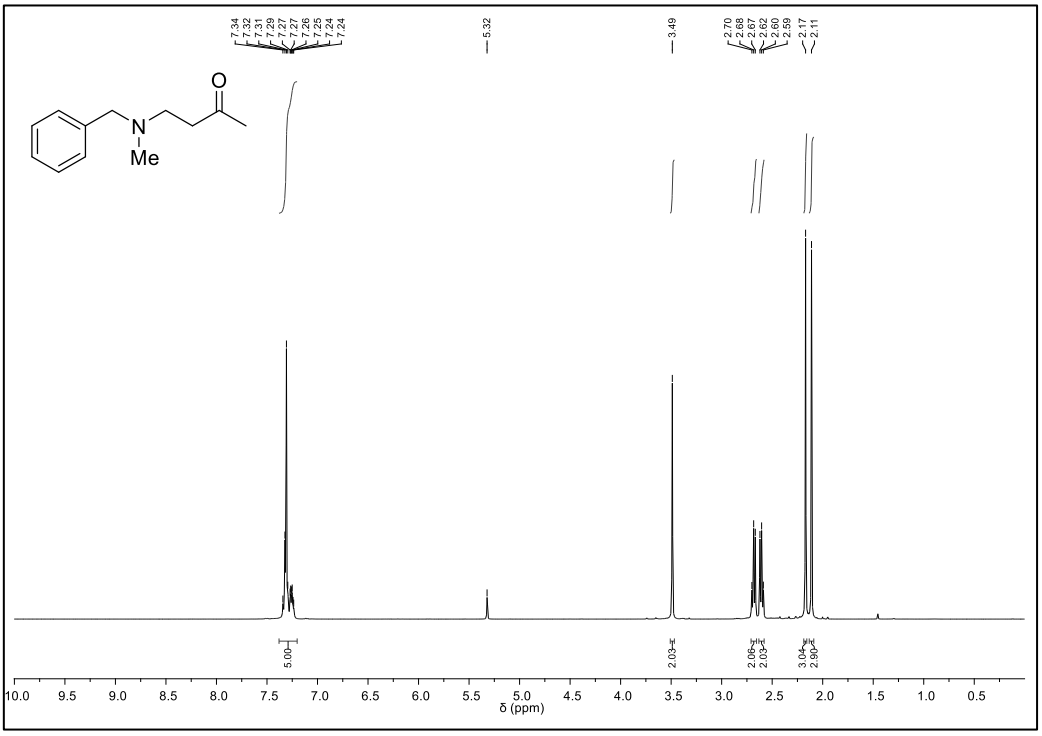

^{13}C-NMR (101 MHz, CD_2Cl_2) of **SM-A**

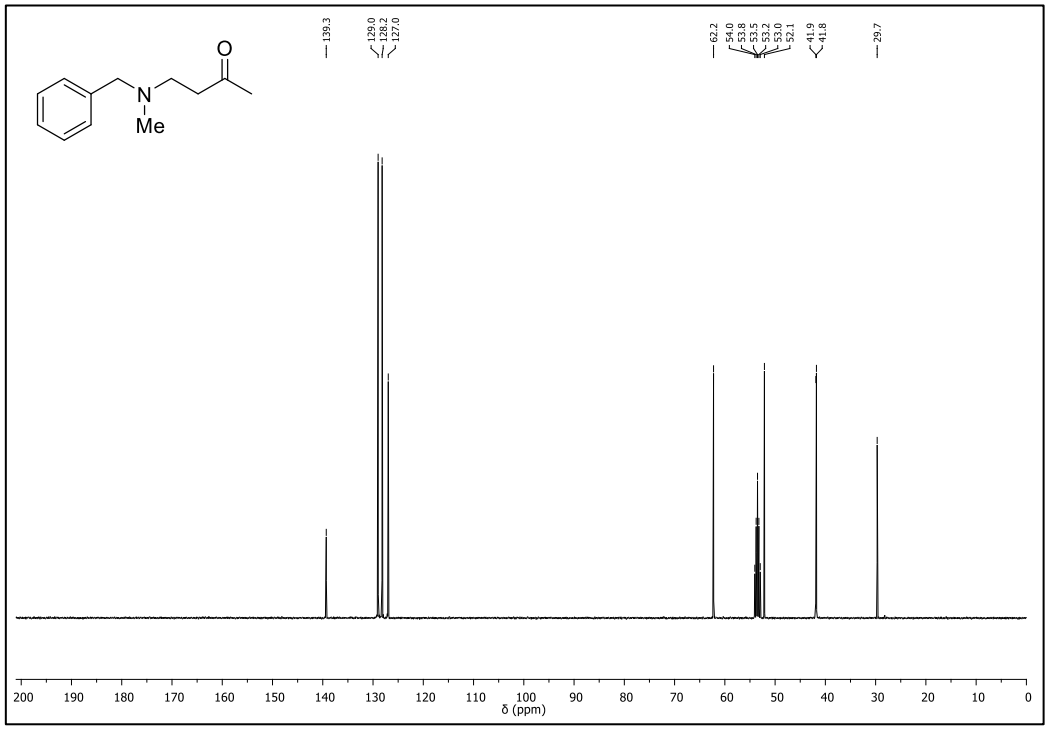

^{1}H-NMR (400 MHz, $CDCl_3$) of **2a**

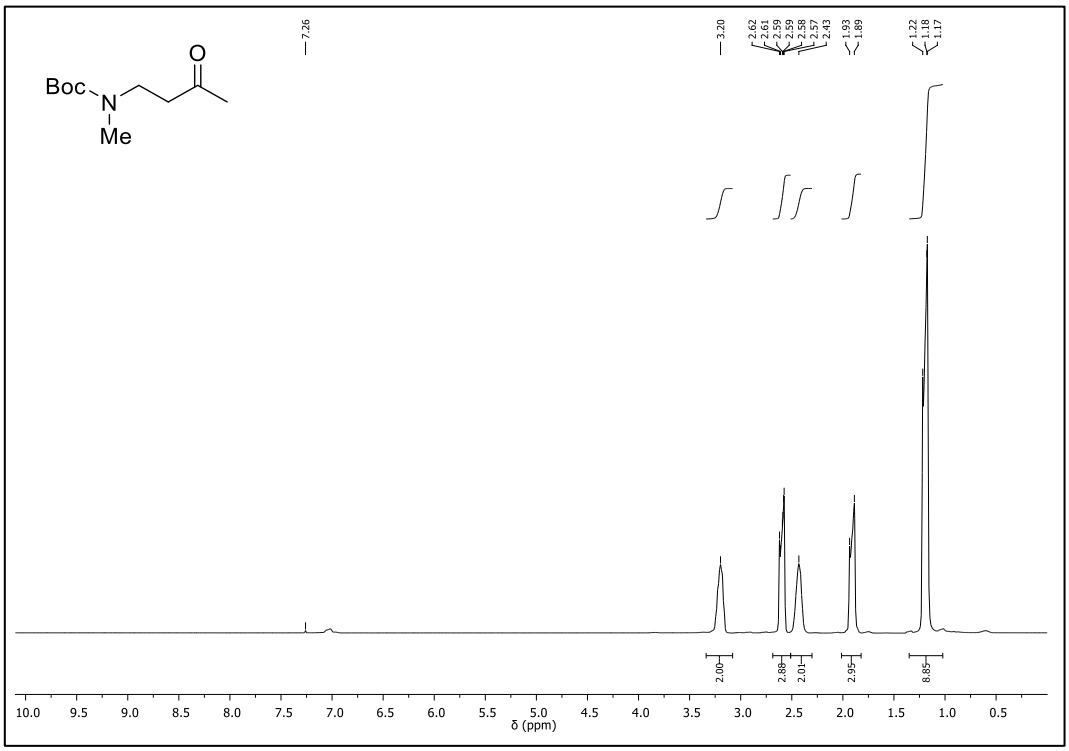

^{13}C-NMR (101 MHz, $CDCl_3$) of **2a**

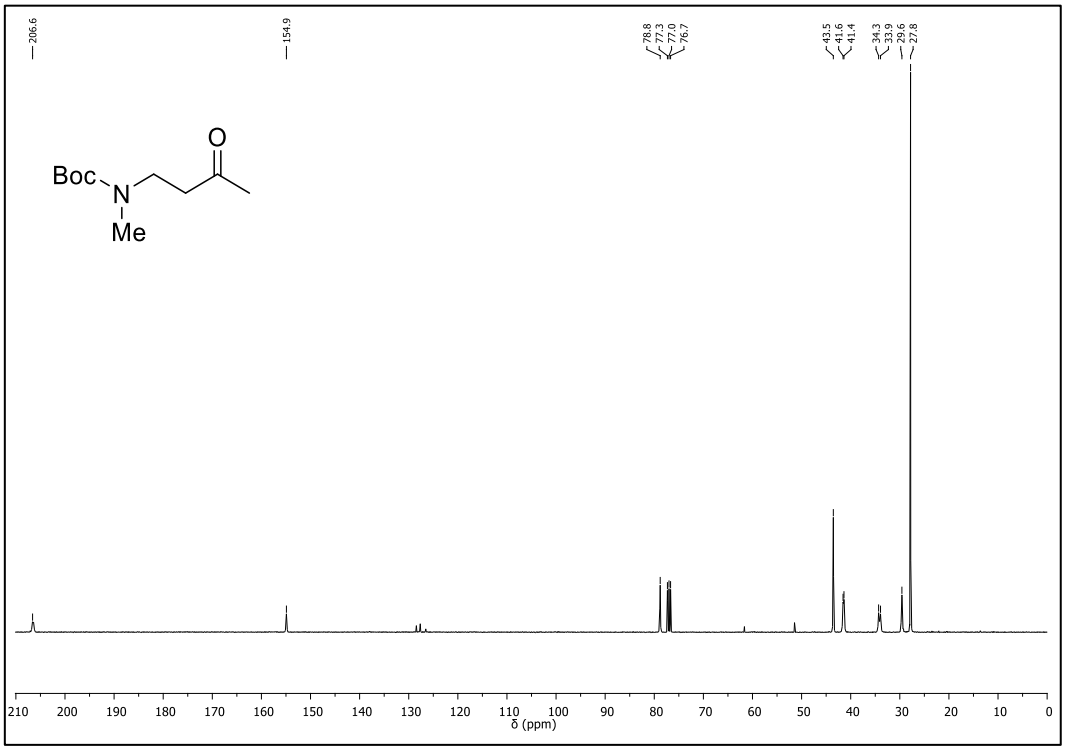

^{1}H-NMR (400 MHz, $CDCl_3$) of **SM-B**

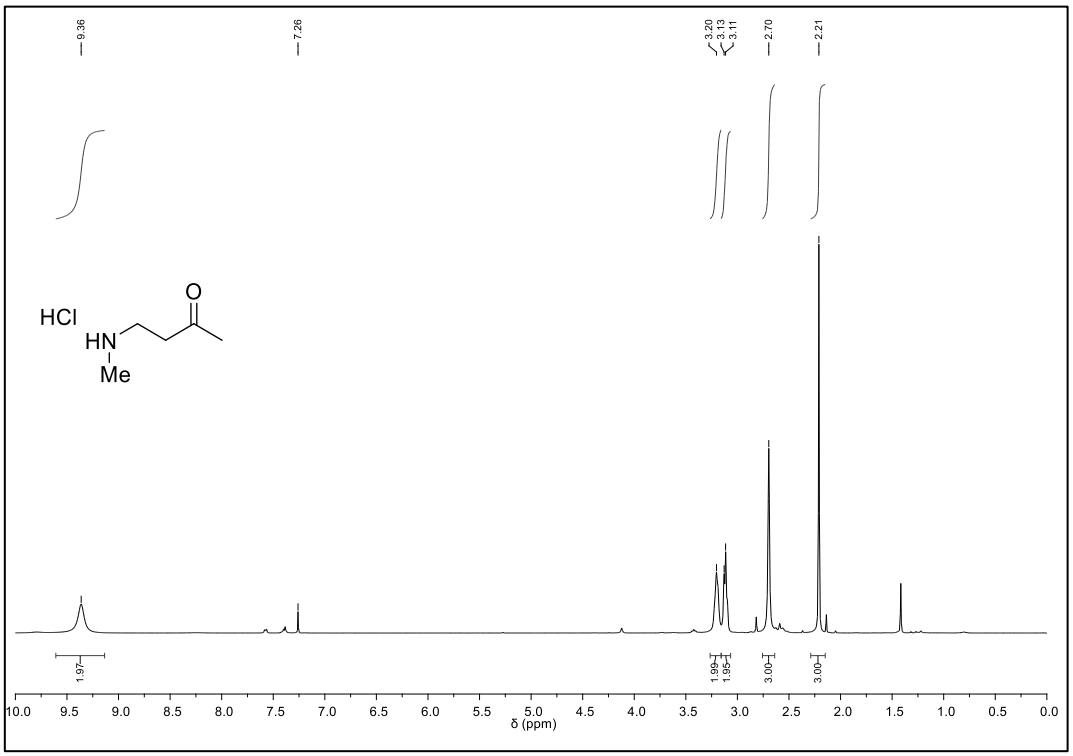

^{13}C-NMR (101 MHz, $CDCl_3$) of **SM-B**

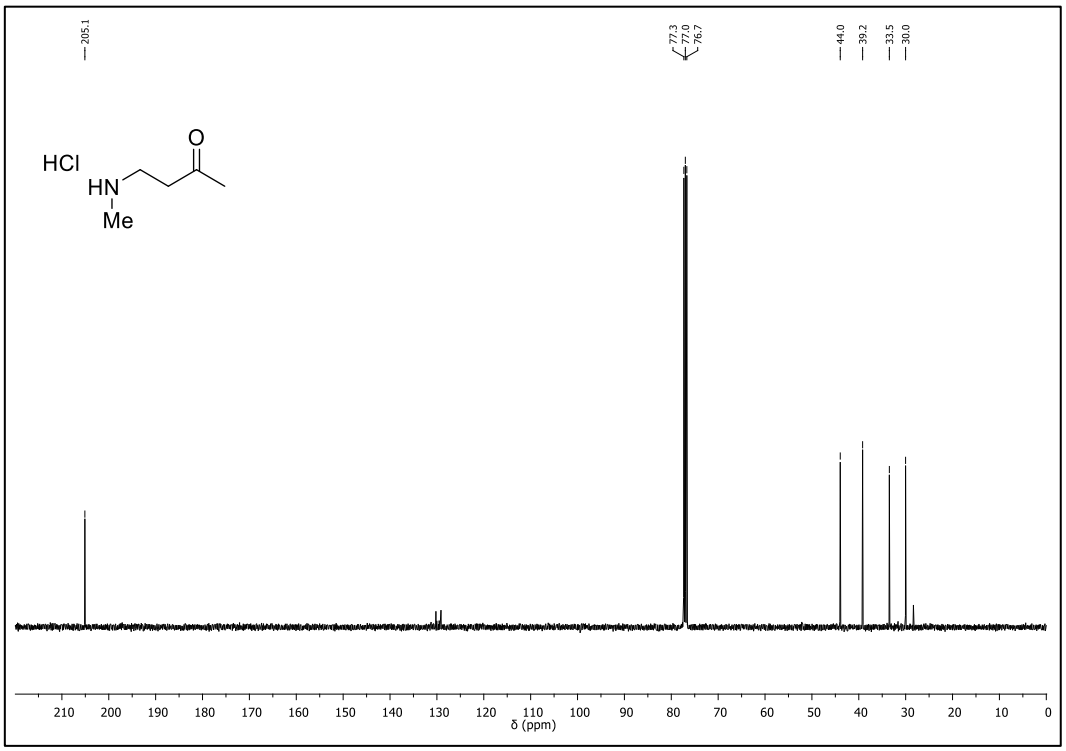

^{1}H-NMR (400 MHz, $CDCl_3$) of **1a**

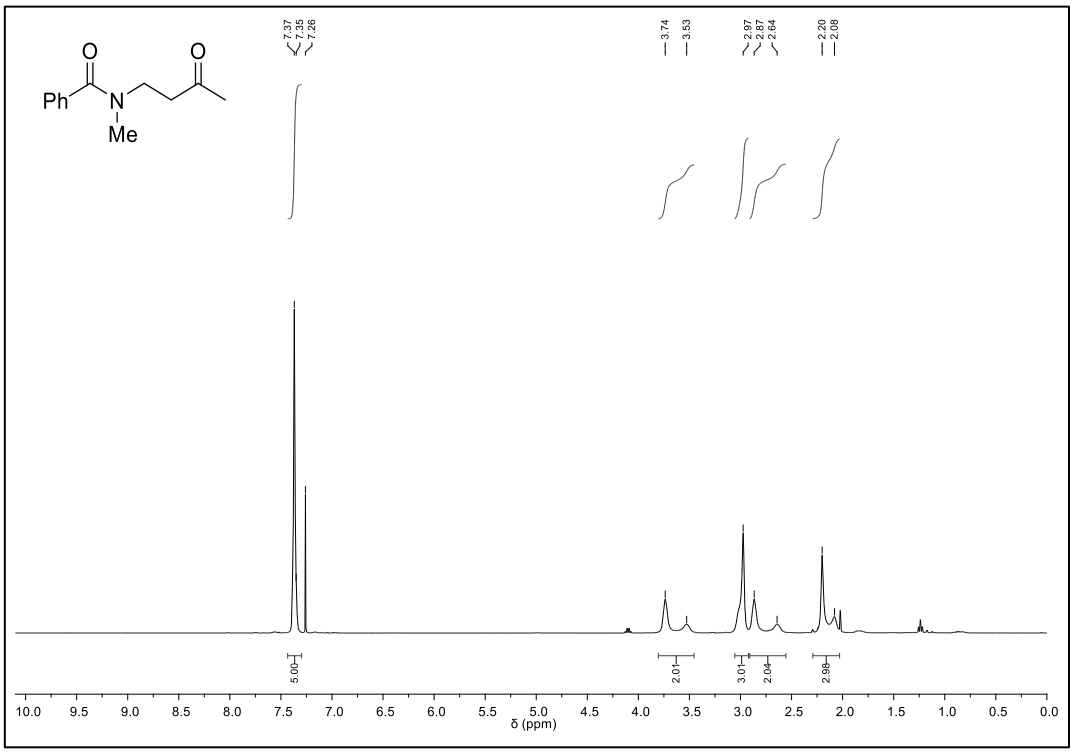

^{13}C-NMR (101 MHz, $CDCl_3$) of **1a**

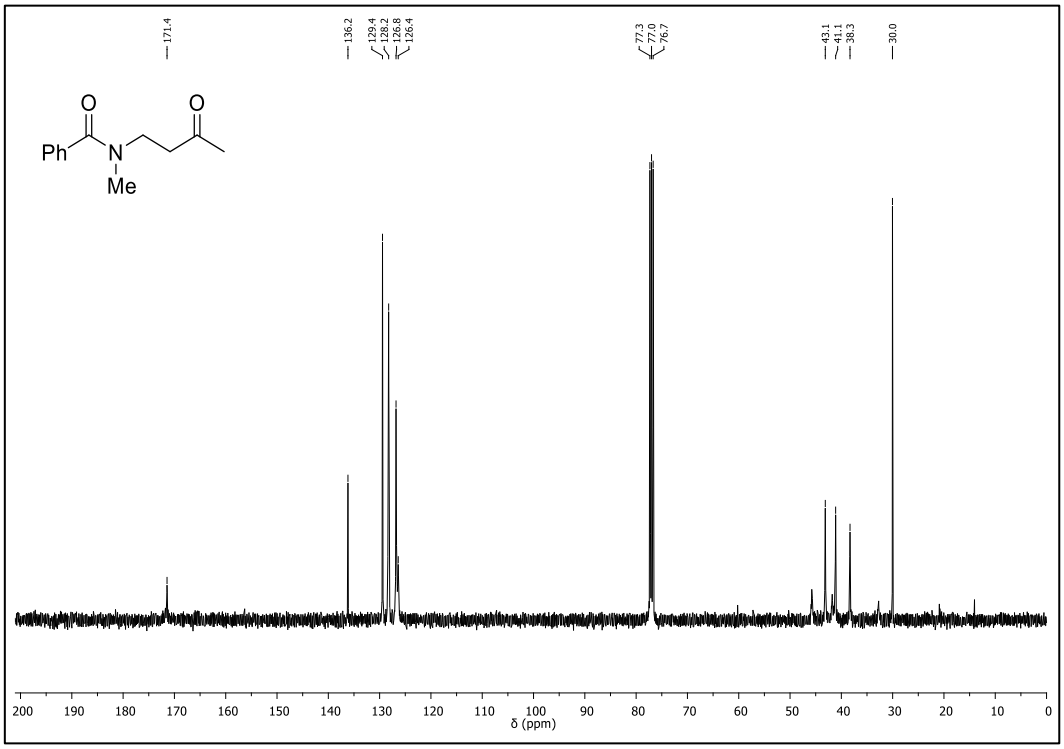

^{1}H-NMR (400 MHz, $CDCl_3$) of **SM-C**

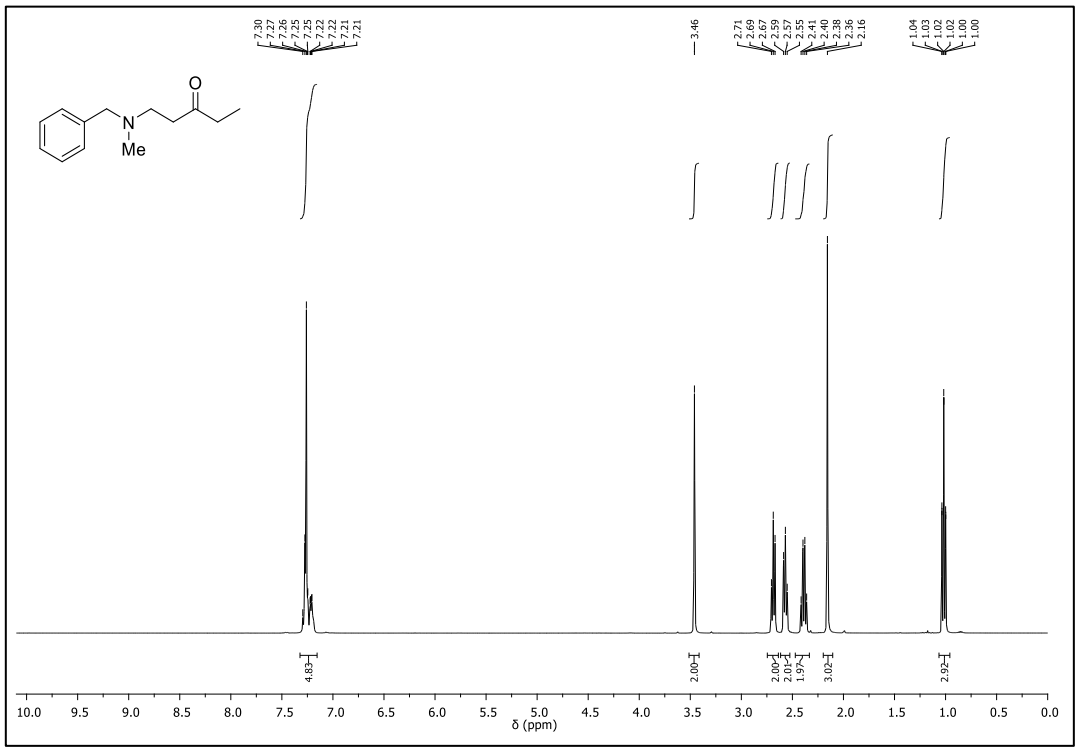

^{13}C-NMR (101 MHz, $CDCl_3$) of **SM-C**

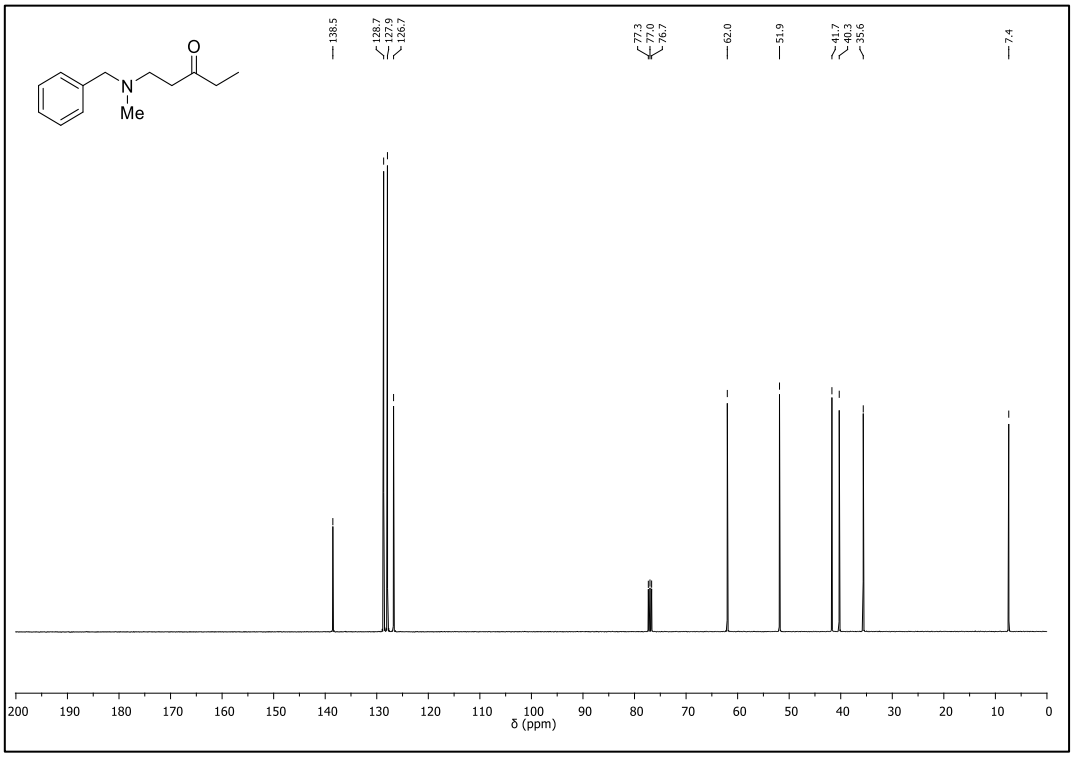

^{1}H-NMR (400 MHz, $CDCl_3$) of **3a**

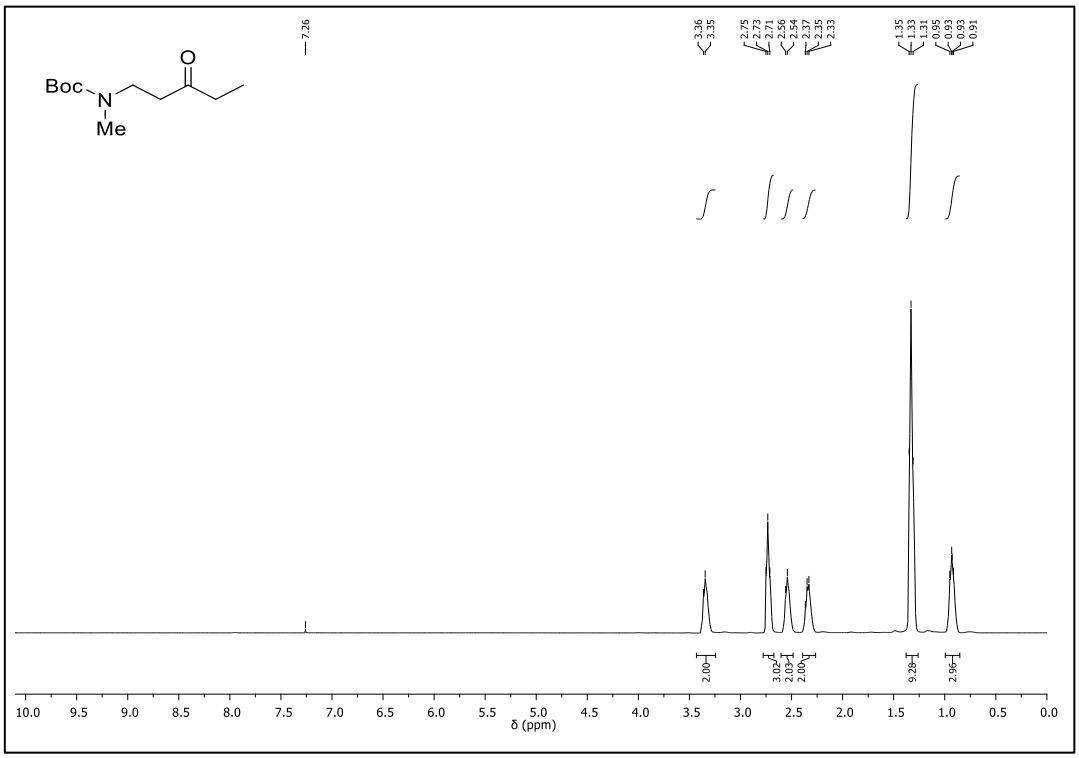

^{13}C-NMR (101 MHz, $CDCl_3$) of **3a**

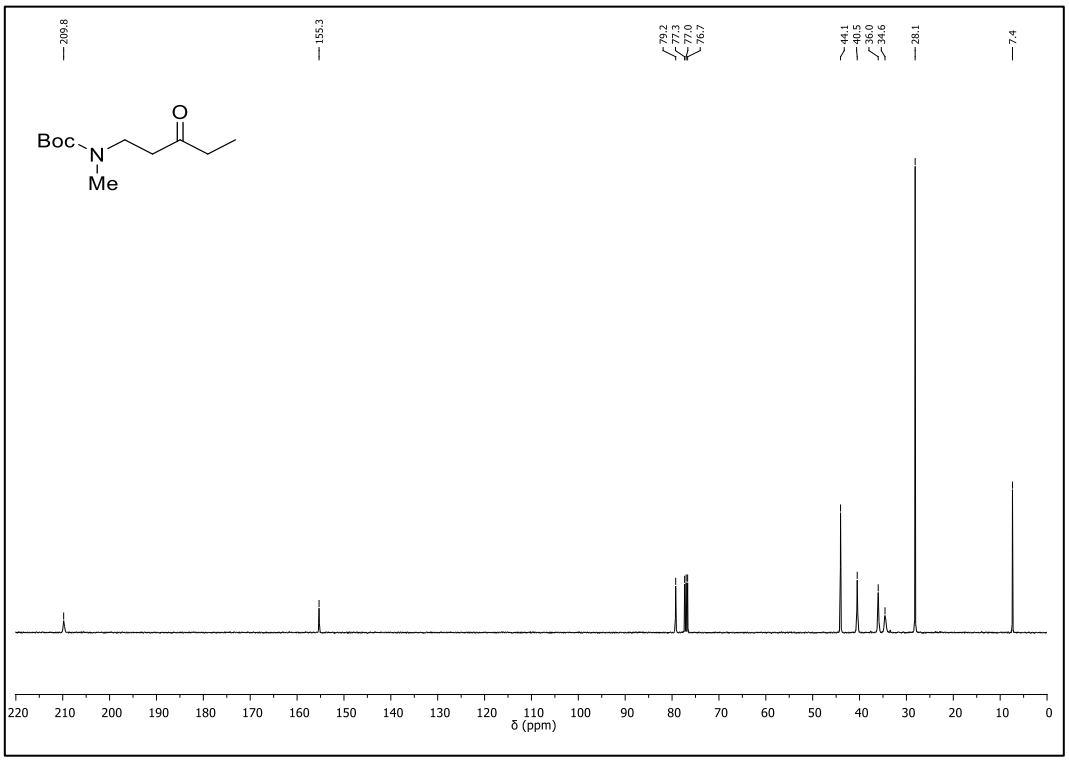

^{1}H-NMR (400 MHz, $CDCl_3$) of **4a**

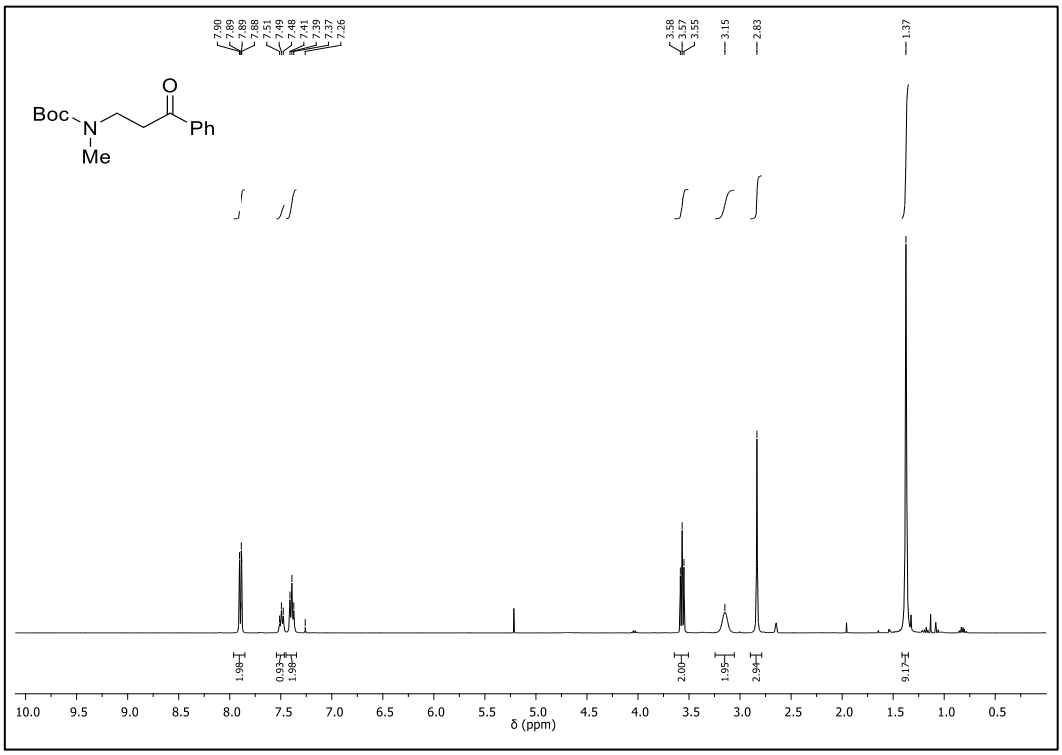

^{13}C-NMR (101 MHz, $CDCl_3$) of **4a**

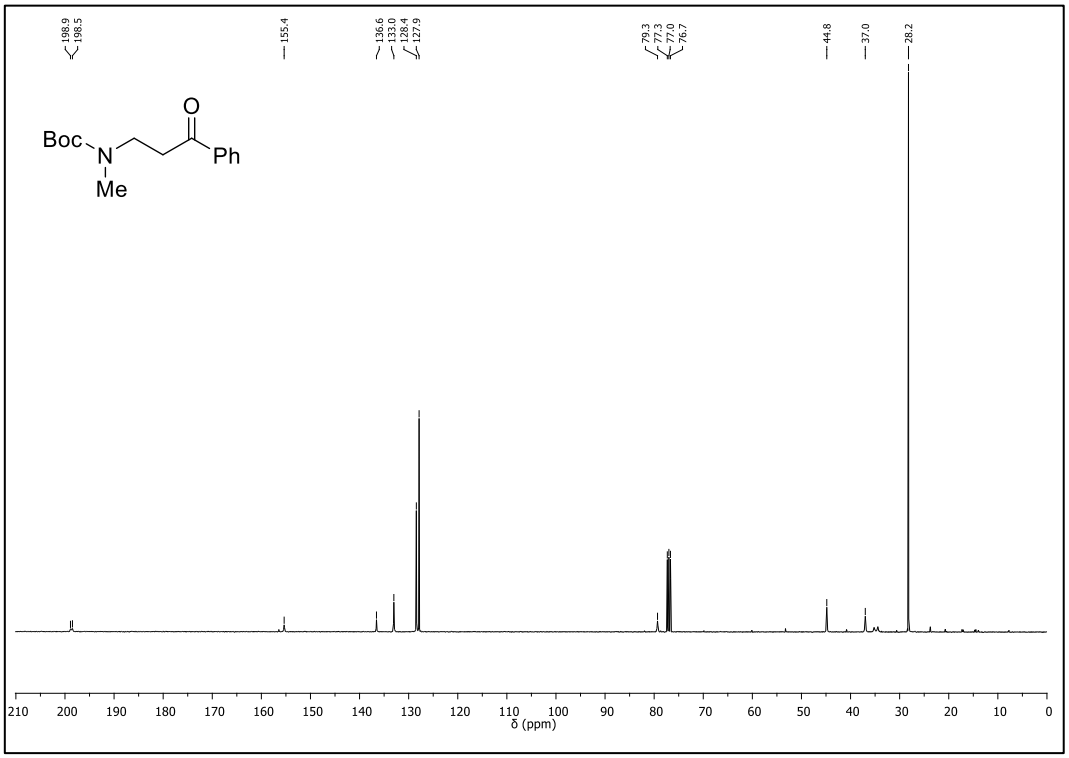

^{1}H-NMR (400 MHz, $CDCl_3$) of **5a**

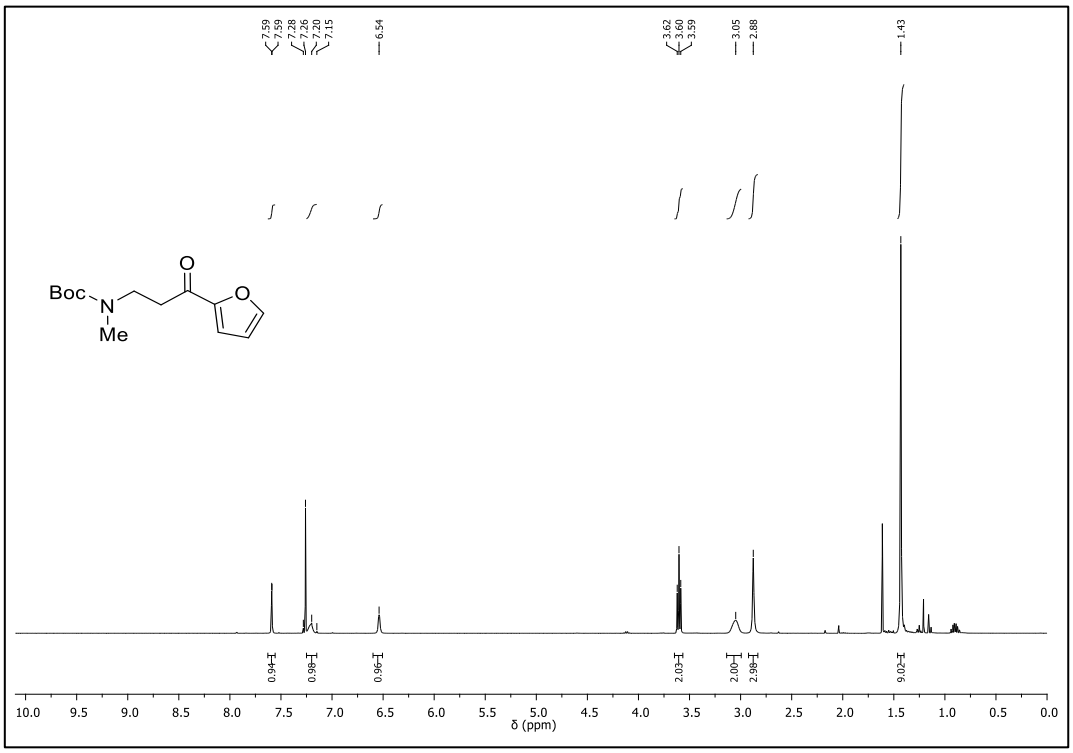

^{13}C-NMR (101 MHz, $CDCl_3$) of **5a**

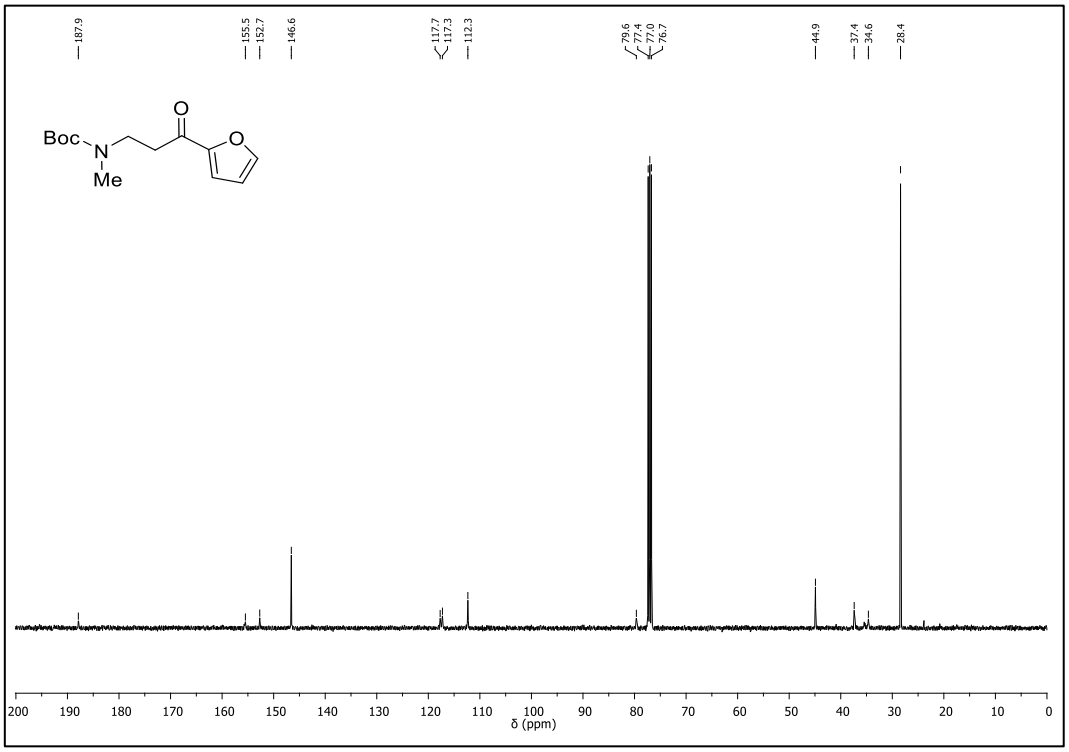

^{1}H-NMR (400 MHz, $CDCl_3$) of **6a**

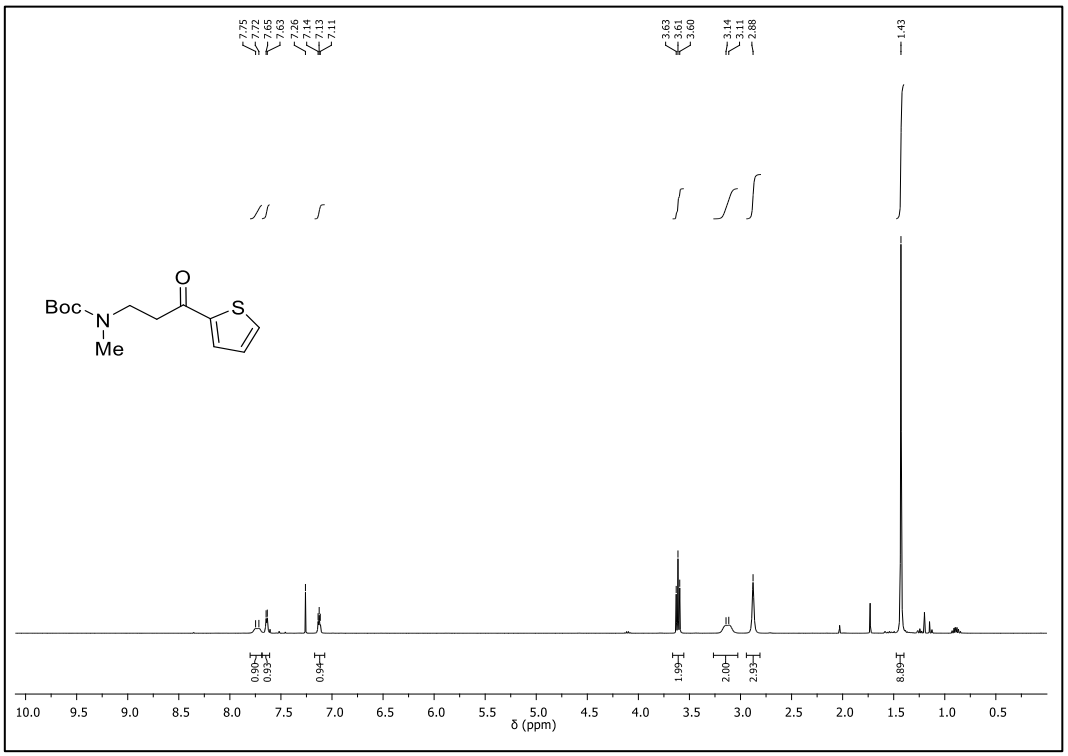

^{13}C-NMR (101 MHz, $CDCl_3$) of **6a**

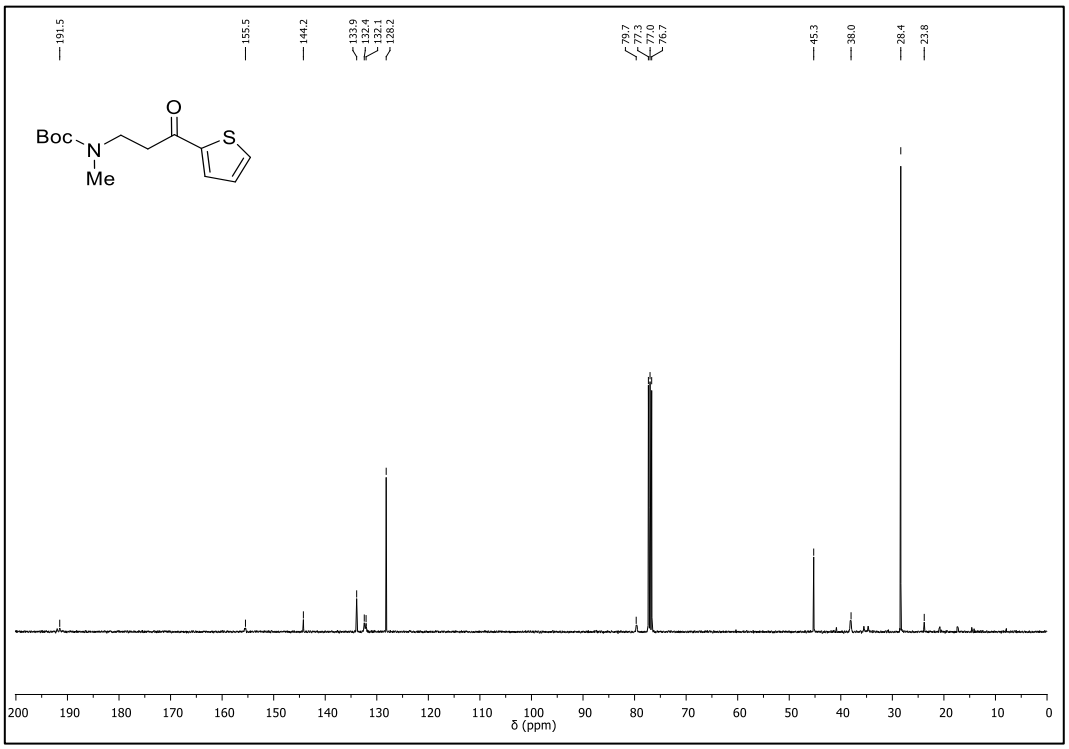

^{1}H-NMR (400 MHz, $CDCl_3$) of **7a**

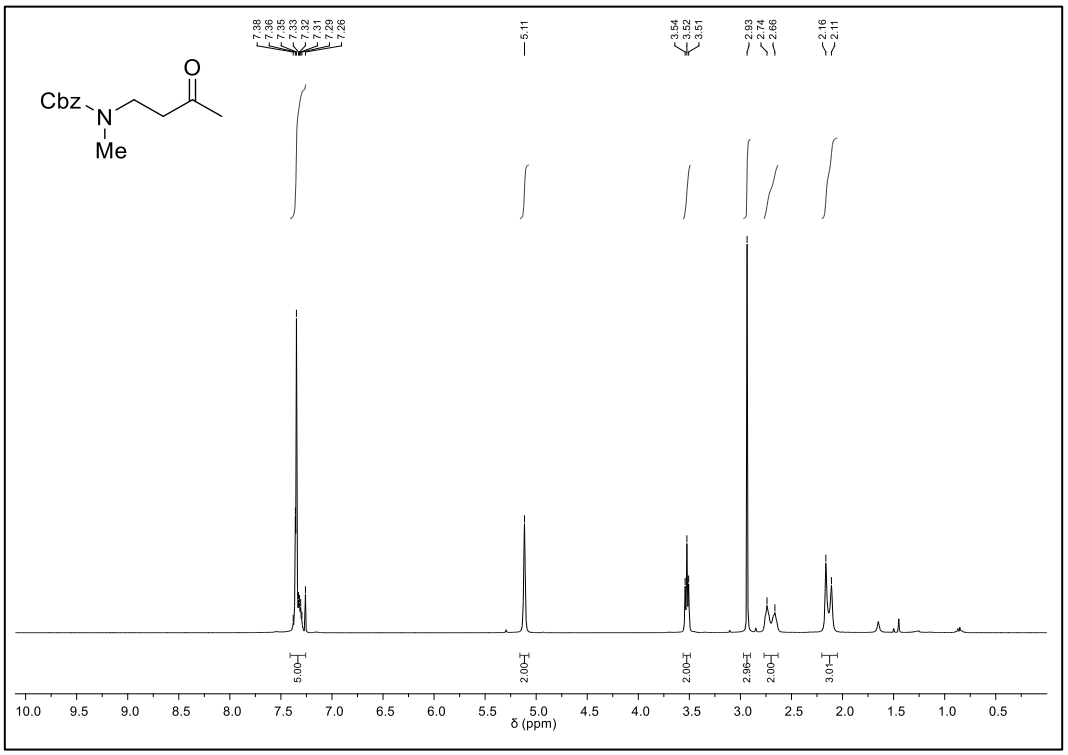

^{13}C-NMR (101 MHz, $CDCl_3$) of **7a**

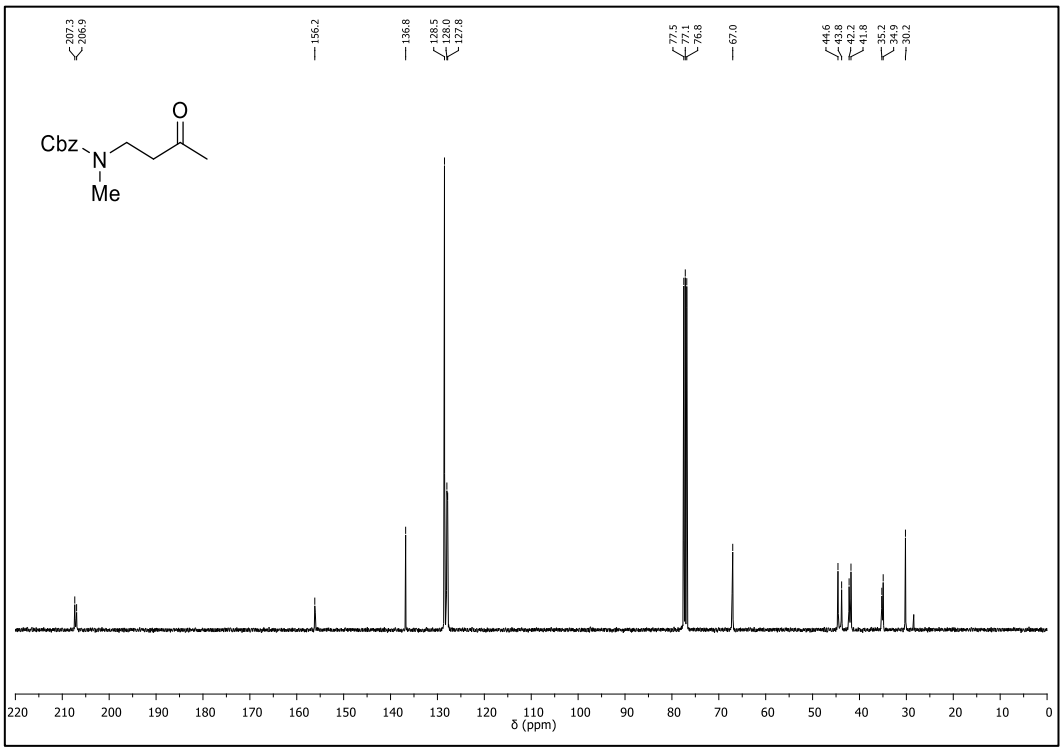

^{1}H-NMR (400 MHz, $CDCl_3$) of **8a**

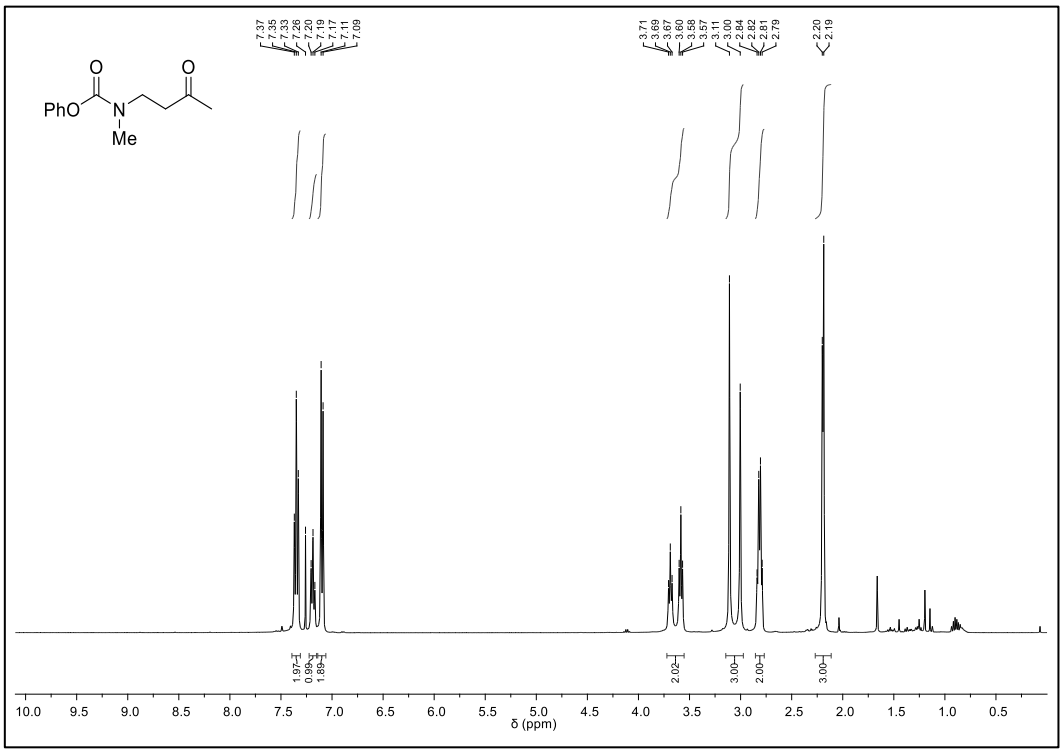

^{13}C-NMR (101 MHz, $CDCl_3$) of **8a**

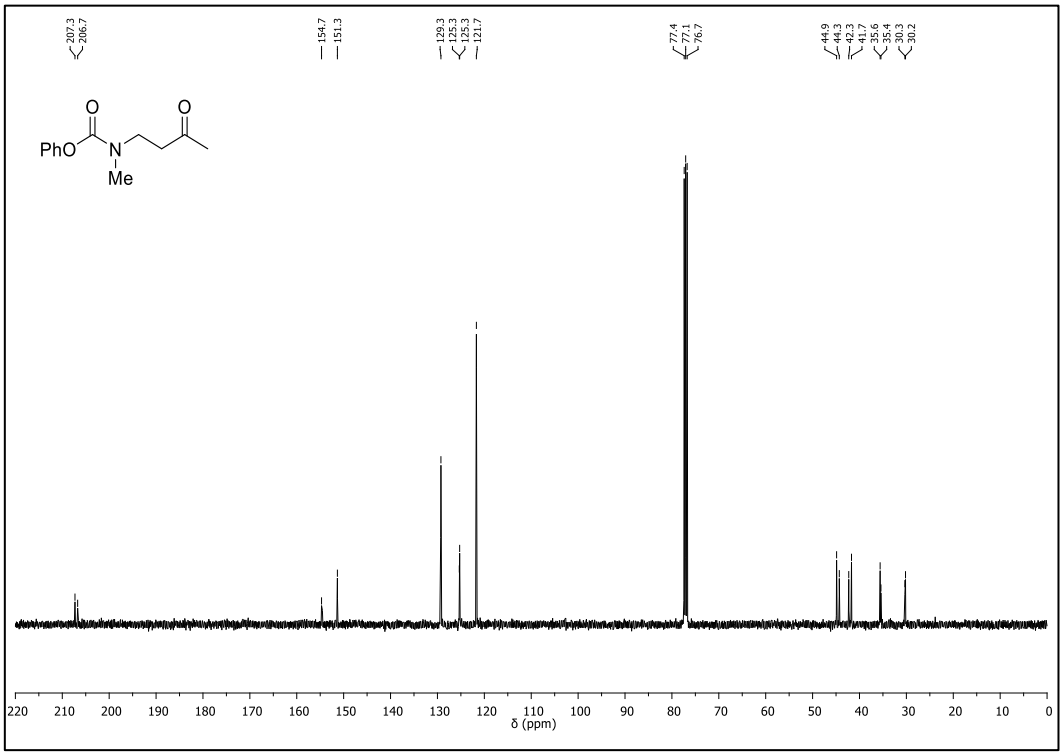

^{1}H-NMR (400 MHz, $CDCl_3$) of **SM-D**

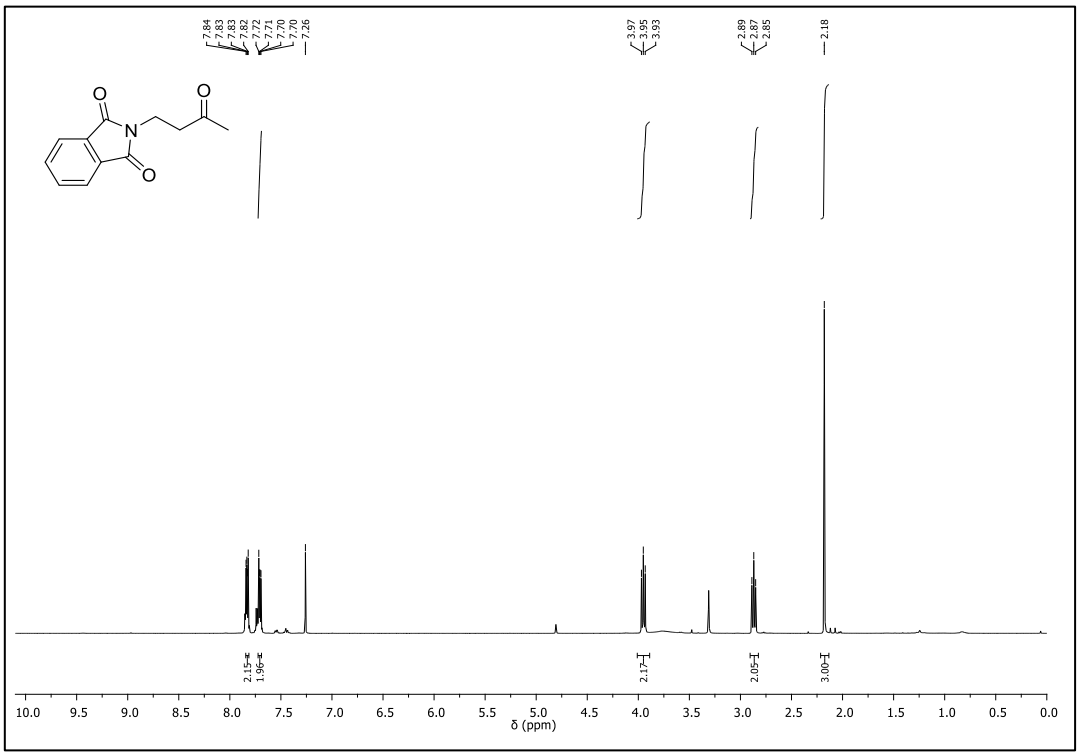

^{13}C-NMR (101 MHz, $CDCl_3$) of **SM-D**

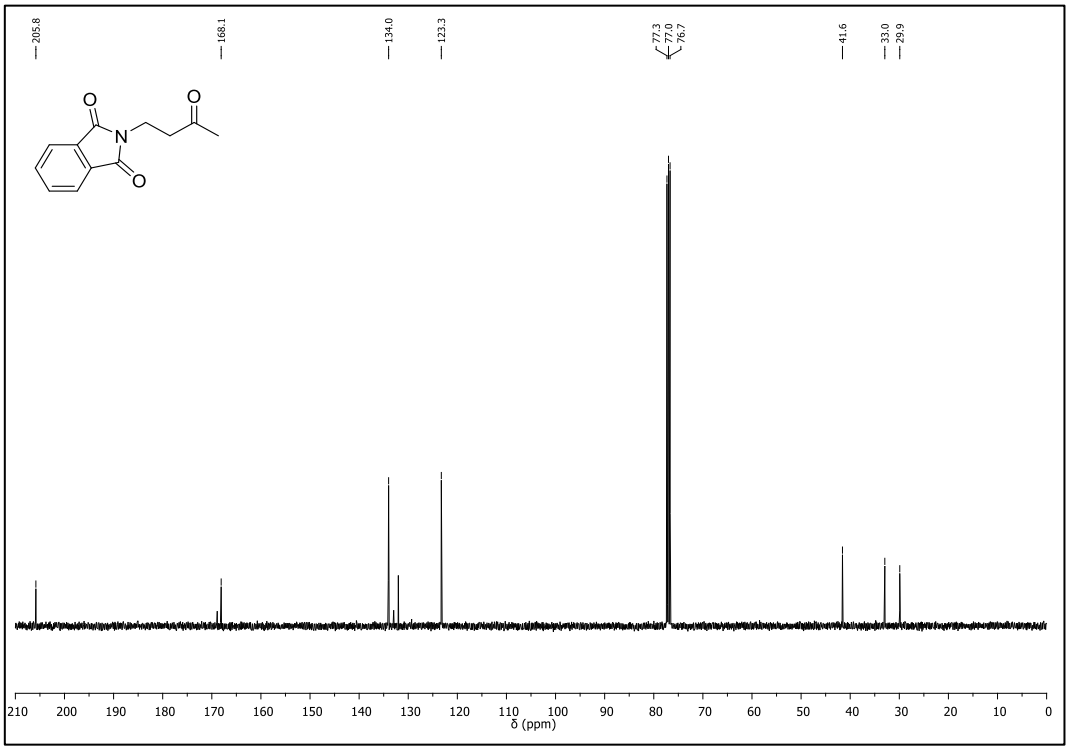

^{1}H-NMR (400 MHz, D_2O) of **SM-E**

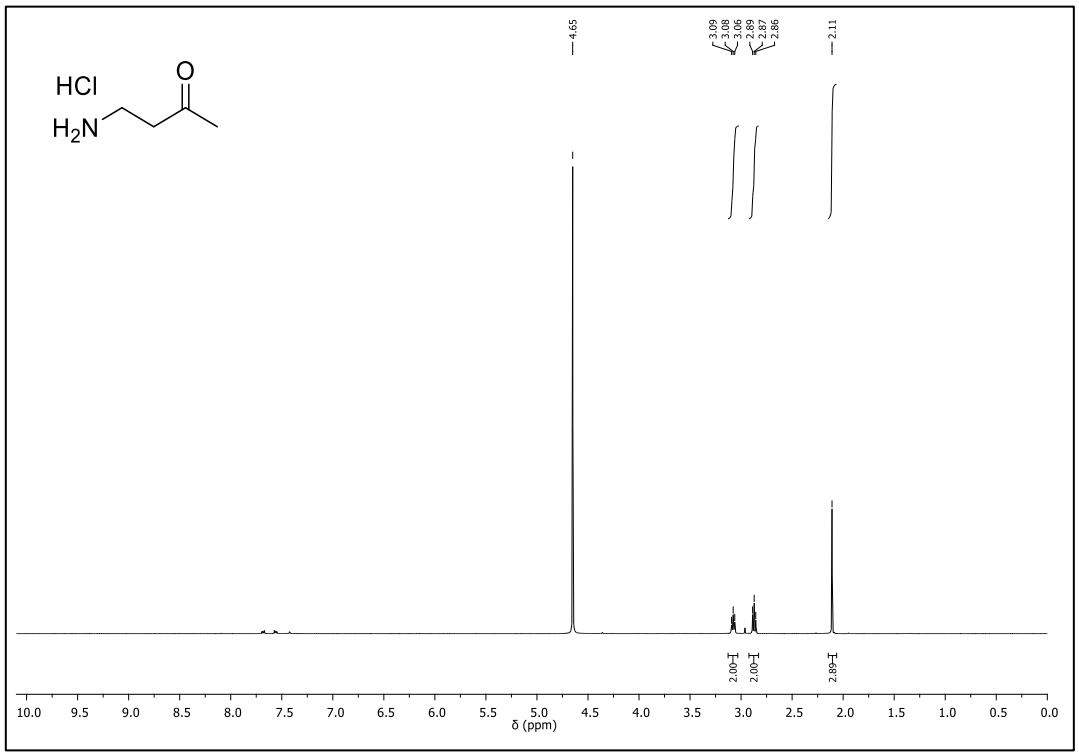

^{13}C-NMR (101 MHz, D_2O) of **SM-E**

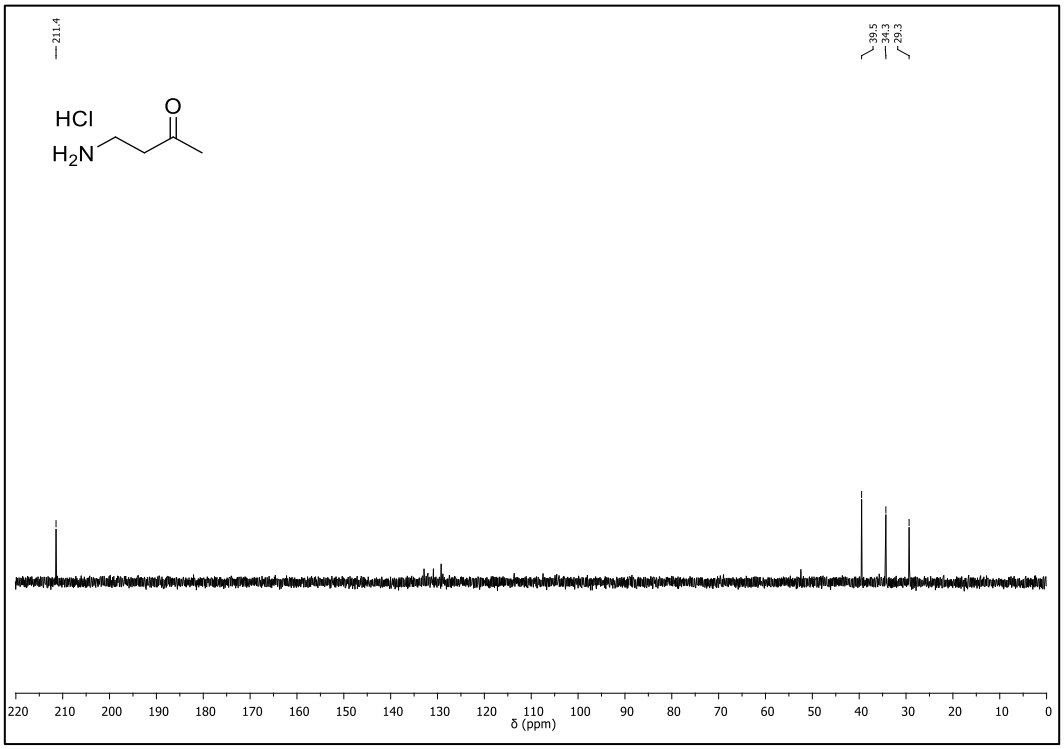

^{1}H-NMR (400 MHz, $CDCl_3$) of **9a**

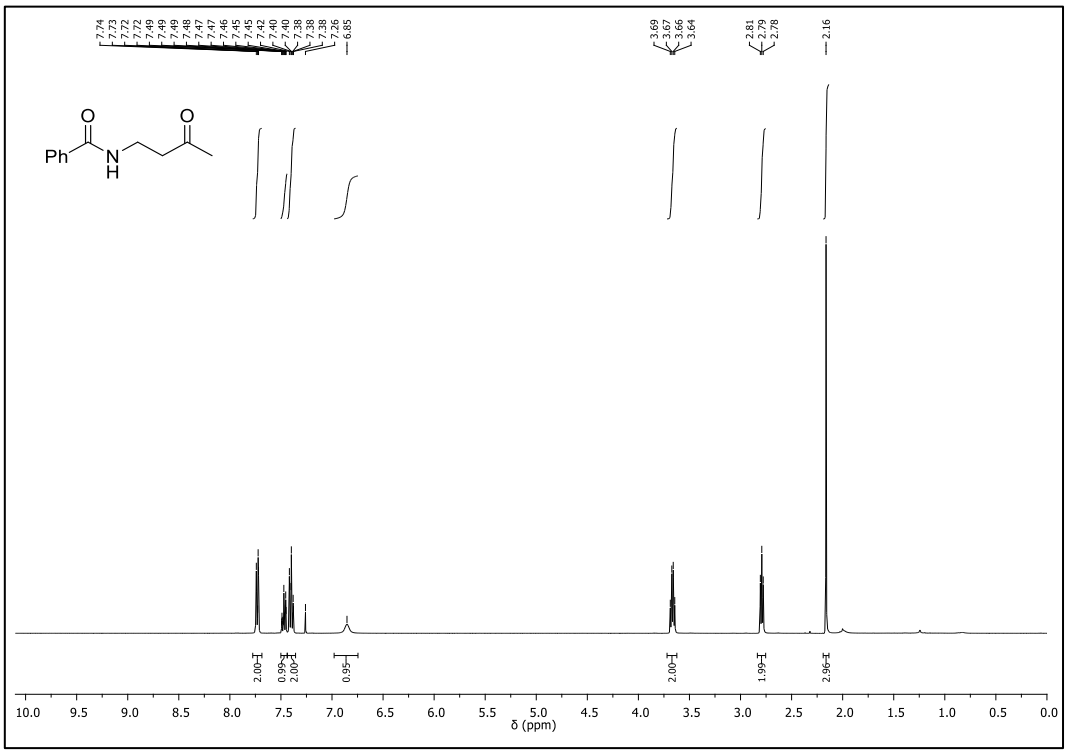

^{13}C-NMR (101 MHz, $CDCl_3$) of **9a**

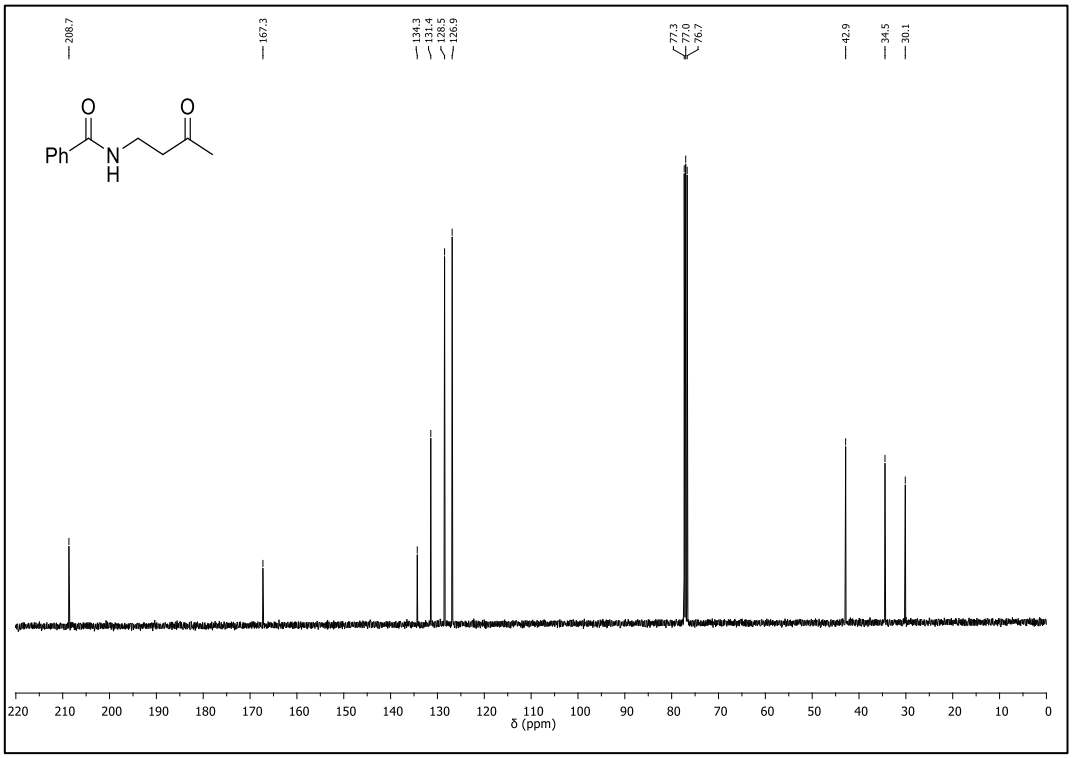

^{1}H-NMR (400 MHz, $CDCl_3$) of **10a**

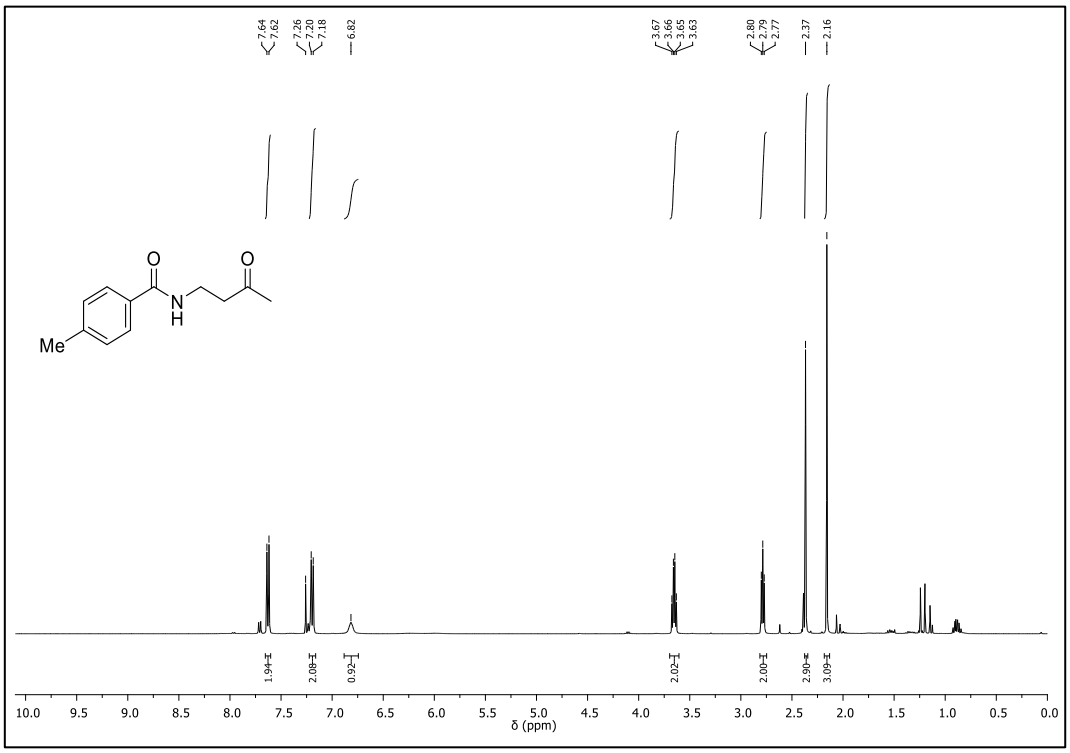

^{13}C-NMR (101 MHz, $CDCl_3$) of **10a**

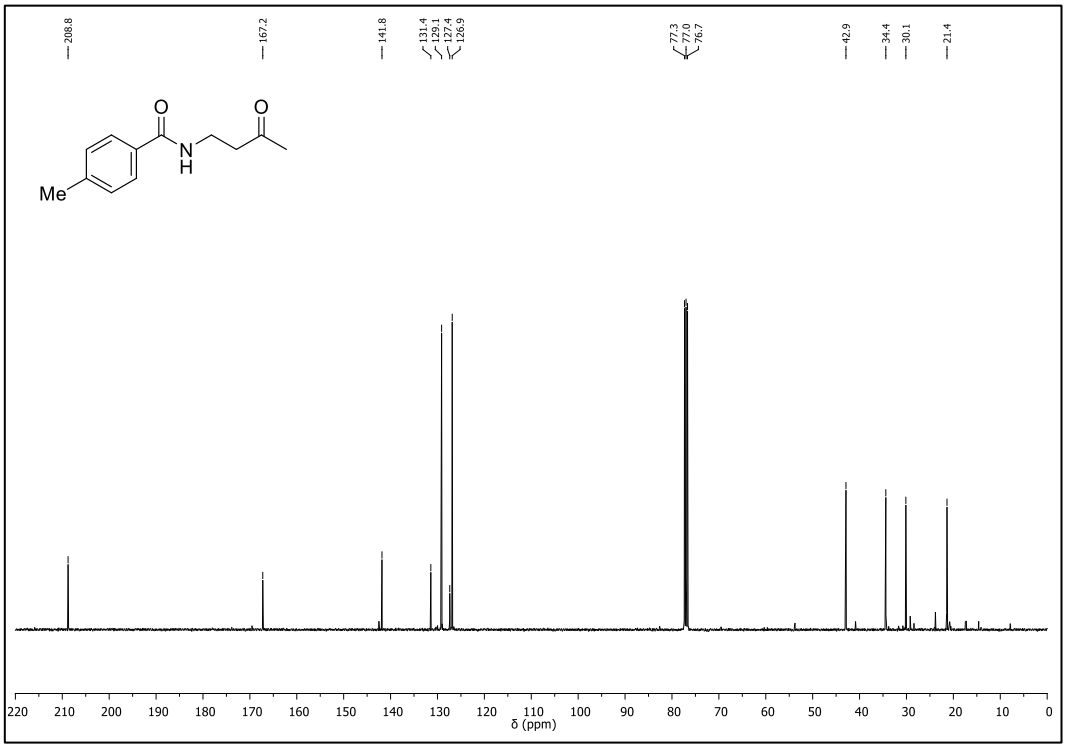

^{1}H-NMR (400 MHz, $CDCl_3$) of **11a**

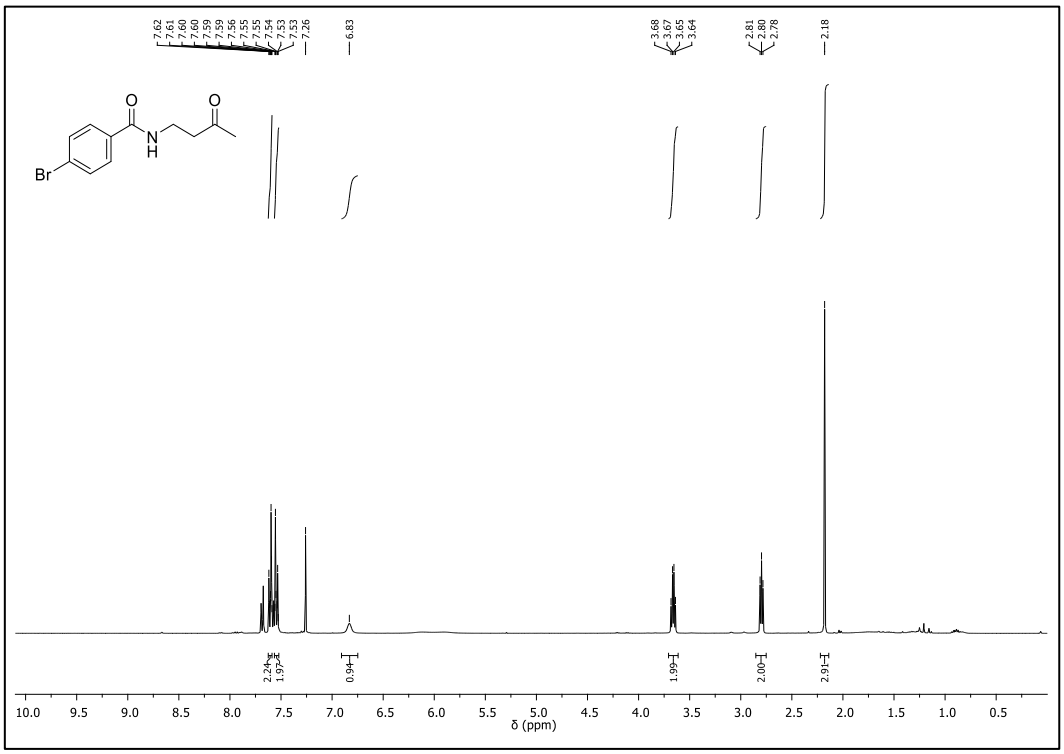

^{13}C-NMR (101 MHz, $CDCl_3$) of **11a**

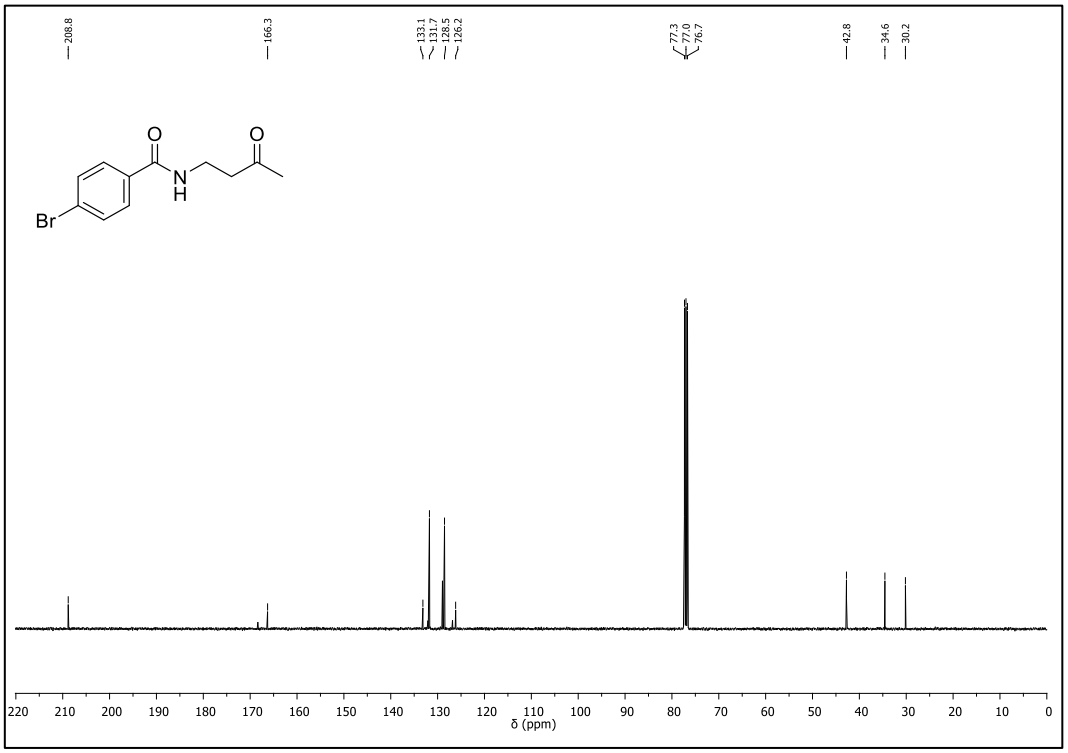

^{1}H-NMR (400 MHz, $CDCl_3$) of **12a**

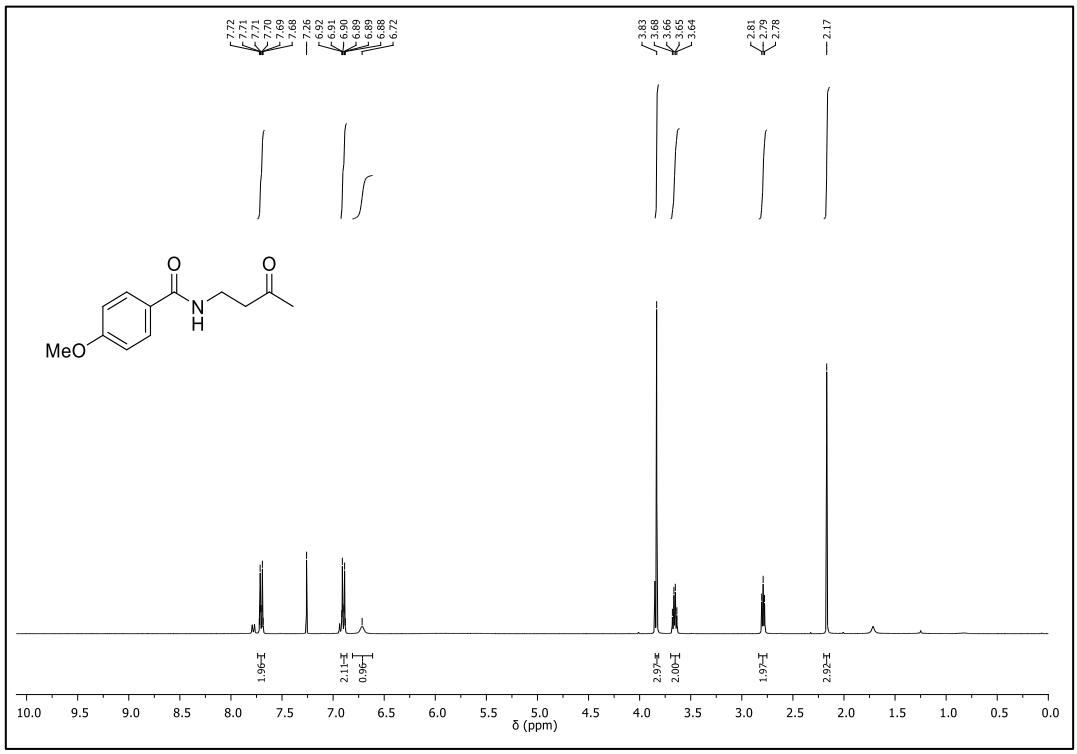

^{13}C-NMR (101 MHz, $CDCl_3$) of **12a**

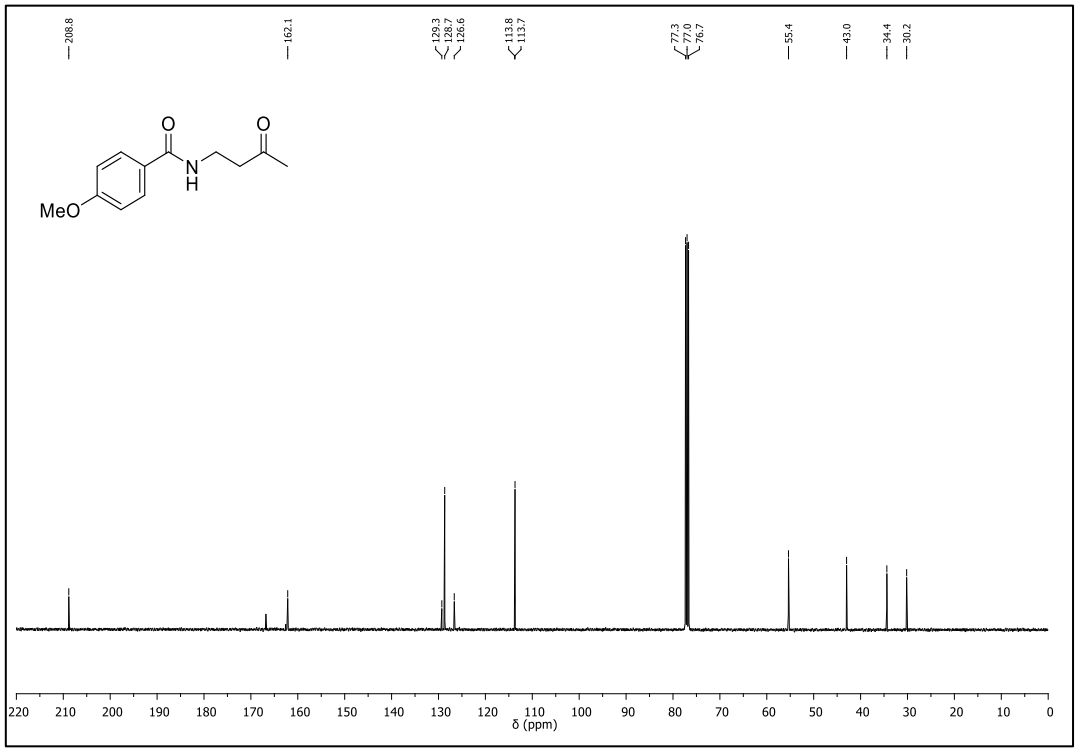

^{1}H-NMR (400 MHz, $CDCl_3$) of **13a**

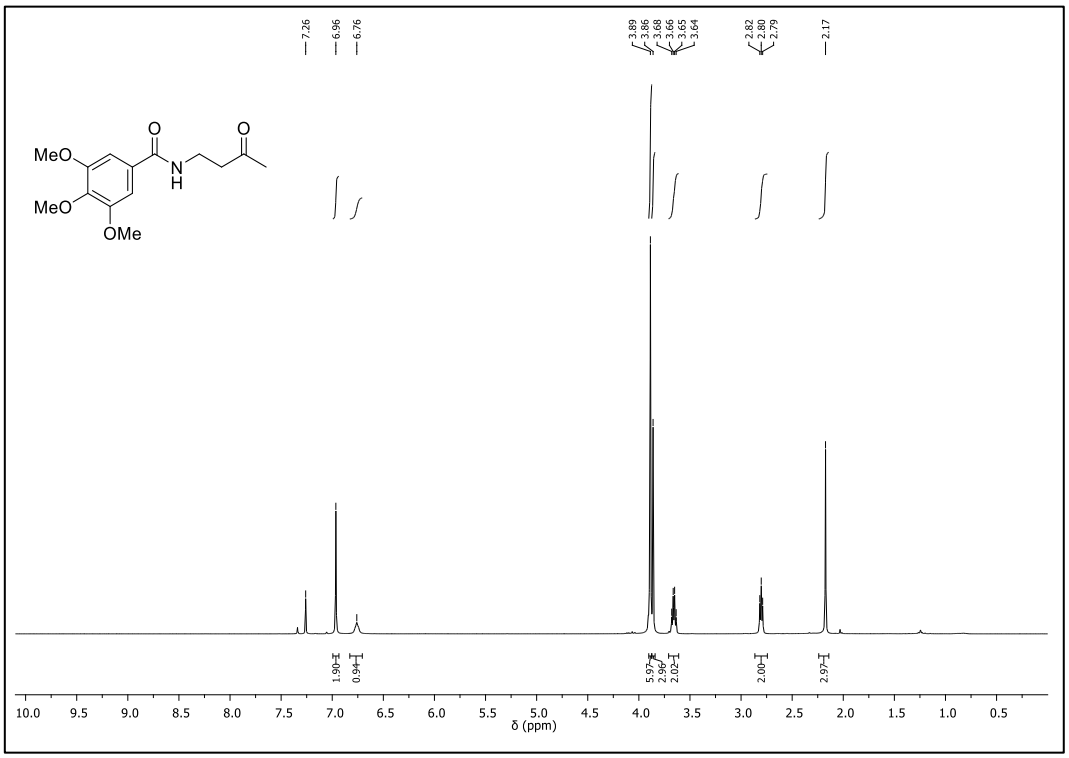

^{13}C-NMR (101 MHz, $CDCl_3$) of **13a**

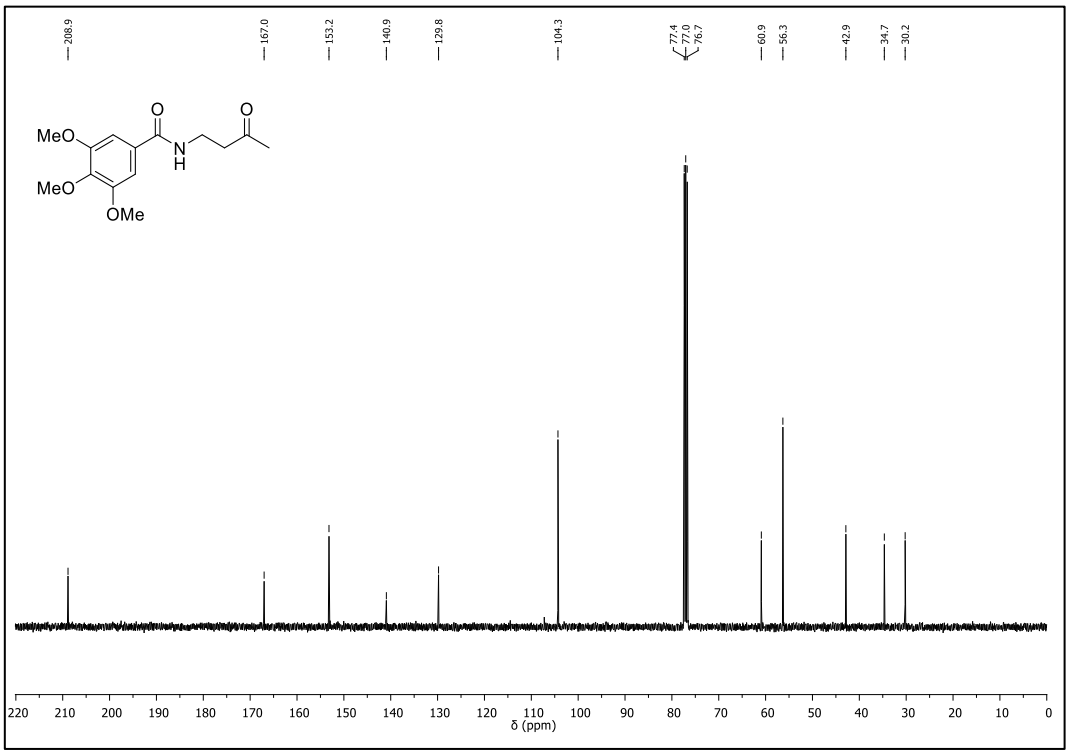

^{1}H-NMR (400 MHz, $CDCl_3$) of **14a**

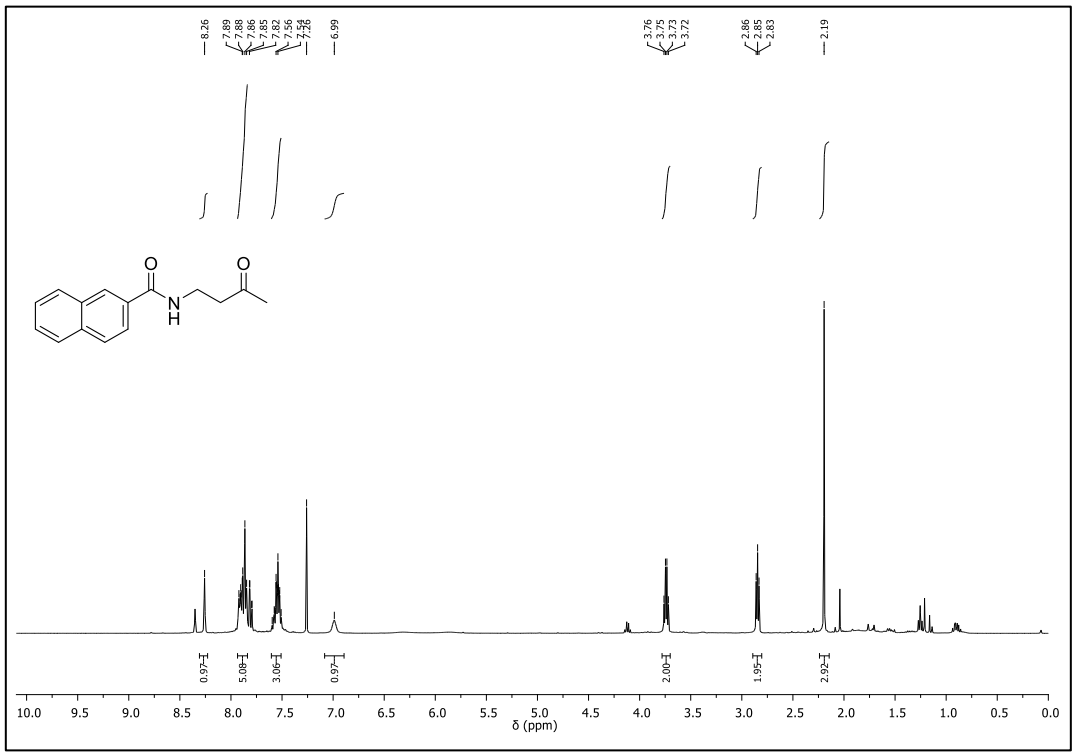

^{13}C-NMR (101 MHz, $CDCl_3$) of **14a**

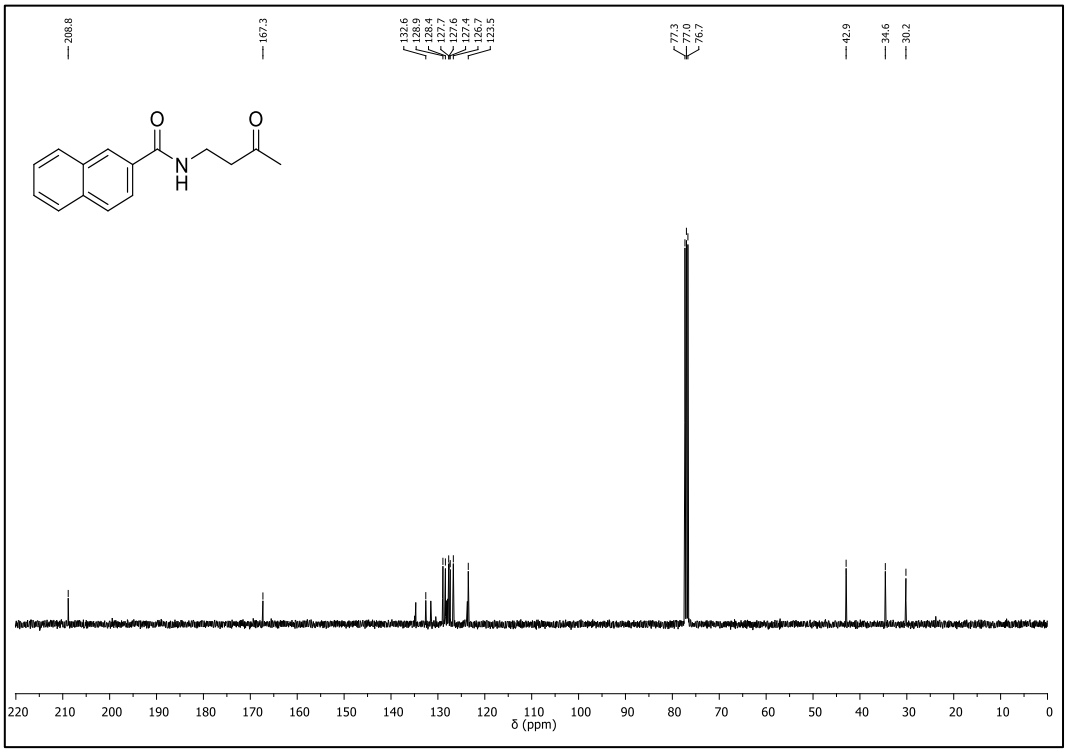

^{1}H-NMR (400 MHz, $CDCl_3$) of **15a**

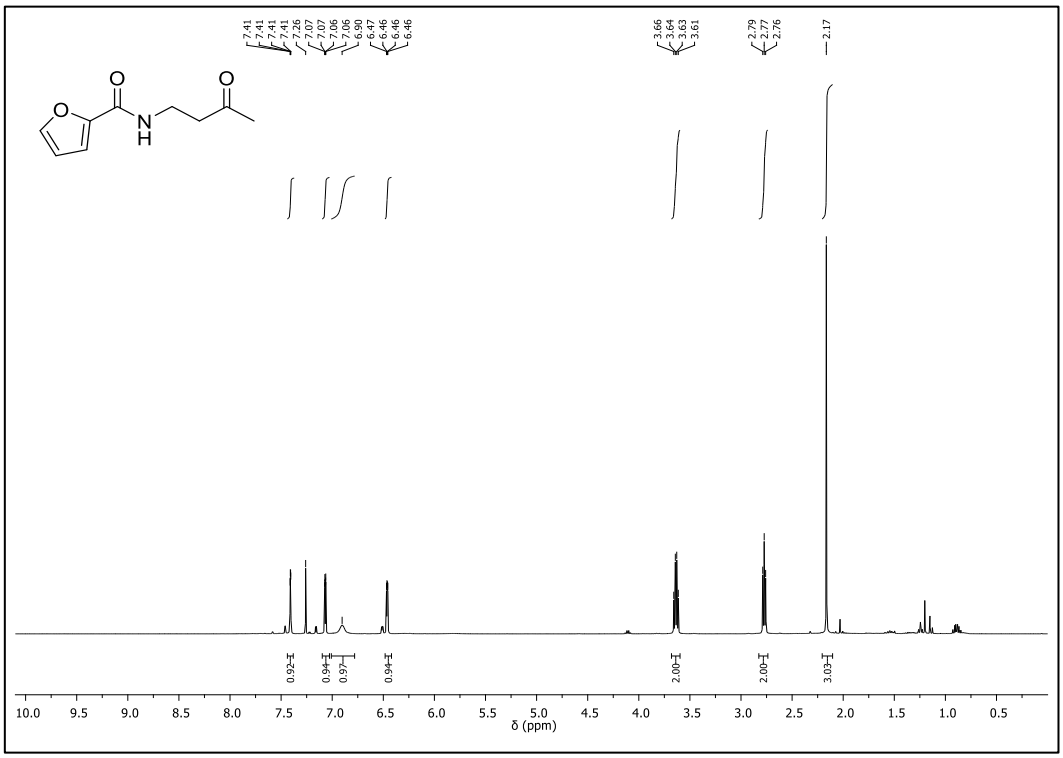

^{13}C-NMR (101 MHz, $CDCl_3$) of **15a**

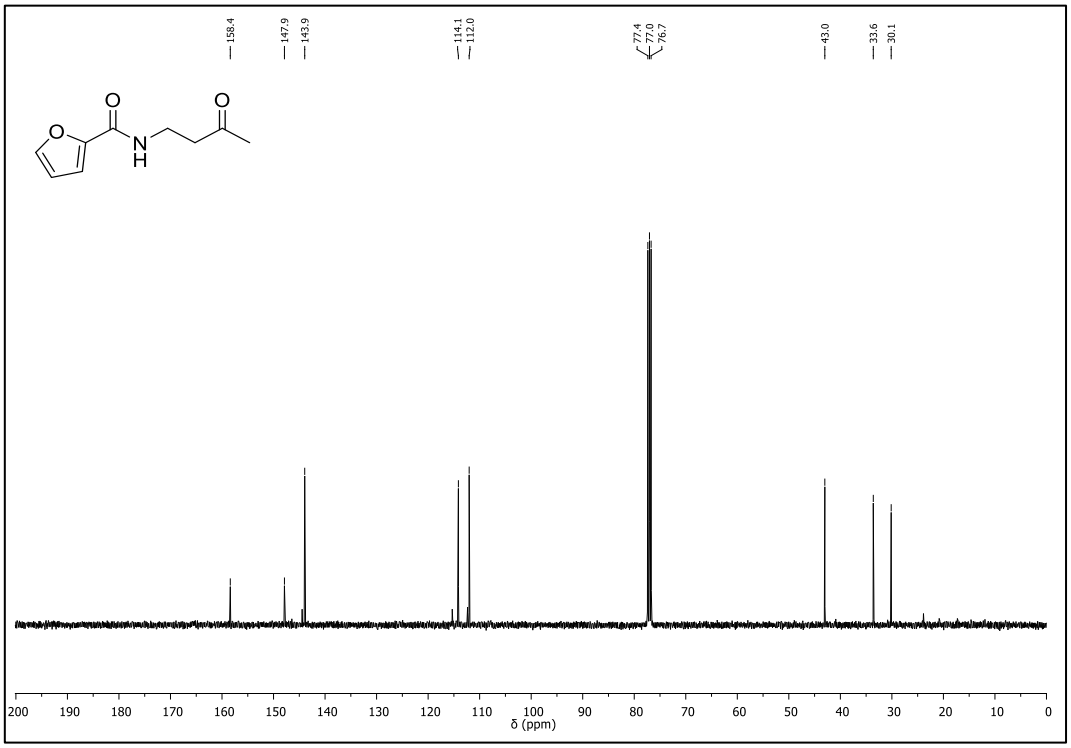

^{1}H-NMR (400 MHz, $CDCl_3$) of **16a**

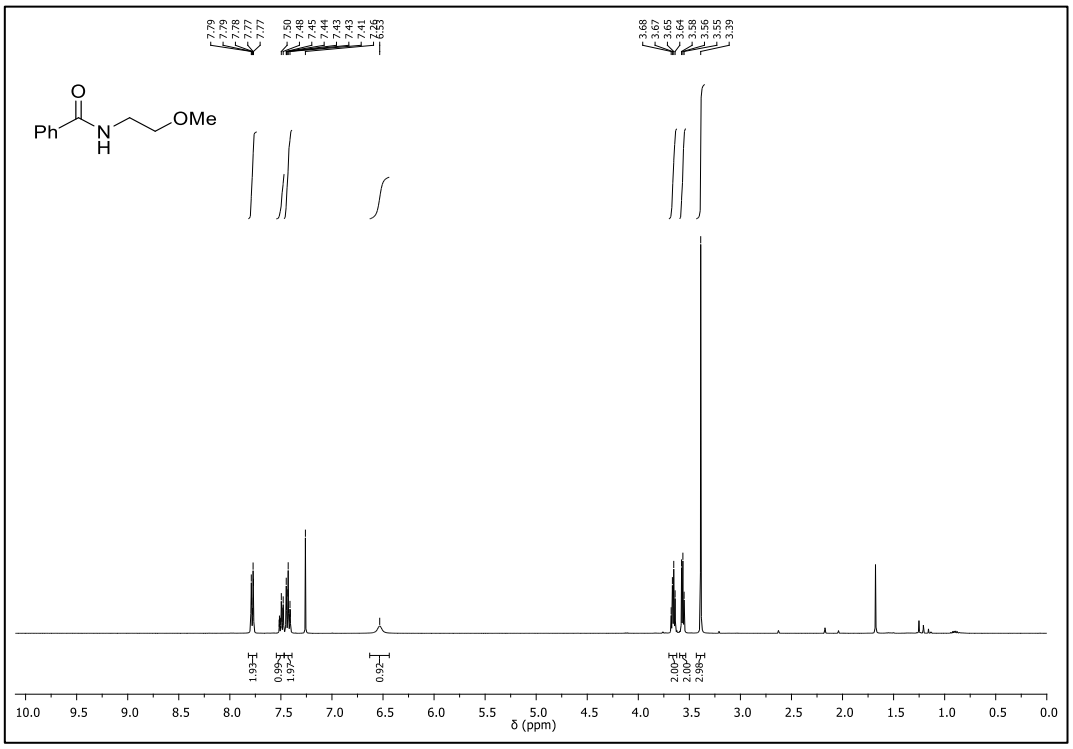

^{13}C-NMR (101 MHz, $CDCl_3$) of **16a**

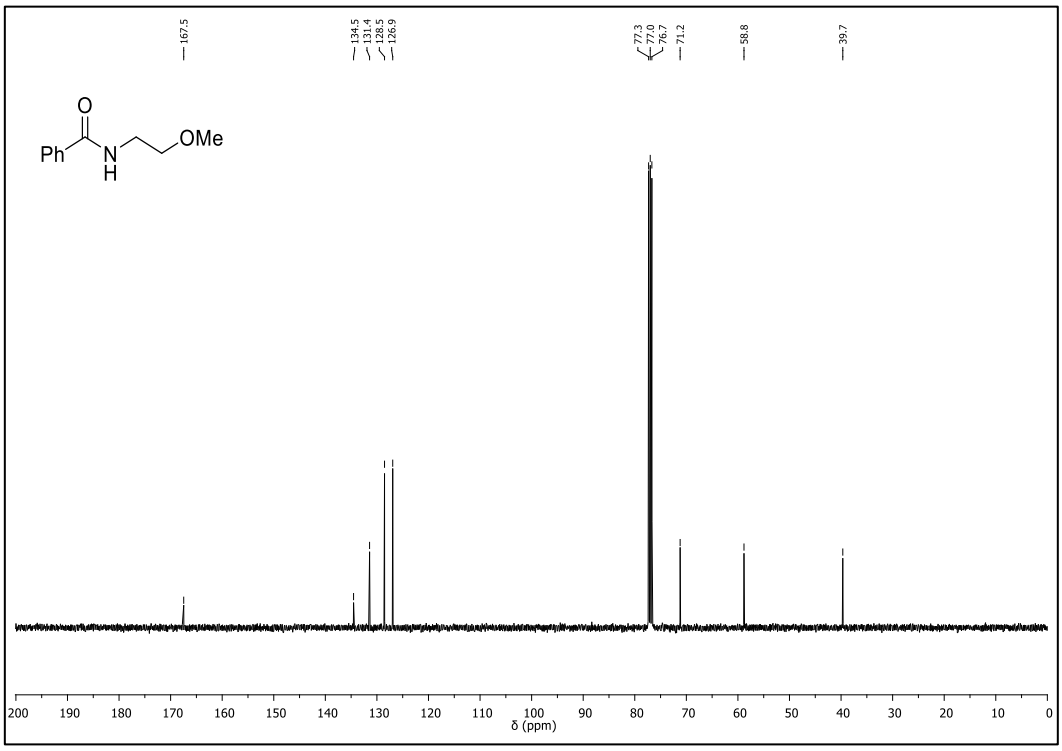

^{1}H-NMR (400 MHz, $CDCl_3$) of **17a**

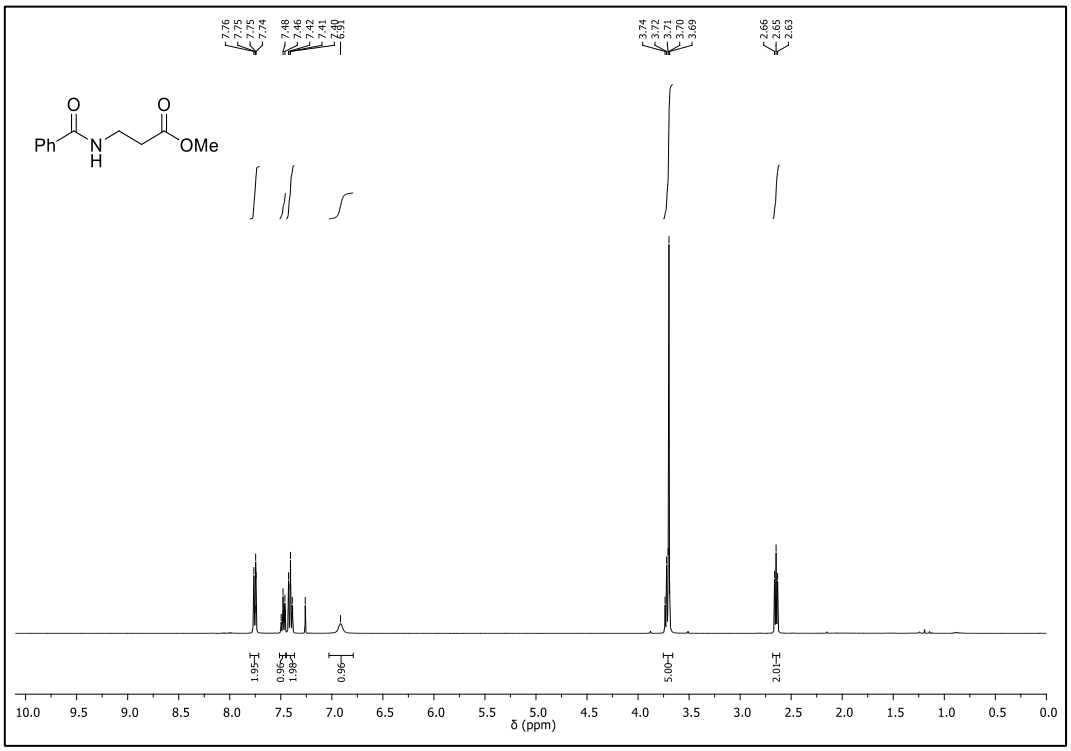

^{13}C-NMR (101 MHz, $CDCl_3$) of **17a**

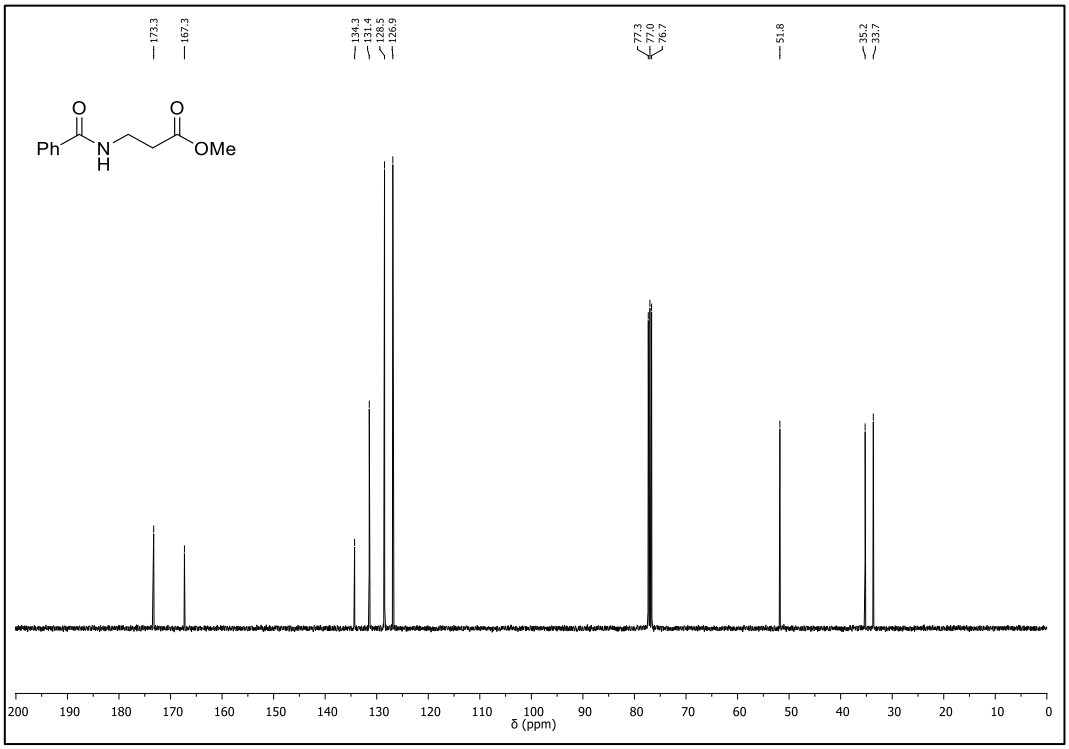

^{1}H-NMR (400 MHz, $CDCl_3$) of **18a**

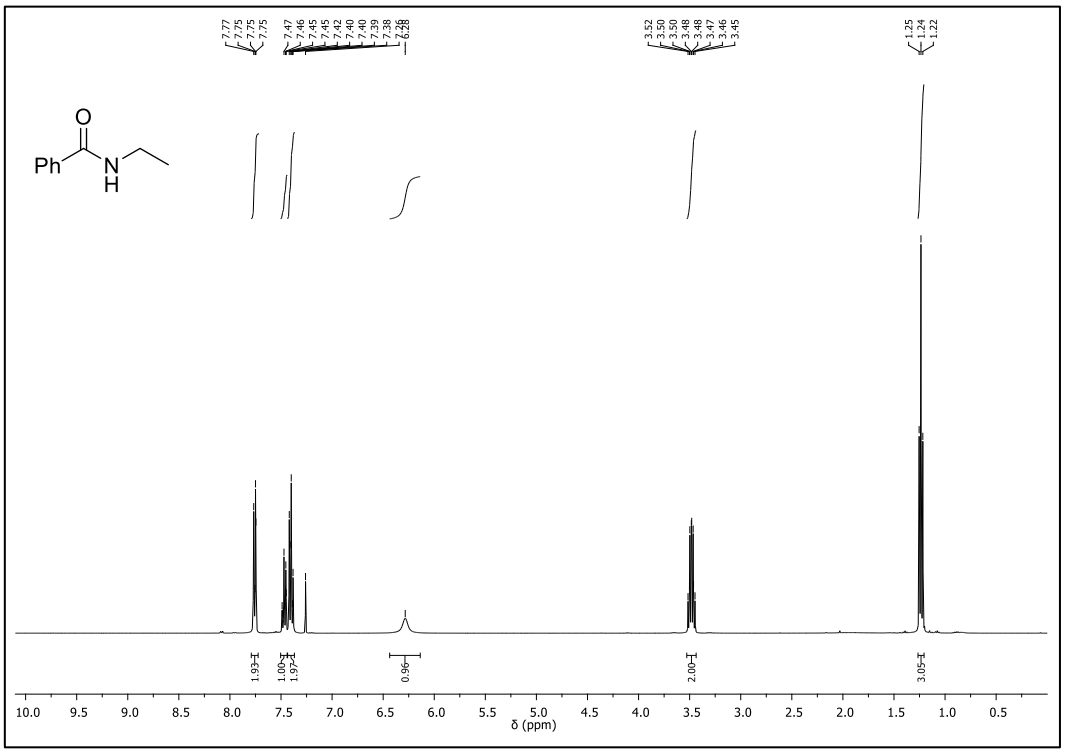

^{13}C-NMR (101 MHz, $CDCl_3$) of **18a**

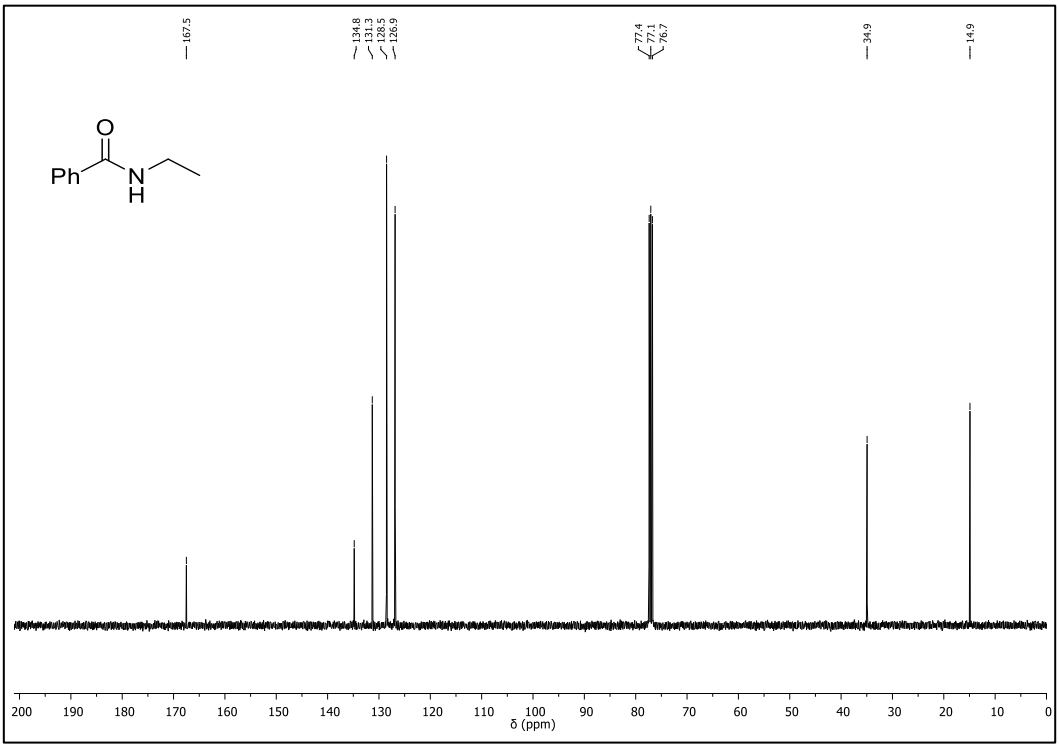

^{1}H-NMR (400 MHz, $CDCl_3$) of **19a**

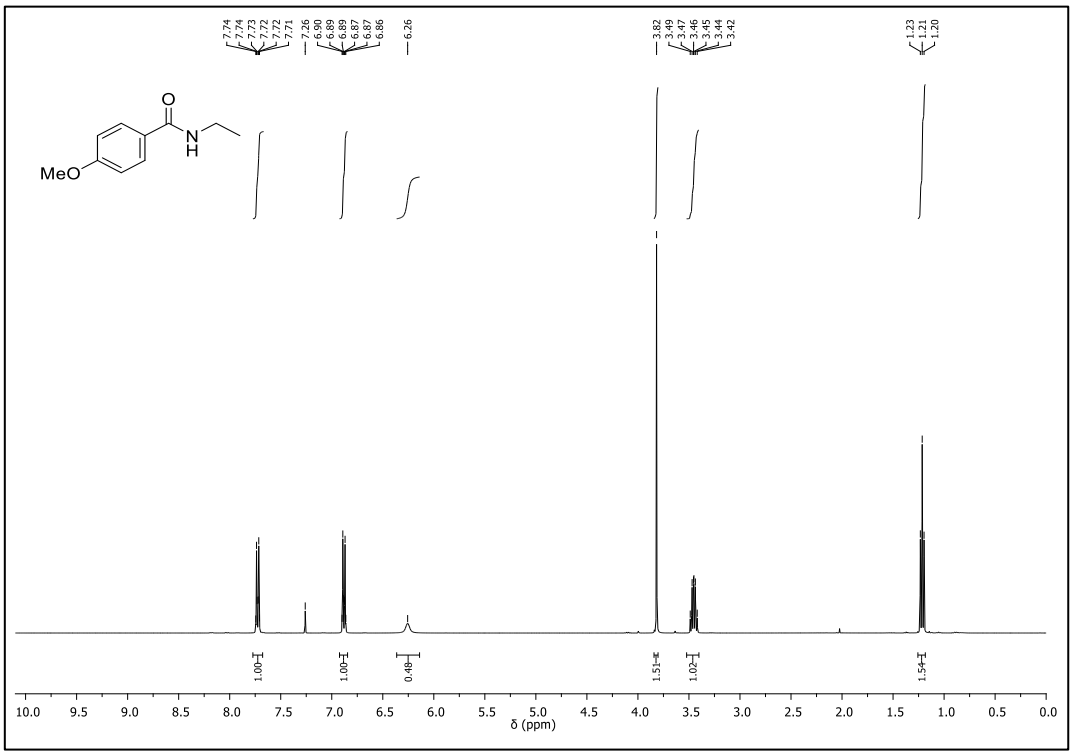

^{13}C-NMR (101 MHz, $CDCl_3$) of **19a**

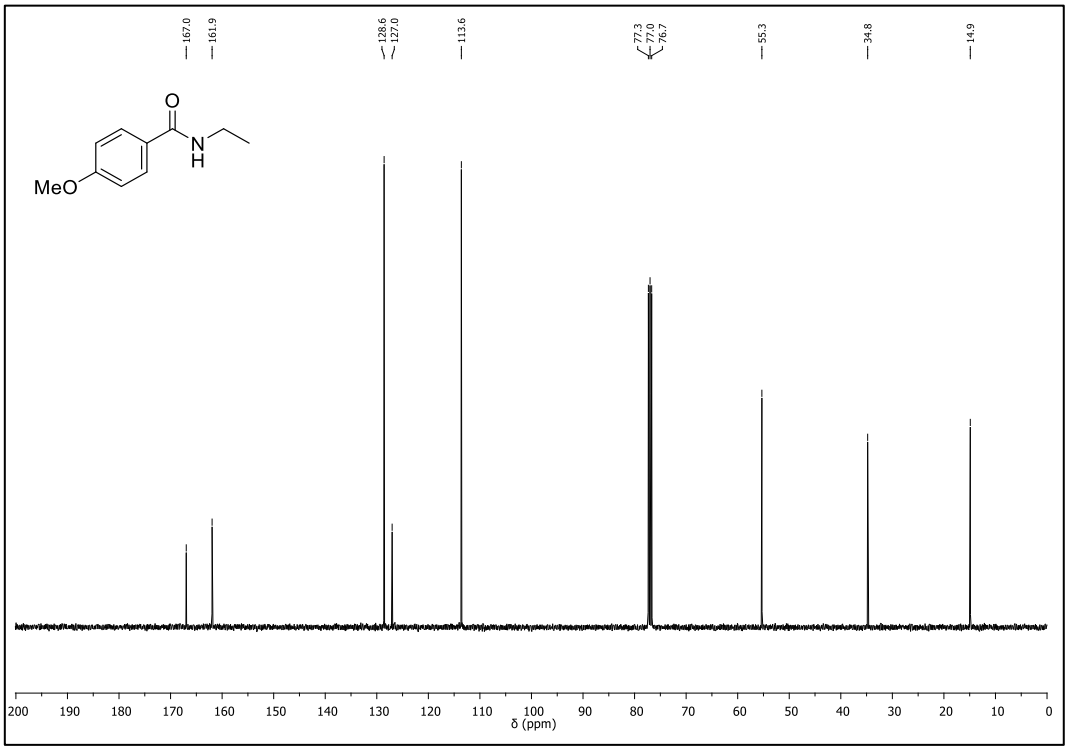

^{1}H-NMR (400 MHz, $CDCl_3$) of **20a**

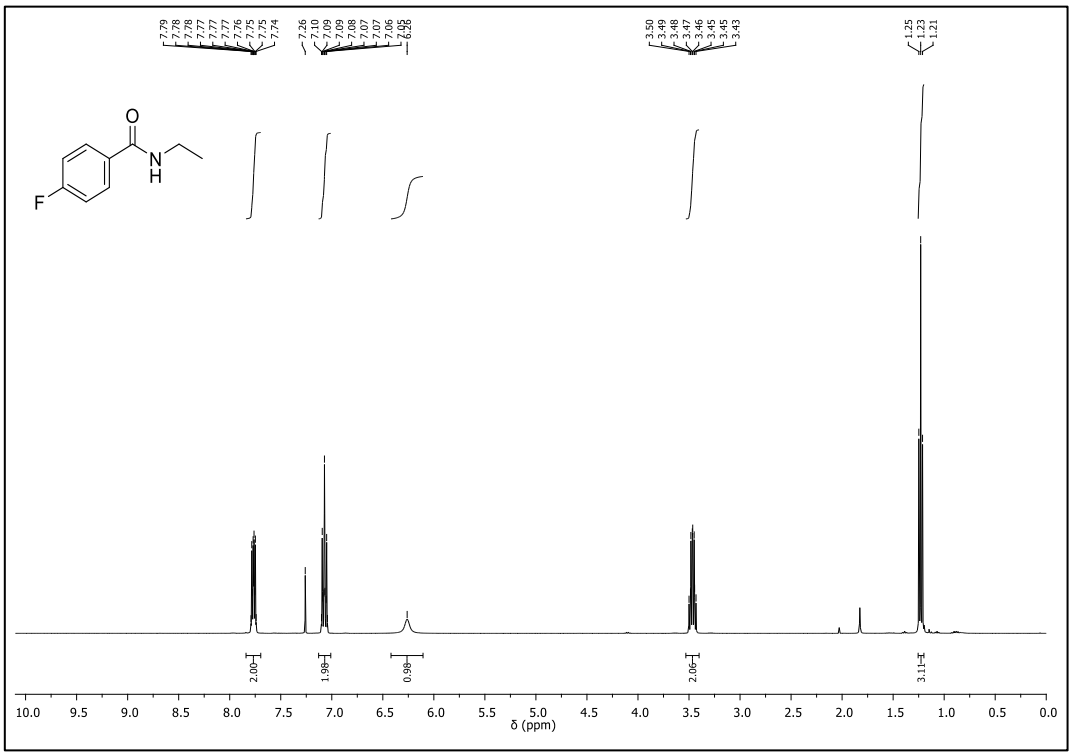

^{13}C-NMR (101 MHz, $CDCl_3$) of **20a**

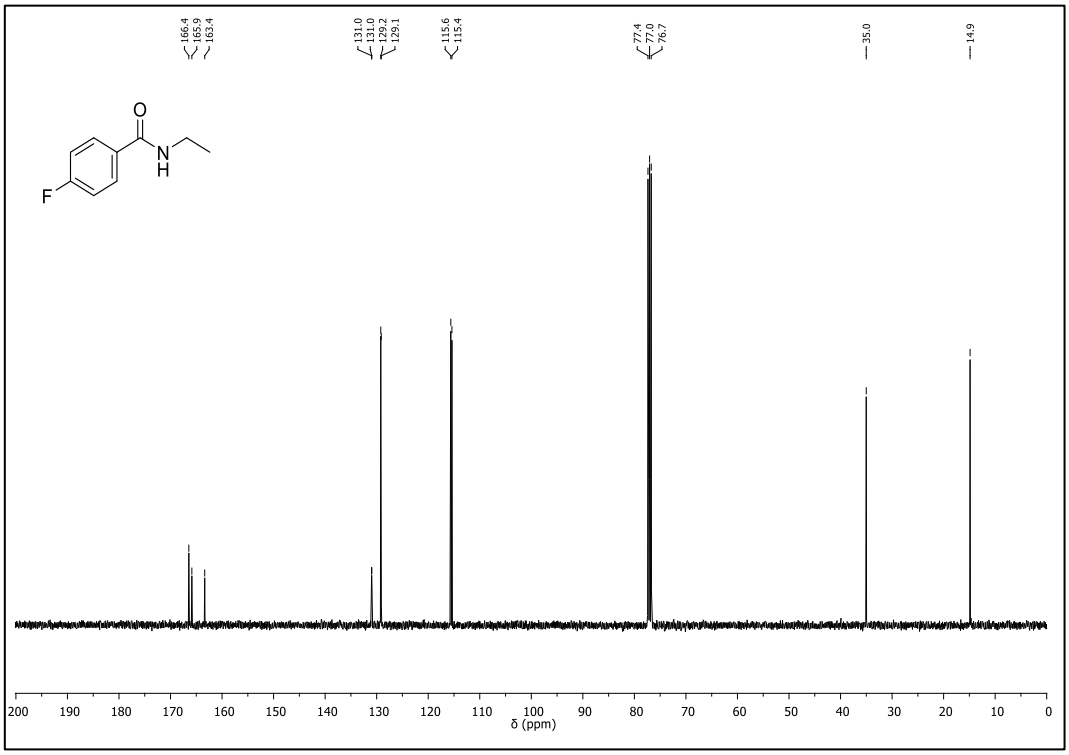

^{19}F-NMR (377 MHz, $CDCl_3$) of **20a**

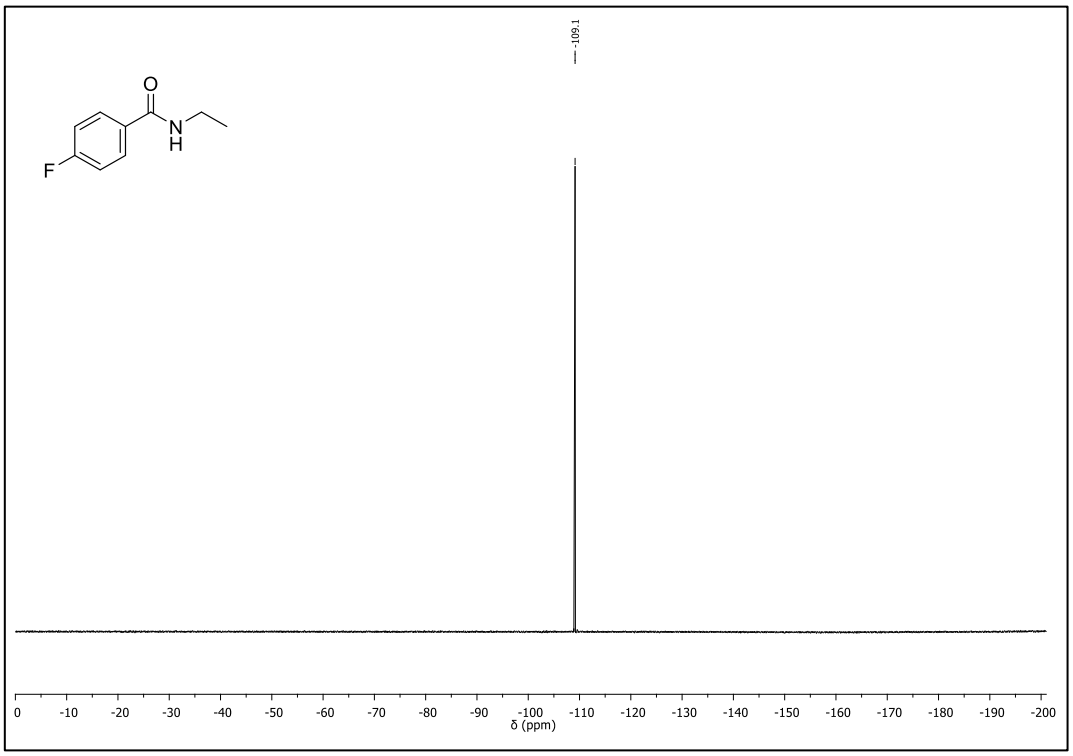

^{1}H-NMR (400 MHz, $CDCl_3$) of **21a**

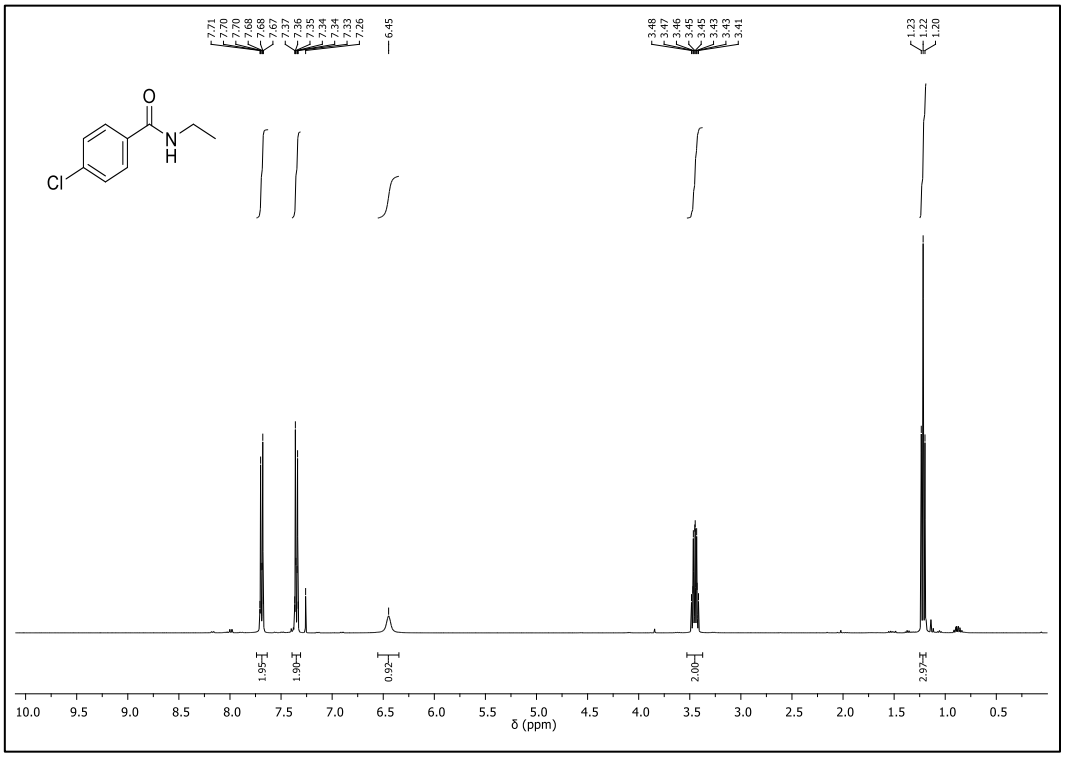

^{13}C-NMR (101 MHz, $CDCl_3$) of **21a**

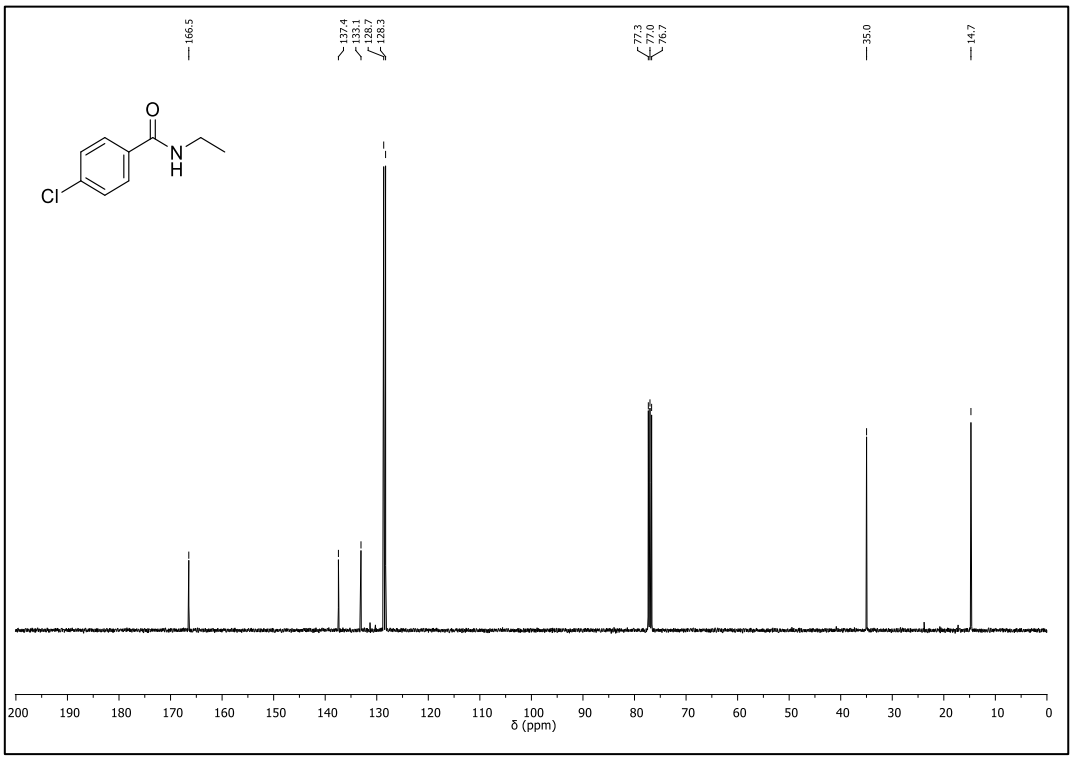

^{1}H-NMR (400 MHz, $CDCl_3$) of **22a**

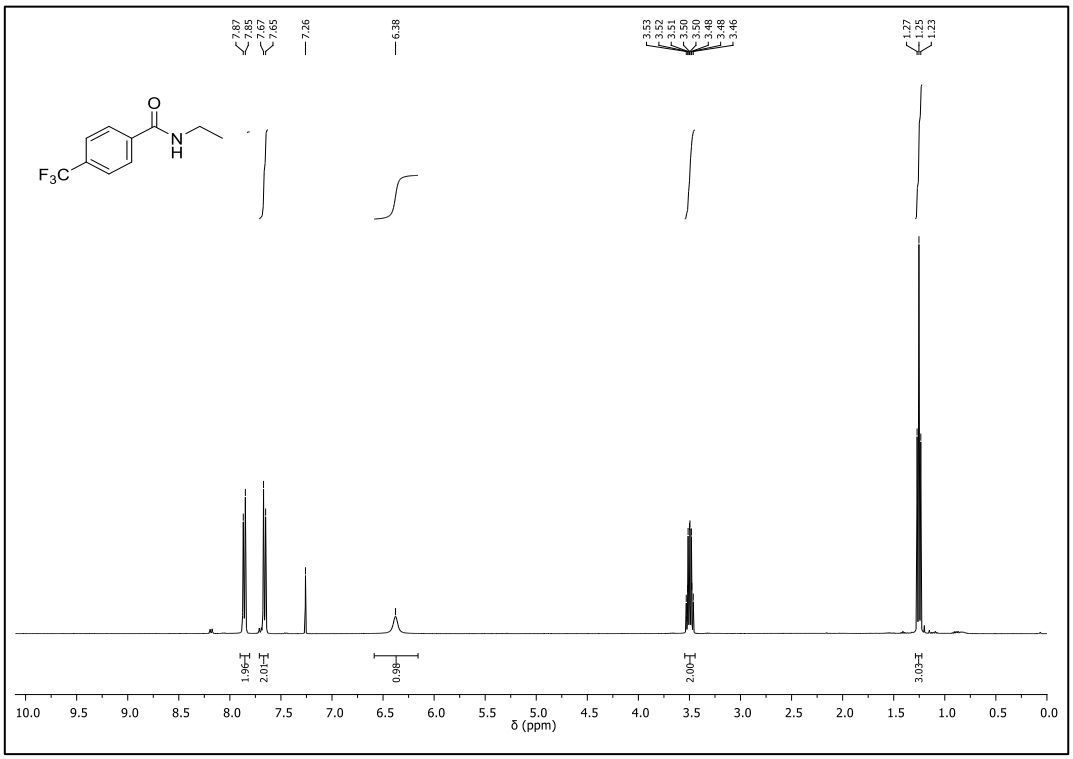

^{13}C-NMR (101 MHz, $CDCl_3$) of **22a**

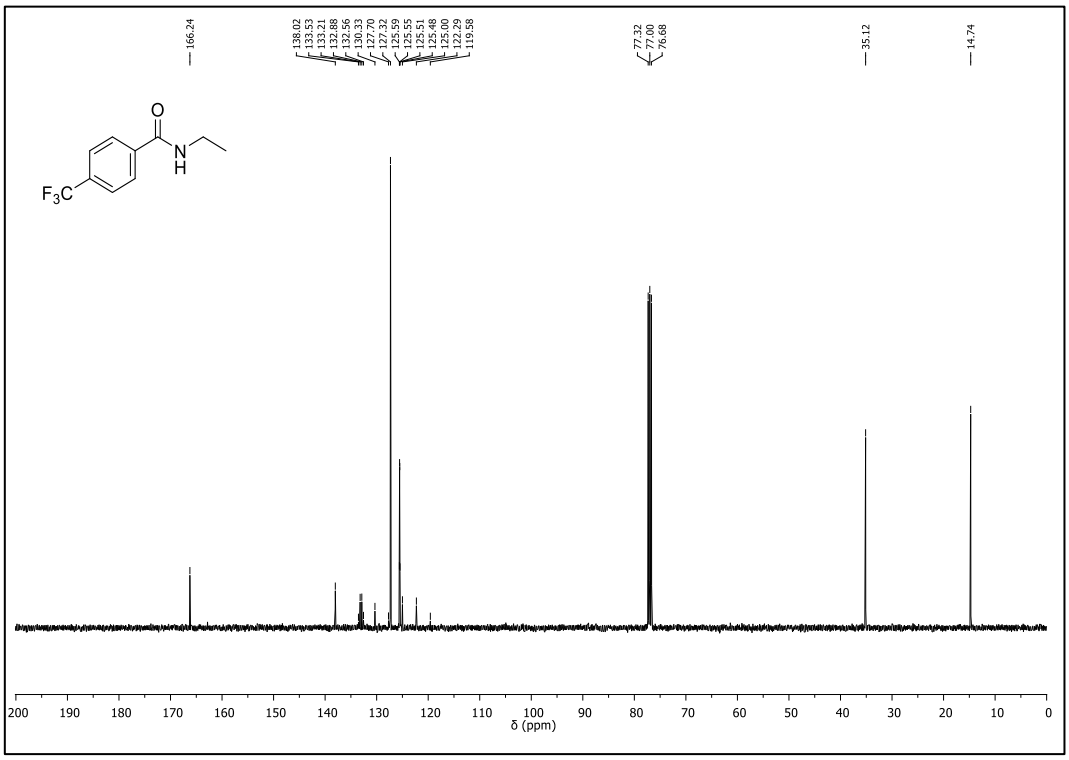

^{19}F-NMR (377 MHz, $CDCl_3$) of **22a**

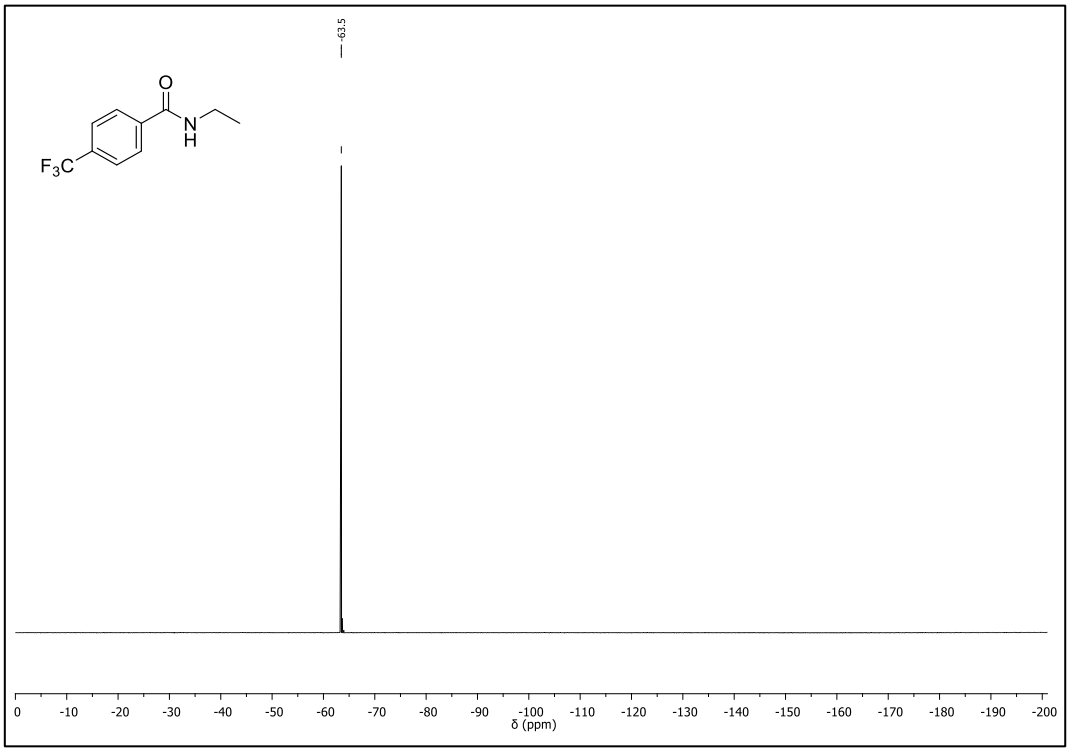

^{1}H-NMR (400 MHz, $CDCl_3$) of **23a**

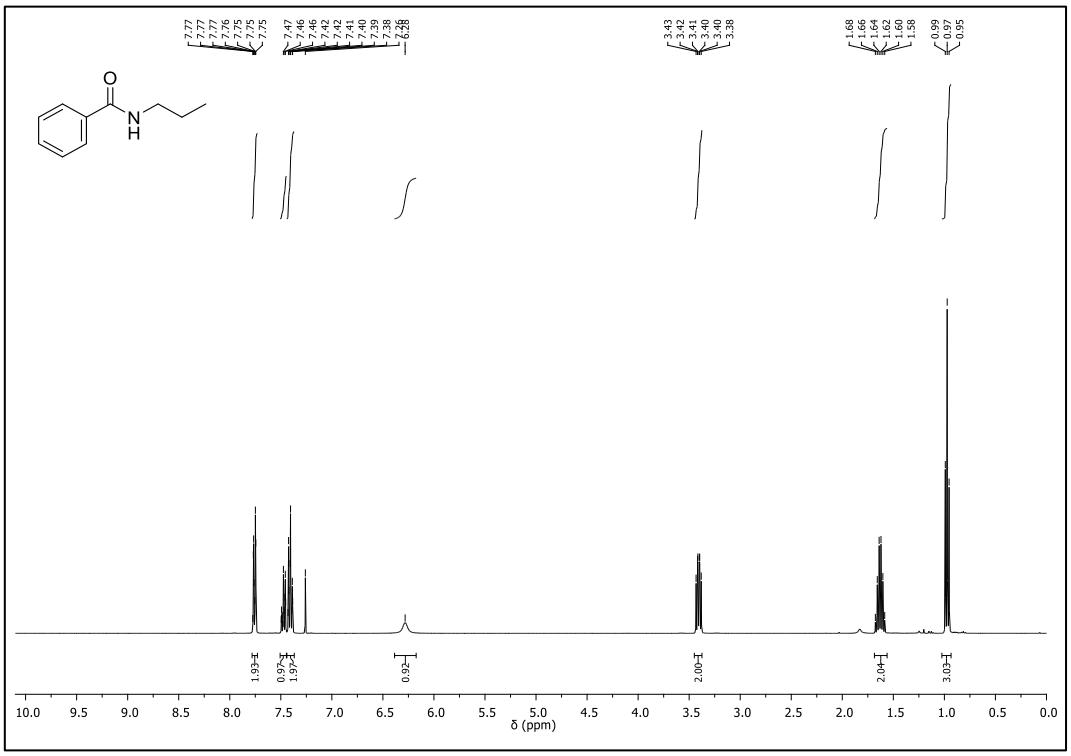

^{13}C-NMR (101 MHz, $CDCl_3$) of **23a**

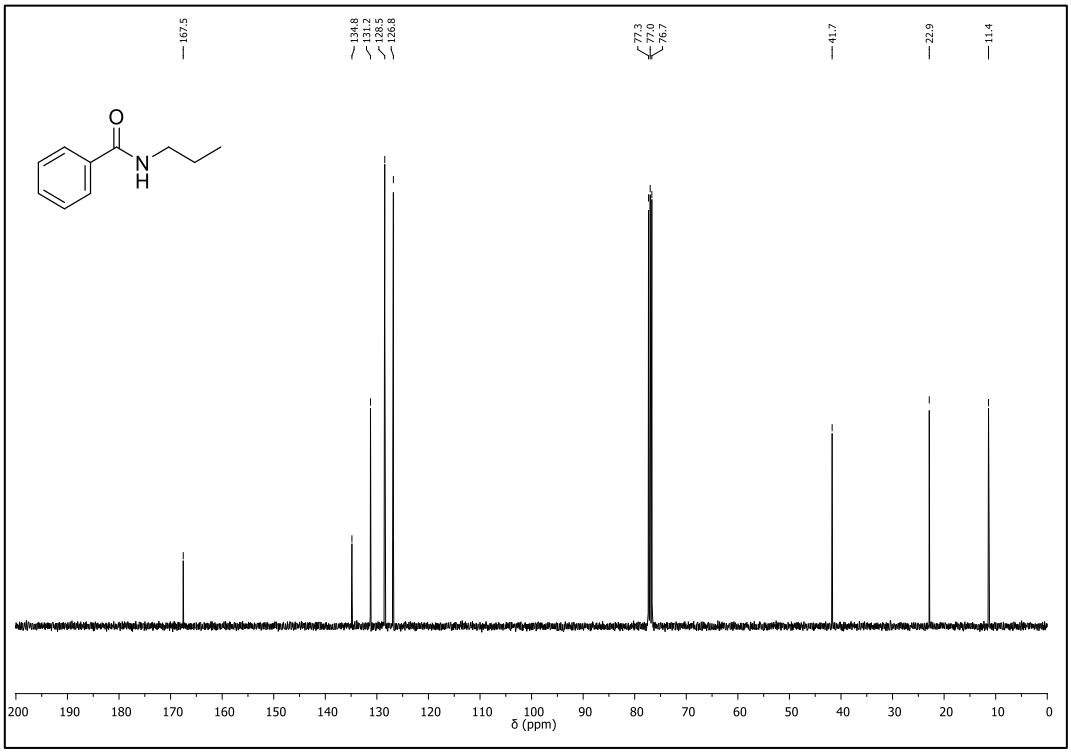

^{1}H-NMR (400 MHz, $CDCl_3$) of **24a**

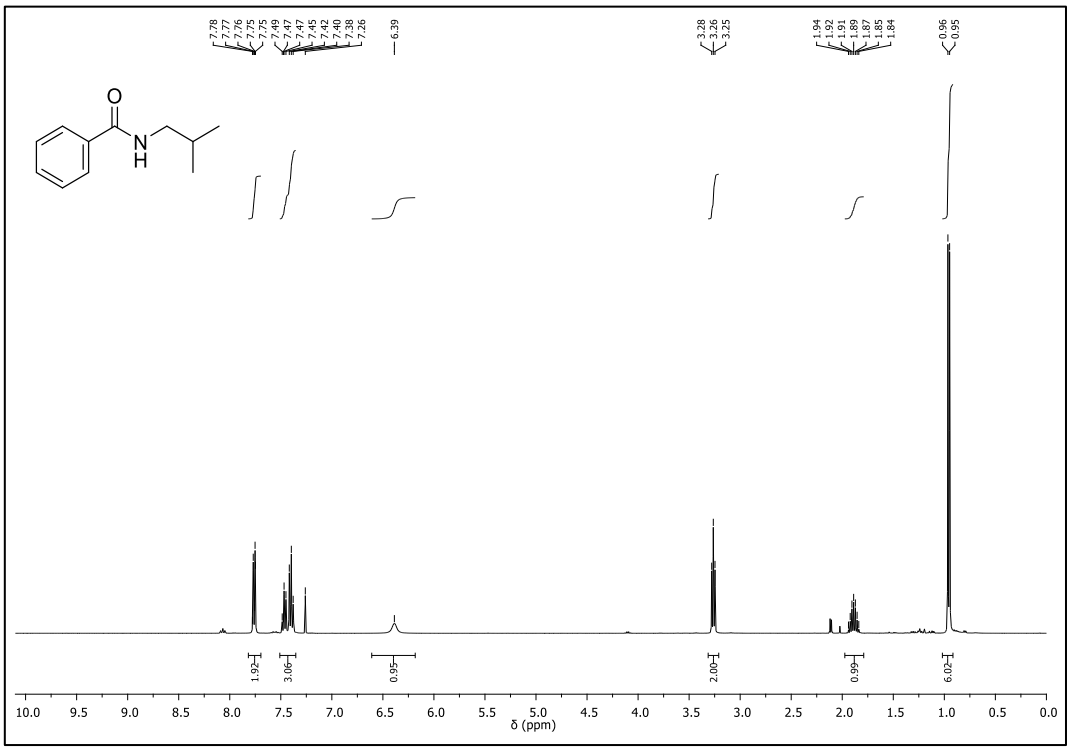

^{13}C-NMR (101 MHz, $CDCl_3$) of **24a**

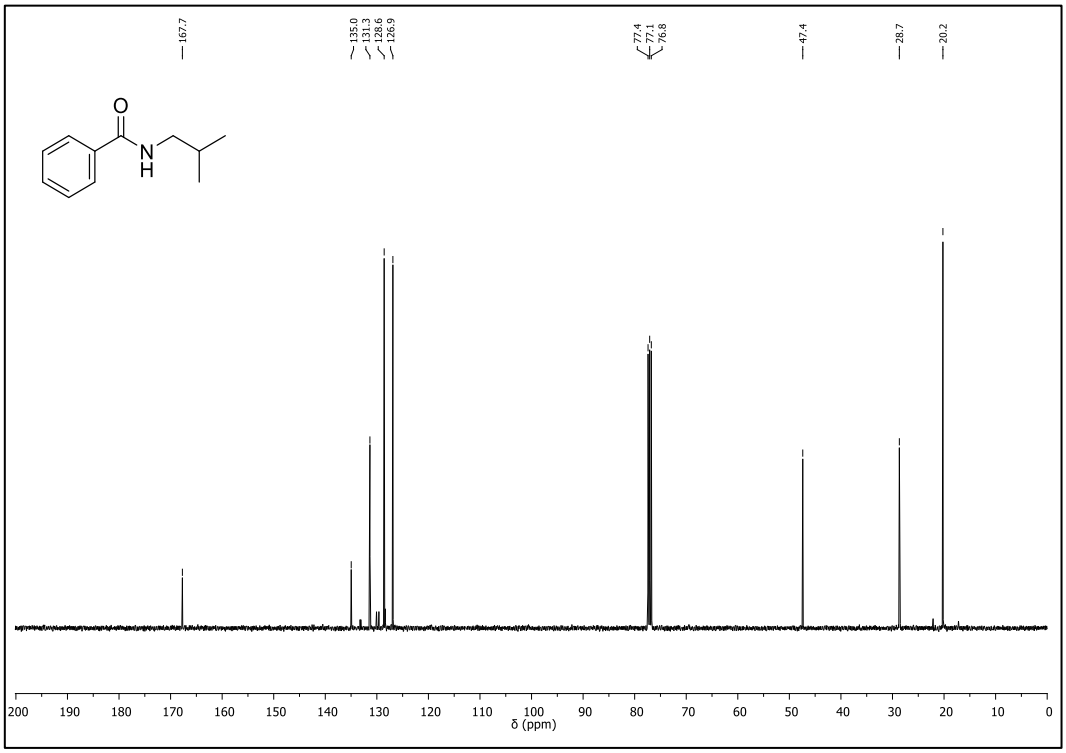

^{1}H-NMR (400 MHz, $CDCl_3$) of **25a**

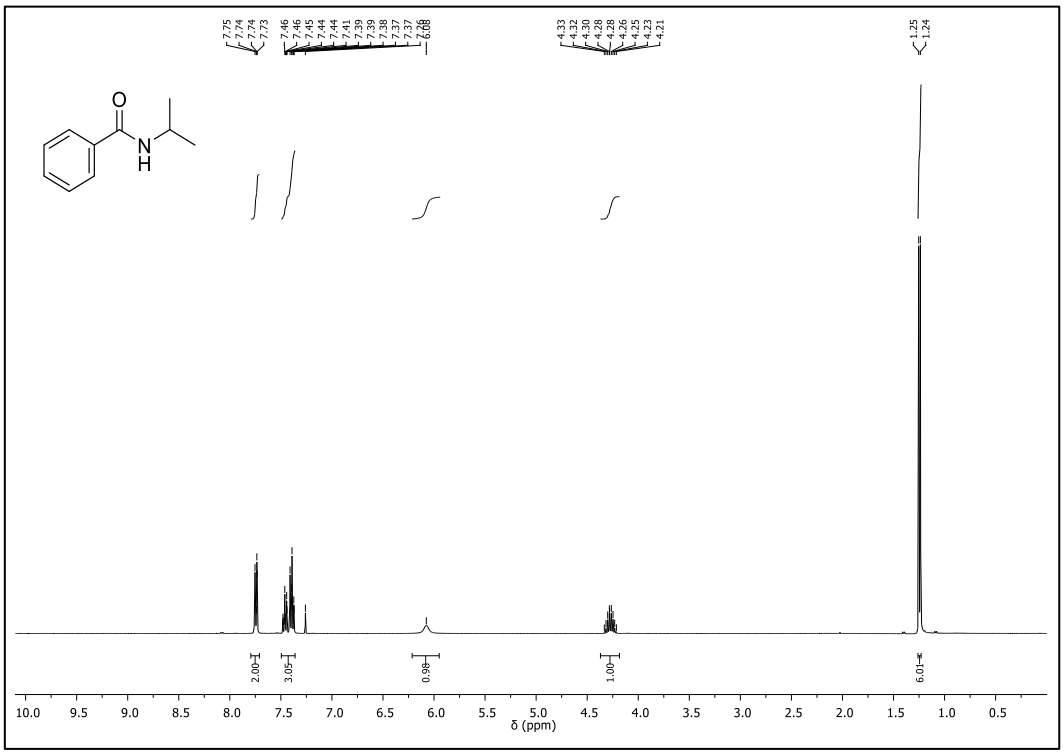

^{13}C-NMR (101 MHz, $CDCl_3$) of **25a**

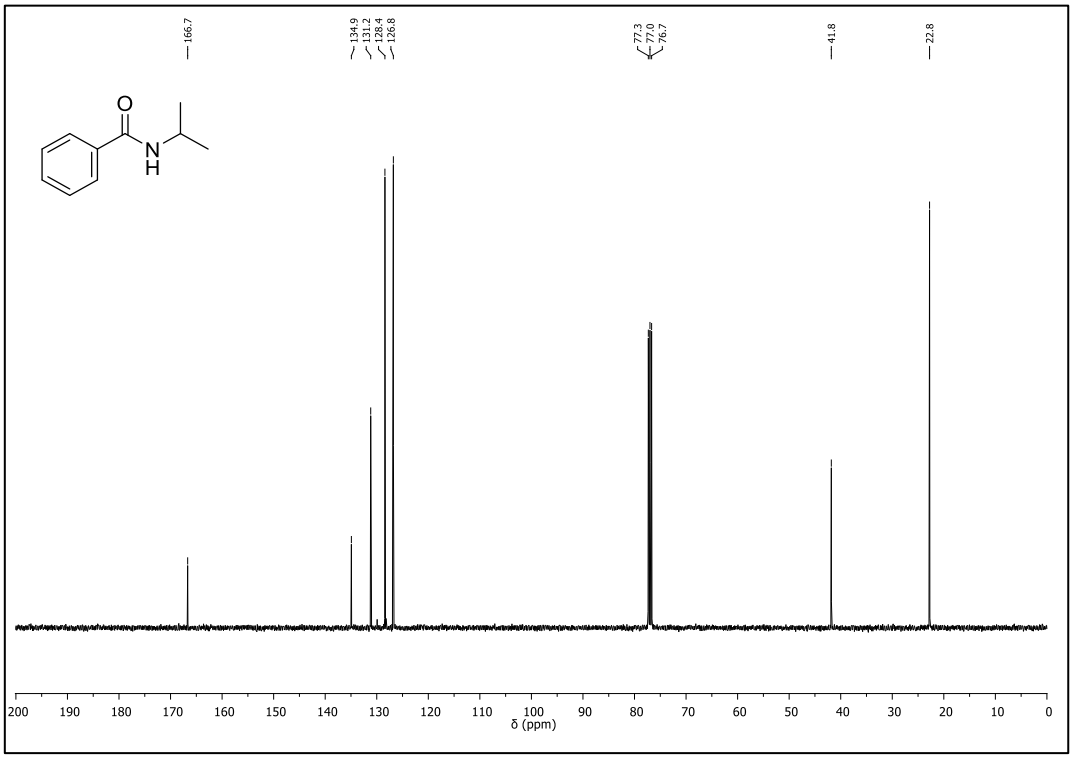

^{1}H-NMR (400 MHz, $CDCl_3$) of **26a**

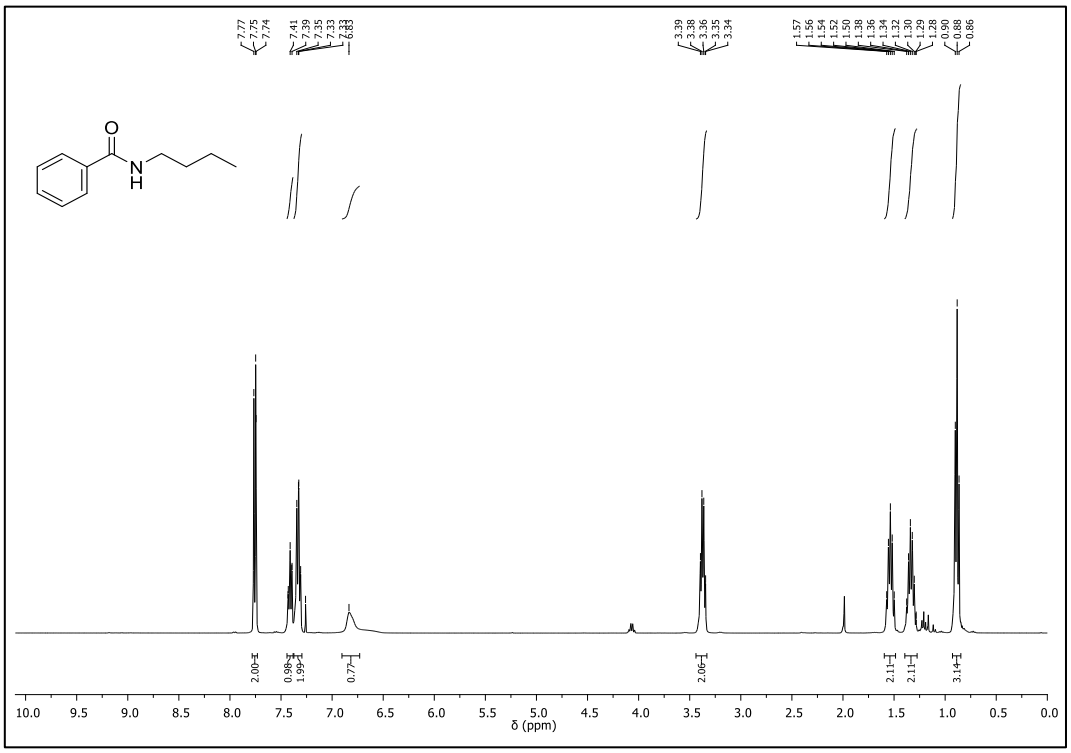

^{13}C-NMR (101 MHz, $CDCl_3$) of **26a**

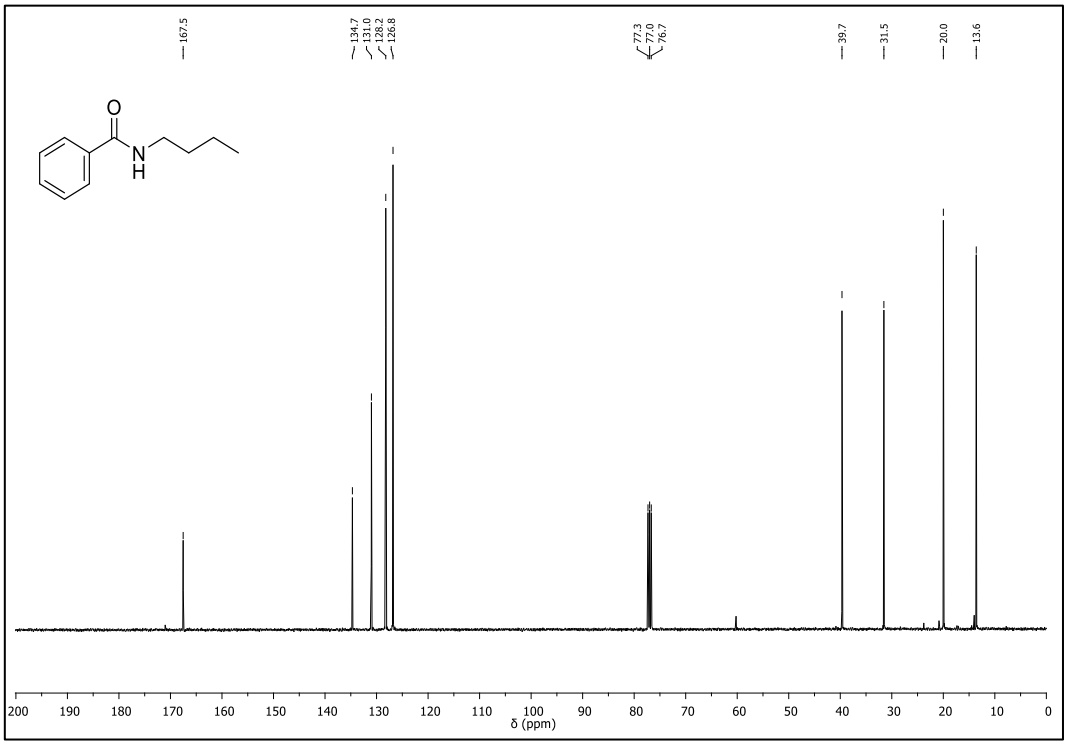

^{1}H-NMR (400 MHz, $CDCl_3$) of **27a**

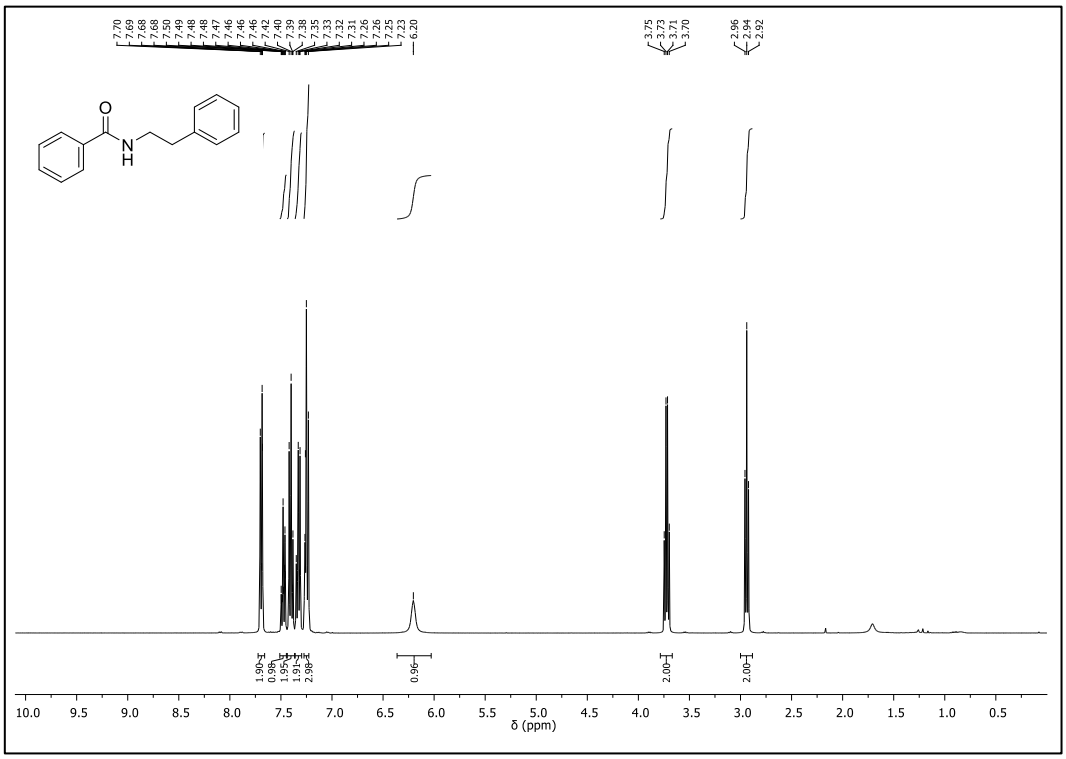

^{13}C-NMR (101 MHz, $CDCl_3$) of **27a**

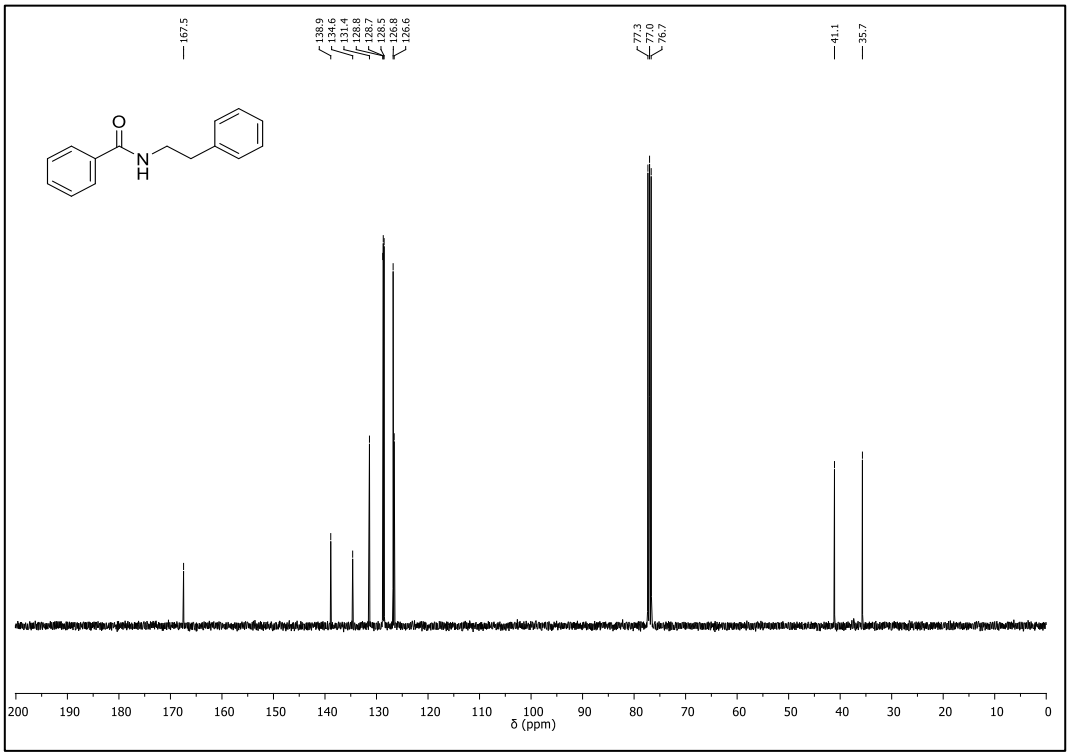

^{1}H-NMR (400 MHz, CD_2Cl_2) of **28a**

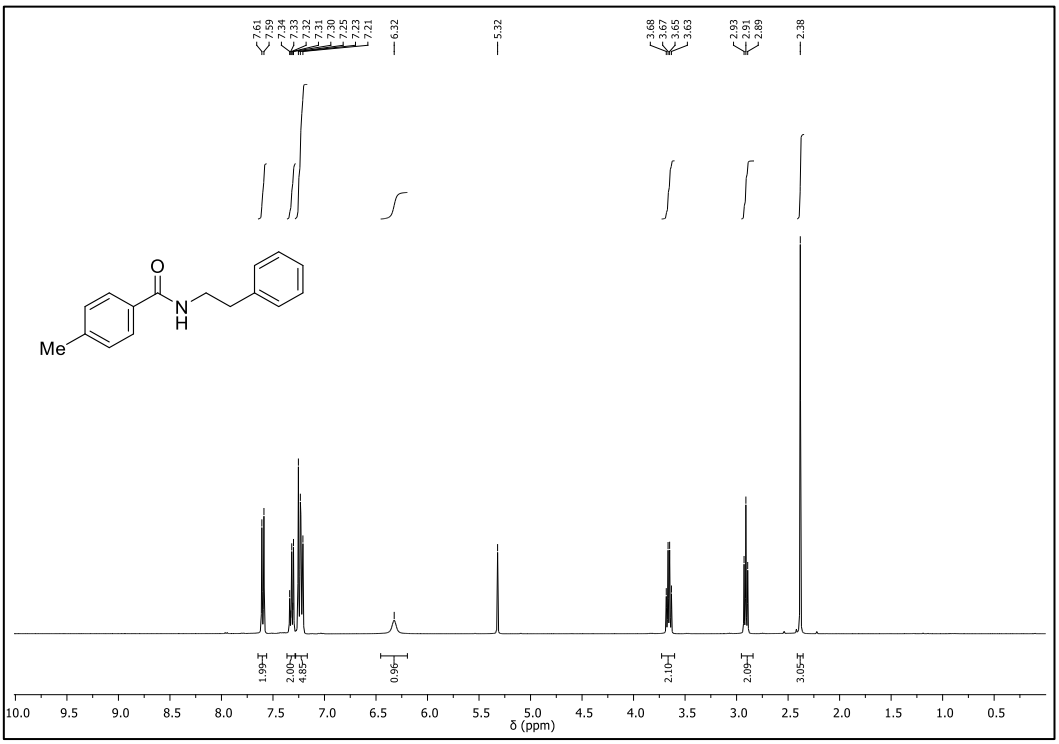

^{13}C-NMR (101 MHz, CD_2Cl_2) of **28a**

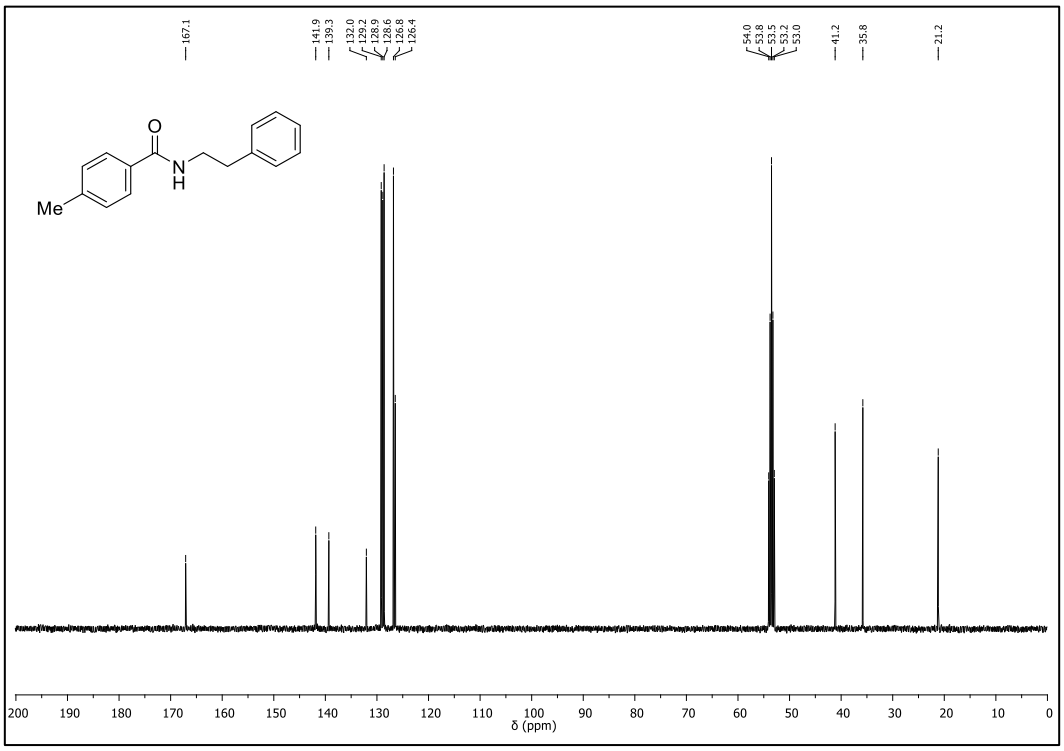

^{1}H-NMR (400 MHz, CD_2Cl_2) of **29a**

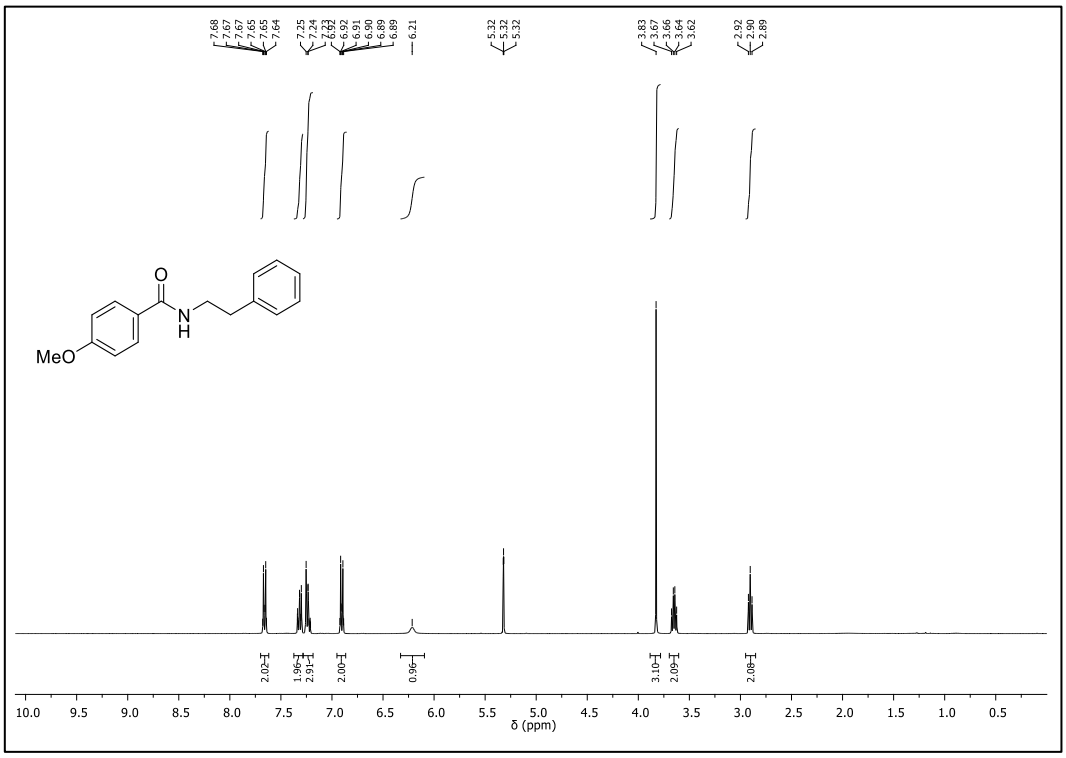

^{13}C-NMR (101 MHz, CD_2Cl_2) of **29a**

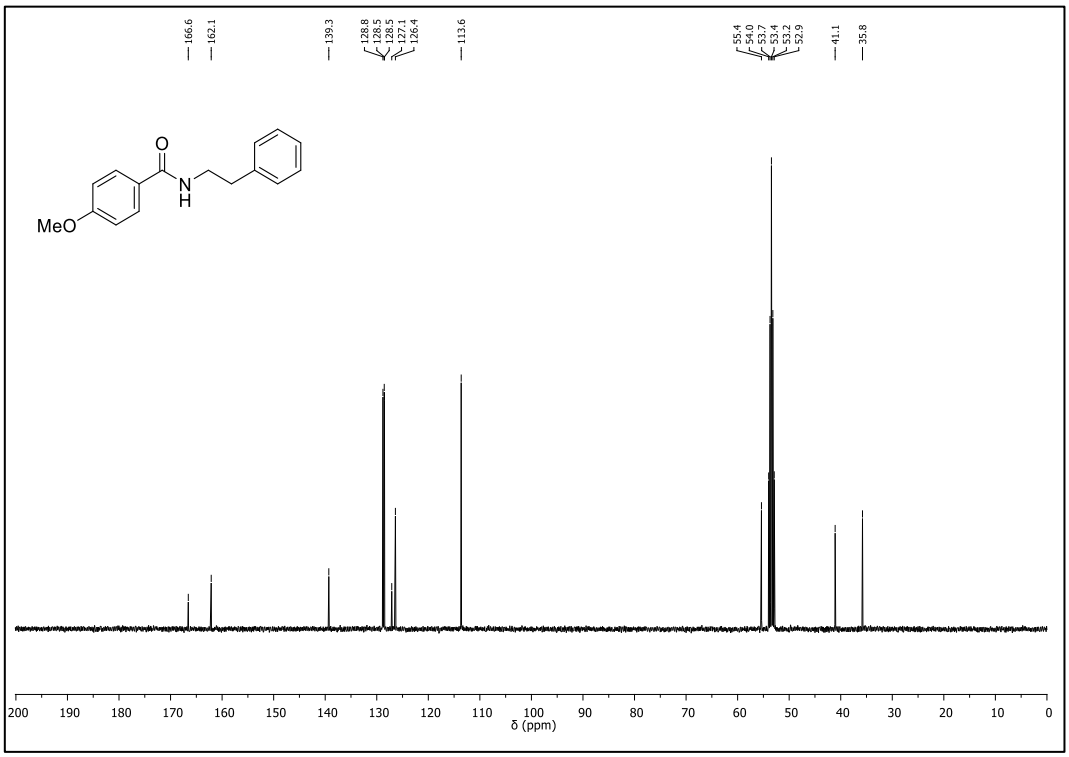

^{1}H-NMR (400 MHz, $CDCl_3$) of **30a**

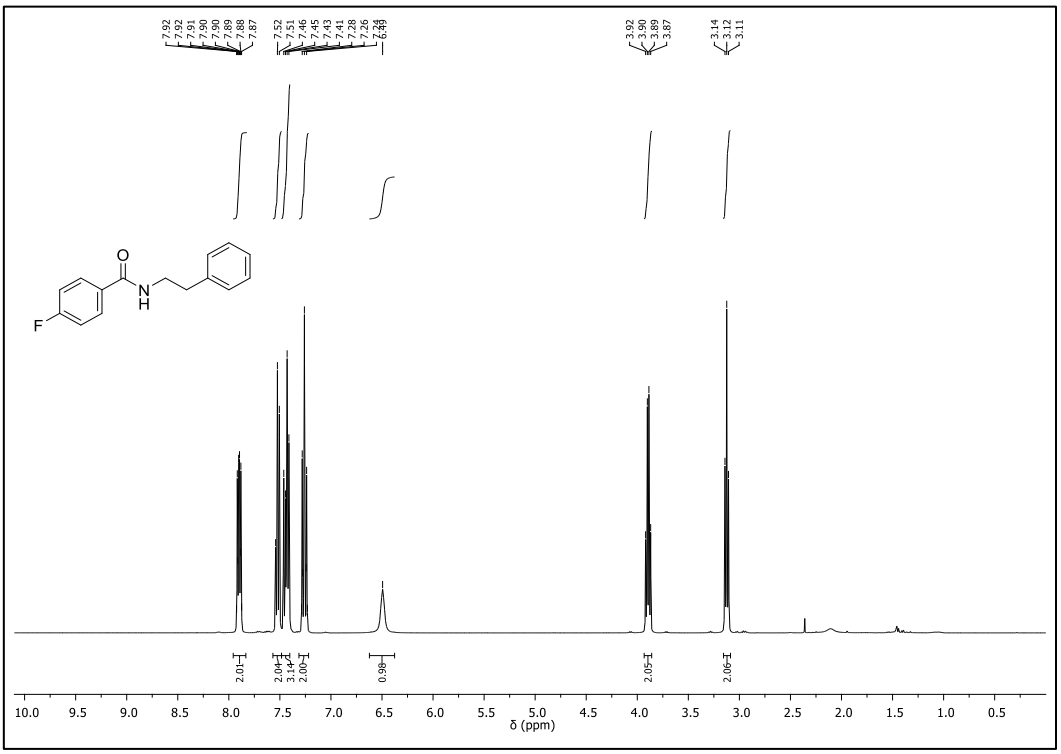

^{13}C-NMR (101 MHz, $CDCl_3$) of **30a**

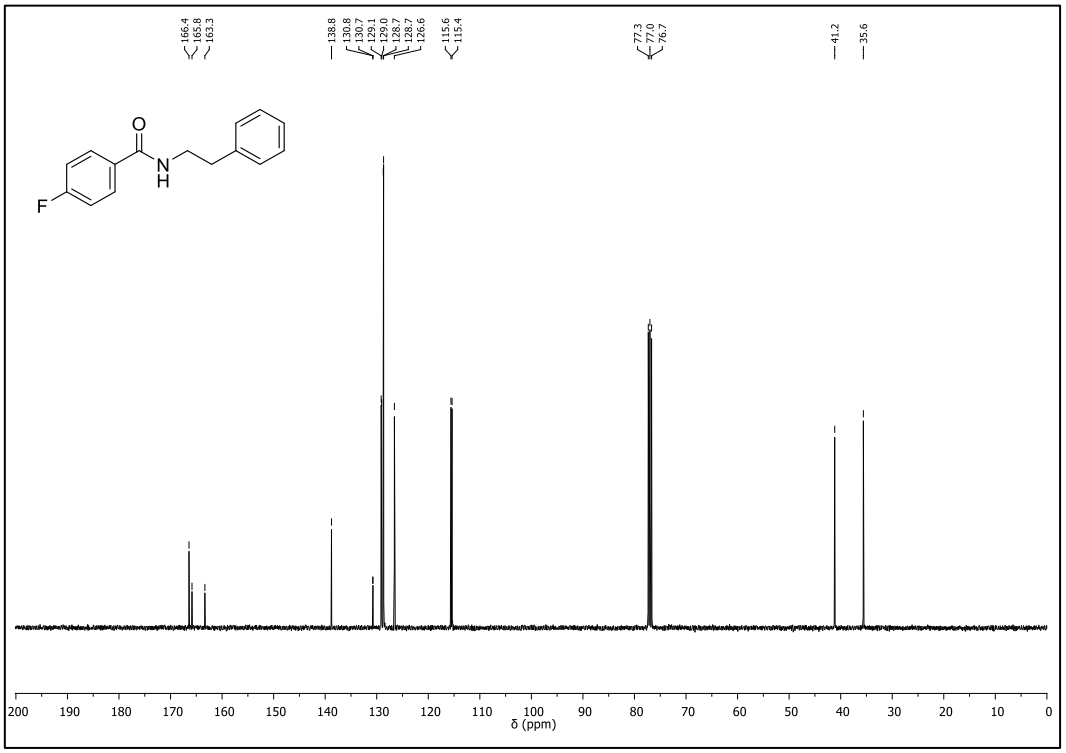

^{19}F-NMR (377 MHz, $CDCl_3$) of **30a**

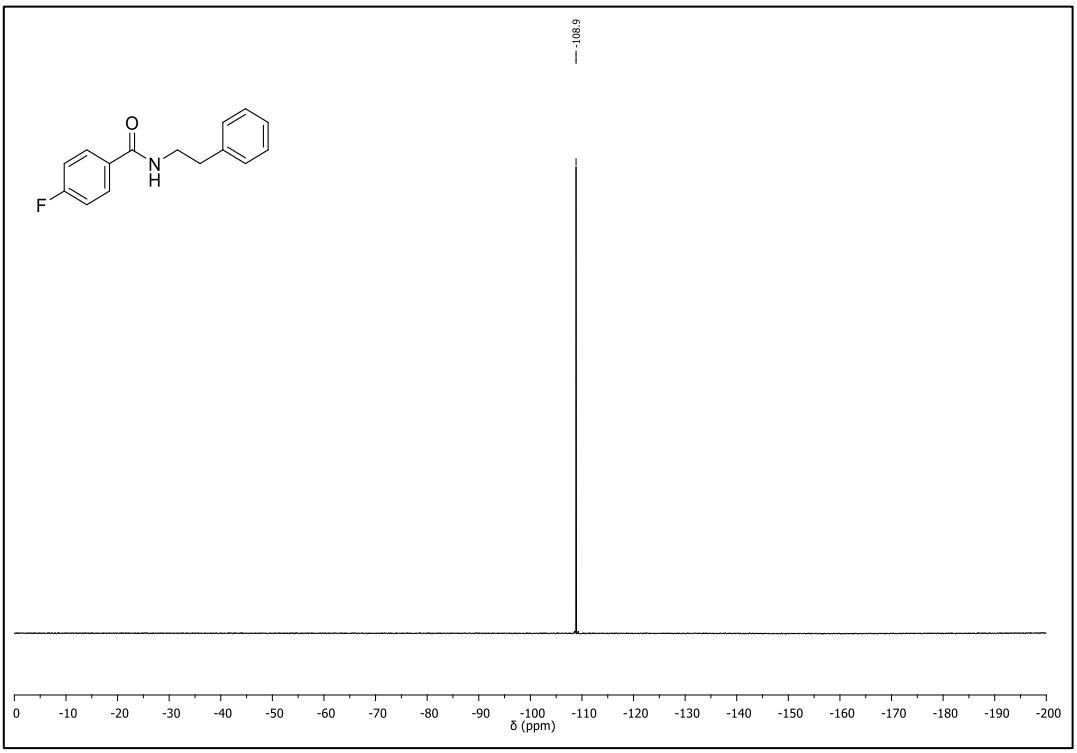

^{1}H-NMR (400 MHz, $CDCl_3$) of **31a**

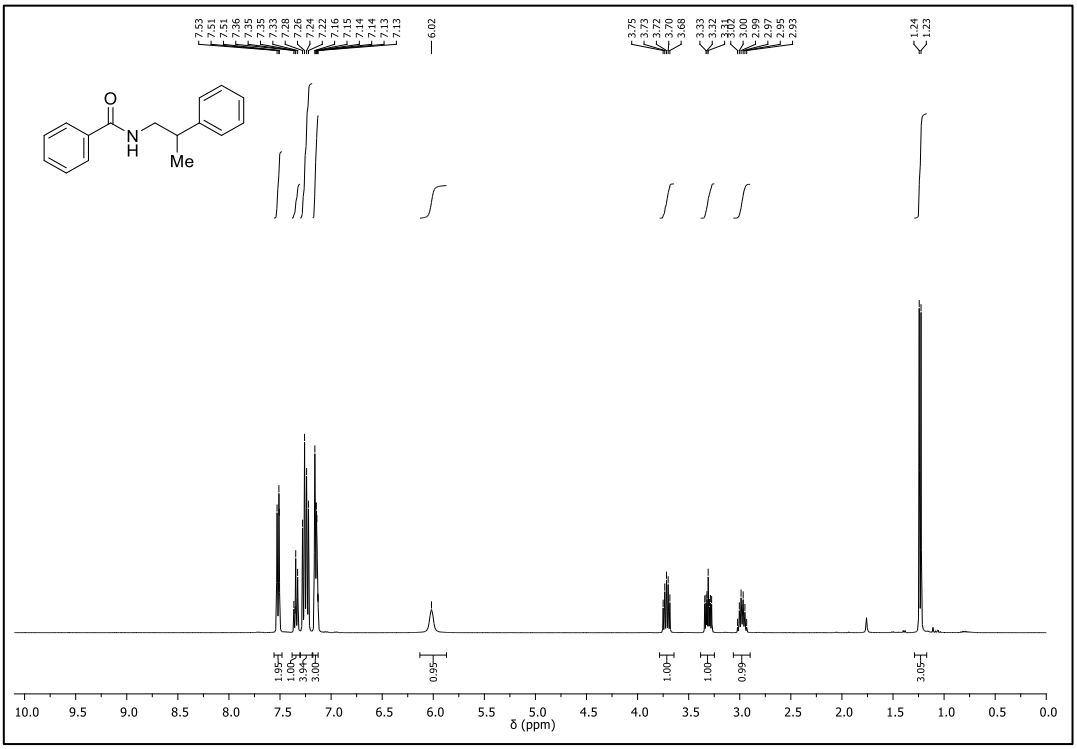

^{13}C-NMR (101 MHz, $CDCl_3$) of **31a**

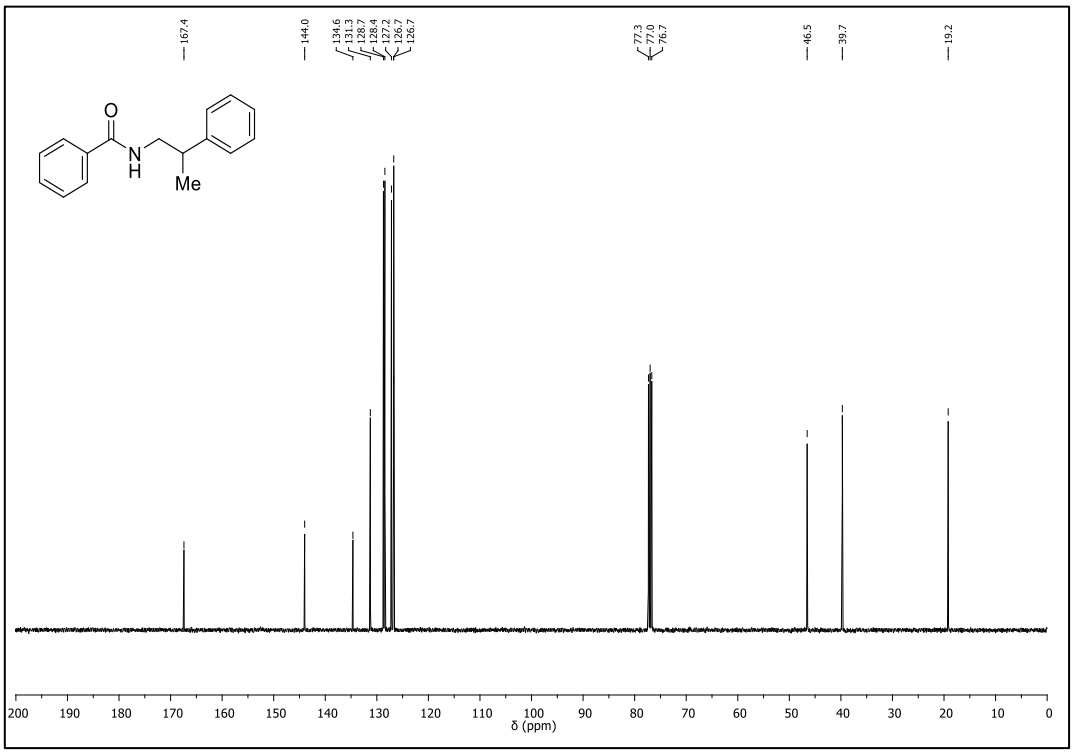

^{1}H-NMR (400 MHz, $CDCl_3$) of **33a**

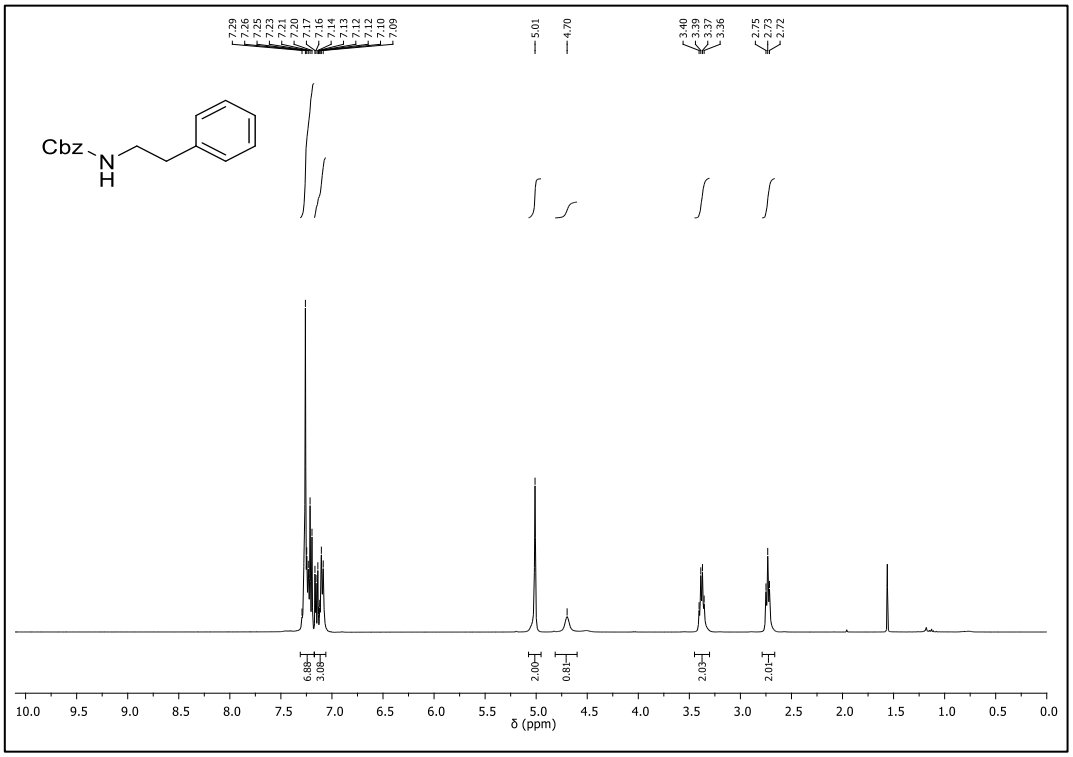

^{13}C-NMR (101 MHz, $CDCl_3$) of **33a**

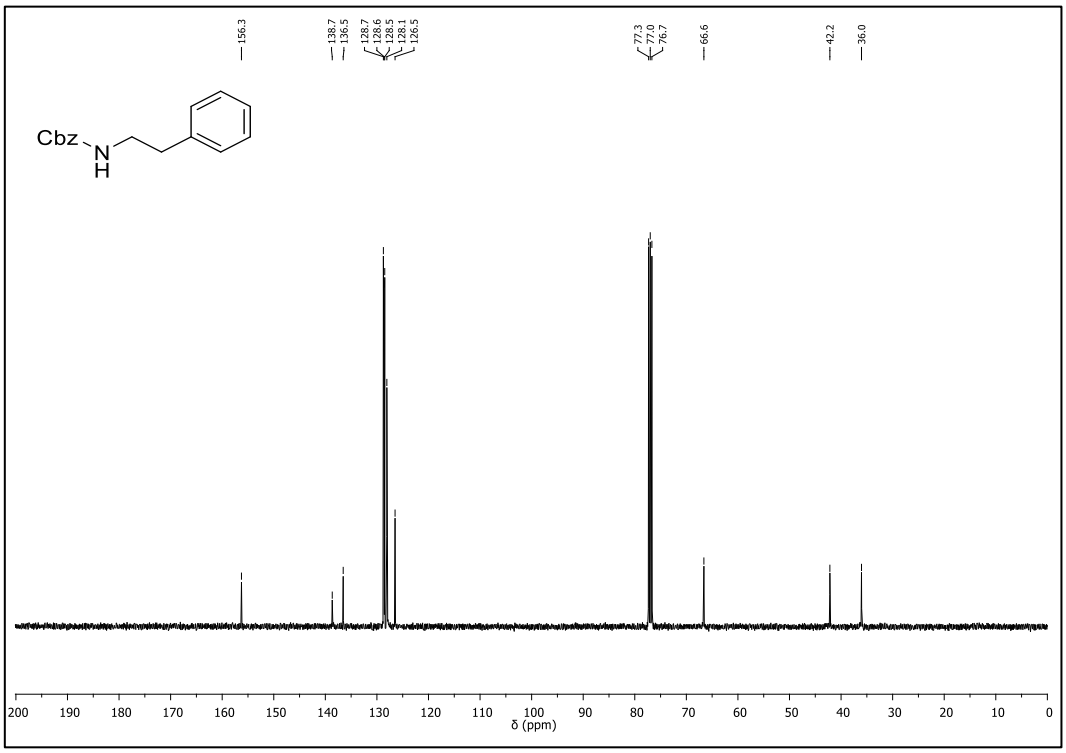

^{1}H-NMR (400 MHz, $CDCl_3$) of **34a**

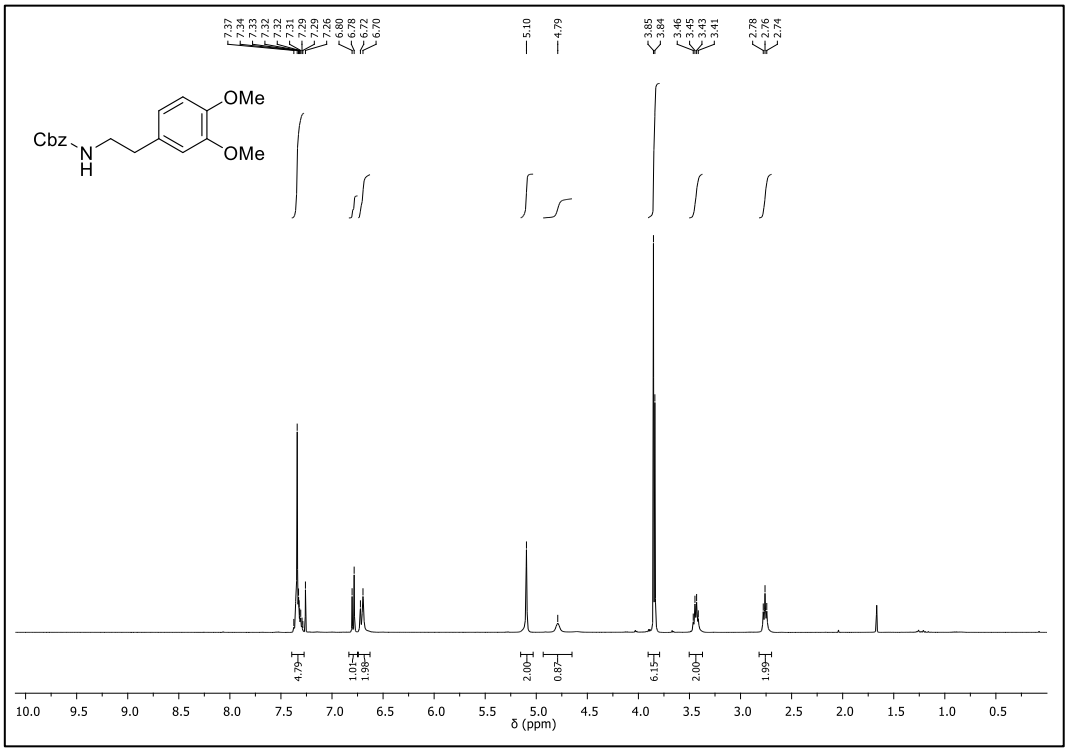

^{13}C-NMR (101 MHz, $CDCl_3$) of **34a**

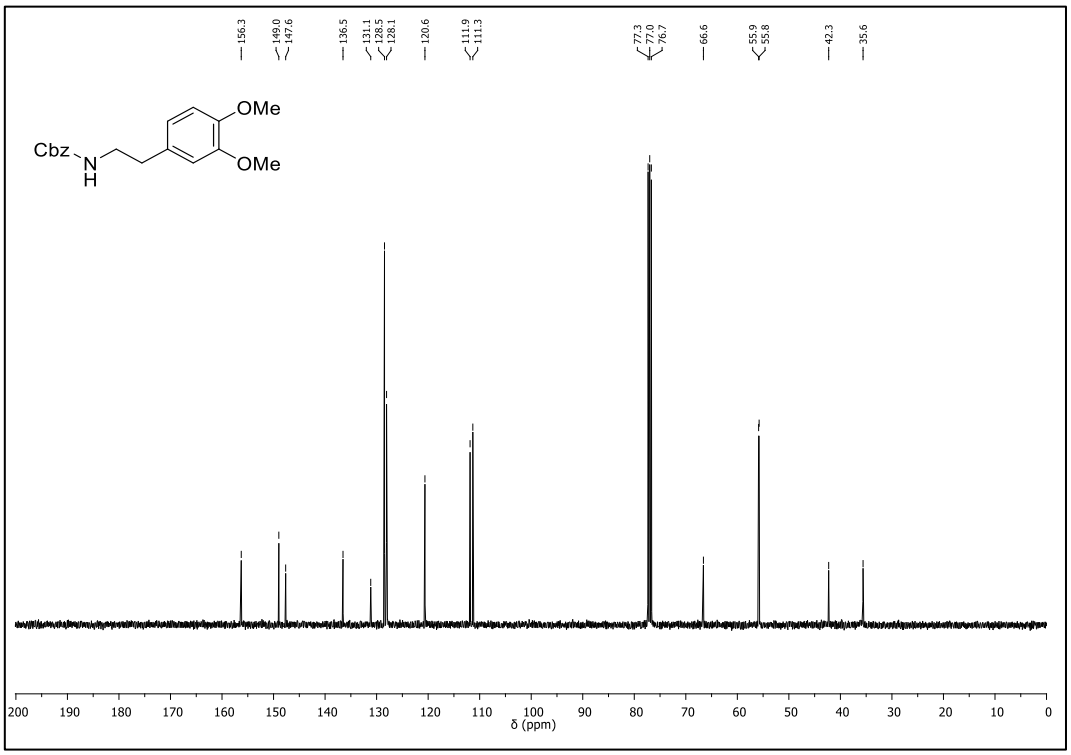

^{1}H-NMR (400 MHz, $CDCl_3$) of **35a**

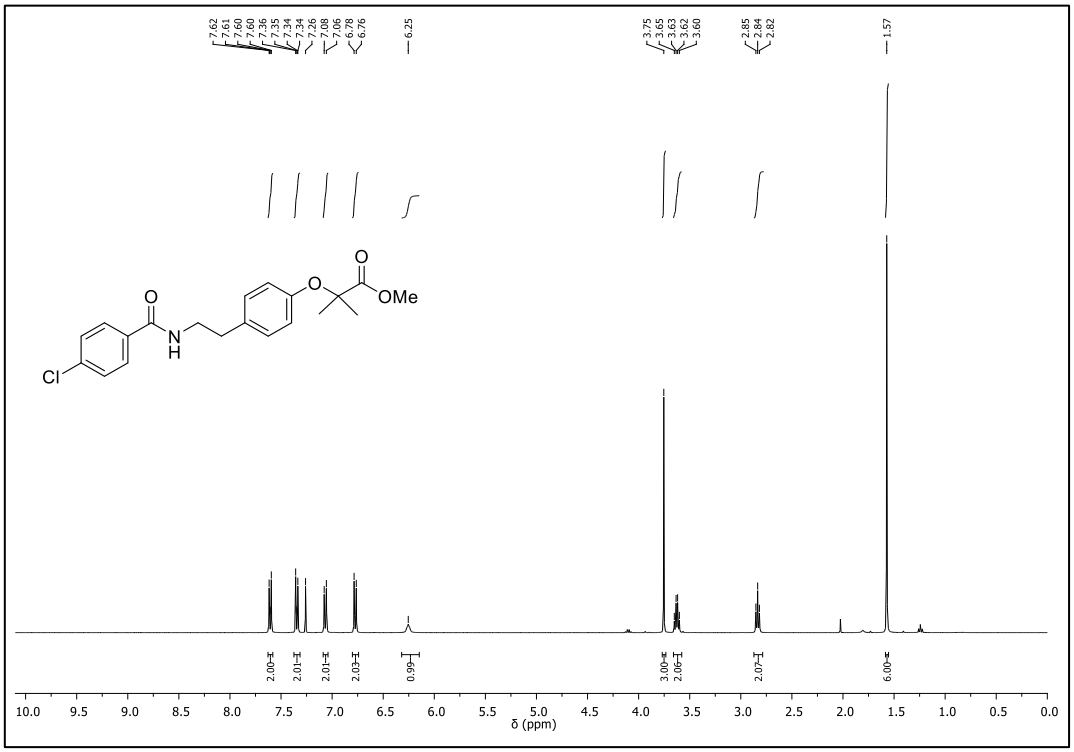

^{13}C-NMR (101 MHz, $CDCl_3$) of **35a**

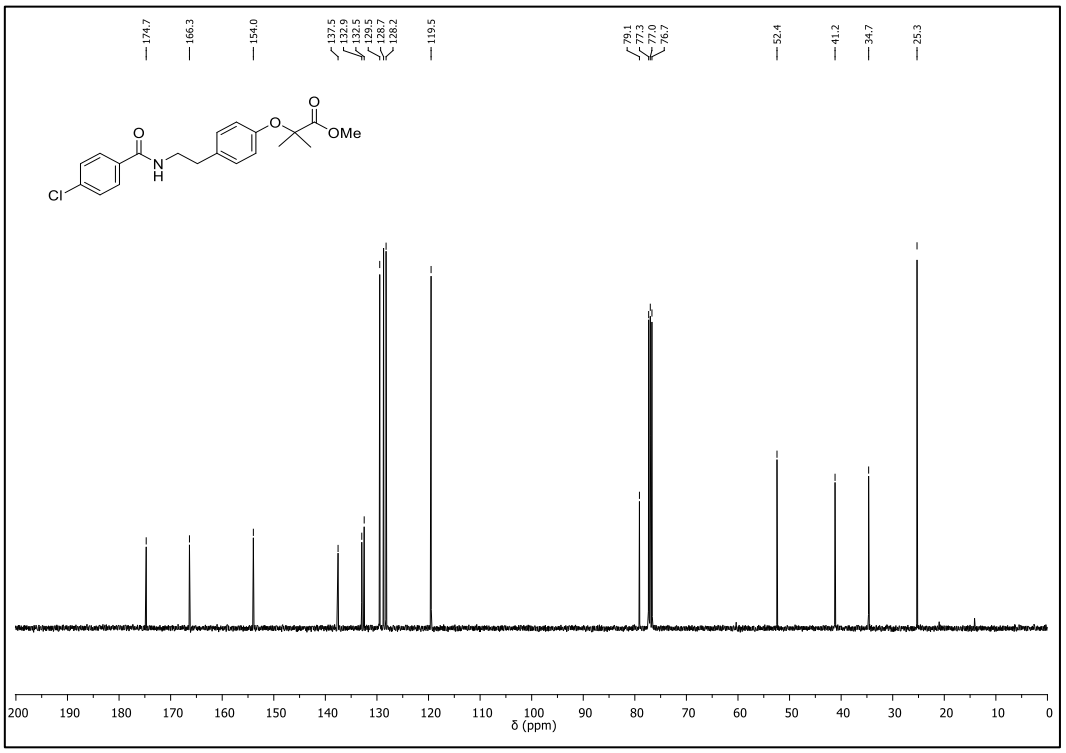

^{1}H-NMR (400 MHz, CD_2Cl_2) of **36a**

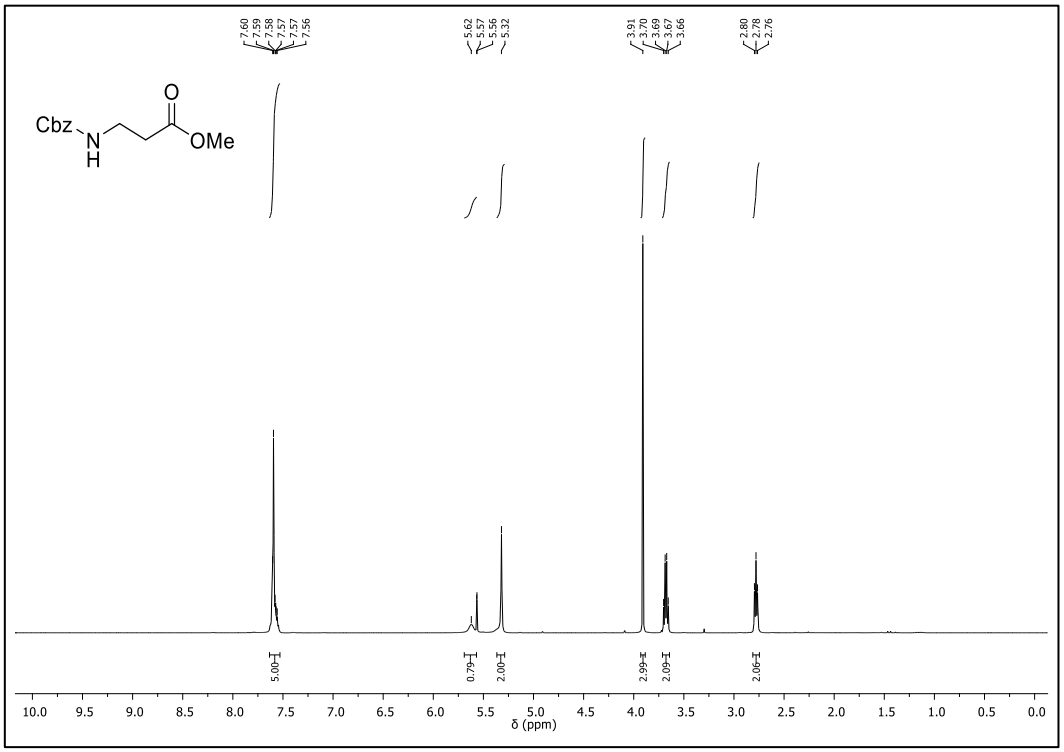

^{13}C-NMR (101 MHz, CD_2Cl_2) of **36a**

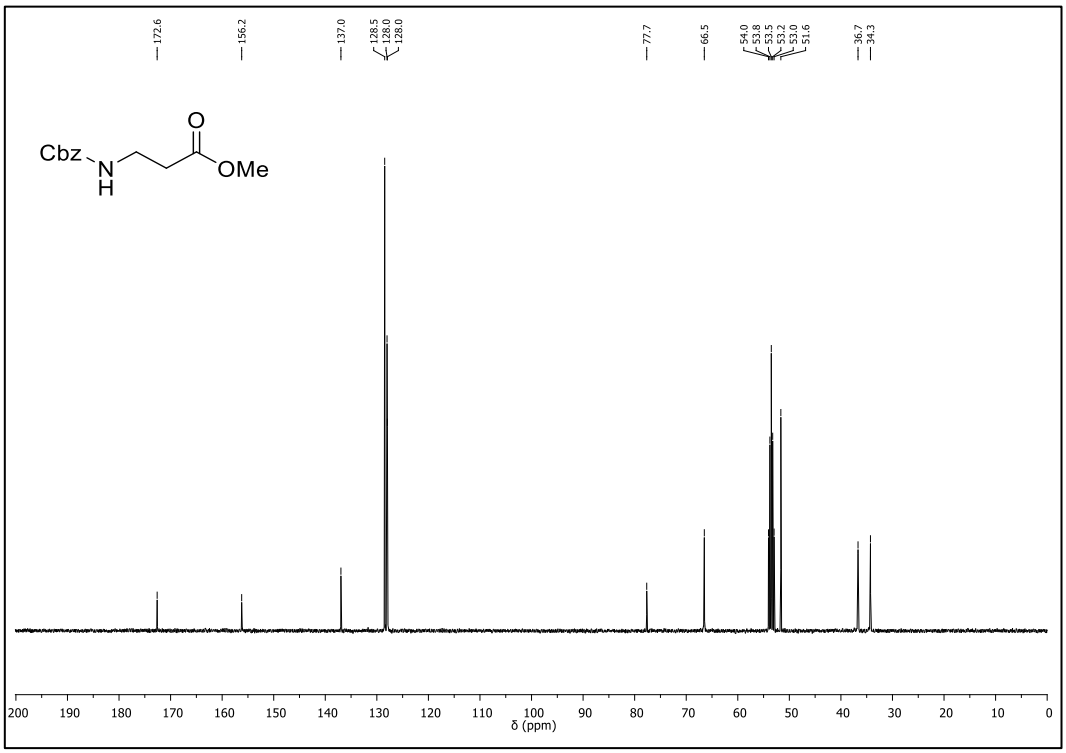

^{1}H-NMR (400 MHz, $CDCl_3$) of **37a**

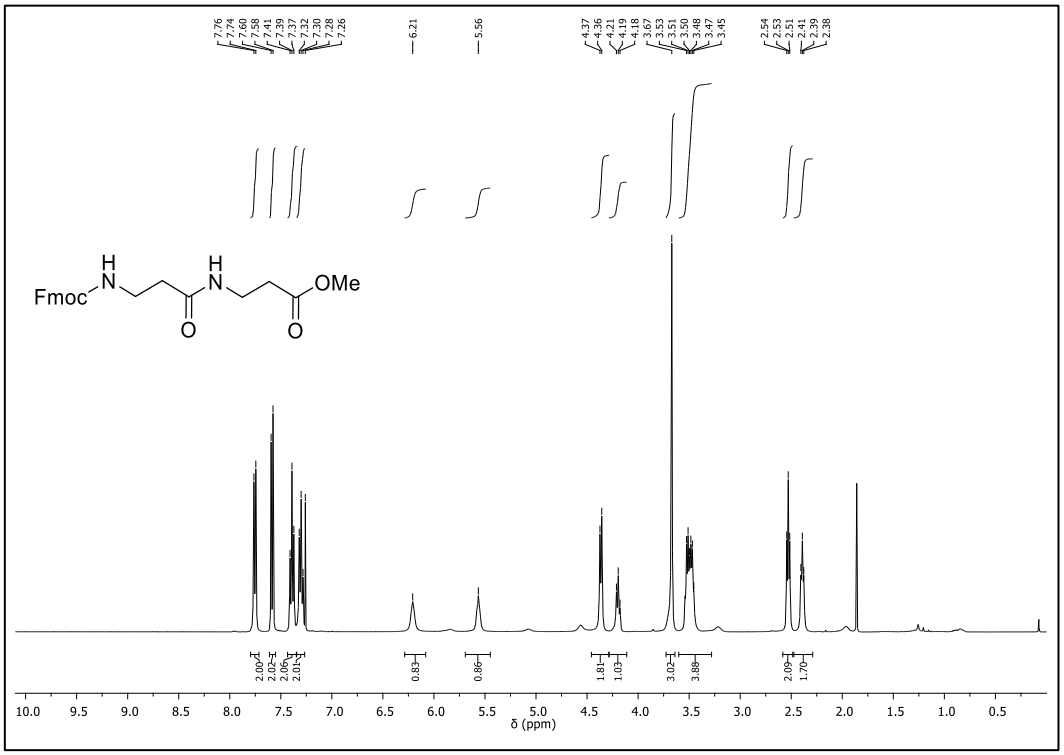

^{13}C-NMR (101 MHz, $CDCl_3$) of **37a**

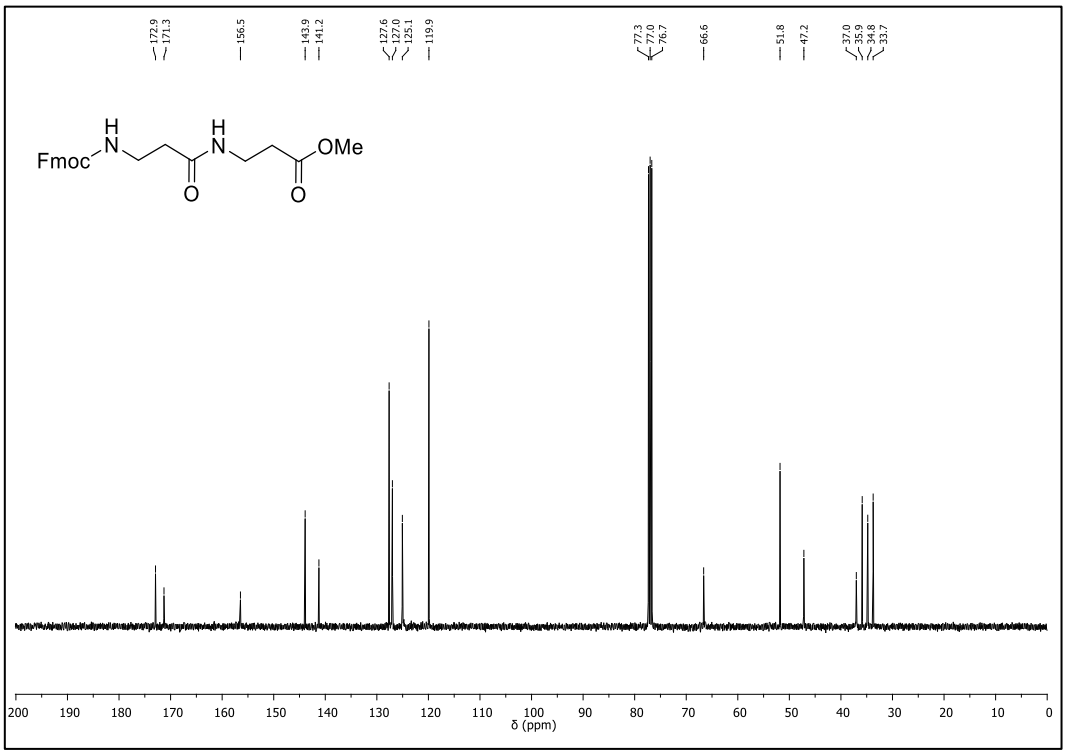

^{1}H-NMR (400 MHz, $CDCl_3$) of **38a**

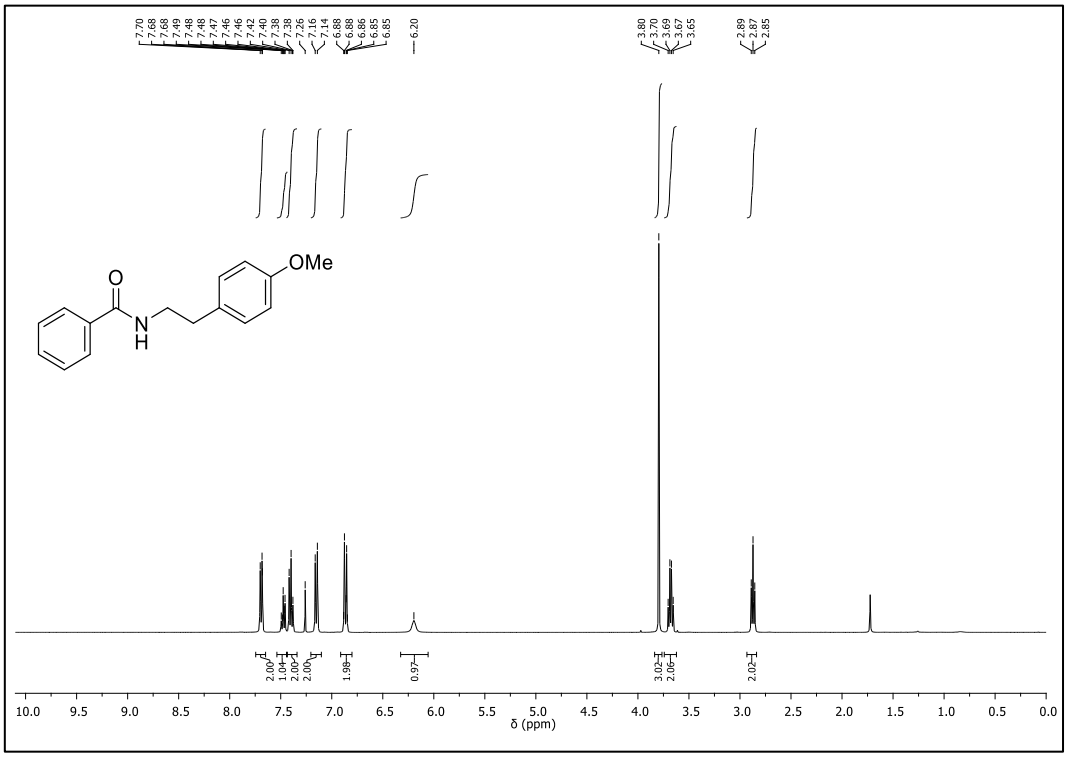

^{13}C-NMR (101 MHz, $CDCl_3$) of **38a**

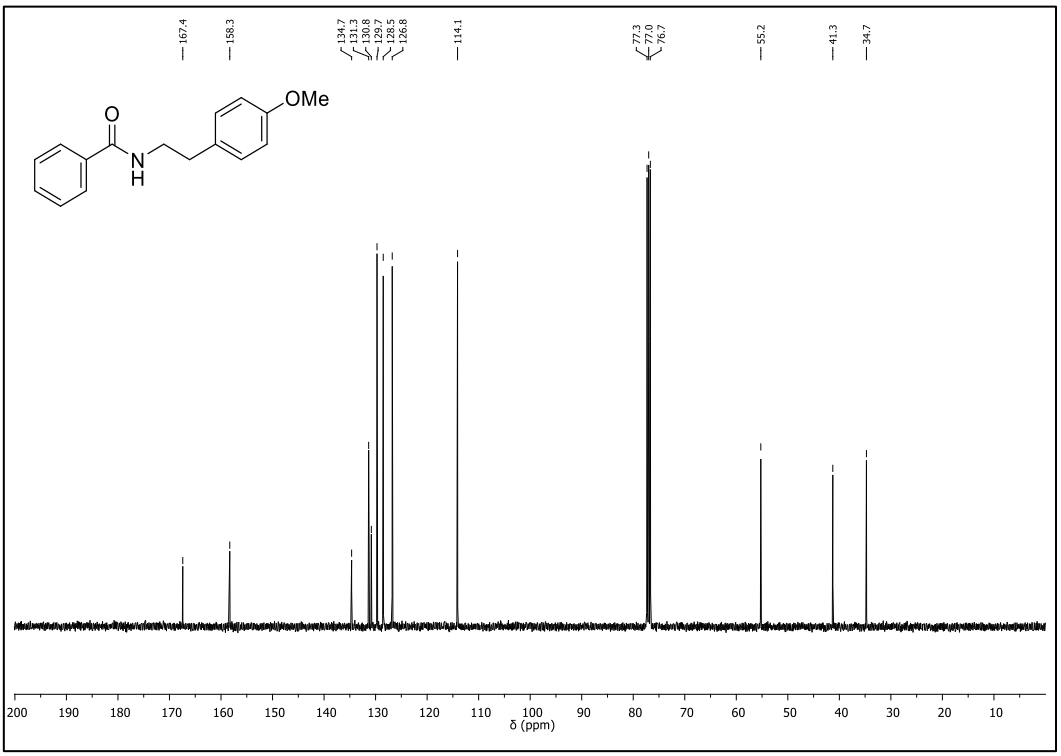

^{1}H-NMR (400 MHz, $CDCl_3$) of **39a**

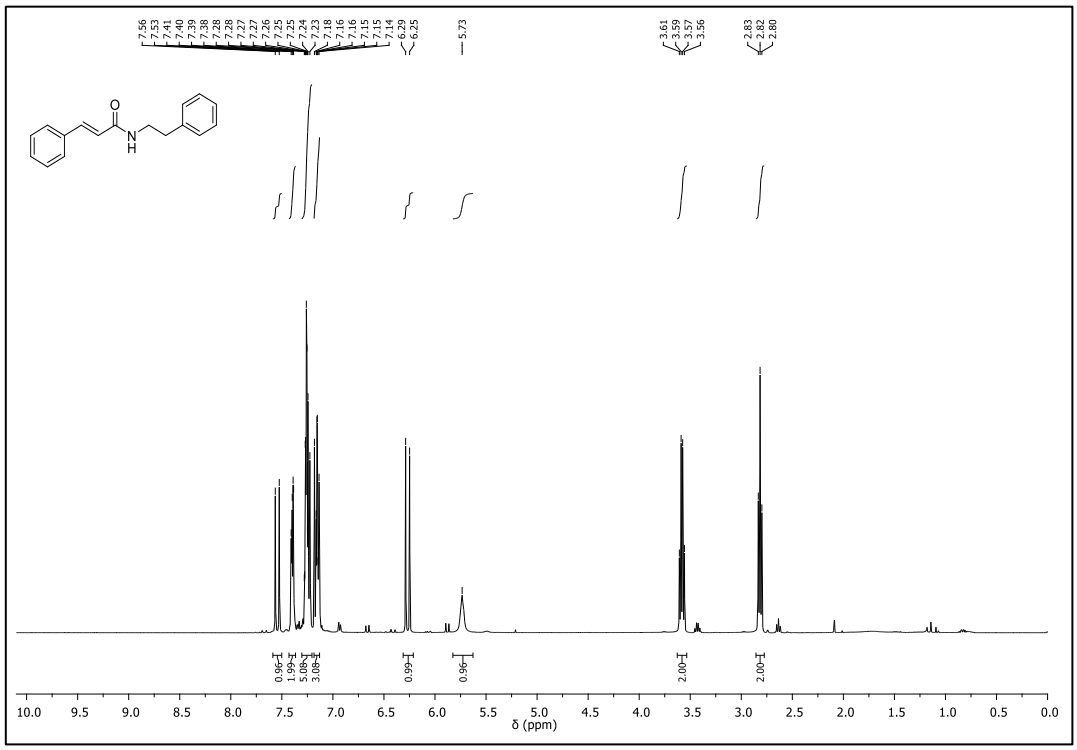

^{13}C-NMR (101 MHz, $CDCl_3$) of **39a**

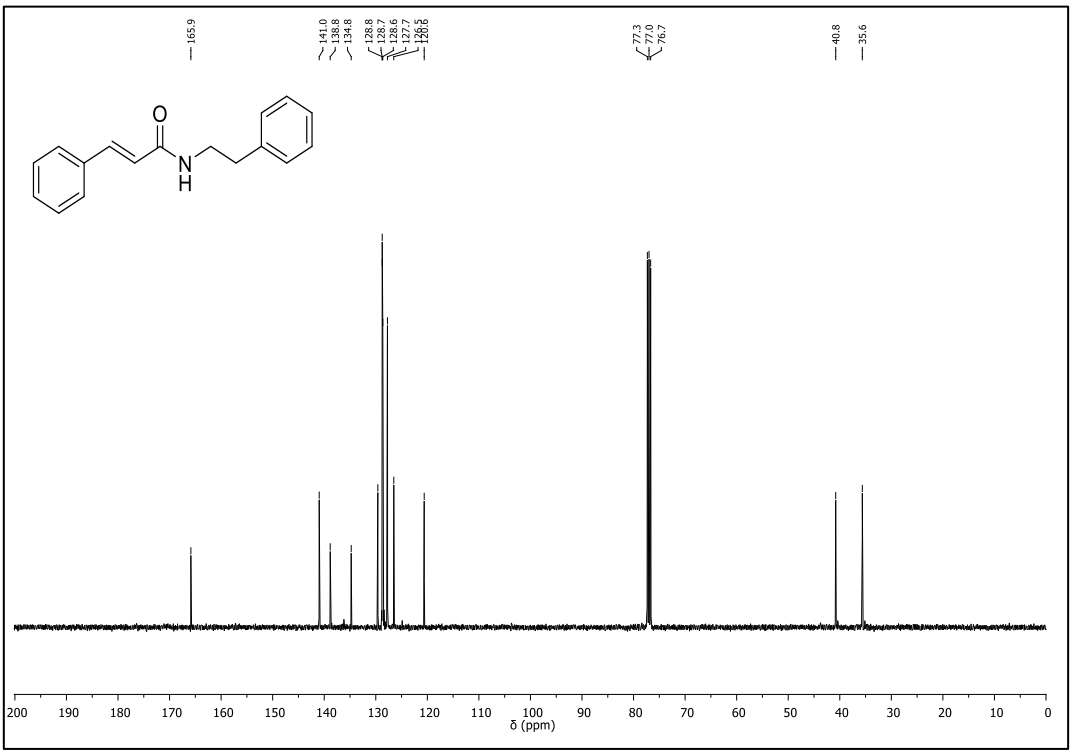

^{1}H-NMR (400 MHz, CD_2Cl_2) of **40a**

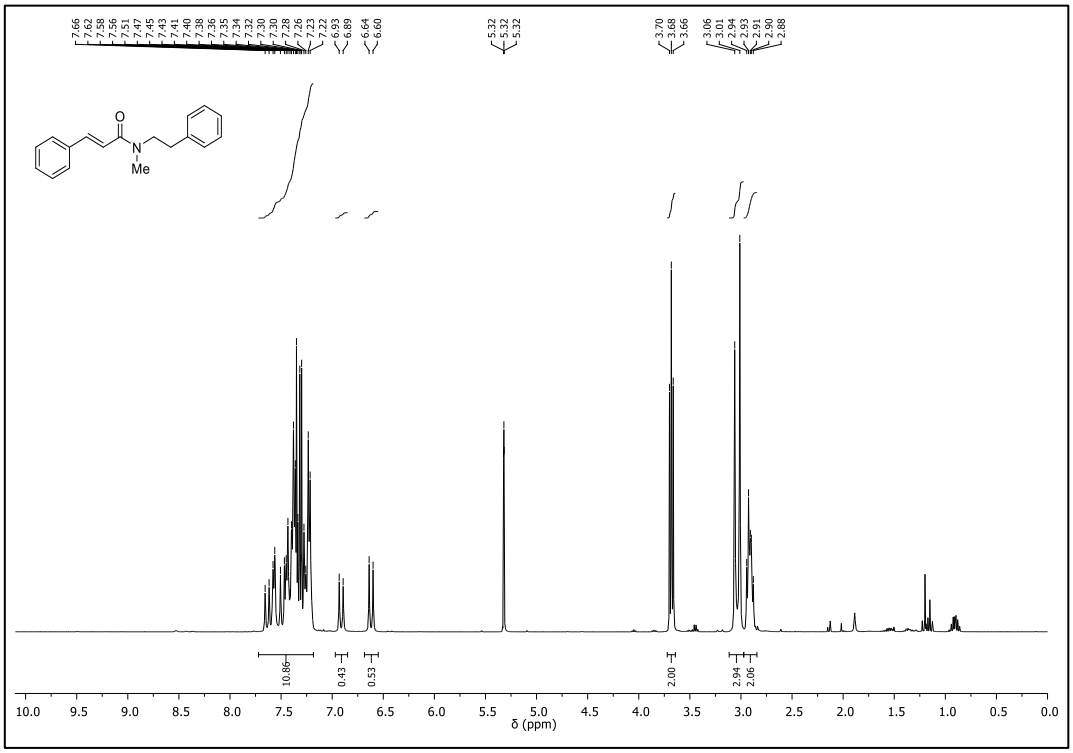

^{13}C-NMR (101 MHz, CD_2Cl_2) of **40a**

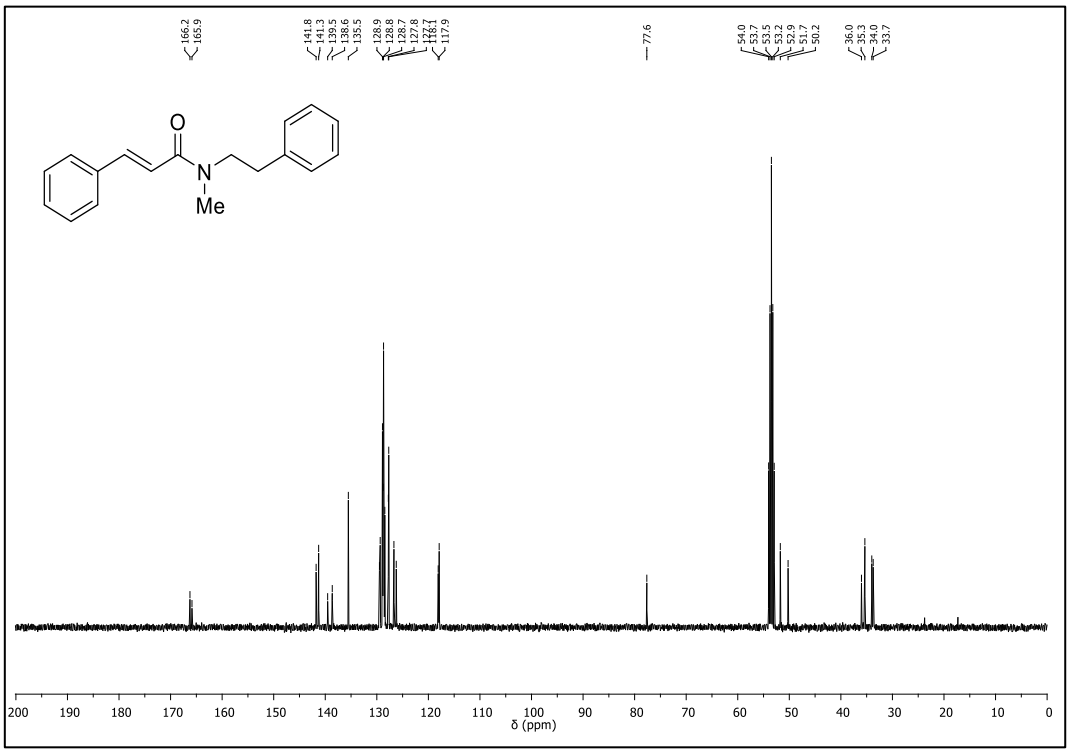

^{1}H-NMR (400 MHz, $CDCl_3$) of **1a-D$_5$**

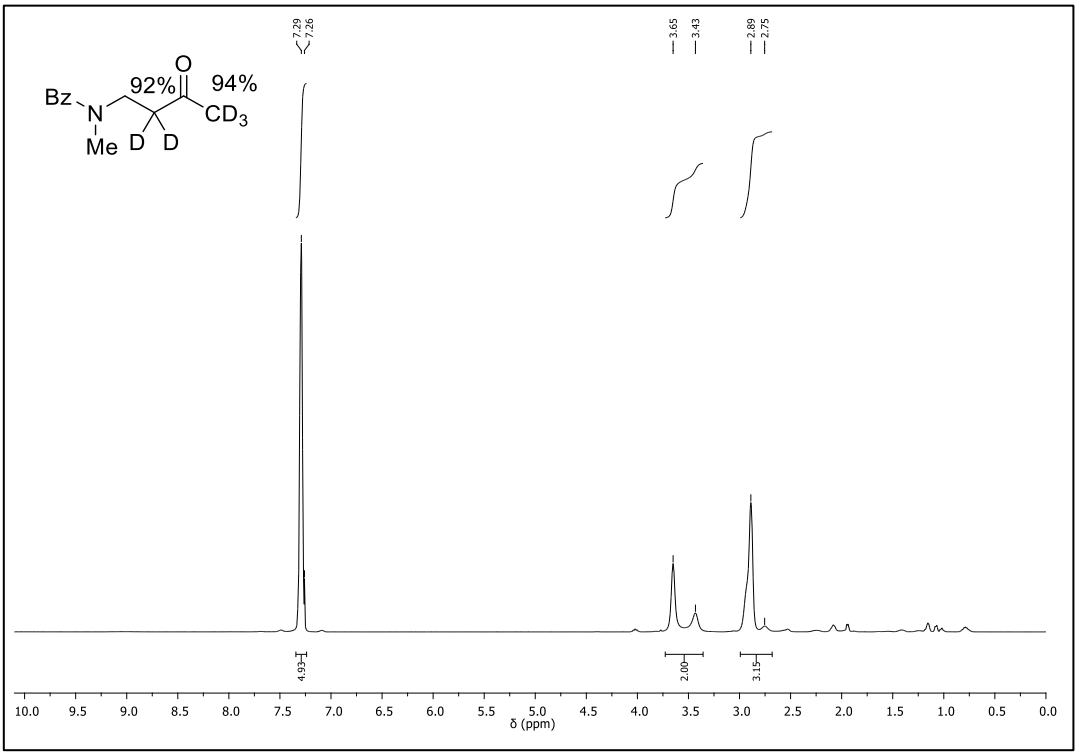

^{13}C-NMR (101 MHz, $CDCl_3$) of **1a-D$_5$**

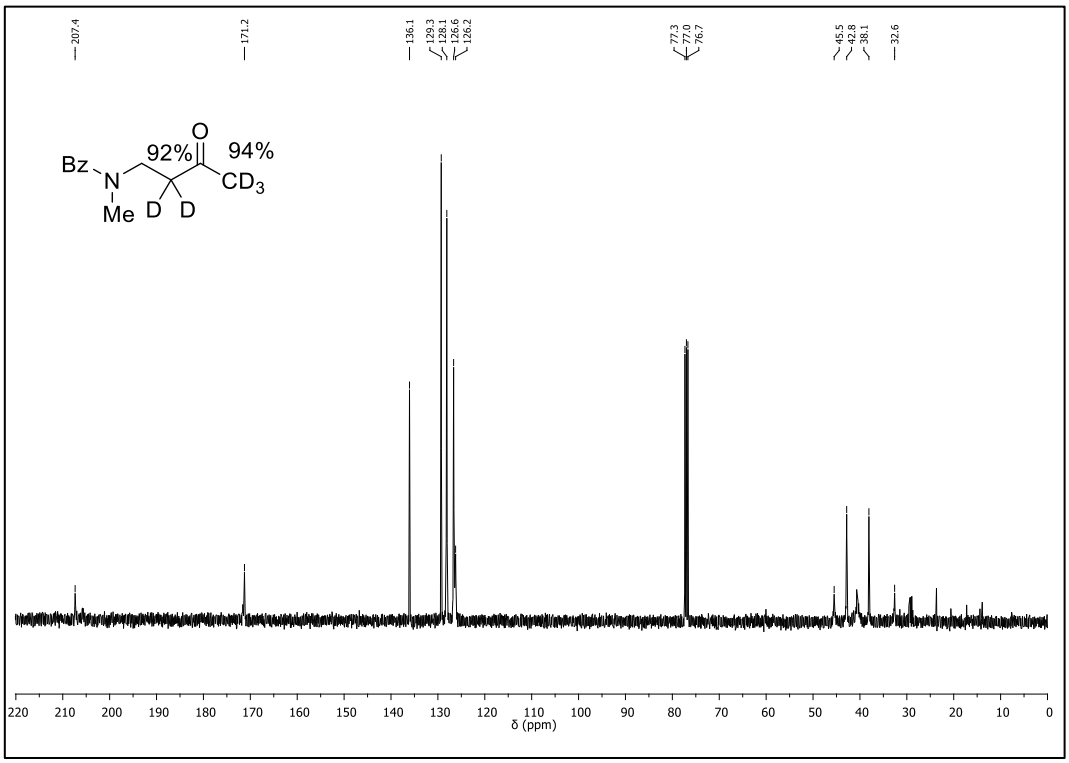

NMR Spectra of Products

^{1}H-NMR (400 MHz, $CDCl_3$) of **1b**

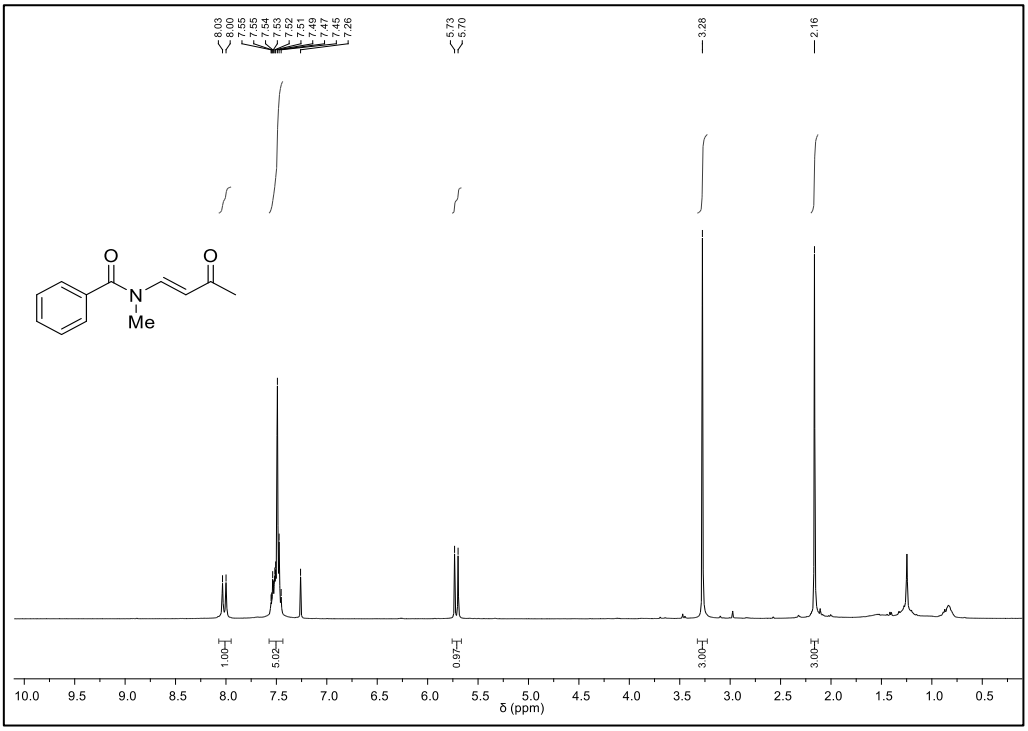

^{13}C-NMR (101 MHz, $CDCl_3$) of **1b**

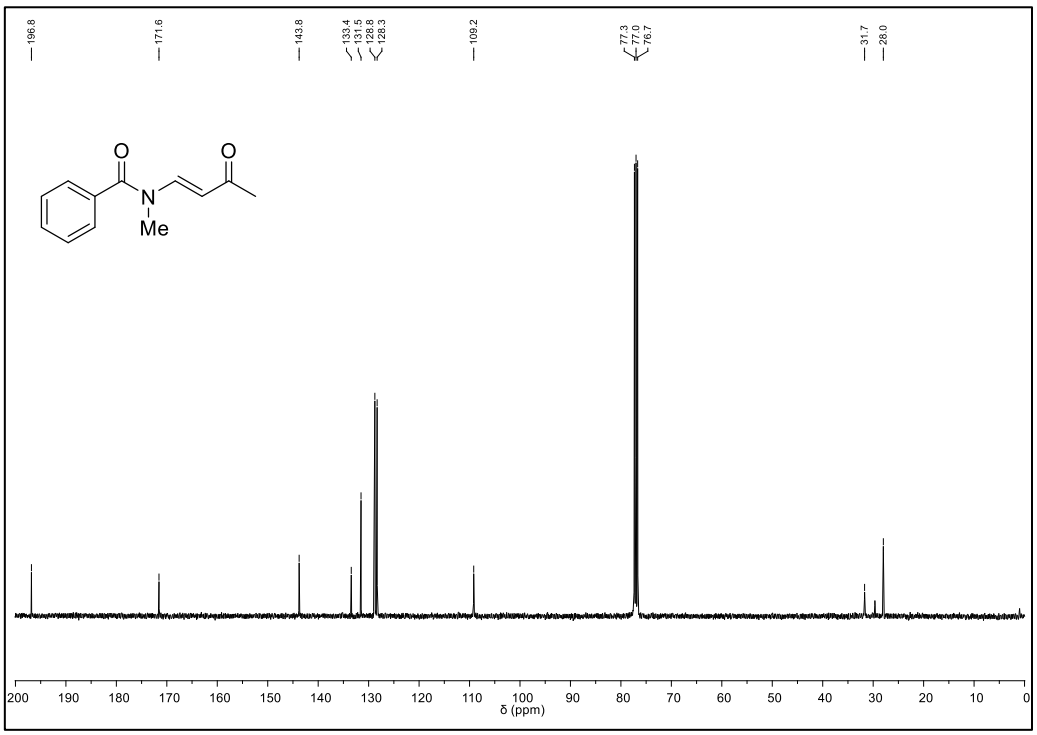

^{1}H-NMR (400 MHz, $CDCl_3$) of **2b**

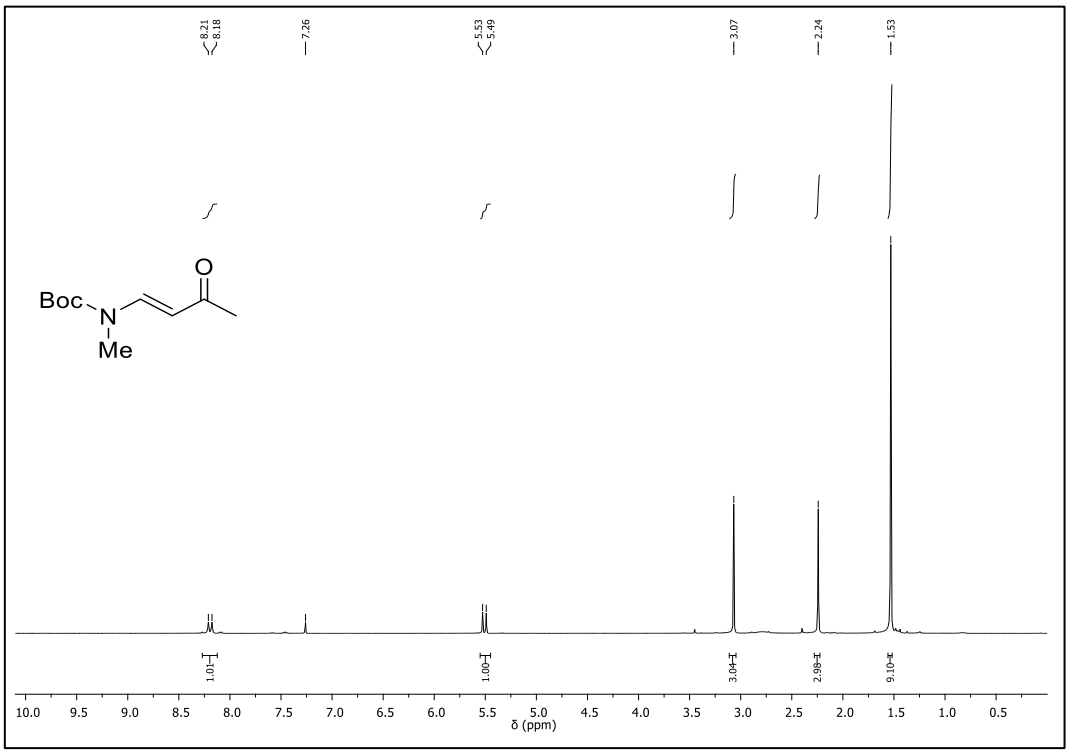

^{13}C-NMR (101 MHz, $CDCl_3$) of **2b**

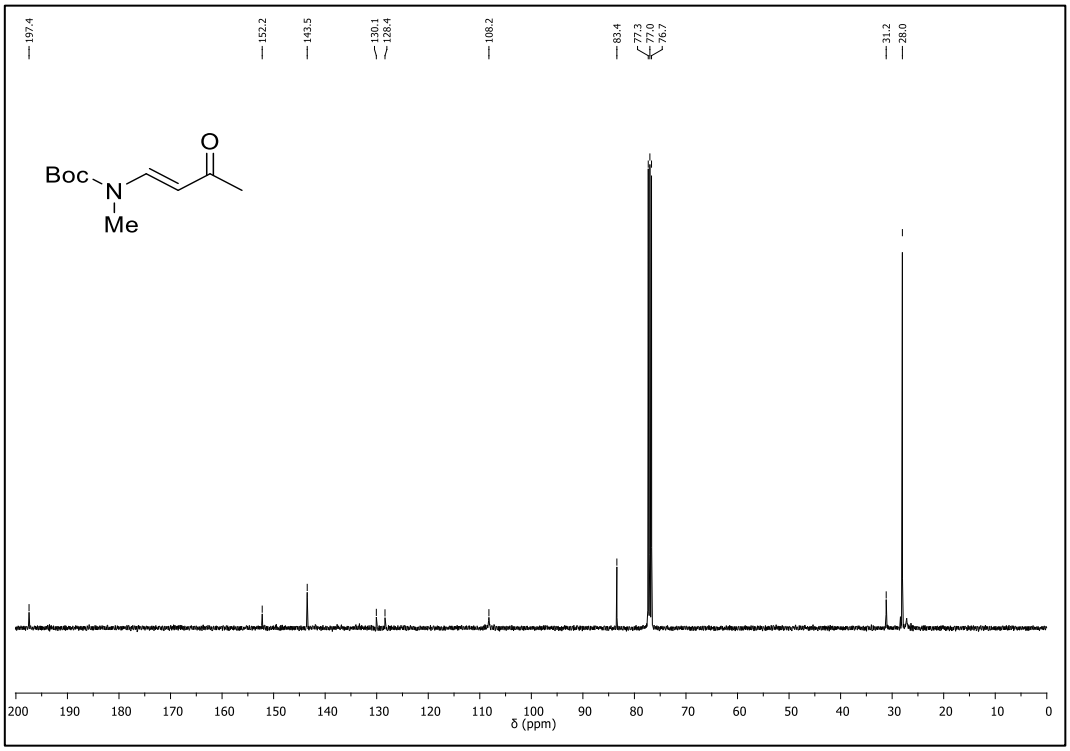

^{1}H-NMR (400 MHz, $CDCl_3$) of **3b**

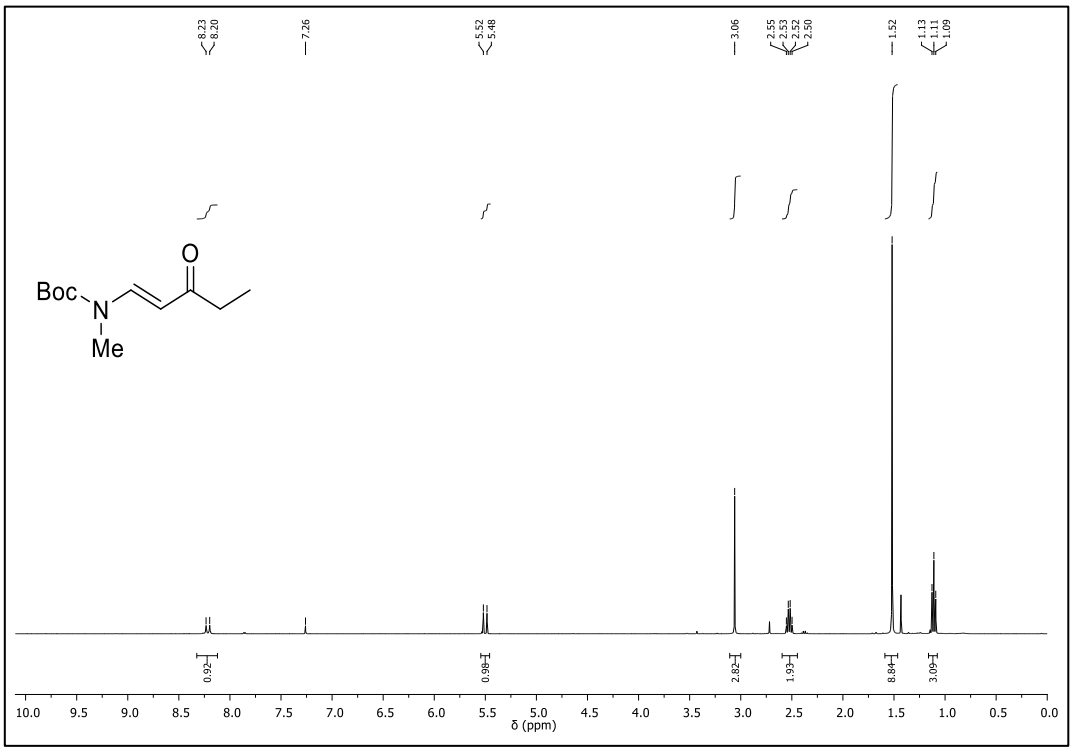

^{13}C-NMR (101 MHz, $CDCl_3$) of **3b**

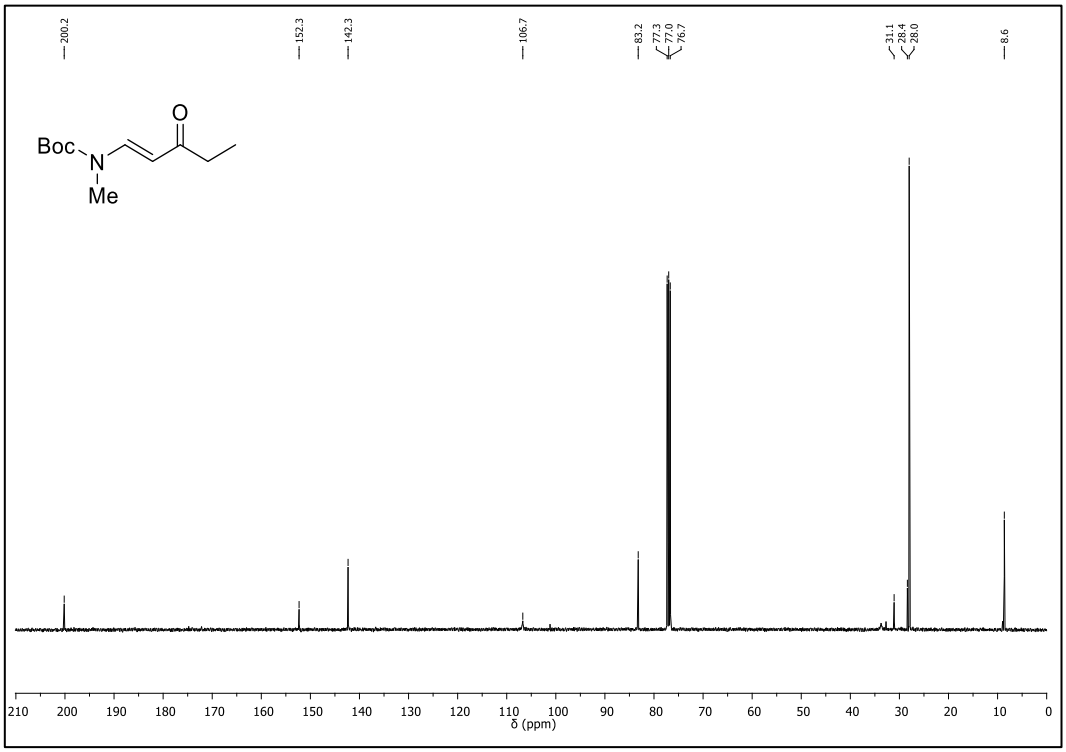

^{1}H-NMR (400 MHz, $CDCl_3$) of **4b**

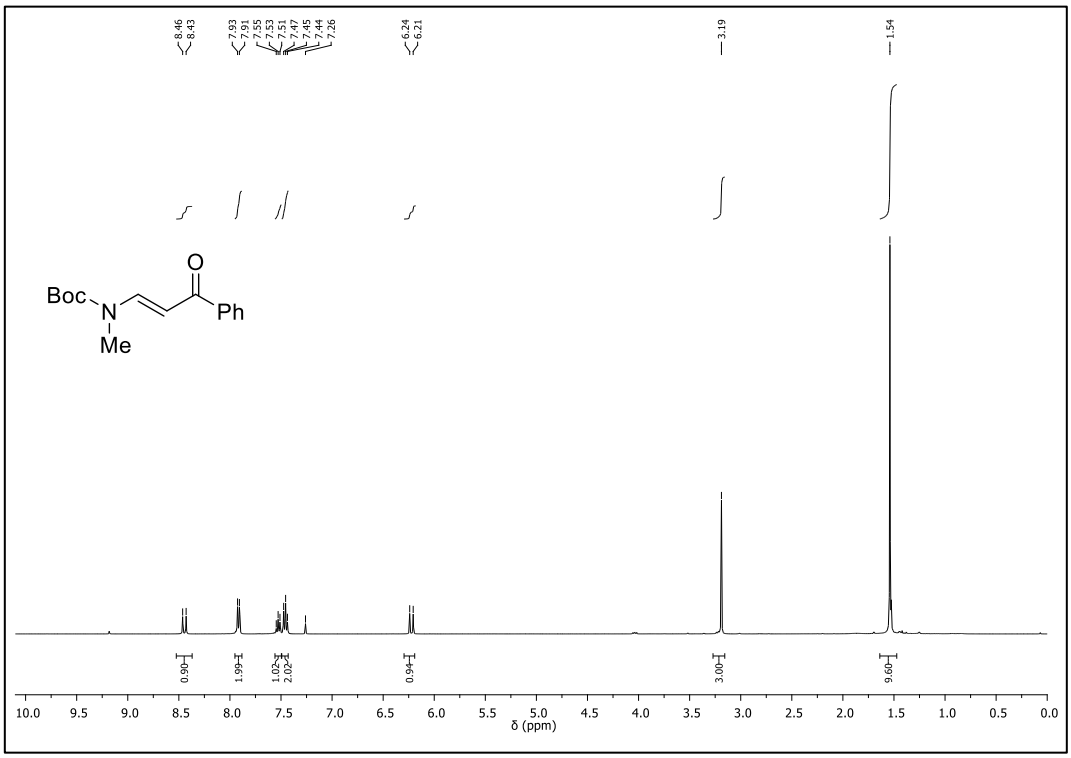

^{13}C-NMR (101 MHz, $CDCl_3$) of **4b**

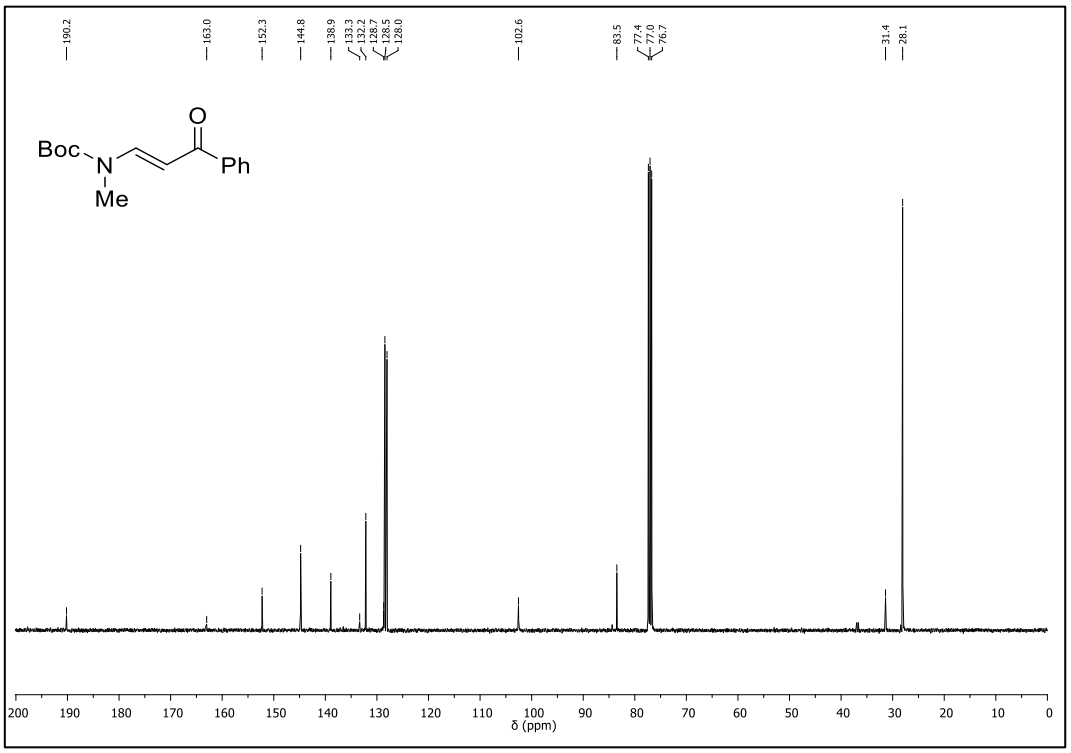

^{1}H-NMR (400 MHz, $CDCl_3$) of **5b**

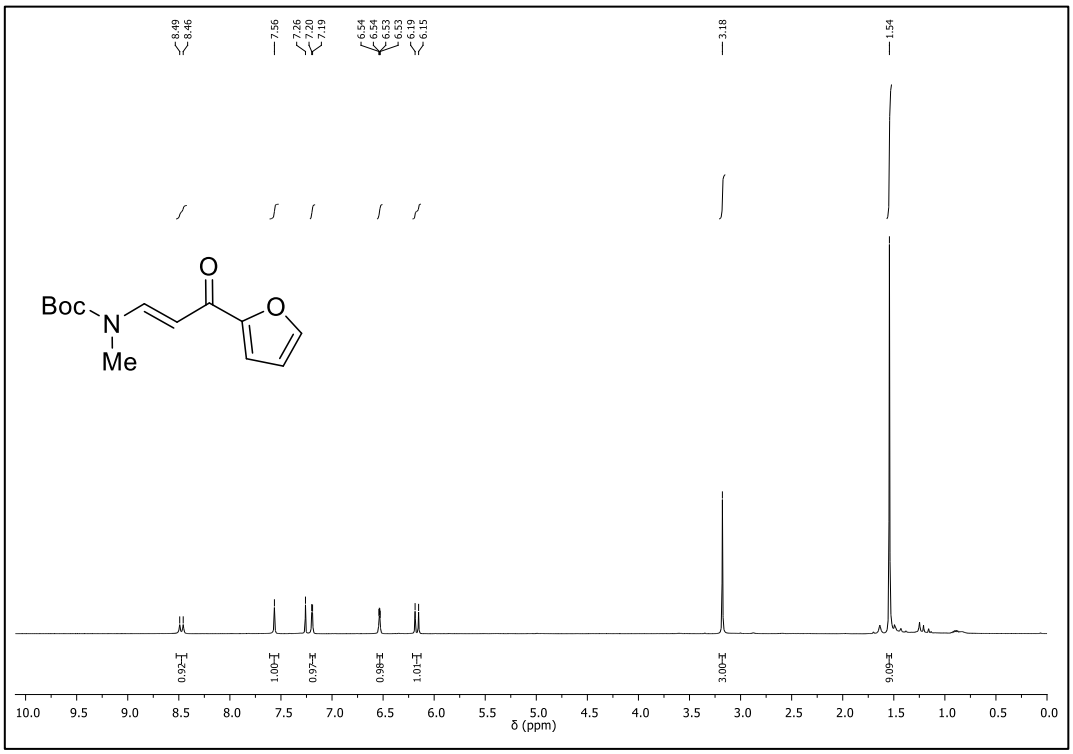

^{13}C-NMR (101 MHz, $CDCl_3$) of **5b**

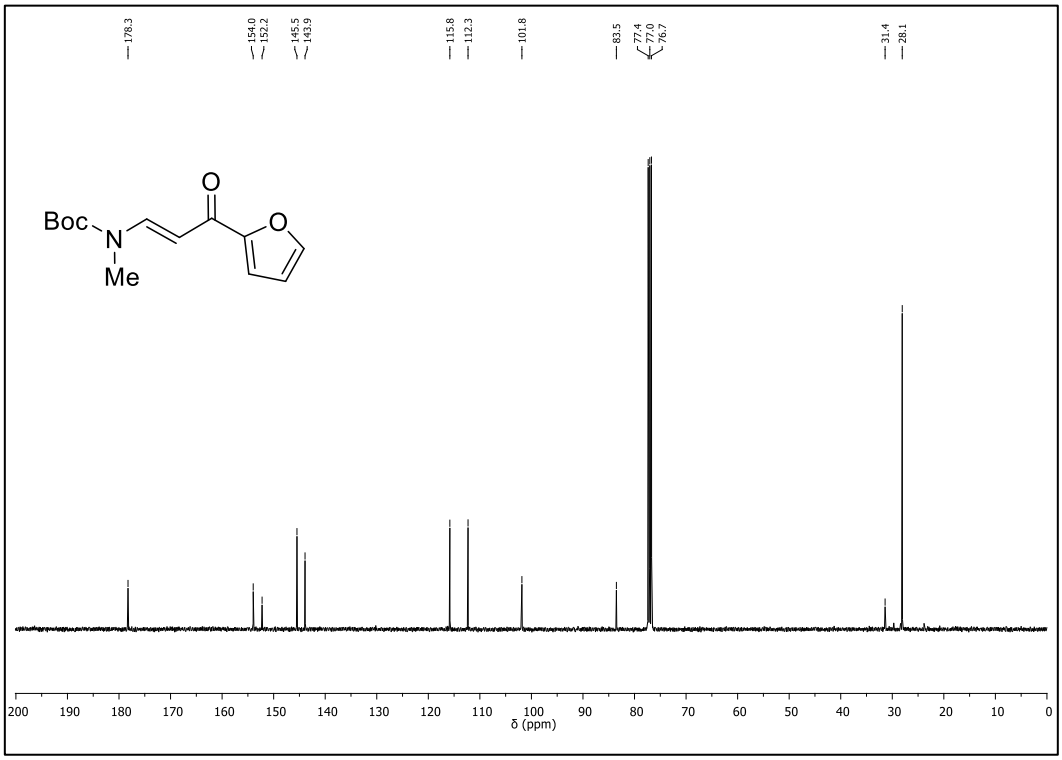

^{1}H-NMR (400 MHz, $CDCl_3$) of **6b**

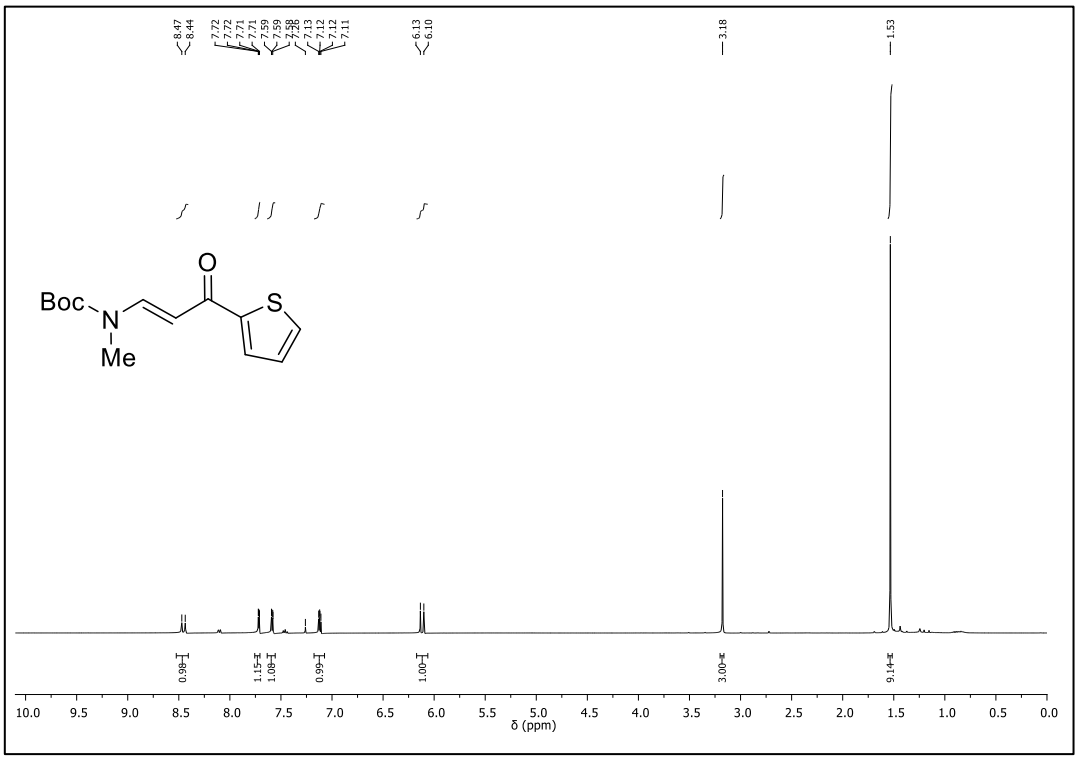

^{13}C-NMR (101 MHz, $CDCl_3$) of **6b**

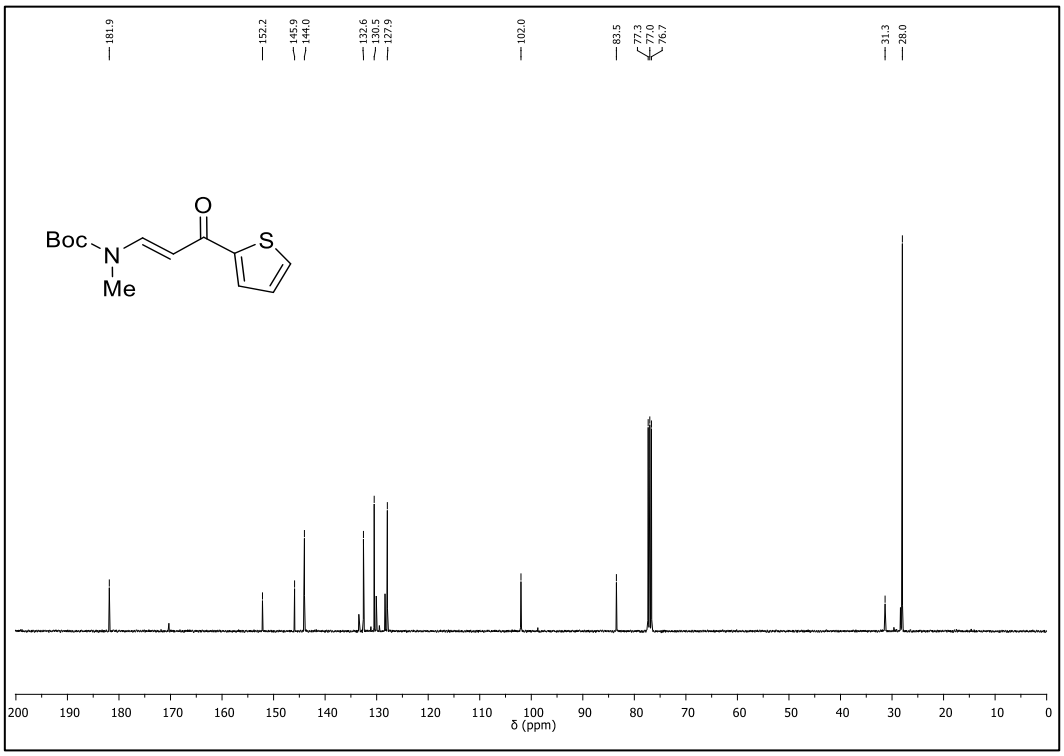

^{1}H-NMR (400 MHz, $CDCl_3$) of **7b**

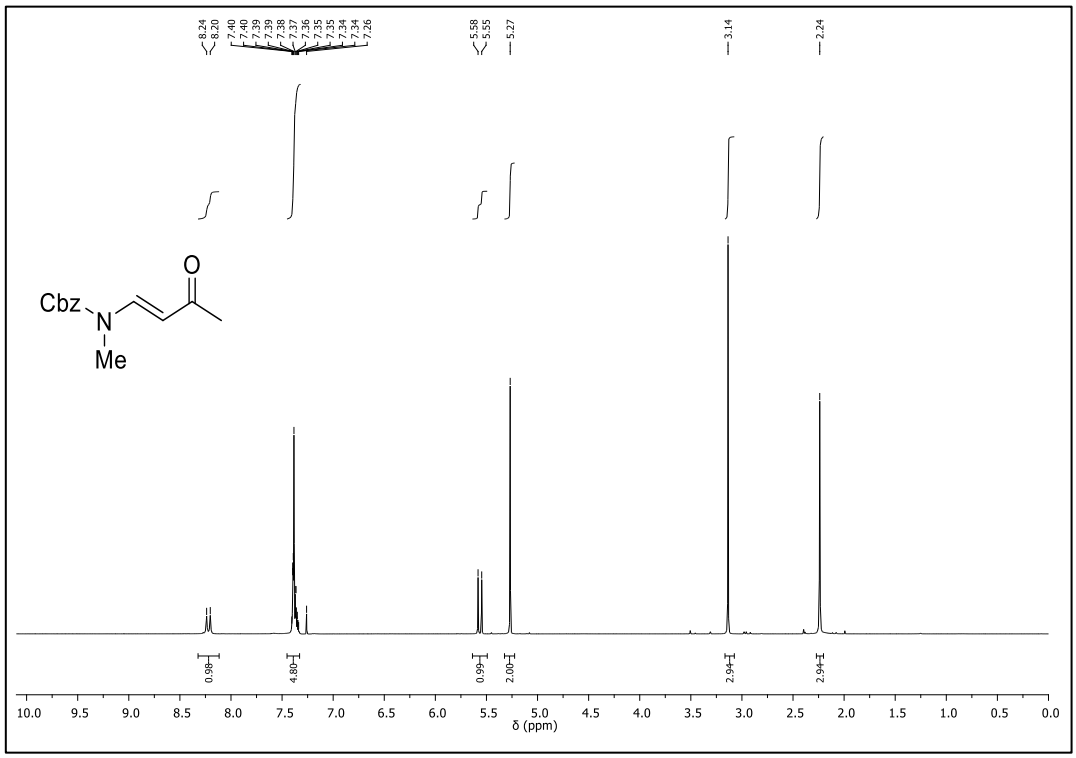

^{13}C-NMR (101 MHz, $CDCl_3$) of **7b**

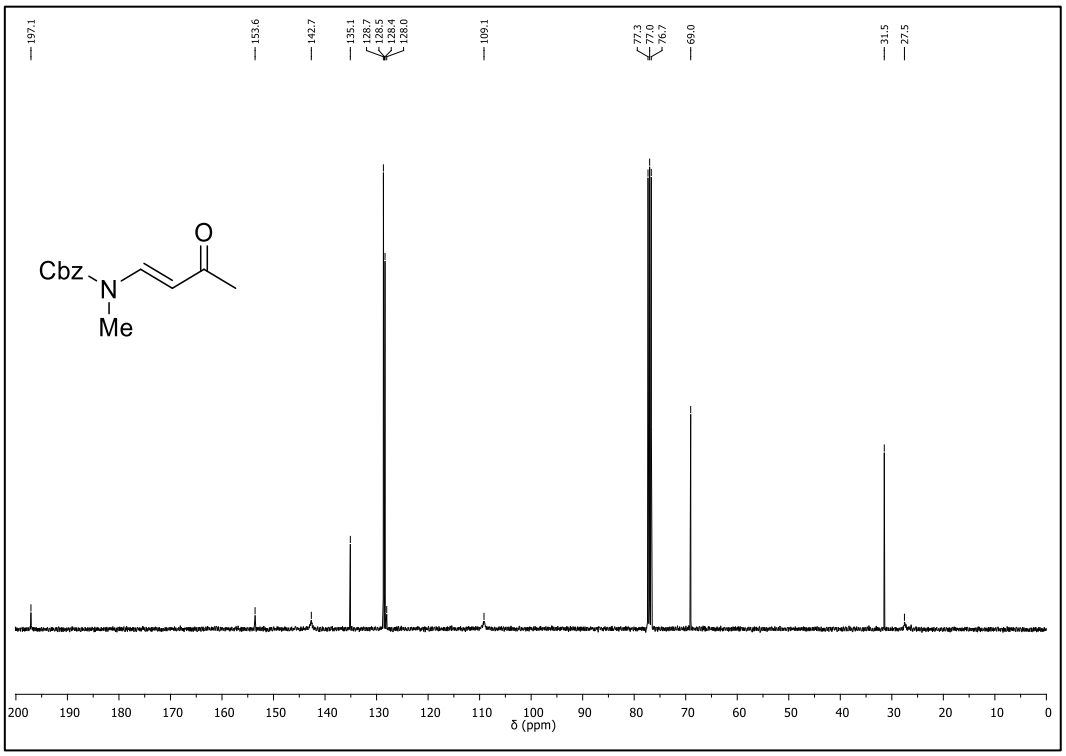

^{1}H-NMR (400 MHz, $CDCl_3$) of **8b**

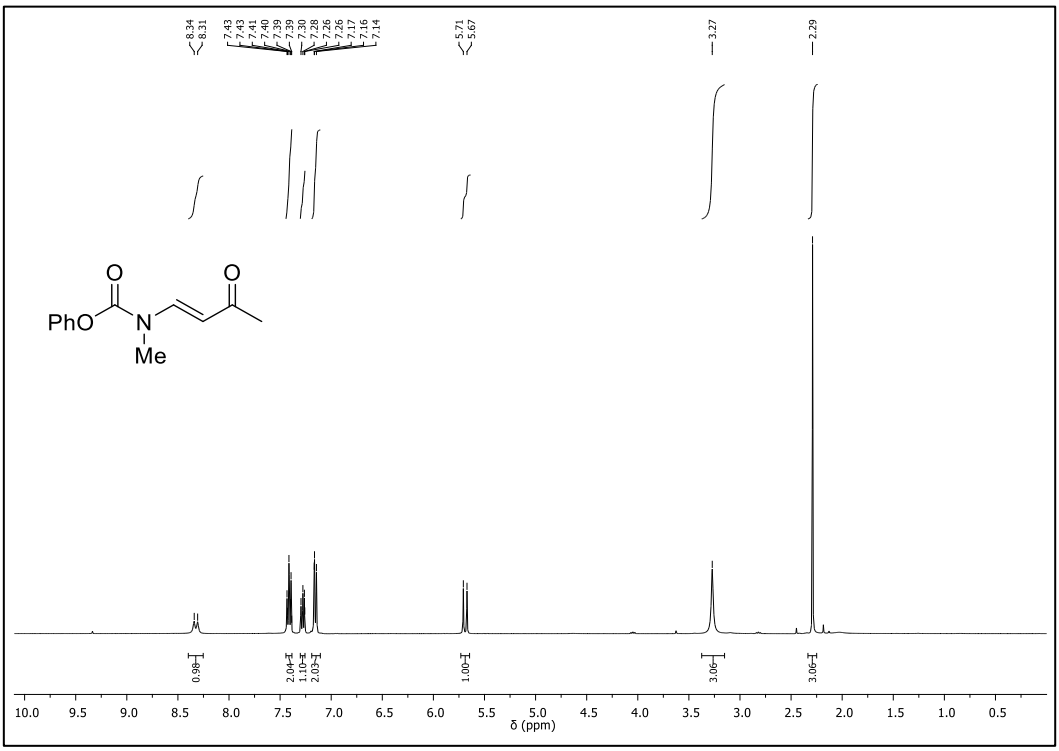

^{13}C-NMR (101 MHz, $CDCl_3$) of **8b**

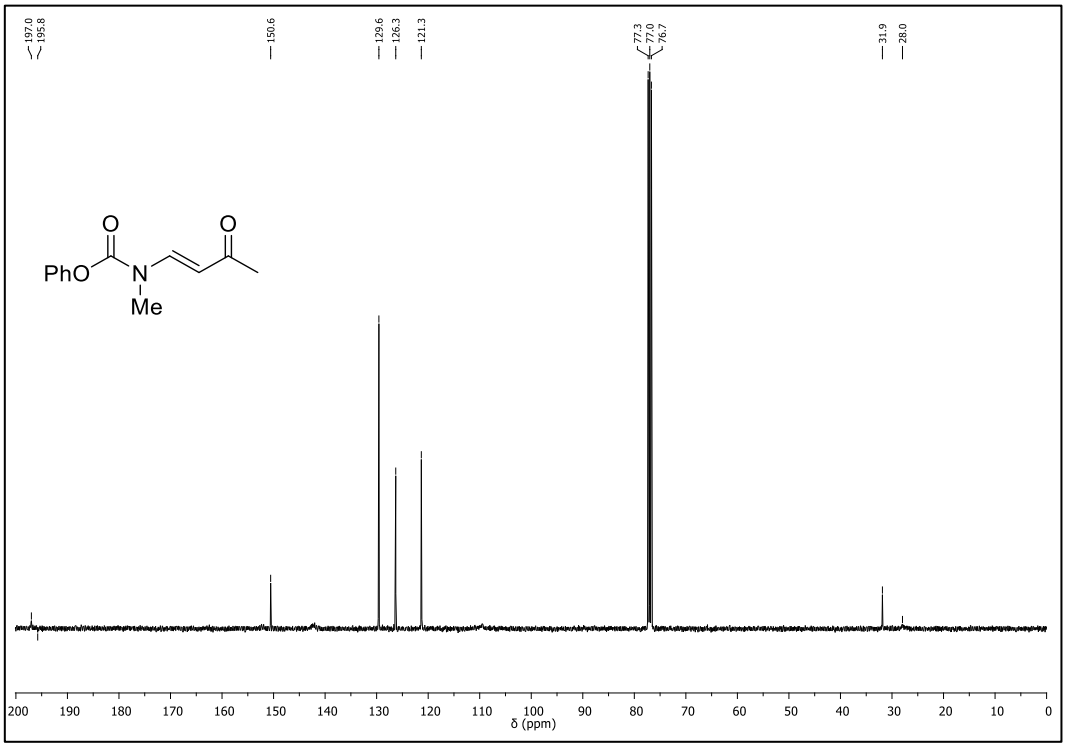

^{1}H-NMR (400 MHz, $CDCl_3$) of **9b**

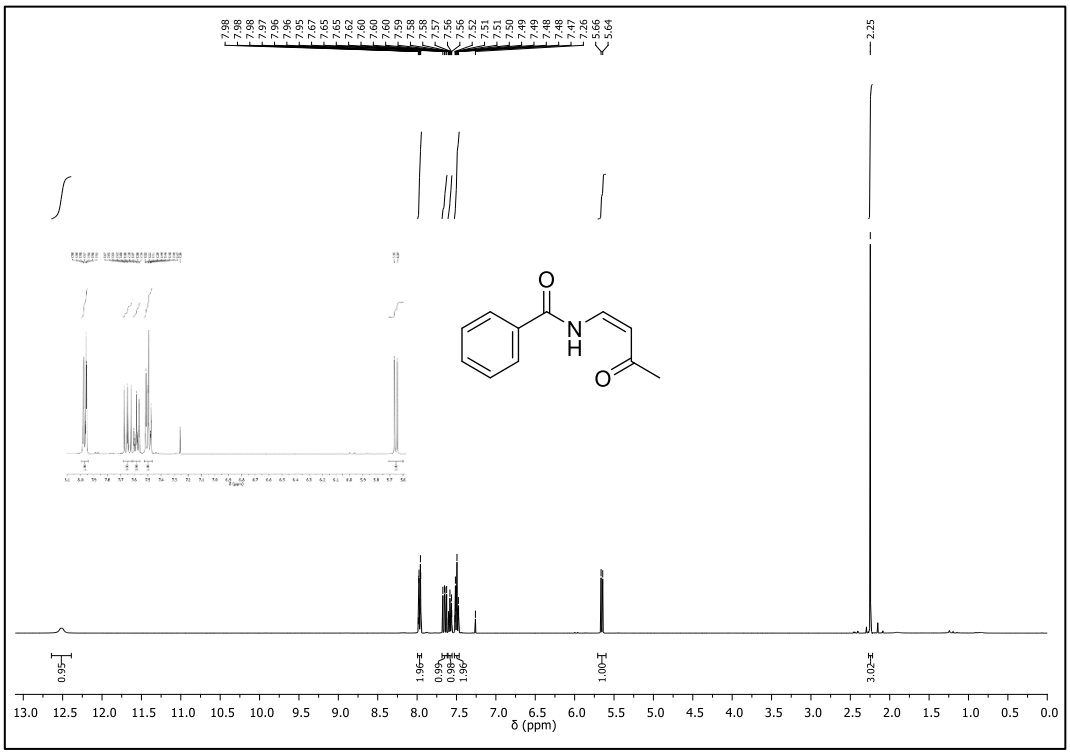

^{13}C-NMR (101 MHz, $CDCl_3$) of **9b**

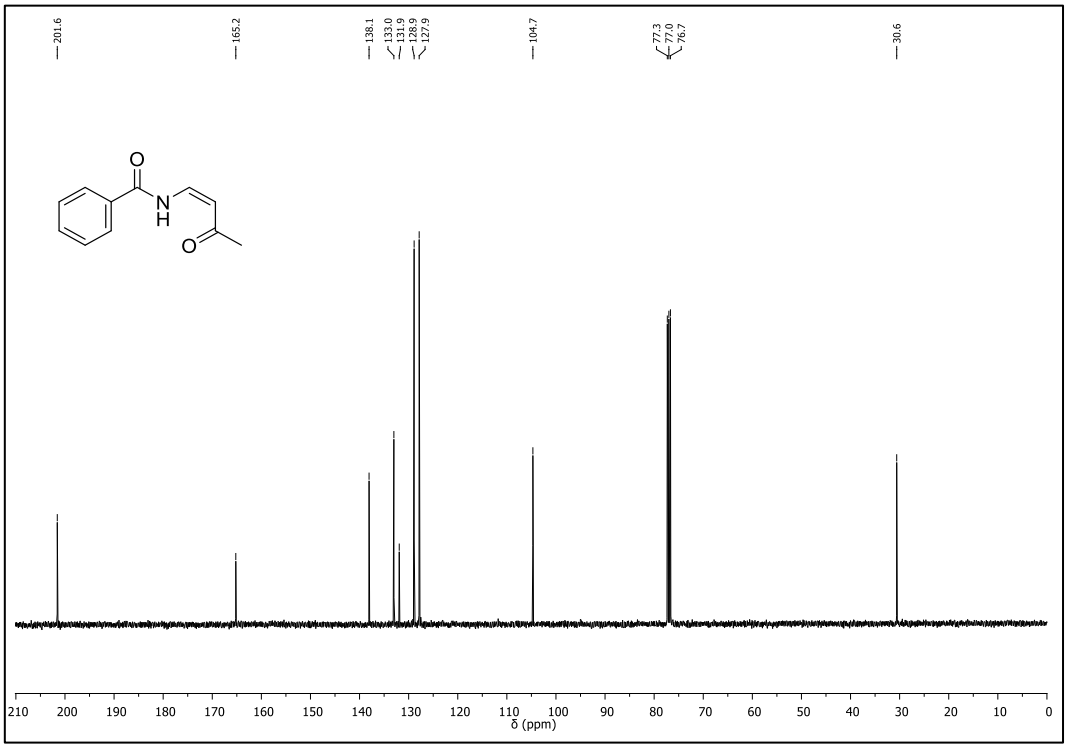

^{1}H-NMR (400 MHz, $CDCl_3$) of **10b**

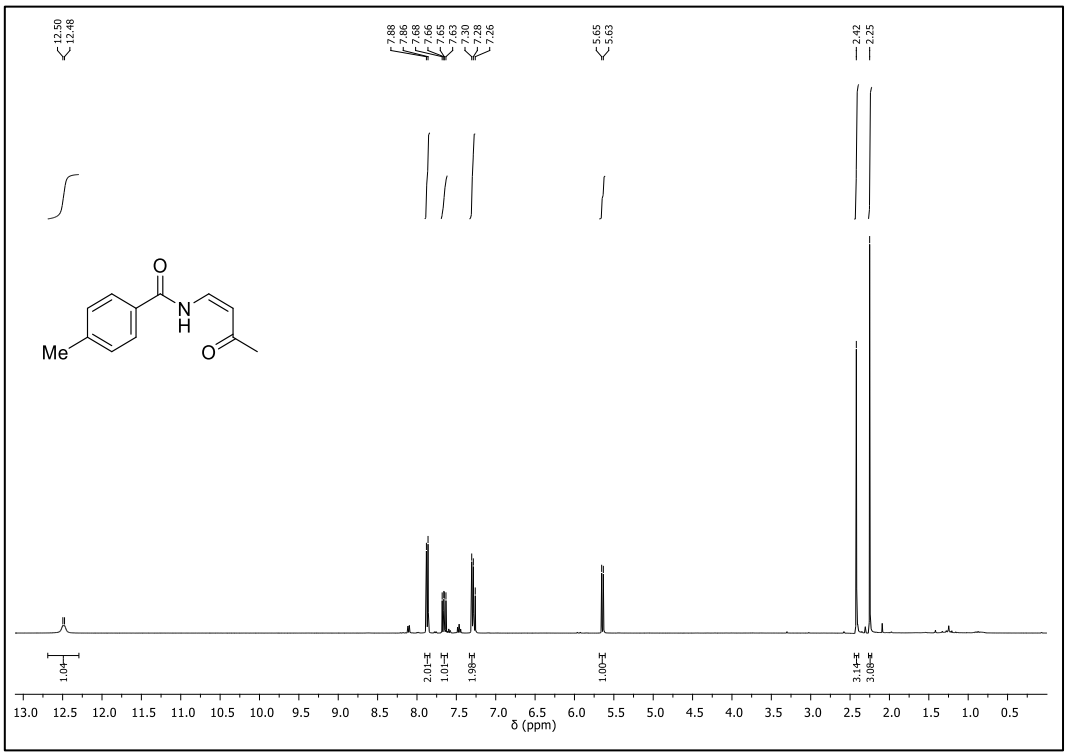

^{13}C-NMR (101 MHz, $CDCl_3$) of **10b**

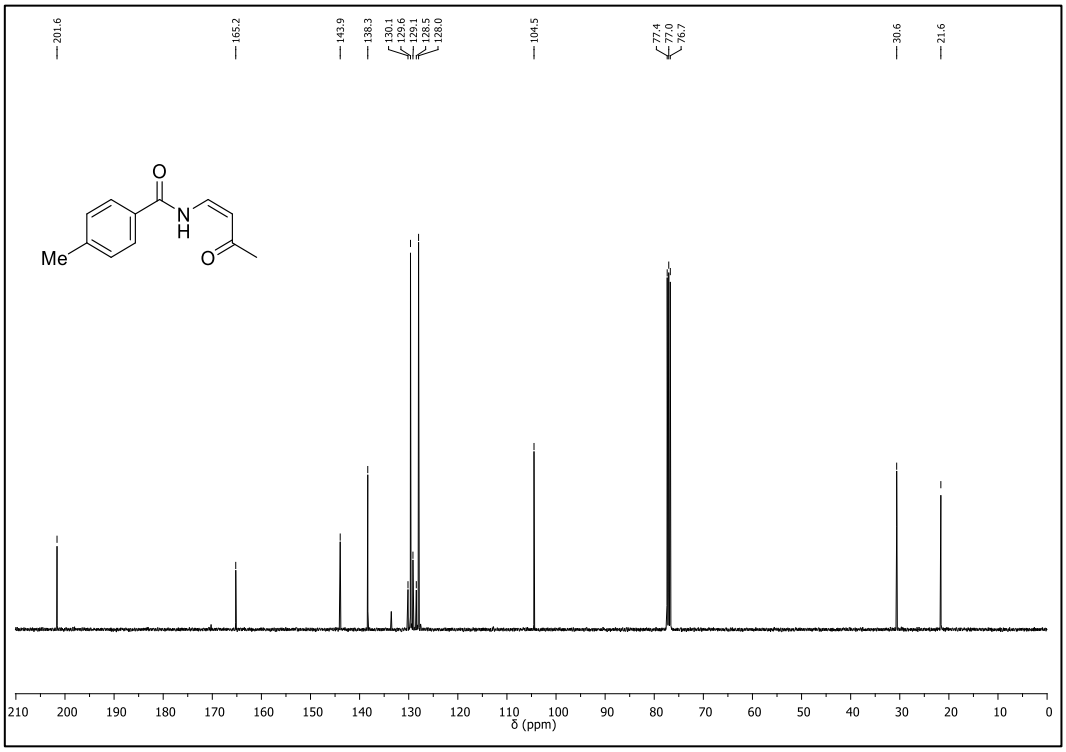

^{1}H-NMR (400 MHz, $CDCl_3$) of **11b**

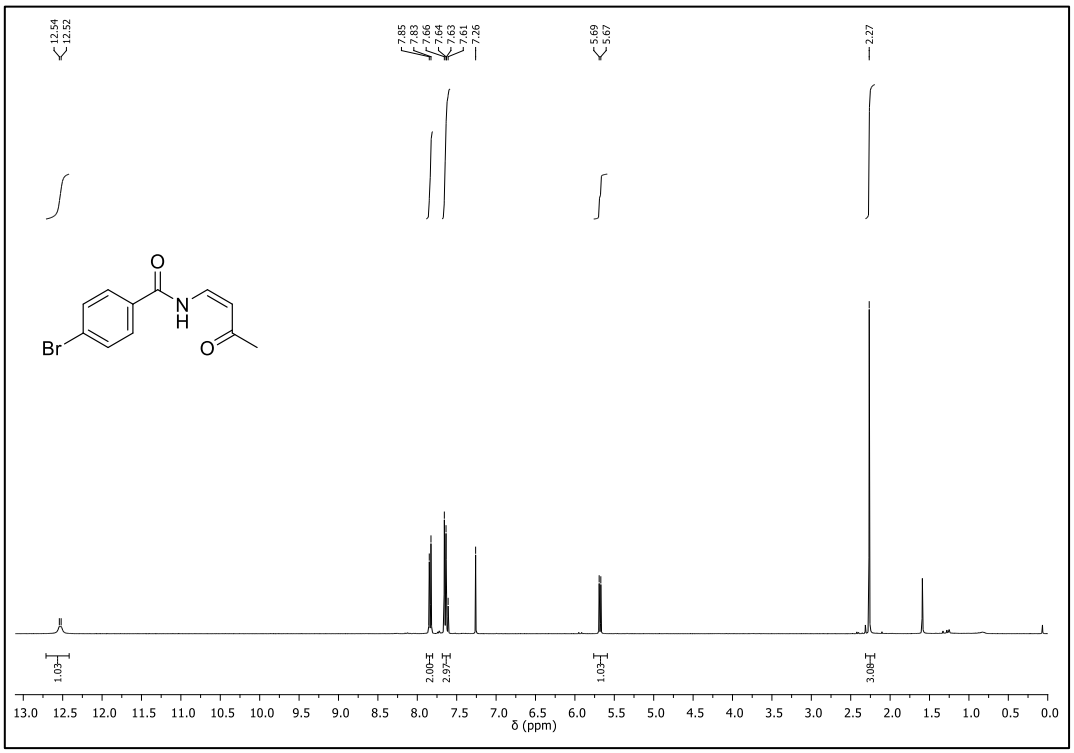

^{13}C-NMR (101 MHz, $CDCl_3$) of **11b**

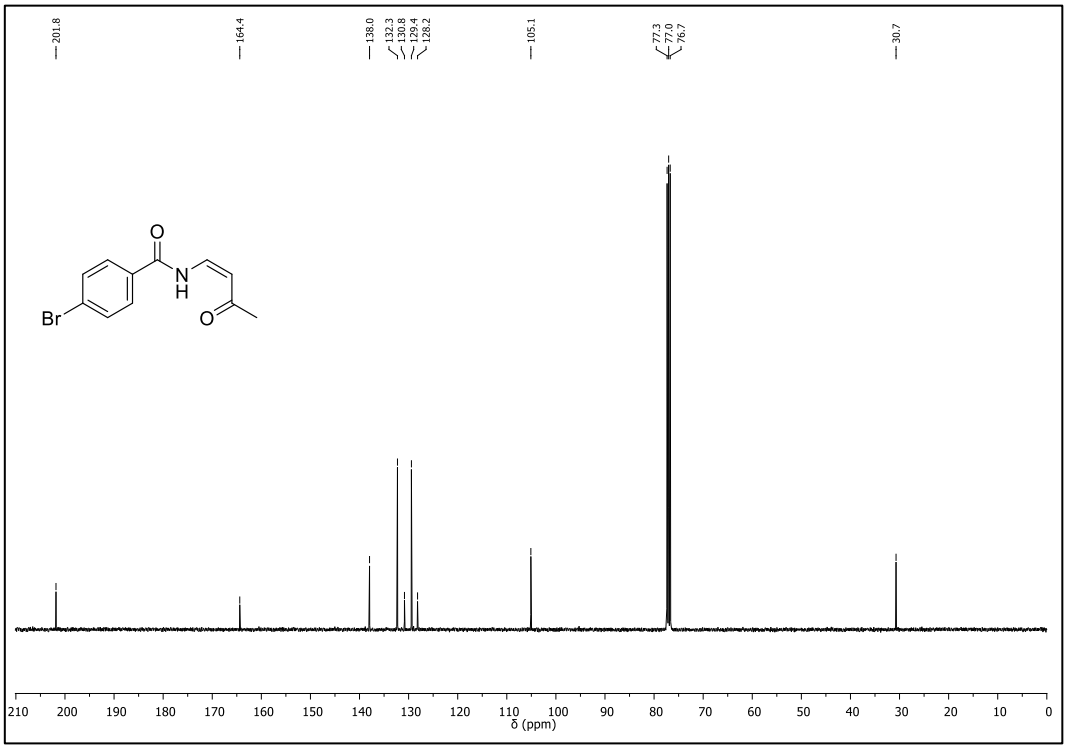

^{1}H-NMR (400 MHz, $CDCl_3$) of **12b**

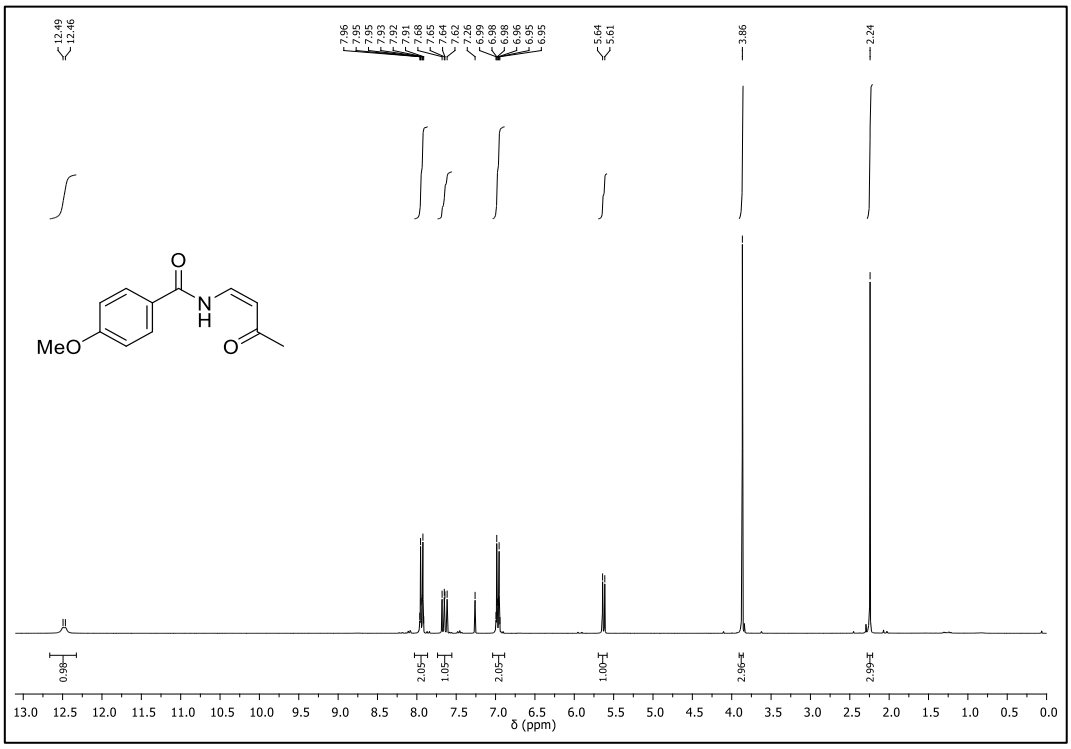

^{13}C-NMR (101 MHz, $CDCl_3$) of **12b**

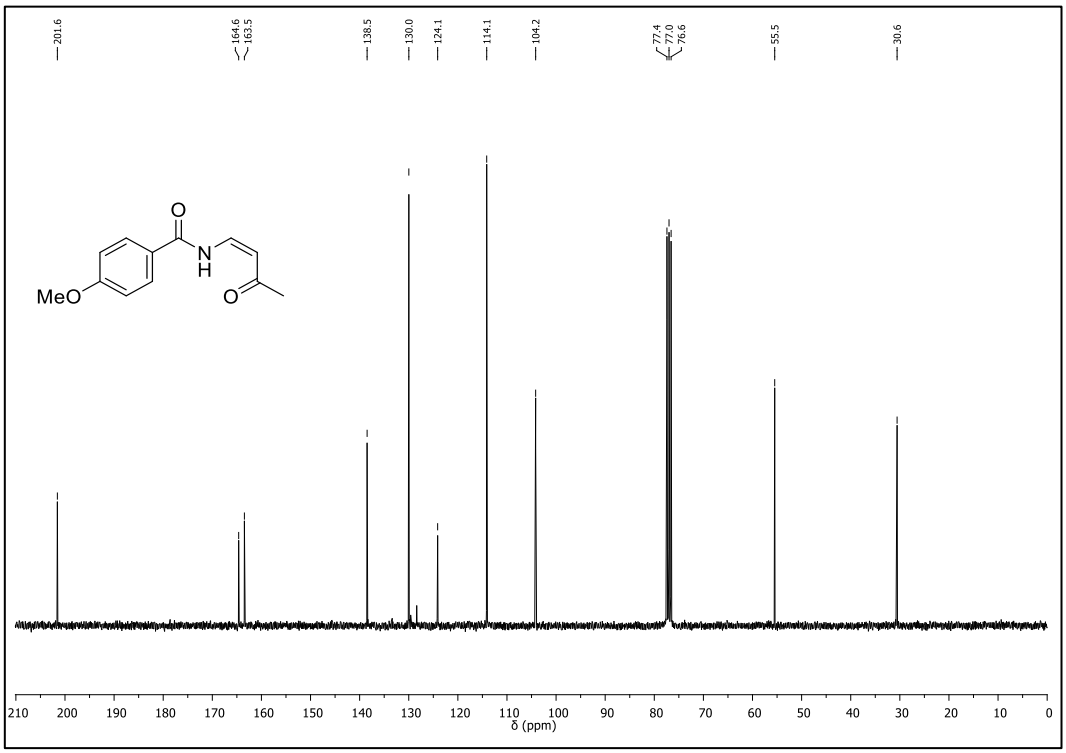

^{1}H-NMR (400 MHz, $CDCl_3$) of **13b**

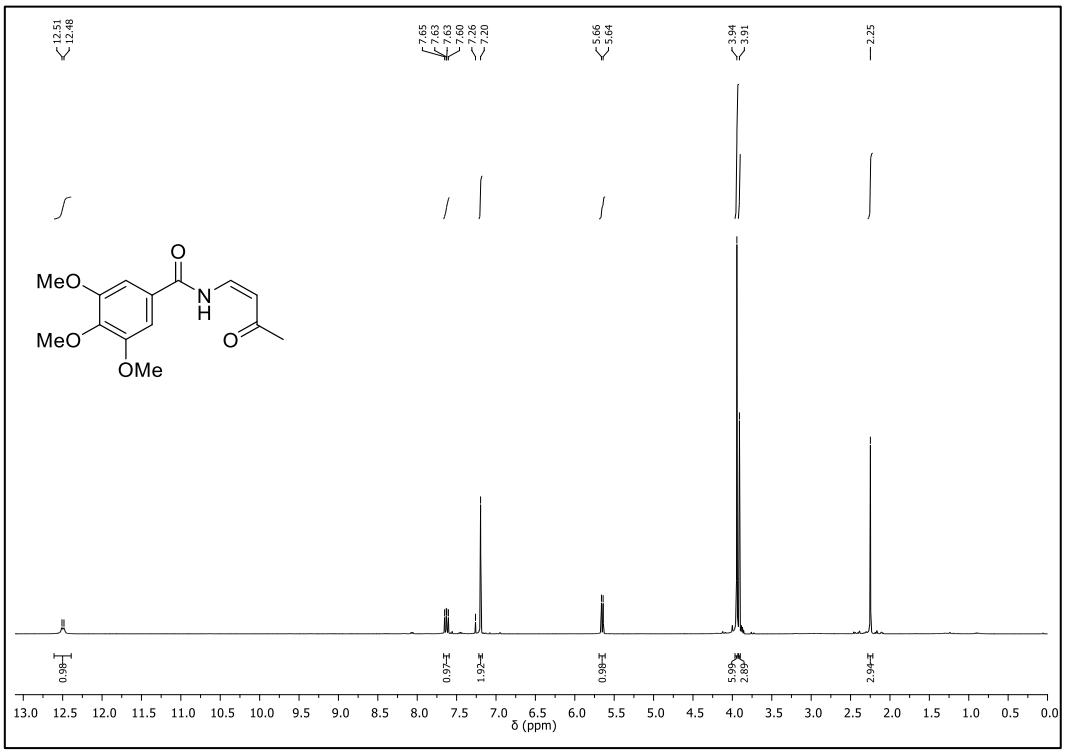

^{13}C-NMR (101 MHz, $CDCl_3$) of **13b**

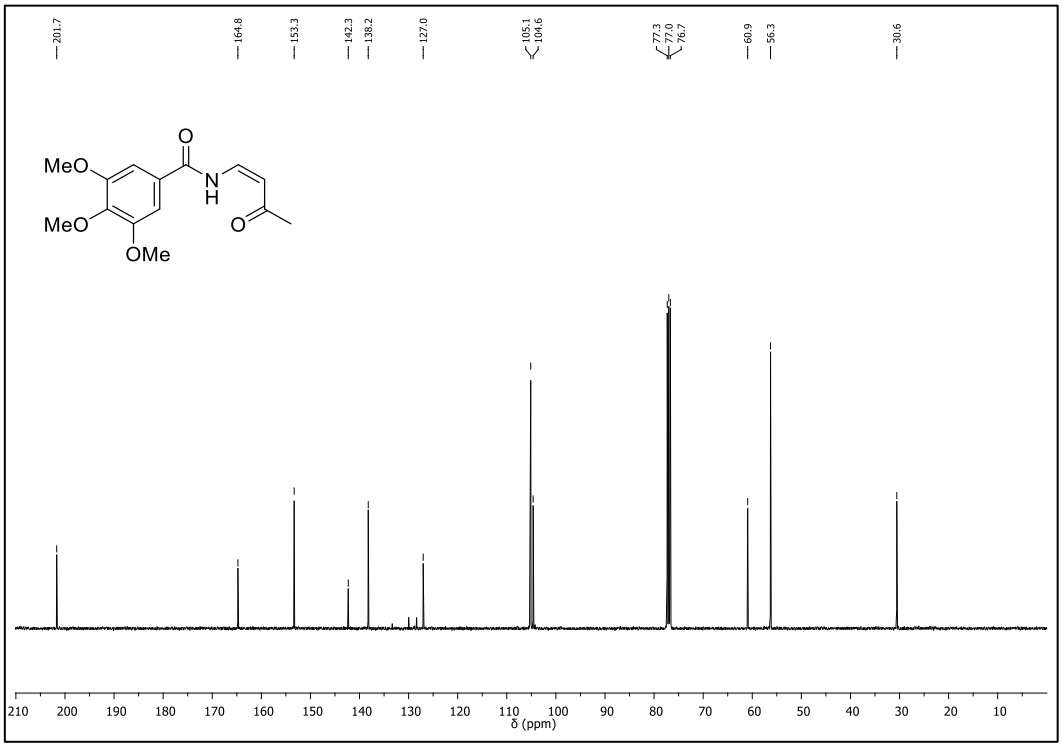

^{1}H-NMR (400 MHz, $CDCl_3$) of **14b**

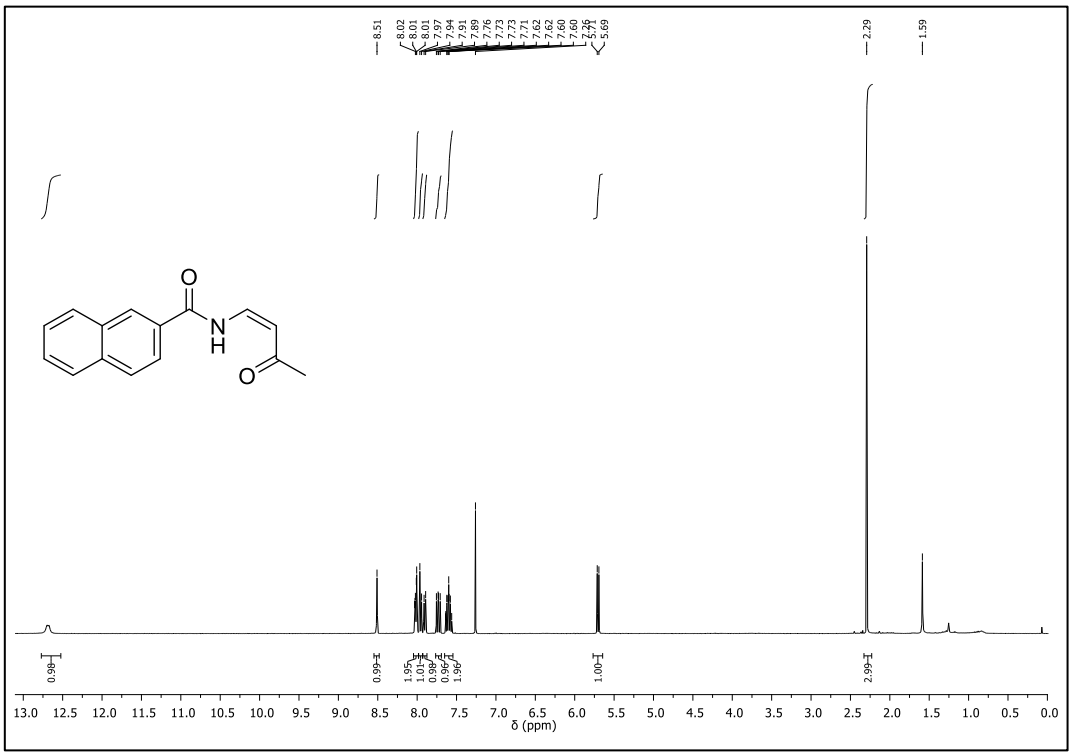

^{13}C-NMR (101 MHz, $CDCl_3$) of **14b**

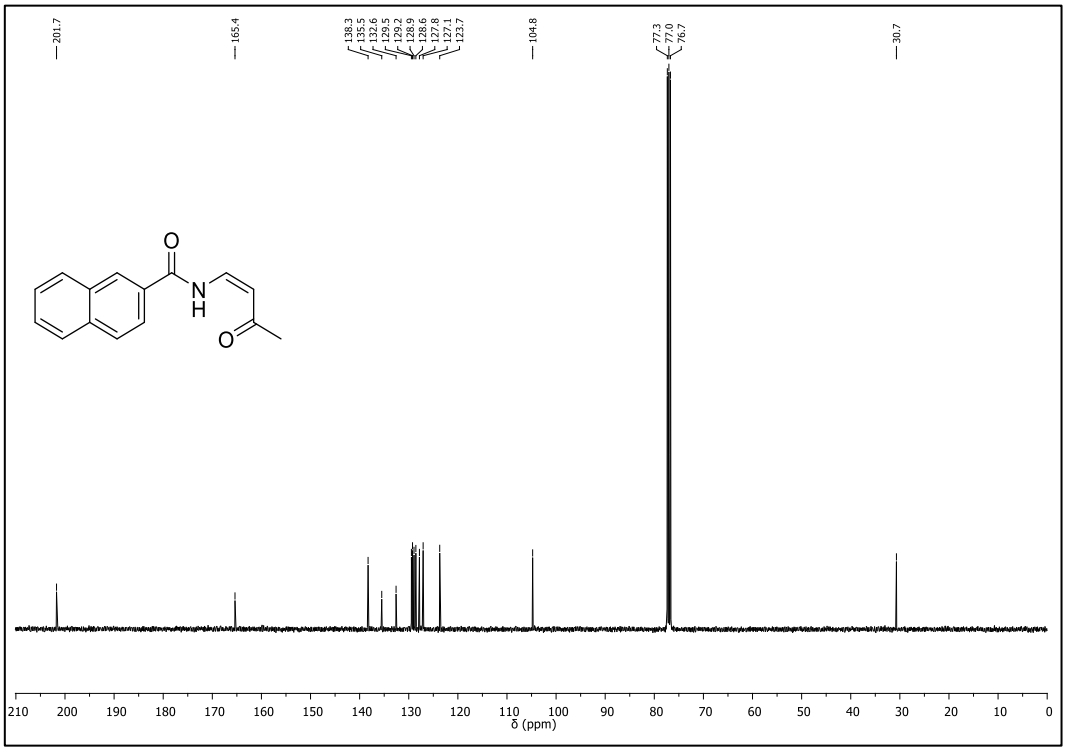

^{1}H-NMR (400 MHz, $CDCl_3$) of **15b**

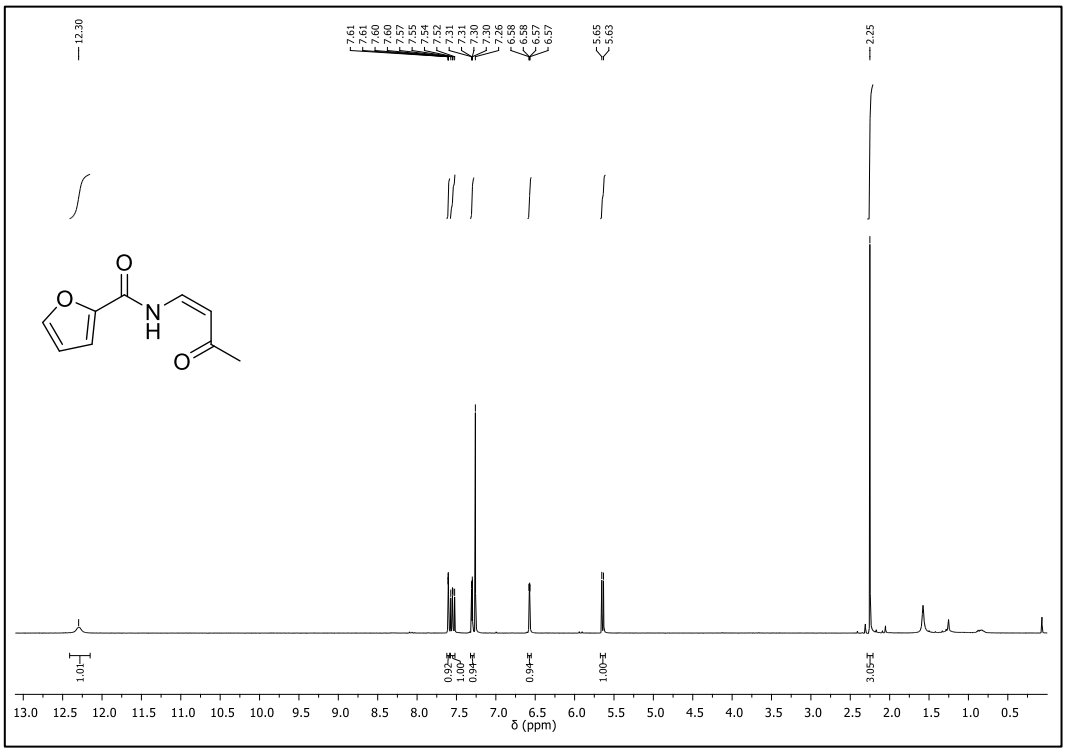

^{13}C-NMR (101 MHz, $CDCl_3$) of **15b**

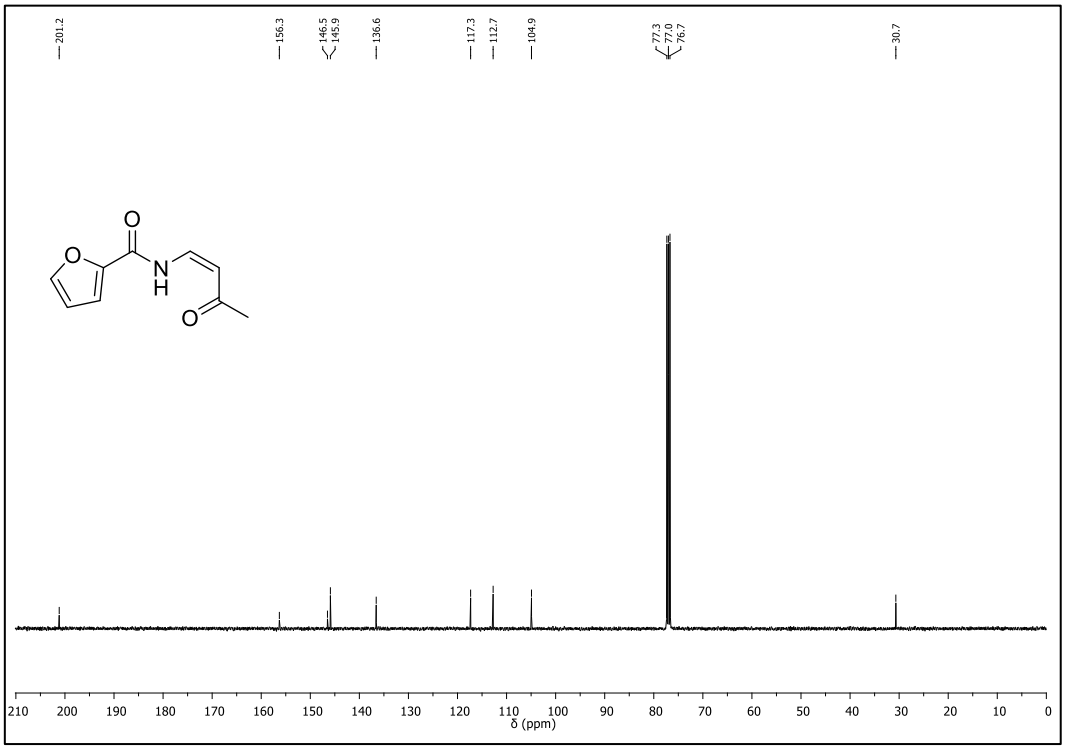

^{1}H-NMR (400 MHz, $CDCl_3$) of **16b** (*Z* isomer)

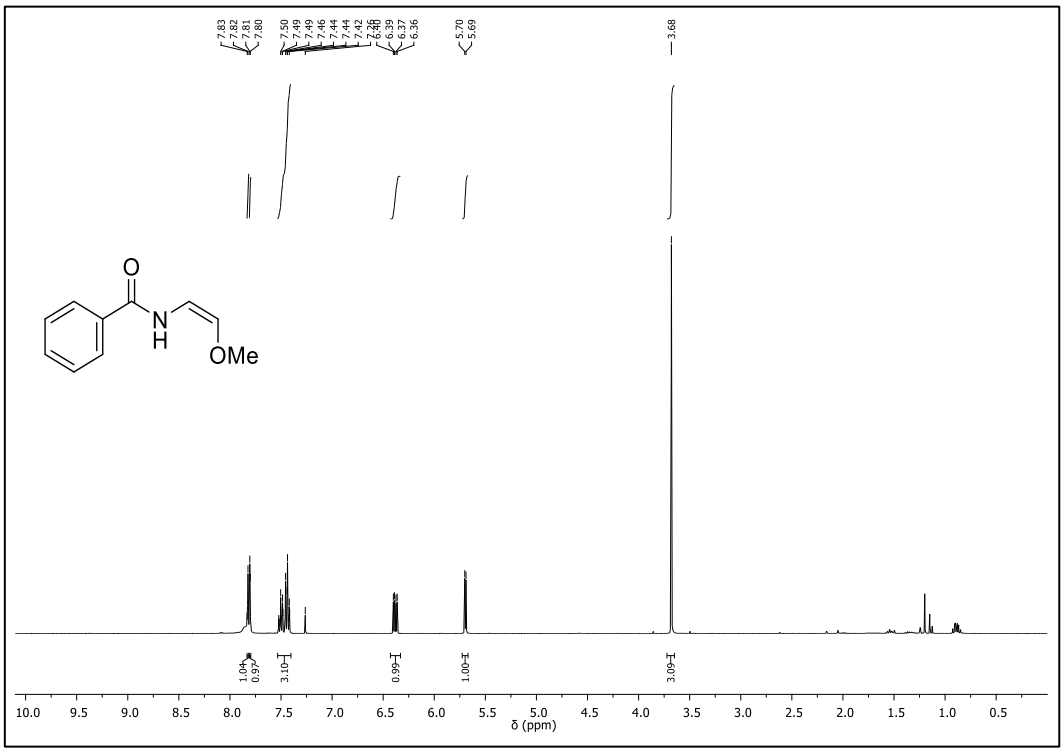

^{13}C-NMR (101 MHz, $CDCl_3$) of **16b** (*Z* isomer)

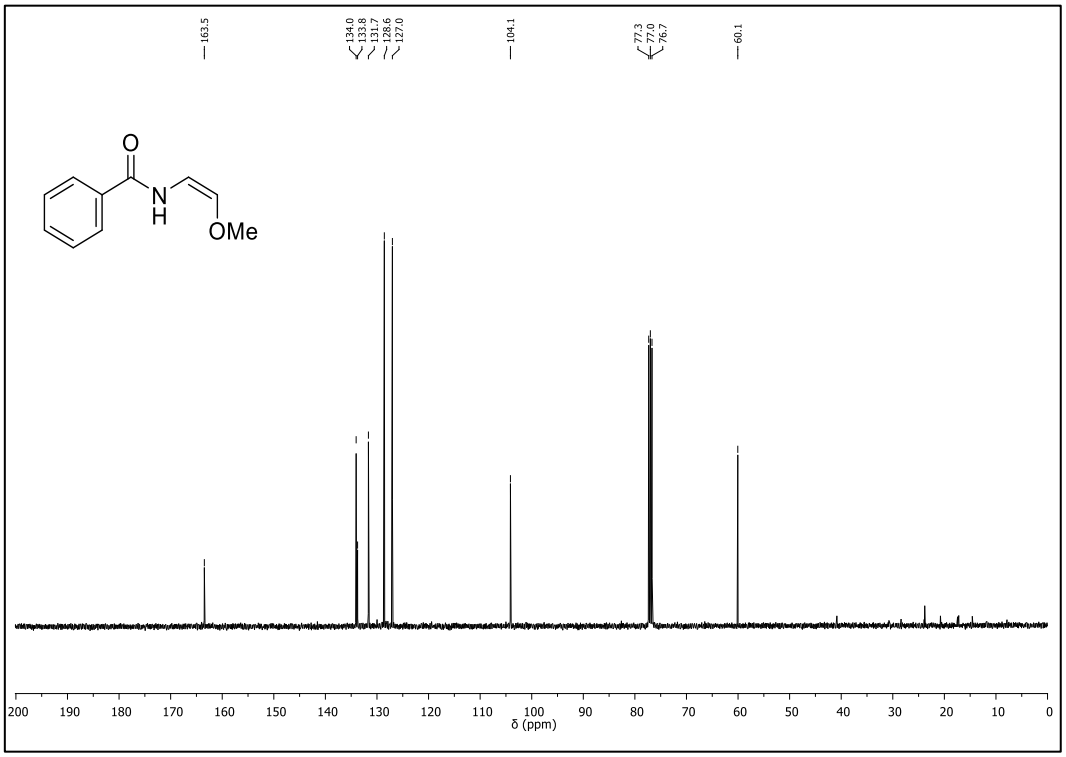

^{1}H-NMR (400 MHz, $CDCl_3$) of **16b** (*E* isomer)

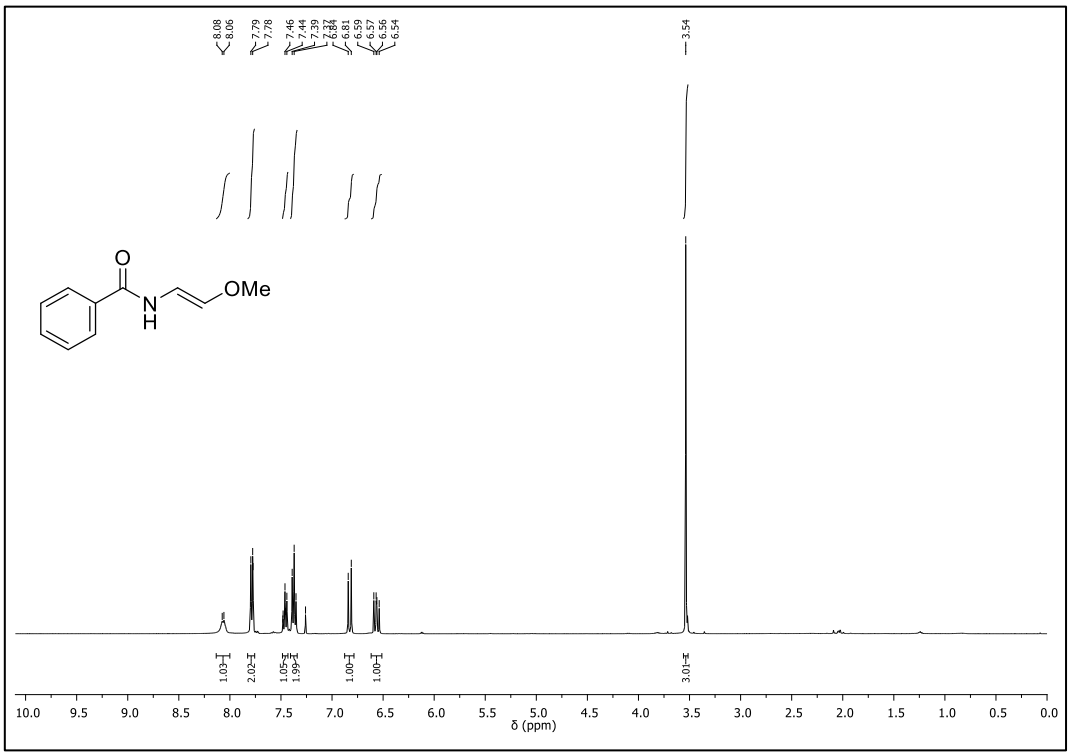

^{13}C-NMR (101 MHz, $CDCl_3$) of **16b** (*E* isomer)

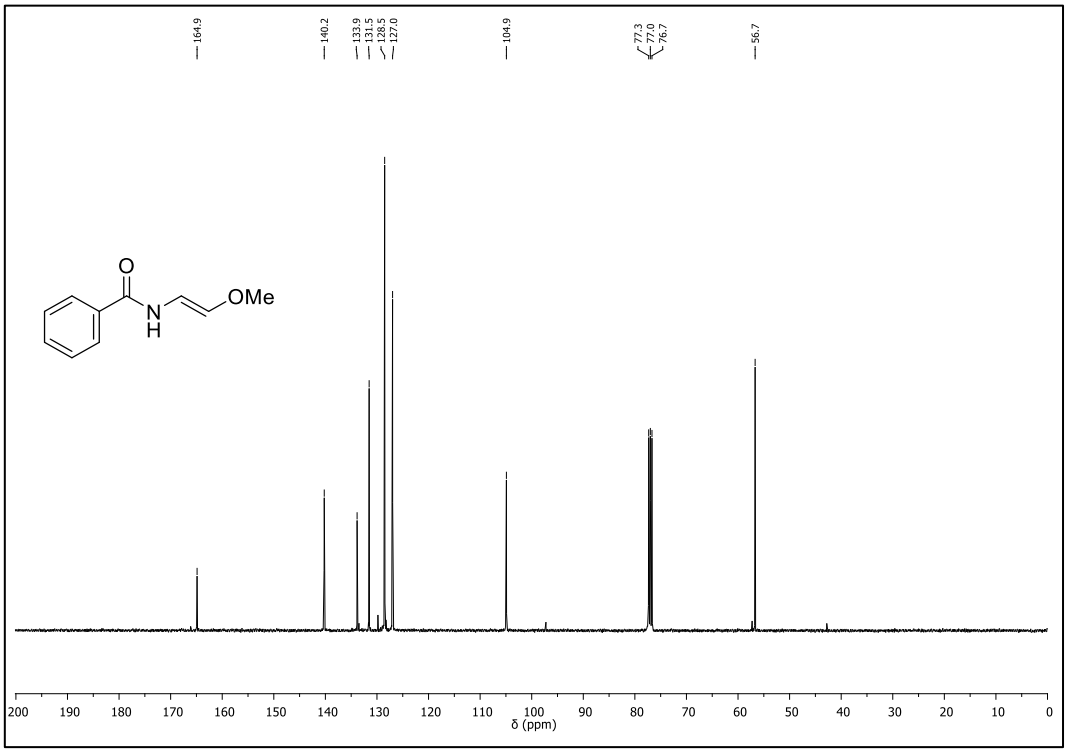

^{1}H-NMR (400 MHz, CD_3CN) of **17b**

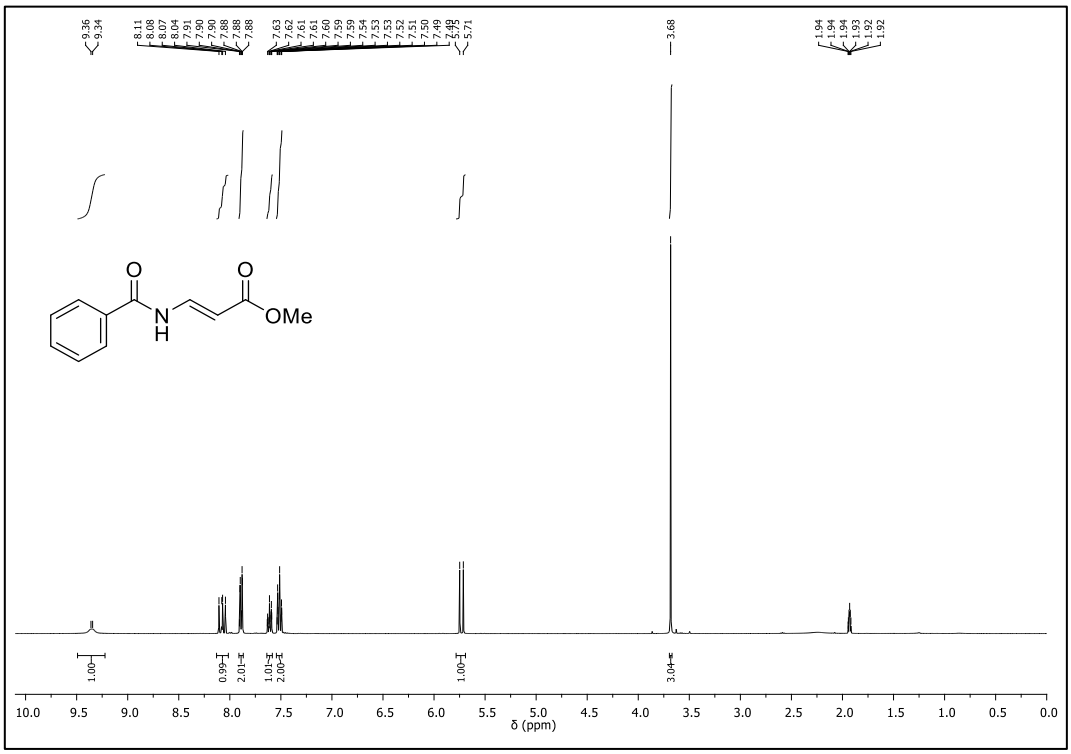

^{13}C-NMR (101 MHz, CD_3CN) of **17b**

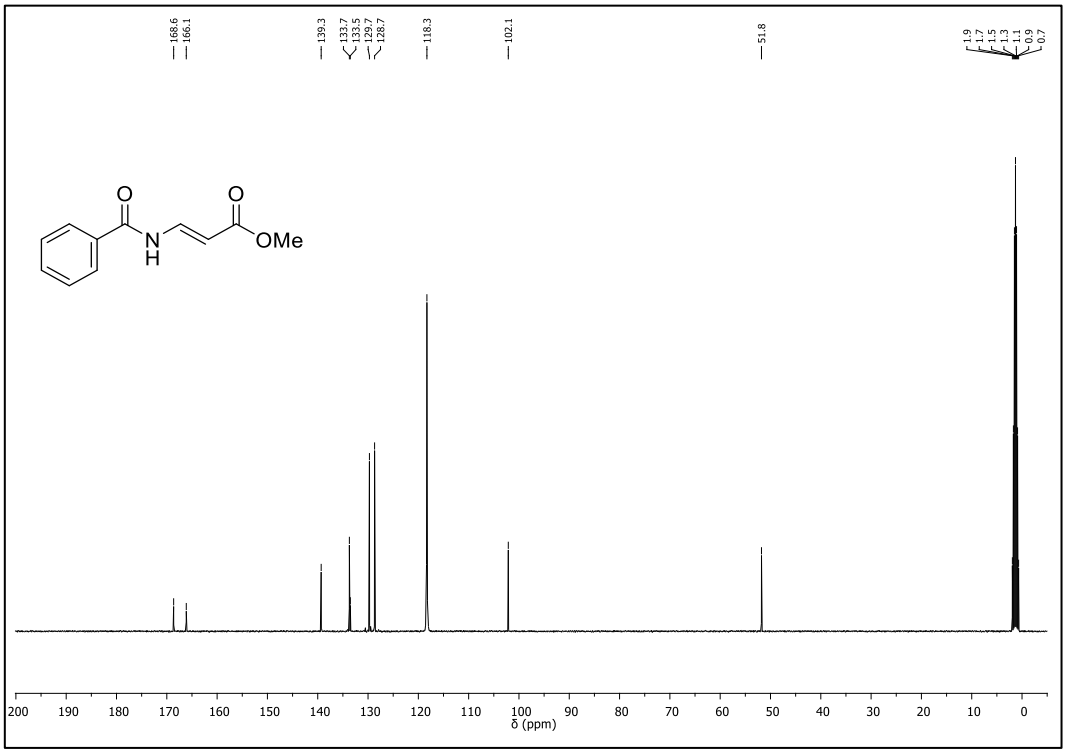

^{1}H-NMR (400 MHz, $CDCl_3$) of **18b**

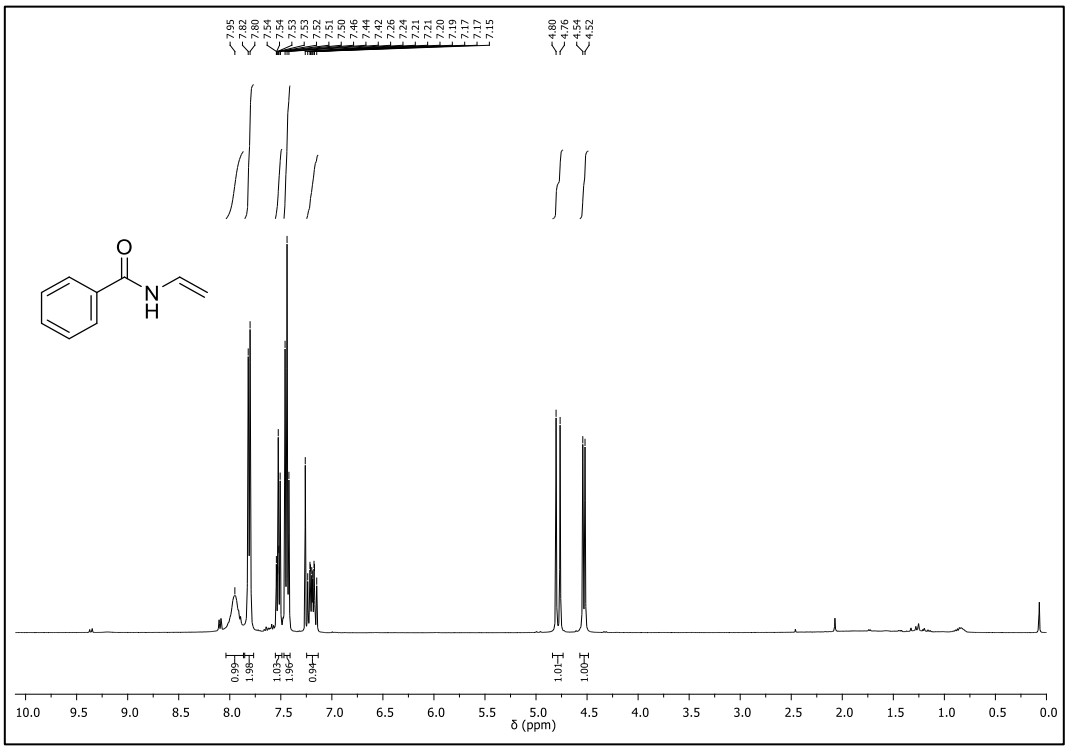

^{13}C-NMR (101 MHz, $CDCl_3$) of **18b**

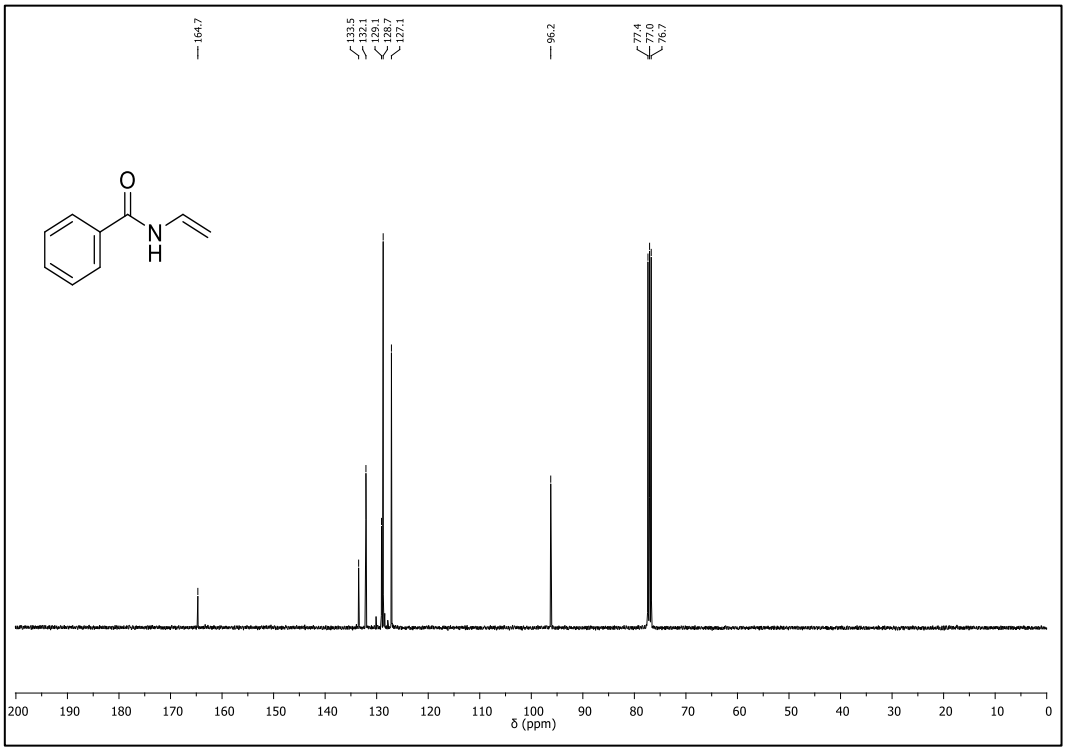

^{1}H-NMR (400 MHz, $CDCl_3$) of **19b**

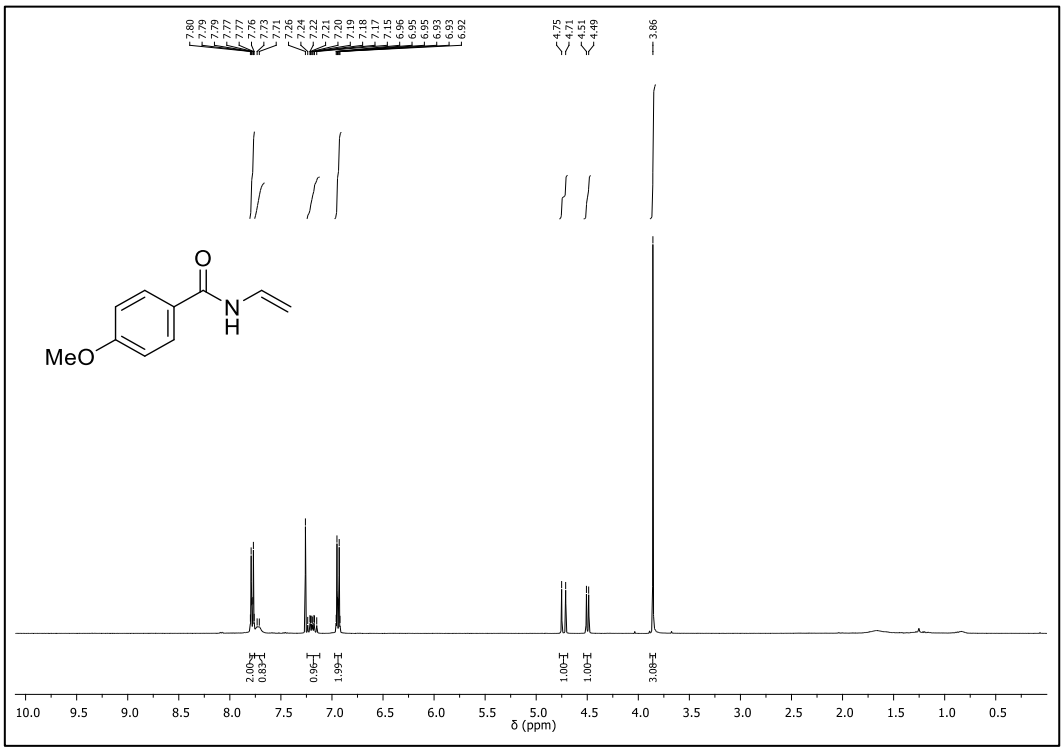

^{13}C-NMR (101 MHz, $CDCl_3$) of **19b**

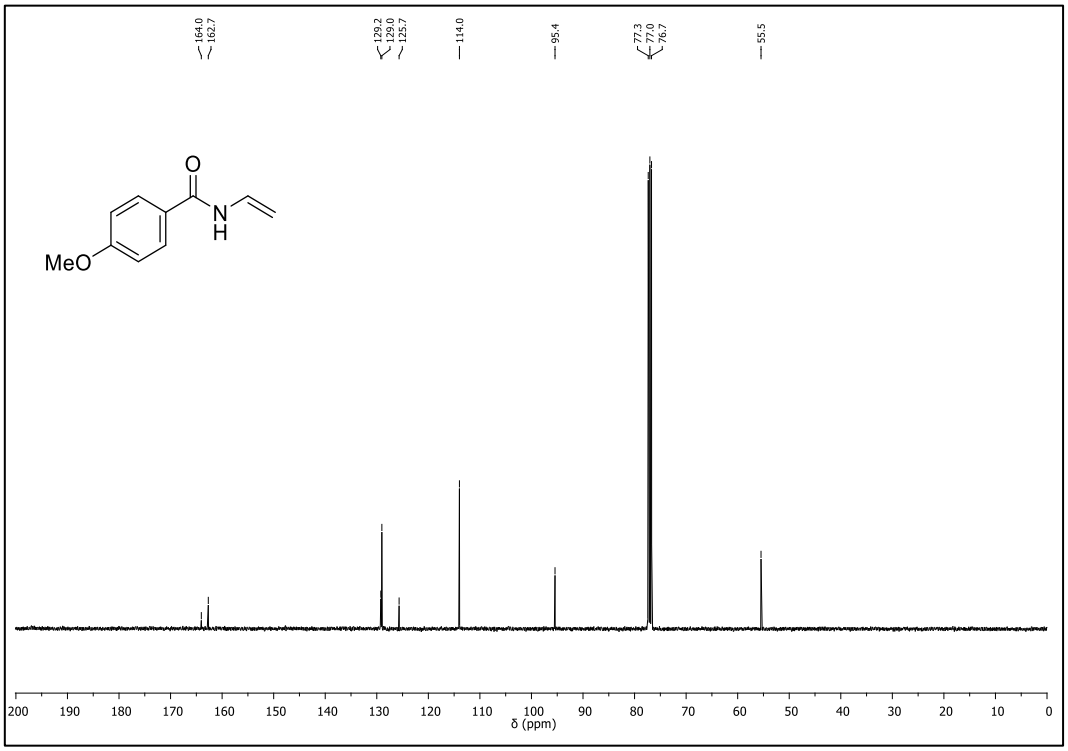

^{1}H-NMR (400 MHz, $CDCl_3$) of **20b**

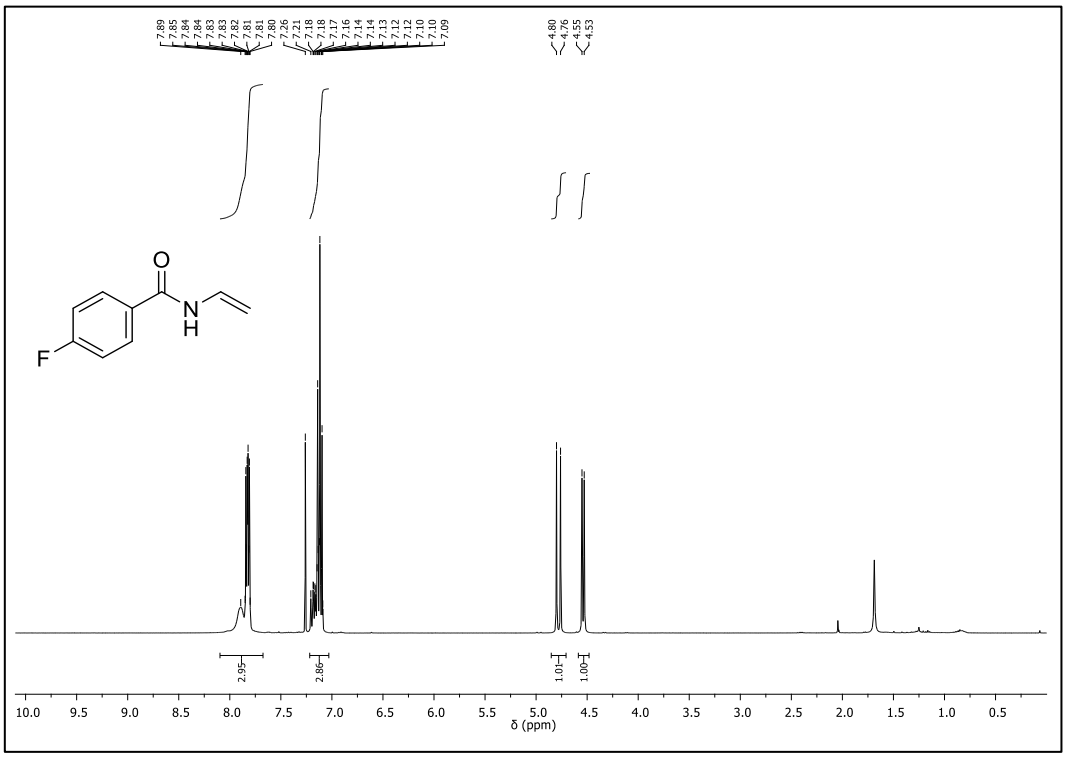

^{13}C-NMR (101 MHz, $CDCl_3$) of **20b**

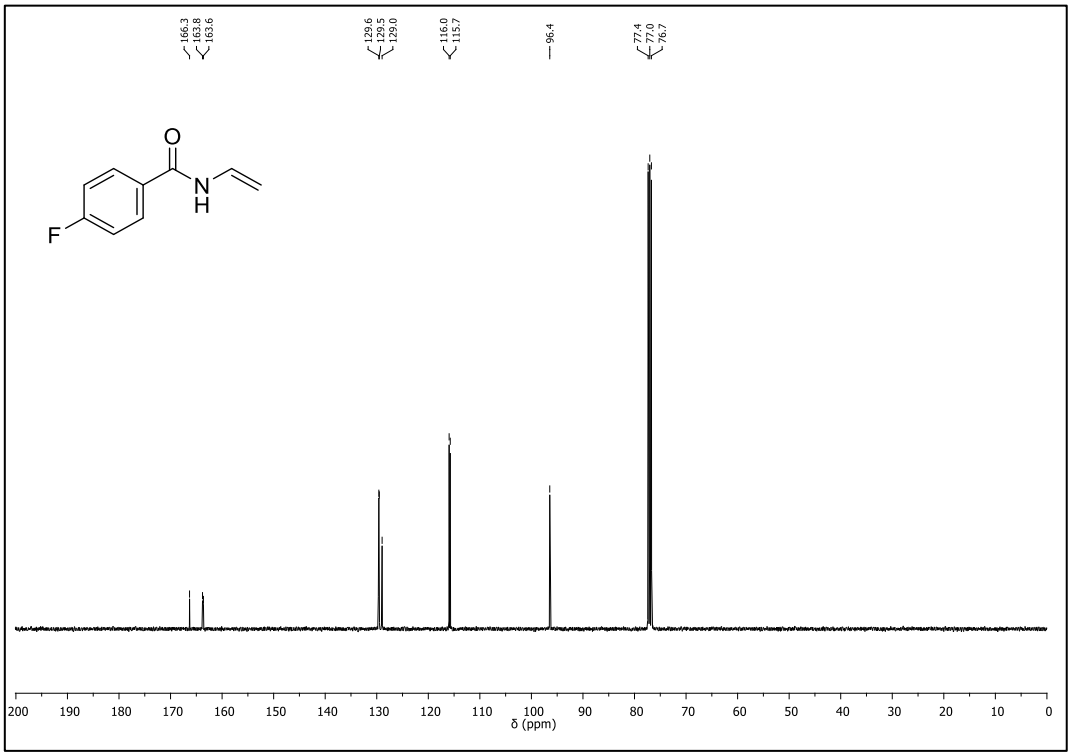

^{19}F-NMR (377 MHz, $CDCl_3$) of **20b**

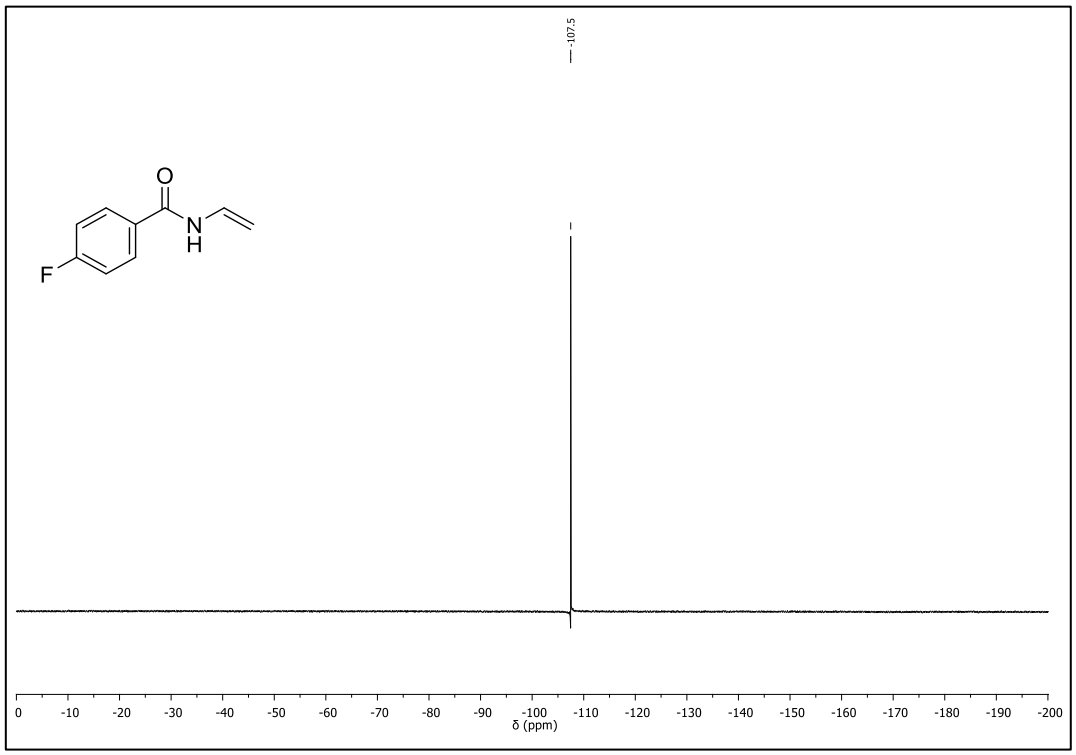

^{1}H-NMR (400 MHz, $CDCl_3$) of **21b**

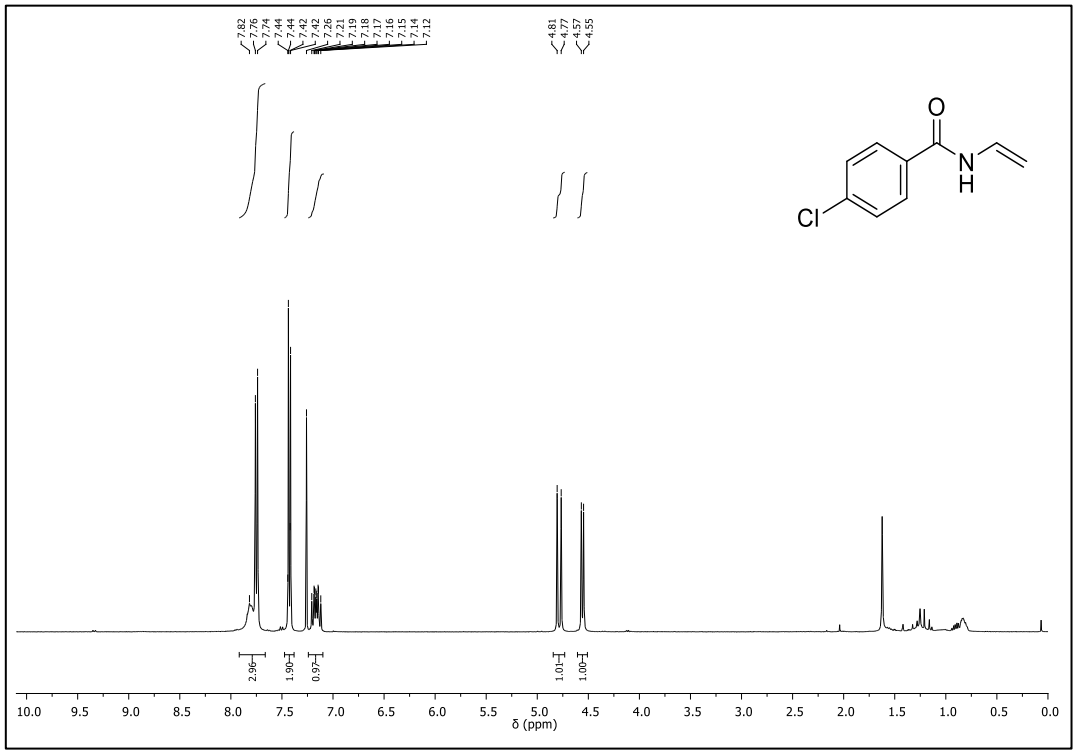

^{13}C-NMR (101 MHz, $CDCl_3$) of **21b**

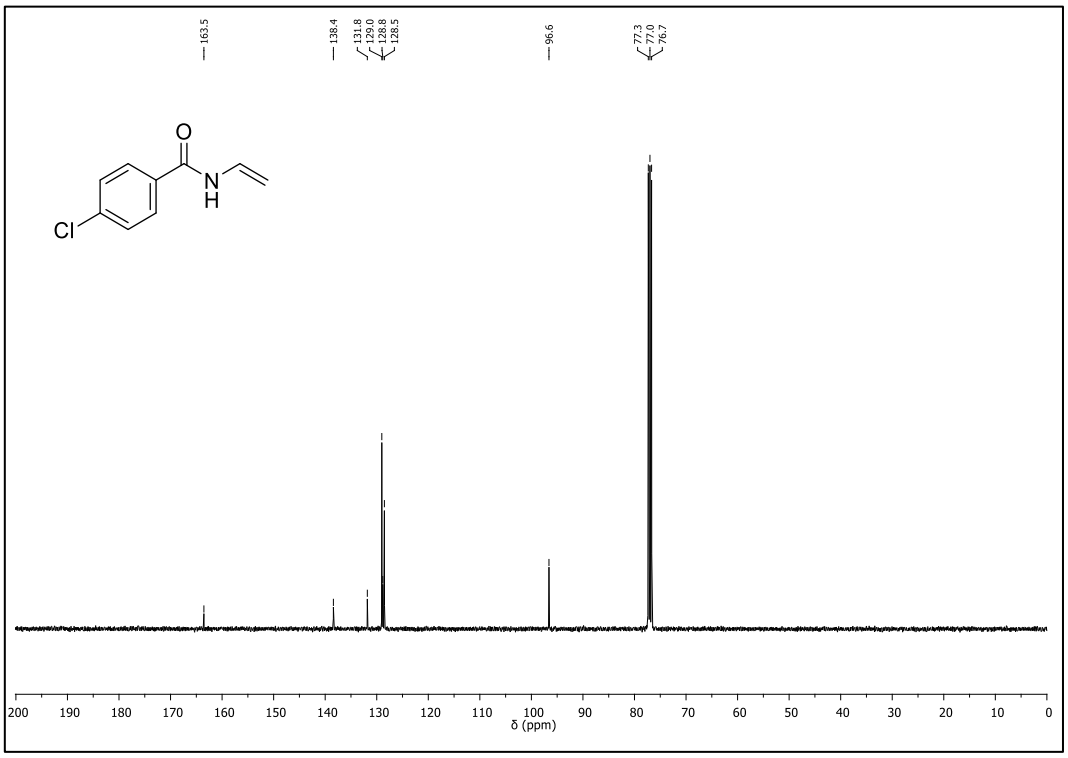

^{1}H-NMR (400 MHz, $CDCl_3$) of **22b**

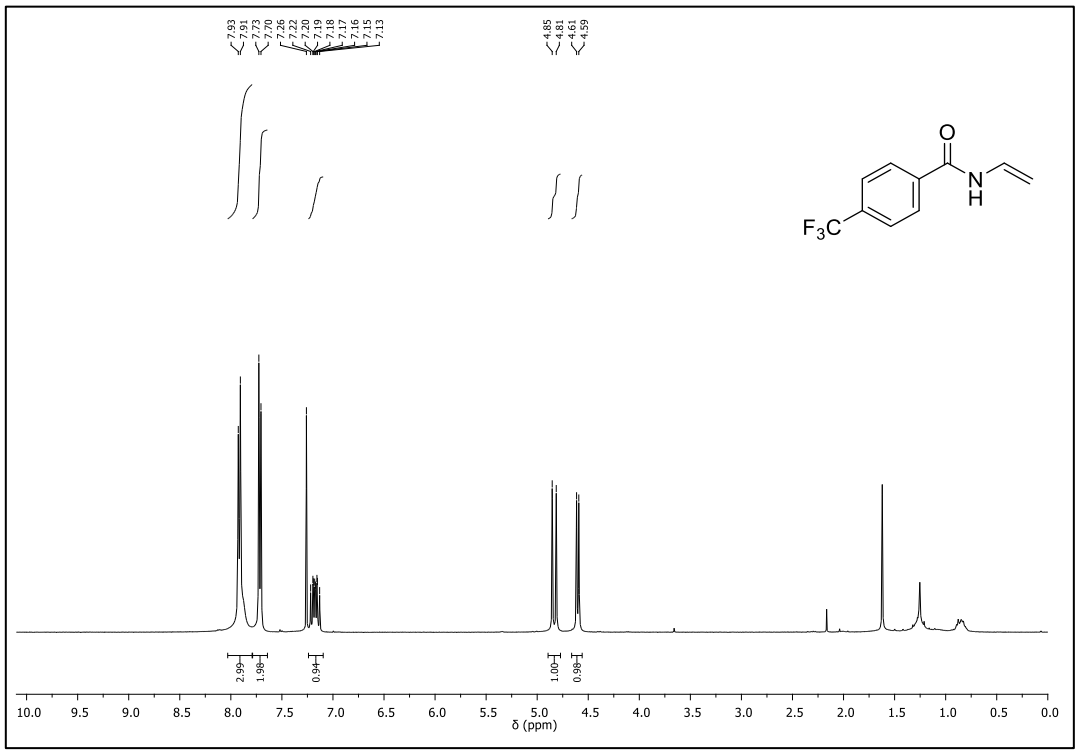

^{13}C-NMR (101 MHz, $CDCl_3$) of **22b**

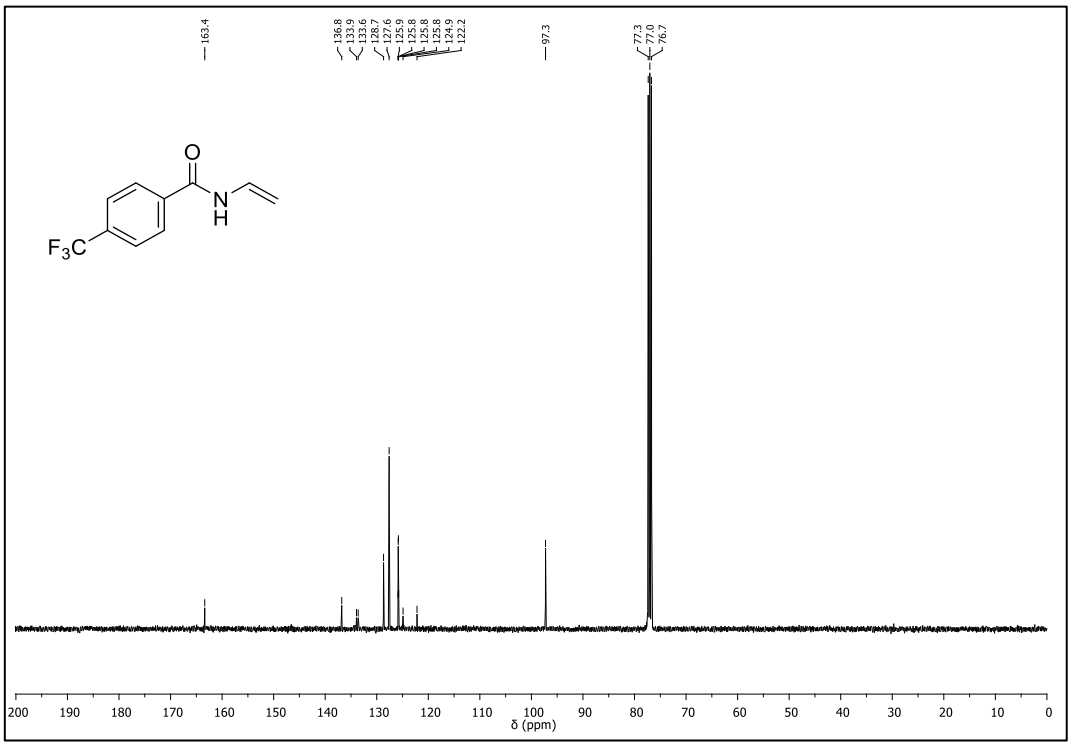

^{19}F-NMR (377 MHz, $CDCl_3$) of **22b**

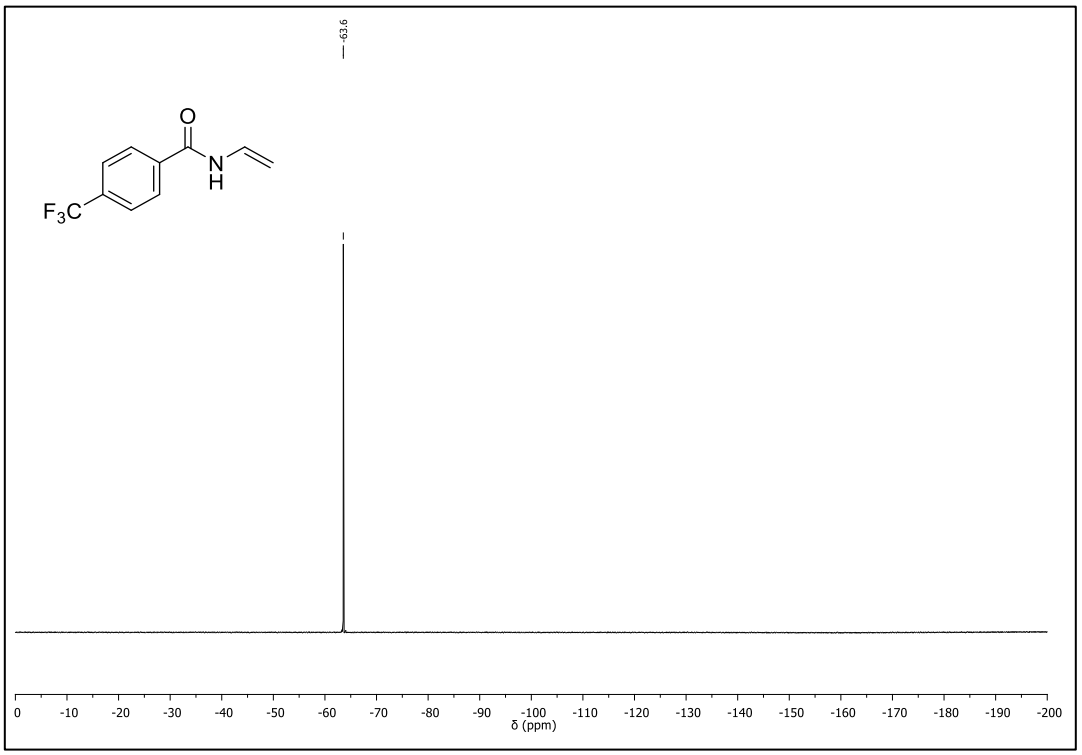

^{1}H-NMR (400 MHz, $CDCl_3$) of **23b**

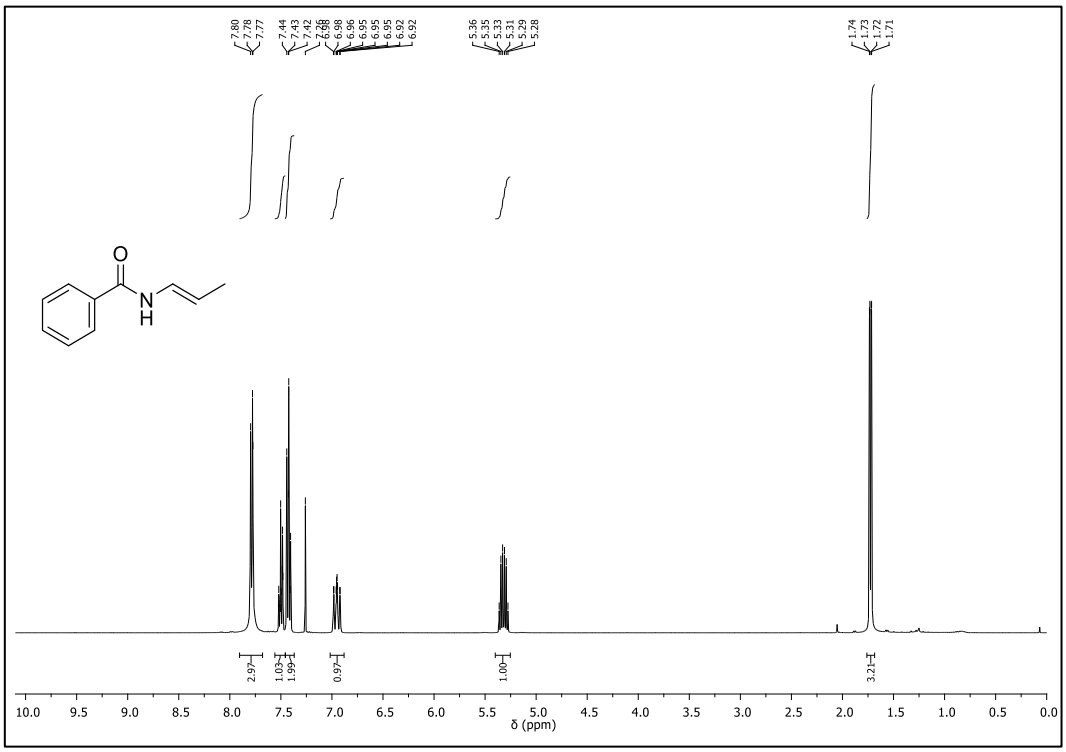

^{13}C-NMR (101 MHz, $CDCl_3$) of **23b**

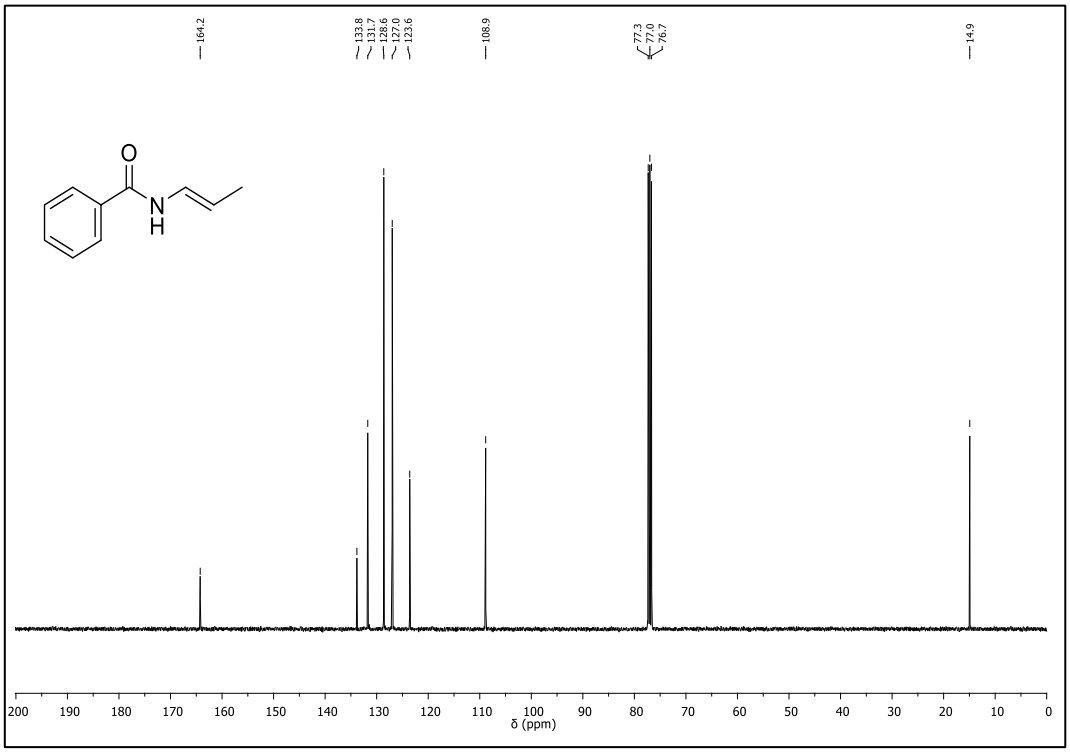

^{1}H-NMR (400 MHz, $CDCl_3$) of **24b**

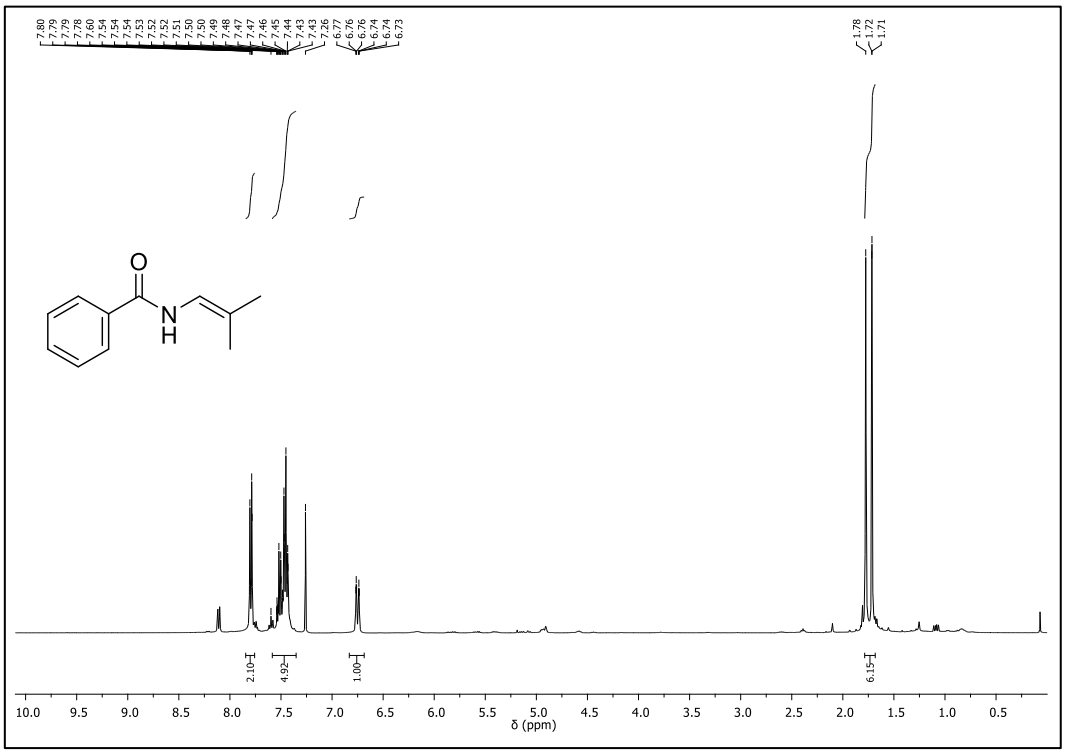

^{13}C-NMR (101 MHz, $CDCl_3$) of **24b**

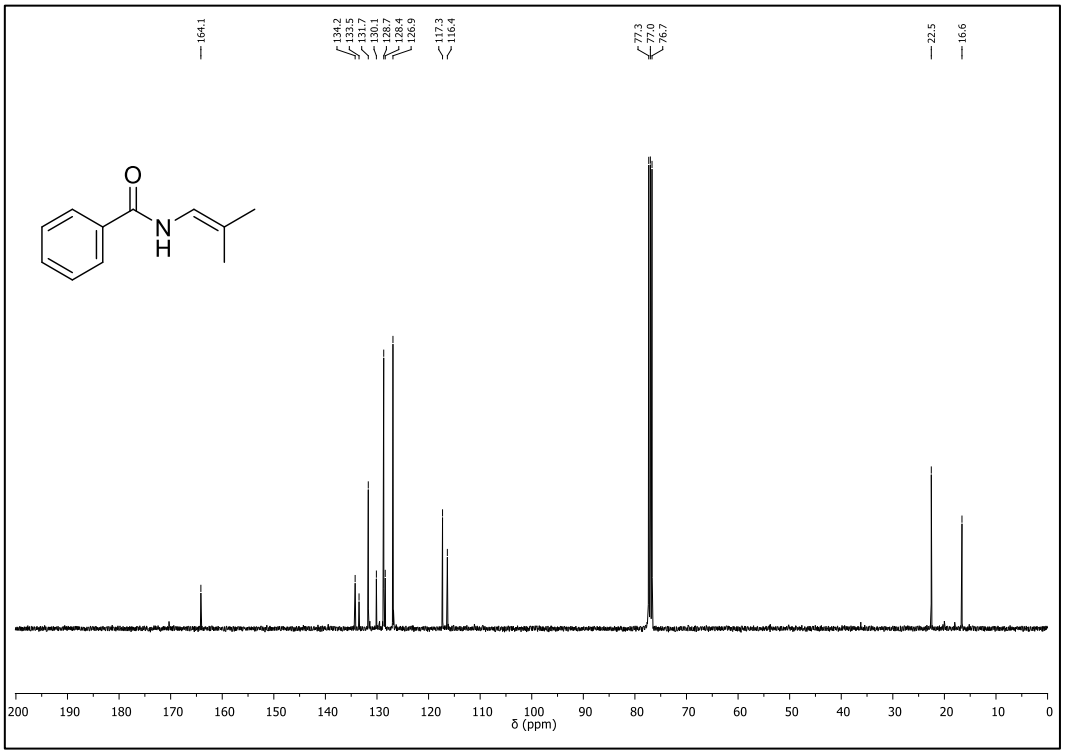

^{1}H-NMR (400 MHz, $CDCl_3$) of **26b**

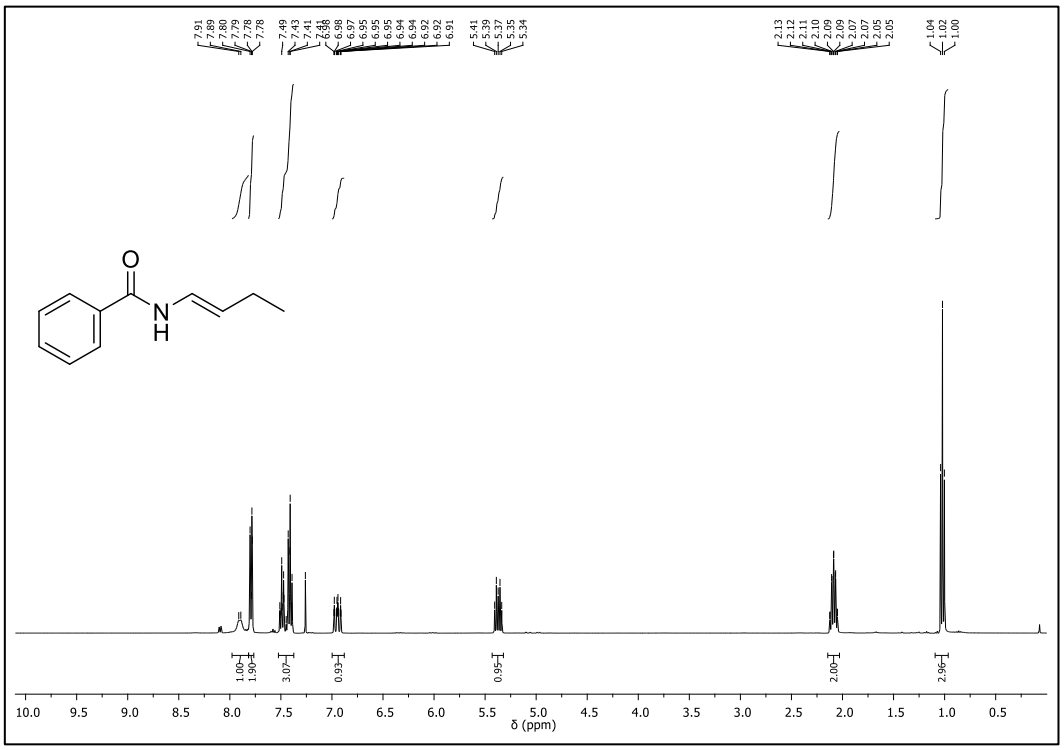

^{13}C-NMR (101 MHz, $CDCl_3$) of **26b**

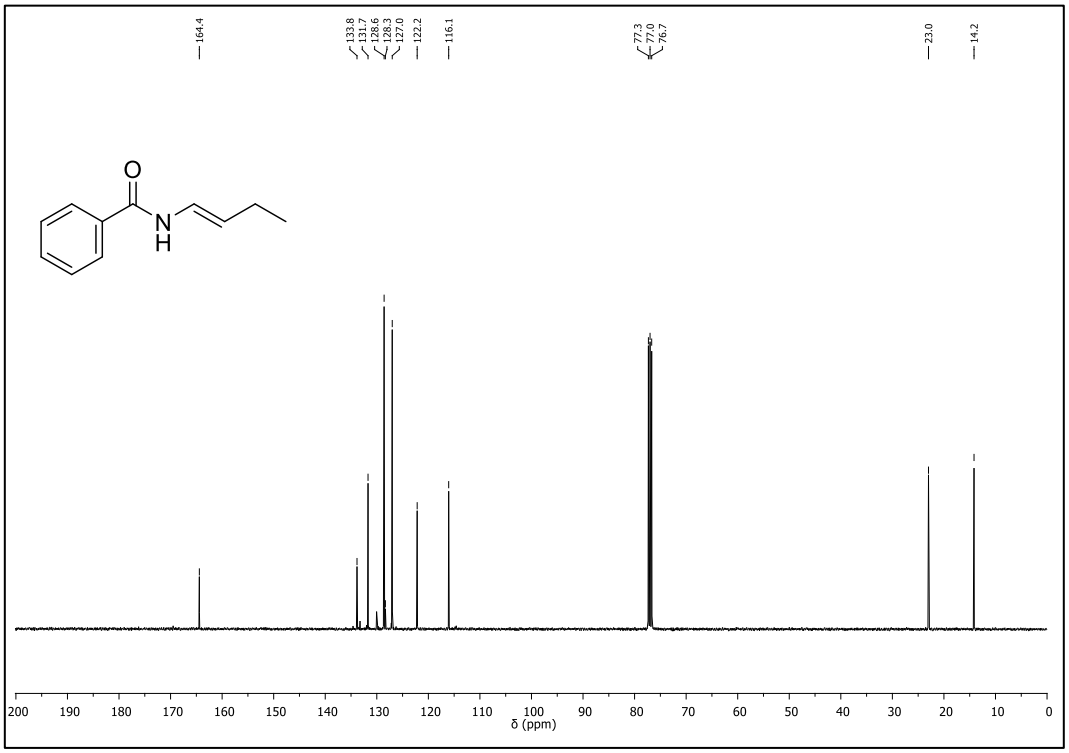

^{1}H-NMR (400 MHz, CD_2Cl_2) of **27b**

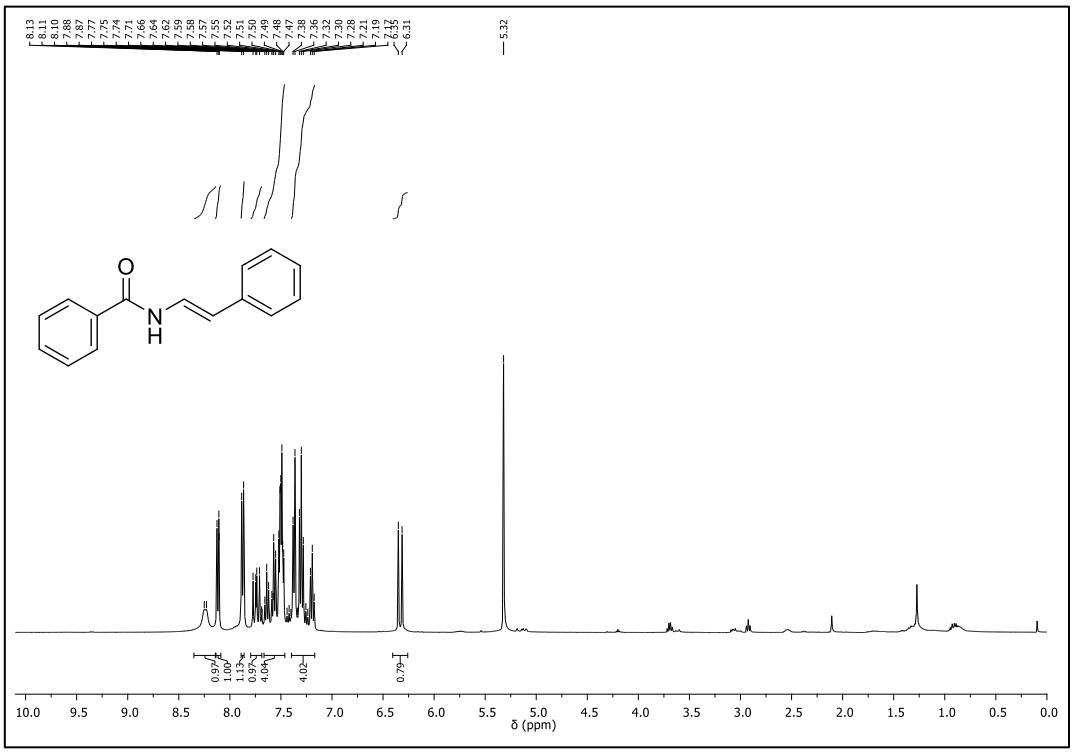

^{13}C-NMR (101 MHz, CD_2Cl_2) of **27b**

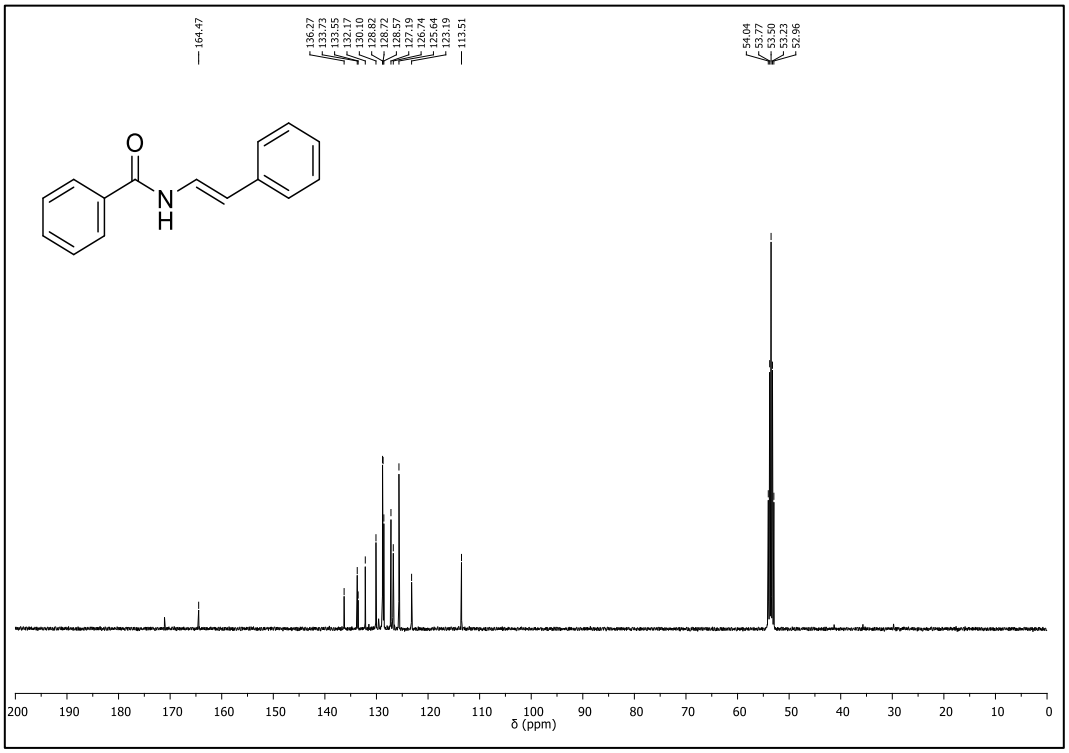

^{1}H-NMR (400 MHz, $CDCl_3$) of **28b**

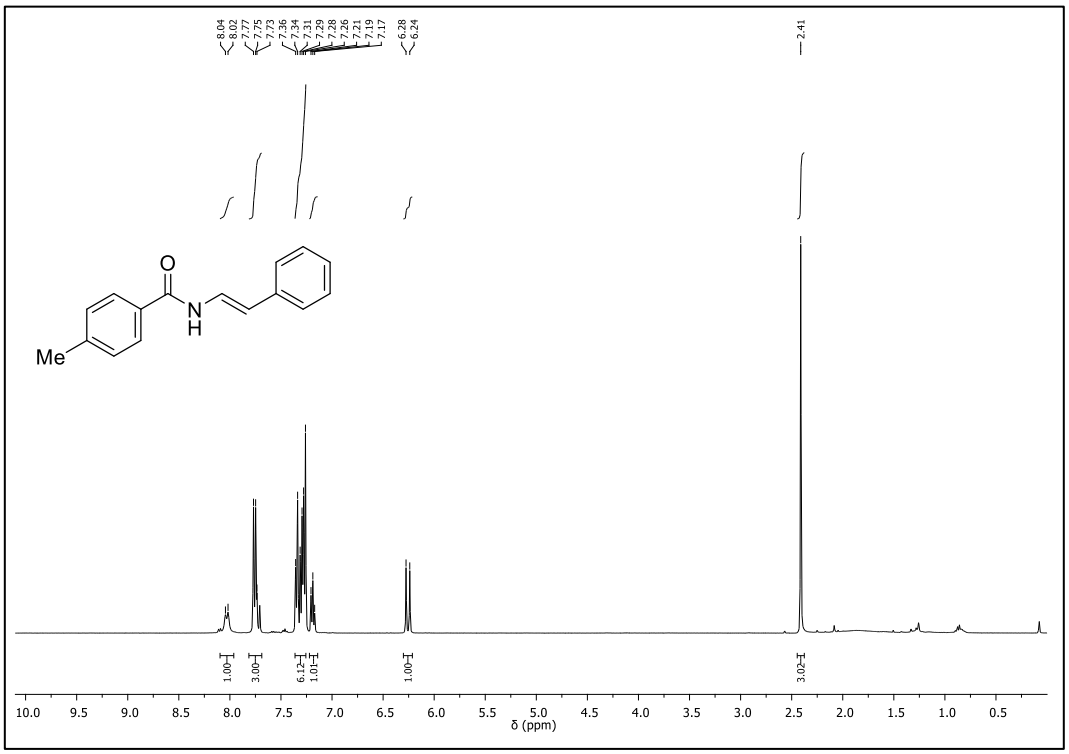

^{13}C-NMR (101 MHz, $CDCl_3$) of **28b**

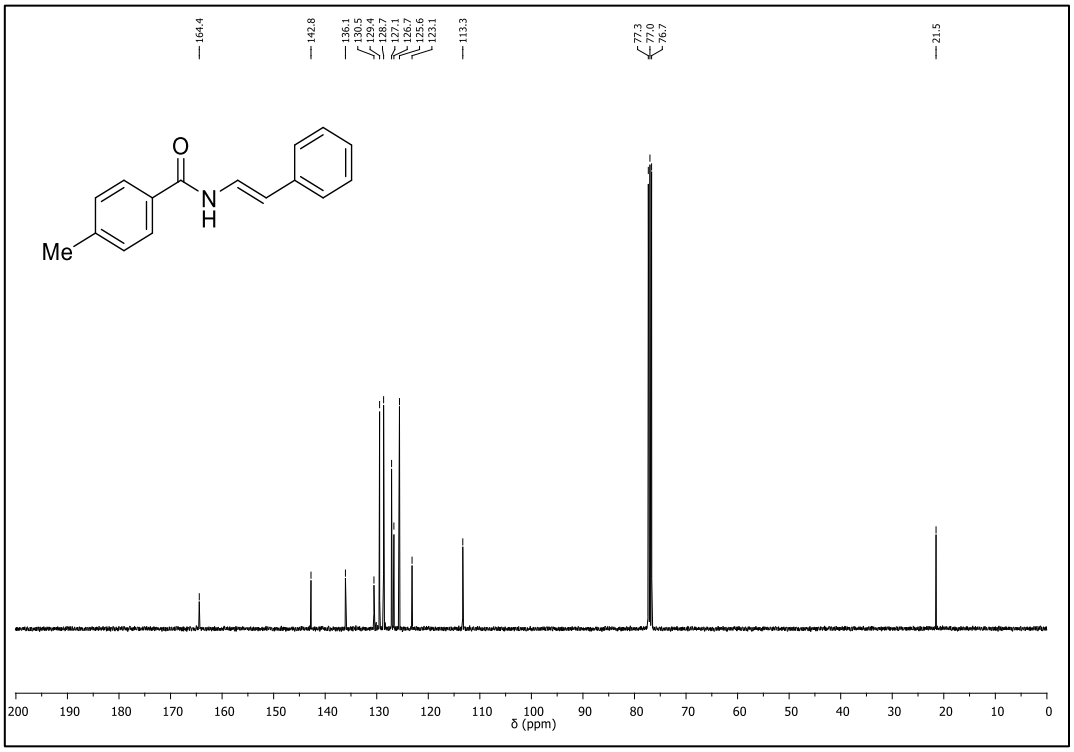

^{1}H-NMR (400 MHz, $CDCl_3$) of **29b**

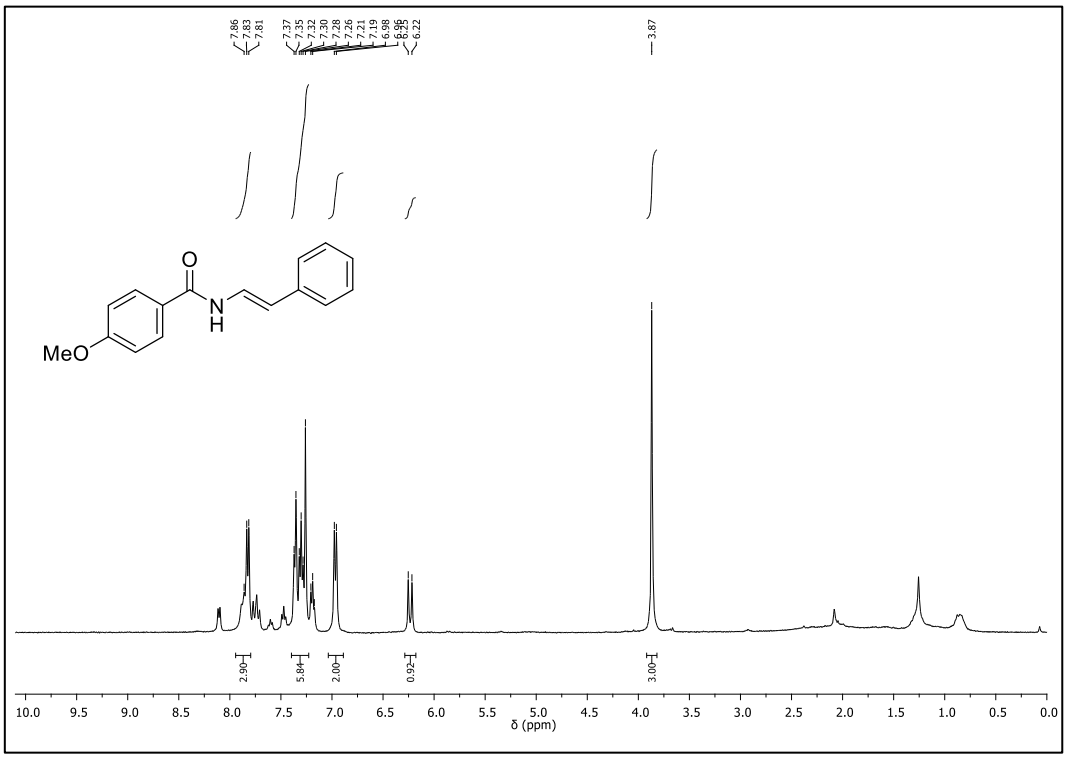

^{13}C-NMR (101 MHz, $CDCl_3$) of **29b**

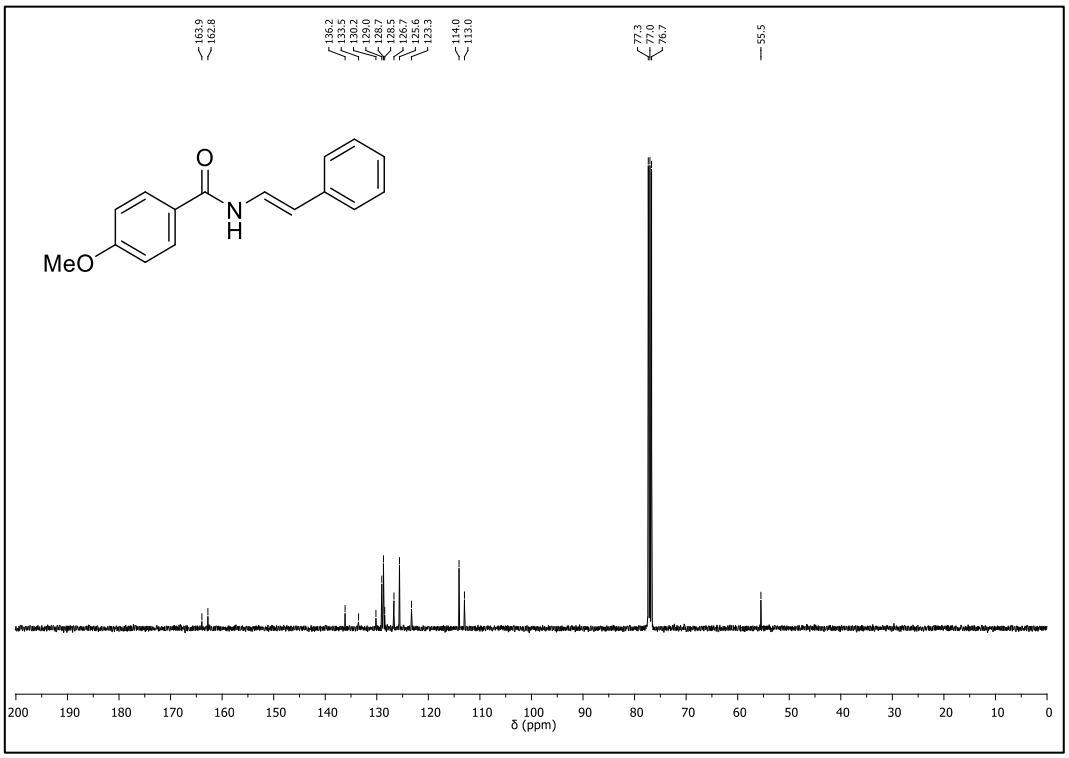

^{1}H-NMR (400 MHz, $CDCl_3$) of **30b** (*E* isomer)

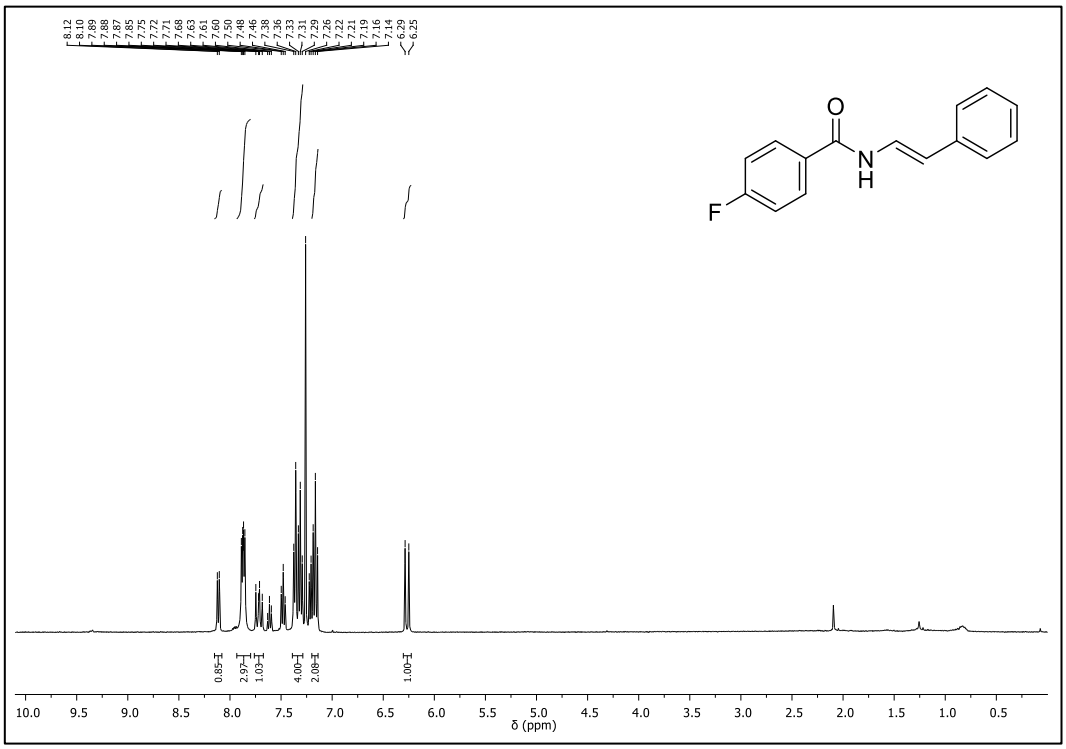

^{13}C-NMR (101 MHz, $CDCl_3$) of **30b** (*E* isomer)

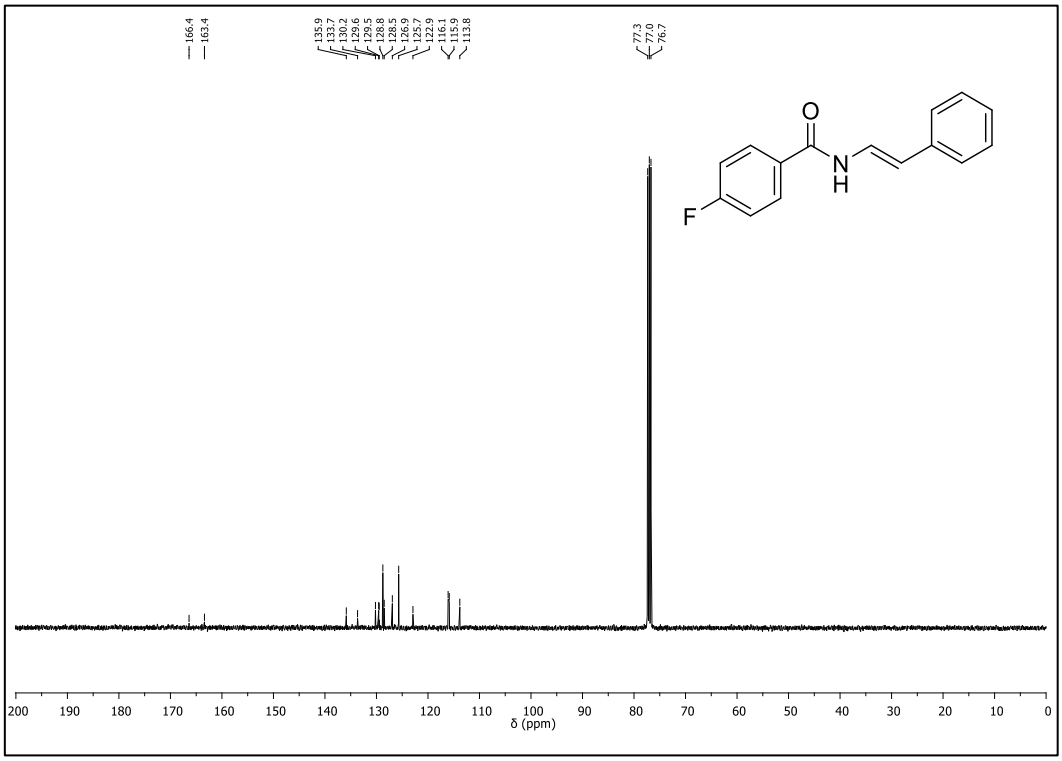

^{19}F-NMR (377 MHz, $CDCl_3$) of **30b** (*E* isomer)

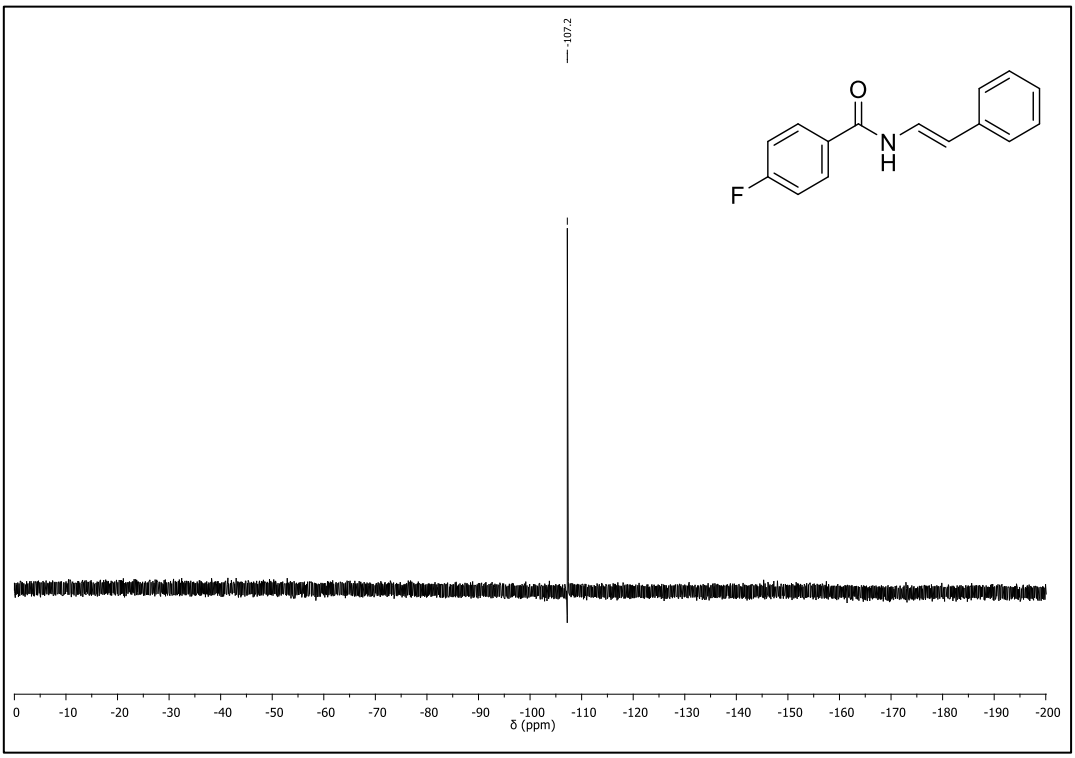

^{1}H-NMR (400 MHz, $CDCl_3$) of **30b** (*Z* isomer)

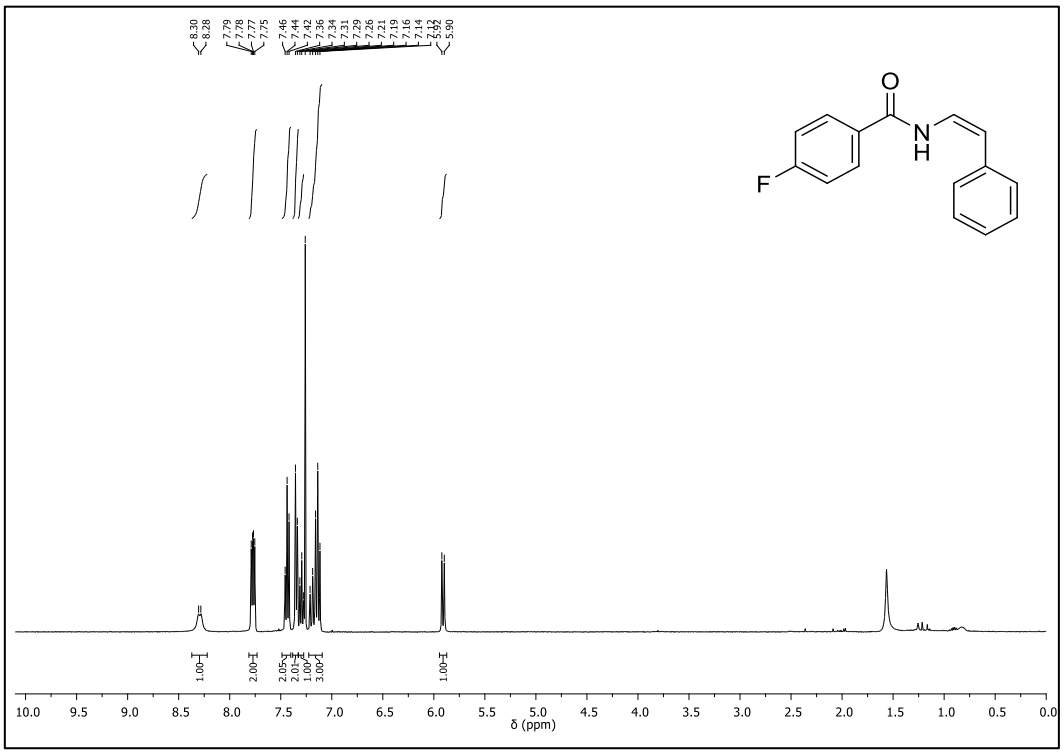

^{13}C-NMR (101 MHz, $CDCl_3$) of **30b** (*Z* isomer)

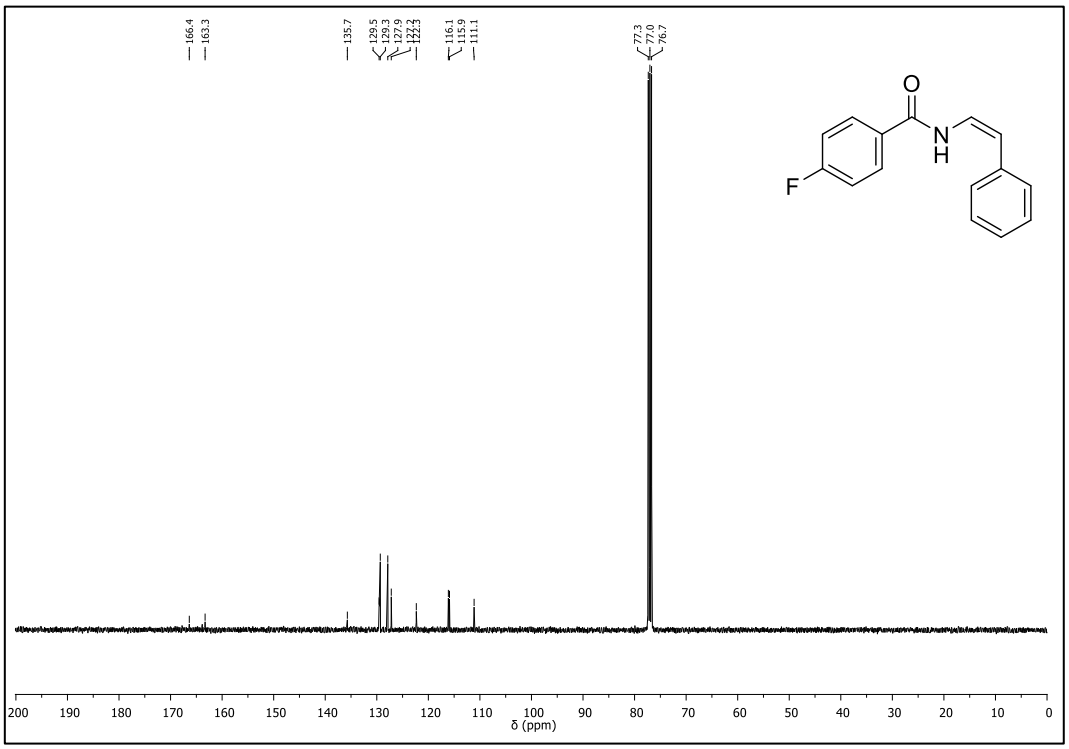

^{19}F-NMR (377 MHz, $CDCl_3$) of **30b** (*Z* isomer)

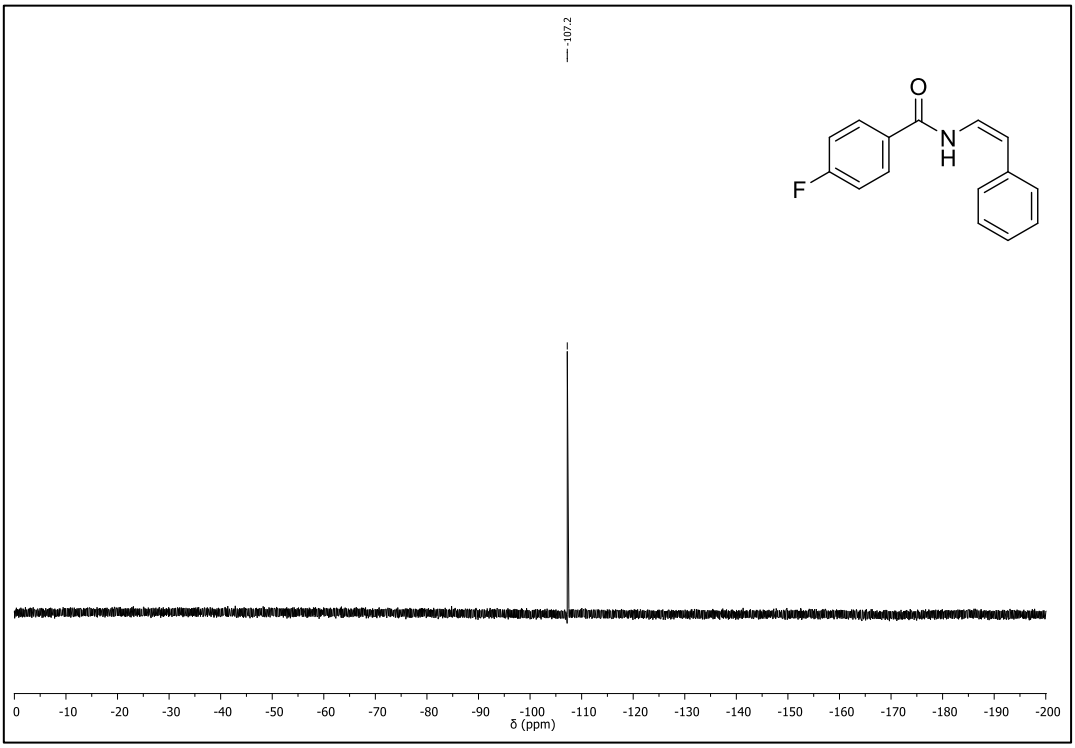

^{1}H-NMR (400 MHz, $CDCl_3$) of **31b** (*E* isomer)

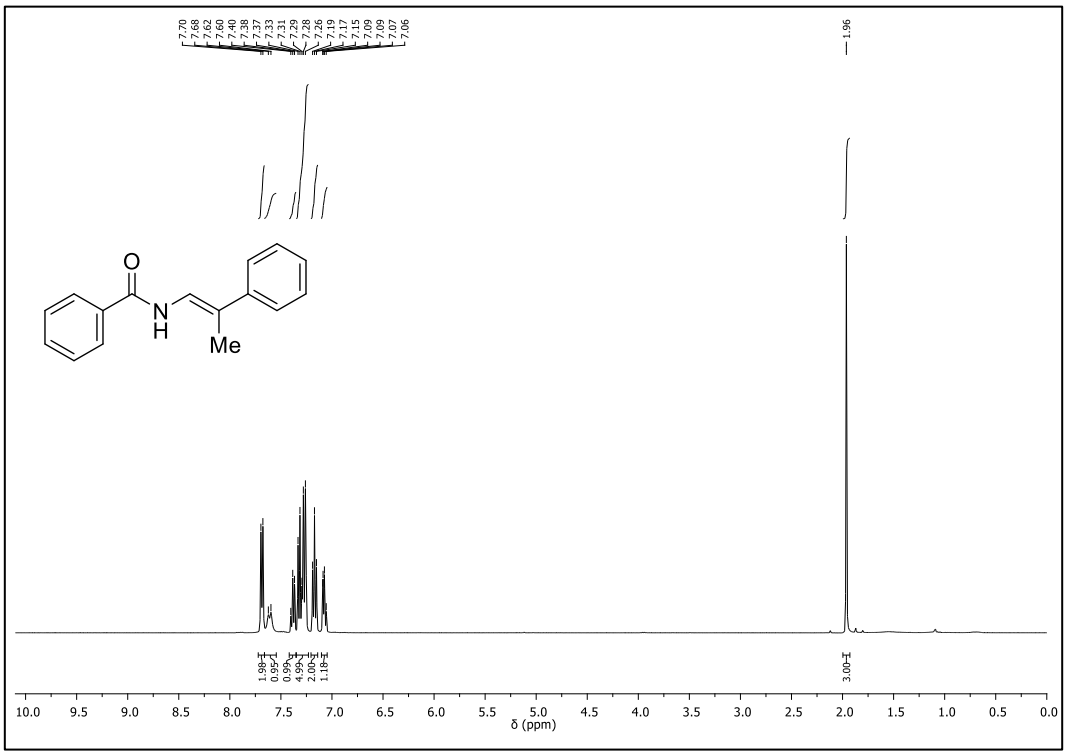

^{13}C-NMR (101 MHz, $CDCl_3$) of **31b** (*E* isomer)

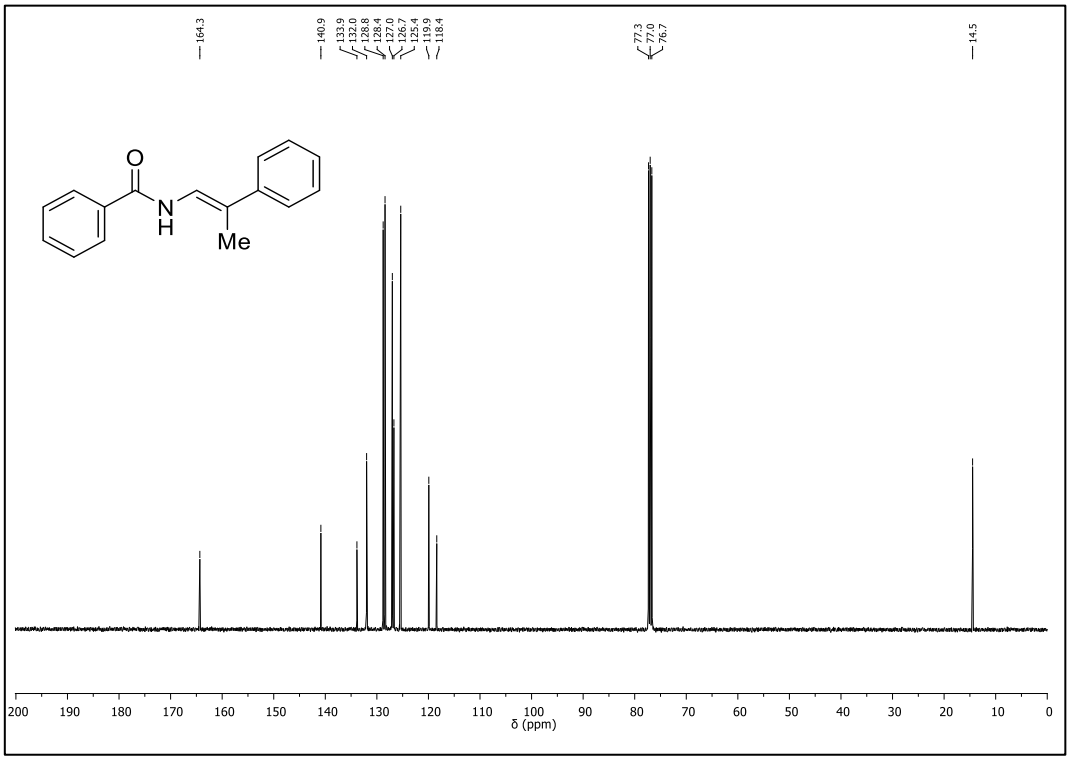

^{1}H-NMR (400 MHz, $CDCl_3$) of **31b** (*Z* isomer)

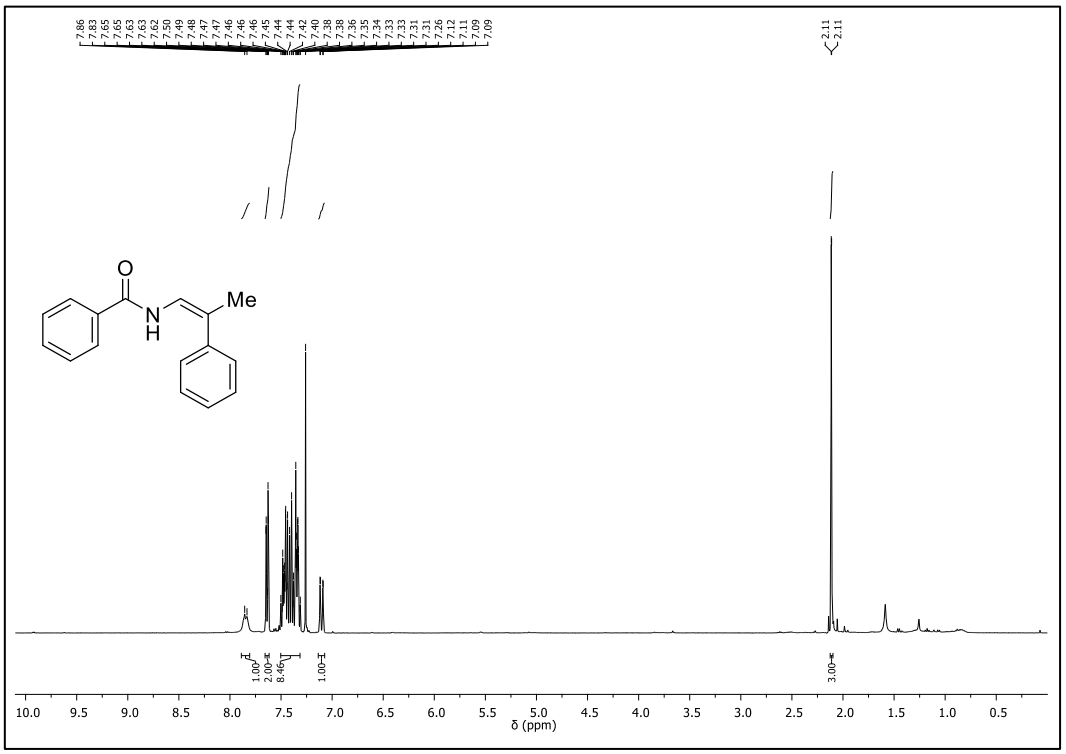

^{13}C-NMR (101 MHz, $CDCl_3$) of **31b** (*Z* isomer)

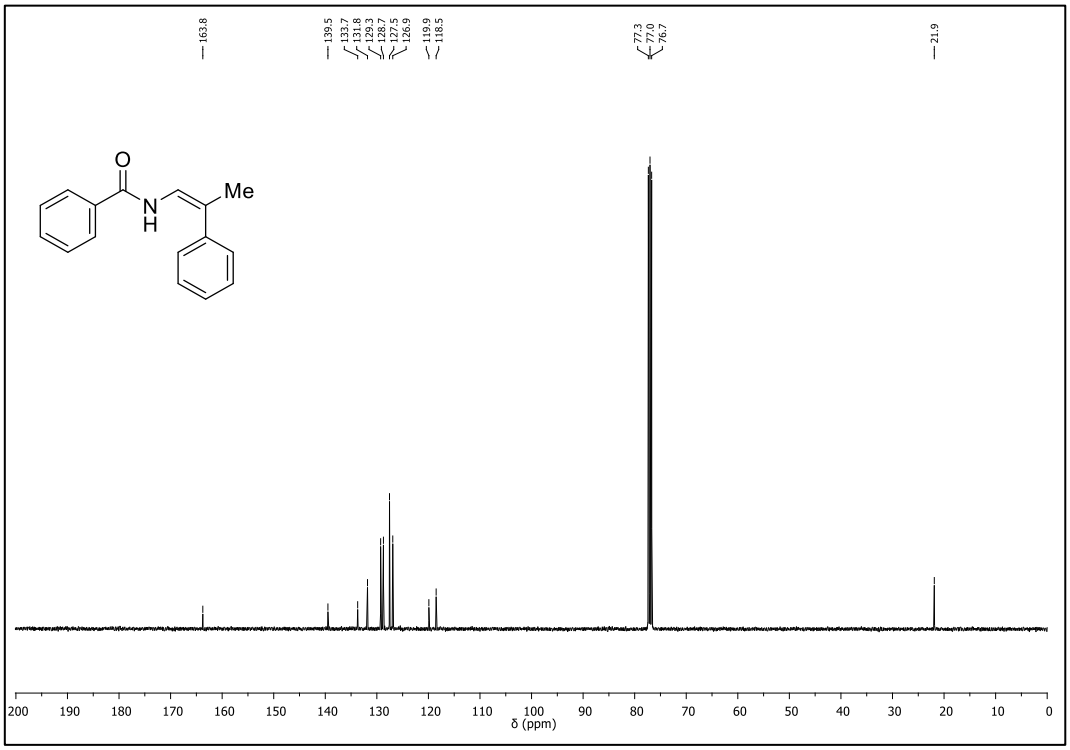

^{1}H-NMR (400 MHz, $CDCl_3$) of **32b** (*E* isomer)

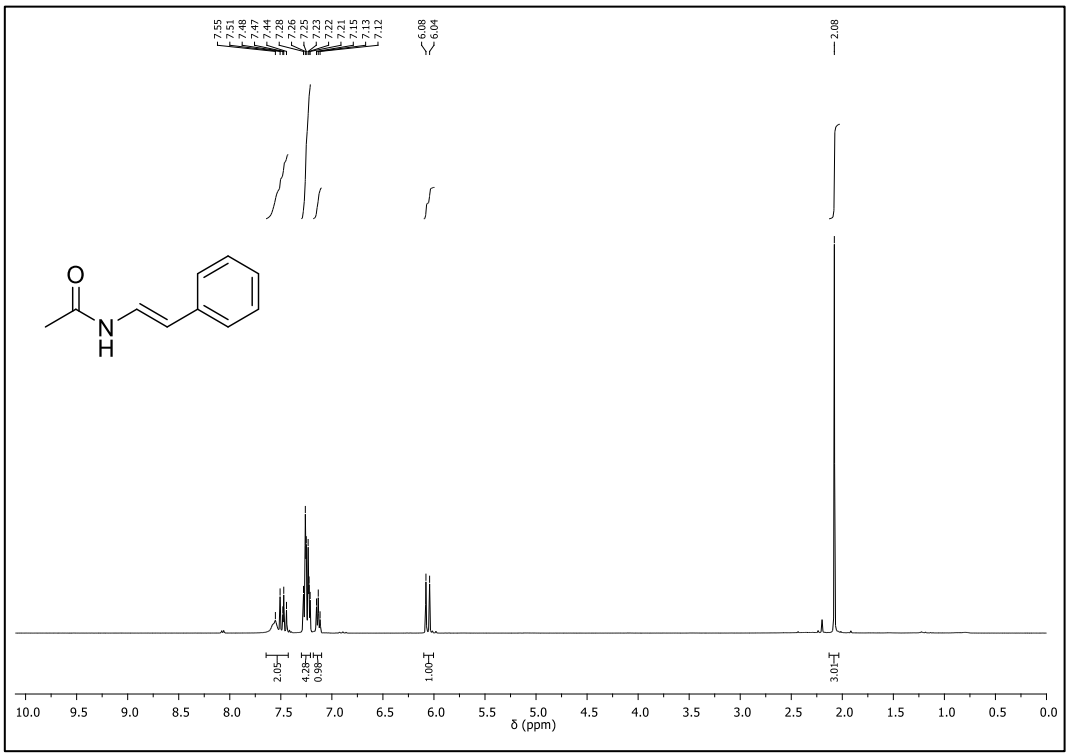

^{13}C-NMR (101 MHz, $CDCl_3$) of **32b** (*E* isomer)

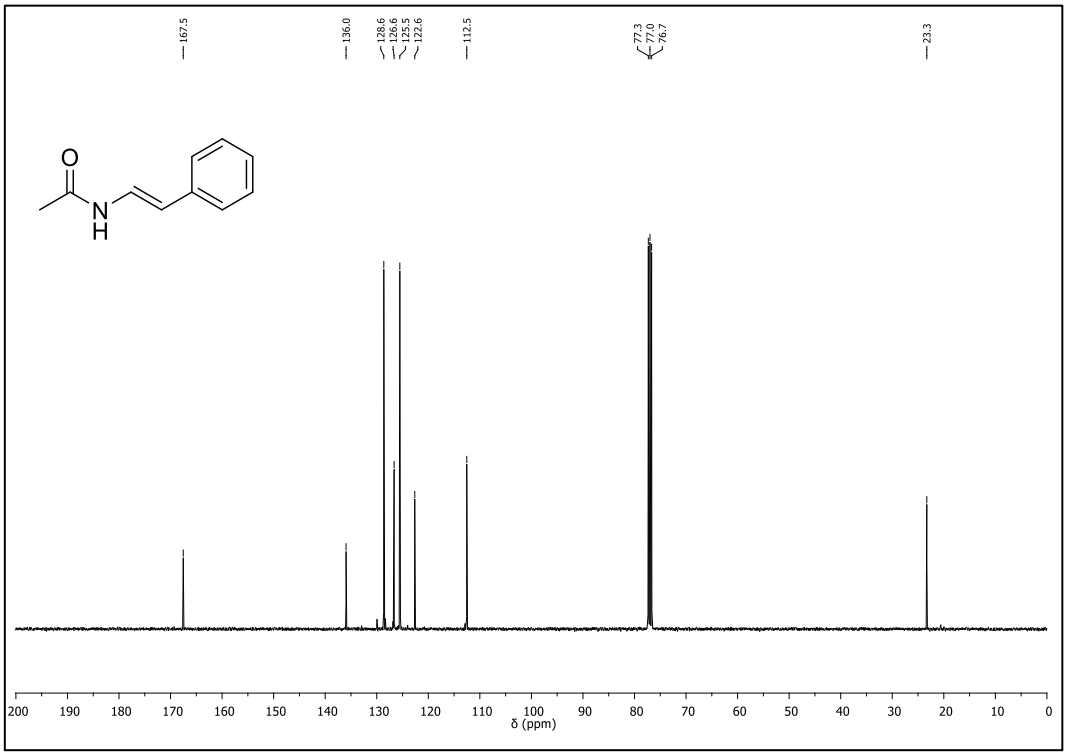

^{1}H-NMR (400 MHz, $CDCl_3$) of **32b** (*Z* isomer)

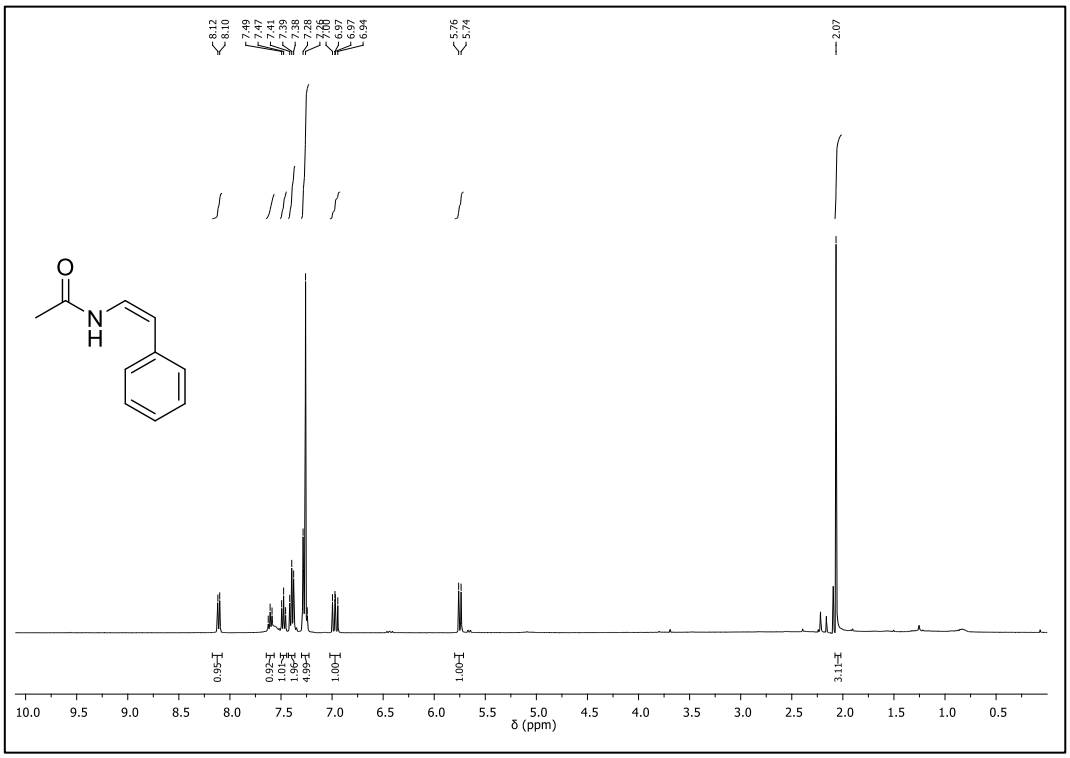

^{13}C-NMR (101 MHz, $CDCl_3$) of **32b** (*Z* isomer)

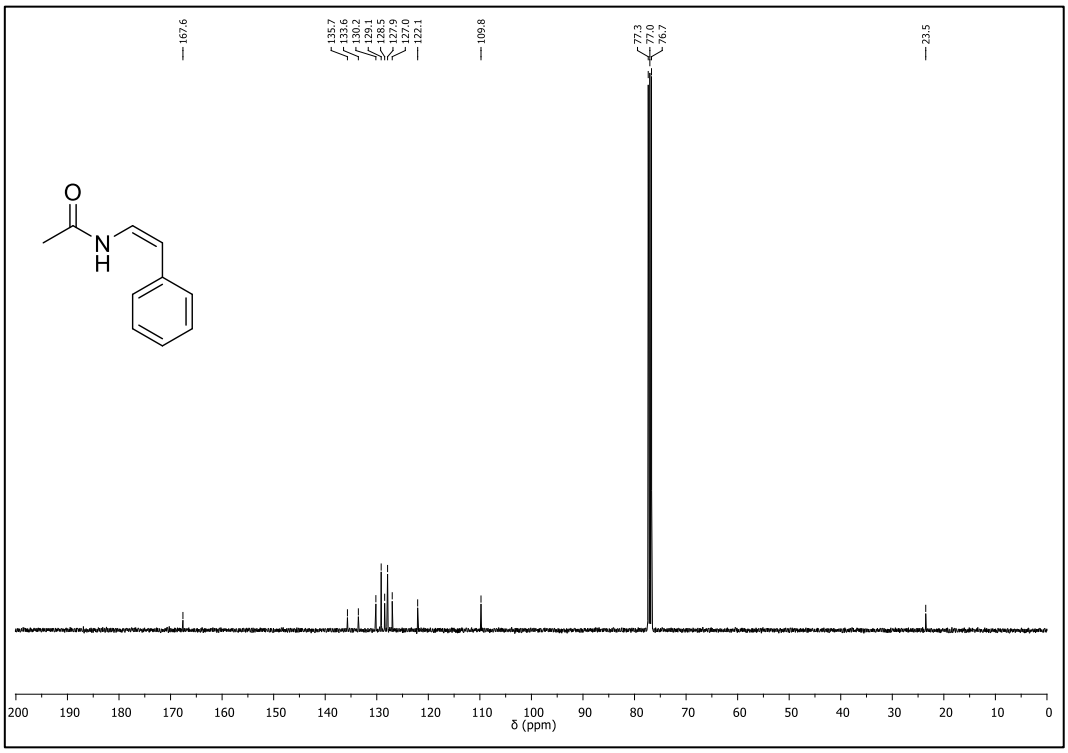

^{1}H-NMR (400 MHz, $CDCl_3$) compound **33b**

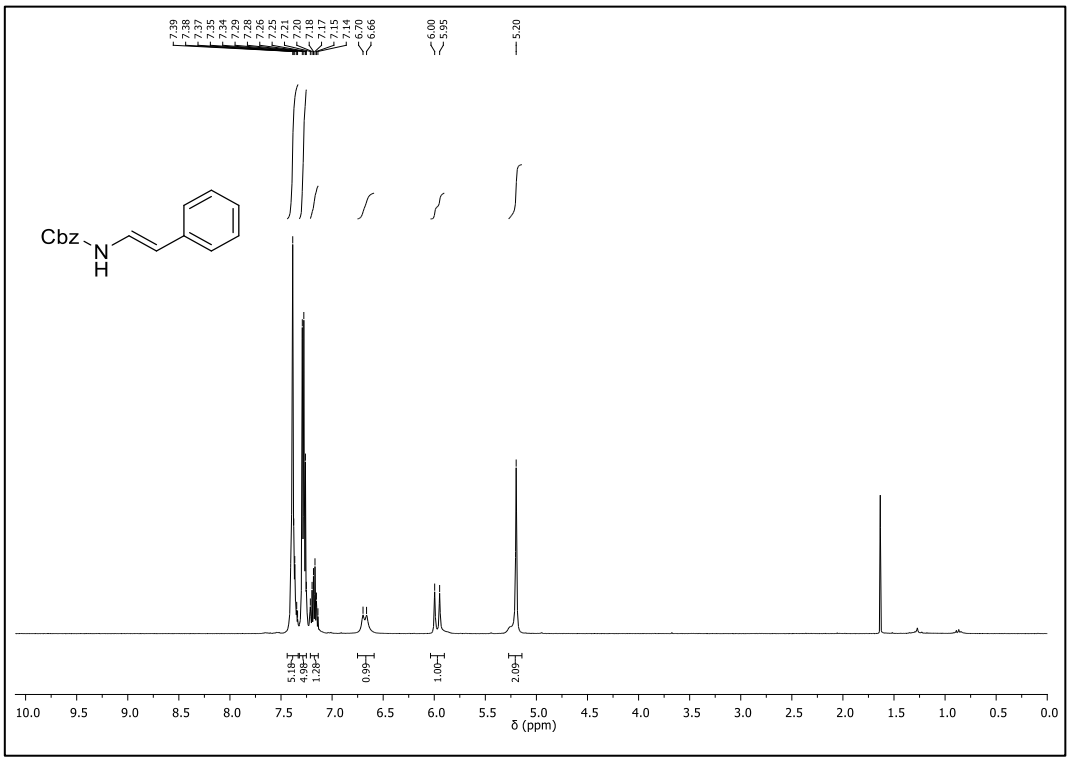

^{13}C-NMR (101 MHz, $CDCl_3$) of **33b**

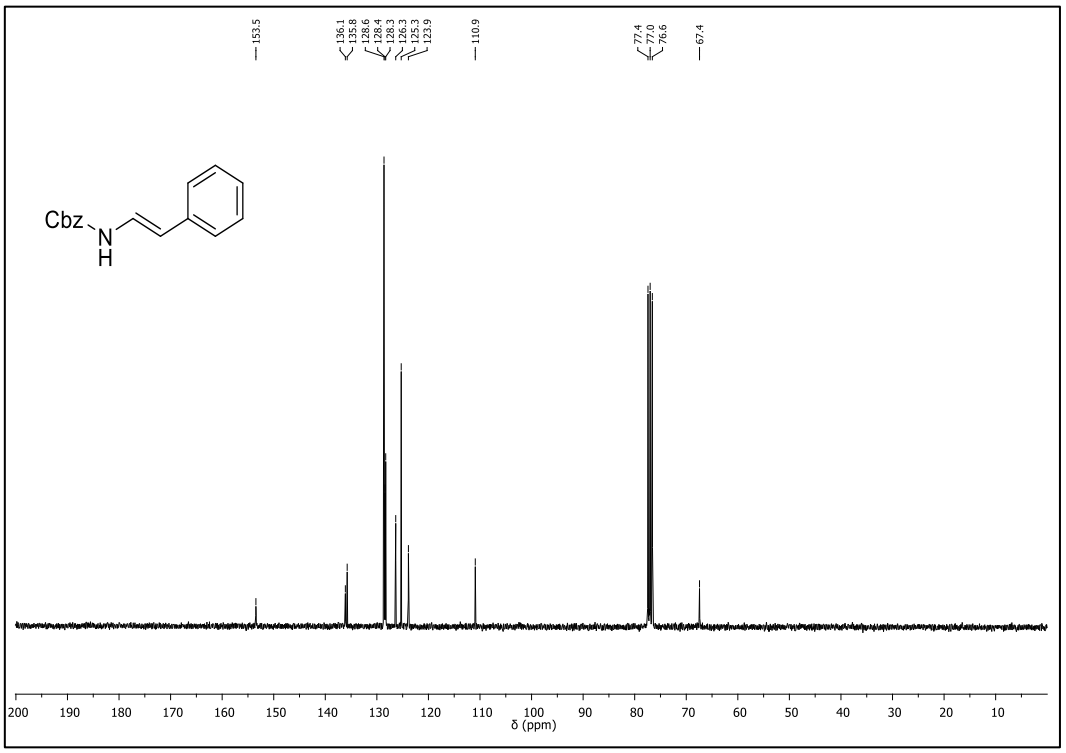

^{1}H-NMR (400 MHz, $CDCl_3$) of **34b**

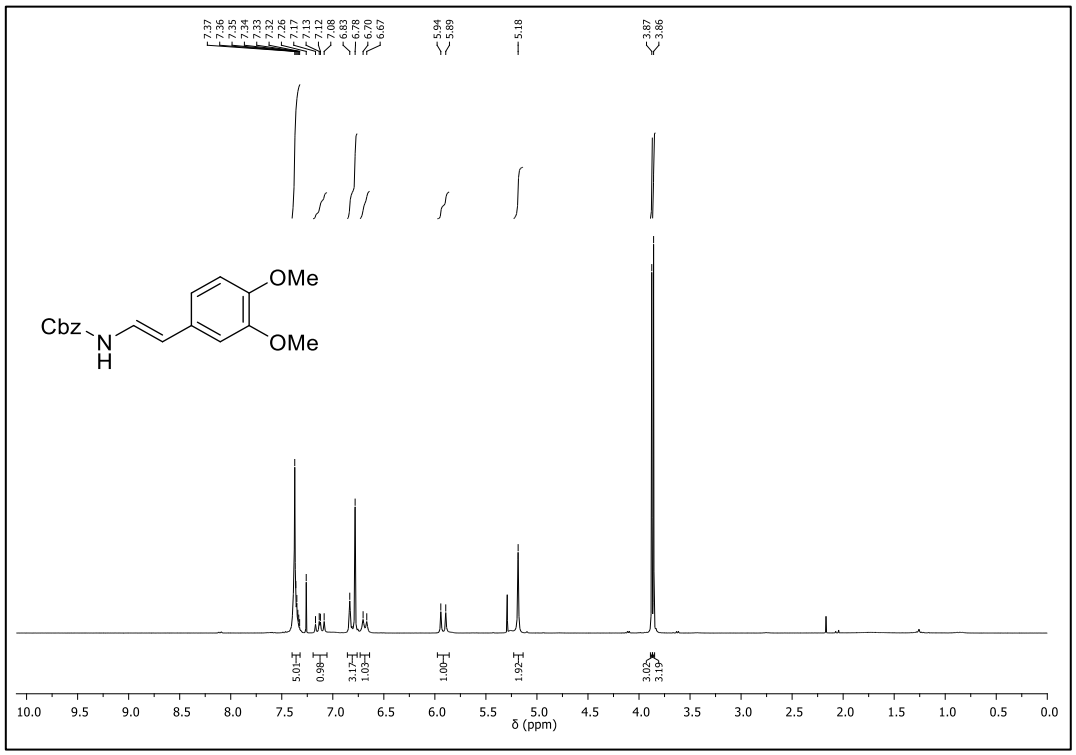

^{13}C-NMR (101 MHz, $CDCl_3$) of **34b**

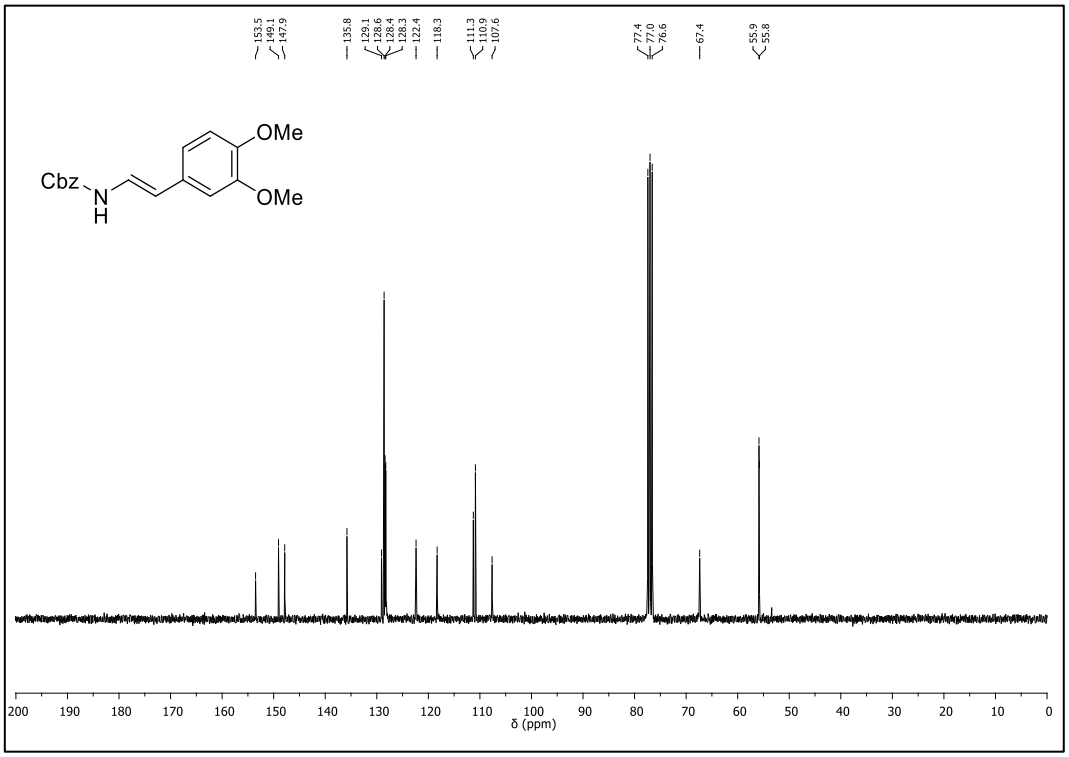

^{1}H-NMR (400 MHz, $CDCl_3$) of **35b** (*E* isomer)

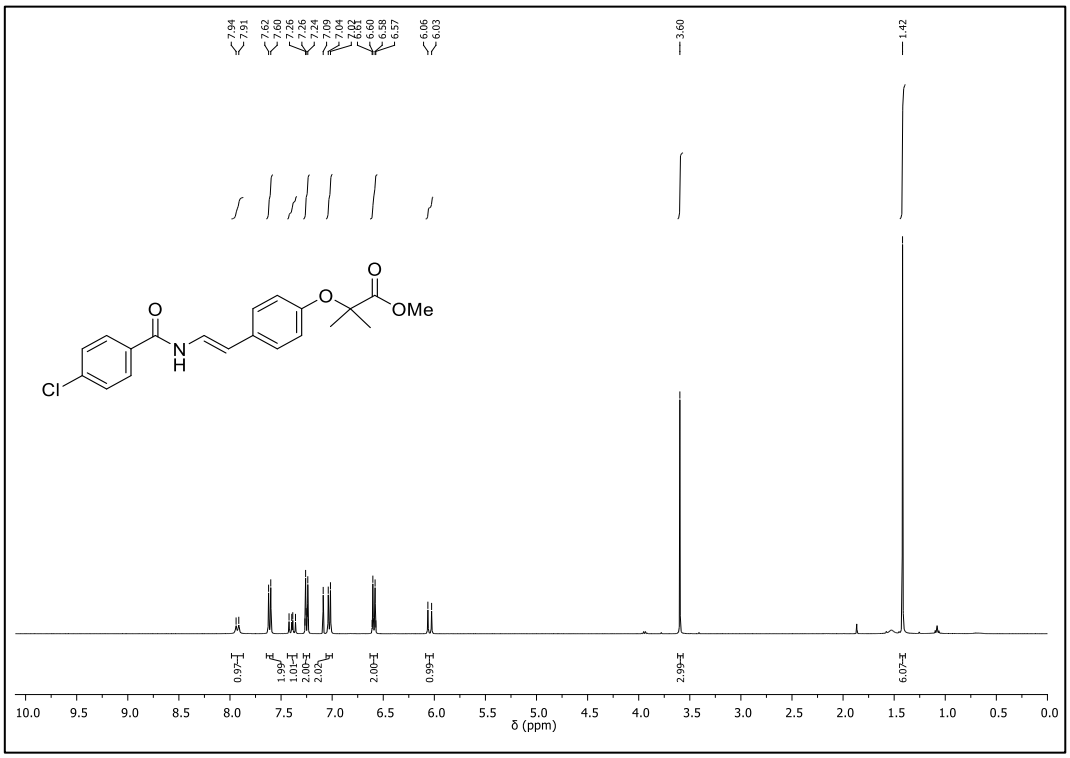

^{13}C-NMR (101 MHz, $CDCl_3$) of **35b** (*E* isomer)

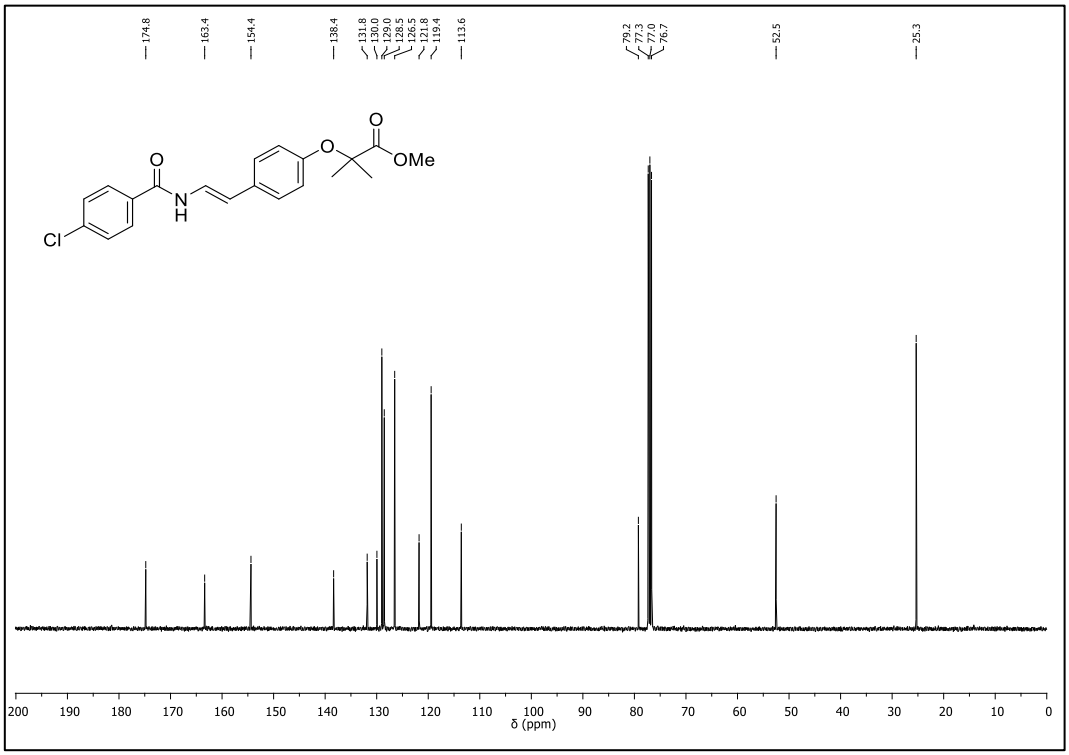

^{1}H-NMR (400 MHz, $CDCl_3$) of **35b** (*Z* isomer)

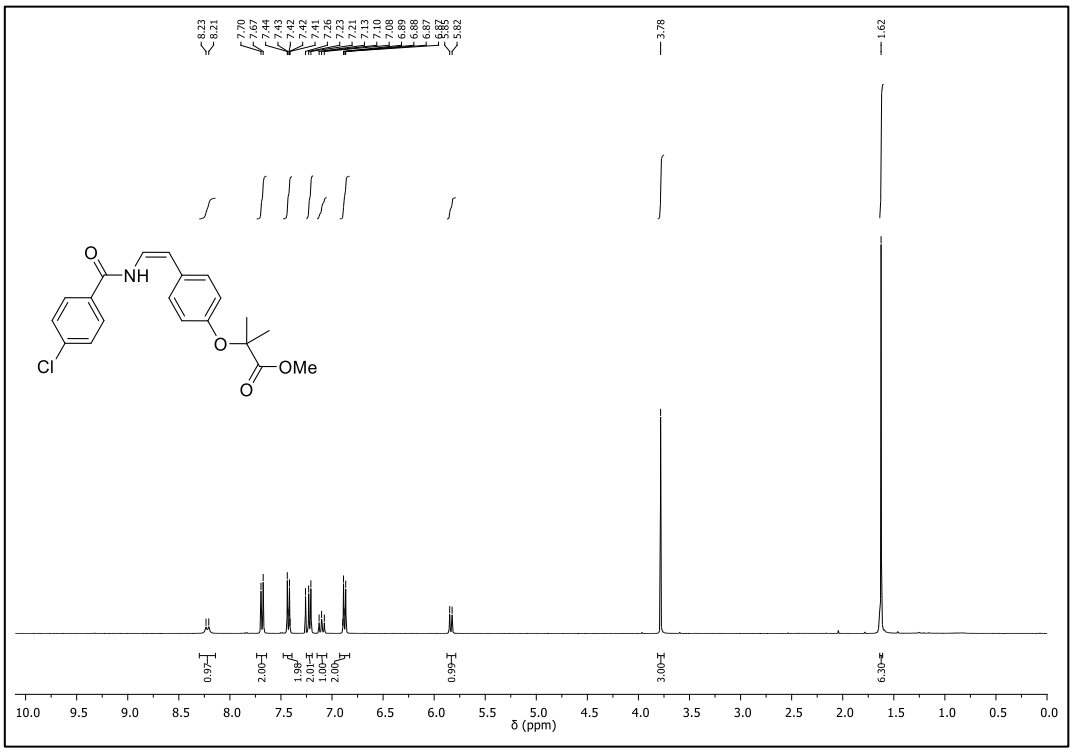

^{13}C-NMR (101 MHz, $CDCl_3$) of **35b** (*Z* isomer)

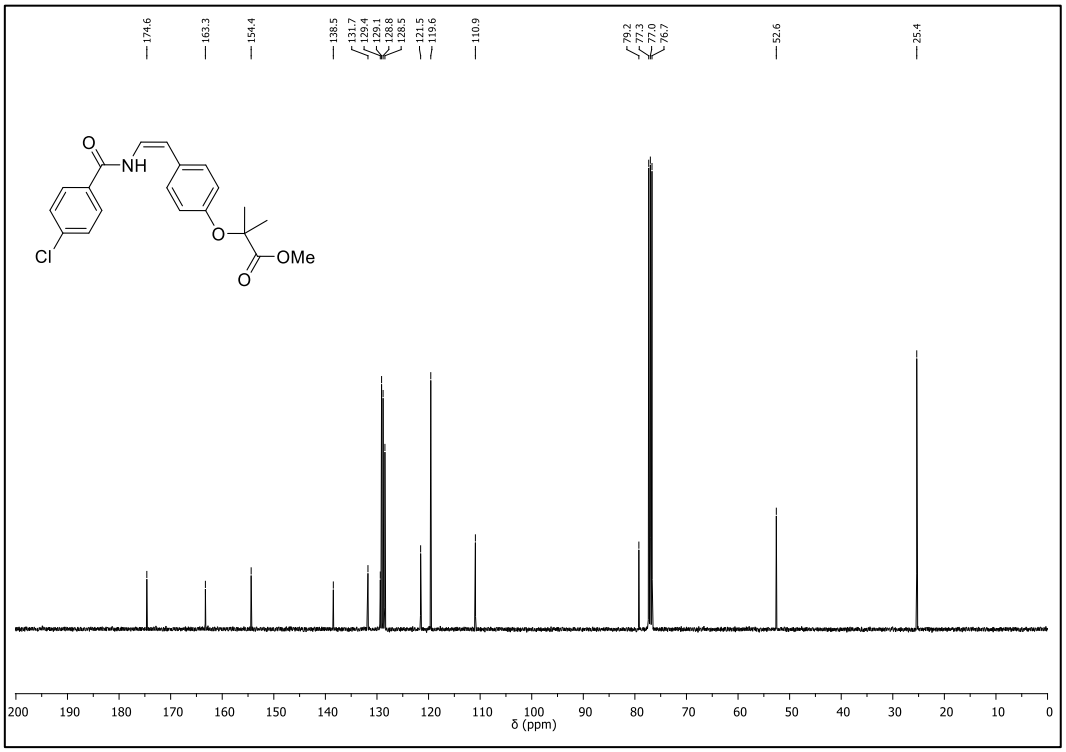

^{1}H-NMR (400 MHz, $CDCl_3$) of **36b** (*E* isomer)

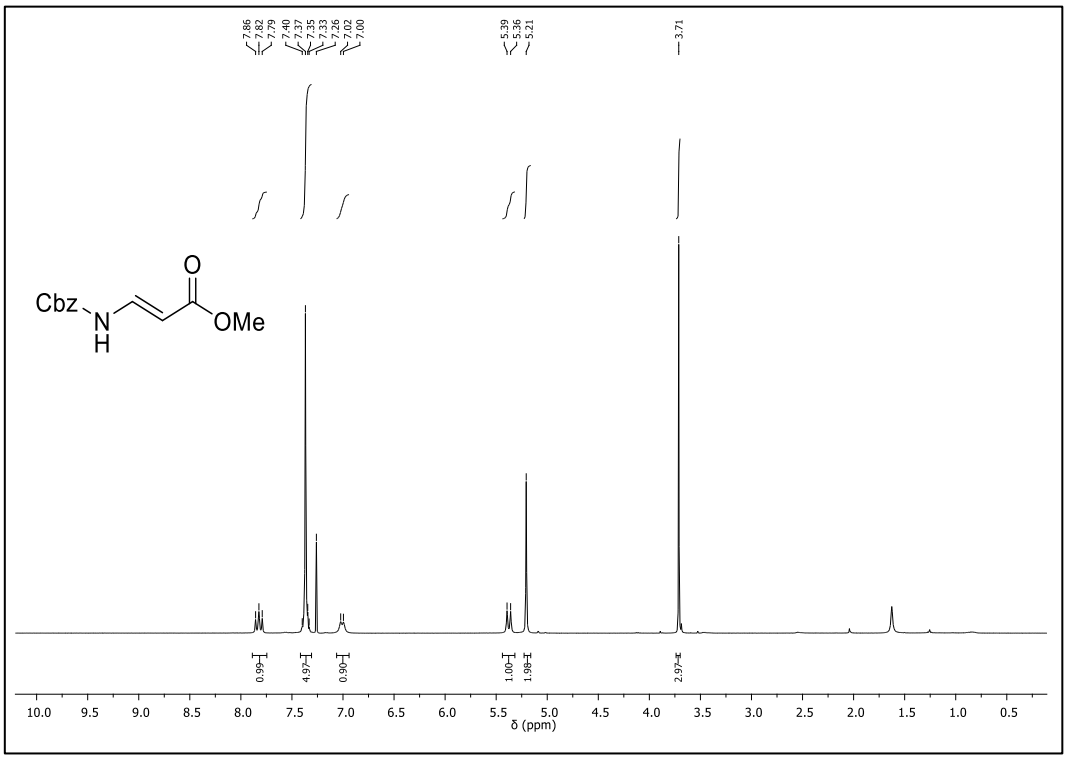

^{13}C-NMR (101 MHz, $CDCl_3$) of **36b** (*E* isomer)

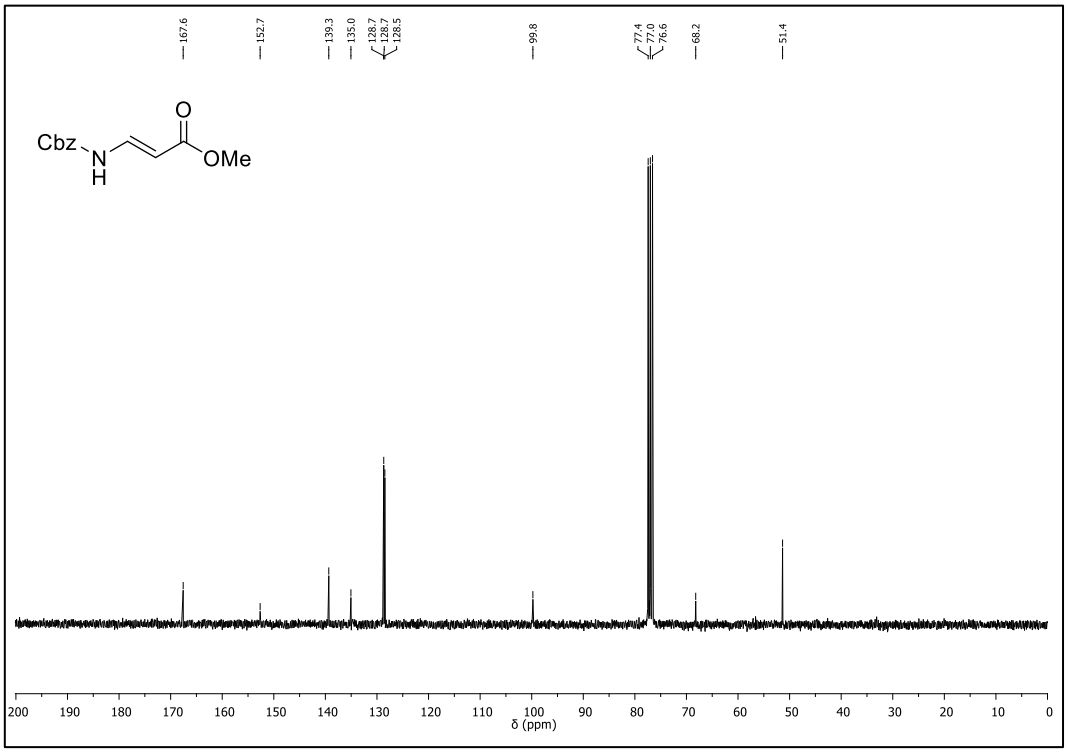

^{1}H-NMR (400 MHz, $CDCl_3$) of **36b** (*Z* isomer)

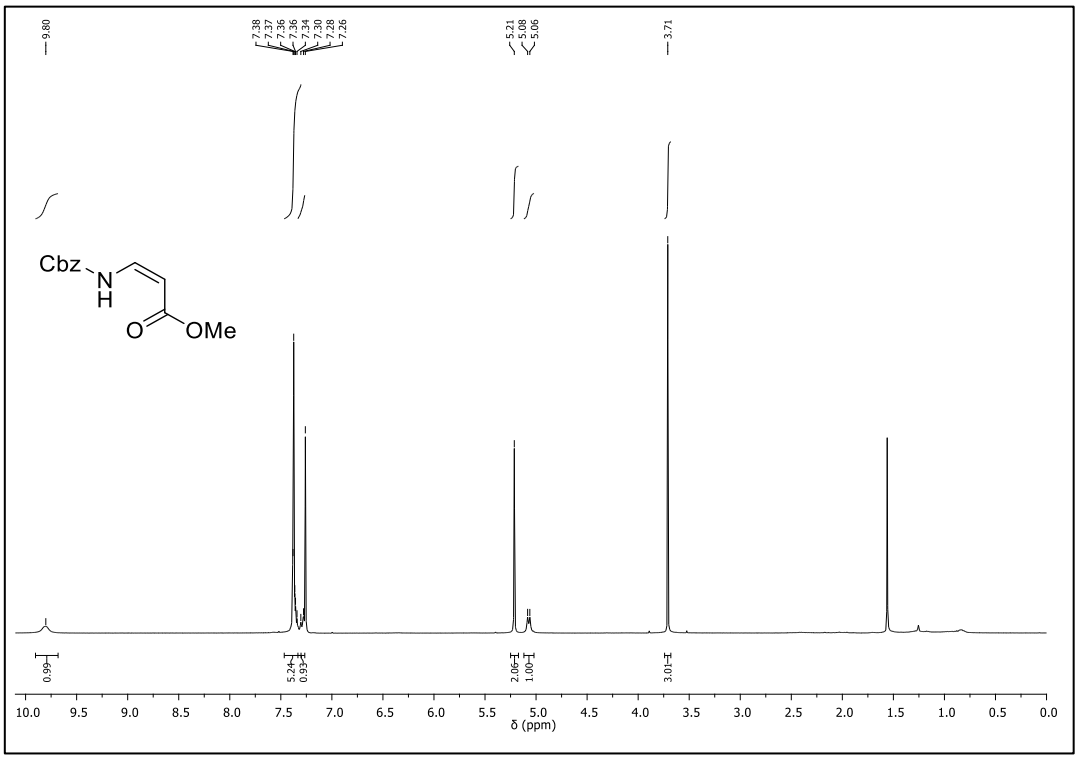

^{13}C-NMR (101 MHz, $CDCl_3$) of **36b** (*Z* isomer)

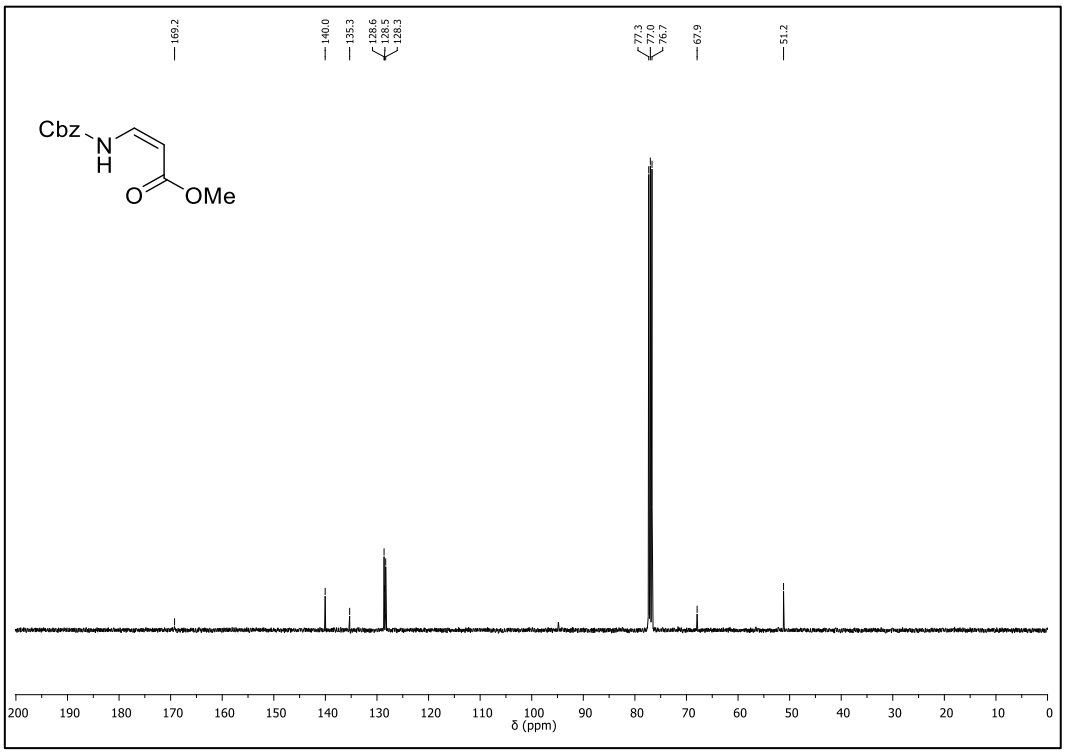

^{1}H-NMR (400 MHz, $CDCl_3$) of **37b**

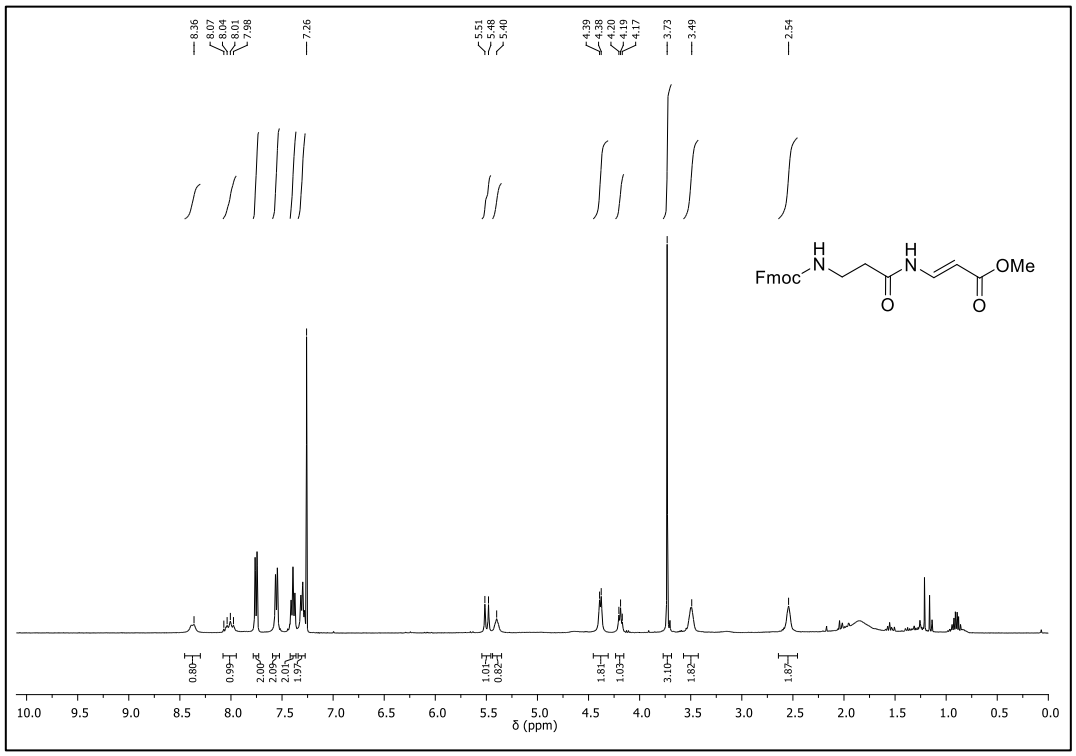

^{13}C-NMR (101 MHz, $CDCl_3$) of **37b**

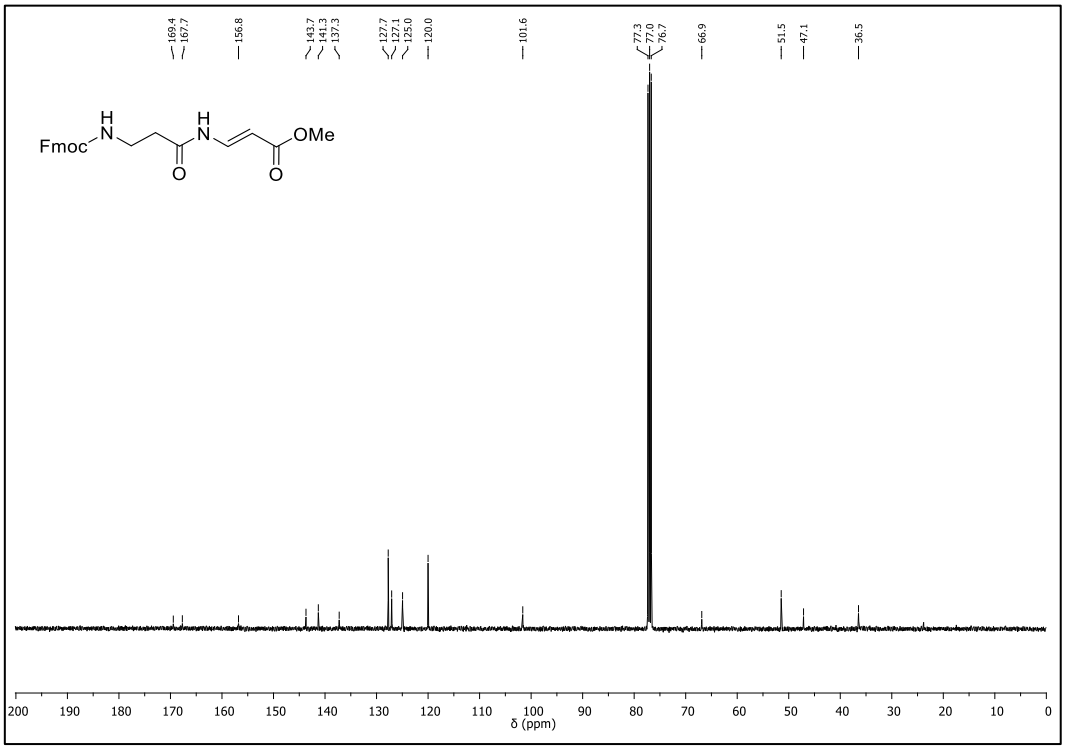

^{1}H-NMR (400 MHz, $CDCl_3$) of **38b** (*E* isomer)

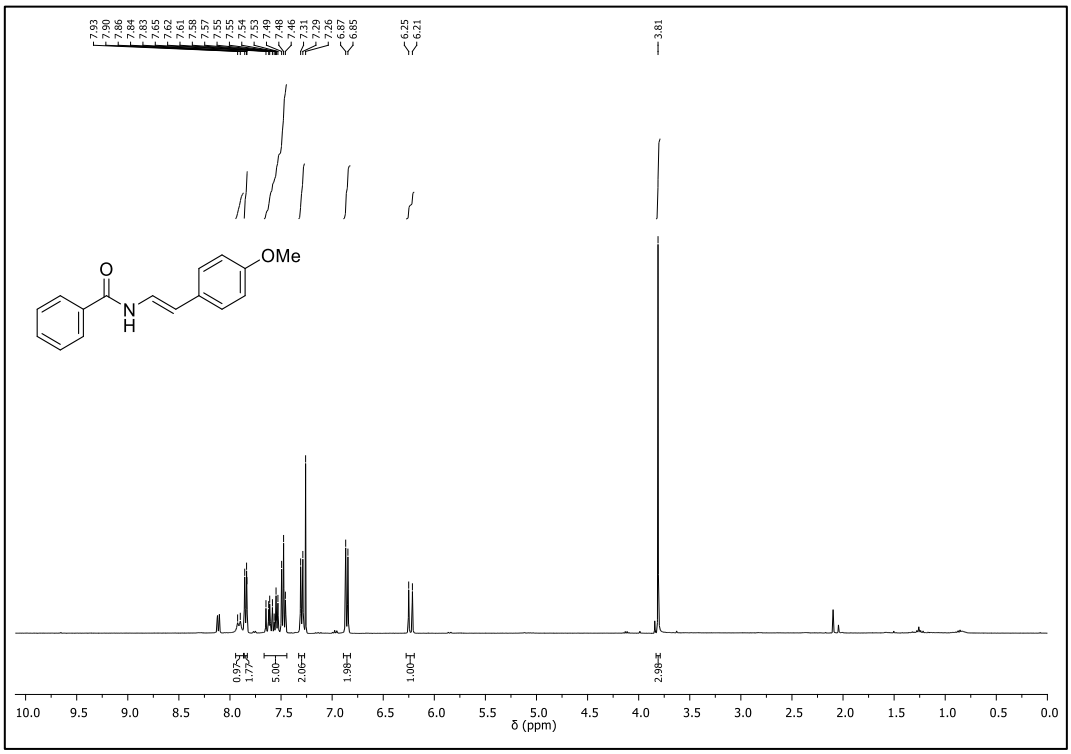

^{13}C-NMR (101 MHz, $CDCl_3$) of **38b** (*E* isomer)

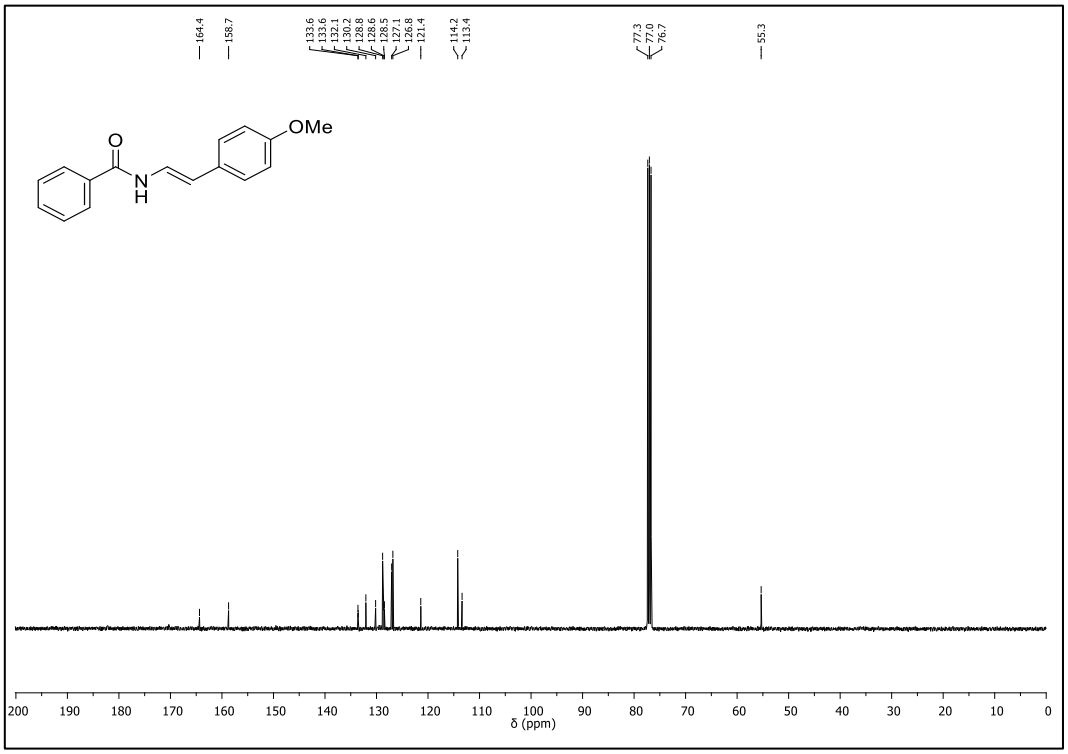

^{1}H-NMR (400 MHz, $CDCl_3$) of **38b** (*Z* isomer)

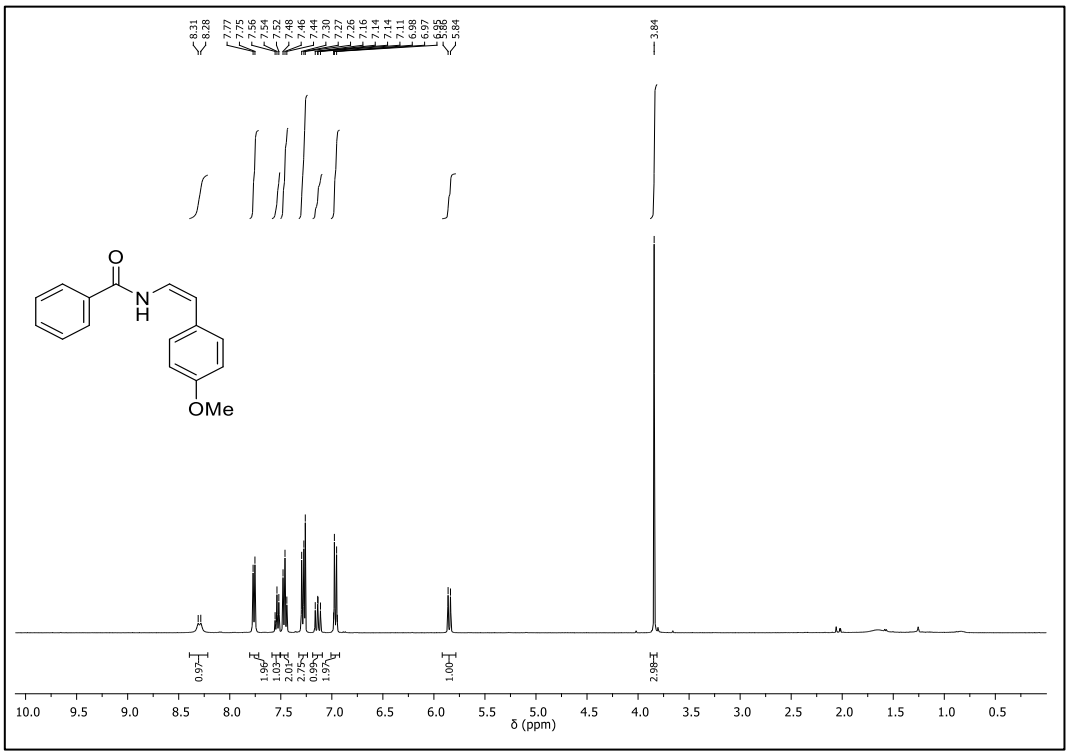

^{13}C-NMR (101 MHz, $CDCl_3$) of **38b** (*Z* isomer)

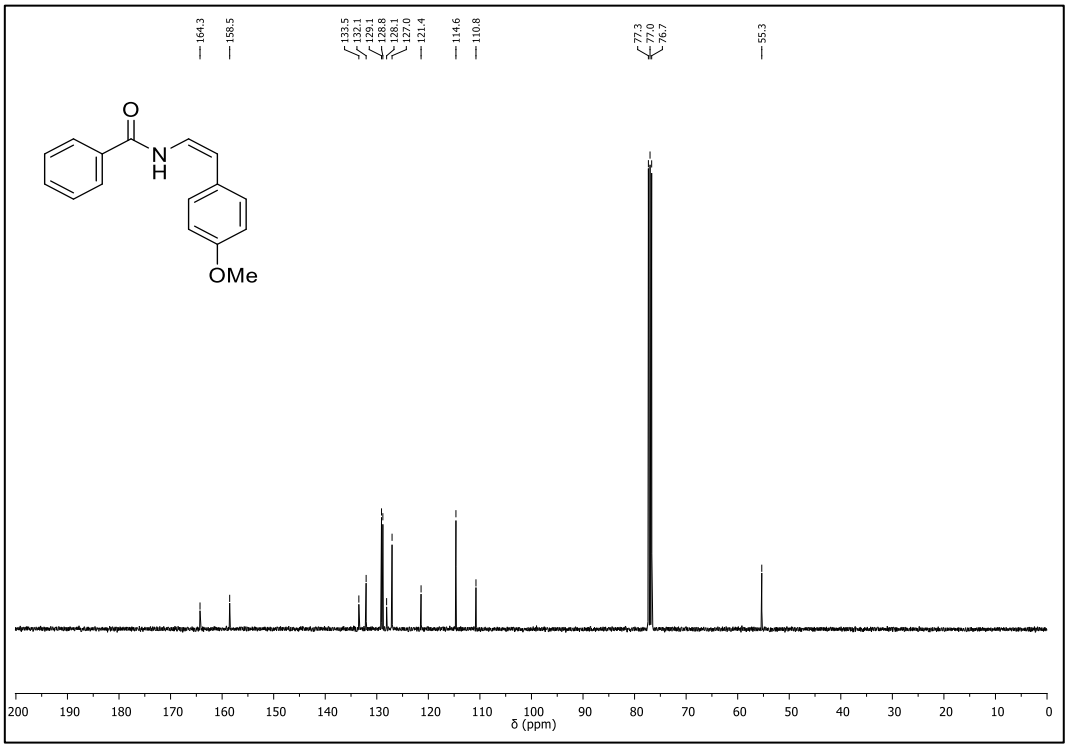

^{1}H-NMR (400 MHz, $CDCl_3$) of **39b**

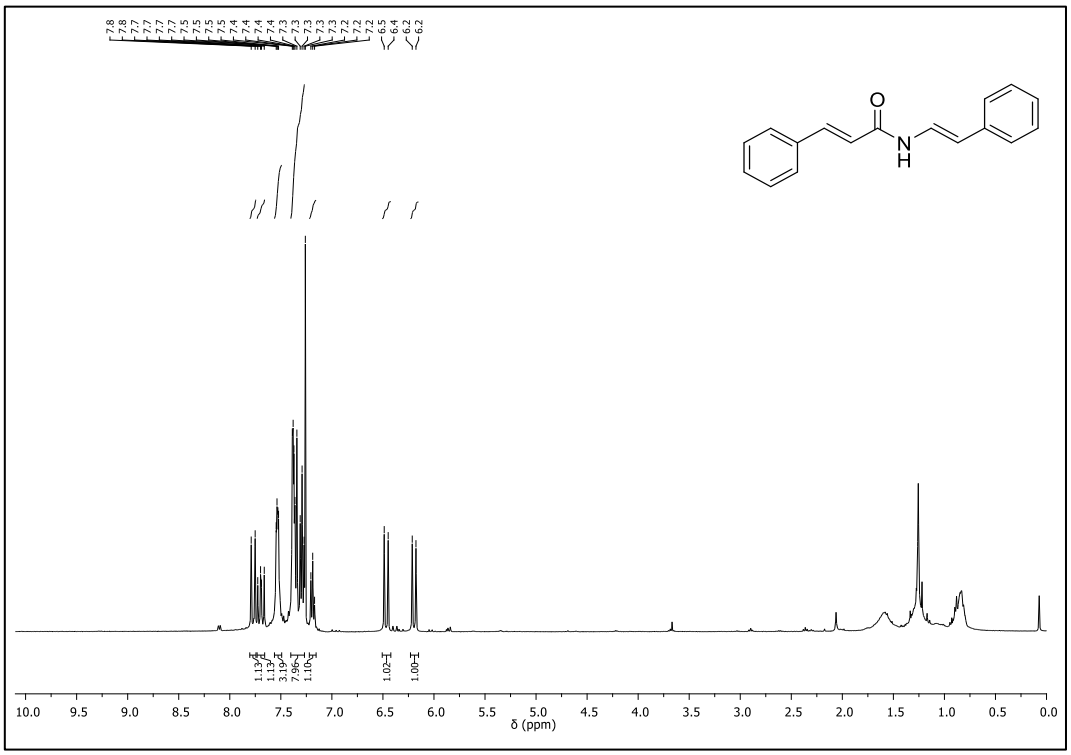

^{13}C-NMR (101 MHz, $CDCl_3$) of **39b**

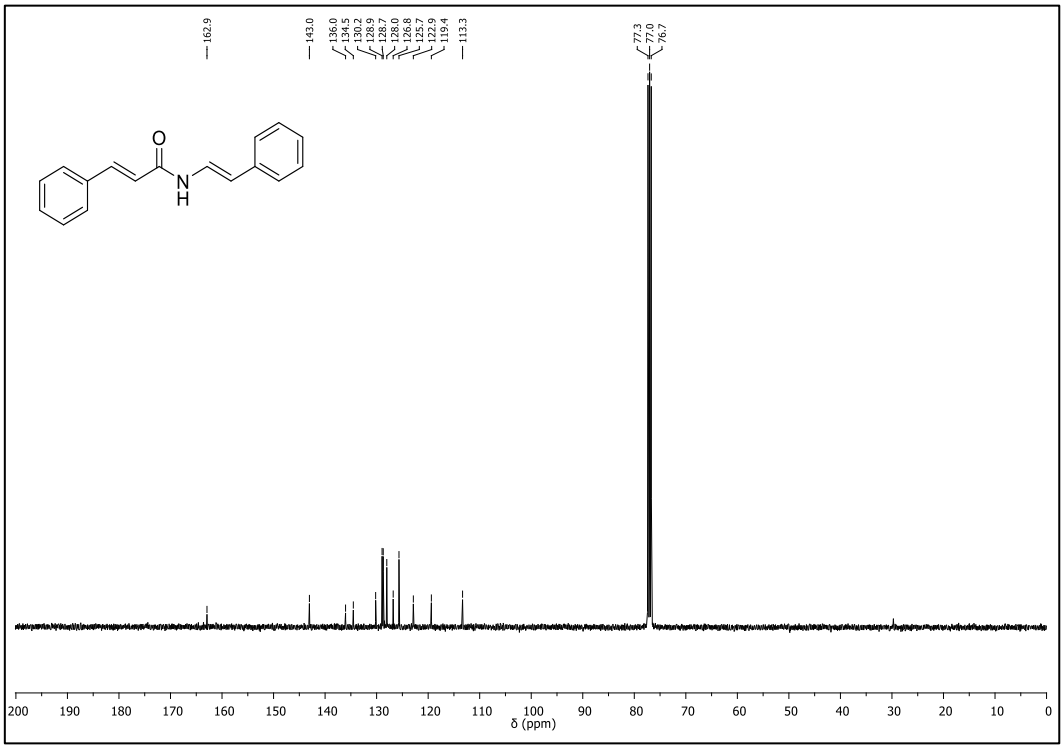

^{1}H-NMR (400 MHz, $CDCl_3$) of **40b**

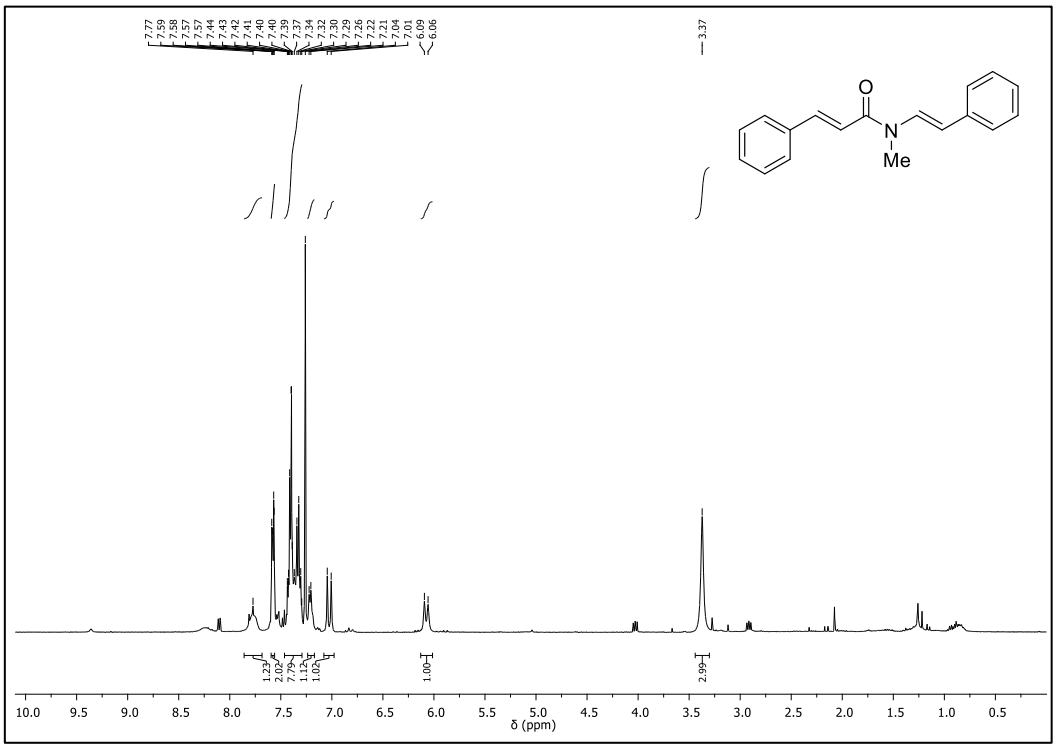

^{13}C-NMR (101 MHz, $CDCl_3$) of **40b**

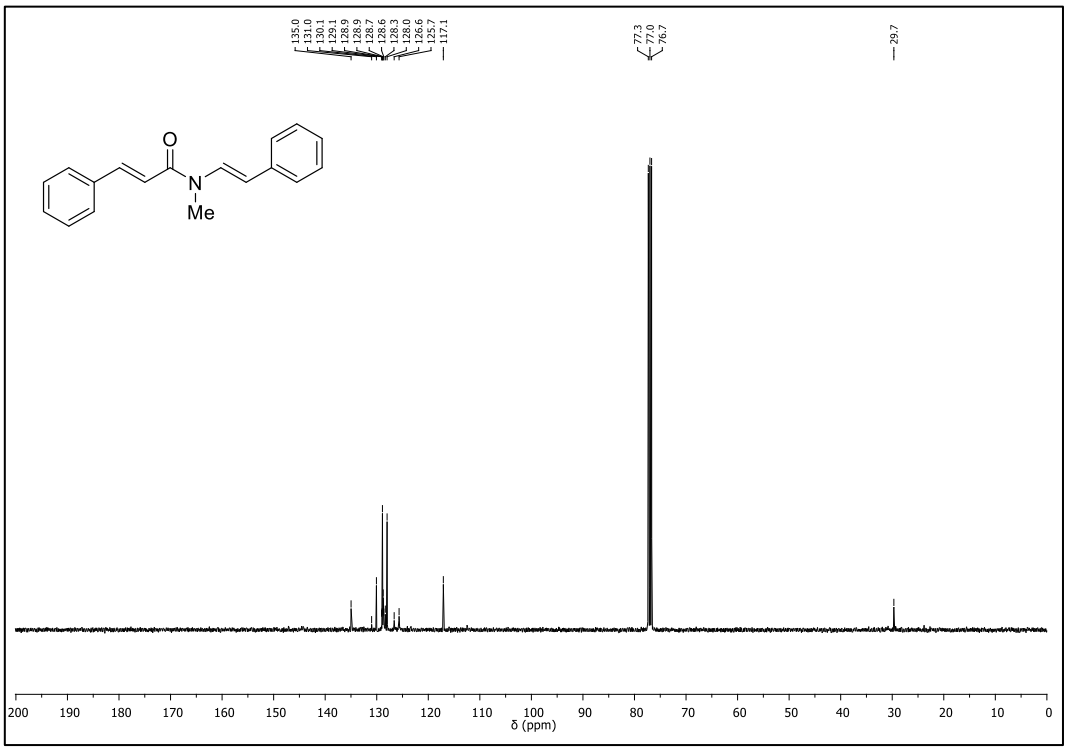

^{1}H-NMR (400 MHz, $CDCl_3$) of **41**

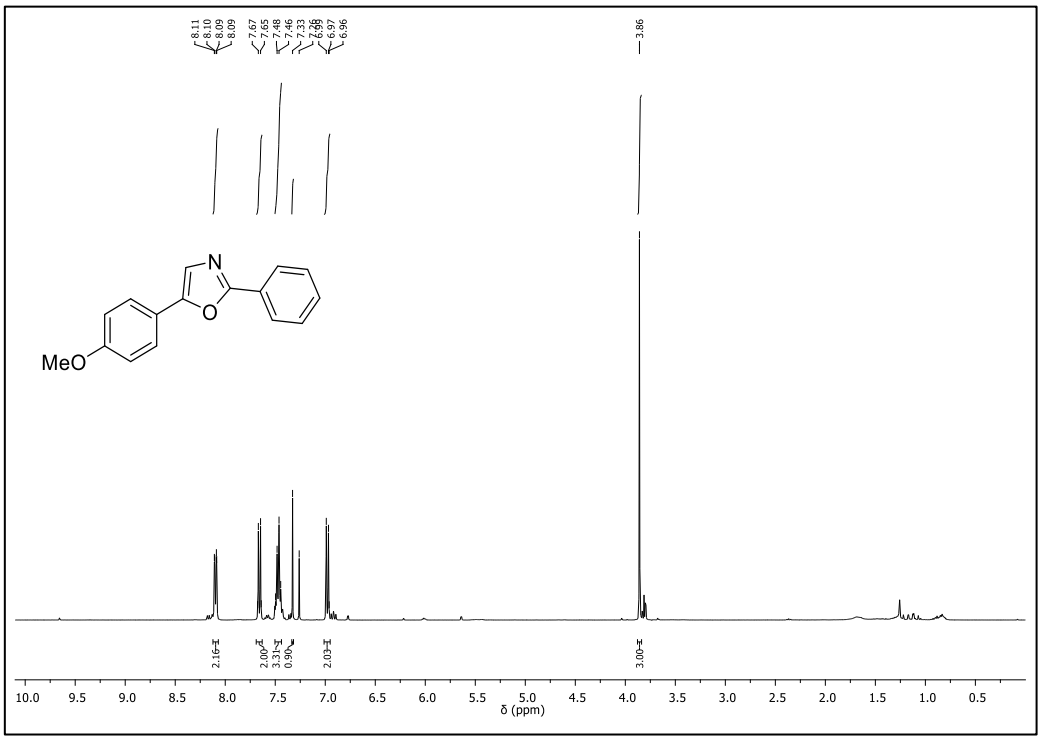

^{13}C-NMR (101 MHz, $CDCl_3$) of **41**

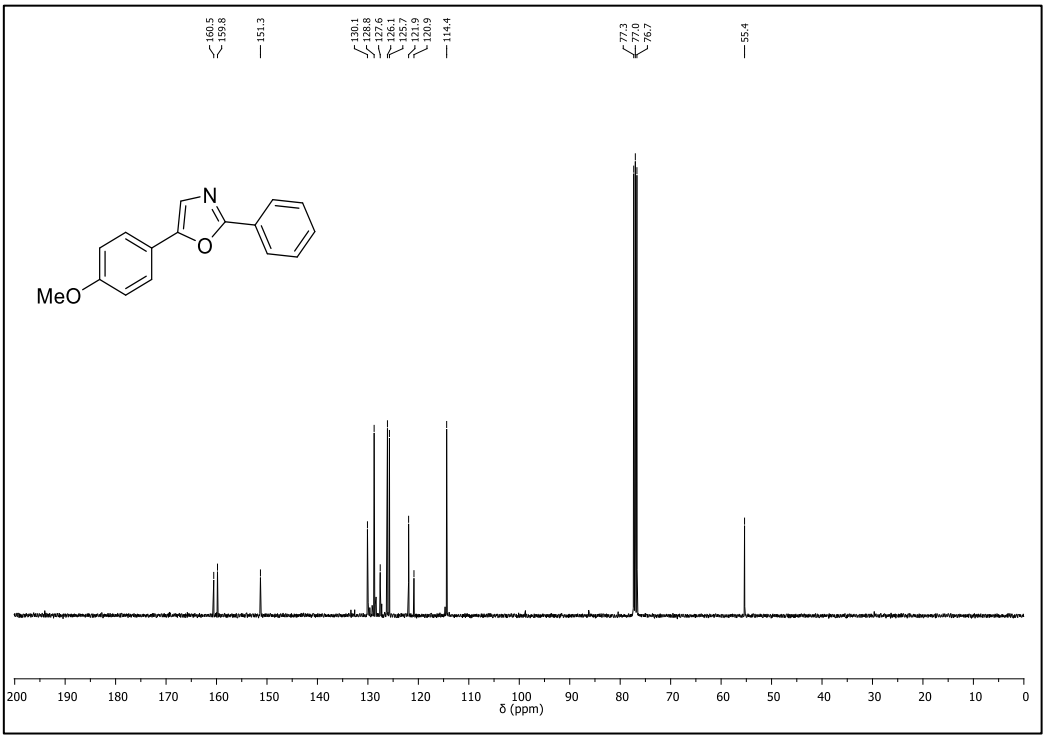

9.4 NMR Spectra of Chapter 4

^{1}H-NMR (400 MHz, $CDCl_3$) of **moclobemide**

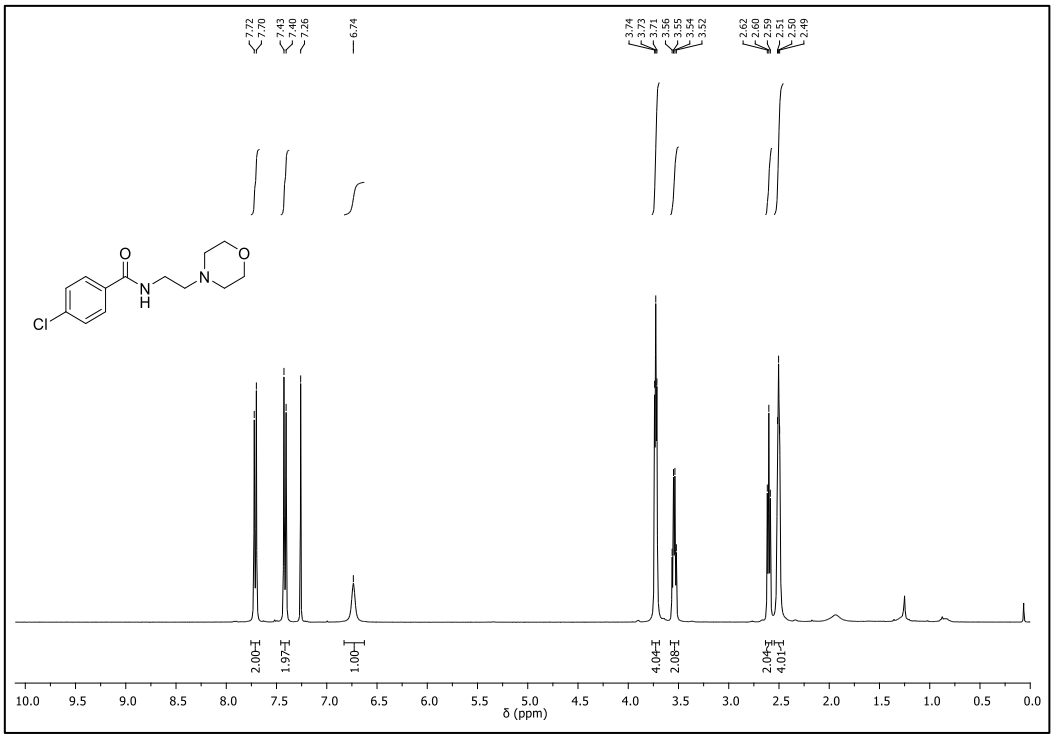

^{13}C-NMR (101 MHz, $CDCl_3$) of **moclobemide**

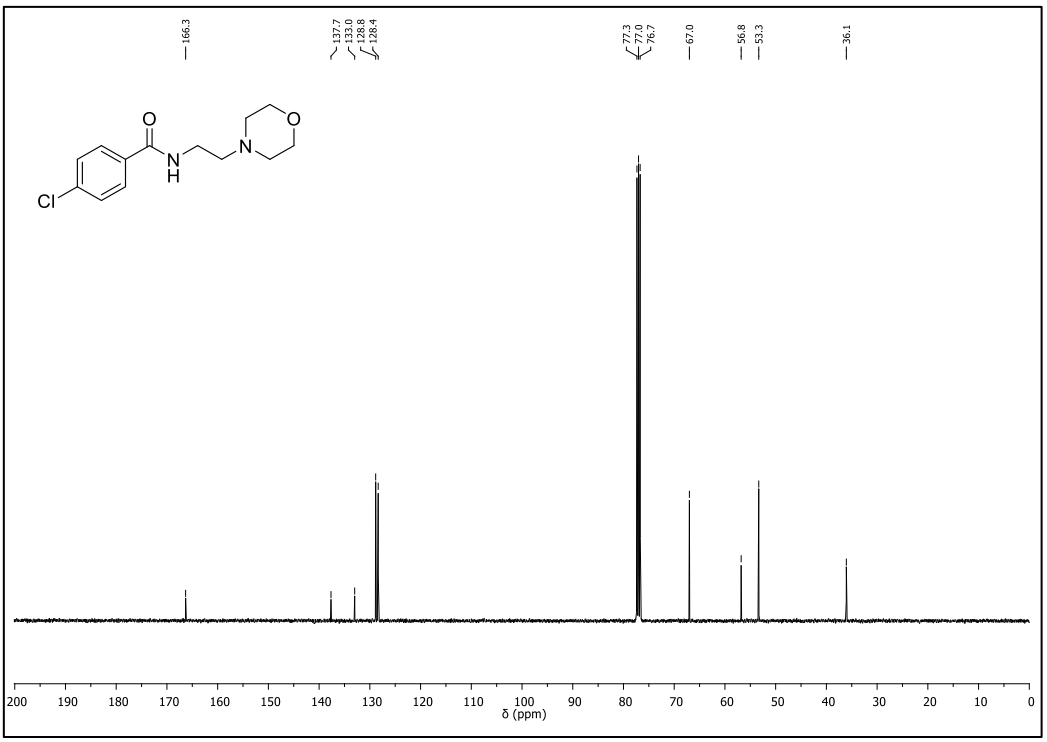

^{1}H-NMR (400 MHz, $CDCl_3$) of **SM-A**

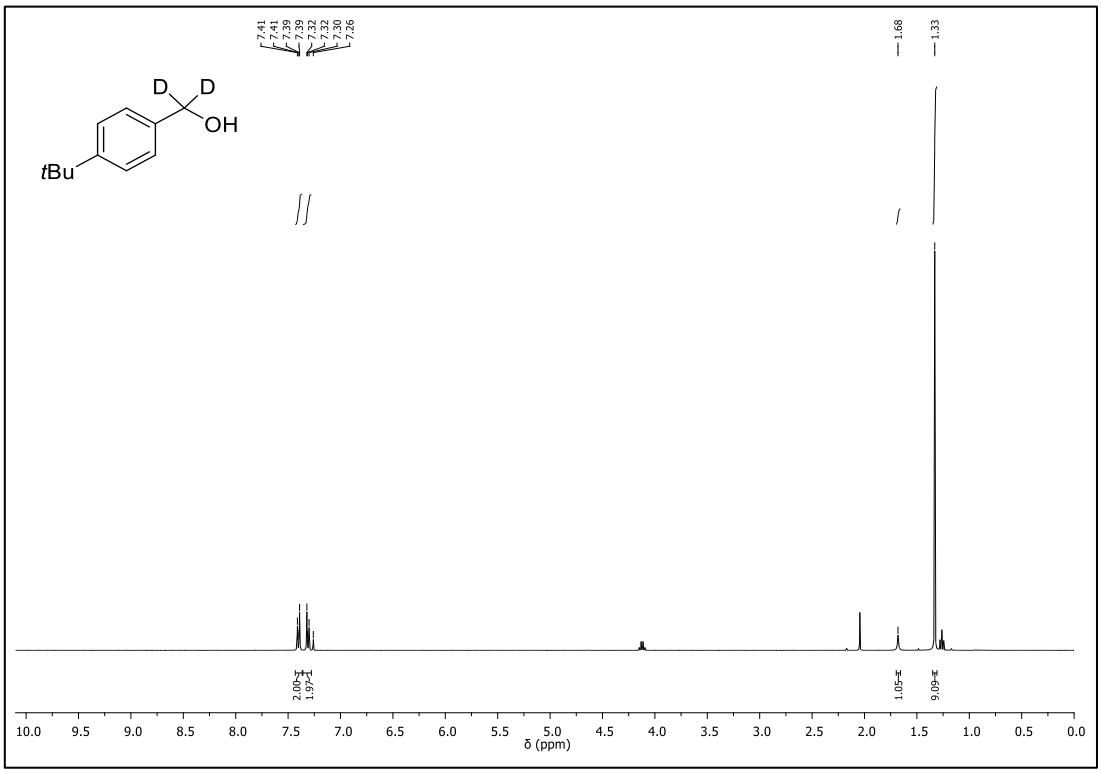

^{13}C-NMR (101 MHz, $CDCl_3$) of **SM-A**

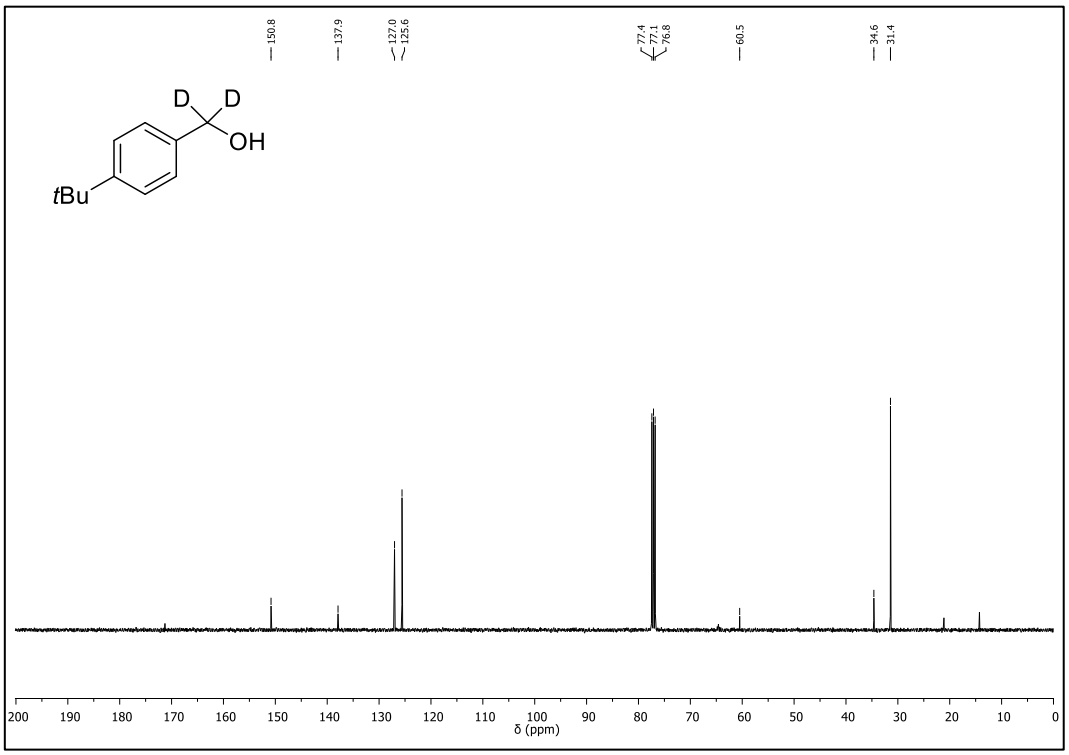

^{1}H-NMR (400 MHz, CD_3CN) of **1a-D**

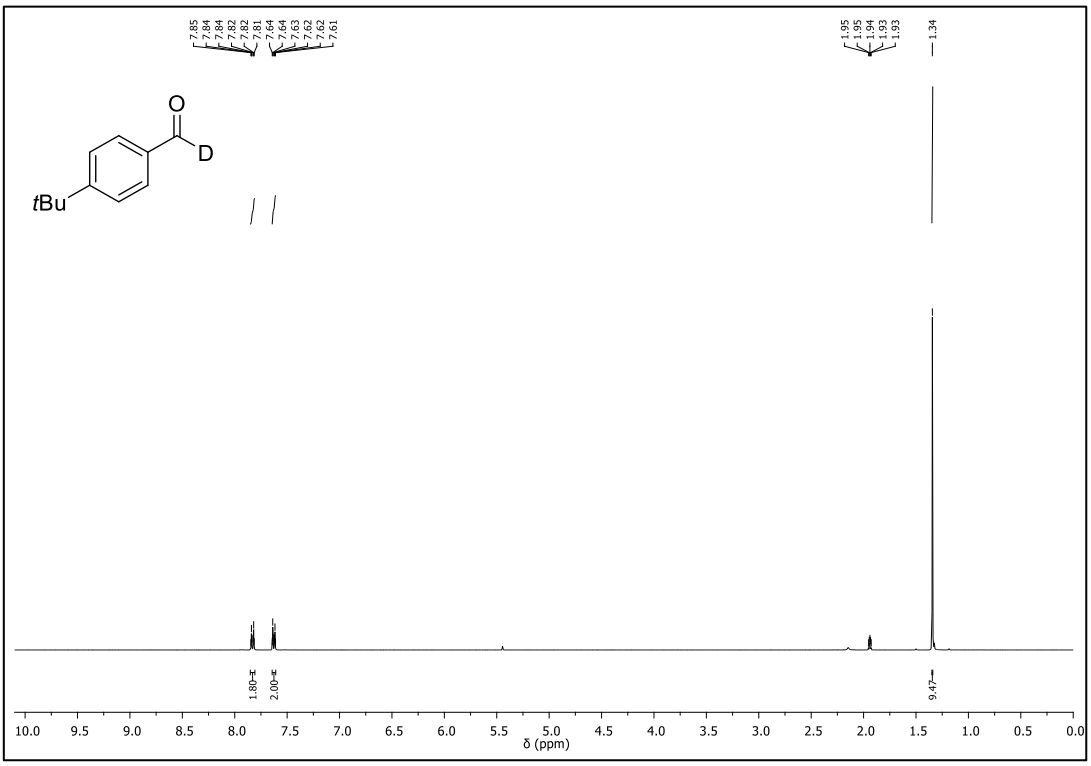

^{13}C-NMR (101 MHz, CD_3CN) of **1a-D**

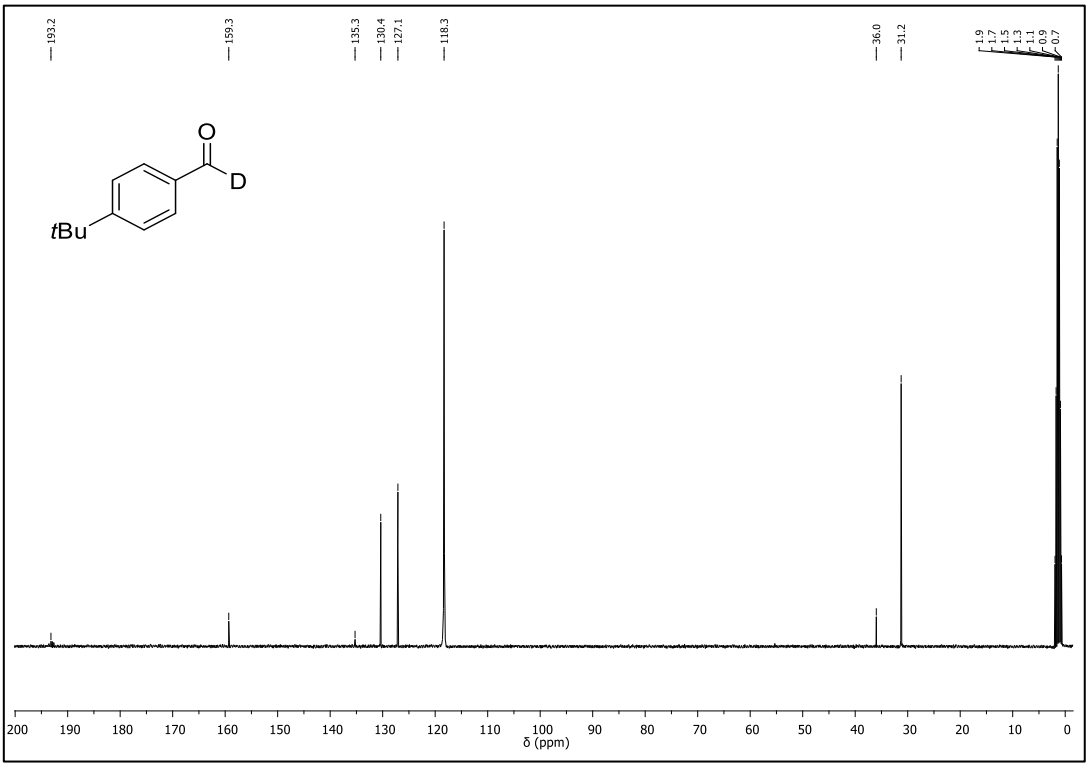

^{1}H-NMR (400 MHz, $CDCl_3$) of **13a**

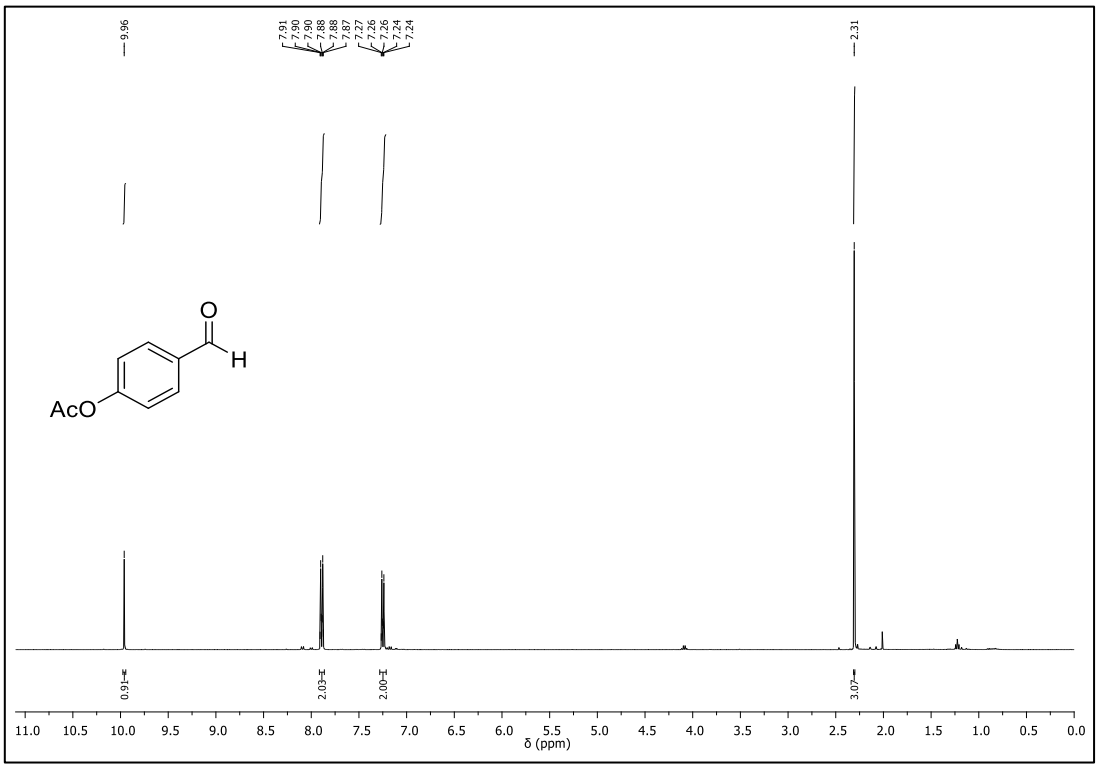

^{13}C-NMR (101 MHz, $CDCl_3$) of **13a**

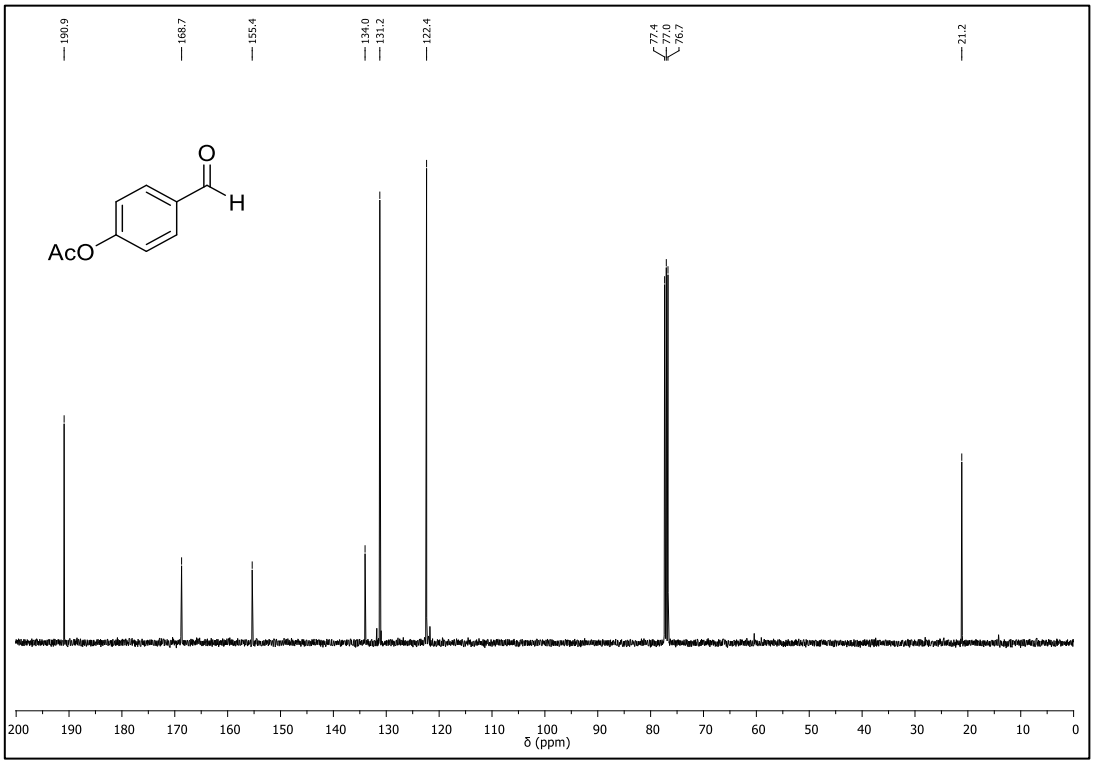

^{1}H-NMR (400 MHz, $CDCl_3$) of **14a**

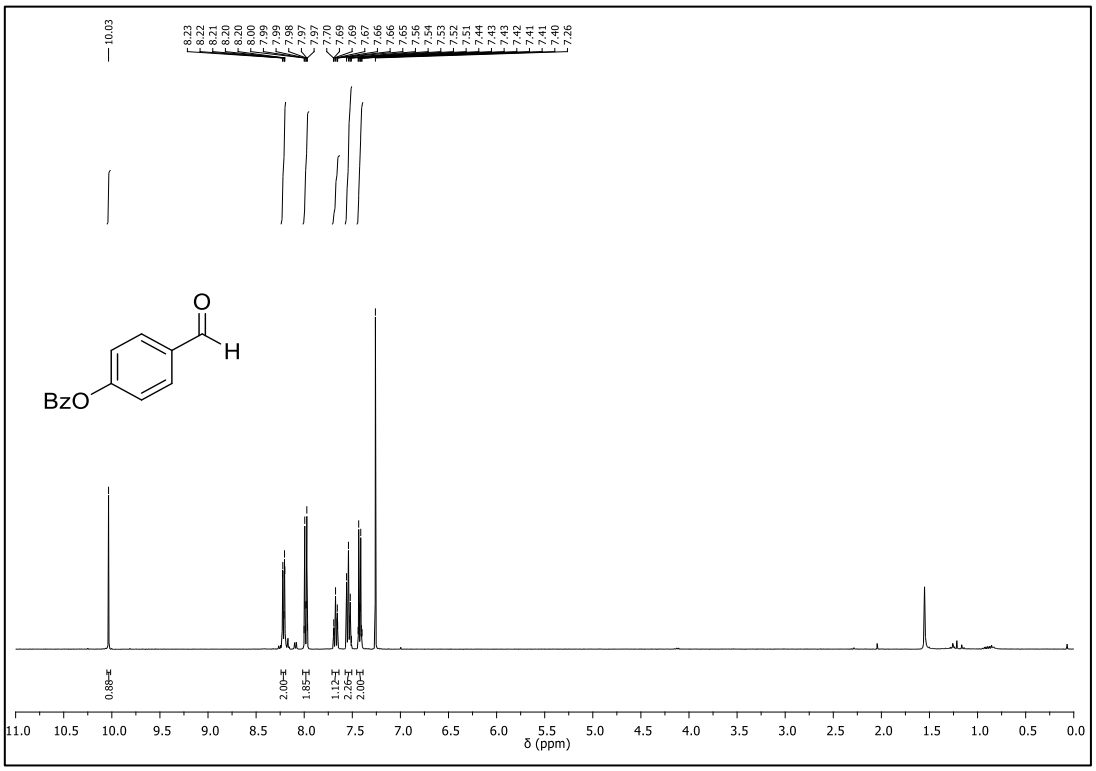

^{13}C-NMR (101 MHz, $CDCl_3$) of **14a**

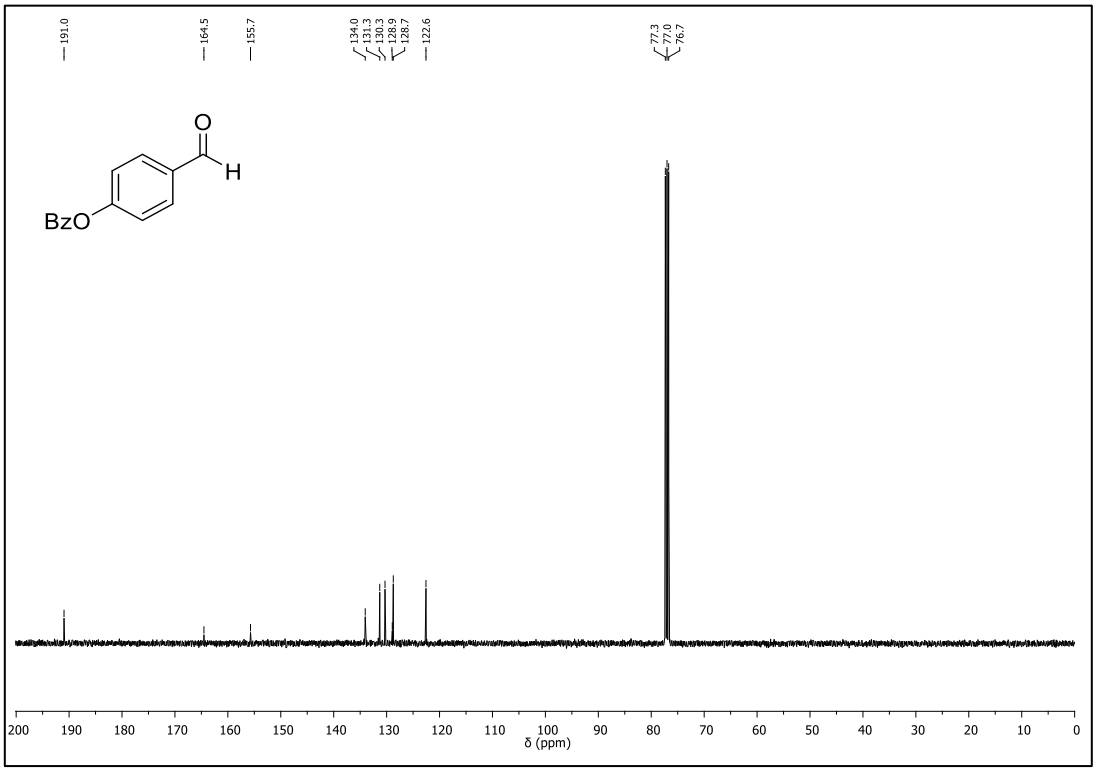

^{1}H-NMR (400 MHz, CD_2Cl_2) of **16b**

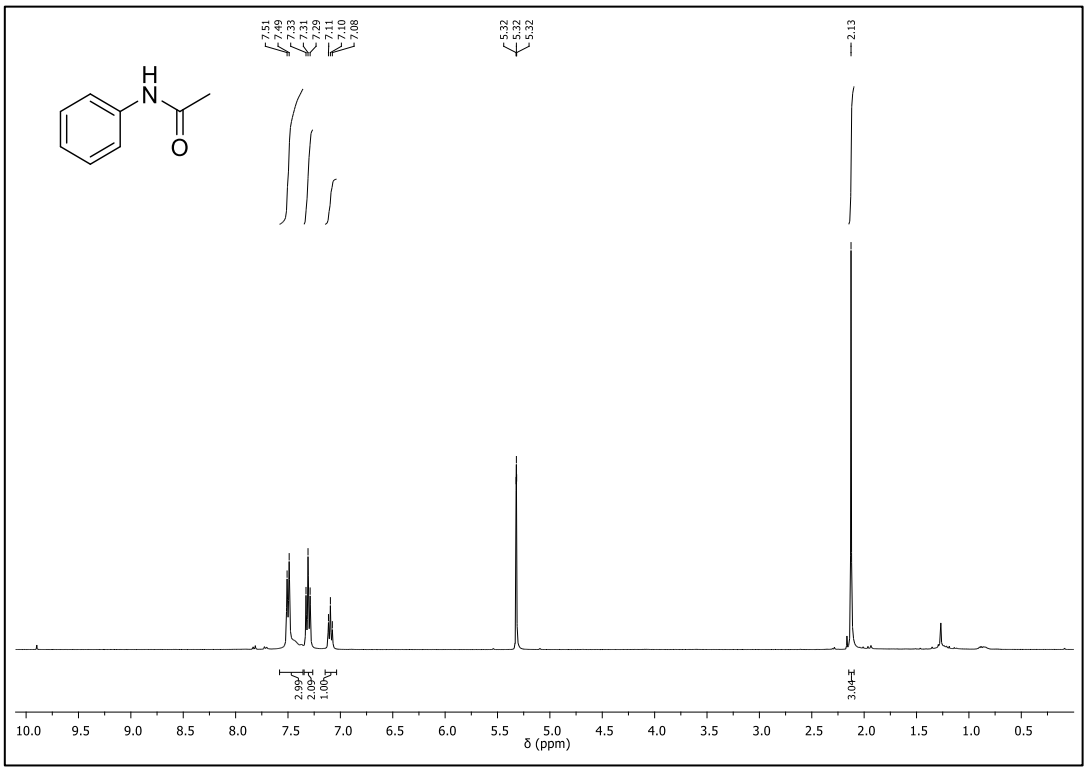

^{13}C-NMR (101 MHz, CD_2Cl_2) of **16b**

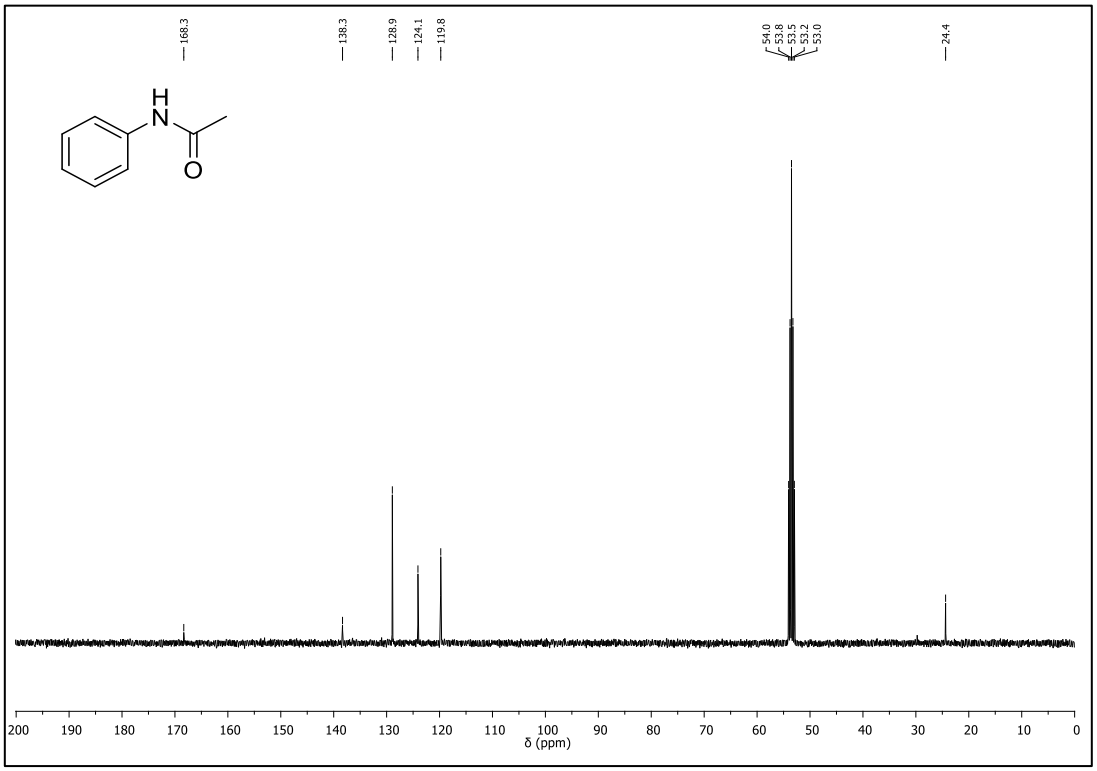

^{1}H-NMR (400 MHz, CD_2Cl_2) of **25b**

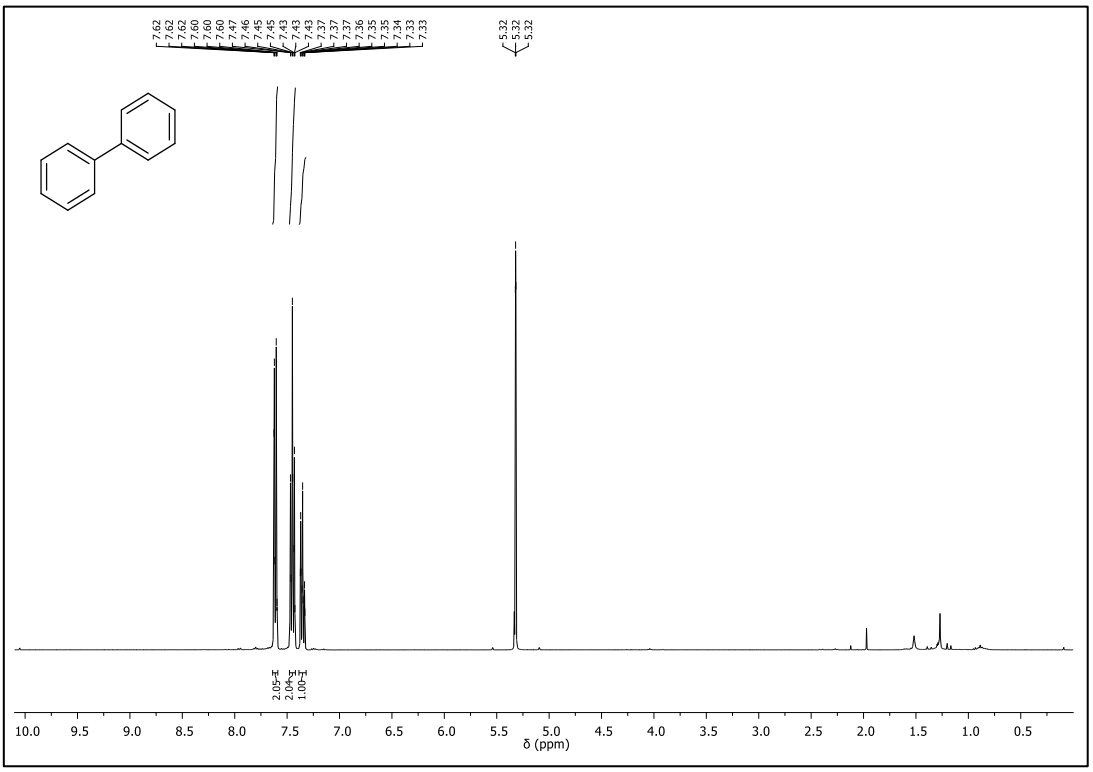

^{13}C-NMR (101 MHz, CD_2Cl_2) of **25b**

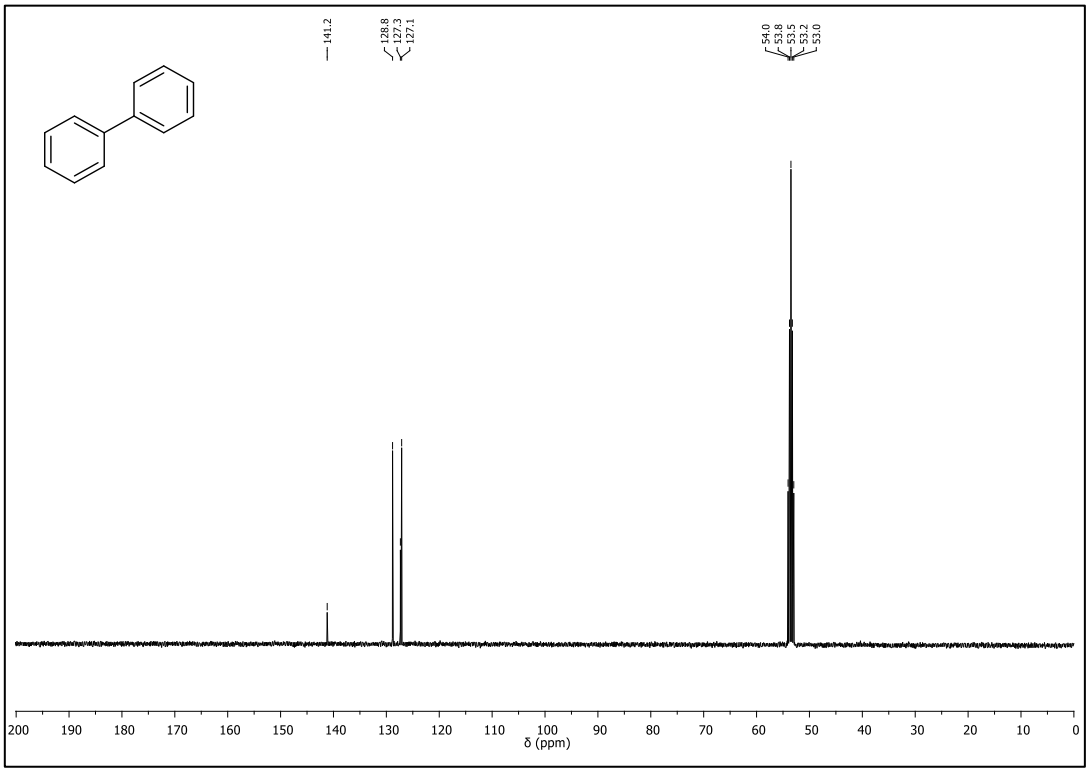

9.5 NMR Spectra of Chapter 5

^{1}H-NMR (400 MHz, $CDCl_3$) of **6a**

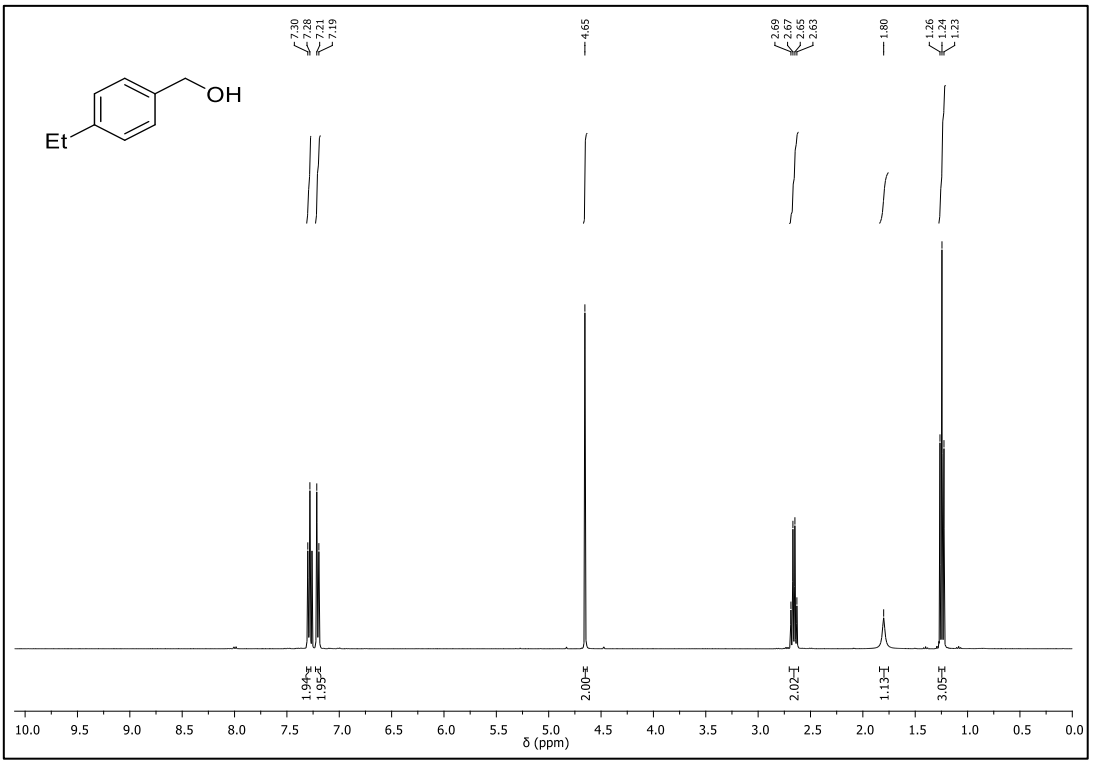

^{13}C-NMR (101 MHz, $CDCl_3$) of **6a**

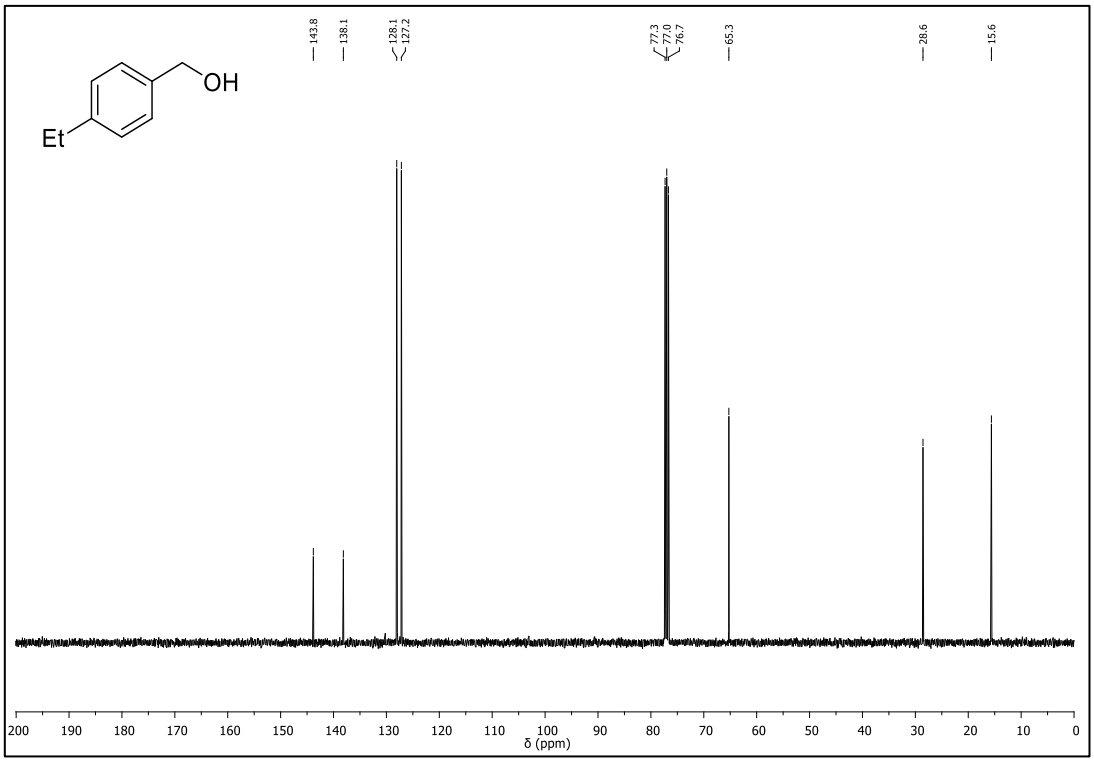

^{1}H-NMR (400 MHz, $CDCl_3$) of **7a**

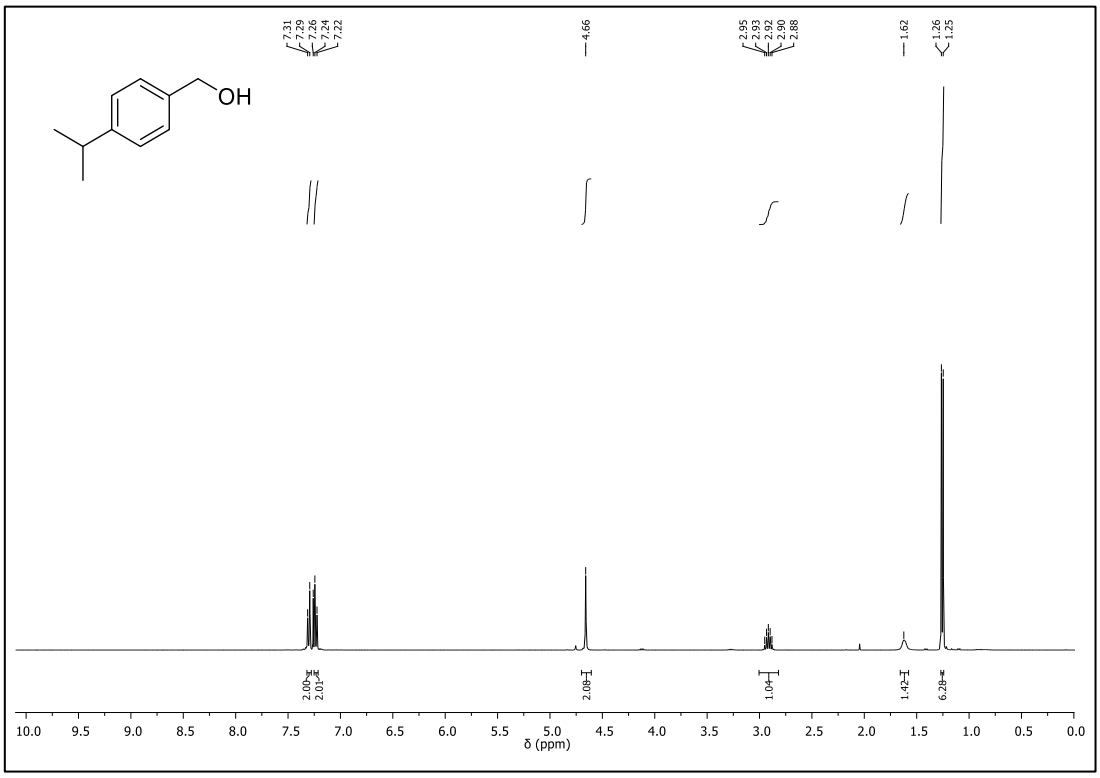

^{13}C-NMR (101 MHz, $CDCl_3$) of **7a**

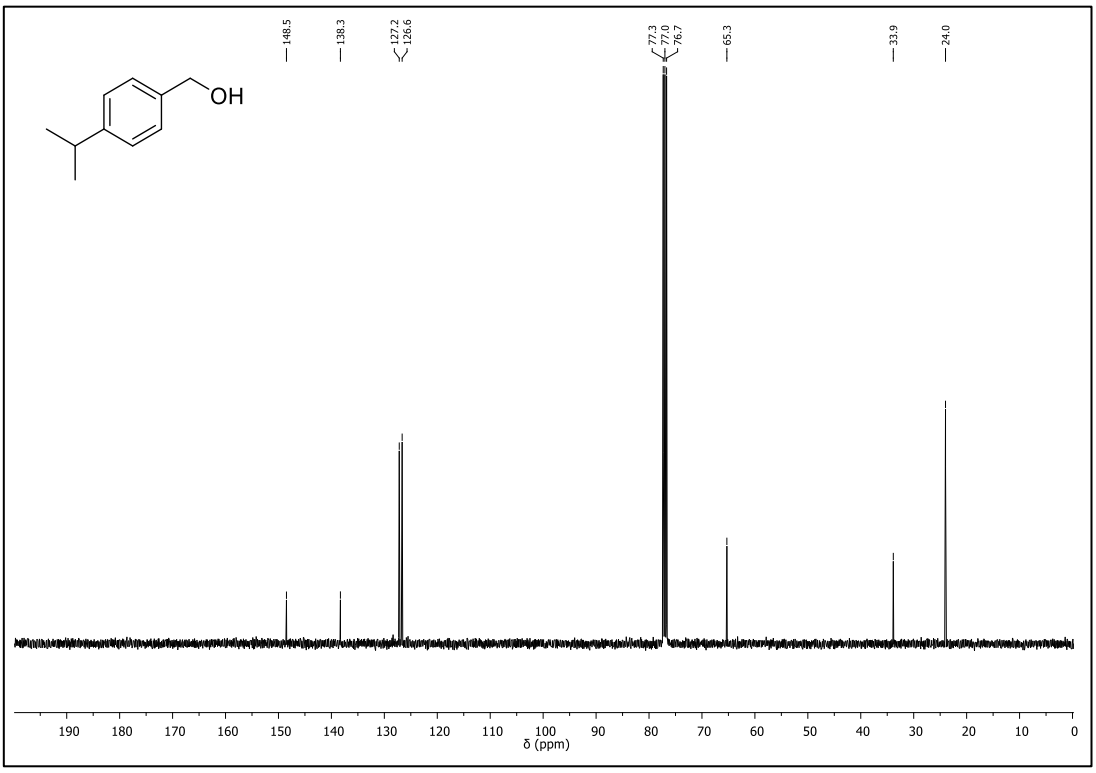

^{1}H-NMR (400 MHz, $CDCl_3$) of **16a**

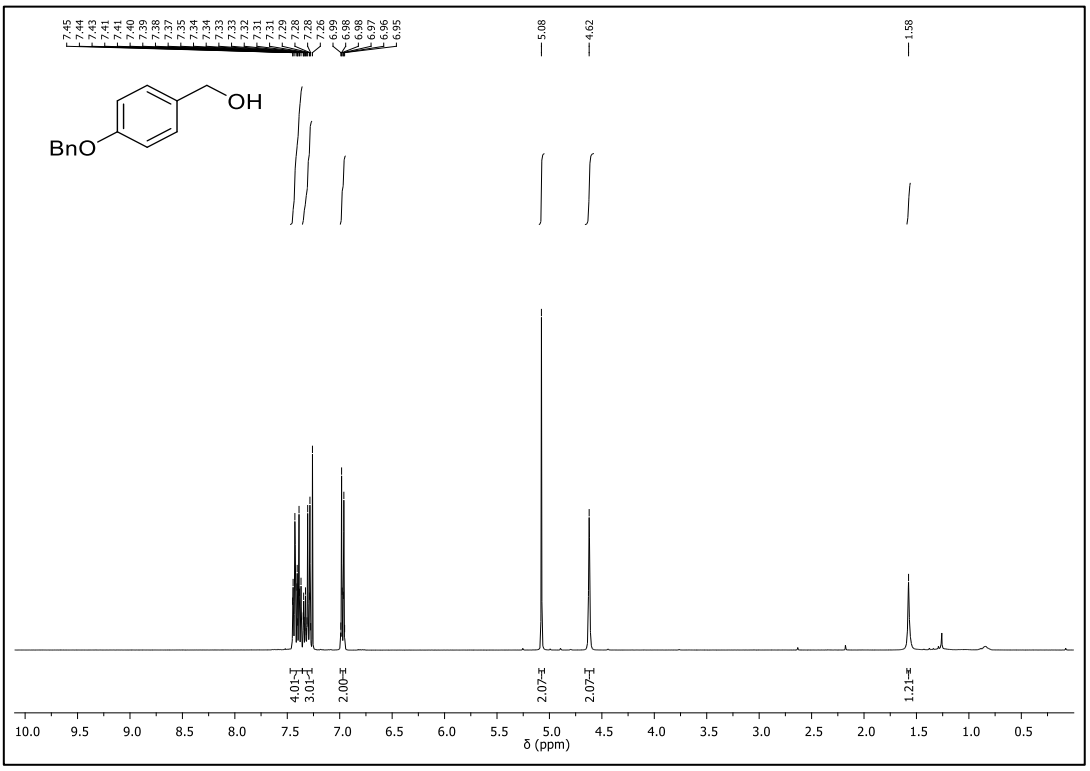

^{13}C-NMR (101 MHz, $CDCl_3$) of **16a**

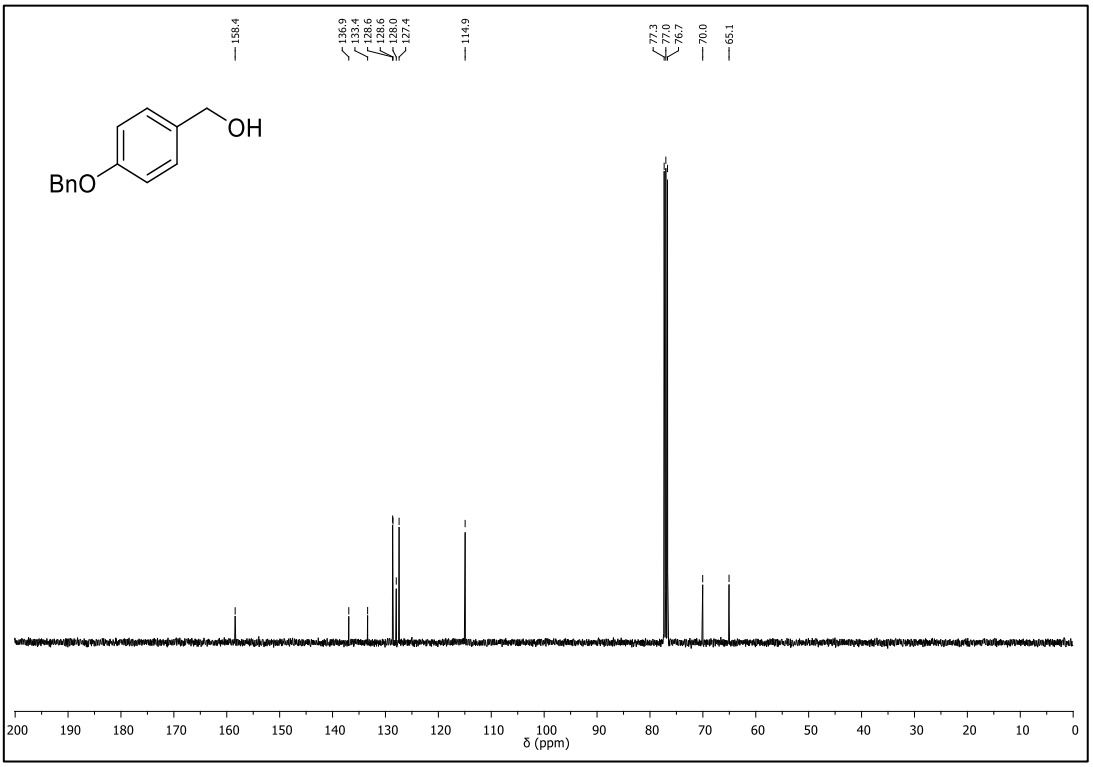

^{1}H-NMR (400 MHz, $CDCl_3$) of **18a**

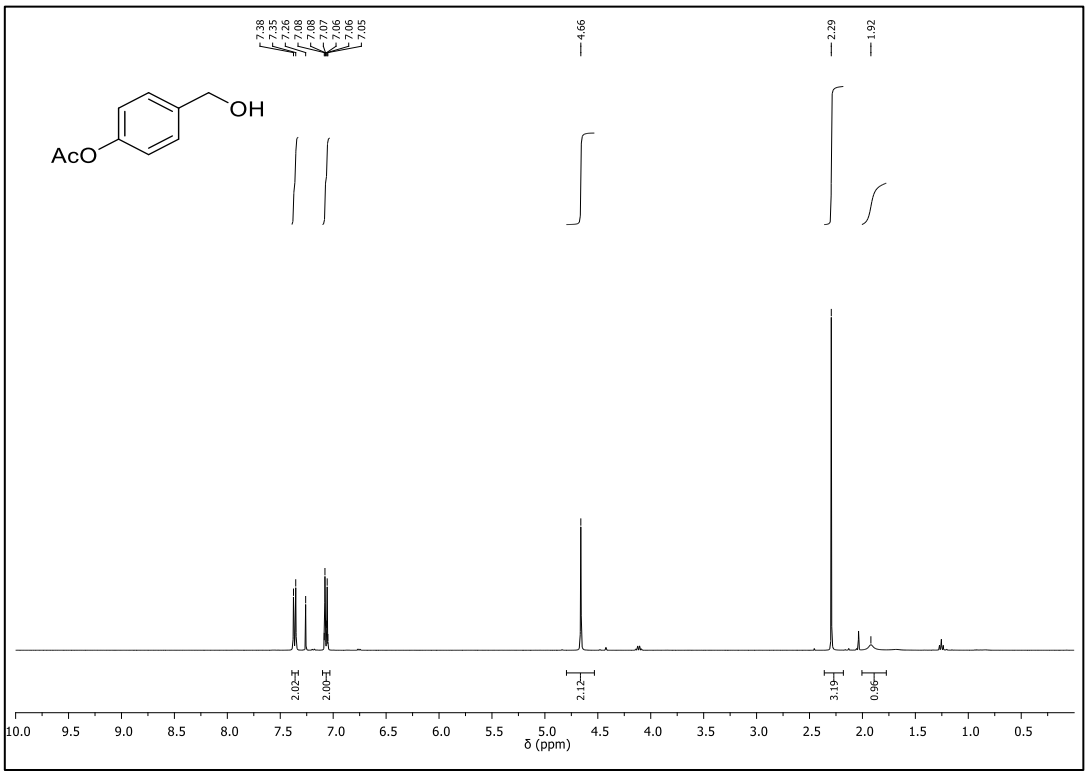

^{13}C-NMR (101 MHz, $CDCl_3$) of **18a**

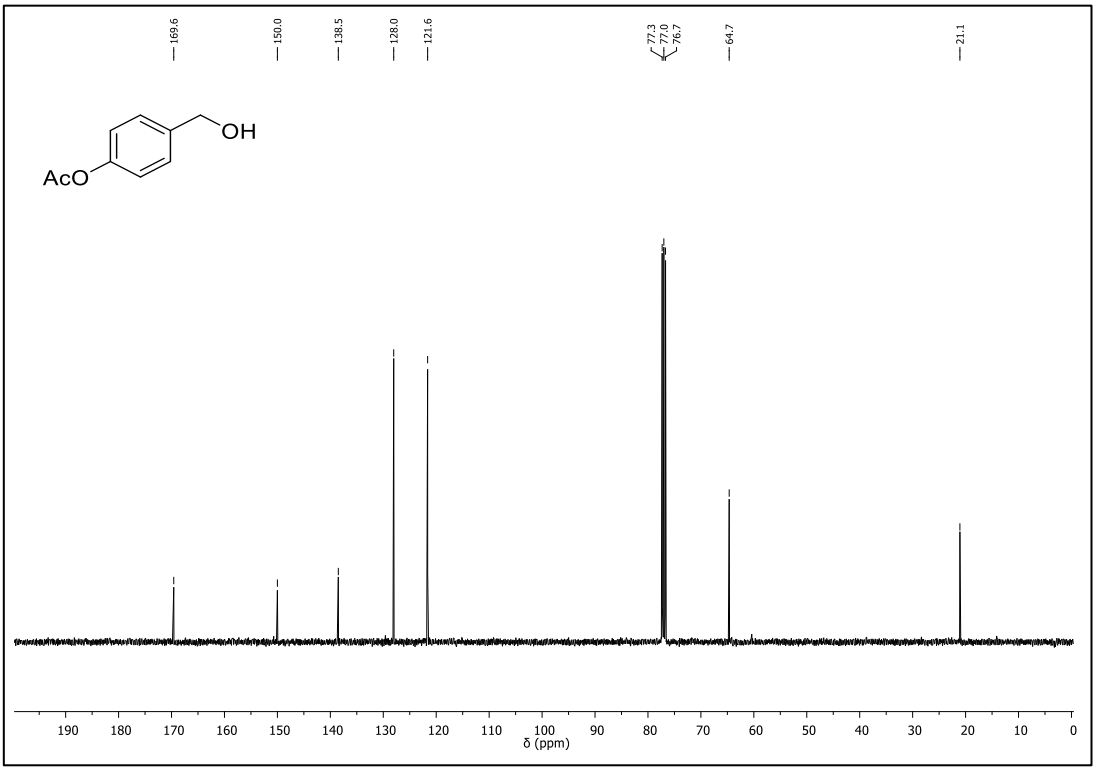

^{1}H-NMR (400 MHz, $CDCl_3$) of **19a**

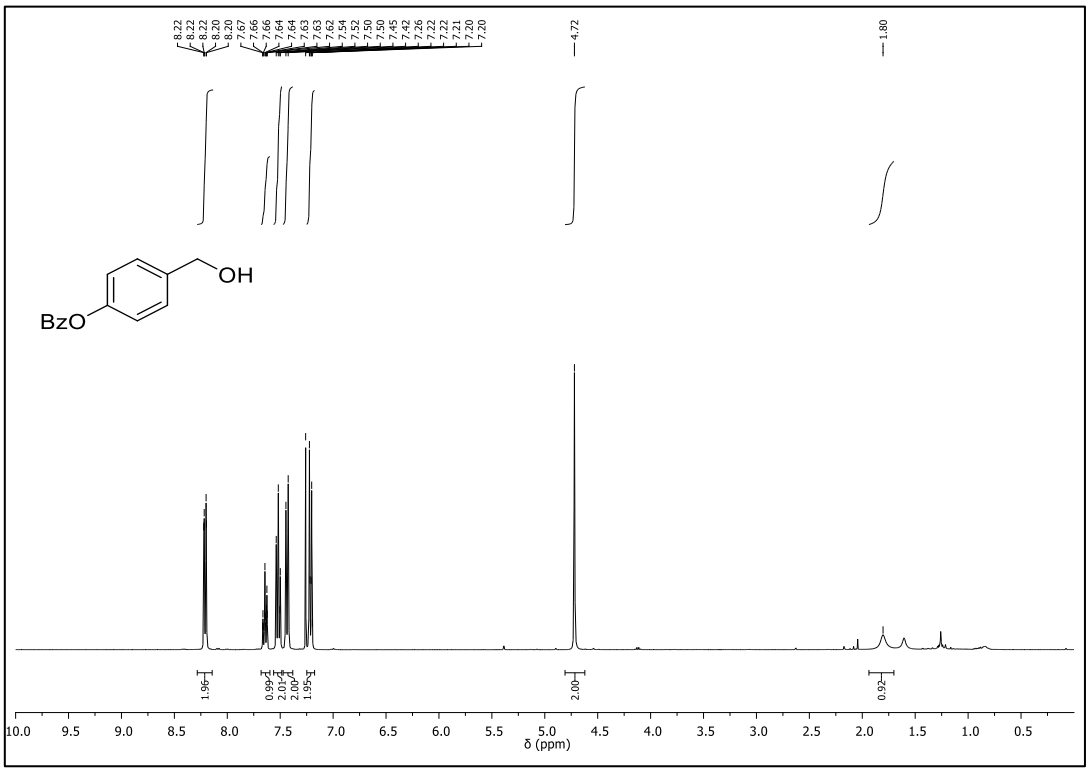

^{13}C-NMR (101 MHz, $CDCl_3$) of **19a**

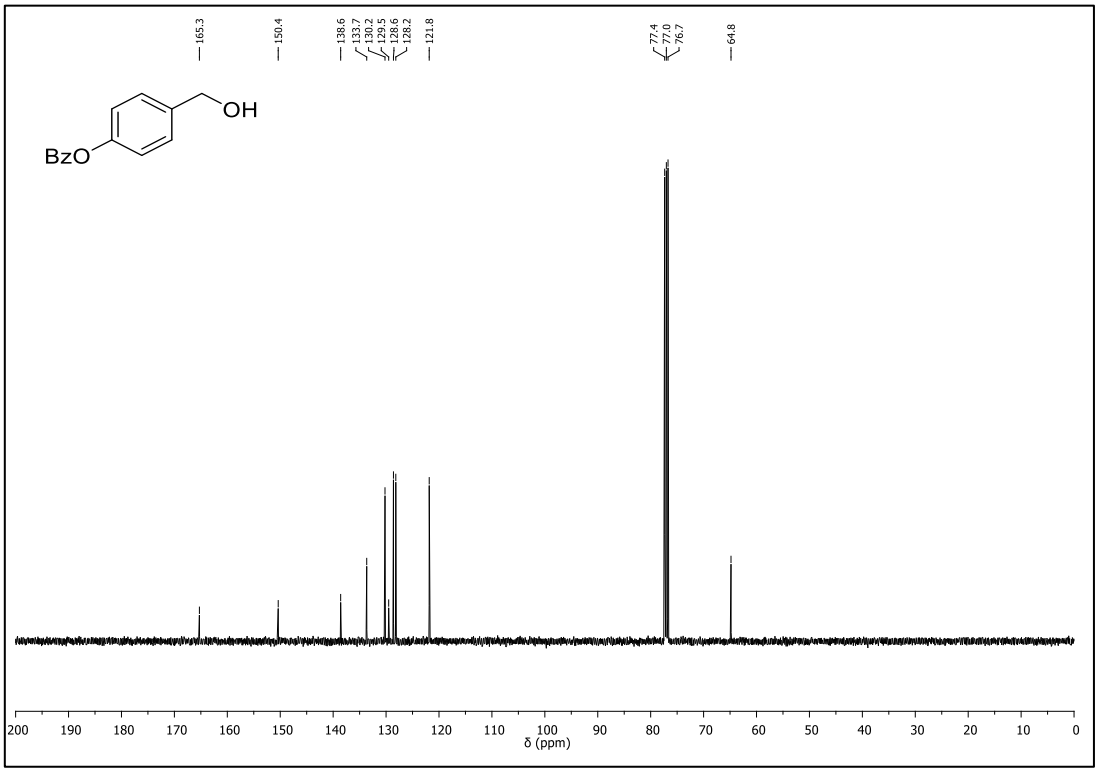

^{1}H-NMR (400 MHz, CD_3OD) of **24a**

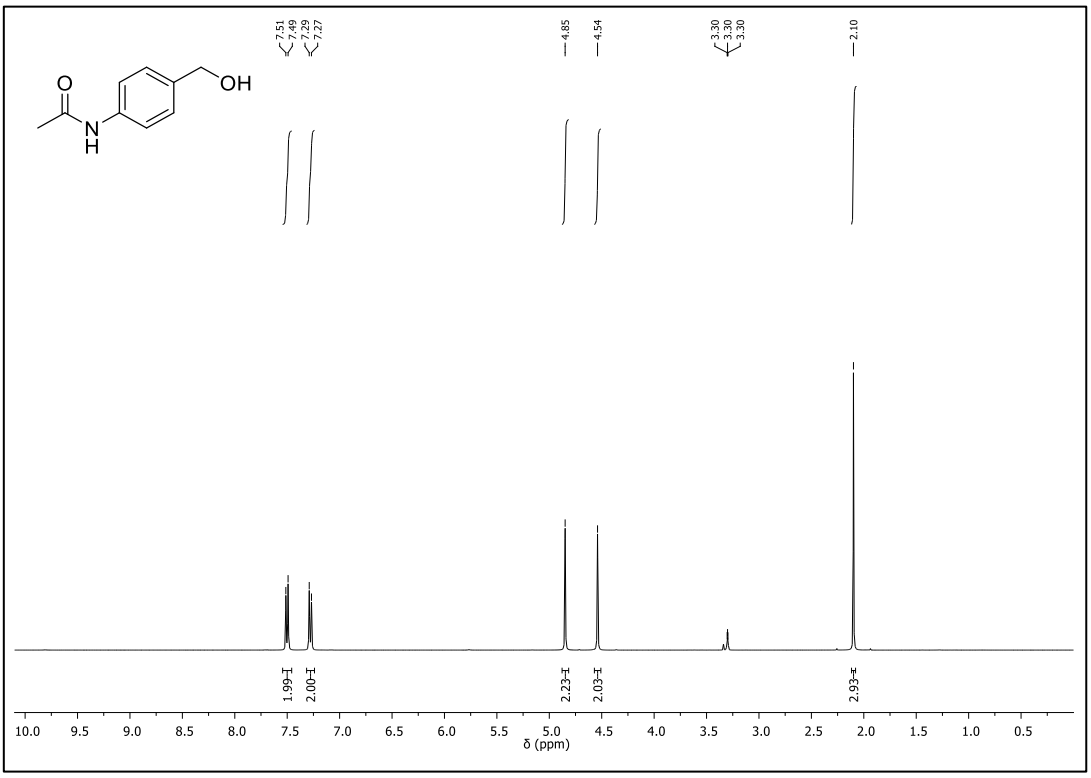

^{13}C-NMR (101 MHz, CD_3OD) of **24a**

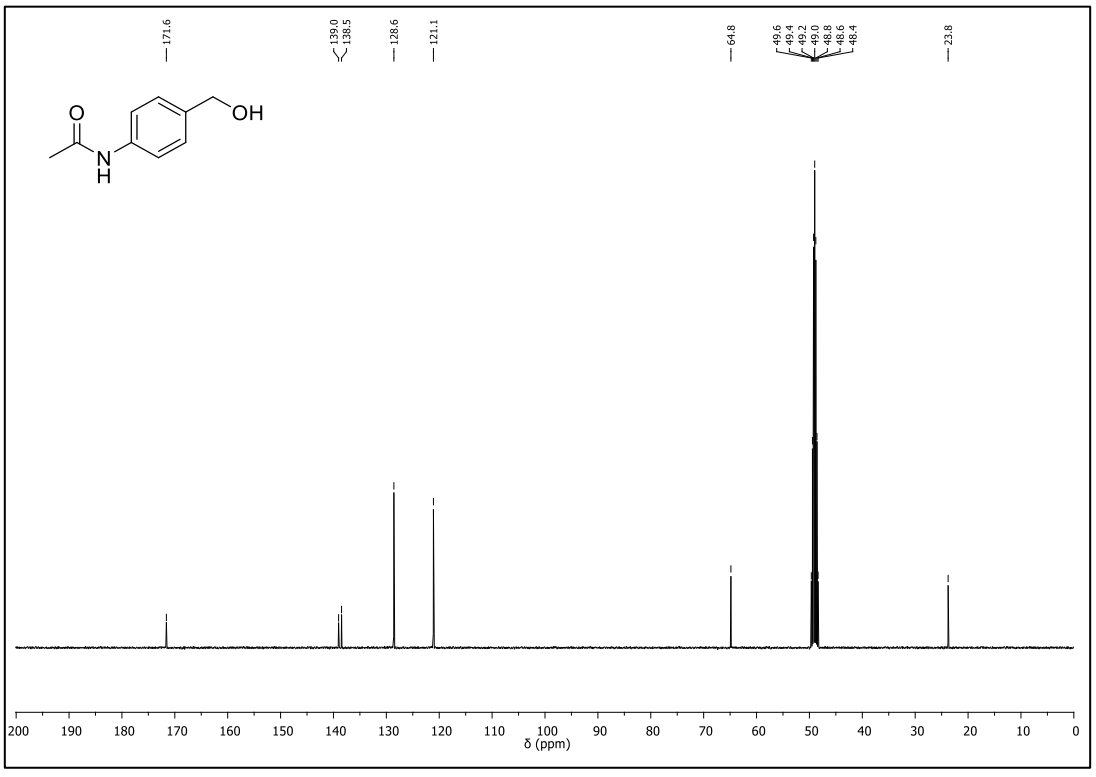

9.6 NMR Spectra of Chapter 6

^{1}H-NMR (400 MHz, $CDCl_3$) of **2e**

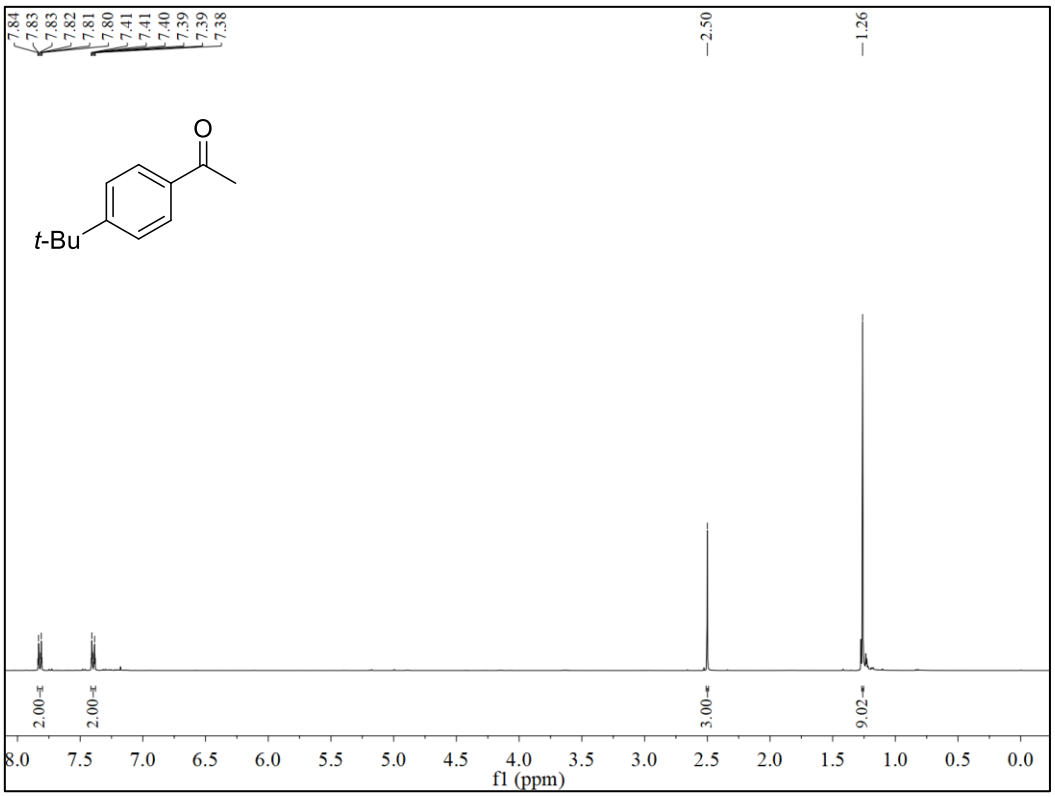

^{13}C-NMR (101 MHz, $CDCl_3$) of **2e**

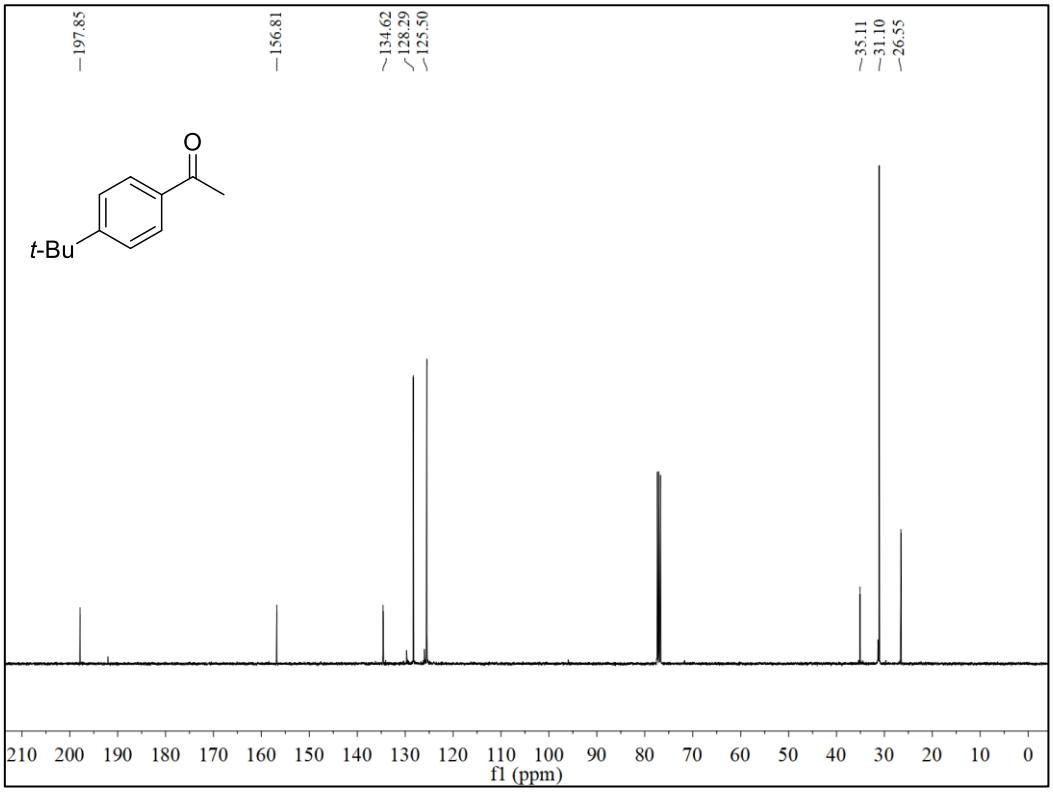

^{1}H-NMR (400 MHz, $CDCl_3$) of **2f**

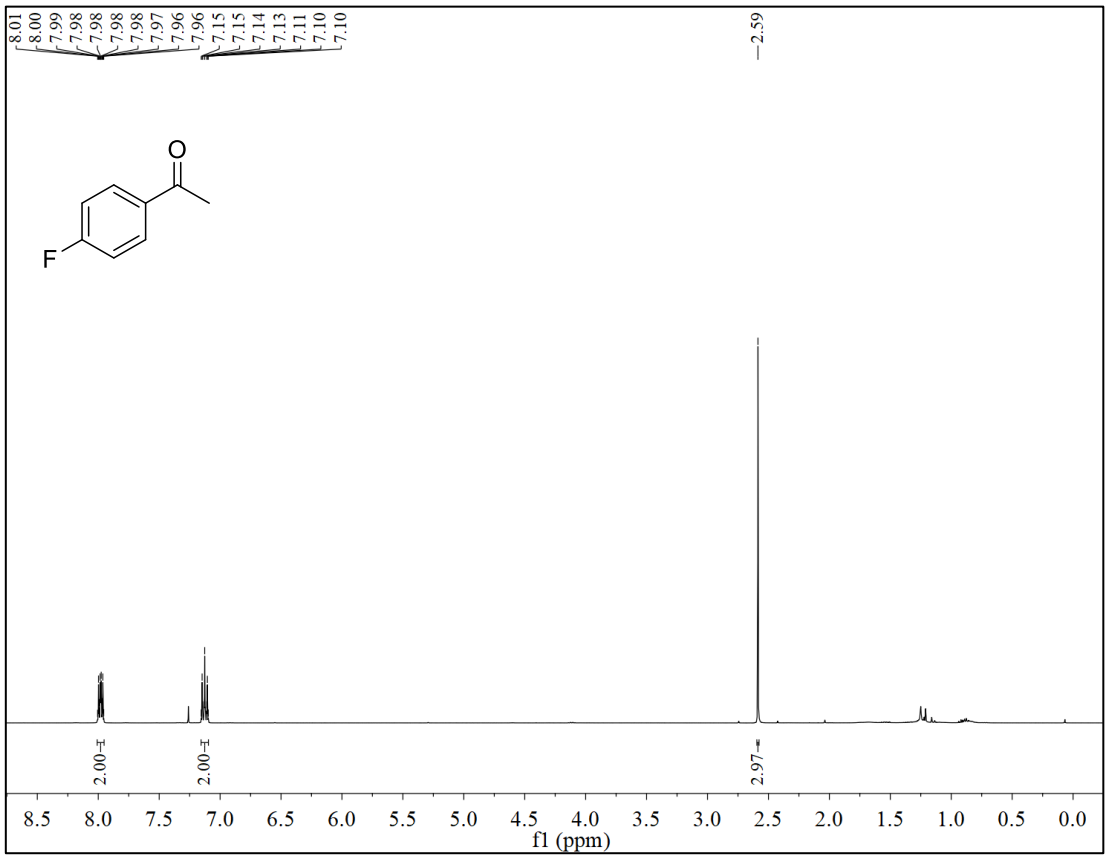

^{13}C-NMR (101 MHz, $CDCl_3$) of **2f**

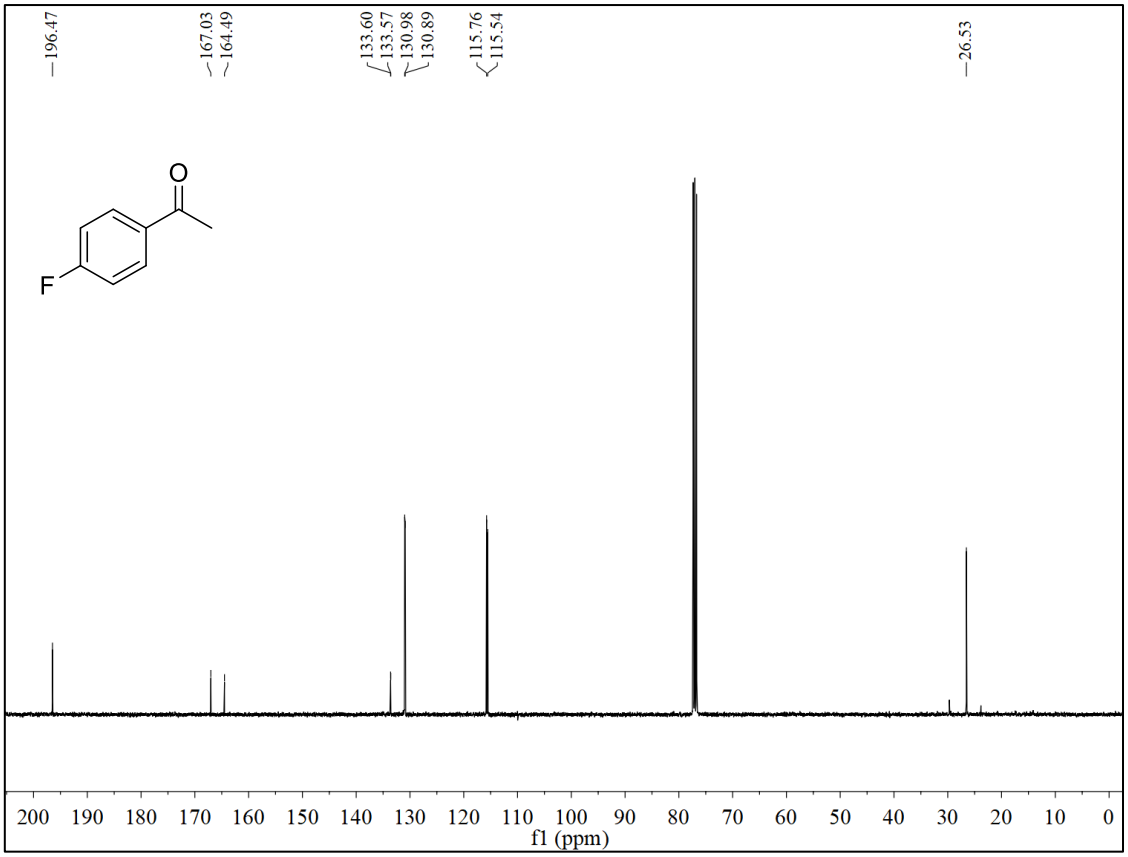

^{19}F-NMR (376 MHz, $CDCl_3$) of **2f** using $PhCF_3$ (δ = –63.72 ppm) as I.S.

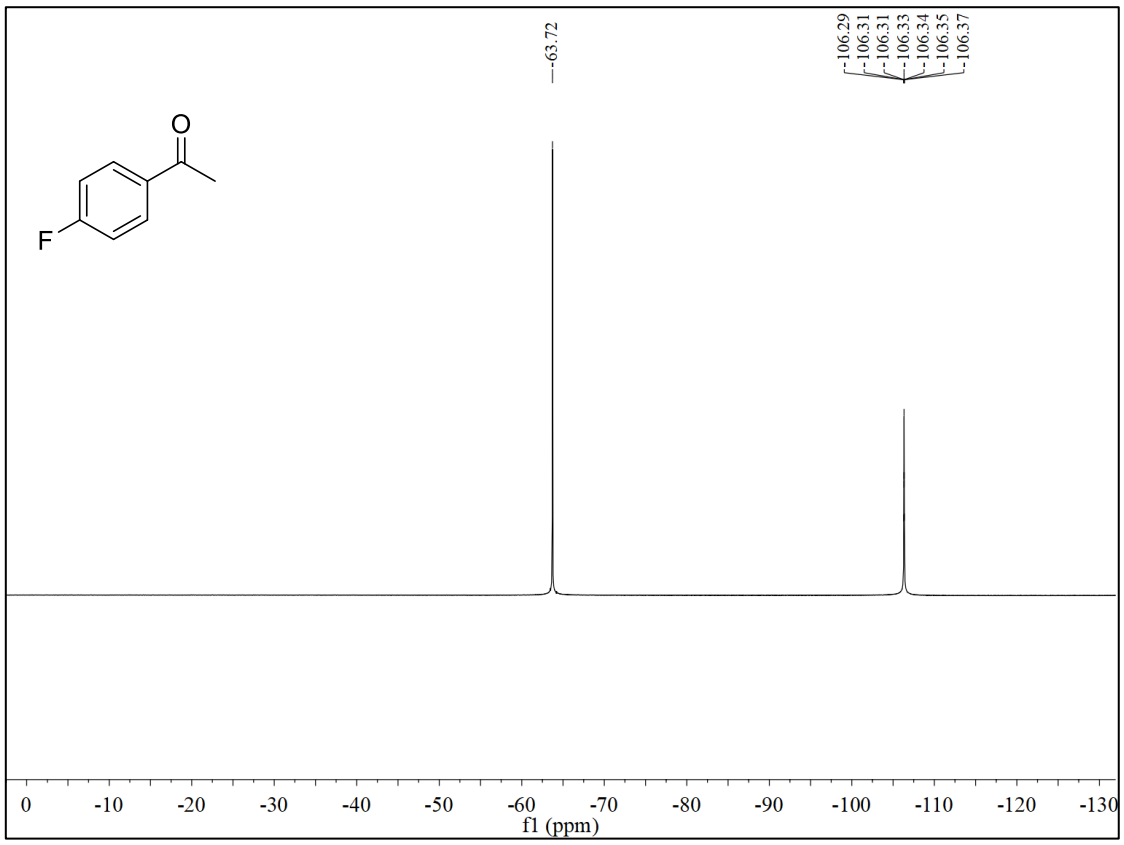

^{1}H-NMR (400 MHz, $CDCl_3$) of **2g**

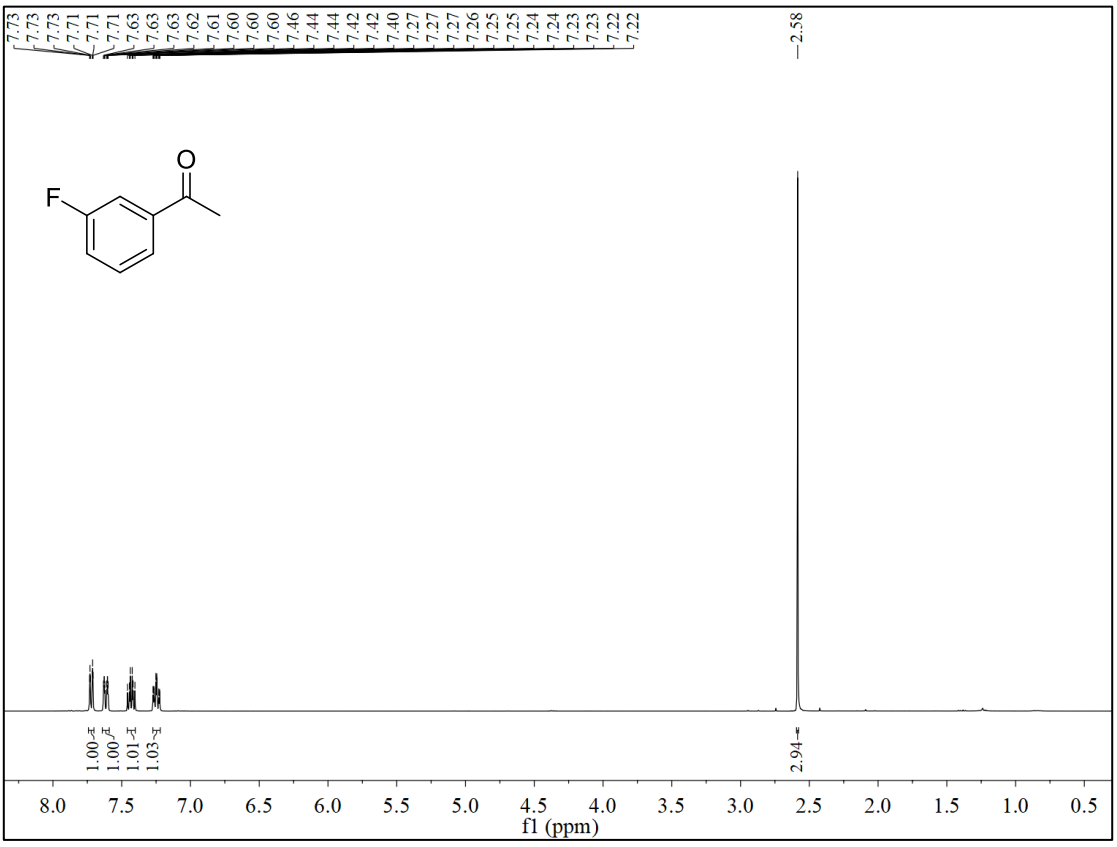

^{13}C-NMR (101 MHz, $CDCl_3$) of **2g**

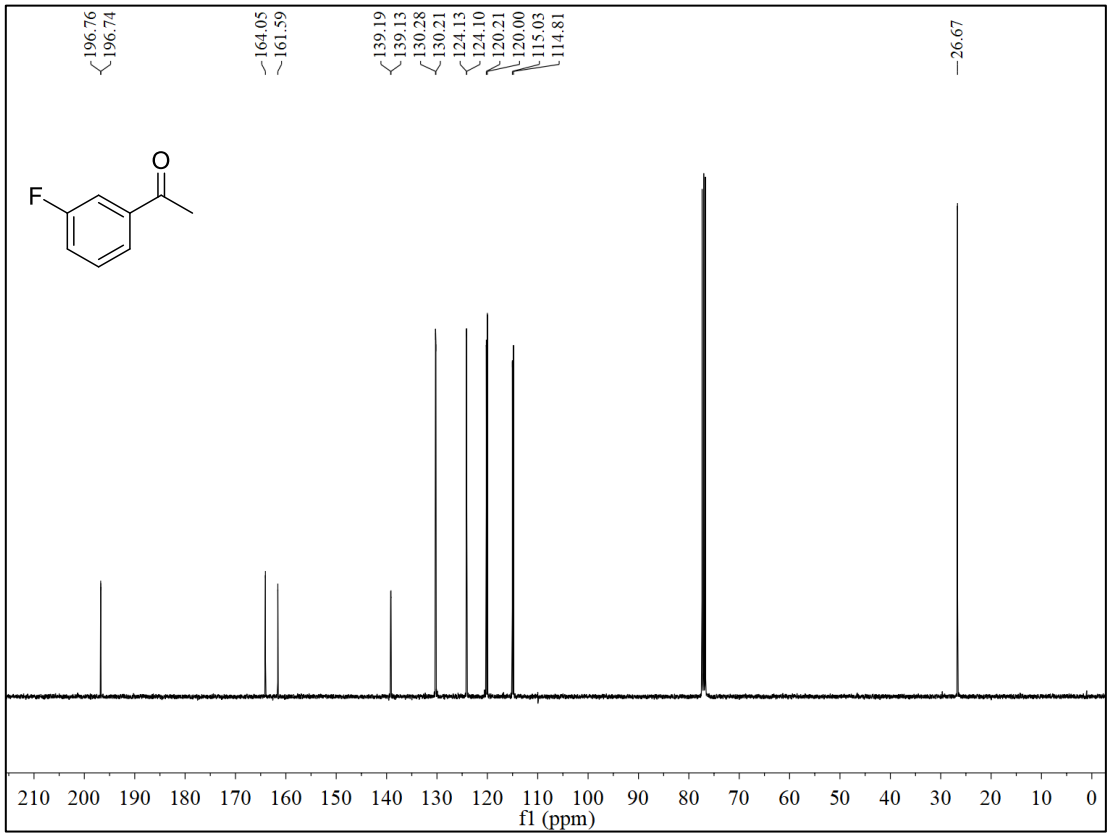

^{19}F-NMR (376 MHz, $CDCl_3$) of **2g** using $PhCF_3$ (δ = –63.72 ppm) as I.S.

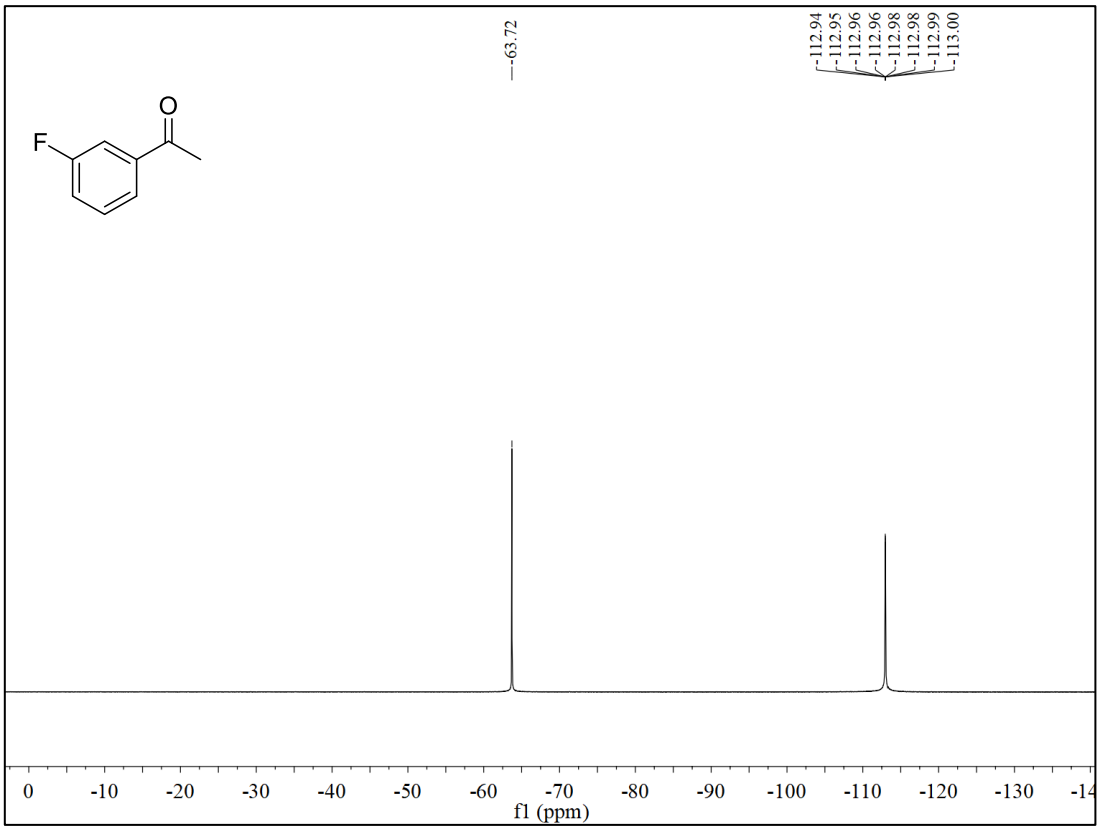

^{1}H-NMR (400 MHz, $CDCl_3$) of **2i**

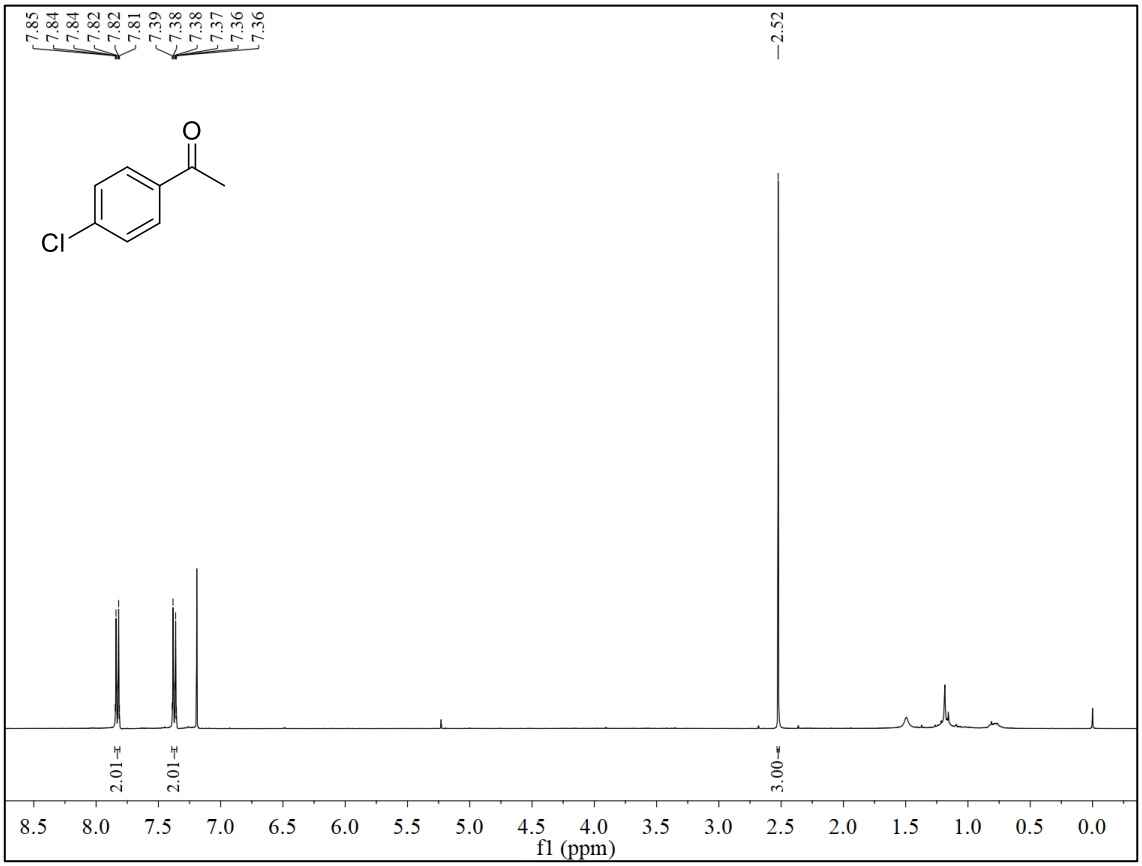

^{13}C-NMR (101 MHz, $CDCl_3$) of **2i**

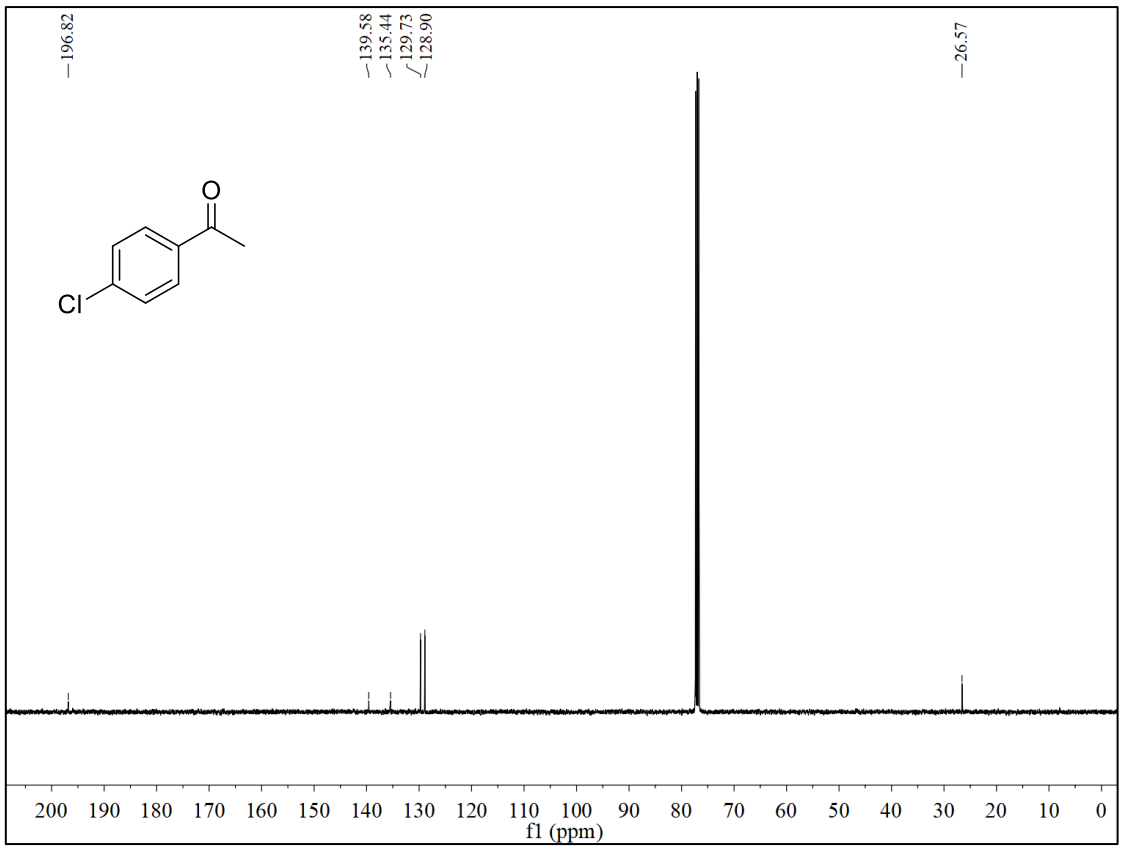

^{1}H-NMR (400 MHz, $CDCl_3$) of **2k**

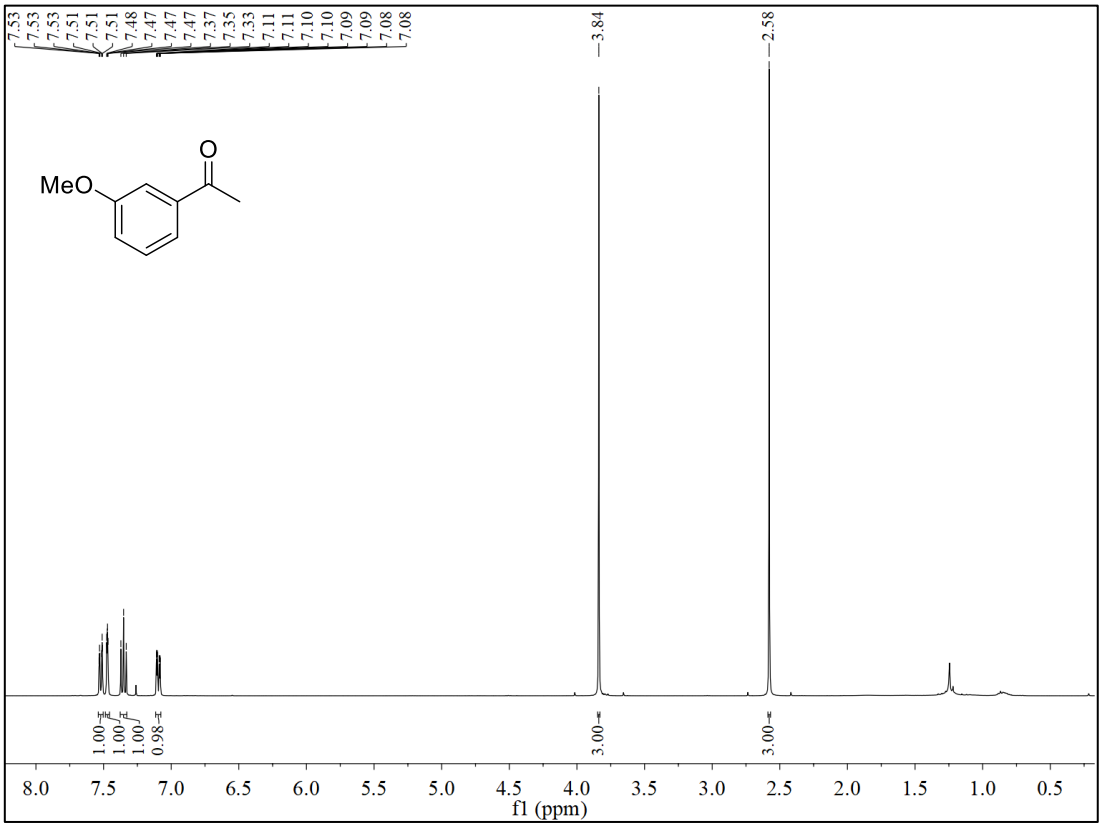

^{13}C-NMR (101 MHz, $CDCl_3$) of **2k**

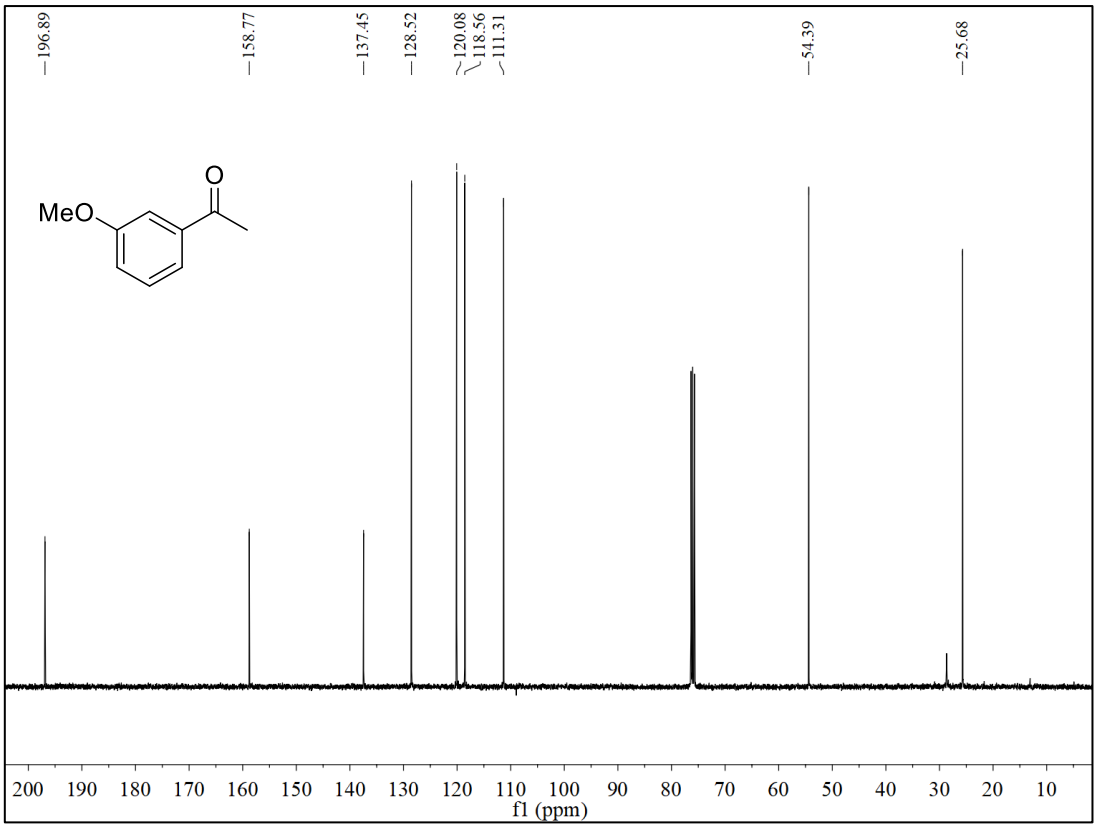

^{1}H-NMR (400 MHz, $CDCl_3$) of **2l**

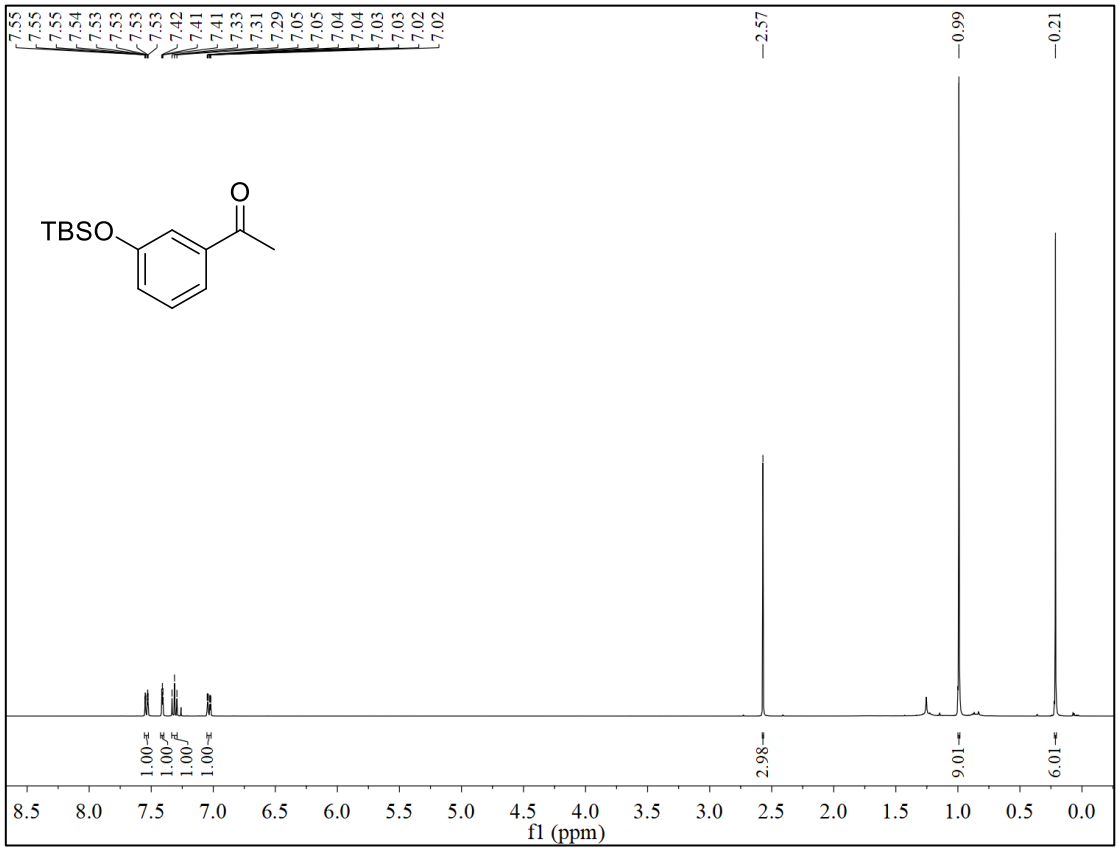

^{13}C-NMR (101 MHz, $CDCl_3$) of **2l**

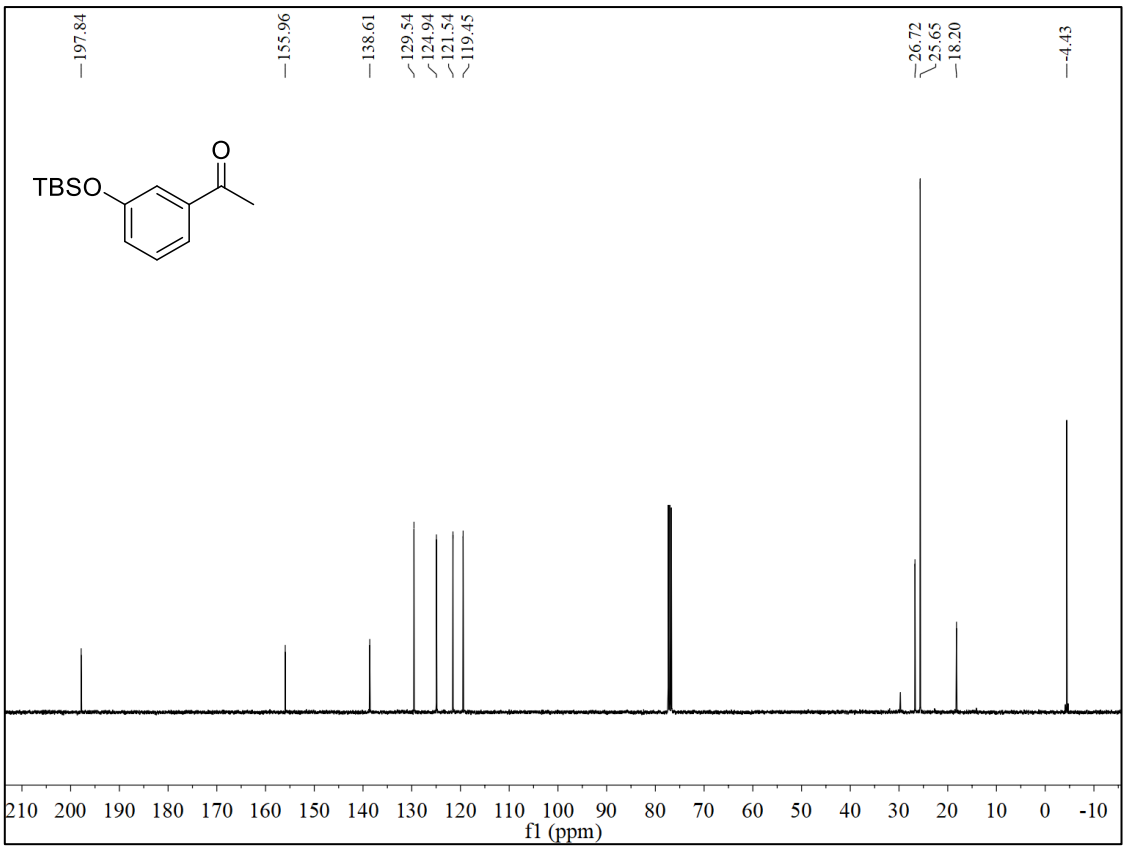

^{1}H-NMR (400 MHz, $CDCl_3$) of **2n**

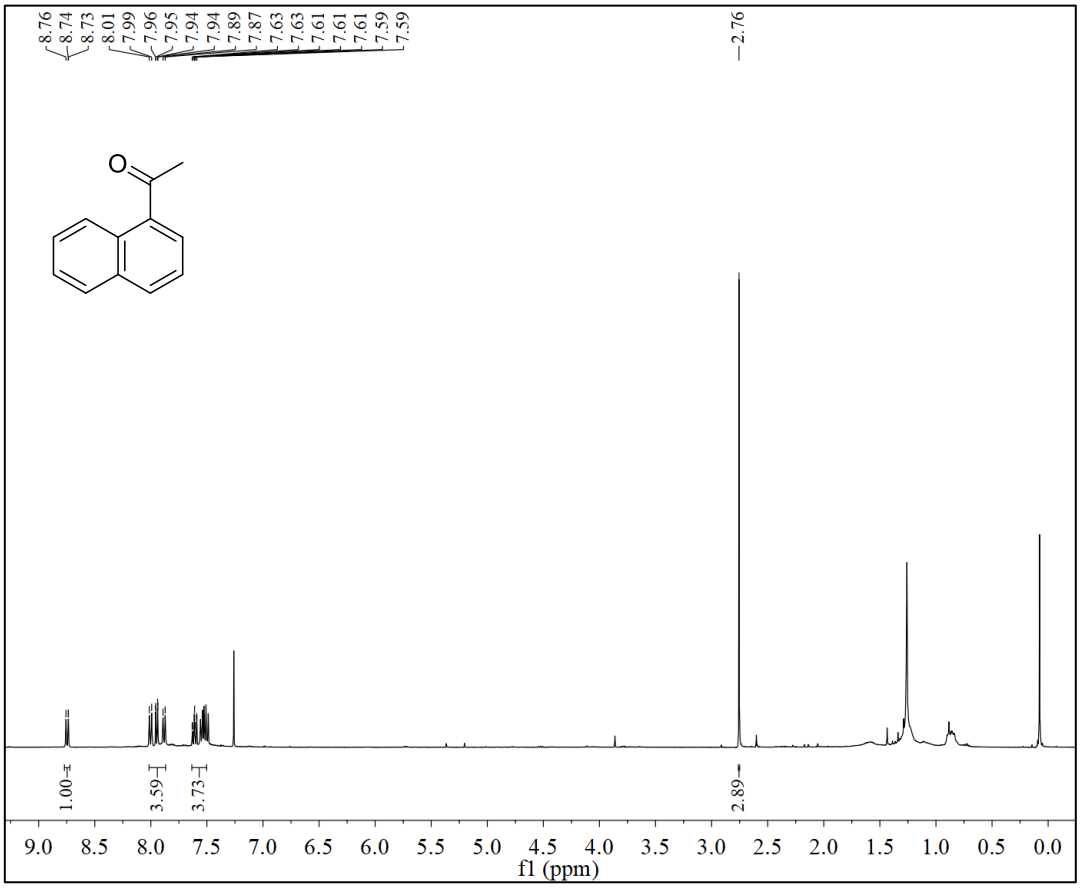

^{13}C-NMR (101 MHz, $CDCl_3$) of **2n**

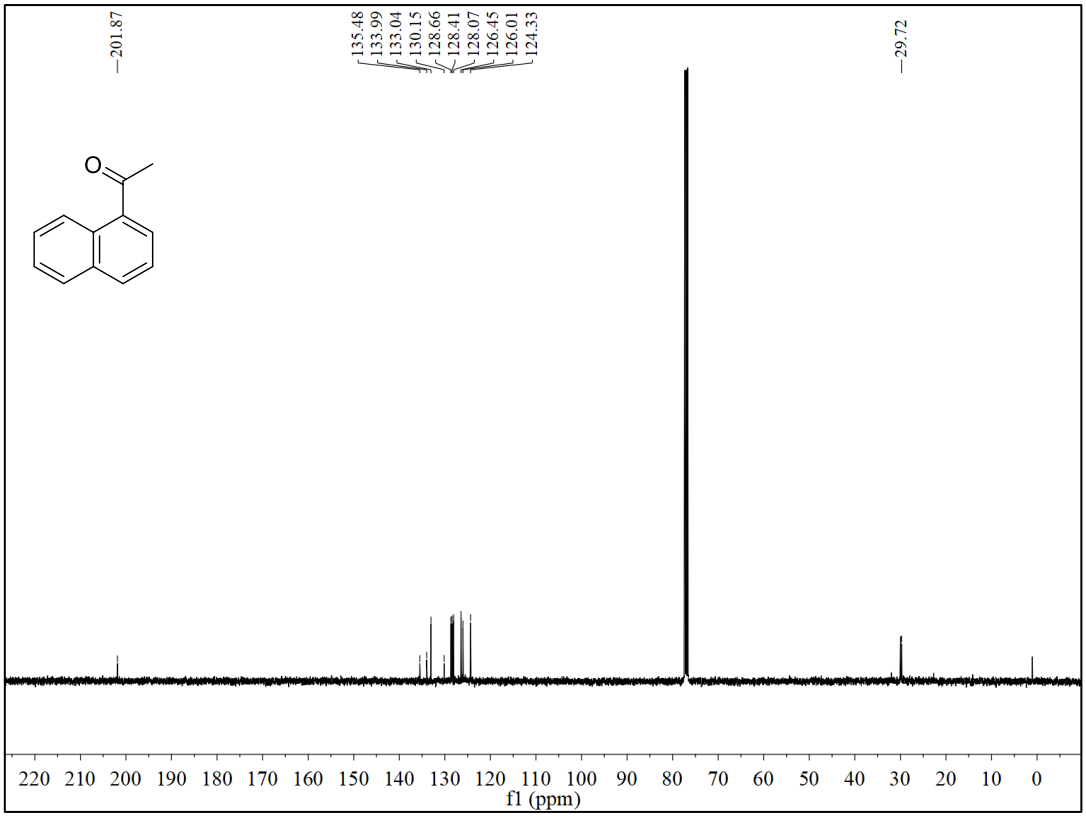

^{1}H-NMR (400 MHz, $CDCl_3$) of **2o**

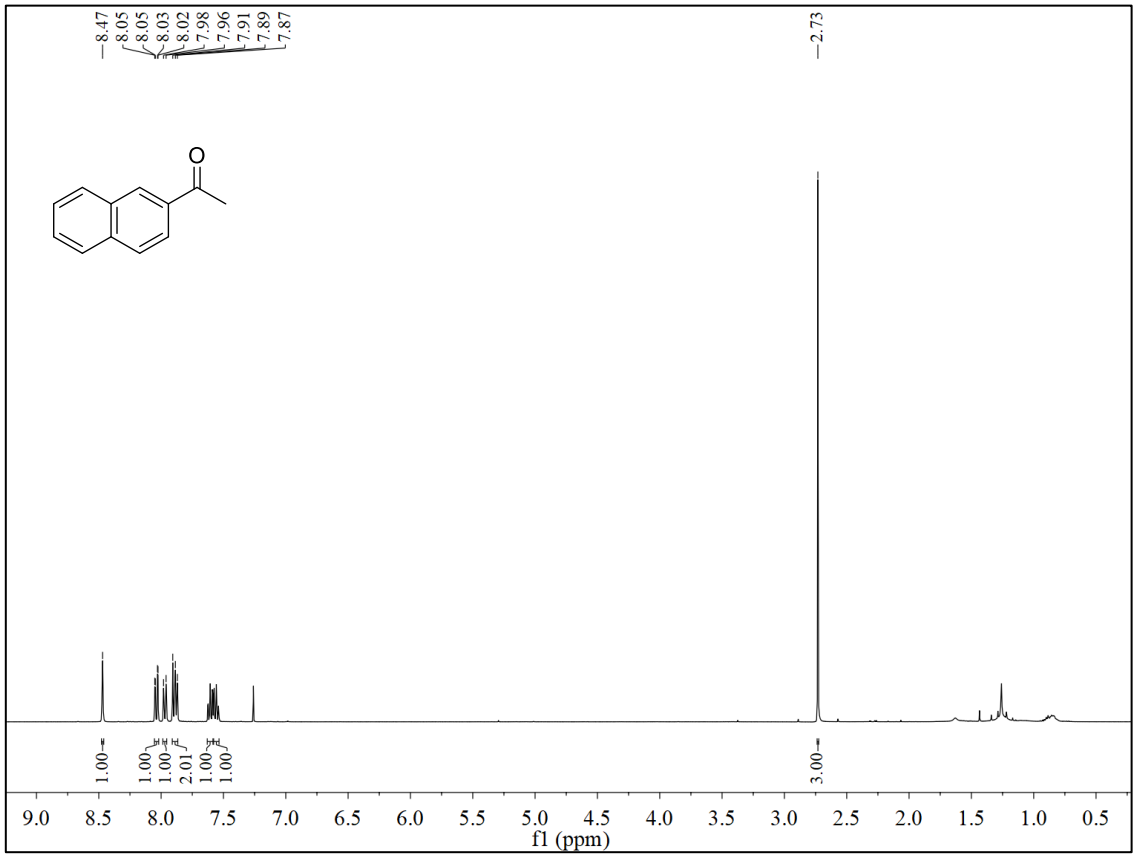

^{13}C-NMR (101 MHz, $CDCl_3$) of **2o**

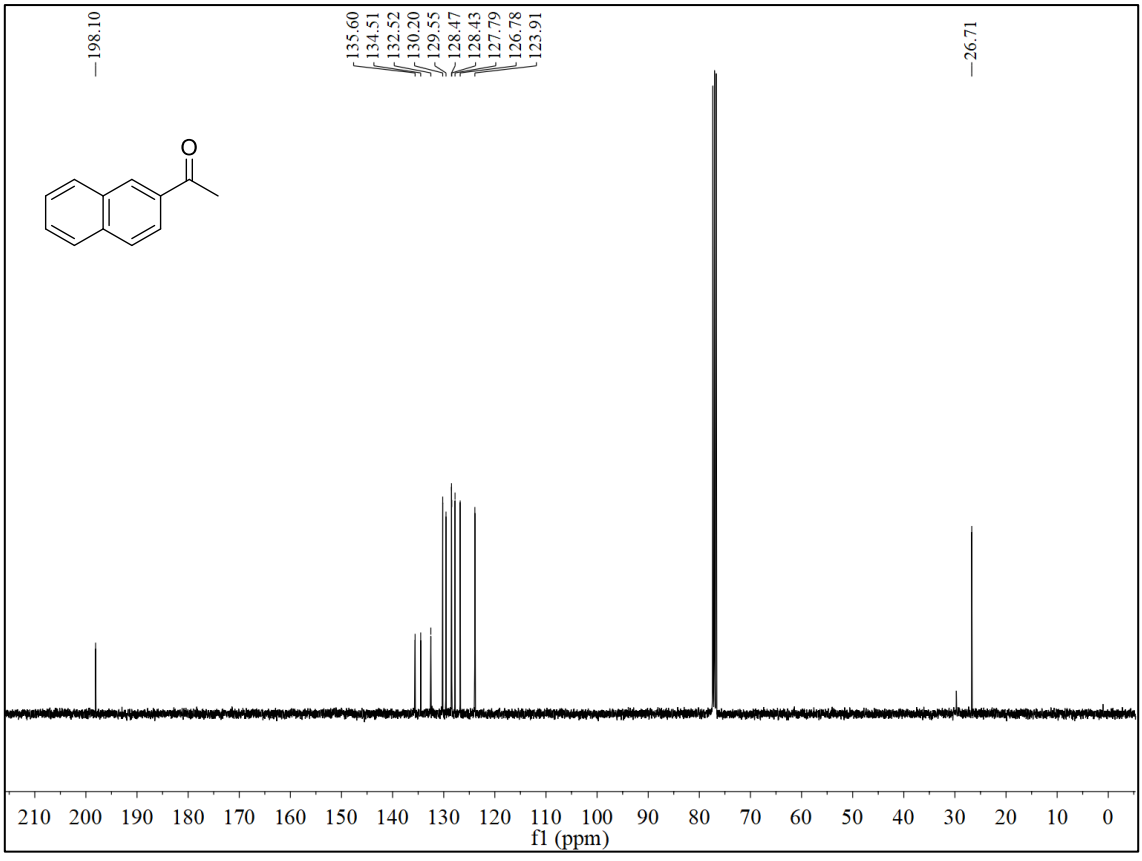

NMR Spectra of Starting Materials

^{1}H-NMR (400 MHz, $CDCl_3$) of **1b**

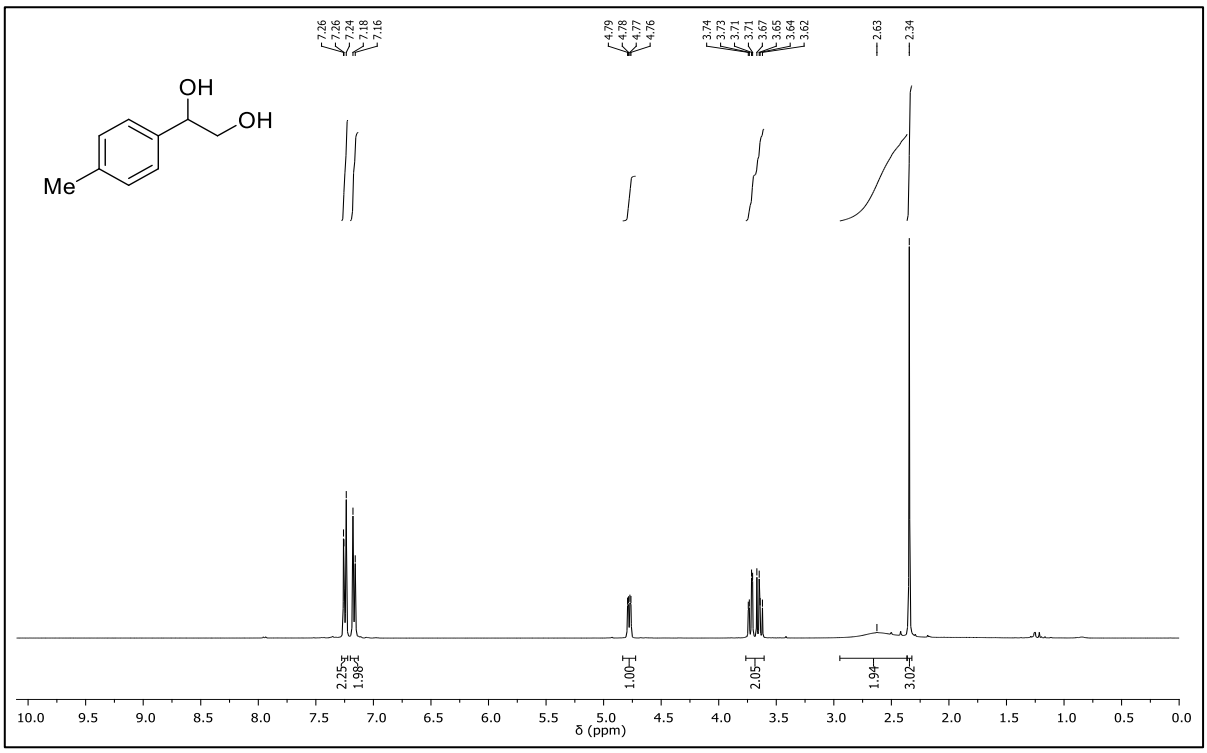

^{13}C-NMR (101 MHz, $CDCl_3$) of **1b**

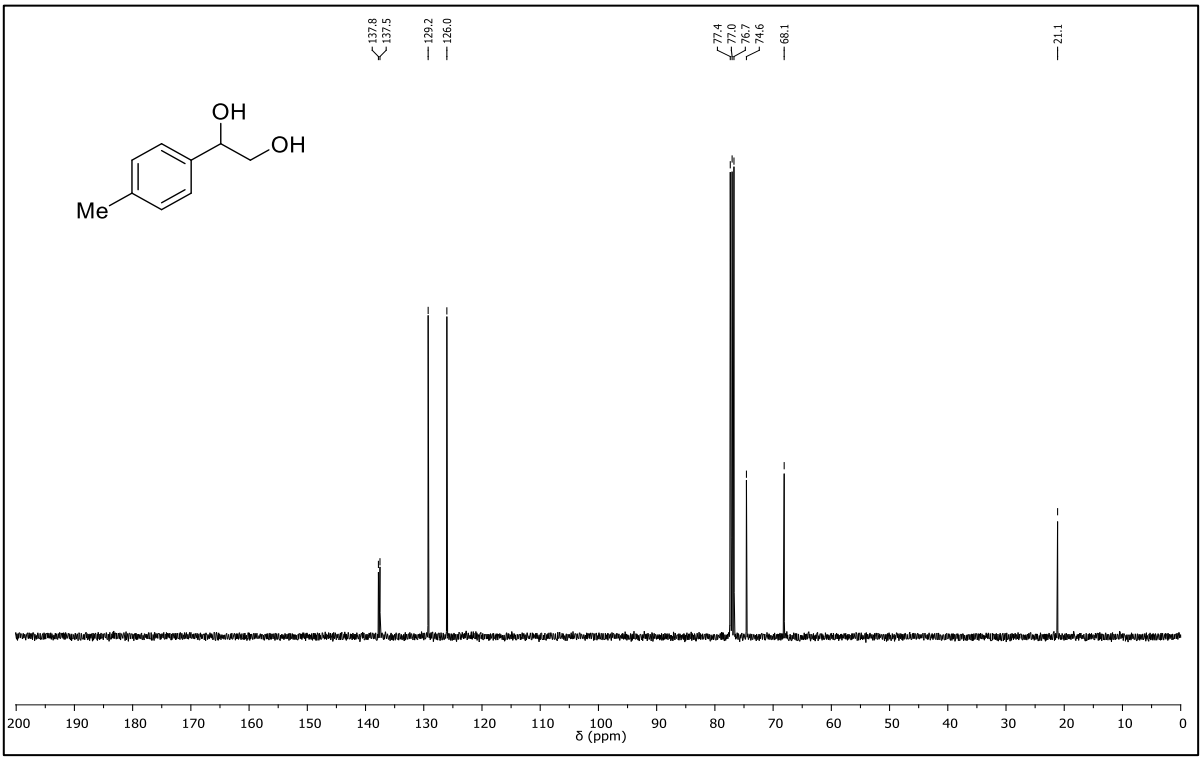

^{1}H-NMR (400 MHz, $CDCl_3$) of **1c**

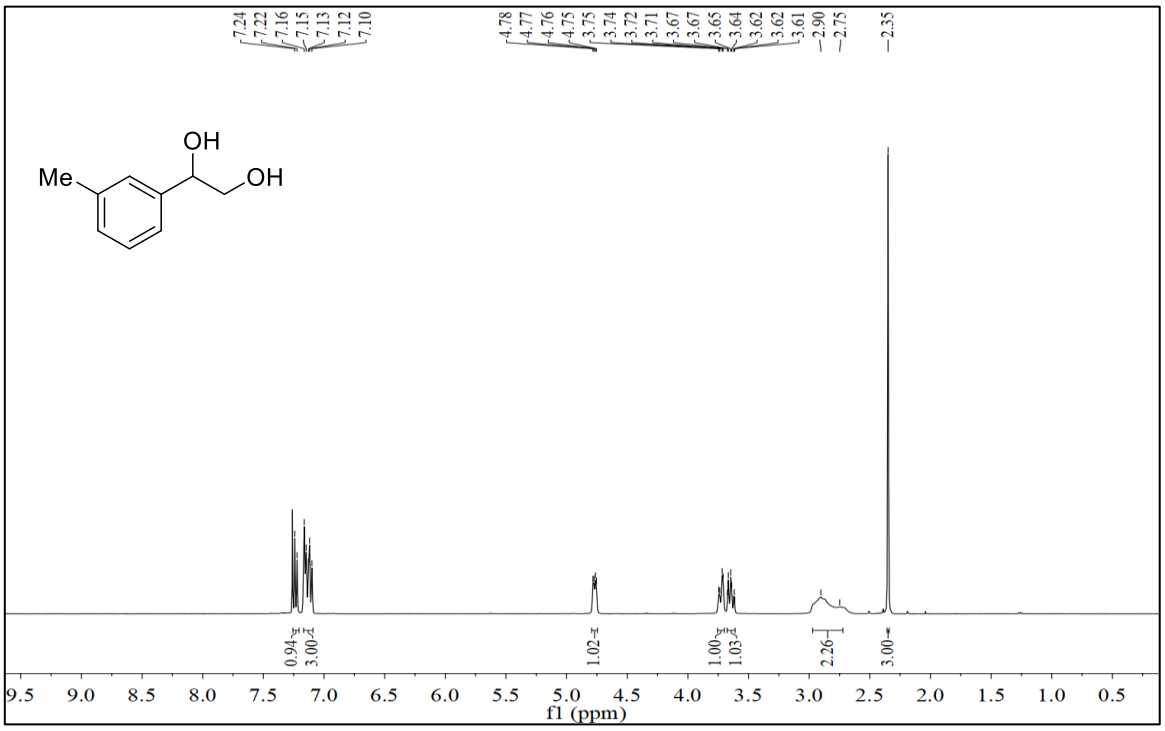

^{13}C-NMR (101 MHz, $CDCl_3$) of **1c**

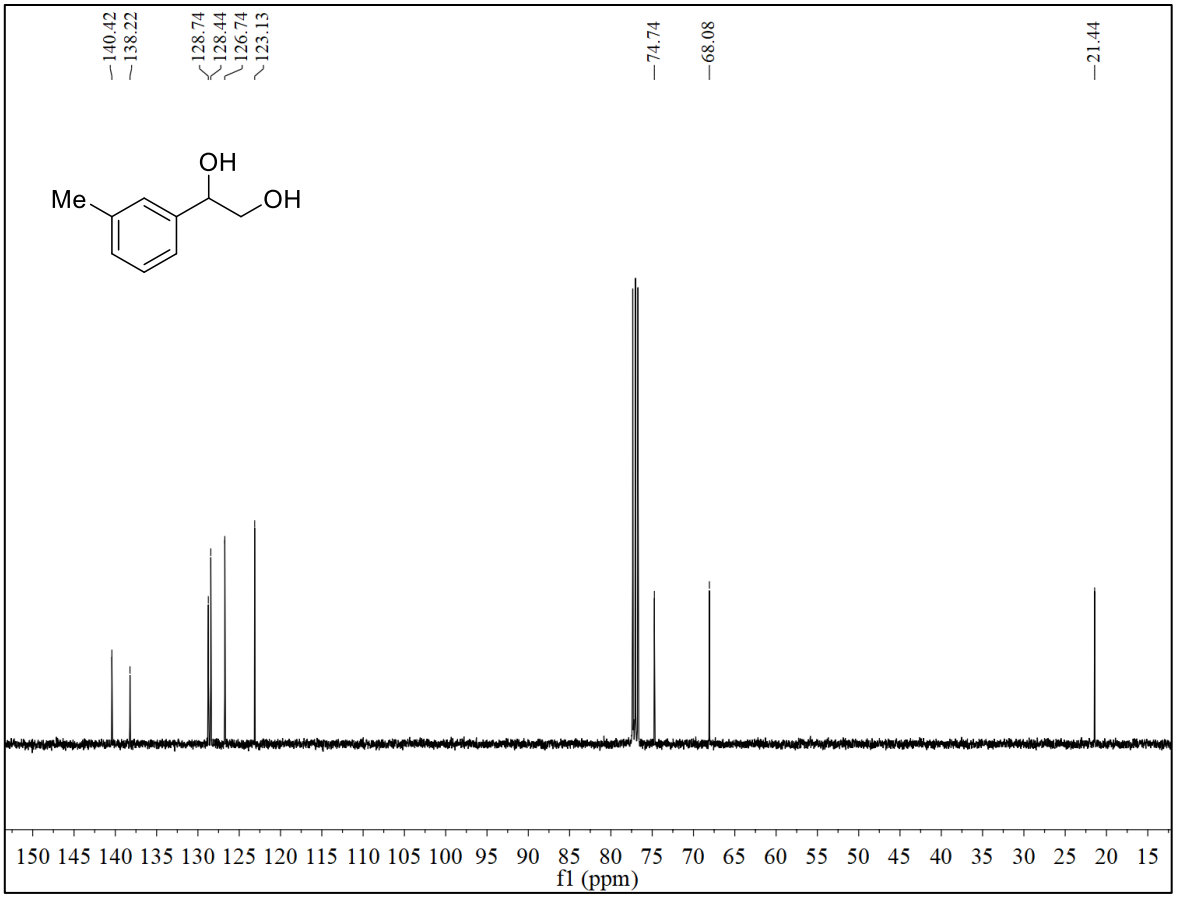

^{1}H-NMR (400 MHz, $CDCl_3$) of **1d**

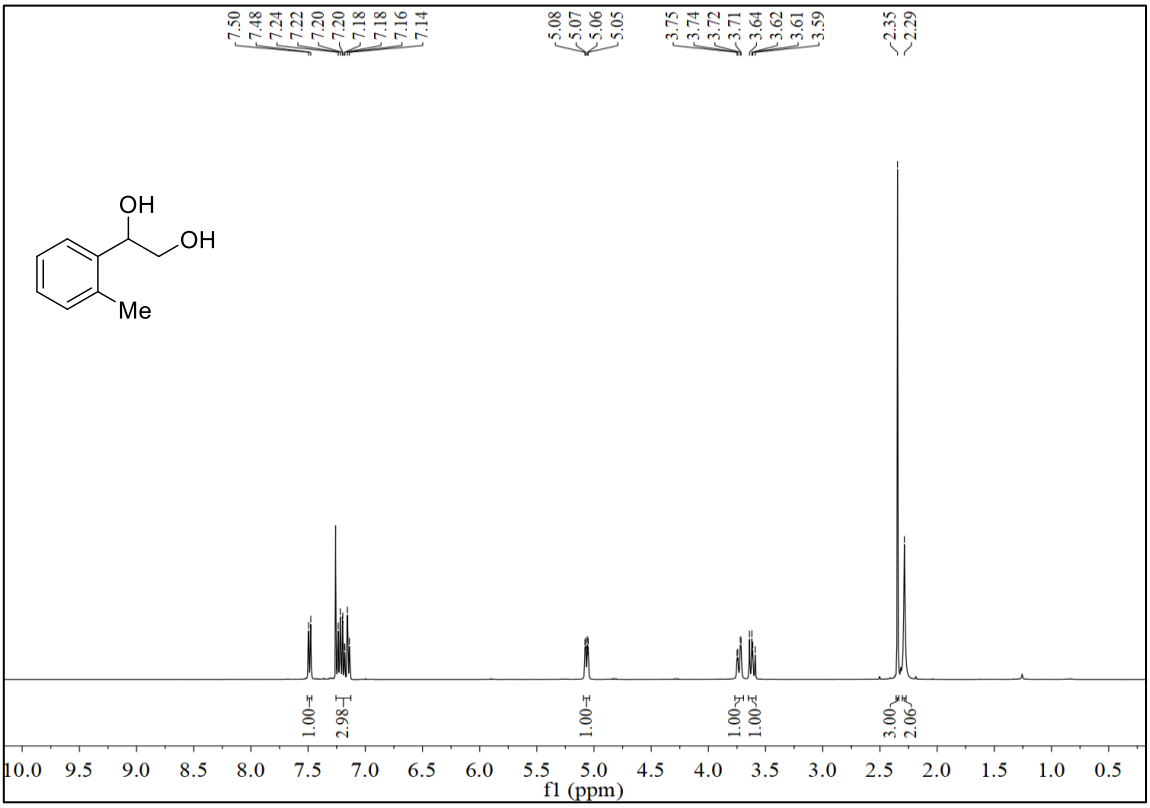

^{13}C-NMR (101 MHz, $CDCl_3$) of **1d**

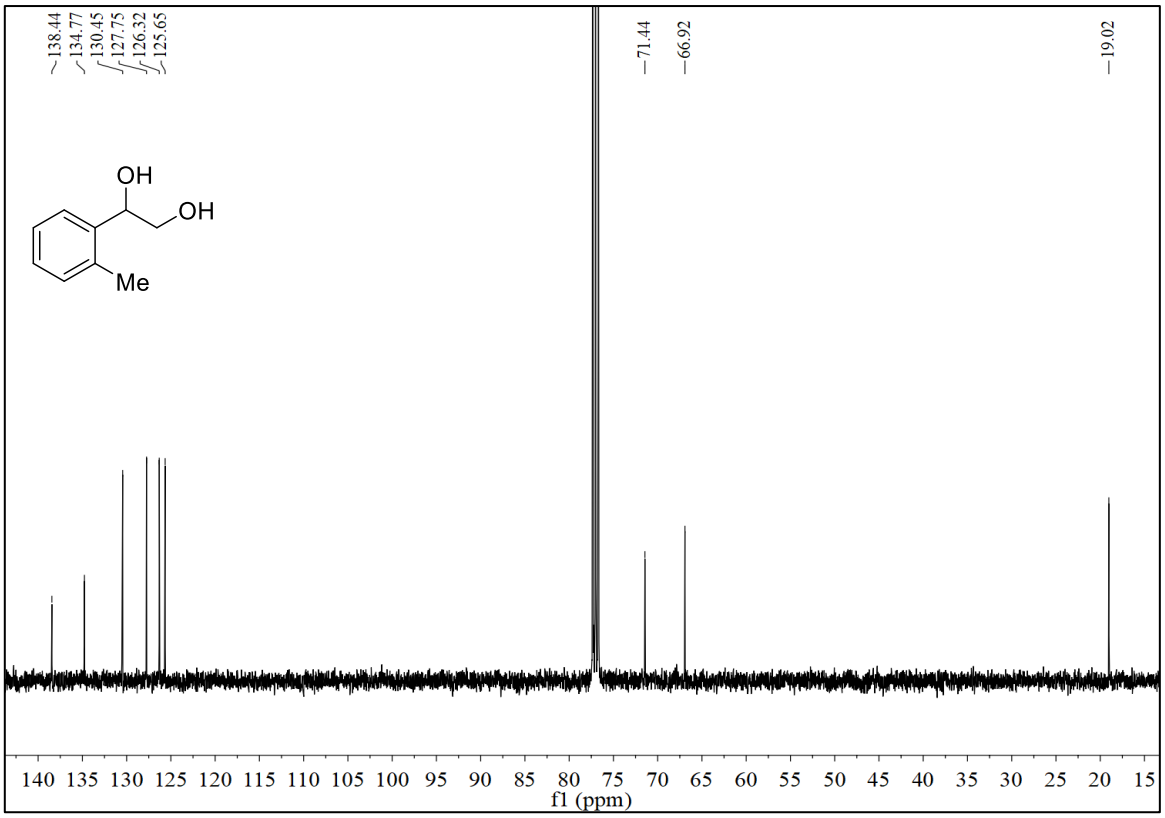

^{1}H-NMR (400 MHz, $CDCl_3$) of **1e**

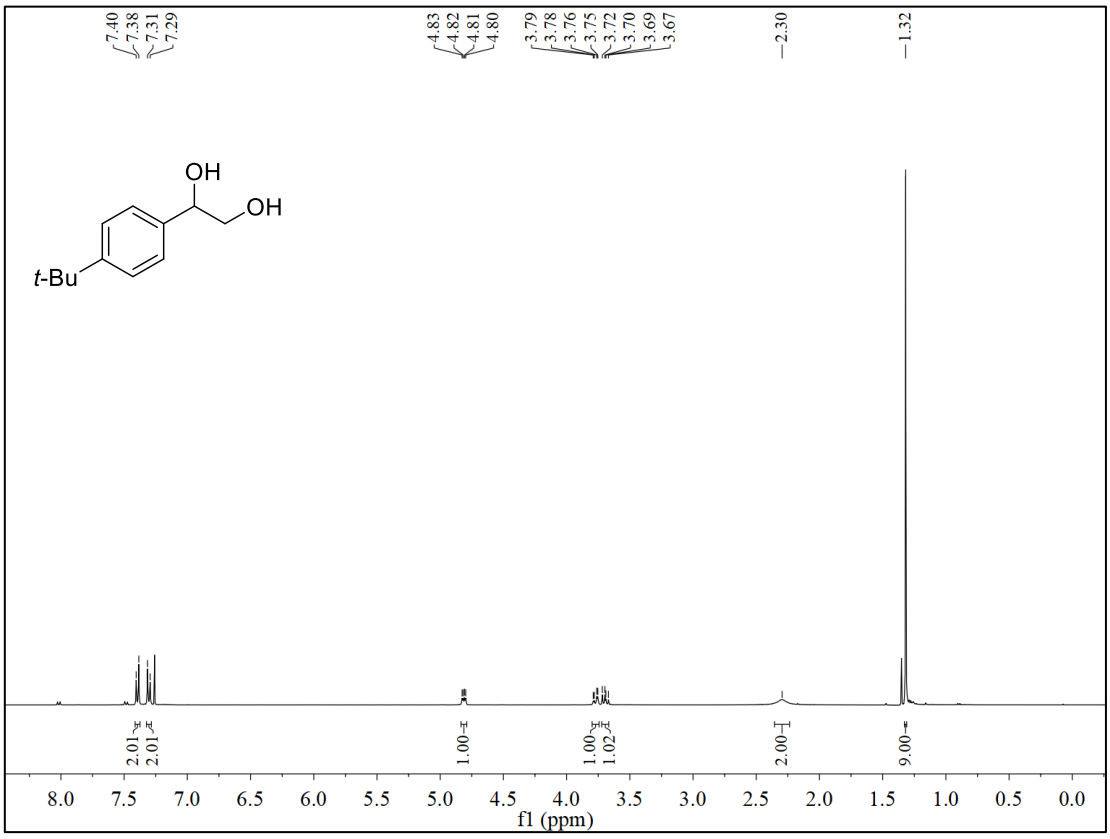

^{13}C-NMR (101 MHz, $CDCl_3$) of **1e**

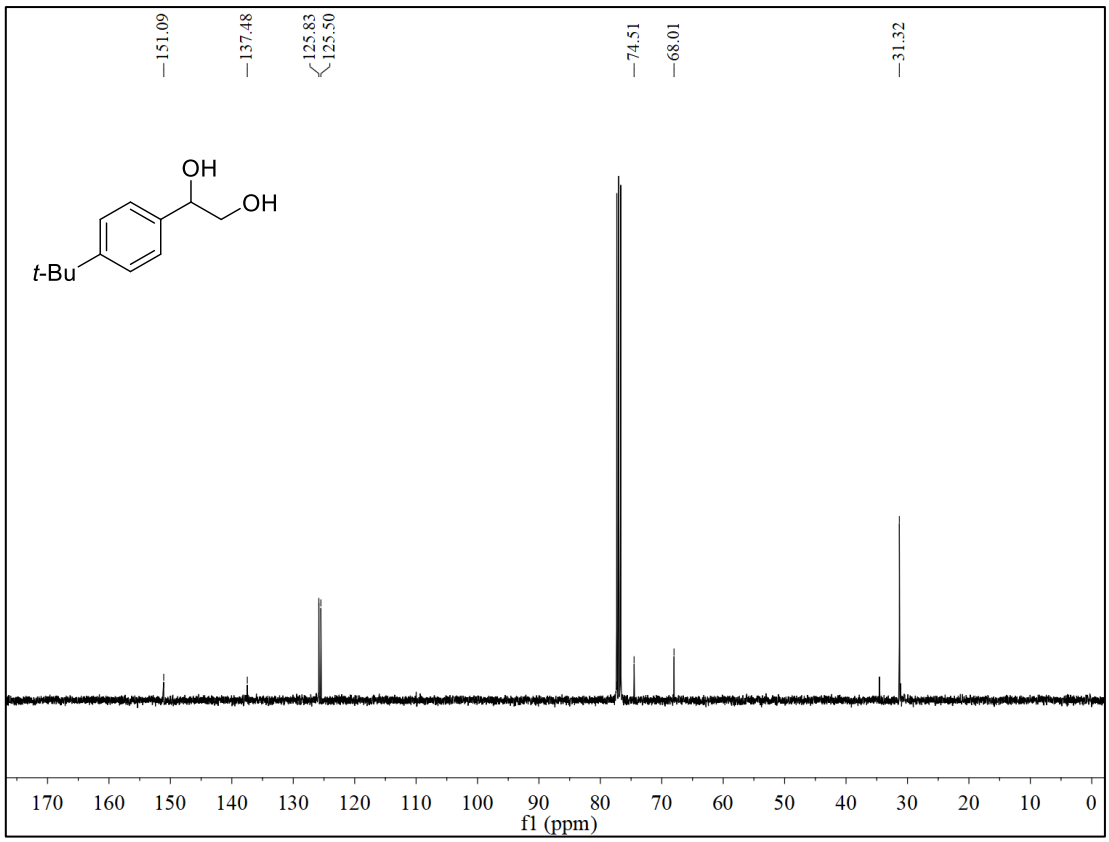

^{1}H-NMR (400 MHz, $CDCl_3$) of **1f**

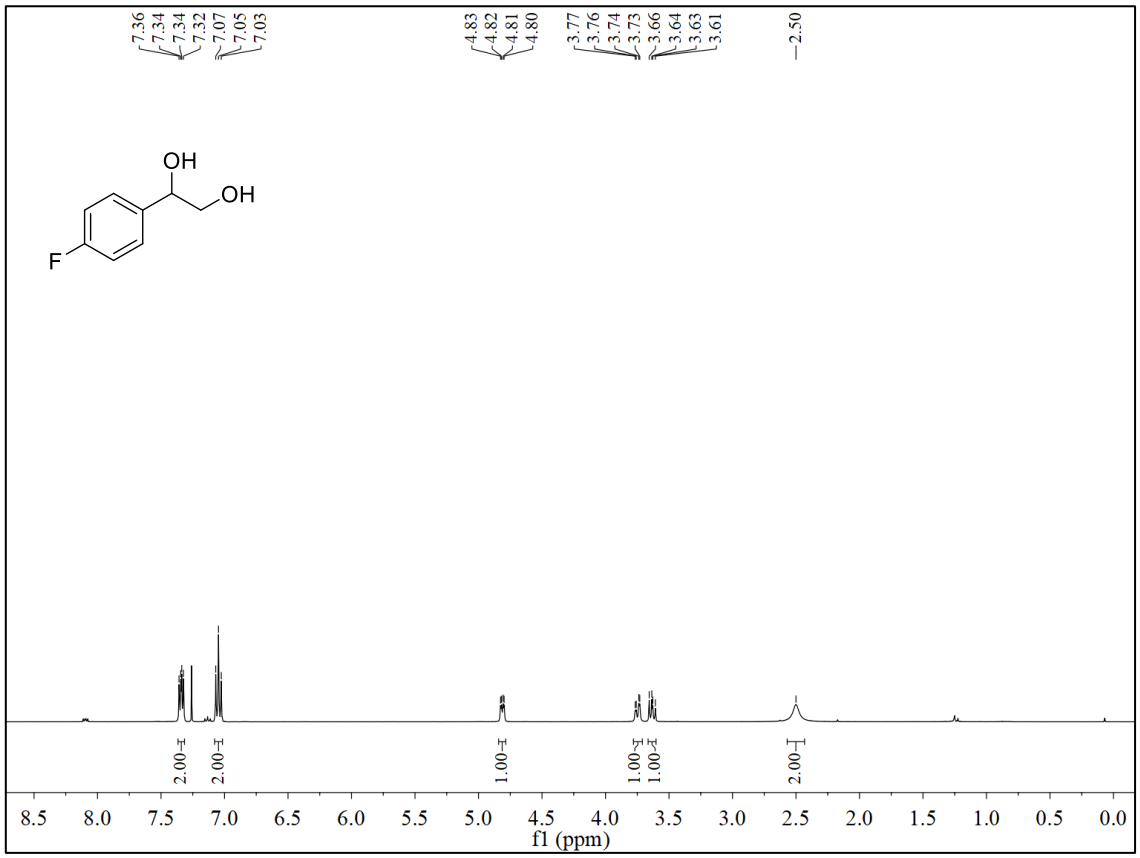

^{13}C-NMR (101 MHz, $CDCl_3$) of **1f**

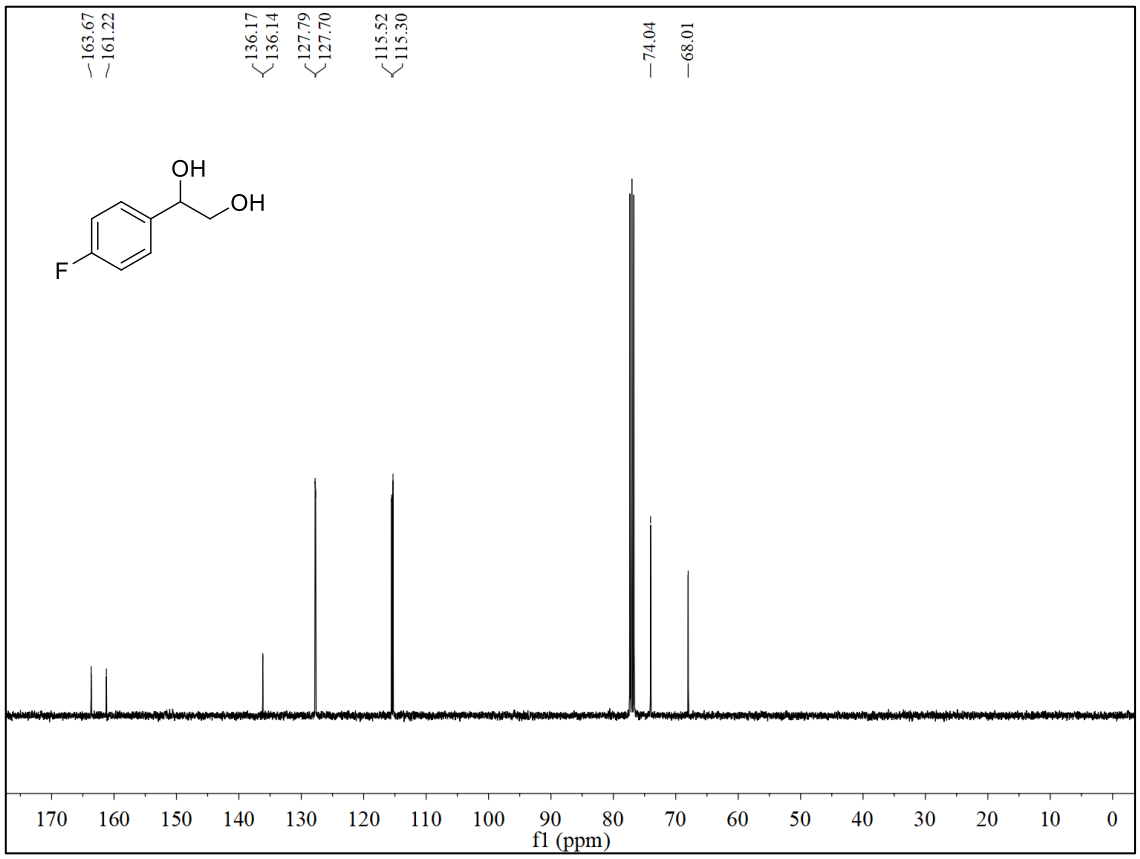

^{19}F-NMR (376 MHz, $CDCl_3$) of **1f** using $PhCF_3$ (δ = –63.72 ppm) as I.S.

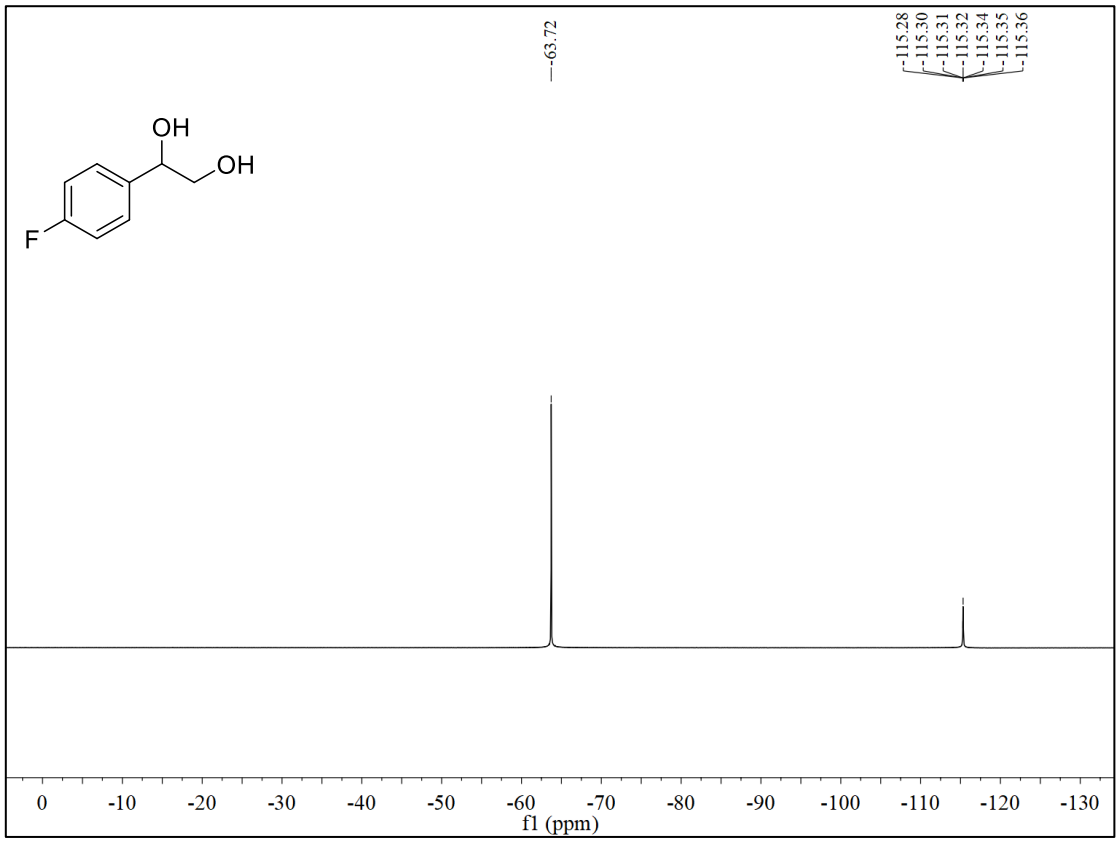

^{1}H-NMR (400 MHz, $CDCl_3$) of **1g**

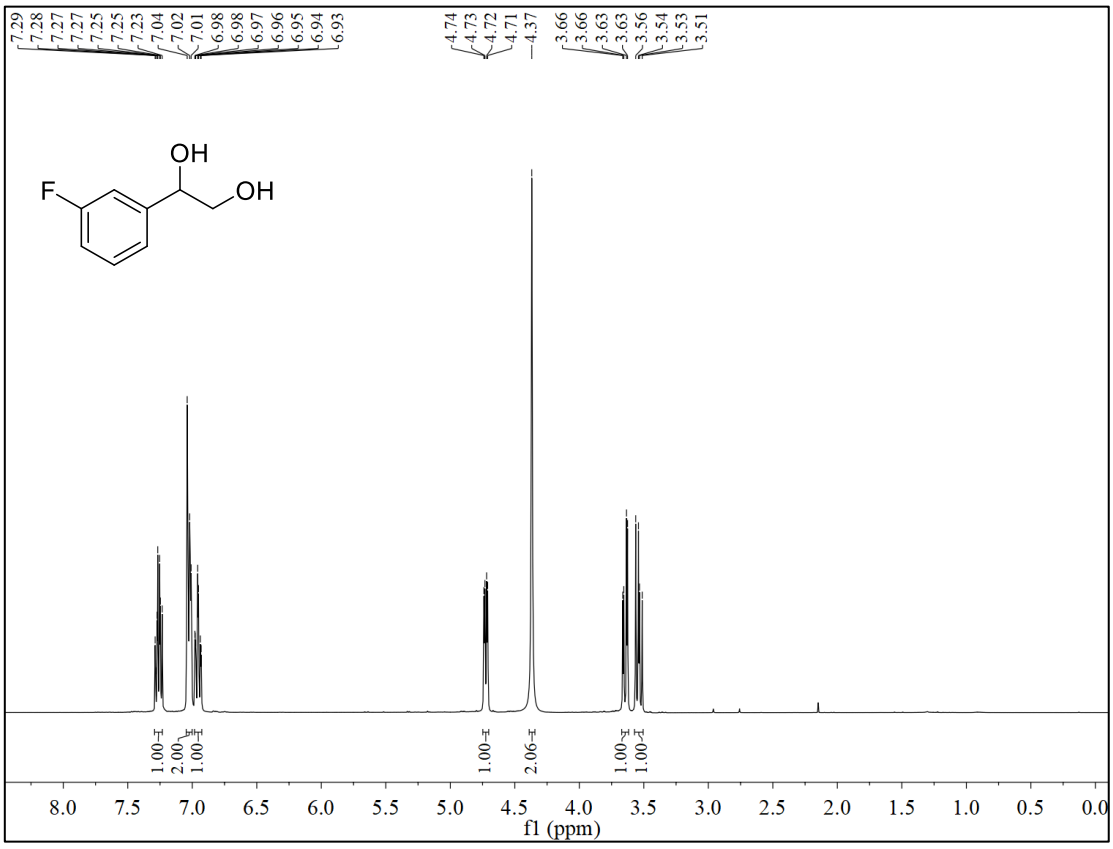

^{13}C-NMR (101 MHz, $CDCl_3$) of **1g**

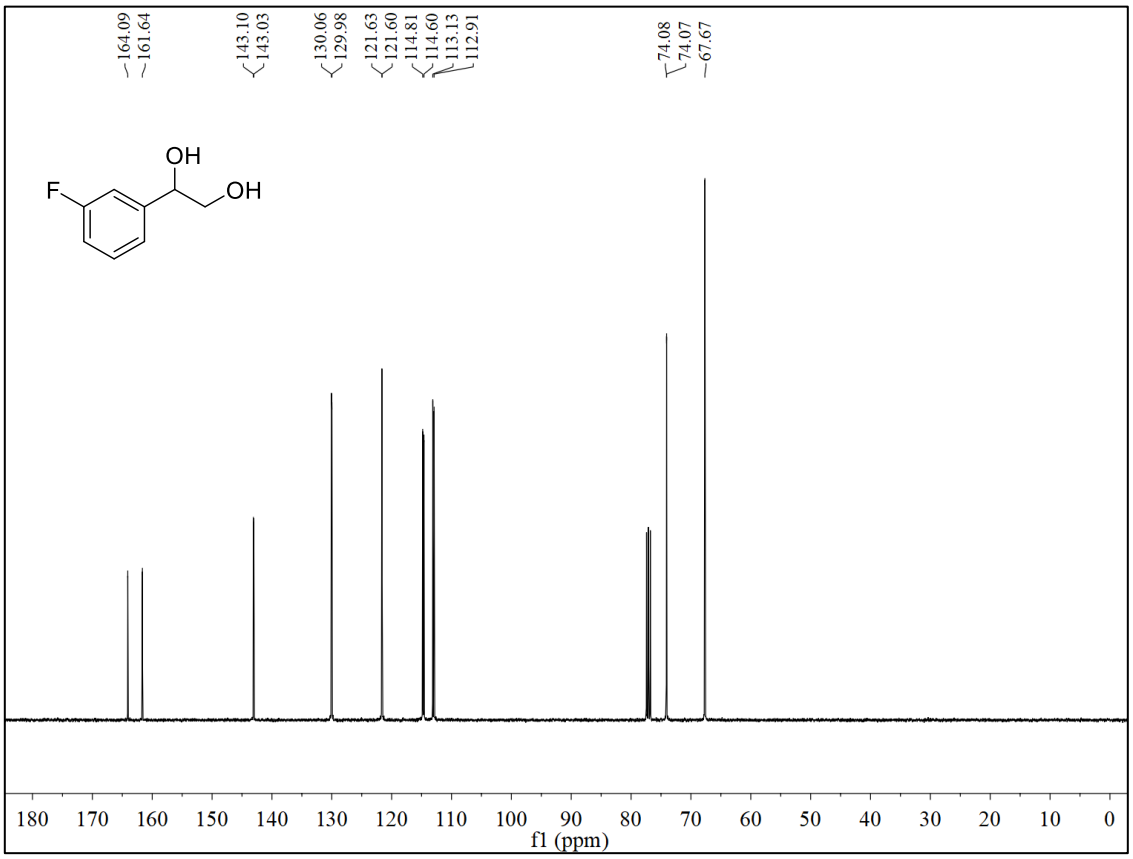

^{19}F-NMR (376 MHz, $CDCl_3$) of **1g** using $PhCF_3$ (δ = –63.72 ppm) as I.S.

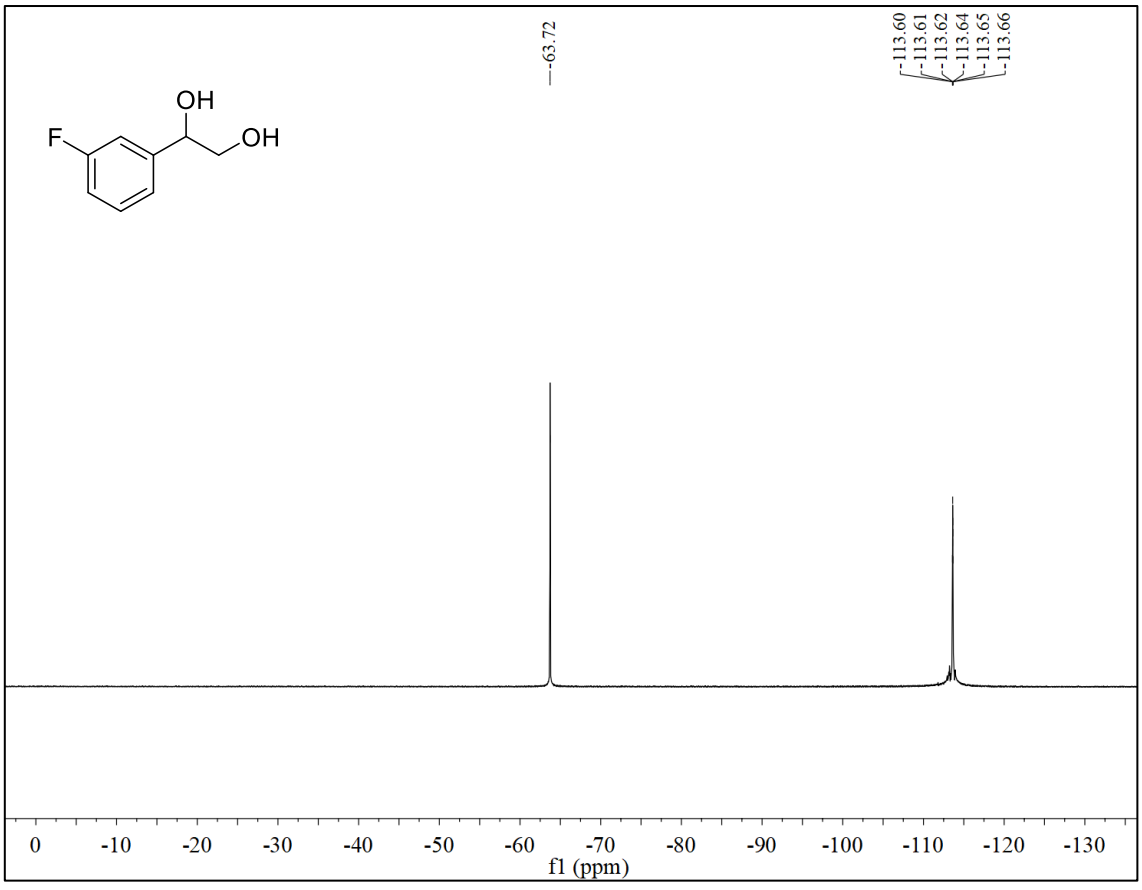

^{1}H-NMR (400 MHz, DMSO-d_6) of **1h**

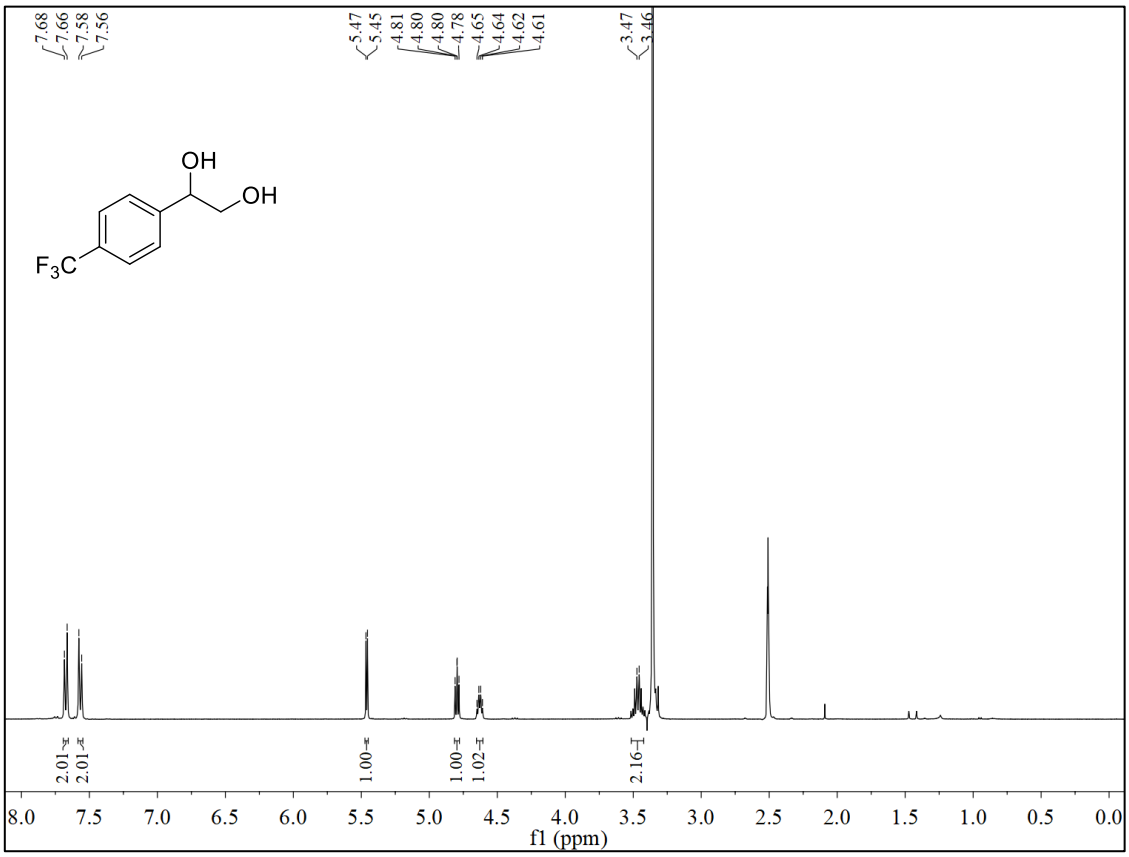

^{13}C-NMR (101 MHz, DMSO-d_6) of **1h**

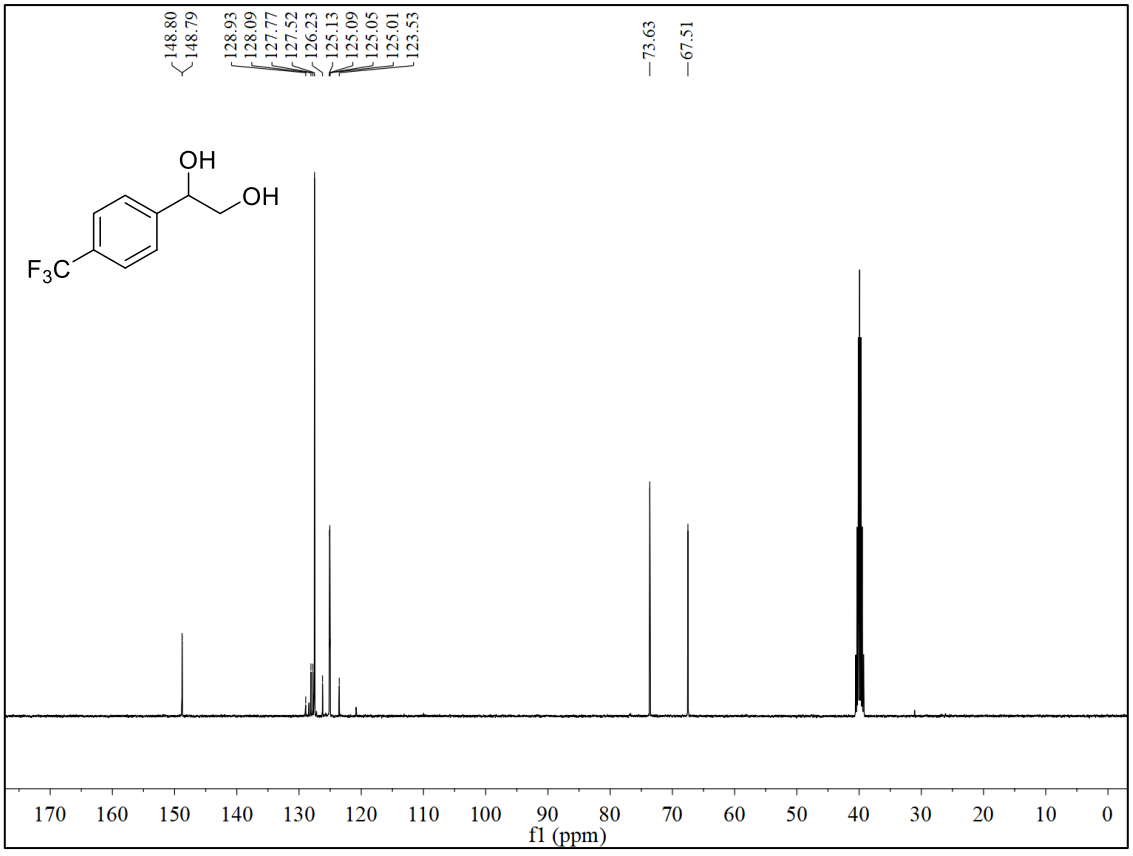

^{19}F-NMR (376 MHz, DMSO-d_6) of **1h** using $PhCF_3$ (δ = –63.72 ppm) as I.S.

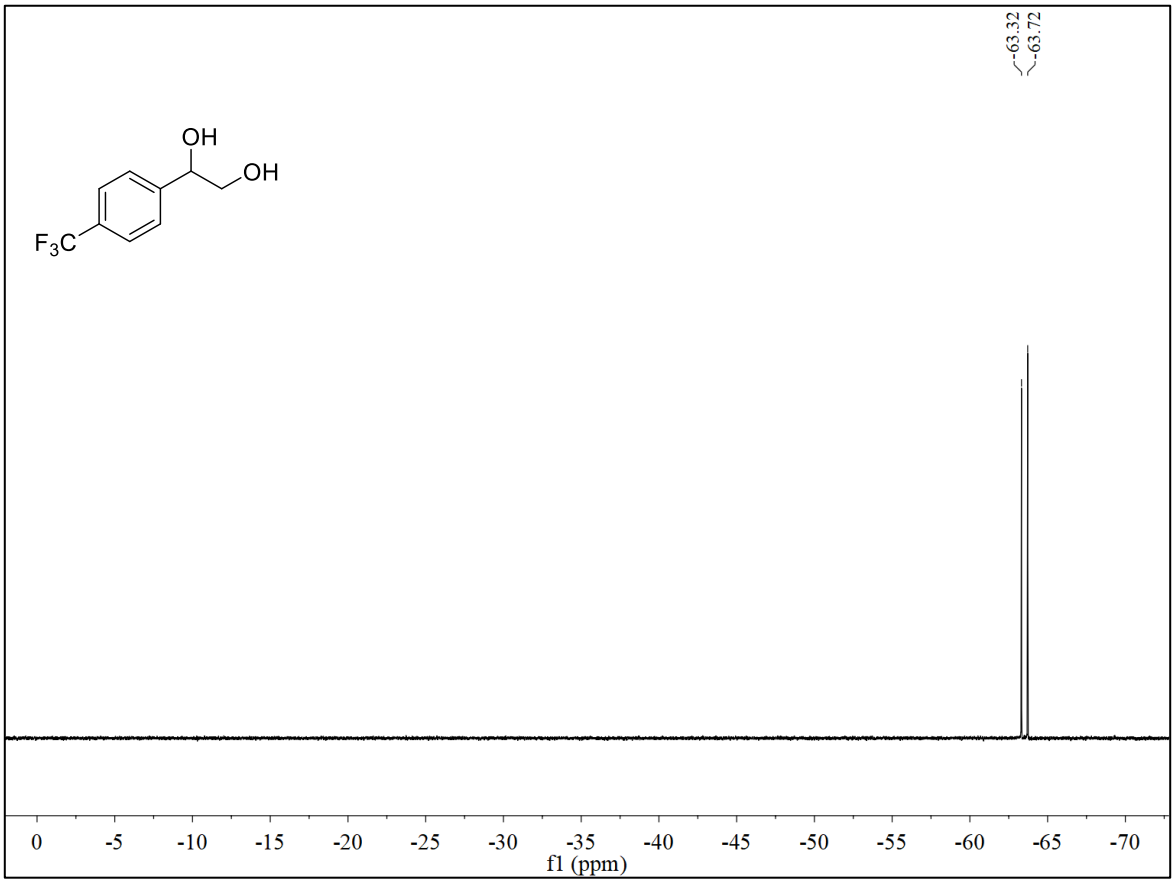

^{1}H-NMR (400 MHz, $CDCl_3$) of **1i**

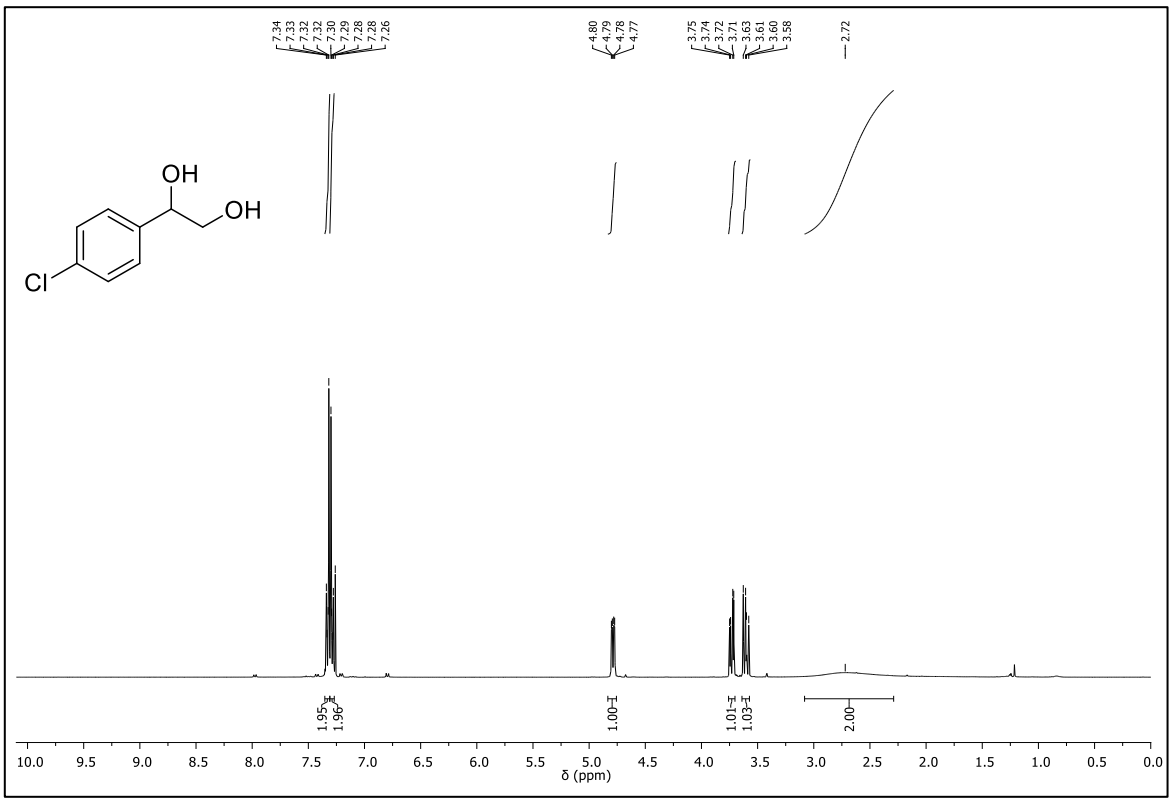

^{13}C-NMR (101 MHz, $CDCl_3$) of **1i**

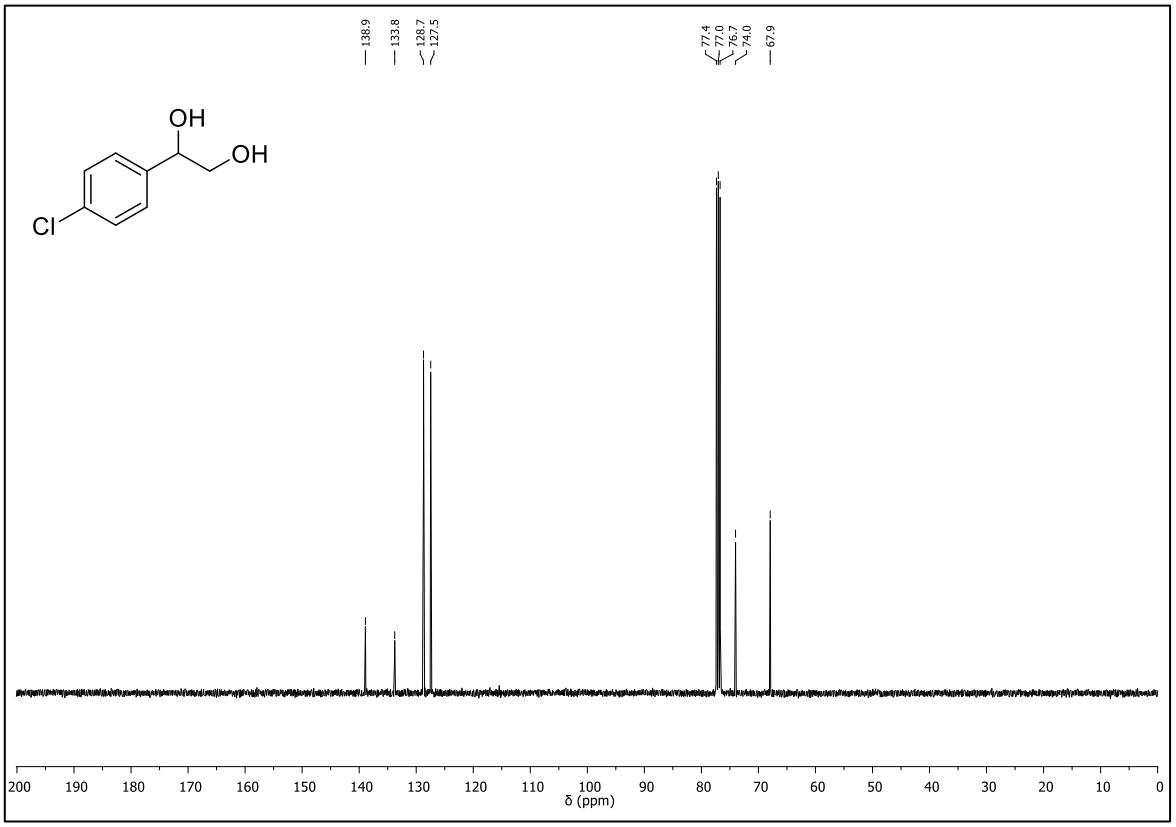

^{1}H-NMR (400 MHz, DMSO-d_6) of **1j**

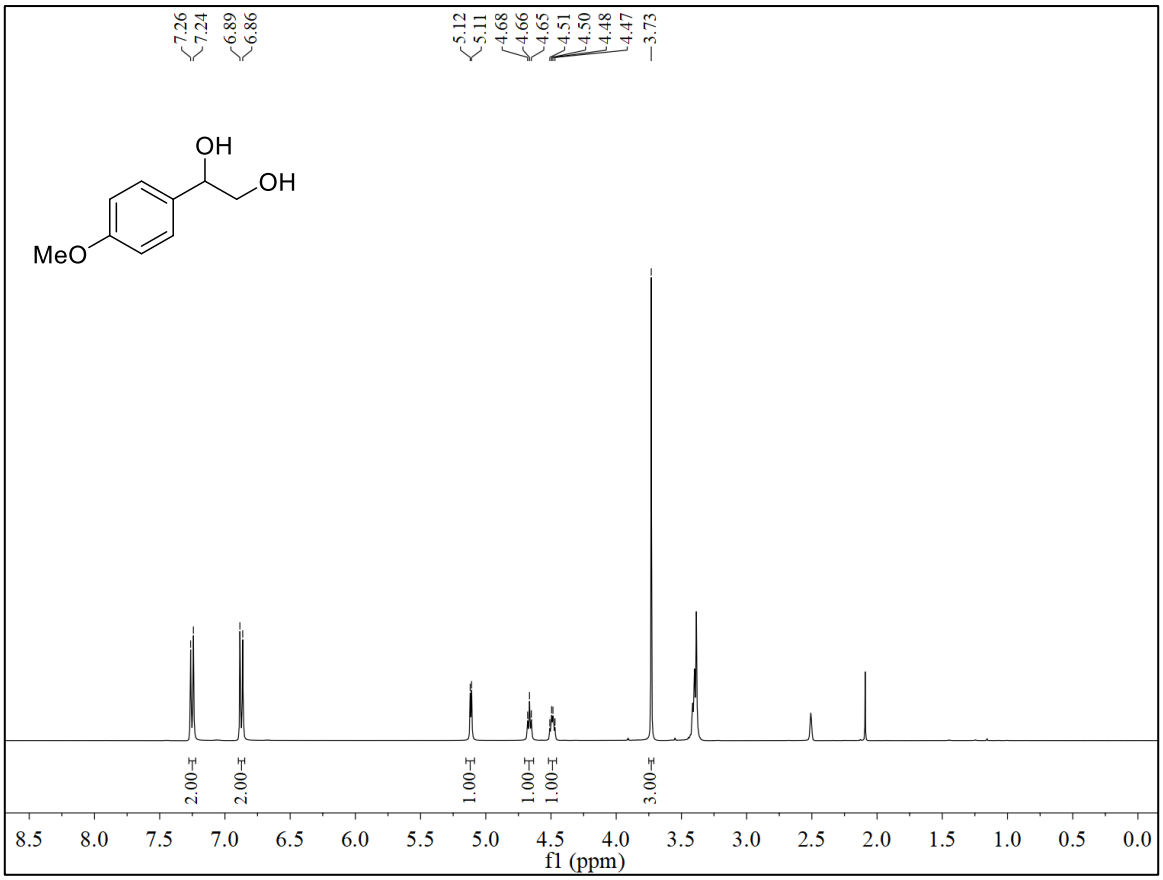

^{13}C-NMR (101 MHz, DMSO-d_6) of **1j**

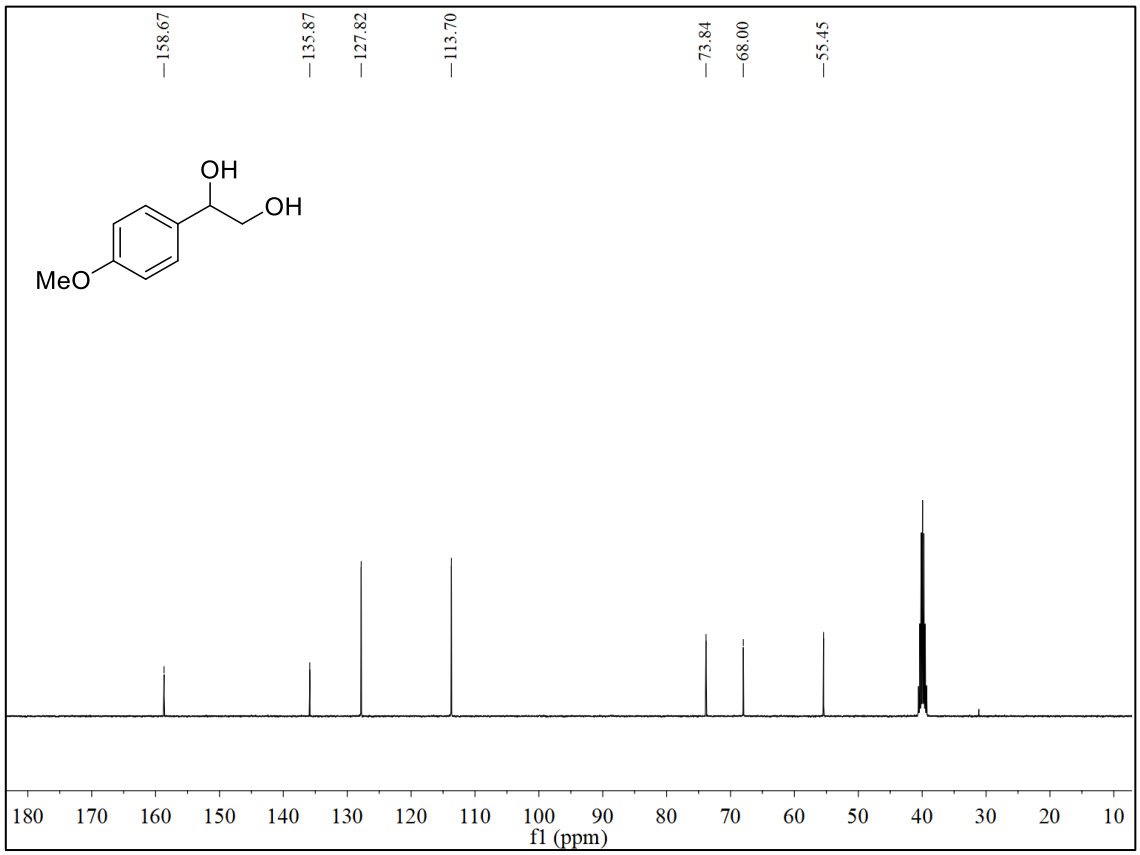

^{1}H-NMR (400 MHz, $CDCl_3$) of **1k**

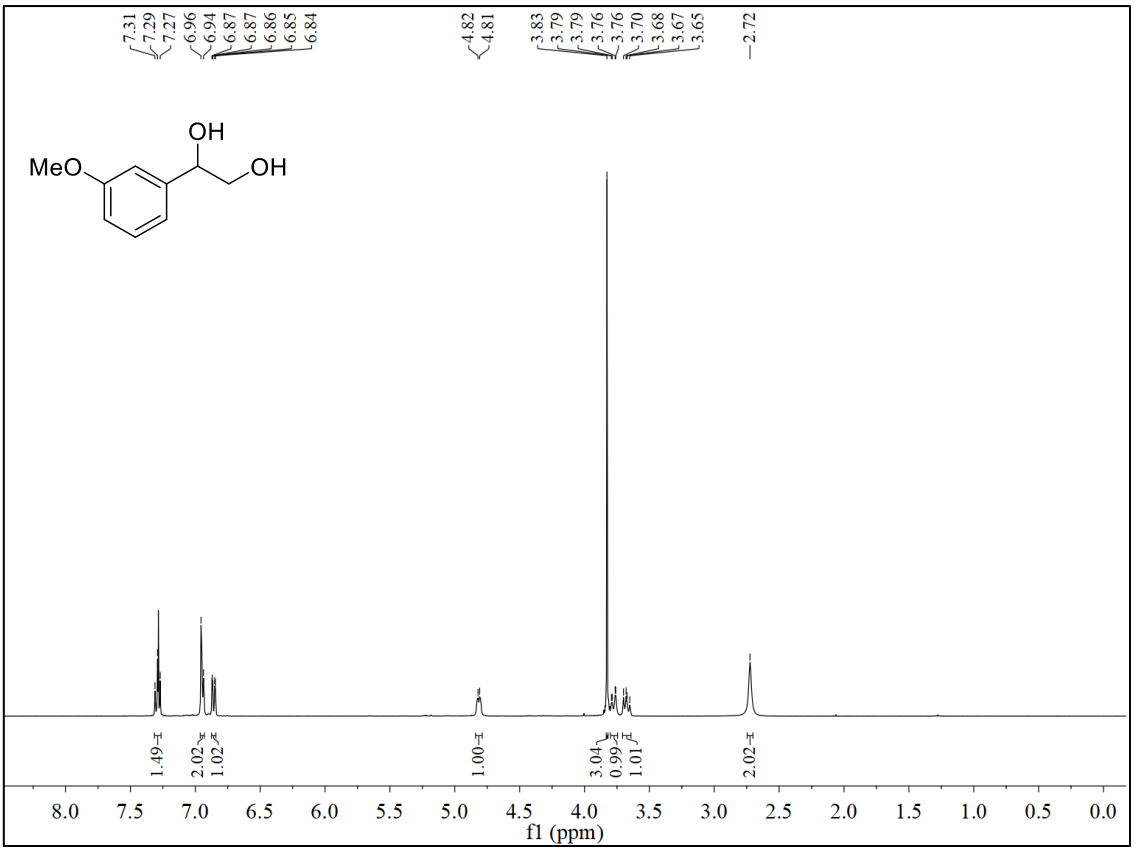

^{13}C-NMR (101 MHz, $CDCl_3$) of **1k**

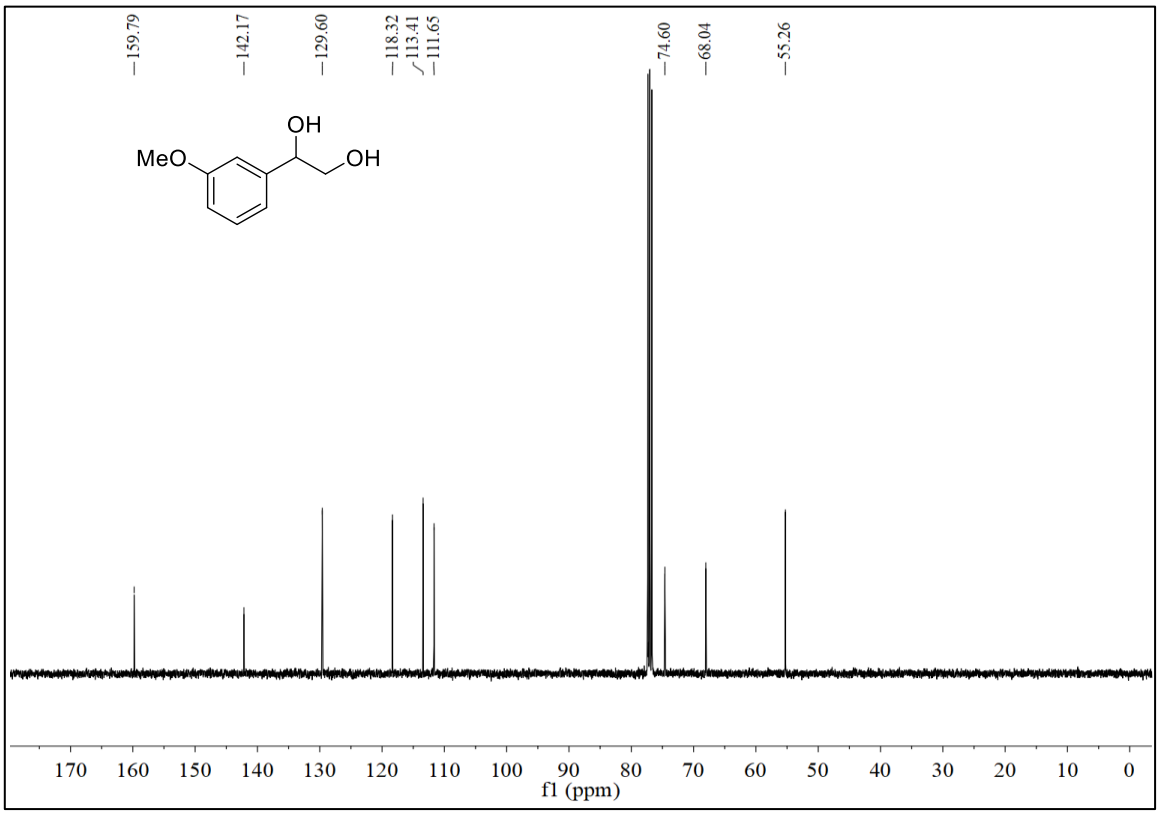

^{1}H-NMR (400 MHz, $CDCl_3$) of **1l**

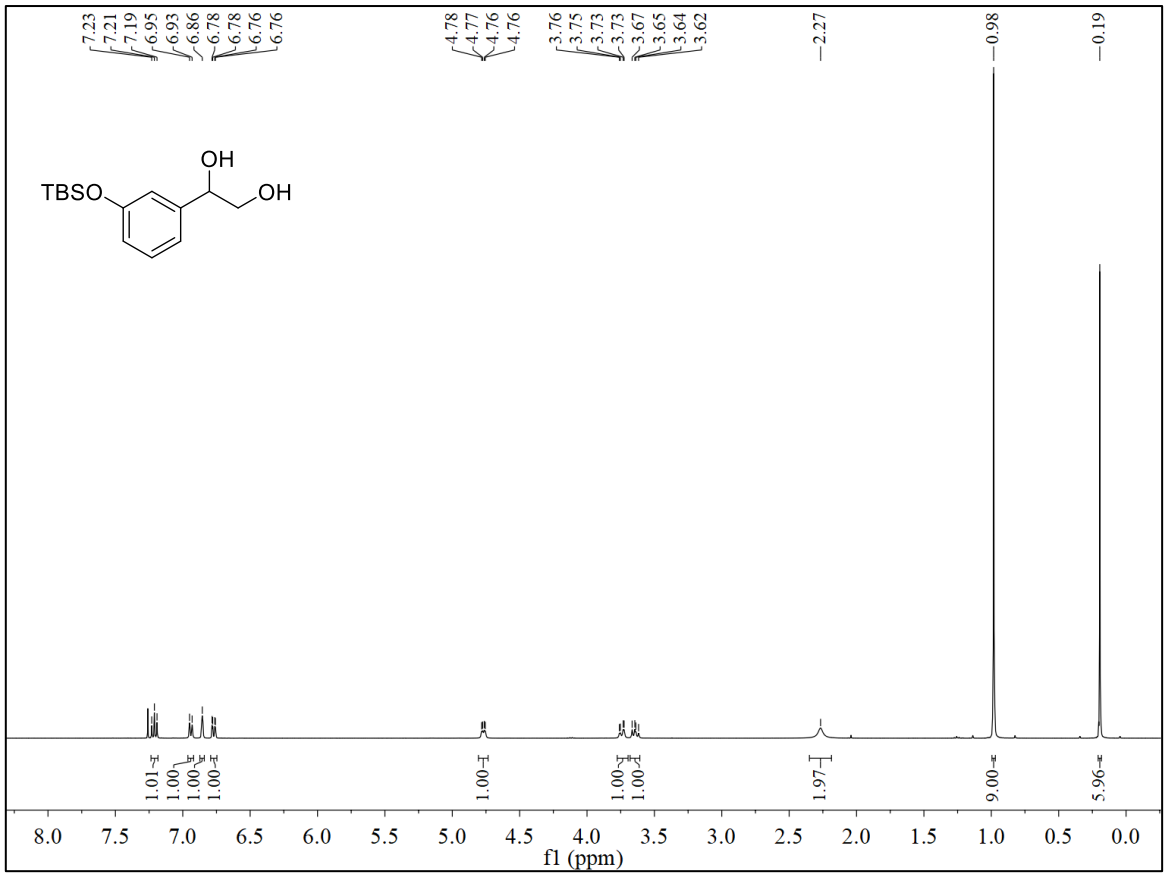

^{13}C-NMR (101 MHz, $CDCl_3$) of **1l**

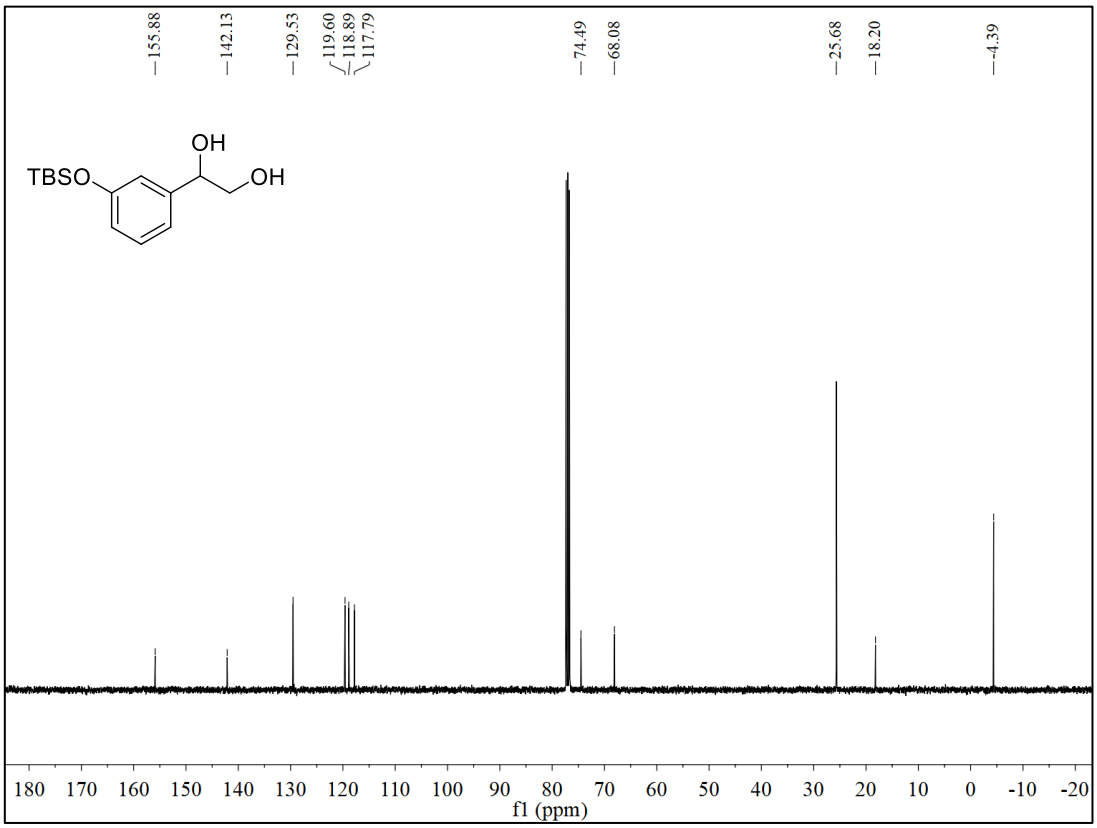

^{1}H-NMR (400 MHz, $CDCl_3$) of **1m**

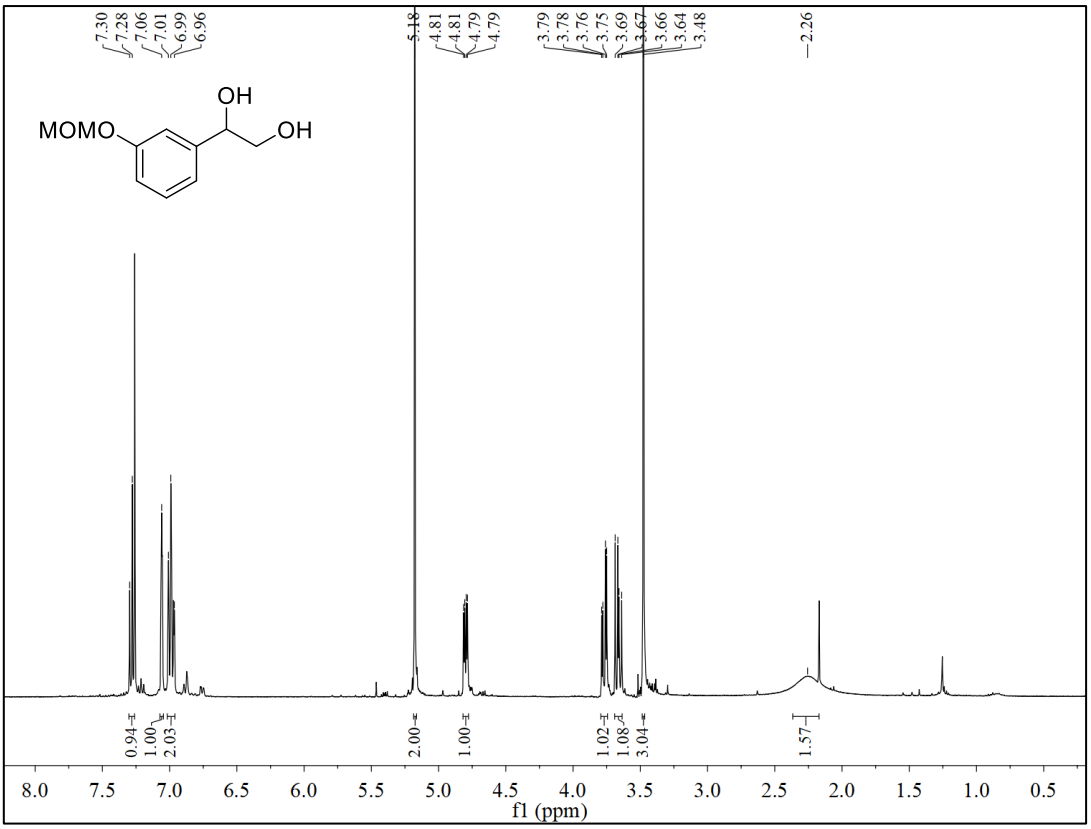

^{13}C-NMR (101 MHz, $CDCl_3$) of **1m**

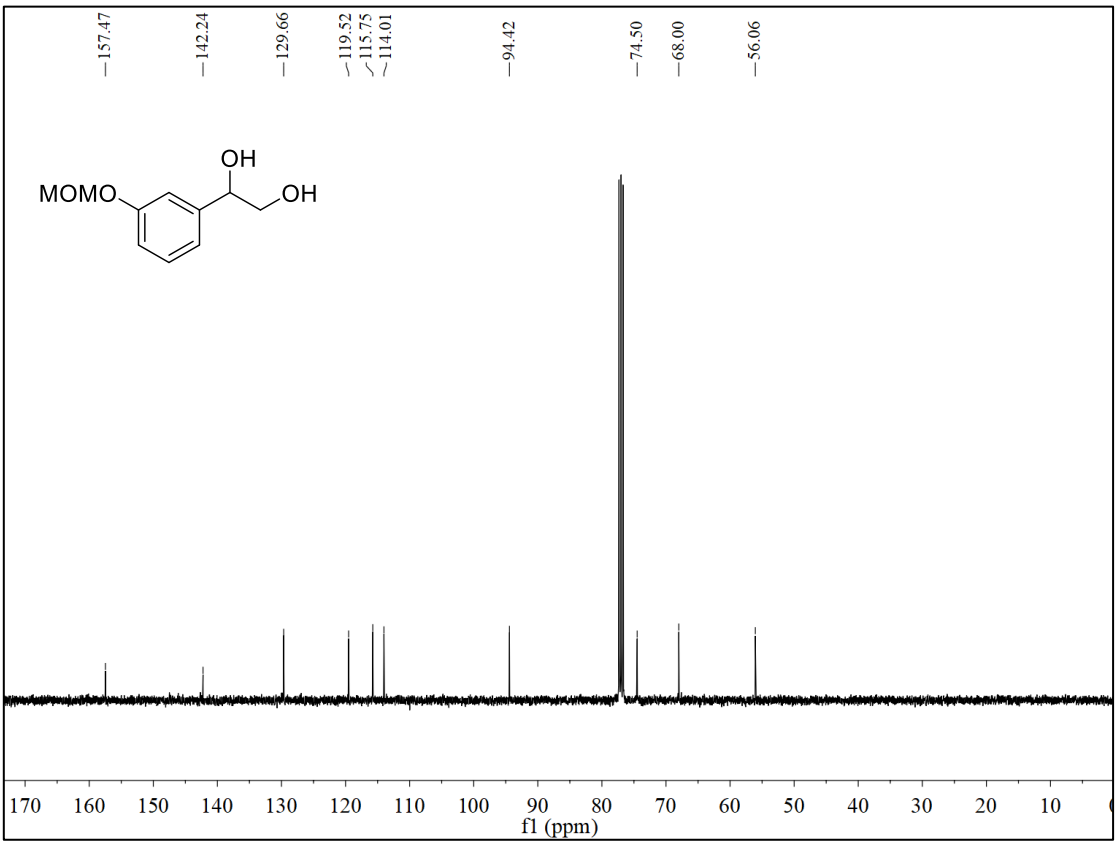

^{1}H-NMR (400 MHz, DMSO-d_6) of **1n**

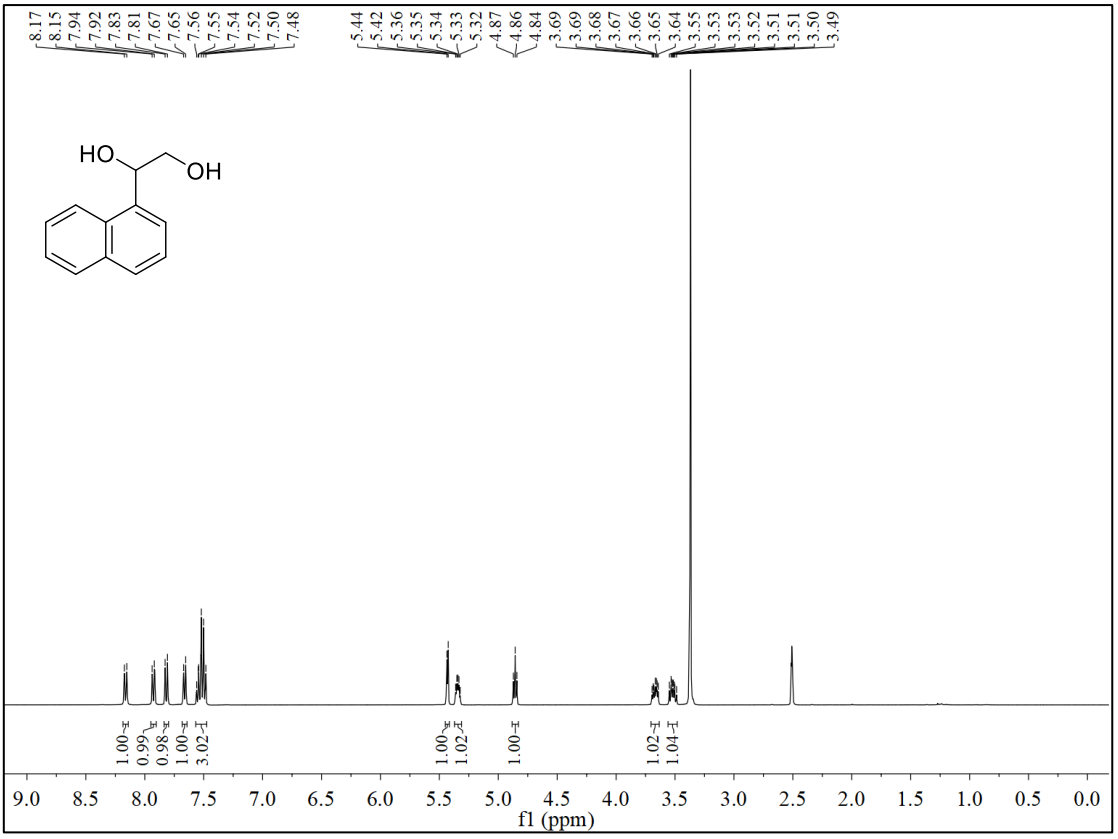

^{13}C-NMR (101 MHz, DMSO-d_6) of **1n**

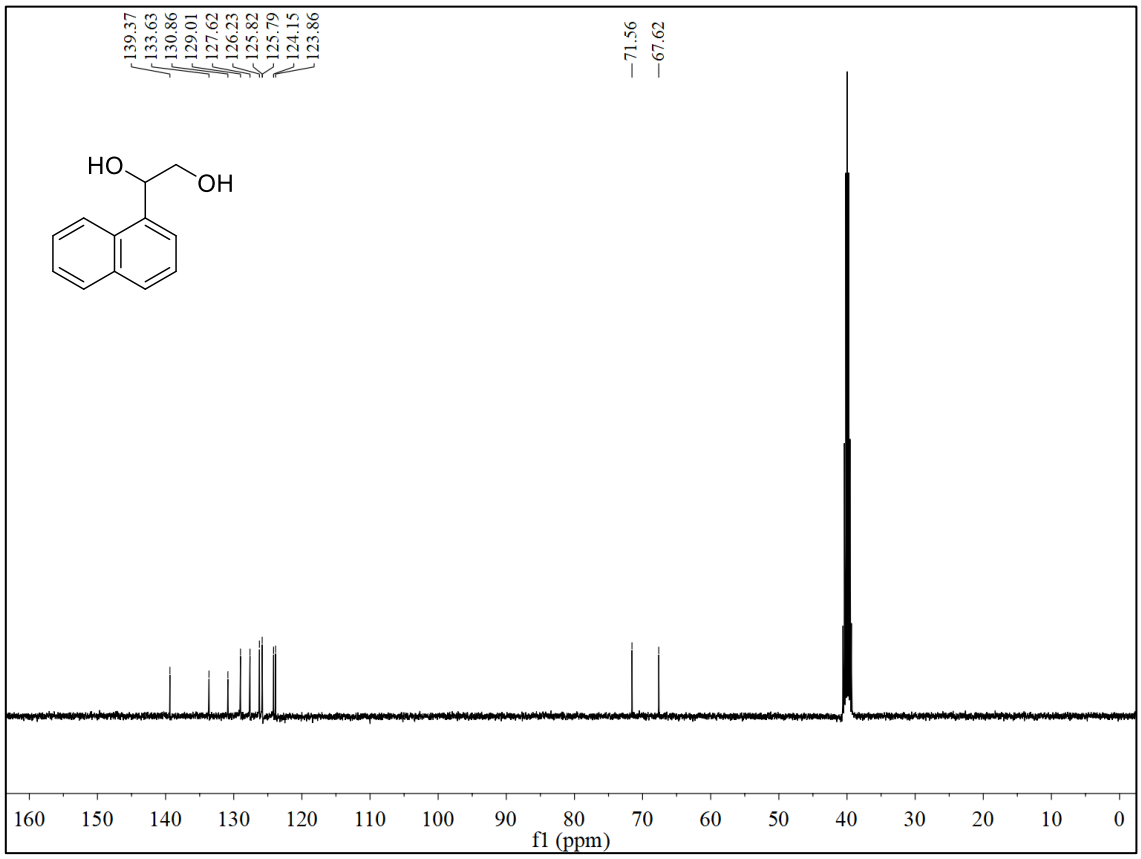

^{1}H-NMR (400 MHz, DMSO-d_6) of **1o**

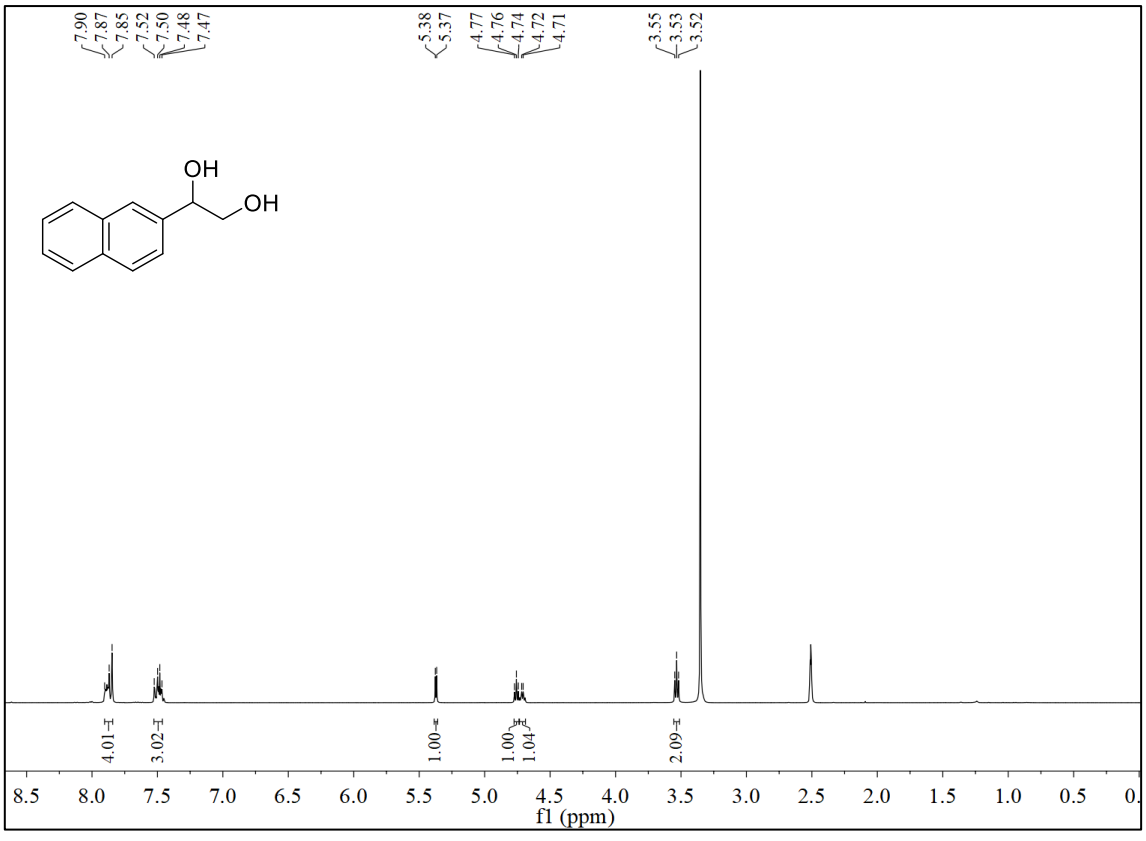

^{13}C-NMR (101 MHz, DMSO-d_6) of **1o**

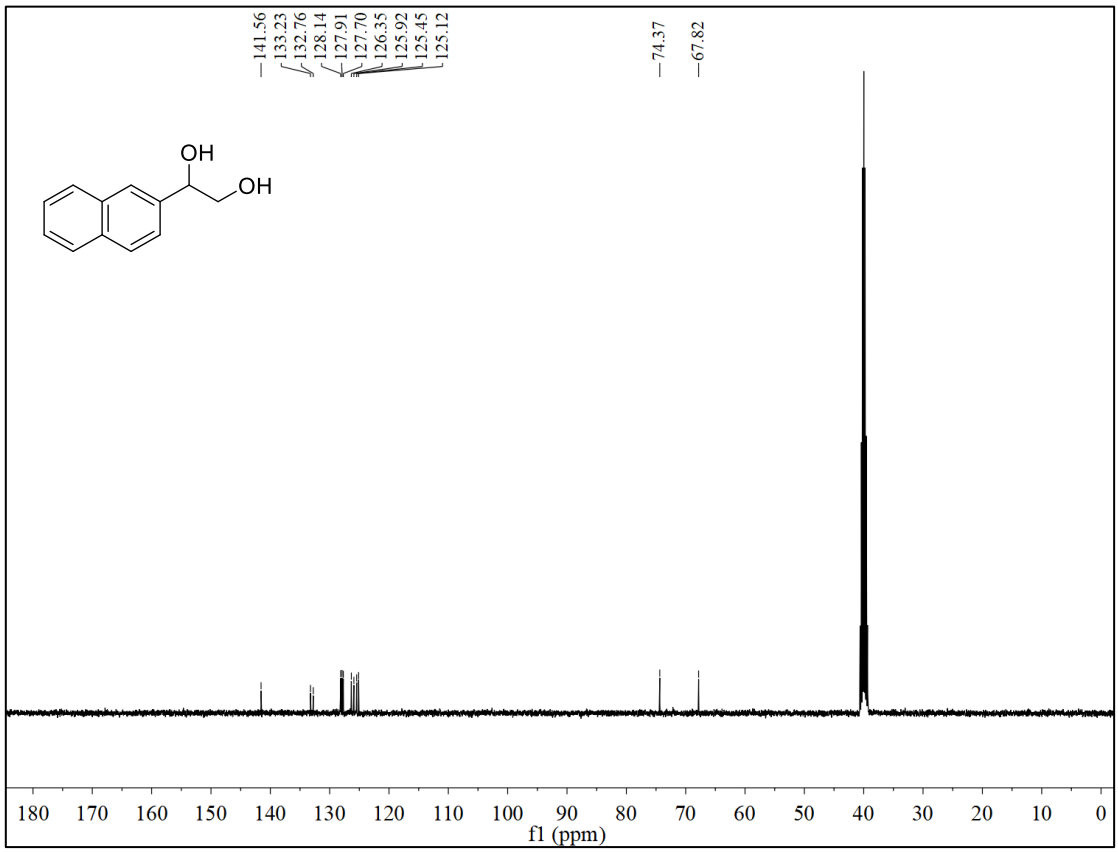

^{1}H-NMR (400 MHz, $CDCl_3$) of **1q**

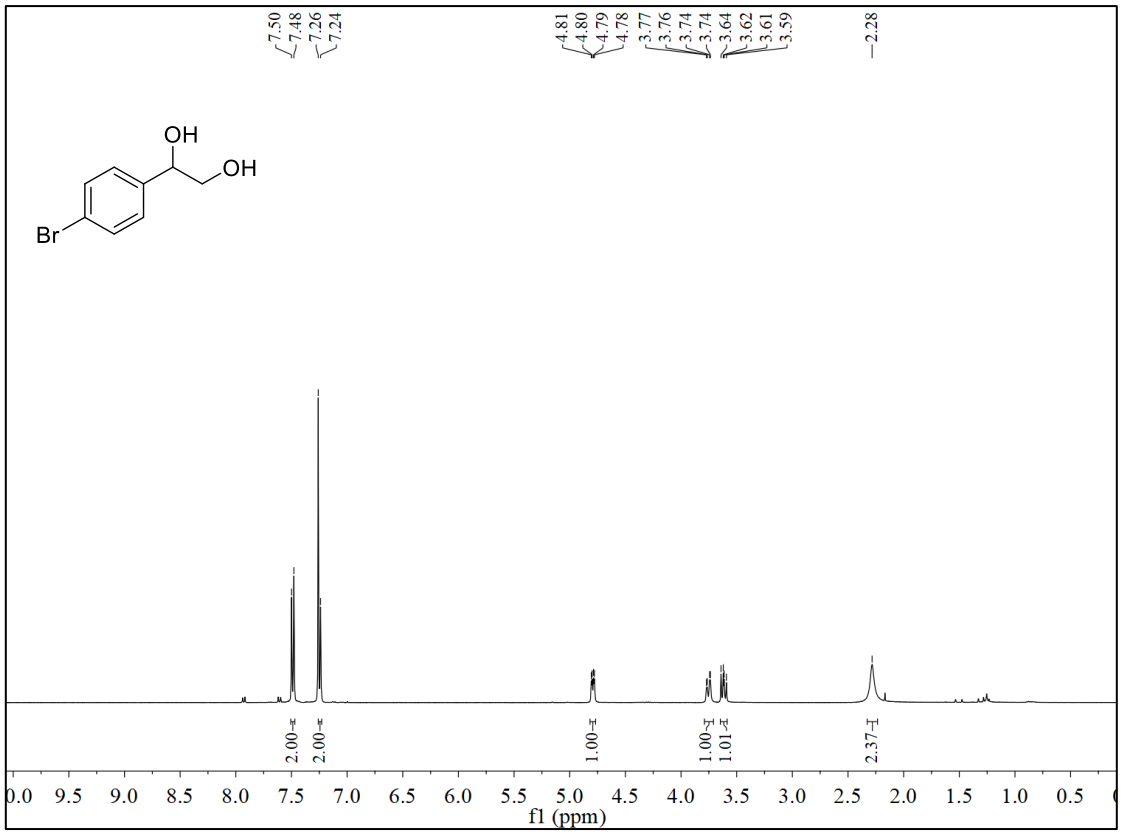

^{13}C-NMR (101 MHz, $CDCl_3$) of **1q**

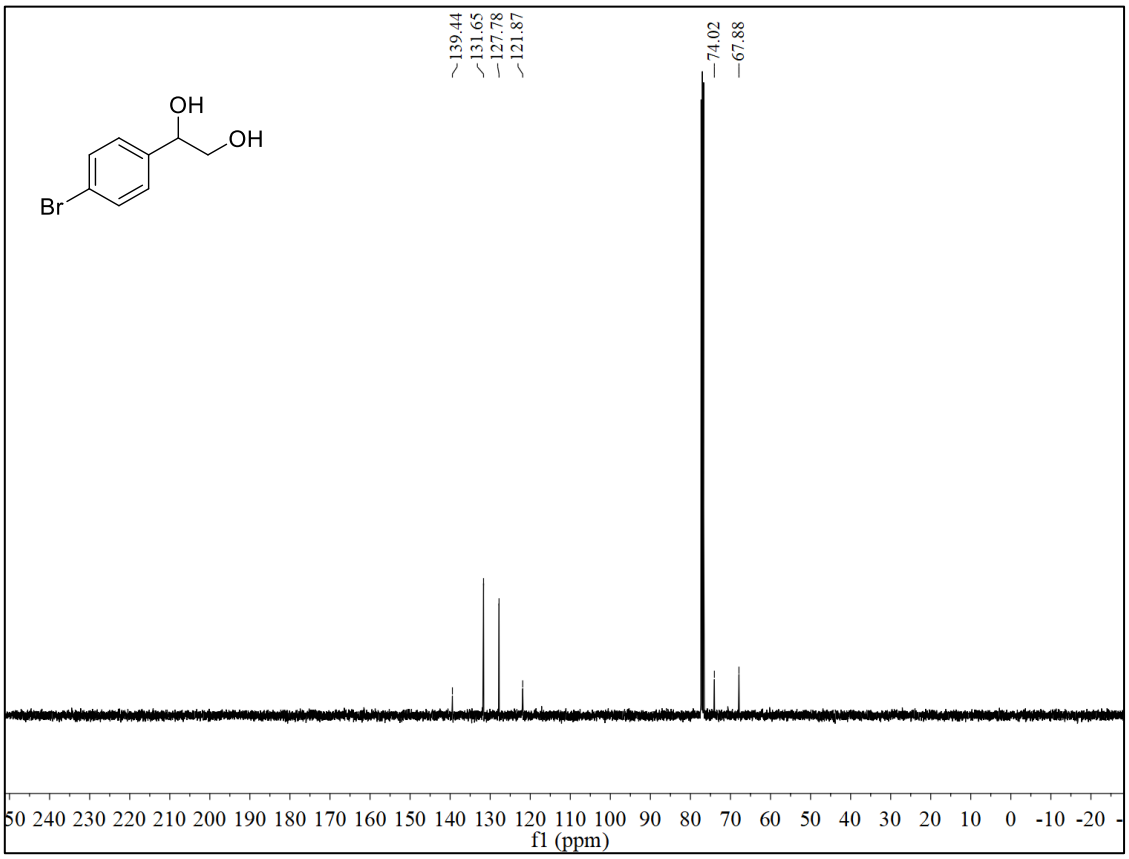

^{1}H-NMR (400 MHz, $CDCl_3$) of **1r**

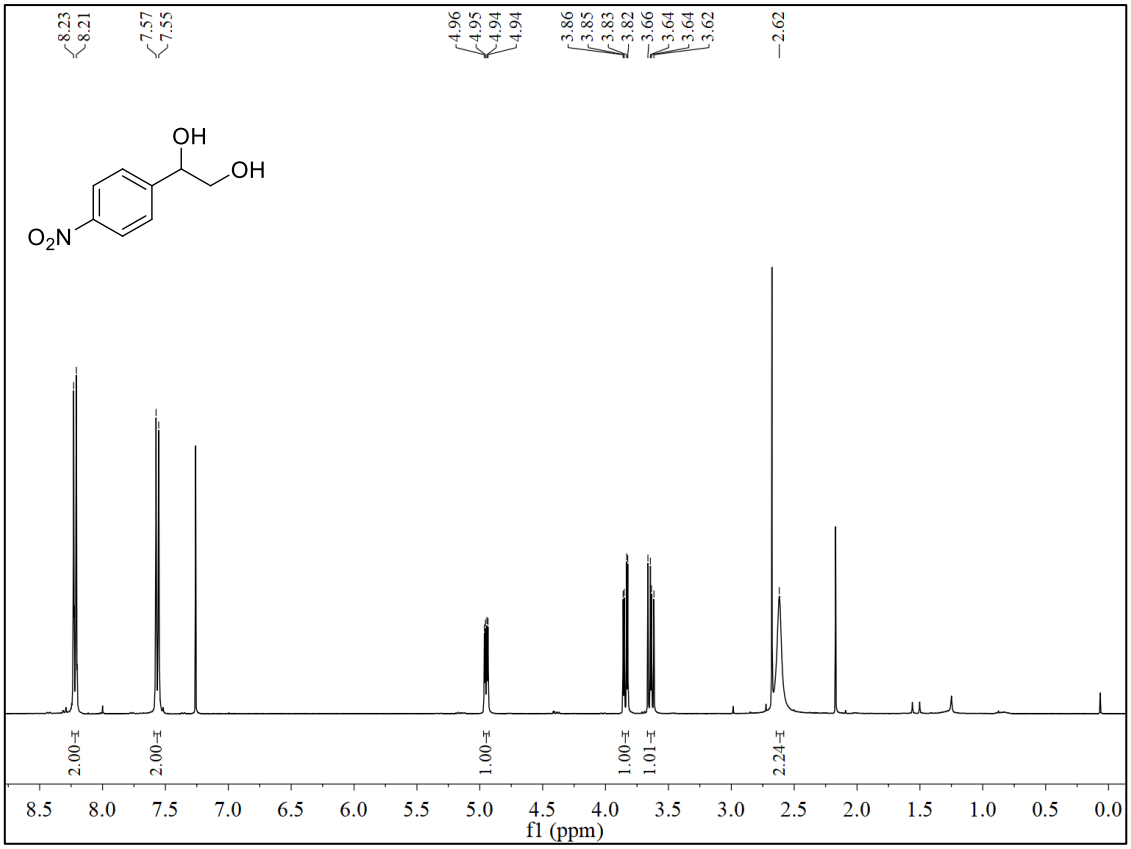

^{13}C-NMR (101 MHz, $CDCl_3$) of **1r**

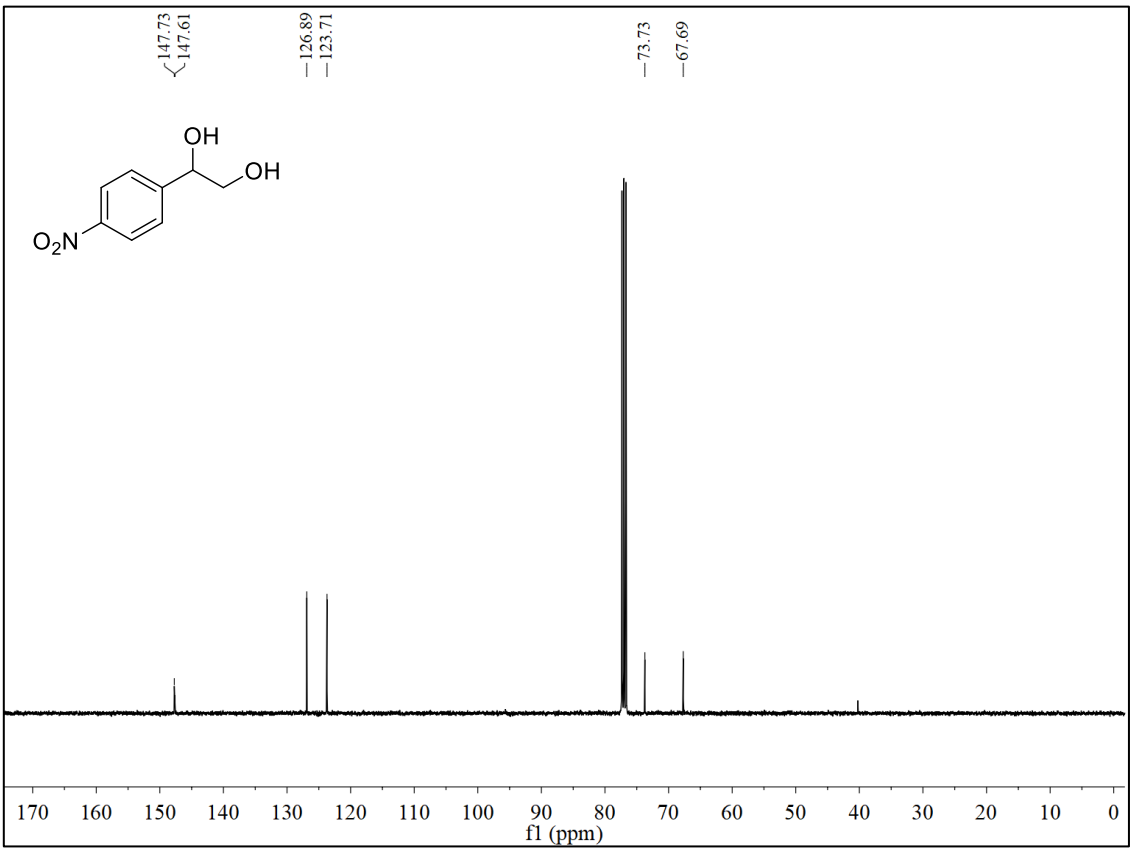

^{1}H-NMR (400 MHz, $CDCl_3$) of **1s**

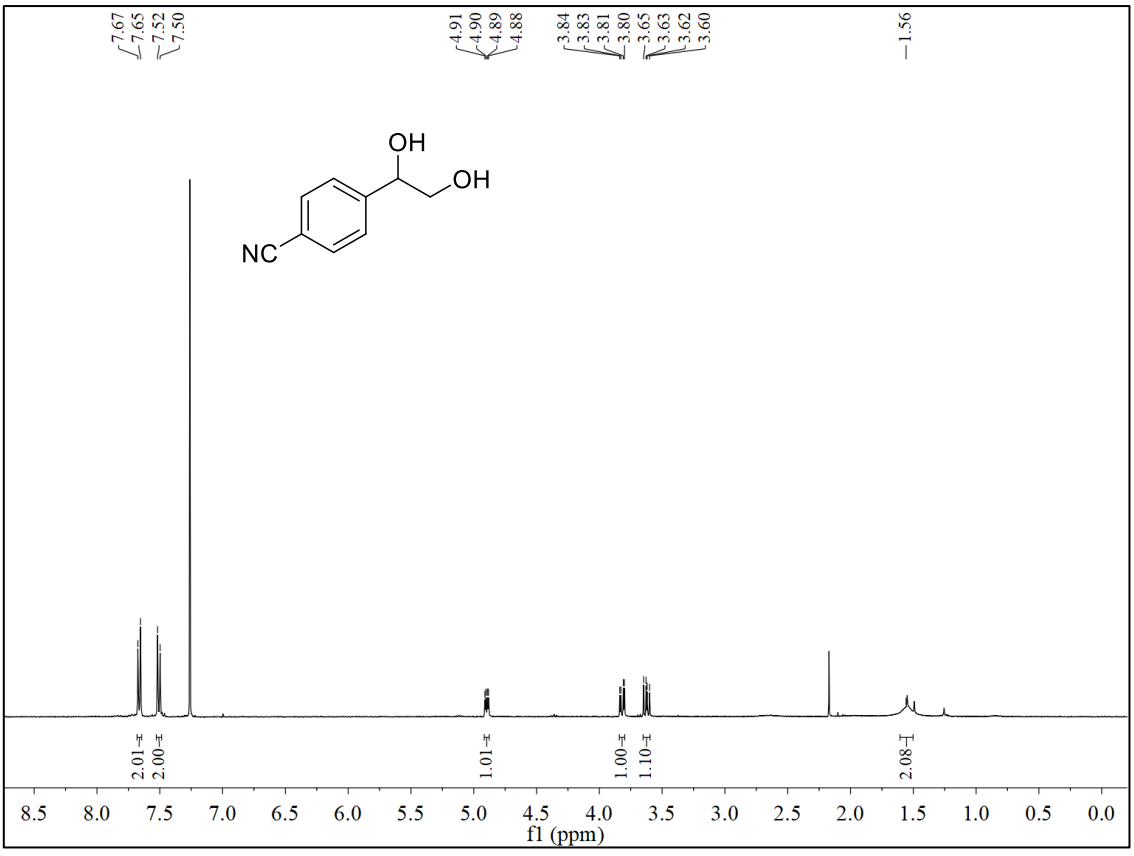

^{13}C-NMR (101 MHz, $CDCl_3$) of **1s**

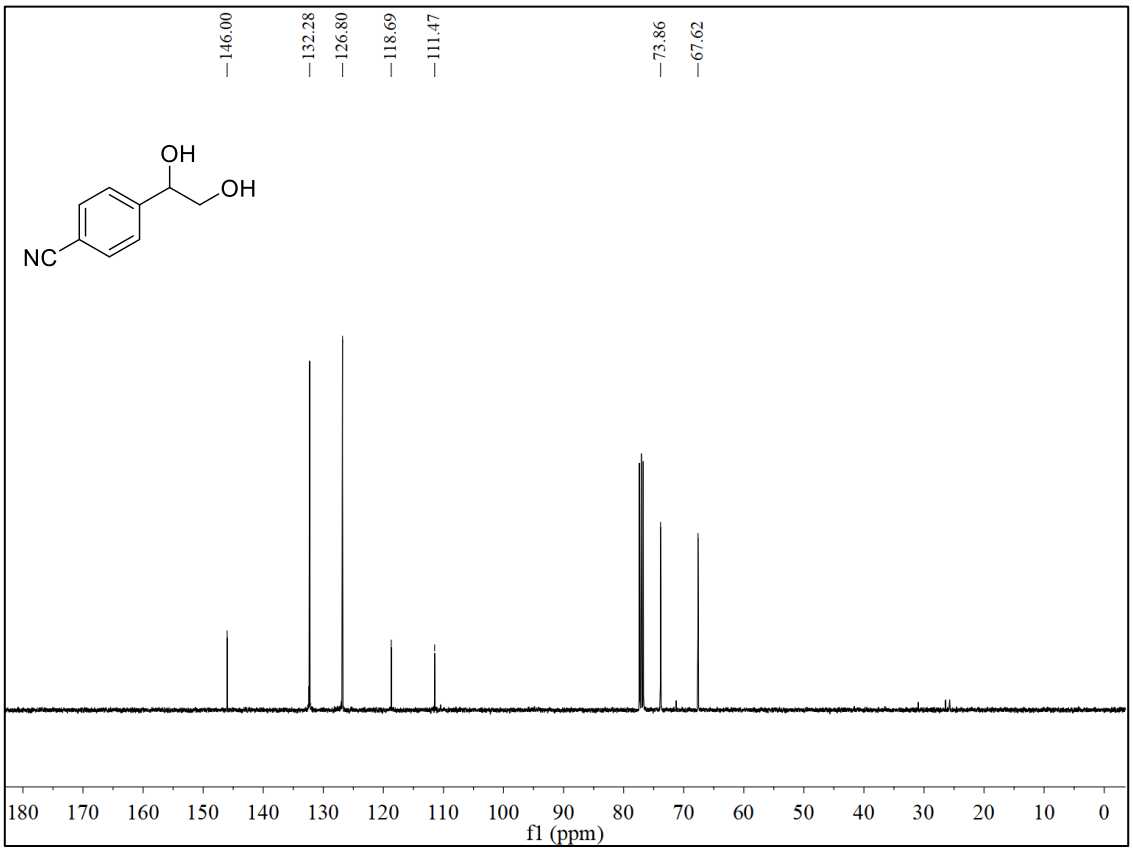

^{1}H-NMR (400 MHz, DMSO-d_6) of **1t**

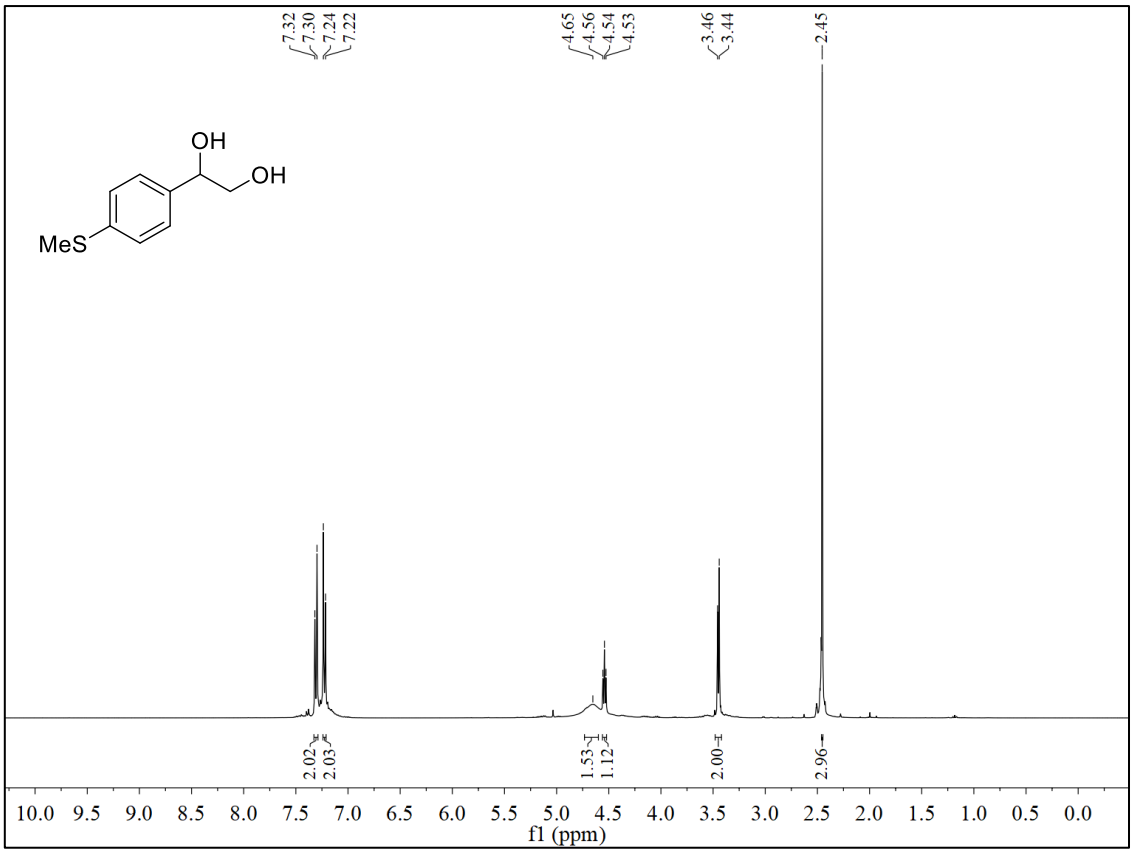

^{13}C-NMR (101 MHz, DMSO-d_6) of **1t**

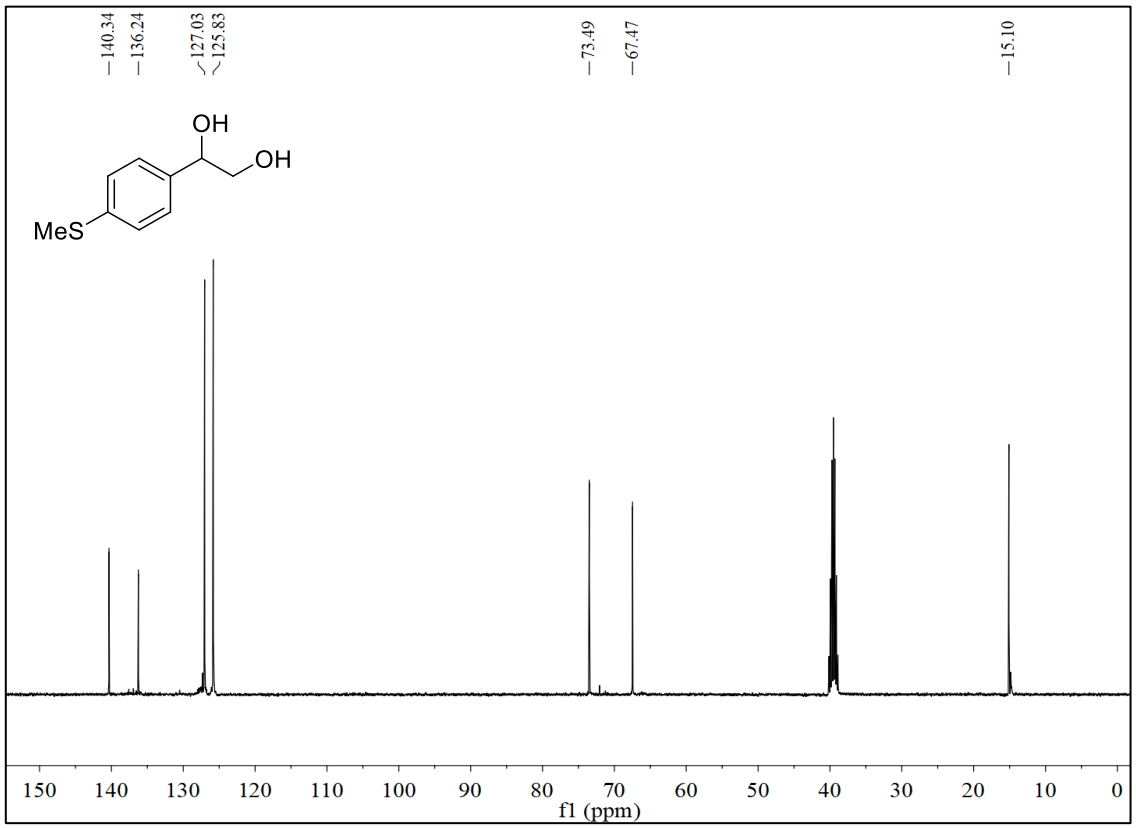

^{1}H-NMR (400 MHz, DMSO-d_6) of **S1**

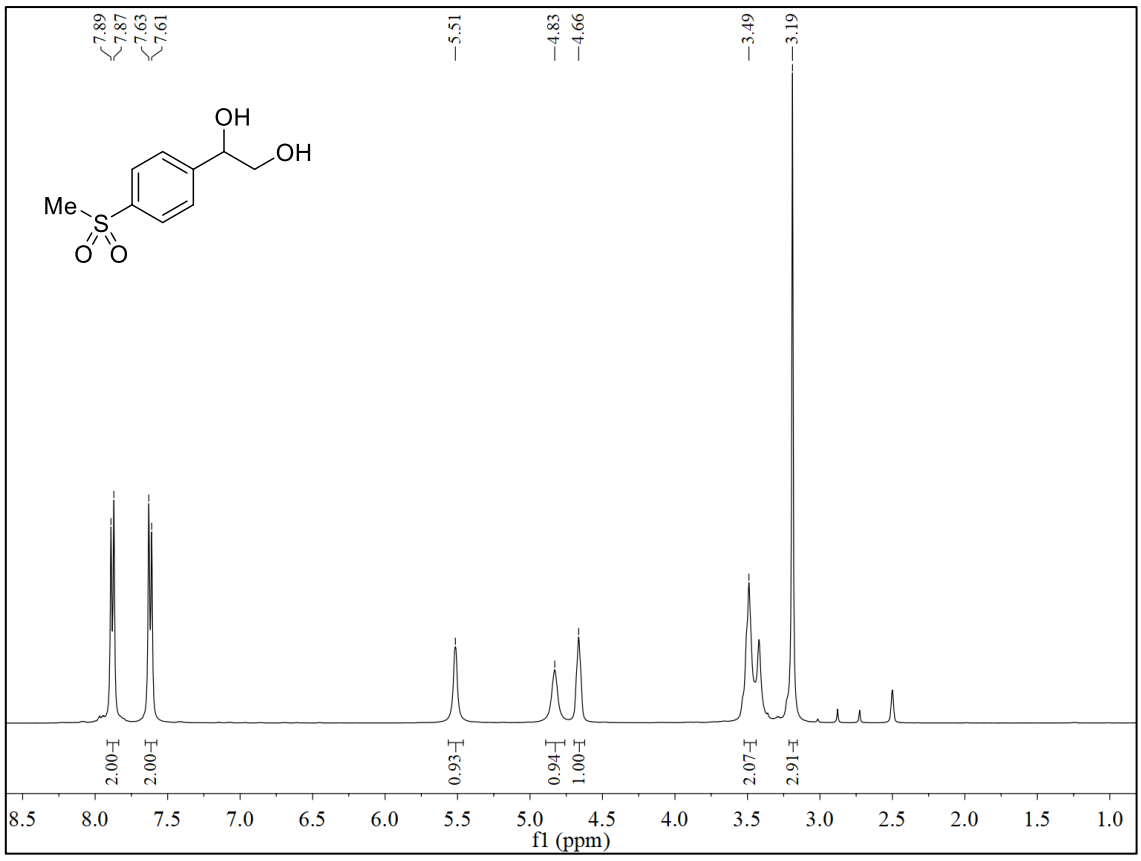

^{13}C-NMR (101 MHz, DMSO-d_6) of **S1**

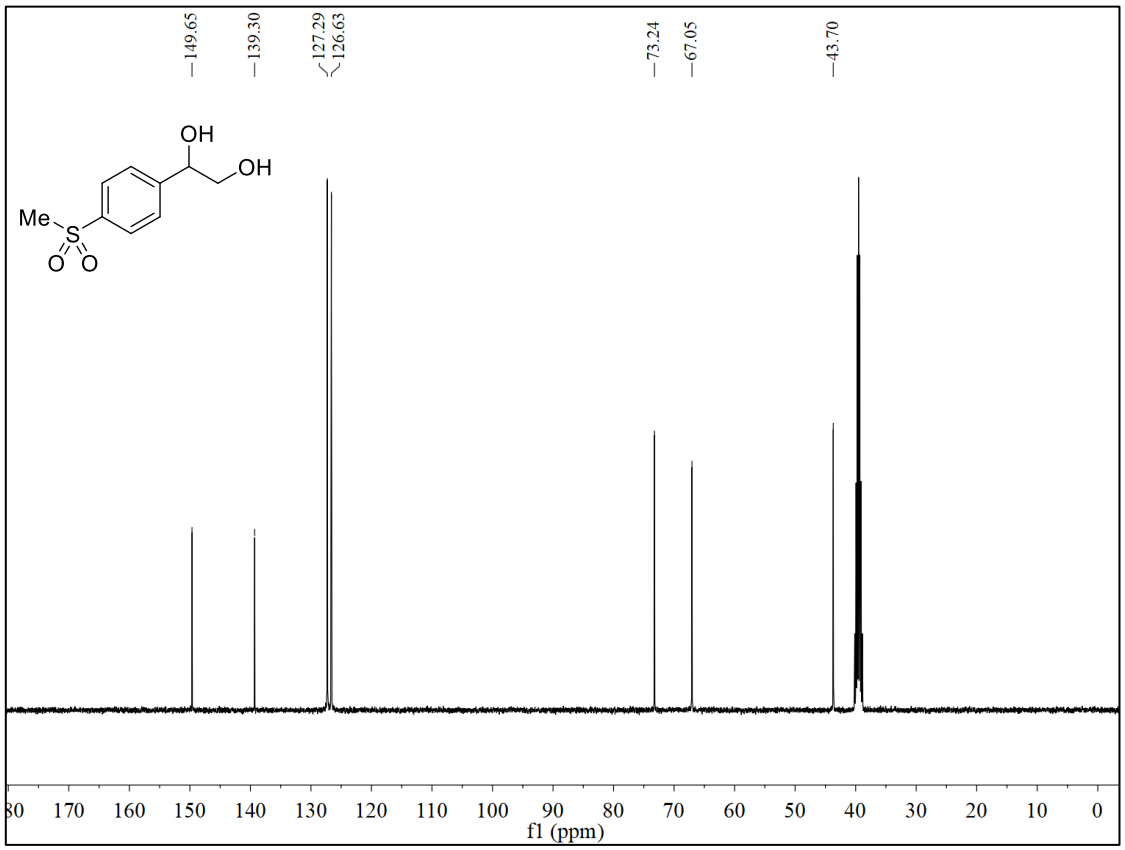

^{1}H-NMR (400 MHz, $CDCl_3$) of **S2**

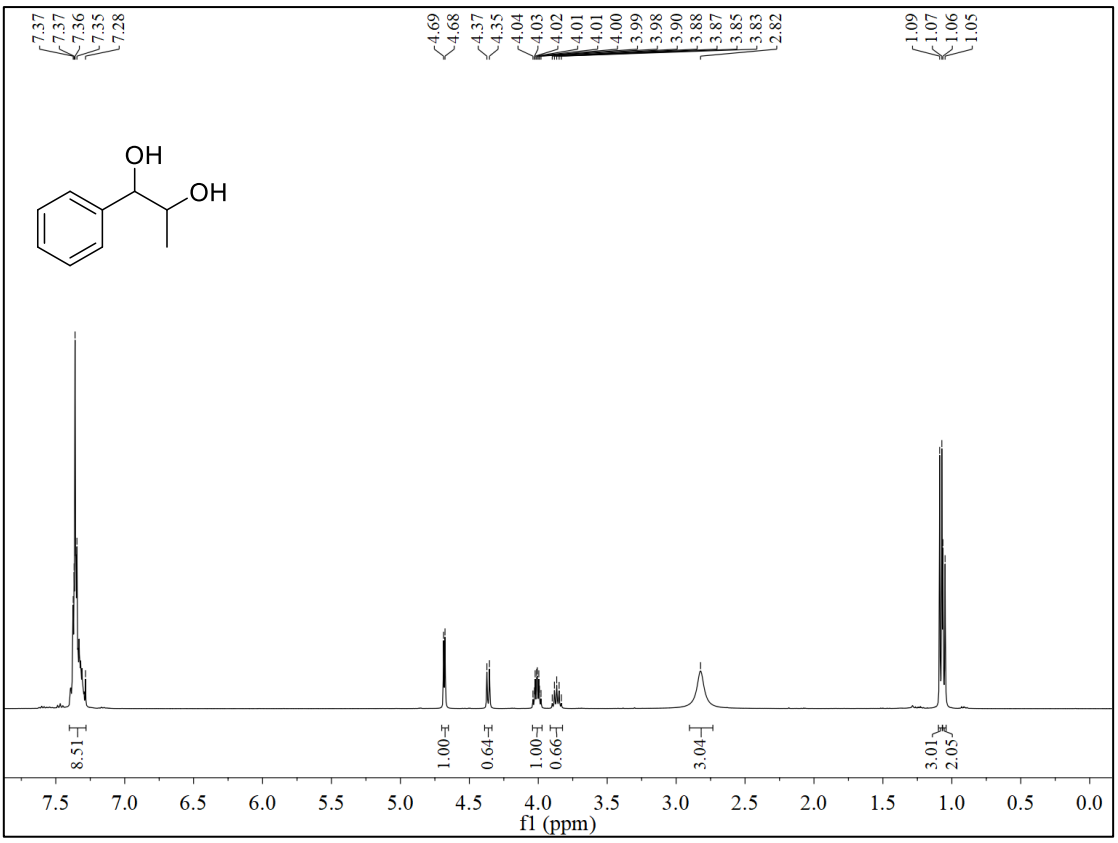

^{13}C-NMR (101 MHz, $CDCl_3$) of **S2**

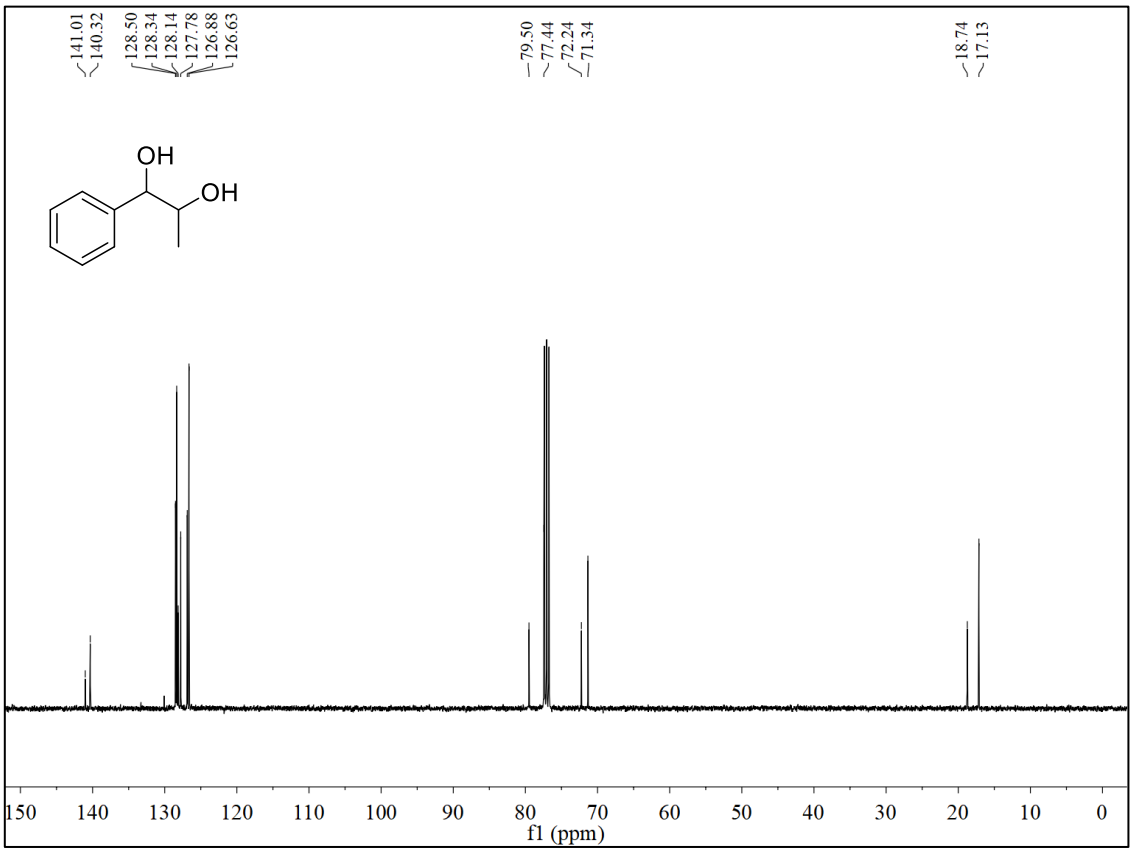

^{1}H-NMR (400 MHz, DMSO-d_6) of **S4**

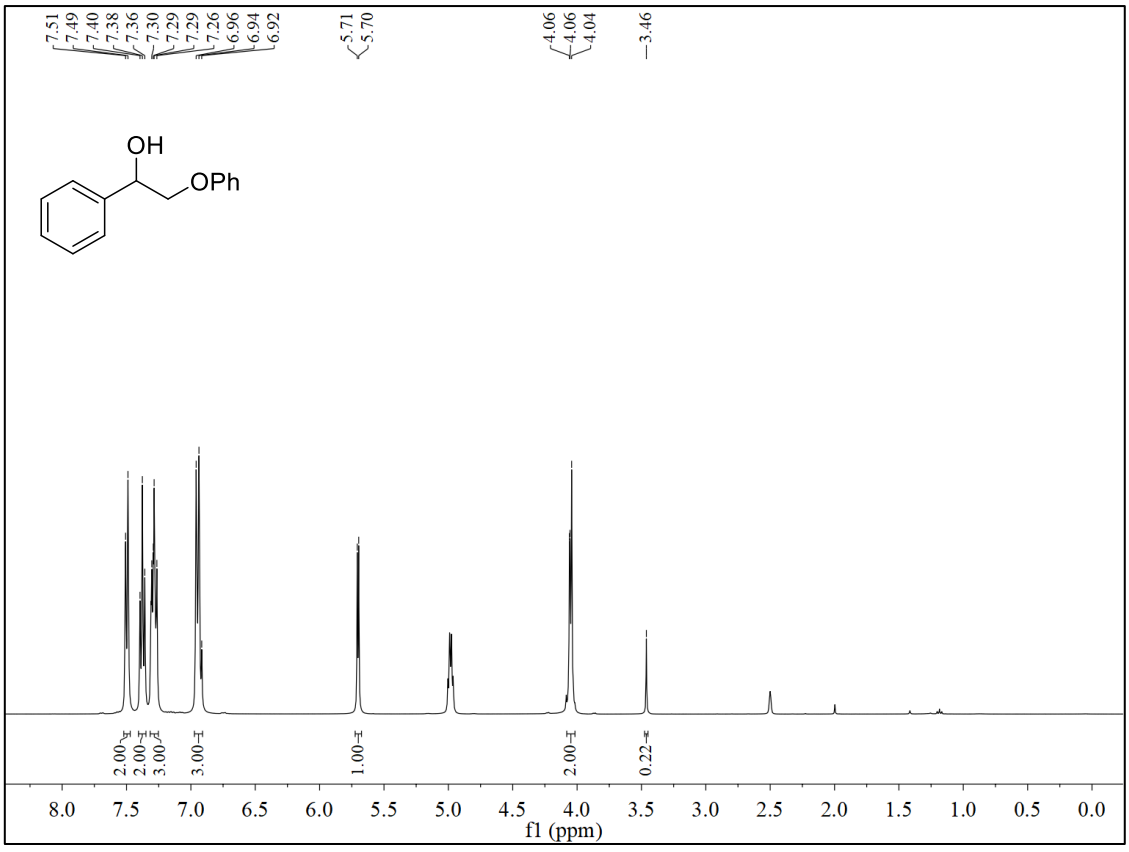

^{13}C-NMR (101 MHz, DMSO-d_6) of **S4**

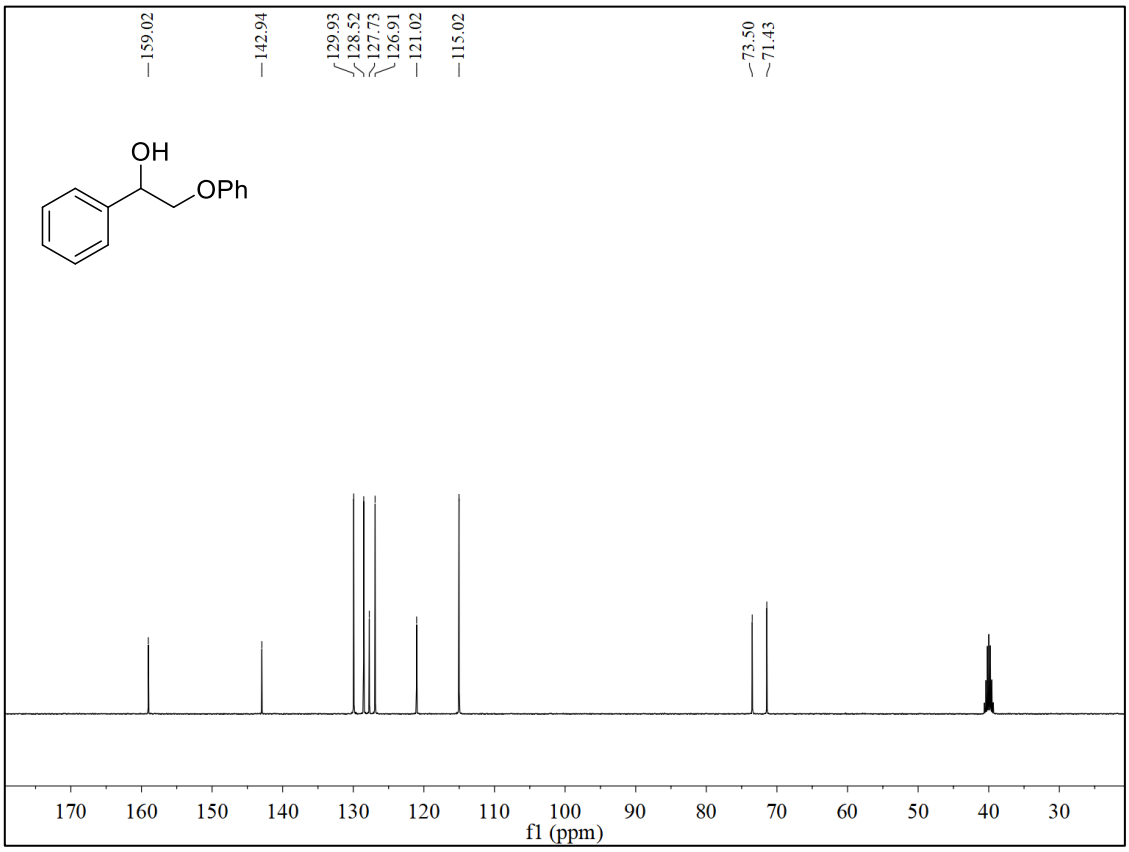

^{1}H-NMR (400 MHz, $CDCl_3$) of **S5**

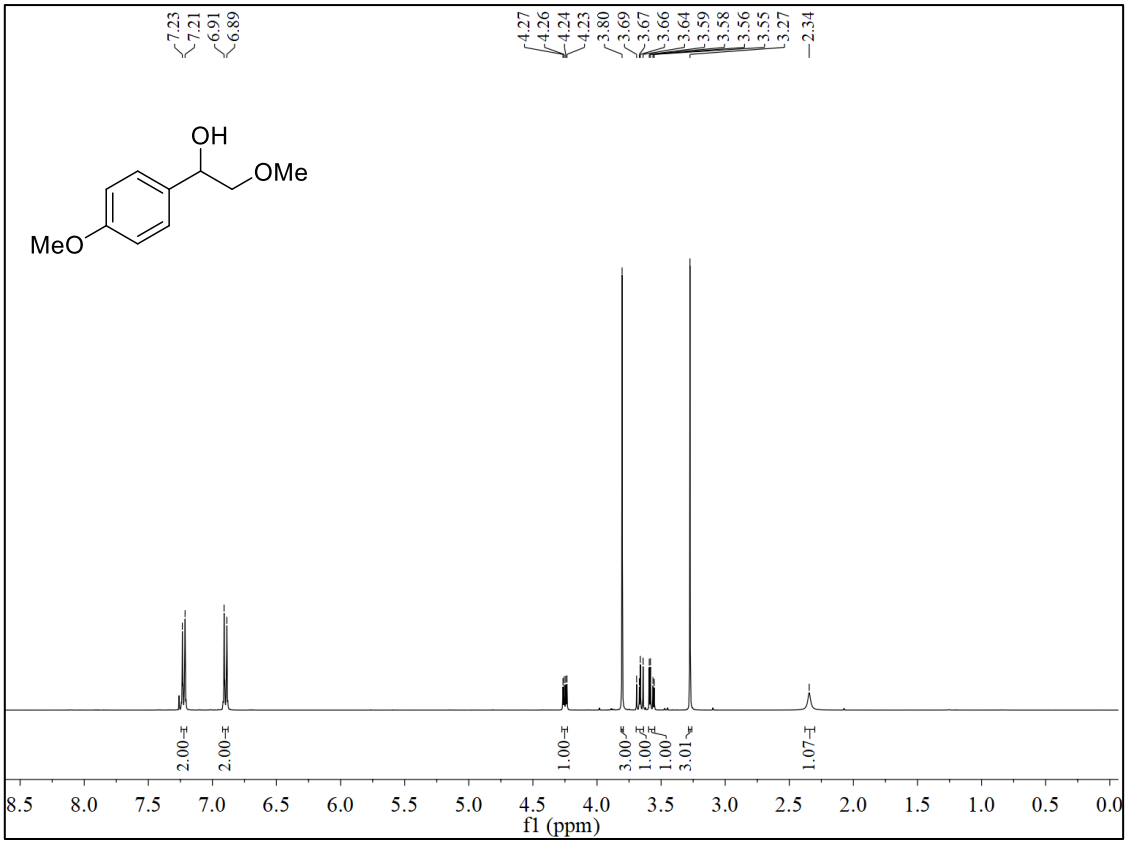

^{13}C-NMR (101 MHz, $CDCl_3$) of **S5**

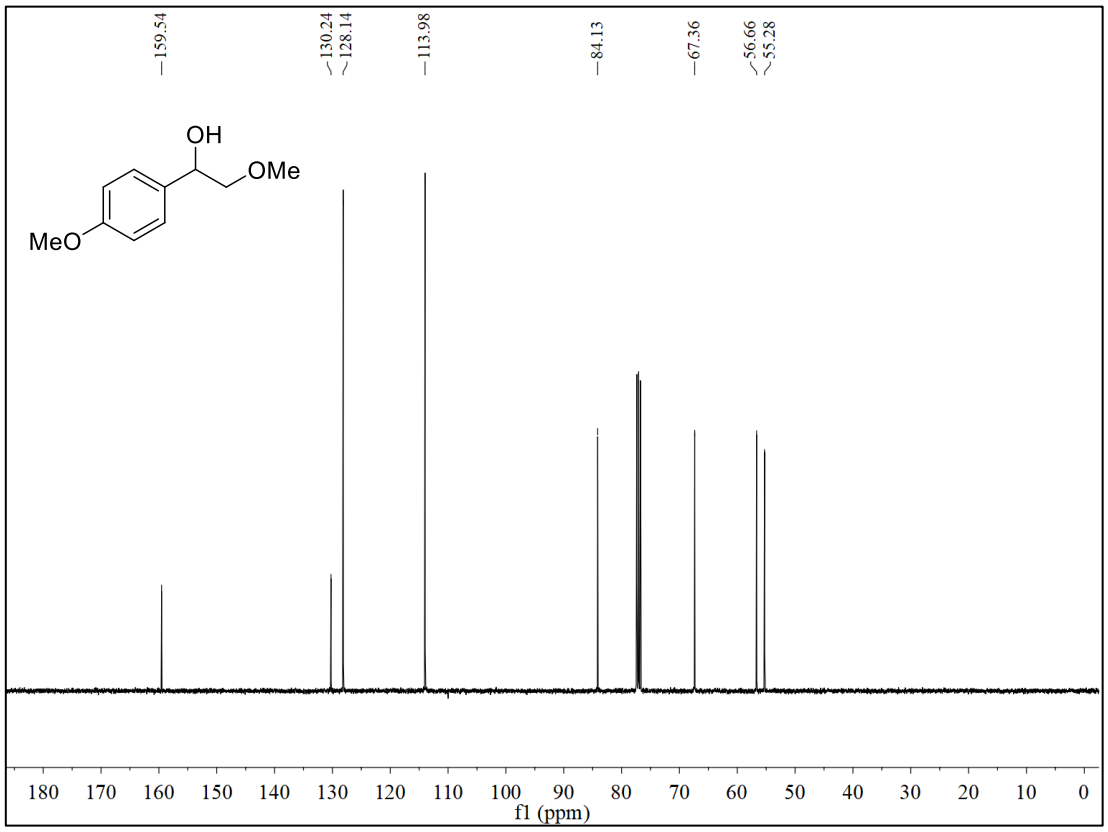

^{1}H-NMR (400 MHz, $CDCl_3$) of **S6**

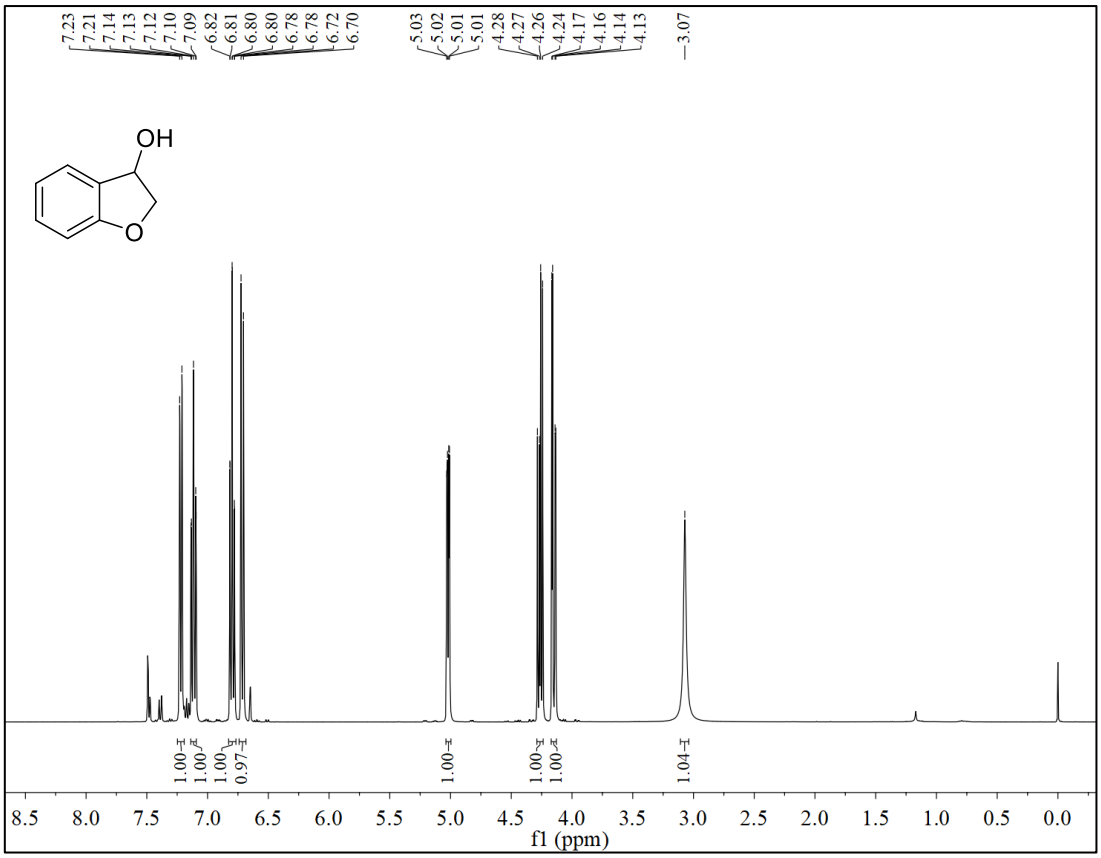

^{13}C-NMR (101 MHz, $CDCl_3$) of **S6**

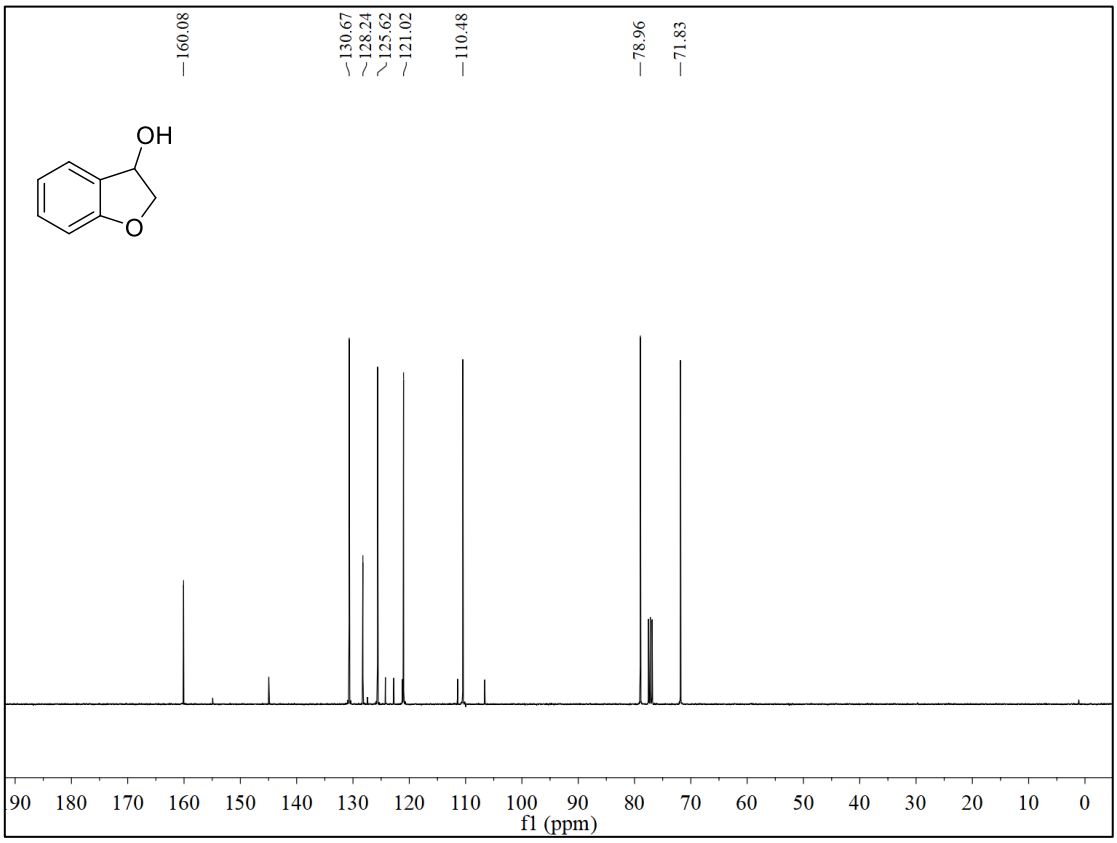

^{1}H-NMR (400 MHz, $CDCl_3$) of **1a_*d*$_1$**

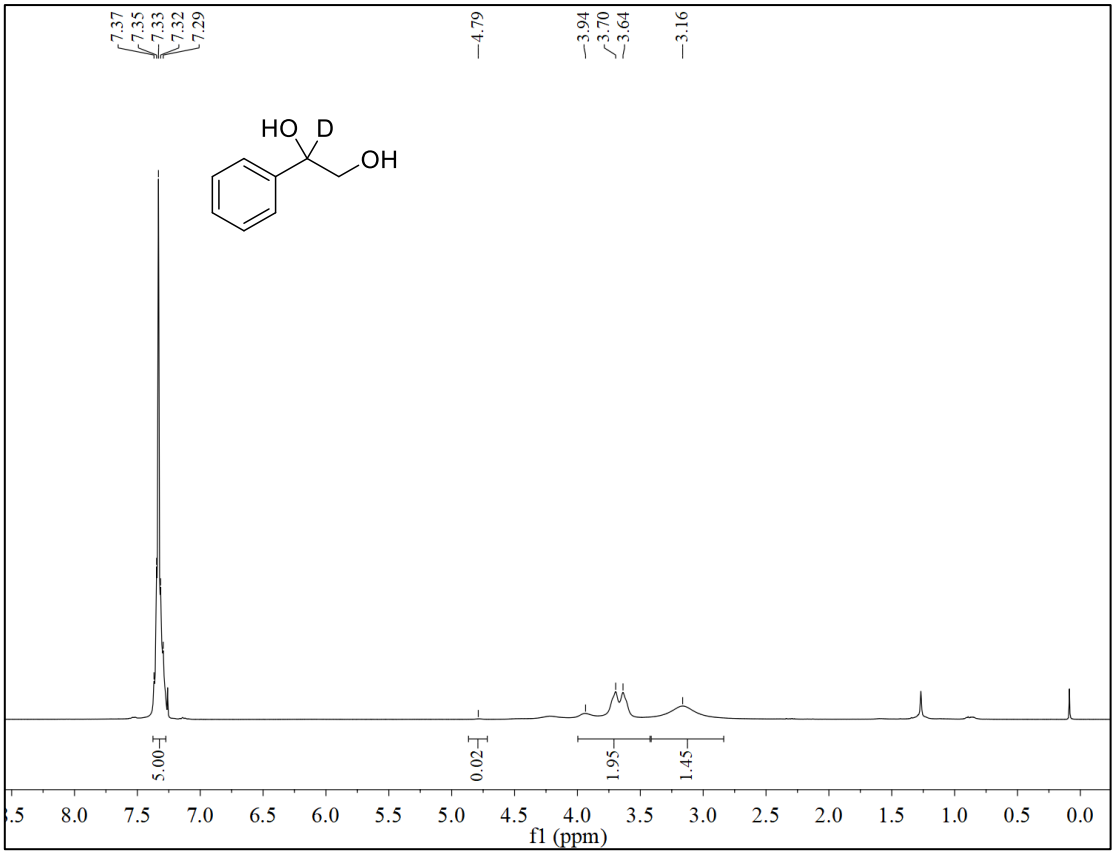

^{13}C-NMR (101 MHz, $CDCl_3$) of **1a**_***d₁***

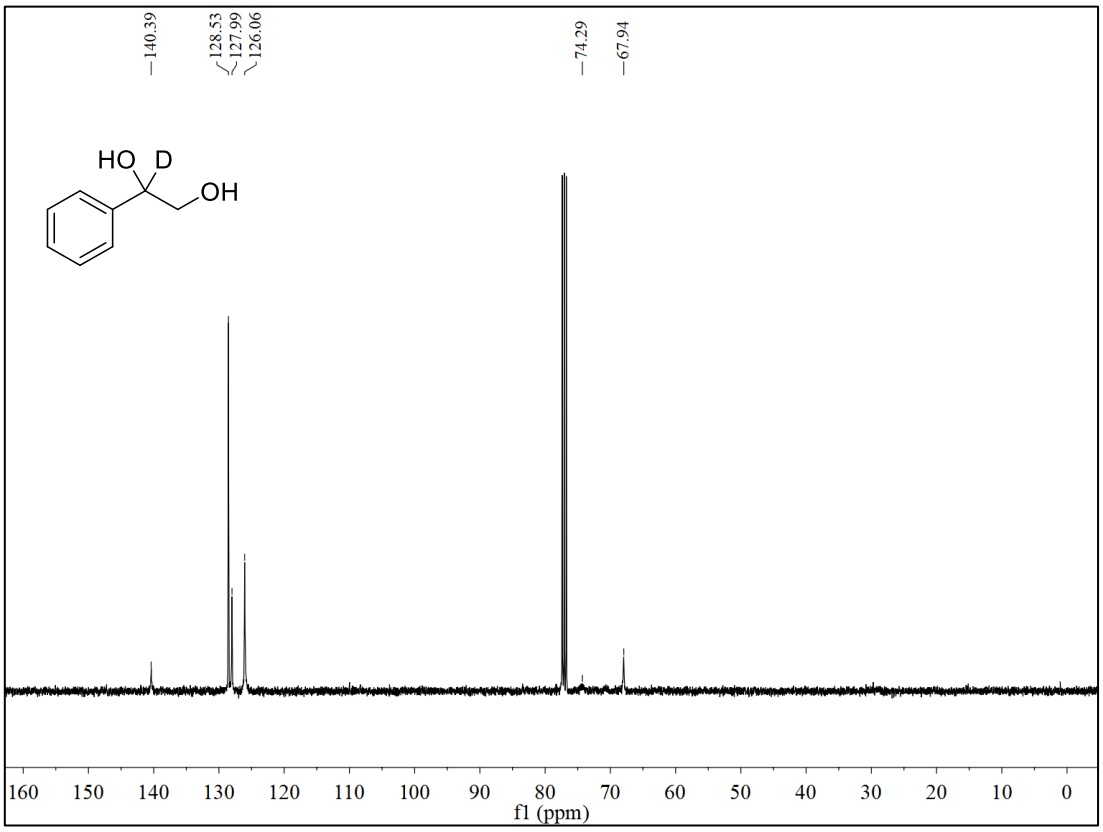

10. Acknowledgements

First, I would like to express my deepest gratitude to my family. This endeavour would not have been possible without your support throughout all these years.

I would also like to extend my sincere thanks to those outstanding teachers, instructors, and supervisors who have inspired and encouraged me to pursue a career in chemistry. Many thanks to Gerardo García Canca, Dr. Iván Cheng Sánchez, Prof. Dr. Francisco Nájera Albendín, Prof. Dr. Enrique Ramírez Losilla, Prof. Dr. María del Pilar Braos García, Prof. Dr. José Santamaría González, and Dr. Sebastian Graf. Special thanks to Prof. María Valpuesta Fernández for her patience and support while introducing me to the synthetic organic laboratory. I would also like to thank all my friends from the University of Malaga and from the University of Regensburg for the great shared moments.

Special thanks to Prof. Dr. Burkhard König for opening the doors of his research group to me and for his exceptional support while exploring the fascinating world of organic chemistry. These years have been a quest full of excitement and intrigue. I would like to express my gratitude for the trust deposited in me and the high degree of freedom I have been able to work during these years. It has been a fun and extremely creative experience. Thank you for your guidance during my master's and PhD thesis.

I would like to thank my collaboration partners for the fruitful discussions and successful projects; Dr. Ritu Chahal, Dr. Martin Morgenstern, Dr. Ahmad Al Barakat Almasalma, Leon Ganser, Isabel Weidacher, Kai Friedmann, and Dr. Andrey Fedulin. Thanks should also go to my colleagues Dr. Kathiravan Murugesan, Asad Shehzad, and Dr. Jessica Stahl for their help during my master's degree and doctoral studies.

I would also like to acknowledge Ernst Lautenschlager and Simone Strauß for technical assistance in our laboratories, Dr. Rudolf Vasold for support with GC measurements, Julia Zach for assistance with LED equipment, Britta Badziura for assistance with orders, Barbara Bauer for administrative support, and the analytical department of the University of Regensburg for their measurements.

Many thanks to the DFG-funded Collaborative Research Centre (CRC) 325 for financial support during my doctoral research and for giving me the opportunity to participate in conferences, seminars, and soft skill workshops to complement my education.

I am very much grateful to all doctoral committee members. Many thanks for their time and effort to Prof. Dr. Burkhard König (1st referee), Prof. Dr. Oliver Reiser (2nd referee), Prof. Dr. Frank-Michael Matysik (examiner), and PD Dr. Jonathan O. Bauer (chair).

11. Curriculum Vitae

Personal Data

Name: Daniel Franz Kolb

Education

PhD in Organic Chemistry May 2022 – May 2025
University of Regensburg, Germany
Thesis under the supervision of Prof. Dr. Burkhard König:
Photoinduced Hydrogen Atom Transfer Strategies for C-H Activation of Organic Molecules

M.Sc. Advanced Synthesis and Catalysis Mar 2020 – Feb 2022
University of Regensburg, Germany
Thesis under the supervision of Prof. Dr. Burkhard König:
Cyclization of Amino Acid Esters via Photocatalytic Carbanion Generation

B.Sc. Chemistry Sep 2015 – Feb 2020
University of Malaga, Spain
Thesis under the supervision of Prof. María Valpuesta Fernández
Synthesis and Conformational Study of Tetrahydro-3-benzazepines

Memberships

Collaborative Research Centre CRC 325 May 2022 – Present

Elite Network of Bavaria Mar 2020 – Present

Conference Contributions

International CataLysis Networking Conference, Pforzheim. Poster presentation Sep 2024

19th Asian Chemical Congress, Istanbul. Poster presentation Jul 2023

Publications

- D. Kolb,‡ A. Fedulin,‡ B. König,* *ChemPhotoChem* 2025, e202500036
- E. K. Taskinen, D. Kolb, M. Morgenstern, B. König,* *Chem. Eur. J.* 2025, *31*, e202404200.
- D. Kolb, K. Friedmann, B. König,* *ChemCatChem* 2024, *16*, e202400936.
- D. Kolb, A. A. Almasalma, M. Morgenstern, L. Ganser, I. Weidacher, B. König,* *ChemPhotoChem* 2023, *7*, e202300167.
- D. Kolb, M. Morgenstern, B. König,* *Chem. Commun*. 2023, *59*, 8592–8595.
- Ritu,‡ D. Kolb,‡ N. Jain,* B. König,* *Adv. Synth. Catal*. 2023, *365*, 605–611.

Eidesstattliche Erklärung

(1) Ich erkläre hiermit an Eides statt, dass ich die vorliegende Arbeit ohne unzulässige Hilfe Dritter und ohne Benutzung anderer als der angegebenen Hilfsmittel angefertigt habe; die aus anderen Quellen direkt oder indirekt übernommenen Daten und Konzepte sind unter Angabe des Literaturzitats gekennzeichnet.

(2) Bei der Auswahl und Auswertung folgenden Materials haben mir die nachstehend aufgeführten Personen in der jeweils beschriebenen Weise unentgeltlich geholfen:

1. Gekennzeichnete Untersuchungen in Kapitel 1 wurden von Dr. Andrey Fedulin durchgeführt.
2. Gekennzeichnete Experimente oder Untersuchungen in Kapitel 2 wurden von Kai Friedmann durchgeführt.
3. Gekennzeichnete Experimente oder Untersuchungen in Kapitel 3 wurden von Ritu durchgeführt. Kristalle wurden von der Röntgenstrukturanalyse der Zentralen Analytik gemessen und bearbeitet.
4. Gekennzeichnete Experimente oder Untersuchungen in Kapitel 4 wurden von Dr. Martin Morgenstern durchgeführt.
5. Gekennzeichnete Experimente oder Untersuchungen in Kapitel 5 wurden von Dr. Ahmad Al Barakat Almasalma, Dr. Martin Morgenstern, Leon Ganser und Isabel Weidacher durchgeführt.
6. Gekennzeichnete Experimente oder Untersuchungen in Kapitel 6 wurden von Elina Taskinen und Dr. Martin Morgenstern durchgeführt.

(3) Weitere Personen waren an der inhaltlich-materiellen Herstellung der vorliegenden Arbeit nicht beteiligt. Insbesondere habe ich hierfür nicht die entgeltliche Hilfe eines Promotionsberaters oder anderer Personen in Anspruch genommen. Niemand hat von mir weder unmittelbar noch mittelbar geldwerte Leistungen für Arbeiten erhalten, die im Zusammenhang mit dem Inhalt der vorgelegten Dissertation stehen.

(4) Die Arbeit wurde bisher weder im In- noch im Ausland in gleicher oder ähnlicher Form einer anderen Prüfungsbehörde vorgelegt.

Regensburg, der 17.06.2025